A journal of exper

Published by the American Institute of Phys
for the
AMERICAN PHYSICAL SOCIETY

Officers

President

M. A. Bitter
Cornell University
Ithaca, New York

Vice-President

R. T. Birge
University of California,
Berkeley, California

Secretary

K. K. Darrow
Bell Telephone Laboratories
Office:
Columbia University
New York 27, New York

Treasurer

G. B. Pegram
Columbia University
New York 27, New York

Local Secretary
for the Pacific Coast

J. Kaplan
University of California at Los
Angeles
Los Angeles, California

Managing Editor

S. A. Goudsmit
Brookhaven National Laboratory
Upton, Long Island
New York

The Physical Review
Entered as second-class matter
acceptance for mailing at special rate of

W

S. L. Nichols in 189

EDITORS

Associate Editors

P. G.
Cambridge
F. J.
P. Kirk
R.
J. C.

communications to S. A. Goudsmit,
Upton, Long Island, New York. The
pay a publication charge of $10 per
to 100 free reprints. Instructions with

corresponding papers in the process of publication
Publication Manager, American Institute of
New York 22, New York.

Subscription Rates

.....$20.00
.....$10.00

Back Numbers

year is available:

1929;
December, 1941;
January, 1943–December, 1945;

back numbers should be addressed to
East 55 Street, New York 22.

members of the American Physical
for the case of other subscribers.

Cornell University, Ithaca, New York.

Easton, Pennsylvania.
, under the Act of March 3, 1879.
P. L. & R. of 1948, authorized January 24, 1942

THE
PHYSICAL REVIEW

A journal of experimental and theoretical physics established by E. L. Nichols in 1893

SECOND SERIES, VOL. 93, No. 6 MARCH 15, 1954

A Generalization of Yang and Lee's Theory of Condensation*

LOUIS WITTEN
Institute for Fluid Dynamics and Applied Mathematics, University of Maryland, College Park, Maryland
(Received November 13, 1953)

Yang and Lee's theory of phase transitions is extended to include a wider class of potential energy functions. In particular, it is shown that the theory does not require a potential with a hard core; the repulsive part of the potential need only be greater than $1/r^n$; $n \geqq 11.4$.

I. INTRODUCTION

YANG and Lee[1] have developed a theory of condensation that describes the condensed as well as the gas phases and the transition regions. They deal with monatomic gases and assume, besides additivity, the following properties for the interaction energy: (1) the atoms have a finite impenetrable core of diameter a, so that $u(r)=+\infty$ for $r \leqq a$; (2) the interaction has a finite range b, so that $u(r)=0$ for $r \geqq b$; (3) $u(r)$ is nowhere minus infinity and has a lower bound $-M$.

They point out that assumption (2) can be relaxed to include forces with a weak long tail such as Van der Waal's force. However, the possibility of relaxing assumption (1) is not mentioned by YL and this assumption seems to play an essential role in their proofs. It seems physically obvious, however, that the existence of condensation phenomena should not depend on the existence of a finite inpenetrable core, but should occur even if the repulsive forces are weaker. It is the purpose of this note to show that assumption (1) can in fact be relaxed. We show that all of the theorems quoted by YL still hold if we replace assumption (1) by the following assumption (1a):

As $r \to 0$, the potential $u(r)$ increases as $1/r^n$; $n > 11.4$. (1a)

We do not believe that 11.4 establishes in fact the smallest value of n for which the theorems are true, but it is the smallest value for which we have established them. Replacing (1) by (1a) in the manner indicated means that the grand partition function is not a polynomial in the fugacity y, and the factorization given by YL does not hold. However, the existence and character of phase transitions still depend on the distribution of zeroes of the grand partition function in the complex y (fugacity) plane.

In Sec. II we discuss the convergence of the grand partition function; the question of convergence did not arise for YL, since their grand partition function is a polynomial. Section III contains the proofs of the theorems of YL using the weaker repulsion of assumption (1a) rather than the core [assumption (1)].

II. CONVERGENCE OF THE GRAND PARTITION FUNCTION

Recall the definition of the grand partition function of the gas in the volume V at the temperature T:

$$\mathcal{Q}_V = \sum_{N=0}^{\infty} \frac{Q_N}{N!} y^N,$$

where

$$y = (2\pi mkT/h^2)^{\frac{1}{2}} \exp(\mu/kT)$$

and

$$Q_N = \int \cdots \int_V d\tau_1 \cdots d\tau_N \exp(-U/kT).$$

The quantities m, k, and h have their usual meanings, μ is the chemical potential per atom, and U is the potential energy.

$\mathcal{Q}_V$ is a power series in y, and it is necessary to talk about its convergence. Q_N is positive for all N; in theorem A, we establish a lower bound for U which holds when the exponent of the repulsive potential n is greater than 3. This in turn establishes an upper bound

* Research supported by U. S. Office of Naval Research.
[1] C. N. Yang and T. D. Lee, Phys. Rev. 87, 404 (1952). This paper and the authors will be referred to in the text as YL.

for Q_N for fixed V, from which the convergence of $\mathcal{Q}_V$ for all y will follow.

Theorem A

Given a vessel of volume V in which any number of particles, N, can be placed. Assume that the intermolecular potential satisfies assumptions (2) and (3) mentioned previously, and that it satisfies assumption (1a), except that n need be only greater than 3. Then for an arbitrary number N of particles, and for any configuration of these particles in the vessel, the inequality $U>-\alpha V$ holds. α is a positive constant independent of V which will further be specified in the proof of the theorem.

Proof of Theorem A

Divide the vessel V into cubical cells of volume r_1^3, where r_1 is some distance such that $u(r_1)>0$. Say there are n_i particles in cell number i. If we define a_{ij} as the smallest value of u that can exist between two particles one of which is in the i cell and the other in the j cell, we can say, if there are N particles in the vessel,

$$U>U'\equiv\sum_i{}' \tfrac{1}{2}n_i(n_i-1)a_{11}+\tfrac{1}{2}\sum_{\substack{i,j\\ i\neq j}}{}' n_in_ja_{ij}, \qquad (1)$$

where $a_{11}=a_{ii}$ for all i and where the prime indicates the restriction

$$\sum_i n_i=N. \qquad (2)$$

There is a further restriction that all the n_i are positive integers. However, we wish only to find a lower bound for U'. Since U' is a continuous function of n_i, if we allow the n_i to assume a continuous range of values and find a lower bound for the resultant U', we have a bound on the original U'. Therefore, allow a continuous variation for the n_i. Now differentiate (1), introducing the undetermined multiplier λ for the restriction (2), and equate the derivative to zero.

$$\frac{\partial U'}{\partial n_i}=n_ia_{11}-\frac{a_{11}}{2}+\sum_{j\neq i}n_ja_{ij}+\lambda=0. \qquad (3)$$

Sum over the cells i to determine λ; there are V/r_1^3 cells

$$\lambda-\frac{a_{11}}{2}=-\frac{r_1^3}{V}[Na_{11}+\sum_i\sum_{j\neq i}n_ja_{ij}]. \qquad (4)$$

So far, (3) describes a stationary point for U'; we will soon show that this stationary point can be made a minimum and we call this minimum $U_{\min}'$. Substituting from (4) and (3) into (1) gives

$$U_{\min}'=\frac{Nr_1^3}{2V}[Na_{11}+\sum_i n_j\sum_{i\neq j}a_{ij}]-\frac{Na_{11}}{2}. \qquad (5)$$

If $-M$ is a lower bound of $u(r)$ and b is the range of interaction (see assumptions 2 and 3), $\sum_{i\neq j}a_{ij}>-Mb^3/r_1^3$. So,

$$U_{\min}'>U''\equiv\frac{N^2r_1^3}{2V}\left[a_{11}-\frac{Mb^3}{r_1^3}\right]-\frac{Na_{11}}{2}. \qquad (6)$$

Now differentiate U'' with respect to N and find the minimum possible value for U'':

$$U_{\min}''=-\frac{a_{11}^2V}{8[a_{11}-Mb^3/r_1^3]r_1^3}. \qquad (7)$$

If we let α be the coefficient of V in expression (7) we have established the theorem, provided we show that we can choose a cell size r_1 independent of V so that the relations (3) will in fact represent a minimum. These relations define a minimum if and only if the matrix $(\partial^2U'/\partial n_i\partial n_j)=(a_{ij})$ corresponds to a positive definite quadratic form. $a_{ii}=a_{11}$ for all i. (a_{ij}) is a symmetric matrix. A necessary and sufficient condition that the form be positive definite is that all the eigenvalues be positive. If we assume that the vessel V is a cube with periodic boundary conditions, (a_{ij}) is a cyclic matrix as well as symmetric. The periodic boundary conditions mean for a one-dimensional system that we would have a ring and for two dimensions, a torus; the three-dimensional cube has an analogous structure. For such a system, the eigenvalues are known[2] and are given by

$$\Lambda_k=a_{11}+2\sum_{p=2,\ p\neq k}^{\frac{1}{2}(V/r_1^3+1)}a_{kp}\cos\left[\frac{2\pi r_1^3}{V}(k-1)(p-1)\right]. \qquad (8)$$

The smallest eigenvalue is obviously such that

$$\Lambda_{\min}>a_{11}-2Mb^3/r_1^3. \qquad (9)$$

If $u(r)$ goes as $1/r_1^n$ with $n>3$, a_{11} will also go as $1/r_1^n$; obviously r_1 can be chosen small enough so that $\Lambda_{\min}$ is positive. This proves the theorem.

The restriction to periodic boundary conditions has been made for simplicity. It is probably not too difficult to show that even without this restriction r_1 can be chosen sufficiently small so that relations (3) represent a minimum. The convergence of the grand partition function for all finite V and y is now obvious.

III. LEMMAS AND THEOREMS

In this section we prove that the lemmas and theorems of YL hold for potentials satisfying (2), (3), and (1a). We use their notation and nomenclature throughout and follow their arguments very closely.

Lemma 1

Let V and W be two cubes of linear dimensions L and $L+b/2$, respectively. Keeping b fixed one has, as $L\to\infty$, $\lim W^{-1}(\log\mathcal{Q}_W-\log\mathcal{Q}_V)=0$.

[2] G. Kowalewskie, *Determinantentheorie* (Chelsea Publishing Company, New York, 1948), third edition, p. 105.

Proof

An essential feature of the proof of YL is that with a hard core, the potential energy of particles in V interacting with those in the shell surrounding V can go to negative infinity no faster than minus W^1. The proof would have been equally valid if the potential had gone as minus W^α with $\alpha<1$ instead of equal to $\frac{2}{3}$. With no hard core the potential energy across the surface of V has no lower bound. However, if n is sufficiently large, it can be shown that those configurations for which the potential across the surface decreases faster than W^α with $\alpha\geqq 1$ will contribute negligibly to the partition function. For the proof of lemma 1, we will use lemma A which is proved in the appendix. Lemma A says that for r_0 sufficiently small so that $u(r_0)$ is well in the repulsive range, and for a fixed volume V, if at least two particles in the vessel are together a distance closer than r_0, then $U>1/r_0^n-\beta V$. β is a positive constant specified in the appendix. We proceed with the proof of lemma 1. Let

$$Q_N(W)=\int\cdots\int_W{}' d\tau_1\cdots d\tau_N \exp(-U/kT)$$
$$+\int\cdots\int_W{}'' d\tau_1\cdots d\tau_N \exp(-U/kT). \quad (10)$$

Call the first integral on the right $Q_N'(W)$, the second integral $Q_N''(W)$. The single prime indicates that this integration is performed for all configurations where no two particles are ever together a distance closer than r_0. The double prime indicates that this integration includes only those configurations for which at least two particles are together a distance closer than r_0. Using lemma A,

$$Q_N''(W)\leqq\exp\left(-\frac{(1/r_0^n-\beta W)}{kT}\right)W^N. \quad (11)$$

If we define the volume between V and W as Δ, we can write

$$Q_N'(W)=\sum_{\alpha=0}^{N}\frac{N!}{\alpha!(N-\alpha)!}\int\cdots\int_V d\tau_1\cdots d\tau_{N-\alpha}\int\cdots$$
$$\times\int_\Delta d\tau_1\cdots d\tau_\alpha \exp\left(-\frac{(U_V+U_\Delta+U_{\Delta V})}{kT}\right), \quad (12)$$

where U_V is the interaction of particles in V with each other, U_Δ is the interaction of particles in Δ with each other, and $U_{\Delta V}$ is the interaction of particles in V with those in Δ.

We now get a lower bound for $U_\Delta+U_{\Delta V}$ in (12). Divide the volume Δ into cubical cells of length r_1 and define a_{ij} as in the proof of theorem A. Considering the restriction that for $Q_N'(W)$ all particles in V are farther apart than r_0 from each other, we can write

$$U_\Delta+U_{\Delta V}>(U_\Delta+U_{\Delta V})'$$
$$=\tfrac{1}{2}\sum_i{}' n_i(n_i-1)a_{11}+\tfrac{1}{2}\sum_{i\neq j}{}' n_in_ja_{ij}-\frac{\alpha Mb^3}{r_0^3}. \quad (13)$$

The last term is a bound on the interaction of the α particles in Δ with the particles in V. The above expression can be minimized with the restriction $\sum n_i=\alpha$ to give

$$U_\Delta+U_{\Delta V}>\frac{\alpha^2r_1^3}{2\Delta}\left[a_{11}-\frac{Mb^3}{r_1^3}\right]-\alpha\left[\frac{a_{11}}{2}+\frac{Mb^3}{r_0^3}\right]. \quad (14)$$

This in turn will yield, when minimized with respect to α,

$$U_\Delta+U_{\Delta V}>-\frac{\Delta}{2r_1^3}\frac{[\frac{1}{2}a_{11}+Mb^3/r_0^3]^2}{[a_{11}-Mb^3/r_1^3]}. \quad (15)$$

Using this in (12) gives

$$Q_N'(W)\leqq\sum_{\alpha=0}^{N}\frac{N!}{\alpha!(N-\alpha)!}Q_{N-\alpha}(V)$$
$$\times\exp\left(\frac{\Delta(\frac{1}{2}a_{11}+Mb^3/r_0^3)^2}{2r_1^3(a_{11}-Mb^3/r_1^3)kT}\right)\Delta^\alpha. \quad (16)$$

From (11) and (16) and the definition of $\mathcal{Q}_W$,

$$\mathcal{Q}_W<\mathcal{Q}_V\exp\left(\frac{\Delta(\frac{1}{2}a_{11}+Mb^3/r_0^3)^2}{2r_1^3(a_{11}-Mb^3/r_1^3)kT}+y\Delta\right)$$
$$+\exp\left(-\frac{(1/r_0^n-\beta W)}{kT}+yW\right). \quad (17)$$

Calling the first term on the right equal to A, we obtain

$$\log\mathcal{Q}_W\leqq\log\mathcal{Q}_V+\frac{\Delta(\frac{1}{2}a_{11}+Mb^3/r_0^3)^2}{2r_1^3(a_{11}-Mb^3/r_1^3)kT}+y\Delta$$
$$+\log\left[1+A^{-1}\exp\left(-\frac{(1/r_0^n-\beta W)}{kT}+yW\right)\right]. \quad (18)$$

In the estimate of $U_\Delta+U_{\Delta V}$ given in (15), the cell size r_1 can be chosen to be a function of W; r_0 can also be chosen as a function of W. a_{11} will become infinite as $1/r_1^n$. As $W\to\infty$, $\Delta\to\infty$ as W^1. Make the following choices for r_1, r_0 as $W\to\infty$:

$$1/r_1^n\sim 1/r_0^3;\quad 1/r_1^{n+3}\sim W^{1-\epsilon};\quad 1/r_0^n\sim W^{1+\epsilon}, \quad (19)$$

where ϵ is a small positive constant. These choices can be made if $1/r_1^{n2/3}\geqq 1/r_0^n>1/r_1^{3n+9}$. Finally, the choices can be made if n is greater than the positive root of $n^2-9n-27=0$, or $n>11.4$. Making the choices (19)

will assure that the second term on the right-hand side of (18) will go to infinity more slowly than W and the last term will vanish as $W\to\infty$. Consequently, since $\mathcal{Q}_W \geqq \mathcal{Q}_V$, $W^{-1}(\log \mathcal{Q}_W - \log \mathcal{Q}_V)\to 0$ as $W\to\infty$.

Lemma 2

Let W_i be a cube of linear dimension 2^iL and $\mathcal{Q}_i$ be an abbreviation of $\mathcal{Q}_{W_i}$. Then, $\lim_{i\to\infty} W_i^{-1}\log \mathcal{Q}_i = K$ exists.

Proof

Consider W_j to be built up from 8^{j-i} smaller cubes, $W_i (j>i)$, and draw within each smaller cube W_i, a concentric cube V_i with linear dimensions $2^iL-(b/2)$. The region between V_i and W_i consists of a contiguous space Γ of volume $\sim 8^j 2^{-i} b$. W_j consists of the volume Γ and the cells V_i. As in the previous lemma, define $Q_N'(W_j)$ and $Q_N''(W_j)$ to refer to configurations having no particles closer together than r_0, and configurations in which at least two particles are closer together than r_0, respectively. In analogy to (11) and (12) we write

$$Q_N''(W_j) \leqq \exp\left(-\frac{(1/r_0^n - \beta W_j)}{kT}\right) W_j^N; \quad (20)$$

$$Q_N'(W_j) = \sum_{\substack{\mu,\nu_1,\nu_2\cdots\nu_{8^{j-i}}-\mu! \\ \mu+\sum\nu_l=N}}{}' \frac{N!}{\mu!\prod_l \nu_l!} \times \int\cdots\int_{V_i} \prod_l d\tau_1\cdots d\tau_{\nu_l} \int\cdots\int_{\Gamma} d\tau_1\cdots d\tau_\mu \times \exp[-(\textstyle\sum_i U_{V_i} + U_\Gamma + \sum_i U_{\Gamma V_i})/kT]. \quad (21)$$

$\sum_i U_{V_i}$ sums the interactions of particles in W_i with each other, U_Γ is the interaction of particles in Γ with each other, and $\sum_i U_{\Gamma V_i}$ is the interaction of particle in Γ with particles in the V_i. In analogy to (16),

$$Q_N'(W_j) \leqq \sum_{\substack{\mu,\nu_1,\nu_2\cdots\nu_{8^{j-i}}-\mu! \\ \mu+\sum\nu_l=N}} \frac{N!}{\mu!\prod_l \nu_l!} \prod_l Q_{\nu_l}(V_i)[8^j 2^{-i} b]^\mu \times \exp\left(\frac{8^j 2^{-i} b(\frac{1}{2}a_{11} + Mb^3/r_0^3)^2}{2r_1^3(a_{11} - Mb^3/r_1^3)kT}\right). \quad (22)$$

From the definition of $\mathcal{Q}_j$ and from (20) and (22),

$$\mathcal{Q}_j \leqq (\mathcal{Q}_{V_i})^{8^{j-i}} \exp\left(y(8^j 2^{-i} b) + \frac{8^j 2^{-i} b(\frac{1}{2}a_{11} + Mb^3/r_0^3)^2}{2r_1^3(a_{11} - Mb^3/r_1^3)kT}\right) + \exp\left(-\frac{(1/r_0^n - \beta W_j)}{kT} + yW_j\right). \quad (23)$$

Letting A be the first expression on the right side of (23) and using $\mathcal{Q}_{V_i} < \mathcal{Q}_i$, we obtain

$$\log \mathcal{Q}_j \leqq 8^{j-i}\log \mathcal{Q}_i + y(8^j 2^{-i} b) + \frac{8^j 2^{-i} b(\frac{1}{2}a_{11} + Mb^3/r_0^3)^2}{2r_1^3(a_{11} - Mb^3/r_1^3)kT} + \log\left[1 + A^{-1}\exp\left(-\frac{(1/r_0^n - \beta W_j)}{kT} + yW_j\right)\right]. \quad (24)$$

Obviously,

$$8^{j-i}\log \mathcal{Q}_{V_i} \leqq \log \mathcal{Q}_j. \quad (25)$$

Equations (24) and (25) give on dividing by $W_j = (W_i)8^{j-i} = 2^{3j}L^3$

$$\frac{1}{W_i}\log \mathcal{Q}_{V_i} \leqq \frac{1}{W_j}\log \mathcal{Q}_j \leqq \frac{1}{W_i}\log \mathcal{Q}_i + \frac{b(\frac{1}{2}a_{11} + Mb^3/r_0^3)^2}{2r_1^3 2^i L^3(a_{11} - Mb^3/r_1^3)kT} + \frac{yb}{2^i L^3} + \frac{1}{W_j}\log\left[1 + A^{-1}\exp\left(-\frac{(1/r_0^n - \beta W_j)}{kT} + yW_j\right)\right]. \quad (26)$$

The last three terms approach zero as $i\to\infty$, providing we make the choice

$$1/r_1^n \sim 1/r_0^3;\ 1/r_1^{n+3} \sim 2^{i-\epsilon};\ j = ai;\ 1/r_0^n \sim 2^{3i+\epsilon}, \quad (27)$$

where a and ϵ are positive constants and $a>1$. These choices can be made if $n>11.4$ precisely, as in the analogous choices of lemma 1. By lemma 1, $W_i^{-1}(\log \mathcal{Q}_i - \log \mathcal{Q}_{V_i})\to 0$. Thus, as $j>i\to\infty$, $W_j^{-1}\log \mathcal{Q}_j - W_i^{-1}\times\log \mathcal{Q}_i \to 0$, and the lemma follows.

Theorem 1

For all positive real values of y, $V^{-1}\log \mathcal{Q}_V$ approaches, as $V\to\infty$, a limit which is independent of the shape of V. This limit is a continuous, monotonically increasing function of y.

Proof

The YL proof of theorem 1, based on the preceding lemmas, holds except for the continuity of the limit as $V\to\infty$ of $V^{-1}\log \mathcal{Q}_V$. Continuity will follow from the fact that the limit not only exists but exists uniformly for all finite positive y, as can be seen from the proofs of the lemmas. Since $V^{-1}\log \mathcal{Q}_V$ is a continuous function of y for all finite positive V and y, the limit function is also a continuous function of y for all finite positive y.

Theorem 2

If in the complex y plane a region R containing a segment of the positive real axis is always free of roots,

then in this region, as $V\to\infty$, all the quantities

$$\frac{1}{V}\log\mathcal{Q}_V,\ \left(\frac{\partial}{\partial\log y}\right)\frac{1}{V}\log\mathcal{Q}_V,\ \left(\frac{\partial}{\partial\log y}\right)^2\frac{1}{V}\log\mathcal{Q}_V,\ \cdots,$$

approach limits which are analytic with respect to y. Furthermore, the operations $(\partial/\partial\log y)$ and $\lim_{V\to\infty}$ commute in R.

Proof

The proof of theorem 2 is somewhat different from that of YL, since their factorization no longer holds. However, the proof still follows from their lemma 3. In our case the expansion $V^{-1}\log\mathcal{Q}_V$ in powers of $y-\eta$ becomes

$$\frac{1}{V}\log\mathcal{Q}_V=\sum_{l=0}^{\infty}b_l(V)(y-\eta)^l, \tag{28}$$

$$b_l(V)=\frac{1}{2\pi iV}\oint\frac{\log\mathcal{Q}_V}{(y-\eta)^l}dy$$

$$=\frac{1}{2\pi iV}\oint\frac{\log\sum_N\dfrac{Q_N(V)y^N}{N!}}{(y-\eta)^l}dy. \tag{29}$$

The path of integration is the circle C, lying inside R, centered at η, where η is a point on the positive real axis. By letting $y-\eta=r\exp(i\theta)$, we obtain

$$b_l(V)=\frac{1}{2\pi V}\int_0^{2\pi}\frac{e^{i(1-l)\theta}\log\sum_N[r^Ne^{iN\theta}Q_N(V)/N!]}{r^{l-1}}d\theta. \tag{30}$$

$|\mathcal{Q}_V(y)|$ has a nonzero lower bound on C, so the absolute value of the log has an upper bound. Hence, for some constant K,

$$b_l(V)\leqq K/Vr^{l-1}. \tag{31}$$

But K/Vr is bounded; hence theorem 2 follows from lemma 3 as shown by YL.

IV. FURTHER REMARKS

The proof of theorem 3 that the density is an increasing function of fugacity, and the other pertinent statements in the text of YL are not changed by the generalization which has been considered. So, a hard repulsive core is not necessary in this theory of condensation; the repulsive potential must only be stronger than $1/r^n$, $n=11.4$. We have not proved the theorems for smaller values of n, but suspect that it can be done. In particular, we believe there may be a connection between the condition $n>3$ for which theorem A is true and the minimum n for which theorems 1, 2, and 3 are true.

The author wishes to thank Dr. C. N. Yang, Dr. T. H. Berlin, and Dr. E. W. Montroll for discussing various aspects of this generalization with him.

APPENDIX

Lemma A

For a fixed volume V and a distance r_0 small enough that $u(r)=1/r_0^n$, if at least two particles in the vessel are together a distance closer than r_0, then for any total number of particles N, and for all possible configurations, the potential energy U has a lower bound such that $U>1/r_0^n-\beta V$. β is a constant independent of V, N, and $n>3$.

Proof

Divide the vessel V into cubical cells of volume r_1^3 as in the proof of theorem A. Assume that at some place in the vessel there are two particles whose distance together is smaller than r_0. Assume that the particles are both in the k cell; the proof is only slightly changed if they are in adjacent cells. Suppose there are n_k other particles in the kth cell and altogether $N\equiv\sum_i n_i$ particles in the vessel in addition to the given two.

$$U>U'\equiv 1/r_0^n+\sum_j{}'\tfrac{1}{2}n_j(n_j-1)a_{11}$$
$$+\tfrac{1}{2}\sum_{l\neq j}{}'n_ln_ja_{lj}+2\sum_{j\neq k}n_ja_{jk}. \tag{31}$$

If we minimize U' with respect to n_i as we have done before,

$$U'>\frac{1}{r_0^n}-\frac{Na_{11}}{2}+\frac{Nr_1^3}{2V}\left\{N\left(a_{11}-\frac{Mb^3}{r_1^3}\right)-\frac{2Mb^3}{r_1^3}\right\}. \tag{32}$$

If we minimize again with respect to N,

$$U'>\frac{1}{r_0^n}-\frac{a_{11}V[\frac{1}{2}a_{11}+2Mb^3/V]}{2r_1^3(a_{11}-Mb^3/r_1^3)}+\frac{V[\frac{1}{2}a_{11}+2Mb^3/V]^2}{2r_1^3(a_{11}-Mb^3/r_1^3)}$$
$$-\frac{Mb^3[\frac{1}{2}a_{11}+2Mb^3/V]}{r_1^3[a_{11}-Mb^3/r_1^3]}, \tag{33}$$

and the lemma obviously holds, as can be seen by going to the limit $V\to\infty$. It can be shown as in theorem A that r_1 can be taken sufficiently small to assure that (32) represents a minimum value for U'.

Diffusion Cooling of Electrons in Ionized Gases

MANFRED A. BIONDI
Westinghouse Research Laboratories, East Pittsburgh, Pennsylvania
(Received December 10, 1953)

The term "diffusion cooling" is used to describe the situation in which the average energy of an electron swarm is reduced by the diffusion of the faster electrons to the container walls. In the present experiment, measurements of the ambipolar diffusion loss of electrons during the afterglow reveal the presence of diffusion cooling by the reduction in the ambipolar diffusion coefficient. In low-pressure neon and argon afterglows the "thermal contact" between electrons and gas atoms is poor; consequently the diffusion loss of the fast electrons causes a large reduction in electron "temperature" with respect to the gas temperature. When small amounts of helium are added, the thermal contact is greatly improved, and therefore the electrons are restored to thermal equilibrium with the gas. These experimental observations confirm the predictions of a qualitative theory given for the process.

THE term "diffusion cooling of electrons" describes the situation in which the average kinetic energy of electrons in an ionized gas is reduced by the diffusion of electrons to the walls of the containing vessel. There are two distinct processes which lead to diffusion cooling of a swarm of electrons. The first results from the fact that in a freely diffusing swarm the fast electrons diffuse more rapidly than the slow electrons.[1] Thus there is a transport of energy to the walls which tends to decrease the average energy of the remaining electrons. If this loss is not compensated by some energy supplying mechanism such as the acceleration of the electrons in an electric field, the electron energy will decrease as the diffusion process continues. The second process responsible for diffusion cooling occurs in an ionized gas (plasma) and is most effective under conditions of ambipolar diffusion. As will be shown in Sec. II, a space-charge field is set up by the excess of positive ions in the plasma which retards the diffusion of the electrons to the walls. This retarding field produces a cooling effect since only the faster electrons in the swarm have sufficient energy to overcome the space charge potential barrier and reach the walls. In the present experiment, we study the cooling which results from the diffusion of electrons against the ambipolar space charge field.

I. EXPERIMENTAL METHOD

The diffusion cooling of electrons is determined from studies of the ambipolar diffusion loss of electrons during the afterglow of a pulsed microwave discharge. Detailed descriptions of the type of experimental apparatus used in these measurements have been published previously.[2] The gas to be studied is contained in a quartz bottle enclosed by a microwave cavity. Application of a pulse of microwave power to the cavity lasting $\sim$100 μsec ionizes the gas. The free electrons in the gas cause a change in resonant frequency which is proportional to the electron concentration. When the microwave maintaining field is removed from the cavity, the electron density decreases as a result of the ambipolar diffusion of the electrons and ions to the walls of the containing vessel. The electron density during the afterglow is determined from measurements of the resonant frequency of the cavity as a function of time by means of a low-energy probing signal.

The gas samples to be studied are introduced to the quartz bottle by means of an ultrahigh vacuum gas handling system.[3] Airco reagent grade gases are used in these measurements.

II. THEORY

In order to relate our ambipolar diffusion measurements to the diffusion cooling of electrons, let us outline briefly a theory for these processes.[4] In the absence of externally applied fields the drift motions of electrons and ions in an ionized gas depend on their concentration gradients and upon the space-charge field which they set up, according to the relations:

$$\Gamma_e = -D_e \nabla n_e - \mu_e n_e \mathbf{E}, \tag{1}$$

$$\Gamma_+ = -D_+ \nabla n_+ + \mu_+ n_+ \mathbf{E}, \tag{2}$$

where Γ is the particle current density, D the diffusion coefficient, n the density, and μ the mobility of the electrons and ions, denoted by the subscripts e and $+$, respectively. $\mathbf{E}$ is the space-charge field. Under ambipolar diffusion conditions $\Gamma_e = \Gamma_+$, $n_e \simeq n_+$, and $\nabla n_e \simeq \nabla n_+$. In addition, $D_e \gg D_+$ and $\mu_e \gg \mu_+$. Consequently, Eqs. (1) and (2) give for the ambipolar space charge field

$$\mathbf{E} \simeq -(D_e/\mu_e)\nabla(\ln n), \tag{3}$$

where n represents the concentration of either particle. This space charge field acts to retard the diffusing electrons.

If we eliminate $\mathbf{E}$ from Eqs. (1) and (2), we find that the current of either particle may be characterized by a

[1] This statement applies when the diffusion cross section of the electrons varies less rapidly than linearly with electron velocity.
[2] See, for example, M. A. Biondi, Rev. Sci. Instr. **22**, 500 (1951); M. A. Biondi and S. C. Brown, Phys. Rev. **75**, 1700 (1949).
[3] D. Alpert, J. Appl. Phys. **24**, 860 (1953).
[4] The concept of the cooling of electrons as a result of ambipolar diffusion was originally developed by T. Holstein, Westinghouse Research Report R-94411-9-A (unpublished), pp. 206–219.

diffusion term alone, i.e.,

$$\Gamma = -D_a \nabla n, \tag{4}$$

where the common diffusion coefficient D_a is the ambipolar diffusion coefficient, given by

$$D_a = (D_+\mu_e + D_e\mu_+)/(\mu_+ + \mu_e). \tag{5}$$

From kinetic theory[5] we have the relation

$$(D/\mu)_{+,e} = (ku)_{+,e}/q, \tag{6}$$

where q is the electronic charge and the subscripts $+$ and e refer to the ions and electrons, respectively, and u is the average kinetic energy of the particles. The quantity k is a number, of order unity, which depends on the form of the velocity distribution of the particles.[6] Equation (5) may now be written in terms of the average energy of the particles:

$$D_a \simeq D_+[1+x(u_e/u_+)], \tag{7}$$

where $x = k_e/k_+$ and is of the order of unity. Equation (7) shows that diffusion cooling may be determined from experimental measurements of the ambipolar diffusion loss of electrons.

During the afterglow the electric field which ionized the gas is no longer present. The electrons therefore do not gain sufficient energy to make inelastic exciting and ionizing collisions with the gas atoms. However, they continue to exchange energy with the gas atoms by elastic recoil collisions. Using the one-electron picture to describe qualitatively the energy balance for the electrons during the afterglow, we have

$$\partial u_e/\partial t \simeq (2m/M)\nu_e(u_{gas} - u_e) - \nu_d(Nu_e), \tag{8}$$

where m and M are the masses of the electron and gas atom, respectively; ν_e and ν_d are the average elastic collision frequency and diffusion frequency[7] of the electrons, and u_{gas} is the average energy of the gas atoms. The first term on the right of Eq. (8) represents the rate of exchange of energy as a result of elastic collisions between electrons and gas atoms. The second term represents the rate of transport of energy to the walls by those electrons which diffuse over the space charge barrier. Only the faster electrons in the distribution can reach the boundary; therefore each electron which diffuses to the walls carries away more than the average energy of the distribution. The factor (Nu_e) represents the excess energy carried to the walls and hence the diffusive energy loss in the one-electron description.

These processes are illustrated schematically in Fig. 1, which shows the diffusion of the electron swarm during the afterglow. The space-charge potential well for the electrons $V_{s.c.}$ reaches a maximum value V_w at the walls of the tube. The energy distribution of the electrons is indicated by the shaded area. If we fix our attention on a particular energy interval in the distribution, electrons (indicated by the dots) are being fed into and out of this interval as a result of elastic recoil collisions with gas atoms. The rate of such feeding depends on the "thermal contact" between the electrons and gas atoms, expressed by the factor $(2m/M)\nu_e$ in Eq. (8); the direction of the net flow of electrons in energy space depends on which is greater, u_{gas} or u_e.

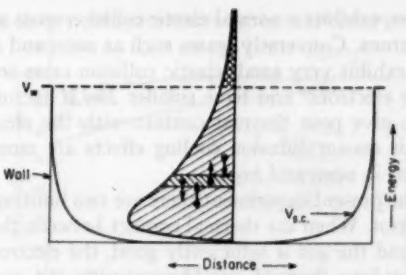

FIG. 1. Diffusion of electrons in the ambipolar space charge well. The electron energy distribution is indicated by the shaded area.

It is clear from the diagram that only those electrons with energy greater than V_w can reach the walls. As a result diffusion to the walls depletes the tail of the electron distribution, the ultimate effect on the shape of the distribution depending on how fast these higher energy electrons are resupplied by means of elastic recoil collisions. In any case the diffusion leads to a reduction in the average energy of the remaining electrons, which may be calculated by use of Eq. (8).

Immediately following a discharge, $u_e \gg u_{gas}$; thus both terms in Eq. (8) contribute to the energy decay.[8] At a later time in the afterglow, energy equilibrium is reached, i.e., $\partial u_e/\partial t = 0$. Equation (8) then gives for the ratio of electron energy to gas energy

$$\frac{u_e}{u_{gas}} \simeq 1 \Big/ \left[1 + N\left(\frac{\nu_d}{\nu_e}\right)\frac{M}{2m}\right]. \tag{9}$$

This equation is at best qualitative since we have only order-of-magnitude knowledge of N and have neglected the dependence of ν_e and ν_d on the average electron energy; however, it does demonstrate that the electron energy drops appreciably below the gas energy when the "thermal contact" between the electrons and the gas atoms is poor and/or the rate of diffusive transport of energy to the walls is large.

A gas such as helium is said to offer good thermal contact with the electrons since, excepting hydrogen, it has the largest value of $2m/M$ of any gas and, in

[5] E. H. Kennard, *Kinetic Theory of Gases* (McGraw-Hill Book Company, Inc., New York, 1938), p. 466.

[6] For example, in the case of the positive ions, which have a Maxwellian velocity distribution $k = \frac{3}{2}$.

[7] See Eq. (11) of Sec. III.

[8] When the energy decay rate due to elastic recoil is small, e.g., in low-pressure mercury afterglows, the diffusion cooling term is primarily responsible for the energy decay immediately following the discharge. G. Mierdel [Z. Physik **121**, 574 (1943)] has observed rapid electron energy decays in mercury afterglows which probably result from diffusion cooling but has incorrectly attributed them to the effects of excitation collisions between fast electrons and mercury atoms.

addition, exhibits a normal elastic collision cross section to electrons. Conversely, gases such as neon and argon, which exhibit very small elastic collision cross sections to slow electrons[9] and have smaller $2m/M$ factors, are said to give poor thermal contact with the electrons. For this reason diffusion cooling effects are more pronounced in neon and argon.

In the present experiment there are two limiting cases of interest. When the thermal contact between the electrons and the gas is sufficiently good, the electrons are brought into thermal equilibrium with the gas, i.e., $u_e = u_{gas}$. In this case Eq. (7) predicts that $D_a = 2D_+$.[10] In the hypothetical limit in which there is *no* thermal contact between electrons and gas atoms (achieved only at zero gas pressure), the electron energy diminishes to zero. In this case Eq. (7) predicts $D_a = D_+$. In the next section we shall compare our measured values of D_a with these limiting values.

III. MEASUREMENTS OF DIFFUSION COOLING

After energy equilibrium is reached in the afterglow the electrons and ions diffuse to the walls with a constant diffusion frequency, ν_d, leading to a decrease in electron (and ion) density given by

$$n_e = (n_e)_0 \exp(-\nu_d t). \tag{10}$$

ν_d is related to the ambipolar diffusion coefficient by

$$\nu_d = D_a/\Lambda^2, \tag{11}$$

where Λ is the characteristic diffusion length of the container[11] and is equal to 0.735 cm in the present

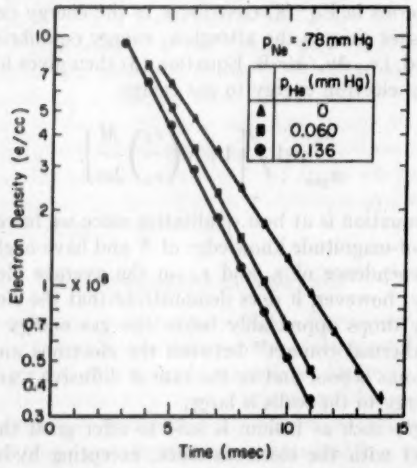

FIG. 2. The effect of the addition of small amounts of helium on the ambipolar diffusion loss of electrons in neon. The gas temperature is 300°K.

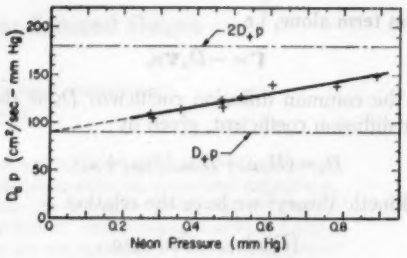

FIG. 3. Diffusion cooling of electrons in neon. The gas temperature is 300°K.

experiment. Measurements are made sufficiently late in the afterglow so that energy equilibrium is reached and Eq. (10) is obeyed.

An example of the experimental data obtained in pure neon is shown by the triangular points of Fig. 2. The slope of the curve gives ν_d, from which we obtain the value of D_a. Since the ambipolar diffusion coefficient is inversely proportional to the gas concentration, we multiply the values of D_a by the pressure p to remove the dependence on gas density. The measured values of $D_a p$ *versus* p for pure neon are shown in Fig. 3.

As predicted in the previous section the measured values of D_a lie between the limits D_+ and $2D_+$[12] which correspond to the respective cases, $u_e = 0$ and $u_e = u_{gas}$. The extrapolation of the experimental data to zero pressure (no thermal contact, infinite diffusion rate) gives the expected value $D_a = D_+$. According to Eq. (7), at the lowest pressure for which measurements were made, the average electron energy corresponds to a "temperature" of ~30°K although the gas temperature was 300°K, illustrating the extreme diffusion cooling which can occur in low pressure afterglow studies.[13]

IV. EFFECT OF HELIUM ON DIFFUSION COOLING

In order to demonstrate that the measured values of $D_a < 2D_+$ result from a reduction in the average electron energy rather than from some other effect, small amounts of helium were added to the neon gas. In low-pressure neon afterglows the dominant process is the ambipolar diffusion of electrons and Ne^+ ions.[14] The addition of small amounts of helium (~0.1-mm Hg) does not affect the type of ions formed since the ionization potential of helium is four volts higher than that of neon. Also, from Eq. (7) it is clear that the ionic diffusion coefficient, rather than that of the electrons, controls the ambipolar diffusion. Since

[9] A. V. Phelps *et al.*, Phys. Rev. 84, 559 (1951).

[10] In the present experiments, the positive ions remain in thermal equilibrium with the gas at all pressures, i.e., $u_+ = u_{gas}$.

[11] A detailed discussion of the electron density decay equation and its solution is given in M. A. Biondi and S. C. Brown, Phys. Rev. 75, 1700 (1949).

[12] The values of D_+ were obtained from theory; T. Holstein, J. Phys. Chem. 56, 832 (1952), and from positive ion mobility measurements, J. Hornbeck, Phys. Rev. 84, 615 (1951); M. A. Biondi and L. M. Chanin, (to be published).

[13] Under these conditions the electron energy distribution will be strongly non-Maxwellian; therefore, the term "temperature" is very loosely used to emphasize the low average energy of the electrons.

[14] The present measurements were confined to pressures sufficiently low to avoid significant conversion of atomic ions to molecular ions during the measurements. Conversion would have seriously complicated the analysis of the experimental data.

experimental measurements[15] show that a helium atom presents only $\frac{1}{8}$ the momentum transfer cross section to a Ne^+ ion that a neon atom does, the added helium has only a slight effect on the ionic diffusion coefficient.[16]

The primary effect of the added helium is on the average electron energy. A helium atom is 29 times more effective in its "thermal contact" with electrons [the factor $(2m/M)\nu_e$ of Eq. (8)] than is a neon atom.[9] Thus, the addition of small amounts of helium to the neon should raise the average electron energy in accordance with Eq. (9) and, consequently, cause D_a to approach the value $2D_+$ as predicted by Eq. (7).

The effect of adding various amounts of helium to a constant pressure of neon is shown in Fig. 2. It will be seen that, as helium is added, the rate of diffusion loss of the electrons *increases*, in agreement with our previous discussion. This behavior is illustrated in greater detail in Fig. 4. Here we plot the ambipolar diffusion coefficient times the neon pressure *versus* the pressure of the added helium for three different neon pressures. The points on the axis are taken from the pure neon data shown in Fig. 3. As helium is added to the 0.78-mm Hg of neon filling (top curve) the value of $D_a p$ increases from its initial value of 137. At approximately 0.09-mm Hg of helium, $D_a p$ reaches the value 180, which is equal to the predicted limit $2D_+ p$.[12] The addition of more helium has no further effect on the measured value of the ambipolar diffusion coefficient, since the electrons were brought into thermal equilibrium with the gas at 0.09-mm Hg of helium and remain in thermal equilibrium thereafter. At a lower neon pressure (0.47-mm Hg) the more rapid diffusion loss of electrons makes the cooling more severe; consequently more helium is required to bring the electrons into thermal equilibrium with the gas. At the lowest neon pressure (0.28-mm Hg) the addition of a nearly equal

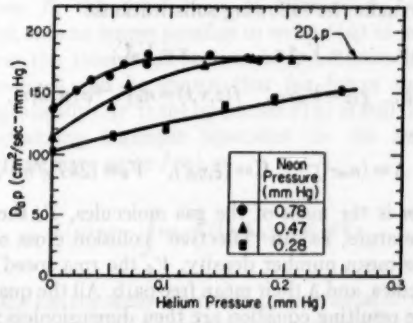

FIG. 4. The effect of helium on the measured ambipolar diffusion of electrons in neon.

[15] See reference 12 and R. J. Munson and A. M. Tyndall, Proc. Roy. Soc. (London) **A172**, 33 (1939).

[16] It may be shown that the resultant diffusion decay time in the mixture, $T_D = 1/\nu_d$ [see Eq. (10)], is simply $T_D = T_{Ne} + T_{He}$, where T_{Ne} is the diffusion decay time of Ne^+ in pure neon at its partial pressure and T_{He} is the value for Ne^+ in pure helium at its partial pressure.

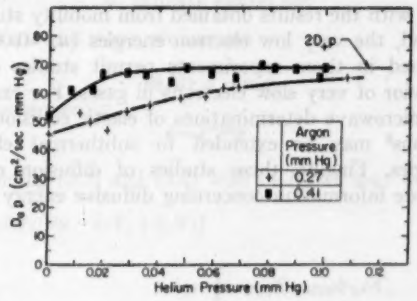

FIG. 5. The effect of helium on the measured ambipolar diffusion of electrons in argon.

amount of helium is insufficient to compensate completely the cooling, although the electron "temperature" is raised from its initial estimated value of ~30°K to ~210°K by the addition of 0.25-mm Hg of helium.

Since argon gas also exhibits a small elastic cross section for slow electrons and has a larger mass than neon, we should also expect diffusion cooling of electrons to take place in low-pressure argon afterglows. The measurements obtained with argon are analogous to the neon results; they are summarized in Fig. 5. In pure argon we again find values of $D_a < 2D_+$. At 0.41-mm Hg of argon it requires approximately 0.05-mm Hg of helium to bring the electrons into thermal equilibrium with the gas, as indicated by the value $D_a = 2D_+$, with the addition of more helium producing no further effect.

V. SUMMARY AND DISCUSSION

The present paper has demonstrated that under special circumstances the average kinetic energy of electrons in an ionized gas may decrease below that of the gas. This effect is attributed to diffusion cooling, a process in which the energy loss by diffusion of the fast electrons to the walls is imperfectly compensated through elastic collisions of the electrons with gas atoms. An elementary theory of the process is developed whose predictions are borne out by experiment. The term "thermal contact" is introduced to describe the rate at which energy is transferred between electrons and gas atoms in elastic recoil collisions. It is shown that helium exhibits good thermal contact, while neon and argon exhibit poor thermal contact with slow electrons. Diffusion cooling effects are experimentally demonstrated in low-pressure neon and argon afterglows. These effects are removed by the addition of small amounts of helium to the neon and argon, which brings the electrons into thermal equilibrium with the gas atoms.

The demonstration of the existence of diffusion cooling effects in afterglow studies serves a twofold purpose. First of all, when care is taken to avoid such effects, the neon and argon ionic diffusion coefficients determined from microwave studies are found to be in good agree-

ment with the results obtained from mobility studies.[12] Second, the very low electron energies ($u_e \sim 0.004$ ev) attained in these experiments permit studies of the behavior of very slow electrons in gases. For example, the microwave determinations of elastic collision cross sections[9] may be extended to subthermal electron energies. Finally, these studies of diffusion cooling provide information concerning diffusive energy transport which supplements that obtained from measurements of positive column characteristics.[17]

The author wishes to thank W. A. Rogers, who assisted in data-taking, and the various members of the Atomic Physics group, especially T. Holstein, for helpful discussions concerning this work.

[17] M. J. Druyvesteyn and F. M. Penning, Revs. Modern Phys. 12, 87 (1940); see Fig. 73.

PHYSICAL REVIEW VOLUME 93, NUMBER 6 MARCH 15, 1954

Variational Formulas in Evaporation Theory*

JOHN GREENSTADT
International Business Machines Corporation, New York, New York
(Received December 4, 1953)

The Laplace transformation is first applied to the linearized one-dimensional Boltzmann equation to enable some remarks on the spectrum of the problem to be made. The original (linearized) equation is then brought into the form of a Fredholm equation, following K. Schwarzschild. A Schwinger variational function is then established for the distribution of molecules returning after being "sprayed" into a gas. Using these results, an integral equation is derived for the probability distribution of molecules at a liquid-vapor interface during slow (steady or time-dependent) evaporation. Finally, this theory is compared with elementary evaporation theory.

1. SCATTERING PROBLEM

IN Fig. 1 is shown a volume of gas with a "molecule spray" imbedded in it. This spray injects molecules into the right-hand volume of gas with a variable but slow rate. Given the probability distribution of the molecules injected, the problem is to find the distribution of the molecules returning from the right as a consequence of collision.

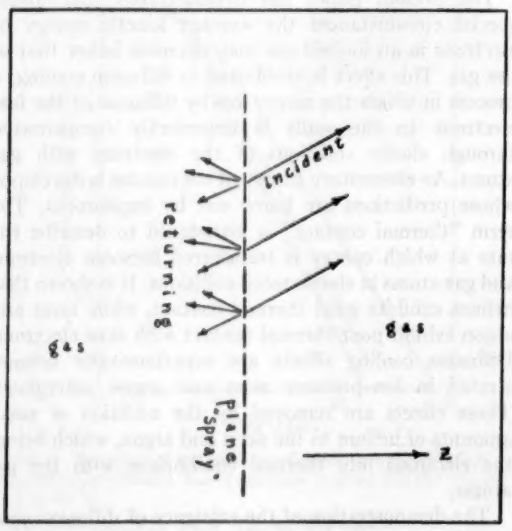

FIG. 1. Diagram of fictitious "spray" with incident and backscattered particles.

2. BOLTZMANN'S EQUATION

The equation for gas transport is Boltzmann's equation:[1]

$$\partial f_1/\partial t + v_{1z}\partial f_1/\partial z = \int \{f_1' f_2' - f_1 f_2\} g_{12} b db d\epsilon d^3\mathbf{v}_2, \quad (2.1)$$

where f is the distribution function (d.f.) for the gas and depends on t, z, v_x, v_y, and v_z. The subscripts refer to the arguments $\mathbf{v}_1$ and $\mathbf{v}_2$ of which f is a function.

We make the following substitutions:

$$\begin{aligned} &z = \Lambda u, \quad t = V_0 \Lambda \tau, \quad \mathbf{v} = V_0 \mathbf{C}, \\ &b = \sigma\beta, \quad g_{12} = V_0 \gamma_{12}, \quad f(z,\mathbf{v},t) = n_0 V_0^{-3} \varphi(u,\mathbf{C},\tau), \end{aligned} \quad (2.2)$$

where

$$\Lambda \equiv (n_0\sigma^2)^{-1}, \quad \mathbf{C} \equiv (\xi,\eta,\zeta), \quad V_0 \equiv (2kT_0/m)^{\frac{1}{2}},$$

and m is the mass of the gas molecules, T_0 the mean temperature, $\pi\sigma^2$ an "effective" collision cross section, n_0 the mean number density, V_0 the rms speed of the molecules, and Λ their mean free path. All the quantities in the resulting equation are then dimensionless:

$$\partial\varphi_1/\partial\tau + \zeta_1 \partial\varphi_1/\partial u = \int \{\varphi_1'\varphi_2' - \varphi_1\varphi_2\} \gamma_{12} \beta d\beta d\epsilon d^3\mathbf{C}_2. \quad (2.3)$$

* Part of a dissertation presented to the faculty of Yale University in candidacy for the degree of Doctor of Philosophy.

[1] See S. Chapman and T. Cowling, *The Mathematical Theory of Non-Uniform Gases* (Cambridge University Press, Cambridge, 1939), p. 66.

3. LINEARIZATION

We assume that the d.f. can be written as

$$\varphi=\varphi_0(1+\psi), \tag{3.1}$$

where $|\psi|\ll 1$ and φ_0 is the d.f. describing the equilibrium state of the gas. This assumption means a "small amplitude" disturbance of equilibrium. φ_0 is then the Maxwellian d.f., *viz.*,

$$\varphi_0=\pi^{-\frac{3}{2}}\exp(-C^2), \quad \left[\int_C \varphi_0 d^3\mathbf{C}=1\right]. \tag{3.2}$$

With this assumption, we obtain

$$\varphi_{01}\{\partial\psi_1/\partial\tau+\zeta_1\partial\psi_1/\partial u\}$$

$$=\int\varphi_{01}\varphi_{02}\{\psi_1'+\psi_2'-\psi_1-\psi_2\}d\Omega d^3\mathbf{C}_2\equiv I(\psi), \tag{3.3}$$

where $d\Omega\equiv\gamma_{12}\beta d\beta d\epsilon$.

Chapman and Cowling[2] show that for $\beta\leq B$, the linear operator $I(\psi)$ can be written as

$$[I(\psi)]_1=-\varphi_{01}k(C_1)\psi(\mathbf{C}_1)$$

$$+\int_{C_2}\varphi_{01}K(\mathbf{C}_1,\mathbf{C}_2)\varphi_{02}\psi_2 d^3\mathbf{C}_2, \tag{3.4}$$

where

$$k(C_1)=\int_{C_2}\int_0^{2\pi}\int_0^B \varphi_0(C_2)|\mathbf{C}_2-\mathbf{C}_1|\beta d\beta d\epsilon d^3\mathbf{C}_2$$

$$=\pi B^2\int_{C_2}\varphi_0(C_2)|\mathbf{C}_2-\mathbf{C}_1|d^3\mathbf{C}_2, \tag{3.5}$$

and $K(\mathbf{C}_1,\mathbf{C}_2)$ is symmetric in $\mathbf{C}_1$ and $\mathbf{C}_2$. Arguments of rotational invariance show that K is really a function of C_1, C_2 and $\epsilon_1\cdot\epsilon_2$ only.[3] Cylindrical symmetry requires that ψ be a function of C and μ only, where $\mu\equiv\zeta/C$.

When B, the outer limit of interaction, becomes infinite, it is no longer possible to write $I(\psi)$ as in (3.4), because the total cross section $k(C)$ becomes infinite. However, it can be shown that for forces that are asymptotically $O(r^{-3})$ the operation $I(\psi)$ is still defined. By admitting improper functions (in the sense of Dirac), we may write $I(\psi)$ as

$$I(\psi)=-\int\varphi_{01}L(\mathbf{C}_1,\mathbf{C}_2)\varphi_{02}\psi_2 d^3\mathbf{C}_2. \tag{3.6}$$

$L(\mathbf{C}_1,\mathbf{C}_2)$ has the same invariance properties as $K(\mathbf{C}_1,\mathbf{C}_2)$.

In addition, $L(\mathbf{C}_1,\mathbf{C}_2)$ is positive semidefinite,[4] i.e.,

$$\int_{C_1,C_2}\psi_1\varphi_{01}L_{12}\varphi_{02}\psi_2 d^3\mathbf{C}_1 d^3\mathbf{C}_2\geq 0. \tag{3.7}$$

[2] Reference 1, p. 129.
[3] A German boldface letter denotes a unit vector.
[4] Reference 1, p. 87.

4. SOUND PROBLEM

For a sound wave, we assume

$$\partial\psi/\partial\tau=-i\alpha\psi, \tag{4.1}$$

and consequently,

$$\psi=\epsilon^{-i\alpha\tau}\Psi. \tag{4.2}$$

Combining (3.3) and (3.4) with (4.2), we may write

$$\varphi_{01}\{\zeta_1\partial\Psi_1/\partial u-i\alpha\Psi_1+k_1\Psi_1\}$$

$$=\int_{C_2}\varphi_{01}K_{12}\varphi_{02}\Psi_2 d^3\mathbf{C}_2. \tag{4.3}$$

This equation will hold for the case when $\beta\leq B$. For the infinite-range case, we may drop k_1 and replace K_{12} by $-L_{12}$.

Note also that there may be a steady-drift solution in a sound wave, i.e., when $\alpha=0$.

5. LAPLACE TRANSFORM

By applying a Laplace transformation to Eq. (4.3) to eliminate the derivative term, we obtain

$$\varphi_{01}\{s\zeta_1\theta_1-i\alpha\theta_1+k_1\theta_1-\zeta_1\Psi_1^0\}$$

$$=\int\varphi_{01}K_{12}\varphi_{02}\theta_2 d^3\mathbf{C}_2, \tag{5.1}$$

where

$$\theta_1(s)\equiv\int_0^\infty\epsilon^{-s u}\Psi_1(u)du, \tag{5.2}$$

$$\Psi_1^0\equiv\Psi_1(u\to 0+). \tag{5.3}$$

For the bounded-range case ($\beta\leq B$) it is simple by using arguments similar to those of Bethe *et al.*[5] to show that the spectrum of permissible values is discrete. For $B\to\infty$ the writer has no proof, but simple analog examples indicate that if the spectrum of L_{12} is itself discrete, then the spectrum of s values is, very likely, also discrete. For Maxwellian central forces (inverse fifth power) the spectrum of L_{12} is known to be discrete, and it is also very likely that the same is true of more rapidly decaying central forces.

Finally, one notes that for $\alpha=0$, the only cylindrically symmetric solutions of the homogeneous equation derived from (5.1) by setting $\Psi_1^0=0$, which correspond to the eigenvalue $s=0$ are the following:

$$\theta_1=1, \quad \theta_1=\zeta_1, \quad \theta_1=C_1^2. \tag{5.4}$$

These three solutions cause the integral in (5.1) to vanish.[6] The probable discreteness of the s spectrum of the operator

$$(\mathcal{O}\theta)_1\equiv\varphi_{01}\{s\zeta_1+k_1-i\alpha\}\theta_1-\int\varphi_{01}K_{12}\varphi_{02}\theta_2 d^3\mathbf{C}_2 \tag{5.5}$$

[5] Bethe, Tonks, and Hurwitz, Phys. Rev. **80**, 11 (1950).
[6] Reference 1, p. 87.

means that decaying exponential solutions are the only others. It is easily demonstrated that waves always decay in the direction of travel.

We shall assume then, that all solutions of (4.3) [and special cases of (4.3)] are either the three nondecaying ones mentioned above or are composed of exponential solutions with a spectrum of decay constants which is separated from the origin.

Therefore, we may write for $\Psi(\mathbf{C})$

$$\Psi(\mathbf{C},u)=\beta+\mu\zeta+\epsilon C^2+\psi(\mathbf{C},u), \tag{5.6}$$

where β, μ, and ϵ are constants and $\psi(\mathbf{C},u)$ represents a wave which decays as $u\to\infty$.

6. INTEGRAL EQUATION

We shall now derive, paralleling Hopf,[7] an integral equation for $\psi(u,\mathbf{C}_1)$. A remark should be made first, however, about some of the properties of the scattering kernel under reflection.

We define the *reflection* of K_{12} as follows:

$$K_{(1)2}\equiv K(\xi_1,\eta_1,-\zeta_1;\,\xi_2,\eta_2,\zeta_2), \tag{6.1a}$$

$$K_{1(2)}\equiv K(\xi_1,\eta_1,\zeta_1;\,\xi_2,\eta_2,-\zeta_2). \tag{6.1b}$$

With cylindrical symmetry, we have

$$K_{(1)2}\equiv K(C_1,-\mu_1;\,C_2,\mu_2), \tag{6.2a}$$

$$K_{1(2)}\equiv K(C_1,\mu_1;\,C_2,-\mu_2). \tag{6.2b}$$

If the properties of the medium in question are invariant under reflection (as they certainly are in a gas), then K_{12}, which characterizes the scattering in this medium, should be subject to the law of dynamical reflectability.[8]

This requires that K_{12} should be invariant under a reflection of the space with respect to the u direction, i.e.,

$$K_{(1)(2)}=K_{12}. \tag{6.3}$$

By replacing ζ_1 by $-\zeta_1$, we have

$$K_{1(2)}=K_{(1)2}. \tag{6.4}$$

A kernel for which $K_{(1)2}=K_{12}$ we call *specular*.

We now denote $k_1-i\alpha$ by A_1 and multiply Eq. (4.3) by $\exp(A_1u/\zeta_1)$. This is an integrating factor and permits us to obtain, by integration from u_a to u_b,

$$\varphi_{01}\{\exp(A_1u_b/\zeta_1)\cdot\zeta_1\psi_1(u_b)-\exp(A_1u_a/\zeta_1)\cdot\zeta_1\psi(u_a)\}$$

$$=\int_{u_a}^{u_b}\int_{C_2}\exp(A_1t/\zeta_1)\cdot\varphi_{01}K_{12}\varphi_{02}\psi_2(t)d^3\mathbf{C}_2dt. \tag{6.5}$$

We now distinguish two different regions for ζ_1, *viz.*, $\zeta_1<0$ and $\zeta_1\geqslant 0$. For the first region ($\zeta_1<0$), we allow $u_b\to\infty$. We must assume that $\exp(A_1u/\zeta_1)\zeta_1\psi_1(u_b)\to 0$ as $u_b\to\infty$. In view of the exponential decay of solutions traveling to the right, this is justified. We replace u_a by u_1, t by u_2, multiply by $\zeta_1^{-1}\exp[(-A_1/\zeta_1)(u_1-u_2)]$ to obtain

$$\varphi_{01}\psi_1^-(u_1)=-\int_{u_1}^{\infty}\int_{C_2}\zeta_1^{-1}\exp[(-A_1/\zeta_1)(u_1-u_2)]$$

$$\times\varphi_{01}K_{12}\varphi_{02}\psi_2(u_2)d^3\mathbf{C}_2du_2. \tag{6.6}$$

(The minus sign on $\psi_1(u_1)$ indicates that (6.6) holds for $\zeta_1<0$.)

When $\zeta_1\geqslant 0$, we set $u_a=0$, $u_b=u_1$, $t=u_2$, we divide by $\zeta_1\exp(A_1u_1/\zeta_1)$ and obtain

$$\varphi_{01}\psi_1^+(u_1)=\exp(-A_1u_1/\zeta_1)\varphi_{01}\psi_1^+(0)$$

$$+\int_0^{u_1}\int_{C_2}\zeta_1^{-1}\exp[-(A_1/\zeta_1)(u_1-u_2)]$$

$$\times\varphi_{01}K_{12}\varphi_{02}\psi_2(u_2)d^3\mathbf{C}_2du_2. \tag{6.7}$$

The plus sign on ψ_1 means that (6.7) holds for $\zeta_1\geqslant 0$.

We now multiply (6.6) and (6.7) by $\varphi_{03}K_{3(1)}$. We then integrate (6.6) over that part of $\mathbf{C}_1$ space in which $\zeta_1<0$, and integrate (6.7) over that part of $\mathbf{C}_1$ space in which $\zeta_1\geqslant 0$. Adding the two together, we obtain

$$\int_{C_1}\varphi_{03}K_{3(1)}\varphi_{01}\psi_1(u_1)d^3\mathbf{C}_1$$

$$=\int_{C_{1+}}\varphi_{03}K_{3(1)}\varphi_{01}\exp(-A_1u/\zeta_1)\psi_1^+(0)d^3\mathbf{C}_1$$

$$+\int_0^{u_1}\int_{C_{2+}}\int_{C_2}\varphi_{03}K_{3(1)}\varphi_{01}$$

$$\times\exp[(-A_1/\zeta_1)(u_1-u_2)]$$

$$\times\zeta_1^{-1}K_{12}\varphi_{02}\psi_2(u_2)d^3\mathbf{C}_2du_2d^3\mathbf{C}_1$$

$$-\int_{u_1}^{\infty}\int_{C_{1-}}\int_{C_2}\varphi_{03}K_{3(1)}\varphi_{01}\exp[(-A_1/\zeta_1)(u_1-u_2)]$$

$$\times\zeta_1^{-1}K_{12}\varphi_{02}\psi_2(u_2)d^3\mathbf{C}_2du_2d^3\mathbf{C}_1. \tag{6.8}$$

In the last integral (which we denote by I) we set $\zeta_1\to-\zeta_1$. We obtain

$$I=\int_{u_1}^{\infty}\int_{C_{1+}}\int_{C_2}\varphi_{03}K_{31}\exp[(A_1/\zeta_1)(u_1-u_2)]$$

$$\times\zeta_1^{-1}K_{(1)2}\varphi_{02}\psi_2(u_2)d^3\mathbf{C}_2du_2d^3\mathbf{C}_1. \tag{6.9}$$

A_1 is unaffected by the sign change in ζ_1. We now note that when $0\leqslant u_2\leqslant u,(u_1-u_2)$ is positive, while when

[7] Hopf, *Mathematical Problems of Radiative Equilibrium* (Cambridge University Press, Cambridge, 1934), p. 20 ff.

[8] Tolman, *Statistical Mechanics* (Oxford University Press, London, 1938), p. 104.

$u_1 \lessgtr u_2$, (u_1-u_2) is negative. Therefore, we can write

$$\int_{C_1} \varphi_{03} K_{3(1)} \varphi_{01} \psi_1(u_1) d^3\mathbf{C}_1$$

$$= \int_{C_{1+}} \varphi_{03} K_{3(1)} \varphi_{01} \exp(-A_1 u_1/\zeta_1) \psi_1^+(0) d^3\mathbf{C}_1$$

$$+ \int_0^\infty \int_{C_2} \varphi_{03} E_{32}(u_1-u_2) \varphi_{02} \psi_2(u_2) d^3\mathbf{C}_2 du_2, \quad (6.10)$$

where, when $0 \lessgtr u_2 \lessgtr u_1$,

$$E_{32}(u_1-u_2) \equiv \int_{C_{1+}} K_{3(1)} \exp[(-A_1/\zeta_1)|u_1-u_2|] \times \zeta_1^{-1} \varphi_{01} K_{12} d^3\mathbf{C}_1, \quad (6.11a)$$

and when $u_1 < u_2$,

$$E_{32}(u_1-u_2) \equiv \int_{C_{1+}} K_{31} \exp[-(A_1/\zeta_1)|u_1-u_2|] \times \zeta_1^{-1} \varphi_{01} K_{(1)2} d^3\mathbf{C}_1. \quad (6.11b)$$

If we define

$$K_{12}^s \equiv \tfrac{1}{2}(K_{12}+K_{1(2)}), \quad (6.12a)$$

$$K_{12}^a \equiv \tfrac{1}{2}(K_{12}-K_{1(2)}), \quad (6.12b)$$

then K_{12}^s is a specular kernel and K_{12}^a is antispecular. We then have

$$E_{32}(u_1-u_2)$$

$$= \int_{C_{1+}} \{(K_{31}^s K_{12}^s - K_{31}^a K_{12}^a) + \operatorname{sgn}(u_1-u_2)(K_{31}^s K_{12}^a - K_{31}^a K_{12}^s)\} \times \exp[-(A_1/\zeta_1)|u_1-u_2|] \zeta_1^{-1} \varphi_{01} d^3\mathbf{C}_1. \quad (6.13)$$

Note the very important fact that $E_{32}(u_2-u_2)$ is not invariant under interchange of $\mathbf{C}_3$ and $\mathbf{C}_2$ or under interchange of u_3 and u_2; it *is* invariant under interchange of $(\mathbf{C}_3,u_3)$ and $(\mathbf{C}_2,u_2)$. Multiplication by $K_{3(1)}$ instead of K_{31} achieves this.

7. MOLECULAR CASE

For this case, $k_1=0$, $K=-L$. We then have

$$\int_{C_1} \varphi_{03} L_{3(1)} \varphi_{01} \psi_1(u_1) d^3\mathbf{C}_1$$

$$= \int_{C_{1+}} \varphi_{03} L_{3(1)} \varphi_{01} \exp(i\alpha u_1/\zeta_1) \psi_1^+(0) d^3\mathbf{C}_1$$

$$- \int_0^\infty \int_{C_2} \varphi_{03} F_{32}'(u_1-u_2) \varphi_{02} \psi_2(u_2) d^3\mathbf{C}_2 du_2, \quad (7.1)$$

where

$$F_{32}'(u_1-u_2) \equiv \int_{C_{1+}} \{(L_{31}^s L_{12}^s - L_{31}^a L_{12}^a) + \operatorname{sgn}(u_1-u_2)(L_{31}^s L_{12}^a - L_{31}^a L_{12}^s)\} \times \exp[(i\alpha/\zeta_1)|u_1-u_2|] \zeta_1^{-1} \varphi_{01} d^3\mathbf{C}_1. \quad (7.2)$$

It can be shown that all of these operations are possible. One of the reasons for this is the absence of nondecaying solutions to (7.1). Moreover, L_{12} is positive definite in the space of solutions of the homogeneous counterpart of (7.1), because the only functions that correspond to the vanishing eigenvalue of L_{12} do not satisfy this equation.

However, in the case of $\alpha=0$, there are nondecaying solutions of the problem which are also annihilated by L_{12}. We may exclude these from the discussion of (7.1) with $\alpha=0$ and determine them separately, since they are not present in (7.1) and are completely independent of it, i.e., they may be assigned arbitrary coefficients and combined with the solution of (7.1). With this in mind, L_{12} becomes positive definite in the space of solutions of (7.1). These considerations enable us to assert that the solution of (7.1) is uniquely defined (in the appropriate subspace).

Unfortunately, the operations in (7.2) are not all defined. The integration over ζ_1 goes from 0 to ∞. At the origin, $L_{31}^s L_{12}^s$ does not vanish, so that at first sight the integral seems to diverge. However, by referring back to the equation from which (7.1) (with $\alpha=0$) came, namely,

$$\varphi_{01}\zeta_1 \partial\psi_1/\partial u = -\int_{C_2} \varphi_{01} L_{12} \varphi_{02} \psi_2 d^3\mathbf{C}_2, \quad (7.3)$$

and by assuming ψ_1 bounded as $\zeta_1 \to 0$, we see that

$$\int_{C_2} \varphi_{0[1]} L_{[1]2} \varphi_{02} \psi_2 d^3\mathbf{C}_2 = 0. \quad (7.4)$$

(A bracket around a suffix indicates that the ζ component has been set equal to zero.) This means that when ψ is a solution of (7.3), (7.4) is true, and, therefore, that the operations in (7.1) are actually possible, provided ψ is combined with F' first. We may also rewrite (7.2) (with $\alpha=0$):

$$F_{32}(u_1-u_2)$$

$$= \int_{C_{1+}} \{(L_{31}^s L_{12}^s - L_{3[1]}^s L_{[1]2}^s - L_{31}^a L_{12}^a) + \operatorname{sgn}(u_1-u_2)(L_{31}^s L_{12}^a - L_{31}^a L_{12}^s)\zeta_1^{-1} \varphi_{01} d^3\mathbf{C}_1. \quad (7.5)$$

$F_{32}(u_1-u_2)$ is then defined also for functions which do not satisfy (7.3).

8. RETURN SCATTERING PROBLEM

The problem stated in Sec. 1 may now be expressed mathematically: one solves (6.10) for $\psi(u)$ and evaluates it at $u=0$ for negative ζ. A formula for this function comes from (6.6). We set $u=0$, $\zeta_1=-\zeta_4$ and define $\varphi_{01}\zeta_1\psi^-(-\zeta_1,0)\equiv\Gamma(\zeta_1)$. Therefore, $\Gamma(\zeta_4)$ (the returning distribution with reversed u axis) is given by

$$\Gamma_4=\int_0^\infty\int_{C_2}\exp[(-A_4/\zeta_4)u_2]\times\varphi_{04}K_{(4)2}\varphi_{02}\psi_2(u_2)d^3\mathbf{C}_2du_2, \quad (8.1)$$

for $\zeta_4\geqslant 0$. The difficulty with (8.1) is, however, that $\psi_2(u_2)$ is unknown. Note that ζ_4 is greater than zero for a particle going to the *left*.

9. VARIATIONAL FORMULA

Let us first restrict the problem by setting

$$\psi_1{}^+(0)=\delta(\xi_1-\xi_5)\delta(\eta_1-\eta_5)\delta(\zeta_1-\zeta_5), \quad (\text{for } \zeta_1,\zeta_5\geqslant 0). \quad (9.1)$$

This is a monochromatic, unidirectional spray all of whose particles have the same velocity $\mathbf{C}_5$. In reality, the problem is not restricted, since a superposition of solutions, each assuming a form (9.1) for $\psi_1{}^+(0)$ can be made equal to a solution with arbitrary $\psi_1{}^+(0)$. When we substitute (9.1) into (6.10), we obtain

$$\int_{C_1}\varphi_{03}K_{3(1)}\varphi_{01}\psi_1{}^5(u_1)d^3\mathbf{C}_1-\int_0^\infty\int_{C_2}\varphi_{03}E_{32}(u_1-u_2)\varphi_{02}\psi_2{}^5(u_2)d^3\mathbf{C}_2du_2=\varphi_{03}K_{3(5)}\varphi_{05}\exp[-(A_5/\zeta_5)u_1]. \quad (9.2)$$

The superscript has been placed on ψ to show that the solution of (9.2) is a function of the parameters (ξ_5,η_5,ζ_5).

We now consider, for conciseness, that the various functions are elements of a linear vector space and that the integrations with kernels are linear operations in this space. The inner product of two elements corresponds to an integration. Thus, we make correspond

$$(a,b)\rightleftarrows\int_0^\infty\int_{C_1}a(\mathbf{C}_1,u_1)b(\mathbf{C}_1,u_1)d^3\mathbf{C}_1du_1. \quad (9.3)$$

Operators correspond to integrals with kernels

$$P\psi\rightleftarrows\int_0^\infty\int_{C_2}P(\mathbf{C}_1,u_1;\mathbf{C}_2,u_2)\psi(\mathbf{C}_2,u_2)d^3\mathbf{C}_2du_2. \quad (9.4)$$

With this shorthand, Eq. (9.2) becomes

$$a_3{}^5=P_{32}\psi_2{}^5, \quad (9.5)$$

where

$$a_3{}^5\equiv\varphi_{03}K_{3(5)}\varphi_{05}\exp[(-A_5/\zeta_5)u_3], \quad (9.6)$$

$$P_{32}\equiv\varphi_{03}K_{3(2)}\varphi_{02}\delta(u_3-u_2)-\varphi_{03}E_{32}(u_3-u_2)\varphi_{02}, \quad (9.7)$$

and P_{32} is symmetric in the space $(\mathbf{C},u)$. Equation (8.1) corresponds, (recalling that ψ is a function of $\mathbf{C}_5$), to

$$\Gamma_{45}=(a_2{}^4,\psi_2{}^5). \quad (9.8)$$

By substituting (9.5) into (9.8), we obtain

$$\Gamma_{45}=(P\psi^4,\psi^5)=(\psi^4,P\psi^5), \quad (9.9)$$

in virtue of the symmetry of P. This shows that Γ_{45} is a symmetric function of $\mathbf{C}_4$ and $\mathbf{C}_5$. Since it was originally defined as equal to $\varphi_{04}\zeta_4\psi^-(-\zeta_4,0)$, it contains ζ_4 as a linear factor. Therefore, it also contains ζ_5 as a linear factor and may be written

$$\Gamma_{45}\equiv\varphi_{04}\zeta_4\Theta_{45}\zeta_5\varphi_{05}, \quad (9.10)$$

where Θ is a bounded function of its arguments.

We set up the following functional according to a prescription of Schwinger:

$$\Gamma_{45}\equiv\frac{(\chi^4,a^5)(a^4,\chi^5)}{(\chi^4,P\chi^5)}. \quad (9.11)$$

This functional is stationary under variations of χ away from the correct solution ψ and is equal to Γ_{45} at this value of χ. When written out, (9.11) becomes

$$\Gamma_{45}=D^{-1}\left\{\int_0^\infty\int_{C_2}\exp[(-A_4/\zeta_4)u]\times\varphi_{04}K_{(4)2}\varphi_{02}\chi_2{}^5(u)d^3\mathbf{C}_2du\right\}\times\left\{\int_0^\infty\int_{C_2}\exp[-(A_5/\zeta_5)u]\times\varphi_{05}K_{(5)2}\varphi_{02}\chi_2{}^4(u)d^3\mathbf{C}_2du\right\}, \quad (9.12)$$

$$D\equiv\int_0^\infty\int_{C_2}\int_{C_3}\chi_2{}^4(u)\varphi_{02}K_{2(3)}\varphi_{03}\times\chi_3{}^5(u)d^3\mathbf{C}_2d^3\mathbf{C}_3du-\int_0^\infty\int_0^\infty\int_{C_2}\int_{C_3}\chi_2{}^4(u_2)\varphi_{02}E_{23}(u_2-u_3)\times\varphi_{03}\chi_3{}^5(u_3)d^3\mathbf{C}_2d^3\mathbf{C}_3du_2du_3.$$

A functional of this form has been found previously for the case of monoenergetic neutron diffusion through a plane slab by S. Borowitz (unpublished).

10. CASE OF $A=0$

Due to the reciprocal of ζ appearing in the exponents in (9.12), Γ_{45} is proportional to $\zeta_4\zeta_5$; this accords with

(9.10). When, however, $A=0$, this will no longer be true, unless χ has the property expressed in (7.4). It is possible, nevertheless, to write down a functional which has this property for arbitrary χ (provided, of course, that all operations with it are defined). We first define

$$L_2^{[4]} \equiv L_{2[4]}, \quad \bar{L}_2^4 \equiv L_{2(4)} - L_{2[4]}, \tag{10.1}$$

also

$$Q_{23} \equiv \varphi_{02} L_{2(3)} \varphi_{03} \delta(u_2 - u_3) + \varphi_{02} F_{23}(u_2 - u_3) \varphi_{03}, \tag{10.2}$$

also

$$\mathfrak{F} \equiv \frac{(\chi^4, L^5)(L^4, \chi^5)}{(\chi^4, Q\chi^5)}, \tag{10.3}$$

and

$$\mathfrak{G}_{45} \equiv \frac{(\chi^4, \bar{L}^5)(\bar{L}^4, \chi^5)}{(\chi^4, \bar{L}^5)(\bar{L}^4, \chi^5) + (\chi^4, L^{[5]})(L^{[4]}, \chi^5)}. \tag{10.4}$$

Then the functional

$$\mathbf{\Gamma}_{45} \equiv \mathfrak{F}_{45} \mathfrak{G}_{45} \tag{10.5}$$

is proportional to $\zeta_4 \zeta_5$ for all χ and is stationary at $\chi = \psi$. Note that $\mathfrak{F}$ has the same form as $\mathbf{\Gamma}_{45}$ for the case $A \neq 0$, while $\mathfrak{G}$ is a stationary factor which reduces to unity for $\chi = \psi$ and is proportional to $\zeta_4 \zeta_5$.

11. TRIAL FUNCTIONS

For the case $A \neq 0$, a linear combination of the function $\exp[(-A_1/\zeta_1)u_1]$ and various products $\exp(-s_i u_1) \cdot N^i(\mathbf{C}_1)$, where s_i are estimated eigenvalues of the operator (5.5). These may perhaps be evaluated from

$$s_i = -\frac{\int_{C_1} \varphi_{01} N_1{}^i \left\{ A_1 N_1{}^i - \int_{C_2} K_{12} \varphi_{02} N_2{}^i d^3\mathbf{C}_2 \right\} d^3\mathbf{C}_1}{\int_{C_1} \varphi_{01} N_1 \zeta_1 N_1{}^i d^3\mathbf{C}_1}, \tag{11.1}$$

or one may choose those values of s_i which actually make $\mathbf{\Gamma}_{45}$ stationary. For the molecular case

$$s_i = -\frac{\int_{C_1}\int_{C_2} \varphi_{01} N_1{}^i L_{12} \varphi_{02} N_2{}^i d^3\mathbf{C}_2 d^3\mathbf{C}_1}{\int_{C_1} \varphi_{01} N_1 \zeta_1 N_1{}^i d^3\mathbf{C}_1}. \tag{11.2}$$

12. CALCULATION OF BACKSCATTERING

The application of the approximate $\mathbf{\Gamma}_{45}$ is very simple. To the incident $\varphi_{01}\zeta_1\psi_1{}^+(0)$ equal to $\varphi_{01}\zeta_1\delta(\mathbf{C}_1 - \mathbf{C}_5)$ corresponds $\varphi_{04}\zeta_4\Theta_{45}\zeta_5\varphi_{05}$. The incident $\varphi_{01}\zeta_1\psi_1{}^+(0)$ is equal to

$$\varphi_{01}\zeta_1\psi_1{}^+(0) = \int_{C_5+} \delta(\mathbf{C}_1 - \mathbf{C}_5)\varphi_{05}\zeta_5\psi_5{}^+(0) d^3\mathbf{C}_5. \tag{12.1}$$

Therefore, by superposition, the backscattered distribution is given by

$$\varphi_{04}\zeta_4\psi_{(4)}{}^-(0) = \int_{C_5+} \varphi_{04}\zeta_4\Theta_{45}\zeta_5\varphi_{05}\psi_5{}^+(0) d^3\mathbf{C}_5. \tag{12.2}$$

This solution to the "spray" problem may be applied to various problems involving nonspecular scattering kernels, such as the following evaporation problem.

13. INTERFACE RELATIONS IN EVAPORATION

We may represent a liquid and vapor separated by an interface as two gases with a potential jump at the interface. The potential increases suddenly from the value zero in the liquid (on the left) to the value W_0, say, in the vapor (on the right).

If a drift of molecules occurs from the liquid to the vapor, one may regard this as a "spray" of molecules into the vapor and use the scattering matrix defined above to calculate the distribution of molecules returning from the vapor. These now fall into the liquid and constitute another spray which will be reflected according to the characteristics of the liquid.

We assume the transition layer between liquid and vapor to be so thin that while the molecules are changing their potential energy, they suffer no collisions. The Boltzmann equation for one dimension, assuming no collisions, is

$$\partial f/\partial t + v_z \partial f/\partial z + \mathfrak{F}_z \partial f/\partial v_z = 0, \tag{13.1}$$

and has the general solution

$$f = G(v_x, v_y, \{v_z^2 - 2z\mathfrak{F}\}^{\frac{1}{2}}, t - \mathfrak{F}^{-1}\{c + 2z\mathfrak{F}\}^{\frac{1}{2}}). \tag{13.2}$$

We are assuming that $\mathfrak{F}_z (\equiv \mathfrak{F})$ is a constant; c is an arbitrary constant. At $z=0$, we assume $(f)_0 = f(v_x, v_y, v_z, t)$ has a known form. We may take $c=0$ and $G \equiv f$ in (13.2). Now we evaluate f at $z=\delta$, the thickness of the interface and we have

$$(f)_\delta = f(v_x, v_y, \{v_z^2 - 2\delta\mathfrak{F}\}^{\frac{1}{2}}, t - \{2\delta/\mathfrak{F}\}^{\frac{1}{2}}). \tag{13.3}$$

Now we take $\mathfrak{F}$ to be <0 and to increase in absolute value with decreasing δ in such a way that $\delta\mathfrak{F}$ remains finite (and is equal to V_0). The product $2\delta\mathfrak{F}$ we denote by $-\kappa^2$. We can then write

$$f(\text{liq.}) = f(v_x, v_y, v_z, t), \tag{13.4}$$

$$f(\text{vap.}) = f(v_x, v_y, \{v_z^2 + \kappa^2\}^{\frac{1}{2}}, t). \tag{13.5}$$

The transition from right to left has the effect

$$g(\text{vap.}) = g(v_x, v_y, v_z, t), \tag{13.6}$$

$$g(\text{liq.}) = g(v_x, v_y, \{v_z^2 - \kappa^2\}^{\frac{1}{2}}, t). \tag{13.7}$$

If we change to dimensionless units as in Sec. 2, we obtain

$$n_0^V\varphi_V(\xi,\eta,\zeta,\tau)=n_0^L\varphi_L(\xi,\eta,\{\zeta^2+\zeta_0^2\}^{\frac{1}{2}},\tau), \quad (13.8)$$

$$n_0^L\varphi_L(\xi,\eta,\zeta,\tau)=n_0^V\varphi_V(\xi,\eta,\{\zeta^2-\zeta_0^2\}^{\frac{1}{2}},\tau), \quad (13.9)$$

where

$$\zeta_0=(m/2kT_0)^{\frac{1}{2}}\kappa, \quad \text{and} \quad \zeta_0>0.$$

The temperatures of the undisturbed media are equal and the densities bear the relation

$$n_0^V=\exp(-\zeta_0^2)\cdot n_0^L. \quad (13.10)$$

In order that all ζ components under discussion shall be nonnegative, we denote ζ by ζ_r when $\zeta>0$ (particle going to right) and by $-\zeta_l$ when $\zeta<0$ (particle going to left). Note that in (13.9), $\zeta^2\geqslant\zeta_0^2$. This means that $\zeta_r>\zeta_0$ and $\zeta_l>\zeta_0$. The reason for this is that molecules in the liquid with a velocity component $\zeta_r<\zeta_0$ cannot escape into the vapor, while molecules in the liquid with a velocity component $\zeta_l<\zeta_0$ did not come from the vapor but came originally from the liquid and were reflected back by the barrier with the same ξ and η components but with a reversed ζ component. If we denote by φ^+ that part of φ defined for $\zeta\geqslant 0$ and by φ^- that part defined for $(-\zeta)>0$, we may describe the above effect by

$$\varphi_L^+(\zeta_r)=\varphi_L^-(\zeta_l) \quad \text{for } \zeta_r<\zeta_0,\ \zeta_l<\zeta_0. \quad (13.11)$$

14. SMALL AMPLITUDE DRIFT

As in Sec. 3, we assume

$$\varphi=\varphi_0(1+\Phi), \quad (14.1)$$

where Φ now consists of two parts: one is a steady, time-independent drift denoted by Ψ; the other is a sound wave of frequency α (in dimensionless units) which we denote by Φ. We set Φ equal to $\mathrm{Rl}\{e^{-i\alpha\tau}\Psi\}$ and deal later with Ψ.

(a) Steady Solution

From Sec. 5, we see that

$$\Psi_L^-=\beta_L-\mu_L\zeta_l+\epsilon_L C_l^2+\psi_L^-(\mathbf{C}_l), \quad (14.2a)$$

$$\Psi_L^+=\beta_L+\mu_L\zeta_r+\epsilon_L C_r^2+\psi_L^+(\mathbf{C}_r), \quad (14.2b)$$

$$\Psi_V^-=\beta_V-\mu_V\zeta_l+\epsilon_V C_l^2+\psi_V^-(\mathbf{C}_l), \quad (14.2c)$$

$$\Psi_V^+=\beta_V+\mu_V\zeta_r+\epsilon_V C_r^2+\psi_V^+(\mathbf{C}_r), \quad (14.2d)$$

where β, μ, and ϵ are constnnts to be determined and ψ is the remainder of Ψ. ψ is a decaying solution which carries no fluxes, since we assume the linear combination of the summational invariants to serve this function.

Using our previous results, we shall trace the flow of molecules back and forth across the barrier, starting from the left side. For $\zeta_r>\zeta_0$, the relation between $\Psi_L^+(\mathbf{C}_r)$ and $\Psi_V^+(\mathbf{C}_r)$ is, following (13.8),[9]

$$\beta_V+\mu_V\zeta_r+\epsilon_V C_r^2+\psi_V^+(\zeta_r)=\beta_L+\mu_L\{\zeta_r^2+\zeta_0^2\}^{\frac{1}{2}}+\epsilon_L(C_r^2+\zeta_0^2)+\psi_L^+(\{\zeta_r^2+\zeta_0^2\}^{\frac{1}{2}}). \quad (14.3)$$

From (12.2), the returning distribution exclusive of summational invariants is given by

$$\psi_V^-(\zeta_l)=\int_{C_r+}\Theta_{lr}{}^V\zeta_r\varphi_0\psi_V^+(\zeta_r)d^3\mathbf{C}_r. \quad (14.4)$$

Now

$$\Psi_V^-(\zeta_l)=\beta_V-\mu_V\zeta_l+\epsilon_V C_l^2+\psi_V^-(\zeta_l) \quad (14.5)$$

describes the molecules going back to the left. These cross the barrier, where their contribution to the distribution in the liquid is obtained using (13.9):

$$\beta_L-\mu_L\zeta_l+\epsilon_L C_l^2+\psi_L^-(\zeta_l)=\beta_V-\mu_V\{\zeta_l^2-\zeta_0^2\}^{\frac{1}{2}}+\epsilon_V(C_l^2-\zeta_0^2)+\psi_V^-(\{\zeta_l^2-\zeta_0^2\}^{\frac{1}{2}}), \quad (14.6)$$

for $\zeta_l\geqslant\zeta_0$.

The part of Ψ_L^- defined for $\zeta_l<\zeta_0$ comes from reflection of the particles described by Ψ_L^+ defined for $\zeta_r<\zeta_0$. From (13.11), we may obtain[10]

$$(\Psi_L^-)_{\zeta_l<\zeta_0}=\beta_L-\mu_L\zeta_l+\epsilon_L C_l^2+(\psi_L^+)_{\zeta_l<\zeta_0}. \quad (14.7)$$

Thus, the decaying part of Ψ_L^- is given by

$$(\psi_L^-)_{\zeta_l<\zeta_0}=-2\mu_L\zeta_l+(\psi_L^+)_{\zeta_l<\zeta_0}. \quad (14.8)$$

Similarly to (14.4), we obtain ψ_L^+ from ψ_L^-

$$\psi_L^+(\zeta_r)=\int_{C_l+}\Theta_{rl}{}^L\zeta_l\varphi_{0l}\psi_L^-(\zeta_l)d^3\mathbf{C}_l. \quad (14.9)$$

This integral must be broken up into two parts

$$\psi_L^+(\zeta_r)=\int_{\zeta_l<\zeta_0}\Theta_{rl}{}^L\zeta_l\varphi_{0l}(\psi_L^-)_{\zeta_l<\zeta_0}d^3\mathbf{C}_l+\int_{\zeta_l\geq\zeta_0}\Theta_{rl}{}^L\zeta_l\varphi_{0l}(\psi_L^-)_{\zeta_l\geq\zeta_0}d^3\mathbf{C}_l. \quad (14.10)$$

To this, we add $\beta_L+\mu_L\zeta_r+\epsilon_L C_r^2$ to obtain Ψ_L^+.

We have now derived Ψ_L^+ in terms of itself implicitly. We can now eliminate all other functions and obtain a rather complicated integral equation for Ψ_L^- (or, more precisely, for ψ_L^-)

$$\psi_L^-(\zeta_l)-\int_{C_{l'}+}\Theta_{ll'}{}^L\zeta_{l'}\varphi_{0l'}\psi_L^-(\zeta_{l'})d^3\mathbf{C}_{l'}=-2\mu_L\zeta_l, \quad \text{for } \zeta_l<\zeta_0; \quad (14.11a)$$

[9] We write $\psi(\zeta)$ for $\psi(\xi,\eta,\zeta)$, since ξ and η remain unchanged in all transformations.

[10] Note the temporary use of ζ_r for the z component of particles going both to right and left.

$$\psi_L^-(\zeta_l)-\int_{C_{l'+}}\left\{\int_{C_{r+}}\Theta^V[(\zeta_l^2-\zeta_0^2)^{\frac{1}{2}},\zeta_r]\varphi_{0r}\right.$$

$$\left.\times\Theta^L[(\zeta_r^2+\zeta_0^2)^{\frac{1}{2}},\zeta_l']d^3\mathbf{C}_r\right\}\zeta_l'\varphi_{0l}'\psi_L^-(\zeta_l')d^3\mathbf{C}_l'$$

$$=(\beta_V-\beta_L)\left[1-\int_{C_{r+}}\Theta^V(\{\zeta_l^2-\zeta_0^2\}^{\frac{1}{2}},\zeta_r)\right.$$

$$\left.\times\zeta_r\varphi_{0r}d^3\mathbf{C}_r\right]-\mu_L\left[\zeta_l+\int_{C_{r+}}\Theta^V(\{\zeta_l^2-\zeta_0^2\}^{\frac{1}{2}},\zeta_r)\right.$$

$$\left.\times\zeta_r\varphi_{0r}\{\zeta_r^2+\zeta_0^2\}^{\frac{1}{2}}d^3\mathbf{C}_r\right]-\mu_V\left[\{\zeta_l^2-\zeta_0^2\}^{\frac{1}{2}}\right.$$

$$\left.+\int_{C_{r+}}\Theta^V(\{\zeta_l^2-\zeta_0^2\}^{\frac{1}{2}},\zeta_r)\zeta_r\varphi_{0r}\zeta_r d^3\mathbf{C}_r\right]$$

$$+(\epsilon_V-\epsilon_L)\left[C_l^2-\int_{C_{r+}}\Theta^V(\{\zeta_l^2-\zeta_0^2\}^{\frac{1}{2}},\zeta_r)\right.$$

$$\left.\times\zeta_r\varphi_{0r}C_r^2d^3\mathbf{C}_r\right]-\zeta_0^2\left[\epsilon_V-\epsilon_L\right.$$

$$\left.\times\int_{C_{r+}}\Theta^V(\{\zeta_l^2-\zeta_0^2\}^{\frac{1}{2}},\zeta_r)\zeta_r\varphi_{0r}d^3\mathbf{C}_r,\right.$$

$$\text{for } \zeta_l\geq\zeta_0. \quad (14.11b)$$

If one could solve these equations, ψ_L^- would be a linear combination of $(\beta_V-\beta_L)$, μ_V, μ_L, ϵ_V and ϵ_L. One could obtain the other functions of interest via Eqs. (14.3) to (14.10).

We have yet to impose conditions on the above constants. We integrate (14.3) over $\mathbf{C}_r$ for $\zeta_r\geq\zeta_0$. To this we add the result of integrating (14.7) over $\mathbf{C}_l$ for $\zeta_l<\zeta_0$. The result is

$$\int_C\varphi_0\zeta\Psi_V d^3\mathbf{C}=\exp(\zeta_0^2)\cdot\int_C\varphi_0\zeta\Psi_L d^3\mathbf{C}, \quad (14.12)$$

and after substituting the values of the Ψ's, we obtain

$$\tfrac{1}{2}\mu_V=\tfrac{1}{2}\exp(-\zeta_0^2)\cdot\mu_L. \quad (14.13)$$

If we multiply (14.3) by ζ_r and integrate over $\mathbf{C}_r$, we obtain similarly,

$$\tfrac{1}{2}\beta_V+(5/4)\epsilon_V=\exp(\zeta_0^2)\left\{\int_{\zeta_r>\zeta_0}\varphi_{0r}\zeta_r\{\zeta_r^2-\zeta_0^2\}^{\frac{1}{2}}\right.$$

$$\left.\times\Psi_L^+(\zeta_r)d^3\mathbf{C}_r\right\}. \quad (14.14)$$

Finally, if we multiply (14.3) by $\{\zeta_r^2+\zeta_0^2\}^{\frac{1}{2}}$ and integrate, we arrive at

$$\int_{C_{r+}}\varphi_{0l}\zeta_l\{\zeta_l^2+\zeta_0^2\}^{\frac{1}{2}}\Psi_V^+(\zeta_r)d^3\mathbf{C}_r$$

$$+\int_{C_{l+}}\varphi_{0l}\zeta_l\{\zeta_l^2+\zeta_0^2\}^{\frac{1}{2}}\Psi_V^-(\zeta_l)d^3\mathbf{C}_l$$

$$=\exp(\zeta_0^2)\left\{\tfrac{1}{2}\beta_L+(5/4)\epsilon_L\right.$$

$$\left.-2\int_{\zeta_l<\zeta_0}\varphi_{0l}\zeta_l^2\Psi_L^-(\zeta_l)d^3\mathbf{C}_l\right\}. \quad (14.15)$$

The last three equations form three linear conditions on the constants in question. The remaining two conditions must come from asymptotic boundary conditions on the flowing fluid.

(b) Time-Dependent Solution

Here we have no nondecaying part, so we simply take over Eqs. (14.11) while setting β, μ, and ϵ to zero for both sides. We now understand by Θ the scattering matrix calculated for this case. For the liquid side, we break Ψ_L up into incident and reflected parts. The equations for Ψ_{LR}^-, the reflected wave, in terms of Ψ_{LI}, the incident wave, are

$$\Psi_{LR}^-(\zeta_l)-\int_{C_{r+}}\Theta_{lr'}{}^L\zeta_l'\varphi_{0l}'\Psi_{LR}^-(\zeta_l')d^3\mathbf{C}_l'$$

$$=\Psi_{LI}^+(\zeta_l)-\Psi_{LI}^-(\zeta_l), \quad \text{for } \zeta_l<\zeta_0, \quad (14.16)$$

$$\Psi_{LR}^-(\zeta_l)-\int_{C_{l'+}}\left\{\int_{C_{r+}}\Theta^V(\{\zeta_l^2-\zeta_0^2\}^{\frac{1}{2}},\zeta_r)\zeta_r\varphi_{0r}\right.$$

$$\left.\times\Theta^L(\{\zeta_r^2+\zeta_0^2\}^{\frac{1}{2}},\zeta_l')d^3\mathbf{C}_r\right\}\times\zeta_l'\varphi_{0l}'\Psi_{LR}^-(\zeta_l')d^3\mathbf{C}_l$$

$$=-\Psi_{LI}^-(\zeta_l)+\exp(\zeta_0^2)$$

$$\times\int_{\zeta_r\geq\zeta_0}\Theta^V(\{\zeta_l^2-\zeta_0^2\}^{\frac{1}{2}},\{\zeta_r^2+\zeta_0^2\}^{\frac{1}{2}})$$

$$\times\zeta_r\varphi_{0r}\Psi_{LI}^+(\zeta_r)d^3\mathbf{C}_r. \quad (14.17)$$

From Ψ_{LR}^-, we may calculate all other distributions of interest.

15. RELATION TO ELEMENTARY THEORY OF EVAPORATION

If one perturbs an equilibrium distribution by introducing slight changes in density, temperature, and mean velocity (in the z-direction), one has

$$f_1(\mathbf{v})=n_0(1+\delta_n)(m/2\pi k)^{-\frac{1}{2}}\{T_0(1+\delta_T)^{-\frac{1}{2}}$$

$$\times\exp\{-m[v_x^2+v_y^2+v_z^2(1-\delta_v)^2]/$$

$$[2kT_0(1+\delta_T)]\}. \quad (15.1)$$

One expands to first order (while changing to dimensionless variables) and obtains

$$\varphi_1=\varphi_0\{1+(\delta_n-\tfrac{3}{2}\delta_T)+2\delta_v\zeta+\delta_T C^2\}. \quad (15.2)$$

If we compare this result with (5.6), we see that $\delta_n-\frac{3}{2}\delta_T=\beta$, $2\delta_v=\mu$, and $\delta_T=\epsilon$.

The interface conditions (14.13)–(14.15) express the number and momentum flux relations which hold at the barrier. Let us now assume that there is no decaying part ψ to Ψ. Then the interface conditions reduce to

$$\mu_V=\exp(-\zeta_0^2)\mu_L, \quad (15.3)$$

$$\tfrac{1}{2}\beta_V+(5/4)\epsilon_V=\tfrac{1}{2}\beta_L+\epsilon_L[\tfrac{3}{4}+\tfrac{1}{2}\zeta_0^2+\tfrac{1}{2}\exp(\zeta_0^2)], \quad (15.4)$$

$$2I_\beta\beta_V+2I_\epsilon\epsilon_V=\exp(\zeta_0^2)\{(\tfrac{1}{2}-2I_\beta^<)\beta_L -2I_\mu^<\mu_L+(5/4-2I_\epsilon^<)\epsilon_L\}, \quad (15.5)$$

where

$$I_\beta\equiv(2\pi^{\frac{1}{2}})^{-1}\{\zeta_0+\exp(\zeta_0^2)G(\zeta_0)\}, \quad (15.6)$$

$$I_\mu\equiv\pi^{-\frac{1}{2}}\exp(\zeta_0^2)H(\zeta_0), \quad (15.7)$$

$$I_\epsilon\equiv(2\pi^{\frac{1}{2}})^{-1}\{(5/2-\zeta_0^2)[\zeta_0+\exp(\zeta_0^2)G(\zeta_0)+\zeta_0^3\}, \quad (15.8)$$

and

$$G(\zeta_0)\equiv\int_{\zeta_0}^{\infty}\exp(-u^2)du;$$

$$H(\zeta_0)\equiv\int_{\zeta_0}^{\infty}\exp(-u^2)\{u^2-\zeta_0^2\}^{\frac{1}{2}}u^2du.$$

Also

$$I_\beta^<\equiv(2\pi^{\frac{1}{2}})^{-1}\{\tfrac{1}{2}\pi^{\frac{1}{2}}-\zeta_0\exp(-\zeta_0^2)-G(\zeta_0)\}, \quad (15.9)$$

$$I_\mu^<\equiv(2\pi^{\frac{1}{2}})^{-1}\{1-\exp(-\zeta_0^2)\cdot(1+\zeta_0^2)\}, \quad (15.10)$$

$$I_\epsilon^<\equiv(2\pi^{\frac{1}{2}})^{-1}\{\tfrac{1}{2}\pi^{\frac{1}{2}}-\zeta_0\times\exp(-\zeta_0^2)\cdot(1+\zeta_0^2)-G(\zeta_0). \quad (15.11)$$

These are the relations that appear in the elementary evaporation theory[11] for slow evaporation. Therefore, the present treatment is a correction to the elementary theory for this case.

16. ACKNOWLEDGMENT

My thanks are due Professor L. Onsager for suggesting this problem and for helpful discussions.

[11] G. Dieterici, Ann. Physik N. F. 66, 826 (1898).

PHYSICAL REVIEW VOLUME 93, NUMBER 6 MARCH 15, 1954

Electron Ejection by Slow Positive Ions Incident on Flashed and Gas-Covered Metallic Surfaces

JAMES H. PARKER, JR.*
Department of Physics, University of California, Berkeley, California
(Received October 19, 1953)

A direct measurement of the ejected electron yield (γ_i) for A^+ incident on flashed and H_2-, N_2- and O_2-treated Ta and Pt and for the singly-charged hydrogen, nitrogen, and oxygen ions incident on Ta and Pt after treatment with the respective parent gas has been made for the kinetic energy range of 2 to 150 ev. The gas treatment for Pt consisted of an exposure to the molecular gas at a pressure of a few mm of Hg, while the treatment for Ta consisted of an exposure plus a glow discharge in which the Ta surface served as the cathode. In general, gas treatment of Ta and Pt was found to produce large decreases in γ_i for A^+ ions, with the effect increasing with decreasing ion energy. For both Ta and Pt the O_2 treatment was found to be the most effective in reducing γ_i while the H_2 treatment was found to be the least effective. γ_i for nitrogen ions on N_2-treated Ta and Pt showed a unique behavior at low ion energy in that it was found to increase with decreasing ion energy. This behavior was not observed for the other ions in this study.

I. INTRODUCTION

THE electrical breakdown of gases is dependent on a primary and a secondary mechanism. Of the active secondary mechanisms, one is photoelectric ionization in the gas near the anode and three more consist of electron liberation from the cathode by photons, metastable atoms, and positive-ion impact. The liberation by positive-ion impact is not only the first of these mechanisms invoked, but it is also exceedingly important for many discharges. Various means have been devised for evaluating γ_i, the coefficient of secondary electron liberation from the cathode, extending from discharge studies to measurements by static or dynamic means in the presence of a gas. Such studies suffer from inadequate control of variables, inability to differentiate between different cathode effects in static studies, and electron loss by back diffusion. The significant first direct studies of the number of electrons liberated per positive ion impact in vacuums with clean electrodes were those of Jackson[1] and more *in extenso* those of Oliphant, and Oliphant

* This work was initially supported under a contract with the U. S. Office of Naval Research. It was carried to its successful conclusion under a grant from the National Science Foundation.

[1] W. J. Jackson, Phys. Rev. 28, 524 (1926).

and Moon.[2] Further studies of this nature have over the years been carried on by Paetow and Walcher,[3] Penning,[4] Rostagni, Helea, and Houtermans, and Hagstrum.[5] The theory of the process has been treated by Kapitza,[6] Oliphant and Moon,[7] Massey,[8] Shekhter,[9] Cobas and Lamb,[10] Hagstrum[11] and Varnerin.[12]

All of these studies dealt with clean metallic surfaces largely with ions above some 50 volts kinetic energy. Although it was recognized that liberation could occur at low kinetic energies of impact if the ionization potential lay above the work function of the surface, (potential liberation), only limited measurements for ions of low kinetic energy had been made when this study began. However, there are many discharges in which secondary cathode emission occurs where ions have energies of the order of 10 volts and perhaps less. Furthermore, little attention was paid in these studies to gas-coated surfaces.

In the electrical breakdown of gases, various gases are obviously present and these tend to create surface films on the cathodes while positive-ion bombardment tends to remove these films. It thus becomes of importance to study the secondary emission from clean and gassy surfaces on cathodes in order to determine the sort of changes to be expected in secondary emission under discharge conditions. So far only Paetow and Walcher[3] using 500-volt Cs^+ ions on W and W coated with Cs, K, O_2, and H_2 and Hagstrum[5] using 200-volt He^+ and Ne^+ ions on H_2- and O_2-coated W as well as He^+ on Mo covered by the condensation of background gases under high vacuum conditions, have attempted such studies. The work of Hagstrum[6,11] was begun and carried out nearly contemporaneously with this investigation.[13] Accordingly this study was undertaken to investigate the secondary electron emission by various ions on clean and contaminated surfaces, using common gases and various ions with energies ranging from about two volts up to two hundred volts. Adopting the very efficient Finkelstein[14] type of ion source producing ion beams of low-energy spread, which permits operation at low gas pressures without differential pumping, direct measurements of γ_i, the positive ion impact coefficient for A^+ ions incident on flashed Ta and Pt as well as on these metals after treatment with H_2, N_2, and O_2 gases, were made. In addition, measurements were made on these metals after exposure to the appropriate gas with singly-charged hydrogen, nitrogen, and oxygen ions.

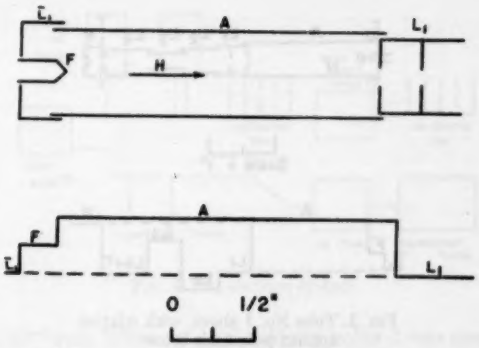

FIG. 1. The Finkelstein ion source above, with relative potentials applied to corresponding electrodes below.

II. EXPERIMENTAL PROCEDURES

A. The Positive Ion Source

The source was of the Finkelstein[14] type shown in Fig. 1 with a diagram of the relative electrode potentials drawn below. In principle the electrons from the hot W filament F are accelerated along the axis of the tubular electrode A by an appropriate potential V_{FA} between A and F. An axial field H of a few hundred gauss causes the electron paths to spiral while the repeller plate L_1 with an aperture and a retarding field relative to A repels electrons and extracts positive ions. At 10^{-5} mm Hg pressure of argon gas with a few μa of electron

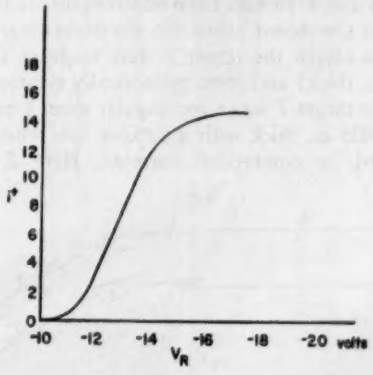

FIG. 2. Retarding potential curve showing two-volt energy spread of ion beam.

[2] M. L. E. Oliphant, Proc. Cambridge Phil. Soc. **24**, 451 (1928); M. L. E. Oliphant and P. B. Moon, Proc. Roy. Soc. (London) **A127**, 373 (1930).

[3] H. Paetow and W. Walcher, Z. Physik. **110**, 69 (1938); W. Ploch and W. Walcher, Z. Physik. **130**, 174 (1951).

[4] F. M. Penning, Proc. Roy. Acad. Sci. (Amsterdam) **31**, 14 (1928); **33**, 841 (1930); Physica **8**, 13 (1928); A. Rostagni, Ricerca sci. **9**, 633 (1938); M. Helea and C. Houtermans, Phys. Rev. **58**, 608 (1940); M. Helea and E. L. Chaffee, Phys. Rev. **49** 925 (1936); I. Okano, J. Phys. Soc. Japan **8**, 362 (1953).

[5] H. D. Hagstrum, Phys. Rev. **89**, 338 (1953).

[6] P. L. Kapitza, Phil. Mag. **45**, 989 (1923).

[7] M. L. E. Oliphant and P. B. Moon, Proc. Roy. Soc. (London) **A127**, 388 (1930).

[8] H. S. W. Massey, Proc. Cambridge Phil. Soc. **26**, 386 (1930); **27**, 460 (1931).

[9] S. S. Shekhter, J. Exptl. Theoret. Phys. (U.S.S.R.) **7**, 750 (1937).

[10] A. Cobas and W. E. Lamb, Phys. Rev. **65**, 327 (1944).

[11] H. D. Hagstrum, Phys. Rev. **89**, 244 (1953); **91**, 541 (1953).

[12] L. J. Varnerin, Jr., Phys. Rev. **91**, 859 (1953).

[13] Quite contemporaneous with this study was one of Okano (see reference 4) in Japan using Mo with common gases at high energies. The results roughly parallel those here although the outgassing and vacuum techniques were not comparable with those of either Hagstrum or the writer.

[14] A. T. Finkelstein, Rev. Sci. Instr. **11**, 97 (1940).

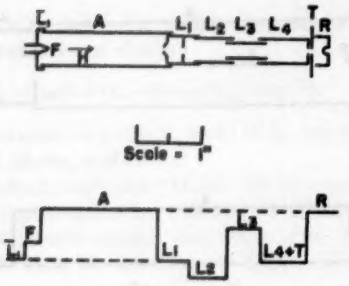

FIG. 3. Tube No. 1 above, with relative applied potentials below.

current from F, the ion beam has a strength of approximately 10^{-8} amp.

The energy spread of the ion beam from this source was about 2 ev as seen in the typical retarding potential curve shown in Fig. 2. From the retarding potential measurements, the potential at which the ions were produced in the source and therefore the energy of the electrons producing them could be ascertained. Thus it appeared that the potential at which the ions were produced was about 10 volts below the potential of electrode A. Experiments revealed that if the electron energy was below 28 ev the ions produced were A^+. Above this, A^{++} ions created by a two-stage process were also present. Thus all measurements were made below 28-ev electron energy. While through the Molnar-Hornbeck[16] process A_2^+ ions might have formed, with pressures of 2×10^{-5} mm these constituted less than 0.5 percent of the total beam. In the measurements of γ_i for ions of gases H_2, N_2, and O_2, the same energy of 28 ev was used. Therefore, while both atomic and molecular ions were present in unknown proportions, only singly-charged ions were produced.

B. The Experimental Tubes

Two tubes were used and these are shown respectively in Figs. 3 and 4. In Fig. 3 the relative potentials on the electrodes are shown below the electrode diagram. All electrodes except the target T were made of Ta sheet (0.015 in. thick) and were cylindrically symmetric. In tube 1 the target T was a rectangular sheet $\frac{1}{2}$ in.$\times$1 in. and 0.00025 in. thick with a circular hole which could be heated by conduction currents. Here R was a repeller electrode at such potential that no positive ions could reach it. The secondary electrons from impact of positive ions on T were drawn to R. L_2 at 10 volts negative to L_1 prevented secondary electrons at L_1 from reaching R. L_3 cut off the lower-energy tail of the positive ion beam. L_4 at the same potential as T prevented positive ions from striking the back side of T. The diameters of holes in L_2 and L_3 were larger than L_4.

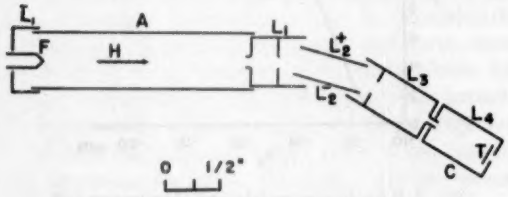

FIG. 4. Tube No. 2.

The retarding potential measurements on the positive ion beam were made by using R as the retarding electrode for ions that pass through L_4 and T. Figure 2 represents the ion current to R as a function of the potential of R with respect to A. Then the potential at which cutoff occurs is the potential with respect to A at which the ions are formed in the source. Both positive ion current to T and electron current to R were measured by separate electrometer tube circuits and potential sources were batteries and potentiometers. Tests ascertained that less than 1 percent of the ejected electrons were returned to the surface by the magnetic field for angles between the normal to the surface and magnetic field from 0 to 45°.

Tube 1 had two defects, these being that the angle of incidence of positive ions on the target was not defined and that secondary electrons produced at L_4 were recorded at R as apparent secondaries from T. Since emission could depend on angles of incidence and as this would generally vary with ion energy, the data on emission as a function of energy were in doubt. That trouble might come from L_4 as secondaries was indicated when a small retarding field for electrons between L_4 and T decreased γ_i by 30 percent. After recourse to tube 2 which avoids these difficulties checked the data on Ta to within 5 percent it was realized that the decrease caused by retarding field on L_4 probably came from positive ions striking the back of the target so that the results were not in doubt.

The source in tube 2 was the same except that the magnetic field of $H\sim200$ gauss was longer in order to envelope the whole electrode assembly. L_2^+ and L_2^- were half-cylinders which acted as deflecting plates. L_3 was a cylinder with two collimating apertures, while L_4 and C were two half-cylinders capped at the ends and separated by 1 mm. The caps toward L_3 formed a circular aperture collinear with those of L_3. Target T was a sheet of $\frac{3}{16}$ in.$\times\frac{3}{8}$ in.$\times$0.00025 in. for Ta and a similar sheet of 0.0004 in. for Pt, placed perpendicular to the axis of L_4 and C which could be heated by conduction currents.

Here the incidence of the beam on the target is normal. If C is positive to T all electrons from T follow the magnetic field and go to C. Electrons from the last aperture in L_3 will be collected by L_4. Excited and metastable atoms from the source are prevented from reaching T. This new arrangement also had its deficiencies as regards the proper potential distributions for L_3, L_4, and C in order to obtain correct data on γ_i for low ion energies. Thus if T was 15 volts or more

[16] J. A. Hornbeck and J. P. Molnar, Phys. Rev. 84, 621 (1951).

negative to the formation potential of the ions in the source and with C set so that ions could not reach it, ions reached T if L_4 was a few volts negative to C. For lower energies the potential of C was lowered so that ions could reach T. However, this meant that ions could now reach C, but by increasing the potential difference between C and L_4 the ions were sufficiently deflected so that measurements extended down to 5 volts.

With the potential of L_4 and C equal and sufficiently negative to T so that ejected electrons from T could not reach them, a positive current was measured at C of 1 percent of the target ion current. This gave an upper limit to the reflection coefficient of positive ions from T. This low value is in qualitative agreement with observations by Hagstrum.[1]

That all electrons ejected from T were collected by C is indicated by results with flashed Ta using He^+ ions which agreed with measurements of Hagstrum[11] under similar conditions to within 7 percent.

C. Vacuum System and Gases

A schematic diagram of the vacuum system is shown in Fig. 5. The vacuum techniques and pressure measurements closely followed those developed by Alpert,[16] the metal valves and ion gauges being on an all borosilicate glass system which could be baked out at 400°C. One Alpert valve served as cutoff, the other as a slow leak. The electrodes of the gauge were outgassed by electron bombardment while those of the measuring tube were outgassed by induction heating. The target could be flashed by conduction current. Absorption and source gases were contained in glass bottles of 2-cc capacity, opened by magnetic-slug-activated breakoffs. Figure 6 shows a photograph of the whole assembly, which is remarkably compact.

The argon came from Linde's one-liter flasks of spectroscopically pure argon. The N_2 and H_2 were prepared by circulating Linde tank gases over hot Cu and through liquid N_2 traps for 24 hours. The O_2 was simply tank O_2 passed through and distilled from a liquid N_2 trap.

D. Procedures

The system was baked at 400°C for periods of 12 to 24 hours. The oven was shut off and the electrodes of the tube were induction heated to 700°–900°C. Pressures at this time with all electrodes cold except the source filament usually ran to $2\text{–}5\times10^{-9}$ mm Hg, (equivalent-N_2 pressure.) Repeated flashing of the target from 30 seconds to several minutes was continued until the maximum pressure after a flash was not over $1\text{–}2\times10^{-8}$ mm Hg. For Pt the flash temperature was 1400°C, while for Ta it was 1400–2000°C. Within a few seconds after flash pressures returned

[16] D. Alpert, Rev. Sci. Instr. 22, 536 (1951); J. Appl. Phys. 24, 860 (1953); R. J. Bayard and D. Alpert, Rev. Sci. Instr. 21, 571 (1950).

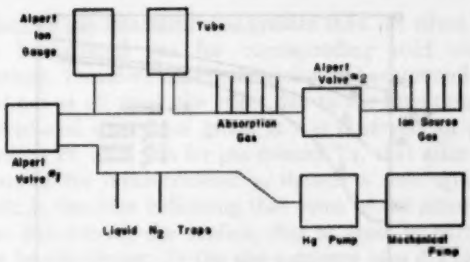

FIG. 5. The vacuum system.

to 10^{-9} mm. When ready the Alpert valve 2 was closed and the source bottle opened. The valve 2 was then opened until the pressure in the tube was $2\text{–}3\times10^{-5}$ mm Hg. Then measurements of γ_i for A^+ began. After study of flashed clean surface, both valves were closed and an absorption bottle was opened, the pressure rising to a few mm of Hg. The Pt was merely exposed to H_2, N_2, or O_2 for 5 minutes except in one case of a 5-minute exposure with 1 minute of glow discharge between target and collector using tube No. 2. In tube No. 1 with Ta target exposure plus glow discharge was routine.

After gas treatment, valve 1 was opened and the absorption gas pumped out to low pressure, or to operating pressure when absorption gas ions were to be used. If A^+ ions were used, the tube after pump-out of absorption gas was filled with A up to operating pressure by opening valve 2. Between each gas treat-

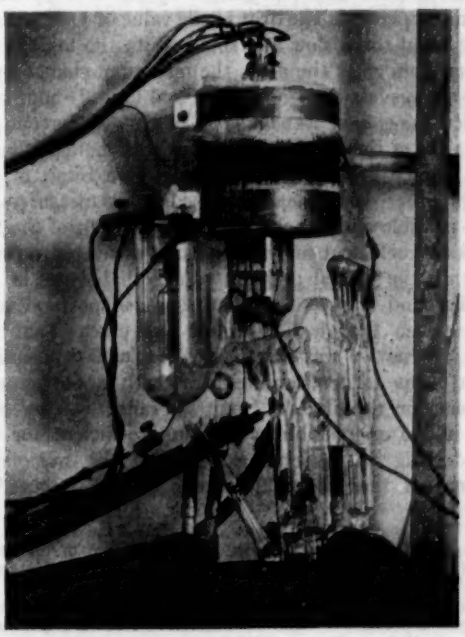

FIG. 6. The whole assembly showing vacuum techniques, and simplicity possible by Finkelstein-type source.

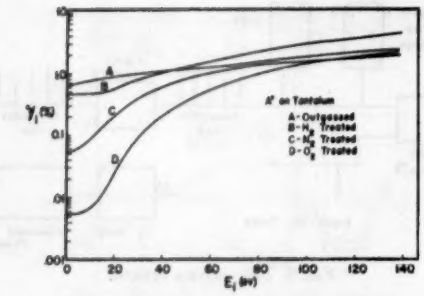

FIG. 7. Ejected electron yield (γ_i) for A^+ ions on outgassed and H_2-, N_2-, and O_2-treated Ta. Note rise to high values irrespective of gas above 100 ev.

ment the entire baking and outgassing procedure was repeated. In operating tube 1 the background pressure during taking of data was in the high 10^{-8} mm range, while that in tube 2 was always between 2 and 5×10^{-9} mm. Measurements in tube 2 could begin 25 seconds after flashing, while in tube 1 they began only after 10 minutes.

III. RESULTS AND DISCUSSION

A^+ on Tantalum

The results obtained with tube No. 1 for A^+ incident on flashed and gas-treated Ta is shown in Fig. 7. Curve *A* is representative of the data obtained after heating and flashing the Ta target to 1400°C. Data taken on different days, for the same target condition, never deviated from that represented by curve *A* by more than ±5 percent. The drift in the value of γ_i after flash was found to be slow and small. With the target cold for an hour after the flash, the maximum change in γ_i was always less than 20 percent and for a 24-hour cold period the change was found to be only 30 percent. At the time of these measurements it was thought that if the surface gas had been removed as a result of the flash, either the film had reformed before measurement was possible and the slow drift was a result of the low sticking coefficient for gas atoms on a covered surface, or that the partial pressure of adsorbable gas in the background was so low that slow redeposition took place even though the surface was clean. That the first alternative was not unlikely for a flash measurement time of ten minutes and with a background pressure in the high 10^{-8} mm Hg range, can be seen, for if one assumes unity sticking coefficient for the condensing background gas atoms, the monolayer formation time is of the order of one minute.[17,18]

However, there was the possibility that the flashing did not remove the gas film and the slow drift in γ_i resulted from the low sticking coefficient of a covered surface. When a Ta target was installed in tube No. 2, not only was the slow drift in γ_i after the flash reproduced but the values obtained for γ_i were within 5 percent of those obtained with tube No. 1. The conditions with tube No. 2 were such that it seemed unlikely that the gas film had *re-formed* before measurement. Therefore, either the gas film was not removed as a result of the flash, or the slow drift was to a low sticking coefficient of the additional atoms, or the film was removed and the slow drift was due to a low partial pressure of adsorbable background gas. The first possibility coincides with Hagstrum's[11] conclusions from recent work on electron ejection by He^+ ions on Ta. From his observations he was forced to conclude that a basic gas film on Ta is not removed by flashing to 1475°C but at the time of the flash it enters into the metal and then returns to the surface as the metal cools. Therefore it seems likely that curve *A* in Fig. 7 is for gas covered Ta and the small drift observed in γ_i after flash was due to the addition to the already covered surface of a few less tightly held atoms. As an added check on the state of the Ta surface used in these studies as compared with that in Hagstrum's studies, a measurement was made of γ_i for He^+ on Ta with tube No. 2. Hagstrum[11] had found γ_i to be essentially constant over the ion energy range of 10–150 ev and equal to 14 percent. With tube No. 2 a constant value of 13 percent was obtained for this same ion energy range.

The only work with which the results for A^+ on Ta may be compared is the pulsed Towsend discharge study by Molnar.[18] In this work for argon and a Ta cathode the value of γ_i at various E/p and p was found to range from 0.5 to 2.6 percent. These results are to be compared with the value of 0.7 percent, obtained in the present study for ions with an energy of a few ev.[19]

The results obtained after gas treatment are shown by curves *B*, *C*, and *D* in Fig. 7. When measurements were started after each gas treatment, γ_i was found, at least for the lower ion energies, to drift slowly upward. This was undoubtedly due in part to the sputtering action of incident argon ions. It is to be noted that after the N_2 and O_2 treatment, γ_i for low ion energy was found to be smaller than that of the flashed surfaces by a factor of approximately 10 to 100, respectively, while at higher energies γ_i for treated surfaces tended to coincide with that obtained for the flashed surface. After the H_2 treatment, γ_i was found to be smaller

[17] This assumes that the gas adsorbed by the target is the background gas and not impurities in the argon or the argon itself. Mass spectrometric analysis of Linde's "spectroscopically pure" argon by Molnar (see reference 18) have shown the impurities to be less than 0.005 percent. This figure would mean that the partial pressure of impurities introduced with the argon would be in the 10^{-9} mm Hg range. While there is not evidence that the thermal argon atoms are adsorbed at room temperature it is known that argon ions of a few ev energy are. However, the effect due to adsorption of argon as ions can be ruled out at least for tube 2 because of the short flash-measurement time (25 seconds), and the low positive-ion beam current densities ($\sim10^{-9}$ amp/cm^2 at the target).

[18] J. P. Molnar, Phys. Rev. 83, 940 (1951).

[19] Molnar's values depend critically on the values of the first Townsend coefficient which are difficult to measure, and thus may not be as reliable as direct values.

at low energy, while being found to be larger at the higher energies. Apparently in the case of the N_2 and O_2 treatment the ions of high energy can penetrate the additional film put on by the gas treatment, and can interact with the surface underneath, while for ions of lower energy the interaction tends to take place at this second film.

A^+ on Platinum

The results for A^+ incident on platinum are shown in Fig. 8. Each point of the top curve represents a measurement made 25 seconds after the target was flashed at 1400°C. With Pt a large drift in γ_i was observed to occur after the flash and a typical plot of γ_i as a function of time after flash is given in Fig. 9. Also the curve labeled "15 minutes after flash" in in Fig. 8 shows the change that has taken place in γ_i for a 15-minute flash measurement time. For the target cold for 24 hours γ_i was found to be reduced to

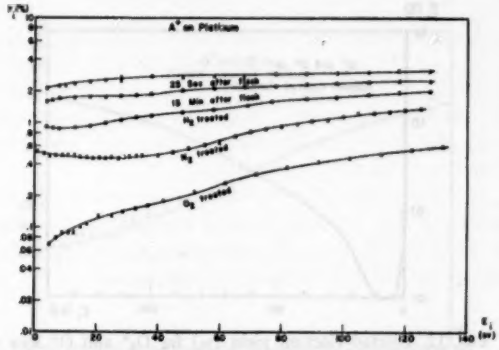

FIG. 8. Ejected electron yield (γ_i) for A^+ ions on outgassed and H_2-, N_2-, and O_2-treated Pt. Note the difference of Pt relative to Ta in that values of γ_i do not merge above 100 ev. Note also decrease in γ_i with time after flash.

$\frac{1}{3}$ of that obtained just after the flash. While it is not maintained that flashing Pt at 1400°C necessarily produced an atomically clean surface, the fact that a large and fast change in γ_i does occur after flash seems to indicate that at least a major part of the surface gas film was removed, the drift indicating the reformation of such. However, even if only a portion of the surface gas was removed by the flash it is still not strange that the drift is fast as contrasted with that found for Ta, since Pt is known to be an active surface catalyst for many gaseous reactions and this activity is directly connected with adsorption.

The other three curves of Fig. 8 show the effect of gas treatment on γ_i for Pt. As was stated before, the treatment in the case of Pt consisted of a five-minute exposure without glow discharge. This time, along with the adsorption gas pump-out time of 10 minutes, meant the time from flash, through the gas treatment, to the measurement on the covered surface was about 15 minutes. From Fig. 8 it can be seen that in all cases the effect of gas treatment was greater than the effect due to background gas for corresponding cold target periods. Therefore the condensation of background gas did not at all mask the effect due to the intentionally introduced adsorption gases. It was observed for gas-treated Pt, as it was for gas-treated Ta, that after the start of the measurements γ_i showed a slow upward drift in the time indicating that some of the adsorbed gas was leaving the surface, due at least in part to ion bombardment. In the one exposure plus discharge treatment in N_2 carried out for Pt, the data was found to lie below that obtained after just an exposure by only about 10 percent. Also, as was the case for gas-treated Ta, the order of increasing effectiveness for the reduction of γ_i was H_2, N_2, and O_2. It is to be noted that the shape of the curves for gas-treated Pt are quite different from those of gas-treated Ta. In the case of Pt the decrease which resulted from gas treatment separated the curves from each other and from that for flashed Pt over the entire ion energy range. This is to be contrasted with the results for Ta where the curves are separated at low ion energy while at higher energy the N_2 and O_2 curves tend to coincide with the flash curve and the H_2 curve rises above.

As a tentative explanation for the difference in results for gas treated Pt and Ta, it is suggested that while with Ta the ions are easily able to penetrate the small additional gas film resulting from treatment, for Pt the treatment results in a complete film over the surface which cannot as easily be penetrated by the ions.

N_2^+ and N^+ on N_2-Treated Ta and Pt

Figures 10 and 11 show the results obtained for a mixture of N_2^+ and N^+ ions incident on N_2-treated Ta and Pt, respectively. The interesting point to be noticed in both of these figures is the increase in γ_i with decreasing ion energy at low ion energies. It would be interesting, of course, to know if this effect is characteristic of both N_2^+ and N^+ or just characteristic of one of these ions. However, in the present studies this

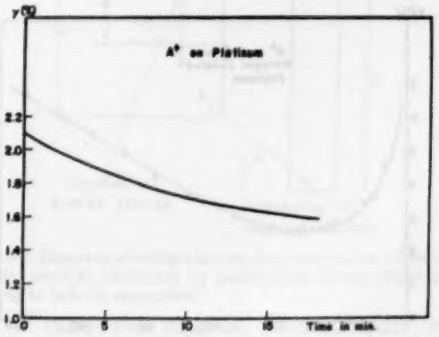

FIG. 9. Ejected electron yield (γ_i) for A^+ ions on outgassed Pt as a function of time. The decrease is due to monolayer formation caused by either residual background tube gases or impurity in the A gas.

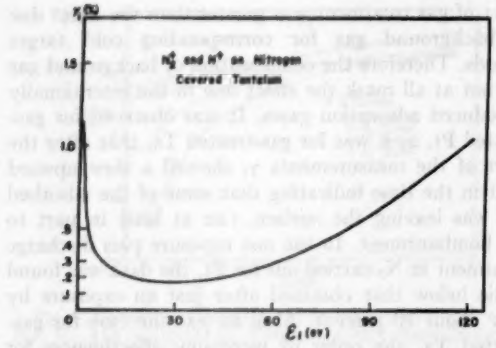

FIG. 10. Ejected electron yield (γ_i) for N_2^+ and N^+ ions on N_2-covered Ta. Note the increase in γ_i at low energies. This may come from emission caused by recombination of N at the surface.

information was impossible to obtain. Also, it is to be noted that the curves for nitrogen ions on Ta and Pt for ion energy greater than approximately 30 ev lie somewhat near the curve for A^+ on the N_2-treated Ta and Pt surfaces, respectively. This is not at all unexpected since the energy available after neutralization of the singly charged nitrogen ions is very close to that for A^+. Therefore, it would be expected that γ_i for nitrogen ions on flashed Ta without a nitrogen surface film would not differ appreciably from the data obtained for A^+ on flashed Ta.

While there is no study that can be directly compared with these results, still it is interesting to note that Huber,[20] using the pulsed Townsend discharge method, has recently found that γ_i for N_4^+ on Ni is of the order of 1 percent when corrected for back diffusion. This is, of the same order as that found in this study for nitrogen ions on Ta at the lowest ion energy.

O_2^+ and O^+ on O_2-Treated Ta and Pt

Figures 12 and 13 show the results obtained for a mixture of O_2^+ and O^+ ions incident on O_2-treated Ta and Pt, respectively. As was found for the nitrogen ions, the curves for oxygen ions on Ta and Pt lie fairly close to those for A^+ on O_2-treated Ta and Pt surfaces, respectively. Here again, this agreement is not unexpected as the energy available after neutralization of the oxygen ions is close to that for A^+. There is to be noticed for low-energy oxygen ions on Ta a slight increase of γ_i for decreasing ion energy; however, the effect is small compared with the similar effect found for nitrogen ions, and in this case its cause may well be instrumental.

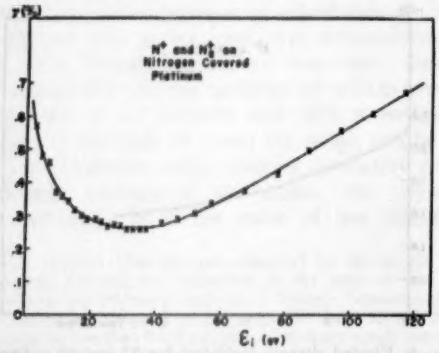

FIG. 11. Ejected electron yield (γ_i) for N_2^+ and N^+ ions on N_2-covered Pt. Here again γ_i increases at low energy.

[20] Elsa Huber, Phys. Rev. 92, 536 (1953).

H_2^+ and H^+ on H_2-Treated Pt

Figure 14 shows the results obtained for a mixture of the singly-charged hydrogen ions incident on H_2-treated Pt. This curve is seen to lie well below that for A^+ on H_2-treated Pt even though the energy after neutralization of the hydrogen ions is reasonably close to that of A^+. No study was made of γ_i for hydrogen ions on Ta.

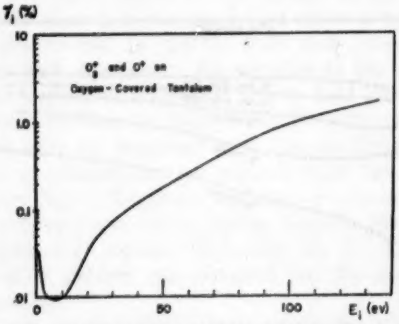

FIG. 12. Ejected electron yield (γ_i) for O_2^+ and O^+ ions on O_2-coated Ta. The increase in γ_i at low energies may be spurious here.

While there are no studies that can be directly compared with these results, still it is interesting to note the observations of Lauer[21] for H_2^+ on Ni using a pulsed Townsend discharge method of measurement with the pressure of H_2 ranging from 100 to 650 mm of Hg. While a photoelectric γ_p was obtained in Lauer's study which was of the order of 0.1 percent to 1 percent (corrected for back diffusion),[22] no positive ion γ_i was observed. Lauer estimated that γ_i had to be at least less than 10^{-4}. The very low γ_i observed in this study, was probably due to the thick H_2 films that form under high-pressure conditions.

IV. CONCLUSIONS

The theoretical interpretation of the γ_i process for slow positive ions incident on clean metals has been fairly clearly qualitatively described, but, as yet, is not on a quantitative basis. In principle the mechanism can best be pictured in terms of the schematic energy level diagram of Fig. 15. Here the levels of electrons in the metal and approaching ion are depicted as for

[21] E. J. Lauer, J. Appl. Phys. 23, 300 (1952).
[22] J. K. Theobald, J. Appl. Phys. 24, 123 (1953).

infinite separation. Actually, as the ion approaches the metal its interaction with the metal alters the levels somewhat. It is seen that what happens is that an electron in the Fermi band is captured into the ground state of the ion and then another metallic electron is excited to an energy level above the Fermi band. The energy *available* to the excited electron depends on the region of the band from which the captured electron comes. Thus the available energies can range from $E_i-\phi$ for the upper limit and E_i-W for the lower limit, where E_i is the ionization potential of the ion, ϕ is the work function, and W is the height of the surface barrier. On close approach the interaction energy decreases the available lower-limit energy, while the upper-limit available energy is unchanged. The method by which the effect of these interactions can be investigated has recently been independently developed by Hagstrum[11] and Varnerin.[12]

The process described above is termed the *direct* process originally proposed and treated by Shekhter.[9]

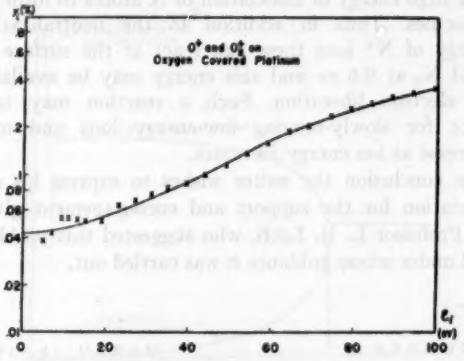

FIG. 13. Ejected electron yield (γ_i) for O_2^+ and O^+ ions on O_2-coated Pt.

Oliphant and Moon,[7] Massey,[8] and Cobas and Lamb[10] proposed and treated a two-stage process. In this the ion is first neutralized to an excited state by resonance capture of a metallic electron. From this state the atom subsequently decays to the ground state with excitation of a second metallic electron. The process active with A^+ ions is only the direct process since the values of ϕ for the surface used are greater than the difference between the lowest excited state and the ionization potential of A.

Now if part of the range of levels that may be occupied by the excited electron lies above the surface barrier, then those of the electrons in these levels that are directed toward the surface and are not reflected at the surface barrier are able to escape. The condition that the upper limit of the range of possible occupied levels lies above the surface barrier is that $E_i>2\phi$.

It is seen, then, that if ϕ increases because of surface contamination the number of excited electrons in levels above the surface barrier will be less and thus γ_i will be decreased. It is thus essential to regard work

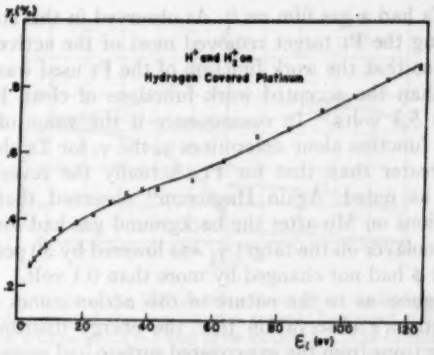

FIG. 14. Ejected electron yield (γ_i) for H_3^+ and H_2 on H_2-covered Pt.

functions and change in work function as gases are adsorbed. No work function data were obtained in these studies. However, Oatley,[23] and others, have found that H_2 *decreases* the work function of Pt slightly while O_2 increases ϕ by at least a volt. Weissler[24] has studied the changes in work function of surfaces of W and Ag after bombardment with hydrogen, nitrogen, and oxygen ions. Quite uniformly bombardment with A^+ or N_2^+ ions cleaned up the surface and restored the work function nearly to its normal value, while H_2 decreased the work function by a few tenths of a volt and O_2 increased it by the order of a volt or more. No data on Ta are available. On the other hand, Bosworth and Rideal[25] report that H_2, N_2, and O_2 films *all* increase the work function of W. Doubtless the conditions of formation and the nature of the films differed from those of Weissler and others. Accepting Oatley and Weissler's conclusion, it appears that there must be another action causing a reduction in γ_i beside that of an increase in ϕ. This is borne out by the following data. Hagstrum,[11] whose Ta was in the same state as that used here, observed a work function of 4.9 volts and

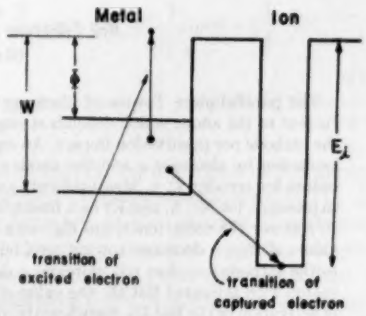

FIG. 15. Diagram showing the one-step mechanism of so-called potential electron liberation by positive-ion energy levels corresponding to infinite separation.

[23] C. W. Oatley, Proc. Phys. Soc. (London), **51**, 318 (1939); A. L. Hughes and Dubridge, *Photoelectric Phenomena* (McGraw-Hill Book Company, Inc., New York, 1932).
[24] G. L. Weissler, J. Appl. Phys. **24**, 472 (1953).
[25] R. C. L. Bosworth and E. K. Rideal, Proc. Roy. Soc. (London) **A162**, 1 (1937); Proc. Cambridge Phil. Soc. **33**, 394 (1937).

the Ta had a gas film on it. As observed in this study, flashing the Pt target removed most of the active gas films so that the work function of the Pt used was not less than the accepted work functions of clean Pt of value 5.3 volts.[26] In consequence if the value of the work function alone determines γ_i the γ_i for Ta should be greater than that for Pt. Actually the reverse is true as noted. Again Hagstrum[11] observed that for He^+ ions on Mo after the background gas had formed a monolayer on the target γ_i was lowered by 30 percent while ϕ had not changed by more than 0.1 volt.

A guess as to the nature of this action comes from Hagstrum's observation that the energy distribution of electrons from the gas-covered surface had more slow electrons than that from the clean surface. This indicates that the probability of the excited electron occupying a low level in the range of levels available to it is greater for the gas covered surface than for the clean one. Such a condition would obviously also lower γ_i. The process active may be crudely envisioned as follows: with a clean surface neutralization involves direct interaction with only one electron of the Fermi band. With a covered surface it could well involve two for the electrons causing neutralization can come from a local state produced by an adsorbed gas atom. In general since such a local level does not lie in the Fermi band it will be refilled after neutralization by a metallic electron. Such a two-step process could well act to lower the energy available to the excited electron. Thus gas coatings not only lower γ_i by raising ϕ, but also lower γ_i by reducing the *available* energy for excitation by a more complicated neutralization process. If the *lowering* of ϕ, for instance by H_2 treatment, is small the value of γ_i can still be decreased by H_2 films because of reduction of available escape energy. Likewise, clean Pt could yield a higher γ_i despite its 0.4-volt higher value of ϕ relatively to Ta, as Ta has a gas film at its surface.

That γ_i increases with ion energy is not surprising since kinetic liberation superposes on potential for all surfaces. For gas treated surfaces the observed increase of γ_i with energy is greater than for clean surfaces. This is to be expected for aside from some "cleanup" of the film by high-energy bombardment more of the high-energy ions penetrate the gas film and interact directly with metallic electrons; i.e., the interaction time with the local gas surface states is decreased relative to that with the lattice.

The initial decrease in γ_i with ion energy, observed *only* with nitrogen ions, can be accounted for by the very high energy of association of N atoms to form N_2 molecules. Thus in addition to the neutralization energy of N^+ ions these can react at the surface to yield N_2 at 9.6 ev and this energy may be available for electron liberation. Such a reaction may take place for slowly-moving low-energy ions and may decrease as ion energy increases.

In conclusion the writer wishes to express his appreciation for the support and encouragement given by Professor L. B. Loeb, who suggested this problem and under whose guidance it was carried out.

[26] H. B. Michaelson, J. Appl. Phys. 21, 536 (1950).

PHYSICAL REVIEW VOLUME 93, NUMBER 6 MARCH 15, 1954

Liberation of Electrons by Positive-Ion Impact on the Cathode of a Pulsed Townsend Discharge Tube

ROBERT N. VARNEY*
Bell Telephone Laboratories, Murray Hill, New Jersey
(Received December 7, 1953)

The parallel-plate Townsend discharge triggered by a flash of ultraviolet light on the cathode gives a current to the anode which depends strongly on the value of γ, the number of new electrons liberated from the cathode per positive-ion impact. An expression is derived relating γ to the first Townsend coefficient for ionization by electrons α and the anode-cathode separation X, which provides an easy experimental procedure for arriving at γ. Measurements are then given for γ as a function of E/p, the ratio of field strength to pressure, for Ne, A, and Kr on a freshly cleaned Mo cathode. The values of γ are essentially independent of E/p above 175 volts/(cm×mm Hg) with values of 0.20 for Ne^+, 0.083 for A^+, and 0.053 for Kr^+. At lower values of E/p, γ decreases toward zero, but this decline is probably related to the back diffusion of electrons to the cathode and does not represent a decrease in the basic γ process. With A^+ ions and a nickel cathode coated with activated $BaCO_3$, the value of γ also leveled off at higher E/p at a γ value related to the degree of activation of the $BaCO_3$. Significantly, the value of γ for this surface did not tend toward zero at zero E/p. This may be attributed to a different distribution of electron velocities for the ejected electrons from the coated surface than for the pure surface.

INTRODUCTION

THE emission of electrons from cathode surfaces as a result of positive-ion impacts has been studied for many years, first as an essential to the understanding of the mechanism of gas discharges and more recently as a challenging problem in the field of atomic interactions. Despite the number of years that the problem

* Now at Washington University, St. Louis, Missouri.

has attracted interest, the resolution of experimental difficulties and uncertainties has only become possible in recent times with the advent of many powerful new tools of electronics research. In the present work, pulsed techniques have been employed with the familiar Townsend type of discharge conditions to yield a highly sensitive measurement of γ, the number of electrons escaping per ion impact. The determination is of significance as a disruptive discharge does not occur, as in the more classical methods of determining γ from the breakdown criterion. A further significance of the present results lies in the correlation with the more direct method of Hagstrum[1] and the extension of his results to a lower-energy domain.

APPARATUS

The pulsed Townsend discharge tube developed by Hornbeck[2] and used by him and by the present writer[3] to measure drift velocities of ions in gases is readily

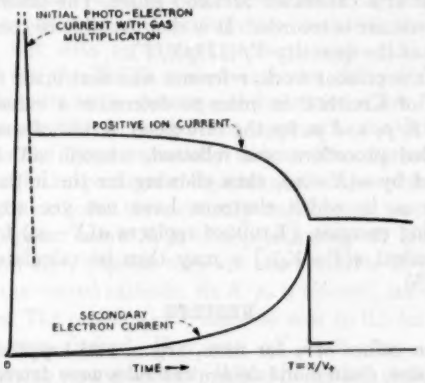

FIG. 1. Schematic resolution of oscilloscope pattern to show positive-ion and electron components of current in the pulsed Townsend discharge tube.

adaptable to the determination of γ, the number of electrons escaping from the cathode per incident ion. As the tube is used, a flash of light of duration approximately 10^{-7} sec liberates photoelectrons from the cathode. The electrons produce positive ions by collision as they drift toward the anode, and the positive ions in turn liberate new electrons as they strike the cathode. A dc potential is maintained across the tube, and a fast oscilloscope is connected to show the current flowing as a function of time following the flash. The current is composed of an electron component and a positive ion component; these are shown schematically in Fig. 1. It is at once clear that the value of γ will strongly influence the pattern appearing on the oscilloscope by its effect on the electron current.

[1] H. D. Hagstrum (private communications). See also Phys. Rev. 89, 244 (1953).
[2] J. A. Hornbeck, Phys. Rev. 83, 374 (1951); 84, 615 (1951).
[3] R. N. Varney, Phys. Rev. 88, 362 (1952); 89, 708 (1953).

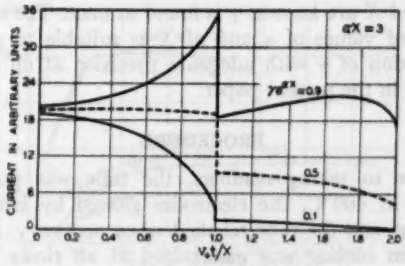

FIG. 2. Graph of Eq. (3) showing three theoretical predictions of oscillograms of the current in a pulsed Townsend discharge tube for a value of $\alpha X=3$ and three values of γ. The calculations applying to times greater than $t=X/v_+$ are not shown in the present paper.

To arrive at a value of γ, a computation has been made of the current to be expected following the flash; it is presented in the appendix. The results of the computation appear below as Eqs. (1)–(3). The current due to electrons i_-, the current due to positive ions i_+, and the total current i which is the sum of i_+ and i_- are given as functions of the time t following the flash, the anode-cathode separation X, and the positive-ion drift velocity v_+. Also appearing in the equations are the electronic charge ϵ, the total number of electrons n_0 emitted by the initial flash, and the first Townsend coefficient α, the number of new electrons liberated by one electron in traveling one cm in the field direction through the gas. The equations are applicable only to the time range, $0\leq t\leq X/v_+$.

$$i_-=\frac{n_0\epsilon v_+}{X}\gamma(e^{\alpha X}-1)e^{\alpha v_+(1+\gamma)t}, \tag{1}$$

$$i_+=\frac{n_0\epsilon v_+}{X}\left[\left(\frac{\gamma}{1+\gamma}e^{\alpha X}-1\right)e^{\alpha v_+(1+\gamma)t}+\frac{e^{\alpha X}}{1+\gamma}\right]. \tag{2}$$

$$i=\frac{n_0\epsilon v_+}{X}\left\{\left[\gamma(e^{\alpha X}-1)+\frac{\gamma}{1+\gamma}e^{\alpha X}-1\right]\times e^{\alpha v_+(1+\gamma)t}+\frac{e^{\alpha X}}{1+\gamma}\right\}. \tag{3}$$

Graphs of Eq. (3) for one value of the parameter αX and for several values of γ are shown in Fig. 2.

The appearance of the horizontal oscilloscope trace in Fig. 2 denotes a constant current, independent of time. Correspondingly, the time-dependent term in Eq. (3) vanishes if the coefficient of that term is zero, or if

$$\gamma(e^{\alpha X}-1)+\frac{\gamma}{1+\gamma}e^{\alpha X}-1=0. \tag{4}$$

Equation (4) may be solved for γ, giving

$$\gamma=[e^{\alpha X}/(e^{\alpha X}-1)]^2-1. \tag{5}$$

If α and X are known, γ is found at once. The normal range of values of α and of X is suitable to permit evaluation of γ with adequate precision at all values arising in the present paper.

PROCEDURE

Prior to taking readings, the tube was pumped, baked at 400°C, the electrodes glowed by induction heating, and the tube rebaked when necessary. Liquid nitrogen cooling was maintained at all times except during actual runs with krypton gas when liquid oxygen replaced the nitrogen to avoid condensation of the krypton. Residual pressures in the tube following treatment were approximately 4×10^{-9} mm.

With pure molybdenum electrodes, gas of the type to be used in the ensuing experiment was admitted from a high-purity commercial source (tested by mass spectrography and found to contain less than 0.01 percent of foreign matter). A glow discharge was then initiated in the tube and caused sputtering of metal from the cathode surface. As this process progressed, higher and higher currents were forced through the tube, reaching 50 to 100 amperes. The highest currents were of necessity limited to bursts of short duration to avoid overheating. Occasional checks of the discharge characteristics showed the sustaining voltage to be dropping for some time. This voltage ultimately reached a limiting value which agreed with minimum values obtained for the corresponding gases in tube manufacture and believed to be characteristic of pure molybdenum surfaces. Repetition of degassing, activating, and degassing procedures in turn was continued with occasional interruptions for measurements until stability of measurements was attained.

The variables available to the operator for a measurement of γ are the type and pressure of gas in the tube, the anode-cathode separation X, and the dc potential V applied across the tube. The intensity of illumination falling on the cathode is subject to slight variation by insertion or removal of screens. The equipment is set into operation with a pre-set plate separation X, gas pressure p, and no applied voltage, and the voltage is then raised slowly by means of a potentiometer control. In due course, a pattern appears similar to the lowest curve in Fig. 2. With higher voltage, traces resembling the higher curves in Fig. 2 are observed. The values of both α and γ are increasing in this process. Figure 3 shows three superposed oscillograms obtained with applied voltages of 177, 182, and 187 volts, respectively (from bottom to top). The trace which is most nearly horizontal along its first straight section is the one desired, and it is estimated that the required voltage may be selected for this condition within approximately ±1 volt.

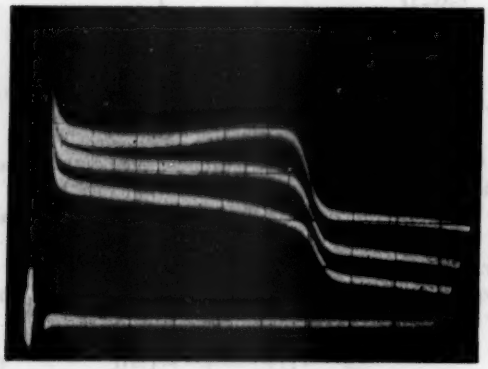

FIG. 3. Three actual oscillograms showing current *vs* time in the Townsend tube for Kr^+ ions in Kr, with a pure Mo cathode. The voltages applied to the tube were, reading upwards, 177, 182, and 187 volts, respectively. Selection of the voltage producing the most nearly horizontal trace may be made much finer than the ±5-volt range illustrated here.

The voltage is then read with a calibrated potentiometer, the plate separation is determined with a measuring microscope, and the pressure is read by means of a calibrated McLeod gauge. The laboratory temperature is recorded. It is then possible to compute E/p_0 as the quantity $V/(273pX/T)$.

In the present work, reference was next made to the work of Kruithof[4] in order to determine a value of α from E/p_0 and p_0 for the rare gases. Kruithof's recommended procedure was followed, wherein αX is replaced by $\alpha(X-x_0)$, thus allowing for the initial distance x_0 in which electrons have not yet acquired ionizing energies. [Kruithof replaces $\alpha(X-x_0)$ by the equivalent $\eta(V-V_0)$.] γ may then be calculated by Eq. (5).

RESULTS

The values of γ for neon, argon, and krypton ions and pure, clean molybdenum cathodes were determined by the procedure described. Additional measurements were made for argon ions in a tube having a cathode coated with $BaCO_3$ and activated partially. The results are plotted in Fig. 4. For the Mo cathode, the value of γ is essentially constant above E/p_0 of 150 to 200, and it takes on value of 0.20 for Ne^+, 0.083 for A^+, and 0.053 for Kr^+. These results may be compared with those of Hagstrum[1] at much higher energies, who has measured γ values on W of 0.24, 0.094, and 0.047 for 10-ev Ne^+, A^+, and Kr^+ ions, respectively. Hagstrum's work shows γ of He^+ (10 ev) on Mo to be about 10 percent less than γ of He^+ (10 ev) on W. One is perhaps justified in concluding that the ion beam experiment would give values for Ne^+, A^+, and Kr^+ on Mo somewhat lower than those quoted above for these ions on W.

At lower values of E/p_0, the values of γ are seen to fall off. While the interpretation of this decline is not assured by the present observations, it is suspected that no change in the basic liberation mechanism is occurring as there is much evidence favoring the independence of γ from the velocity of the incident ions. It is believed,

[4] A. A. Kruithof, Physica 7, 519 (1940).

however, that at low E and high p, the back reflection of electrons by gas atoms in close proximity to the cathode becomes a mechanism of appreciable significance and may be responsible for the apparent decline in γ.

The observation shown in Fig. 4 for the cathode coated with $BaCO_3$ and activated by a glow discharge in argon is included because of the interest in its shape rather than in the absolute values of γ. The surface is extremely sensitive to virtually any electric current through the tube and may become more strongly activated or deactivated in a short interval of measuring time. The curve shown, however, was traced and retraced several times to establish its validity and the constancy of the surface characteristic throughout the run. Change in the activity of the surface is recognized by a change in the value of γ which has been seen to approach values of 0.5 at the upper limit and to drop below 10^{-3} under less favorable circumstances. The curve shown is an intermediate one.

Surfaces activated to a higher or a lower degree were found to yield curves essentially identical with the one shown but with an altered ordinate scale. All such curves for the $BaCO_3$-coated cathodes differed from those for pure Mo in the shape of the section at low E/p; the former definitely did not approach the origin, whereas the latter essentially did so. The distinction has practical experimental significance because with the pure Mo cathode, the necessary oscilloscope patterns fail to appear below E/p_0 of approximately 40 (volts/cm×mm Hg), whereas they are observable to E/p_0 of 22 for the coated cathode. As E/p_0 is lowered, αX also declines. The product $\gamma e^{\alpha X}$ must be near to 0.5 for the oscillograms desired. If γ and αX both drop, this requirement cannot be met. With the coated cathode, it can be met as γ does not fall toward zero with E/p_0.

The explanation of this behavior of γ at lower values of E/p_0 is believed to be associated with the velocity of ejection of the secondary electrons. If, on the average, the secondary electrons leave at higher speed from the coated cathode than from the pure metal, the back diffusion from the gas is reduced and the apparent value of γ remains higher. Further study of this process is thus indicated.

SOURCES OF ERROR

The uncertainty concerning the origin of the secondary electrons common in determinations of γ is at least partially resolved in the present work. Thus, the emission of secondaries by impact of metastable atoms is completely eliminated from the present observations by the choice of time scales. In the few microseconds during which oscillograms are recorded, metastable atoms drifting at thermal speeds reach the cathode in such trifling numbers as to be insignificant. By the same token, neutral atoms can only be conceivably effective

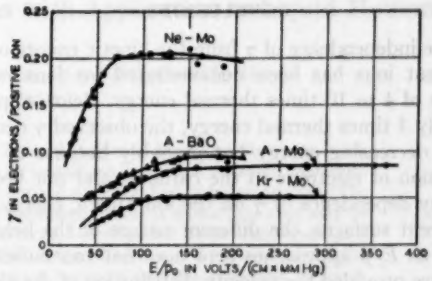

FIG. 4. The values of γ as a function of E/p_0 for Ne^+, A^+ and Kr^+ incident on a clean Mo cathode and for A^+ on a partially activated coated cathode. The degree of cleanness or of activation alters the ordinate scale but not the shape of the curves.

in influencing the observed secondary emission when they are formed from positive ions in the last free path. Radiation originating in the gap from de-excitation and reaching the cathode may influence the apparent secondary emission if it occurs rapidly, that is, in the range of 10^{-8} sec. Molnar[6] indicates that it may account for 7 percent of the total secondary emission. It is a potential factor in the present work, and if Molnar's data are applicable, the values of γ in Fig. 4 must be reduced by the indicated amount.

The rapid aging of clean molybdenum surfaces reported by Molnar in reference 5 did not appear to influence the present results. No decline in γ was observable over a period of several hours during which a curve such as appears in Fig. 4 could be traced and retraced. After 24 hours, with pumping, the values of γ were usually some 10 percent below the previous day's values. Any of a number of seemingly trivial abuses of the tube, however, could precipitate the value of γ to 10^{-3} or even 10^{-4}.

The accuracy of Kruithof's values of α become of significant interest in the determination of γ by the present method. An important question therefore arises whether α cannot be determined directly from these observations. An additional relation connecting αX and γ may be found by comparing the height of the discontinuity at $t=X/v_+$ with the current just before or just after this jump. In theory at least, the simultaneous solution of the new equation with Eq. (5) should yield both αX and γ. In practice, the fractional change in current at the discontinuity as depicted on the oscilloscope screen is sufficiently insensitive to changes in αX or in γ to make it of little practical value for determination of one of these variables. Hornbeck in reference 2 has made some investigation of α by measuring the area under the initial peak of the oscillogram arising from the photoelectron current. Still other procedures for finding α directly in the same experiment are possible, but none has been developed to a suitable precision at the present time.

[6] J. P. Molnar, Phys. Rev. 83, 933 (1951).

CONCLUSIONS

The independence of γ from the kinetic energy of the incident ions has been demonstrated for ions in the range of 4 to 10 times thermal energy. Below approximately 4 times thermal energy, the observed γ declines with decreasing energy but probably because of back diffusion of electrons to the cathode, and not because of any dependence of γ on the ion kinetic energy. For different surfaces, the different nature of the behavior of γ as E/p approaches zero does not contradict this picture provided the velocity distribution of the ejected electrons is also different for different surfaces.

The writer is indebted to Dr. J. A. Hornbeck who designed and constructed the original apparatus and to Dr. B. T. McClure who kindly provided the high-current unit for activating the molybdenum cathode. Dr. McClure and Dr. M. A. Townsend also assisted greatly by providing information on the discharge to molybdenum cathodes which indicated when the cleaning process had reached its limit. Dr. D. J. Rose and Dr. K. G. McKay were most helpful in discussions of the work and criticism of the manuscript. It is also a pleasure to acknowledge the assistance of Mr. F. D. Dolezal who aided extensively with apparatus maintenance, readings, reduction of observations, photography of oscilloscope patterns, and skillful stabilization of the apparatus preceding and during runs.

APPENDIX

The current flowing in the Townsend tube following a very short irradiation of the cathode by ultraviolet light may be analyzed as follows: if the oscilloscope sweep time is adjusted roughly to correspond to the time of transit of positive ions across the tube, electron transit will be so rapid that the regulating feature of the electron current observation will be the rate of liberation of electrons. The current due to positive ions, by contrast, will be determined by the density of ions in the tube at each instant according to the classic Lorentz formula:

$$i_+/A=\rho v_+, \tag{6}$$

where A is the cross-section area of the current.

Initially then, the oscilloscope will show a sharp peak of short duration corresponding to the initial burst of photoelectrons. Whereas the electron burst then vanishes from the picture it has produced a cloud of positive ions, the Townsend avalanche, which is now swept toward the cathode and is responsible for a current component given by

$$i_{+1}=(n_0\epsilon v_+/X)(e^{\alpha X}-e^{\alpha v_+ t}). \tag{7}$$

This equation and all subsequent ones are applicable only to the time interval $0\leq t\leq X/v_+$.

As each ion of Eq. (7) reaches the cathode there is a probability γ that it will release a new electron from the cathode. Such an electron, if it is released, will produce a new avalanche of positive ions yielding a new term in the positive-ion current equation:

$$i_{+2}=(\epsilon v_+/X)\int_0^t \gamma n_+(t')[e^{\alpha X}-e^{\alpha v_+(t-t')}]dt'. \tag{8}$$

The entire integral represents the number of ions formed between 0 and t by the secondary electrons and not yet swept out. The factor $n_+(t)$ represents the number of positive ions per second striking the cathode so that $\gamma n_+(t)$ becomes the number of secondary electrons emitted per second. The electron current from these secondaries is just this amount augmented by the gas multiplication factor (see reference 2) and is thus

$$i_-=n_+(t)\gamma(e^{\alpha X}-1)/\alpha X. \tag{9}$$

Because $n_+(t)$ is as yet undetermined, the positive-ion current which is the sum of (7) and (8) is thus given by an integral equation.

A further relation between i_+ and n_+ is needed. This may be written in the form that the rate of change of i_+ arises from creation of new ions by ionization and sweeping out of old ions by the field. The result is

$$di_+/dt=(\epsilon v_+/X)[n_+(t)\gamma(e^{\alpha X}-1)-n_+(t)]. \tag{10}$$

If the sum of Eqs. (7) and (8) giving i_+ is now differentiated with respect to t under the integral sign and placed on the left side of Eq. (10), the result after clearing is

$$n_+(t)=n_0\alpha v_+e^{\alpha v_+ t}+\gamma\alpha v_+\int_0^t n_+(t')e^{\alpha v_+(t-t')}dt'. \tag{11}$$

Equation (11) is a linear integral equation in n_+ and its solution is

$$n_+(t)=n_0\alpha v_+e^{\alpha v_+(1+\gamma)t}. \tag{12}$$

The values of i_+ and i_- are at once obtained by substitution of Eq. (12) into (7), (8), and (9).

The Nature of Higher-Order Phase Transitions with Application to Liquid Helium*

O. K. RICE
Department of Chemistry, University of North Carolina, Chapel Hill, North Carolina
(Received December 1, 1953)

A general discussion is given of the relation between transitions of various order, especially those which are not concerned with solid lattices. It is shown that third-order transitions bear much the same relation to anomalous first-order transitions as second-order transitions bear to ordinary first-order transitions. The conditions under which higher-order transitions can occur are considered, and it is shown that they may be associated with a dispersed phase. If the transition is second order, the dispersed phase must undergo a transition in itself. The ideas concerning second-order transitions are applied to the λ transition in liquid helium. An argument is given, based on energetic grounds, which indicates that the superfluid in liquid helium is in the form of clusters which are separated in ordinary space as well as in momentum space. If this view is correct, the λ transition corresponds to the appearance of much larger clusters, essentially marking the beginning of long-range orders. It is shown that the Bose-Einstein statistics is quite essential for the formation of the clusters; they cannot appear in He^3, and no λ transition is to be expected in He^3. Finally, a possible explanation is given for Taconis' hypothesis that He^3 is not soluble in the superfluid part of He^4.

1. INTRODUCTION

THE λ-point transformation in liquid helium seems to be connected in some way with the Bose-Einstein condensation, as originally suggested by London, and it has been frequently assumed that a qualitative understanding of these phenomena may be obtained if the liquid forces are ignored completely, except insofar as they result in an effective pressure which holds the atoms together in the liquid phase. There are, however, quite definite differences between the behavior of liquid helium and that of the Bose-Einstein gas, which may perhaps best be seen by considering the character of the isotherms. The nature of the isotherms for a Bose-Einstein gas is indicated by Fig. 1. The transition is an anomalous first-order transition, in the nomenclature of Mayer and Streeter,[1] the effective volume of the condensed phase being zero.[2] On the other hand, the transition in liquid helium is second order, and the isotherms are schematically presented in Fig. 2, which takes into account the negative value of the thermal expansion coefficient, $(\partial V/\partial T)_p$, and of the pressure coefficient, $(\partial p/\partial T)_V$, below the λ point. In the latter figure, the effect of the liquid forces is clearly shown. Certainly, considerable modification of the simple Bose-Einstein transformation will be needed before it can be used as a prototype for the transition in liquid helium.

However, since the intermolecular forces depend on the volume, it might be supposed that if the volume is held constant the intermolecular forces would be at least approximately constant, and so perhaps would not contribute to the specific heat at constant volume, C_v. Thus it is suggested that we compare the ideal Bose-Einstein gas with liquid helium at constant volume. This is what is usually done and this procedure has very recently received some theoretical backing, since

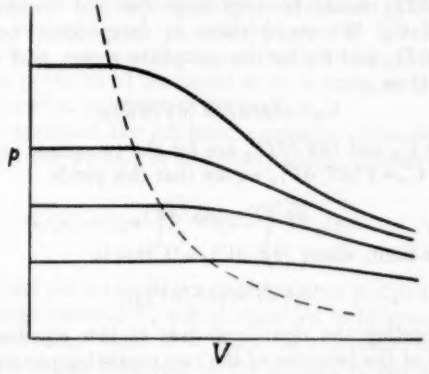

FIG. 1. Isotherms for a Bose-Einstein gas. The broken line is the transition line.

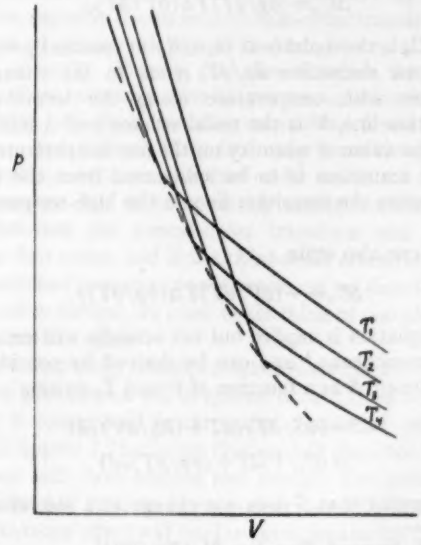

FIG. 2. Isotherms (schematic) for liquid helium. $T_4>T_3>T_2>T_1$. The broken line is the λ line.

* Work supported by the U. S. Office of Naval Research.
[1] J. E. Mayer and S. F. Streeter, J. Chem. Phys. **7**, 1019 (1939).
[2] B. Kahn and G. E. Uhlenbeck, Physica **5**, 399 (1938).

work of Feynman[3] has indicated that a λ transition should occur even though there are strong interatomic forces. Feynman's general argument is that the motion of the atoms is not sufficiently altered by the interatomic forces but that the general character of the transition remains unaltered. He effectively assumes that the attractive forces do not have any specific effect, only the general effect of holding the atoms together. Within the liquid, the atoms would act much like hard spheres. Feynman then finds that the λ transition should be like the transition in the Bose-Einstein gas, in that there should be no break in C_v, but only a change in slope. Actually, of course, C_v shows a break rather than a mere change in slope, and it is quite possible that this arises from the attractive forces. It was shown by Bijl, de Boer, and Michels[4] that such a break in C_v would appear if the lowest energy level into which the molecules "condense" were lower compared with the higher energy levels than would be the case with the ideal gas, this lowering of the lowest energy being produced by the liquid forces.

Under the circumstances it *may* be profitable to consider the difference between the λ phenomenon in helium and the transition in an ideal Bose-Einstein gas in the light of the available experimental data, still bearing in mind, however, the great probability that the phenomena are related. The first step will be to consider the general characteristics of second-order transitions, especially those which are not concerned with solid lattices, and in particular to note some of the relationships between transitions of various types.

Before turning to this development, however, we wish to set down the Keesom-Ehrenfest equation, for future reference, in the following form:

$$\Delta C_p = (dp/dT)T\Delta(\partial V/\partial T)_p. \tag{1}$$

Here C_p is the molal heat capacity at constant pressure, the total derivative dp/dT refers to the change of pressure with temperature along the second-order transition line, V is the molal volume and Δ indicates that the value of quantity on the low-temperature side of the transition is to be subtracted from the value just across the transition line on the high-temperature side.

We can also write

$$\Delta C_v = -(dV/dT)T\Delta(\partial p/\partial T)_V. \tag{2}$$

This equation is implied but not actually written down by Semenchenko,[5] and can be derived by considering the entropy S as a function of V and T, writing

$$dS = (\partial S/\partial T)_V dT + (\partial S/\partial V)_T dV$$
$$= (C_v/T)dT + (\partial p/\partial T)_V dV.$$

Now noting that S does not change at a second-order transition, so that along the transition line,

$$d\Delta S = (\Delta C_v/T)dT + \Delta(\partial p/\partial T)_V dV = 0,$$

we see that Eq. (2) follows immediately.

For helium, we may note that application of Eqs. (1) and (2) makes it highly probable that C_p and C_v actually have definite breaks rather than merely sharp maxima at the λ point. For both $(\partial V/\partial T)_p$ and $(\partial p/\partial T)_V$ actually change sign at the λ-point, and there is no evidence to indicate that they do not change suddenly. In fact, they appear to increase in magnitude as the λ point is approached from below, and not to change rapidly as it is approached from above.[6] Though it is impossible to prove a point of this sort absolutely, the evidence is thus exceedingly good that we are dealing with a true second-order transition.

2. GENERAL DISCUSSION OF PHASE TRANSITIONS OF VARIOUS ORDERS

Gorter[7] has pointed out that if we cooled a vapor in a closed, opaque container of constant volume, we would find a discontinuity in the slope, $(\partial p/\partial T)_V$, of the pressure-temperature curve when we reached the point of condensation. If we were unaware of the separation of phases, we might infer that a second-order transition had occurred. If we tried the experiment with systems of different density we could find dp/dT and dV/dT for the transition, and it would, in fact, be entirely proper to apply Eqs. (1) and (2). However, we would also find, that, in what we know to be the two-phase region, $(\partial p/\partial V)_T = 0$. Since $(\partial p/\partial T)_V$ does not vanish, this means that $(\partial T/\partial V)_p = 0$ or $(\partial V/\partial T)_p$ is infinite. C_p, which, in the transition region, includes the heat effects arising from evaporation or condensation, also becomes infinite, so that dp/dT cannot be determined from Eq. (1). However, we can consider this to be a limiting case in the application of Eq. (1). If $(\partial p/\partial V)_T$ in the two-phase region were very small but not zero, $(\partial V/\partial T)_p$ would be very large but not infinite, as would C_p. We could then, in comparison, neglect $(\partial V/\partial T)_p$ and C_p for the one-phase region, and write Eq. (1) as

$$C_p = (dp/dT)T(\partial V/\partial T)_p,$$

where C_p and $(\partial V/\partial T)_p$ are for the two-phase region. Since $C_p = T(\partial S/\partial T)_p$ we see that this yields

$$dp/dT = (\partial S/\partial V)_p.$$

In the limit, where $(\partial p/\partial V)_T = 0$, this is

$$dp/dT = (\partial S/\partial V)_T.$$

Interpreting the right-hand side of this equation in terms of the behavior of the two coexisting phases, we see that $(\partial S/\partial V)_T = \Delta S/\Delta V$, and we recover the Clapeyron equation.

[3] R. P. Feynman, Phys. Rev. **91**, 1291 (1953).
[4] Bijl, de Boer, and Michels, Physica **8**, 655 (1941).
[5] V. K. Semenchenko, Zhur. Fiz. Khim. **21**, 1461 (1947).
[6] W. H. Keesom, *Helium* (Elsevier Publishing Company, New York, 1942), Sec. 4.7.
[7] See reference 6, p. 259.

In the case of Eq. (2) there is no difficulty in applying the equation when $(\partial p/\partial V)_T=0$, for, as we have noted $(\partial p/\partial T)_V$ remains finite, and so, unless dV/dT is infinite, C_v will remain finite also.

This discussion will indicate the desirability of considering a little more closely the relation between first- and second-order transitions. Let us suppose that we have a transition which resembles a first-order transition, except that the slope of an isotherm in the transition region is not quite zero. Then the isotherms will appear as shown in Fig. 3. This represents a set of ordinary second-order transitions, or rather two sets of such transitions, one set on the left-hand branch of the transition curve and the other on the right-hand branch. Is there any way that we can still interpret the transition at the right-hand branch (vapor) as the formation of some of the left-hand phase (liquid)? Suppose that the Gibbs free energy of the vapor at some given temperature is G_g and that it is at a pressure p_g. The free energy of liquid at pressure p_l is

$$G_g+\int_{p_g}^{p_l} V dp.$$

The free energy of liquid at p_g is

$$G_l(p_g)=G_g+\int_{p_g}^{p_l} V dp-\int_{p_g}^{p_l} V_l dp. \tag{3}$$

Since the average value of V involved in the first integral is greater than the average value of V_l in the second, we see that

$$G_l(p_g)>G_g. \tag{4}$$

Of course this is why an ordinary liquid phase does not appear at the transition line. Unless some device can be found to lower the free energy of the liquid, the interpretation we have proposed cannot stand. However we know that if the liquid is dispersed in the gas its entropy will be increased and its enthalpy *may* be lowered. Both effects can contribute to the lowering of the chemical potential of the liquid so as to bring it down to the chemical potential of the gas.[8]

If we approach the left-hand transition curve from the liquid side we find, in an entirely similar manner,

$$G_g(p_l)=G_l+\int_{p_l}^{p_g} V dp-\int_{p_l}^{p_g} V_g dp. \tag{5}$$

In this case the integrals are negative since $p_g<p_l$ and the average value of V_g will be expected to be greater than the average value of V, since the compressibility of the gas is less than that of the mixture of gas and liquid. Therefore, in this case,

$$G_g(p_l)>G_l. \tag{6}$$

[8] Compare V. K. Semenchenko, Zhur. Fiz. Khim. **21**, 1461 (1947).

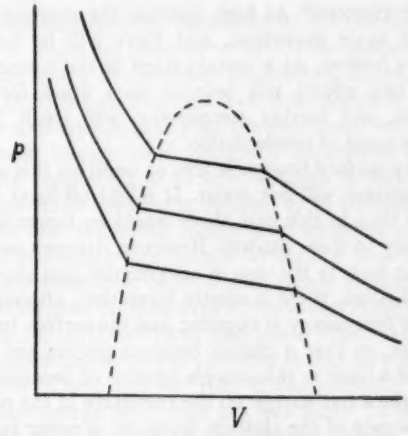

FIG. 3. Isotherms, illustrating a possible type of second-order transition. The broken line is the transition line.

Again we are led to the idea of a dispersed phase, this time gas in liquid. Of course a dispersion of gas in liquid could merge gradually, as the proportion of gas increased, into a dispersion of liquid in gas.

If there were no discontinuity in the slope $(\partial p/\partial V)_T$ of the isotherms at the transition line of Fig. 3, but only a discontinuity in $(\partial^2 p/\partial V^2)_T$, then the transition would be third order instead of second order. It is seen that when $(\partial p/\partial V)_T$ in the transition region within the transition line approaches zero the third-order transformation approaches an anomalous first-order transition. In this case $(\partial V/\partial T)_p$ and C_p increase without limit and become infinite at the transition line, but $(\partial p/\partial T)_V$ and C_v [by Eq. (2)] remain continuous and finite. However, since $(\partial p/\partial T)_V$ is constant in the transition region in the anomalous first-order transition, the rates of change of $(\partial p/\partial T)_V$ and, hence, of C_v, change abruptly. This is just the situation in the Einstein-Bose transition. The Clapeyron equation in its usual form will hold for the anomalous first-order transition, as for the ordinary first-order transition.

The relation between the third-order transition and the anomalous first order is exactly similar to the relation between the second-order transition and the ordinary first order, and if the third-order transition is to be described in terms of two phases, as we described the second-order one, we must again think of one phase dispersed in the other.

When a first-order transition takes place certain pretransition phenomena will in general occur. Thus, when a vapor is compressed isothermally clusters of molecules will appear.[9] The larger clusters will resemble the liquid but will have surface free energy. The surface free energy will tend to favor coalescence of clusters, but the entropy effect will tend to favor separation into

[9] J. Frenkel, J. Chem. Phys. **7**, 200, 538 (1939); W. Band, J. Chem. Phys. **7**, 324, 927 (1939).

smaller clusters.[10] At high dilution the entropy effect will be more important, and there will be but few clusters formed. At a certain stage in the compression these two effects will balance each other for large clusters, and further compression will result in the sudden onset of condensation.

If the surface tension is zero or negative this sudden condensation will not occur. It might off-hand be expected that in this case there would no longer be any tendency to form clusters. However, it seems probable that, at least in the case of compression just above the critical point, there is cluster formation; although the surface free energy is negative and the surface tends to increase, so that a cluster becomes porous and open, there is a limit to this process because of dependence of the surface free energy on the curvature of the surface. Coalescence of the clusters, however, is never favored, and will not occur until the free volume of large clusters is reduced to zero. The size of the clusters simply increases gradually up to this point, and then there is just one big, but spongy cluster. This can be further compressed, but with a somewhat different law of compression. However, it appears from a discussion of this case,[11] and especially because the individual clusters are already subject to compression even before coalescence so that the whole process takes place gradually, that $(\partial p/\partial V)_T$ will probably be continuous, though $(\partial^2 p/\partial V^2)_T$ may very well not be. Except in the special case when the surface tension is zero $(\partial p/\partial V)_T$ should not become zero, so this situation corresponds to the third-order transition. It will be seen that the spongy coalesced cluster is really a dispersion, but depends for stabilization on its negative surface tension, as well as upon its configurational entropy, which arises because it does not have a fixed shape. Indeed, the two factors are closely interrelated, and one can say that the fact that the convoluted surfaces of the dispersed phase are mobile adds to the surface entropy.

To have a second-order transition an intermediate situation must exist.[12] The tendency for dispersal must exist, as though the system had a negative or at least near-zero surface tension. On the other hand, there must also be some special stability of a condensed phase, which is in this case an extended dispersed phase with configuration entropy. Thus clusters would be formed on compression, but they would not be compact, but rather disperse clusters. But on further compression, as their entropy of translation as a whole decreased so that the entropy of coagulation would not be so great, there would begin to appear a very large cluster, a condensed but still dispersed phase, as though for this process of coalescence the surface tension were positive. This large cluster is the "condensed phase." The question which now arises is why this condensed phase does not continue to form on compression without change of free energy, until it fills the volume and encompasses all the dispersed clusters. If this happened the transition would have a, perhaps small but nonetheless real, first-order region with a finite latent heat. The answer is that the large cluster described still has an entropy of mixing, for it is not confined to any one part of the system, in essential contrast to the condensed phase in an ordinary condensation. Thus the coalescence of the clusters really occurs simply when the point arises at which much larger, but not "infinite" or macroscopic clusters reach as low a free energy as the already large, but not *that* large (intermediate sized) clusters which were previously present. The sudden appearance of clusters of a much larger size signals the second-order transition, after which further compression results in the further building up of the much larger clusters, both by having them grow at the expense of the intermediate clusters, and ultimately (and to some extent simultaneously) at the expense of the vapor molecules, i.e., molecules which are not combined into clusters, or which are present in very small clusters. Since the intrinsic free energy involved in going from intermediate clusters to very large clusters is certain to be very small, it is not to be expected that such a transition would occur until the concentration of the intermediate clusters was sufficiently large so that their free volume would be greatly restricted.

3. THE λ TRANSITION IN LIQUID HELIUM

We shall base our discussion of liquid helium upon the fundamental assumption that the λ phenomenon depends upon some of the atoms going into a low-energy state, and that the superfluid properties result from these atoms. These atoms, then, essentially form the superfluid, and in using the language of the two-fluid hypothesis of Tisza we shall assume that it has some actual physical significance. With this fairly definite picture in mind we desire to inquire how it can be fitted into the general picture of a second-order transition, as presented in the preceding section.

If, below the normal λ temperature, we start with helium I at a high pressure which is gradually lowered, we will eventually reach the transition curve where the change to helium II occurs. The situation is not very different from that which we find at the left-hand side of Fig. 3. The transition is, as we have seen, presumably a second-order one; therefore the pressure will continue to decrease after it occurs. In terms of the two-fluid theory we will say that superfluid appears at the transition, or at least that it there first takes a form in which the superfluid properties become evident, and the amount of superfluid continues to increase as the pressure is lowered, until at some pressure (which may be negative but practically is around zero pressure

[10] See O. K. Rice, J. Phys. and Colloid. Chem. **54**, 1293 (1950).
[11] O. K. Rice, J. Chem. Phys. **15**, 314 (1947); *Thermodynamics and Physics of Matter* (Vol. I of *High Speed Aeronautics and Jet Propulsion*) (Princeton University Press, Princeton, to be published), Sec. 7, Art. 6.
[12] There are of course other ways that second-order transitions can occur, especially in solid lattice.

below 1°K) the system consists almost entirely of superfluid.

Though the isobars given by Keesom[6] indicate $-(\partial p/\partial V)_T$ decreases discontinuously at the transition line, the situation at the other end of the transition (i.e., corresponding to the right-hand branch of Fig. 3) is not so clear since there is no definite sign of another transition. However, the slope of the isobars $(\partial p/\partial T)_\rho$ (where ρ is the density) becomes practically zero around 1°K where presumably the liquid has become pure superfluid. We therefore conclude that the properties of the superfluid do not depend appreciably on the temperature, but only upon the pressure or density. Furthermore, we find that at any pressure $(\partial p/\partial V)_T$ is greater for superfluid (i.e., near 0°K) than it is where there is a mixture of superfluid and normal fluid near the λ-transition pressure. Also V is larger for superfluid than for normal fluid. Thus the conditions by which the inequality (6) is derived from Eq. (5) (with the superfluid taking the place of the gas and the normal fluid taking the place of the liquid) are fulfilled. Thus, where the transition occurs, the superfluid must have a lower chemical potential than pure superfluid would have. In other words, in terms of partial molal quantities (with subscript s referring to superfluid and subscript λ referring to the condition at the transition line) we must have either

$$\bar{S}_{s,\lambda} > S_s, \tag{7}$$

or

$$\bar{H}_{s,\lambda} < H_s, \tag{8}$$

or both, where the quantities on the right-hand side refer to the pure superfluid. From consideration of the conditions of equilibrium in the two-fluid theory, I have already come to these conclusions, and I have developed the thermodynamics of liquid helium[13] on the basis of the assumption $\bar{S}_{s,\lambda} > S_s$ and $\bar{H}_{s,\lambda} = H_s$, which implies an entropy of mixing, while Gorter[14] has developed the thermodynamics on assumptions which are equivalent to taking $\bar{S}_{s,\lambda} = S_s$ and $\bar{H}_{s,\lambda} < H_s$, implying an enthalpy of mixing.

This is a difference between the transition in liquid helium and the transition in the Bose-Einstein gas which is of some importance, and should be taken into account in any theory of liquid helium. It arises because of the fact that the transition in helium is not first-order, at least over an observable range of thermodynamic conditions, whereas that in the Bose-Einstein gas is. If there is to be an entropy of mixing, it would seem that some separation in ordinary space of superfluid and normal fluid, such as I have already suggested[13] would be necessary. This would be in general accord with the idea of dispersion, mentioned in Sec. 2 above. The possibility that helium II involves a dispersion has also been suggested by Semenchenko.[8,15] On the other hand, it might be possible to avoid the separation in ordinary space if the other alternative, $\bar{S}_{s,\lambda} = S_s$ and $\bar{H}_{s,\lambda} < H_s$ is the correct one. The Bose-Einstein transition is a unique one, in that the condensed state, i.e., the lowest energy level, though it apparently has an effective volume equal to zero, actually is spread out over the entire containing volume. It is, perhaps, conceivable that the lowest energy level would be affected by the molecular interactions in such a way that it was lower when most of the atoms were in excited states than when most of them were in the lowest energy level. Certain calculations[16] have been made which are based on symmetrization of free particles or Bloch-type wave functions. These indicate that if two particles are in the same energy level they are less likely to be close together than if they are in different energy levels. Depending upon whether one supposes that the repulsive or attractive forces are more important one will conclude that the mutual energy of the two particles will be relatively lowered or raised by the interatomic forces when they are in the same energy level. These conclusions are based, however, upon the general ideas of small perturbation theory.

Since the strong repulsive forces can scarcely be handled by small perturbation theory, and since they will profoundly affect the wave function, it seems to me better to approach the problem by the standard method of handling a two-particle problem, separating off the coordinates of the center of gravity, and considering then the relative radial or vibrational motion and the relative rotational motion. In the case of helium the attractive forces are relatively weak and it seems quite likely that one or two degrees above the λ point the atoms are only rarely held in any fixed position, the motion being mostly translational. This translational motion is superimposed upon a large zero-point energy; there is a potential energy well near every helium atom, but its neighbors have sufficient energy to escape from it. The unbalanced forces at the edge of the liquid, however, are sufficient to keep the average atom from escaping, so that there is a nonzero energy of evaporation. For any helium atom to go into its lowest energy level actually involves a cooperative phenomenon which

[13] O. K. Rice, Phys. Rev. **76**, 1701 (1949); **79**, 1024 (1950).
[14] C. J. Gorter, Physica **15**, 523 (1949).

[15] V. K. Semenchenko, Doklady Akad. Nauk S.S.S.R. **74**, 335 (1950). Other writers have developed theories which involve clusters of one sort or another, e.g., H. N. V. Temperley, Proc. Phys. Soc. (London) **A65**, 619 (1952); M. Toda, Progr. Theoret. Phys. (Japan) **6**, 458 (1951). The latter assumes that the excitations in helium above 1°K consist of groups of about eight atoms in a solid-like cluster, which would involve separation in ordinary space. This is a possible type of excitation around 1°K; however, Toda assumes that the λ point occurs when the liquid consists entirely of such "molecules," and in such dense packing they would not have the statistical properties ascribed to them, so this can scarcely be a theory of the λ point. The idea that the excitation in liquid helium is connected with "molecules" is also suggested by the interesting analysis of T. Matsubara, Progr. Theoret. Phys. (Japan) **6**, 714 (1951). However, since he neglects interactions between the molecules, it would seem that the same difficulties would appear at the λ point.

[16] N. F. Mott, Phil. Mag. **40**, 61 (1949).

requires the interaction of more than one atom. Thus it takes at least two atoms to abandon their mutual translational energy for mutual vibration. Indeed, in the case of helium, it must require more than this, because the potential-energy minimum of the van der Waals attraction is hardly deep enough for there to be discrete energy levels. However, we do know that it is possible for a group of helium atoms to condense together in a lowest energy level (liquid helium at 0°K). There must be a smallest number of atoms which will do this. So in the liquid it is quite possible that a group of atoms can be firmly, though temporarily, bound together in their lowest energy level.[17] The surrounding liquid would of course be expected to alter the situation quantitatively, and the cluster would be continually exchanging atoms with neighboring portions of the liquid, either through excitation and de-excitation, or through an atom in one part of the cluster leaving while simultaneously another atom joins the group at another location. Nevertheless, the idea of low-energy clusters seems to be a reasonable speculation.

It is probably not a very good approximation to consider normal modes of vibration of such a group of atoms, as in a crystal lattice; however, such an approximation may serve to give some idea of the placing of the energy levels. In a crystal lattice if all the atoms are fixed except one, that atom would vibrate with a frequency of say, ν_0. The average value of the squares of the actual frequencies obeys the relation $\langle\nu^2\rangle_{Av}=\nu_0^2$. The greater the number of atoms cooperating in the lattice the greater the spread of frequencies. Now the maximum of the sum of all the frequencies occurs when all the frequencies are equal if the frequencies are constrained in such a way that the sum of their squares has a fixed value. Thus the interaction will lower the zero-point energy, and presumably the greater the number of cooperating atoms the lower will be the zero-point energy; furthermore, this discussion would lead to the inference that the low energy atoms will occur in spatially connected groups. In any event, it seems to be unlikely that the lowest energy level for a single atom could extend spatially throughout the vessel in the case of liquid helium, because the atoms would be scattered on account of the repulsive forces. I remarked on this some years ago,[18] and it has recently been discussed with some amplification by Ziman.[18]

It is doubtful that any calculation based on the idea of lattice vibrations could have any quantitative application to liquid helium. Nevertheless it will be of interest to attempt to calculate the difference in zero-point energy between a Debye lattice and a lattice in which all the frequencies are the same and equal to $\nu_0=(\langle\nu^2\rangle_{Av})^{\frac{1}{2}}$ (i.e., the corresponding Einstein lattice). Going from an Einstein lattice to a Debye lattice involves a spread in the frequency spectrum, something like that which occurs when additional atoms are added to a cluster. The Debye characteristic temperature Θ is given by the relation[19]

$$k\Theta=(5/3)^{\frac{1}{2}}h(\langle\nu^2\rangle_{Av})^{\frac{1}{2}}=(5/3)^{\frac{1}{2}}h\nu_0; \tag{9}$$

the zero-point energy, E_D, is given by

$$E_D=(9/8)k\Theta. \tag{10}$$

The zero point of the corresponding Einstein lattice is

$$E_E=\tfrac{3}{2}h\nu_0=\tfrac{3}{2}(\tfrac{3}{5})^{\frac{1}{2}}k\Theta=1.03E_D. \tag{11}$$

Since the zero-point energy of liquid helium is 30 to 40 cal per mole,[20] the energy of the Debye lattice is around 1 cal per mole less than that of the Einstein lattice. It is of interest that the difference is of the order of magnitude of the energy content of helium at its λ point, which is about 3 cal per mole. It appears that the energy lowering arising from cooperative vibration of the atoms can easily be great enough to furnish considerable incentive for the "condensation" of atoms in their lowest energy level into considerable groups. It is to be noted that since this energy effect increases with increasing number of superfluid atoms (which would of course result in larger conglomerates) the change of $\bar{H}_s$ with temperature would be in the opposite direction to that required by the inequality (8) and noted in the next paragraph following (8).

The attractive forces between the helium atoms clearly play quite a decisive role in the picture we have just presented. If we elected to neglect specific effects of attractive forces between individual pairs of neighboring atoms, there would be no incentive to consider modes of vibration, and the idea of clusters would not present itself. It is in this way that the present discussion differs from most previous treatments. In particular, we may mention that it seems to differ in this way from the recent work of Feynman.[3]

The above discussion would seem to lend some weight to the idea that the high specific heat just above the λ point arises from the presence of superfluid globules, which have not yet coalesced into sufficiently large clusters to bring the superfluid properties into evidence. I showed that the trend of the specific heat required that there be 60 to 80 atoms in such globules.[21] My

[17] Phonon excitations in the clusters would, of course, not be excluded, and this could occur without breaking up the cluster, but it is known that this type of excitation is not of great importance near the λ point.

[18] J. M. Ziman, Phil. Mag. 44, 548 (1953).

[19] See O. K. Rice, J. Am. Chem. Soc. 63, 3 (1941).

[20] F. London, J. Phys. Chem. 43, 49 (1939).

[21] There is perhaps other evidence for globules of superfluid above the λ point, namely, the absorption and dispersion of sound just above the λ point. A. B. Pippard, Phil. Mag. 42, 1209 (1951), has explained this in terms of fluctuations involving large regions composed of helium II; it seems probable that this is equivalent to small regions of pure superfluid and, indeed, H. Satô, Busseiron Kenkyû 35, 15 (1951), has attempted to explain the same phenomenon on the basis of my original theory. However, Satô found that to obtain agreement it was necessary to assume only five atoms in the globules, which is entirely too low to explain the specific heat data, and there appeared to be other quantitative discrepancies.

theory, however, could not tell much about the transition itself. It now appears likely that the transition may be described in much the same terms as we described a second-order transition at the end of Sec. 2. The globules need not be spherical clusters but could be rod-like or filament-like, or of irregular shape. Since the energy decreases with increasing cluster size, a point could be reached as the temperature is lowered (or, isothermally, as the pressure is lowered) where, rather suddenly, a much larger size of globule, or perhaps a network which extends for a long distance in at least one direction, becomes stable. If such a network is practically macroscopic in one direction, the superfluid properties would be expected to come into evidence when it appears. As the temperature (or pressure) is lowered, these extended networks would rapidly fill the liquid volume, and so grow at the expense of smaller clusters, which now have less free volume, and at the same time also grow at the expense of the normal fluid.

The formation of extended networks corresponds to the appearance of long-range order in the ordinary type of order-disorder transition. There is, of course, a considerable resemblance between our description of the helium transition, and the usual type of order-disorder process. The effective attraction of two neighboring atoms of superfluid is an essential element. A lattice approximation, however, would scarcely be applicable, and the situation also differs from that of the Ising lattice, for example, in that the interactions are not additive, the interactions depending on how many are already in the low-energy group.[22] The latter difference is quite important, for according to the picture given here, the apparent attraction between the superfluid atoms will actually effectively exist only between a certain minimum number of them, and will become stronger rather rapidly for a while as more are added to the group; then after a certain number are present the attraction will approach an asymptotic value. It is this fact which is responsible for the appearance of definite clusters. In spite of these differences, it is interesting that the specific heat of an Ising lattice with a simple cubic arrangement, according to calculations of Wakefield[23] closely parallels that of liquid helium, except very close to the transition point, where the specific heat of the Ising lattice probably becomes infinite.

In my earlier paper I estimated that only 4 or 5 percent of the helium was in the form of superfluid at the λ point. This seems rather a small fraction of locally ordered material to bring about the onset of long-distance order. For example, the quasi-chemical approximation for the simple cubic lattice gives 14 percent local order at the transition point, while Wakefield's calculations, judging from the specific heat curves, indicate even more. This point, therefore, may merit some elaboration.

Let us derive an expression for the molal heat capacity at constant pressure C_p on the basis of the two-fluid hypothesis. We will use the subscript n to denote normal fluid, the subscript s to denote superfluid. Mole fractions will be designated by x.

The molal enthalpy is given by

$$H=x_n\bar{H}_n+x_s\bar{H}_s. \tag{12}$$

To obtain C_p we differentiate this expression, remembering that $dx_s=-dx_n$, and that $x_n(\partial\bar{H}_n/\partial x_n)_T+x_s(\partial\bar{H}_s/\partial x_n)_T=0$:

$$C_p=(\bar{H}_s-\bar{H}_n)dx_s/dT+x_n(\partial\bar{H}_n/\partial T)_{x_s}+x_s(\partial\bar{H}_s/\partial T)_{x_s}. \tag{13}$$

We have taken x_s and T as the variables, and p is, of course, always assumed constant. This is the situation, practically, when helium is heated under its own vapor pressure. If there were no superfluid, we should have $C_p=\partial\bar{H}_n/\partial T$. Therefore, subtracting this from Eq. (13), and noting that $1-x_n=x_s$, we find for the "anomalous" part of the specific heat,

$$C_{p,a}=(\bar{H}_s-\bar{H}_n)dx_s/dT+x_s[(\partial\bar{H}_s/\partial T)_{x_s}-(\partial\bar{H}_n/\partial T)_{x_s}]. \tag{14}$$

Since x_s is small above the λ point, since $(\partial\bar{H}_s/\partial T)_{x_s}$, i.e., the specific heat of superfluid at constant mole fraction, should presumably be zero and even $(\partial\bar{H}_n/\partial T)_{x_s}$, roughly the "nonanomalous" part of the specific heat, is relatively small, we may write, approximately

$$C_{p,a}=(\bar{H}_s-\bar{H}_n)dx_s/dT. \tag{15}$$

Hence x_s at the λ point, T_λ, will be given by

$$-x_{s,\lambda}=\int_{T_\lambda}^{\infty}[C_{p,a}/(\bar{H}_s-\bar{H}_n)]dT. \tag{16}$$

On the basis of the assumption that the normal part of the specific heat was 2.2 cal deg^{-1} mole^{-1}, I estimated that $C_{p,a}=3.0\exp[(T_\lambda-T)/0.05]$. Substituting this in Eq. (16) and assuming that $\bar{H}_n-\bar{H}_s$ is approximately equal to the enthalpy of the liquid at the λ point, which is about 3.0 cal mole^{-1}, one finds $x_{s,\lambda}=0.05$.

The difficulty may well lie with the estimate of the normal value of C_p, hence of $C_{p,a}$. If we examine the specific heat curves for the order-disorder case[23] we notice that they drop rapidly near the transition point, then tail off very slowly at higher temperatures. This corresponds to a decrease in the average size of the clusters as the temperature increases. The temperature coefficient for the number of clusters of any given size depends on the difference between the energy of the entire cluster and the energy of the same number of atoms without local order. This energy difference is

[22] I. Prigogine and J. Philippot, Physica **19**, 508 (1953) have considered the λ transition to be an order-disorder phenomenon in a treatment which is based on a discussion of fluctuations, and which apparently takes no direct account of the two-fluid hypothesis. See also H. Fröhlich, Physica **4**, 639 (1937).

[23] A. J. Wakefield, Proc. Cambridge Phil. Soc. **47**, 419, 799 (1951).

approximately proportional to the size of the cluster. Thus the number of small clusters will fall off much less rapidly with increasing temperature than the number of large clusters, and as the small clusters remain after the large ones disappear the specific heat decreases less rapidly. Thus, we should not really expect a simple exponential falling off of $C_{p,a}$ with T, and this suggests that our normal specific heat should have been taken somewhat lower than 2.2 cal deg^{-1} mole^{-1}. If $C_{p,a}$ were an average of 0.2 to 0.3 greater over a range of 1 to 1.5 degrees, this would make a considerable difference in the percentage of superfluid at the λ point.

4. PROPERTIES OF He^3 AND OF He^3–He^4 SOLUTIONS

Although there has been little mention thus far in the discussion of the Bose-Einstein statistics, it is easily shown that this type of statistics actually plays a most important role in determining the possibility of the occurrence of clusters. We will discuss this in terms of the rotational states of pairs. Since such pairs are in close contact with other atoms and interact with them in such a way that angular momentum will not be conserved, it is clear that this procedure involves an approximation. There seems little doubt, however, that we touch in this way on the essence of the matter. If a cluster of atoms is to be in its lowest state, it would appear that, in terms of the above approximation, any pair should be in its lowest possible rotational state.[24] In the case of an atom with no nuclear spin no complication can result, since the state of zero relative angular momentum is allowed. He^3, however, has a nuclear spin of $\frac{1}{2}$ and obeys the Fermi statistics, that is, the wave function of a pair of atoms is antisymmetrical. The situation is similar to that which occurs with H_2, which results in the distinction between *ortho-* and *para-*hydrogen. With any pair of atoms there is only one chance in four that their nuclear spins will have the proper relation, so as to allow them to have no mutual angular momentum. In any group of atoms, a large fraction of the adjacent pairs must have an angular momentum with respect to each other, and, in view of the small mass, this will be associated with a considerable energy. Because of the small depth of the potential-energy well in which any He^3 atom is vibrating, this energy would be expected to be sufficient to cause "dissociation" by rotation. Thus we do not expect a group of He^3 atoms to be bound together in a low-energy cluster.

It is interesting to speculate on the effect of a He^3 atom if introduced into a cluster of He^4 superfluid. Since there are no symmetry requirements, in a pair consisting of a He^3 and a He^4 atom, there would be no bar to the He^3 atom going into a state of zero angular momentum. On account of its smaller mass, however, it would be expected to have a higher zero-point energy than the He^4 atoms. Indeed, its zero-point energy would be greater than it would be in pure He^3, since He^3 has a considerably lower density than He^4. It is probable that an He^3 atom could not be accommodated in the potential energy wells available in He^4. Indeed, London and F[25] thought that He^3 could not liquify at all, on account of its higher zero-point energy. This was not a good prediction, as it proved possible to circumvent this high zero-point energy by forming a liquid of lower density. However, it is not to be expected that a single He^3 could ordinarily cause a sufficient lowering of density in its neighborhood to enable it to fit into a superfluid cluster. Certainly if it did so, and probably in any event, it would tend to disrupt the cooperative action of the atoms in the cluster, and so effectively raise the energy more than if it were dissolved in normal fluid. Thus we may have found some basis for Taconis' hypothesis,[26] that He^3 is not soluble in superfluid, but only in normal fluid, although it has recently been suggested[27] that the abnormally high vapor pressure of He^3 from solutions of He^4 is only what is to be expected from a mixture of ideal gases, one obeying Einstein-Bose and the other Fermi-Dirac statistics. In other words, it is supposed that in the explanation of this phenomenon, the liquid forces could be neglected entirely. On the other hand, Morrow[28] has shown that Taconis' assumption, combined with rather usual ideas about nonideal solutions, can account for many of the experimental results.

Note added in proof.—Since this paper went to press, L. Guttman and J. R. Arnold, Phys. Rev. **92**, 547 (1953), have presented evidence that He^6 participates only slightly in the superfluidity of He^4. This may be because of the effect of a particle of higher mass on the zero-point energy of a cluster of superfluid. A particle of infinite mass, introduced into a linear array of atoms, would effectively cut the array into two pieces, thus increasing the zero-point energy. Introduction of an He^6 atom into a superfluid cluster of He^4 would have a considerably smaller, but nevertheless similar, effect, and might increase the zero-point energy sufficiently so that He^6 would tend to be expelled from the superfluid.

[24] See E. G. D. Cohen, quoted by I. Prigogine and J. Philippot, Physica **18**, 747 (1952).

[25] F. London and O. K. Rice, Phys. Rev. **73**, 1188 (1948).

[26] Taconis, Beenakker, Nier, and Aldrich, Phys. Rev. **75**, 1966 (1949).

[27] C. V. Heer and J. G. Daunt, Phys. Rev. **81**, 447 (1951); Daunt, Tseng, and Heer, Phys. Rev. **86**, 911 (1952); A. Harasima, J. Phys. Soc. Japan **6**, 271 (1951).

[28] J. C. Morrow, Phys. Rev. **84**, 502 (1951).

The Connection between the Smoluchowski Equation and the Kramers-Chandrasekhar Equation*

R. W. DAVIES
American Institute of Aerological Research, Pasadena, California
(Received October 19, 1953)

It is shown that the Kramers and Chandrasekhar extension of the Fokker-Planck equation to phase space leads to a modified Telegraph or hyperbolic-type diffusion equation in configuration space. The solution of this equation at large times asymptotically approaches the solution of the Smoluchowski equation. The hyperbolic diffusion equation and the Smoluchowski equation differ by one term which is related to the fact that particle velocities exist in the former case whereas in the latter case they do not.

LET $W(x,v;t)$ represent the probability density for a Brownian particle in phase space x,v. Using the assumption that Brownian motion is a simple Markoff process in phase space, Kramers[1] and Chandrasekhar[2] have demonstrated that $W(x,v;t)$ satisfies the equation

$$W_t+vW_x=((\beta v-K(x))W)_v+(kT\beta/m)W_{vv}, \quad (1)$$

where $K(x)$ is an external force, T is temperature, β is a friction constant, m is mass, and k is Boltzmann's constant. [Equation (1) is an extension of the Fokker-Planck equation to phase space.]

If it is assumed that Brownian motion is a simple Markoff process in configuration space x, then the probability density

$$\rho(x,t)=\int_{-\infty}^{+\infty}W(x,v;t)dv$$

satisfies

$$\rho_t+\left(\frac{K(x)\rho}{\beta}\right)_x=\frac{kT}{m\beta}\rho_{xx}, \quad (2)$$

which is known as Smoluchowski's equation. It has been argued that the description given by Eq. (2) approximates that given by (1) for $t\gg\beta^{-1}$. M. Kac pointed out to me that a truly satisfactory explanation remains to be given. I shall attempt to give such an explanation here.

Equation (1) is an approximation to the Boltzmann equation for Brownian motion. Thus, integrating (1) over velocity space gives

$$\rho_t+(\rho\bar{v})_x=0, \quad (3)$$

where

$$\rho\bar{v}=\int_{-\infty}^{+\infty}vWdv.$$

This is the equation of continuity. Multiplying by v and integrating over velocity space gives

$$(\rho\bar{v})_t+(\rho\langle v^2\rangle)_x+\beta\rho\bar{v}=K(x)\rho, \quad (4)$$

where

$$\rho\langle v^2\rangle=\int_{-\infty}^{+\infty}v^2Wdv.$$

This is the momentum equation. Now eliminating $\rho\bar{v}$ from (4) by means of (3) leads to the exact diffusion equation in configuration space

$$\frac{1}{\beta}\rho_{tt}+\rho_t+\left(\frac{K(x)\rho}{\beta}\right)_x=\left(\frac{\rho\langle v^2\rangle}{\beta}\right)_{xx}. \quad (5)$$

Now $\rho(\langle v^2\rangle-kT/m)\simeq O(e^{-2\beta t})$. It is clear then that for $t\gg\beta^{-1}$ the Smoluchowski Eq. (2) differs from (5) "only" by the term $(1/\beta)\rho_{tt}$.

Equation (5) is hyperbolic while Eq. (2) is parabolic indicating that the term $(1/\beta)\rho_{tt}$ is very important irrespective of its relative magnitude. It is well known that the model which Smoluchowski's equation represents has a particle path for which the velocity does not exist. The model represented by Eq. (1) is set up so that the particle velocity does have meaning although the particle acceleration does not exist. Clearly Eq. (1) is the more accurate representation of the phenomena for small times. An even more refined model of diffusion would have to include the existence of a particle acceleration.

The above paragraph can be profitably restated in the following way. Let β be a parameter which can be varied. Then take the limit of Eq. (5) as β approaches infinity. The resulting equation will make sense and reduce to equation (2) if $\langle v^2\rangle$ and $K(x)$ also approach infinity in such a way that

$$\lim_{\beta\to\infty}\frac{\langle v^2\rangle}{\beta}=\frac{kT}{6\pi a\eta},$$
$$\lim_{\beta\to\infty}\frac{K(x)}{\beta}=U(x), \quad (6)$$

where $U(x)$ is the "drift" velocity, η is the absolute viscosity of the liquid surrounding the particles, and a is the particle radius.

The solutions of Eqs. (2) and (5) can be compared for one simple case. Let $K(x)=0$, $\bar{v}(0)=0$ everywhere, $\langle v^2(0)\rangle=kT/m$ and $\rho(x,0)=\delta(x)$, where $\delta(x)$ is the Dirac delta function. In other words there is no external force,

* This work was supported by the U. S. Office of Scientific Research, Baltimore, Maryland.
[1] H. Kramers, Physica 7, 284 (1940).
[2] S. Chandrasekhar, Revs. Modern Phys. 15, 41 (1943).

the Brownian particles are in kinetic equilibrium with the surrounding medium, their initial velocities are symetrically distributed and they are all initially located at the origin. Then for Eq. (2) the initial value is $\rho(x,0)=\delta(x)$, and for Eq. (5) the values are $\rho(x,0)=\delta(x)$, $\rho_t(x,0)=0$. Equation (2) is now the heat equation, and its solution for above initial values is given by

$$\rho_1(x,t)=\left(4\pi\frac{kT}{m\beta}t\right)^{-\frac{1}{2}}\exp\left[-x^2\Big/\left(2\frac{kT}{m\beta}t\right)\right]. \quad (7)$$

Equation (5) is now the telegraph equation, and its solution is given by

$$\rho_2(x,t)=\begin{cases}\frac{1}{2}e^{-\frac{1}{2}\beta t}\beta[I_0(X)+\frac{1}{2}\beta t\, I_1(X)/X]; & x<(kT/m)^{\frac{1}{2}}t\\ 0; & x>(kT/m)^{\frac{1}{2}}t\\ \frac{1}{2}e^{-\frac{1}{2}\beta t}\delta; & x=\pm(kT/m)^{\frac{1}{2}}t\end{cases} \quad (8)$$

and

$$X=\tfrac{1}{2}\beta(t^2-mx^2/kT)^{\frac{1}{2}},$$

where I_0 and I_1 represents the Bessel functions of imaginery argument. For large time ρ_2 is asymptotic to ρ_1, which is to be expected since both Eqs. (2) and (5) have the same steady-state solution.

As stated in the first paragraph, Eq. (1) represents a simple Markoff process-type diffusion in phase space. However when the problem is reduced to configuration space in the representational form of Eq. (5), the diffusion is a Markoff process of order two. In fact it is possible to derive the Telegraph equation from a random-walk problem in configuration space which is a multiple Markoff process. This was first done by Goldstein.[3]

[3] S. Goldstein, Quart. J. Mech. Appl. Math. 4, 129 (1951).

PHYSICAL REVIEW VOLUME 93, NUMBER 6 MARCH 15, 1954

Quantum Statistics of Closed and Open Systems

P. T. LANDSBERG*
Randal Morgan Laboratory of Physics, University of Pennsylvania, Philadelphia, Pennsylvania
(Received September 21, 1953)

In this note an ideal Bose-Einstein and an ideal Fermi-Dirac gas are considered in the "limit L," i.e., in the limit in which the number of particles N and the volume V of the system are allowed to tend to infinity so as to keep N/V a finite and nonzero constant. It is shown that, whatever the system of energy levels, the mean occupation numbers calculated on the basis of the grand canonical ensemble are in the limit L the same as those calculated on the basis of the canonical ensemble. The only requirement is that the mean total number of particles for the grand canonical ensemble be equal to the fixed total number of particles for the canonical ensemble.

IT is well known that for an open system of non-interacting quantum-mechanical particles, treated on the basis of the grand canonical ensemble (g.c.e.), the mean occupation number of the jth quantum state of a particle is[1]

$$\bar{\nu}(\bar{N},j)=1/\{\exp[\eta(j)-\alpha]\pm 1\}, \quad (1)$$

where $\eta(j)$ is the energy of the jth quantum state divided by kT, the top sign refers to fermions, the bottom signs to bosons, and α is determined by

$$\bar{N}=\textstyle\sum_j \bar{\nu}(\bar{N},j). \quad (2)$$

$\bar{N}$ is the fixed average number of particles in the fixed volume V of the system. The corresponding mean occupation number $\bar{n}(N,j)$ for a closed system, having N particles in a volume V and treated on the basis of a canonical ensemble (c.e.), is similar,[2,3] except that α is replaced by α_j, where

$$\exp(-\alpha_j)\equiv Z_{N+1}\bar{n}(N+1,j)/Z_N\bar{n}(N,j),$$
$$\text{and} \quad (3)$$
$$N=\textstyle\sum_j \bar{n}(N,j).$$

Z_N and Z_{N+1} are the partition functions of the system when it has N or $N+1$ particles in the volume V. The two treatments (g.c.e. and c.e.) will not in general lead to the same results, although, if one assumes $\bar{N}=N$, the difference is usually small. We are not aware, however, of any general investigation into the conditions which must be fulfilled if these two treatments (with $\bar{N}=N$) are to yield *exactly* similar results for the main physical properties of the system. We shall show that *one such condition is that the properties of the system be considered in the "limit L."* This limit is defined by the requirement that N and V be allowed to tend to infinity while their ratio $\rho=N/V$ remains a finite and nonzero constant. The symbol $\sim$ shall denote equality in the limit L.

In the case of bosons a restricted proof of our propo-

* On leave of absence from the Department of Natural Philosophy, the University of Aberdeen, Aberdeen, Scotland.
[1] R. C. Tolman, *Statistical Mechanics* (Cambridge University Press, Cambridge, 1938), p. 503.
[2] T. Sakai, Proc. Phys. Math. Soc. Japan 22, 193 (1940).
[3] F. Ansbacher and W. Ehrenberg, Phil. Mag. 40, 626 (1949).

sition is implied in previous work.[4] The restriction resides in the fact that certain assumptions concerning the spectrum of energy levels were made throughout this paper, since they were required for the subject then under discussion. The demonstration that these restrictions are not in fact required for the present purpose is quite straightforward, but will be briefly given here for convenience of exposition. It suffices to appeal to the important result[5]

$$\bar{n}(N+1,\,j)>\bar{n}(N,\,j) \quad \text{(for finite systems)}, \tag{4}$$

whence[4]

$$1<\bar{n}(N+1,\,j)/\bar{n}(N,\,j)<[\textstyle\sum_K \bar{n}(N+1,\,K)]/[\sum_K \bar{n}(N,\,K)]=1+1/N \quad \text{(finite systems)}. \tag{5}$$

It follows that $\bar{n}(N+1,\,j)\sim\bar{n}(N,\,j)$, so that

$$\rho\sim V^{-1}\textstyle\sum_j[1/\{x\exp\eta(j)-1\}] \tag{6}$$

must be satisfied by both $x=e^{-\alpha}$ and $x=Z_{N+1}/Z_N$ in the limit L, so that $e^{-\alpha}\sim Z_{N+1}/Z_N$ and $\bar{\nu}(N,j)\sim\bar{n}(N,j)$ (all N, all j).

In the case of fermions the analog of (4) does not appear to be available in the literature. We shall, therefore, indicate a method of establishing it. Let $S(N;r,\lambda)$[6] denote the sum of all those terms in the partition function Z_N of the system which are obtained by allowing distributions of N particles over all the quantum states j, subject to the condition $n(N,\lambda)=r$, where r is a given nonnegative integer (which must be 0 or 1 for fermions). It is known[2,3] that

$$S(N;\,1,\,\lambda)=e^{-\eta(\lambda)}S(N-1;\,0,\,\lambda).$$

We establish first an auxiliary result. Let

$$X\equiv\frac{S(N;\,0,\,\lambda)S(N+1;\,1,\,\lambda)}{S(N;\,1,\,\lambda)S(N+1;\,0,\,\lambda)}=\frac{e^{-\eta(\lambda)}\sum_{\alpha_1}\cdots\sum_{\alpha_N}\sum_{\beta_1}\cdots\sum_{\beta_N}\exp[-\eta(\alpha_1)\cdots-\eta(\alpha_N)-\eta(\beta_1)\cdots-\eta(\beta_N)]}{e^{-\eta(\lambda)}\sum_{\gamma_1}\cdots\sum_{\gamma_{N-1}}\sum_{\delta_1}\cdots\sum_{\delta_{N+1}}\exp[-\eta(\gamma_1)\cdots-\eta(\gamma_{N-1})-\eta(\delta_1)\cdots-\eta(\delta_{N+1})]}.$$

The summations on the right are subject to the following restrictions: (1) For each term in the sum no two of the α suffixes must be equal, and the same applies to the β, γ, δ suffixes, since an equality of this kind would indicate the presence of two particles in the same quantum state. (2) The λth quantum state must be omitted from all summations, as it is either empty or, if it is occupied, has already been accounted for by the factors $e^{-\eta(\lambda)}$. Thus,

$$X=\{\sum_{a_1}\cdots\sum_{a_{2N}}\exp(-\sum_{p=1}^{2N}\eta(a_p))\}/\{\sum_{b_1}\cdots\sum_{b_{2N}}\exp(-\sum_{q=1}^{2N}\eta(b_q))\}.$$

In this summation, (1) a_p, $b_q\neq\lambda$ for all p and q, and (2) relations of the form $a_j\neq a_k$, $b_j\neq b_k$ $(j\neq k)$ must be imposed. There are $\frac{1}{2}N(N-1)+\frac{1}{2}N(N-1)=N^2-N$ of them for the numerator, and $\frac{1}{2}(N-1)(N-2)+\frac{1}{2}(N+1)N=N^2-N+1$ of them for the denominator. Thus, for each term in the sum of the denominator there exists an equal term in the sum of the numerator, but the latter has additional terms, since its suffixes are subject to a smaller number of restrictions. Hence our auxiliary result,

$$X>1 \quad \text{(finite system)}. \tag{7}$$

Since

$$\bar{n}(N,\lambda)=S(N;1,\lambda)/\{S(N;0,\lambda)+S(N;1,\lambda)\},$$

therefore,

$$\frac{1}{\bar{n}(N,\lambda)}-\frac{1}{\bar{n}(N+1,\lambda)}=1+\frac{S(N;\,0,\,\lambda)}{S(N;\,1,\,\lambda)}-1-\frac{S(N+1;\,0,\,\lambda)}{S(N+1;\,1,\,\lambda)}>0,$$

so that (4) holds in virtue of (7) also in the case of fermions. The argument now continues as for bosons, and the required proposition is established.

Further properties of quantum statistical systems in the limit L will be established in a subsequent communication.

[4] P. T. Landsberg, Proc. Cambridge Phil. Soc. **50**, 65 (1954).
[5] A. R. Fraser, Phil. Mag. **42**, 165 (1951).
[6] This notation was devised in conjunction with Dr. F. Ansbacher, University of Aberdeen, Aberdeen, Scotland.

Energy Spectrum Resulting from Electron Slowing Down*

L. V. SPENCER AND U. FANO
National Bureau of Standards, Washington, D. C.
(Received December 3, 1953)

The equation for the slowing down of electrons is cast in a form suitable for numerical calculations. Pilot calculations have been performed for source energies of $4mc^2$ and $80mc^2$ in Al and Pb. The spectrum of slowed-down electrons, which would be the reciprocal of the stopping power under the assumption of continuous slowing down, departs substantially from this elementary solution at the upper and lower energy ends of the spectrum. The departures are large throughout when bremsstrahlung is important. The accumulation of secondary knock-on electrons is also included in the calculations.

1. INTRODUCTION

HIGH-ENERGY particles (or photons) traversing a material generally dissipate their energy through a succession of collisions. Therefore, even though the radiation source be monochromatic with energy E_0, particles of all energies $E \leqslant E_0$ will be found in the material. The determination of the energy spectrum of all particles in the material, irrespective of their position and direction, constitutes a first task in a systematic study of the degradation, penetration, and diffusion of high-energy radiations.[1,2]

The spectrum resulting from the slowing down of neutrons has been studied by Placzek, in part by analysis and in part by numerical procedures.[3] The spectrum resulting from repeated Compton scattering of x-ray photons is derived by straightforward numerical procedures.[4] The problem of the slowing down of charged particles appears trivial only under the assumption of continuous slowing down; it has been discussed extensively in F (Secs. 1, 2, and 3), but accurate results were obtained in that paper only for heavy charged particles. The slowing down of electrons will be treated in the present paper. The solution of this problem may find direct application, for example, to the study of the total x-ray emission of electrons and to the analysis of the chemical and biological actions of x, γ, and β rays which depend on the spectrum of electrons traversing a material. However, the present work was undertaken primarily as a stepping stone to the theory of penetration and diffusion.

In the overwhelming majority of collisions a fast electron loses a minimal fraction of its energy. If larger energy losses were disregarded, the slowing down of electrons could be treated as a continuous process and the resulting spectrum would be simply the reciprocal of the stopping power (see, e.g., F, Sec. 3a). This solution of the problem is often accepted as self-evident. However, occasional large energy losses due to knock-on collisions against atomic electrons produce an error which has been discussed, but not calculated adequately, in F. This error is corrected in the present paper. It amounts to a few percent over most of the spectrum but becomes much larger in the portions of the spectrum near the source energy and at low energies. At high energies, bremsstrahlung emission makes the continuous slowing-down model unrealistic.

The probability of large energy losses by knock-on or by radiative collisions is given by rather complicated analytical formulas. Hence, the effects of these collisions should be treated, presumably, by numerical methods of direct integration similar to those employed in the x-ray problem.[4] On the other hand, the overwhelming number of small energy losses makes such a direct procedure unworkable (see also F, Sec. 3b). Therefore, our problem consists of developing a procedure suited to the contrasting requirements of large and of small energy losses.

This objective appears to have been achieved, and a few pilot calculations have been performed numerically. Source energies of $4mc^2$ and $80mc^2$ were considered, and aluminum and lead were chosen as representative materials. The calculations were performed by first disregarding and then taking into account the energy jumps due to bremsstrahlung. Knock-on collisions were first treated only as a source of large energy losses, but then also as additional sources of fast secondary electrons. For consistency, one should also include as sources the Compton and pair electrons generated by the bremsstrahlung and thereby solve the complete problem for a cascade shower; however, the application has not been carried that far. Some error has been

* Work supported by the U. S. Office of Naval Research and the U. S. Atomic Energy Commission.

[1] See, e.g., U. Fano, Phys. Rev. **92**, 328 (1953), which will be referred to as F.

[2] The following experimental arrangement may serve as a means of investigating the spectrum of slowed-down particles and of their secondaries, if any, which flow through a material loaded with a distributed source of particles. If a cavity is dug inside the material (the cavity being empty or filled with a gas of the same composition as the material), the flux in the cavity will be exactly the same as in the surrounding material, as shown in a general manner, by one of us [U. Fano, *Radiation Research* (to be published)]. A small aperture through the cavity walls will let through the same flux of radiation that would flow through an equal area within the material, except for edge effects which can be minimized. The emerging flux can be measured and analyzed.

[3] G. Placzek, Phys. Rev. **69**, 423 (1946); see also R. E. Marshak, Revs. Modern Phys. **19**, 185 (1947).

[4] P. R. Karr and J. E. Lamkin, Phys. Rev. **76**, 1843 (1949); the same procedure has been applied routinely in a large number of later applications.

incurred by disregarding the "Blunck-Leisegang correction."[5] This is discussed in the Appendix.

The numerical procedures were eventually so developed as to reduce the labor for each calculation to moderate proportions (see Sec. 8). Most of the remaining labor goes into the tabulation of collision cross sections; given these tabulations, some of the curves in Figs. 1–4 were calculated by one man in a day.

2. THE DEGRADATION EQUATION

Assuming that electrons are generated within a uniform infinite medium with initial energy T_0,[6] we inquire about the resulting spectrum $y(T)$ of electrons. Call $k(T,\tau)$ the probability per unit path length that an electron of energy T experiences an energy loss τ. The statistical balance of electrons of energy T is governed by the equation

$$y(T)\int_0^T k(T,\tau)d\tau=\int_0^\infty y(T+\tau)k(T+\tau,\tau)d\tau + S\delta(T_0-T), \quad (1)$$

with the boundary condition $y(\infty)=0$, where S represents the strength of the electron source and the Dirac δ represents the source spectrum.

The normalization of $y(T)$ depends on the physical situation and proves liable to misunderstandings. If the source is uniform in space and constant in time, S is expressed in particles cm^{-3} sec^{-1}; $y(T)$ is then expressed in particles cm^{-2} sec^{-1} $energy^{-1}$ and represents the flux of electrons of energy T traversing a small spherical probe per unit cross-sectional area of the probe, per unit time per unit energy range of the spectrum. The spectral density of electrons in space (particles cm^{-3} $energy^{-1}$) is given by $y(T)/v$, where v is the velocity corresponding to T. However, the time element is irrelevant and S may be expressed as particles cm^{-3} emitted at all times; $y(T)$ has then the dimensions particles cm^{-2} $energy^{-1}$ and represents the flux through the probe integrated over the time of traversal. The space element is irrelevant also, and S may represent the total number of particles emitted over the whole medium without regard to uniformity; $y(T)$ has then the dimensions cm $energy^{-1}$ and represents the track length covered by electrons of the stated energy, per unit energy range. This is actually the same quantity that is called differential track length in shower theory. This last normalization is adopted here, with $S=1$ (see also F, Sec. 2).

If the electron source is not monochromatic but generates $S(T)dT$ electrons of energies between T and $T+dT$, the expected value $y(T)dT$ of the track length traveled by all electrons between T and $T+dT$ is the solution of

$$y(T)\int_0^T k(T,\tau)d\tau=\int_0^\infty y(T+\tau)k(T+\tau,\tau)d\tau+S(T). \quad (2)$$

The degradation equation (1) or (2) determines $y(T)$ directly once $y(T+\tau)$ is known for all $\tau>0$. This circumstance leads one naturally to stepwise methods of solution, beginning with the highest source energy T_0, such that $y(T_0+\tau)$ vanishes, and progressing from high to low energies along the course of energy degradation. Direct numerical evaluation of the integrals in (1) is, however, not workable for electrons owing to the very steep increases of $k(T,\tau)$ for small τ. Therefore, one must, in this range, manage to exploit analytical properties of the equation.

3. GENERAL FEATURES OF THE PROBABILITY OF SMALL AND MODERATE ENERGY LOSSES

We shall consider separately the contributions to $k(T,\tau)$ from bremsstrahlung $k_b(T,\tau)$ and from collisions against atomic electrons $k_c(T,\tau)$. For small τ, the bremsstrahlung contribution is always comparatively unimportant and can anyhow be represented in a simple analytical form, such as

$$k_b(T,\tau)=a/\tau+A, \text{ for } \tau\ll T, \quad (3)$$

where a and A depend on T only. The collisions against atomic electrons yield a simple Rutherford contribution for values of τ much larger than the binding energy I of the electrons and much smaller than T or mc^2, namely,

$$k_c(T,\tau)=(2\pi N_e e^4/mv^2)/\tau^2=\kappa/\tau^2, \quad \tau\gg I, \quad \tau\ll T, \quad \tau\ll mc^2. \quad (4)$$

Here e and m are the charge and rest mass of an electron, N_e is the number of atomic electrons per unit volume of the material, and v is the speed corresponding to T.

For $\tau\sim I$, $k_c(T,\tau)$ does not have a simple analytical form. However, small energy losses τ can be treated, in effect, according to a continuous slowing-down model so that the detailed dependence of k_c on τ is irrelevant but only the total rate of energy dissipation in low-τ collisions, $\int_0^\tau \tau' k_c(T,\tau')d\tau'$, matters. Analytical treatments which take advantage of this circumstance are presented in the following sections.

Owing to (4), we can write

$$\int_0^\tau \tau' k_c(T,\tau')d\tau'=\kappa\ln(\tau/\bar{Q}), \quad \tau\gg I, \quad \tau\ll T, \quad \tau\ll mc^2, \quad (5)$$

where $\bar{Q}$ is a constant determined by the theory of stopping power which, for $v\ll c$, equals Bethe's $Q_{min}=(I_0Z)^2/2mv^2$, with $I_0\approx 10$ ev.[7] In so far as all relevant data on k_c for low τ are represented by (5), one may consider for analytical purposes that (4) holds down to $\tau=\bar{Q}$ and that k_c vanishes for $\tau<\bar{Q}$.

The preceding arguments do not hold as well for the

[5] O. Blunck and S. Leisengang, Z. Physik 128, 500 (1950).

[6] The letter T will serve to specify "kinetic energy."

[7] H. A. Bethe, *Handbuch der Physik* (Springer, Berlin, 1933), Vol. 24, Part 1, 491 ff; Ann. Physik 5, 325 (1930).

heaviest materials, where the binding energy of the K electrons is $\sim 0.2mc^2$ and there is hardly any range of τ for which the conditions of (3) are fully satisfied. (However, the K electrons in Pb are only 2 out of a total of 82.) This difficulty has been pointed out by Blunck and Leisegang[5] in connection with the Landau theory[8] of straggling of energy loss, which treats small energy losses in the manner indicated above. These authors gave a method for correcting the Landau theory. In the Appendix the size of the Blunck-Leisegang correction is estimated in connection with our results.

4. LANDAU-TYPE THEORY[9]

In order to learn how to solve the problem with regard to small energy losses without having yet to face the complications arising from the behavior of $k(T,\tau)$ for large τ, a solution of (1) was first sought in the range $T_0-T\ll T_0$, $T_0-T\ll mc^2$, $T_0-T\gg I$. Within this range one may perform the same simplifications as in the Landau theory,[8] i.e., assume $k(T,\tau)$ to be given by (4) from $\tau=\bar{Q}$ to $\tau=\infty$, and extend the integral on the left of (1) to $\tau=\infty$ since the resulting error is negligible. (See also F, Appendix V.) The equation becomes, then,

$$I(T_0-\Delta)\int_{\bar{Q}}^{\infty} d\tau/\tau^2=\int_{\bar{Q}}^{\Delta} I(T_0-\Delta+\tau)d\tau/\tau^2+\delta(\Delta), \quad (6)$$

where Δ represents T_0-T, and $I(T)$ represents $\kappa y(T)$.

The Laplace transform of $I(T)$ is then defined as follows:[10]

$$v(p)=\int_0^{\infty} d\Delta \exp(-p\Delta)I(T_0-\Delta). \quad (7)$$

Provided $\bar{Q}$ is effectively independent of T,[10] the transform of (6) is[11]

$$1=v(p)\int_{\bar{Q}}^{\infty} d\tau[1-\exp(-p\tau)]/\tau^2\approx v(p)p\ln(e/\gamma p\bar{Q}), \quad (8)$$

TABLE I. Comparison between approximate solutions to the Landau-type problem.

$(T_0-T)/\bar{Q}$	$I(T)$, expression (11)	$I(T)$, expression (24)
10	0.2069	0.2258
10^2	0.1435	0.1485
10^3	0.1086	0.1107
10^4	0.08718	0.08821
10^5	0.07272	0.07332
10^6	0.06235	0.06273

[8] L. Landau, J. Phys. (U.S.S.R.) 8, 201 (1944).
[9] U. Fano and L. V. Spencer, Phys. Rev. 91, 240 (1953).
[10] The possibility of incorporating the variable factor κ into the $I(T)$ extends the range of accuracy of the present calculation beyond that of the Landau theory. The limit of accuracy is now set by the assumed validity of (4) and the assumed constancy of $\bar{Q}$.
[11] The evaluation of the integral in this equation assumes that $p\bar{Q}\ll 1$, which is very well fulfilled for values of p of interest to this calculation.

with $e=2.718\cdots$ and $\gamma=1.781\cdots$. The solution of (6) is, therefore,[12]

$$I(T_0-\Delta)=(2\pi i)^{-1}\int_{c-i\infty}^{c+i\infty} dp \exp(p\Delta)/p\ln(e/\gamma p\bar{Q}). \quad (9)$$

Deformation of the path of integration to loop along the negative real axis yields

$$I(T_0-\Delta)=\int_0^{\infty}(du/u)\exp(-u)/[\pi^2+\ln^2(e\Delta/\gamma u\bar{Q})]$$

$$=\pi^{-1}\int_0^{\infty} du\exp(-u)\times\arctan[\pi/\ln(e\Delta/\gamma u\bar{Q})]. \quad (10)$$

Since $\ln u$ is small throughout the important range of the last integration, the arctangent can be expanded into powers of $\ln u$. Recalling that

$$\int_0^{\infty} du\exp(-u)\ln^n u=\Gamma^{(n)}(1),$$

the nth derivative of the gamma function at $x=1$, and setting $\bar{B}=\ln(e\Delta/\gamma\bar{Q})$, we find

$$I(T_0-\Delta)=\{\pi^{-1}\arctan(\pi/\bar{B})+\Gamma^{(1)}(1)/(\pi^2+\bar{B}^2)+\bar{B}\Gamma^{(2)}(1)/(\pi^2+\bar{B}^2)^2+\cdots\}. \quad (11)$$

This expansion converges very rapidly. A short tabulation of the bracketed quantity in (11) is given in the second column of Table I. Notice that, for $\bar{B}\gg\pi$, $y(T_0-\Delta)\approx 1/\kappa\bar{B}$, which is the reciprocal of the stopping power calculated by excluding all energy losses $\tau>e\Delta/\gamma$. This consideration, as well as an inspection of (9), illustrates the relationship of the result of this calculation to the prediction of the model of continuous slowing down. Notice also the rise of y for very small Δ indicating that the "effective stopping power" becomes quite small. This rise constitutes the "transient" discussed in F, Sec. 3c.

5. GENERAL ANALYTICAL TREATMENT

We now want to return to the general problem of formulating an equation which is amenable to numerical treatment. To do this we utilize an integral form which is equivalent to (1), namely,

$$\int_T^{T_0} dT'y(T')K(T',T)=1, \quad (12)$$

where

$$K(T',T)=\int_{T'-T}^{\infty} k(T',\tau)d\tau \quad (13)$$

expresses the probability per unit path that an electron's

[12] This equation results from Landau's Eqs. (5) and (10) by integrating $f(x,\Delta)$ over all values of the path length x.

kinetic energy drops from T' to a value *below* T. [It is implied, of course, that $k(T,\tau)$ vanishes for $\tau>T$.] Equation (12) states that the energy of every electron must drop below T somewhere along its path. The form (12) minimizes an undesireable feature of Eq. (1): the integral on the left side of (1) represents the total probability of collision, which is excessively large owing to the contribution of small energy losses but whose value is irrelevant since only the rate of energy dissipation through small losses matters. The integral cross section $K(T',T)$ in (12) is large only for a very small range of values of T' (very near to T) and thus does not contribute excessively to the integral.

The integral form of Eq. (2) is

$$\int_T^\infty dT'y(T')K(T',T)=\int_T^\infty S(T')dT'. \quad (14)$$

In order to simplify the integration over T' in the critical range $T'\approx T$, we strive to smooth out and reduce in magnitude the integrand in this range by adding and subtracting from (12) some suitable expression. We indicate with $\bar{K}(T',T)$ a function[13] to be chosen according to criteria indicated below and write

$$y(T)\int_T^{T_0} dT'\bar{K}(T',T)$$
$$+\int_T^{T_0} dT'[y(T')K(T',T)-y(T)\bar{K}(T',T)]=1. \quad (15)$$

Consider now the expression in brackets. As T' approaches T, $y(T')$ approaches $y(T)$ because it is a continuous function. The bracket will then tend to be small and finite, as T' approaches T, provided $\bar{K}(T',T)$ approximates $K(T',T)$ in this range. More specifically, we are interested in minimizing the integral over the difference between these expressions, in the critical range. Accordingly we set as a main consideration for the choice of $\bar{K}(T',T)$ that[14]

$$\int_T^{T+\delta} dT'[K(T',T)-\bar{K}(T',T)]=0,$$
$$\text{for } \delta\gg I,\ \delta\ll T,\ \delta\ll mc^2. \quad (16)$$

In terms of the differential cross section $k(T,\tau)$, this condition reads

$$\int_0^\delta \tau k(T+\tau,\tau)d\tau-\int_0^\delta \bar{K}(T+\delta,T)d\delta$$
$$=-\delta\int_\delta^\infty k(T+\delta,\tau)d\tau+\int_T^{T+\delta} dT'(T'-T)$$
$$\times\int_{T'-T}^{T'}[\partial k(T',\tau)/\partial T']d\tau. \quad (17)$$

[13] One may express $\bar{K}(T',T)$ in the form $\int_{T'-T}^{\infty}\bar{k}(T,\tau)d\tau$ and regard $\bar{k}(T,\tau)$ as a "mock cross section."

[14] The variation of κ between T and $T+\delta$, which is small owing to $\delta\ll T$, will often be disregarded in the following formulas.

The terms on the right side of (15) are small or of incidental significance. The first of them, which yields κ in the limit of small δ, materially improves the convergence of the numerical procedure; otherwise it could have been removed by modifying details of the condition (16). The essential point of the condition is that the integral over $\bar{K}(T',T)$ must approximate the other term on the left side of (17), namely the *stopping power, limited to small or moderate energy losses*. In addition, it will clearly be convenient that $\bar{K}(T',T)$ remain rather close to $K(T',T)$ even for $T'\gg T$ and that it be integrable analytically.

Setting

$$F(T_0,T)=\int_T^{T_0} dT'\bar{K}(T',T), \quad (18)$$

we recast (15) in the form

$$y(T)=[1/F(T_0,T)]$$
$$\times\left\{1-\int_T^{T_0} dT'[y(T')K(T',T)-y(T)\bar{K}(T',T)]\right\}, \quad (19)$$

which is suited to numerical integration. In fact, one may regard $1/F(T_0,T)$ as a first approximation estimate of $y(T)$. The first term on the right of (19), which is the largest one, represents indeed a reciprocal stopping power. The important point is then that the whole integral in the braces of (19) be much smaller than 1. Thus the structure of (19) lends itself also to an iteration procedure. In fact (19) can be integrated directly by numerical methods proceeding stepwise from high to low energies, as in the x-ray problem,[4] iteration being used to a minor extent in performing each integration step. The important conditions on the choice of $\bar{K}$, as stated before, are (1) that the numerical integration over T' be easy, and (2) that the whole integral over T' remain much smaller than 1.

6. A SIMPLE APPLICATION TO THE LANDAU-TYPE PROBLEM

As a first test of (19), this equation was solved under the assumption that the probability of energy losses is the same as in the Landau-type theory of Sec. 4, i.e., $k(T,\tau)=\kappa(T)/\tau^2$ for $\tau\gtrsim\bar{Q}$. Equation (13) yields, then,

$$\begin{aligned} K(T',T)&=\kappa(T')/(T'-T), \quad \text{for } T'-T\gtrsim\bar{Q},\\ K(T',T)&=K(T+\bar{Q},T), \quad \text{for } T'-T\lesssim\bar{Q}. \end{aligned} \quad (20)$$

We choose $\bar{K}(T',T)$, for this problem, as identical with $K(T',T)$ except for the replacement of $\kappa(T')$ with $\kappa(T)$, namely,

$$\begin{aligned} \bar{K}(T',T)&=\kappa(T)/(T'-T), \quad \text{for } T'-T\gtrsim\bar{Q},\\ \bar{K}(T',T)&=\bar{K}(T+\bar{Q},T), \quad \text{for } T'-T\lesssim\bar{Q}. \end{aligned} \quad (21)$$

Equation (18) yields, then,

$$F(T_0,T)=\kappa(T)\{1+\ln[(T_0-T)/\bar{Q}]\}. \quad (22)$$

If we enter (20), (21), and (22) into (19) and define, as in Sec. 4, $I(T)=\kappa(T)y(T)$, (19) reduces to

$$I(T)=\{1+\ln[(T_0-T)/\bar{Q}]\}^{-1}\times\left\{1-\int_0^{T_0-T}(d\tau/\tau)[I(T+\tau)-I(T)]\right\}. \quad (23)$$

A first approximation to $I(T)$ is obtained by neglecting the integral in comparison with unity

$$I(T)\approx\{1+\ln[(T_0-T)/\bar{Q}]\}^{-1}. \quad (24)$$

Table I compares $I(T)$ obtained from this expression with values for $I(T)$ obtained from (11). The agreement is excellent.[16] Further, expressions (24) and (11) can be shown to be asymptotically the same as (T_0-T) increases.

7. DISCUSSION OF CROSS SECTIONS

For the purpose of a realistic calculation, we have utilized cross sections with the following improvements with respect to the Landau-type theory. (1) The nonrelativistic Rutherford cross section for knock-on collisions has been replaced by the relativistic Møller formula. The energy loss is limited to $\tau\leqslant T/2$ for electrons of energy T since an electron emerging from a knock-on collision with energy lower than $T/2$ is classified as a secondary. (2) Energy losses by bremsstrahlung have been added. (3) The production of secondary electrons has been entered as an additional source on the right side of (14). Notice that the production of secondaries of energy T depends upon the presence of primaries of energy greater than $2T$ and therefore on previous determination of $y(T')$ for $T'>2T$.

For very small energy losses the Møller formula has been arbitrarily assumed to remain valid down to $\tau=\bar{Q}$ for the reasons discussed in Sec. 3, thus causing the small error considered in the Appendix.

A. Probability of Knock-on Collisions

The probability of collisions with energy loss τ, according to the Møller relativistic calculation,[16] may be written

$$k_M(T,\tau)=(2\pi N\mathscr{r}_0^2/\beta^2)\{\tau^{-2}+(T-\tau)^{-2}-[(2+T^{-1})/(T+1)^2]\times[\tau^{-1}+(T-\tau)^{-1}]+(T+1)^{-2}\}, \quad (25)$$

for $\tau\leqslant T/2$, where T and τ are in mc^2 units, $\mathscr{r}_0=e^2/mc^2$ and $\beta=v/c=[T(T+2)]^{\frac{1}{2}}/(T+1)$. As in Secs. 3 and 6 we assume this law to hold for small τ down to $\tau=\bar{Q}$, where $\bar{Q}$ is chosen so as to give the correct stopping power, limited to moderate energy losses. The value of $\bar{Q}$ was chosen, on the basis of stopping power theory,[7] supplemented by experimental data, as

$$\bar{Q}=\tfrac{1}{2}(ZI_0/mc^2)^2[T(T+2)]^{-1}\exp(\beta^2), \quad (26)$$

in units of mc^2, with I_0 equal to 11.5 ev for Al and to 10.2 ev for Pb. This value of $\bar{Q}$ fails to take into account the density effect, a simplification which seemed warranted in a pilot calculation.[17]

According to (13), the contribution of collisions to $K(T',T)$ is, then,

$$K_c(T',T)=0, \quad \text{for } T'\geqslant 2T,$$

$$K_c(T',T)=\int_{T'-T}^{T'/2}k_M(T',\tau)d\tau=(2\pi N\mathscr{r}_0^2/\beta'^2)\{(T'-T)^{-1}-T^{-1}-[(2+T'^{-1})/(T'+1)^2]\ln[T/(T'-T)]+(T'+1)^{-2}(T-T'/2)\}, \quad (27)$$

$$\text{for } T+\bar{Q}\leqslant T'\leqslant 2T,$$

$$K_c(T',T)=K_c(T+\bar{Q},T), \quad \text{for } T'\leqslant T+\bar{Q}.$$

For the corresponding function $\bar{K}_c(T',T)$ we took

$$\bar{K}_c(T',T)=0, \quad \text{for } T'\geqslant 2T,$$

$$\bar{K}_c(T',T)=(2\pi N\mathscr{r}_0^2/\beta^2)\{(T'-T)^{-1}-T^{-1}-[(2+T^{-1})/(T+1)^2]\ln[T/(T'-T)]+(T+1)^{-2}(T-T'/2)\}, \quad \text{for } T+\bar{Q}\leqslant T'\leqslant 2T, \quad (28)$$

$$\bar{K}_c(T',T)=\bar{K}(T+\bar{Q},T), \quad \text{for } T'\leqslant T+\bar{Q}.$$

The contribution to $F(T_0,T)$ arising from $\bar{K}_c(T',T)$ is

$$F(T_0,T)=\int_T^{T_0}dT'\bar{K}_c(T',T)=(2\pi N\mathscr{r}_0^2/\beta^2)\{1+\ln(\Delta/\bar{Q})-\Delta/T-[(2+T^{-1})/(T+1)^2]\Delta[1+\ln(T/\Delta)]+(T+1)^{-2}(\Delta/2)(T-\Delta/2)\}, \quad (29)$$

where Δ equals T_0-T or T, whichever is smaller, and terms of the order of $\bar{Q}$ have been disregarded in the braces.

B. Production of Secondary Electrons

The Møller expression (25), $k_M(T,\tau)$, also represents the probability of production of secondary electrons of energy $T-\tau$ when evaluated for $\tau>T/2$. Therefore, the additional "source" of secondary electrons, to be entered as $S(T')$ in (14) is given by $\int_{2T'}^{\infty}dT''y(T'')$

[16] A second approximation can easily be calculated by inserting the approximate solution (24) into the integral in (23). This second approximation, which agrees to at least four significant figures with column 1 of Table I, in the following:

$$I(T)\approx\{1+\ln(\Delta/\bar{Q})\}^{-1}\{1-(\pi^2/6)[1+\ln(\Delta/\bar{Q})]^{-2}\},$$

where $\Delta=T_0-T$.

[16] C. Møller, Z. Physik 70, 686 (1931).

[17] Owing to the density effect, $\bar{Q}$ should not decrease indefinitely as T increases but should approach the minimum value $2\pi e(137)^2N\mathscr{r}_0^3$, with $e=2.71828\cdots$.

$\times k_M(T'', T''-T')$. When this expression is entered in (14) together with the "true" source $S(T')=\delta(T'-T_0)$ we find, by changing the order of integrations,

$$\int_T^\infty S(T')dT' = 1+\int_{2T}^{T_0} dT' y(T') K_s(T',T), \quad \text{for } T<T_0/2, \quad (30)$$

where

$$K_s(T',T)=\int_{T'/2}^{T'-T} k_M(T',\tau)d\tau$$
$$=(2\pi N_a r_0^2/\beta'^2)\{T^{-1}-(T'-T)^{-1}$$
$$-[(2+T'^{-1})/(T'+1)^2]\ln[(T'-T)/T]$$
$$+(T'+1)^{-2}(T'/2-T)\}. \quad (31)$$

Notice that $k_M(T,\tau)=k_M(T,T-\tau)$, and $K_s(T',T)=\int_T^{T'/2}k_M(T',\tau)d\tau$.

C. Bremsstrahlung Energy Losses

The cross section for energy losses by bremsstrahlung has been calculated by Bethe and Heitler.[18] This treatment relies upon the Born approximation and yields a cross section of the form

$$k_b(T,\tau)=(ZN_a r_0^2/137)[28.1-(16/9)\ln Z]$$
$$\times[T/(T+1)][\tau^{-1}-f(T,\tau)], \quad (32)$$

where T,τ are in mc^2 units and $f(T,\tau)$ is a positive function, containing no singularity, which is known only numerically.[19] Since $k_b(T,\tau)$ vanishes for $\tau>T$ the integral (13) over this cross section yields

$$K_b(T',T)=(ZN_a r_0^2/137)[28.1-(16/9)\ln Z]$$
$$\times[T'/(T'+1)]\left\{\ln[T'/(T'-T)]-\int_{T'-T}^{T'} d\tau f(T',\tau)\right\}. \quad (33)$$

Since $K_c(T',T)$ vanishes for $T'>2T$, according to (27), and since $K_b(T',T)$ is small in the same range of $T'>2T$, it is possible and, in fact, convenient, to modify again the integral of Eq. (14). We limit the integral on the left side to $T\leqslant T'\leqslant 2T$ and transfer the remaining portion,[9] $\int_{2T}^\infty y(T')K_b(T',T)dT'$ to the right side, to be treated in effect as a "negative source."

Following this idea, we take

$$\bar{K}_b(T',T)=0, \quad \text{for } T'>2T,$$
$$\bar{K}_b(T',T)=(ZN_a r_0^2/137)[28.1-(16/9)\ln Z]$$
$$\times[T/(T+1)]\left\{\ln[T'/(T'-T)]-\int_{T'-T}^{T'} d\tau f(T',\tau)\right\}, \quad \text{for } T'<2T, \quad (34)$$

and, therefore,

$$F_b(T_0,T)=\int_T^{T_0} dT' \bar{K}_b(T',T)$$
$$=(ZN_a r_0^2/137)[28.1-(16/9)\ln Z]$$
$$\times[T/(T+1)]\left\{\Delta\ln[(\Delta+T)/\Delta]\right.$$
$$+T\ln[(\Delta+T)/T]$$
$$\left.-\int_T^{T+\Delta} dT'\int_{T'-T}^{T'} d\tau f(T',\tau)\right\}, \quad (35)$$

where Δ equals T_0-T or T, whichever is smaller, as in (29). In the integrations over $f(T',\tau)$, the approximate analytical expressions by Schiff[20] were entered instead of the numerical tables of Bethe and Heitler.

D. Final Form of the Equation

We combine the preceding formulas by setting

$$K(T',T)=K_c(T',T)+K_b(T',T), \quad \text{for } T'\leqslant 2T, \quad (36)$$
$$\bar{K}(T',T)=\bar{K}_c(T',T)+\bar{K}_b(T',T), \quad \text{for } T'\leqslant 2T, \quad (37)$$
$$K^*(T',T)=K_s(T',T)-K_b(T',T), \quad \text{for } 2T\leqslant T'\leqslant T_0, \quad (38)$$
$$F(T_0,T)=F_c(T_0,T)+F_b(T_0,T), \quad (39)$$

where K_c, $\bar{K}_c$, K_s, K_b, $\bar{K}_b$, F_c, and F_b are given, respectively, by (27), (28), (31), (33), (34), (29), and (35). We take (30) as the source term and treat the large bremsstrahlung losses as a "negative source," as explained above. Equation (19) takes now the form

$$y(T)=[F(T_0,T)]^{-1}\left\{1+\int_{2T}^{T_0} dT' K^*(T',T)y(T')\right.$$
$$\left.-\int_T^{T+\Delta} dT'[y(T')K(T',T)-y(T)\bar{K}(T',T)]\right\}, \quad (40)$$

where Δ equals T_0-T or T, as before.

8. SOME DETAILS OF THE CALCULATION

The usual method for solving numerically a Volterra integral equation like that of expression (40) involves writing finite sums for the integrals. This reduces the integral equation to a triangular system of linear equations which can be easily solved in succession. A set of points T_i must be chosen, one per interval of integration, at which the integrand is evaluated. A suitable integration formula must likewise be selected (e.g., trapezoidal, Simpson's Rule). The first step in the integration (i.e., the first linear equation) often requires special attention.

[18] H. Bethe and W. Heitler, Proc. Roy. Soc. (London) **A146**, 83 (1934).

[19] Notice that bremsstrahlung in the field of an electron has not been included in (32).

[20] L. I. Schiff, Phys. Rev. **83**, 252 (1951).

In our calculations the T_i were distributed evenly on a scale of $\log T$, that is, according to the formula T_0, ζT_0, $\zeta^2 T_0$, etc. There were three reasons for this: (1) the population of secondary electrons might increase so rapidly at low energies that the solution would diverge, perhaps as some inverse power of T, as $T\to 0$. If this happened, the integration could nevertheless proceed owing to the smaller and smaller intervals of T. (2) The choice of ζ according to $\zeta^n=\frac{1}{2}$, where n is an integer, would enable us to take into account very simply the special behavior at $T'=2T$. (3) Owing to the logarithmic distribution, the same set of points is equally suited to different primary energies.

As a first trial, ζ was chosen so that $\zeta^3=\frac{1}{2}$. (Too small a value for ζ means coarse intervals which tend to yield inaccurate results. On the other hand, a ζ near unity means many steps and a long calculation. We decided that for the first calculation it would be better to err in the direction of small ζ.) Fortunately, later experience indicated that this was a fairly good choice, and most of the calculations were accomplished using this interval.

For an integration formula we took Simpson's Rule which means approximation by parabolas. Simpson's Rule is especially suited to an even number of integration intervals as well as to *equal-sized* intervals. We therefore modified Simpson's Rule to apply to equal-sized intervals in a logarithmic sense. Where the number of integration intervals was odd, we fitted the last two intervals with a parabola and integrated this parabola over the last interval only.

For the first calculations we tabulated $K(T',T)$, $\bar{K}(T',T)$, and $K^*(T',T)$, neglecting the bremsstrahlung part, from $T_0=80$ (in mc^2 units) to $T=1.25$. (Later this was extended to $T=0.0124$.) In these tabulations the points $T'=T$ were left blank, since for $T'\to T$,

$$[y(T')K(T',T)-y(T)\bar{K}(T',T)]\to (\partial/\partial T)\{2\pi N_a r_0^2 y(T)/\beta^2\}. \quad (41)$$

(See the Appendix.)

While accomplishing the first solutions, we tabulated the quantity $[y(T')K(T',T)-y(T)\bar{K}(T',T)]$ for each step $T=T_n$ in order to make sure that it is sufficiently well behaved to allow an accurate evaluation of the integral over T' by our numerical integration scheme. We also decided to use a step-by-step iteration scheme as follows. Having determined $y(T)$ at T_0, T_1, $\cdots T_{n-1}$ we estimated what $y(T_n)$ will be. Making use of this, we then tabulate the quantity $[y(T')K(T',T)-y(T)\bar{K}(T',T)]$ for $T=T_n$, and for $T'=T_n$, T_{n-1}, T_{n-2}, T_{n-3}.[21] We then evaluate the integral and thereby obtain from (40) a new estimate of $y(T_n)$. These estimates converge extremely rapidly to a unique value.

The remaining questions concern the start of the integration from $T\sim T_0$. The approximate solutions (24) and (11) are accurate near T_0 and can be used to give nearly correct values for the $y(T_i)$ for T_i near T_0. Unfortunately, $y(T)$ has a peak of logarithmic type at T near T_0. However, this peak contributes a negligible amount to the integral. In most calculations it was found adequate to clip off the peak at the level of $y(0.95T_0)$, the more so since the integral of $[y(T')K(T',T)-y(T)\bar{K}(T',T)]$ is very small compared with unity near T_0. For greater accuracy at the beginning of the calculation an extra point was inserted between T_0 and ζT_0.

[21] To calculate the derivative in (41) we merely fitted a parabola to the points T_n, T_{n-1}, and T_{n-2} and differentiated. This proved adequate because the solution is not very sensitive to the value of the derivative.

9. FURTHER DETAILS—BREMSSTRAHLUNG

Calculations involving bremsstrahlung have two unpleasant features: (1) the quantity $\int_{T'-T}^{T'} f(T',\tau)d\tau$ must be tabulated, and (2) the approximate solution, $1/F(T_0,T)$, is less accurate than in calculations not involving bremsstrahlung.[22]

To tabulate the quantity $\int_{T'-T}^{T'} f(T',\tau)d\tau$, we established a fairly coarse grid of values of $f(T',\tau)$. We then carried out the integration numerically by fitting parabolas. Finally, we did a double interpolation, first in the variable $(1-T/T')$ and then in the variable T', in order to establish the table needed for the solution of the integral equation.[23] The tabulations were not carried below $T=1.25mc^2$. At this energy the sudden omission of bremsstrahlung introduces a discontinuity in $y(T)$ which amounts to about 5 percent in Pb and to less than 1 percent in Al. We made a rough extrapolation of the bremsstrahlung correction for energies somewhat lower than $1.25mc^2$ in order to reduce the discontinuity in Pb to a smaller value.

In problems involving bremsstrahlung, the integration was started at energies so near T_0 that bremsstrahlung modified the $y(T)$ given by expressions (24) and (11) by no more than a percent or so. In the $80mc^2$ Pb problem, this meant setting $T_1/T_0\approx 0.998$. Thereafter, to expand the interval of integration, the T_i's were distributed uniformly in a scale of $\log(T_0-T)$. In order to join this system of exponentially increasing intervals with the set of *decreasing* intervals previously established for lower energies, the last of the increasing intervals was arranged to coincide with the interval $\zeta T_0 \geq T \geq \zeta^2 T_0$, i.e., with the second interval of the set discussed in the preceding section. This procedure proved workable because $1/F(T_0,T)$ is always a fairly good estimate of $y(T)$ for $T>T_0/2$.

An appropriate integration formula was established for this rather unusual sequence of intervals, a weight being assigned to each pair of values (T',T).

[22] For example, in the $80mc^2$ calculation with bremsstrahlung in Pb, $y(T)$ and $1/F(T_0,T)$ differ by as much as 12 percent, whereas neglecting bremsstrahlung they differ by no more than a percent or so.

[23] The tabulation of $f(T',\tau)$ for Pb utilized the spectrum of Schiff with $\theta_0=0$. The $f(T',\tau)$ so obtained was normalized to agree with that of Bethe and Heitler at $\tau=0$. This procedure appeared justified by expedience in a first pilot calculation. The tabulation for Al used the Schiff spectrum integrated over all angles.

As mentioned previously, much of the numerical work involves tabulating and integrating numerically the function $[y(T')K(T',T)-y(T)\bar{K}(T',T)]$. Having determined that this is a reasonably well-behaved function, the integrals $\int_T^{T_0-2T}dT'y(T')K(T',T)$ and $\int_T^{T_0-2T}dT'\bar{K}(T',T)$ were calculated separately, using the same integration weights for both integrals and assuming that the first integrand is

$$(\partial/\partial T)[2\pi N_s r_0^2 y(T)/\beta^2]$$

at $T'=T$, whereas the second integrand is zero at that point. This separation makes it possible to perform first the integrations and then independently the determination of $y(T_0)$.

TABLE II. Comparison between $y(T)$ and the reciprocal stopping power neglecting both bremsstrahlung and secondary electrons.

T, mc^2 units	Reciprocal stopping power, Pb	$y(T)$, Pb	Reciprocal stopping power, Al	$y(T)$, Al
79.86	0.0293	0.0366	0.0892	0.1065
63.50	0.0302	0.0304	0.0914	0.0921
50.40	0.0310	0.0307	0.0936	0.0927
40.00	0.0319	0.0314	0.0960	0.0947
20.00	0.0350	0.0344	0.1039	0.1024
10.00	0.0385	0.0378	0.1126	0.1109
5.00	0.0421	0.0414	0.1211	0.1192
2.50	0.0448	0.0440	0.1263	0.1242
1.25	0.0443	0.0433	0.1218	0.1195
0.625	0.0387	0.0379	0.1037	0.1020
0.3125	0.0295	0.0290	0.0769	0.0757
0.1563	0.0203	0.0199	0.0510	0.0502
0.07813			0.0318	0.0310
0.03906			0.0193	0.0186
0.01953			0.0116	0.0110

TABLE III. Comparison between $y(T)$ and the reciprocal stopping power when bremsstrahlung is included but secondary electrons are not.

T, mc^2 units	Reciprocal stopping power, Pb	$y(T)$, Pb	Reciprocal stopping power, Al	$y(T)$, Al
79.86	0.00584	0.0336	0.0555	0.1065
63.50	0.00703	0.00704	0.0617	0.0658
50.40	0.00853	0.00668	0.0679	0.0633
40.00	0.0104	0.00779	0.0740	0.0664

10. DISCUSSION OF RESULTS

Tables II and III and Figs. 1 through 4 summarize the results of our calculations. In all tables and figures the differential track length in units of cm/mc^2 is presented as a function of the electron kinetic energy in mc^2 units.

Each of the Figs. 1 through 4 presents the electron slowing down spectra calculated with different refinements, namely, neglecting both secondary electrons and bremsstrahlung (curve I), neglecting only the bremsstrahlung (curve II), and including both bremsstrahlung and secondary electrons (curve III). In Fig. 4 the bremsstrahlung influence is so small that curves II and III coincide. In all figures curves I and II coincide

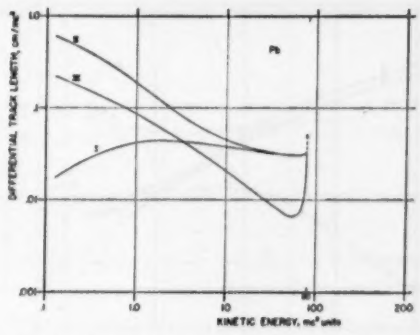

FIG. 1. Electron slowing-down spectra for an $80mc^2$ source in Pb.

at energies higher than one-half the initial energy since all secondaries have energies less than one half the initial energy.

A comparison of curves I and II shows the buildup of secondary electrons. All four figures indicate that neglecting bremsstrahlung the secondary electrons become as numerous as the primary electrons at about 4 percent of the initial energy. There are 10 percent as many secondaries as primaries at about 16 percent of the initial energy. Notice also that at the lowest energies there are up to 300 times as many secondary electrons as there are primary electrons.

A comparison of curves II and III demonstrates the influence of bremsstrahlung. This is overwhelming at high energies in Pb and negligible at low energies in Al. Bremsstrahlung has been treated only as a mechanism for energy loss and electrons resulting from cascade processes have *not* been included.

Notice that curves II and III tend to separate at energies at which the secondaries begin to dominate ($\sim 1mc^2$ for the $80mc^2$ source problems). This is because the generation of secondaries of energy T depends upon the spectrum at energies greater than $2T$. In the bremsstrahlung calculations there are always fewer electrons

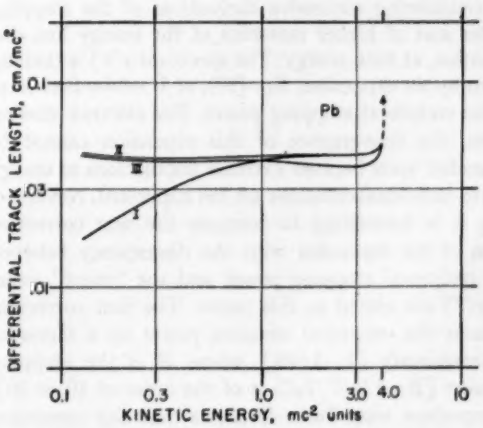

FIG. 2. Electron slowing-down spectra for a $4mc^2$ source in Pb.

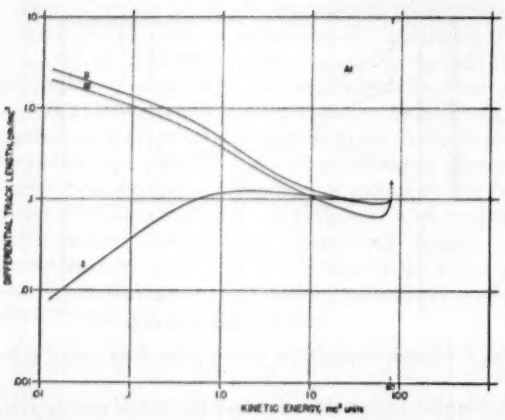

FIG. 3. Electron slowing-down spectra for an $80mc^2$ source in Al.

at high energies than in the bremsstrahlung-neglected calculations, hence fewer secondaries are generated and the spectrum at low energies rises somewhat more slowly. On the other hand, at *very* low energies curves II and III tend to become parallel, indicating an approach to an equilibrium spectrum.

Table II compares spectra (which do not involve secondary electrons or bremsstrahlung) with the reciprocal stopping power, which is the spectrum obtained on the assumption that the electrons lose their energy continuously. The model of continuous slowing down disregards the possibility that an electron loses much energy in a single process and thereby overlooks the interlinkage between the values of $y(T)$ for different values of T. It stands to reason that this oversimplification will not have drastic effects in regions of the spectrum where $y(T)$ remains fairly constant. The data in Table II verify this surmise.

The model of continuous slowing down was improved in F, Sec. 5, by a procedure of successive approximations. This procedure takes partial account of the interlinkage between different portions of the spectrum by considering successive derivatives of the stopping power and of higher moments of the energy loss distribution, at each energy. The spectrum $y(T)$ is thereby given by an expansion, Eq. (30), of F whose first term is the reciprocal stopping power. For electron slowing down, the convergence of this expansion cannot be depended upon because extreme fluctuations of energy loss in individual collisions are too important. Nevertheless, it is interesting to compare the first corrective term of the expansion with the discrepancy between the reciprocal stopping power and the "exact" value of $y(T)$ calculated in this paper. The first correction reduces the reciprocal stopping power by a factor of approximately $[1-1/4B]$, where B is the stopping number $[B\sim 2\ln(T/I_0Z)$ is of the order of 10 or 20]. Comparison with Table II shows that this correction has the proper sign and order of magnitude for most values of T and displays the increasing trend of the discrepancy at lower values of T. The large discrepancy between the reciprocal stopping power and $y(T)$ in the upper portion of the spectrum derives from the "transient" effect for which no allowance was made in Eq. (30) of F.

Table III gives a comparison similar to that of Table II between the reciprocal stopping power and $y(T)$ when bremsstrahlung is included in the calculation. As in Table II, the continuous slowing down model gives a low value in the transient range, near T_0, and a high value in the broad range of lower energies. However, in this range, the discrepancy is quite large, when bremsstrahlung is important, as expected in view of the extreme type of energy fluctuations that is characteristic of the bremsstrahlung process.

We wish to thank Miss Ida E. Hornstein and Mr. John Hubbell for much help in the numerical work.

APPENDIX

The Blunck-Leisegang correction concerns the evaluation of the integral of $[y(T')K(T',T)-y(T)K(T',T)]$ for $T'\sim T$ in (19). We rewrite this expression in the form

$$[y(T')-y(T)]K(T',T)+y(T)[K(T',T)-\bar{K}(T',T)]. \tag{42}$$

The second bracket in this expression can be taken as zero at $T'=T$ owing to the condition (16).[14] Since $K(T',T)$ peaks near $T'=T$, the first bracket in (42) must be replaced with $[dy(T)/dT](T'-T)$ for $T'\sim T$. (Higher-order terms in the expansion of $y(T')-y(T)$ are not significant in this approximation.) Since the important quantity is not (42) itself but its integral over a range of T' near T we calculate, as in (17),

$$\left(\frac{dy}{dT}\right)\int_T^{T+\delta} dT'(T-T')K(T',T)$$

$$=\frac{1}{2}\left(\frac{dy}{dT}\right)\left\{\int_0^{\delta}\tau^2 k(T+\tau,\tau)d\tau + \delta^2\int_{\delta}^{T+\delta} k(T+\delta,\tau)d\tau - \int_T^{T+\delta} dT'(T'-T)^2 \times\int_{T'-T}^{T'}[\partial k(T',\tau)/\partial T']d\tau\right\}. \tag{43}$$

For the purpose of evaluating the integral in (19) we are interested only in those terms of (43) that are small of order δ as δ grows smaller. The last term in the braces of (43) is, accordingly, negligible. The second term in the braces yields $\kappa(T)\delta$, if one assumes k to be given by (4) for the relevant values of the variables.[14] With regard to the first term, we have been assuming since Sec. 3 that $k(T,\tau)$ is represented adequately by (4) also

for low values of τ when it is multiplied by τ^n, with $n>1$, and integrated. Under this assumption, the first term in the braces yields $\kappa(T)\delta$, like the second term, and the total value of (43), to within δ^2 corrections, is $(dy/dT)\kappa(T)\delta$, which justifies (41).[14]

The Blunck-Leisegang correction consists in evaluating $\int_0^\delta \tau^2 k(T+\tau,\tau)d\tau$ to a better accuracy than is done by taking k according to (4). The following evaluation is believed to represent an improvement with respect to the rough estimation given by the original authors.

The collision probability is given, for low or moderate τ, by the Bethe formula[7]

$$k(T,\tau)=\kappa\int_{Q_{\min}}^{Q_{\max}}|F_\tau(Q)|^2 dQ/Q^2. \tag{44}$$

Here, $|F_\tau(Q)|^2$ represents the generalized form factor, i.e., the probability that an atom absorbs the energy τ when one of its electrons has absorbed the momentum corresponding to a free recoil energy Q. Since, for large Q, $|F_\tau(Q)|^2\sim\delta(Q-\tau)$, and since $Q_{\min}$, which depends on τ, may be replaced with an effective value $\bar{Q}$, we have with adequate accuracy

$$\int_0^\delta \tau^2 k(T+\tau,\tau)d\tau\sim\kappa\int_{\bar{Q}}^\delta dQQ^{-2}\int_0^\infty |F_\tau(Q)|^2\tau^2 d\tau. \tag{45}$$

The last integral over τ can be evaluated by a closure theorem (sum rule) and yields $Q^2+(4/3)Q\langle T\rangle_{\text{at}}$, where $\langle T\rangle_{\text{at}}$ is the mean kinetic energy of the atomic electrons. When this expression is entered in (45), the first term Q^2 yields the same result that was obtained by taking $k(T,\tau)$ according to (4) instead of (44). The second term, $(4/3)Q\langle T\rangle_{\text{at}}$, yields the desired correction. We have then

$$\int_0^\delta \tau^2 k(T+\tau,\tau)d\tau\sim\kappa[\delta+(4/3)\langle T\rangle_{\text{at}}\ln(\delta/\bar{Q})], \tag{46}$$

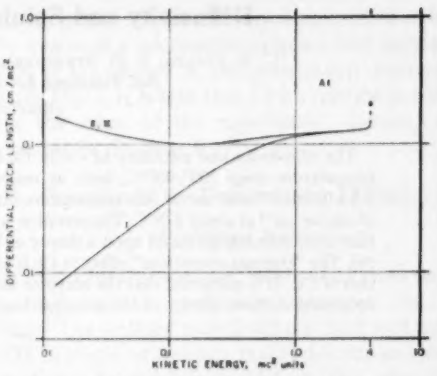

FIG. 4. Electron slowing-down spectra for a $4mc^2$ source in Al.

where $\bar{Q}$ has been disregarded as compared to δ. Thus, recalling (42) and (43), we find that the integral in (19) has been underestimated, in the range $T'\sim T$, by an amount approximately equal to

$$\tfrac{1}{2}(dy/dT)\kappa(4/3)\langle T\rangle_{\text{at}}\ln(\delta/\bar{Q}). \tag{47}$$

This quantity may be expressed, according to (5), in terms of the stopping power of nonradiative collisions

$$(2/3)(dy/dT)\langle T\rangle_{\text{at}}\int_0^\delta k_c(T,\tau)\tau d\tau. \tag{48}$$

The residual dependence of (47) and (48) on δ indicates that the departures from the free-electron collision formula (4) due to the bound motion of atomic electrons cause our earlier evaluation of (19) to be somewhat in error even for T' substantially larger than T. The total error is given approximately by (48) with the integral replaced with the full stopping power of nonradiative collisions. Therefore, it is clearly of the order of magnitude of the relative variation of $y(T)$ over a spectral interval $\langle T\rangle_{\text{at}}$. According to the Thomas-Fermi model $\langle T\rangle_{\text{at}}$ is of the order of $10Z^{4/3}$ ev.

Diffusivity and Solubility of Copper in Germanium

C. S. Fuller, J. D. Struthers, J. A. Ditzenberger, and K. B. Wolfstirn
Bell Telephone Laboratories, Murray Hill, New Jersey

(Received December 2, 1953)

The diffusivity and solubility of Cu in Ge have been investigated as a function of temperature in the temperature range 700°–900°C, both by resistivity and radio-activity methods. The average diffusivity is $2.8\pm0.3\times10^{-6}$ cm²/sec in this temperature interval. The solubility shows a maximum of 4.0×10^{16} atoms of copper cm^{-3} at about 875°C. The precision is not sufficient to determine an activation energy for diffusion. However, calculations based upon a theory of Wert and Zener, indicate an activation energy of about 4000 cal. The "thermal conversion" effect in Ge is explained by a temperature-dependent solution and precipitation of Cu. It is suggested that the acceptor and diffusional properties of Cu in Ge can be accounted for by decreased electron affinity of Cu at higher temperatures.

INTRODUCTION

DURING the development of germanium rectifiers, Scaff and Theuerer[1] found that it was possible to modify reversibly the electrical conductivity of germanium by heat treatment. Later, they carried out a more detailed study[2] of this phenomenon, which they termed "thermal conversion." They proposed that their observations could be explained either by a change in solubility of an acceptor impurity or of lattice defects introduced by the heat treatment.

More recent experiments by Fuller, Theuerer, and van Roosbroeck[3] established the additional fact that thermal conversion is attended by rapid diffusion of a *p-n* boundary from the germanium surface into the interior when *n*-type germanium of resistivity above approximately 1 ohm cm is heated to conversion temperatures. They determined the rate of diffusion and the solubility of a postulated acceptor, termed "thermal acceptor," as a function of temperature.

Still later work by one of the authors established by means of surface cleaning procedures that the thermal acceptor was usually present on the surface as an impurity and that surface cleaning prevented or greatly retarded the conversion of high-resistivity germanium. Attempts to find surface impurities which would reproduce the effects observed, pointed strongly to copper as the acceptor impurity.[4,5] This identity was securely established by means of experiments carried out by Fuller and Struthers[6] through the use of radioactive copper-64.

The purpose of this article is to give more precise results on the solubility and the diffusivity of copper in germanium and to show how these results are able to account for the changes which occur in the resistivity of germanium upon heat treatment. Two methods of determining diffusivity, one based on the measurement of electrical resistivity[7] and the other on radioactive copper, are described and the results compared. In Sec. II methods for determining the solid solubility of copper are described and results given. A discussion of the role of copper in the "thermal conversion" effect is given in Sec. IV. A discussion of the results is given in Sec. V which shows good agreement with the theory of interstitial diffusion proposed by Wert and Zener (see reference 24). An anomaly between the electrical and diffusional behavior of copper is discussed on the basis of recent results on the mobility of copper ions in germanium. The final quantitative results presented for the diffusivity differ appreciably from those previously given.[3]

I. DIFFUSION OF COPPER IN GERMANIUM

The diffusivity of copper in germanium has been determined by two independent methods. One is based on electrical resistance and assumes that each copper atom contributes a constant number of carriers. The other makes use of radioactive copper-64 and involves no assumptions. As will be shown, the agreement between the two methods is well within the estimated errors.

A. Test of Fick's Law

When the times required to reach a fixed arbitrary copper concentration c are determined at successively greater distances, Fick's second law, $\partial c/\partial t = D\partial^2 c/\partial x^2$, requires that x vary linearly with the square root of the time t. The movement of a *p-n* junction in a slab of *n*-type Ge of homogeneous resistivity enables this

[1] H. C. Torrey and C. A. Whitmer, *Crystal Rectifiers* (McGraw-Hill Book Company, Inc., New York, 1948), pp. 365–67.
[2] H. C. Theuerer and J. H. Scaff, J. Metals **191**, 59 (1951).
[3] Fuller, Theuerer, and van Roosbroeck, Phys. Rev. **85**, 678 (1952).
[4] This work also showed that water, except for carefully distilled samples, contained sufficient impurity to convert high-resistivity germanium.
[5] Experiments by W. P. Slichter and E. D. Kolb, Phys. Rev. **87**, 526 (1952), likewise showed similar effects of impurities, notably copper, on the surface of Ge. Recently, Seiler, Geist, Keller, and Blank, Naturwiss. **40**, 56 (1953) have found a surface impurity to be responsible for thermal conversion. Cu is mentioned as a possibility. Recent experiments by R. A. Logan, Phys. Rev. **91**, 757 (1953), have further confirmed the role of copper as a surface impurity. See also George Finn, Phys. Rev. **91**, 754 (1953); W. C. Dunlap, Jr., Phys. Rev. **87**, 190 (1952); S. Mayburg and L. Rotondi, Phys. Rev. **91**, 1015 (1953).
[6] C. S. Fuller and J. D. Struthers, Phys. Rev. **87**, 526 (1952).
[7] Variations of this method are given in references 3 and 26. See also R. N. Hall and W. C. Dunlap, Jr., Phys. Rev. **80**, 467 (1950); W. C. Dunlap, Jr., Phys. Rev. **87**, 615 (1952).

one-dimensional relation to be tested for copper. This is because the p-n junction marks a boundary at which the electron concentration just equals the hole concentration introduced by the copper atoms. The carrier concentration is simply derived from the relation

$$1/\rho = q(n\mu_n + p\mu_p), \tag{1}$$

in which ρ = resistivity in ohm cm; $q = 1.60 \times 10^{-19}$ coulombs; n,p = number of electrons or holes per cm^3, respectively; μ_n,μ_p = mobility of electrons or holes in cm^2/volt sec, respectively. Since for our purposes the minority carrier concentration is negligible compared to the majority carrier concentration, (1) may be written,

$$1/\rho_n = qn\mu_n, \tag{2}$$

$$1/\rho_p = qp\mu_p, \tag{3}$$

where now ρ_n and ρ_p are the resistivities of n-type and p-type germanium, respectively. The mobilities,[8] μ_n and μ_p at 25°C, the temperature of measurement, were taken as 3900 and 1900 cm^2 per volt sec, respectively, for high-resistivity germanium. In the calculations, these mobilities were corrected for impurity scattering by means of empirical curves determined by Debye and Conwell and independently by Prince.[9]

In the present instance, the resistivity ρ_n of the original n-type specimen provides n from (2). This is equal to the number of holes per cm^3 at the boundary which in turn is proportional to the number of copper atoms per cm^3. It is therefore a simple matter to determine the distances and times for equal concentrations of the diffused copper.

To test this relation two specimens ($0.8 \times 0.8 \times 0.25$ cm) of n-type single-crystal germanium[10] of uniform resistivity (ρ at 25°C = 0.7 ohm cm) were cleaned of surface impurities by grinding on fresh, dry Aloxite No. 400 abrasive paper. The exposed faces were treated with 1 percent (by weight) copper nitrate solution and each specimen was subjected to a series of heatings for known times in helium. Two runs were made, one at 815° and one at 915°C. After each heating, a cross-sectional cut was made perpendicular to the slab face in order to expose a fresh p-n boundary. This was necessary in order to avoid edge effects. The amounts removed did not affect materially the heat-up time curves. A heat-up time correction, chosen so as to meet the condition of zero distance at zero time, was applied to all points. No correction for cooling was required because of the rapid quenching to near room temperature in less than 1 second. The corrections used were 20 seconds at 815°C and 10 seconds at 915°C. The p-n boundary penetration distances were determined by means of a sharpened tungsten wire which served as a rectifying probe. Distances were measured to ±0.0001 cm by means of a micrometer eyepiece and microscope.

Plots of $\sqrt{t}$ against x, the penetration distance, are shown in Fig. 1. It is seen that Fick's relation is followed within the error of the experiment, namely, about ±2 percent in the time t.

B. Procedures for Determining Diffusivity

1. *Resistance Method*

Specimens for this method, were cut as cross sections from single-crystal germanium prepared by zone leveling.[11] The sections were 0.625 cm thick and roughly circular in shape of average radius 1.9 cm and ranged in resistivity (n-type) from 14.1 to 38.1 ohm cm at 25°C. Copper was applied as a 1 percent by weight nitrate solution to one surface of each of five specimens of the germanium, which were previously carefully cleaned of surface impurities.[12] In this manner, a very thin layer of metallic copper was deposited on one face of each specimen. Each specimen was then heated on a freshly split mica support in a resistance-type furnance with the copper treated surface toward the mica. The specimens and the mica support could be introduced into the furnance and removed therefrom in a time of about 1 second. Heating was carried out in

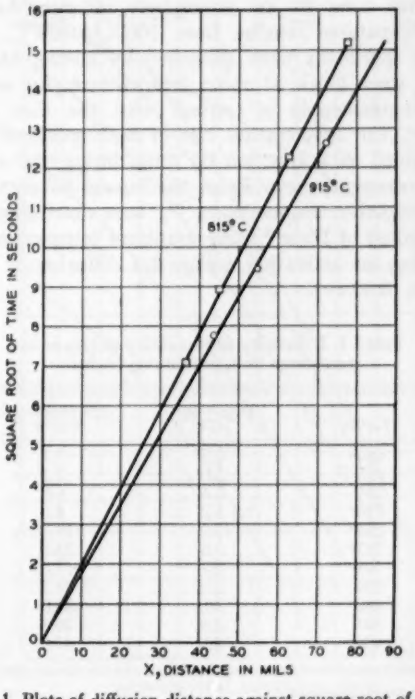

FIG. 1. Plots of diffusion distance against square root of time to reach a fixed concentration at 815° and 915°C.

[8] J. R. Haynes and W. Shockley, Phys. Rev. **85**, 678 (1952).
[9] M. Prince, Phys. Rev. **92**, 681 (1953); P. P. Debye and E. M. Conwell, Phys. Rev. **93**, 693 (1954); Esther Conwell, Proc. Inst. Radio Engrs. **40**, 1327 (1952).
[10] G. K. Teal and J. B. Little, Phys. Rev. **78**, 647 (1950).
[11] W. G. Pfann and K. W. Olsen, Phys. Rev. **89**, 322 (1952).
[12] The purpose of cleaning was to minimize diffusion from the back and side surfaces.

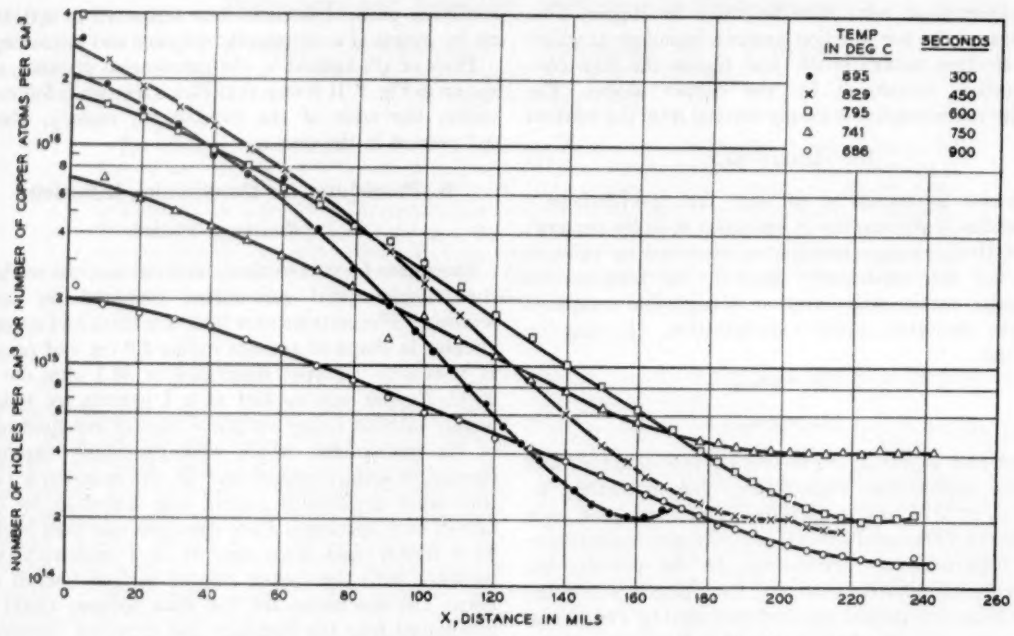
TEMP IN DEG C
SECONDS
• 695 300
× 829 450
□ 795 600
△ 741 750
○ 686 900
NUMBER OF HOLES PER CM³ OR NUMBER OF COPPER ATOMS PER CM³
X, DISTANCE IN MILS

FIG. 2. Penetration curves for Cu in Ge at various temperatures as determined from resistivity.

a quartz tube in an atmosphere of pure helium at temperatures ranging from 700° to 914°C. The heated specimens were quenched by sliding onto a heavy steel block at room temperature. By means of a thermocouple in contact with the thin mica support, the temperature rise of each specimen was determined as a function of time during the entire heat treatment cycle. From the curves so obtained, mean effective temperatures, T_e, were determined by the method of Ham,[13] using graphical integration and assuming an activation energy for diffusion of 8000 calories (0.35 ev).

TABLE I. Diffusivity and solubility of copper in germanium from penetration curves.

T_e(°C)	D(cm²/sec) $\times 10^5$	C_0(Cu atoms/cm³) $\times 10^{-18}$
680[a]	2.7	2.7
686	3.0	2.1
741	2.4	6.6
770[a]	3.2	8.0
780[a]	2.7	19.0
785[a]	3.6	26.0
795[a]	2.7	17.0
829	2.2	27.2
880[a]	3.1	36.0
895	2.9	20.8
900[a]	2.5	47.0

[a] Radiotracer determinations.

[13] J. L. Ham, Trans. Am. Soc. Metals 31, 877 (1943). The value of ΔH^* of 8000 cal assumed in these calculations is probably high, but large errors can be tolerated without appreciable influence on T_e.

Bars 0.125×0.125×0.625 cm were next cut perpendicular to the plane faces of each specimen. Without injury to the ends, solder was applied to them to form ohmic contacts for the passage of current. Each bar was mounted in turn on a traveling stage under a microscope in such a manner that contact could be made along the sides of the bar at measured distances from the ends. A sharp tungsten probe was employed for the contact and the distance was measured to ±0.002 cm by means of a micrometer screw. Thus, with a current of 1 milliampere flowing down the bar, the change in potential at each point along the bar, and therefore the change in resistivity could be measured. A type-K potentiometer was used to measure potential differences. Potential differences were taken in steps of 5, and sometimes 10 mils, along all four sides of each bar and the results averaged for the resistivity calculations.

The number of holes per cm³ added at each step during the diffusion is given by the sum of the electron concentrations of the original n-type germanium specimens [Eq. (2)] and the hole concentrations corresponding to the resistivity at each step along the test bars as derived from Eq. (3). The assumption (justified later on in this paper) is made here that one hole is introduced by each diffusing copper atom.

From plots, at each mean effective temperature, of the number of copper atoms per cm³ as a function of distance into the specimen, C_0 the surface copper concentration, and D the diffusivity were determined

by a method suggested by Bardeen.[14] This consists of matching the penetration curves, with log distance plotted *vs* log concentration, to the curve obtained by plotting, on log-log paper to the same scale, erfc$u$ against u, where erfc$u$ is

$$1-\frac{2}{\sqrt{\pi}}\int_0^u \exp(-\beta^2)d\beta.$$

C_0 then corresponds to the point where erfc$u=1$ and D is derived from the point where $u=x/[2(Dt)^{\frac{1}{2}}]=1$.

2. Radiotracer Method

Specimens, approximately 0.5 in. thick and 1 in. in diameter, were cut from n-type single-crystal germanium.[8] Radioactive copper[15] (Cu^{64}) was deposited on all surfaces by immersing the specimens for two minutes in a 0.1 percent (by weight) copper nitrate solution containing Cu^{64}. Diffusion anneals were carried out in helium gas in a quartz tube furnace at temperatures ranging from 680° to 900°C. The heated specimens were quenched in air by sliding onto a heavy steel block at room temperature. Blocks the full thickness of the specimen and $\frac{3}{8}$-in. square cross section were cut from the center of the heated samples, giving for the diffusion measurements specimens in which copper was diffused from two surfaces only. Grindings were taken, using No. 400 or No. 320 Aloxite paper, at measured distances from the surface of the block and the activity of the grindings measured by the usual counting techniques. The concentration of copper in the grindings was calculated from the activity making suitable corrections for absorption and decay, and the penetration curves plotted in the usual way. Because of the short half-life of Cu^{64} (12.8 hr) it was necessary to complete the work within 72 hours to obtain the desired counting precision.

3. Diffusion Results

In Table I are given the essential results from both the resistance and radiotracer measurements. Figure 2 shows the penetration curves obtained at each temperature by the resistance method, and Fig. 3 gives similar curves for the radiotracer results. In calculating diffusivity and surface concentration, corrections were applied to the penetration curves of Fig. 2 by subtracting from each ordinate the final concentration level approached in each case.[16] The corrected penetration curves fit the u, erfc$u$ curves within the error of experiment in all cases.[17] No such corrections are needed for the curves of Fig. 3 which descend normally.

When log D is plotted against $1/T$ in the usual manner to determine ΔH^*, the activation energy for diffusion, the scatter in the results as shown in Fig. 4 is too great to allow an accurate estimate of ΔH^* to be made. This is in spite of the fact that the precision of the determinations is rather good, namely a probable error of ±10 percent, for this type of measurement. The average diffusivity of copper in germanium, taking all of the results, is $2.8\pm0.3\times10^{-5}$ cm²/sec, at all temperatures investigated. If we assume a maximum positive deviation of 2σ at 900°C and a maximum negative deviation of the same amount at 700°C, the maximum expected ΔH^* is 4900 cal. We may suppose the true value, therefore, to fall between 0 and 4900 cal.[18] Obviously a higher precision will be required to estimate ΔH^* more accurately than this.

II. SOLID SOLUBILITY OF COPPER IN GERMANIUM

Indirect determinations of the solubility of copper as a function of temperature are obtainable, as already

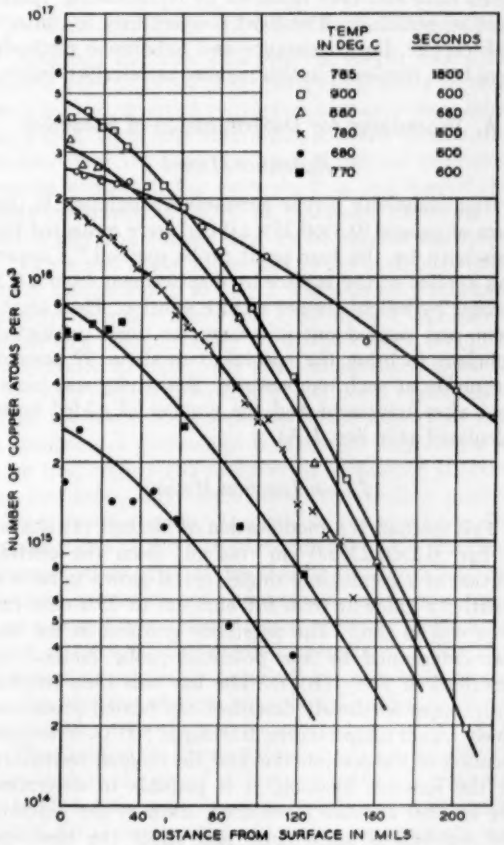

FIG. 3. Penetration curves at various temperatures determined by means of radioactive copper.

[14] W. G. Pfann (private communication).

[15] The isotopes were obtained from the Oak Ridge and Brookhaven National Laboratories on allocation from the U. S. Atomic Energy Commission.

[16] The finite concentration levels reached at large distances are believed due to residual copper from the sides and backs of the specimens.

[17] This is the equivalent of a straight-line plot on probability paper. See C. Wells, *Atom Movements* (Am. Soc. Metals, 1951), p. 33.

[18] The previously reported ΔH^* of 12 000 cal (reference 3) is too high, probably because of the limited number of determinations available at the time and the lack of sufficiently pure Ge (see IV).

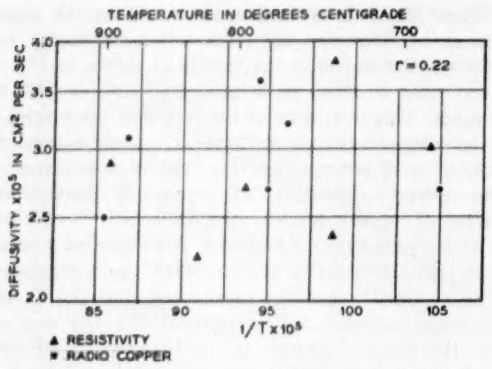

FIG. 4. Scatter diagram of diffusivity *versus* reciprocal of absolute temperature.

mentioned, from the penetration curves (Figs. 2 and 3). These have been included in Table I for both the resistance and radiotracer methods. Direct measurements have also been obtained by equilibrating specimens of germanium[19] at fixed temperatures in contact with copper. Both resistance and radiotracer methods have been employed in this manner as described below.

A. Procedures for Determination of Solubility

1. Resistance Method

High-resistivity *n*-type germanium specimens in the form of prisms (0.5×0.25×1.0 cm) were measured for resistivity by the four point probe method.[20] Copper was applied to the surface by displacement from a 0.5 percent by weight copper nitrate solution. Heat treatment was carried out in helium for times calculated sufficient to bring the specimens to above 99 percent saturation at each temperature. Resistivity was measured after treatment and the number of added holes calculated as in Sec. I(A).

2. p-n Junction Method

This method is a modification of method (1) above. A bar, 0.2×0.2×5.0 cm was cut from the central portion of a germanium single crystal grown to have a resistivity gradient from 0.1 ohm cm to 25.0 ohm cm from end to end.[17] The resistivity gradient in the bar was determined by the potential probe method as described in Sec. I(B)(1). The bar was then treated with copper as already described and heated at successively higher temperatures, starting at 500°C. From the location of the *p-n* junction and the original resistivity at the junction location, it is possible to determine the number of holes introduced, since at the junction the number of holes must just equal the electrons originally present. It is assumed none of the other impurities in the Ge are altered by the experiment. By heating until an equilibrium was established at a given temperature, approached from above and below, and determining the *p-n* boundary positions, solubility was determined as a function of temperature under the assumption that each copper atom supplies one hole to the filled band. An advantage of this method is that it enables solubilities to be determined below the eutectic temperature of Cu-Ge (650°C).[29]

3. Radiotracer Method

The method employed and the results have already been published.[6] These results are included in Fig. 5.

B. Solubility Results

Figure 5 shows a plot of all of the experimental data on solid solubility of copper in Ge as a function of temperature. The solid curve has been drawn favoring the determinations made by extrapolation of the curves of Fig. 2 and the previously published[6] radiotracer results which are believed to be the most accurate of the measurements.

As can be seen from Fig. 5, the direct resistivity methods give lower solubilities at temperatures in the range 700°–850°C. This is believed to be due to variations in resistivity near the surfaces of the specimens as a result of copper precipitation (see below). All of the measurements are in substantial agreement at the lower temperatures. Likewise, at the higher temperatures a definite solubility maximum is indicated at about 875°C.

The agreement between the radiotracer results and those obtained by extrapolation of the curves of Fig. 2, which are considered the most accurate of the resistivity results, provides evidence that each copper atom supplies substantially one conducting hole in germanium at room temperature. Other evidence for this is reported in references 5 and 6.

III. DISCUSSION OF ERRORS

Because of the extremely high rate of diffusion of copper in Ge and its very low solubility (less than 3 atoms per million of Ge at the maximum), precise determinations of these quantities are difficult. Further complications arise from the presence of temperature gradients at the start and finish of the heating periods, from the possibility of precipitation from the supersaturated solution during the quench, from previous contamination of the germanium with copper, and from surface reactions which may influence rate.[21] The presence of inhomogeneities in resistivity can also influence the results obtained by the methods depending on resistance measurement, especially at lower temperature where low copper concentrations prevail. A

[19] The authors are indebted to E. Buehler for the single crystals from which these specimens were prepared.

[20] L. B. Valdes, Proc. Inst. Radio Engrs. 42, 420 (1954).

[21] The presence of oxygen or nitrogen in the gas atmosphere has been found to reduce the diffusion rate.

discussion of the influence of these factors upon the reliability of the determinations is therefore in order.

The method[13] of correcting for the temperature rise upon insertion of the specimens in the furnace is recognized as not being entirely adequate. Surface concentration changes occurring during the heat-up period will also effect the results. These errors will lower the values of the diffusivity at the higher temperatures relative to those at the lower temperatures. The effects, however, do not exceed 10 percent of the diffusivity values reported.

Tests have shown that the errors arising from precipitation are small provided quenching is sufficiently fast.[22] Because of the maximum in the solubility curve at about 875°C, there is the possibility that the solubilities determined above 875°C will show solubilities which are too high. Small variations may likewise occur in the diffusion because of changes in surface solubility near this temperature.

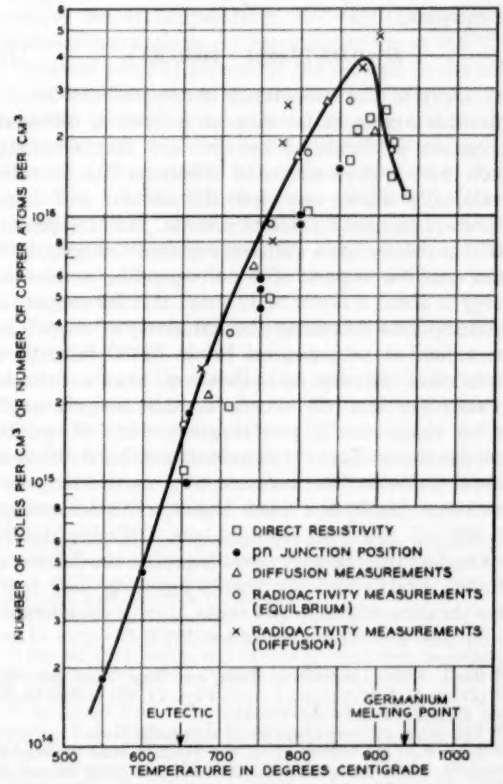

FIG. 5. Plot of number of conducting holes or number of copper atoms per cm³ against temperature.

[22] A possibility of a small error entering because of other acceptors or defects being retained by very rapid quenching [see R. A. Logan, Phys. Rev. 91, 757 (1953)] exists. Tests on copper-free specimens of the Ge employed showed, however, less than 10^{14} carriers retained.

Errors from copper contamination, while present, are small except at the lower temperatures where the effect is to give apparently higher diffusivities than actual. At the lowest temperature (686°C) this may amount to as much as 10 percent error in D. Such contamination should not, however, influence appreciably the solubility results.

Errors caused by random inhomogeneities in the resistivity of the germanium contribute to the scatter of the data. These errors are, however, relatively small compared to those mentioned above except possibly at the lowest temperatures.

Likewise the random errors in the measurement of resistivity (±2) percent, time (±1 percent), distance (±0.5 percent), radio count (±1–10 percent), mobility (±5 percent) are less important than the errors incidental to heat-treatment mentioned above. The over-all probable error in the determination of D is therefore largely determined by the latter and is estimated to be about ±10 percent. The same applies to the best determinations of C_0.

IV. PRECIPITATION OF COPPER IN GERMANIUM

Although the high diffusivity of copper established by the work reported in the paragraphs above accounts well for the observed conversion of n-type germanium to p-type upon heat treatment, it is not immediately evident how the other features[2] of thermal conversion can be explained. For example, it is well known that heat treatment at 500°C of thermally converted Ge will result in a change back to its original resistivity.

This is now easily understood on the basis of the solubility results shown in Fig. 5. The solubility of copper rapidly decreases below 875°C so that, if equilibrium conditions prevail, nearly all of the copper should be precipitated at sufficiently low temperatures. Evidence that such precipitation does in fact occur is obtainable from resistivity measurements. These show that once a specimen of germanium is saturated with copper at high temperature and reconverted by heating at 500°C in the usual way, subsequent conversions proceed almost homogeneously throughout the specimen. Determinations of the rate of movement of p-n junctions, likewise, show that in previously converted and annealed specimens of germanium, the conversion proceeds at a much higher rate at the same temperature that it does in the original germanium. The high diffusivities previously reported[3] are now believed due to the presence of some precipitated copper in the Ge employed.

The proof of the precipitation of copper, however, is provided by the use of radioactive copper. Germanium saturated with radiocopper at 900°C was annealed at 520°C for 17 hours, after which time the specimen was cut in two and radioautographs taken of the interior surfaces. Figure 6 shows the results. It is evident that the copper is no longer as uniformly distributed, as is shown by the mottled appearance of the annealed as

compared to the unannealed specimens. This is especially evident at the surfaces. Quantitative measurements of activity in fact show that except near the surface, precipitation occurs throughout the specimen. That the surface is an especially good locus for nucleation is shown not only by the radioactivity measurements, but also by the early observation[2] of thin n-type layers on heat converted specimens of germanium which were slowly cooled.

The reversal of conductivity type and the return of the heat-converted germanium to its original resistivity, which occurs on annealing is therefore made understandable by the precipitation of copper.

V. DISCUSSION—MECHANISM OF DIFFUSION

The characteristic features about the diffusion of copper into germanium are its extremely high diffusivity, approaching that of liquid diffusions, and its relatively low activation energy of diffusion. One is tempted on this basis to postulate an interstitial mechanism for this diffusion.[23] Wert and Zener[24] have examined the case for interstitial diffusion generally, and have shown that for many diffusions, supposedly interstitial, ΔS^* for diffusion is positive. They give the following expression for D_0:

$$D_0=\lambda a_0^2\nu \exp(\Delta S^*/R), \tag{4}$$

in which λ is a constant depending on lattice geometry, a_0 is the lattice constant for Ge, ν= vibration frequency, ΔS^* is the entropy of diffusion, and $R=1.99$ calories. They further have indicated how $\Delta S^*/R$ may be determined in terms of ΔH^* for diffusion from a knowledge of the temperature coefficient of the shear modulus, μ, of the solvent including the magnitude of this modulus, μ_0, at absolute zero:

$$\Delta S^*=-\Delta H^*(1/\mu_0)(d\mu/dT). \tag{5}$$

Here μ_0 is the extrapolated modulus, and ΔH^* is the activation energy for diffusion. The temperature coefficient of the rigidity modulus, has been determined for germanium as a function of temperature.[25] From the high-temperature slope of the curves for the shear modulus in the (110) plane,[26] $d\mu/d=-0.00060\times10^{11}$ dynes/cm^2/°C and the extrapolated value of the modulus, $\mu_0=4.2\times10^{11}$ dynes/cm^2. According to Eq. (4), where $\lambda=\frac{1}{8}$ for the germanium lattice,[27] $a_0=5.62\times10^{-8}$ cm, and ν, taken as the average lattice vibration frequency, is 0.45×10^{12} sec^{-1}, one obtains

$$\log D_0=-3.75+0.000031\Delta H^*. \tag{6}$$

The average experimental value for D is 2.8×10^{-5} cm^2/sec at 1073°K. By substituting these values in the general diffusion equation, using D_0 from (4), ΔH^* comes out to be 4100 cal for copper in Ge. This value is in agreement with the results reported here and suggests the equation,

$$D=0.00019\exp(-4100/RT), \tag{7}$$

may apply in the temperature range 700°–900°C.

Another argument favoring an interstitial diffusion mechanism is furnished by the fact that elements which there is good reason to believe go into Ge substitutionally show very low diffusivities and high activation energies for diffusion in Ge. For example, at 800°C antimony has a diffusion constant[28] roughly 10^{-6} times that for copper. The corresponding activation energy is about a factor of 12 times that for copper.

Attempts to determine the diffusivity of copper in germanium at temperatures below 650°C indicate a much lower diffusion rate. However, since a eutectic between Cu and Ge occurs at this temperature,[29] the low values may be a consequence of lack of equilibrium conditions. Esaki[30] has recently published diffusion constants due to "thermal acceptors" in this temperature range. He finds a much higher activation energy (35 000 cal) than that reported here. Diffusion limited by a surface reaction may possibly explain the difference between Esaki's and our results assuming they both have the same origin. In any event, there is considerable doubt that Eq. (7) applies below 650°C.[31]

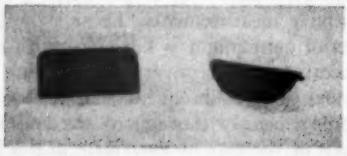

(a)

(b)

FIG. 6. Radioautographs of copper in Ge.

[23] C. Wagner, Z. phys. Chem. **B38**, 325 (1937).
[24] C. A. Wert and C. Zener, Phys. Rev. **76**, 1169 (1949); C. Zener, J. Appl. Phys. **22**, 373 (1951).
[25] Bond, Mason, McSkimin, Olsen, and Teal, Phys. Rev. **78**, 176 (1950); H. J. McSkimin, J. Appl. Phys. **24**, 988 (1953). M. E. Fine, J. Appl. Phys. **24**, 338 (1953).
[26] This is the shearing plane for an interstitial jump.
[27] λ in Eq. (4) follows from the random walk expression $1/6(\Delta x)^2\nu$, where Δx is jump distance and ν is jump frequency, taking into account the number, $n=4$, of alternate paths and the fact that $\Delta x=\sqrt{3}a_0/4$.
[28] D. E. Brown and W. C. Dunlap, Jr., Phys. Rev. **87**, 616 (1952); C. S. Fuller, Phys. Rev. **86**, 136 (1952).
[29] M. Hansen, *Der Aufbau der Zweistofflegierungen* (Springer, Berlin, 1936), p. 565.
[30] Leo Esaki, Phys. Rev. **89**, 1026 (1953).
[31] As C. Goldberg, Phys. Rev. **88**, 920 (1952), has indicated, Eq. 7 and that previously published (reference 3) do not appear

The nature of the copper particle which diffuses is of interest. If copper of itself is the acceptor, one might expect, analogously to other acceptors in Ge, that it would be present as a negative ion. However, the diameter of such a negative copper ion would appear to be too large ($>1.5A$) to permit interstitial diffusion, since the interstitial space (Fig. 7) is just sufficient to accommodate a Ge atom (1.22A).[32]

No firm explanation of this apparent discrepancy can be given until more is known about the behavior of copper in Ge. Since there are indications of a trapping level[33] as well as an acceptor level for copper,[34] the true state of the dissolved atom may be complicated. Furthermore, little is known of the effect of temperature on the ionization processes of copper under these circumstances. It is for example, conceivable that copper may diffuse at high temperatures as Cu^+ or Cu^0, and assume the role of acceptor only at lower temperatures. Evidence for this has recently been obtained through experiments on the diffusion of copper in a dc field.[35] It is found that copper behaves as a positive ion at temperatures 850°–900°C and there is evidence that little or no migration occurs at 700°C.

Another point of interest is the reversal in the solid solubility of copper in Ge as shown in Fig. 5. Such behavior in solid systems is rather rare and at first might suggest nonideal solution behavior of copper. Recently Thurmond[36] has shown that the above solubility behavior ("retrograde solubility") follows normally from thermodynamic treatment of the copper-germanium system. We are led to conclude therefore that copper in Ge behaves as a Henry's-law dilute solution.

The authors have carried out similar work on silicon to that described above for germanium. Preliminary results[6] indicate Cu to be an acceptor in Si. However, as yet the magnitude of the resistivity changes has not allowed determinations of D or C_0 to be made by this method. On the other hand, the radiotracer method shows that $D_{900°C}$ is of the same order as that for Cu in Ge (5×10^{-6} cm²/sec) and C_0 is roughly ten times that observed for Ge at 850°C.[34] We hope to publish details of this work in a later paper.

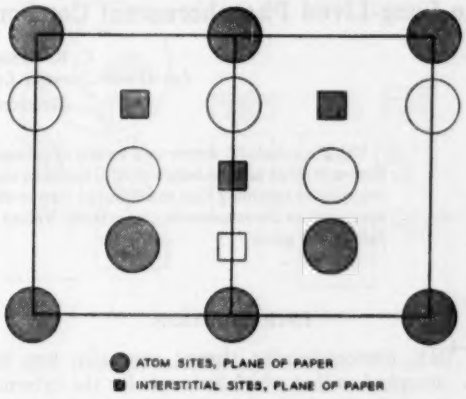

FIG. 7. Projection of atom and interstitial sites of diamond lattice on (110) plane.

SUMMARY

1. The diffusivity of Cu in Ge has been determined in the temperature range 700°–900°C by two independent methods, one based on electrical resistivity and the other on copper radioactivity. Both methods agree within the limit of error, for a value of $D=2.8\pm0.3\times10^{-6}$ cm²/sec in this temperature interval. From the elastic constants for Ge and the theory of Wert and Zener an activation energy of 4100 cal per mol is derived leading to the relation

$$D=0.00019\exp(-4100/RT).$$

2. The solid solubility of copper in Ge as a function of temperature has also been determined by both electrical and radioactive methods. The best results support the conclusion that one copper atom contributes one conducting hole at room temperature.[37]

3. The role the precipitation of Cu plays in the reversible resistivity changes observed during the "thermal conversion" of Ge is discussed.

4. It is pointed out that the acceptor properties of Cu in Ge are in disagreement with the diffusional properties. It is suggested that the anomaly may be resolved by assuming a different state of ionization for copper at room temperature and at the temperature of diffusion.

ACKNOWLEDGMENT

The authors are indebted to J. A. Burton, W. C. Ellis, Conyers Herring, J. N. Hobstetter, W. P. Slichter, R. G. Shulman, and R. G. Treuting for helpful discussions during the preparation of this paper.

to account for the slow process observed at lower temperatures (560°C). However, it must be pointed out that the solubility of Cu at this temperature is very low and so far, no determinations have been made at these temperatures.

[32] C. Herring has suggested to the authors that the Cu atom and its accepted electron may behave as separate entities.

[33] Burton, Hull, Morin, and Severiens, *Symposium on Impurity Phenomena* (Schnectady, New York, 1953); J. Phys. Chem. **57**, 853 (1953).

[34] An energy level for copper ionization of 0.04 ev has been reported. F. J. Morin and J. P. Maita, Phys. Rev. **90**, 337 (1953); W. DeSorbo and W. C. Dunlap, Jr., Phys. Rev. **83**, 879 (1951). G. L. Pearson in W. Shockley, *Electrons and Holes in Semiconductors* (D. Van Nostrand Company, Inc., New York, 1950), p. 227.

[35] J. C. Severiens and C. S. Fuller, Phys. Rev. **92**, 1322 (1953).

[36] C. D. Thurmond and J. D. Struthers, Symposium on Impurity Phenomena, Schenectady, New York (1953); J. Phys. Chem. **57**, 831 (1953). Retrograde solubility of Cu in Si was observed in this work.

[37] Some recent work indicates that the second level (see reference 34) may contribute to the conductivity in strongly *n*-type Ge.

The Long-Lived Phosphorescent Components of Thallium-Activated Sodium Iodide

C. R. EMIGH AND L. R. MEGILL*
Los Alamos Scientific Laboratory, Los Alamos, New Mexico
(Received October 28, 1953)

Using a cobalt-60 source as a means of primary irradiation, the long-lived phosphorescent decay of thallium-activated sodium iodide crystal has been studied at several crystal temperatures. The results have been interpreted assuming that the different trap levels act independently of each other and that each trap decays according to the monomolecular process. Values for the experimental trap depths and vibrational frequency factors are given.

INTRODUCTION

THE monomolecular theory generally has been accepted as that which accounts for the extremely long-lived phosphorescent decay of the heavy-metal activated alkali halides.[1,2] As these crystals usually have a complex decay scheme, a thorough investigation of the decay characteristics must be made to substantiate convincingly the presence of the monomolecular decay process for the different trap levels. This decay is characteristic of a phosphor which shows no photoconductivity. Therefore, the luminescence may be thought of as being produced as a result of excitation and subsequent delayed optical emission arising from the transition characteristics of the heavy activator. In thallium-activated sodium iodide, which is assumed to be an ionic crystal, the emission spectrum will be that of the thallium ion which is substituted in dilute concentrations for the sodium ion in the lattice structure.[3]

The results of experiments[4–6] on the thermoluminescence of KI(Tl) and NaI(Tl) crystals indicate that these alkali halides probably have many traps which take part in the decay. These traps are considered to be in the neighborhood of the thallium ions; consequently the electrons, on escaping, are captured by the same luminescent centers from which they were originally emitted.[7]

The decay curves necessarily will be complex because of the many traps. If the primary decay process were of a bimolecular nature, the procedure for finding the components due to various traps by an analysis of the decay characteristics would be indeed most difficult, if not impossible. However, the monomolecular process for the different traps gives a mixture of exponential decay components. Therefore, the phosphorescent decay is subject to simple analysis by a "peel-off" of these components. It might be argued that any monotonically decreasing curve can be represented by a superposition of exponential components. This of course is true. However, if the initial intensities of the exponential components are varied relative to each other and if all the resulting decay curves can be resolved into terms with a consistent set of mean lives for the exponential components, then considerable support is given to the exponential decay hypothesis. Furthermore, if the initial intensities of the different traps behave in a manner consistent with a simple exponential theory in their relationship to the exposure times, then added support is obtained. The initial intensities may be varied relative to each other by varying the irradiation time of the crystal. This effect will be made clear by the experimental results which are explained in a later section.

THE MONOMOLECULAR THEORY

The monomolecular theory for phosphorescence decay is reviewed here to bring out some of the underlying assumptions which are made in its development. As retrapping and radiationless transitions between traps are to be considered negligible, each trapping process will act independently of all the other traps. For each trap level the decay process can be considered identical and the following remarks will apply to all the trap levels.

We need not go into detail about the nature of the traps themselves or about their relationships with the lattice structure. It is assumed that the trap exists, that a transitional state through which a trapped electron must pass to reach an excited state of the luminescent center exists, and that in order to free an electron from a trap an energy of activation is required to raise the trapped electron to the transitional state. Whether or not this transitional state is a localized conduction band has no effect, as the entire process is assumed to occur in the region of the luminescent center. After making these simplifying assumptions, the absolute rate theory[8] can be applied. Therefore, the specific reaction rate k_i is

$$k_i = s_i e^{-\epsilon_i/kT}. \quad (1)$$

In this expression, s_i is the frequency factor for transi-

* Now at the University of Colorado, Boulder, Colorado.
[1] J. T. Randall and M. H. F. Wilkins, Proc. Roy. Soc. (London) **A184**, 347 (1945).
[2] F. Seitz, J. Chem. Phys. **6**, 150 (1938).
[3] J. E. Mayer, J. Chem. Phys. **1**, 270, 327 (1933).
[4] B. Smaller and E. Avery, Phys. Rev. **85**, 766 (1952).
[5] Smaller, May, and Freedman, Phys. Rev. **79**, 94 (1950).
[6] J. Bonanomi and J. Rossel, Helv. Phys. Acta **24**, 310 (1951).
[7] F. Seitz, in *Preparation and Characteristics of Solid Luminescent Materials* (Cornell Symposium of the American Physical Society, John Wiley and Sons, Inc., New York, 1948), Paper 1, p. 14.
[8] Glasstone, Laidler, and Eyring, *Theory of Rate Processes* (McGraw-Hill Book Company, Inc., New York, 1941).

tions from the trap, or the metastable state, to the emitting state and ϵ_i is the experimental trap depth.

Under the condition of constant irradiation, the buildup of electrons in a given trap can be expressed approximately by the differential equation

$$dn_3/dt = -k_1 n_3 - k_2 n_3 + B_3 n_1, \quad (2)$$

where n_3 represents the number of electrons in the metastable state at a given time t_0, $B_3 n_1$ is the number of electrons raised into the metastable state per unit time, k_1 is the specific reaction rate for the radiationless transition to the normal state, and k_2 is the specific reaction rate for the transition to the emitting state (Fig. 1). This equation is based on n_3 being at all times much smaller than the total number of unfilled traps.

The buildup of electrons in the emitting state can be

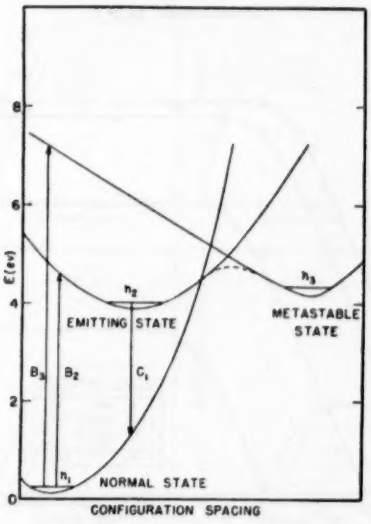

FIG. 1. Configurational coordinate diagram for NaI(Tl).

expressed approximately by the differential equation

$$dn_2/dt = -C_1 n_2 + B_2 n_1 + \mu_1 k_1 n_3 + (1-\mu_2) k_2 n_3, \quad (3)$$

where n_2 is the number of electrons in the emitting state at the time t_0, $B_2 n_1$ is the number of electrons raised into the emitting state per unit time, μ_1 is the fraction of trapped electrons which go over the nonradiative barrier into the normal state but are captured by the emitting state before losing their energy by elastic waves, μ_2 is the fraction of trapped electrons which go over the barrier into the emitting state and are captured immediately by radiationless transitions into the normal state, and C_1 is the optical transition rate from the emitting state to the ground state.

As the measured phosphorescent intensity is assumed proportional to the optical transition rate, the buildup intensity due to one given trap at a given exposure

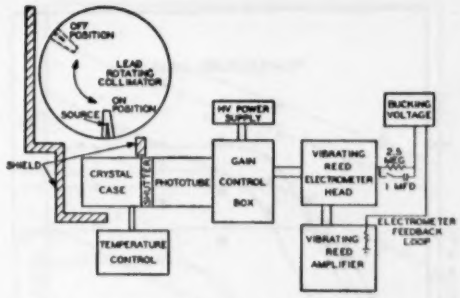

FIG. 2. Schematic diagram of experimental setup.

time, t_0, in terms of the solutions to Eqs. (2) and (3) is

$$I_0(t_0) = DC_1 n_2(t_0) = DB_3 n_1 \frac{\mu_1 k_1 + (1-\mu_2) k_2}{k_1 + k_2} (1 - e^{-(k_1+k_2)t_0}), \quad (4)$$

where D is a constant relating the observed intensity to the electron transition rate from the emitting state to the normal state. When the crystal exposure is terminated, the phosphorescent intensity due to each trap will fall off exponentially from the initial intensity $I_0(t_0)$ and can be expressed approximately by

$$I(t) = I_0(t_0) e^{-(k_1+k_2)t}. \quad (5)$$

The irradiation time is given by t_0 while the time of decay after cessation of irradiation is given by t.

It is the primary purpose of this experiment to analyze decay curves obtained from various irradiation exposure times, t_0, into a series of terms of the type given by Eq. (5), then to apply the experimentally determined mean lives and initial intensities for the different traps to equations of type (4) to show the internal consistency of these experimentally determined constants.

EXPERIMENTAL SETUP

A thallium-activated sodium iodide crystal was obtained from the Larco Nuclear Instrument Company for this experiment. The crystal has a thallium-activator concentration of 0.20 percent by weight. It has a square

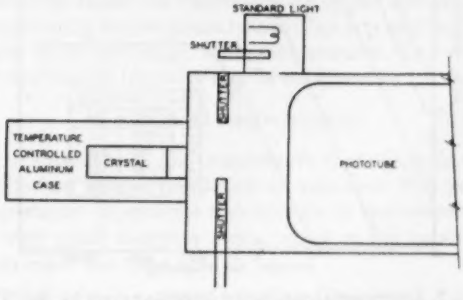

FIG. 3. Detailed schematic diagram of the crystal container.

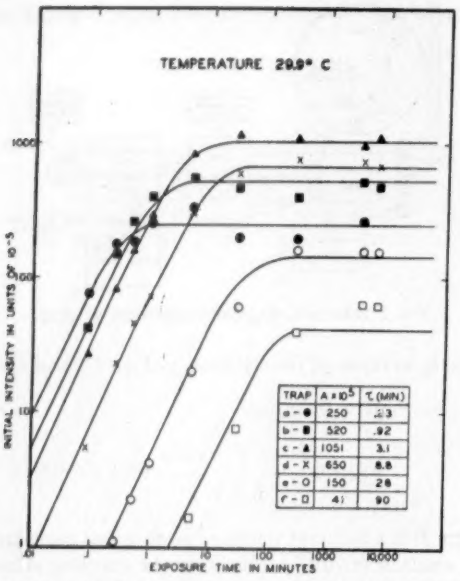
TEMPERATURE 29.9° C
INITIAL INTENSITY IN UNITS OF 10^-5
EXPOSURE TIME IN MINUTES
TRAP | A x10^5 | τ (MIN)
a - ● | 250 | .33
b - ■ | 520 | .92
c - ▲ | 1051 | 3.1
d - X | 650 | 8.8
e - O | 150 | 28
f - □ | 41 | 90

FIG. 4. Experimental equilibrium intensity curves for NaI(Tl) at a temperature of 29.9°C.

cross section of 2.5 cm on a side and is 1 cm thick. The temperature of the crystal was controlled throughout the experiment to ±0.03°C.

A cobalt-60 source was used to irradiate the crystal. The source is kept in a collimator which can be rotated into position for irradiation of the crystal (Fig. 2). The collimator is 7 cm long and has a 1.25-cm aperture. The crystal was placed 28 cm from the source and was oriented so that the radiation was incident normally on the larger surface. The time required to direct the radiation onto or off the crystal was less than 0.1 second, allowing the time of irradiation to be determined to this degree of accuracy.

A 5819 photomultiplier was used to detect the light from the crystal. The signal from the photomultiplier was fed into a vibrating reed electrometer used as a current measuring device. The circuit used is discussed in greater detail elsewhere in regard to another application.[9] The electrometer operates a recording millivoltmeter so that data may be obtained automatically.

The gain of the system was checked occasionally by use of a standard light. The dark current from the photomultiplier was measured periodically by closing a modified camera lens shutter between the crystal and the photomultiplier (Fig. 3). The background from the crystal due to extraneous radiation—cosmic rays and scattered radiation from the cobalt-60 source—was determined before a run was made. The value of this background remains quite constant. The data are corrected for small variations in gain, dark current, and background before analysis. The accuracy of the corrected data is somewhat better than 3 percent except at signals which are of the same order of magnitude as the background and dark current.

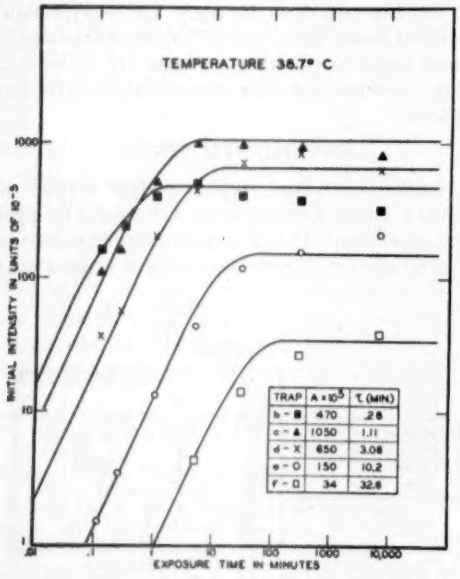
TEMPERATURE 38.7° C
INITIAL INTENSITY IN UNITS OF 10^-5
EXPOSURE TIME IN MINUTES
TRAP | A x10^5 | τ (MIN)
b - ■ | 470 | .28
c - ▲ | 1050 | 1.11
d - X | 650 | 3.08
e - O | 150 | 10.2
f - □ | 34 | 32.8

FIG. 5. Experimental equilibrium intensity curves for NaI(Tl) at a temperature of 38.7°C.

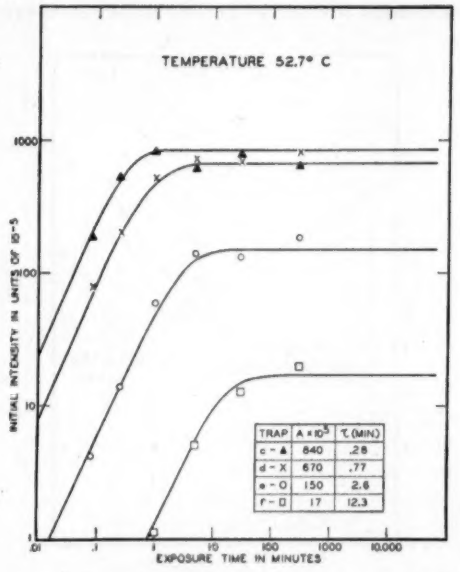
TEMPERATURE 52.7° C
INITIAL INTENSITY IN UNITS OF 10^-5
EXPOSURE TIME IN MINUTES
TRAP | A x10^5 | τ (MIN)
c - ▲ | 840 | .28
d - X | 670 | .77
e - O | 150 | 2.6
f - □ | 17 | 12.3

FIG. 6. Experimental equilibrium intensity curves for NaI(Tl) at a temperature of 52.7°C.

RESULTS

The phosphorescent decay data for a given temperature and for various exposure times were analyzed by

[9] C. R. Emigh and L. R. Megill, Non-Destructive Testing 11, No. 3, 30 (1953).

the exponential "peel-off" procedure into a series of terms of the type given by Eq. (5). A set of values for the initial intensities and mean lives of the various traps involved are obtained by a preliminary peel-off cut through the data. This entire analyzing procedure is repeated in a slightly different manner. Before the constants for each trap are determined, the exponential term which represents the next shallower trap and which is obtained from the preliminary cut is subtracted out of the data. This results in a longer straight line on a log intensity *versus* time plot. Consequently, a somewhat better determination of the constants for each trap is obtained. Repetition of this procedure two or three times results in a set of values which do not change by successive cuts through the data.

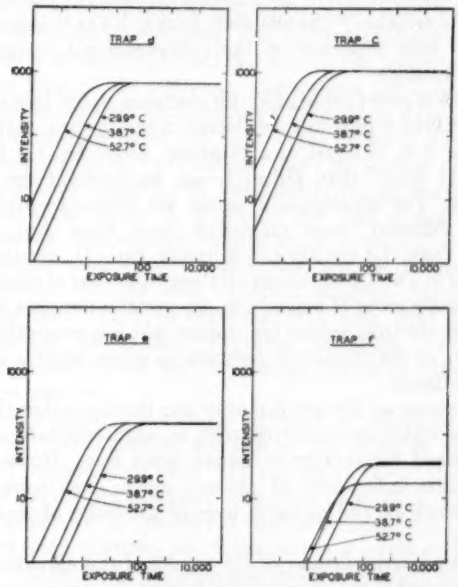

FIG. 7. Equilibrium intensity curves grouped as to trap designations.

The results of such analysis are shown in Figs. 4, 5, and 6 for crystal temperatures of 29.9°C, 38.7°C, and 52.7°C, respectively. Here, the initial intensities relative to the total intensity from the crystal during irradiation are plotted *versus* the irradiation exposure time. For each trap and at all three temperatures, the initial intensity levels off with increasing exposure times indicating an equilibrium between the rate of trapping electrons and the rate of losing electrons from each trap. The experimental mean lives τ's and the equilibrium intensities A's are given in the tables accompanying the figures. The τ's are the averaged values obtained for each trap by averaging the values of τ obtained at the various exposure times. The solid curves through the experimental points are obtained by using the experimentally determined τ's and the values of A which best fit all

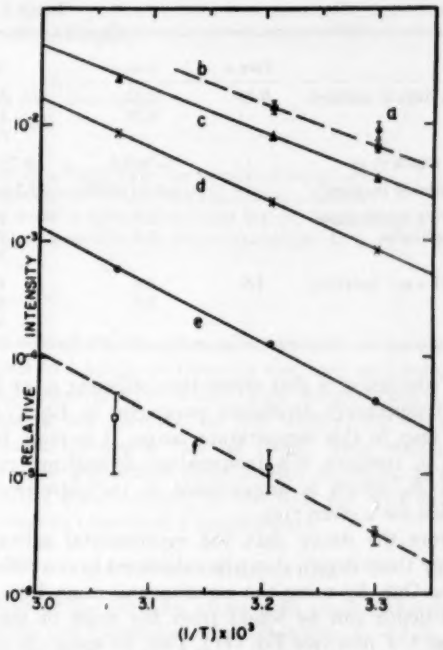

FIG. 8. Semilogarithmic plot of relative intensity *versus* reciprocal temperature.

the experimental points in equations of the type given by Eq. (4), where τ is set equal to $1/(k_1+k_2)$, and the equilibrium intensity is set equal to

$$A = DB_3n_1\frac{\mu_1k_1+(1-\mu_2)k_2}{k_1+k_2}. \tag{6}$$

Figure 7 shows the equilibrium curves grouped as to trap designation for the traps *c*, *d*, *e*, and *f*. For traps *c*, *d*, and *e* the equilibrium intensities are temperature independent within the experimental error. It is felt that the same is probably true for the *a* and *b* traps although the experimental evidence is not conclusive. If indeed these equilibrium intensities are temperature independent, then the relation (6) implies that only one specific reaction rate is employed in the decay process for each trap. It is therefore assumed that radiationless transitions from either the emitting state or the metastable state directly to the ground state play a negligible role in the decay process at these temperatures. Therefore, the equilibrium intensity can be expressed by

$$A = DB_3n_1(1-\mu_2) = \text{constant}. \tag{7}$$

In the case of trap *f*, a temperature dependence in the equilibrium intensity is definitely indicated. This same temperature dependence also appears in the intensities for very small exposure times, which is, for exposure times much less than $1/k_2$,

$$I = DB_3n_1(1-\mu_2)k_2I_0. \tag{8}$$

TABLE I. Trap characteristics.

	Trap *a*	Trap *b*	Trap *c*	Trap *d*	Trap *e*	Trap *f*	Temp in °C
Mean lives in minutes	0.23	0.92	3.1	8.8	28	90	29.9
	...	0.28	1.11	3.06	10.2	32.6	38.7
	...	...	0.28	0.77	2.6	12.3	52.7
Trap depth in ev	...	0.7±0.2	0.75±0.05	0.88±0.05	1.00±0.05	1.1±0.2	...
Vibrational frequency	...	$(1\pm0.8)\times10^{10}$	$(2.2\pm1)\times10^{10}$	$(7.3\pm3)\times10^{11}$	$(2.2\pm1)\times10^{13}$	$(3\pm2)\times10^{14}$	...
Relative equilibrium amplitudes	1.7	3.5	7.0	4.3	1.00	0.27	29.9
	...	3.1	7.0	4.3	1.00	0.23	38.7
	...	...	5.6	4.5	1.00	0.11	52.7
$B_3n_1(1-\mu_2)$ (relative)	1.5	4.6	8.1	5.5	0.90	0.22	29.9
	...	3.6	6.8	5.0	1.00	0.22	38.7
	...	...	5.4	5.0	1.16	0.12	52.7

The conclusion is that either the coefficient μ_2 or B_3 is the temperature dependent parameter in Eq. (7) for this trap in this temperature range. It is more likely that μ_2 contains this temperature dependence rather than B_3, which is proportional to the capture cross section for a given trap.

From the decay data the experimental activation energy (trap depth, ϵ) can be calculated in two different ways. One, by using the experimental mean lives, the trap depth can be found from the slope of the $\ln\tau$ *versus* $1/T$ plot (see Eq. (1)]. Two, by using the equation for the intensity for very small exposure times, Eq. (8), the trap depth can be found from the slope of the $\ln I$ *versus* $1/T$ plot, suitable corrections being made for the temperature dependence of μ_2 in the case of the *f* trap. Of the two methods, the latter appears to give a more consistent set of results. This is probably because in the peel-off analysis the initial intensities are percentage-wise more accurately determined than the mean lives. Figure 8 is a plot of $\ln I$ *versus* $1/T$. The values of intensities which were used were obtained by extrapolating the linear portion of the intensity curves at low exposure times to the 1-minute exposure time. The values of the trap depths with an estimate of their probable errors are tabulated in Table I. Using these values for the trap depths, the values for the frequency factor s_i in Eq. (1) are calculated from the experimental τ's. These are also tabulated in Table I.

The experimental trap depths are in essential agreement with those values obtained by Smaller[5] in his experiment on KI(Tl). This is not surprising as the luminescent center consists of a thallium ion whose nearest neighbors are iodine ions for both the NaI(Tl) and KI(Tl) crystals. As the traps are probably formed by a displacement of the thallium ion with respect to an iodine neighbor,[10] the relatively distant Na or K ions will have little influence on the configurational potential relationships.

The *a priori* probability for electrons to fall into any given trap is generally considered to be constant, that is, $I\tau$ or I/k_1 is equal to a constant. From Eq. (8) this would imply that $DB_3n_1(1-\mu_2)$ be constant for all traps. The experimental values for $DB_3n_1(1-\mu_2)$ for the different traps calculated both from Eq. (8) and from the equilibrium intensity Eq. (7), are tabulated in Table I. Although all these values are of roughly the same order of magnitude, the variation implies that either the cross section for capture, which is proportional to B_3, or the cross-over coefficient μ_2 varies slightly with trap depth.

Because of the low intensity due to traps other than those which are herein reported, no consistent data were obtained for shorter or longer mean lives. However, definite indications of shorter mean lives were in evidence as well as mean lives of the order of several days.

Our interpretations of the results of this experiment indicate that the process is fundamentally a monomolecular one and that retrapping and radiationless transitions to the ground state are negligible, or at least, they do not change the process into one of a bimolecular nature.

[10] F. E. Williams, in *Preparation and Characteristics of Solid Luminescent Materials* (Cornell Symposium of the American Physical Society, John Wiley and Sons, Inc., New York, 1948), Paper 20, pp. 338, 339.

PHYSICAL REVIEW VOLUME 93, NUMBER 6 MARCH 15, 1954

Electrical Properties of α-Fe_2O_3

F. J. MORIN
Bell Telephone Laboratories, Murray Hill, New Jersey
(Received December 7, 1953)

The conductivity, Seebeck effect, and optical transmission of α-Fe_2O_3 have been analyzed using two alternative models. The first model assumes conduction to occur in the *d* levels of Fe ions and yields a quantitative fit to the data. Mobility behavior determined with this model is explained in terms of wavy bands. The second model assumes conduction in the *sp* bands of oxygen in addition to *d*-level conduction. It is shown qualitatively to be a reasonable model.

1. INTRODUCTION

IN a previous paper on α-Fe_2O_3,[1] conductivity and Seebeck effect data were presented. An attempt was made to interpret the data in terms of the usual band theory for semiconductors. The behavior of α-Fe_2O_3 differs in several important ways from the predictions of the theory. The following observations are difficult to explain. Intrinsic-like samples can be made *n* type or *p* type (judging from the sign of the Seebeck effect) without changing their conductivity; no normal Hall effect is found; mobility as determined from application of the band theory is unusually low and shows an anomalous temperature dependence; impurity concentration predicted from electrical results disagrees by several decades with chemical analysis. Similar results[2] for NiO have confirmed the idea that the conduction mechanism in these materials differs fundamentally from the mechanism found in silicon and germanium.

In this paper the results reported in reference 1 together with chemical analysis of the samples and optical transmission data are discussed. Two alternative models are proposed to explain these data. The first model to be considered assumes conduction to involve only electrons and holes in the *d* levels of Fe ions. This is consistent with low mobility carriers and the fact that no normal Hall effect is detected. The model leads to a quantitative fit of the data. Impurity concentration determined electrically agrees with that determined by chemical analysis. Mobility varies over the range 10^{-5} to 10^{-1} cm²/volt sec. It varies with impurity concentration and increases exponentially with temperature. This behavior suggests the presence of wavy bands. At high temperatures and at high-impurity concentrations, where wavy bands may be said to have been smoothed out by high carrier concentration, a mobility behavior is found in both Fe_2O_3 and NiO having an apparent activation energy of $\sim$0.1 ev. The question is raised as to whether 0.1 ev represents the energy required to transfer a charge carrier from one Fe ion to another and whether this energy is related to the antiferromagnetic exchange energy kT_C.

The second model assumes conduction to involve *d* electrons and holes, and also *sp* electrons and holes in the bands associated with the O ions. So many unknown parameters are involved in this model that only a qualitative discussion can be given. This model is shown to be reasonable when applied to Fe_2O_3. It has been fitted quantitatively to the data for NiO which is believed to constitute a simpler case.

2. *d* LEVEL CONDUCTION

Results of the previous attempt to analyze the data suggested the possibility that mobility in Fe_2O_3 is unusually low. A rough estimate of the magnitude of mobility may be made by the following consideration. It is observed that about 10^{-2} atom percent Ti must be added to Fe_2O_3 in order to change its room temperature conductivity appreciably. To produce a comparable change in the conductivity of germanium only about 10^{-7} atom percent of As need be added. It is concluded that the mobility of carriers in Fe_2O_3 is the order of $10^3\times10^{-7}/10^{-2}=10^{-2}$ cm²/volt sec. Failure to detect a Hall effect is consistent with this low mobility. Such behavior suggests that conduction is occurring in exceedingly narrow bands or in localized levels. The results of the analysis do not depend upon whether narrow bands or localized levels are assumed. However, in Sec. 2.3, mobility is shown to have an apparent activation energy. This suggests that conduction involves localized levels. These levels can probably be identified as the *d* levels of iron since the levels of oxygen constitute a wide band in ionic oxides such as Fe_2O_3.

An energy-level scheme is shown in Fig. 1. The *d* levels are shown lying between the filled and empty *sp* bands of oxygen. These bands are assumed in this section to be so far from the *d* levels that they play no part in conduction. The intrinsic ionization energy E_G represents the energy required to create an electron-hole pair, that is an Fe^{2+} and an Fe^{4+}. These diffuse from one cation site to the next by the exchange of an electron. Donor and acceptor ionization energies are represented in Fig. 1 by E_D and E_A. The distance of the Fermi level above the filled levels is represented by E_F.

Where energy bands are wide, carrier concentration depends upon the level density near the band edge. For bands less than kT wide or for localized levels, carrier

[1] F. J. Morin, Phys. Rev. **83**, 1005–1010 (1951).
[2] F. J. Morin, following paper [Phys. Rev. **93**, 1199 (1954)].

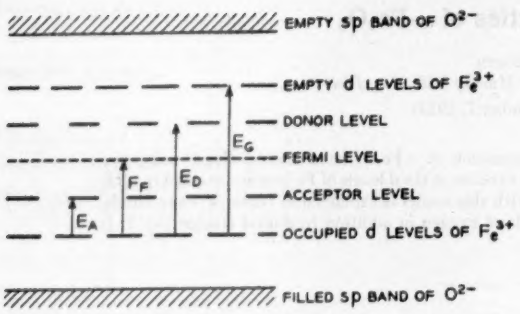

FIG. 1. Energy-level scheme assumed in the analysis of the data.

concentration must depend upon the total level density. It is assumed, therefore, that electron and hole concentrations are given by

$$n=N\exp[-(E_G-E_F)/kT], \tag{1}$$

$$p=N\exp(-E_F/kT), \tag{2}$$

where $N=4\times10^{22}$ iron atoms per cm³ of crystal. The assumption of narrow bands or localized levels also leads to the assumption that the kinetic energy term in the Seebeck effect is negligible so that for electrons alone,

$$QT=E_G-E_F, \tag{3}$$

and for holes alone,

$$QT=E_F, \tag{4}$$

where Q is the Seebeck effect in volts per degree. When both holes and electrons are involved two expressions are necessary, that for conductivity,

$$\sigma=\sigma_n+\sigma_p, \tag{5}$$

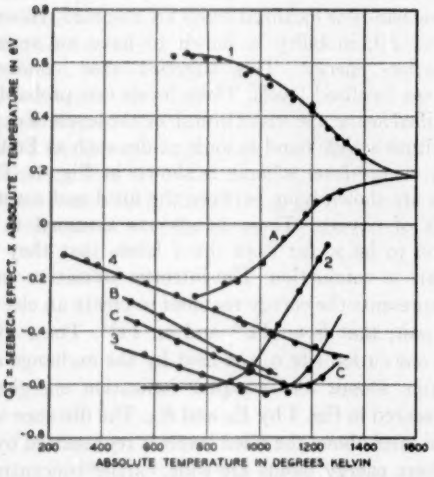

FIG. 2. The product of Seebeck effect and absolute temperature as a function of absolute temperature for samples of α-Fe_2O_3. Sample composition given in Table I.

and that for Seebeck effect,

$$QT\sigma=-(E_G-E_F)\sigma_n+E_F\sigma_p. \tag{6}$$

Combining (5) and (6) yields

$$\sigma_n=\sigma(E_F-QT)/E_G. \tag{7}$$

One more equation is needed in fitting the data:

$$\sigma_n/\sigma_p=(\mu_n/\mu_p)\exp[(2E_F-E_G)/kT], \tag{8}$$

where μ_n and μ_p are electron and hole mobilities.

2.1 SEEBECK EFFECT

Seebeck effect data from reference 1 is shown replotted in Fig. 2. Sample D has been omitted for clarity. Sample 1 is p type, the others are n type. QT increases (negatively) with temperature in the range of impurity conductivity. It tends toward a positive value as conduction enters what is assumed to be the intrinsic range. An extrapolation of the data suggests that QT (sample 1)$=QT$ (sample A) when $T>1600°$.

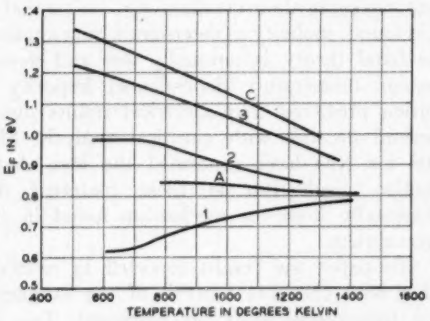

FIG. 3. Fermi energy as a function of absolute temperature computed as described in Sec. 2.1.

If this is assumed to represent an intrinsic region where $E_F=E_G/2$ and $n=p$, then a positive QT may mean that $\mu_p>\mu_n$. By assuming a value for E_G, the ratio μ_n/μ_p can be computed from σ and QT measured in this range using Eqs. (5) and (7). The assumed value for E_G can then be checked using Eqs. (5) and (8) by computing a fit to measured σ and QT in the range where $n\neq p$ but both are important. When this is done it is found that a fit can be obtained for samples 1, 2, and A when $E_G=1.6$ ev and $\mu_n/\mu_p=0.635$, and a fit for samples 3 and C when $E_d=1.7$ ev and $\mu_n/\mu_p=0.650$. The solid lines drawn on the QT plot represent values of QT used in the computation. Values of E_F found by this computation are shown in Fig. 3. For samples 4, B, and D it is assumed that $QT=E_G-E_F$.

The ionization energy of the impurities seems to change with impurity concentration. The flat portion of the E_F curves indicates an impurity level at 0.99 ev in sample 2, 0.85 ev in sample A, and 0.61 ev in sample 1. For the other samples, E_F behavior indicates the impurity levels to lie within 0.4 ev of the empty levels.

In these samples, E_F has left the neighborhood of the impurity level and is moving toward $E_G/2$. Consequently, the slopes of the carrier concentration curves for samples 3, 4, *B*, *C*, and *D* do not represent ionization energies of impurities.

2.2 CARRIER CONCENTRATION

Conduction electron concentration, computed from E_F values found in Sec. 2.1 and Eq. (1), is shown in Fig. 4. Impurity concentration can be estimated directly from the curves of Fig. 4 for samples 3, 4, *B*, *C*, and *D*. It can be determined for samples 1, 2, and *A* by fitting the curves using an expression of electrical neutrality. It should be recalled that, in addition to the titanium, donor centers were added to samples, *A*-*D* by reduction and acceptor centers added to samples 1–4 by oxidation. These additional centers are present in unknown amounts. However, because of the approximate way in which the data are being treated it seems worth while to compare the electrically determined impurity concentrations with those determined by chemical analysis. The comparison is made in Table I. The conclusion drawn from these data is

TABLE I. Impurity concentrations.

Sample No.	Titanium content in 10^{19} atoms/cm^3	Electrical impurities in 10^{19} atoms/cm^3
1	1.0	0.6
A	0.88	1.0
2	2.8	2.0
B	4.4	8.0
3	13.	2.5
C	13.	5.5
4	43.	46
D	72.	50

that there is good agreement between the electrical and chemical determination of impurity concentration. Since results obtained from the band model disagreed by several decades, the present agreement supports the assumptions leading to Eqs. (1), (2), (3), and (4).

2.3 MOBILITY AND WAVY BANDS

From n obtained in Sec. 2.2 and σ_n obtained by fitting *QT* data in Sec. 2.1 or measured directly, μ_n has been calculated and is shown in Fig. 5. Two things are unusual about these results: the low values found for mobility, and the temperature dependence which suggests an activation energy associated with mobility. Two regions of different temperature dependence can be distinguished. At low temperature the activation energy depends upon impurity concentration. At high temperatures it decreases with temperature tending toward an activation energy of 0.1 ev. This same behavior is found for NiO, reference 2, Fig. 5, the mobility reaching an activation energy of 0.1 ev at high-impurity concentrations and at high temperature.

A reasonable explanation for some of this behavior is suggested by the idea of "wavy bands" as described

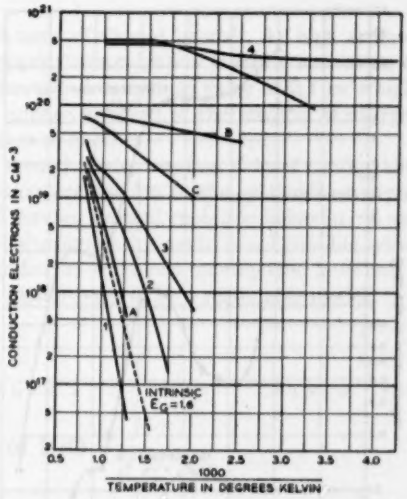

FIG. 4. Concentration of conduction electrons as a function of reciprocal absolute temperature computed with Eq. (1).

by Wannier[3] and James.[4] These are potential fluctuations produced by crystal imperfections and inhomogeneous distribution of impurities. In the present case, the potential fluctuations give rise to an activation energy for the motion of holes and electrons. If the potential wells are filled with carriers the fluctuations are smoothed out and the mobility activation energy decreased. This is brought about by increasing impurity concentration and by increasing temperature. The residual activation energy of 0.1 ev may be the energy

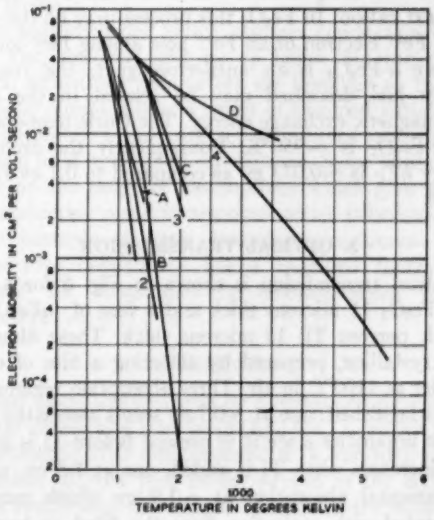

FIG. 5. Mobility of conduction electrons as a function of reciprocal absolute temperature computed from conductivity and conduction electron concentration.

[3] G. H. Wannier, Phys. Rev. **76**, 438–439 (1949).
[4] H. M. James, Science **110**, 254–256 (1949).

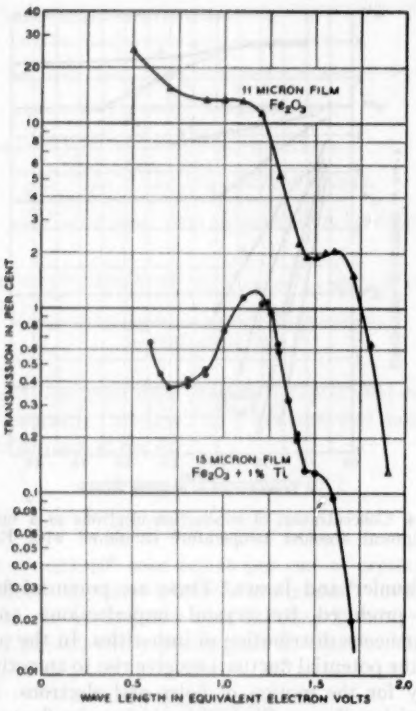

FIG. 6. Optical transmission as a function of wavelength for polycrystalline films of α-Fe_2O_3 sintered at 1100°C in air.

required for the fundamental transfer process of conduction, that is the energy required to transfer a carrier from the potential well of one cation to that of the next cation. In Fe_2O_3 this process may be the drift of an Fe^{2+} electron or an Fe^{4+} hole among Fe^{3+} ions.

Since α-Fe_2O_3 is an antiferromagnet, the transfer energy just described may be related to the antiferromagnetic exchange energy. The Curie temperature for α-Fe_2O_3 is $\sim$950°K. Consequently the exchange energy kT_C is $\sim$0.073 ev as compared to 0.1 ev found above.

3. OPTICAL TRANSMISSION

Optical transmission is shown in Fig. 6 for a film of α-Fe_2O_3 11 microns thick and a film of (αFe_2O_3+1 atomic percent Ti) 15 microns thick. These films are polycrystalline, prepared by sintering a film of oxide powder at 1100°C in air. Three absorption regions can be distinguished: one at $\sim$0.7 ev seems associated with donor impurities since it is present before Ti is added and increases when Ti is added, one at 1.5 ev, and a fundamental absorption at $\sim$1.9 ev which may be associated with excitation from the filled sp band of oxygen to empty d levels or to empty sp levels.

In Sec. 2.1 it was pointed out that Fermi level behavior indicated donor levels at 0.85 ev and 0.99 ev above the filled levels. The separation of filled and empty d levels was found to be 1.6–1.7 ev. This locates donor levels at 0.6–0.8 ev below the empty levels in agreement with the optical result of 0.7 ev. The results also suggest the absorption at 1.5 ev to be excitation from filled to empty d levels.

4. sp BAND CONDUCTION

Assuming the optical absorption at 1.9 ev to involve the sp bands of oxygen leads to the possibility of conduction by sp holes and electrons. Judging from experience with sp band conduction in oxides such as ZnO and Cu_2O, sp charge carriers can be expected to have mobilities in the range 10–100 cm²/volt sec at 1000°. This mobility range is greater than that found for d carriers by a factor of 10^2–10^4 at 1000° in pure αFe_2O_3. Thus the sp carrier concentration can be small compared to d carrier concentration and still contribute to conduction.

In Fig. 1 the d levels are shown between the bands of oxygen. If the d levels lie near enough to the filled band, excitation from sp to d will occur. At high temperature this situation will provide high-mobility holes and low-mobility electrons in addition to the low-mobility carriers from d to d excitation. The conduction, with increasing temperature, may become dominated by high-mobility holes. Measured QT will tend to become large and positive as it becomes increasingly influenced by high-mobility holes lying far below the Fermi energy. Such QT behavior is observed in NiO.

If the d levels lie about midway between the sp bands and the sp bands are near enough together, sp to sp excitation can be expected. In this case the contribution to conduction by sp electrons will more or less balance that by sp holes and QT will be small. Its sign will depend upon location of the d levels with respect to the sp bands and upon the relative mobilities of sp holes and electrons. This seems to be the situation in Fe_2O_3 assuming sp band conduction. The introduction of sp electrons in addition to sp holes prevents a quantitative fit to the data being made for Fe_2O_3 because too many unknown parameters are involved. If the d levels are assumed to be midway between the sp bands, and the absorption at 1.9 ev is assumed to be an sp to sp transition, the Fermi level in pure Fe_2O_3 will be at $\sim 1.9/2 = 0.95$ ev above the filled sp band. Then sp carrier concentration will be $\sim 4\times10^{15}$ cm^{-3}. For the sp carrier to make a contribution to conduction at 1000° equal to that of the d carriers, the sp mobility will have to be

$$\mu_{sp} = (n+p)_d \mu_d / (n+p)_{sp}$$
$$= 8\times10^{18}\times10^{-2}/4\times10^{15} = 20 \text{ cm}^2/\text{volt sec},$$

which is a reasonable result.

5. SUMMARY

Conductivity, Seebeck effect, and optical transmission of α-Fe_2O_3 have been analyzed using two

alternative models. The first model assumes the following: conduction is in the d levels of iron; the Seebeck effect depends only on the location of the Fermi level; the level density involved in conduction equals the cation density. The model yields a quantitative fit to the data. Impurity concentration determined electrically agrees with that determined chemically. Electrical and optical results are consistent. Carrier mobility is found to be below 0.1 cm²/volt sec. It has an activation energy dependent upon impurity concentration and temperature which is explained on the basis of "wavy bands". At high temperature and impurity concentration mobility activation energy tends towards a minimum value of 0.1 ev which may be the energy involved in the transfer of charge from one cation to another.

The second model assumes d level conduction and, in addition, conduction in the sp bands of oxygen by carriers having normal mobility behavior. A quantitative discussion of this model is not possible because of the number of unknown parameters involved. It is shown qualitatively to be a reasonable model.

PHYSICAL REVIEW VOLUME 93, NUMBER 6 MARCH 15, 1954

Electrical Properties of NiO

F. J. MORIN
Bell Telephone Laboratories, Murray Hill, New Jersey
(Received December 7, 1953)

The conductivity, Seebeck effect, and optical transmission of NiO have been analyzed using two alternative models. The first model assumes conduction to occur in the d levels of Ni ions and yields a quantitative fit to the data. Mobility behavior determined with this model is explained in terms of wavy bands. The second model assumes conduction in the filled sp band of oxygen in addition to d-level conduction. It also yields a quantitative fit to the data which, however, is unsatisfactory because the concentrations and mobilities which result for d carriers appear unreasonable. Examples of grain boundary conduction are analyzed.

1. INTRODUCTION

ELECTRICAL conductivity, Seebeck effect, and optical transmission have been measured on sintered polycrystalline samples of NiO. This was done in continuation of the work on α-Fe_2O_3[1,2] with the object of understanding the conduction mechanism in oxides having partially filled d levels. NiO containing lithium or excess oxygen[3,4] provides a p-type system for comparison with the n-type system: α-Fe_2O_3 containing titanium. NiO also provides a simpler subject for study than α-Fe_2O_3; it is not ferromagnetic, its structure is NaCl cubic, and conduction is believed to involve fewer unknown parameters.

The general behavior of NiO is very similar to that of α-Fe_2O_3. Conductivity is insensitive to impurities in concentrations below $\sim 10^{18}$ cm^{-3}. No Hall effect is observed. NiO differs in one essential way from α-Fe_2O_3: no n-type NiO is known. The data are analyzed in terms of the two models described in reference 2. The assumption of d-level conduction alone leads to the result that electron mobility is less than hole mobility by a factor of at least two decades.

Impurity ionization energy decreases with increasing impurity concentration. Lithium concentration determined electrically agrees with that determined chemically. Mobility activation energy decreases with increasing impurity concentration and temperature to the minimum value of 0.1 ev found for α-Fe_2O_3. This behavior is described in reference 2 in terms of a wavy-band model.

The second model, which assumes conduction by d holes and electrons and by sp holes, fits the data. Several adjustable parameters are involved so that a fit can be obtained over a range of assumed values for some parameters. Only one set of assumed parameters has been used in detailed calculations. Some limits can be set on the range of assumptions which give a fit.

A conduction result is described which is believed to be an example of grain boundary conduction. Its temperature dependence fits a modified theory of Henisch[5] for conduction in inhomogeneous semiconductors.

2. METHODS

Nickel oxide was prepared by thermal decomposition of either chemically pure $Ni(NO_3)_2$, $NiCO_3$, or NiC_2O_4. Stoichiometric NiO was prepared with difficulty since NiO tends to exist with excess oxygen in the lattice. It was found that the oxygen content of the sintered sample depended upon the salt from which it was prepared as well as upon sintering conditions. Stoichiometry was approched more closely using $NiCO_3$ and NiC_2O_4. This seems reasonable when the oxygen

[1] F. J. Morin, Phys. Rev. **83**, 1005–1010 (1951).
[2] F. J. Morin, preceding paper [Phys. Rev. **93**, 1195 (1954)].
[3] J. H. DeBoer and E. J. W. Verwey, Proc. Phys. Soc. (London) **49**, (extra part) (1937).
[4] E. J. W. Verwey, Chem. Weekblad **44**, 705–708 (1948).
[5] H. K. Henisch, Phil. Mag. **42**, 734 (1951).

TABLE I. Sintering conditions.

Sample No.	Starting material	Temperature °C	Atmosphere	Time hours	Lithium concentration Spectro.	Electrical
1	$NiCO_3$	1150	1000 N_2+1 H_2	15		
	resintered	1250	1000 N_2+1 H_2	15	slight trace	...
2	NiC_2O_4	1250	1000 N_2+0.3 H_2	15	slight trace	3.6×10^{17}
3	$NiCO_3$	1150	500 N_2+1 H_2	15	slight trace	3×10^{18}
4	$NiC_2O_4+Li_2CO_3$[a]	1250	1000 N_2+0.3 H_2	15	$\sim6\times10^{18}$	3×10^{18}
5	$NiC_2O_4+Li_2CO_3$[a]	1250	1000 N_2+0.3 H_2	15	6.0×10^{19}	5×10^{19}
6	$Ni(NO_3)_2+LiNO_3$[b]	1100	O_2	16	4.2×10^{20}	7×10^{21}
7	$Ni(NO_3)_2$	1200	O_2	16	...	...
8	$Ni(NO_3)_2$	1500	air	2	...	...

[a] Mechanical mixing.
[b] Melted together.

content and gaseous decomposition products of the salt are considered. Stoichiometry is roughly indicated by the color of the sample. Pure stoichiometric NiO is a pale green. After some experience had been obtained, conductivity and Seebeck effect were used as indicators of very close approach to stoichiometry.

Grain boundary behavior must be considered in polycrystalline oxide samples. When such samples are cooled from sintering temperature in an atmosphere containing oxygen, they oxidize more rapidly at grain boundaries than within grains. This produces grain boundary resistance in n-type oxides and grain boundary conductivity in p-type oxides. To eliminate grain boundary conductivity, samples to be studied were sintered in a reducing atmosphere. To check the absence of grain boundary conductivity, the conductivity temperature-dependence of these samples is compared in Sec. 3 with that of a single crystal (assumed to contain no boundaries) and with samples sintered and cooled in oxygen to produce grain boundary conductivity. Table I summarizes sample preparation conditions and lithium concentration determined electrically and by spectrochemical analysis.

3. CONDUCTIVITY

Conductivity is shown in Fig. 1. Samples 1, 2, and 3 represent attempts to achieve stoichiometry. Samples 4, 5, and 6 contain increasing amounts of lithium and unknown amounts of excess oxygen. The fact that the conductivity of samples 2, 3, and 4 blend into sample 1 above 1000° suggests that the conductivity of 1 in this region represents intrinsic behavior and, therefore, that 1 is the most nearly stoichiometric sample. Samples 4 and 5 were sintered under the same conditions as 2 so that, judging from conductivity, the amount of excess oxygen in 4 and 5 is much smaller than the amount of lithium. Sample 6 was sintered under the same conditions as 7 in which the major impurity is excess oxygen. Therefore, judging from conductivity, the amount of excess oxygen in 6 is much less than the amount of lighium. The single-crystal conductivity is included for comparison with polycrystalline conductivity. Samples 7 and 8 were sintered and cooled in oxygen to produce examples of grain boundary conductivity. A qualitative comparison of the conductivity curves supports the idea that samples 1, 2, 3, and 4 have no grain boundary conductivity and that samples 7 and 8 do have grain boundary conductivity. Samples 7 and 8 are described in detail in Sec. 9.

4. SEEBECK EFFECT

Seebeck results are shown in Fig. 2. QT indicates the movement of the Fermi level with temperature and impurity concentration. QT is found to be always positive. Ordinarily it will decrease at high temperature as the Fermi level nears the middle of the forbidden energy region and carriers of opposite sign become appreciable in number. This was the case for α-Fe_2O_3. The high-temperature behavior of samples 1, 2, and 3 is unusual, therefore, and suggests that electron mobility is less than hole mobility by a factor of at least two decades. The tendency of QT for samples 1, 2, and 3 to approach the same value at high temperature is consistent with their conductivity behavior and the idea that they are entering the range of intrinsic conductivity.

The Fermi level tends to level off with temperature when passing through an impurity level. The low temperature QT behavior for samples 4, 5, and 6 indicate the location of acceptor levels whose ionization energy changes with lithium concentration from 0.10 to 0.46 ev. QT for samples 2 and 3 indicates an impurity level around 0.5 ev and the hump in 4 indicates a higher-lying level around 0.7 ev. The slowness with which QT for 2, 3, and 4 approaches QT for 1 at high temperature suggests levels lying around 0.8–0.9 ev. These are more easily seen on examination of carrier concentration curves.

5. HALL EFFECT

No Hall effect was observed on the sintered samples. There was the possibility, however, that grain boundaries reduced mobility enough to make the Hall effect undetectable. Accordingly an attempt was made to measure Hall effect on the single crystal. Measurement was made at 600°K. Hall coefficient is given by

$$R_H = V_H t\times10^8/HI \text{ cm}^3/\text{coul},$$

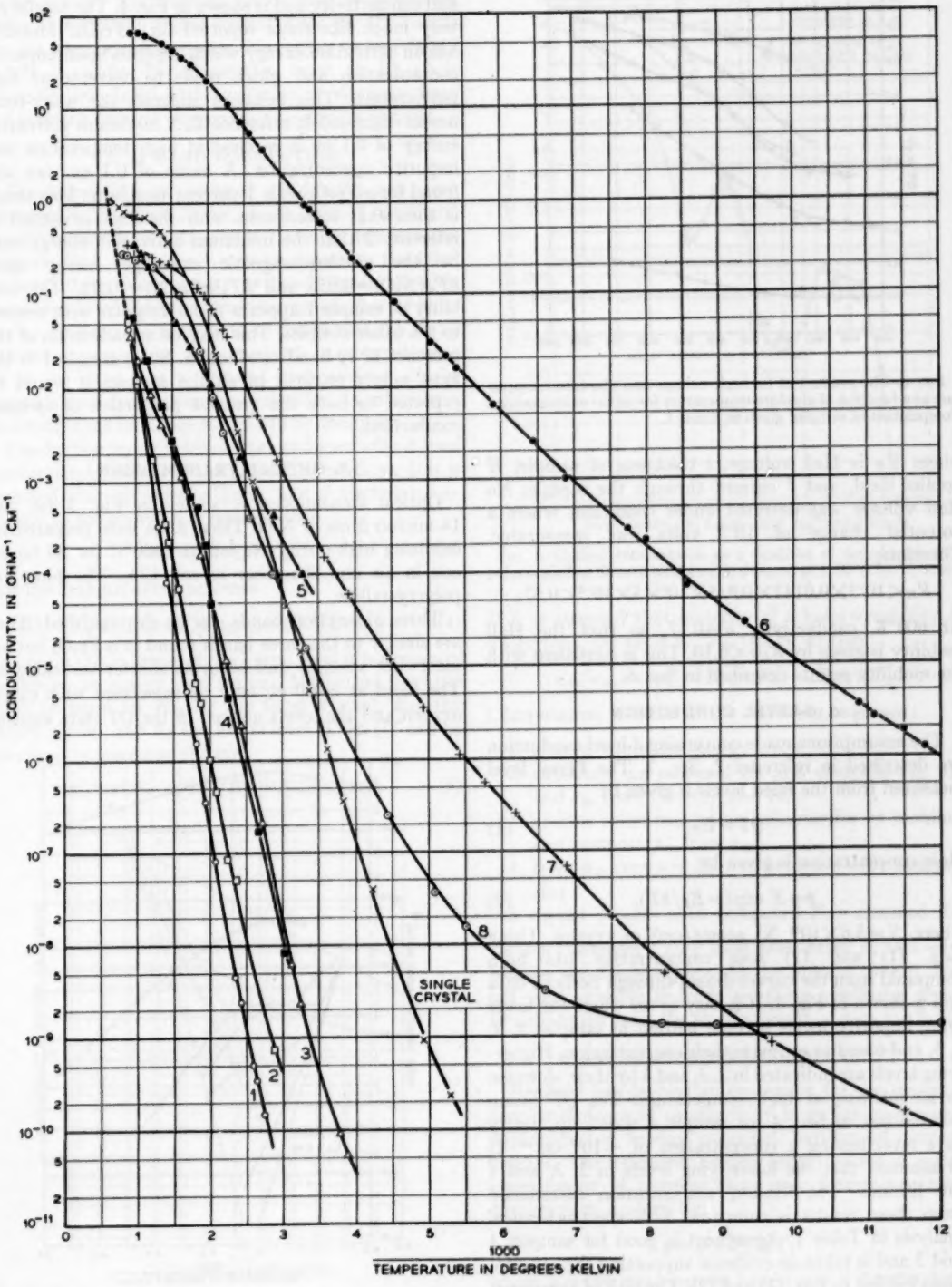

FIG. 1. Conductivity of nickel oxide samples as a function of reciprocal absolute temperature. Composition of samples given in Table I.

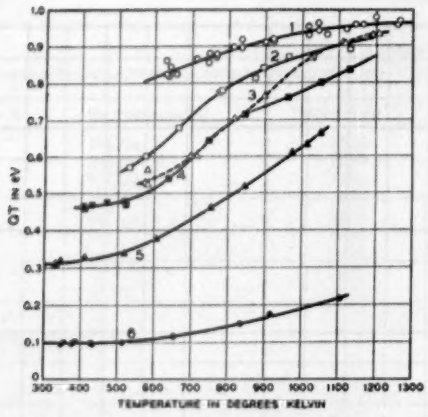

FIG. 2. The product of Seebeck voltage and absolute temperature as a function of absolute temperature for nickel oxide samples. Composition of samples given in Table I.

where V_H is Hall voltage, t thickness of sample, H applied field, and I current through the sample. No Hall voltage was detected under conditions where a potential change of 10^{-5} volts was measurable. Therefore,

$$R_H < 10^{-5} \times 0.0142 \times 10^8 / 5 \times 10^3 \times 5 \times 10^{-8} < 0.57.$$

At 600°K conductivity $\sigma = 0.17$, so that the Hall mobility is given by $R_H \sigma < 0.10$. This is consistent with the mobility results described in Sec. 6.

6. *d*-LEVEL CONDUCTION

The assumptions made concerning *d*-level conduction are described in reference 2, Sec. 2. The Fermi level measured from the filled levels is given by

$$QT = E_F. \tag{1}$$

Hole concentration is given by

$$p = N \exp(-E_F/kT), \tag{2}$$

where $N = 5.6 \times 10^{22}$ Ni atoms/cm³ of crystal. Using Eqs. (1) and (2) hole concentration has been computed from the curves drawn through Seebeck data and is shown in Fig. 3. It is easy to see where the lower lying impurity levels become ionized in samples 2, 3, 4, 5, and 6 and to estimate their concentration. Higher-lying levels are indicated in 2, 3, and 4 by their slowness to go intrinsic at high temperature. The QT hump pointed out in Sec. 4 for sample 4 shows up clearly as a level having a concentration of $\sim 10^{19}$ cm^{-3}. It is assumed that the lower-lying levels in 2, 3, and 4 are lithium. The lithium concentration determined from these results is compared with spectrochemical analysis in Table I. Agreement is good for samples 4 and 5 and is taken as evidence supporting the assumptions leading to Eqs. (1) and (2). The lack of agreement found for sample 6 has not been explained.

Mobility has been computed from hole concentration and conductivity and is shown in Fig. 4. The results are very much like those reported for α-Fe_2O_3.[3] Mobility has an activation energy which depends upon impurity concentration and which tends to decrease at high temperature. This behavior suggests the wavy-band model discussed in reference 2. A minimum activation energy of 0.1 ev is reached at high temperature and impurity concentration. A value of 0.1 ev was also found for α-Fe_2O_3 with 1 percent titanium. This result is somewhat inconsistent with the idea advanced in reference 2 that the minimum activation energy may be the antiferromagnetic exchange energy since $kT_C(\text{NiO}) = 0.056$ and $kT_c(\alpha\text{Fe}_2\text{O}_3) = 0.073$. The mobility of sample 1 appears to be irregular with respect to the other samples. This may be an indication of the presence of *sp*-band conduction. Since sample 1 is the most nearly intrinsic of all the samples it would be expected to have the greatest proportion of *sp*-band conduction.

7. OPTICAL TRANSMISSION

Optical transmission is shown in Fig. 5 for two 14-micron films of NiO. These films were prepared by oxidizing high-purity Ni foil at 1100°C for 20 hours, one in air and the other in wet CO_2. The films are polycrystalline.

Three absorption bands can be distinguished. They are similar to the three bands found in α-Fe_2O_3 but are somewhat stronger and occur at shorter wavelengths. The band at $\sim$1.0 ev may be associated with excess oxygen and the levels noticed in the QT data existing

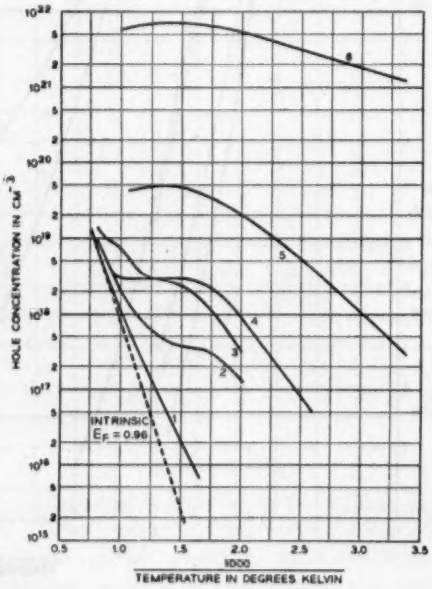

FIG. 3. Concentration of conduction holes as a function of reciprocal absolute temperature computed from Seebeck effect using Eq. (2).

at 0.8–0.9 ev. The band at 1.9 ev may be associated with the forbidden region indicated by the QT results for sample 1 which suggests this region to be $0.96\times2=1.92$ ev wide. The absorption band at 2.7 ev is probably associated with excitation of electrons from the filled sp band of oxygen into an empty sp band.

8. sp BAND CONDUCTION

The possibility of sp-band conduction has been discussed in reference 2, Sec. 4. As pointed out there, the QT behavior of NiO sample 1 at high temperature suggests that the d levels may be nearer to the filled sp band then to the empty sp band. Several models have been investigated on the assumption that sp holes but no sp electrons contribute to conduction. So many unknown parameters are involved in computing a fit to the data that a detailed discussion of all the computations does not seem worthwhile. As an example of the methods used, one model will be described.

Conduction by sp holes can be combined with d-level conduction by means of the following equations. If it is assumed that sp holes, d holes, and d electrons contribute to the conduction process, then

$$\sigma=\sigma_{sp}+\sigma_{dp}+\sigma_{dn}, \tag{3}$$

and the Seebeck effect becomes

$$QT=[(QT)_{sp}\sigma_{sp}+(QT)_{dp}\sigma_{dp}-(QT)_{dn}\sigma_{dn}]/\sigma. \tag{4}$$

To obtain QT in terms of the Fermi level it is necessary to assume an energy level system. Measuring from the filled sp band let E_{dp} be the filled d level, E_{dn} the empty d level, and E_F the Fermi level. Then QT can be rewritten in more useful form

$$\sigma_{dp}=\sigma(E_F-QT)/(E_{dp}+E_{dn}\sigma_{dn}/\sigma_{dp}). \tag{5}$$

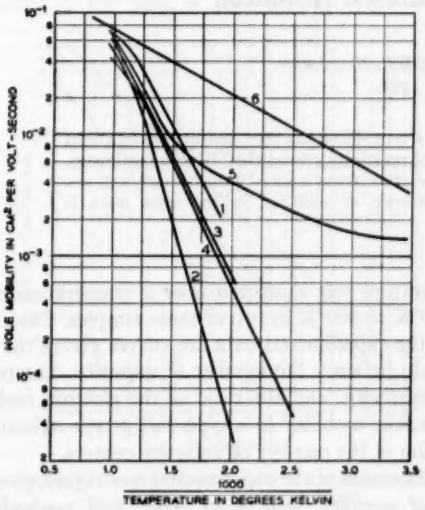

FIG. 4. Mobility of conduction holes as a function of reciprocal absolute temperature computed from conductivity and carrier concentration.

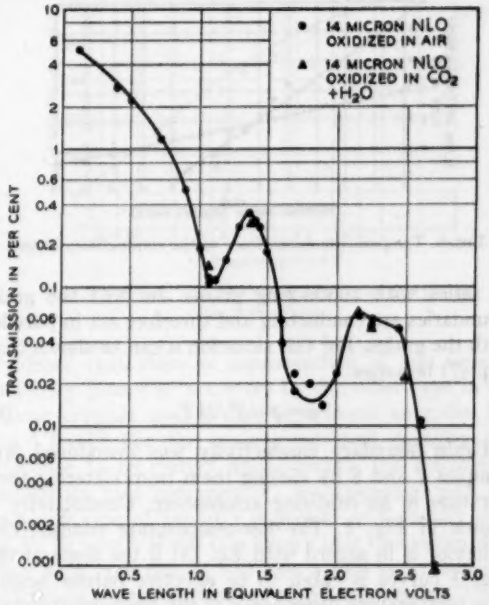
14 MICRON NiO OXIDIZED IN AIR
14 MICRON NiO OXIDIZED IN CO₂ +H₂O
TRANSMISSION IN PER CENT
WAVE LENGTH IN EQUIVALENT ELECTRON VOLTS

FIG. 5. Optical transmission as a function of wavelength for polycrystalline films of nickel oxide sintered at 1100°C for 20 hours.

If it is assumed that mobility of d holes = mobility of d electrons, the ratio σ_{dn}/σ_{dp} can be written

$$\sigma_{dn}/\sigma_{dp}=\exp[-(E_{dn}+E_{dp}-2E_F)/kT]. \tag{6}$$

Computation is made in the following sequence:

1. assume values for energy levels;
2. substitute an assumed E_F and compute σ_{sp}, σ_{dn} and σ_{dp} from (3), (5), and (6);
3. assume some reasonable behavior for sp mobility and compute p_{sp} from σ_{sp};
4. from p_{sp} compute E_F and compare with assumed E_F;
5. repeat process until computed E_F = assumed E_F.

Data for samples 1 to 5 have been fitted in this way. Results are disappointing. At the present time it does not seem possible to learn anything conclusive about sp conduction from the small amount of data available.

9. GRAIN BOUNDARY CONDUCTIVITY

Henisch[8] has derived an expression for the temperature dependence of conductivity in an inhomogeneous semiconductor having potential barriers of various heights. The effective barrier height φ for a series arrangement of barriers along any filamentary conduction path is given by

$$\varphi=\bar{\varphi}+S^2/2kT, \tag{7}$$

where $\bar{\varphi}$ is the mean barrier height and S the standard deviation in barrier height. This situation applies to α-Fe_2O_3 in which high-resistance grain boundaries are

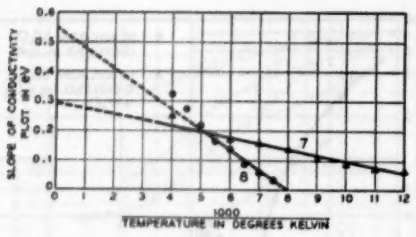

FIG. 6. Temperature dependence of the conductivity slope.

in series with conducting grains. In NiO the grain boundaries are conducting and therefore act in parallel with the grains. For this situation it can be shown that Eq. (7) becomes

$$\varphi = \bar{\varphi} - S^2/2kT. \tag{8}$$

Grain boundary conductivity was introduced into samples 7 and 8 by cooling them from sintering temperature in an oxidizing atmosphere. Conductivity is shown in Fig. 1. The low-temperature conductivity behavior is in accord with Eq. (8) if the slope of the Fig. 1 curves is taken to be effective barrier height. The temperature dependence of the conductivity slope is shown in Fig. 6 as plotted points. Straight lines are drawn through the points to determine the intercept at $1/T=0$ which is $\bar{\varphi}$ and the slope which is $S^2/2k$. Points deviate from straight line behavior at 200°K probably because the normal conductivity process becomes comparable to grain boundary conductivity. From these results $\bar{\varphi}=0.30$ ev and $S=0.059$ ev for sample 7, and $\bar{\varphi}=0.55$ ev and $S=0.108$ ev for sample 8.

10. SUMMARY

Conductivity, Seebeck effect, and optical transmission of NiO have been analyzed using two alternative models. The first model assumes the following: conduction is in the d levels of nickel; the Seebeck effect depends only upon the location of the Fermi level; the level density involved in conduction equals the cation density. The model yields a quantitative fit to the data. Impurity concentration determined electrically agrees with that determined chemically. Electrical and optical results are consistent. Carrier mobility is found to be below 0.1 cm²/volt sec. It has an activation energy dependent upon impurity concentration and temperature which is explained on the basis of wavy bands. At high temperature and impurity concentration mobility activation energy tends towards a minimum value of 0.1 ev which may be the energy involved in the transfer of charge from one cation to another.

The second model assumes d-level conduction and, in addition, conduction in the filled sp band of oxygen by holes having normal mobility behavior. A quantitative investigation has been made of this model with unsatisfactory results. The idea of sp-band plus d-level conduction is shown to be reasonable.

Two instances of grain boundary conduction are presented and analyzed in terms of a modified theory of Henisch.

PHYSICAL REVIEW VOLUME 93, NUMBER 6 MARCH 15, 1954

Drift Mobilities in Semiconductors. II. Silicon

M. B. Prince
Bell Telephone Laboratories, Murray Hill, New Jersey
(Received December 4, 1953)

The drift mobility of holes in n-type silicon and electrons in p-type silicon has been measured as functions of impurity concentration and temperature. In single crystals of resistivity greater than 10 ohm-centimeter, the mobility at 300°K of holes is $\mu_P=500\pm50$ cm²/volt-sec and of electrons is $\mu_N=1200\pm100$ cm²/volt-sec. For this high-resistivity material, the temperature dependence of mobility in the same units is $\mu_N=5.5\times10^8T^{-1.6}$ and $\mu_P=2.4\times10^8T^{-2.3}$.

INTRODUCTION

THIS paper constitutes a companion paper to one dealing with the drift mobilities in germanium.[1] The drift mobility of holes and electrons has been measured in silicon single crystals grown from starting material of relatively high purity. Drift measurements were made on samples that were cut from crystals whose resistivity values ranged from 0.3 to 30 ohm-centimeter at 300°K. The variation of mobility with temperature was measured over a temperature range of 150°K to 300°K in two of these samples. Calculated from the experimental data are curves giving the relationship between the number of impurity centers and the resistivity, and the ratio of the electron mobility to the hole mobility in n-type and p-type silicon as a function of the number of impurity centers.

A discussion of the experimental techniques, preparation of samples, sources of error, and methods for combining the results of various scattering mechanisms is given in I.

[1] M. B. Prince, Phys. Rev. 92, 681 (1953) hereinafter referred to as I.

MOBILITY *VERSUS* IMPURITY CENTER DENSITY

A. Experimental Results

The experimental results showing the mobility of electrons in p-type silicon and of holes in n-type silicon are given in Fig. 1 as a function of the resistivity of the sample. All the data presented in this section have been corrected to 300°K by using the temperature variation of the mobility which is discussed in a later section. Each experimental point represents the average of several individual measurements. In the case of electron mobility these results agree with the value

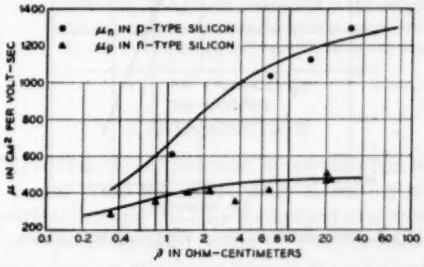

FIG. 1. Drift mobility *versus* resistivity for electrons in p-type silicon and holes in n-type silicon.

obtained by Haynes and Westphal[2] over the range of their resistivity values.

B. Interpretation

Less information can be extracted from the experimental data in the case of silicon than in the case of germanium.[1] The reason for this is twofold. Firstly, the data for silicon are fewer and extend over a smaller range than for germanium. Secondly, the art of purifying silicon has not at present reached the high degree attained in the case of germanium. There is some

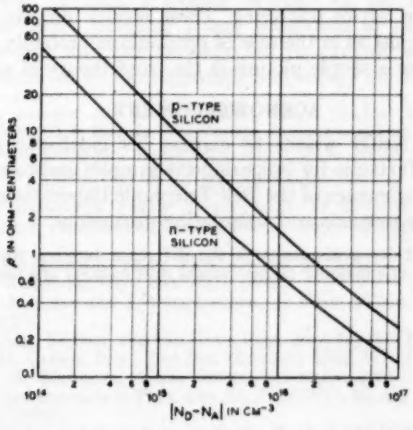

FIG. 2. Resistivity *versus* density of uncompensated impurities for n- and p-type silicon.

[1] J. R. Haynes and W. C. Westphal, Phys. Rev. **85**, 680 (1952).

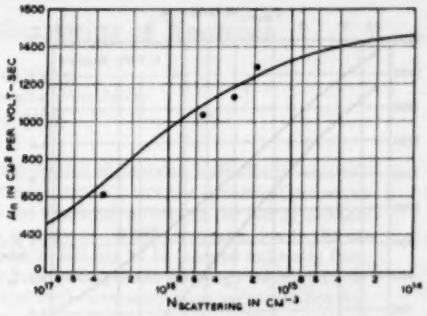

FIG. 3. Electron mobility *versus* density of scattering centers in silicon.

evidence that there is compensation of one type of impurity (donor or acceptor) by the other type in the silicon crystals used in this experiment near the 10^{16} cm^{-3} level.[3] For the present we shall consider this evidence to be correct and calculate the number of impurities in a specimen N_I by assuming that the minority type of impurity is present at a density level of 5×10^{14} cm^{-3}. While it is known that this assumption may be a poor one, it will give a first order approximation to the parameters we wish to determine. Using the relations $N_A-N_D=1/\rho_P q\mu_P$ and $N_D-N_A=1/\rho_N q\mu_N$ together with estimates of $b=\mu_N/\mu_P$, as explained in

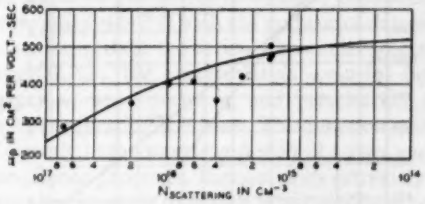

FIG. 4. Hole mobility *versus* density of scattering centers in silicon.

I, one can then obtain the density of majority impurities ($|N_A-N_D|+5\times10^{14}$) and the total density of impurities $N_I(=N_D+N_A=|N_D-N_A|+10^{15})$. N_D and N_A represent the density of donors and acceptors, ρ_N and ρ_P the resistivity of n- and p-type material, μ_N and μ_P the mobility of electrons and holes, and q the charge on an electron. With this information a plot of ρ *versus* $|N_D-N_A|$ can be obtained for p- and n-type silicon (Fig. 2), and plots of μ_N and μ_P *versus* N_I can be obtained (Figs. 3 and 4).

The solid curves in Figs. 1, 3, and 4 are empirical and have the same general shape as theoretical curves that include impurity scattering of the Conwell-Weisskopf[4] type. In drawing these curves, the higher values of mobility in the various parts of the plots are weighted more heavily due to the compensation effect

[3] Fuller, Theuerer, and Morin (unpublished).

[4] E. Conwell and V. F. Weisskopf, Phys. Rev. **69**, 258 (1946); **77**, 388 (1950).

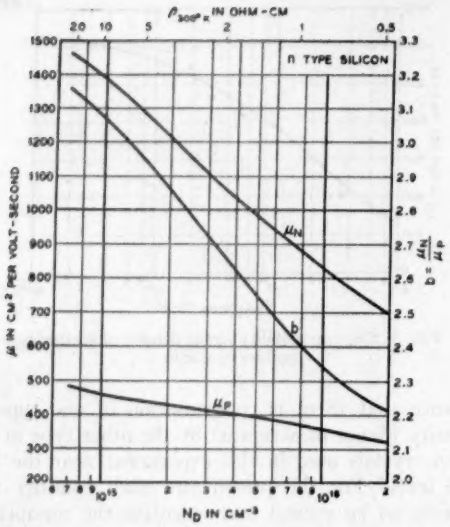

FIG. 5. Electron and hole mobilities in *n*-type silicon.

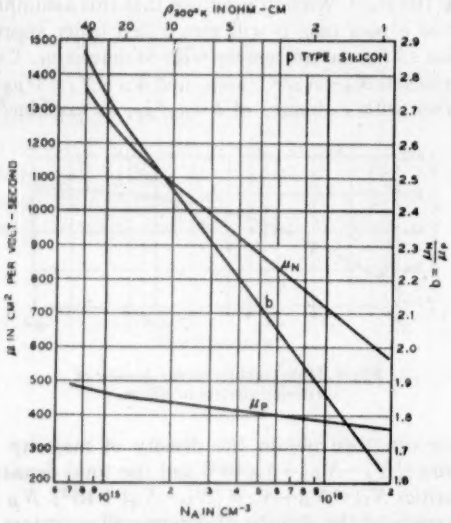

FIG. 6. Electron and hole mobilities in *p*-type silicon.

of impurities on the mobility (see I). Extrapolation of these curves to near the intrinsic range yields a lattice-scattering mobility of 1500 and 500 cm²/volt-second, respectively, for electrons and holes. Using these curves, one can obtain curves of drift mobility of the majority carrier and *b* for *n*-type and *p*-type silicon.[5] These are given as Figs. 5 and 6.

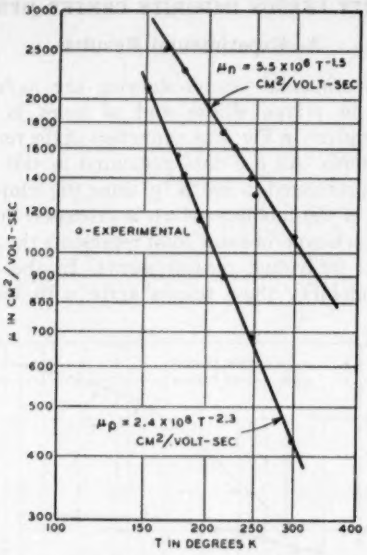

FIG. 7. Drift mobility *versus* temperature in silicon.

MOBILITY *VERSUS* TEMPERATURE

The results of measuring the temperature dependence of the drift mobility of electrons in *p*-type and of holes in *n*-type silicon are shown in Fig. 7. Down to 150°K the results are consistent with the lines $\mu_N = 5.5 \times 10^8 T^{-1.5}$ cm²/volt-sec and $\mu_P = 2.4 \times 10^8 T^{-2.33}$ cm²/volt-sec. Since there was appreciable impurity scattering in the *p*-type sample, the exponent for pure lattice scattering of electron mobility may be larger than the given -1.5. In the case of the *n*-type sample, the impurity scattering was negligible and therefore the exponent -2.3 is probably the correct exponent for pure lattice scattering. These results indicate that silicon, just as in the case of germanium, probably does not have a simple picture in the band theory of solids.

ACKNOWLEDGMENT

The writer wishes to express his indebtedness to A. A. Tartaglia for preparing the samples and to many of his colleagues of the Bell Telephone Laboratories for their suggestions and stimulating discussions.

[5] See I for a discussion of the difference between the drift mobility of a majority carrier and the drift mobility of a minority carrier.

Crystal Dynamics and Inelastic Scattering of Neutrons

G. PLACZEK AND L. VAN HOVE
Institute for Advanced Study, Princeton, New Jersey
(Received December 10, 1953)

A general discussion is given for the angular and energy distribution of neutrons inelastically scattered by a crystal, with special emphasis on those features of the distribution in which the dynamical properties of the crystal manifest themselves most immediately. The direct relationship between the energy changes in scattering and the dispersion law of the crystal vibrations is analyzed. While for x-rays, due to the extremely small relative size of these energy changes, the dispersion law has to be inferred indirectly from intensity measurements, it is shown that the very much larger relative magnitude of energy transfers in the case of slow neutrons opens the possibility of direct determination of the frequency-wave vector relationship and the frequency-distribution function of the crystal vibrations by energy measurements on scattered neutrons. The general properties of the outgoing neutron distribution in momentum space which are relevant for this purpose are derived by first considering the particularly instructive limiting case of neutrons initially at rest and subsequently generalizing the results to incident neutrons of arbitrary energy.

I. INTRODUCTION

THE diffraction of neutrons by crystals has been in recent years the object of an increasing number of investigations and has been recognized as a promising tool for crystallographic research.[1] Considerable work has been done on elastic scattering, the coherent part of which exhibits Bragg reflections in full analogy with x-rays, and on transmission measurements, dealing with total cross sections. The influence of crystal dynamics on neutron scattering was discussed by various authors[2–14a] and quantitative calculations of total cross sections were carried out on the basis of a greatly simplified model for the crystal elastic vibrations, the familiar Debye model, in which the velocity of sound waves (phonons) is assumed independent of wavelength, direction, and polarization.

From its success in describing specific heats, the Debye model is known to be a fair approximation for effects which involve the average of a smooth function over all crystal vibrations. It gives, therefore, at least for cubic crystals, a reliable estimate of the Debye-Waller factor affecting Bragg reflections of neutrons and x-rays and can be expected to provide a good orientation as to the magnitude and energy dependence of total inelastic neutron cross sections for the incoherent[15] part of the scattering. For other effects, however, in particular for the angular and energy distribution of inelastically scattered neutrons, the details of the vibration spectrum play a much more important role and the theoretical discussion has to take them into account. It is the aim of the present investigation to show how they manifest themselves in this distribution.

The analogous problem for the inelastic scattering of x-rays has been the object of detailed theoretical and experimental study[16–23] with the purpose of determining from scattering data the actual vibrational spectrum of the crystal, i.e., the exact relation $\omega=\omega_j(\mathbf{q})$ between frequency ω, wave vector $\mathbf{q}$, and polarization j of a plane wave vibration (phonon). This function manifests itself directly in the wavelength shift of x-rays scattered by one-phonon processes. Because of its extremely small relative size, however, this shift is not readily accessible to measurement, and hence the function $\omega_j(\mathbf{q})$ has to be inferred from measurements of the scattered intensity.

Because of the different relation between energy and momentum the energy balance is entirely altered in the case of slow neutrons. While this is generally true, it may be exemplified more concretely by considering the important particular case of coherent one-phonon processes. For an incident wavelength of the order of the lattice constant the absolute energy changes in a

[1] For surveys see: J. M. Cassels, Progr. Nuclear Phys. **1**, 185 (1950); D. J. Hughes, *Pile Neutron Research* (Addison-Wesley Publishing Company, Cambridge, 1953); G. E. Bacon and K. Lonsdale, Repts. Progr. in Phys. **16**, 1 (1953).
[2] G. C. Wick, Physik. Z. **38**, 403, 689 (1937).
[3] I. Pomeranchuk, Physik. Z. Sowjetunion **13**, 65 (1938).
[4] Halpern, Hamermesh, and Johnson, Phys. Rev. **59**, 981 (1941).
[5] R. Seeger and E. Teller, Phys. Rev. **62**, 37 (1942).
[6] R. Weinstock, Phys. Rev. **65**, 1 (1944).
[7] A. Akhiezer and I. Pomeranchuk, J. Phys. (U.S.S.R.) **11**, 167 (1947).
[8] Placzek, Nijboer, and Van Hove, Phys. Rev. **82**, 392 (1951).
[9] J. M. Cassels, Proc. Roy. Soc. (London) **A208**, 527 (1951).
[10] D. A. Kleinman, thesis, Brown University, 1951 (unpublished) and abstracts in Phys. Rev. **81**, 326 (1951); **86**, 622 (1952); **90**, 355 (1953).
[11] I. Waller and P. O. Fröman, Arkiv. Fysik **4**, 183 (1951).
[12] P. O. Fröman, Arkiv. Fysik **4**, 191 (1951); **5**, 53 (1952).
[13] G. Placzek, Phys. Rev. **86**, 377 (1952).
[14] G. L. Squires, Proc. Roy. Soc. (London) **A212**, 192 (1952).
[14a] G. Placzek, Phys. Rev. **93**, 897 (1954).
[15] Using the same terminology as Hughes, reference 1, we call coherent the interferent part of the slow neutron scattering, and incoherent the noninterferent part due to spin and isotope disorder. The existence of these two types of scattering has been discussed first by Wick (reference 2). Both types comprise elastic as well as inelastic processes.
[16] J. Laval, Bull. soc. franç. minéral. **64**, 1 (1941).
[17] K. Lonsdale, Repts. Progr. in Phys. **9**, 256 (1943).
[18] M. Born, Repts. Progr. in Phys. **9**, 294 (1943).
[19] W. H. Zachariasen, *Theory of X-Ray Diffraction in Crystals* (John Wiley and Sons, Inc., New York, 1945).
[20] P. Olmer, Acta Cryst. **1**, 57 (1948); Bull. soc. franç. minéral. **71**, 144 (1948).
[21] H. Curien, thèse, Paris, 1952; Acta Cryst. **5**, 393 (1952).
[22] H. Cole and B. E. Warren, J. Appl. Phys. **23**, 335 (1952).
[23] H. Cole, J. Appl. Phys. **24**, 482 (1953).

general direction are, for neutrons, not radically different from those for x-rays, being in both cases of the order of average phonon energies. For neutrons, however, the energy corresponding to such an incident wavelength is of the same order of magnitude and the relative change in energy or wavelength is therefore of order one, which considerably reduces the difficulty of its direct measurement.

As the incident wavelength increases, the contrast between the x-ray and neutron cases becomes even more pronounced. For x-rays, in the case of a Bravais lattice, the absolute energy change in a given scattering direction becomes proportional to the incident energy, with a relative change of the order of the ratio of sound velocity to light velocity. For neutrons, on the other hand, the absolute energy changes in a given scattering direction do not systematically decrease with increasing incident wavelength; in fact, they ultimately become independent of it, tending to finite values. Thus, a limiting case is approached for which the incident energy and momentum can be put equal to zero both in the conservation laws which determine the energy shift, and in the transition probabilities. Physically, this is the case of a neutron initially at rest which takes up energy and momentum by absorbing a phonon. For finite incident wavelength this description will be adequate if the outgoing wavelength is small compared to the incoming one. Under this condition the transition probability is approximately constant, and hence the scattering cross section becomes proportional to the wavelength. The actual wavelength beyond which the condition is satisfied depends on the scattering direction and on crystal structure, but it often lies in the accessible region of the subthermal neutron spectrum in which transmission experiments are already quite common. Scattering experiments in this region[24] still present a certain intensity problem and may be easier at somewhat shorter wavelengths, which, as we shall see, have to be used anyhow if one wishes to determine the function $\omega_j(\mathbf{q})$ for all $\mathbf{q}$.

In the above remarks we have been concerned with coherent one-phonon scattering only. The energy distribution of neutrons incoherently scattered by one-phonon processes is also of considerable interest in connection with crystal dynamics, especially for cubic crystals, for which, as will be shown later, it is directly connected with the frequency-distribution function of the crystal. For multiphonon processes, coherent as well as incoherent, the relation between neutron scattering and dynamical properties of the crystal is much more complicated, except for the limiting of high incident energies.[13] For the purpose of the determination of the frequency spectrum of the crystal from scattering data these processes are therefore of less interest, and for this reason we shall concentrate on one-phonon processes.

One has, however, to inquire under what conditions one-phonon scattering can be experimentally separated from multiphonon processes. For a single crystal, one-phonon coherent scattering is distinguishable from all other processes by its energy distribution in each outgoing direction, which will be seen to comprise a finite number of discrete energy values, appearing as sharp peaks above the continuous background of one-phonon incoherent and multiphonon scattering. No such direct distinction is possible between neutrons scattered in one-phonon incoherent and multiphonon processes. While the contribution of the latter to the cross section is always decisive at high incident energies and often appreciable even in the limiting case of zero incident energy,[25] it would, however, seem quite feasible to carry out scattering experiments under conditions (moderately low temperature and incident energy and high nuclear mass) which make multiphonon effects either entirely negligible or reduce them to the size of a manageable correction, thus allowing the isolation of the incoherent one-phonon processes.

In the following sections, we discuss the angular and energy distribution of neutrons scattered by one-phonon processes, both coherent and incoherent. Sections II and III deal with the limiting case of infinite incident wavelength. Apart from its direct interest, this case illustrates with particular clarity the essential aspects of the problem. The complications arising for finite incident wavelength are of a purely formal nature and are taken care of in Sec. IV.

Regarding the crystal structure, we consider for convenience a Bravais lattice, with one nucleus per cell. For a lattice with more particles per cell, our discussion has to be supplemented by consideration of a structure factor and of optical branches in the frequency spectrum. With minor modifications, our treatment can also be extended to neutron scattering by spin waves in ferromagnetic crystals, a problem already studied by Moorhouse[26] from a slightly different point of view.

II. ANGULAR AND ENERGY DISTRIBUTION FOR INFINITE INCIDENT WAVELENGTH

In the limiting case of infinite incident wavelength, energy can only be transferred from the crystal to the neutron, and inelastic scattering is therefore possible only if the crystal is at a nonvanishing temperature. In one-phonon scattering, a phonon initially excited in the crystal is absorbed by the neutron initially at rest which picks up its energy. Energy conservation is expressed by

$$k^2 = (2m/\hbar)\omega_j(\mathbf{q}), \tag{1}$$

where m and $\mathbf{k}$ are the mass and final wave vector of the neutron; $\mathbf{q}$, j, and $\hbar\omega_j(\mathbf{q})$ are the wave vector, polarization index ($j=1, 2, 3$ for a Bravais lattice), and energy of the absorbed phonon.

Equation (1) holds for both coherent and incoherent

[24] P. Egelstaff, Nature 168, 290 (1951).

[25] For estimates see Squires, reference 14.

[26] R. G. Moorhouse, Proc. Phys. Soc. (London) 64, 1097 (1951).

scattering. For the latter it is the only condition relating the phonon variables to the momentum $\hbar\mathbf{k}$ transferred to the neutron; Eq. (1) has then only to be supplemented by an intensity formula given in Sec. III. For coherent scattering, the interference between waves scattered by the various nuclei imposes a further relation

$$\mathbf{k}=\mathbf{q}+2\pi\boldsymbol{\tau}, \tag{2}$$

where $\boldsymbol{\tau}$ is an arbitrary vector of the reciprocal lattice.[7] It is well known that the wave vector $\mathbf{q}$ of a lattice vibration is only defined apart from 2π times an arbitrary reciprocal lattice vector $\boldsymbol{\tau}$; the frequency $\omega_j(\mathbf{q})$ is accordingly a periodic function of $\mathbf{q}$,

$$\omega_j(\mathbf{q}+2\pi\boldsymbol{\tau})=\omega_j(\mathbf{q}). \tag{3}$$

To a phonon of wave vector $\mathbf{q}+2\pi\boldsymbol{\tau}$ can be attributed a momentum $\hbar(\mathbf{q}+2\pi\boldsymbol{\tau})$, and in this sense Eq. (2) is conventionally regarded as expressing momentum conservation.[27]

The conservation laws determine the main features of the angular and energy distribution of scattered neutrons. To show this, we shall use the following properties of the $\omega_j(\mathbf{q})$ function, valid for any Bravais lattice: for each $j=1, 2, 3$, $\omega_j(\mathbf{q})$ is a continuous function with the periodicity (3) of the reciprocal lattice; for $\mathbf{q}$ approaching $2\pi\boldsymbol{\tau}$, it has the form

$$\omega_j(\mathbf{q})=c_j(\boldsymbol{\xi}/\xi)\xi; \quad \boldsymbol{\xi}=\mathbf{q}-2\pi\boldsymbol{\tau}, \tag{4}$$

where $c_j(\boldsymbol{\xi}/\xi)$, the sound velocity for long wavelengths in the direction $\boldsymbol{\xi}/\xi$, can be calculated from the elastic constants.[28]

For incoherent scattering, the energy equation (1) shows that the length of $\mathbf{k}$ is restricted to the interval

$$0\leqslant k\leqslant k_{\max}=(2m\omega_{\max}/\hbar)^{\frac{1}{2}}, \tag{5}$$

where $\omega_{\max}$ is the maximum of $\omega_j(\mathbf{q})$ for all $\mathbf{q}$ and j; the direction of $\mathbf{k}$ is unrestricted. Equation (5) defines in $\mathbf{k}$ space a sphere Σ of radius $k_{\max}$ and center $\mathbf{k}=0$. Any vector with endpoint inside or on Σ is a possible value for the outgoing neutron wave vector. Hence, neutrons are scattered in all directions, with energies ranging continuously from 0 to $\hbar\omega_{\max}$. This conclusion holds for single crystals as well as for powders.

The restrictions affecting $\mathbf{k}$ are more severe for coherent scattering. Combining Eqs. (1), (2), (3) one obtains them in the simple form

$$k^2=(2m/\hbar)\omega_j(\mathbf{k}). \tag{6}$$

For each j, (6) defines in $\mathbf{k}$ space a surface S_j, which may be composed of several disconnected parts. The surfaces S_1, S_2, S_3 in general cross each other, and the set of all three will be called S. We suppose the origin $\mathbf{k}=0$ not to be counted as a point of S. For neutrons scattered coherently with absorption of one phonon, the outgoing wave vector is thus restricted to have its endpoint on S.

In order to discuss the general properties of the surface S, let us call lattice vectors in $\mathbf{k}$ space the reciprocal lattice vectors $\boldsymbol{\tau}$ multiplied by 2π, and let us speak accordingly of lattice points and cells in $\mathbf{k}$ space. We state

(i) The surface S is entirely contained in the sphere Σ.

(ii) Each radius of the sphere Σ crosses S at least once and in general a finite number of times not smaller than 3.

(iii) Each connected region of $\mathbf{k}$ space inside Σ which contains a lattice point $2\pi\boldsymbol{\tau}\neq 0$ and a point $\mathbf{k}_1$, where $\omega_j(\mathbf{k}_1)=\omega_{\max}$ for some j, is crossed by S; in particular, S crosses any cell of $\mathbf{k}$ space, centered at a lattice point $2\pi\boldsymbol{\tau}\neq 0$ and fully contained in Σ.

Property (i) is obvious. To establish (ii), we notice first that, S being a two-dimensional surface, if a radius of Σ crosses it at all, it will in general do so a finite number of times. To show that every radius crosses S, consider

$$\varphi_j(\mathbf{k})=k^2-(2m/\hbar)\omega_j(\mathbf{k})$$

as a function of k for fixed direction of $\mathbf{k}$ and fixed j: for small k, Eq. (4) gives

$$\varphi_j(\mathbf{k})=k^2-(2m/\hbar)c_j(\mathbf{k}/k)\cdot k<0,$$

whereas, for $k=k_{\max}$,

$$\varphi_j(\mathbf{k})=k_{\max}{}^2-(2m/\hbar)\omega_j(\mathbf{k})=(2m/\hbar)[\omega_{\max}-\omega_j(\mathbf{k})]\geqslant 0.$$

Since the function is continuous, it must vanish for at least one value k_j of k, giving a point on S. For general directions of $\mathbf{k}$, the three k_j's will be different. Property (iii) is established by a similar continuity argument, considering $\varphi_j(\mathbf{k})$ for the polarization j which gives $\omega_j(\mathbf{k}_1)=\omega_{\max}$, along a path in $\mathbf{k}$ space from $2\pi\boldsymbol{\tau}$ to $\mathbf{k}_1$.

The physical meaning of property (i) is quite trivial: it states that the outgoing neutron energy never exceeds the maximum phonon energy $\hbar\omega_{\max}$. Property (ii) determines the main features of the angular and energy distribution for coherent one-phonon scattering by a single crystal: neutrons are scattered in every direction and for each direction the outgoing energy has a finite number of discrete values, in general three or more. Measurement of outgoing energy as function of direction determines the surface S and thus yields $\omega_j(\mathbf{k})$.[29] This type of scattering is, therefore, particularly well fitted to give information on the crystal vibrations.

As mentioned in the introduction, the discrete nature of their energy spectrum allows an experimental separation of neutrons scattered in one-phonon coherent processes. It is, indeed, easily established that in

[27] The momentum $\hbar\mathbf{q}$ thus attributed to a vibration is not to be confused with the momentum of the crystal considered as a system of particles, and Eq. (2) has nothing in common with momentum conservation in the sense of particle dynamics.

[28] H. A. Jahn, Proc. Roy. Soc. (London) **A179**, 320 (1941).

[29] In order to measure in this way $\omega_j(\mathbf{q})$ for every $\mathbf{q}$ and j, one has to use neutrons with nonvanishing initial momentum. See Eqs. (17) and (18) below.

multiphonon coherent processes, as well as in incoherent inelastic scattering, the final wave vector $\mathbf{k}$ depends on three or more parameters, giving in each direction an outgoing energy which ranges continuously over one or more finite intervals. The latter type of energy distribution is also obtained for coherent one-phonon scattering by a powder, as is shown by averaging over orientations the energy distribution for a single crystal. In this respect, powders are less convenient than single crystals for study of the elastic vibrations by means of neutron scattering.

Returning to one-phonon coherent scattering by a single crystal, we have still to consider the implications of property (iii) above. (iii) is of interest particularly when the sphere Σ contains a rather large number of lattice points of $\mathbf{k}$ space. It then shows that the surface S is distributed in Σ with a certain uniformity, since it passes through every cell inside Σ, except possibly the cell centered at the origin. In every direction, the discrete values of the outgoing wave vector $\mathbf{k}$ will be distributed over the interval $0 \leqslant k \leqslant k_{\max}$ with a corresponding amount of uniformity.

While such conclusions are bound to be rather vague, it is instructive to compare the size of the sphere Σ with the size of the lattice cell in $\mathbf{k}$ space. The ratio of their volumes is

$$\frac{(4\pi/3)k_{\max}^3}{(2\pi)^3/v_0} = \frac{v_0}{6\pi^2}\left(\frac{2m\omega_{\max}}{\hbar}\right)^{\frac{1}{2}} = F, \tag{7}$$

where v_0 is the volume per particle in the crystal.

The parameter F plays an important role in determining the general shape of the surface S. When F is very small compared to 1, the sphere Σ is entirely in the region where the approximation (4) applies with $\tau=0$. Equation (6) reduces to

$$k = (2m/\hbar)c_j(\mathbf{k}/k), \quad (j=1, 2, 3). \tag{8a}$$

Hence, S is formed of three closed surfaces around the origin of $\mathbf{k}$ space, intersecting each other and fully contained in the lattice cell of center $\mathbf{k}=0$. For slightly larger F, S can be expected to have the same general shape, but Eq. (8a) will have to be completed with correction terms of relative order $F^{\frac{1}{2}}, F^{\frac{1}{2}}, \cdots$. For $F \gg 1$ on the other hand, the shape of S is again simple in the region of $\mathbf{k}$ space where k is small compared to $k_{\max}$. S is there composed of three closed surfaces around each lattice point $2\pi\tau \neq 0$, of approximate equation

$$\xi = 4\pi^2\hbar\tau^2[2mc_j(\xi/\xi)]^{-1} + \cdots, \quad (j=1, 2, 3), \qquad \xi = \mathbf{k} - 2\pi\tau, \tag{8b}$$

with correction terms of relative order $F^{-\frac{1}{2}}, F^{-\frac{1}{2}}, \cdots$. In the region where k is comparable to $k_{\max}$, S behaves quite differently: it runs continuously from cell to cell in $\mathbf{k}$ space.

For actual crystals F seems to be larger than one, but in general not large enough for (8b) to apply. This is thus the case intermediate between those considered above. Here even the general shape of S cannot be predicted without a fairly accurate knowledge of the $\omega_j(\mathbf{q})$ function. Conversely this case would appear to be all the more favorable for the determination of the $\omega_j(\mathbf{q})$ function from the measured shape of the surface S.

The calculation of F for an actual substance requires the knowledge of $\omega_{\max}$, which is accurately available only for a very few crystals. It is, however, only the order of magnitude of F which is of interest, and this is easily obtained by remarking that the order of magnitude of $\omega_{\max}$ is given by the Debye temperature θ

$$\omega_{\max} \simeq k_B\theta/\hbar,$$

(k_B = Boltzmann constant).[30] The approximate value of F thus obtained, defined by

$$F_D = \frac{v_0}{6\pi^2}\frac{(2mk_B\theta)^{\frac{1}{2}}}{\hbar^3}, \tag{9}$$

is given in Table I for a few substances.

III. INTENSITY FORMULAS FOR LONG INCIDENT WAVELENGTH

The discussion of Sec. II has to be supplemented by the consideration of the scattered intensity per unit angular and energy range. This intensity is simply expressed in terms of the differential cross section $d\sigma/d\mathbf{k}$ per unit volume in $\mathbf{k}$ space.

We consider a single crystal and measure the coherent cross section per nucleus in units of $\langle a\rangle_{\text{Av}}^2$ and the incoherent cross section per nucleus in units of $\langle a^2\rangle_{\text{Av}} - \langle a\rangle_{\text{Av}}^2$. a is the spin- and isotope-dependent scattering length. The units are, respectively, the coherent and incoherent scattering cross sections of the bound nucleus per unit solid angle. With the aid of standard methods[7] it is then found that

$$\frac{d\sigma_1^{\text{inc}}}{d\mathbf{k}} = \frac{2}{Mk_0}\exp[-\langle(\mathbf{k}\cdot\mathbf{u})^2\rangle_{\text{Av}}]\frac{v_0}{(2\pi)^3}\sum_j\int d\mathbf{q} \times \frac{[\mathbf{k}\cdot\mathbf{e}_j(\mathbf{q})]^2}{k^2}\frac{\delta[k^2-2m\hbar^{-1}\omega_j(\mathbf{q})]}{\exp[\beta\omega_j(\mathbf{q})]-1}, \tag{10}$$

$$\frac{d\sigma_1^{\text{coh}}}{d\mathbf{k}} = \frac{2}{Mk_0}\exp[-\langle(\mathbf{k}\cdot\mathbf{u})^2\rangle_{\text{Av}}]\sum_j\frac{[\mathbf{k}\cdot\mathbf{e}_j(\mathbf{k})]^2}{k^2} \cdot \frac{\delta[k^2-2m\hbar^{-1}\omega_j(\mathbf{k})]}{\exp[\beta\omega_j(\mathbf{k})]-1}. \tag{11}$$

The suffix 1 in σ_1^{inc} and σ_1^{coh} refers to one-phonon scattering. M is the ratio of nuclear to neutron mass. In the Debye-Waller factor $\exp[-\langle(\mathbf{k}\cdot\mathbf{u})^2\rangle_{\text{Av}}]$, $\mathbf{u}$ is the displacement vector of any nucleus in the crystal from its equilibrium position, and the average is taken over

[30] For tungsten, calculations by P. C. Fine [Phys. Rev. **56**, 355 (1939)] give $\hbar\omega_{\max}/k_B = 336°$, as compared to $\theta = 373°$ from the elastic constants and $\theta = 310°$ from specific heats.

the thermal equilibrium distribution. $\mathbf{e}_j(\mathbf{q})$ is the polarization vector of the phonon defined by j and $\mathbf{q}$, β is the reciprocal temperature multiplied by hk_B^{-1}. The integration over $\mathbf{q}$ in (10) extends over one cell in $\mathbf{k}$ space. The argument of the δ function in (11) gives directly the Eq. (6) of the surface S discussed in the previous section and the functions $\mathbf{e}_j(\mathbf{k})$ as well as $\omega_j(\mathbf{k})$ are defined for all $\mathbf{k}$ through the periodicity condition corresponding to (3).

The cross sections (10) and (11) correspond to transition probabilities for a neutron initially at rest, in conformity with the limiting case discussed in the previous section. The incident momentum hk_0 thus appears only in the factor relating transition probability to cross section. This limiting case applies if $k \gg k_0$. For coherent scattering, as follows from our discussion of the surface S, k has a nonvanishing minimum, and hence (11) holds for all outgoing energies as soon as $k_0 \ll k_{\min}$. For incoherent scattering, on the other hand, there is no such minimum. However small k_0 may be, therefore, the limiting case will not apply in the small region of the outgoing energy spectrum where k is not large compared to k_0. Here (10) must be replaced by the general expression (15).

Equation (10) can be considerably simplified for cubic crystals. As is well known, a quadratic form $\Sigma_{xy} A_{xy} k_x k_y$ invariant under the operations of any of the cubic point groups is a multiple of $\Sigma_x k_x^2$, i.e., $A_{xy} = A\delta_{xy}$ (δ_{xy} = Kronecker symbol). For cubic crystals, this fact implies, firstly,[19]

$$\langle (\mathbf{k}\cdot\mathbf{u})^2 \rangle_{\text{Av}} = k^2 \langle u_0^2 \rangle_{\text{Av}},$$

where u_0 is the component of $\mathbf{u}$ in an arbitrary direction. The Debye-Waller factor is thus independent of the direction of $\mathbf{k}$. Secondly,

$$\sum_j \int d\mathbf{q} e_j^x(\mathbf{q}) e_j^y(\mathbf{q}) \frac{\delta[k^2 - 2mh^{-1}\omega_j(\mathbf{q})]}{\exp[\beta\omega_j(\mathbf{q})] - 1} = A\delta_{xy},$$

with

$$A = \frac{1}{3} \sum_j \int d\mathbf{q} \frac{\delta[k^2 - 2mh^{-1}\omega_j(\mathbf{q})]}{\exp[\beta\omega_j(\mathbf{q})] - 1}.$$

Introducing the frequency distribution function $g(\omega)$, defined as the number of normal vibrations per unit frequency interval, divided by the total number of vibrations,

$$g(\omega)d\omega = \frac{1}{3} \frac{v_0}{(2\pi)^3} \sum_j \int_{\omega \le \omega_j(\mathbf{q}) \le \omega + d\omega} d\mathbf{q}, \qquad g(\omega) = 0 \quad \text{for} \quad \omega > \omega_{\max},$$

we find:

$$\frac{d\sigma_1^{\text{inc}}}{d\mathbf{k}} = \frac{2}{Mk_0} \exp[-k^2\langle u_0^2 \rangle_{\text{Av}}] \times \int_0^{\omega_{\max}} \frac{\delta(k^2 - 2mh^{-1}\omega)}{\exp(\beta\omega) - 1} g(\omega) d\omega,$$

TABLE I. The parameter F_D.

Substance	Lattice type	10^{24} v_0 in cm^3	θ in °K	F_D
Pb	cu face-cent.	30.0	88	3.6
W	cu body-cent.	15.7	310	12
Fe	cu body-cent.	11.7	462	17
Al	cu face-cent.	16.5	398	19

or

$$\frac{d\sigma_1^{\text{inc}}}{d\mathbf{k}} = \frac{h}{Mmk_0} \exp[-k^2\langle u_0^2 \rangle_{\text{Av}}] \frac{g(hk^2/2m)}{\exp(\beta hk^2/2m) - 1}. \quad (12)$$

For cubic crystals the one-phonon incoherent scattering has thus, for small k_0, an energy distribution independent of direction and simply expressed in terms of the frequency distribution $g(\omega)$ of the crystal.

It has been shown elsewhere[31] that the $g(\omega)$ function of a general crystal contains a finite number of singularities resulting from the periodic structure; they are singular points ω_c in the neighborhood of which $g(\omega)$ has one of the two forms

$$g(\omega) = g(\omega_c) + \begin{cases} A|\omega - \omega_c|^{\frac{1}{2}} + O(\omega - \omega_c) & \text{for } \omega < \omega_c \\ O(\omega - \omega_c) & \text{for } \omega > \omega_c \end{cases}, \quad (13)$$

or the same with $\omega < \omega_c$ and $\omega > \omega_c$ interchanged. The constant A can have either sign; it is usually negative for $\omega_c < \omega_{\max}$ and positive for $\omega_c = \omega_{\max}$ [$\omega_{\max}$ is in general a singular point of $g(\omega)$]. The symbol $O(\omega - \omega_c)$ denotes a rest term of order $|\omega - \omega_c|$ for $\omega \to \omega_c$. The singular frequencies ω_c are simply related to the $\omega_j(\mathbf{q})$ function of the crystal: apart from exceptional cases, they are the values of $\omega_j(\mathbf{q})$ at the points where grad $\omega_j(\mathbf{q}) = 0$, $(j = 1, 2, 3)$.[31] We shall call them the singular frequencies of the crystal. The general shape of the energy distribution $(2mk/h^2)(d\sigma_1^{\text{inc}}/d\mathbf{k})$ (for fixed direction of $\mathbf{k}$) can be predicted from the behavior of $g(\omega)$ and a typical distribution is given in Fig. 1. Its singularities are of the same analytical type as (13), ω being replaced by k or the energy $E = h^2k^2/2m$.[32]

Apart from (10), the inelastic incoherent cross section contains terms due to multiphonon processes. In general they depend on the direction of $\mathbf{k}$, but the energy distribution in each direction can be shown to be continuously differentiable. The energy distribution in each direction for inelastic incoherent scattering by a cubic

[31] L. Van Hove, Phys. Rev. 89, 1189 (1953); in the formulas on p. 1191 of this paper $(\nu - \nu_c)^{\frac{1}{2}}$ must be replaced by $|\nu - \nu_c|^{\frac{1}{2}}$. The vector $\mathbf{q}$ there used is our present vector $\mathbf{q}$ divided by 2π. The frequency distribution of a simple cubic crystal has been calculated with its correct singularities by G. F. Newell, J. Chem. Phys. 21, 1877. See also H. B. Rosenstock and G. F. Newell, J. Chem. Phys. 21, 1607 (1953); H. B. Rosenstock and H. M. Rosenstock, J. Chem. Phys. 21, 1608 (1953).

[32] All our statements concerning singularities in the $g(\omega)$ function and in energy distributions of scattered neutrons hold for general values of the force constants of the crystal. The origin and nature of possible exceptions have been discussed by Van Hove (reference 31).

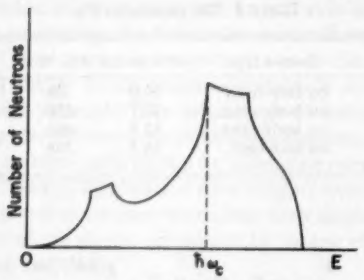

FIG. 1. Schematic shape of the energy distribution of scattered neutrons for long incident wavelength in the case of one-phonon incoherent scattering. E is the outgoing neutron energy, and ω_c a singular frequency of the crystal.

crystal has, therefore, still the shape illustrated in Fig. 1; its singularities in the first derivative are all due to one-phonon processes and are the same in all directions.

For noncubic crystals, the one-phonon incoherent cross section cannot be expressed in terms of the frequency distribution $g(\omega)$ of the crystal. The polarization terms of Eq. (10) cannot be eliminated, and the energy distribution of scattered neutrons varies with direction. In each direction, however, it has the shape illustrated in Fig. 1 and its singularities, unaffected by multiphonon processes occur, as for cubic crystals, at neutron energies E_c independent of direction and related by $E_c=\hbar\omega_c$ to the singular frequencies of the crystal.[33] As mentioned later, the singular frequencies of the crystal do not show up in coherent cross sections. Incoherent scattering of neutrons, for crystals where it is appreciable, seems to be the simplest phenomenon singling out these frequencies, which are important in determining the analytical singularities of the frequency distribution of the crystal.

The foregoing discussion was concerned with single crystals. For inelastic scattering by a powder, according to (12) nothing is changed for a cubic crystal, whereas Eq. (10) must be averaged over orientations in the noncubic cases. As we have seen, however, the singularities in the energy distribution occur at energies independent of direction and are thus retained in the averaging; consequently, the qualitative behavior shown in Fig. 1 remains unchanged.

Turning now to coherent scattering, we note that in one-phonon processes, the neutrons scattered in a given direction have a discrete energy spectrum, corresponding to outgoing wave vectors $\mathbf{k}_1, \mathbf{k}_2, \cdots$. From (11) the cross section per unit solid angle for the outgoing beam of energy $\hbar^2k_i^2/2m$ is

$$\left(\frac{d\sigma_1^{\text{coh}}}{d\Omega}\right)_{k_i}=\frac{2}{Mk_0}\exp[-\langle(\mathbf{k}_i\cdot\mathbf{u})^2\rangle_{\text{Av}}]\cdot\frac{[\mathbf{k}_i\cdot\mathbf{e}_j(\mathbf{k}_i)]^2}{\{\exp[\beta\omega_j(\mathbf{k}_i)]-1\}\cdot|2k_i-2m\hbar^{-1}d\omega_j/dk|}, \quad (14)$$

[33] L. Van Hove (to be published).

where j is the polarization index for which $k_i^2=2m\hbar^{-1}\omega_j(\mathbf{k}_i)$, and the derivative of $\omega_j(\mathbf{k})$ is taken at $\mathbf{k}=\mathbf{k}_i$, for fixed orientation of $\mathbf{k}$. For a powder, Eq. (14) must be averaged over all crystal orientations, producing in each direction an outgoing energy distribution continuous over finite intervals.

As mentioned before, multiphonon coherent scattering by a single crystal gives in each direction a continuous energy distribution of outgoing neutrons. Without entering into its detailed discussion, we shall mention that the energy distribution contains again, in general, singularities of type (13), produced by two-phonon processes. In this case the singularities occur at energies unrelated to the singular frequencies of the crystal and varying with the outgoing direction considered. They are thereby distinguishable from the singularities resulting from one-phonon incoherent scattering (which occur at the same energies in all directions), and for a powder they disappear by directional averaging.

To summarize the results obtained in the previous sections, we shall now briefly recall the main properties derived for the angular and energy distribution of inelastically scattered neutrons by single crystals in the limit of long incident wavelengths. In each outgoing direction the energy distribution of scattered neutrons contains a discrete part, resulting from one-phonon coherent scattering, and a continuous part produced by incoherent and multiphonon coherent scattering. The discrete part gives direct information on the crystal vibrations: the outgoing momentum $\mathbf{k}$ verifies Eq. (6) for some j. The continuous part has singularities of the analytical type (13) (with ω replaced by outgoing energy), the shape of which is illustrated in Fig. 1. Some of these singularities occur at energies E_c independent of direction: they are produced by incoherent one-phonon scattering and $\hbar^{-1}E_c$ are the singular frequencies of the crystal. The other singularities, which occur at energies varying with direction, originate from two-phonon coherent scattering.

IV. EXTENSION TO ARBITRARY INCIDENT WAVELENGTHS

The previous considerations are easily extended to the inelastic scattering of neutrons of arbitrary initial momentum $\hbar\mathbf{k}_0$. The only important change is the occurrence of scattering with energy transfer from the neutron to the crystal. Apart from this fact, we shall see that all essential features of the angular and energy distribution are retained. As the discussion runs entirely parallel to that presented in Secs. II and III, we shall make it very brief and restrict ourselves to scattering by a single crystal.

Considering first one-phonon incoherent scattering, we find for the case of energy gain by the neutron that the final wave vector $\mathbf{k}$ has in every direction a length ranging from k_0 to $(k_0^2+2m\hbar^{-1}\omega_{\max})^{\frac{1}{2}}$, whereas for energy loss by the neutron, k ranges from k_0 down

to 0 if $k_0^2 \leqslant 2mh^{-1}\omega_{\max}$, or to $(k_0^2-2mh^{-1}\omega_{\max})^{\frac{1}{2}}$, if $k_0^2 > 2mh^{-1}\omega_{\max}$. The differential cross sections are

$$\frac{d\sigma_1^{\text{ine}}}{d\mathbf{k}} = \frac{2}{Mk_0}\exp[-\langle(\boldsymbol{\kappa}\cdot\mathbf{u})^2\rangle_{\text{Av}}]\frac{v_0}{(2\pi)^3}\sum_j \int d\mathbf{q} \times \frac{[\boldsymbol{\kappa}\cdot\mathbf{e}_j(\mathbf{q})]^2}{|k^2-k_0^2|}\times\left[\frac{1}{\exp[\beta\omega_j(\mathbf{q})]-1}+\tfrac{1}{2}(1\mp 1)\right] \cdot\delta[k^2-k_0^2\mp 2mh^{-1}\omega_j(\mathbf{q})]. \quad (15)$$

The upper (lower) signs correspond to scattering with energy gain (loss) by the neutron, i.e., to $k>k_0$ ($k<k_0$). The integration is extended over one cell in $\mathbf{k}$ space. $h\boldsymbol{\kappa}$, with $\boldsymbol{\kappa}=\mathbf{k}-\mathbf{k}_0$, is the momentum transfer.

For cubic crystals, Eq. (15) can be simplified with the help of the frequency distribution function $g(\omega)$:

$$\frac{d\sigma_1^{\text{ine}}}{d\mathbf{k}} = \frac{h}{Mmk_0}\exp[-\kappa^2\langle u_0^2\rangle_{\text{Av}}]\times\frac{\kappa^2}{|k^2-k_0^2|} \times\left(\frac{1}{\exp(\beta h|k^2-k_0^2|/2m)-1}+\tfrac{1}{2}(1\mp 1)\right) \times g(h|k^2-k_0^2|/2m). \quad (16)$$

For cubic as well as noncubic crystals, the energy distribution in each outgoing direction has singularities of the type shown in Fig. 1 and Eq. (13) (ω being replaced by the neutron energy), occurring at energies

$$h^2k^2/2m = (h^2k_0^2/2m) \pm \hbar\omega_e,$$

where the ω_e are the singular frequencies of the crystal. Multiphonon incoherent scattering produces no such singularities.

For coherent scattering the situation is again similar to that prevailing in the limiting case of $k_0=0$. For one-phonon processes with energy gain by the neutron, momentum and energy conservation are expressed by the single equation

$$k^2-k_0^2 = (2m/h)\omega_j(\mathbf{k}-\mathbf{k}_0), \quad j=1,2,3, \quad (17)$$

the obvious generalization of Eq. (6). Equation (17) defines in $\mathbf{k}$ space a surface located between the spheres of radii k_0 and $(k_0^2+2mh^{-1}\omega_{\max})^{\frac{1}{2}}$, centered at the origin. Each radius of the large sphere intersects the surface at least once, in general a finite number of times, and each cell of $\mathbf{k}$ space contained between the two spheres is crossed by the surface [compare properties (i), (ii), (iii) in Sec. II]. Some points of the surface may, however, correspond to a vanishing energy transfer: they give rise to elastic coherent scattering. If we include them, the main feature of the angular and energy distribution is, therefore, retained: neutrons are scattered in each direction with a discrete energy spectrum.

The situation is slightly more complicated for one-phonon coherent scattering with energy loss by the neutron, which is governed by the equation

$$k_0^2-k^2 = (2m/h)\omega_j(\mathbf{k}-\mathbf{k}_0). \quad (18)$$

This equation has no solution, and the type of scattering considered is thus impossible when k_0 is smaller than a minimum value $k_0^{(1)}$; it is only for k_0 larger than a value $k_0^{(2)}>k_0^{(1)}$ that neutrons are scattered in *every* direction. Both for $k_0>k_0^{(2)}$ and $k_0<k_0^{(2)}$ the scattered neutrons have a discrete energy spectrum in each outgoing direction. The actual values of $k_0^{(1)}$ and $k_0^{(2)}$ depend on the details of the $\omega_j(\mathbf{q})$ function. It is, however, generally true that

$$k_0^{(1)} \leqslant \pi\tau_0, \quad (19)$$

$$k_0^{(2)} \leqslant (2mh^{-1}\omega_{\max})^{\frac{1}{2}}, \quad (20)$$

where τ_0 is a reciprocal lattice vector of minimum length.[34]

The differential cross section for one-phonon coherent scattering is

$$\frac{d\sigma_1^{\text{coh}}}{d\mathbf{k}} = \frac{2}{Mk_0}\exp[-\langle(\boldsymbol{\kappa}\cdot\mathbf{u})^2\rangle_{\text{Av}}]\sum_j \frac{[\boldsymbol{\kappa}\cdot\mathbf{e}_j(\boldsymbol{\kappa})]^2}{|k^2-k_0^2|} \times\left[\frac{1}{\exp[\beta\omega_j(\boldsymbol{\kappa})]-1}+\tfrac{1}{2}(1\mp 1)\right] \times\delta[k^2-k_0^2\mp 2mh^{-1}\omega_j(\boldsymbol{\kappa})], \quad (21)$$

with the same use of double signs as in Eq. (15). An expression similar to (14) is easily deduced from Eq. (21).

There exists for one-phonon coherent scattering a special case deserving a discussion of its own: it is the case when $\mathbf{k}_0$ approximately verifies the Bragg condition

$$|\mathbf{k}_0+2\pi\boldsymbol{\tau}|^2 \simeq k_0^2.$$

Inelastic scattering with $\boldsymbol{\kappa}$ nearly equal to $2\pi\boldsymbol{\tau}$ and with small energy transfer is then taking place, with a large differential cross section increasing proportionally to $(k^2-k_0^2)^{-2}\sim|\boldsymbol{\kappa}-2\pi\boldsymbol{\tau}|^{-2}$ when the Bragg condition is approached. This is seen from Eq. (21) by using

$$\exp[\beta\omega_j(\boldsymbol{\kappa})-1] \simeq \beta\omega_j(\boldsymbol{\kappa}) = \frac{\beta h}{2m}|k^2-k_0^2| \simeq \beta c_j\left(\frac{\boldsymbol{\kappa}-2\pi\boldsymbol{\tau}}{|\boldsymbol{\kappa}-2\pi\boldsymbol{\tau}|}\right)|\boldsymbol{\kappa}-2\pi\boldsymbol{\tau}|.$$

The nature of the conservation laws for this special case was discussed by Seeger and Teller;[5] Waller and Fröman[11] gave a detailed treatment of the differential cross section.[34a]

[34] The condition $k_0 \geqslant \pi\tau_0$ insures the possibility of the type of scattering under discussion for some but not all orientations of the crystal. It can be written $\lambda_0 \leqslant \lambda_B$ where λ_0 is the incident wavelength and $\lambda_B=(2\tau_0)^{-1}$ the Bragg cut-off wavelength. It was first given by Wick (reference 2). The inequality (20) applies to an arbitrary orientation of the crystal.

[34a] *Note added in proof.*—See also the recent paper by R. D. Lowde, Proc. Roy. Soc. (London) **A221**, 206 (1954).

Regarding multiphonon coherent scattering, the general situation is again the same as in the case of long incident wavelength: in each outgoing direction the scattered neutrons have a continuous energy spectrum, with singularities resulting from two-phonon processes and occurring at energies which vary with direction.

It has been the main purpose of this paper to put in evidence the direct relationship between the energy changes of neutrons scattered by a crystal and the dispersion law of the crystal vibrations as expressed by the $\omega_j(\mathbf{q})$ and $g(\omega)$ functions. We hope to have shown that energy measurements on scattered neutrons provide a new approach to the problem of determining these functions from scattering data. While the few experimental data so far available[34,35,36] do not as yet permit an analysis along these lines, the foregoing discussion indicates that further experimental work in this field would be of considerable interest.

[35] B. N. Brockhouse and D. G. Hurst, Phys. Rev. **88**, 542 (1952).
[36] R. D. Lowde, Proc. Phys. Soc. (London) **A65**, 857 (1952) and reference (34a).

PHYSICAL REVIEW VOLUME 93, NUMBER 6 MARCH 15, 1954

Calculation of the Energy Band Structures of the Diamond and Germanium Crystals by the Method of Orthogonalized Plane Waves*

FRANK HERMAN
RCA Laboratories Division, Radio Corporation of America, Princeton, New Jersey
(Received October 22, 1953)

The mathematical procedure employed in recent exploratory calculations of the energy band structures of the diamond and germanium crystals is described. Some of the symmetry properties of the eigensolutions of diamond-type lattices and the construction of an approximate potential for the diamond crystal are reviewed.

The relative order of the crystal eigenvalues $E_\gamma(\mathbf{k})$ for a particular $\mathbf{k}$ was found to depend more upon the symmetry of the crystal potential than upon the detailed nature of this potential. On the other hand, the curvatures of the energy surfaces calculated by perturbation theory were found to depend in a rather critical manner upon the exact form of the crystal potential.

It would appear that more reliable estimates of the energy band structures of actual crystals can be obtained with the aid of Herring's method of orthogonalized plane waves than by means of other approximational methods requiring comparable effort provided (1) reliable crystal potentials are employed, (2) calculations are carried to the point where the eigensolutions are satisfactorily "convergent," and (3) eigensolutions for more than just the points of high symmetry in the reduced zone are investigated.

A more elaborate calculation of the energy band structure of the germanium crystal has been undertaken; the work is now in progress.

1. INTRODUCTION

RECENT developments in the field of semiconductor physics[1,2] have stimulated widespread interest in the diamond-type valence crystals. Although the general behavior of these crystals can be readily understood in terms of simple phenomenological models, a detailed knowledge of their energy band structures should prove useful in many problems.

This paper describes the mathematical procedure employed in recent exploratory calculations of the electronic structures of the diamond[3,4] and germanium[5] crystals. The method of orthogonalized plane waves (OPW), first proposed by Herring[6] and already successfully applied to metallic lithium[7,8] and beryllium,[9] is used here for the first time to study valence crystals.

The exploratory studies of diamond and germanium have revealed some hitherto unexpected features in the energy band structures of these crystals.

In particular, the lowest conduction band states at the central point of the reduced zone in each case were found to be triply degenerate, rather than nondegenerate, as earlier work on diamond,[10,11] and silicon[12,13] had suggested. Moreover, by means of perturbation-type calculations, it was found that the states normally

* This paper is based on a dissertation submitted in partial fulfillment of the requirements for the degree of Doctor of Philosophy, in the Faculty of Pure Science, Columbia University, January, 1953.
[1] W. Shockley, *Electrons and Holes in Semiconductors* (D. Van Nostrand Company, Inc., New York, 1950).
[2] *Semi-Conducting Materials*, edited by H. K. Henish (Butterworths Scientific Publications, London, 1951).
[3] F. Herman, Phys. Rev. **88**, 1210 (1952).
[4] F. Herman, Ph.D. thesis, Columbia University, January, 1953 (unpublished); available on microfilm through University Microfilms, University of Michigan, Ann Arbor, Michigan.
[5] F. Herman and J. Callaway, Phys. Rev. **89**, 518 (1953).
[6] C. Herring, Phys. Rev. **57**, 1169 (1940).
[7] C. Herring, Phys. Rev. **55**, 598 (1939).
[8] R. H. Parmenter, Phys. Rev. **86**, 552 (1952).
[9] C. Herring and A. G. Hill, Phys. Rev. **58**, 132 (1940).
[10] G. E. Kimball, J. Chem. Phys. **3**, 560 (1935).
[11] A. Morita, Science Repts. Tôhoku Univ. **33**, 92 (1949). A numerical error has recently been detected in this work by J. C. Slater and G. F. Koster (see reference 18).
[12] J. F. Mullaney, Phys. Rev. **66**, 326 (1944).
[13] D. K. Holmes, Ph.D. thesis, Carnegie Institute of Technology, 1949 [Phys. Rev. **87**, 782 (1952)].

occupied by electrons, i.e., the conduction band states of lowest energy, did not occur at the central zone point but along the six (1,0,0) axes somewhere within the reduced zone.

In the neighborhood of each of these six energy minima, the surfaces of constant energy were approximately ellipsoids of revolution. Since eigensolutions associated with only a limited number of reduced wave vectors were actually determined, the exact locations along the (1,0,0) axes of these energy minima were not deduced.

The present computations also indicate that the valence states of maximum energy in both diamond and germanium occur at the central point of the reduced zone. In each case these states are triply degenerate. Unlike some earlier results,[10,14] each of the four valence bands in diamond was found to have finite width.

In view of the strong current interest in the exact shape of the energy surfaces in the diamond-type valence crystals,[15–19] a more elaborate calculation of the band structure of the germanium crystal has been undertaken. The work is now in progress.

2. CRYSTAL EIGENFUNCTIONS AND EIGENVALUES

The electronic structure of a crystal can be determined by solving the Hartree-Fock equations for all the states belonging to the core and valence bands and the low-lying conduction bands. In the ground state, a cyclic crystal of the diamond type containing M^3 unit cells must have as many occupied states as there are occupied states in the $2M^3$ atoms forming the crystal, namely, $2ZM^3$, where Z is the nuclear charge. These $2ZM^3$ states can be arranged into $Z-4$ core bands and 4 valence bands. Each energy band contains M^3 doubly degenerate states corresponding to the M^3 allowed values of the reduced wave vector $\mathbf{k}$.

In actual numerical studies, it is not possible to work with so many electronic states. Instead, one may consider a limited number of eigensolutions which correspond to a representative set of $\mathbf{k}$ uniformly distributed throughout the reduced zone. (Since the reciprocal lattice of the diamond-type crystals is body-centered cubic, the reduced zone is the truncated octahedron shown in Fig. 1.) For example, one might choose the 256 $\mathbf{k}$ forming the simple cubic lattice one octant of which is shown in Fig. 2. Only 19 of these 256 reduced wave vectors are nonequivalent because the reciprocal lattice is invariant to the symmetry operations of the crystallographic point group O_h. Thus, a reasonably detailed picture of the form of a particular energy band could be obtained by evaluating 19 crystal eigensolutions.

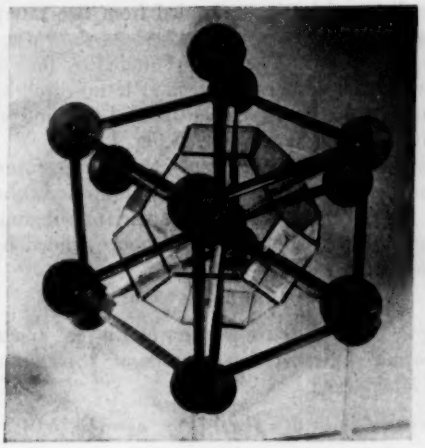

FIG. 1. Crystal model showing reduced zone.

As a further simplification, one could evaluate the energy eigenvalues and the slopes and curvatures of the energy surfaces at certain points of high symmetry in the reduced zone. The energy band structure could then be deduced from these results. Since the approach outlined in the previous paragraph represents a formidable computational task, the treatment just mentioned was utilized. In the study of the germanium crystal now under way, the eigensolutions at each ot the 19 nonequivalent points on the mesh shown in Fig. 2 and listed in Table I are being determined.

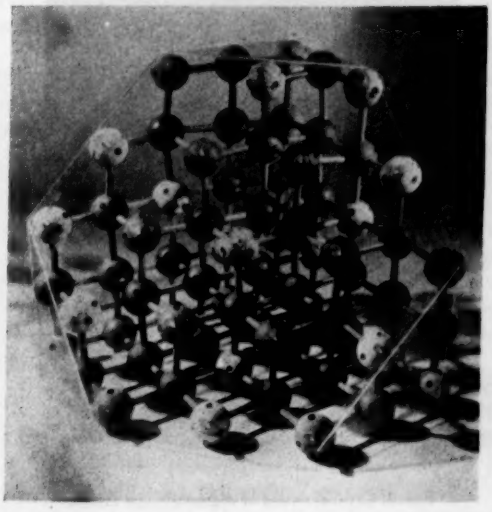

FIG. 2. Crystal model of one octant of a 256-point mesh representing the reduced zone.

[14] G. G. Hall, Phil. Mag. **43**, 338 (1952).
[15] W. Shockley, Phys. Rev. **78**, 173 (1950); **90**, 491 (1953).
[16] Portis, Kip, and Kittel, Phys. Rev. **90**, 988 (1953).
[17] E. N. Adams II, Phys. Rev. **92**, 1063 (1953); E. M. Conwell, Phys. Rev. (to be published).
[18] J. C. Slater and G. F. Koster, Quarterly Progress Report, Solid-State and Molecular Theory Group, Massachusetts Institute of Technology, July 15, 1953 (unpublished), pp. 6–10.
[19] J. C. Slater, Technical Report No. 4, Solid-State and Molecular Theory Group, Massachusetts Institute of Technology, July 15, 1953 (unpublished), pp. 76–89.

The diamond lattice is formed from two interpenetrating face-centered cubic lattices. As shown in Figs. 3 and 4, each lattice site is surrounded by four others situated at the vertices of a regular tetrahedron having the first site as center. The outlines of the unit cell are indicated, though not in full, in Fig. 4.

The symmetry operations which transform the diamond lattice into itself form a group known as the space group O_h^7.[20] One of the invariant subgroups of O_h^7 is the (infinite) translation group defined by the displacements

$$\mathbf{d}=d_1\mathbf{a}_1+d_2\mathbf{a}_2+d_3\mathbf{a}_3, \tag{2.1}$$

where d_1, d_2, and d_3 are integers and $\mathbf{a}_1$, $\mathbf{a}_2$, and $\mathbf{a}_3$ are the primitive translation vectors of a face-centered cubic lattice, i.e.,

$$\mathbf{a}_1=(0,\tfrac{1}{2}a,\tfrac{1}{2}a);\quad \mathbf{a}_2=(\tfrac{1}{2}a,0,\tfrac{1}{2}a);\quad \mathbf{a}_3=(\tfrac{1}{2}a,\tfrac{1}{2}a,0). \tag{2.2}$$

The Born-von Karman cyclic boundary conditions can be used to replace the infinite translation group (2.1) by a finite translation group. The cyclic crystal is assigned M^3 unit cells by restricting the integers d_i $(i=1, 2, 3)$ to the range $-\frac{1}{2}M\leq d_i\leq+\frac{1}{2}M$, where M is a large integer.

Another invariant subgroup of O_h^7, known as the factor group of O_h^7, is composed of 48 operations which may be enumerated as follows. First, there are 24 pure rotations about any lattice site. These form the crystallographic point group T_d. Secondly, there are 24 compound operations each consisting of three successive operations: (a) a pure rotation of T_d about any lattice site, (b) an inversion about the same lattice site, and (c) a nonprimitive translation $\tau=(a/4,a/4,a/4)$. All other symmetry operations transforming the diamond lattice into itself and not included in the factor group defined above can be resolved into two successive operations, the first belonging to the above factor group, and the second to the finite translation group specified by the displacements (2.1) and the large interger M.

Some of the symmetry properties of crystal eigensolutions of diamond-type lattices will now be reviewed.

Crystal eigenfunctions may be written in the form

$$X_\gamma(\mathbf{k},\mathbf{r})=e^{2\pi i\mathbf{k}\cdot\mathbf{r}}U_\gamma(\mathbf{k},\mathbf{r}), \tag{2.3}$$

where the functions $U_\gamma(\mathbf{k},\mathbf{r})$ are required to have the same translational symmetry as the crystal potential, i.e.,

$$U_\gamma(\mathbf{k},\mathbf{r}+\mathbf{d})=U_\gamma(\mathbf{k},\mathbf{r}), \tag{2.4}$$

where $\mathbf{d}$ is a direct lattice vector defined by (2.1). γ is a band identification index.

Crystal eigenfunctions associated with a particular reduced wave vector $\mathbf{k}$ can be arranged into mutually orthogonal sets.[21–23] The members of each set have distinctive symmetry properties. The symmetry of a crystal eigenfunction can be described in terms of the symmetry operations which transform the reduced wave vector $\mathbf{k}$ into an equivalent reduced wave vector $\mathbf{k}'$. (The reduced wave vector $\mathbf{k}'$ is said to be equivalent to $\mathbf{k}$ if $\mathbf{k}'=\mathbf{k}+\mathbf{h}$, where $\mathbf{h}$ is a reciprocal lattice vector, or if $\mathbf{k}'=R\{\mathbf{k}\}$, where R is a symmetry operation belonging to the crystallographic point group O_h.)

TABLE I. List of nonequivalent reduced wave vectors $\mathbf{k}=a^{-1}(k_1,k_2,k_3)$ belonging to 256-point mesh. $N(\mathbf{k})$ denotes the number of distinct $\mathbf{k}$ that can be generated from the listed $\mathbf{k}$ by the symmetry operations of O_h. $W(\mathbf{k})$ is a weighting factor: $\Sigma(\text{nonequiv. }\mathbf{k})N(\mathbf{k})W(\mathbf{k})=256$. The eigensolutions for $\mathbf{k}=a^{-1}(\frac{1}{4},\frac{1}{4},0)$ can be shown to be identical to those for $\mathbf{k}=a^{-1}(1,\frac{1}{4},\frac{1}{4})$.

$4k_1$	$4k_2$	$4k_3$	$N(\mathbf{k})$	$W(\mathbf{k})$	$4k_1$	$4k_2$	$4k_3$	$N(\mathbf{k})$	$W(\mathbf{k})$
0	0	0	1	1	3	1	0	24	1
1	0	0	6	1	3	1	1	24	1
1	1	0	12	1	2	2	2	8	$\frac{1}{2}$
1	1	1	8	1	3	2	0	24	1
2	0	0	6	1	3	2	1	48	$\frac{1}{2}$
2	1	0	24	1	4	0	0	6	$\frac{1}{2}$
2	1	1	24	1	4	1	0	24	$\frac{1}{2}$
2	2	0	12	1	4	1	1	24	$\frac{1}{2}$
2	2	1	24	1	3	3	0	12	$\frac{1}{2}$
3	0	0	6	1	4	2	0	24	$\frac{1}{2}$

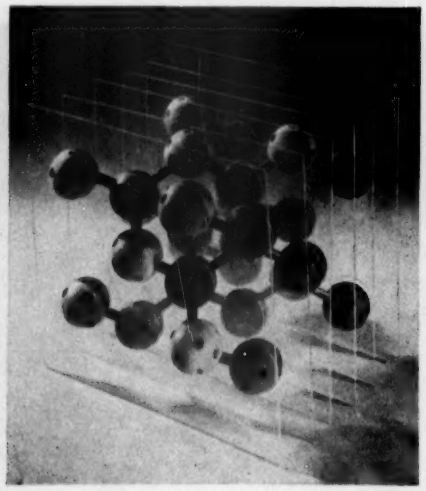

FIG. 3. Crystal model of diamond-type lattice.

The collection of symmetry operations transforming a wave vector $\mathbf{k}$ into an equivalent wave vector forms a group known as the group of the wave vector $\mathbf{k}$ which may be denoted by the symbol $G(\mathbf{k})$. Let the number of symmetry operations belonging to $G(\mathbf{k})$ be $g(\mathbf{k})$, the number of orthogonal sets formed by the crystal wave functions be $c(\mathbf{k})$, and the degeneracy of a member i, $i=1, 2, \cdots c(\mathbf{k})$ be f_i. In the language of group theory,[24] f_i denotes the dimensionality of the irreducible representation (IR) i.

[20] F. Seitz, Z. Krist. 88, 433 (1934); 90, 289 (1935); 91, 336 (1935); 94, 100 (1936).

[21] Bouckaert, Smoluchowski, and Wigner, Phys. Rev. 50, 58 (1936).

[22] F. C. Von der Lage and H. A. Bethe, Phys. Rev. 71, 612 (1947).

[23] G. F. Koster, Phys. Rev. 89, 67 (1953).

[24] Eyring, Walter, and Kimball, *Quantum Chemistry* (John Wiley and Sons, Inc., New York, 1944), Chap. X.

Using the notation just developed, we may now classify[25] the crystal wave functions $X_\gamma(\mathbf{k},\mathbf{r})$ according to the set of symmetry types $G_i^j(\mathbf{k})$, where the index $i=1, 2, 3, \cdots c(\mathbf{k})$ and the index $j=1, 2, \cdots f_{g(\mathbf{k})}$. For the general point in the reduced zone, $g(\mathbf{k})=1$, the identity operation being the only element of $G(\mathbf{k})$. The sole symmetry type is then $G_1^1(\mathbf{k})$. For the central point of the reduced zone, $\mathbf{k}=a^{-1}(0,0,0)$, $g(\mathbf{k})=48$, since each of the 48 members of the factor group of the space group O_h^7 transforms $\mathbf{k}=a^{-1}(0,0,0)$ into an equivalent wave vector. It can be shown[21,25] that $c(0,0,0)=10$ and that there are 4 nondegenerate, 2 doubly-degenerate, and 4 triply-degenerate irreducible representations belonging to $G(0,0,0)$.

Other typical points of high symmetry in the reduced zone are: $\mathbf{k}=a^{-1}(1,0,0)$, the midpoint of a square face, where there are 4 doubly-degenerate IR; $\mathbf{k}=a^{-1}(\frac{1}{2},\frac{1}{2},\frac{1}{2})$, the midpoint of a hexagonal face, where there are 4 nondegenerate and 2 doubly-degenerate IR; $\mathbf{k}=a^{-1}(1,\frac{1}{2},0)$, a corner point on the zone surface, where there are 2 doubly-degenerate IR; $\mathbf{k}=a^{-1}(\frac{1}{4},\frac{1}{4},0)$ and $a^{-1}(1,\frac{1}{4},\frac{1}{4})$, the midpoints of edges on the zone surface, where there are 4 nondegenerate IR.

Symmetry classification is also possible if $\mathbf{k}$ lies on lines or planes of symmetry in the reduced zone. Thus, for $\mathbf{k}=a^{-1}(k,0,0)$, $0<k<1$, there are 4 nondegenerate and 1 doubly-degenerate IR; for $\mathbf{k}=a^{-1}(k,k,k)$, $0<k<\frac{1}{2}$, there are 2 nondegenerate and 1 doubly-degenerate IR; for $\mathbf{k}=a^{-1}(k,k,0)$, $0<k<\frac{1}{2}$, there are 4 nondegenerate IR; for $\mathbf{k}=a^{-1}(1,k,0)$, $0<k<\frac{1}{2}$, there is 1 doubly-degenerate IR; for $\mathbf{k}=a^{-1}(1,k,k)$, $0<k<\frac{1}{2}$, there are 4 nondegenerate IR; for $\mathbf{k}=a^{-1}(k_x,\frac{1}{2},k_z)$, $k_x+k_z=1$, $\frac{1}{2}<k_x<1$, $0<k_z<\frac{1}{2}$, there are 2 nondegenerate IR; finally, for $\mathbf{k}$ lying on the plane $k_x=0$ or on the plane $k_x=k_y$, there are 2 nondegenerate IR.

The energy $E_\gamma(\mathbf{k})$ possesses certain important symmetry properties. $E_\gamma(\mathbf{k})$ is invariant to any symmetry operation which transforms the reciprocal lattice into itself. Thus, $E_\gamma(\mathbf{k}+\mathbf{h})=E_\gamma(\mathbf{k})$ and $E_\gamma[R\{\mathbf{k}\}]=E_\gamma(\mathbf{k})$, where R is an operation belonging to the group O_h. The energy is a continuous function of $\mathbf{k}$ within the reduced zone. If discontinuities in $E_\gamma(\mathbf{k})$ *vs* (unreduced) $\mathbf{k}$ occur at all, they occur at the boundaries of a Brillouin zone in the extended reciprocal lattice.[26] Since the four valence bands are fully occupied in the ground state and the lowest conduction band is separated from each of these valence bands by a finite energy gap for all values of the reduced wave vector, the diamond-type crystals are insulators (diamond) or semiconductors (silicon, germanium, grey tin).[1]

The principal objective of the present study is to determine the form of the valence and conduction bands, in particular, to find where in the reduced zone the band limits occur. On the basis of symmetry considerations alone, it is not possible to predict the values of $\mathbf{k}$ for which the valence states of maximum energy and the conduction band states of minimum energy occur. Rather, it is necessary to solve the Hartree-Fock equations, as will be described more fully in later sections.

[25] The following discussion is based on the work of C. Herring, J. Franklin Inst. **233**, 525 (1942). Table XI of that paper is in error. A corrected form of this table is available from Dr. C. Herring. Dr. Herring has kindly called to the author's attention a useful but unpublished manuscript by T. Sugita entitled "On the representation of crystallographic space-group diamond-type lattice."

[26] L. Brillouin, *Wave Propagation in Periodic Structures* (McGraw-Hill Book Company, Inc., New York, 1946).

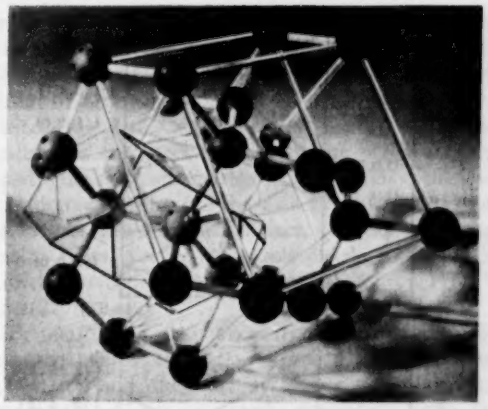

FIG. 4. Another model of diamond-type lattice. The transparent rods indicate two interpenetrating unit cubes. All the hexagonal and only a few of the triangular faces of the unit cell are shown.

It is instructive, however, to consider the energy band structure of an "empty" diamond-type lattice, i.e., the eigensolutions of a crystal having zero potential but retaining its symmetry properties in ghost form. These eigensolutions are the free-electron eigensolutions

$$X(\mathbf{h},\mathbf{k},\mathbf{r})=\exp[2\pi i(\mathbf{h}+\mathbf{k})\cdot\mathbf{r}];$$
$$E(\mathbf{h},\mathbf{k})=(2\pi)^2|\mathbf{h}+\mathbf{k}|^2, \tag{2.6}$$

where the energy bands are denoted by $\mathbf{h}$ instead of γ and $\mathbf{k}$ represents the reduced wave vector.

For the empty lattice, the energy profiles are parabolic, as indicated in Fig. 5. The "crystal" symmetry introduces considerable degeneracy at $\mathbf{k}$ occupying positions of high symmetry in the reduced zone. Since various energy bands overlap, some accidental degeneracies also arise.

If a perturbing potential having the symmetry of the diamond lattice is introduced, producing a "nearly-empty" lattice, many but not all the energy degeneracies are resolved. For example, the eightfold degeneracy at $\mathbf{h}=a^{-1}(1,1,1)$ is decomposed into two nondegenerate states and two triply-degenerate states. In the notation of references 21, 22, and 25, these correspond to symmetry types Γ_1, $\Gamma_{2'}$ and $\Gamma_{25'}$, Γ_{15}, respectively. The symmetry properties of the eigensolutions for the "nearly-empty" lattice, including the degeneracies, can be deduced by standard group-theoretical methods from the character tables given in references 21 and 25.

As the perturbing potential is increased in strength, so that it approaches the actual crystal potential, the four valence bands are fully separated from the remaining (conduction) bands. That the band limits do not necessarily occur at the central point of the reduced zone is suggested by the complicated structure of the energy bands for the "empty" and the "nearly-empty" lattices.

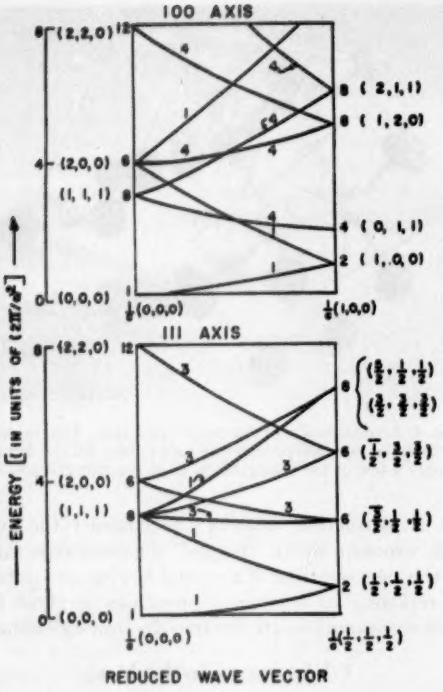

FIG. 5. Energy profiles for "empty" diamond-type lattice. The integers shown in and immediately alongside the diagrams give the degeneracies of the various eigensolutions. Typical crystal eigensolutions [see Eq. (2.6)] are listed in the abbreviated form $(h_1+k_1,\ h_2+k_2,\ h_3+k_3)$.

In the case of the "nearly-empty" lattice, the four degenerate states marked (0,1,1) are resolved into two doubly-degenerate sets, one belonging to the valence bands, the other, to the conduction bands. Similarly, the six degenerate states marked (3/2,1/2,1/2) separate into a doubly-degenerate set of valence band states, a doubly-degenerate set of conduction band states, and two nondegenerate conduction band states.

3. CONSTRUCTION OF AN APPROXIMATE CRYSTAL POTENTIAL

In the calculation of the electronic structure of a crystal, there are two main problems. The first, the determination of a suitable crystal potential, is treated in this section; the second, the numerical solution of the crystal wave equations, is discussed in the next section.

As recently emphasized by Slater[27] and earlier pointed out by Brillouin,[28] the Hartree-Fock equations for a crystal may be written in the form

$$[-\nabla^2-V_{\text{crystal}}{}^{\gamma}(\mathbf{k},\mathbf{r})]X_{\gamma}(\mathbf{k},\mathbf{r})=E_{\gamma}(\mathbf{k})X_{\gamma}(\mathbf{k},\mathbf{r}), \quad (3.1)$$

where the crystal potential appropriate to the state $(\mathbf{k},\gamma)$, $V_{\text{crystal}}{}^{\gamma}(\mathbf{k},\mathbf{r})$, is assumed to contain all Coulomb and exchange terms. The crystal eigenfunctions of (3.1) will be assumed normalized in the volume of the cyclic crystal, i.e.,

$$\int_{M^3\Omega}|X_{\gamma}(\mathbf{k},\mathbf{r})|^2dr=1, \quad (3.2)$$

where Ω denotes the volume of the unit cell $(=a^3/4)$ and $M^3\Omega$ indicates the region of integration.

At the first stage of a self-consistent calculation, it is necessary to construct a suitable crystal potential. Similarly, in a less ambitious undertaking, where no attempt is made to obtain a self-consistent set of eigensolutions, an assumed crystal potential must be employed. The physical reliability of investigations of the second type depends in large measure upon how successfully the actual crystal potential can be approximated at the outset.

We now describe how the crystal potential used in the exploratory study of diamond[3,4] was devised. In the study of the germanium crystal,[5] a similar procedure was followed; however, an approximate exchange potential was not included in the crystal potential for Ge.

In the study of diamond, a crystal model was constructed by arranging neutral carbon atoms in the form of a diamond lattice having the experimental lattice constant ($a=3.5597$A[29]). Each constituent atom was assumed to be in the valence state, i.e., in the $(1s)^2(2s)^1(2p)^3\ {}^5S$ state. This is the lowest state of the free atom for which the four valence orbitals can be hybridized into four tetrahedrally equivalent directed orbitals.

The crystal charge density was then set equal to the sum of the charge densities of each of the $2M^3$ atoms forming the cyclic crystal

$$\rho_{\text{crystal}}{}^{\text{elec}}(\mathbf{r})=\sum_{\mathbf{d}}^{M^3}\sum_{\omega=1}^{2}\rho_{\text{atom}}{}^{\text{elec}}(\mathbf{r}-\mathbf{d}-\mathbf{t}_{\omega}), \quad (3.3)$$

where the electronic charge density of a free carbon atom was assumed to be

$$\rho_{\text{atom}}{}^{\text{elec}}(\mathbf{r})=2[R_{1s}(r)]^2+[R_{2s}(r)]^2+3[R_{2p}(r)]^2. \quad (3.4)$$

In (3.3), the summation on $\mathbf{d}$ is taken over the M^3 direct lattice vectors of the cyclic crystal, the summation on ω, over the two basis vectors $\mathbf{t}_1=(a/8,a/8,a/8)$ and $\mathbf{t}_2=(-a/8,-a/8,-a/8)$ locating the two atoms in the unit cell. (In what follows, the origin of coordinates is chosen at the midpoint of the unit cell.) The $R_{nl}(r)$ appearing in (3.4) are normalized radial wave functions, i.e.,

$$\int_0^{\infty}[R_{nl}(r)]^2r^2dr=1; \quad nl=1s,\ 2s,\ 2p.$$

These were obtained from Jucys' self-consistent field calculations for the valence state of the free carbon atom.[30]

[27] J. C. Slater, Phys. Rev. 81, 385 (1951).
[28] L. Brillouin, J. phys. 5, 413 (1934).

[29] *Handbook of Chemistry and Physics* (Chemical Rubber Publishing Company, Cleveland, Ohio, 1943), twenty-seventh edition.
[30] A. Jucys, J. Phys. (U.S.S.R.) 11, 49 (1947).

Since the tightly bound ($1s$) electrons are probably not strongly affected by crystal formation, the core contribution to the crystal charge density is undoubtedly given quite reliably by the approximation (3.3). On the other hand, the valence contribution should be somewhat different from that estimated by (3.3) because the valence states are modified by the bonding associated with crystal formation. For the sake of mathematical simplicity, no attempt to improve upon (3.3) was made. Recent work by McWeeny[31] and by Schmid[32] describes methods for obtaining improved estimates of the charge densities of atoms in bonded systems.

The crystal Coulomb potential (including the self-Coulomb potential of the state under consideration) is a periodic function and thus can be represented by a three-dimensional Fourier series:

$$V_{\text{crystal}}^{\text{coul}}(\mathbf{r})=\sum_{\mathbf{h}} v(\mathbf{h})^{\text{coul}} \exp(2\pi i\mathbf{h}\cdot\mathbf{r}). \quad (3.5)$$

It is easily shown, by expanding the crystal charge density in a similar form and applying Poisson's equation, that the Fourier coefficients of the crystal Coulomb potential are given by the following relations:[33]

$$v(000)^{\text{coul}}=A\int_0^{\infty}\rho_{\text{atom}}^{\text{elec}}(r)r^4dr \text{ ry}; \quad (3.6)$$

$$v(\mathbf{h})^{\text{coul}}=\frac{B[Z-f(\mathbf{h})]\cos(2\pi\mathbf{h}\cdot\mathbf{t}_1)}{h_1^2+h_2^2+h_3^2} \text{ ry}. \quad (3.7)$$

For diamond, $A=1.3832$, $B=0.7576$; for germanium, $A=0.3446$, $B=0.4767$. Z is the nuclear charge and $f(\mathbf{h})$ the atomic scattering factor:

$$f(\mathbf{h})=\int_{\infty}\rho_{\text{atom}}^{\text{elec}}(\mathbf{r})\exp(-2\pi i\mathbf{h}\cdot\mathbf{r})d\tau. \quad (3.8)$$

As before, $\mathbf{h}=a^{-1}(h_1,h_2,h_3)$ is a reciprocal lattice vector. Since the reciprocal lattice is body-centered cubic, the three indices h_1, h_2, h_3 must be chosen either all even or all odd. According to the approximation (3.4), the atomic charge density is spherically symmetrical. Therefore, the following simplification may be made:

$$f(\mathbf{h})=4\pi\int_0^{\infty}\rho_{\text{atom}}^{\text{elec}}(r)\frac{\sin(2\pi|h|r)}{(2\pi|h|r)}r^2dr. \quad (3.9)$$

In writing Eqs. (3.6) and (3.7), it has been assumed that the charge density per atom is spherically symmetrical. Even though experimental evidence[34] suggests that this is not exactly the case, we elected to work with Eqs. (3.6) and (3.7) since our numerical results for $f(\mathbf{h})$ obtained from Eq. (3.9) agree reasonably well with Brill's experimental results[34] as well as with the $f(\mathbf{h})$ computed by McWeeny[35] using an atomic model similar to our own.

Since the core charge density per atom is more localized in the atomic cell than the valence charge density, the core contribution to the Fourier coefficients (3.7) decreases more slowly with increasing $|\mathbf{h}|$ than the valence contribution. In fact, the valence charge density plays a significant role in determining the numerical values of the coefficients $v(000)^{\text{coul}}$, $v(111)^{\text{coul}}$, and $v(220)^{\text{coul}}$ only.

If $v(000)^{\text{coul}}$ is not known exactly, as is certainly the case, the energy separation between the core band eigenvalues and the valence and conduction band eigenvalues will be incorrectly predicted. Since the separation between the core states and the lowest valence states is about 20 rydbergs in diamond, an incorrect value for $v(000)^{\text{coul}}$ would have a negligible effect upon the calculated energy band structure itself. [Because the top-most core states lie quite close to the bottom-most valence states in germanium, the choice of $v(000)^{\text{coul}}$ in this case is more critical.]

If the assumed crystal charge density leads to a significant error in $v(111)^{\text{coul}}$, the calculated energy band structure for diamond or germanium would be seriously affected. According to our estimates, the probable error in $v(111)^{\text{coul}}$ in each case is small enough not to be troublesome but large enough not to be entirely ignored. Finally, it would appear that the probable error in $v(220)^{\text{coul}}$ is so small that it need not be considered further.

In summary, then, we have obtained the Fourier coefficients of the crystal Coulomb potential on the basis of our crystal model. The need for such computations would disappear if very precise x-ray work could be performed to yield unambiguous numerical values for the atomic scattering factors, for then the $v(\mathbf{h})^{\text{coul}}$ could be obtained directly from the experimental $f(\mathbf{h})$.[36]

We must now attempt to devise some method for estimating the potential acting upon a valence or conduction band electron due to exchange effects. Although general treatments of the exchange terms in the Hartree-Fock equations for crystals have been given, rigorous solutions have been obtained to date only for the case of a free-electron gas.[27,28,37,38] In studies of actual crystals, exchange effects have been taken into account by various forms of the free-electron approximation.[39]

[31] R. McWeeny, Acta Cryst. 5, 463 (1952).
[32] L. A. Schmid, Ph.D. thesis, Princeton University, July, 1953 (unpublished); Phys. Rev. 92, 1373 (1953).
[33] H. Fröhlich, *Electronen Theorie der Metalle* (J. Springer, Berlin, 1936).
[34] R. Brill, Acta Cryst. 3, 333 (1950).
[35] R. McWeeny, Acta Cryst. 4, 513 (1951). In this reference, McWeeny does not include the effect of bonding as he does in his later papers (see reference 31).
[36] The author wishes to acknowledge an illuminating conversation with Professor Brill on this point.
[37] P. A. M. Dirac, Proc. Cambridge Phil. Soc. 26, 376 (1930).
[38] F. Seitz, *The Modern Theory of Solids* (McGraw-Hill Book Company, Inc., New York, 1940), Sec. 75.
[39] G. V. Raynor, Repts. Progr. in Phys. 15, 173 (1952). This excellent review article contains a very comprehensive survey of energy band calculations for actual crystals.

In our study of diamond, we have employed a technique recently discussed by Slater[37] and already applied to a numerical study of the singly ionized copper atom by Pratt.[40] According to Slater, the exchange potential for an actual crystal can be represented to a good degree of approximation by the exchange potential appropriate to a free electron gas having the same local charge density at all points in space as the actual crystal. Slater's expression for the (approximate) exchange potential is

$$V_{\text{crystal}}^{\text{exch}}(\mathbf{r}) = 6\left\{\frac{3}{4\pi}\cdot\frac{1}{2}\rho_{\text{crystal}}^{\text{elec}}(\mathbf{r})\right\}^{\frac{1}{3}} \text{ry}. \quad (3.10)$$

The factor of $\frac{1}{2}$ appears in front of $\rho_{\text{crystal}}^{\text{elec}}(\mathbf{r})$ because only half the electrons in the crystal have the same spin as the state under consideration.

The free electron exchange potential (3.10) is the same for each state. Thus, the total crystal potential,

$$V_{\text{crystal}}^{\gamma}(\mathbf{k},\mathbf{r}) = V_{\text{crystal}}^{\text{coul}}(\mathbf{r}) + V_{\text{crystal}}^{\text{exch}}(\mathbf{r}), \quad (3.11)$$

is independent of $\mathbf{k}$ and γ. In what follows, we will replace the symbol $V_{\text{crystal}}^{\gamma}(\mathbf{k},\mathbf{r})$ by the more appropriate symbol $V_{\text{crystal}}(\mathbf{r})$.

The numerical methods employed in calculating the Fourier coefficients of the total crystal potential, defined by the relation

$$V_{\text{crystal}}(\mathbf{r}) = \sum_{\mathbf{h}} v(\mathbf{h}) \exp(2\pi i \mathbf{h}\cdot\mathbf{r}), \quad (3.12)$$

are discussed in detail in reference 4. To conserve space, they will not be described here. The results indicate that the exchange terms contribute to all the important $v(\mathbf{h})$ to the extent of about 10 percent of the respective numerical values of the various $v(\mathbf{h})$.

It is difficult to estimate the reliability of the Slater approximation for the crystal exchange potential. According to Pratt's study of the Cu^+ ion,[40] the free-electron approximation (3.10) leads to eigensolutions about as good as one could obtain by solving Hartree's equations except in the case of the $1s$ and the $3d$ states. For these states, Pratt's eigensolutions based on (3.10) are somewhat poorer and better, respectively, than the solutions based on Hartree's equations.

In their work on beryllium,[9] Herring and Hill estimated that use of the free-electron approximation led to a result for the total exchange energy correct to within about 6 percent. In his recent work on diamond, Schmid[23] concludes that use of the same approximation yields results having a still smaller uncertainty.

It would appear that further work is required in order to establish on a firm quantitative basis the precision with which the free-electron exchange potential can represent the exchange potential appropriate to the exact Hartree-Fock equations.[41] Also, the concept of a unipotential,[42] such as (3.11), assumed to be the same for all states, deserves serious study.

For the present, however, we will make use of our assumed crystal potential. Although this potential can certainly be improved upon, we believe that it represents a reasonable approximation to the true crystal potential.

4. NUMERICAL SOLUTION OF THE CRYSTAL WAVE EQUATIONS BY THE OPW METHOD

A wide variety of numerical methods has been proposed for determining the eigensolutions for a periodic potential. Many of these have already been applied to studies of actual crystals.[39] The method of orthogonalized plane waves[6] was selected as the most suitable for the investigations of the diamond and germanium crystals for the following reasons:

(a) In studies based on the Wigner-Seitz-Slater cellular method,[43] Slater's modified cellular method,[44] and certain forms of the scattering matrix method,[45,46] the potential within all or part of an atomic cell must be assumed spherically symmetric. Since in diamond-type crystals each atom has only four nearest neighbors, it is desirable to avoid what may in fact be unrealistic approximations. In the method of orthogonalized plane waves, as in other methods employing Fourier series representations of the crystal potential,[26] the cellular potential may have any symmetry properties whatever.

(b) In calculations based on various forms of the cellular method[43,44] and on methods utilizing difference and integral equation formulations (see Appendix I), special attention must be paid to boundary conditions. On the other hand, since orthogonalized plane waves automatically satisfy all the periodicity conditions required by crystal symmetry, the numerical work associated with the OPW method is considerably simplified.

(c) It is difficult to estimate the mathematical and physical reliability of the results of energy band structure studies not carried to the point where the eigensolutions are self-consistent in the Hartree-Fock sense. However, by standard perturbation theory techniques, it is possible (1) to estimate the truncation errors associated with nearly convergent eigensolutions and (2) to estimate the dependence of the results upon the exact form of the assumed crystal potential. Such calculations are particularly easy to execute in conjunction with the OPW method.

(d) The computational labor required for the determination of a fixed number of crystal eigensolutions would appear to be about the same whether the Wigner-Seitz-Slater cellular method or the OPW method is employed. On the other hand, the difference and

[40] G. W. Pratt, Jr., Phys. Rev. 88, 1217 (1952).
[41] E. P. Wohlfarth, Phil. Mag. 44, 281 (1953).
[42] G. K. Horton and R. T. Sharp, Phys. Rev. 89, 885 (1953).
[43] J. C. Slater, Phys. Rev. 45, 794 (1934).
[44] J. C. Slater, Phys. Rev. 51, 846 (1937).
[45] J. Korringa, Physica 13, 392 (1947).
[46] R. J. Harrison, Phys. Rev. 84, 377 (1951).

integral equations cited in Appendix I require considerably more calculational effort. For practical numerical computations, the OPW method appears to offer greater convenience than localized orbital treatments[10,14,23] in their present states of development.

We now describe how the problem of determining the electronic structure of a diamond-type crystal is formulated according to Herring's orthogonalized plane wave method. We assume that a crystal potential has been determined, for example, in the manner described in the previous section, and that $V_{\text{crystal}}(\mathbf{r})$ has been expanded as a three-dimensional Fourier series [see Eq. (3.12)]. In what follows, the band index for core states will be represented by β and the band index for valence and conduction band states by α.

According to the OPW method, crystal wave functions for core states are expressed as linear combinations of suitably chosen atomic orbitals, i.e.,

$$X_\beta(\mathbf{k},\mathbf{r})=M^{-\frac{1}{2}}\sum_{\mathbf{d}}^{M^3} e^{2\pi i\mathbf{k}\cdot\mathbf{d}}\sum_{\omega=1}^{2} b_\beta(\mathbf{k},\omega)\psi_\beta(\mathbf{k},\mathbf{r}-\mathbf{d}-\mathbf{t}_\omega). \quad (4.1)$$

In (4.1), $\psi_\beta(\mathbf{k},\mathbf{r}-\mathbf{d}-\mathbf{t}_\omega)$ is a localized orbital centered at the lattice site specified by the direct lattice vector $\mathbf{d}$ and the basis vector $\mathbf{t}_\omega$; $b_\beta(\mathbf{k},\omega)$ is a phase factor. It will be assumed that the $\psi_\beta(\mathbf{k},\mathbf{r})$ form an orthonormal set and that the $\mathbf{k}$ dependence of the $\psi_\beta(\mathbf{k},\mathbf{r})$ may be neglected. Thus, $\psi_\beta(\mathbf{k},\mathbf{r})=\psi_\beta(\mathbf{r})$ and

$$\int_\infty \psi_{\beta'}^*(\mathbf{r}-\mathbf{d}'-\mathbf{t}_{\omega'})\psi_\beta(\mathbf{r}-\mathbf{d}-\mathbf{t}_\omega)d\mathbf{r} =\delta(\beta',\beta)\delta(\mathbf{d}',\mathbf{d})\delta(\omega',\omega). \quad (4.2)$$

In addition, it is assumed that the phase factors are so chosen that the eigenfunctions (4.1) are normalized to unity in the following sense

$$\int_{M^3\Omega} X_\beta^*(\mathbf{k},\mathbf{r})X_\beta(\mathbf{k},\mathbf{r})d\mathbf{r}=1. \quad (4.3)$$

Since there are two atoms per unit cell, (4.3) is satisfied provided we set $|b_\beta(\mathbf{k},\omega)|^2=\frac{1}{2}$ for all β, $\mathbf{k}$, and ω.

Crystal wave functions for valence and conduction band states are represented by linear combinations of plane waves each of which has been orthogonalized to all core wave functions (4.1) by the Schmidt process. Writing the valence and conduction band wave functions in the form

$$X_\alpha(\mathbf{k},\mathbf{r})=\sum_{\mathbf{h}} a^\alpha(\mathbf{h},\mathbf{k})[(M^3\Omega)^{-\frac{1}{2}}\exp\{2\pi i(\mathbf{h}+\mathbf{k})\cdot\mathbf{r}\} - \sum_{\beta}^{\text{core}} A_\beta(\mathbf{h}+\mathbf{k})X_\beta(\mathbf{k},\mathbf{r})], \quad (4.4)$$

the orthogonality coefficients $A_\beta(\mathbf{h}+\mathbf{k})$ are determined by imposing the orthogonality conditions

$$\int_{M^3\Omega} X_\beta^*(\mathbf{k},\mathbf{r})X_\alpha(\mathbf{k},\mathbf{r})d\mathbf{r}=0 \quad \text{(for all } \beta \text{ and } \alpha), \quad (4.5)$$

whence

$$A_\beta(\mathbf{h}+\mathbf{k})=\sum_{\omega=1}^{2} b_\beta^*(\mathbf{k},\omega)\exp[2\pi i(\mathbf{h}+\mathbf{k})\cdot\mathbf{t}_\omega] \times\int\psi_\beta^*(\mathbf{r})\exp[2\pi i(\mathbf{h}+\mathbf{k})\cdot\mathbf{r}]\Omega^{-1}d\mathbf{r}. \quad (4.6)$$

In the OPW expansion (4.4), the $a^\alpha(\mathbf{h},\mathbf{k})$ are (as yet) undetermined linear coefficients; the summation on β is taken over all core bands whose spin assignment is the same as that of the state under consideration; the summation on $\mathbf{h}$ ranges from $\mathbf{h}=(0,0,0)$ over all reciprocal lattice vectors $\mathbf{h}$ having moduli less than some $|\mathbf{h}|_{\max}$. Finally, let us denote by N the number of orthogonalized plane wave terms admitted to the expansion (4.4).

To obtain approximate core eigenfunctions, the atomic orbitals $\psi_\beta(\mathbf{k},\mathbf{r})$ may be replaced by the corresponding (normalized) free atomic orbitals $\varphi_{nlm}(\mathbf{r})$. For the core states, the band index β may now be replaced by the four indices n, l, m, p, where p is a parity index which may have the values $+1$ and -1. If negligible overlapping occurs between atomic orbitals centered on different lattice sites, as is actually the case, the phase factors $b_\beta(\mathbf{k},\omega)$ may be set equal to $\pm 1/\sqrt{2}$, the choice of sign depending upon the indices l, p, and ω. For a particular choice of the set n, l, m, two nonequivalent crystal wave functions may be formed using the relation (4.1), these being distinguished by the parity index p. For the special case $\mathbf{k}=(0,0,0)$, the crystal wave functions corresponding to $p=+1$, -1 are even and odd, respectively, with respect to inversion about the midpoint of any unit cell.

To this degree of approximation, each of the states belonging to a particular core band has the same energy eigenvalue. In addition, core states constructed from different indices m and p but from the same indices n and l are degenerate. Denoting the crystal potential appropriate to the core band β by $V_{\text{crystal}}^\beta(\mathbf{r})$, we may write

$$E_\beta=E_{nlmp} =\int_{\substack{\text{atomic}\\ \text{cell}}}\varphi_{nlm}^*(\mathbf{r})[-\nabla^2-V_{\text{crystal}}^\beta(\mathbf{r})]\varphi_{nlm}(\mathbf{r})d\mathbf{r}. \quad (4.7)$$

As a rough approximation, $E_\beta=E_{nl}$, where E_{nl}, the free atomic energy eigenvalue, is defined by

$$E_{nl}=\int_\infty\varphi_{nlm}^*(\mathbf{r})[-\nabla^2-V_{\substack{\text{free}\\ \text{atom}}}^{nlm}(\mathbf{r})]\varphi_{nlm}(\mathbf{r})d\mathbf{r}. \quad (4.8)$$

On the second cycle of a calculation employing self-consistent iteration, the approximation that $E_\beta=E_{nl}$ must be abandoned in favor of more reliable values for $E_\beta(\mathbf{k})$. Although it is reasonable to expect that the

most tightly bound electrons give rise to energy bands having zero width, it is likewise to be expected that the least tightly bound core electrons in a crystal, such as the (3*d*) electrons in germanium, produce energy bands having finite width. Recent work by Fletcher[47] on the (3*d*) bands in nickel indicates a possible approach to the problem of obtaining an accurate representation of the eigenstates of the loosely bound core states. In the present work, such refinements were not attempted.

As first shown by Herring,[6] the energy eigenvalues $E(\mathbf{k})$ and the components of the eigenvectors $X_\alpha(\mathbf{k},\mathbf{r})$ can be determined by evaluating the Nth order determinantal equation:

$$|H(\mathbf{h}',\mathbf{h};\mathbf{k})-E(\mathbf{k})J(\mathbf{h}',\mathbf{h};\mathbf{k})|=0, \tag{4.9}$$

where the matrix elements are defined as follows:

$$H(\mathbf{h}',\mathbf{h};\mathbf{k})=(2\pi)^2|\mathbf{h}+\mathbf{k}|^2\delta(\mathbf{h}',\mathbf{h})-v(\mathbf{h}-\mathbf{h}') + \sum_{\beta}^{\text{core}}|E_\beta(\mathbf{k})|A_\beta^*(\mathbf{h}'+\mathbf{k})A_\beta(\mathbf{h}+\mathbf{k}); \tag{4.10}$$

$$J(\mathbf{h}',\mathbf{h};\mathbf{k})=\delta(\mathbf{h}',\mathbf{h})-\sum_{\beta}^{\text{core}}A_\beta^*(\mathbf{h}'+\mathbf{k})A_\beta(\mathbf{h}+\mathbf{k}). \tag{4.11}$$

In these expressions, $\mathbf{h}'$ denotes the row and $\mathbf{h}$ the column of the matrix elements of $H(\mathbf{k})$ and $J(\mathbf{k})$. $\delta(\mathbf{h}',\mathbf{h})$ is the usual Kronecker delta function.

Because orthogonalized plane waves do not form an orthonormal set, the energy parameter $E(\mathbf{k})$ appears on the off-diagonal matrix elements of the secular determinant (4.9), as may be seen from the relation (4.11). In actual numerical calculations, one may reduce (4.9) to the canonical form [$E(\mathbf{k})$ appearing only on main diagonal] by finding the inverse matrix $J^{-1}(\mathbf{k})$ and then premultiplying the matrix equation (4.9) by $J^{-1}(\mathbf{k})$. In setting up a calculation in this manner, about as much computational labor is required to obtain the inverse matrix $J^{-1}(\mathbf{k})$ as to evaluate the eigensolutions of the canonical form of (4.9). We will not discuss computational details here except to say that the actual work was carried out with the aid of the IBM Calculating Punch 602A using iterative matrix multiplication schemes.[48–50]

In the matrix element (4.10), $(2\pi)^2|\mathbf{h}+\mathbf{k}|^2$ is the (repulsive) kinetic energy term, $v(\mathbf{h}-\mathbf{h}')$, the (attractive) potential energy term. The remaining terms represent a (repulsive) pseudopotential arising from the orthogonalization.

In general, it is found in actual studies[3–5] that the orthogonality terms nearly cancel the potential energy terms. Consequently, the off-diagonal matrix elements in (4.10) are considerably reduced in absolute magnitude by the orthogonality process. It is thus possible to represent a crystal wave function by considerably fewer orthogonalized plane waves than by ordinary plane waves. In the latter case, there are no orthogonality terms present. Thus, extremely high order secular determinants must be solved before satisfactorily convergent eigensolutions are obtained.

From another viewpoint,[6,8] the atomic orbitals appearing in the OPW's (4.4) account for most of the atomic-like behavior which a crystal wave function exhibits in the neighborhood of the crystal nuclei. The remaining portion of the crystal wave function, being relatively smooth, can be represented by a reasonably small number of plane wave terms.

The partial cancellation of the potential energy terms by the orthogonality terms has its disadvantages. Unless both the crystal potential and the core eigensolutions are known with considerable precision, the off-diagonal matrix elements cannot be accurately determined. In the work on diamond[3,4] and germanium,[5] it was found that one significant figure was lost in the off-diagonal matrix elements as a consequence of this partial cancellation. Because there are more core states in the germanium crystal than in the diamond crystal, there are also more orthogonality terms. For this reason, the cancellation was more complete in germanium than in diamond. However, this is not necessarily the general rule.

Even though the OPW method converges more rapidly than the straightforward Fourier series method,[26] very high order secular determinants must be evaluated if reliable results are to be obtained. It is therefore essential to simplify the problem by taking full advantage of the symmetry properties of the crystal eigensolutions.

We now focus our attention on the eigensolutions corresponding to those reduced wave vectors which occupy positions of high symmetry in the reduced zone. These eigensolutions may be arranged in mutually orthogonal sets, as noted earlier. The $N\times N$ secular determinant for a particular $\mathbf{k}$ may then be factored into $c(\mathbf{k})$ separate secular determinants, one for each irreducible representation in the wave vector group $G(\mathbf{k})$. If a certain IR is f-fold degenerate, the corresponding (separated) secular determinant may be additionally factored into f identical and separate secular determinants. Thus, instead of solving one very high order secular determinant for each $\mathbf{k}$ investigated, it is necessary only to evaluate several relatively low order secular determinants.

To factor the Nth order secular determinant for a particular $\mathbf{k}$, the linear combinations of orthogonalized plane waves belonging to the various symmetry types $G_i^j(\mathbf{k})$ must be found. This is accomplished by applying standard group-theoretical methods.[24] Some typical "symmetrized" orthogonalized plane waves are listed in Table II.

It is easily shown that the core wave functions

[47] G. C. Fletcher, Proc. Phys. Soc. (London) **A65**, 192 (1952).
[48] W. M. Kincaid, Quart. Appl. Math. 5, 320 (1947).
[49] H. E. Fettis, Quart. Appl. Math. 8, 206 (1950).
[50] P. S. Dwyer, *Linear Combinations* (John Wiley and Sons, Inc., New York, 1951), Chap. 15.

arising from s, p, and d atomic orbitals belong to the irreducible representations $(\Gamma_1,\Gamma_{2'})$, $(\Gamma_{25'},\Gamma_{15})$, and $(\Gamma_{25'},\Gamma_{15},\Gamma_{12},\Gamma_{12'})$, respectively, at $\mathbf{k}=a^{-1}(0,0,0)$. Consequently, the triply-degenerate valence band state $\Gamma_{25'}$ and the lowest triply-degenerate conduction band state Γ_{15} are automatically orthogonal to all the core states in the case of diamond but not in the case of germanium.

For states automatically orthogonal to all core states, all the orthogonality terms in the symmetrized OPW's vanish identically and the OPW method becomes fully equivalent to the ordinary Fourier series method.[26]

As suggested to the author by Herring,[51] it is possible to treat such cases as follows. To the symmetrized (ordinary) plane wave expansion, a suitable set of atomic orbitals is added. Each atomic orbital is required to behave properly near the nucleus, have the appropriate symmetry properties in the atomic cell, and vanish within half an interatomic spacing of its center. Since both the atomic part and the plane wave part are separately orthogonal to all core wave functions, the augmented plane wave expansion is itself orthogonal to all core wave functions.

In the study of diamond,[3,4] augmented plane wave expansions were not employed since it was thought worthwhile to study the convergence of the ordinary plane wave expansions for these special states and then compare this behavior to the convergence of the OPW expansions for the remaining states. In retrospect, it appears that use of the augmented plane wave expansions would have been desirable since the ordinary plane wave expansions converged very slowly. On the other hand, as already noted in the earlier announcement,[3] the convergence of the OPW expansions containing nonvanishing orthogonality terms was quite rapid.

After determining the crystal eigensolutions for $\mathbf{k}$ occupying positions of high symmetry in the reduced zone, the slope and curvature of the energy surfaces passing through these points were calculated by a well-known perturbation method.[41,52,53] The effect of the 4 valence bands and the 10 lowest conduction bands was included in the calculation leading to the curvatures of the various energy surfaces at the central point of the reduced zone. The apparent discrepancy between the form of our estimated energy bands and those recently obtained by Slater[19] might arise from the fact that Slater considers an energy band system containing four valence bands and only four conduction bands.

5. DISCUSSION OF RESULTS

In judging the reliability of the results,[3-5] three factors must be kept in mind. First, the calculations were based on assumed crystal potentials. Secondly, the eigensolutions obtained were nearly but not fully "convergent." Finally, the energy band structures were deduced from the energy eigenvalues, the estimated slopes and the estimated curvatures of the energy surfaces at a limited number of points in the reduced zone.

Since it does not appear possible to determine in any simple manner how closely the assumed crystal potentials approximate the actual crystal potentials, certain auxiliary calculations were performed. In these, the assumed potentials were modified slightly and new sets of crystal eigensolutions determined by perturbation theory. The range of allowed variation of the

[51] C. Herring (private communication).
[52] F. Seitz, Phys. Rev. 47, 400 (1935).
[53] W. Shockley, Phys. Rev. 78, 173 (1950).

TABLE II. Typical linear combinations of orthogonalized plane waves belonging to some of the symmetry types of $G(0,0,0)$ and $G(1,0,0)$. The column headings of the form Γ_i and X_i denote irreducible representations in the notation of references 21 and 25. The various symmetry types are also expressed in the form G_i^j. In this table, each row corresponds to a particular orthogonalized plane wave. Each orthogonalized plane wave [see the bracketed quantity in Eq. (4.4)] is shown in the abbreviated form $[h_1+k_1\ h_2+k_2\ h_3+k_3]$. To illustrate the notation, we write out in full the three leading terms of the crystal wave functions belonging to symmetry type $G_1^1(1,0,0)$:

$$X_1^1(100,\mathbf{r})=a_1^1(100)[100]+a_1^1(011)\{[011]-[0\bar{1}\bar{1}]+[0\bar{1}1]+[01\bar{1}]\}+a_1^1(120)\{[\bar{1}20]-[\bar{1}\bar{2}0]+[\bar{1}02]-[\bar{1}0\bar{2}]\}.$$

In this expression, the $a_1^1(\mathbf{h}+\mathbf{k})$ are undetermined linear coefficients.

	Γ_1	$\Gamma_{2'}$		$\Gamma_{25'}$			Γ_{15}		$\Gamma_{12'}$	
$(\mathbf{h}+\mathbf{k})$	G_1^1	G_2^1	G_3^1	G_3^2	G_2^2	G_4^1	G_4^2	G_4^3	G_5^1	G_5^2
[0 0 0]	+1									
[1 1 1]	+1	+1	+1	+1	+1	+1	+1	+1		
[1 $\bar{1}$ $\bar{1}$]	−1	−1	+1	+1	−1	+1	+1	−1		
[$\bar{1}$ 1 $\bar{1}$]	−1	−1	+1	−1	+1	+1	−1	+1		
[$\bar{1}$ $\bar{1}$ 1]	−1	−1	−1	+1	+1	−1	+1	+1		
[$\bar{1}$ $\bar{1}$ $\bar{1}$]	+1	−1	+1	+1	+1	−1	−1	−1		
[$\bar{1}$ 1 1]	−1	+1	+1	+1	−1	−1	−1	+1		
[1 $\bar{1}$ 1]	−1	+1	+1	−1	+1	−1	+1	−1		
[1 1 $\bar{1}$]	−1	+1	−1	+1	+1	+1	−1	−1		
[2 0 0]		+1	0	0	+1				+2	0
[0 2 0]		+1	0	+1	0				−1	+1
[0 0 2]		+1	+1	0	0				−1	−1
[$\bar{2}$ 0 0]		−1	0	0	−1				−2	0
[0 $\bar{2}$ 0]		−1	0	−1	0				+1	−1
[0 0 $\bar{2}$]		−1	−1	0	0				+1	+1

	X_1		X_3		X_3		X_4	
[h+k]	G_1^1	G_1^2	G_2^1	G_2^2	G_2^1	G_2^2	G_4^1	G_4^2
[1 0 0]	+1	0						
[$\bar{1}$ 0 0]	0	+1						
[0 1 1]	+1	+1					+1	0
[0 $\bar{1}$ $\bar{1}$]	−1	−1					+1	0
[0 $\bar{1}$ 1]	+1	−1					0	+1
[0 1 $\bar{1}$]	+1	−1					0	−1
[1 2 0]	0	+1	+1	0	0	+1	+1	+1
[1 $\bar{2}$ 0]	0	−1	−1	0	0	+1	+1	+1
[$\bar{1}$ 2 0]	+1	0	0	+1	−1	0	+1	+1
[$\bar{1}$ $\bar{2}$ 0]	−1	0	0	−1	−1	0	+1	+1
[1 0 2]	0	+1	−1	0	+1	0	+1	−1
[1 0 $\bar{2}$]	0	−1	+1	0	+1	0	+1	−1
[$\bar{1}$ 0 2]	+1	0	0	−1	0	−1	+1	−1
[$\bar{1}$ 0 $\bar{2}$]	−1	0	0	+1	0	−1	+1	−1

crystal potential was $\pm 0.1 v_{111}$, a reasonable measure of the major uncertainty in the assumed potentials.

It was found that these changes in the assumed value of v_{111} altered the various energy eigenvalues considerably. The magnitude and direction of these shifts of $E_\alpha(\mathbf{k})$ depended upon the symmetry type of the eigensolution in question as well as upon the order of the secular determinant from which $E_\alpha(\mathbf{k})$ was obtained. Fortunately, the relative order of sufficiently convergent eigenvalues at $\mathbf{k}=(0,0,0)$ did not change as a result of these arbitrary modifications of v_{111}. It appears safe to conclude, therefore, that the lowest conduction band states at the central zone point in diamond and germanium are the triply degenerate states $\Gamma_{25'}$ rather than the nondegenerate state $\Gamma_{2'}$ even if our assumed crystal potentials are slightly in error. The recent work of Slater and Koster,[18] reported in detail by Slater,[19] offers additional support to our conclusion in the case of diamond.

On the other hand, the curvatures of the energy surfaces at $\mathbf{k}=(0,0,0)$ were found to change only under large modifications of the assumed potential in diamond but under relatively small modifications in germanium. Thus, it appears that the predicted energy band structure of germanium is much more sensitive to the physical assumptions than that of diamond.

The convergence of the crystal eigensolutions was rapid for all eigenstates in germanium and for the eigenstates in diamond which were not automatically orthogonal to all core states. Thus, the eigenvalues for these states could be obtained to at least two significant figures by solving eighth-order secular determinants.

The valence state $\Gamma_{25'}$ and the conduction band state Γ_{15} in diamond required special attention because these symmetry types were not represented among the core states. The eigensolutions of 16th-order secular determinants for these states were nearly but not fully convergent. The secular determinants for these symmetry types were set up to 24th and even higher orders and solved by perturbation theory using the 16th-order eigensolutions as the "unperturbed" eigensolutions. In this manner, the truncation errors for the 16th-order eigensolutions were found to be not more than a few percent.

The present work indicates that the estimated curvatures depend critically upon the numerical values of the crystal eigensolutions and thus in turn upon the exact form of the assumed crystal potentials. Although the use of slope and curvature information to predict the shape of the energy bands reduces the magnitude of a computation considerably, the results are not to be trusted to the same extent as those leading, for example, to the relative order of the eigensolutions at a particular $\mathbf{k}$.

A more detailed investigation of the energy band structure of the germanium crystal has been undertaken. In the study now in progress, an approximate exchange potential is included in the assumed crystal potential in addition to an approximate Coulomb potential. Some refinements have been introduced in order to improve the initial choice of the crystal Coulomb potential. Considerable pains are being taken to insure that the initial set of core eigenstates approximate the actual state of affairs closely. Instead of relying upon curvature calculations, the energy band structure will be deduced in the new work by determining the eigensolutions at each of the reduced wave vectors listed in Table I.

6. ACKNOWLEDGMENTS

The author wishes to express his gratitude to Professor Henry M. Foley of Columbia University and to Dr. Dwight O. North of the RCA Laboratories for valuable guidance and constructive criticism. It is a pleasure to acknowledge enlightening discussions with Dr. Conyers Herring of the Bell Telephone Laboratories, Dr. Arnold R. Moore of the RCA Laboratories, and Dr. Leon Brillouin of the International Business Machines Corporation.

For permission to use the IBM facilities at the Watson Scientific Computing Laboratory at Columbia University, the author is grateful to Professors Wallace J. Eckert and Llewellyn H. Thomas. The author appreciates the help of Professor Francis J. Murray of Columbia University and Mr. Eric V. Hankam of the Watson Laboratory in programming the calculation.

Finally, the author wishes to thank Dr. Irving Wolff, Mr. Edward W. Herold, and Dr. Lloyd P. Smith of the RCA Laboratories for their continued interest and encouragement.

APPENDIX I. DIFFERENCE AND INTEGRAL EQUATION METHODS

The unit cell of the direct lattice can be represented by a set of points $\mathbf{u}$ arranged in some convenient array. All physically interesting quantities such as the crystal potential and the crystal wave functions are defined only at these points $\mathbf{u}$. Let us assume that the crystal potential is known. Then, with the aid of the variational principle, we seek to determine the set of values $X_\gamma(\mathbf{k},\mathbf{u})$, one for each $\mathbf{u}$, for which the energy

$$E_\gamma(\mathbf{k})=\frac{\sum_{\mathbf{u}} X_\gamma^*(\mathbf{k},\mathbf{u})[-\nabla^2-V_{\text{crystal}}{}^\gamma(\mathbf{k},\mathbf{u})]X_\gamma(\mathbf{k},\mathbf{u})}{\sum_{\mathbf{u}} X_\gamma^*(\mathbf{k},\mathbf{u})X_\gamma(\mathbf{k},\mathbf{u})} \quad (1.1)$$

is a minimum, subject to two conditions: First, the crystal wave function must satisfy the periodicity properties imposed by crystal symmetry, and secondly, the crystal wave function must be orthogonal to all crystal eigenfunctions having lower energies and the same reduced wave vector $\mathbf{k}$.

The crystal eigenvalue problem thus formulated can be solved, in principle, by difference equation methods

exemplified by systematic iteration,[54,55] relaxation,[55,56] or dynamical analogs[57] or by various iterative integral equation techniques.[58] Unfortunately, even if the crystal symmetry properties are fully exploited, reliable results can be obtained only if extremely fine meshes are employed.

A rough estimate of the number of nonequivalent mesh points **u** required for satisfactory convergent eigensolutions may be made as follows. First, assume that the crystal eigenfunctions for the valence and low-lying conduction band states resemble atomic (2*s*) orbitals in any atomic cell. Secondly, assume that the interval of a suitable mesh at a distance r from the nucleus is approximately equal to the corresponding interval used in tabulating the (2*s*) radial wave functions in Hartree-Fock computations. The number of nonequivalent **u** of a mesh thus constructed is found to be so large that calculations by the methods just described appear to require the aid of the largest automatic computing machines now available.

[54] G. E. Kimball and G. H. Shortley, Phys. Rev. **45**, 815 (1934).
[55] J. B. Scarborough, *Numerical Mathematical Analysis* (The Johns Hopkins Press, Baltimore, 1950), second edition, Chap. XII.
[56] R. V. Southwell, *Relaxational Methods in Theoretical Physics* (Oxford University Press, London, 1946).
[57] G. Kron, Phys. Rev. **67**, 39 (1945).
[58] W. A. Bowers, Phys. Rev. **82**, 766 (1951); D. Slepian, Ph.D. thesis, Harvard University, Sept., 1949 (unpublished); M. Dank and H. B. Callen, University of Pennsylvania Technical Report No. 4, September, 1951 (unpublished); M. Dank, University of Pennsylvania Technical Report No. 2, December, 1952 (unpublished).

PHYSICAL REVIEW VOLUME 93, NUMBER 6 MARCH 15, 1954

A Variational Calculation of the Elastic Scattering of Electrons by Hydrogen Atoms*

HOWARD BOYET † AND SIDNEY BOROWITZ
Department of Physics, College of Engineering, New York University, New York 53, New York
(Received August 4, 1953; revised manuscript received December 11, 1953)

The Schwinger variational method for three-body collisions is applied to the calculation of elastic scattering of electrons by hydrogen atoms in the energy range 0–10 volts. When a Born trial field is used, the contributions of the ground state and all the excited states including the continuum can be calculated. The former contribution is equivalent to the static field approximation and the latter contributions give the corrections to it. When these are included, the results do not agree with those of Massey and Moiseiwitsch who use a different approximation. We conclude that the Schwinger variational method with a Born trial field is unsatisfactory in this energy range.

I. INTRODUCTION

PROBLEMS involving elastic three-body collisions present two complications not encountered in two-particle scattering problems. The first is the polarization of the charge distribution of the scatterer by the incoming particle. The second is the phenomenon of exchange scattering, in which the incoming particle and one of the particles of the scatterer exchange roles after scattering. This is especially complicated when these two particles are identical, and thus, by the Pauli principle, there are interference terms in the scattering cross section between the direct and the exchange scattered wave.

Heretofore, three-particle scattering problems have been treated by the Born approximation,[1] by a static-field approximation,[1] and by a generalization of the Hulthén[2] variational method which is due to Kohn.[3] The first of these methods is not likely to be very accurate at low energies. The static-field approximation, by its very nature, cannot treat the complications mentioned above. In using the last method, one can include the effect of polarization and exchange by suitable choice of trial function.

Recently, the Schwinger variational method has been extended to cover three-particle collisions.[4] In principle this method has the advantage that cruder trial functions could be used, since some of the features of the problem (polarization effects, for example) are automatically taken into account when one iterates the trial solution with the Green's function of the unperturbed problem. This advantage is part of the limitation of the method, since the integrations involving the Green's function are extremely difficult to carry out.

In the present paper, we shall apply this last method to the elastic scattering of slow electrons by hydrogen atoms. This particular problem has already been treated by several different approaches. It has been solved approximately by the Kohn-Hulthén method.[5] It has been

* This work was performed at Washington Square College of Arts and Science, New York University, and was supported in part by a contract with the U. S. Air Force through sponsorship of the Geophysics Research Directorate of the Air Force Cambridge Research Center, Air Research and Development Command.
† Now at Bell Telephone Laboratories, Whippany, New Jersey.
[1] N. F. Mott and H. S. W. Massey, *The Theory of Atomic Collisions* (Clarendon Press, Oxford, 1949).
[2] L. Hulthén, Kgl. Fysiograf. Sällskap. Lund Förh. **14**, 21 (1944).
[3] W. Kohn, Phys. Rev. **74**, 1763 (1948).
[4] S. Borowitz and B. Friedman, Phys. Rev. **89**, 441 (1953).
[5] H. S. W. Massey and B. Moiseiwitsch, Proc. Roy. Soc. (London) **A205**, 483 (1951).

formulated in the static-field approximation and then solved exactly;[6] and this formulation has also been solved approximately by the Schwinger variational method with a Born trial field.[7] The results given by the Kohn-Hulthén method agree fairly well with those of reference 6 at energies above 2 electron volts, and in the static-field formulation the approximate results are reasonably close to the exact ones at energies above 3 electron volts.

When the method of reference 4 is applied to this problem, the result is an infinite series, the first term of which is the same as the result of reference 7. The remaining terms, as was mentioned earlier, give the polarization effects. We have evaluated this series and found that with the polarization terms included the results barely agree with those of Massey and Moiseiwitsch (Kohn-Huthén method) to within an order of magnitude.

There are no experimental data which would enable one to choose between the results of reference 5 and those obtained here. However, the Born trial field is so crude at low energies that we must conclude that the results using the Schwinger variational method are not to be trusted. This conclusion is disappointing. We had expected that since the Born trial field was successful in duplicating the exact result in the static-field formulation, that a similar success could be achieved in the exactly formulated problem. Apparently, however, the choice of a trial function is much more critical in the higher-dimensional problems.

II. CALCULATIONS AND RESULTS

The following expression for the direct scattered amplitudes f_n has been shown[4] to be stationary with respect to variations of Ψ_0 and Ψ_n around their correct values:

$$-4\pi f_n(\theta)=\frac{(\Psi_n,\exp(ik_0\mathbf{n}_0\cdot\mathbf{r}_1)\phi_0(\mathbf{r}_2)V)(\exp(ik_n\mathbf{n}\cdot\mathbf{r}_1)\phi_n(\mathbf{r}_2)V,\Psi_0)}{(\Psi_n,V\Psi_0)-(\Psi_nV,GV\Psi_0)}. \tag{1}$$

The following notational conveniences have been used in (1): (a, b) denotes the inner product, $\int a^*bd\tau$; G is the Green's function of the differential operator $[\nabla_1^2+\nabla_2^2+2mE/\hbar^2+(2/a_0)(1/r_1)]$, appropriate to the boundary conditions of the problem, and is given by

$$G(\mathbf{r}_1,\mathbf{r}_2;\mathbf{r}_1',\mathbf{r}_2')=-\left(\sum_m+\int\right)\phi_m(\mathbf{r}_2)\phi_m^*(\mathbf{r}_2')\times\exp(ik_n|\mathbf{r}_1-\mathbf{r}_1'|)(4\pi|\mathbf{r}_1-\mathbf{r}_1'|)^{-1}; \tag{2}$$

$V=V(\mathbf{r}_1,\mathbf{r}_2)=(2/a_0)[1/r_{12}-1/r_1]$, with $a_0=$ Bohr radius $=\hbar^2/me^2$; ϕ_m are the hydrogenic wave functions; $\mathbf{n}_0$ and $\mathbf{n}$ are unit vectors in the direction of the incident and scattered wave, respectively; the angle between $\mathbf{n}_0$ and $\mathbf{n}$ is called θ; k_0 and k_n are the wave numbers of the incident and scattered waves, respectively.

The use of a Born trial field for elastic scattering means that we set

$$\Psi_0=\exp(ik_0\mathbf{n}_0\cdot\mathbf{r}_1)\phi_0(\mathbf{r}_2),\qquad \Psi_n=\exp(ik_n\mathbf{n}\cdot\mathbf{r}_1)\phi_0(\mathbf{r}_2). \tag{3}$$

With this trial function, the elastic scattered amplitude is given by

$$f_0(\theta)=\frac{-\frac{1}{4\pi}\int\exp[ik_0(\mathbf{n}_0-\mathbf{n})\cdot\mathbf{r}]W_{00}(\mathbf{r})d\tau}{1-I(\theta)\Big/\left\{\int\exp[ik_0(\mathbf{n}_0-\mathbf{n})\cdot\mathbf{r}]W_{00}(\mathbf{r})d\tau\right\}}, \tag{4}$$

where

$$I(\theta)=\int\exp(-ik_0\mathbf{n}\cdot\mathbf{r}_1)\left(\sum_m+\int\right)W_{0m}(\mathbf{r}_1)\times\frac{\exp(ik_m|\mathbf{r}_1-\mathbf{r}_2|)}{-4\pi|\mathbf{r}_1-\mathbf{r}_2|}W_{m0}(\mathbf{r}_2)\exp(ik_0\mathbf{n}_0\cdot\mathbf{r}_2)d\tau_1d\tau_2, \tag{5}$$

and

$$W_{nm}(\mathbf{r}_1)=\int\phi_n^*(\mathbf{r}_2)V(\mathbf{r}_1,\mathbf{r}_2)\phi_m(\mathbf{r}_2)d\tau_2. \tag{6}$$

The work involved in evaluating (4) for an arbitrary scattering angle is formidable and not necessary. We can make use of the following theorem for the total scattering cross section:[8]

$$Q=(4\pi/k_0)\ \mathrm{Im}f_0(0), \tag{7}$$

where $\mathrm{Im}f_0(0)$ is the imaginary part of the elastic scattering amplitude in the forward direction, $\mathbf{n}_0=\mathbf{n}$.

In terms of the scattered amplitudes,

$$Q=\int(|f_0|^2+|g_0|^2)d\Omega, \tag{8}$$

where g_0 is the elastic exchange-scattered amplitude. The correct expression for the total elastic-scattering cross section is given as

$$Q'=\int(\tfrac{3}{4}|f_0-g_0|^2+\tfrac{1}{4}|f_0+g_0|^2)d\Omega. \tag{9}$$

It is not difficult to show[9] that $Q/2\leq Q'\leq 3Q/2$. For our

[6] S. Chandrasekhar and F. H. Breen, Astrophys. J. **103**, 41 (1946); J. Macdougall, Proc. Roy. Soc. (London) **A136**, 549 (1932).

[7] S. Altschuler, Phys. Rev. **89**, 1278 (1953); L. Mower, Phys. Rev. **89**, 947 (1953).

[8] E. Feenberg, Phys. Rev. **40**, 40 (1932).

[9] H. Boyet and S. Borowitz, Research Report No. CX-7, Mathematics Research Group, Washington Square College, New York University.

TABLE I. Numerical results.

Volts	k_0a_0	I_0	I_1	I_2	I_3	I_4	I_c	$I(0)$
0.135	0.1	$0.769+i(0.099)$	0.966	0.167	0.060	$\sim$0.029	0.783	$2.774+i(0.099)$
0.54	0.2	$0.734+i(0.189)$	0.970	0.171	0.061	$\sim$0.029	0.788	$2.753+i(0.189)$
1.21	0.3	$0.683+i(0.264)$	0.984	0.171	0.061	$\sim$0.029	0.793	$2.720+i(0.264)$
3.38	0.5	$0.554+i(0.361)$	1.001	0.177	0.063	$\sim$0.029	0.815	$2.639+i(0.361)$
6.75	0.707	$0.425+i(0.397)$	1.090	0.187	0.068	$\sim$0.029	0.837	$2.636+i(0.397)$
9.45	0.835	$0.357+i(0.397)$	1.227	0.204	0.071	$\sim$0.029	0.879	$2.767+i(0.397)$

purposes this knowledge of Q' to within $\pm Q/2$ is sufficiently accurate.

The only difficult integral that has to be evaluated in (4) is $I(0)$. The contributions to $I(0)$ may be considered to be made up of three parts:

$$I(0)=I_0+\sum_{n>0} I_n+I_c. \tag{10}$$

The first contribution arises from the ground-state term in the sum. This is the only contribution that one gets in the static-field formulation. The remaining terms obtained in this approximation are corrections to the static-field formulation: the second term is the contribution of the discrete states, and the third is the contribution of the continuum. The integrals have all been carried out;[9] Table I gives the numerical results. A comparison of I_0 and $I(0)$ in Table I indicates the extent of the polarization corrections.

We have not evaluated the contributions of the discrete states beyond I_4, since they seem to converge quite rapidly. In fact the I_n are products of integrals of the order of magnitude unity and coefficients whose ratios are as the ratio of the line intensities of the Lyman series. It is interesting to note that the virtual transitions to the continuum states contribute quite considerably to $I(0)$.

TABLE II. Cross sections for elastic scattering of electrons by hydrogen atoms, in units of $4\pi a_0^2$.

Volts	k_0a_0	Q(ordinary Born-static field)	Q(variational-static field)	Q(exact-static field)[a]	Q[Eq. (4) of this paper]	Q(Kohn-Huthén)[b]
0.135	0.1	0.99	15.66	44.50	0.31	13.36
0.54	0.2	0.95	8.88	17.00	0.30	8.91
1.21	0.3	0.88	5.17	8.28	0.29	6.17
3.38	0.5	0.72	2.19	2.99	0.26	3.28
	0.6					2.40
6.75	0.707	0.56	1.15	1.42	0.20	
	0.8					1.39
9.45	0.835	0.48	0.83	0.98	0.15	

[a] See reference 7.
[b] See reference 6.

Table II gives the values of the cross sections calculated from the values of $I(0)$ in Table I; they are compared with the static field approximation as well as the computations of Massey and Moiseiwitsch. The polarization corrections to the static-field formulation reduce the cross section to a point where there is virtually no agreement with the more plausible results based on the Kohn-Huthén method.

III. CONCLUSIONS

We see thus that despite the fact that a Born trial field can be used successfully with the Schwinger variational method at low energies in the static-field formulation, its use in the six-dimensional problem does not give very good values for the total cross section. The Born trial is one of the simplest that can be used analytically, and yet the integrals involved when it is used in our problem are very complex, and the results poor. This would seem to discourage the use of this method in problems such as these.

At higher energies, this trial function would undoubtedly give better results. However, once we exceed the first excitation energy in hydrogen, namely 10.17 volts, the calculations, though feasible, are considerably more involved. In this case too, the cross section Q as given by (7) would include the sum of the total elastic and inelastic cross sections.

Finally we should like to point out that the use of a static-field formulation in a three-body problem can be justified only if the polarization terms are small. We have demonstrated here, however, that these terms can be surprisingly large; hence this approach to a three-body problem must be used with circumspection.

IV. ACKNOWLEDGMENTS

We should like to thank Professor E. Gerjuoy for several cogent comments.

Paramagnetic Resonance in Gases at Low Fields

M. A. GARSTENS
Electricity Division, U. S. Naval Research Laboratory, Washington, D. C.
(Received September 2, 1953)

A classical analysis has been made of the paramagnetic resonance of a gas composed of a collection of magnetic dipoles in an external static magnetic field H_0 for both circularly and linearly polarized radio-frequency fields at right angles to H_0. Assuming that during collisions the dipoles have components only along the H_0 direction one obtains for the circularly polarized case equations similar to those of Bloch with the single parameter τ, the mean time between collisions. The expression for paramagnetic absorption thus obtained suffers from the defect that at zero external field it does not reduce to the Debye formula, as it should. If a Boltzmann distribution of the x and y components of the magnetization is assumed during collisions, the absorption formula is modified and correctly reduces to the Debye formula. For a linearly polarized radio-frequency field, one obtains as the absorption formula the sum of two terms [Eq. (17)]. This again does not reduce to the Debye formula. Introducing a Boltzmann distribution of magnetization during collisions one obtains a corrected formula in which absorption does not vanish at low fields.

I. INTRODUCTION

EXAMINATION of the macroscopic paramagnetic absorption formula of Bloch[1] indicates that it does not reduce to the Debye formula at zero field, as it should and as experiment indicates,[2] but instead predicts zero absorption at zero field. This suggests that it is subject to the same restriction which troubles the Lorentz theory of line broadening for a harmonic oscillator which restriction was eliminated by the revision carried through by Van Vleck and Weisskopf.[3] We have been interested in carrying through in detail a similar revision of the Bloch equations. We consider the case of a gas which is composed of a collection of dipoles with τ the mean time between collisions. Instead of the harmonic oscillator treated by Lorentz and Van Vleck-Weisskopf we follow the precessional motion of the magnetic dipoles in the external field during and between collisions as defined by their equations of motion.

II. THE CIRCULARLY POLARIZED CASE

If the dipole collection is placed in an external field H_0 in the z direction and subjected to a circularly polarized radio-frequency field in the plane at right angles to z, the motion of each dipole is governed by the following differential equations

$$\frac{d\mu_x}{dt}=\gamma[\mu_y H_0+\mu_z H_1\sin\omega t], \tag{1a}$$

$$\frac{d\mu_y}{dt}=\gamma[\mu_z H_1\cos\omega t-\mu_z H_0], \tag{1b}$$

$$\frac{d\mu_z}{dt}=\gamma[-\mu_z H_1\sin\omega t-\mu_y H_1\cos\omega t], \tag{1c}$$

where μ is the constant magnetic moment of each dipole, μ_x, μ_y, μ_z are the components of μ in the x, y, z direction, H_1 the amplitude of the rf field, γ the gyromagnetic ratio, ω the angular frequency, and $H_x=H_1\cos\omega t$, $H_y=-H_1\sin\omega t$, $H_z=$ the external field H_0. A simple solution of (1) can be obtained by assuming that $\mu_x=\mu_y=0$, $\mu_z=\mu$ during collisions[4] and that μ_x and $\mu_y\ll\mu_z$ between collisions. The latter assumption implies that $\mu_z\sim\mu$ so that μ_z may be considered constant.

The solution of these equations under the above assumptions is

$$\mu_+=Ke^{-i\omega t}+B_1e^{-i\omega_0 t}, \tag{2a}$$

$$\mu_-=Ke^{i\omega t}+B_2e^{i\omega_0 t}, \tag{2b}$$

where

$$K=\gamma H_1\mu_z/(\omega_0-\omega),\quad \omega_0=\gamma H_0,\quad \mu_+=\mu_x+i\mu_y,$$

and

$$\mu_-=\mu_x-i\mu_y.$$

If collisions are assumed to occur at the time $t-\theta$, then $\mu_+=\mu_-=0$ at this time. Thus

$$B_1=-Ke^{i(t-\theta)(\omega_0-\omega)},\quad B_2=-Ke^{-i(t-\theta)(\omega_0-\omega)},$$

and Eqs. (2) become

$$\mu_+=Ke^{-i\omega t}[1-e^{i\theta(\omega-\omega_0)}], \tag{3a}$$

$$\mu_-=Ke^{+i\omega t}[1-e^{-i\theta(\omega-\omega_0)}]. \tag{3b}$$

To average the components of the magnetic moments over varying times of last collision, assuming random occurrence of collisions with the mean time τ between them, we multiply μ_+ and μ_- by $(1/\tau)e^{-\theta/\tau}$ and integrate θ from zero to infinity. We thus obtain

$$\langle\mu_+\rangle=\int_0^\infty\frac{\mu_+}{\tau}e^{-\theta/\tau}d\theta=Ke^{-i\omega t}\left(\frac{(\omega-\omega_0)^2\tau^2-i(\omega-\omega_0)\tau}{1+\tau^2(\omega-\omega_0)^2}\right),$$

$$\langle\mu_-\rangle=\int_0^\infty\frac{\mu_-}{\tau}e^{-\theta/\tau}d\theta=Ke^{i\omega t}\left(\frac{(\omega-\omega_0)^2\tau^2+i(\omega-\omega_0)\tau}{1+\tau^2(\omega-\omega_0)^2}\right).$$

[1] F. Bloch, Phys. Rev. 70, 460 (1946).
[2] C. J. Gorter, *Paramagnetic Relaxation* (Elsevier Publishing Company, New York, 1947).
[3] J. H. Van Vleck and V. F. Weisskopf, Revs. Modern Phys. 17, 227 (1945).
[4] Such collisions are known as strong collisions since the dipoles have no memory of their orientation before collision (see reference 3). They are also assumed to be adiabatic (occurring in a time short compared to the Larmor period). With these two assumptions it is permissible to use, as we later do, a Boltzmann distribution of magnetization during collisions.

Here the angular brackets around μ_+ and μ_- represent their mean values, so that the total magnetization of the collection of dipoles is obtained by multiplying the mean value by N, the number of dipoles per cm³. Thus the x and y components of magnetization M_x and M_y are given by the expressions

$$M_x = N\frac{\langle\mu_+\rangle+\langle\mu_-\rangle}{2} = \omega_0\chi_0\tau\frac{(H_1\cos\omega t)\tau(\omega_0-\omega)+H_1\sin\omega t}{1+\tau^2(\omega_0-\omega)^2},$$
$$M_y = N\frac{\langle\mu_+\rangle-\langle\mu_-\rangle}{2i} = \omega_0\chi_0\tau\frac{(-H_1\sin\omega t)\tau(\omega_0-\omega)+H_1\cos\omega t}{1+\tau^2(\omega_0-\omega)^2}, \quad (4)$$

where χ_0 represents the static susceptibility. These are similar to the Bloch equations[1] with T_2 replaced by τ. Thus the imaginary portion of the susceptibility χ'' corresponding to the out of phase component of magnetization is given by

$$\chi'' = \tfrac{1}{2}\chi_0\omega_0\tau\frac{1}{1+\tau^2(\omega_0-\omega)^2}. \quad (5)$$

We now lift the restriction μ_x, $\mu_y \ll \mu_z$ (i.e., $\mu_z \sim \mu_0$). If the times between collisions are sufficiently long this restriction will not hold since μ_x, μ_y, μ_z can have all values between $\pm\mu$. We transform Eqs. (1) by means of the definitions[5]

$$\mu_x+i\mu_y = Se^{-i\omega t}, \quad \alpha^2=\omega_1^2+\Delta^2, \quad \Delta=\omega-\omega_0, \quad \omega_1=\gamma H_1,$$

into

$$dS/dt = i\Delta S+i\omega_1\mu_z, \quad d\mu_z/dt = \tfrac{1}{2}i\omega_1(S-\bar{S}). \quad (6)$$

These have the solution

$$\mu_z = A\cos(\alpha t+B)+C,$$
$$S-\bar{S} = (2iA\alpha/\omega_1)\sin(\alpha t+B), \quad (7)$$
$$S+\bar{S} = (2\Delta A/\omega_1)\cos(\alpha t+B)+D,$$

where A, B, C, and D are the constants of integration. If we now assume that at time $t-\theta$, $\mu_x=\mu_y=0$, $\mu_z=\mu$, then $S=(\mu_x+i\mu_y)e^{i\omega(t-\theta)}=0$, and

$$\mu_z=\mu=A\cos[\alpha(t-\theta)+B]+C,$$
$$S-\bar{S}=0=\frac{2iA\alpha}{\omega_1}\sin[\alpha(t-\theta)+B], \quad (8)$$
$$S+\bar{S}=0=\frac{2\Delta A}{\omega_1}\cos[\alpha(t-\theta)+B]+D$$

[5] W. J. Archibald, Am. J. Phys. **20**, 368 (1952).

From these and the relationship $\mu_x^2+\mu_y^2+\mu_z^2=\mu^2$, the four constants of integration can be evaluated as

$$A=\mu\omega_1^2/\alpha^2, \quad B=-\alpha(t-\theta), \quad C=\mu\Delta^2/\alpha^2, \quad D=-2\Delta A/\omega_1.$$

substituting these back into (7) we obtain

$$\mu_z = (\mu/\alpha^2)(\omega_1^2\cos\alpha\theta+\Delta^2),$$
$$S-\bar{S} = (2i\omega_1\mu/\alpha)\sin\alpha\theta, \quad (9)$$
$$S+\bar{S} = (2\Delta\mu\omega_1/\alpha^2)(\cos\alpha\theta-1).$$

To obtain the mean value of these quantities we must now average them over varying times of last collision assuming again a random occurrence of collisions with mean time τ between them. Thus

$$\langle S-\bar{S}\rangle = \int_0^\infty \frac{1}{\tau}(S-\bar{S})e^{-\theta/\tau}d\theta = \frac{2i\omega_1\mu\tau}{1+\alpha^2\tau^2}$$
$$\langle S+\bar{S}\rangle = \int_0^\infty \frac{1}{\tau}(S+\bar{S})e^{-\theta/\tau}d\theta = -\frac{2\Delta\mu\omega_1\tau^2}{1+\alpha^2\tau^2}.$$

From these, since

$$\langle\mu_x+i\mu_y\rangle = \tfrac{1}{2}e^{-i\omega t}(\langle S-\bar{S}\rangle+\langle S+\bar{S}\rangle),$$

we obtain

$$\langle\mu_z\rangle = \frac{\omega_1\mu\tau}{1+\alpha^2\tau^2}(\sin\omega t-\Delta\tau\cos\omega t),$$

from which

$$M_z = N\langle\mu_z\rangle = \chi_0\omega_0\tau\frac{(\omega_0-\omega)\tau H_1\cos\omega t+H_1\sin\omega t}{1+\tau^2(\omega_0-\omega)^2+\gamma^2H_1^2\tau^2}. \quad (10)$$

We thus note the appearance of the saturation term $\gamma^2H_1^2\tau^2$ as a result of lifting the restrictions on μ_x, μ_y, μ_z.[6]

III. THE LINEARLY POLARIZED CASE

If the radio-frequency field is linearly polarized, then the equations of motion to be solved are

$$d\mu_z/dt = \gamma\mu_y H_0,$$
$$d\mu_y/dt = \gamma(2\mu_z H_1\cos\omega t-\mu_z H_0), \quad (11)$$

with $H_x=2H_1\cos\omega t$, $H_y=0$, and $H_z=H_0$ representing the external field. We again make the assumption that collisions are frequent so that $\mu_z \sim \mu$. If $\mu_+=\mu_x+i\mu_y$, then (11) reduces to

$$d\mu_+/dt+i\gamma H_0=2i\gamma\mu H_1\cos\omega t. \quad (12)$$

[6] If the saturation term is small compared to 1 the previous equation reduces to Eq. (4). It is of interest to ask what the saturation term means in the collision broadening picture. Thus, if in Eq. (7) one sets $\Delta=0$ (i.e., resonance), then $\alpha=\gamma H_1$. The time taken for μ_z to change from its extreme positive to its extreme negative value is then $1/\gamma H_1$. If $\tau \ll 1/\gamma H_1$, collisions occur much more frequently than the flip frequency, thus preventing the dipoles from diverging much from their collision values $\mu_x=\mu_y=0$, $\mu_z=\mu$, and reducing the solution for M_z to that previously obtained [i.e., Eq. (4)].

The solution of this equation is

$$\mu_+ = \int_{-\infty}^{t} dt'(2i\gamma\mu H_1 \cos\omega t') \times \exp\left(-\int_{t'}^{t} i\gamma H_0 dt''\right) + C_1 e^{-i\omega_0 t}$$

$$= 2i\gamma\mu H_1 \frac{i\gamma H_0 \cos\omega t + \omega \sin\omega t}{(i\gamma H_0)^2 + \omega^2} + C_1 e^{-i\omega_0 t}. \quad (13)$$

C_1 may again be evaluated by assuming that $\mu_+ = 0$ at the time $(t-\theta)$. Then

$$\mu_+ = \frac{2\gamma\mu H_1}{\omega_0^2 - \omega^2}\{\omega_0 \cos\omega t - i\omega \sin\omega t - [\omega_0 \cos\omega(t-\theta) - i\omega \sin\omega(t-\theta)]e^{-i\omega_0\theta}\}, \quad (14)$$

and

$$\langle\mu_+\rangle = \int_0^\infty \frac{\mu_+}{\tau} e^{-\theta/\tau} d\theta$$

$$= \frac{2\gamma\mu H_1}{\tau(\omega_0^2 - \omega^2)}\left\{\tau\omega_0 \cos\omega t - i\omega\tau \sin\omega t - \omega_0 \cos\omega t \frac{\tau(1+i\tau\omega_0)}{(1+i\tau\omega_0)^2+\omega^2\tau^2} - \omega_0 \sin\omega t \frac{\omega\tau^2}{(1+i\tau\omega_0)^2+\omega^2\tau^2} + i\omega \sin\omega t \frac{\tau(1+i\tau\omega_0)}{(1+i\tau\omega_0)^2+\omega^2\tau^2} - i\omega \cos\omega t \frac{\omega\tau^2}{(1+i\tau\omega_0)^2+\omega^2\tau^2}\right\}. \quad (15)$$

The imaginary component of the susceptibility can now be evaluated using the μ_x component of μ_+ in (15) and the formula for the total absorption of energy per unit volume per second

$$A_0 = \frac{\omega}{2\pi}\int_{t-0}^{t-2\pi/\omega} \mathbf{H}\cdot d\mathbf{M} = \frac{\omega}{2\pi}\int_0^{2\pi/\omega} H_x dM_x$$

$$= \frac{N\omega}{2\pi}\int_0^{2\pi/\omega} 2H_1 \cos\omega t d\langle\mu_x\rangle = 2H_1^2\omega\chi''.$$

Substituting from (15) into the latter expression one obtains for χ'':

$$\chi'' = \tfrac{1}{2}\chi_0\omega_0\tau\left(\frac{1}{1+\tau^2(\omega_0-\omega)^2} - \frac{1}{1+\tau^2(\omega_0+\omega)^2}\right), \quad (16)$$

which can be written in the equivalent but more suggestive form

$$\chi'' = \tfrac{1}{2}\chi_0\omega_0\tau\left(\frac{2\omega\omega_0\tau^2}{1+\tau^2(\omega_0+\omega)^2}\right) \times \left(\frac{1}{1+\tau^2(\omega_0-\omega)^2} + \frac{1}{1+\tau^2(\omega_0+\omega)^2}\right). \quad (17)$$

Both the circularly and linearly polarized expressions for χ'' thus vanish as the external field H_0 or ω_0 approaches zero, the linearly polarized one doing so much more rapidly according to (17). Since neither formula shows any zero field absorption as they should, the assumption that the x and y components vanish during collision appears to be the one to be modified. Assuming a Boltzmann distribution for the x and y components of magnetization after collision[3] we correct C_1 in Eq. (13). This correction to C_1 for the linearly polarized case, to be added to the solution (14) is given by the expression

$$\Delta C_1 e^{-i\omega_0(t-\theta)} = \frac{\int\int \mu e^{-\mu H\cos\theta'/kT}\cos\theta' d\Omega}{\int\int e^{-\mu H\cos\theta'/kT} d\Omega} = \frac{2\chi_0 H_1}{N}\cos\omega(t-\theta),$$

where $-\mu H\cos\theta'$ represents the potential energy of the magnetic moment μ in the field $H = 2H_1\cos\omega(t-\theta)$ and θ' is the angle between μ and the x axis. Thus

$$\Delta C_1 e^{-i\omega_0 t} = (2\chi_0 H_1/N)\cos\omega(t-\theta)e^{-i\omega_0\theta}.$$

A correction ΔC_2, corresponding to the integration constant C_2 in the solution of the equation defining μ_-, similar to that which defines μ_+, is given by

$$\Delta C_2 e^{i\omega_0 t} = (2\chi_0 H_1/N)\cos\omega(t-\theta)e^{i\omega_0\theta}.$$

The correction to μ_x is obtained by adding ΔC_1 and ΔC_2, i.e.,

$$\Delta\mu_x = \tfrac{1}{2}(\Delta C_1 e^{-i\omega_0 t} + \Delta C_2 e^{i\omega_0 t}) = (2\chi_0 H_1/N)\cos\omega(t-\theta)\cos\omega_0\theta.$$

If this is averaged over θ with the weighting factor $(1/\tau)e^{-\theta/\tau}$ we obtain

$$\langle\Delta\mu_x\rangle = \text{Real Part}\left\{\frac{\chi_0 H_1}{\tau N}\int_0^\infty e^{i\omega(t-\theta)} \times (e^{i\omega_0\theta} + e^{-i\omega_0\theta})e^{-\theta/\tau} d\theta\right\}$$

$$= \frac{\chi_0 H_1}{\tau N}\left(\frac{(1/\tau)\cos\omega t - (\omega_0-\omega)\sin\omega t}{(1/\tau)^2 + (\omega_0-\omega)^2} + \frac{(1/\tau)\cos\omega t + (\omega_0+\omega)\sin\omega t}{(1/\tau)^2 + (\omega_0+\omega)^2}\right).$$

Since as the expression for the total absorption of energy A_0 indicates, only the sine terms in $\langle\Delta\mu_x\rangle$ contribute to the absorption, we select those and obtain as the correction to χ'':

$$\langle\Delta\chi''\rangle=-\tfrac{1}{2}\chi_0\tau\left(\frac{\omega_0-\omega}{1+\tau^2(\omega_0-\omega)^2}-\frac{\omega_0+\omega}{1+\tau^2(\omega_0+\omega)^2}\right),$$

yielding, when added to (16), the revised expression for χ'':

$$\chi''=\tfrac{1}{2}\chi_0\omega\tau\left(\frac{1}{1+\tau^2(\omega_0-\omega)^2}+\frac{1}{1+\tau^2(\omega_0+\omega)^2}\right). \quad (18)$$

In effect ω_0 in the coefficient of (16) has been replaced by ω and the sign between the two terms has been changed. If now ω_0 is allowed to approach zero, χ'' approaches the expression:

$$\chi''=\chi_0\omega\tau/(1+\tau^2\omega^2),$$

which is the Debye formula for zero field absorption.

Figure 1 is a logarithmic plot, of the relative variation $\Delta g/g$ of g from its free spin value as a function of $\omega\tau$, obtained from Eq. (18) by maximizing χ'' as a function of $\omega_0\tau$ for constant $\omega\tau$. This is in conformity with experiment, the field $H_0=\omega_0/\gamma$ being the variable parameter used in determining the maximum of χ'' for different constant frequencies ω. τ is assumed to be constant over the observed range of frequencies and field. $\Delta g/g$ is then defined as the deviation of ω_0 at maximum χ'' from ω divided by ω. For $\omega\tau>1$ an inverse fourth power variation with $\omega\tau$ is indicated. This diminishes as $\omega\tau$ approaches the value 1 and then increases again when $\omega\tau<1$. Of interest is the disappearance of a maximum in absorption when $\omega\tau$ is less than 0.58.

No measurements have been made in paramagnetic gases at low enough fields to check the above formula. At this laboratory,[7] however, this variation of g as a function of frequency at low fields, has been measured in the free radical diphenyl-picryl-hydrazyl in the range $1<\omega\tau<2$. The inverse variation of $\Delta g/g$ with $\omega\tau$ was found to be slightly larger than fourth power. This appears to be consistent with the values indicated by Fig. 1.

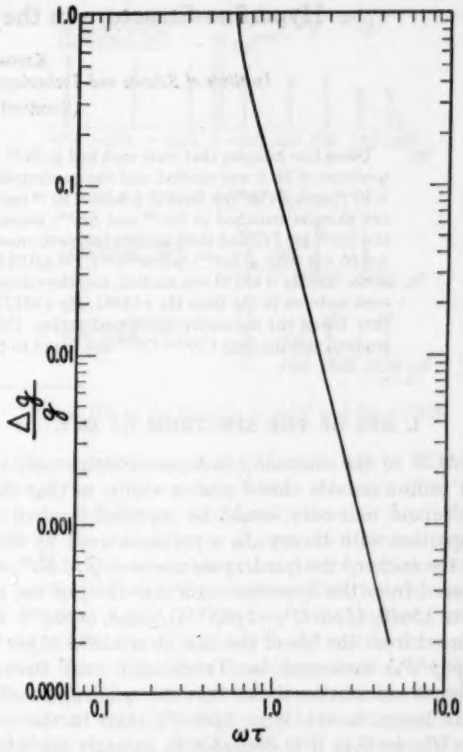

FIG. 1. Variation of g from the free-spin value. The slope measures n in $\Delta g/g\sim 1/(\omega\tau)^n$.

SUMMARY

An analysis has been made of the motion of magnetic dipoles in a gas immersed in a magnetic field H_0 and a cross rf field either circularly or linearly polarized. In the first case, assuming zero x and y components of magnetization during collision, the usual Bloch equation for absorption is obtained; in the second the difference between two Bloch type terms is found. Both, however, predict no absorption at zero field. By assuming a Boltzmann distribution during collisions one obtains for the linearly polarized case the sum of two terms which show zero field absorption and reduce correctly to the Debye formula. The absorption formula thus derived predicts a change of g from the free spin value varying inversely with $\omega\tau$ from the fourth power when $\omega\tau>1$, decreasing as $\omega\tau$ approaches the value 1 and then increasing as $\omega\tau$ sinks below 1. This is verified approximately for diphenyl-picryl-hydrazyl in the range $1<\omega\tau<2$.

[7] A. H. Ryan and L. S. Singer (private communication).

Hyperfine Structure in the Spectra of Sb, Sm, Hg, and Cd†

KIYOSHI MURAKAWA
Institute of Science and Technology, Komaba-machi, Meguro-ku, Tokyo, Japan
(Received December 4, 1953)

Using two samples that were enriched in Sb^{121} and Sb^{123}, respectively, the hyperfine structure (hfs) of the spectrum of Sb II was studied, and the quadrupole moments were determined to be $Q(Sb^{121}) = (-0.52 \pm 0.10) \times 10^{-24}$ cm², $Q(Sb^{123}) = (-0.67 \pm 0.10) \times 10^{-24}$ cm². Study of the hfs of the spectra of Sm I and Sm II, using two samples enriched in Sm^{147} and Sm^{149}, respectively, yielded the result that the nuclear spins of Sm^{147} and Sm^{149} are 7/2 and their nuclear magnetic moments are $\mu(Sm^{147}) = -0.76 \pm 0.08$ nm and $\mu(Sm^{149}) = -0.64 \pm 0.06$ nm with $\mu(Sm^{147})/\mu(Sm^{149}) = 1.198 \pm 0.015$. Using a sample containing 1.5 percent of Hg^{196}, the hfs of the line Hg II λ6150 was studied, and the existence of the Hg^{196} component was just observed. Shifts of the even isotopes in the lines Hg I λ5461, Hg I λ6123, and Hg III λ4797 were measured, and it was found that they follow the regularity mentioned earlier. Using natural cadmium, the hfs of the line Cd II λ4415 was studied, and the shift $Cd^{114} - Cd^{116}$ was found to be anomalously small compared with the shift $Cd^{112} - Cd^{114}$.

I. HFS OF THE SPECTRUM OF Sb II

EACH of the antimony isotopes contains only one proton outside closed proton shells, so that their quadrupole moments would be especially suited for comparison with theory. In a previous work by Suwa and the author,[1] the quadrupole moment Q of Sb^{121} was deduced from the hyperfine structure (hfs) of the line Sb II λ5640 ($5p6s\ ^3P_2 - 5p6p\ ^3S_1$),[2] and $Q(Sb^{123})$ was deduced from the hfs of the line Sb II λ5895 ($5p6s\ ^3P_1 - 5p6p\ ^3P_0$) measured by Tomboulian and Bacher.[3] A simple calculation shows that the quadrupole effect is far larger in the term $5p6s\ ^3P_2$ than in the term $5p6s\ ^3P_1$, so that it is desirable to measure the hfs of $5p6s\ ^3P_2$ for Sb^{123}, but this was almost impossible owing to the complexity of the hfs of the line λ5640, if natural antimony only was used.

The separated isotopes Sb^{121} and Sb^{123} were available to the author in 1951. Using a hollow cathode discharge tube[4] and a Fabry-Pérot etalon the hfs of λ5640 was examined. All the important components could be measured, but some weak components could not owing to the ghosts of the strong helium line λ5876. The hfs diagram of λ5640 for the natural antimony could now be completely constructed and is shown in Fig. 1. A number in parentheses was calculated, because the expected component was disturbed by the ghost and could not be measured accurately. The components b, c, e, $\bar{b}$, $\bar{c}$, $\bar{e}$, $\bar{g}$, and $\bar{i}$ were measured on plates that were taken using separated isotopes. The other components were measured on plates that were taken using natural antimony.

From Fig. 1 we get

$$A^{121} = 73.8 \times 10^{-3}\ \text{cm}^{-1}, \quad B^{121} = -0.159 \times 10^{-3}\ \text{cm}^{-1};$$
$$A^{123} = 40.0 \times 10^{-3}\ \text{cm}^{-1}, \quad B^{123} = -0.098 \times 10^{-3}\ \text{cm}^{-1}$$

for the term $5p6s\ ^3P_2$. From the ratio of B^{121} and B^{123}, we get the ratio of the quadrupole moments of Sb^{121} and Sb^{123}:

$$Q^{123}/Q^{121} = 21B^{123}/10B^{121} = 1.29 \pm 0.10.$$

This value is in agreement with that published by Loomis and Strandberg[5] (1.263) and that published by Dehmelt and Krüger[6] (1.2689). Putting the values

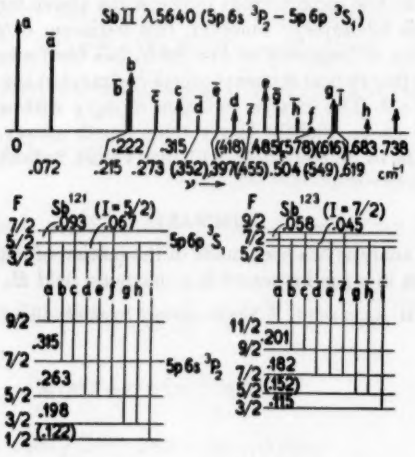

FIG. 1. Hfs of the line Sb II λ5640.

† The work with enriched isotopes was performed at the University of Wisconsin in 1950–1951 and was supported by the U. S. Office of Naval Research. The work with natural samples was performed in Tokyo. The enriched isotopes were produced by the Y-12 plant, Carbide and Chemicals Division, Oak Ridge, and were obtained by allocation from the U. S. Atomic Energy Commission.

[1] K. Murakawa and S. Suwa, Phys. Rev. **76**, 433 (1949).

[2] The Sb II spectrum was classified by J. S. Badami, Z. Physik **79**, 224 (1932) and extensively by R. J. Lang and E. H. Vestine, Phys. Rev. **42**, 233 (1932). In the course of the study of the hfs of Sb II it was found that the classifications of a considerable number of lines given by Lang and Vestine should be modified, and the modified and extended classification was published by K. Murakawa and S. Suwa, Rept. Inst. Sci. Tech. Univ. Tokyo **1**, 90 (1947) in Japanese.

The spins of Sb are known to be $I^{121} = 5/2$ and $I^{123} = 7/2$ from the works of Badami (reference 2) and of M. F. Crawford and Bateson, Can. J. Research **10**, 693 (1934).

[3] D. H. Tomboulian and R. F. Bacher, Phys. Rev. **58**, 52 (1940).

[4] O. H. Arroe and J. E. Mack, J. Opt. Soc. Am. **40**, 386 (1950).

[5] C. C. Loomis and M. W. P. Strandberg, Phys. Rev. **81**, 798 (1951).

[6] H. G. Dehmelt and H. Krüger, Z. Physik **130**, 385 (1951).

of B in Casimir's formula (quoted in reference 1) we get

$$Q^{121}=(-0.52\pm0.10)\times10^{-24}\ \text{cm}^2,$$
$$Q^{123}=(-0.67\pm0.10)\times10^{-24}\ \text{cm}^2.$$

These values are more accurate than those given in the previous work.[1] Loomis and Strandberg set the upper limit of Q^{121} and Q^{123} at -0.50 and -0.62 (in unit of 10^{-24} cm^2), respectively and the lower limit of Q^{121} and Q^{123} at -0.35 and -0.45, respectively. Their estimates are in essential agreement with the values deduced here. Quite recently Sprague and Tomboulian[7] have deduced the values $Q^{121}=-1.3\times10^{-24}$ cm^2 and $Q^{123}=-1.7\times10^{-24}$ cm^2. From their short description it is not possible to find source of the discrepancy.

II. HFS OF THE SPECTRA OF Sm I AND Sm II

In a previous work by Ross and the author[8] the hfs of the spectra of Sm I and Sm II was examined, using two samples that were enriched in Sm^{147} and Sm^{149} (see Table I and reference 9), respectively; and it was concluded Sm^{147} and Sm^{149} have the same spins equal to 5/2, that because the maximum number of hyperfine components of any Sm line with a flag pattern was observed to be six. This conclusion was based unfortunately on the assumption that the contribution of the complex $4f^6$ to the hfs splitting of the configuration $4f^66s$ or $4f^66p$ was negligible, so that the hfs of the transition $4f^66s-4f^66p$ represented directly the approximate hfs of $4f^66s$. The contribution of $4f^6$ is small only when the J value of the term is small, for example, equal to 1 or ½. However, in order to determine the nuclear spin, just those lines[10] that involve sufficiently high J values should be chosen. In this case the aforementioned finding leads to the conclusion that the spin is probably equal to 5/2 or larger, because the hfs of any line attributed to the transition $4f^66s-4f^66p$ does not represent the splitting of the term $4f^66s$ directly, it being possible that both the upper and the lower term have the same order of magnitude of hfs splitting. It is, therefore, necessary to determine the nuclear spins and magnetic moments, keeping these points in mind.

TABLE I. Isotopic constitution (percent) of the samples of samarium.

Sample label	Isotope 144	147	148	149	150	152	154
149	0.55	5.09	11.88	71.53	3.98	4.85	2.13
147	1.10	81.63	6.96	3.94	1.20	3.41	1.77
Natural	3.16	15.07	11.27	13.84	7.47	26.63	22.53

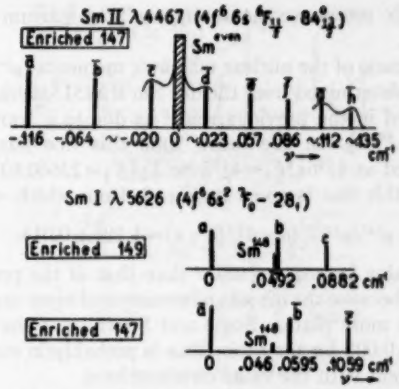

FIG. 2. Hfs of the lines Sm II λ4467 and Sm I λ5626.

After measurement of the hfs splittings of numerous terms of Sm II, it was found that the term $4f^66s\ ^6F_{11/2}$ has a small splitting, and finally the line Sm II λ4467 ($4f^66s\ ^6F_{11/2}-84^\circ_{13/2}$) was chosen for determining the spin. This line is so weak that it was overlooked in the previous work.[8] The measured hfs for the sample 147 is given in Fig. 2. The two tail components were not so well resolved, but they could still be recognized as two. From Fig. 2 we can conclude that the term $84^\circ_{13/2}$ of Sm^{147} is inverted (hfs level with the largest F lies deepest) and splits into eight hfs levels, so that the spin of Sm^{147} is 7/2. The hfs of λ4467 of the sample 149 is quite similar to that of the sample 147; however, the scale is somewhat smaller. The spin of Sm^{149} is, therefore, also 7/2. The hfs of the line Sm I λ5626 ($4f^66s^2\ ^7F_0-28_1$) shown in Fig. 2 also supports qualitatively this spin value. This conclusion is in agreement with that of Bogle and Scovil,[11] who found the spins from para-

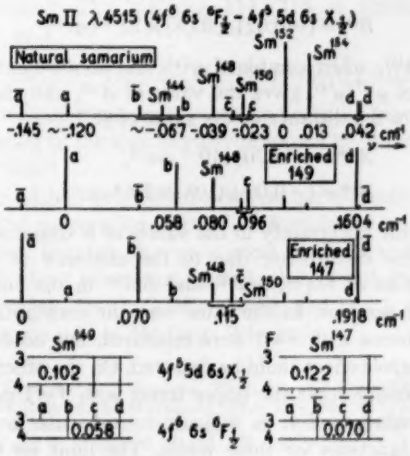

FIG. 3. Hfs of the line Sm II λ4515.

[7] G. Sprague and D. H. Tomboulian, Phys. Rev. **91**, 476 (1953).
[8] K. Murakawa and J. S. Ross, Phys. Rev. **82**, 967 (1951).
[9] The isotropic constitution of natural samarium was taken from Inghram, Hayden, and Hess, Phys. Rev. **73**, 180 (1948).
[10] The classification of the spectra of Sm I and Sm II was published by W. Albertson, Phys. Rev. **47**, 370 (1935); **52**, 644 (1937) and Astrophys. J. **84**, 26 (1936), respectively. That of Sm I was extended by P. Brix, Z. Physik **126**, 431 (1949). The literature concerning the shift of even isotopes was summarized by D. D. Smith and J. R. McNally, J. Opt. Soc. Am. **40**, 878 (1950).
[11] G. S. Bogle and H. E. D. Scovil, Proc. Phys. Soc. (London) **65**, 368 (1952).

magnetic resonance measurements of samarium ethyl sulfate.

The ratio of the nuclear magnetic moments (μ^{147}/μ^{149}) can be determined from the line Sm II λ4515, which was classified in the previous work[8] as due to a transition $J=\frac{1}{2}\rightarrow J'=\frac{1}{2}$. In the mean time this line has been classified as $4f^6 6s\ {}^6F_{\frac{1}{2}}-4f^5 5d6s\ X_{\frac{1}{2}}(X_{\frac{1}{2}}=23660.03)$. The hfs of this line is given in Fig. 3, from which we get

$$\mu^{147}/\mu^{149}=(\bar{d}-\bar{a})/(d-a)=1.198\pm0.015.$$

This value is more accurate than that of the previous work,[8] because the hfs was now measured more carefully and on more plates. Bogle and Scovil[11] got the value 1.222 ± 0.008 for the ratio. This is probably in essential agreement with the value obtained here.

From Fig. 3 we get $A^{147}(4f^6 6s\ {}^6F_{\frac{1}{2}})=-0.0175$ cm^{-1}. In the previous work[8] it was found that the splitting of the term $4f^6 6s\ {}^8F_{\frac{1}{2}}$ of Sm^{147} is -0.120 cm^{-1}. We, therefore, get $A^{147}(4f^6 6s\ {}^8F_{\frac{1}{2}})=-0.0300$ cm^{-1}. $A({}^8F_{\frac{1}{2}})+A({}^6F_{\frac{1}{2}})$ should be independent of coupling, and is equal to $\frac{7}{8}a(6s)$, where the contribution of the complex $4f^6$ is neglected. We get, therefore, $a^{147}(6s)=-0.0712$ cm^{-1}. Putting this value and $n^{*3}/(dn^*/dn)=9.85$ in the Fermi-Segrè-Goudsmit formula, we get finally

$$\mu^{147}=-0.76\pm0.08 \text{ nm}.$$

Using the above-mentioned value of μ^{147}/μ^{149}, we get

$$\mu^{149}=-0.64\pm0.06 \text{ nm}.$$

Elliott and Stevens[12] obtained $|\mu^{147}|=0.68\pm0.1$ nm and $|\mu^{149}|=0.55\pm0.1$ nm from the data of Bogle and Scovil.[11]

From the hfs of the line Sm I λ5626 ($4f^6 6s^2\ {}^7F_0-28_1$) shown in Fig. 2, the following constants for the term 28_1 are obtained:

$$A^{147}=-13.33\times10^{-3} \text{ cm}^{-1},$$
$$B^{147}=(-0.021\pm0.08)\times10^{-3} \text{ cm}^{-1}.$$

This A^{147}, when combined with the above-mentioned value of μ^{147}/μ^{149}, gives the value of A^{149}, and then we get from the distance ac the value of B^{149}:

$$A^{149}=-13.20\times10^{-3} \text{ cm}^{-1},$$
$$B^{149}=(-0.00\pm0.08)\times10^{-3} \text{ cm}^{-1},$$

where the uncertainty in the values of B comes mainly from the disturbance due to the existence of minor quantities of Sm^{150}, Sm^{152}, and Sm^{154} in the enriched isotope samples. In the same way the constants B in some terms with $J=1$ were measured, but no definite quadrupole effect could be detected. On the other hand it is possible that the upper terms with $J=1$ perturb each other, and it is difficult to calculate accurate wave functions for these terms. The limit for Q was roughly estimated, and it is possible at the present time

[13] R. J. Elliott and K. W. H. Stevens, Proc. Phys. Soc. (London) 65, 370 (1952).

TABLE II. Isotopic constitution (percent) of the samples of mercury.

Sample label	Isotope 196	198	199	200	201	202	204
196	1.46	7.48	9.03	13.15	7.87	25.24	35.78
Natural	0.15	10.1	17.0	23.3	13.2	29.6	6.7

to give the estimates only:

$$|Q^{147}|,\ |Q^{149}|<1\times10^{-24} \text{ cm}^2.$$

Elliott and Stevens[12] got the limit $|Q^{147}|,\ |Q^{149}|\leqq0.72\times10^{-24}$ cm^2.

In order to get more accurate values of Q, it would be necessary to get the sample in an isotopically pure state. Especially Sm^{147} would deserve further study in view of the discussion by Hill and Wheeler[13] about the nuclear deformation in connection with the alpha activity[14] of Sm^{147}.

III. ISOTOPE SHIFT IN THE SPECTRA OF Hg I, Hg II, AND Hg III

In order to study the isotope shift of Hg^{196}, the enriched 196 sample (see Table II) was placed in an iron hollow cathode discharge tube and, using helium as the carrier gas, the line Hg II λ6150 ($7s\ {}^2S_{\frac{1}{2}}-7p\ {}^2P_{\frac{3}{2}}$) was obtained with strong intensity. The hfs of λ6150 is shown in Fig. 4, in which the calculated relative intensity (in percent) is given under the notation of each component. If the shift 198–196 were of the same order of magnitude as 204–202, the 196 component should lie about midway between 198 and a, but this is not the case. The 198 component is somewhat diffuse to the smaller-frequency side, and this was interpreted as due to the unresolved 196 component, whose position was estimated to be about -0.110 cm^{-1}. The shift 198–196 is then about 0.019 cm^{-1}.

Since the 196 sample contains larger percentage of Hg^{204} than natural mercury, shift of even isotopes in

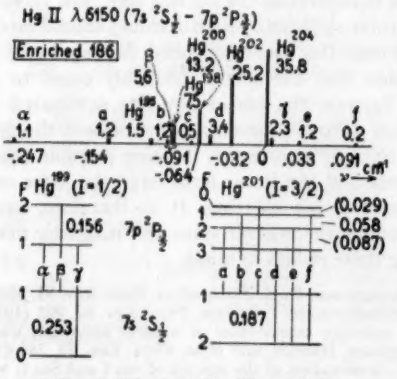

FIG. 4. Hfs of the line Hg II λ6150.

[13] D. L. Hill and J. A. Wheeler, Phys. Rev. 89, 1102 (1953).
[14] Rasmussen, Reynolds, Thompson, and Ghiorso, Phys. Rev. 80, 475 (1950).

the line Hg I λ5461 ($6s6p\,^3P_2-6s7s\,^3S_1$) was also measured. The shift 204−202 was measured to be 0.0306 cm^{-1}. Since the 202 component (intensity 25.2) is expected to have superimposed on it a partial component (intensity 5.4) of Hg^{199} lying 0.0299 cm^{-1} to the smaller-frequency side of the 204 component, the corrected shift 204−202 is 0.0309 cm^{-1}. The shift of the even isotopes is given in Table III, together with the measurement of Sterner[15] for the same line. The position of Hg^{198} given by Sterner deviates somewhat from that of the present author, but the source of the discrepancy is difficult to find at present.

In the measurement using natural mercury, a high-frequency electrodeless discharge tube was used. This light source was found to give sharper lines than a hollow cathode tube. Hg I λ6123 ($7s\,^3S_1-5d^9 6s^2 6p\,^1D_2$) and Hg III λ4797 ($5d^9 6s^2\,12_4-5d^9 6p\,2_3^0$)[16] were especially strong, and the result of the measurement is given in Table III. The present measurement for λ6123 is more accurate than the previous one.[17,18] From Table III we see that the ratio $\Delta\nu(198-200):\Delta\nu(200-202):\Delta\nu(202-204)$ is constant at least as a first approximation, as was inferred in references 17 and 18. If the result of Sterner[15] were accepted, $\Delta\nu(198-200)/\Delta\nu(202-204)$ for λ5461 would have the anomalous value 0.805. Such an anomalous value for λ5461 only is very improbable, however.

TABLE III. Isotopic shift of the even isotopes of mercury[a] ($\Delta\nu$ in cm^{-1}).

Line		Isotope 198	200	202	204
Hg I λ5461	$\Delta\nu$(J.S.)[b]		0.0240	0.0326	0.0298
	$\Delta\nu$(K.M.)[c]		0.0276	0.0311	0.0309
	Ratio(K.M.)[c]		0.89 ±0.03 :	1.01 ±0.03 :	1
Hg I λ6123	$\Delta\nu$		0.1886	0.2131	0.2090
	Ratio		0.902 ±0.012 :	1.020 ±0.012 :	1
Hg III λ4797	$\Delta\nu$		0.552	0.604	0.599
	Ratio		0.922 ±0.006 :	1.009 ±0.006 :	1

[a] In all three lines listed the 204 component lies on the highest-frequency side.
[b] J. Sterner (see reference 15).
[c] Our results.

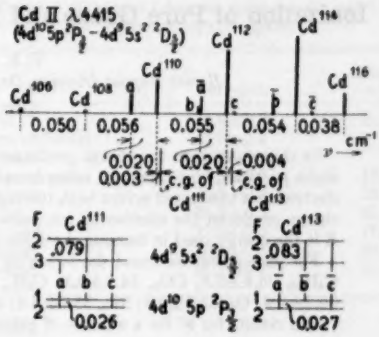

FIG. 5. Hfs of the line Cd II λ4415 (c.g. means center of gravity).

IV. ISOTOPE SHIFT IN THE SPECTRUM OF Cd II

Koch and Rasmussen[19] and Ross and the author[20] found an anomalous shift of the even isotopes in the spectra of Xe I and of Te II, respectively. The neutron numbers of the Cd isotopes are fairly near to those of the Te isotopes, and the isotope shift in the spectrum of Cd deserves investigation. This was studied by previous workers,[21] but they detected components due to Cd^{110}, Cd^{112}, and Cd^{114} only.

In the present work the hfs of the line Cd II λ4415 ($4d^{10}5p\,^2P_{\frac{1}{2}}-4d^9 5s^2\,^2D_{\frac{3}{2}}$)[22] was studied, using natural cadmium and a liquid-air-cooled hollow-cathode discharge tube. The result of measurement is shown in Fig. 5. The hfs splittings of the odd isotopes were calculated, using the magnetic moments given in the literature.[23] The distance 114−116 is anomalously small, and

$$\Delta\nu(114-116)/\Delta\nu(112-114)=0.70\pm0.02.$$

This kind of anomaly would be probably interpreted according to the idea recently proposed by Wilets, Hill, and Ford.[24]

The author would like to express his appreciation for the kind cooperation of Dr. J. S. Ross in the work with enriched isotopes. It was a great pleasure to be able to talk about interesting related subjects with Professor J. E. Mack, Dr. J. G. Hirschberg, and Dr. J. S. Ross during my stay in Madison, Wisconsin.

[15] J. Sterner, Phys. Rev. **86**, 139 (1952). All the data of previous workers concerning λ5461 are listed in his article. See also K. Burns and K. B. Adams, J. Opt. Soc. Am. **42**, 56, 716 (1952).
[16] The hfs of the line Hg III λ4797 was interpreted by S. Mrozowski, Phys. Rev. **57**, 207 (1940), and later the classification was published by E. W. Foster, Proc. Roy. Soc. (London) **A200**, 429 (1950). E. W. Foster [Proc. Roy. Soc. (London) **A208**, 367 (1951)] also measured the hfs of λ4797, but, since he employed a small resolving power, he could resolve the structure only incompletely. In the present work the hfs of λ4797 could be resolved completely, and the result of the measurement is: −1.1560 (198), −1.0746 (199), −0.6043 (200), −0.4293 (201), 0 (202), 0.5994 (204) cm^{-1}, the accuracy being ±0.0012 cm^{-1}. Contrary to the calculation of Foster, the 199 and 201 components are sharp and each of them has a splitting smaller than about 0.010 cm^{-1}.
[17] K. Murakawa, Phys. Rev. **78**, 480 (1950).
[18] K. Murakawa and S. Suwa, J. Phys. Soc. Japan **5**, 429 (1950).
[19] J. Koch and E. Rasmussen, Phys. Rev. **77**, 722 (1950).
[20] J. S. Ross and K. Murakawa, Phys. Rev. **85**, 559 (1952).
[21] H. Schüler and H. Westmeyer, Z. Physik **82**, 685 (1933); P. Brix and A. Steudel, Z. Physik **128**, 260 (1950).
[22] This and other lines of Cd II were classified by Y. Takahashi, Ann. Physik **3**, 27 (1929).
[23] J. E. Mack, Revs. Modern Phys. **22**, 64 (1950); P. F. A. Klinkenberg, Revs. Modern Phys. **24**, 63 (1952).
[24] Wilets, Hill, and Ford, Phys. Rev. **91**, 1488 (1953).

Ionization of Pure Gases and Mixtures of Gases by 5-Mev Alpha Particles

T. E. BORTNER AND G. S. HURST
Health Physics Division, Oak Ridge National Laboratory, Oak Ridge, Tennessee
(Received November 13, 1953)

In this experiment the charge produced in a large ionization chamber, by the complete stopping of Pu^{239} alpha particles, was measured using an accurately calibrated capacitor in series with a potentiometer. An electrometer connected across both the capacitor and potentiometer was used as a null indicator. From the charge produced the number of ion pairs n was deduced and W, defined by the equation $W=E/n$ where E is the energy used in forming the n ion pairs, was computed.

For pure gases, we found the following values of W (in ev per ion pair): A, 26.4±0.3; BF_3, 36.0±0.4; C_4H_{10}, 26.4±0.3; CO_2, 34.3±0.3; C_2H_4, 28.0±0.3; He, 46.0±0.5; H_2, 37.0±0.4; CH_4, 29.4±0.3; N_2, 36.3±0.4; O_2, 32.2±0.3; SF_6, 35.7±0.4; air, 35.0±0.3; freon 12, 29.5±0.3.

Our results for W for a mixture of gases are described by the formula

$$\frac{1}{W_m}=\left(\frac{1}{W_1}-\frac{1}{W_2}\right)z+\frac{1}{W_2},$$

where $z=P_1/(P_1+aP_2)$, and W_m is the W for the gas mixture having two components of pressure P_1 and P_2 with W values for the pure gases equal to W_1, and W_2, respectively. For the following mixture a has the values shown: N_2-H_2, 0.28; N_2-A, 0.53; N_2-O_2, 1.06; He−A, 0.75; He−H_2, 3.55; He−N_2, 8.47; He−CH_4, 0.68; A−H_2, 0.56; H_2-CH_4, 4.03.

In the case of He the W of 46.0 is not used in the above equation, since small traces of impurities reduce W(He) to 30.0 electron volts, and this latter value is appropriate for using in the formula for gas mixtures.

INTRODUCTION

SOME of the practical radiation dosimetry units are defined in terms of the energy delivered by the radiation to a gram of soft tissue. Methods of measuring dose, on the other hand, involve the use of Bragg-Gray cavities filled with various gases in which ionization is collected. Thus, to have a consistent system of definitions and measurements, the value of W (electron volts required to produce an ion pair) must be known. It is known that the value of W depends, in general, on the mass and energy of the ionizing particle, and the gas used. It is the purpose of this work to study a large number of gases and gas mixtures, using a fixed particle and energy; namely, Pu^{239} alpha particles. Many of these gases have been studied previously, but unfortunately some of the work has been hampered by impure gases and other difficulties.

APPARATUS AND METHOD

The method used for measuring the ionization produced by alpha particles is shown in Fig. 1. The parallel plate ionization chamber is enclosed in a steel case which may be held at positive pressures so that the range of alpha particles will be entirely inside the collecting volume even for gases such as hydrogen or helium. The rate of ionization in the chamber is measured by the voltage change on an accurately calibrated capacitor. The voltage change is determined

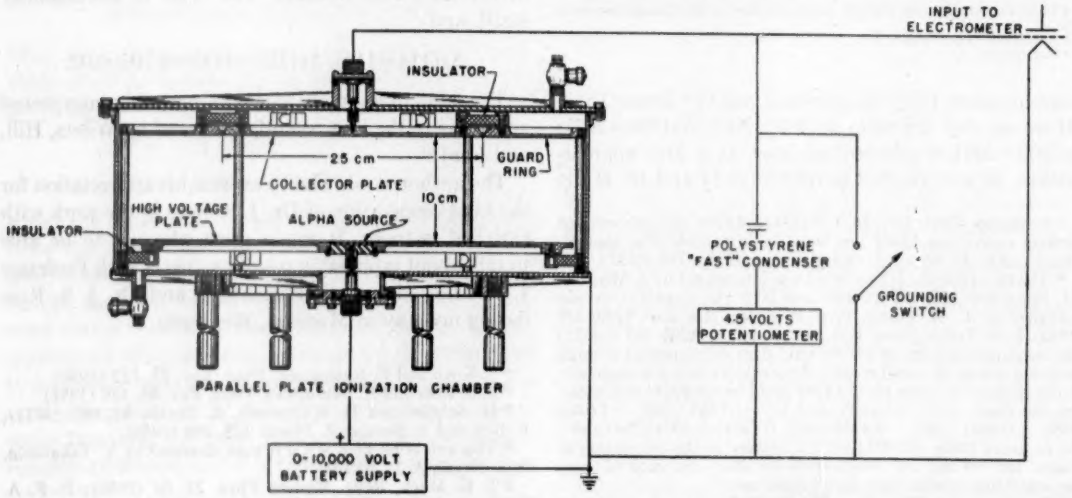

FIG. 1. Block diagram of the apparatus for measuring W for alpha particles.

with a potentiometer, using an ac-operated electrometer[1] as a null indicator. The capacitor is of such size that the readings are several hundred millivolts per minute, a rate of drift which is much greater than that due to the inherent variations in the electrometer. For this system, the formula appropriate for computing W is:

$$W = N \times E \times 1.59 \times 10^{-19} / CV, \qquad (1)$$

where N = counts per minute of alpha source with 2π geometry, E = energy of alpha particles in electron volts, C = capacitance of the condenser in farads, V = rate of drift of the condenser (volts/minute), and 1.59×10^{-19} = charge of the electron in coulombs. An alpha source of Pu^{239} is electroplated on platinum and calibrated by counting with a methane flow proportional counter connected to a linear amplifier and discriminator circuit. The source plate is used without a collimator since with a collimator some ionization is formed in the sensitive volume by alpha particles which terminate

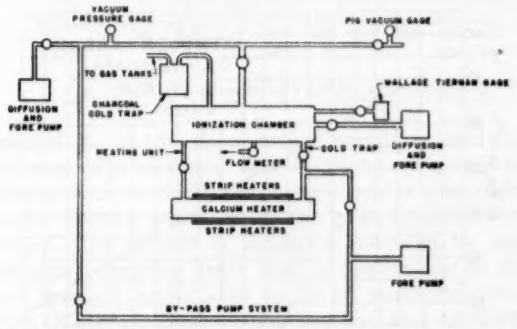

FIG. 2. Block diagram of gas filling and purification system. All circles, unless otherwise designated, are cut-off valves.

in the collimator wall without losing all their energy in the gas. These pulses would not be detected with the proportional counter but do contribute to the ionization.

An extremely stable high-voltage supply is required and for this reason a series of 300-volt batteries, connected by resistors for safety, is mounted in a polystyrene box. This system gives results that are reproducible to within 0.1 percent.

Purification of the different gases is accomplished by means of the apparatus in Fig. 2. Gases which condense in a trap of liquid nitrogen are redistilled, while others are run through activated charcoal at liquid nitrogen temperature. Figure 2 also shows a calcium trap attached by one-inch stainless steel tubes to the ion chamber. Convection of the gas through the calcium trap and the chamber was increased by placing a heating coil on one of the chamber outlets, which was kept at 300°C and by a liquid nitrogen trap on the other chamber port. If the gas itself does not unite with hot

[1] F. M. Glass, Nucleonics **10**, No. 2, 36 (1952).

TABLE I. W values (electron volts per ion pair) for nonelectronegative gases.

Gas	Our result	Reference result
Argon	26.4±0.3	26.4[a]
Boron trifluoride	36.0±0.4	
Butane	26.4±0.3	
Carbon dioxide	34.3±0.3	34.5[a]
Ethylene	28.0±0.3	28.0[b]
Helium	46.0±0.5	42.7[a]
Hydrogen	37.0±0.4	37.0[b]
Methane	29.4±0.3	29.0[b]
Nitrogen	36.3±0.4	36.3[c]

[a] See reference 3.
[b] See reference 4.
[c] See reference 2.

calcium, this method of purification is often used to remove certain impurities. In the case of helium, the calcium is kept at a temperature of 400°C and proved to be very effective in removing oxygen. Argon contamination is removed by flowing through a trap of charcoal at liquid nitrogen temperature.

RESULTS WITH PURE NONELECTRONEGATIVE GASES

Nonelectronegative gases are defined as those in which the probability of electron attachment to form a heavy negative ion is small. Thus, the chances of columnar recombination are small at moderate electric fields, and the ionization current *versus* voltage curve quickly saturates. Table I shows the W values obtained for pure gases.[2-4]

Helium requires very careful purification; with no purification grade A helium[5] taken from different tanks gave a spread of W values from 31 to 43 electron volts. Two different methods of purification gave W for helium equal to 46.0±0.4 electron volts. One method consisted of flowing helium over cocoanut charcoal at

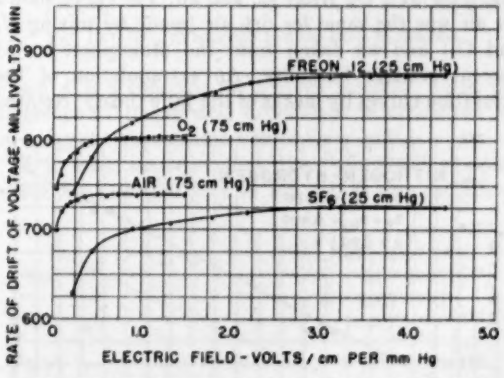

FIG. 3. Saturation curves for SF_6, air, O_2, and freon 12.

[2] Alder, Huber, and Metzger, Helv. Phys. Acta **20**, 234 (1947).
[3] W. P. Jesse, and J. Sadauskis, Phys. Rev. **90**, 1120 (1953).
[4] J. M. Valentine and S. C. Curran, Phil Mag. **43**, 964 (1952).
[5] According to information supplied by Dr. M. M. Deaton, Chief, Research Branch, Helium Division, Region IV, Bureau of Mines, grade A helium has a purity of 99.9+ percent when bottled.

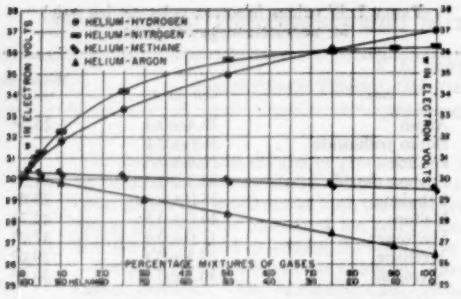

FIG. 4. W for mixtures of He with H_2, N_2, CH_4, and A.

liquid nitrogen temperature; the ionization being measured during flow. Stopping the flow results in a rapid decrease in W (increase in ionization) after a few minutes. This was probably due to outgassing of the chamber even though no gas other than helium had been in the chamber for over 90 days. The second method of purification consisted of a continuous convection of the helium over metallic calcium held at 400°C.

TABLE II. W values for electronegative gases.

Gas	W in ev
O_2	32.2±0.3
SF_6	35.7±0.4
Air	35.0±0.3
Freon 12	29.5±0.3

RESULTS WITH ELECTRONEGATIVE GASES

For electronegative gases columnar recombination is quite appreciable even with high electric fields in the ionization chamber. Results of ionization current *versus* electric field (in volts per cm per mm Hg) are shown in Fig. 3 for SF_6, O_2, freon 12, and air. The curve shown for air was the same for dry air (made by mixing N_2 and O_2) and air taken from the atmosphere at 53 percent relative humidity. An extrapolation of the saturation curves by means of the Jaffe theory[6] resulted

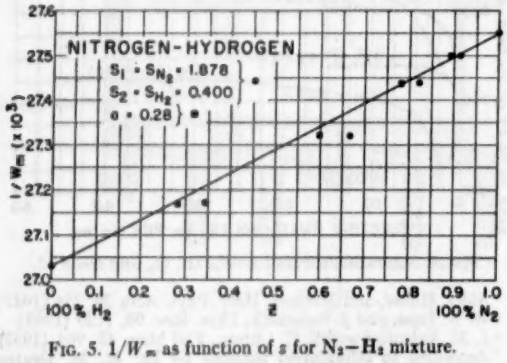

FIG. 5. $1/W_m$ as function of z for N_2-H_2 mixture.

[6] G. Jaffe, Ann. Physik 42, 303 (1913). A convenient application was made by H. Zanstra, Physica 2, 817 (1935).

in only a very minor increase in current above its value at the highest fields; thus the chamber was known to be very near saturation. Values for W can be computed using the upper value for the current, and these values for electronegative gases are given in Table II.

RESULTS WITH GAS MIXTURES

Since the W for He depends so critically on the amount of gas impurity it is of interest to obtain W curves as a function of gas mixture for He with several other gases. In Fig. 4 these values are shown for H_2, N_2, CH_4, and A, in helium. In each case the W is reduced from 46.0 ev for pure He to approximately 30 ev by the addition of small traces (less than one percent) of the contaminating gas. This behavior is consistent with the suggestion by Jesse and Sadauskis[7] that the low reported values for W of He are due to the fact that the energy in the well-known metastable state in He

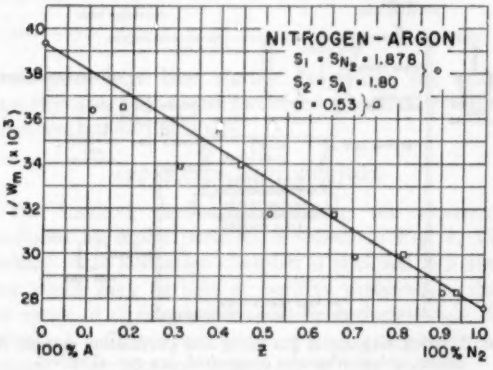

FIG. 6. $1/W_m$ as function of z for N_2-A mixture.

(19.7 volts) can be transferred to a contaminating gas and produce extra ionization in gases where the ionization potential is less than the metastable potential.

If it is assumed that the presence of a second gas does not contribute ionization to the first, then a formula may be written for the W of a gas mixture. Such a formula,[8] based on the energy lost to the two gases according to the partial pressures P_1 and P_2, and the molecular stopping powers S_1 and S_2, may be written as:

$$\frac{1}{W}=\left(\frac{1}{W_1}-\frac{1}{W_2}\right)z+\frac{1}{W_2}, \qquad (2)$$

where

$$z=S_1P_1/(S_1P_1+S_2P_2).$$

Plotting the measured values of $1/W$ as a function of z should give a straight line according to Eq. (2). Our results for several gas mixtures are shown in Figs.

[7] W. P. Jesse and J. Sadauskis Phys. Rev. 88, 417 (1952).

[8] Huber, Baldinger, and Haeberli, Helv. Phys. Acta, 23, Suppl. III (1949).

5–13, where it is seen that using reported[9] values for (RaC alpha) molecular stopping powers gives large deviations (small circle in figures) for almost all cases except for N_2-O_2 and H_2-CH_4 mixtures. In a subsequent article, Haeberli, Huber, and Baldinger[10] noticed small deviations from Eq. (2) for mixtures N_2-He and $He-A$. Our difference for the $He-A$ mixture is much larger and is not due entirely to the fact that we use $S_{He}=0.308$ while they use a relative value of 0.430.

In order to account for the small differences in theory and experiment, Haeberli *et al.*, assumed that a certain

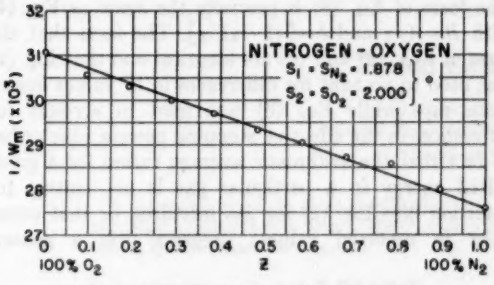

FIG. 7. $1/W_m$ as function of z for N_2-O_2 mixture.

portion E_s of the alpha-particle energy is used in forming delta rays, and that the delta-ray energy is divided between the two gas components in proportion to the stopping powers of the two gases for delta rays (σ_1,σ_2). The amount of ionization produced by the secondary electrons (delta rays) is proportional to E_s and inversely proportional to the W values for delta rays (W_{s1},W_{s2}). These assumptions lead to a modified

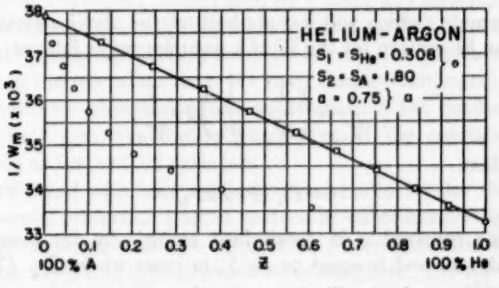

FIG. 8. $1/W_m$ as function of z for $He-A$ mixture.

formula for the W of a gas mixture:

$$\frac{1}{W_m}=\left(\frac{1}{W_1}-\frac{1}{W_2}\right)z+\frac{1}{W_2}+\Delta, \tag{3}$$

where

$$\Delta=\left(\frac{1}{W_{s1}}-\frac{1}{W_{s2}}\right)(k_2-k_1\gamma_{12})\frac{z(1-z)}{\gamma_{12}+z(1-\gamma_{12})},$$

[9] H. R. von Taubenberg, Z. Physik 2. 268 (1920).
[10] Haeberli, Huber, and Baldinger, Helv. Phys. Acta, 26, 145 (1953).

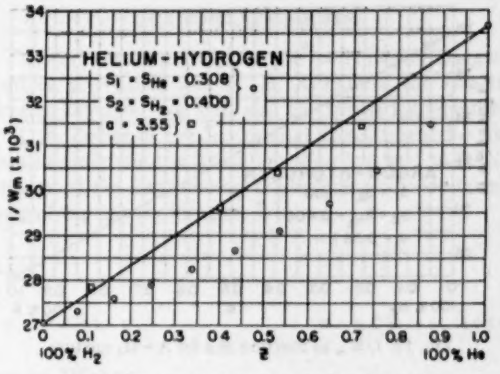

FIG. 9. $1/W_m$ as function of z for $He-H_2$ mixture.

with $\gamma_{12}=s_1\sigma_2/s_2\sigma_1$; k_2 and k_1 are defined by $E_s=k_1E_1+k_2z_2$, where $E_1=zE_0$, $E_2=(1-z)E_0$, and E_0 is the initial energy of the alpha particle. For a given gas mixture, the Δ term should depend on pressure (or z) as

$$\Delta=A\frac{z(1-z)}{\gamma+z(1-\gamma)}, \tag{4}$$

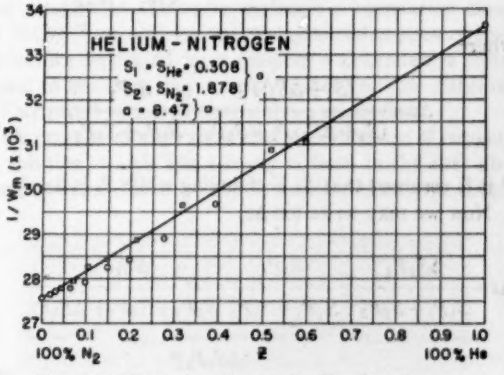

FIG. 10. $1/W_m$ as function of z for $He-N_2$ mixture.

where A is a constant for a given mixture. Thus, the difference in theory and experiment is accounted for by using the appropriate values for γ and A.

If it were assumed that the "effective" stopping power for insertion in z in Eq. (2) is not the actual

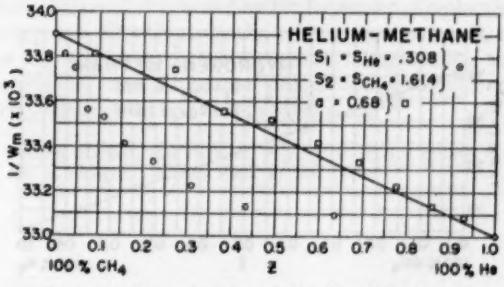

FIG. 11. $1/W_m$ as function of z for $He-CH_4$ mixture.

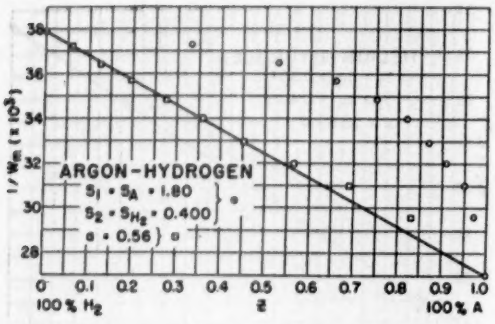

FIG. 12. $1/W_m$ as function of z for A$-$H$_2$ mixture.

stopping power reported in the literature, but differs from S_1 by an amount ΔS, then we would write

$$\Delta\left(\frac{1}{W_m}\right)=\frac{1}{W_m}-\left(\frac{1}{W_1}-\frac{1}{W_2}\right)z-\frac{1}{W_2}$$

$$=\left(\frac{1}{W_1}-\frac{1}{W_2}\right)\Delta z, \quad (5)$$

where

$$\Delta z=\frac{(S_1+\Delta S_1)P_1}{(S_1+\Delta S_1)P_1+S_2P_2}-\frac{S_1P_1}{S_1P_1+S_2P_2},$$

if it is assumed that S_1 is changing while S_2 is fixed.

Now we may write for Δz,

$$\Delta z=\frac{\Delta S_1P_1}{S_1P_1+S_2P_2}-\frac{S_1P_1}{S_1P_1+S_2P_2}\cdot\frac{\Delta S_1P_1}{S_1P_1+S_2P_2+\Delta S_1P_1}$$

$$-\frac{(\Delta S_1P_1)^2}{(S_1P_1+S_2P_2)(S_1P_1+S_2P_2+\Delta S_1P_1)}, \quad (6)$$

and if the term in $(\Delta S_1)^2$ is neglected,

$$\Delta z=\frac{\Delta S_1}{S_1}\times\frac{z(1-z)}{1+(\Delta S_1/S_1)z}, \quad (7)$$

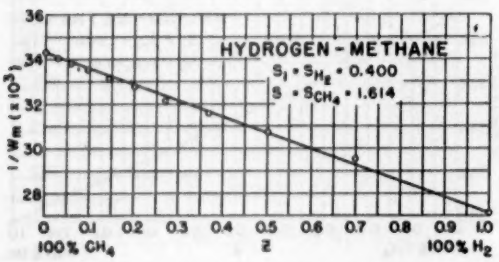

FIG. 13. $1/W_m$ as function of z for H_2-CH_4 mixture.

and

$$\Delta\left(\frac{1}{W_m}\right)=\left(\frac{1}{W_1}-\frac{1}{W_2}\right)\times\frac{\Delta S_1}{S_1}\times\frac{z(1-z)}{1+(\Delta S_1/S_1)z}$$

$$=\frac{Bz(1-z)}{1+bz}, \quad (8)$$

where

$$B=\left(\frac{1}{W_1}-\frac{1}{W_2}\right)\frac{\Delta S_1}{S_1} \quad \text{and} \quad b=\frac{\Delta S_1}{S_1}.$$

The form of Eq. (8) is precisely the same as Eq. (4) with $B=A/\gamma$ and $b=[(1-\gamma)/\gamma]$. The facts that the form of Eqs. (8) and (4) are identical and that Eq. (4) was used to account for differences in W values due to delta rays while Eq. (8) was used to account for differences in the effective stopping powers (due either to fact that the arithmetic average values for a given initial energy in a particular gas is not correct for insertion into Eq. (2) for gas mixtures, or that errors exist in reported values) suggests that a general

TABLE III. Values of a compared to S_2/S_1.

Mixture	Figure	S_2/S_1	a
N_2-H_2	5	0.21	0.28
N_2-A	6	0.95	0.53
N_2-O	7	1.06	1.06
He$-$A	8	5.85	0.75
He$-H_2$	9	1.30	3.55
He$-N_2$	10	6.10	8.47
He$-CH_4$	11	5.24	0.68
A$-H_2$	12	0.22	0.56
H_2-CH_4	13	4.03	4.03

formula (which will include both of the above effects) can be written for the W of a gas mixture as follows:

$$\frac{1}{W_m}=\left(\frac{1}{W_1}-\frac{1}{W_2}\right)z+\frac{1}{W_2},$$

where

$$z=P_1/(P_1+aP_2). \quad (9)$$

The constant a is determined empirically for every mixture and is equal to S_2/S_1 in cases where Eq. (2) holds.

As seen from the curves in Figs. 5–13, the agreement between measurements and Eq. (9) is good when the correct value of a is used. Comparisons of a with S_2/S_1 are made in Table III. It should be noted that for He the W for "contaminated He" was used as 30.0 ev.

Strictly speaking, the approximation made in deducing Eq. (7) is not justified in view of some of the values of a in Table III. In any case, the argument presented is not intended to be a proof that the empirical Eq. (9) holds for every mixture. However, the identical form of Eqs. (4) and (8) implies that not all the devia-

tions found by Haeberli *et al.*, should be attributed to delta-ray formation. Furthermore, Eq. (9) has some value in that it is not only an extremely simple way to represent large amounts of experimental data, but is useful in attempting to separate sudden changes (due, for example, to the discharge of metastable states) in $(1/W)$ as a function of z from the more gradual ones that Eq. (9) is intended to represent.

ACKNOWLEDGMENTS

The authors are grateful for the many helpful suggestions of J. Neufeld and R. H. Ritchie of the Health Physics Division. We wish also to express appreciation to R. E. Zedler of the Instrument Department for his work in designing the ionization chamber, and to P. N. Hensley of the Engineering Department who designed parts of the gas purification system.

PHYSICAL REVIEW VOLUME 93, NUMBER 6 MARCH 15, 1954

Proton Relaxation in Water

G. CHIAROTTI AND L. GIULOTTO
Istituto di Fisica dell'Università di Pavia, Pavia, Italy
(Received November 2, 1953)

A determination of the thermal relaxation time of protons in pure water gives the value 3.6±0.2 sec, in very good agreement with theory. The O_2 molecule in aqueous solution seems to have a μ_{eff} of 1.2 Bohr magnetons for the relaxation processes.

WE have recently performed a series of measurements of the thermal relaxation time of protons in pure water and in water containing oxygen in solution. The methods used are based on measurements of amplitude of the "in phase" nuclear signals caused by the total reversal of the magnetization. Two observations with different sweep frequencies and with resonance field centered with respect to the sweep, or one observation with resonance field not centered (Fig. 1), enable one to determine the relaxation time. This latter method is similar to that used by Conger and Selwood.[1] To obtain good accuracy with the first method, one of the two sweep periods must be several times greater than the relaxation time. We have therefore arranged a device for observation and registration of the nuclear signals with modulation frequencies of the constant field as low as 0.02 cycle/sec.

We find with both methods $T_1=3.6\pm0.2$ sec for the thermal relaxation time of protons in water completely free of oxygen and $T_1=1.4\pm0.1$ sec for water saturated with oxygen at a pressure of one atmosphere. The time we find for pure water is considerably different from that found by Purcell *et al.*[2] (2.3 sec), but it is in very good agreement with their theory if one assumes for the rotation of the water molecule a correlation time of 1×10^{-11} sec and for the translational motion of two molecules separated by a distance r a correlation time equal to the time they take to travel over the distance r. Our result seems to justify this assumption.

Our measurements show that the influence of oxygen in solution, which was already noticed in the first observations of Bloch *et al.*,[3] is smaller than one could expect from the magnetic moment of the oxygen molecule which is 2.8 Bohr magnetons. The μ_{eff} of the O_2 in the relaxation processes seems to be 1.2 Bohr magnetons. This could be caused by the formation of molecular complexes (like O_4 molecules with a zero moment), or by the influence of the electronic relaxation on the correlation time. This latter process seems to influence the nuclear relaxation also in other cases.[2,4]

FIG. 1. "In phase" proton signals in pure water due to total reversal of the magnetization. Resonance field not centered with respect to the sweep. Sweep period, 5.7 sec.

[1] R. L. Conger and P. W. Selwood, J. Chem. Phys. **20**, 383 (1952).
[2] Bloembergen, Purcell, and Pound, Phys. Rev. **73**, 679 (1948); N. Bloembergen, *Nuclear Magnetic Relaxation* (M. Nijhoff, The Hague, 1948).
[3] Bloch, Hansen, and Packard, Phys. Rev. **70**, 474 (1946).
[4] R. L. Conger, J. Chem. Phys. **21**, 937 (1953).

Line Width of Rotational Spectra of Some Symmetric Top Molecules Due to Nuclear Quadrupole Moments*

TAKASHI ITO AND YUKITO TANABE, *Department of Physics, Faculty of Science, University of Tokyo, Tokyo, Japan*

AND

MASATAKA MIZUSHIMA, *Department of Physics, Duke University, Durham, North Carolina*

(Received September 16, 1953)

The hyperfine structure of rotational spectra is sometimes so complicated that it cannot be analyzed easily. In many other cases it is difficult to resolve the hfs and the whole spectrum is observed as a somewhat broad single line. In these cases the line width or the mean-square frequency deviation may have a more practical significance. In this paper explicit formulas are given for the mean-square frequency deviation as a function of the nuclear quadrupole coupling constant and the quantum numbers I, J, K. Thus by means of these formulas we shall be able to obtain the nuclear quadrupole coupling constant from the line width of the rotational line without analyzing hfs. Calculations were made on symmetric top molecules which have one or three identical nuclei with electric quadrupole moments. The effect of other nuclei which have electric quadrupole moments can be easily taken into account. The method of separating the present line width from that of the pressure broadening and that due to the centrifugal distortion is discussed.

I. INTRODUCTION

THE hfs of the rotational spectrum is usually due to the coupling between the nuclear electric quadrupole moment and the surrounding electrons. The coupling constant which is obtained by analyzing the hfs is important in two points. First it can be used to estimate the nuclear quadrupole moment, which has a close relation with the nuclear structure. Actually the nuclear shell model was much improved when the simple nuclear shell model was found to be not able to account the value of the nuclear quadrupole moment.[1] On the other hand it is known that the coupling constant has a close relation to the property of the chemical bond.[2] From this constant one can estimate, for example, the contribution of the ionic structure and the extent of s-p hybridization of the chemical bond.

Unfortunately sometimes the hfs is so complicated that it cannot be analyzed, or cannot even be resolved experimentally. This happens, especially, in the case of molecules with more than one nucleus which has a quadrupole moment. Bersohn[3] and Mizushima and Ito[4] have proposed theories of the hfs of symmetric top molecules with three identical nuclei which have quadrupole moments. The theory was applied to the $J=0\rightarrow1$ transition of the $CHBr_3$ molecule with success.[5] However, it was pointed out[4] that the hfs in the rotational spectra with larger J is very complicated and is practically impossible to analyze. Actually there are many experimental data on the rotational lines of this type of molecule ($AsCl_3$,[6] PCl_3,[6] PBr_3,[7] $CHBr_3$,[7,8] $CHCl_3$,[9,10] CH_3CCl_3,[10] $POCl_3$,[11] $PSCl_3$,[11] $HSiCl_3$,[12] CH_3SiCl_3),[12] but in none of these cases is the hfs resolved.

Even in these cases where the hfs is extremely complicated, it must be possible to obtain the quadrupole coupling constant from the over-all line width. The Van Vleck formula,[13]

$$\langle\Delta\nu^2\rangle_{Av}=-\mathrm{Tr}(H\mathbf{S}-\mathbf{S}H)^2/h^2\,\mathrm{Tr}\mathbf{S}^2, \tag{1}$$

will give the mean-square frequency deviation of the rotational line due to the hfs, where H is the nuclear quadrupole coupling energy and S is the dipole moment of the molecule.

II. SYMMETRIC TOP MOLECULE WITH ONE NUCLEUS WHICH HAS A QUADRUPOLE MOMENT

a. Hamiltonian of the Quadrupole Coupling

The interaction of the nucleus and the electrons is

$$V=\sum_{i,j}e_ie_j/r_{ij}, \tag{2}$$

where e_i is the charge of the ith proton and e_j is that of the jth electron. Taking the origin at the center of charge of the nucleus, V can be expanded as (assuming $r_i>r_j$):

$$V=\sum_{i,j}\sum_{k=0}^{\infty}e_ie_j(r_i^k/r_j^{k+1})P_k(\cos\theta_{ij}), \tag{3}$$

* This research was supported in part by The United States Air Force under a contract monitored by the Office of Scientific Research, Air Research and Development Command.

[1] J. Rainwater, Phys. Rev. 79, 432 (1950); A. Bohr, Phys. Rev. 81, 134 (1951).
[2] C. H. Townes and B. P. Dailey, J. Chem. Phys. 17, 783 (1949).
[3] R. Bersohn, J. Chem. Phys. 18, 1124 (1950).
[4] M. Mizushima and T. Ito, J. Chem. Phys. 19, 739 (1951).
[5] Kojima, Tsukada, Hagiwara, Mizushima, and Ito, J. Chem. Phys. 20, 804 (1952).
[6] P. Kisliuk and C. H. Townes, Phys. Rev. 78, 347 (1950); J. Chem. Phys. 18, 1109 (1950).
[7] Q. Williams and W. Gordy, Phys. Rev. 79, 195 (1950).
[8] Williams, Cox, and Gordy, J. Chem. Phys. 20, 1524 (1952).
[9] Unterberger, Trambarulo, and Smith, J. Chem. Phys. 18, 565 (1950).
[10] Ghosh, Trambarulo, and Gordy, J. Chem. Phys. 20, 605 (1952).
[11] Williams, Sheridan, and Gordy, J. Chem. Phys. 20, 164 (1952).
[12] Mockler, Bailey, and Gordy, Phys. Rev. 87, 172 (1952).
[13] J. H. Van Vleck, Phys. Rev. 74, 1168 (1948).

where θ_{ij} is the angle between the vectors $\mathbf{r}_i$ and $\mathbf{r}_j$ and $P_k(\cos\theta_{ij})$ is the Legendre function. By means of the addition theorem, formula (3) can be written as

$$V=\sum_{i,j}\sum_{k=0}^{\infty} e_ie_j(r_i^k/r_j^{k+1})\mathbf{C}^{(k)}(i)\cdot\mathbf{C}^{(k)}(j), \quad (4)$$

where

$$\mathbf{C}^{(k)}(i)\cdot\mathbf{C}^{(k)}(j)=\sum_{q=-k}^{k}(-1)^qC_q^{(k)}(i)C_{-q}^{(k)}(j), \quad (5)$$

and

$$C_q^{(k)}=[4\pi/(2k+1)]^{\frac{1}{2}}Y_k^q(\cos\theta,\phi). \quad (6)$$

The $k=0$ term in the formula (4) is the interaction of the electrons and the nucleus, where the nucleus is assumed to have no structure. The $k=1$ term vanishes identically by the definition of the origin. The $k=2$ term is the interaction of the nuclear quadrupole moment and the electrons; it can be written as

$$V_Q=\mathbf{Q}\cdot\nabla\mathbf{E}, \quad (7)$$

where

$$\mathbf{Q}=\sum_i e_ir_i^2\mathbf{C}^{(2)}(i), \quad (8)$$

and

$$\nabla\mathbf{E}=\sum_j(e_j/r_j^3)\mathbf{C}^{(2)}(j). \quad (9)$$

The matrix element of V_q can be obtained by the Racah formulas.[14] By his formula (29) of reference 14, we obtain

$$\begin{aligned}&(IM_I|Q_q|IM_I')\\&=(-1)^{I+M_I}(I\|Q\|I)V(II2;-M_IM_I'q)\\&=(-1)^{2I+M_I}(II|Q_0|II)V(II2;-M_IM_I'q)/V(II2;-II0)\\&=\tfrac{1}{2}(-1)^{2I+M_I}eQV(II2;-M_IM_I'q)/V(II2;-II0),\end{aligned} \quad (10)$$

where eQ is the nuclear quadrupole moment and V is the function defined by Racah.[14]

In the same way we obtain

$$\begin{aligned}&(JKM|\nabla E_q|J'K'M')\\&=(-1)^{J+M}(JK\|\nabla E\|J'K')V(JJ'2;-MM'q)\\&=\tfrac{1}{2}(-1)^{2J+M}(JKJ|\partial^2V/\partial Z^2|J'K'J)\\&\quad\times V(JJ'2;-MM'q)/V(JJ'2;-JJ0),\end{aligned} \quad (11)$$

where $\partial^2V/\partial Z^2$ is the second derivative of the electric potential V at the position of the nucleus under consideration with respect to the Z coordinate which is the axis of quantization fixed in the space. Since the second-order effect in the hfs which comes from the different rotational state ($J'\neq J$) is usually small, we shall neglect it in this paper, and consider only the $J'=J$ case. It can be shown easily that[15]

$$\begin{aligned}&(JKJ|\partial^2V/\partial Z^2|JKJ)\\&=\{3K^2-J(J+1)\}\{(J+1)(2J+3)\}^{-1}\partial^2V/\partial z^2,\end{aligned} \quad (12)$$

$$\begin{aligned}&(J1J|\partial^2V/\partial Z^2|J-1J)\\&=-\{J/2(2J+3)\}(\partial^2V/\partial x^2-\partial^2V/\partial y^2),\end{aligned} \quad (13)$$

and all the other matrix elements are zero. In these formulas z is the symmetry axis of the molecule and x and y are perpendicular to z axis. In the case of the molecule considered in this section $\partial^2V/\partial x^2-\partial^2V/\partial y^2$ is usually zero; thus we shall neglect the matrix element (13) in this section.

b. Calculation of $\mathrm{Tr}(H\mathbf{S}-\mathbf{S}H)^2$

The Van Vleck formula (1) can be applied to our problem if we put

$$H=V_Q\equiv\mathbf{Q}\cdot\nabla\mathbf{E}, \quad (14)$$

and take only the $J\leftrightarrow J+1$ matrix elements of $\mathbf{S}$, which is given by the Racah formula[14] as

$$\begin{aligned}&(JKM|S_q|J+1KM')=(-1)^{J+M}\\&\quad\times(JK\|S\|J+1K)V(JJ+11;-MM'q).\end{aligned} \quad (15)$$

We obtain

$$\begin{aligned}\mathrm{Tr}(H\mathbf{S}-\mathbf{S}H)^2&=\mathrm{Tr}(\mathbf{Q}\cdot\nabla\mathbf{E}\mathbf{S}-\mathbf{S}\mathbf{Q}\cdot\nabla\mathbf{E})^2\\&=\mathrm{Tr}\{\textstyle\sum_q(-1)^q(Q_q\nabla E_{-q}\mathbf{S}-\mathbf{S}Q_q\nabla E_{-q})\}^2\\&=\mathrm{Tr}\{\textstyle\sum_q(-1)^qQ_q(\nabla E_{-q}\mathbf{S}-\mathbf{S}\nabla E_{-q})\}^2\\&\quad\sum_{q,q'}\mathrm{Tr}^s\{(-1)^qQ_qQ_{-q'}\}\,\mathrm{Tr}^r\{(-1)^{q'}\\&\quad\times(\nabla E_{-q}\mathbf{S}-\mathbf{S}\nabla E_{-q})(\nabla E_{q'}\mathbf{S}-\mathbf{S}\nabla E_{q'})\}.\end{aligned} \quad (16)$$

It can easily be shown that

$$\mathrm{Tr}^s\{(-1)^qQ_qQ_{-q'}\}=\delta(q,q')\,\mathrm{Tr}^s(\mathbf{Q}\cdot\mathbf{Q})/5. \quad (17)$$

Thus, formula (16) is

$$\mathrm{Tr}(H\mathbf{S}-\mathbf{S}H)^2=\tfrac{1}{5}\,\mathrm{Tr}^s(\mathbf{Q}\cdot\mathbf{Q})\,\mathrm{Tr}^r(\nabla\mathbf{E}\mathbf{S}-\mathbf{S}\nabla\mathbf{E})^2. \quad (18)$$

By our formula (10) and using the Racah formulas (20a) and (19) of reference 14, we obtain

$$\begin{aligned}\mathrm{Tr}^s(\mathbf{Q}\cdot\mathbf{Q})&=\sum_{M_I}\sum_q(-1)^{q+2I+M_I+M_I'}(I\|Q\|I)^2\\&\quad\times V(II2;-M_IM_I'q)V(II2;-M_I'M_I-q)\\&=(I\|Q\|I)^2=\{eQ/2V(II2;-II0)\}^2.\end{aligned} \quad (19)$$

By means of the definition of the V function, this is

$$\mathrm{Tr}^s(\mathbf{Q}\cdot\mathbf{Q})=e^2Q^2(2I+1)(I+1)(2I+3)/4I(2I-1). \quad (20)$$

[14] G. Racah, Phys. Rev. **62**, 438 (1942).

[15] It is helpful to note that

$$\partial^2V/\partial Z^2=\sum_{i,j=1}^{3}\Phi_{zi}\Phi_{zj}\partial^2V/\partial a_i\partial a_j,$$

where $a_1=x$, $a_2=y$, $a_3=z$, and Φ_{zi} is the direction cosine between the Z axis and the a_i axis.

The trace over the rotational states in formula (17) can be obtained as follows: In

$$\begin{aligned}\mathrm{Tr}^r(\nabla\mathbf{ES}-\mathbf{S}\nabla\mathbf{E})^2 &= \mathrm{Tr}^r(\nabla\mathbf{ES}\cdot\nabla\mathbf{ES})+\mathrm{Tr}^r(\mathbf{S}\nabla\mathbf{E}\cdot\mathbf{S}\nabla\mathbf{E})\\ &\quad -\mathrm{Tr}^r(\nabla\mathbf{ES}\cdot\mathbf{S}\nabla\mathbf{E})-\mathrm{Tr}^r(\mathbf{S}\nabla\mathbf{E}\cdot\nabla\mathbf{ES}),\end{aligned}\tag{21}$$

the last term, for example, can be written [using formulas (11) and (15)] as:

$$\begin{aligned}&\mathrm{Tr}^r(\mathbf{S}\nabla\mathbf{E}\cdot\nabla\mathbf{ES})\\ &=\sum_M\sum_q\sum_{q'}(-1)^{q+q'}\langle JM|S_q|J+1M'\rangle\\ &\quad\times\langle J+1M'|\nabla E_{q'}|J+1M''\rangle\\ &\quad\times\langle J+1M''|\nabla E_{-q'}|J+1M'\rangle\langle J+1M'|S_{-q}|JM\rangle\\ &=(JK\|S\|J+1K)(J+1K\|S\|JK)\\ &\quad\times(J+1K\|\nabla E\|J+1K)^2\\ &\quad\times\sum_M\sum_q V(JJ+11;-MM'g)\\ &\quad\times V(JJ+11;-M'M-q)\\ &\quad\times\sum_{q'}V(J+1J+12;-M'M''g')\\ &\quad\times V(J+1J+12;-M''M'-q'),\end{aligned}$$

which is, again using the orthogonality of the V function [formulas (19) and (20a) of reference 14],

$$\begin{aligned}\mathrm{Tr}^r(\mathbf{S}\nabla\mathbf{E}\cdot\nabla\mathbf{ES}) &= -(JK\|S\|J+1K)(J+1K\|S\|JK)\\ &\quad\times(J+1K\|\nabla E\|J+1K)^2(2J+3)^{-1}.\end{aligned}\tag{22}$$

In the same way,

$$\begin{aligned}\mathrm{Tr}^r(\nabla\mathbf{ES}\cdot\mathbf{S}\nabla\mathbf{E}) &= -(JK\|S\|J+1K)(J+1K\|S\|JK)\\ &\quad\times(JK\|\nabla E\|JK)^2(2J+1)^{-1}.\end{aligned}\tag{23}$$

In calculating the other terms of the formula (21), it is necessary to use the Racah formula:[14]

$$\begin{aligned}&\sum_{\alpha\beta\gamma\delta\varphi}(-1)^{f+\varphi}V(abc;\alpha\beta-\epsilon)V(acf;-\alpha\gamma\varphi)\\ &\quad\times V(bdf;-\beta\delta-\varphi)V(cdg;\gamma\delta-\eta)\\ &=(-1)^{e+\epsilon+f+d-b}W(abcd;ef)\delta(e,g)\delta(\epsilon,\eta)/(2e+1),\end{aligned}\tag{24}$$

where W is the function defined in the Racah paper.[14] The result of the calculation is

$$\begin{aligned}&\mathrm{Tr}^r(\nabla\mathbf{ES}\cdot\nabla\mathbf{ES})=\mathrm{Tr}^r(\mathbf{S}\nabla\mathbf{E}\cdot\mathbf{S}\nabla\mathbf{E})\\ &=-(JK\|S\|H+1K)(J+1K\|S\|JK)\\ &\quad\times(JK\|\nabla E\|JK)(J+1K\|\nabla E\|J+1K)\\ &\quad\times W(JJ+1JJ+1;12).\end{aligned}\tag{25}$$

Thus we obtain

$$\begin{aligned}&\mathrm{Tr}^r(\nabla\mathbf{ES}-\mathbf{S}\nabla\mathbf{E})^2=(JK\|S\|J+1K)\\ &\times(J+1K\|S\|JK)\{(JK\|\nabla E\|JK)^2(2J+1)^{-1}\\ &+(J+1K\|\nabla E\|J+1K)^2(2J+3)^{-1}\\ &-2(JK\|\nabla E\|JK)(J+1K\|\nabla E\|J+1K)\\ &\quad\times W(JJ+1JJ+1;12)\}.\end{aligned}\tag{26}$$

Quantities such as $(JK\|\nabla E\|JK)$ are obtained in the formulas (11) and (12), and W can be calculated by the Racah formula.[14] Thus we finally obtain

$$\begin{aligned}&\mathrm{Tr}^r(\nabla\mathbf{ES}-\mathbf{S}\nabla\mathbf{E})^2=(JK\|S\|J+1K)(J+1K\|S\|JK)\\ &\times\Big\{\frac{\{3K^2-J(J+1)\}^2}{4J(J+1)(2J-1)(2J+3)}\\ &+\frac{\{3K^2-(J+1)(J+2)\}^2}{4(J+1)(J+2)(2J+1)(2J+5)}\\ &-\frac{\{3K^2-J(J+1)\}\{3K^2-(J+1)(J+2)\}}{2(J+1)^2(2J+1)(2J+3)}\Big\}\left(\frac{\partial^2V}{\partial z^2}\right)^2,\\ &\equiv(JK\|S\|J+1K)(J+1K\|S\|JK)\\ &\quad\times F(J,K)(\partial^2V/\partial z^2)^2.\end{aligned}\tag{27}$$

By the formulas (18), (20), and (27) we obtain

$$\begin{aligned}\mathrm{Tr}(H\mathbf{S}-\mathbf{S}H)^2 &= \tfrac{1}{5}e^2Q^2(\partial^2V/\partial z^2)^2\{(2I+1)(I+1)\\ &\quad\times(2I+3)/4I(2I-1)\}(JK\|S\|J+1K)\\ &\quad\times(J+1K\|S\|JK)F(J,K).\end{aligned}\tag{28}$$

Another quantity, $\mathrm{Tr}\mathbf{S}^2$, which is necessary to obtain the line-width formula, can be obtained easily by using the formula (15) and the orthogonality of the V function. The result is

$$\begin{aligned}\mathrm{Tr}\mathbf{S}^2=\mathrm{Tr}^s\,\mathrm{Tr}^r\mathbf{S}^2 &= -(2I+1)(JK\|S\|J+1K)\\ &\quad\times(J+1K\|S\|JK).\end{aligned}\tag{29}$$

Thus from the formulas (28), (29), and (1) we obtain the final formula for the transition $J,K\rightarrow J+1,K$:

$$h^2\langle\Delta\nu^2\rangle_{hw}=\tfrac{1}{5}e^2Q^2(\partial^2V/\partial z^2)^2Z(I)F(J,K),\tag{30}$$

where

$$Z(I)\equiv(I+1)(2I+3)/4I(2I-1),\tag{31}$$

and

$$\begin{aligned}F(J,K)=&\frac{\{3K^2-J(J+1)\}^2}{4J(J+1)(2J-1)(2J+3)}\\ &+\frac{\{3K^2-(J+1)(J+2)\}^2}{4(J+1)(J+2)(2J+1)(2J+5)}\\ &-\frac{\{3K^2-J(J+1)\}\{3K^2-(J+1)(J+2)\}}{2(J+1)^2(2J+1)(2J+3)}.\end{aligned}\tag{32}$$

When J is very large, it can be approximated by

$$F(J,K)\sim\tfrac{3}{16}(21K^4J^{-6}-6K^2J^{-4}+J^{-2}).\tag{32'}$$

The numerical value of the I-dependent part of the formula (30) is given in the last column of Table II. From the fact that $\mathrm{Tr}^s\mathbf{Q}=0$, we can quite easily show that $h\langle\Delta\nu\rangle_{hw}=0$; thus the nuclear quadrupole moment does not change the mean frequency.

III. SYMMETRIC TOP MOLECULE WITH THREE IDENTICAL NUCLEI WHICH HAVE QUADRUPOLE MOMENTS

There are many molecules which belong to this group and whose hfs are not yet analyzed or resolved. Some of their quadrupole coupling constants are obtained from the pure quadrupole absorption in the solid state.[16] Thus, if we can obtain the corresponding values in the gas state, we shall be able to obtain some information on how the nature of the chemical bond changes from state to state. It has been pointed out[2] that the coupling constant is determined by the nature of the chemical bond in which the nucleus under consideration partakes, and the direct effect of the other part of the molecule is very small. Thus the coupling constants in $CHCl_3$ and CH_3Cl, for example, may be assumed to be about the same. Actually this was found to be the case in $CHBr_3$ and CH_3Br,[5] but at present this is the only case confirmed experimentally.

We can calculate the mean-square frequency deviation for this kind of molecule by the same procedure as followed in the last section.

The nuclear quadrupole coupling energy is

$$V_Q=\mathbf{Q}_1\cdot\nabla\mathbf{E}_1+\mathbf{Q}_2\cdot\nabla\mathbf{E}_2+\mathbf{Q}_3\cdot\nabla\mathbf{E}_3, \tag{33}$$

instead of the formula (7) or (14). In this case we had better consider the matrix element explicitly from the beginning. If the JK, JK' matrix element is denoted by a superscript K, K', then

$$H^{K,K'}=\mathbf{Q}_1\cdot\nabla\mathbf{E}_1^{K,K'}+\mathbf{Q}_2\cdot\nabla\mathbf{E}_2^{K,K'}+\mathbf{Q}_3\cdot\nabla\mathbf{E}_3^{K,K'}. \tag{34}$$

It can be seen from the relative position of each nucleus that the relation

$$\begin{aligned}\nabla\mathbf{E}_1^{K,K'}&=e^{(2\pi i/3)(K-K')}\nabla\mathbf{E}_2^{K,K'}\\&=e^{(4\pi i/3)(K-K')}\nabla\mathbf{E}_3^{K,K'}\equiv\nabla\mathbf{E}^{K,K'}\end{aligned} \tag{35}$$

holds. Thus

$$\begin{aligned}H^{K,K'}=(\mathbf{Q}_1&+e^{(2\pi i/3)(K'-K)}\mathbf{Q}_2\\&+e^{(4\pi i/3)(K'-K)}\mathbf{Q}_3)\cdot\nabla\mathbf{E}^{K,K'}.\end{aligned} \tag{36}$$

If we define

$$\mathbf{Q}^{K,K'}=\mathbf{Q}_1+e^{(2\pi i/3)(K'-K)}\mathbf{Q}_2+e^{(4\pi i/3)(K'-K)}\mathbf{Q}_3, \tag{37}$$

we can write

$$H^{K,K'}=\mathbf{Q}^{K,K'}\cdot\nabla\mathbf{E}^{K,K'}, \tag{38}$$

which is the same expression as (14).

It must be remarked that the matrix element (13), which was zero in the previous case, is not zero in the present case. Actually, if we assume that the charge distribution is cylindrical around the chemical bond under consideration it can be shown that

$$\partial^2V/\partial z^2=\tfrac{1}{2}(3\cos^2\theta-1)(\partial^2V/\partial a^2), \tag{39}$$

$$\partial^2V/\partial x^2-\partial^2V/\partial y^2=\tfrac{3}{2}\sin^2\theta(\partial^2V/\partial a^2), \tag{40}$$

[16] R. Livingston, J. Chem. Phys. 19, 1434 (1951).

TABLE I. Symmetry of the spin function.

Vibrational state	$K=3m$	$K=3m\pm1$
A_1	A_1+A_2	E
A_2	A_1+A_2	E
E	$2E$	A_1+A_2+E

where a is the coordinate parallel to the chemical bond, and θ is the angle between this a axis and the z axis which is the symmetry axis of the molecule. Thus in this section we must consider the $K=1$, $K'=-1$ matrix element in addition to the $K'=K$ case. We shall consider the $K=1$ and $K\neq1$ cases separately.

a. $K\neq1$

Since in this cese only $K'=K$ is to be considered, the superscript in the formula (37) is not necessary if we define

$$\mathbf{Q}=\mathbf{Q}_1+\mathbf{Q}_2+\mathbf{Q}_3. \tag{41}$$

By the same procedure as in Sec. II, we obtain the same formula as (18) with this definition. However, in calculating

$$\mathrm{Tr}^s\mathbf{Q}\cdot\mathbf{Q}=\sum_i\mathrm{Tr}^s\mathbf{Q}_i\cdot\mathbf{Q}_i+2\sum_{i>j}\mathrm{Tr}^s\mathbf{Q}_i\cdot\mathbf{Q}_j, \tag{42}$$

the Pauli principle must be taken into account.

The permutation group of three particles $\mathfrak{S}_3$ has three representations, A_1, A_2, and E, where A_1 is the symmetric, A_2 is the antisymmetric, and E is the two-dimensional representation. According to Dennison,[17] the rotational wave function with $K=3m$ (m being an integer) belongs to A_1+A_2, and when $K=3m\pm1$ it belongs to E. Since the Pauli principle requires that the total wave function must belong to the A_1 representation when I is an integer, and that it must belong to the A_2 representation when I is a half-integer, the symmetry of the spin function of each rotational vibrational state is fixed as in Table I.[4]

The number of spin functions which belong to each representation is given by Dennison[17] as

$$\begin{aligned}&A_1\cdots\tfrac{1}{3}(2I+1)(I+1)(2I+3),\\&A_2\cdots\tfrac{1}{3}(2I+1)I(2I-1),\\&E\cdots(8/3)(2I+1)I(I+1).\end{aligned} \tag{43}$$

If all the spin functions were allowed, we would obtain from the formula (19):

$$\mathrm{Tr}^s\mathbf{Q}_i\cdot\mathbf{Q}_i=(2I+1)^2(I\|Q\|I)^2. \tag{44}$$

If the symmetry is restricted, the above quantity will be divided in proportion to the number shown in (43) as

$$\mathrm{Tr}^s(A_1)\mathbf{Q}_i\cdot\mathbf{Q}_i=\tfrac{1}{3}(I+1)(2I+3)(I\|Q\|I)^2, \tag{45a}$$

$$\mathrm{Tr}^s(A_2)\mathbf{Q}_i\cdot\mathbf{Q}_i=\tfrac{1}{3}I(2I-1)(I\|Q\|I)^2, \tag{45b}$$

$$\mathrm{Tr}^s(E)\mathbf{Q}_i\cdot\mathbf{Q}_i=(8/3)I(I+1)(I\|Q\|I)^2. \tag{45c}$$

[17] D. M. Dennison, Revs. Modern Phys. 3, 280 (1931).

By the discussion shown in the Appendix one can see that

$$\mathrm{Tr}^{\nu}(A_1)\mathbf{Q}_i\cdot\mathbf{Q}_j=\tfrac{1}{6}(2I+3)(I\|Q\|I)^2, \quad (46a)$$

$$\mathrm{Tr}^{\nu}(A_2)\mathbf{Q}_i\cdot\mathbf{Q}_j=-\tfrac{1}{6}(2I-1)(I\|Q\|I)^2, \quad (46b)$$

$$\mathrm{Tr}^{\nu}(E)\mathbf{Q}_i\cdot\mathbf{Q}_j=-\tfrac{2}{3}(I\|Q\|I)^2, \quad (46c)$$

where $i\neq j$. Thus we obtain from the formulas (42), (45), and (46):

$$\mathrm{Tr}^{\nu}(A_1)\mathbf{Q}\cdot\mathbf{Q}=(I+2)(2I+3)(I\|Q\|I)^2, \quad (47a)$$

$$\mathrm{Tr}^{\nu}(A_2)\mathbf{Q}\cdot\mathbf{Q}=(I-1)(2I-1)(I\|Q\|I)^2, \quad (47b)$$

$$\mathrm{Tr}^{\nu}(E)\mathbf{Q}\cdot\mathbf{Q}=\{8I(I+1)-4\}(I\|Q\|I)^2. \quad (47c)$$

Since $\mathrm{Tr}^{r}(\boldsymbol{\nabla}\mathbf{E}\mathbf{S}-\mathbf{S}\boldsymbol{\nabla}\mathbf{E})^2$ has exactly the same value as before [formula (27)], we obtain

$$\mathrm{Tr}(H\mathbf{S}-\mathbf{S}H)^2=\tfrac{1}{3}e^2Q^2(\partial V^2/\partial z^2)^2X(I)(JK\|S\|J+1K)\times(J+1K\|S\|JK)F(J,K), \quad (48)$$

where

$$X(I)=(2I+1)(I+2)(2I+3)^2(I+2)/4I(2I-1)$$ for the A_1 spin state, (49a)

$$=(2I+1)(2I+2)(2I+3)(I-1)/4I$$ for the A_2 spin state, (49b)

$$=(2I+1)(2I+2)(2I+3)\{2I(I+1)-1\}/I(2I-1)$$ for the E spin state. (49c)

In calculating $\mathrm{Tr}\mathbf{S}^2=\mathrm{Tr}^{\nu}\,\mathrm{Tr}^{r}\mathbf{S}^2$, the symmetry requirement again appears. In this case Tr^{ν} means the number shown in formula (43). $\mathrm{Tr}^{r}\mathbf{S}^2$ is again

$$-(JK\|S\|J+1K)(J+1K\|S\|JK).$$

From Table I we see the final results can be given for three cases: the cases where the spin function is A_1+A_2, E, and A_1+A_2+E, respectively. Thus

$$h^2\langle\Delta\nu^2\rangle=\tfrac{1}{3}e^2Q^2(\partial^2V/\partial z^2)^2Y(I)F(J,K), \quad (50)$$

where

$$Y(I)=\{\tfrac{2}{3}(I+1)(2I+3)/I(2I-1)\}\times\{(I+2)(2I+3)+(I-1)(2I-1)\}\times\{(I+1)(2I+3)+I(2I-1)\}^{-1}\equiv Y(I)_a,$$ for the A_1 or A_2 vibrational state with $K=3m$. (51a)

$$=\tfrac{2}{3}(2I+3)(2I^2+2I-1)/I^2(2I-1)\equiv Y(I)_b,$$ for the E vibrational state with $K=3m$, or the A_1 or A_2 vibrational state with $K=3m\pm1$. (51b)

$$=\tfrac{2}{3}\{(I+1)(2I+3)(8I^2+8I+5)/I(2I-1)(8I^2+8I+3)\}\equiv Y(I)_c,$$ for the E vibrational state with $K=3m\pm1$. (51c)

$F(J,K)$ is given by the formulas (31) and (32). Sometimes the formula (39) for $\partial^2V/\partial z^2$ will be useful. The numerical values of the function $Y(I)$ are shown in Table II.

b. $|K|=1$

It can be seen from the formulas (11), (13), and (40) that when $|K|=1$, the matrix element between the K and $-K$ states does not vanish and this gives us a new kind of terms. In this case,

$$\mathrm{Tr}(H\mathbf{S}-\mathbf{S}H)^2=\sum_{K'=\pm K}\mathrm{Tr}(H^{K,K'}\mathbf{S}-\mathbf{S}H^{K,K'})\times(H^{K',K}\mathbf{S}-\mathbf{S}H^{K',K}), \quad (52)$$

where the superscripts K, K' indicate the matrix element. Since the term with $K'=K$ is given by the formula (48), we have only to calculate the term with $K'=-K=1$. In this case the formula (38) is

$$H^{1,-1}=\mathbf{Q}^{1,-1}\cdot\boldsymbol{\nabla}\mathbf{E}^{1,-1}, \quad (53)$$

and $\mathbf{Q}^{1,-1}$ is, from the formula (37),

$$\mathbf{Q}^{1,-1}=\mathbf{Q}_1+e^{(2\pi i/3)}\mathbf{Q}_2+e^{(4\pi i/3)}\mathbf{Q}_3, \quad (54)$$

which gives

$$\mathbf{Q}^{1,-1}\cdot\mathbf{Q}^{-1,1}=\sum_i\mathbf{Q}_i\cdot\mathbf{Q}_i-\sum_{i>j}\mathbf{Q}_i\cdot\mathbf{Q}_j. \quad (55)$$

Thus from the formulas (45), (46), and (55) we obtain

$$\mathrm{Tr}^{\nu}(A_1)\mathbf{Q}^{1,-1}\cdot\mathbf{Q}^{-1,1}=(I+\tfrac{1}{2})(2I+3)(I\|Q\|I)^2, \quad (56a)$$

$$\mathrm{Tr}^{\nu}(A_2)\mathbf{Q}^{1,-1}\cdot\mathbf{Q}^{-1,1}=(I+\tfrac{1}{2})(2I-1)(I\|Q\|I)^2, \quad (56b)$$

$$\mathrm{Tr}^{\nu}(E)\mathbf{Q}^{1,-1}\cdot\mathbf{Q}^{-1,1}=\{8I(I+1)+2\}(I\|Q\|I)^2, \quad (56c)$$

which correspond to the formulas (47a), (47b), and (47c), respectively. The $\mathrm{Tr}^{r}(\boldsymbol{\nabla}\mathbf{E}\mathbf{S}-\mathbf{S}\boldsymbol{\nabla}\mathbf{E})^2$ part will be by

$$\mathrm{Tr}^{r}(\boldsymbol{\nabla}\mathbf{E}\mathbf{S}-\mathbf{S}\boldsymbol{\nabla}\mathbf{E})^2=\mathrm{Tr}^{r}(\boldsymbol{\nabla}\mathbf{E}^{1,-1}\mathbf{S}\cdot\boldsymbol{\nabla}\mathbf{E}^{-1,1}\mathbf{S})+\mathrm{Tr}^{r}(\mathbf{S}\boldsymbol{\nabla}\mathbf{E}^{1,-1}\cdot\mathbf{S}\boldsymbol{\nabla}\mathbf{E}^{-1,1})-\mathrm{Tr}^{r}(\boldsymbol{\nabla}\mathbf{E}^{1,-1}\mathbf{S}\cdot\mathbf{S}\boldsymbol{\nabla}\mathbf{E}^{-1,1})-\mathrm{Tr}^{r}(\mathbf{S}\boldsymbol{\nabla}\mathbf{E}^{1,-1}\cdot\boldsymbol{\nabla}\mathbf{E}^{-1,1}\mathbf{S}). \quad (57)$$

By the same procedure as in Sec. II, we obtain

$$\mathrm{Tr}^{r}(\boldsymbol{\nabla}\mathbf{E}\mathbf{S}-\mathbf{S}\boldsymbol{\nabla}\mathbf{E})^2=(J1\|S\|J+11)(J+11\|S\|J1)\times[(J1\|\nabla E\|J-1)(J-1\|\nabla E\|J1)(2J+1)^{-1}+(J+11\|\nabla E\|J+1-1)(J+1-1\|\nabla E\|J+11)\times(2J+3)^{-1}-\{(J1\|\boldsymbol{\nabla}E\boldsymbol{\nabla}J-1)\times(J+1-1\|\nabla E\|J+11)+(J+11\|\nabla E\|J+1-1)\times(J-1\|\nabla E\|J1)\}W(JJ+1JJ+1;12)]. \quad (58)$$

We obtain from the formulas (11) and (13) that

$$(J1\|\nabla E\|J-1)=(J-1\|\nabla E\|J1)=-\tfrac{1}{2}\{J/2(2J+3)\}^{\frac{1}{2}}\times(\partial^2V/\partial x^2-\partial^2V/\partial y^2)/V(JJ2;-JJ0)=-\tfrac{1}{4}\{J(2J+1)(J+1)/(2J-1)(2J+3)\}^{\frac{1}{2}}\times(\partial^2V/\partial x^2-\partial^2V/\partial y^2), \quad (59)$$

from which the formula

$$\mathrm{Tr}^r(\nabla\mathbf{E}\mathbf{S}-\mathbf{S}\nabla\mathbf{E})^2=(J1\|S\|J+11)(J+11\|S\|J1)\times(\partial^2V/\partial x^2-\partial^2V/\partial y^2)^2\frac{1}{16}\left\{\frac{J(J+1)}{(2J-1)(2J+3)}+\frac{(J+1)(J+2)}{(2J+1)(2J+5)}-\frac{2J(J+1)}{(2J+1)(2J+3)}\right\} \quad (60)$$

is obtained. Since $\mathrm{Tr}\mathbf{S}^2$ has the same value as before, we finally obtain the contribution from the $K'=-K$ matrix elements as

$$\hbar^2\langle\Delta\nu^2\rangle=\tfrac{1}{5}e^2Q^2(\partial^2V/\partial x^2-\partial^2V/\partial y^2)^2Y''(I)F'(J), \quad (61)$$

where

$$F'(J)=\frac{1}{16}\left\{\frac{J(J+1)}{(2J-1)(2J+3)}+\frac{(J+1)(J+2)}{(2J+1)(2J+5)}-\frac{2J(J+2)}{(2J+1)(2J+3)}\right\}. \quad (62)$$

When $J\to\infty$, it is

$$F'(J)\sim 3/(64J^2). \quad (63)$$

The mean-square frequency deviation for the case $|K|=1$ is obtained by adding the formulas (5) and (61); that is,

$$|K|=1$$

$$\hbar^2\langle\Delta\nu^2\rangle=\tfrac{1}{5}e^2Q^2\{Y(I)(\partial^2V/\partial z^2)^2F(J,1)+Y'(I)(\partial^2V/\partial x^2-\partial^2V/\partial y^2)^2F'(J)\}, \quad (64)$$

where $Y(I)$ is given by the formulas (51b) and (51c), $F(J,1)$ is given by the formulas (31) and (32) by putting $K=1$, and $F'(J)$ is given by the formulas (62) and (63). Also the formulas (39) and (40) may be useful in some cases.

TABLE II. $Y(I)$ and $Z(I)$.

I	$Y(I)_a$	$Y(I)_b$	$Y(I)_c$	$Z(I)$
1	7.16	5.625	7.89	2.5
3/2	3.69	3.25	3.86	1.25
2	2.61	2.41	2.68	0.875
5/2	1.31	1.4	2.13	0.7

IV. EFFECT OF OTHER KINDS OF NUCLEI WHICH HAVE QUADRUPOLE MOMENT

Sometimes there are more than one kind of nuclei which have quadrupole moments within a molecule. This will make the hfs very complicated, and, especially when the value of the coupling constant is about the same, the analysis is very difficult. Let us assume that there are two nuclei which have quadrupole moments; then the Hamiltonian is

$$H=\mathbf{Q}_1\cdot\nabla\mathbf{E}_1+\mathbf{Q}_2\cdot\nabla\mathbf{E}_2. \quad (65)$$

In this case,

$$\begin{aligned}\mathrm{Tr}(H\mathbf{S}-\mathbf{S}H)^2&=\mathrm{Tr}\{(\mathbf{Q}_1\cdot\nabla\mathbf{E}_1\mathbf{S}-\mathbf{S}\mathbf{Q}_1\cdot\nabla\mathbf{E}_1)+(\mathbf{Q}_2\cdot\nabla\mathbf{E}_2\mathbf{S}-\mathbf{S}\mathbf{Q}_2\cdot\nabla\mathbf{E}_2)\}^2\\&=\mathrm{Tr}(\mathbf{Q}_1\cdot\nabla\mathbf{E}_1\mathbf{S}-\mathbf{S}\mathbf{Q}_1\cdot\nabla\mathbf{E}_1)^2+\mathrm{Tr}(\mathbf{Q}_2\cdot\nabla\mathbf{E}_2\mathbf{S}-\mathbf{S}\mathbf{Q}_2\cdot\nabla\mathbf{E}_2)^2\\&\quad+2\,\mathrm{Tr}(\mathbf{Q}_1\cdot\nabla\mathbf{E}_1\mathbf{S}-\mathbf{S}\mathbf{Q}_1\cdot\nabla\mathbf{E}_1)\times(\mathbf{Q}_2\cdot\nabla\mathbf{E}_2\mathbf{S}-\mathbf{S}\mathbf{Q}_2\cdot\nabla\mathbf{E}_2)\\&=\tfrac{1}{5}\{\mathrm{Tr}^s\mathbf{Q}_1\cdot\mathbf{Q}_1\,\mathrm{Tr}^r(\nabla\mathbf{E}_1\mathbf{S}-\mathbf{S}\nabla\mathbf{E}_1)+\mathrm{Tr}^s\mathbf{Q}_2\cdot\mathbf{Q}_2\,\mathrm{Tr}^r(\nabla\mathbf{E}_2\mathbf{S}-\mathbf{S}\nabla\mathbf{E}_2)\\&\quad+2\,\mathrm{Tr}^s\mathbf{Q}_1\cdot\mathbf{Q}_2\,\mathrm{Tr}^r(\nabla\mathbf{E}_1\mathbf{S}-\mathbf{S}\nabla\mathbf{E}_1)\times(\nabla\mathbf{E}_2\mathbf{S}-\mathbf{S}\nabla\mathbf{E}_2)\}. \quad (66)\end{aligned}$$

If two nuclei under consideration are different, then since there are no symmetry requirements, apparently $\mathrm{Tr}^s\mathbf{Q}_1\mathbf{Q}_2=0$. Thus one can easily show that the total mean-square frequency deviation is simply the sum of the mean-square deviations due to each nucleus which is given by the formula (30). The additivity also holds when a different nucleus is added to a group of identical nuclei.

Thus if we know the coupling constant of one nucleus, we can easily obtain the value for the other nucleus.

V. WIDTH DUE TO PRESSURE BROADENING AND CENTRIFUGAL STRETCHING

The width $(\langle\Delta\nu^2\rangle)^{\frac{1}{2}}$ due to the quadrupole moment is of the order of $|eQ\partial^2V/\partial z^2|$, as can be seen from the formulas (30), (50), and (61). This quadrupole coupling constant has a value from about 5 Mc/sec to 600 Mc/sec depending on nuclei and molecules. The width due to the pressure broadening, on the other hand, has the value from about 5 Mc/sec per mm Hg to 50 Mc/sec per mm Hg. Since experiments can be done under pressure much lower than 1-mm Hg, the pressure broadening must be usually smaller than the width due to the nuclear quadrupole moment. Even if the pressure broadening is large, we can separate it easily if the line shape due to the pressure broadening is the Lorentz type or symmetric on a frequency scale. In this case we can easily prove that

$$\langle\Delta\nu^2\rangle_{\text{total}}=\langle\Delta\nu^2\rangle_{\text{hfs}}+\langle\Delta\nu^2\rangle_{\text{pressure}}. \quad (67)$$

Since, as is well known, $\langle\Delta\nu^2\rangle_{\text{pressure}}$ is proportional to the second power of pressure, while $\langle\Delta\nu^2\rangle_{\text{hfs}}$ does not depend on pressure, we can separate them easily by measuring the pressure dependence of $\langle\Delta\nu^2\rangle_{\text{total}}$.

In most of the heavy molecules which have been measured, the fine structure due to the centrifugal deformation was not resolved. If the rotational energy levels can be expressed by the formula

$$F=BJ(J+1)+(A-B)K^2-DJ^2(J+1)^2 -D_{JK}J(J+1)K^2-D_KK^4, \quad (68)$$

the frequency of J, $K\rightarrow J+1$, K line is

$$h\nu=2B(J+1)-2D_{JK}(J+1)K^2. \quad (69)$$

Thus, if D_{JK} which gives the K dependence of the moment of inertia is not zero, each $K\rightarrow K$ line must have a slightly different frequency. Since the intensity of the $K\rightarrow K$ transition is proportional to $(J+1)^2-K^2$, the mean of the above frequency over K is

$$h\langle\nu\rangle=2B(J+1)-\tfrac{2}{3}D_{JK}J(J+1)(J+2). \quad (70)$$

The frequency deviation of each line from the above mean value is

$$h\Delta\nu=\tfrac{2}{3}D_{JK}(J+1)\{J(J+2)-5K^2\}. \quad (71)$$

Thus the mean-square deviation is

$$h^2\langle\Delta\nu^2\rangle=(8/175)D_{JK}{}^2J(J+1)^2(J+2) \times(2J-1)(2J+5), \quad (72)$$

which will tend to

$$h^2\langle\Delta\nu^2\rangle\sim(32/175)D_{JK}{}^2J^6 \quad (73)$$

when $J\rightarrow\infty$. This formula gives the width due to the centrifugal deformation.

Since the mean frequency deviation of the hfs is zero, the total mean-square frequency deviation is the sum of those of the hfs and the K semidegeneracy.

$$h^2\langle\Delta\nu^2\rangle_{\text{total}}=h^2\langle\Delta\nu^2\rangle_K+h^2\langle\Delta\nu^2\rangle_{\text{hfs}}, \quad (74)$$

where $h^2\langle\Delta\nu^2\rangle_K$ is given by the formula (72) or (73). The quantity $h^2\langle\Delta\nu^2\rangle_{\text{hfs}}$ is given as follows (for large J): one-nucleus case,

$$h^2\langle\Delta\nu^2\rangle_{\text{hfs}}=(3/25)e^2Q^2(\partial^2V/\partial z^2)^2Z(I)J^{-2}; \quad (75)$$

three-nucleus case,

$$h^2\langle\Delta\nu^2\rangle_{\text{hfs}}=(9/25)e^2Q^2(\partial^2V/\partial z^2)^2Z(I)J^{-2}, \quad (76)$$

where $Z(I)$ is defined in the formula (31). The numerical values of $Z(I)$ are listed in Table II for some cases. The contribution from the $K=1$ state is neglected. In these formulas $F(J,K)$ was averaged over K, and gave $3/(10J^2)$.

Since the first term in the formula (74) is proportional to J^6 while the second term is proportional to J^{-2}, we can easily separate these terms by observing the J dependence of $h^2\langle\Delta\nu^2\rangle$.

APPENDIX I. $\mathrm{Tr}^s\mathbf{Q}_i\cdot\mathbf{Q}_j$

If there is no symmetry requirement, evidently

$$\mathrm{Tr}^s\mathbf{Q}_i\cdot\mathbf{Q}_j=0, \quad (78)$$

but if we adopt a spin function which has a definite symmetry in permutation then this quantity will have a finite value, which gives a certain correlation between different nuclei.

We can divide the whole spin functions into two groups: symmetric and antisymmetric functions in exchanging i and j nuclei. (Let us ignore the third nucleus for a while.) The symmetric function has forms, $\Psi(M_I,M_I)$ and $[\Psi(M_I,M_I)+\Psi(M_I,M_I)]$, while the antisymmetric function has a form

$$[\Psi(M_I,M_I)-\Psi(M_I,M_I)].$$

The trace over symmetric functions is

$$\mathrm{Tr}^s{}_+\mathbf{Q}_a\cdot\mathbf{Q}_b=\sum_{M_I}(M_IM_I|\mathbf{Q}_a\cdot\mathbf{Q}_b|M_IM_I) +\sum_{M_I>M_I'}\{(M_IM_I'|\mathbf{Q}_a\cdot\mathbf{Q}_b|M_IM_I')\}$$
$$=\tfrac{1}{2}\sum_{M_I,M_I'}\{(M_I|\mathbf{Q}_a|M_I)(M_I'|\mathbf{Q}_b|M_I') +(M_I|\mathbf{Q}_a|M_I')(M_I'|\mathbf{Q}_b|M_I)\}. \quad (79)$$

Since

$$\sum_{M_I}(M_I|\mathbf{Q}_a|M_I)=0, \quad (80)$$

$$\sum_{M_I,M_I}(M_I|\mathbf{Q}_a|M_I)(M_I|\mathbf{Q}_b|M_I)=(I\|\mathbf{Q}\|I)^2, \quad (81)$$

we obtain

$$\mathrm{Tr}^s{}_+\mathbf{Q}_a\cdot\mathbf{Q}_b=\tfrac{1}{2}(I\|Q\|I)^2. \quad (82)$$

In the same way, the trace over antisymmetric functions is

$$\mathrm{Tr}^s{}_-\mathbf{Q}_a\cdot\mathbf{Q}_b=-\tfrac{1}{2}(I\|Q\|I)^2. \quad (83)$$

The number of symmetric functions considered above is $(2I+1)(I+1)$; thus the trace over all functions which belongs to the A_1 representation of $\mathfrak{S}_3$ is

$$\mathrm{Tr}^s(A_1)\mathbf{Q}_a\cdot\mathbf{Q}_b=\tfrac{1}{6}(2I+3)(I\|Q\|I)^2, \quad (84)$$

since there are $\frac{1}{3}(2I+1)(I+1)(2I+3)A_1$ functions. In the same way we obtain

$$\mathrm{Tr}^s(A_2)\mathbf{Q}_a\cdot\mathbf{Q}_b=-\tfrac{1}{6}(2I-1)(I\|Q\|I)^2. \quad (84)$$

Since the trace over all functions must be given by the formula (78), we obtain

$$\mathrm{Tr}^s(E)\mathbf{Q}_a\cdot\mathbf{Q}_b=-\tfrac{2}{3}(I\|Q\|I)^2. \quad (85)$$

The Band Fluorescence of Mercury Vapor*

A. O. McCoubrey
University of Pittsburgh, Pittsburgh, Pennsylvania, and Westinghouse Research Laboratories, East Pittsburgh, Pennsylvania
(Received December 3, 1953)

The band fluorescence of mercury vapor excited by the 2537A atomic line has been studied during the afterglow. Time sampling techniques were employed to overcome difficulties attending the measurement of very low-intensity radiations. The two main band constituents (centered at 4850A and 3350A) were found to decay simultaneously under all conditions investigated. The temporal structure of the decaying fluorescence was found to be characterized by two time constants and has the form associated with chain types reactions. The two time constants and the relative intensities of the 4850A and 3350A bands were measured for a range of vapor densities at a fixed vapor temperature. In order to evaluate the role of diffusion in the lifetime of the excited particles involved, measurements were made in vessels of two different sizes.

The experimental results have led to an interpretation according to which the optically excited $Hg(^3P_1)$ atoms are converted into metastable $Hg(^3P_0)$ atoms by inelastic collisions. The $Hg(^3P_0)$ atoms are then converted in a three-body collision reaction to metastable $Hg_2(^3O_u^-)$ molecules which, in turn, may be destroyed in the vapor by either one of two processes, i.e., by spontaneous radiation to the ground state, giving rise to the 3350A band, or by a second three-body collision through which the emission of the 4850A band is induced. An analysis based upon this picture has permitted the quantitative evaluation of several properties of the particles involved. The diffusion coefficient of the $Hg(^3P_0)$ atom was found to be 210 cm²/sec for a density of 10^{16} atoms/cc and a temperature of 200°C; the diffusion coefficient of the $Hg_2(^3O_u^-)$ molecules is 88 cm²/sec under the same conditions. The spontaneous radiation rate of the $Hg_2(^3O_u^-)$ molecules is 20 sec^{-1} and the three-body collision induced radiation rate is 21×10^{-32} $(atoms/cc)^{-2}$ sec^{-1}. The three-body destruction rate for the $Hg(^3P_0)$ atoms is 100×10^{-32} $(atoms/cc)^{-2}$ sec^{-1}. It was also found that the $Hg_2(^3O_u^-)$ molecules are approximately 90 percent reflected by the glass walls of the enclosure. The diffusion coefficient obtained for $Hg(^3P_0)$ atoms is in agreement with the results of other work and the three-body collision rates are comparable with those for similar processes investigated elsewhere.

I. INTRODUCTION

WHEN mercury vapor is excited by the 2537A resonance line it emits, in addition to imprisoned resonance radiation,[1] a continuous band spectrum whose intensity depends strongly upon the vapor density. This band fluorescence[2] consists of two main constituents, one in the visible region centered at 4850A, and the second in the near ultraviolet region centered at about 3350A. The spectral distribution of these bands is shown in Fig. 1. A third band of much less intensity and smaller spectral extent is associated with the fluorescence at a wavelength of 2650A. When the radiation exciting the vapor is extinguished, there is an afterglow during which the fluorescent bands persist for several milliseconds. Phillips[3] first discovered the persistence and Rayleigh[4] carried out a number of qualitative studies using a moving vapor stream technique. In this work Rayleigh estimated the persistence times and found some evidence for the simultaneous decay of the 3350A and the 4850A components.

FIG. 1. The band fluorescence of mercury vapor at a density of about 6×10^{15} atoms/cc. The line on the left is the 2537A exciting line; the center band extends from about 3000A to 3700A with maximum intensity at 3350A; the band on the right extends from 4000A to 5300A with maximum intensity at 4850A.

Rayleigh later found that the 4047A mercury line was absorbed[5] by the fluorescing vapor and the visible triplet, 4047A, 4358A, and 5461A was thereby excited (see Fig. 2). He therefore concluded that metastable $Hg(^3P_0)$ atoms were present in the fluorescing vapor. From the absorption of the 5461A line he found that metastable $Hg(^3P_2)$ atoms were also present at much smaller concentration.

Frank and Grotrian[6] first associated the continuous bands with excited levels of the Hg_2 molecule. In a recent interpretation of the mercury vapor fluorescence, due to Mrozowski,[7] the 4850A band was considered to arise by direct radiation from the $Hg_2(^3O_u^-)$ state.[8] While this molecular state is metastable, a small but finite transition probability is considered to be due to the gyroscopic effect of molecular rotation which spoils the quantization of electronic angular momentum parallel to the internuclear axis. On account of the metastability, it was presumed that the $Hg_2(^3O_u^-)$ state acts as the primary reservoir for the long-lived molecular excitation. The 3350A band was accounted for in terms of transitions from the $Hg_2(^3\Pi_u)$ state. This

* The research reported here was submitted to the Graduate School of the University of Pittsburgh in partial fulfillment of the requirements for the degree of Doctor of Philosophy. The work was performed at the Westinghouse Research Laboratories.

[1] T. Holstein, Phys. Rev. **72**, 1212 (1947).

[2] For a short survey and bibliography, see W. Finkelnburg, *Kontinuierliche Spektren* (Julius Springer, Berlin, 1938), Sec. 60.

[3] F. S. Phillips, Proc. Roy. Soc. (London) A89, 39 (1913).

[4] Lord Rayleigh, Proc. Roy. Soc. (London) A114, 620 (1927).

[5] Lord Rayleigh, Proc. Roy. Soc. (London) A137, 101 (1932).

[6] J. Frank and W. Grotrian, Z. Physik 4, 89 (1921).

[7] S. Mrozowski, Z. Physik 106, 458 (1937).

[8] The classification of the electronic states of diatomic molecules adopted here is described in G. Herzberg, *Spectra of Diatomic Molecules* (D. Van Nostrand Company, Inc., New York, 1950).

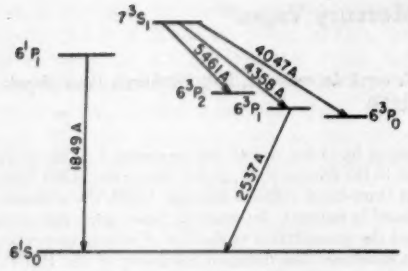

FIG. 2. The energy levels of mercury.

state is thought to have a lifetime of the order of 10^{-7} second. The persistence of the 3350A band was held to be due to a continual repopulation of the $Hg_2(^3\Pi_u)$ state from the lower-lying $Hg_2(^3\Sigma_u^-)$ reservoir as a result of inelastic collisions. Because of the short lifetime of the $Hg_2(^3\Pi_u)$ state, both bands were considered to decay with the population of $Hg_2(^3\Sigma_u^-)$. In this way the common persistence times of the 3350A band and the 4850A band were explained as required by the experiments of Rayleigh.

Recently, in this laboratory, the fluorescence of mercury vapor was observed in connection with experiments on the imprisonment of resonance radiation.[9] While the apparatus was not well suited to the study of fluorescence, several significant observations were made. It was confirmed that the 3350A band and the 4850A band decay together. At constant vapor temperature, the persistence time was found to decrease rapidly as vapor density increased. However, at constant vapor density the temperature had no observable effect on the persistence. It was also found that the intensity of the 4850A band relative to that of the 3350A band, $I(4850)/I(3350)$, increased with vapor density. This result is in agreement with a similar observation by Mrozowska.[10]

The experimental observations have shown the Mrozowski picture to be incorrect in several respects. In particular, it is of interest to note that the rate of transitions from the $Hg_2(^3\Sigma_u^-)$ reservoir to the $Hg_2(^3\Pi_u)$ state would be expected to increase with temperature with a consequent decrease in persistence time. As mentioned previously, such a decrease is not observed. Also, an increase in vapor density would be expected to increase the frequency of transitions from the $Hg_2(^3\Sigma_u^-)$ state to the $Hg_2(^3\Pi_u)$ state. As a result, $I(4850)/I(3550)$ should decrease with an increase in vapor density. The experiments reveal that the opposite occurs.

In order to lay the groundwork for a better theoretical explanation, an experimental program was undertaken to obtain quantitative information concerning the persistent band fluorescence of mercury vapor. The present paper describes these experiments and presents the results within the framework of new theoretical hypotheses.

[9] Holstein, Alpert, and McCoubrey, Phys. Rev. **76**, 1259 (1949).
[10] I. Mrozowska, Acta. Phys. Polonica **2**, 81 (1933).

II. EXPERIMENTAL METHOD

a. General Technique

In the experimental method, a vessel containing mercury vapor is irradiated with 2537A resonance radiation. After a time interval during which the concentration of imprisoned resonance radiation builds up in the vessel, the incident light is turned off. The afterglow contains not only the escaping resonance radiation, but also the continuous bands associated with the persistent fluorescence. Through the use of optical filters these different spectral components may be separated for individual study.

The detailed procedure may be understood with reference to the block diagram in Fig. 3. Radiation from a mercury discharge lamp is periodically interrupted by a rotating shutter. A monochromator selects the 2537A resonance line and focuses it on a cylindrical tube containing mercury. This vessel, the "fluorescence tube," is surrounded by a furnace which controls the temperature and pressure of the mercury vapor. The intensity of radiation emitted by the vapor in the fluorescence tube is measured by means of an electron-multiplier phototube. Optical filters are used in front of the phototube to separate the band fluorescence from imprisoned resonance radiation, and also to resolve the band spectrum. The intensity signal from the photomultiplier tube is indicated by a method to be discussed in detail in later paragraphs. The indicating circuits are synchronized to operate during the afterglow periods by a trigger voltage derived photoelectrically from the rotating shutter.

The fluorescence tubes were of cylindrical geometry having a length at least ten times the radius. The main body of the tube was made of Corning 7911 glass which is transparent to the ultraviolet radiation used for excitation. The lower end of the tube, which served as the reservoir for liquid mercury, included a graded seal terminating in Pyrex glass. This construction permitted the tubes to be prepared on a standard Pyrex vacuum system. Using techniques described in detail by Alpert,[11] the tubes were evacuated and filled with triply

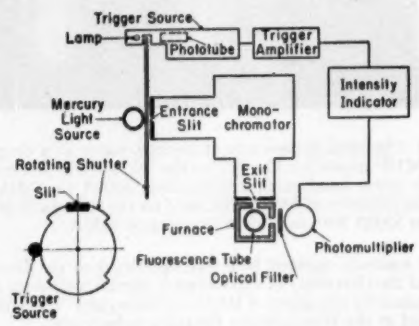

FIG. 3. The schematic diagram of the apparatus.

[11] D. Alpert, J. Appl. Phys. **24**, 860 (1953).

distilled mercury. At the time of sealoff the pressure of residual gases was never greater than 10^{-8} mm Hg.

Fluorescence tubes having two different sizes were prepared. The larger tube was 2.35 cm in radius and 25 cm long, and the smaller tube was 0.64 cm in radius and 14 cm long.

To accomodate the two fluorescence tube sizes, two furnaces of similar design were constructed. Figure 4 is a sketch showing the important details of the larger furnace. The furnace consisted of an upper and lower section, both of which were constructed of heavy copper cylinders. The heating element consisted of nichrome wires embedded in the walls of the cylinders with quartz tubing for electrical insulation. The heating elements in the two sections were supplied from independent current sources. Thus the pressure of mercury vapor in equilibrium with the liqiud was controlled by the temperature of the lower section, while the vapor temperature above was that of the upper furnace section. To prevent drafts of cool air from entering the furnace, quartz windows covered the openings in the upper section through which passed the incident exciting light and the emerging radiation. Temperatures were measured with thermocouples strapped to the glass as illustrated.

The optical filters used to resolve the fluorescent radiation were Corning 5840 for the 3350A band and Corning 3389 for the 4850A band. Data supplied by the manufacturer indicated that each filter allowed less than one percent of the rejected band to pass, while transmission of the 3350A band was about 50 percent and transmission of the 4850A band was about 85 percent.

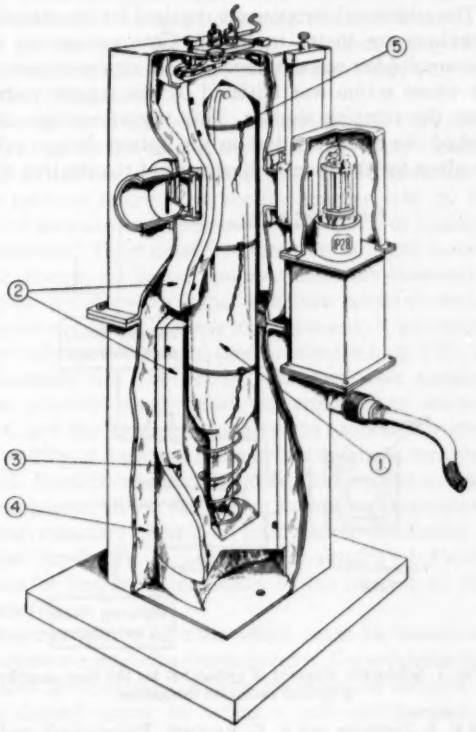

FIG. 4. The furnace and fluorescence tube details: 1. fluorescence tube; 2. copper heating units; 3. heating element; 4. thermal insulation; 5. thermocouple.

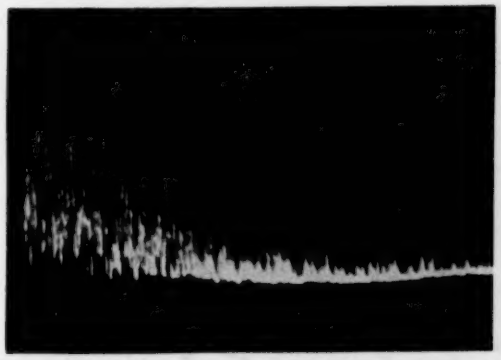

FIG. 5. An oscilloscope trace of a fluorescence decay cycle. The shot effect is due to the random arrival of optical quanta at the photomultiplier. The trace in this photo is about 30 milliseconds long.

b. Time Sampling Technique

In the preliminary experiments,[6] the intensity signals from the photomultiplier were indicated directly on an oscilloscope. Thus one observed a continuously decaying signal; a photograph of a typical trace is given in Fig. 5. While even these traces represented new data, they were obviously not suitable for good quantitative measurements. The very low optical intensities involved and the consequent statistical variations or "shot effect" made such a method inadequate for the observation of the fine structure in the decay. The limitations imposed by the statistics in the decaying radiation presented the outstanding experimental problem in the research. To meet this problem, a time sampling technique was devised in which the circumstance that a photomultiplier tube is sensitive only when proper voltages are applied to its electrodes is used to advantage.

The operation of the time sampling technique may be discussed with reference to Figs. 6A and 6B, in which the voltage applied to the photomultiplier is shown in its phase relationship to a hypothetical time varying light signal. In Fig. 6A, the photomultiplier supply voltage is gated on for a short fixed time interval, Δt, at a relative time $t=t_1$. The charge which flows from the photomultiplier tube under these conditions during one cycle is

$$q(t_1)=AG\int_{t_1-\frac{1}{2}\Delta t}^{t_1+\frac{1}{2}\Delta t} I(t)dt,$$

where A is the calibration factor which relates the instantaneous photocathode current to the instantan-

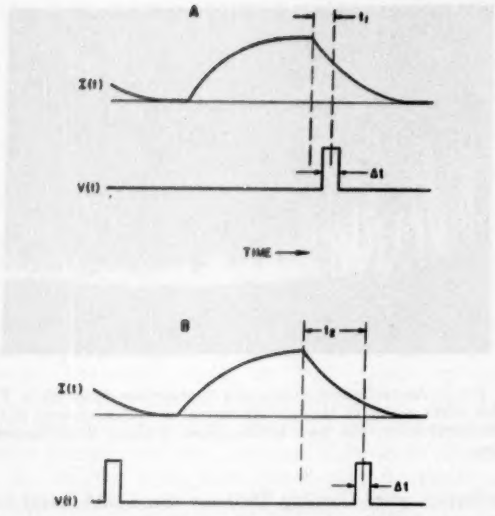

FIG. 6. Time sampling of light signal.

eous light intensity and G is the photomultiplier gain. The charge $q(t_1)$ is proportional to the average intensity during the time interval $(t_1-\frac{1}{2}\Delta t)<t<(t_1+\frac{1}{2}\Delta t)$, and for Δt sufficiently small this charge may be used as a measure of $I(t_1)$. As indicated in Fig. 6B, the intensity $I(t_2)$ at a relative time $t=t_2$, is obtained by relative displacement of the photomultiplier voltage gate. Thus, the time dependence of the radiation intensity may be obtained by a point by point procedure.

If the intensity $I(t)$ contains large random fluctuations, which is the case of interest here, it is necessary to collect a sufficient number of photomultiplier charge samples $q(t_1)$ to obtain an average over the fluctuations. This procedure amounts to taking intensity samples at a selected relative time t from a large number of intensity cycles which are identical in every respect except for the random fluctuations; the average sample value then yields the required experimental point. By this method, the average time dependence of an intensity variation may be obtained which contains fluctuations having a mean period large compared to the period of the intensity variation. If the mean intensity for a given relative time t is $\langle I(t)\rangle_{Av}$, the root-mean-square deviation expected in a series of charge measurements each of which requires S intensity cycles to obtain is $\delta=[A\langle I(t)\rangle_{Av}\Delta tS/e]^{\frac{1}{2}}$, and the fractional error in the information is

$$\delta/A\langle I(t)\rangle_{Av}\Delta tS=[A\langle I(t)\rangle_{Av}\Delta tS/e]^{-\frac{1}{2}},$$

where e is the electronic charge.

An example may serve to better establish the ideas above. Consider a case in which it is desired to measure the time dependence of a decay which extends over a time interval of ten milliseconds. To resolve the fine structure of such a decay, it might be necessary to use a photomultiplier gate interval $\Delta t=0.1$ millisecond. The limit of useful sensitivity of a photomultiplier tube depends upon its dark current which, for a selected RCA Type 1P28 photomultiplier operating at a gain of 10^6, may be 10^{-9} ampere. In the case of an easily measured instantaneous signal current of ten times this dark current, the instantaneous primary photoelectric current is about 5×10^4 electrons/second, or about five photoelectrons during one gate interval Δt. If these five electrons are regarded as a measure of the instantaneous intensity, the root mean square error will be about 45 percent. However, if the photoelectrons which are emitted during 1000 identical gate intervals are collected the rms error may be reduced almost to one percent. Since the quantum efficiency of the photosurface in the Type 1P28 phototube is about ten percent in the ultraviolet,[12] the optical radiation intensity considered in this example corresponds to about 50 quanta entering the photomultiplier during each gate interval Δt.

It should be pointed out that the preceding considerations neglect the statistics in the electron multiplication process in the phototube. This effect is due to the random fluctuations in the number of secondary electrons emitted from the phototube dynodes per incident primary electron. An estimate based upon an analysis by Shockley and Pierce[13] indicates that this source of noise is small compared to the "shot effect" considered above.

The additional components required for the sampling technique are shown in Fig. 7. Gate voltage for the photomultiplier was obtained from an electronic generator whose action was initiated by the trigger voltage from the rotating shutter. This trigger voltage established the reference time in the optical decay cycles. To allow for the rough adjustment of the relative time

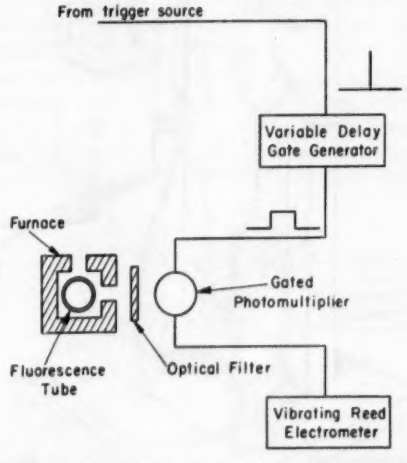

FIG. 7. Schematic diagram of apparatus for the time sampling of optical radiation intensities.

[12] V. K. Zworykin and E. G. Ramberg, *Photoelectricity and Its Application* (John Wiley and Sons, Inc., New York, 1949).
[13] W. Shockley and J. R. Pierce, Proc. Inst. Radio Engrs. **26**, 321 (1938).

of the trigger, the angular position of the trigger source was adjustable about the axis of the rotating shutter. In addition, the gate generator was equipped with a manual control by means of which the gate could be electrically delayed relative to the trigger for any period up to half of an optical cycle. The width of the gate voltage was adjustable from 0.05 to one millisecond. Charge samples from the photomultiplier tube were collected on a capacitor whose potential was measured by a vibrating reed electrometer.

The relative occurrence time of the photomultiplier gate was measured by observing its position relative to the beginning of the optical decay cycle with the aid of a cathode-ray synchroscope. The time axis of the synchroscope was continuously calibrated by means of an accurate time mark generator.

It may here be remarked that gating a photomultiplier is not only a convenient way to achieve time sampling, but it also provides a method for observing very weak optical signals immediately following intense phenomena. This technique is free of the saturation effects which render sensitive wideband electronic amplifiers inoperative for relatively long periods of time following intense signals. While these difficulties have been overcome by gating the amplifier or by other special techniques, it is usually more convenient to gate the photomultiplier. The time resolution available depends upon the speed of application and removal of the gate voltage. With modern pulse-generating techniques the method may be extended to study very fast optical phenomena.

One of the major sources of uncertainty in the experiment was in the determination of the vapor density. Vapor densities were obtained from the temperature of the mercury reservoir on the fluorescence tube by the use of saturated vapor pressure data given in Landolt-Börnstein.[14] These density values were adjusted to take into account the higher temperature in the observation region. To maintain vapor densities constant within ten percent during a decay measurement, it was necessary to keep the temperature constant within 2°C. To accomplish this the heating elements were supplied from a current source which was regulated to one percent, and the furnace was allowed to reach steady state by waiting at least two hours before making a measurement. Precautions were also taken to keep the exterior environment of the furnace at constant temperature. These measures served to limit the uncertainties in vapor density to 2½ percent at a density of 4×10^{16} atoms/cc and to a maximum of ten percent at 10^{16} atoms/cc.

Another source of error which must be considered concerns the intensity measurements. Uncertainties due to shot fluctuations could, in principle, be reduced to any desired extent by taking a sufficient number of intensity samples. However, limitations were encountered due to fluctuations in photomultiplier gain as a result of variations in gate pulse voltage and fluctuations in intensity of the 2537A source of excitation. It is felt that, due to all causes, uncertainties in intensity measurements amounted to no more than three percent.

[14] Landolt-Börnstein, *5 Auflage II* (Julius Springer, Berlin, 1923), p. 1334.

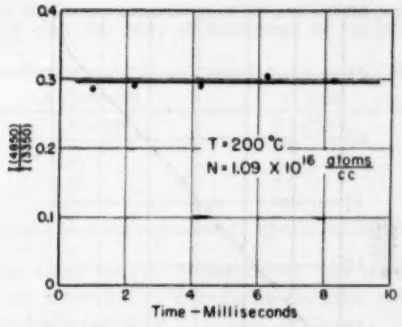

FIG. 8. The relative intensity of the visible and near ultraviolet bands in the afterglow. The curve demonstrates the simultaneous decay of the two bands.

III. RESULTS

The early experimental work indicated several aspects of the band fluorescence which required quantitative investigation. In the first place, it was of interest to check carefully the result that the radiation in the two principal bands decays simultaneously. Also, since early experiments had shown strong pressure effects, it seemed imperative to obtain quantitative data on the density variation of the band intensities as well as the persistence times. Finally, the long persistence times encountered in the mercury fluorescence suggested that diffusion might be an important feature. In order to make a thorough test of this possibility, the experiments were carried out in fluorescence tubes of two different sizes. Measurements were made with a vapor temperature of 200°C; as a result of this choice the vapor temperature remained in excess of the mercury condensation temperature over a wide range of densities.

The ratio of the intensity of the 4850A band to that of the 3350A band was measured at various times in the afterglow and for different vapor densities. For all mercury vapor densities investigated, i.e., for densities between 7×10^{15} atoms/cc and 5×10^{16} atoms/cc, this ratio was found to be constant with respect to time in the afterglow period. This particular result was also obtained for several vapor temperatures between 150°C and 200°C. A plot of measurements made for a density of 1.09×10^{16} atoms/cm³ and a temperature of 200°C is given in Fig. 8.

The variation with vapor density of the ratio, $I(4850)/I(3350)$, as measured during the afterglow is given in Fig. 9.

The intensity of fluorescent radiation as a function of time in the afterglow was measured using the large

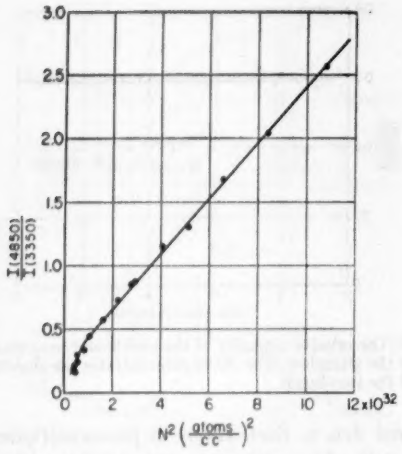

FIG. 9. The ratio of the band intensities as a function of the square of the vapor density.

(2.35-cm radius) tube. Since the intensity of the two bands had previously been found to decay simultaneously, the total radiation from the 3350A and the 4850A bands was included in these measurements. A Corning 7740 filter (Pyrex glass) was used to cut out the imprisoned resonance radiation escaping during the initial stages of the decay.

Figure 10 illustrates the data of a typical decay measurement taken with a photomultiplier sampling gate width of 100 μsec. As indicated, the curve consists of an initial relatively slow decay rate, going finally into a constant slope characteristic of the exponential form. It is found that the difference $\Delta I(t)$ between the final decay curve extrapolated to early time and the actual decay curve is also exponential in nature. These decay

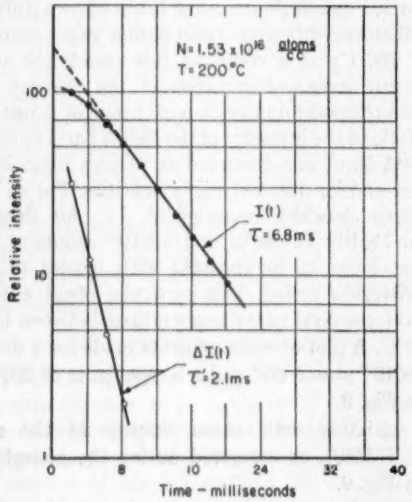

FIG. 10. The measured intensity $I(t)$ and difference intensity $\Delta I(t)$ in the afterglow of Hg_2 fluorescence.

curves, are therefore, characterized by an initial time constant τ_1' and a fina time constant τ_1 both of which depend upon the vapor density. Tables I and II give the values τ_1' and τ_1 measured at different densities for the constant vapor temperature of 200°C.

The effect of enclosure geometry on the rate of fluorescence decay was evaluated by comparing the rate of decay of radiation from the large tube with that emitted by the smaller tube (0.64-cm radius). Table III lists the values of the final time constant τ_2 for decays in the small tube. To facilitate a comparison of the observations, the same values of vapor temperature and density were used in both tubes. Typical data comparing the decays are plotted in Fig. 11. In the case of the small tube, the initial structure of the decay was too fast to measure accurately with the equipment designed for the longer decays.

IV. DISCUSSION

The more complete experimental information just described has made new theoretical considerations possible. Before discussing these in detail it is desirable to review some consequences of the experiments.

TABLE I. Density dependence of the final time constant τ_1 associated with the decay of fluorescence in the large tube. $T=200$°C.

M (atoms/cc)	τ_1 (sec)
1.17×10^{16}	7.2×10^{-3}
1.53	6.8
1.91	6.25
2.00	5.8
2.56	4.2
2.56	4.3
3.18	3.1
3.58	2.35
4.19	1.82

If the 4850A band and the 3350A band had their origins in different excited molecular reservoirs, the persistence of each band would depend upon the depopulation rate of its associated reservoir. The circumstance that the two bands decay simultaneously, therefore, suggests the hypothesis that there is a common persistent reservoir of molecular excitation which feeds both bands. Furthermore, the complex decays which are observed in the afterglow are characteristic of chain reactions involving "parent-daughter" processes. The fact that two exponential parameters are associated with the decay suggests two reservoirs of excitation, one feeding the other which, in turn, radiates the observed fluorescent bands.

Figure 11 demonstrates the strong influence which enclosure size has on the persistence time of the fluorescence. This result suggests that diffusion plays a part in determining the lifetimes of the persistent reservoirs.

The influence which the vapor density exerts upon the persistence time is evident in Tables I and II. This data was taken in the larger tube in which diffusion

would be expected to play a relatively less important role. The increase in the rate of decay with the vapor density indicates that collision destruction processes affect the life of both persistent reservoirs. The operation of a collision process is also evident in Fig. 9, which gives the density dependence of the relative intensities of the 4850A band and the 3350A band.

Finally, it should be noted that the entire fluorescence phenomenon is density dependent. Though further quantitative measurements have not been made, it has been observed that while band radiation is detected with difficulty at a density of 6×10^{15} atoms/cc, it becomes easily detectable at a density of 1×10^{16} atoms/cc and the total intensity continues to increase.

The generalities discussed above have led to an interpretation suggested by Holstein. According to this interpretation, the first stage leading to the fluorescence is the absorption of the mercury resonance radiation by normal $Hg(^1S_0)$ atoms

$$h\nu(2537)+Hg(^1S_0)\rightarrow Hg(^3P_1). \quad (1)$$

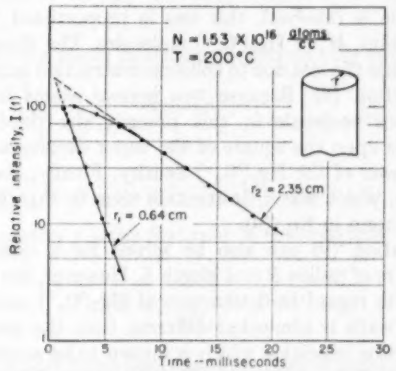

FIG. 11. The effect of geometry on the rate of fluorescence decay.

As a consequence of the imprisonment of resonance radiation,[15] the effective lifetime of a quantum of 2537A radiation is of the order of 100 microseconds in the enclosures considered. Knowing the excitation power entering the fluorescence tube, one can compute that the concentration of $Hg(^3P_1)$ builds up to the order of 10^{10} (atoms/cc).

The next step in the process is considered to be the collision conversion of resonance atoms to metastable atoms, which constitute the nonradiating reservoir of excitation, i.e.,

$$Hg(^3P_1)+Hg(^1S_0)\rightarrow Hg(^3P_0)+Hg(^1S_0)+0.21\text{ ev}. \quad (2)$$

The presence of $Hg(^3P_0)$ metastable atoms in the fluorescing vapor has been observed,[5] and it has long been known[16] that such metastables may be created as a result of the collision quenching of the $Hg(^3P_1)$ resonance state.

[15] T. Holstein, Phys. Rev. **72**, 1212 (1947).
[16] W. Arthman and P. Pringsheim, Z. Physik **35**, 626 (1926).

TABLE II. Density dependence of the initial time constant τ_1' associated with the decay of fluorescence in the large tube. $T=200°C$.

N (atoms/cc)	τ_1' (sec)
1.53×10^{16}	2.1×10^{-3}
1.91	2.0
2.00	2.37
2.56	1.4
3.58	0.75

As the third step, it is postulated that metastable atoms are converted to metastable diatomic molecules by three-body collisions

$$Hg(^3P_0)+2Hg(^1S_0)\rightarrow Hg_2(^3O_u^-)+Hg(^1S_0). \quad (3)$$

These diatomic molecules are considered to be the radiating reservoir mentioned above. The mechanics of this reaction may be outlined with reference to the potential energy diagram in Fig. 15. The considerations upon which this diagram is based will be taken up later; it is sufficient now to point out that the first excited level, $Hg_2(^3O_u^-)$ arises from the $Hg(^1S_0)$ and the $Hg(^3P_0)$ states of the separated atoms. In reaction (3) it is considered that an atom $Hg(^1S_0)$ collides with a metastable $Hg(^3P_0)$ atom. While these atoms are in close association a third body $Hg(^1S_0)$ also collides, taking away enough energy to stabilize the system in a vibrational state of the electronic $Hg_2(^3O_u^-)$ configuration.

It is next proposed that the 3350A band arises from spontaneous radiation by the metastable molecules

$$Hg_2(^3O_u^-)\rightarrow 2Hg(^1S_0)+h\nu(3350). \quad (4)$$

While the $Hg_2(^3O_u^-)$ state is metastable according to molecular theory,[17] it is considered possible that the metastability may be slightly broken down as the result of a gyroscopic disturbance of the electronic motion arising from the nuclear rotation.[6,18,19]

The 4850A band is explained as arising from an alternate mode of decay of the $Hg_2(^3O_u^-)$ state, namely,

TABLE III. Density dependence of the final time constant τ_2 associated with the decay of fluorescence in the small tube. $T=200°C$.

N (atoms/cc)	τ_2 (sec)
1.17×10^{16}	1.45×10^{-3}
1.53	1.57
1.91	1.65
2.00	1.6
2.56	1.70
2.56	1.65
3.18	1.6
3.58	1.45
4.06	1.35

[17] G. Herzberg, *Spectra of Diatomic Molecules* (D. Van Nostrand Company, Inc., New York, 1950).
[18] S. Mrozowski, Revs. Modern Phys. **16**, 160 (1944).
[19] This effect will be referred to more briefly hereafter as "gyroscopic perturbation."

collision induced radiation

$$Hg_2(^3O_u^-)+2Hg(^1S_0)\rightarrow 4Hg(^1S_0)+h\nu(4850). \quad (5)$$

The participation of two normal mercury atoms in this reaction is required to explain the N^2 dependence of the intensity ratio, $I(4850)/I(3350)$, as well as the effect of the higher densities on the persistence time. While there may be intermediate steps in reaction (5), there is so far no experimental evidence by which they might be identified. Since the 4850A band and the 3350A band decay at the same rate, whatever intermediate steps may be involved must consume a very small amount of time compared to the lifetime of $Hg_2(^3O_u^-)$.

Proceeding to a quantitative description of the theory, it is possible to set up the differential equations which describe the population of the excited particles in the volume elements of the enclosure. While the imprisonment time of the resonance radiation is about 100 microseconds, this is small compared to the milliseconds required for fluorescence decay. Hence, the simplifying assumption may be made that at time zero, that is, when the exciting radiation is cut off, the concentration of $Hg(^3P_1)$ drops immediately to zero and the production of $Hg(^3P_0)$ ceases. It is then necessary to specify first, the rate at which metastable $Hg(^3P_0)$ atoms are lost, and second, the rate at which metastable $Hg_2(^3O_u^-)$ molecules are lost.

In a given volume element of the enclosure, metastable atoms are lost by diffusion to neighboring volume elements and by collision destruction according to reaction (3). In equation form these losses are given by

$$\partial m/\partial t = D_m\nabla^2 m - C_m N^2 m, \quad (6)$$

where m is the density of $Hg(^3P_0)$ atoms, D_m is the diffusion coefficient of these metastable atoms, and C_m is a constant of proportionality. The first term on the right represents the rate of change of density due to diffusion, while the second term expresses the rate of collision destruction of metastable $Hg(^3P_0)$ atoms. Because two normal atoms are involved in a collision with one metastable atom, the second term depends upon the square of the vapor density N and is linearly proportional to m.

Equation (6) can readily be solved for a given initial distribution of metastable $Hg(^3P_0)$ atoms in a cylindrical enclosure of length L and radius R, under the condition shown to be reasonable by Coulliette[20] that the metastable atoms are destroyed upon reaching the boundary. The solution is given by

$$m(r,t) = m_0(r)e^{-t/\tau'}, \quad (7)$$

where

$$1/\tau' = D_m[(2.41/R)^2+(\pi/L)^2]+C_m N^2, \quad (8)$$

and the quantity $m_0(r)$ specifies the initial spatial distribution of $Hg(^3P_0)$ atoms. In Eq. (7) and Eq. (8), it is assumed that the fundamental mode of the decay is predominant. The justification of this assumption rests upon the fact that the experimentally measured fluorescence decays could be resolved into two clearly exponential components (see Fig. 10). If higher modes were important, the logarithmic plots for the late parts of $I(t)$ and $\Delta I(t)$ would be expected to be nonlinear.

The metastable $Hg_2(^3O_u^-)$ molecules in any given volume element are lost by diffusion, by spontaneous radiative decay, and by collision induced radiation. In addition, $Hg_2(^3O_u^-)$ molecules are created according to reaction (3). These processes are expressed by the equation

$$\partial M/\partial t = D_M\nabla^2 M - BM - C_M N^2 M + C_m N^2 m, \quad (9)$$

where M is the density of $Hg_2(^3O_u^-)$ molecules, D_M is their diffusion coefficient, and B and C_M are factors of proportionality. The first term on the right represents the rate of change of molecular density due to diffusion. The second term represents the loss due to spontaneous radiation according to reaction (4). Since only one molecule is involved, this loss is proportional to the population, M, of $Hg_2(^3O_u^-)$ molecules. The third term represents the loss due to collision destruction according to reaction (5). Because two normal atoms interact with one molecule in this process, the third term depends upon the square of the vapor density and the first power of the $Hg_2(^3O_u^-)$ density. Finally, the term $C_m N^2 m$, which was a destruction term in Eq. (6), is a supply term in Eq. (9).

Equation (9) can also be solved for a cylindrical enclosure of radius R and length L. However, the condition with regard to destruction of $Hg_2(^3O_u^-)$ molecules at the walls is somewhat different than the complete destruction condition which is known to be accurate in the case of the metastable $Hg(^3P_0)$ atoms. This situation first became evident when Eq. (9) was solved assuming complete destruction at the walls. When the solution was compared with the experimental data, it was found that the density dependence of the diffusion loss was correctly predicted at high densities, but not at the lower densities. Experiment and theory were brought into good agreement by assuming that a fraction A of the moecules which strike the bounding walls are destroyed, while the remainder $(1-A)$ are reflected back into the interior of the enclosure.

Quantitatively, the incomplete destruction boundary condition may be expressed in terms of the molecular diffusion current reaching the walls. The current density of excited molecules striking the walls is given to a sufficiently good approximation by the kinetic theory relation $M\bar{v}/4$, where $\bar{v}$ is the mean molecular speed. The net current density to the walls is, then, $\frac{1}{4}M\bar{v}A$. The desired boundary condition is obtained by equating this quantity to the diffusion current density; thus, at the walls,

$$-D_M\nabla M = \tfrac{1}{4}M\bar{v}A. \quad (10)$$

[20] J. H. Coulliette, Phys. Rev. 32, 636 (1928).

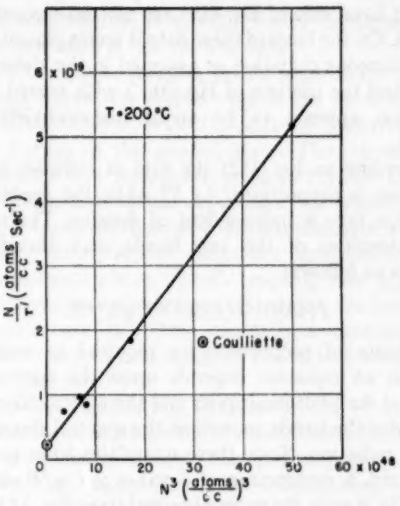

FIG. 12. The destruction of metastable mercury atoms, $Hg(^3P_0)$, in mercury vapor.

With the above boundary conditions, the solution of Eq. (9) is

$$I(t) \propto M(t) = \frac{\text{constant}}{\tau - \tau'}\left[\tau e^{-t/\tau} - \tau' e^{-t/\tau'}\right], \quad (11)$$

where

$$1/\tau = D_M[(j/R)^2 + (\pi/L)^2] + B + C_M N^2. \quad (12)$$

The quantity j is the first root of the equation,[21]

$$jJ_1(j) - \frac{R\bar{v}A}{4D_M}J_0(j) = 0, \quad (13)$$

where J_1 and J_0 are the Bessel functions of order one and zero, repectively. A mode analysis has been used and again, in Eqs. (11)–(13) it has been assumed that the fundamental decay mode predominates.

It should be noted that while Eq. (11) has the same form as the experimental decays, there is nothing in the theory to indicate whether τ or τ' is the larger time constant. It has already been implied that τ, which has been identified with the $Hg_2(^3O_u^-)$ molecules, is the larger of the two. However, the justification of this identification rests upon the experimental results. In particular, it will be shown that this choice results in the correct prediction of the diffusion coefficient for the metastable $Hg(^3P_0)$ atoms.

In order to compare the experimental time constants associated with $\Delta I(t)$ in Table II with the theory, it is convenient to rewrite Eq. (11) as follows

$$K\tau e^{-t/\tau} - I(t) = K\tau' e^{-t/\tau'}, \quad (14)$$

where K is a constant. The quantity on the left now corresponds to the experimental $\Delta I(t)$. To further facilitate the comparison, Eq. (8) is multiplied by N:

$$N/\tau' = ND_m[(2.41/R)^2 + (\pi/L)^2] + C_m N^3. \quad (15)$$

In this form N/τ' depends linearly on N^3 because ND_m is constant. The zero density intercept is related to the diffusion coefficient. In Fig. 12, the experimental data has been plotted in this way. The zero density intercept yields a value, $ND_m = 2.1\times10^{18}$ (atoms/cc) (cm²/sec) for a temperature of 200°C. It is of interest to compare this value with other experimental results. Measurements have been made for $Hg(^3P_0)$ atoms by Coulliette[20] whose result, corrected to the above temperature assuming a constant mean free path, is $ND_m = 2.11\times10^{18}$ (atoms/cc) (cm²/sec). Biondi[22] has obtained a value of $ND_m = 1.7\times10^{18}$ (atoms/cc) (cm²/sec) for the nearby $Hg(^3P_2)$ metastable state. This value is also corrected to a temperature of 200°C. This good agreement constitutes strong evidence for the correctness of the basic concepts of the theory.

For $t > \tau'$ the first term on the right side of Eq. (11) predominates and $\log I(t)$ becomes a straight line on a time plot. The slope of the line is $1/\tau$. This characteristic behavior is demonstrated by the data as shown in Fig. 10. The variation of τ with density is given for the large tube in Table I, and for the small tube in Table III.

Equation (12) may be applied to the large (subscript 1) and small (subscript 2) fluorescence tubes, yielding

$$1/\tau_1 = D_M[(j_1/R_1)^2 + (\pi/L_1)^2] + B + C_M N^2, \quad (16)$$

$$1/\tau_2 = D_M[(j_2/R_2)^2 + (\pi/L_2)^2] + B + C_M N^2. \quad (17)$$

Subtracting (16) from (17) and multiplying the result

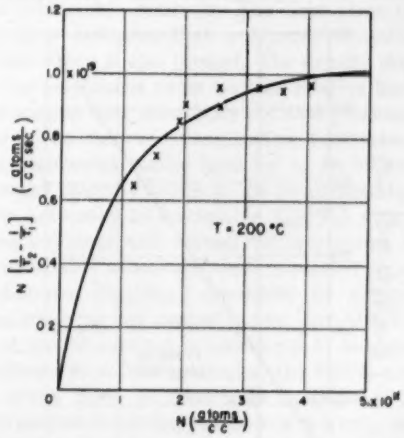

FIG. 13. The destruction of the diatomic mercury molecules at the enclosure walls. The solid curve is obtained from diffusion theory which includes a destruction coefficient at the walls of $A = 0.11$ and a density-diffusion coefficient product of $ND_M = 0.88\times10^{18}$(atoms/cc)(cm²/sec) at 200°C.

[21] Solutions of Eq. (13) are tabulated in H. S. Carslaw and J. C. Jaeger, *Conduction of Heat in Solids* (Oxford University Press, London, 1947), p. 379.

[22] M. A. Biondi, Phys. Rev. **90**, 730 (1953).

by N leads to

$$N\left(\frac{1}{\tau_2}-\frac{1}{\tau_1}\right)$$

$$=ND_M\left[\left(\frac{j_2}{R_2}\right)^2-\left(\frac{j_1}{R_1}\right)^2+\left(\frac{\pi}{L_2}\right)^2-\left(\frac{\pi}{L_1}\right)^2\right]. \quad (18)$$

The extra factor of N is included for convenience since ND_M is constant. The right-hand side of Eq. (18) depends upon N only through j_1 and j_2. It is also these quantities that bring in the effect of reflection of the molecules from the bounding walls. It is worth noting that if the molecules were entirely destroyed upon striking the walls, j_1 and j_2 would both become the first root of the Bessel function of order zero. In this case the right-hand side of Eq. (18) would be constant.

Using the data in Tables I and III, the values of $N(1/\tau_2-1/\tau_1)$ are plotted as a function of N in Fig. 13. Equation (18) is also plotted in this figure. Fitting the theoretical curve to the data required the variation of two parameters, the destruction coefficient A and ND_M. The solid curve represents the best fit and corresponds to a value of $ND_M=0.88\times10^{18}$ (atoms/cc) (cm²/sec) and a destruction coefficient of $A=0.11$.

Having now determined the rate of loss of $Hg_2(^3O_u^-)$ molecules by diffusion, the volume destruction processes may be considered. Equation (12) may be rewritten as follows:

$$1/\tau_1-D_M[(j_1/R_1)^2+(\pi/L_1)]=B+C_MN^2. \quad (19)$$

On an N^2 plot the right-hand side of Eq. (19) is a straight line with a zero density intercept corresponding to the rate of spontaneous radiation by the $Hg_2(^3O_u^-)$ molecules. The experimental values corresponding to the left hand side of Eq. (19) are plotted against N^2 in Fig. 14. On the basis of these data it seems plausible that a spontaneous radiation as assumed in the theory does exist, and the lifetime of $Hg_2(^3O_u^-)$ with regard to this radiation appears to be about one-twentieth of a second.

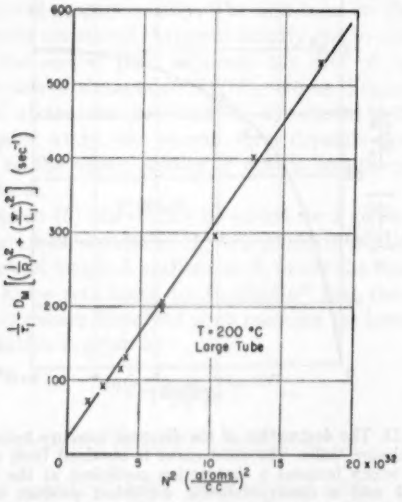

FIG. 14. The volume destruction of diatomic mercury molecules. The zero density intercept corresponds to a spontaneous radiation rate of 20 sec⁻¹.

According to Eq. (12) the rate of collision induced radiation is proportional to N^2 while the spontaneous radiation rate is independent of density. The ratio of the intensities of the two bands may therefore be written as follows:

$$I(4850)/I(3350)\propto C_MN^2/B. \quad (20)$$

The factor of proportionality required to make this relation an equation depends upon the spectral response of the photomultiplier and the optical filters used to resolve the bands, as well as the spectral distribution of the radiation. Since these quantities have not been evaluated, a comparison of a value of C_M/B obtained from Fig. 9 with the value obtained from Fig. 14 has not been made. On the other hand, the intensity ratios have been measured as a function of density. While the straight line in Fig. 9 does not quite intersect the origin, and there is a small unexplained curvature at the lowest densities, it is evident that $I(4850)/I(3350)$ is proportional to N^2 over the major part of the density range.

From the slopes of the curves in Figs. 12 and 14 the three-body collision coefficients, $C_m=100\times10^{-32}$ (atoms/cc)$^{-2}$ sec^{-1} and $C_M=21\times10^{-32}$ (atoms/cc)$^{-2}$ sec^{-1}, have been obtained for reactions (3) and (5), respectively. These coefficients can be compared with those for similar reactions which have been reported in the literature. Phelps and Molnar[25] have found that helium, neon, and argon metastable atoms are destroyed in three-body collisions with the parent gas atoms. The coefficients in these cases vary from 0.02×10^{-32} (atoms/cc)$^{-2}$ sec^{-1} for $He(^3S_0)$ to 0.9×10^{-32} (atoms/cc)$^{-2}$ sec^{-1} for $A(^3P_2)$. These values were measured at room temperature while the mercury coefficients given above were obtained at 200°C. In recombination studies three-body collision coefficients of the order of 10^{-32} (atoms/cc)$^{-2}$ sec^{-1} have been observed in hydrogen[24] and also in iodine[25–27] when noble gases are present. When more complex additives are available as third bodies, iodine recombines at a much greater rate, e.g., 138×10^{-32} (molecules/cc)$^{-2}$ sec^{-1} when CH_3CH_2I is present. Finally, Phelps and Brown[28] have measured a three-body coefficient of 6.5×10^{-32} (ions/cc)$^{-2}$ sec^{-1} for the reaction $He^+ + 2He \rightarrow He_2^+ + He$

[25] A. V. Phelps and J. P. Molnar, Phys. Rev. **89**, 1202 (1953). The author is indebted to A. V. Phelps for a discussion of the available experimental results pertaining to three-body reactions.
[26] I. Amdur, J. Am. Chem. Soc. **60**, 2347 (1938).
[27] Christie, Norrish, and Porter, Proc. Roy. Soc. (London) **A216**, 152 (1953).
[28] R. Marshall and N. Davidson, J. Chem. Phys. **21**, 659 (1953).
[27] H. E. Russell and J. Simons, Proc. Roy. Soc. (London) **A217**, 271 (1953).
[28] A. V. Phelps and S. C. Brown, Phys. Rev. **86**, 102 (1952).

at room temperature. A suitable theory for three-body collision processes is not yet available.

It is of interest to consider briefly some of the potential energy curves for Hg_2 in view of the identification of the 3350A band with electronic transitions from the $Hg(^3O_u^-)$ state to the ground state. The curves suggested by the new results are given in Fig. 15. On the right, at large internuclear separation, the states of the separated atoms are specified. At intermediate nuclear separation, the molecular states are identified by the notation appropriate to Hund's coupling case (c).[29] At small internuclear separations the states are specified by Hund's case (a). The correlations between the molecular states and the states of the excited atoms are given by Mulliken.[30]

The ground state of Hg_2 is characteristic of van der Waals molecules in which the relatively weak binding is due to polarization forces. The known properties of this state are summarized by Finkelnburg.[31] The dissociation energy is about 0.08 electron volt and the potential minimum occurs at a nuclear separation of about 3A.

Some quantitative information concerning the $Hg_2(^1\Sigma_u)$ state has been obtained by Kuhn and Freudenberg.[32] These authors measured the properties of the absorption band which begins at the 2537A atomic line and extends in the long wave direction to a limit at 3300A. It was found that the intensity of absorption at the long wave limit increases with the square of the atomic vapor density and with temperature, indicating that positive energy levels of the molecular ground state are responsible for the absorption. It was assumed that these positive energy levels are populated according to the Maxwell-Boltzman law and that absorption at the long wave limit involves transitions to the minimum of the $Hg_2(^1\Sigma_u)$ potential curve in accordance with the Frank-Condon principle. On this basis the position of the potential minimum of the $Hg_2(^1\Sigma_u)$ curve was calculated to be directly above the 0.27 electron volt point on the ground-state curve. From the value of the long wave limit and the wavelength of the atomic line, $Hg(^3P_1) \rightarrow Hg(^1S_0)$, it was determined that the dissociation energy of $Hg_2(^1\Sigma_u)$ is 0.84 electron volt.

The $Hg_2(^3O_u^-)$ potential curve has been added to the diagram in a manner consistent with the results of the present paper. It has been assumed that the minimum of the $Hg_2(^3O_u^-)$ curve lies beneath the minimum of the $Hg_2(^1\Sigma_u)$ curve. This procedure is based upon the recognition that at small internuclear separation spin-orbit interaction becomes a small perturbation and the two potential curves must approach each other very closely; it seems reasonable that for increasing internuclear distance the spin-orbit energy separation of the two curves increases monotonically to the value for the separated atoms. Using, therefore, the 0.27-electron volt level of the ground potential curve as the final state for the 3350A emission, it follows from the known energy of the $^3P_0$ atomic state that the dissociation energy of $Hg_2(^3O_u^-)$ is 0.71 electron volt.

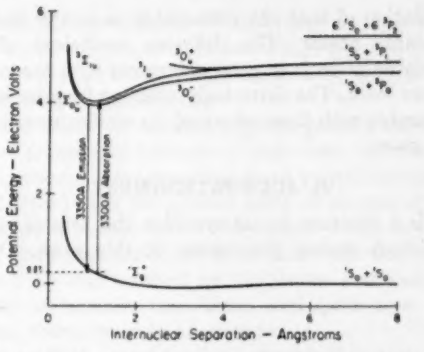

FIG. 15. The potential energy levels of Hg_2 constructed on the basis of considerations discussed in the text.

V. SUMMARY

The intensities of the principal fluorescent bands of mercury excited by the 2537A atomic resonance line have been measured quantitatively as a function of time in the afterglow. Observations have been made at a fixed vapor temperature and over a range of vapor densities within which the character of the fluorescence goes through extensive alteration. The results of the experiments reveal that the two principal bands centered at 3350A and 4850A, have their origin in a common metastable reservoir. The time structure of the afterglow indicates that a second, nonradiating metastable entity is also present. The density dependence of the persistence times and the relative band intensities suggest that three-body collision processes are involved in the chain of events leading to fluorescence.

The experimental results have led to an interpretation in which mercury atoms in the resonance $Hg(^3P_1)$ state are converted to metastable $Hg(^3P_0)$ atoms by quenching collisions with normal mercury atoms. Some of the metastable atoms are then converted to metastable diatomic $Hg_2(^3O_u^-)$ molecules by three-body collisions involving two normal atoms. The 3350A component of the fluorescence is considered to be spontaneous radiation from the molecules; the 4850A compoponent arises from a three-body collision induced radiation process involving two normal mercury atoms.

A detailed analysis based upon this scheme has made it possible to obtain from the data diffusion coefficients for the metastable molecules and the metastable atoms, the lifetime of the metastable molecules with respect to spontaneous radiation, and the frequencies of the three-body collision processes responsible for the

[29] The various angular momentum coupling cases for diatomic molecules are described in G. Herzberg, *Spectra of Diatomic Molecules* (D. Van Nostrand Company, New York, 1950).
[30] R. S. Mulliken, Revs. Modern Phys. 2, 92 (1930).
[31] W. Finkelnburg, *Kontinuierliche Spektren* (Julius Springer, Berlin, 1938).
[32] H. Kuhn and K. Freudenberg, Z. Physik **76**, 38 (1932).

annihilation of both the metastable molecules and the metastable atoms. The diffusion coefficient of the metastable atom is in good agreement with the results of other work. The three-body collision frequencies are comparable with those obtained for similar reactions in other gases.

VI. ACKNOWLEDGMENT

It is a pleasure to acknowledge the help of several individuals during the course of this work. Dr. T. Holstein, who first recognized the interesting nature of the problem, guided the theoretical interpretation of the experimental results. Dr. D. Alpert has maintained an interest in the program since its inception and has contributed many helpful discussions. C. G. Matland assisted with the preparation of the experimental tubes and also helped with the tedious task of taking data. Finally, seminar discussions with the members of the Physics Department of the Westinghouse Research Laboratories have been invaluable.

PHYSICAL REVIEW VOLUME 93, NUMBER 6 MARCH 15, 1954

Dipole and Quadrupole Transition Probabilities in Neutron-Capture Gamma Radiation

B. B. KINSEY AND G. A. BARTHOLOMEW
Physics Division, Atomic Energy of Canada Limited, Chalk River, Ontario, Canada

(Received November 30, 1953)

An analysis of the intensities of neutron-capture γ rays in even-charge nuclei shows that at high energies the emission probability of $E1$ radiation is greater than that of any other multipole order. This conclusion is supported by additional evidence from odd-charge nuclei. In three nuclei (Mg^{25}, Si^{29}, and S^{33}) a direct comparison shows that (at the same energy) the emission probability of $E1$ is 200 times greater than that of $M1$ radiation. The rate of emission of $E2$ radiation has been compared directly with $E1$ radiation in only one instance, *viz.*, Mg^{25}, where (at 7 Mev) it was found to be lower by a factor of 2000. Further evidence is adduced to show that this ratio is not exceptional and that the rate of emission of $E2$ radiation (at 7 Mev) is less than that of $M1$ radiation. The absolute rates of emission for $E1$ and $M1$ γ rays are evaluated in those instances where the radiation width of the capturing state is known. When corrected for the level spacing near the initial state (and for the nuclear radius, in the case of $E1$ radiation), the rates of emission are remarkably constant; they are independent of the nuclear charge and mass over a range where the level spacing may vary by a factor of 10^4 or more. The emission rates of $E1$ and $M1$ radiation are generally ten times lower than those predicted by the formula of Weisskopf, which is based on the independent-particle model. The emission rates do not exceed those expected from that formula in the case of the exceptionally strong $M1$ ground-state γ rays from F^{20} and Al^{28}. It is shown that the identification of the spins and parities of excited states in many nuclei can be made on the basis of intensity measurements. Finally, the influence of closed shells on the γ-ray spectra is discussed.

INTRODUCTION

A DETERMINATION of the relative emission probabilities of different multipole orders of γ radiation is of considerable interest for it throws a direct light on the mechanism responsible for the emission of radiation. In the absence of selection rules or other limitations, one would expect that the probability of detection of low-energy electric dipole ($E1$) radiation,[1] would far exceed that of higher multipole orders, for, theoretically, the relative probabilities of emission of the various multipoles should decrease by successive factors of the order of $(R/\lambda)^2$, where R is a quantity of the order of the nuclear radius and $2\pi\lambda$ is the wavelength of the radiation. For 1-Mev radiation and for a nucleus of mass 100, this factor is about 0.1 percent.

Now the greater part of the experimental data on the relative rates of emission of the various multipoles has been derived from the study of the γ rays following β decay. It became increasingly apparent that, among the observed γ rays, far more are of $M1$ and $E2$ types than $E1$. Until recently, this fact has not been fully appreciated because of the tendency of early experimenters working with the heavy elements to obtain internal photoelectric conversion coefficients which were too low. Since the coefficients increase with increasing multipole order, and since they are generally greater for magnetic than for electric radiations, $E2$ radiations were mistaken for $E1$, and $M1$ radiations for $E2$. That these radiations are actually $E2$ and $M1$ is confirmed by more exact calculations[2] of internal conversion coefficients which have given results which are lower than early estimates.[3] Consequently, the few examples of $E1$ radiations following β decay have become fewer still, and, although some well-authenticated

[1] We follow here the notation for electric and magnetic multipole radiation introduced by M. Goldhaber and A. W. Sunyar, Phys. Rev. 83, 906 (1951).

[2] Rose, Goertzel, and Spinrad, Phys. Rev. 83, 79 (1951).

[3] H. R. Hulme, Proc. Roy. Soc. (London) A138, 643 (1932); H. M. Taylor and N. F. Mott, Proc. Roy. Soc. (London) A138, 665 (1932); J. B. Fisk and H. M. Taylor, Proc. Roy. Soc. (London) A143, 274 (1933); A146, 178 (1934); H. M. Taylor, Proc. Cambridge Phil. Soc. 32, 291 (1936).

examples remain,[4] the occurrence of $E1$ radiations at low energies is exceptional. As a result, the rather widespread belief has arisen that some mechanism inhibits the emission of $E1$ radiation.

The emission of $E1$ radiation from a given state may be forbidden by selection rules, e.g., if all states of lower energy have the same parity, or it may be suppressed because of peculiarities of nuclear structure. Delbrück and Gamow[5] were the first to point out that if all the nuclear constituents have the same specific charge, no relative displacement of the centroids of mass and charge can occur and no $E1$ radiation will be emitted. For example, no $E1$ radiation can be emitted as a result of the relative motion of the constituents of a nucleus consisting entirely of α particles. A similar inhibition of $E1$ radiation must hold for the radiations emitted by the oscillations of a liquid-drop nucleus in which strong correlations exist between the motions of protons and neutrons. Therefore, if it were found that the ratio of the transition probabilities of $E2$ to $E1$ radiation were much greater than $(R/\lambda)^2$, or if the ratio of $M1$ to $E1$ were unexpectedly large, it might be concluded that the emission of $E1$ radiation was being suppressed by some such correlated motion. Conversely, if the relative emission probabilities of $E2$ to $E1$ radiations were of the order of $(R/\lambda)^2$ or less, at least part of the energy emitted as $E1$ radiation would have to be attributed to a single particle moving in an orbit with a size comparable to that of the nucleus, or to groups of particles with a specific charge very different from that of the rest of the nucleus. If the emission is due entirely to the displacement of a neutron, it can be shown[1] that the ratio of $E2$ to $E1$, or the relative emission probabilities of any two successive electric multipoles, is less than $(R/\lambda)^2$ by a factor of the order of the square of the atomic weight. This, in effect, would make undetectable all electric multipoles above the first.

The rates of emission of multipoles of orders higher than $E1$ have been examined by Goldhaber and Sunyar.[1] In some instances, e.g., $M4$ radiations, these authors show that the emission probability is in good agreement with the estimates of Weisskopf.[6] In others, e.g., $E3$ radiations (and more recently, $M1$ radiations[7]), the emission probability is consistently less than that given by Weisskopf's formula, while for $E2$ radiation there are wide variations in emission probability, some $E2$ γ rays being faster and some slower than is expected from that formula. Although some examples of very slow $E1$ radiations of low energy are known, it is probably unsafe as yet to conclude that the rate of emission of low-energy $E1$ radiation is always much lower than that expected theoretically. The infrequent detection of $E1$ radiation following β decay is probably better ascribed to the absence of low-lying excited states which have the proper spin and which differ in parity from the ground state, rather than to an inhibition of the emission of $E1$ radiation.

In the study of neutron-capture gamma rays, we observe transitions between a state near the neutron binding energy (corresponding to an excitation usually near 7 Mev) and the ground state or excited states. The range of energy covered by these γ rays is much higher than that produced in β decay and also much higher than that covered by Goldhaber and Sunyar's analysis of isomeric transitions, and quite new phenomena, therefore, may be expected.

In an earlier paper[8] we have described very briefly certain regularities occurring in the emission of neutron-capture γ rays, which suggest that, in even-charge nuclei at excitations of several Mev, the predominant feature is the emission of $E1$ radiation. These data are discussed in greater detail in the present paper (Sec. 2).

Since the earlier paper[8] was written, the angular distributions of the protons in the (d,p) reaction have been measured in some nuclei of special interest. These results give the orbital angular momentum carried by the neutron in the formation of the ground state and some excited states of the product nucleus and thus provide the means for identifying the multipole type of the γ rays producing these states in the (n,γ) reaction. This additional evidence confirms our conclusions about the strength of $E1$ radiation. In particular, three examples were found where the emission probability of $E1$ and $M1$ γ rays emitted by the same state could be directly compared. The results show that the transition probability for $E1$ radiation is 200 times greater than that for $M1$ radiation. In one instance, where $E1$ and $E2$ γ rays could be directly compared, the transition probability for $E1$ radiation was found to be 2000 times greater than that for $E2$ radiation at 7 Mev. These results are discussed in detail in Sec. 3.

In certain cases the absolute value of the transition probability for $E1$ and $M1$ γ rays can be compared with the theoretical predictions of Weisskopf. It is found that the theoretical predictions give values which are too high by an order of magnitude for both types of radiation. These results also confirm the conclusion, obtained from the direct comparison, that the transition probability for $E1$ radiation is about 200 times greater than that for $M1$ radiation. A detailed discussion is given in Sec. 4.

2. THE INTENSITY OF GROUND-STATE GAMMA RAYS

The multipole order of high-energy γ rays can be directly determined from measurements of the internal conversion coefficient for the production of pairs or from angular or polarization correlations of successive γ rays. For neutron-capture γ rays such measurements are difficult and none have yet been reported. In the

[4] Beling, Newton, and Rose, Phys. Rev. **87**, 670 (1952); A. W. Sunyar, Phys. Rev. **90**, 387 (1953).
[5] M. Delbrück and G. Gamow, Z. Physik **72**, 492 (1931).
[6] V. F. Weisskopf, Phys. Rev. **83**, 1073 (1951).
[7] R. L. Graham and R. E. Bell, Can. J. Phys. **31**, 377 (1953).
[8] B. B. Kinsey and G. A. Bartholomew, Physica **18**, 1112 (1952).

absence of such information, we know the multipole orders of only those γ rays for which the spins and parities of the initial and final states are known. Except for a very few excited states, this information is available only for the ground states of nuclei and consequently, the nature of only those γ rays which are emitted in direct transitions from the initial state of the compound nucleus to the ground state can generally be determined. For want of a better name we shall call these γ rays the "ground-state" γ rays, a term which we have used consistently in other communications. Now, the present results have been obtained under conditions where the capture of thermal neutrons predominates. Since the capture of thermal neutrons occurs only for s waves, the parities of the ground-state γ rays are determined uniquely by the parities of the ground states of the target and of the product nucleus. The angular momentum radiated is determined by a combination of the spins of these states and the spin of the neutron.

In general, two alternative ways of emitting the ground-state γ ray will exist in all cases where a neutron is captured by an even-odd[9] or by an odd-charge nucleus, corresponding to the neutron spin being added parallel or antiparallel to the spin of the target nucleus. Except for a very few instances (e.g., the gamma rays produced by capture in Cd) in which thermal neutron capture is of a specifically resonant type, the extent to which the compound nucleus is formed with the one spin or the other is unknown, and with certain exceptions (which we shall discuss later) the resulting ground-state radiation consists of an undetermined mixture of γ rays of two multipole orders. We shall refer to this mixture as "composite" radiation. The intensity of this composite radiation is not characteristic of a γ ray of any particular multipole order. When thermal capture is not resonant, it is perhaps not strictly correct to refer to the "state" of the compound nucleus. However, hereafter we shall call this level of excitation the "capturing state," whether the capture is resonant or not.

TABLE I. Spins and parities of states which combine with emission of $E1$ radiation.

Type of product nucleus	Configuration or spin and parity: Target nucleus	Capturing state	Ground-state product nucleus	Possible types or multipole radiation
Even-odd	$0(+)$	$1/2(+)$	$p_{1/2}(-)$	$E1$ only
	$0(+)$	$1/2(+)$	$p_{3/2}(-)$	$E1$, $M2$
Even-even	$p_{1/2}(-)$	$0(-)$	$0(+)$	Forbidden
		$1(-)$	$0(+)$	$E1$ only
	$p_{3/2}(-)$	$1(-)$	$0(+)$	$E1$ only
		$2(-)$	$0(+)$	$M2$ only
		$J+1/2(\pm)$	$J\pm1/2(\mp)$	$E1, M2, E3, \cdots$
		$J-1/2(\pm)$	$J\pm1/2(\mp)$	$E1, M2, E3, \cdots$
Odd-odd	$J(\pm)$	$J+1/2(\pm)$	$J+3/2(\mp)$	$E1, M2, E3, \cdots$
		$J-1/2(\pm)$	$J+3/2(\mp)$	$M2, E3, \cdots$
		$J+1/2(\pm)$	$J-3/2(\mp)$	$M2, E3, \cdots$
		$J-1/2(\pm)$	$J-3/2(\mp)$	$E1, M2, E3, \cdots$

Theoretically, the probability of emission of radiation increases rapidly with the energy, and, therefore, the occurrence of relatively strong ground-state γ rays is to be expected in nuclei which radiate exclusively γ rays of the same multipole order. Such nuclei, of course, are exceptional. In general, the neutron-capture γ-ray spectra contain radiations of many different multipole orders which, presumably, have very different emission probabilities. Consequently, relatively strong ground-state γ rays should occur, in general, only when the multipole emitted is the one with the highest transition probability.

Prominent ground-state γ rays are the exception rather than the rule. We find, in fact, that the only even-charge nuclei which produce a ground-state γ ray of exceptional strength are those which, according to the shell model,[10] have an odd neutron in a p state in the ground state of either the target or product nucleus. In the even-odd product nuclei up to zinc which we have so far examined, we have found no exception to this rule.

In the upper part of Table I the possible multipole types of ground-state γ rays are given for even-charge nuclei where the odd neutron (in the target or product nucleus) is in a p state. Assuming that all even-even nuclei have zero spin and even parity, it is clear that for even-odd product nuclei the capturing state must have a spin of $1/2$ and even parity. For $p_{1/2}$ states the ground-state γ ray will be of $E1$ type. This is also true for $p_{3/2}$ states, for, although the radiation may have an $M2$ component, it is to be expected theoretically that the rate of emission of $M2$ radiation is much lower than that of $E1$ radiation. The association of strong ground-state γ rays with p states in even-odd nuclei, therefore, suggests that this strength is due to their $E1$ character.

Three even-even product nuclei have been studied which have been produced by neutron capture by nuclei in $p_{3/2}$ states. In these nuclei, which form a special class, the ground-state γ rays are usually weaker than those producing the first-excited state. This is to be expected if the emission of $E1$ radiation is the most probable process, as the even-odd product nuclei appear to show. For even-even product nuclei, the capturing state can have one of two possible spins. As Table I shows, the resulting composite radiation always has an $E1$ component, the other component being $M2$ or entirely absent; and the observed intensity, in photons per capture, will depend on the proportion in which the two spin states are formed. However, the parity of the first-excited state is probably even and its spin is 2 units. For a $p_{3/2}$ target nucleus, then, both components

[9] In this adjective and in similar adjectives mentioned hereinafter, we describe the proton number (Z) first, and the neutron number (N) second.

[10] We use the strong-coupling model of M. G. Mayer, Phys. Rev. 78, 16 (1950), and Haxel, Jensen, and Suess, Z. Physik 128, 301 (1950).

of the composite radiation emitted to this state will be $E1$. Disregarding the energy dependence of emission probability, it follows that, if the matrix elements of the two transitions are equal, the intensity of the ground-state γ ray will be the weaker (for it will consist, in part, of $M2$ radiation).

In odd-odd product nuclei the relationship between the multipolarity of the ground-state γ ray and the configuration of the product nucleus is less simple, for now both target and product nuclei have spins greater than zero. In Table I are listed all possible combinations of spin and parity of the target and product nuclei for which the emission of an $E1$ component in the ground-state radiation is possible. As in the case of even-even product nuclei, composite ground-state γ rays are emitted. If the spin of the ground state of the product nucleus is $J\pm1/2$, where J is the spin of the target nucleus, both components of the composite ground-state γ ray will contain $E1$ radiation. If the spin of the ground state is $J\pm3/2$, $E1$ radiation will be emitted from only one of the two possible capturing states.

The experimental results will now be considered in detail. Since the γ rays emitted by odd-charge nuclei are weaker and more numerous than those emitted by even-charge nuclei, and since also they are more difficult to interpret, we shall deal separately with even- and odd-charge nuclei. We shall consider the light even-charge elements first, because for these nuclei there is usually sufficient data from other sources to determine the neutron binding energies or the positions of excited states. The "light" elements will be defined as those with atomic numbers equal to or less than that of zinc. The remainder will be called "heavy" elements.

2.1. Intensities of Ground-State γ Rays of Even-Charge Light Elements

The experimental results for the ground-state γ rays of all even-charge nuclei up to zinc are listed in Table II.[11] The first column gives the category under which it will be convenient to discuss these results in some detail, the second, the neutron number (N), and the third, the configuration of the ground state of the even-odd nucleus according to the shell structure theories,[10] regardless of whether this nucleus happens to be the target or the product nucleus. The product nucleus responsible for the emission of the γ ray observed is listed in columns four and five, the designation of the γ ray used in previous publications in the sixth, and its intensity in the seventh. The last two mentioned were taken from the published tables[12–14] of the intensities of the ground-state γ rays from the natural element, corrected for the contribution to the thermal neutron capture caused by the isotope in question.[15]

TABLE II. Intensities of ground-state γ rays of even-charge nuclei up to zinc. In those marked with an asterisk, it is not yet certain whether the γ ray listed is correctly identified.

Group	Neutron number N	Ground state of even-odd nucleus	Product odd N	Nucleus even N	γ ray	Intensity in photons per 100 captures	Reference
1	6	$p_{3/2}$		Be^{10}	A	75	a
	7	$p_{1/2}$	C^{13}		A	70	a
2	13	$d_{5/2}$	Mg^{25}		C	0.4	b
	14	$d_{5/2}$		Mg^{26}		<0.2	b
	15	$s_{1/2}$	Mg^{27}		F_1	~13	c
	15	$s_{1/2}$	Si^{29}		B	2	b
	16	$s_{1/2}$		Si^{30}	A	3	b
	17	$d_{3/2}$	Si^{31}			<15	b
	17	$d_{3/2}$	S^{33}		A	1	d
3	21	$f_{7/2}$	Ca^{41}			<0.2	d
	23	$f_{7/2}$	Ca^{43}			<1	d
	26	$f_{7/2}$		Ti^{48}		<1	e
	27	$f_{7/2}$	Ti^{49}			<0.2	e
	27	$f_{7/2}$	Cr^{51}			<1	e
	28	$f_{7/2}$		Ti^{50}		<1	e
4	29	$p_{3/2}$	Cr^{53}		D	40	e
	29	$p_{3/2}$	Fe^{55}		B	~50	e
	30	$p_{3/2}$		Cr^{54}	A	13	e
	31	$p_{3/2}$	Fe^{57}		E	40	e
	31	$p_{3/2}$	Ni^{59}		A	50	e
	32	$p_{3/2}$		Fe^{58}	A	~5	e
	33	$f_{5/2}$	*Ni^{61}		B	80	e
	35	$f_{5/2}$	*Zn^{65}		E	40	e
	38	$f_{5/2}$		Zn^{66}	A	0.3	e

* See reference 16.
[b] See reference 12.
[c] See reference 25.
[d] See reference 13.
[e] See reference 14.

A casual inspection of Table II clearly shows that strong ground-state γ rays are associated for the most part with those nuclei which, according to the shell model, are in p states, while weak ground-state γ rays are associated with nuclei in d states, s states, or $f_{7/2}$ states. The table suggests, therefore, that the strength of the ground-state γ rays in Groups 1 and 4 is due to the greater emission probability of $E1$ radiation and that the weakness of the ground-state γ rays in Groups 2 and 3 is caused, respectively, by the relative weakness of $M1$, or $E2$, and of $E3$ radiation.

While the absolute intensity of a γ ray is not in itself a criterion of emission probability, the above interpretations would appear to be correct, for, in the even-odd nuclei in Groups 2 and 3, very strong γ rays are found which lead to excited states, and which will be shown, on the basis of independent evidence, to be of the $E1$ type. We shall now discuss the experimental evidence in more detail and we shall commence with a consideration of the nuclei-producing strong ground-state γ rays, *viz.*, those contained in Groups 1 and 4.

[11] This table contains all those nuclei up to zinc which we have so far been able to investigate with existing apparatus. The γ rays of some nuclei, such as C^{14} or Si^{31}, have still to be determined, while for others, e.g., O^{17} and S^{35}, the cross sections are so low that the capture γ rays have not been detected.

[12] Kinsey, Bartholomew, and Walker, Phys. Rev. **83**, 519 (1951).

[13] Kinsey, Bartholomew, and Walker, Phys. Rev. **85**, 1012 (1952).

[14] B. B. Kinsey and G. A. Bartholomew, Phys. Rev. **89**, 375 (1953).

[15] H. Pomerance, Phys. Rev. **88**, 412 (1952).

2.1.1. Group 1

In Group 1 there is only one even-odd nucleus, C^{13}. In this nucleus only three states are known to exist which can be excited by transitions from the neutron binding energy at 4.95 Mev. It is significant, as has been shown elsewhere,[16] that only those transitions have been detected which can take place with the emission of $E1$ radiation.

2.1.2. Group 4

In Group 4 the identification of the strong γ rays with the direct transition to the ground state in even-odd nuclei is certain only in Cr^{53}, Fe^{55}, and Ni^{59}, and probable in Fe^{57}. In Ni^{61} and Zn^{65} strong ground-state γ rays appear to be associated with $f_{5/2}$ states. Such γ rays, if indeed they are ground-state γ rays,[17] are of $M2$ type. However, in the absence of information on the positions of the excited states in these nuclei, it is quite possible that the γ rays observed are not, in fact, ground-state γ rays but are emitted in $E1$ transitions to low-lying excited states. [This explanation accounts for the strength of the strong γ ray originally ascribed to the ground-state transition of K^{40} (see Sec. 2.3.3).]

It is interesting to note that the decay of Fe^{55} and Ni^{59} is consistent[18] with the assignment of a $p_{3/2}$ configuration to the ground states of these nuclei and with the known spins of Mn^{55} (5/2) and Co^{59} (7/2). The spin of the stable isotope, Cr^{53} which has been found[19] to be 3/2, also indicates a $p_{3/2}$ state. That the ground states of Cr^{53} and Fe^{57} are, in fact, p states has recently been demonstrated by studies of the (d,p) reaction.[20] Also, existing data on the decay of Co^{57} show that both the ground state and the 14-kev state[21,22] of Fe^{57} should be p states. Both, therefore, should be produced by the emission of $E1$ radiation from the capturing state. It has already been shown[14] that the strong γ ray at 7.639 ± 0.004 Mev can be identified with either transition. Further analysis of the shape and width[23] of the coincidence peak suggests that this γ ray is indeed the ground-state γ ray (see Appendix A).

The γ rays produced in the ground-state transitions in the even-even nuclei Cr^{54} and Fe^{58} are relatively weak. While the γ ray producing the first-excited state in Fe^{58} has not been detected separately from the ground-state γ ray of Fe^{55}, the γ ray leading to the first-excited state of Cr^{54} is stronger than the ground-state γ ray in that nucleus. (This is also true of Be^{10} if the intensities of the γ rays are corrected by the cubes of the energies.) For these nuclei it is very probable that the spin of the first-excited state is 2 units;[24] and the γ ray producing this state, therefore, is $E1$, regardless of the spin of the capturing state, whence it follows that the ground-state γ rays can be relatively weak as explained in a previous section.

2.1.3. Group 2

The weak ground-state γ rays in this group have intensities of the order of a few photons per 100 captures. The isotopic neutron capture cross sections of Mg^{26}, Si^{29}, and Si^{30} are low.[15] Consequently, only the ground-state γ ray has been identified in[25] Mg^{27} and in Si^{30}, while no γ rays have been detected in Si^{31} for which the intensity of the ground-state γ ray given in Table II is an upper limit. The remaining even-odd nuclei, Mg^{25}, Si^{29}, and S^{33}, all have one striking characteristic, *viz.*, in the spectrum of each there is one γ ray of exceptional strength produced in a transition from the capturing level to a highly excited state. Since the ground-state γ rays of the nuclei of Group 2 produce no change in parity (they are $E2$ or $M1$ or mixtures of both), it is probable that the outstanding γ ray must be a multipole of a much higher emission probability, i.e., it must be $E1$. Recently this conclusion has been confirmed in measurements by Holt and Marsham[26,27] on the angular distribution of the protons in the (d,p) reaction in these three even-odd nuclei. From these measurements it appears that the state excited by the strong γ ray in the neutron capture process is the lowest state for which the neutron is absorbed in the (d,p) process with unit orbital angular momentum. Since the target nucleus, in each instance, has zero spin and even parity, it is clear that this state is a p state. The strong γ rays, therefore, are indeed $E1$, while the relatively weaker γ rays, producing directly the ground state or other even states, are $M1$ or $E2$. The latter are also emitted from the capturing state and, therefore, compete with the $E1$ γ ray. A study of the intensities of the even- and odd-parity γ rays, therefore, gives directly the ratio of the emission probabilities of $E2$ or $M1$ relative to $E1$ radiations. A detailed account of the γ rays emitted by these three nuclei is given in Appendixes B, C, and D.

---

[16] G. A. Bartholomew and B. B. Kinsey, Can. J. Phys. **31**, 49 (1953).

[17] Ni^{61}: It is not yet established (reference 14) whether the strong γ ray in question (8.532 Mev) is the ground-state γ ray of Ni^{61} or whether it represents a transition to an excited state of Ni^{59}. Zn^{65}: The strong γ ray E (7.876 Mev) has an energy close (100 kev) to the estimated neutron binding energy of Zn^{66}. The positron decay of Zn^{65}, suggests that the spin of Zn^{66} is very different from that of Cu^{65}, which is 3/2 ($p_{3/2}$ proton).

[18] The decay of both nuclei takes place by electron capture between ground states. The β decay of Fe^{55} is presumably allowed ($\log ft = 5.9$), while that of Ni^{59} is clearly forbidden ($\log ft = 11$). This is to be expected, for the spin of Co^{59} is greater than that of Mn^{55} by one unit.

[19] B. Bleaney and K. D. Bowers, Proc. Phys. Soc. (London) **A64**, 1035 (1951).

[20] C. F. Black, Phys. Rev. **90**, 381 (1953).

[21] E. H. Plesset, Phys. Rev. **62**, 181 (1942).

[22] M. Deutsch and W. E. Wright, Phys. Rev. **77**, 139 (1950).

[23] B. B. Kinsey and G. A. Bartholomew, Can. J. Phys. **31**, 537 (1953).

[24] This is certainly true of Be^{10} [see E. Bedewi, Proc. Phys. Soc. (London) **A65**, 64 (1952); see also reference 16] and also of Fe^{58} [see Bishop, Daniels, Goldschmidt, Halban, Kurti, and Robinson, Phys. Rev. **88**, 1432 (1952)].

[25] B. B. Kinsey and G. A. Bartholomew, Can. J. Phys. **31**, 901 (1953).

[26] J. R. Holt and T. N. Marsham, Phys. Rev. **89**, 665 (1953).

[27] J. R. Holt and T. N. Marsham, Proc. Phys. Soc. (London) **A66**, 258 (1953).

No strong γ rays leading to excited states have been detected in the spectrum of the even-even nucleus Mg^{26}. No odd states were found by Holt and Marsham in Mg^{26} below an excitation of 6 Mev. This explains the absence of unusually strong γ rays in that nucleus: all those detected with the pair spectrometer which can be identified with this nucleus are $M1$ radiations.

2.1.4. Group 3

The ground-state γ rays have not been detected from any of the nuclei in this group. In all cases, the intensity is less than 1 percent per capture. Now, the unpaired neutron in the ground state of an even-odd nucleus in this group is in an $f_{7/2}$ state. The ground state, therefore, has odd parity and its spin is probably either 7/2 or 5/2.[28] The weakness of the ground-state γ ray in these nuclei, therefore, demonstrates the relatively low probability of emission of $E3$ or $M2$ radiation in comparison with γ rays of lower multipole order.

It has been possible to attempt an analysis of the capture radiations from only two nuclei in this group, *viz.*, Ca^{41} and Ti^{49}. In both, an exceptionally strong γ ray is emitted leading to the first-excited state, and a somewhat weaker γ ray to the second-excited state. Holt and Marsham[29] have shown that in Ca^{41} both excited states are p states. In Ca^{41}, therefore, it is certain, and in Ti^{49} it is very probable, that the strong γ ray is $E1$. The level systems of both nuclei are probably very similar, for in Ca^{41} the unpaired neutron is the only occupant of the $f_{7/2}$ shell, and in Ti^{49} there is one neutron less than that required to fill the shell. Therefore, the ground states of both nuclei almost certainly have spin 7/2 and the ground-state γ rays must be $E3$. The ratio of the measured upper limit of the intensity of this γ ray to the intensity of the $E1$ γ ray gives an upper limit for the emission probability of $E3$ radiation relative to $E1$. A detailed account of the γ rays emitted by these nuclei is given in Appendixes E and F.

2.2. Intensities of Ground-State γ Rays in Heavy Even-Charge Nuclei

The investigation of these nuclei is still incomplete.[30] Those even-charge nuclei which have already been studied are listed in Table III according to the multipole order of the ground-state γ ray expected from shell structure.[31]

An inspection of Table III shows that the ground-state γ rays, like those in the lighter elements, are relatively strong when the shell model predicts that they are of $E1$ type and relatively weak when they are of $M1$ type or of higher order, in agreement with the conclusions of the previous section. This is confirmed by a few examples, such as Sr^{87}, where a very strong γ ray[30] is observed producing an excited state which is known to be a p state from the evidence of isomeric transitions.

There are two exceptions: Se^{78}, where the ground-state γ ray (10.6 Mev) is some fifteen times weaker than that producing a low-energy excited state, and Hg^{200}, where the ground-state γ ray apparently is not detected, for the highest-energy γ ray observed has an energy much less than that expected of the neutron binding energy in that nucleus. Both nuclei are even-even, and, according to the shell model, the ground states of the even-odd target nuclei are $p_{1/2}$ states. It can be seen from Table I that a weak ground-state γ ray would indicate that the thermal capture occurs predominantly in a state with zero spin. In mercury, the greater part of the thermal neutron capture cross section appears to be caused by a negative energy resonance[32] in Hg^{200}. The above evidence that the spin of this resonance is zero is not consistent with the interpretation of measurements of the scattering of neutrons at thermal energies[33] which indicate spin 1.

The outstanding intensities of the lead γ rays will be discussed in a later section.

TABLE III. Lowest multipole orders and intensities (reference 30) of ground-state γ rays in heavy even-charge nuclei in photons per 100 captures in the separated isotope.

$E1$		$M1$		Higher orders		
Se^{77}	4	Cd^{114}	0.14	Sr^{87}	($E4$)	<1[a]
Se^{78}	0.3	Sn^{118}	0.3[a,b]	Sr^{88}	($E4$)	<0.05[a]
W^{183}	10[a]	Ba^{138}	0.3	Zr^{92}	($E2$)	1
W^{184}	3			Mo^{96}	($E2$)	0.05
W^{187}	4[a]			Sm^{150}	($E3$ or $M4$)	<0.05[a]
Pt^{194}	0.3[b]			Gd^{158}	($E3$)	<0.03[a]
Hg^{200}	<0.1[a]					
Pb^{207}	100					
Pb^{208}	100					

[a] γ ray not detected.
[b] Minimum value; contribution of isotope to total capture cross section unknown.
[c] Identification of γ ray not certain.

2.3. The Intensity of Ground-State γ Rays in Odd-Charge Nuclei

The products of neutron capture in odd-charge nuclei are mainly nuclei of the odd-odd type. (The only odd-even nucleus which has been examined in detail is N^{15}; to a lesser extent the γ rays of K^{41} and V^{51} have been studied.) The identification of the capture γ rays produced by odd-odd nuclei is more difficult than the identification of those of even-charge nuclei, for the density of levels and, therefore, the total number of γ rays emitted, is much greater. In many heavy odd-odd nuclei, the highest energy γ rays have not been resolved. Furthermore, the ground-state radiation is generally

[28] This is true if the nucleus contains three or five $f_{7/2}$ neutrons. For example, it would appear that the spin of 5/2 for Mn^{55} is caused by the coupling of five $f_{7/2}$ protons. See Mayer, reference 10.
[29] J. R. Holt and T. N. Marsham, Proc. Phys. Soc. (London) **A66**, 565 (1953). We are indebted to Dr. Holt for the privilege of seeing these results before publication.
[30] B. B. Kinsey and G. A. Bartholomew, Can. J. Phys. **31**, 1051 (1953).
[31] See P. F. A. Klinkenburg, Revs. Modern Phys. **24**, 63 (1952).
[32] W. W. Havens and J. Rainwater, Phys. Rev. **70**, 154 (1946).
[33] Hibdon, Muehlhause, Ringo, and Robillard, Phys. Rev. **82**, 560 (1951).

TABLE IV. Intensities of the ground-state γ rays in odd-charge nuclei in photons per 100 captures in the separated isotope. For those γ rays marked with an asterisk the multipolarity is the same regardless of the spin of the capturing state. For the others, the lowest multipole order of the "composite" radiation is given.

E1		*M1*		Higher orders		
*N^{15}	20[a]	*F^{20}	20[b]	Na^{24}	(*E2*)	<1[b]
*K^{42}	30[c]	*Al^{28}	35[b]	K^{40}	(*M2*)	<0.3[c]
Sc^{46}(?)	0.3[d]	P^{32}	0.5[b]	Nb^{94}	(*E2*)(?)	0.4[c]
*V^{52}	7[f]	*Cl^{36}	3[b]	In^{114}	(*E4*)	<0.05[e]
*Mn^{56}	12[d]	Sb^{122}	1[e]	Au^{198}	(*M2*)	<0.3(?)[e]
*Co^{60}	3[d]					
*Cu^{64}	24[d]					
*Cu^{66}	50[d]					
*Rh^{104}	0.2[c]					
*Ag^{108}	1.2[c]					
*Pr^{141}	2[c]					
Ta^{182}	0.7[c]					
*Tl^{204}	5[c]					

[a] See reference 34.
[b] See reference 12.
[c] See reference 48.
[d] See reference 36.
[e] See reference 46.
[f] The intensities for vanadium in reference 12 are too large by a factor of 1.6.

composite. This last difficulty is removed when thermal capture is dominated by one resonance or, for dipole radiation, when the spin of the final state in the product nucleus is equal to $J\pm1/2$ (see Table I). In such cases, the multipole order of the ground-state γ rays or those leading to some low-lying states may be determined when the relevant spins and parities are known. The ground-state spin has been directly measured for only a very few odd-odd nuclei, but in many cases it can be inferred from the β activity. In others, recent measurements of the angular distribution of the protons in the (d,p) reaction are of assistance.

The intensities and multipolarities of the ground-state γ rays from odd-charge nuclei are listed in Table IV. A casual inspection of this table will show that there is no obvious regularity of the kind shown in the even-charge nuclei (Table II).

2.3.1. *The E1 γ Rays*

In the lighter elements, the *E*1 ground-state γ rays are generally strong, although that of Sc^{46} is an exception. For the remaining nuclei, excepting Cu^{64} and Cu^{66}, the *E*1 ground-state γ rays do not dominate the spectrum as they do in the even-charge nuclei. We shall now consider some of the salient features of these spectra.

The γ rays produced by N^{15} have been described elsewhere.[34] An unexplained feature is the relative weakness of the *E*1 ground-state γ ray: it is weaker than the γ ray of half the energy emitted in the transition to the first excited state. Moreover, it is not much stronger than the γ rays producing highly excited states, some of which, according to the results of Gibson and Thomas,[35] must be *M*1.

[34] Kinsey, Bartholomew, and Walker, Can. J. Phys. **29**, 1 (1951).
[35] W. M. Gibson and E. E. Thomas, Proc. Roy. Soc. (London) **A210**, 543 (1952).

feature of N^{15} is the relative weakness of the ground-state γ ray: it is weaker than the γ ray of half the energy emitted in the transition to the first excited state.

If correctly identified as an *E*1 γ ray, the weakness of the ground-state γ ray in Sc^{46} is unusual. This weakness might result from the high density of excited states in this nucleus.[36] It is, however, much weaker than other γ rays leading to excited states. It is quite possible that its multipole order has not been correctly identified,[37] for the assumption that this γ ray is *E*1 is based on the spin of Sc^{46} being 4 units.[38]

The three nuclei V^{52}, Mn^{56}, and Co^{60} produce rather similar γ-ray spectra.[36] In each case the thermal neutron capture cross section appears to be derived mainly from the lowest resonance, and in each case the ground-state γ ray, or the γ ray with the highest energy, is almost certainly of *E*1 type (see Appendix G). An interesting feature common to these three nuclei is that many other γ rays are produced with very similar intensities; presumably, they also are *E*1.

The nuclei Cu^{64} and Cu^{66} differ from all other odd-charge nuclei in that the *E*1 ground-state γ rays (see Appendix G) like those of the even-charge nuclei in Group 4, are by far the strongest in the spectra. Moreover, the spectra appear simpler than those of neighboring odd-odd nuclei. This simplicity, together with the great strength of these ground-state γ rays, may be caused by a wider spacing of the levels near the ground-state.

2.3.2. *The M1 γ Rays*

The *M*1 γ rays emitted by the odd-charge nuclei show some wide variations in intensity and some interesting anomalies.

In the two nuclei P^{32} and Cl^{36} the *M*1 ground-state γ rays are of relatively low intensity. In P^{32} the ground-state γ ray is much weaker than a number of other high-energy *M*1 γ rays which are also emitted by the capturing state (see Appendix G). The fact that neutron capture in P^{31} is nonresonant might account for the weakness of the ground-state γ ray and for the lack of uniformity in the intensities of other high-energy *M*1 γ rays in P^{32}. In Cl^{36}, where the thermal neutron capture

[36] G. A. Bartholomew and B. B. Kinsey, Phys. Rev. **89**, 386 (1953).
[37] The spin of Sc^{45} being 7/2, this γ ray will be *E*1 regardless of the spin of the capturing state, provided that the spin of the ground state of Sc^{46} is 4 units. The assignment of 4 units for the spin rests on the assumption that the spin of the isomeric state is 7 units, for the isomeric transition is *E*3 or *M*3. If the spin of the ground state were 5, which would be consistent with its β decay, the spin of the isomeric state would have to be 8 or 2, of which the former is inconsistent with any simple interpretation of the shell model. Such evidence as exists on the decay of the isomeric state, however, does not exclude the possibility that its spin is 2. In that event, it is quite possible that the ground state (with spin 5) is produced by neutron capture more often from a compound state of spin 3 than from spin 4. This could account for the observed weakness of the ground-state γ ray.
[38] M. Goldhaber and R. D. Hill, Revs. Modern Phys. **24**, 179 (1952).

is resonant,[39] the intensities of the high-energy γ rays are much more uniform.

The $M1$ ground-state γ rays in F^{20} and in Al^{28} are exceptionally strong[12] and dominate the spectrum of these nuclei. This is peculiar in that the level systems of both nuclei are more complicated than in even-charge nuclei of similar atomic weight.

The spin[40] of the ground state of F^{20} is probably 1, and therefore the ground-state γ ray is $M1$. It is possible that the anomalous strength of this γ ray is connected in some way with the unusual configuration of the ground state, which does not decay to the ground state of Ne^{20} except by a forbidden transition. Such a conclusion, however, is purely speculative, for no similar explanation is appropriate to Al^{28}.

In Al^{28}, the strength of the ground-state γ ray is especially striking, for this nucleus possesses the most complicated level system of any light nucleus yet examined.[41] Recent measurements show that the energy of this γ ray is indeed that of the neutron binding energy of Al^{28}, and is not to be confused with the transition to the low-lying excited state at 31 kev.[42] The ground-state γ ray is probably (but not certainly) $M1$, for measurements on the angular distribution of the (d,p) reaction (which do not resolve the ground-state doublet) show that the configuration of the unpaired neutron in the ground-state, in the 31-kev state, or in both, is that of an s state.[43] However, it is not clear from the measurements that, if the unpaired neutron in the 31-kev state is in an s state, the ground-state could not be a p state; but in view of the even parities of the ground-states and of low-lying states in this region of the periodic table, this possibility seems most unlikely.[44] It is most probable that both the ground-state and the 31-kev state are s states for the unpaired neutrons. The great strength of the ground-state γ ray and the relative weakness of the remaining γ rays is difficult to explain. The latter cannot all be $E2$ radiations, for at least one component of the doublet at 1.0 Mev appears to have a spin of either 2 or 3 units.[45] We conclude that most of these γ rays also must be $M1$ radiations and that the remarkable prominence of the ground-state γ ray is due to some peculiar property of the ground state possibly associated with the presence of the unpaired proton.[45]

2.3.3. E2, M2, and Higher-Order γ Rays

No γ rays which are known to be of the $E2$ or $M2$ type or of higher orders have been observed in studying the light odd-charge nuclei. Among the heavy elements, the identification of the highest energy γ ray with the ground-state transition is usually uncertain, because the higher-energy γ rays detected are seldom completely resolved, even when the line width of the instrument is 100 kev, and the errors in the neutron binding energies (obtained from other sources) are usually less than the mean spacing of the levels near the ground state. In gold,[46] where the highest-energy γ ray, A, has an energy close to the known neutron binding energy, we do not know for certain whether this γ ray is the $M2$ ground-state γ ray or whether it is emitted in a transition to a low-lying excited state. From a consideration of the absolute intensities of the gold γ rays it seems much more probable that the observed high-energy gold radiations are all $E1$, and that the $M2$ ground-state γ ray was not detected.

Until recently, the ground-state γ ray in the nucleus K^{40} seemed anomalous. The existence of a strong γ ray with an energy near the known neutron binding energy of K^{40} has been pointed out in a previous communication.[13] Since the spin of K^{40} is known to be 4 units[47] and that of K^{39} is $3/2$, it follows that the ground-state γ ray is composite with $M2$ and $E3$ components. It is now known that a low-lying state exists in K^{40} near 30 kev, and that the energy of the strong γ ray is in good agreement with the energy expected for a direct transition to this state.[48] If, as seems probable, the spin of this state were 2 units, the γ ray would be $E1$ regardless of the spin of the capturing state. The coincidence peak produced by this γ ray is very well defined and there is no evidence of a peak lying just above it which could be due to the $M2$ γ ray.

3. RELATIVE EMISSION PROBABILITIES

It is impossible to obtain reliable information on the relative emission probabilities of different multipoles

[39] C. T. Hibdon and C. O. Muehlhause, Phys. Rev. **79**, 44 (1950).
[40] Bromley, Bruner, and Fulbright, Phys. Rev. **89**, 396 (1953).
[41] Enge, Buechner, and Sperduto, Phys. Rev. **88**, 963 (1952).
[42] The energy corresponding to the end point of the coincidence peak is in good agreement with that corresponding to the neutron binding energy of Al^{28} (see reference 23). The equivalent energy displacement between the peak of the coincidence curve and the observed end point is normal. If the greater part of the peak coincidence counting rate were due to a transition to the 31-kev state, this displacement would be greater than the normal value by 31 kev, and such a difference would be easily detected (see Appendix A).
[43] H. R. Holt and T. N. Marsham, Proc. Phys. Soc. (London) **A65**, 763 (1952); Proc. Phys. Soc. (London) **A66**, 249 (1953).
[44] An indication that the ground-state γ ray must have a lower rate of emission than that expected of $E1$ radiation is afforded by the existence of a γ ray with an energy of 7.34 Mev and an intensity fifty times lower. As pointed out in a previous communication (see reference 12), this γ ray must arise from a transition from a highly excited state, which, in turn, is excited in a transition of 0.38 Mev. If the 0.38-Mev transition and the ground-state transition were of the same multipole order, the intensity of the former should be lower by a factor of 10^4. The fact that it is only 50 times lower suggests very strongly that it is $E1$, while the ground-state γ ray is $M1$.
[45] It has been pointed out by M. Vosko [thesis, McGill University, 1952 (unpublished)] that the relative strengths of the Al^{28} $M1$ γ rays might be explained on the basis of an extension of the single particle selection rules to take account of the odd neutron and odd proton. For an allowed transition, then, $\Delta J = \pm 1$ and for a forbidden transition, $\Delta J = 0$. There is as yet little evidence to show whether these selection rules apply.
[46] G. A. Bartholomew and B. B. Kinsey, Can. J. Phys. **31**, 1025 (1953).
[47] Z. A. Zacharias, Phys. Rev. **61**, 270 (1942).
[48] G. A. Bartholomew and B. B. Kinsey, Can. J. Phys. **31**, 927 (1953); Buechner, Sperduto, Browne, and Bockelman, Phys. Rev. **91**, 1502 (1953).

TABLE V. Ratios of emission probabilities of pure $M1$ and $E1$ radiation.

Nucleus	$E1$ γ Ray	$E1$ Energy	$E1$ Intensity	$M1$ γ Ray	$M1$ Energy	$M1$ Intensity	Ratios of corrected intensities
Mg^{25}	J	3.92 Mev	0.90	E	6.75 Mev	0.020	0.5 percent
Si^{29}	M	3.54 Mev	0.60	B	8.47 Mev	0.022	0.3 percent
S^{33}	G	5.43 Mev	0.60	B	7.78 Mev	0.016	0.9 percent
						Mean	0.6 percent

except in even-odd nuclei or such odd-odd or even-even nuclei for which the thermal neutron energy lies close to that of a resonance. There are as yet very few data on the parities and spins of the excited states of odd-charge nuclei which exhibit resonant capture, and consequently it is not yet possible to compare the emission probabilities for γ rays emitted by elements in this group. Among the few even-even nuclei which are known to capture thermal neutrons in one spin state only, there is only one, Cd^{114}, for which something is known about the character of the low-lying states.

3.1. Relative Emission Probabilities of $E1$ and $M1$ Radiation

In the even-odd nuclei we have found three examples of $E1$ radiation in competition with pure $M1$ radiation. We list these examples in Table V. In the last column of this table we give the ratios ($M1$ to $E1$) of the emission probabilities; these quantities are equal to the ratios of the intensities divided by the ratios of the cubes of the respective energies.

The mean ratio of the emission probabilities is of the order of magnitude expected theoretically[6,49] on the single-particle model, *viz.*, $10(\hbar/McR)^2$, which, for a nucleus of mass 30, is about 2 percent.

It is important to note that all three $M1$ γ rays given in Table V violate the orbital angular momentum selection rules for single-particle transitions. In each case, the transition is $s_{1/2} \rightarrow s_{1/2}$ for the odd neutron.[50] Among the even-even and odd-odd product nuclei we have found, unfortunately, no examples in which an $E1$ and a competing allowed $M1$ γ ray can be compared.

3.2. Relative Emission Probabilities of $E2$ and $E1$ Radiation

Only one nucleus, Mg^{25}, has been found[12] in which a pure $E2$ γ ray (the γ ray C) is in competition with an $E1$ γ ray (J). (The γ ray C is 7.32 Mev and the γ ray J, 3.92 Mev.) Since the emission probability of $E2$ radiation increases as the fifth power of the energy, while that of $E1$ radiation increases as the cube, such a comparison has meaning only at one energy. If we choose 7 Mev, we find that the ratio of emission probabilities of $E2$ to $E1$ radiation is 0.05 percent.

It would appear from this result that, at 7 Mev, the emission probability of $E2$ is an order of magnitude less than that of $M1$ radiation and of the same order as that given by Weisskopf's formula.[6] Although this instance is the only one in which such a direct measurement can be made, there is additional evidence which shows that the emission probability of $E2$ is not greater than that of $M1$ radiation. For example, near 7 Mev, if the emission probability of $E2$ radiation were greater than that of $M1$ radiation, the intensities of those γ rays which could, theoretically, consist of mixtures of $M1$ and $E2$ components, would be greater than that of pure $M1$ γ rays. In Cd^{114}, the γ ray B (8.48 Mev)[30] could contain both $E2$ and $M1$ components arising from a transition from an initial state of spin 1 and a final state of spin 2. This γ ray is only a little stronger than the pure $M1$ γ ray leading to the ground state (9.046 Mev). Similar instances occur in Si^{29} and S^{33}. In Si^{29}, the mixed γ ray, E (7.19 Mev), has an intensity only four times that of the pure $M1$ ground-state γ ray (8.47 Mev). In S^{33}, the mixed ground-state γ ray is nearly equal in intensity to that of the pure $M1$ γ ray producing the first-excited state. However, the mixed transitions in Si^{29} and S^{33} involve a change in the orbital angular momentum of 2 units (they are transitions of the type $s_{1/2} \rightarrow d_{3/2}$), which on the single-particle model are forbidden for $M1$ radiation. It would be possible to argue, therefore, that the mixed transitions emit exclusively $E2$ radiation, and that the relative intensities observed are the relative intensities of $E2$ to $M1$ radiation. However, the apparent absence of suppression of $M1$ radiation in the $s_{1/2} \rightarrow s_{1/2}$ transition in Si^{29} and Mg^{27}, and the strength of $E2$ γ rays corresponding to single-neutron transitions both suggest that the single-particle selection rules do not hold.

3.3. Relative Emission Probabilities of $E3$ (or $M2$) and $E1$ Radiation

In the few nuclei in which $E3$ radiations might be detected (e.g., those of Group 3 of Table II), these γ rays are in some instances in competition with $E1$ radiations of comparable energy. The emission probability at 7 Mev is certainly less than 0.1 percent of that of $E1$ radiation. This upper limit, however, is of the same order of magnitude as the relative emission probability of $E2$ to $E1$ radiation. To improve upon the measured upper limit for the intensity of $E3$ radiation emitted in competition with $E1$ radiation is extremely difficult, even in the most favorable case, *viz.*, Ca^{41}. A reliable estimate of the emission probability of $E3$ radiation can be made best by comparison with $M1$ or $E2$ radiation in a nucleus in which $E1$ radiation does not contribute appreciably to the total radiation width. No suitable nucleus has yet been found.

[49] J. M. Blatt and V. F. Weisskopf, *Theoretical Nuclear Physics* (John Wiley and Sons, Inc., New York, 1952).

[50] All $M1$ γ rays emitted by the capturing states formed by the capture of thermal neutrons in even-even nuclei must violate such selection rules. The only other single-particle transition which can give rise to $M1$ radiation from the capturing state is $s_{1/2} \rightarrow d_{3/2}$, which is also forbidden.

It is not possible, from the existing data, to compare directly the strength of $M2$ radiation with that of $E1$ or any higher multipole. Only two even-odd nuclei, Ni^{61} and Zn^{65}, have been examined in which $M2$ ground-state γ rays are expected to occur. It has already been shown (Sec. 2.1.1) that there is some doubt that the γ rays observed are actually ground-state γ rays. Resonant capture occurs in the odd-odd nucleus, Au^{198}, and the ground-state γ ray emitted must be of the $M2$ type.[46] However, in this instance also, there is no direct proof that the γ ray detected is the ground-state γ ray (see Sec. 2.3.3).

4. ABSOLUTE EMISSION PROBABILITIES

It is of interest to examine the nuclear properties which determine the absolute emission probability or, in other words, the experimental radiation width Γ_r for a γ ray r. The widths of transitions of the same type in different nuclei may be compared among themselves and with theoretical predictions. If radiation is assumed to be emitted through the motion of a single proton or a neutron in the nucleus, the theoretical widths $\Gamma_{th}(E1)$ and $\Gamma_{th}(M1)$, for electric and magnetic dipole radiation, according to Weisskopf,[6] may be expressed in terms of the energy E and the radius of the nucleus R, as follows:

$$\Gamma_{th}(E1)=0.047E^3R^2,$$
$$\Gamma_{th}(M1)=0.021E^3,$$

where the units are so chosen that E must be expressed in Mev, R in units of 10^{-13} cm, and Γ_{th} in ev. The complete expressions for the widths include statistical factors which depend on the quantum numbers of the initial and final single particle states. These quantities are not included in the above expressions.

For purposes of comparison it is convenient to use the quantity $(2J_i+1)|M|^2$, where J_i is the spin of the initial state,[51] and $|M|^2$ is the ratio of the observed radiation width to Γ_{th}, the width predicted by the individual particle formula, and is a measure of the matrix element of the transition.

For emission by highly excited states, where the single-particle approximation is not expected to hold, Blatt and Weisskopf[10] have predicted that the radiation width will also be proportional to D, the average level spacing near the initial state between levels which combine with the lower state with the emission of radiation of the same multipole order. An order of magnitude estimate for the proportionality constant, as shown by Blatt and Weisskopf, is 2 Mev^{-1}. Therefore, for high-energy neutron capture γ rays, the quantity $(2J_i+1)(|M|^2/2D)$ is a better measure of the matrix element.

If the total radiation width of a nuclear state is Γ_γ, then $\Gamma_r=I_r\Gamma_\gamma$, where I_r is the intensity of the γ ray in photons per disintegration. Thus, the partial width of any γ ray emitted by the capturing state may be obtained if the radiation width of a low-lying s-wave resonance is known, and if it can be assumed that the observed absolute intensity of the γ ray produced by thermal-neutron capture is identical with that which would be observed for neutron capture at exact resonance. Such an assumption is probably justified in relation to s-wave resonances in even-odd product nuclei, for, in these nuclei, the spin of all s-wave resonances is 1/2. In even-even or odd-odd product nuclei, we can assume that the observed γ-ray intensities are those which apply at exact resonance only when it is known that the thermal neutron capture cross section is determined entirely by the nearest resonance. Unfortunately, a calculation of the radiation width can be made for only a few nuclei, and, even in these, the validity of the calculation is difficult to estimate. However, in odd-odd nuclei if the spin of the final state differs from that of the ground state of the target nucleus by 1/2, both components of the composite radiation will be of the dipole type. In such a case it is probably sufficient (though not strictly correct) to take the radiative width of any s resonance as the appropriate width for the calculation of the partial width of the ground-state γ ray even though thermal capture is not resonant. The error committed will certainly be small in heavy nuclei where the radiation widths for the two types of s resonance should be almost identical.

In the heavy elements, there is no difficulty in estimating the radiation width, for the greater part of the total width is due to radiation and the low-lying resonances can all be taken as s resonances. The total widths are remarkably constant and for the present purposes no serious error is committed if we assume that $\Gamma_\gamma\simeq 0.1$ ev. However, such an assumption is probably incorrect for lead and bismuth, which have abnormally simple capture γ-ray spectra. In the lighter elements, from atomic weight 80 downwards, the radiation width usually contributes only a small fraction to the total widths of low-lying resonances. The radiation width can be determined by measurement of the absorption cross section by activation methods at the resonance energy, from a measurement of the resonance absorption integral, or by a direct measurement of the resonance yield of capture γ rays. The last method is very difficult and has not yet been accomplished. The activation methods are usually applicable to the odd-charge nuclei but are not suitable to the even-charge nuclei of interest here, for these are either stable, or have activities which are unsuitable for measurement. In these cases, the only available quantity is the thermal neutron capture cross section, and the radiation width may be calculated from this only if a nearby resonance is assumed to be responsible for it. This restriction reduces the number of nuclei which can be examined and eliminates all of the interesting nuclei in Group 4 of Table II.

[51] We adopt here the procedure used by Goldhaber and Sunyar (see reference 1) and others. Although $(2J_i+1)$ is not the correct statistical factor (see references 49 and 62) we include it for convenience in comparing the present results with other data (see reference 56).

TABLE VI. Emission probabilities of $E1$ radiation. Where relevant, the energy of the resonance presumed responsible for the thermal neutron capture is given in the second column and its parameters in the third and fourth. D is the estimated mean level spacing at the neutron binding energy. The γ ray is designated according to the system used in previous communications and its intensity is given in photons per capture in the separate isotope.

Nucleus	Resonance energy	Γ_n	Γ_γ ev	D Mev	γ ray	E Mev	I_γ photons per capture	$(2J_i+1)\|M\|^2$	$(2J_i+1)\|M\|^2/2D$
Even-charge nuclei:									
Si^{30}	170 kev[a]	37 kev[a]	14	0.5	M	3.54	0.6	0.4	0.4
S^{32}	108 kev[b]	18 kev[b]	26	0.3	G	5.43	0.6	0.2	0.3
W^{183}			0.07[d]	1×10^{-5}[d]	D	6.18	0.13	2.3×10^{-5}	1.2
W^{184}			0.1[e]	4×10^{-5}[d]	A	7.42	0.036	$\geq 5\times10^{-6}$	0.06
W^{187}			0.15[d]	1×10^{-4}[d]	F	5.24	0.06	4×10^{-5}	0.2
Odd-charge nuclei:									
V^{52}	2700 ev[e]	780 ev[e]	1.0	2×10^{-2}	A	7.31	0.07	1×10^{-3}	0.02
Mn^{56}	345	22[f]	0.6[f]	2×10^{-3}	A	7.26	0.12	8×10^{-4}	0.2
Co^{60}	120	4[g]	0.27[g]	1×10^{-3}	A	7.48	0.03	1×10^{-4}	0.05
Cu^{64}			0.2[g]	1×10^{-3}[e]	A	7.91	0.25	2×10^{-4}	0.1
Cu^{66}			0.2[g]	1×10^{-3}[e]	B	7.63	0.5	5×10^{-4}	0.3
Rh^{104}	1.3		0.16[b]	1×10^{-4}[e]	A	6.79	0.002	1×10^{-6}	0.006
Ag^{108}			0.1[e]	5×10^{-5}	A	7.27	0.01	3×10^{-6}	0.03
Ag^{110}	5.2		0.17[d]	5×10^{-5}	D	6.67	$\leq$0.004	$\leq 2\times10^{-6}$	$\leq$0.02
								Mean	0.26

[a] See U.S. Atomic Energy Commission Report AECU-2040, 1952 (unpublished).
[b] See reference 57.
[c] Assumed value.
[d] Calculated from results obtained by W. Selove, Phys. Rev. **84**, 869 (1951).
[e] See reference 83.
[f] See reference 84.
[g] See Appendix G.
[h] V. L. Sailor, Phys. Rev. **91**, 53 (1953).

Now, D is the average spacing near the neutron binding energy between states which have the same spin and parity as the initial state.[52] In the heavy elements such spacings are not difficult to estimate, for only s resonances are detected in neutron transmission measurements. In the light elements, however, where the spacing of resonances may be 50 kev apart, p-wave and higher-wave resonances are detected, and D must be estimated from those resonances which show the characteristic s-wave interference with the potential scattering. Since only a few of these are usually recognizable, estimates of their spacing are less reliable than those obtained from the heavy elements.

It is well known that a quantity depending on the ratio of the radiation width to the spacing can be obtained from the capture cross sections of medium-fast neutrons. For s-wave neutrons, this capture cross section is related to Γ_γ/D through the equation $\bar{\sigma}=2\pi^2\lambda^2\Gamma_\gamma/D$, where D is a mean level spacing for s resonances. The observed values of $\bar{\sigma}$, however, for neutrons of 200 kev and 1 Mev,[53] give values for Γ_γ/D which are too high by factors between 2 and 10. This discrepancy is due mainly to the contributions of higher orbital angular momenta, which, in elements such as nickel, are large even for neutrons with energies as low as a few tens of kilovolts.[54] It is not possible, however, to estimate the contributions to $\bar{\sigma}$ made by the different angular momenta, and for this reason we have found it necessary here to reject all data based on fast neutron capture cross sections and to use only those results which give separately the two quantities required. Even if this method were free from objection, it would not, in general, yield the information required for the capture cross sections for fast neutrons have been determined by activation measurements which exclude most even-charge nuclei.[55]

4.1. $E1$ Radiation

The results of the comparison of $E1$ radiations are listed in Table VI. It will be seen that the quantities $(2J_i+1)|M|^2$ (column 9) vary over a range of 10^5 while division by $2D$ (column 10) eliminates the greater part of this variation. The matrix elements for the odd-charge nuclei tend to be rather lower than those for even-charge nuclei, but, as will be shown below, none of these entries is completely reliable for one reason or another, and, therefore, this apparent dependence on Z may be spurious. A similar constancy in the rate of emission of $E1$ radiations produced by proton capture in the lightest elements has been reported by Wilkin-

[52] To calculate D, we assume that the spacing between states with spins $J+1/2$ is identical with that between states with spin $J-1/2$, where J is the spin of the target nucleus. Then D is equal to the spacing of s-wave resonances when $J=0$ and twice this spacing when $J\neq0$.

[53] H. Halban and L. Kowarski, Nature **142**, 393 (1938); J. H. E. Griffiths, Proc. Roy. Soc. (London) **A170**, 513 (1939); Hughes, Spatz, and Goldstein, Phys. Rev. **75**, 1781 (1949); L. E. Beghian and H. Halban, Nature **163**, 366 (1949).

[54] A detailed and consistent analysis of some fast-neutron capture cross-section measurements has been given by B. Margolis, Phys. Rev. **88**, 327 (1952).

[55] An exceptionally large value for the radiation width of Ni^{59} has been obtained by E. P. Wigner [Am. J. Phys. **17**, 99 (1949)]. However, it is now known that the activity observed was almost certainly not that of Ni^{59}, which has a very long period; see H. W. Wilson, Phys. Rev. **82**, 548 (1951).

son,[56] although no variation with even or odd Z was noted. The agreement of the theoretical predictions with experiment is perhaps surprising in view of the approximate nature of the theory.

Only those nuclei have been included in Table VI for which the radiation widths or the level spacings near the binding energy can be estimated with some assurance. Probably for neither quantity can such estimates be made to better than a factor of two. As already pointed out, no data are available suitable for the calculation of radiation widths of those nuclei in Group 4 of Table II and the same difficulty is encountered for the two nuclei Be^{10} and C^{13} in Group 1 of that table. Of the heavier nuclei in Table III, the isotopes of lead also are unsuitable, since the radiation widths are not available. The isotope Se^{77} cannot be used because nothing is known about the level spacing D. In Se^{78} the degree to which capture occurs in a state of spin zero is not known. The nucleus Pt^{196} is not included because the capture cross section of Pt^{195} has not been measured, because the radiation width in Pt^{196} is unknown, and because the radiation is composite.

Both silicon and sulfur show a marked resonance at low energies which is responsible for their low scattering cross sections at thermal energies. In S^{33} the shape and energy dependence of the scattering cross section at low energies has been studied by Adair, Bockelman, and Peterson,[57] who showed that the 108-kev resonance was responsible for it; the scattering length at thermal energies can also be accounted for by this resonance.[58] Silicon is similar but no detailed analysis has yet been made. For both nuclei we assume that the thermal neutron capture is due to the lowest resonance and we have calculated the value of the radiation width from the thermal capture cross section and the measured neutron width. There is, as yet, no quantitative check on the validity of this procedure and the results obtained, therefore, must be taken as a rough indication only of the required width. For W^{183} and W^{187} we have assumed without any direct confirmatory evidence that the γ rays listed are the ground-state γ rays. The identification of the ground-state γ ray in W^{184} is certain, but it appears that thermal capture cannot be accounted for entirely by the parameters of the resonance at 4 ev, and, therefore, the value of $|M|^2$ is a lower limit.

Among the odd-charge elements, thermal neutron capture in vanadium, manganese, and cobalt appears to be caused in the main by a low-lying resonance in each case (see Appendix G). The spacings assumed for these nuclei, however, are very rough, and may well be overestimated. For the copper isotopes, the radiation width (0.2 ev) is a very rough value consistent with slow-neutron measurements (see Appendix G). The spacings assumed for the copper nuclei are mere estimates. In the silver isotopes, the identification of the ground-state γ ray is not absolutely certain. The same is true of rhodium. In this element the spacing is uncertain, for only one resonance (at 1.3 ev) has been detected in a range of 100 ev.

Other nuclei which are expected to emit $E1$ ground-state γ rays but which have not been examined are those of Br, Y, Tm, Hf, and Ir. The two nuclei Pr^{142} and Tl^{204} emit $E1$ ground-state γ rays which have been studied, but these nuclei are excluded from the table because they both lie near closed shells and may, therefore, have somewhat larger level spacings than neighboring nuclei and may possess radiation widths which differ considerably from 0.1 ev. Both quantities are unknown for both nuclei. The nucleus Ta^{182} is excluded because it seems probable that the ground-state γ ray was not resolved.

4.2. $M1$ Radiation

The matrix elements for $M1$ radiations and the data from which they were calculated are listed in Table VII. It will be seen that, except for the F^{20} and Al^{28} ground-state γ rays, the correction for the level spacing yields remarkably constant values while the spacing varies over a factor of nearly 10^4. The matrix elements agree with the predictions of Blatt and Weisskopf[49] for F^{20} and Al^{28} but are lower by an order of magnitude for most of the other nuclei shown.

The cadmium data are unsatisfactory in that only one resonance has been detected; the values for D in Table VII were obtained on the assumption that the spacing of all s resonances is 50 ev, a value consistent with that deduced from the neutron width[49] of the 0.17-ev resonance.

The radiation widths of the F^{20} and Al^{28} nuclei have been obtained by direct methods. Rough (and possibly too high) values have been given by Henkel and Barschall.[59] For Al, these authors give $\Gamma_\gamma = 5$ to 15 ev; their results were obtained from the ratio of peak absorption to peak scattering cross sections and are rather smaller than those which can be derived from slow-neutron measurements.[60] We adopt the low value $\Gamma_\gamma = 5$ ev.

5. MECHANISM OF THE RADIATIVE PROCESS

The ratio of the rates of emission of $M1$ and $E1$ radiation, in the few cases where they have been directly compared (Sec. 3. 1), are in agreement with Weisskopf's formula. The absolute values of the emission rates of $M1$ and $E1$ radiation tend to be lower than (but within an order of magnitude of) the values given by the single-particle formula when that formula is modified to take into account the complexity of the initial state. This agreement is remarkable in view of the very large corrections which have been made.

It is clear that the complexity of the initial state must

[56] D. H. Wilkinson, Phil. Mag. 44, 450 (1953).
[57] Adair, Bockelman, and Peterson, Phys. Rev. 76, 308 (1949).
[58] D. C. Peaslee, Phys. Rev. 85, 555 (1952).
[59] R. K. Henkel and H. H. Barschall, Phys. Rev. 80, 145 (1950).
[60] Harris, Muehlhause, and Thomas, Phys. Rev. 79, 11 (1950).

TABLE VII. Emission probability of $M1$ radiation. For explanation of headings, see caption of Table VI.

Nucleus	Resonance energy	Γ_n	Γ_γ ev	D Mev	γ ray	E Mev	I_γ photons per capture	$(2J_i+1)\lvert M\rvert^2$	$(2J_i+1)\lvert M\rvert^2/2D$
Even charge									
Si^{29}	170 kev[a]	37 kev[a]	14	0.5	B	8.47	0.02	0.04	0.04
Si^{29}	170 kev	37 kev	14	0.5	E	7.19	0.08	0.3	0.3
S^{33}	108 kev[b]	18 kev[b]	26	0.3	A	8.65	0.012	0.05	0.08
S^{33}	108 kev	18 kev	26	0.3	B	7.78	0.016	0.08	0.14
Cd^{114}	0.17 ev		0.11[c]	$\sim 10^{-4}$	A	9.05	0.0014	3×10^{-5}	0.15
Cd^{114}	0.17 ev		0.11	$\sim 10^{-4}$	B	8.48	0.0023	6×10^{-5}	0.3
Odd charge									
F^{20}			15[d]	0.4	A	6.63	0.2	1.0	1.2
Al^{28}			5[e]	0.3	A	7.72	0.35	1.1	1.8
Al^{28}			5[e]	0.3	C	6.77	0.014	0.06	0.1
Cl^{36}			0.3[f]	0.04[g]	A	8.56	0.03	2.7×10^{-3}	0.03
								Mean	0.4

[a] See U.S. Atomic Energy Commission Report AECU-2040, 1952 (unpublished).
[b] See reference 57.
[c] B. V. Brockhouse, Can. J. Phys. 31, 432 (1953).
[d] See reference 60.
[e] See text.
[f] See reference 39.
[g] See Kiehn, Goodman, and Hansen, Phys. Rev. 91, 66 (1953).

obliterate to a large extent any simple picture of the radiative process in terms of the motion of a single particle. It is not surprising, therefore, that no major reduction of the rate of emission is apparent in cases where such might be expected on the basis of a strict single-particle model. For example, the matrix elements of the $E1$ ground-state γ rays in Rh^{104}, Ag^{108}, and Ag^{110} (Table VI) are rather small though perhaps not significantly smaller than those of the other γ rays listed. For these three nuclei, the transition must involve a shift in the configuration of both the unpaired neutron and the unpaired proton.[61] Such a simultaneous displacement of two particles should, in the single-particle model, reduce the transition probability. (This hypothesis has been invoked by Moszkowski[62] to account for the weakness of isomeric $E3$ transitions and by Trocheris[63] to account for the absence of β decay in the isomeric state of Y^{87}.) Furthermore, the $M1$ γ rays observed in Mg^{25}, Si^{29}, and S^{33} violate the single-particle selection rule for change of orbital angular momentum. The matrix elements for such transitions (Table VII) are an order of magnitude smaller than those of the F^{20} and Al^{28} ground-state γ rays. However, as yet there is insufficient evidence to show that this difference is derived from single-particle selection rules. Finally, the ratio of the rates of emission of $E2$ to $E1$ radiation in the odd-neutron nucleus Mg^{25} indicates that the radiative mechanism cannot be identified with the simple displacement of a neutron in that nucleus, for in that event the intensity of the $E2$ radiation would be so low that it would be undetectable.

For heavy elements, the initial highly excited state must contain many different configurations, and presumably some always exist which make possible a radiative transition of any given type. The interpretation of the relative emission probabilities of different multipoles would require a detailed knowledge of the density and the distribution in energy of the levels with the appropriate spin and parity; in the absence of such information it is perhaps surprising that the ratio of the transition probabilities of $M1$ and $E1$ radiations follows so closely that predicted by Weisskopf's formula. An understanding of such details requires a complex model of the nucleus; a start in this direction has been made by Bohr and Mottelson.[64]

6. DISCUSSION

It has been shown in Tables VI and VII that the values for the matrix elements for $E1$ and $M1$ radiation tend to be lower than the estimates of Blatt and Weisskopf by about the same amount (an order of magnitude). It follows, therefore, that the ratio of the matrix element for $M1$ radiation to that for $E1$ radiation agrees with the predicted value, *viz.*, $10(\hbar/McR)^2$, which for medium weight nuclei is about 1 percent. (The same result was obtained directly in Table V.)

The difference between the emission probability of $E1$ and $M1$ radiation is sufficiently great and the variations of emission probability in each group are sufficiently low by comparison to make possible a guess of the multipolarity of other high-energy capture γ rays

[61] From shell structure it would appear that the ground state of the odd proton in the odd-even target nucleus is a $p_{1/2}$ state. From β-decay evidence the ground state of the product nucleus has a spin of 1 and even parity. From the shell model the only way such a state could be produced for these three nuclei is by the combination of a $g_{9/2}$ proton with a $g_{7/2}$ neutron. Therefore, in the $E1$ transition the odd proton must change configuration. It should be pointed out again that there is no conclusive evidence in any of these cases that the ground-state γ ray was observed; it is still possible that weak γ rays with higher energies remain to be detected.

[62] S. A. Moszkowski, Phys. Rev. 89, 474 (1953).

[63] M. Trocheris, Physica 18, 1094 (1952).

[64] A. Bohr, Kgl. Danske Videnskab. Selskab, Mat.-fys. Medd. 26, No. 14 (1952); A. Bohr and B. Mottleson, Physica 18, 1066 (1952).

in certain cases. The data required are the absolute intensity of the γ ray, the density of states near the initial state, and the total radiation width. Alternatively, if the multipole order of one γ ray in the spectrum is known, that of the others may be deduced with some certainty. In the spectra of nuclei such as V^{52}, Fe^{57}, Co^{60}, where the ground-state γ ray is $E1$, all competing γ rays with comparable intensities and lower energy are probably of the same type. Thus, the capture γ-ray spectrum should reveal the sequence of levels which differ in parity and by one unit in spin from that of the capturing state; in even-odd nuclei such as Fe^{57} the spectrum reveals the sequence of p states. In nuclei such as Mg^{25} or S^{33}, where the ground-state γ ray has even parity, a similar argument applies to those γ rays emitted by the capturing state with energies less than that of the $E1$ γ ray with the highest energy. As pointed out in Appendix C, this conclusion is verified in the case of S^{33}. We cannot conclude, however, that all low-energy γ rays are $E1$, for many of these must be emitted by states other than the capturing state, and their intensity may depend on factors other than multipole order, e.g., the extent to which the initial state is excited.

The weakness of second-order radiation and the fail ure to detect any γ rays of higher order shows that the greater part of the energy emitted in neutron-capture radiation is carried by $E1$ and $M1$ γ rays, for which the emission probability varies as the cube of the energy. Blatt and Weisskopf[40] have attempted to calculate the total radiation width to be expected from Al, Ag, and W, on the assumption that the radiation emitted is entirely of one multipole order. Except for W, the results obtained even for $M1$ radiation are all too high. If the radiation is predominantly $E1$, as our measurements appear to show, their results are about 100 times too high. We have seen that the partial radiation widths predicted by the single-particle model are too high by about an order of magnitude. If allowance is made for this fact, the theoretical result might be reduced by a factor of 10. However, we have seen that the parities of the low-lying levels tend to be the same as those of the ground state, at least for the lighter elements, and in one nucleus (S^{33}) there is evidence that they are distributed in bands. The effect of such an uneven distribution on the calculation of the total width is difficult to estimate and a large measure of disagreement is not surprising.

While the finer details of the distribution of energy levels cannot easily be deduced from the observed spectra of neutron-capture radiation mainly because the experimental resolution has been insufficient, some general effects have been observed. The gross shape of the spectrum expected theoretically has been calculated by Margolis.[65] The net result is a peaked distribution, the peak being at a relatively lower energy when the density of the levels is high. Owing to the insensitivity of the pair spectrometer to low-energy γ rays, the spectrum is difficult to trace reliably near 3 Mev, and in only a few instances is there evidence of the peak in the distribution. In most cases the number of γ rays emitted per unit energy range appears to increase continuously as the energy is reduced to 2.5 Mev, the lowest energy at which it is possible to make measurements with a pair spectrometer. An attempt has been made to determine the variation of level density with energy from the observed shape of the spectrum, but the results are probably unreliable.[66]

There is some evidence for a general reduction in the level density near the closed neutron shells. In the spectra of Zr (50 neutrons) and Ba and Pr (82 neutrons), a decrease in the relative number of high-energy γ rays and an increase in their intensity is indicative of a decrease in level density. A more obvious effect is shown in the γ ray spectra of Au, Hg, and Tl, in which the maximum in the γ ray spectrum is clearly shifted to high energies. However, the level densities near the ground states of Au^{198} and Hg^{200} are very different, and the observed effect could be produced by a concentration of $E1$ radiation in γ rays leading to low-lying excited states with appropriate spin and parity. The effect is most striking in the γ-ray spectrum produced by the two isotopes of lead, Pb^{207} and Pb^{208}, for which the intensities of the ground-state γ rays appear to be near 100 percent. It is well known that the spacing of the levels in Pb^{208} is exceptionally wide. It is noticeable that tin[20] shows no peculiar characteristics, although at this element the 50-proton shell is closed; however, it is doubtful whether any conclusion can be drawn from this observation, for it is not yet known whether the capture spectrum is derived from essentially one isotope or whether all the numerous isotopes of tin make their contribution.

ACKNOWLEDGMENT

We wish to thank Dr. J. R. Holt of the University of Liverpool and Dr. W. W. Buechner and Dr. D. M. Van Patter of the Massachusetts Institute of Technology for their cooperation and for the privilege of seeing many of their results before publication.

APPENDIX A. Fe^{57}

It seems certain[20] that the ground state of Fe^{57} is odd and must have a spin of 1/2 or 3/2. If the energy difference of 14 kev between the energies of the two principal γ rays emitted in the decay of Co^{57} is really due to the excitation of a state only 14 kev above the ground state of Fe^{57} (and this is probable, although published evidence[21,22] does not prove it), the $M1$ character of the 14-kev transition shows that the spin of that state must be 1/2, 3/2, or 5/2. The last alternative can be ruled

[65] B. Margolis (private communication).

[66] J. D. Jackson (private communication); J. D. Jackson and B. B. Kinsey, Phys. Rev. 82, 345 (1951).

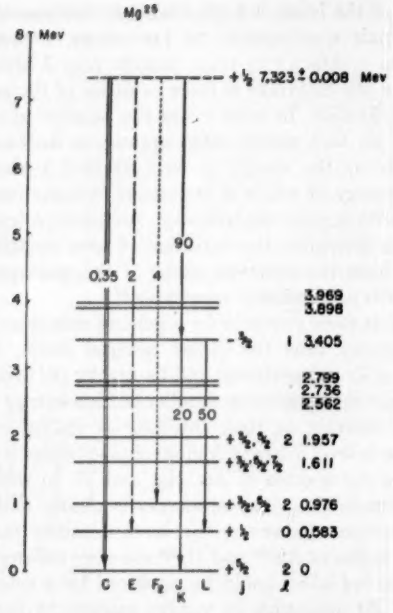

FIG. 1. Decay scheme for the capture γ rays of Mg^{25}. For explanation, see reference 70, Appendix B.

out, for this state is not excited directly in the decay of Co^{57}, for which the spin[67] is 7/2.

That the spin of the ground state is 1/2 and that of the 14-kev state is 3/2 can be shown from a consideration of the internal conversion of the two principal γ rays (133 kev and 119 kev) emitted in the decay of Co^{57}. The number of conversion electrons produced by these γ rays are about equal, although the ratio of the intensities of the 133-kev to the 119-kev γ ray is roughly[68] 1 to 3. If the lifetime of the 133-kev state is short (as would appear from reference 22) neither γ ray can be $E3$ as has been claimed.[69] In iron, at this energy, the conversion coefficients of electric and magnetic radiations of the same multipole order are approximately the same. It follows that the two γ rays are of different multipole orders, one being electric and the other magnetic, for they have the same parity. The 119-kev γ ray has the highest intensity and is, therefore, of the lowest multipole order; and since this γ ray must excite the 14-kev state, it follows that the spin of the 14-kev state must be greater than that of the ground state, which, therefore, must be 1/2. It then also follows that the 133-kev state has spin 5/2.

Since both the ground state and the 14-kev state are p states, both should be produced by emission of $E1$ radiation. The 7.6-Mev peak, however, appears to be normal in all respects:[14] the energy equivalent of its width and the displacement between the peak and its end point are just those expected of a homogeneous γ ray (100±5 kev and 60±5 kev, respectively). One of the two γ rays, therefore, must be weaker than the other. If the weaker γ ray is the ground-state γ ray, it must be at least 20 times weaker than the other because otherwise its existence would have been detected in the latter of the two parameters just mentioned. It seems much more likely, therefore, that the ground-state γ ray is the stronger of the two, for in that case the presence of a weaker γ ray (with lower energy) would not be revealed as an increase in the width of the peak, if its intensity were less than one third of the other.

APPENDIX B. Mg^{25}

The decay scheme for this nucleus is shown in Fig. 1, which has been constructed[70] from the positions of the energy levels found by Endt and co-workers.[71] The parities and spins of some of these levels are shown on the right, together with the orbital angular momentum found by Holt and Marsham.[27] The 1.611-Mev state was not examined by Holt and Marsham. It is excited in the decay[72] of Na^{25}, from which it may be deduced that its spin is 3/2, 5/2, or 7/2.

Recent measurements on the energy of the strong γ ray J gives the value[25] 3.918±0.004 Mev and identify it with the transition from the capturing state at 7.323 Mev to the state at 3.405 Mev. A recalculation of the intensity of the γ ray J, based on a more reliable estimate of the energy dependence of the coincidence counting rate of the spectrometer,[23] gives 0.7 photon per capture in natural magnesium. This is equivalent to 1.4 photons per capture in Mg^{24}, which is obviously too high.[73] We adopt the more realistic figure 0.9.

The 3.405-Mev state is the lowest p state found by Holt and Marsham; its spin must be 1/2 or 3/2. There exist two strong γ rays K and L which have energies which correspond to transitions from this state to the ground state and to the first excited state, respectively. The sum of their intensities is roughly equal to that of the γ ray J. Since both of these γ rays must also be of odd parity, and since the ground state of Mg^{25} has a spin of 5/2, it follows that the spin of the 3.405-Mev state is 3/2, for otherwise the transition from it to the ground state (the γ ray K) would be $M2$ and would not be expected to compete with the γ ray L. The existence

[67] Baker, Bleaney, Bowers, Shaw, and Trenam, Proc. Phys. Soc. (London) A66, 305 (1953).
[68] L. G. Elliott (private communication).
[69] Cheng, Dick, and Kurbatov, Phys. Rev. 88, 887 (1952).

[70] In this and subsequent decay schemes, electric and magnetic radiations are represented by full and by broken lines, respectively, dipoles by single lines, quadrupoles by double lines, etc. Unidentified γ rays are shown by dotted lines. The figures in the middle of the lines give the intensities in photons per 100 captures; vertical figures are those obtained with the pair spectrometer and slanting figures are those obtained by Braid (reference 74).
[71] Endt, Enge, Haffner, and Buechner, Phys. Rev. 87, 27 (1952).
[72] E. Bleuler and W. Zünti, Helv. Phys. Acta 20, 195 (1947).
[73] This result is incompatible with the equality of the contributions made by Mg^{24} and Mg^{25} to the total magnesium thermal-capture cross section, as found by Pomerance (reference 15); the errors in that determination were large (about 30 percent) and may account for the discrepancy.

of the γ ray L has been confirmed by Braid[74] and its intensity measured by him with results in rough agreement with our own. Braid has also found weaker γ rays (at 1.9 and at 1.1 Mev) which can probably be assigned to Mg^{26}. One might expect to observe the γ ray produced in the transition from the 3.405-Mev state to that at 1.611 Mev. Part of the 1.9-Mev γ ray might be emitted in this transition.

The γ rays ascribed to Mg^{25} account for the greater part of the de-excitation of this nucleus. It will be seen from Fig. 1 that the sequence of events is determined very largely by the emission of $E1$ radiation.

APPENDIX C. Si^{29}

The decay scheme of this nucleus is shown in Fig. 2, which is constructed from the positions of the energy levels determined by Endt *et al.*[75] The main feature of the γ-ray spectrum is a cascade of two very strong γ rays (K and M) of nearly equal intensity. Recent measurements[23] of the energies of these γ rays give the values (K) 4.933±0.005 Mev and (M) 3.540±0.006 Mev. Added together, these energies are in agreement with that of the ground-state γ ray B, which is 8.468 ±0.008 Mev. The accuracy of these measurements is sufficient to identify the intermediate level as that at 4.934 Mev.[75] As in Mg^{25}, the strong γ ray M excites the lowest p state found by Holt and Marsham.[26] In Si^{29}, this p state is the highest member of a close triplet. While it is not clear from the work of Holt and Marsham whether or not the other two states of the triplet also have odd parity, the energy measurements make it certain that the strong γ ray M excites only the highest component, and that the transitions to the others are much less frequent.

A recalculation of the intensities of these γ rays, based on the original data[12] and on the new counting efficiency curve,[23] shows that the intensity of the γ ray M is a little less than that of K. Roughly the intensity of both is about 0.7 photon per capture in Si^{28}. The equality of the intensities of the γ rays K and M shows that the transition from the 4.934-Mev state to lower intermediate states are relatively infrequent. Transitions from this state to the first and second excited states would produce γ rays with the energies 3.656 and 2.907 Mev. Neither has been detected although the detection of a weak γ ray with the latter energy is difficult experimentally. The 3.656-Mev γ ray, however, would produce a peak in the coincidence spectrum partly resolved from that of M but lying just above it. Such a peak has not been found; its intensity is less than one-tenth of that of M (or K). It seems certain that the 3.656-Mev transition must also be $E1$, for of the two possibilities for the spin of the first excited state obtained from the results of Holt and Marsham, only a spin of 3/2 is consistent with an allowed decay of P^{29}

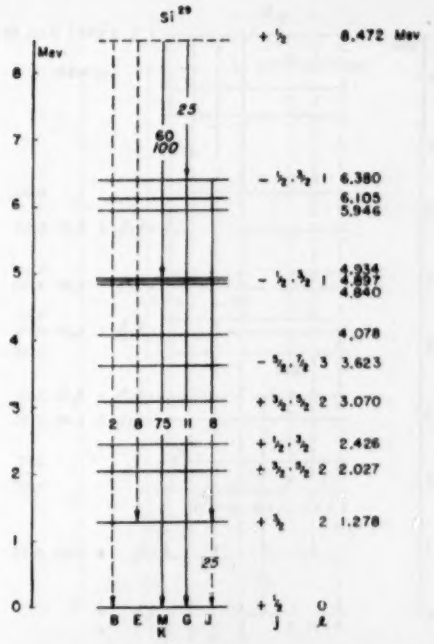

FIG. 2. Decay scheme for the capture γ rays of Si^{29}. For explanation, see reference 70, Appendix B.

to this state.[76] It is not surprising that the 3.656-Mev γ ray is not observed, for it is only necessary that the matrix element of this transition be less than one-third of that for the γ ray K.

Few of the other intermediate states appear to be excited to an appreciable extent by transitions from that at 4.934 Mev, for of the three low-energy γ rays found by Braid,[74] one corresponds to a transition from the first excited state to the ground state, another to a transition from the capturing state to the p state at 6.38 Mev, and the third cannot as yet be fitted into this decay scheme. The intensity of the former (25 percent per capture in Si^{28}) is somewhat greater than the intensities of the two γ rays known to be feeding this level. The intensity of the latter is somewhat greater than that of the γ rays produced by the 6.38-Mev level, which, as is to be expected, produces transitions to the ground state and to the first-excited state.

APPENDIX D. S^{33}

Most of the numerous γ rays emitted by sulfur can be accounted for by the excitation of the nucleus S^{33}. The contribution of S^{33} to the thermal capture cross section is unknown; presumably it is small like that of S^{34} and S^{36}. A tentative decay scheme is shown in Fig. 3, in which the positions of the excited states found by

[74] T. H. Braid (private communication).

[75] Endt, Van Patter, Buechner, and Sperduto, Phys. Rev. **83**, 491 (1951).

[76] Roderick, Lönsjö, and Meyerhof, Phys. Rev. **90**, 371 (1953). The spin of P^{29} must be 1/2, for the β decay to the ground state of Si^{29} is of the super-allowed type.

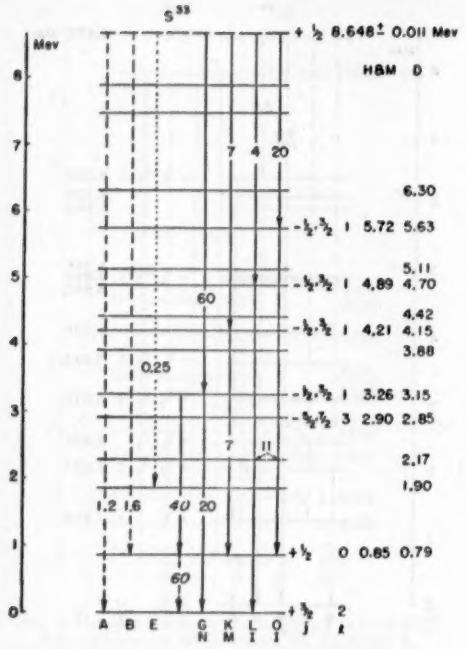

FIG. 3. Decay scheme for the capture γ rays of S^{33}. For explanation, see reference 70, Appendix B.

Holt and Marsham[26] and by Davison[77] are shown on the right. The energies of these states are not known with the precision of those of the nuclei discussed above and for this reason the identification of the sulfur γ rays is less certain.

Excepting the two weak $M1$ transitions, A, producing directly the ground state, and B, the first-excited state, and another of unknown multipolarity producing the second excited state, the remainder of the γ-ray spectrum is obviously derived from transitions to a succession of p states found by Holt and Marsham.

The strongest γ ray is the γ ray G, which excites the lowest of these p states (at 3.2 Mev). The γ ray G is followed by the emission to the ground state of the γ ray N, which is noticeably weaker than G. It is clear from this that some of the excitation of the 3.2-Mev state is relieved by the emission of γ rays in transitions to intermediate states. These γ rays have energies too low for detection by the pair spectrometer, but a 2.3-Mev γ ray has been detected by Braid[74] which may be identified as the transition between the 3.2-Mev level and the first excited state at 0.8 Mev. The intensity of this γ ray, when added to that of N, is roughly equal to the intensity of G.

Similar transitions to the ground state and to the first excited state are to be expected from the higher p states, for they will all be of $E1$ type, and some of these can be identified. (Those which have not been recorded are such that the coincidence peaks which they would produce are masked by the tails of much stronger γ rays.) It follows that the first level is excited very frequently in the neutron capture process. The γ ray emitted by this state (0.8 Mev) has been detected and measured by Braid;[74,75] its intensity (0.6 photon per capture)[74] is in agreement with the sum of the intensities of the γ rays known to be feeding this level.

[77] P. W. Davison, Phys. Rev. 75, 757 (1949).

APPENDIX E. Ca^{41}

A decay scheme for this nucleus is shown in Fig. 4, in which the positions of the energy levels are those obtained by Sailor,[79] and the spins and parities of the levels are those obtained by Holt and Marsham.[29] It is clear that the two strong γ rays C and D are of $E1$ type, and account for the greater part of the neutron captures producing Ca^{41}. A recalculated value for the intensity of the γ ray C is 40 photons per 100 captures in natural calcium; this value corresponds roughly to 80 photons per 100 captures in Ca^{40}, for about half[15] of the natural capture cross section of this element is derived from Ca^{42}. None of the remaining calcium γ rays can be identified with certainty, for the positions of the excited states of Ca^{43} are mostly unknown.

A strong γ ray with an energy of 1.9 Mev has been detected by Braid.[74] This γ ray clearly represents the decay of the first excited state. No γ ray was found by Braid at 2.4 Mev, which would correspond to the

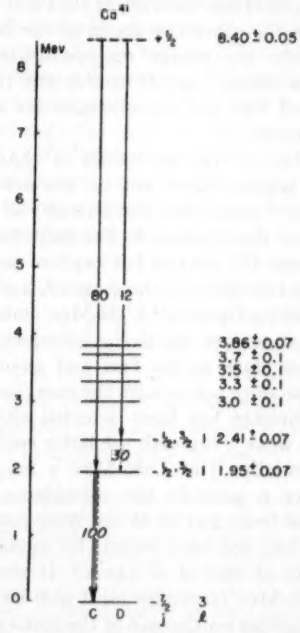

FIG. 4. Decay scheme for the capture γ rays of Ca^{41}. For explanation, see reference 70, Appendix B. The transition from the first excited state to the ground state is shown as either $E2$ or $M3$.

[78] T. H. Braid, Phys. Rev. 90, 355 (1953).
[79] V. L. Sailor, Phys. Rev. 75, 1836 (1949).

transition between the second excited state and the ground state. This transition is evidently forbidden (as in Ti^{49}, discussed below) and the excitation of the second state is relieved by a transition to the first, for a γ ray of 0.48 Mev has been measured by Braid. The spins of the first two states could be both 1/2, both 3/2, or one 1/2 and the other 3/2. The transition from the first excited state to the ground state, therefore, is $E2$ or $M3$.

APPENDIX F. Ti^{49}

The decay scheme for this nucleus is shown in Fig. 5, in which the energies of the levels shown on the right are those obtained by Pieper.[80] This nucleus has not been examined by Holt and Marsham; the γ-ray spectrum, however, is very similar to that of Ca^{41}, and since the nucleus Ti^{48} contributes the greater part of the capture cross section of natural titanium, the γ rays have been measured with some precision and their identification is not in doubt.

As in Ca^{41}, Braid[78] has measured two strong γ rays with energies equal to that of the first excited state (1.4 Mev) and to the difference (0.3 Mev) in the energies between that state and the second excited state. In addition, he has found some evidence[74] for the existence of a 1.7-Mev γ ray, corresponding to a direct transition from the second state to the ground state. The intensity of this γ ray, if it exists, is 0.1 photon per capture or less. If this is indeed its origin, then the spins of the first and second excited states must be 1/2 and 3/2, respectively, and the competing γ rays are $M1$ and $E2$, contradicting a suggestion made by Breit[80] that the spins of these states are in the reverse order.

APPENDIX G. NOTES ON SOME ODD-CHARGE NUCLEI

V^{52}

The parity of the ground state of V^{52} is certainly even, for it decays by an allowed transition to the first excited state of Cr^{52}, which, presumably, is even and has a spin of 2 units. This conclusion has been verified by recent measurements on the (d,p) reaction.[81] The spin of V^{52} is probably 3 units. If this is true, the ground-state γ ray is $E1$ whatever the spin of the capturing state. The scattering of thermal neutrons seems to be determined largely by the resonance at 2700 ev,[82] and we assume that the thermal absorption cross section is likewise derived from this resonance.

Mn^{56}

In manganese the thermal-neutron scattering and absorption cross sections seem to be derived mainly[83] from the 345-ev resonance, for which the spin is 3 units.

[80] G. Pieper, Phys. Rev. **88**, 1299 (1952).
[81] J. S. King and E. H. Beach, Phys. Rev. **90**, 381 (1953).
[82] M. Hamermesh and C. O. Muehlhause, Phys. Rev. **78**, 175 (1950).
[83] Harris, Hibdon, and Muehlhause, Phys. Rev. **80**, 1014 (1950).

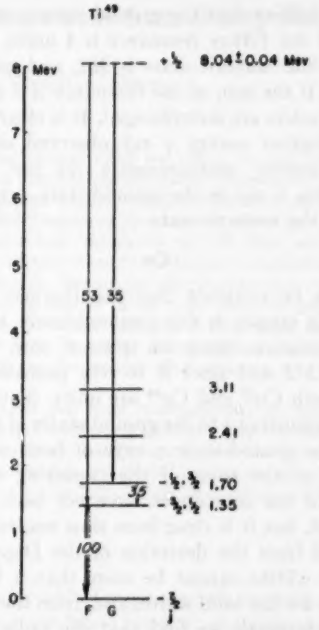

FIG. 5. Decay scheme for the capture γ rays of Ti^{49}. For explanation, see reference 70, Appendix B. The transition from the first excited state to the ground state is shown as either $E2$ or $M3$.

The spin of Mn^{56} is 5/2. While the classification of the β decay of Mn^{56} is uncertain ($\log ft \simeq 7$), the spin of the ground state is probably 3 units and at most does not differ from this by more than 1 unit. Provided that the spin of Mn^{56} is not more than 3 units, the ground-state γ ray must be $E1$ regardless of the spins of the resonances which contribute to the thermal neutron capture cross section.

Co^{60}

The neutron scattering in cobalt at low energies seems to be derived[58] from the 120-ev resonance and is consistent with a spin of 4 units. The total cross section at exact resonance has been measured by Seidl[84] and is consistent only with a spin of 4 units. However, the value of the neutron width obtained from the strength of the resonance ($\sigma_0\Gamma'^2$)[85] is about 4 ev, which suggests that the spin is 3 units. The actual value of the spin, therefore, is still uncertain. The radiation width is obtained from this value of Γ' after multiplication by the ratio of the resonance absorption and scattering integrals.[60] It is 0.27 ev and accounts for about one-half of the thermal absorption cross section. The remainder must be due to the tails of other resonances.

Assuming that the spin of the ground state of Co^{60} is 5 units and that that of the isomeric state at 59 kev is

[84] F. G. P. Seidl, Phys. Rev. **75**, 1508 (1949).
[85] W. W. Havens and L. J. Rainwater, Phys. Rev. **83**, 1123 (1951); A. W. Merrison and E. R. Wiblin, Proc. Roy. Soc. (London) **A215**, 278 (1952).

2 units, it follows that the ground-state γ ray is $E1$, if the spin of the 120-ev resonance is 4 units, while that leading to the isomeric state is $M2$, and, presumably, forbidden. If the spin of the resonance is 3 units, these multipole orders are interchanged. It is clear, therefore, that the highest energy γ ray observed must be $E1$ although energy measurements do not determine whether this γ ray is the ground-state γ ray or that leading to the isomeric state.

Cu

There is no evidence that the thermal capture of neutrons in copper is due predominantly to any particular resonance. Since the spins of both copper isotopes are 3/2 and since it is very probable that the spins of both Cu^{64} and Cu^{66} are unity (both decay by allowed β transitions to the ground states of the product nuclei), the ground-state γ rays of both must be $E1$ regardless of the spins of the capturing states. The positions of the resonances have not been accurately determined, but it is clear from slow neutron measurements and from the detection of the Doppler-effect[86] that their widths cannot be more than a few ev. We adopt 5 ev for the total width, and, from the ratio of the resonance integrals we find that the radiation widths are of the order of 0.2 ev.

P^{32}

The shape of the angular distribution[81] of the protons in the (d,p) reaction suggests that the spin of the ground state of P^{32} is 1 or 2. If the latter, the weakness of the ground-state γ ray might be explained by its composite character. King and Beach[87] have found that the first excited state is produced by ingoing neutrons with an orbital angular momentum of 2 units, the second, third, and fourth (0.51, 1.15, and 1.32 Mev) by a mixture of $l=0$ and $l=2$. The spins of the last three states, therefore, would appear to be unity, and the γ rays producing them are $M1$, regardless of the spin of the capturing state. Of these γ rays, those producing the second (C) and the third (D) are much stronger than those producing either the ground state or the first excited state; the γ ray D (6.76 Mev) is some fifty times stronger than the ground-state γ ray. The excited states at 2.18 and 2.23 Mev are again mixed s and d states for the odd neutron, and the γ rays producing them are less powerful. The first odd states to appear are at 3.26 and 3.32 Mev and seem to be mixed p and f states for the odd neutron. If these states are indeed of mixed character, their spin is 2, and the γ ray producing them can contain $E1$ radiation. The strong γ ray L (4.68 Mev) can be identified with one of these γ rays. Its intensity is about the same as that of the $M1$ γ ray D; it is, however, very different from the preponderant intensities of the $E1$ γ rays in the even-odd nuclei. As yet, it is not possible to determine whether this weakness is due to the admixture of $M2$ radiation derived from nonresonant capture or whether, like the ground-state γ ray in N^{15}, it is due to some other cause.

[86] Coster, DeVries, and Diemer, Physica **20**, 281 (1943).

[87] J. S. King and E. H. Beach, see reference 81; and E. H. Beach (private communication).

Energy Spectra and Angular Distributions of Photoneutrons from Heavy Nuclei*†

GLENN A. PRICE‡
Physics Research Laboratory, University of Illinois, Champaign, Illinois
(Received November 9, 1953)

The energy spectra of photoneutrons from the absorption of 22-Mev bremsstrahlung by silver and bismuth have been measured with nuclear emulsions. Comparisons are made between the observed photoneutron spectra and those predicted on the basis of a statistical nuclear model. Energy level densities are assumed proportional to $\exp[(a\epsilon)^{\frac{1}{2}}]$ and $\ln(A\epsilon/20+1)$, where ϵ is the excitation energy of the residual nucleus. The exponential form of the energy level density is in better agreement with the data than is the logarithmic form. However, for neutron energies greater than 4 Mev there are more photoneutrons observed than predicted by the exponential energy level density scheme.

The angular distributions of photoneutrons from several elements have been measured with a variety of neutron detectors. The moderated neutron detector, which is equally sensitive to neutrons of most energies, indicates the photoneutron flux to be predominately isotropic. The small anisotropic component has a maximum at 90 degrees to the x-ray beam. Photoneutrons from bismuth have a larger anisotropic component than photoneutrons from any other element which was tested. In that case 21 percent of the neutron flux is in the anisotropic component.

The $Al(n,p)$ and $Si(n,p)$ reactions have been used to measure the angular distributions of photoneutrons from several elements. These reactions have thresholds at 1.95 Mev and 2.69 Mev, respectively and are primarily sensitive to neutrons with more than 4-Mev energy. The angular distributions thus observed have a maximum at 90 degrees to the x-ray beam. In general, photoneutrons from the heavy elements deviate more from isotropy than do the light elements. An epithermal neutron detector indicates that the low-energy photoneutrons are emitted isotropically.

It is concluded that most photoneutrons are generated in a manner consistant with the statistical nuclear model. The high-energy photoneutrons, which constitute a small fraction of the total photoneutron flux, are ejected predominately at right angles to the x-ray beam as expected by dipole absorption of the photons.

I. INTRODUCTION

PREVIOUS measurements of the angular distribution of photoneutrons by Price and Kerst[1] indicated that photoneutrons from heavy nuclei are predominately isotropic in space. Byerly[2] has measured the photoneutron energy spectra from copper and found the measurement to be in agreement with a statistical nuclear model. However, detailed examination of the angular distributions of photoneutrons from heavy nuclei by Poss[3] and by Demos, Fox, Halpern, and Koch[4] has shown that the high-energy photoneutrons are emitted anisotropically in space with a maximum at right angles to the x-ray beam. Experiments by other investigators have revealed similar characteristics in gamma-proton reactions.[5–10] The experiments described in this paper were performed to gain more information concerning gamma-neutron reactions in heavy nuclei using 22-Mev bremsstrahlung from a betatron.

II. PHOTONEUTRON ENERGY SPECTRA

The presence of knock-on protons in nuclear emulsions was used to measure the energy and number of photoneutrons which were ejected at right angles to the 22-Mev x-ray beam incident on silver and bismuth targets. The Ilford C-2, 200-micron emulsions were wrapped in black paper and placed with their leading edges 6 in. from the target. A lead shield, $\frac{1}{32}$ in. thick, was placed between the target and the emulsion to absorb a soft ionizing radiation which otherwise would have excessively fogged the plates. The lead shield was sufficiently transparent to neutrons so that no correction was required in computing the neutron flux. The emulsion was tilted 3 degrees from the target so that the leading edge of the emulsion would not shield the rest of the emulsion. The emulsions were shielded from x-rays and neutrons originating at the betatron by thick walls of concrete and paraffin.

The silver target was a sphere, 1.75 cm in diameter and weighed 27.9 grams. After correcting for x-ray absorption in the target the integrated exposure for the silver target was 134.2 mole-"r." The bismuth target was 1.615 cm in diameter and weighed 21.5 grams. After correcting for x-ray absorption in the target the integrated exposure for the bismuth target was 45.2 mole-"r." In both cases the correction for x-ray absorption in the targets amounted to about 36 percent. Exposure times for all runs were 105 minutes. The total number of "r" in each run was monitored by comparing the intensity of 8.2-hour beta activity induced in a tantalum foil at the exit port of the lead collimator with the tantalum activity when a Victoreen ion chamber (in an aluminum block) was placed in the x-ray beam.

After the emulsions were developed by appropriate procedures they were scanned with an E. Leitz Wetzlar binocular microscope, 12× ocular and 8-mm objective. All proton tracks which started and stopped in the

* Assisted by the joint program of the U. S. Office of Naval Research and the U. S. Atomic Energy Commission.
† Part of a thesis submitted in partial fulfillment of the requirement for the degree of Doctor of Philosophy in Physics in the Graduate College of the University of Illinois.
‡ Now at Brookhaven National Laboratory, Upton, New York.
[1] G. A. Price and S. W. Kerst, Phys. Rev. **77**, 806 (1950).
[2] P. R. Byerly, Jr., thesis, University of Pennsylvania, 1950 (unpublished).
[3] H. L. Poss, Phys. Rev. **79**, 539 (1950).
[4] Demos, Fox, Halpern, and Koch, Phys. Rev. **86**, 605 (1952).
[5] B. C. Diven and G. M. Almy, Phys. Rev. **80**, 407 (1950).
[6] Curtis, Hornbostel, Lee, and Salant, Phys. Rev. **77**, 290 (1950).
[7] J. Halpern and A. K. Mann, Phys. Rev. **83**, 370 (1951).
[8] Rothman, Mann, and Halpern, Phys. Rev. **86**, 629 (1952).
[9] M. E. Toms and W. E. Stephens, Phys. Rev. **82**, 709 (1951).
[10] M. E. Toms and W. E. Stephens, Phys. Rev. **85**, 728 (1952).

emulsion, and whose directions were within 15 degrees of the neutron direction were accepted. The neutron energy was determined from the range and direction of the knock-on proton in the emulsion. The number of neutrons in any energy interval in calculated from the number of proton tracks observed in that energy interval, the hydrogen content of the emulsion, and the neutron-proton scattering cross section. Appropriate corrections were made for the probability of protons leaving the emulsion before the ends of the range, probability that the proton angle is less than 15 degrees, and the scattering of neutrons by heavy nuclei in the nuclear emulsion.

The photoneutron energy spectra are shown in Figs. 1 and 2. In the case of the bismuth photoneutron spectrum, Fig. 1, the neutrons were computed in 1-Mev intervals. However, for the silver photoneutrons spectrum, Fig. 2, the neutrons were put into 2-Mev intervals because of the larger probable errors involved. The probable errors as indicated by vertical lines through the experimental points represent variations in neutron intensity if the number of proton tracks, N, which contribute to each point is varied by $\pm\sqrt{N}$.

The photoneutron energy spectrum with the silver target was taken from 129 acceptable proton tracks found in 462 mm² of emulsion. The bismuth photoneutron spectrum was calculated from 196 proton tracks in 467 mm² of emulsion. The background plates yielded 61 tracks for a corresponding area. 58 of the 61 background tracks were in the energy range from 1 to 2 Mev. The background plates were exposed in a manner similar to the regular plates but with no target in the x-ray beam. Unexposed nuclear emulsions revealed a large number of one, three, four, and five prong alpha stars which were attributed to thorium contamination. The one-prong alpha tracks could not be easily distinguished from short proton tracks. Consequently, most of the 58 background tracks from 1 to 2 Mev could be attributed to single-prong alpha stars. If fresh nuclear emulsions had been used the effect of thorium contamination would have been much less.

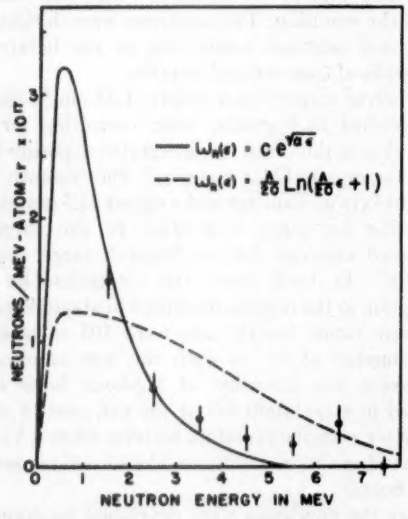

FIG. 1. Energy spectrum of photoneutrons emitted from bismuth when irradiated by 22-Mev bremsstrahlung. Solid and dashed curves indicated predicted spectra as calculated on the statistical model of the nucleus with indicated energy level densities, $\omega_R(\epsilon)$.

The solid and dashed curves in Figs. 1 and 2 represent photoneutron spectra which would be expected on the basis of a statistical nuclear model. The number of neutrons/Mev-atom-"r," $F(\epsilon_n)$, was calculated from the following formula, which is analogous to one derived by Diven and Almy for photoproton spectra,

$$F(\epsilon_n)=\epsilon_n\sigma_{n\beta}\int_{B_n+\epsilon_n}^{E_{\max}}\frac{\sigma(\gamma,n)N(E,E_{\max})\omega_R(E-B_n-\epsilon_n)}{\int_0^{E-B_n}\epsilon_n\sigma_{n\beta}\omega_R(E-B_n-\epsilon)d\epsilon_n}dE,$$

where ϵ_n is the neutron energy, $\sigma_{n\beta}$ is the neutron penetration factor, E is the photon energy, B_n is the neutron binding energy, $\sigma(\gamma,n)$ is the gamma-neutron cross section, $N(E,E_n)$ is the number of photons/Mev-"r" in the bremsstrahlung spectrum, and $\omega_R(E-B_n-\epsilon_n)$ is the energy level density of the residual nucleus. The quantity, $E-B_n-\epsilon_n$, is the excitation energy of the residual nucleus.

The solid curves are the theoretical photoneutron energy spectra which would be expected with an energy level density,

$$\omega_R(E-B_n-\epsilon_n)=C\exp\{[a(E-B_n-\epsilon_n)]^{\frac{1}{2}}\},$$

where C is a constant, $a=1.6(A-40)^{\frac{1}{2}}$, and A is the atomic mass number.

The dashed curves are the theoretical photoneutron energy spectra which would be expected with an energy level density,

$$\omega_R(E-B_n-\epsilon_n)=(A/20)\ln[(A/20)(E-B_n-\epsilon_n)+1].$$

The exponential form of the energy-level density is suggested by Weisskopf and Ewing,[11] whereas the logarithmic form is the Schiff[12] regular energy-level density.

$\sigma(\gamma,n)$ for silver was taken from the results of Diven and Almy. The gamma-neutron cross section for bismuth has not been measured; therefore an assumed cross section was used. The bismuth gamma-neutron cross section was assumed to have a threshold at 7.5 Mev, a peak at 13.5 Mev, a full width at half-maximum of 6 Mev, and an integrated cross section of 7.5 Mev-barns. The bismuth threshold has been measured by Sher, Halpern, and Mann,[13] and the integrated cross section is inferred from the total photoneutron yields

[11] V. F. Weisskopf and D. H. Ewing, Phys. Rev. **57**, 472 (1940).
[12] L. I. Schiff, Phys. Rev. **73**, 1311 (1948).
[13] Sher, Halpern, and Mann, Phys. Rev. **84**, 149 (1951).

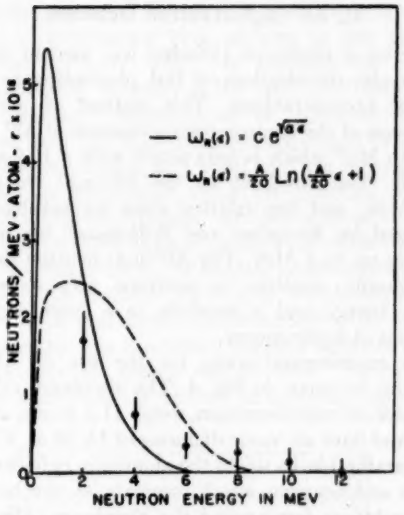

FIG. 2. Energy spectrum of photoneutrons emitted from silver when irradiated by 22-Mev bremsstrahlung. Solid and dashed curves indicate predicted spectra as calculated on the statistical model of the nucleus with indicated energy level densities, $\omega_R(\epsilon)$.

by Kerst and Price.[14] The photoneutron energy spectrum is quite insensitive to the shape of the gamma-neutron cross section to the assumption concerning the shape of the cross section is not a crucial one. The neutron penetration factor $\sigma_{n\beta}$ was calculated from a formula given by Weisskopf.[15]

III. ANGULAR DISTRIBUTIONS OF PHOTONEUTRONS

A. Moderated Neutron Detector

The moderated neutron detector is the same one which was used by Price and Kerst to measure the angular distribution of photoneutrons. It is patterned after the shielded long counter of Hanson and McKibben[16] except that it uses a rhodium foil instead of a BF_3 counter for detecting slow neutrons. It consists of a cylindrical rhodium foil in a hole in a block of paraffin, $2\frac{3}{4}$ in.$\times 2\frac{3}{4}$ in.$\times 5\frac{1}{4}$ in. The paraffin block is surrounded by $\frac{1}{32}$ in. cadmium foil and is placed in a paraffin cylinder, 12 in. in diameter and 15 in. long. The action of the detector is as follows: photoneutrons having more energy than 0.1 ev pass through the cadmium, are slowed down by collisions with hydrogen nuclei in the smaller paraffin block and are captured by the rhodium foil. Neutrons which come in toward the side of back of the detector are slowed down in the paraffin cylinder and then are captured in the cadmium foil. Thus, the action of the paraffin cylinder and cadmium foil make the detector sensitive to neutrons from one direction only. The energy spectrum of photoneutrons is such that eliminating neutrons less than 0.1 ev in energy has a negligible effect on the results. When a normal Rh^{103} nucleus captures a slow neutron it forms Rh^{104} which decays by beta emission with a 44-second half-life. Consequently, a measure of the 44-second beta activity gives a relative yield figure for the photoneutron intensity from the target.

A large concrete wall shields the neutron detector from x-rays and neutrons which originate at the betatron. Another rhodium foil was placed in a crevice in the concrete wall for the purpose of measuring the relative intensity of the x-ray beam. The hydrogen in the concrete wall has a moderating action on the neutrons which are generated at the electron target in the betatron, the x-ray collimator, and in the concrete wall by x-rays. Consequently, the slow neutron flux in the concrete wall is proportional to the intensity of the x-ray beam passing through the collimator, provided that the direction of the beam does not shift. Thus, the intensity of 44-second beta activity in the monitor foil is proportional to the integrated x-ray intensity at the target. This type of x-ray monitor has the particular advantage that it has the same rate of decay as the neutron detector. Therefore, fluctuations in photoneutron yield due to fluctuations in x-ray intensity during a run are nullified.

The procedure in making a run was to expose a sample to three minutes radiation by the betatron with rhodium foils in place. Then 30 seconds were allowed to move the rhodium foils to two thin-walled cylindrical Geiger counters. The total counts on the two Geiger counters for the next three minutes give the relative

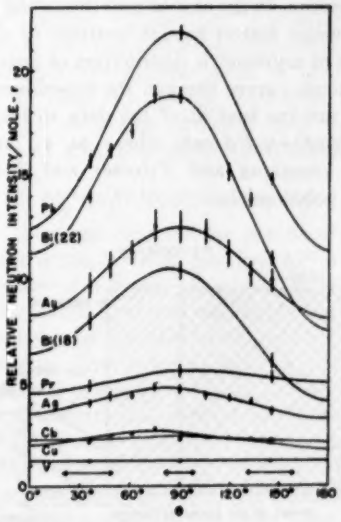

FIG. 3. Angular distributions of high-energy photoneutrons created by 22-Mev bremsstrahlung on various targets as observed with the $Al^{27}(n,p)$ detector. The bismuth target was also irradiated with 18-Mev bremsstrahlung.

[14] D. W. Kerst and G. A. Price, Phys. Rev. **79**, 725 (1950).
[15] McMillan, Segrè, Teller, Bloch, Williams, Critchfield, Weisskopf, and Christy, U. S. Atomic Energy Commission Report, MDDC-1175, 1947 (unpublished).
[16] W. Sleator, Jr., Phys. Rev. **72**, 207 (1947).

measure of the neutron yield and the x-ray intensity, respectively. Then a background run was made by repeating the previous procedure with no target in the x-ray beam. The cycle for one run was completed in 10 minutes, which allowed plenty of time for the decay of activity in the foils between runs.

The angular distributions of total neutron intensity as observed with the moderated neutron detector are shown in figure.[3] Each point in Fig. 3 represents the average of three runs with the exception of silver and gold. The silver and gold values are averages of two complete series which were taken on separate days, or an average of six runs each. The agreement between the repeated values was well within the probable errors as calculated from the statistics of counting rates. Target sizes varied from 0.15-gram mole for the gold and bismuth targets to 9.1-gram mole for the beryllium target, although most of the targets contained less than one gram mole.

An estimate of the fraction of neutrons scattered by the bismuth target into the moderated neutron detector was made. This was done because the neutron detector cannot distinguish photoneutrons which originate at the target from other neutrons, say, which originate at the betatron and are scattered by the target into the detector. The moderated neutron detector was used without its cadmium shield and outer paraffin cylinder to measure the neutron flux in the x-ray beam at the target position. If the mean scattering cross section of bismuth is taken to be 8 barns, then the fraction of scattered neutrons observed at the 90-degree position would be 1.3 percent of the photoneutron yield observed at that position. In the case of gold the strong resonance at 4.8 ev might scatter enough neutrons to account for the observed asymmetric distribution of neutrons.

The smooth curves through the experimental points of Fig. 3 are the best fit of the data to the function, $a_0+a_1P_1(\cos\theta)+a_2P_2(\cos\theta)$ where a_0, a_1, and a_2 are arbitrary constants and $P_1(\cos\theta)$ and $P_2(\cos\theta)$ are Legendre polynomials.

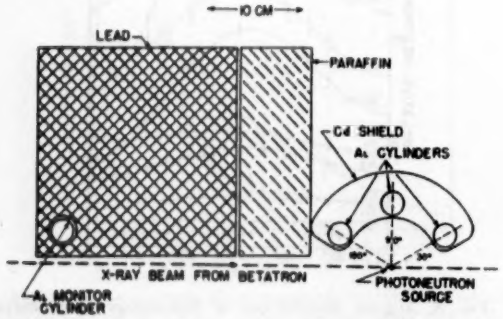

FIG. 4. Experimental setup for observation of angular distributions of photoneutrons with threshold detectors.

B. $Al^{27}(n,p)$ Neutron Detector

A series of aluminum cylinders was used to observe the angular distributions of fast photoneutrons using 22-Mev bremsstrahlung. This method of detection makes use of the neutron-proton reaction in Al^{27} which leads to Mg^{27} which is beta-active with a 10.2-minute half-life. The threshold for the $Al^{27}(n,p)$ reaction is 1.95 Mev, and the relative cross section has been measured by Bretscher and Wilkinson[17] for neutron energies up to 4 Mev. The $Al^{27}(n,p)$ neutron detector is primarily sensitive to neutrons with more than 4-Mev energy and is sensitive to a lesser degree to neutrons of lower energy.

The experimental setup for the use of $Al^{27}(n,p)$ detectors is shown in Fig. 4. The aluminum cylinders are made of pure aluminum, weigh 11.1 grams, are 3 in. long, and have an inside diameter of 13/16 in. The lead and paraffin blocks shield the aluminum cylinders from x-rays and neutrons which originate at the betatron. The cadmium box around the aluminum cylinders is necessary to absorb slow neutrons coming from the lead, the paraffin, and the room in general. Aluminum cylinders are positioned in the cadmium box by annular slots in a lucite sheet. Slow neutron capture in aluminum produces Al^{28} which is beta active with a 2.4-minute half-life. The 2.4-minute activity would confuse the analysis of the 10.2-minute activity if it were not eliminated. Tests with a Ra-Be neutron source, in which a paraffin reflector was used to increase the number of thermal neutrons, indicated that a $\frac{1}{16}$-in. cadmium shield would completely eliminate the 2.4-min activity induced in the aluminum by slow neutrons without affecting the 10.2-minute activity.

The standard operating procedure included the use of three aluminum cylinders simultaneously at three different angles. All targets were cylinders less than $\frac{3}{8}$ in. in diameter and less than 2 in. high and oriented with the x-ray beam perpendicular to the axis of the cylinder. All targets were in the pure metallic form except for the praesodymium target in which case PrO_2 was used. Target weights varied from 30.6 grams for the PrO_2 to 92.9 grams for the Cu target. The betatron was on for 15 minutes, followed by a 5-minute waiting period, during which time the aluminum cylinders were transfered to cylindrical Geiger counters, and then the total count for the next 15 minutes was taken as relative intensity of fast neutrons. There were nine aluminum cylinders, and they were alternated so that the 10.2-minute activity had sufficient time to decay between successive uses. The neutron flux at a particular angular position was taken from the average activity of the nine aluminum cylinders at that position. All runs were normalized to a constant x-ray intensity by means of an aluminum cylinder in a cadmium lined cavity in the lead block. Fast neutrons from the betatron

[17] E. Bretscher and D. H. Wilkinson, Proc. Cambridge Phil. Soc. 45, 141 (1949).

and those generated in the lead block by x-rays give rise to a 10.2-minute beta activity in the monitor aluminum cylinder which is proportional to the integrated x-ray intensity at the target position.

The angular distributions of photoneutrons as observed with $Al^{27}(n,p)$ detectors are shown in Fig. 5. Vertical lines through each point indicate the standard deviation as determined from the counting statics. The smooth curves represent the least squares fit of the data to the function $a_0+a_1P_1(\cos\theta)+a_2P_2(\cos\theta)$. Figure 6 gives the values of B/A if the fast photoneutron yield is fitted to the function $A+B^2\sin^2\theta$. The betatron was operated with a maximum photon energy of 22 Mev in all cases except one run with a bismuth target in which case the betatron energy was 18 Mev. The relative neutron intensities are plotted in arbitrary units per

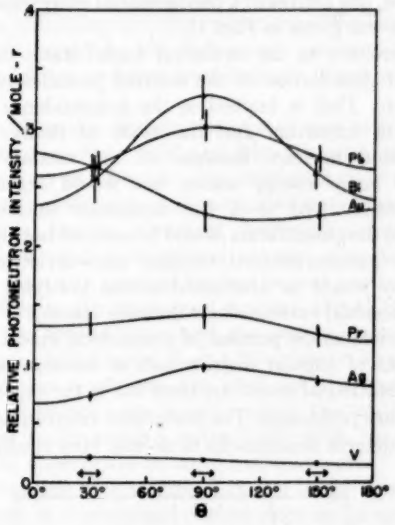

FIG. 5. Angular distributions of photoneutrons created by 22-Mev bremsstrahlung as observed with the moderated neutron detector. θ is the angle at the target between the incident bremsstrahlung and the neutron detector.

mole-"r." On the same scale of arbitrary units a 500-mg RaBe source gives 3.29×10^{-6} arbitrary units per Ra-Be neutron. However, it is not possible to compare absolute numbers of fast photoneutrons with fast Ra-Be neutrons since the energy distributions of the two sources are not the same. The geometrical centers of the aluminum cylinders nearest the x-ray beam were at angles of 30 degrees and 150 degrees from the beam taken at the target. However, the mean angles of the detectors for the detection of neutrons were actually 36 degrees and 144 degrees. The mean angle of each detector was calculated with a $\sin^2\theta$ weighting factor since there was a large $\sin^2\theta$ component in the photoneutron intensities. The mean angle for detection differs from the geometrical center of the

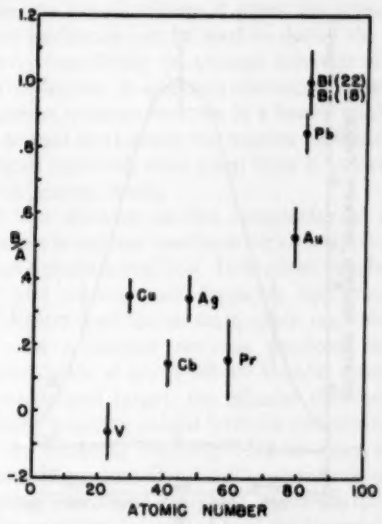

FIG. 6. Anisotropy of photoneutrons as observed with the $Al^{27}(n,p)$ threshold detector when the angular distributions are fitted to the function $A+B\sin^2\theta$.

cylinder because of the relatively large size in comparison to the distance from the photoneutron source.

The fast neutron detector was checked by means of a 500-mg Ra-Be neutron source. The Ra-Be source, which emits 6.17×10^6 neutrons per second, was put at the normal target position. Runs were made with the same time sequence as for a photoneutron run. Fast neutrons from Ra-Be were observed at nine angles from 30 degrees to 150 degrees. The probable error due to counting statistics was ±0.75 percent and a maximum variation of 5 percent from the mean was observed from one position to another. Consequently the variations are real and can be attributed to errors in the positions of the annular slots of about $\frac{1}{32}$ in. Therefore, all observed neutron intensities were corrected for the variations observed with the Ra-Be neutrons, which should be emitted isotropically.

C. $Si^{28}(n,p)$ Neutron Detector

Another threshold detector for the observation of fast neutrons is the $Si^{28}(n,p)$ reaction. Al^{28} is unstable to the emission of a β particle with a half-life of 2.4 minutes. The threshold of the (n,p) reaction is 2.69 Mev and is probably most sensitive to neutrons of more than 5.5-Mev energy. The detectors were actually in the form of quartz cylinders, SiO_2, about $1\frac{3}{4}$ in. long, $\frac{3}{4}$-in. inside diameter, and $\frac{1}{32}$-in. wall thickness. The method of using these SiO_2 detectors was similar to the method employed for $Al^{27}(n,p)$ detectors except that no cadmium box was used to stop slow neutrons since they do not create a competing activity. The intensity of the 2.4-minute beta activity in the quartz cylinders gives a relative value for the intensity of fast neutrons from the irradiated sample.

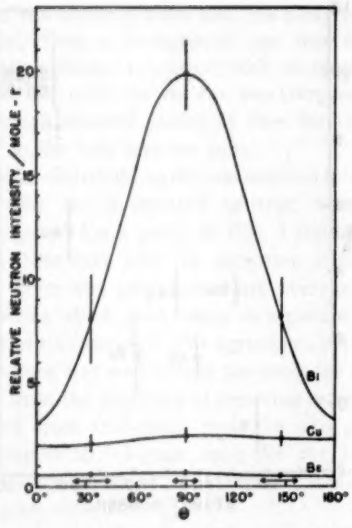

FIG. 7. Angular distributions of photoneutrons from 22-Mev bremsstrahlung on several targets as observed with the $Si^{28}(n,p)$ threshold detector.

The angular distributions of fast photoneutrons as observed with $Si^{28}(n,p)$ detectors are shown in Fig. 7. The smooth curves are the best fit of the data to the function, $a_0+a_1P_1(\cos\theta)+a_2P_2(\cos\theta)$. The units of relative neutron intensity as observed with different types of neutron detectors in this paper bear no relationship to each other.

D. Epithermal Neutron Detector

A neutron detector was constructed which consisted of a rhodium foil in a paraffin cylinder 4.5 cm in diameter and 6 cm long. Moderately slow neutrons are slowed down in the paraffin to an energy at which they are reasily captured by the rhodium. A measurement of the 44-second beta activity in the rhodium gives a relative yield value for the neutron flux. The paraffin block is small enough so that neutrons of more than a few hundred kev energy do not suffer collisions in passing through the paraffin and therefore are not detected.

In such a neutron detector the sensitivity should be fairly uniform for neutron energies from zero up to some value ϵ_0, and above that value decrease rather rapidly. A measurement was made in which a small sample of heavy water was irradiated with 7-Mev bremsstrahlung, and the angular distribution of photoneutrons from deuterium was observed with the epithermal neutron detector. The ratio of neutron intensity at right angles to the intensity parallel to the x-ray beam was found to be 1.60 ± 0.07. From this observed ratio and the known variation of photoelectric and photomagnetic cross sections of the deuteron near threshold the value of ϵ_0 for the epithermal neutron detector was calculated to be 130 kev.

Samples of gold and bismuth were irradiated with 10-Mev bremsstrahlung, and the epithermal photoneutrons from these samples do not show any anisotropy outside probable error. Figure 8 shows the photoneutron yield from $Be(\gamma,n)$ as measured with the epithermal neutron detector as a function of maximum betatron energy.

IV. DISCUSSION

The concept of a statistical model of the nucleus has been developed in great detail by Weisskopf and others. One of the basic premises of the statistical model is that the mode of decay of an excited nucleus is independent of the mode of formation. Another requirement is that the energy-level density of the compound nucleus and the residual nucleus may be expressed by continuous functions. When these requirements are satisfied, one arrives at a photoneutron energy spectrum such as was given in Part II.

A corollary to the statistical model states that the angular distribution of the emitted particles must be isotropic. That is implied in the independence of the mode of formation and the mode of decay of the compound nucleus. Because of the random phase of the many energy states, one would expect that particles emitted from the compound nucleus, not going to the ground state, would be emitted isotropically. In the gamma-neutron reaction any deviation from isotropy would be attributed to the low-lying states of the residual nucleus where the wide spacing of energy levels violates the premise of a statistical model. These concepts of angular distributions of reaction particles in the statistical model are born out in the experiments which are performed. The moderated neutron detector, which detects neutrons up to several Mev equally well,

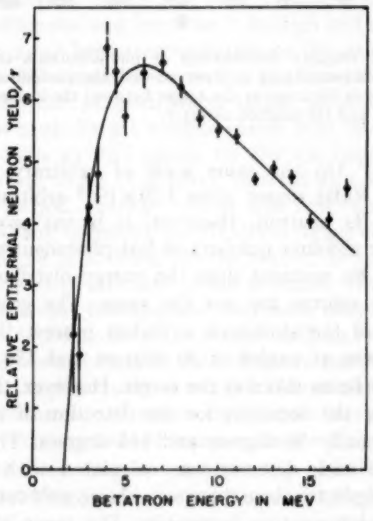

FIG. 8. Relative yield of photoneutrons from beryllium as observed with the epithermal neutron detector.

indicated that the intensity of photoneutrons is very nearly independent of direction. If the angular distributions are expressed in the form $A+B\sin^2\theta$, then the ratio of neutrons contributing to the anisotropic term, $B\sin^2\theta$, to the total number of neutrons is $1.67B/A$. For example, in the case of photoneutrons from bismuth 21 percent of all the neutrons are emitted in a $\sin^2\theta$ distribution (anisotropic), whereas the rest are emitted isotropically. The other elements which were tested with the moderated neutron detector showed smaller anisotropic terms than did bismuth.

Measurements of the angular distributions of photoneutrons with the threshold detectors, $Al^{27}(n,p)$ and $Si^{28}(n,p)$, showed a much more pronounced anisotropy than did the moderated neutron detector. The threshold detectors are sensitive to the very energetic neutrons, around 4 Mev, which represent transitions of the compound nucleus to low-lying levels in the residual nucleus. In keeping with the restrictions of the statistical model, it would be the high-energy neutrons which could exhibit a deviation from isotropy if any neutrons did so.

The epithermal neutron detector showed isotropy of photoneutrons from gold and bismuth with energies from zero up to a few kev. The maximum cross section for nuclear absorption of photons is about 6 Mev above the gamma-neutron threshold. Just such a peak has been observed in most gamma-neutron cross sections. This means than most of the epithermal neutrons are emitted from the compound nucleus about 14 Mev above the ground state and the residual nucleus is left in an excited state, 5 or 6 Mev above its ground state. These conditions are ideal for the statistical model; therefore, one would expect the epithermal neutrons to be emitted isotropically with an energy spectrum appropriate to the statistical model.

The concept of a statistical model in the formation and decay of a compound nucleus does not in any way contradict the principles of quantum mechanics. The nucleus and its reaction products must still be considered as a quantum mechanical system. The absorption of the photon to form the compound nucleus and the subsequent emission of a neutron must still conform to the principles of conservation of parity, energy, angular momentum, etc. Under certain conditions however, certain average quantities can be examined, just as in the kinetic theory of gases the principles of statistical mechanics can be used to derive the general gas laws by considering the average behavior of a large group of molecules. A quantum-mechanical description of the gamma-neutron reaction in a heavy nucleus can disclose several facts about the angular distributions of the particles involved, even when little is known about the specific energy levels.

There is a theorem on the complexity of angular distributions in nuclear reactions which is applicable to the gamma-neutron reaction. It is given implicitly by Myers[18] and shown more explicitly by Eisner and Sachs.[19] Eisner and Sachs state their conclusions as follows: "In a nuclear reaction produced with an unpolarized beam of given orbital angular momentum on an unpolarized target, the angular distribution of the outgoing intensity cannot be more complicated then that of the incoming intensity." To be more explicit, the highest Legendre polynomial necessary to describe the outgoing intensity is $P_{2L}(\cos\theta)$, where L is the orbital angular momentum, in units of $\hbar$, of the incoming wave. The theorem does not in any way restrict the angular momentum of the outgoing neutron to values equal to, or less then, L, but rather, the limitation on the degree of the highest Legendre polynomial in the intensity arises out of interference between outgoing neutron waves.

Photon absorption usually goes by dipole transition in which case $L=1$. Then the outgoing neutron intensity can be expressed as $a_0+a_1P_1(\cos\theta)+a_2P_2(\cos\theta)$, where a_0, a_1, and a_2 are arbitrary constants. For the purpose of comparison, the observed angular distributions are fitted in the best possible way to the above function. It can be shown that the existence of the second term $a_1P_1(\cos\theta)$ may be attributed to a mixture of dipole and quadrapole absorption of the photon. Strictly speaking, terms up to $P_4(\cos\theta)$ should be included to account for quadrapole effects. However, $P_3(\cos\theta)$ and $P_4(\cos\theta)$ were omitted since some of the data could not be specified uniquely by more than three arbitrary constants.

The author is indebted to D. W. Kerst for his interest and encouragement in this problem.

[18] R. D. Myers, Phys. Rev. **54**, 361 (1938).
[19] E. Eisner and R. G. Sachs, Phys. Rev. **72**, 680 (1947).

Nuclear Cross Sections at Low Energies

J. L. JOHNSON AND H. M. JONES*
Yale University,† New Haven, Connecticut
(Received December 7, 1953)

The note is concerned with estimates of the accuracy of the one-term formula for the energy dependence of the reaction cross section for charged particles. The second term in an expansion of the cross section in powers of the energy is worked out for a one-body model. Comparison with data of Sawyer and Phillips on the bombardment of Li and Be with protons and deuterons shows that the deviations from the one-term formula are of the correct order of magnitude to be accounted for by the second term. This term was compared with the effect of the 107-kev resonance on the cross section of $H^3(d,n)He^4$. Employing a conservative central-field model the correction term to the one-body asymptotic form is found to be smaller than the effect of the resonance expected from the Breit-Wigner formula. The f-function generalization to $L>0$ which has been made by Breit is studied and a table facilitating its use for the calculation of reaction cross sections is given.

I. INTRODUCTION

THE present note is concerned primarily with the influence of the Coulomb field on the dependence of nuclear reaction cross sections σ on energy. It was first pointed out by Gamow[1] that the cross sections should depend critically on the energy if the Coulomb barrier prevents direct contact between the colliding particles. In this somewhat qualitative approach it was not important to specify the mechanism of the nuclear reaction, since the Coulomb barrier effect is to some degree independent of the interaction between the particles at distances smaller than that corresponding to contact. On a tentative picture of the flux of relative motion being the determining factor, Breit[2] worked out the asymptotic form of the cross section at low energies in connection with estimates on the possibility of nuclear transmutations by artificial sources of charged particles. This work has been extended by Ostrofsky, Breit, and Johnson,[3] employing a more detailed view of the reaction mechanism. It was supposed by them that the influence of interactions in the region of configuration space corresponding to distances smaller than the contact radius b may be schematically represented through the introduction of an imaginary part of the potential energy and this quantity was related to the inherent probability of distintegration P by means of the conservation theorem for the number of particles. The quantity P represents the probability per second and per unit volume of the space of relative motion of the colliding particles that a disintegration should take place. This quantity is used also in the present work, although its effect on the damping of the incident wave is not taken into account so as to simplify the form of the answers. In the work of OBJ it was shown that the asymptotic form of σ is independent of the value of the orbital angular momentum L even though the centrifugal barrier depends on this quantity. Their paper also shows that, except for the entrance of a factor of proportionality in σ, the same asymptotic form applies independently of the value of P. Generalizations of these results both regarding generality of derivation and of applicability to a wide variety of situations have been made by Wigner.[4] The asymptotic form is in good agreement with experimental data as has been shown by OBJ and later work.

One of the main objects of the present note is to present estimates of the energy region in which deviations from the asymptotic one term form are negligible and to assign approximate values to its probable accuracy. This purpose is accomplished by deriving the second term in the expansion of the ratio of σ to the value of the one term approximation of OBJ in powers of the energy of relative motion E. Since the principal interest here is to have an approximate estimate, the effect of P on the internal function is neglected. There being no special reason for believing that the main term and the correction term are affected very differently by the imaginary part of the potential energy, it is probable that the estimates are valid also for non-negligible absorptions.

For small absorption inside b the behavior of the phase shift as a function of E can be represented conveniently through the employment of the f function of Breit, Condon, and Present[5] and its generalization to $L\neq 0$ made by Breit.[6] In this representation the critical dependence of K_L on E at low E does not interfere with a convenient graphical treatment of experimental material somewhat as in the effective range plots for p-p and p-n scattering. Since the phase shift determines the value of the wave function at the nuclear boundary it is possible to estimate the energy

* Now at Lincoln Laboratory, Massachusetts Institute of Technology, Cambridge, Massachusetts.
† Assisted by the joint program of the U. S. Office of Naval Research and the U.S. Atomic Energy Commission and the Office of Ordnance Research, U. S. Army.
[1] G. Gamow, Z. Physik 52, 510 (1928).
[2] G. Breit, Phys. Rev. 34, 817 (1929).
[3] Ostrofsky, Breit, and Johnson, Phys. Rev. 49, 22 (1936). Hereafter this paper will be referred to as OBJ. The same point of view regarding the role of nuclear absorption has been taken by Feshback, Peaslee, and Weisskopf, Phys. Rev. 71, 145 (1947).
[4] E. P. Wigner, Phys. Rev. 73, 1002 (1948).
[5] Breit, Condon, and Present, Phys. Rev. 50, 825 (1936).
[6] G. Breit, Revs. Modern Phys. 23, 238 (1951).

dependence of σ by means of the f_L function. The present note contains, therefore, a table and a few graphs facilitating the calculation of f_L and showing effects of varying L and other parameters on the (f_L,E) curves.

Notation

The notation for the Coulomb functions is the same as that used by Yost, Wheeler, and Breit,[7] and by Bloch, Hull, Broyles, Bouricius, Freeman, and Breit.[8]

F_L,G_L regular and irregular Coulomb functions for angular momentum $L\hbar$ normalized to be asymptotic to the sine and cosine of the same phase at large r with $F_L>0$ at small r. Where no ambiguity arises the subscript L is omitted in this note.

$\nu=2L+1$.

r,v relative distance and velocity.

$k=\mu v/\hbar$, where μ is the reduced mass.

$\rho=kr$. In this note it is in most cases taken at the nuclear boundary, $r=b$.

$\eta=ZZ'e^2/\hbar v=1/ka$.

$x=(8\rho\eta)^{\frac{1}{2}}$.

$C_L=\{2^L/(2L+1)!\}\{[L^2+\eta^2][(L-1)^2+\eta^2]\cdots\times[1+\eta^2]\}^{\frac{1}{2}}C_0$.

$C_0=[2\pi\eta/(e^{2\pi\eta}-1)]^{\frac{1}{2}}$.

u regular solution of the radial equation for $r<b$, normalized so that $u(b)=1$.

$\delta=F'/F-u'/u$; $'=d/d\rho$.

P adjustable parameter representing probability of reaction occurring if the bombarding particle is inside the nuclear boundary. In general different values of P can be chosen for different L.

U depth of square well representing internal potential in Mev. In all applications the centrifugal potential is supposed to extend in to the origin and is superimposed on this square-well potential.

II. EXPANSION OF THE LOW-ENERGY CROSS SECTION

OBJ derived the formula for the partial cross section for distegration on the one-body model without spin in the limiting case of no absorption, obtaining[9]

$$\sigma_L=\frac{4\pi Pb^3}{v}\frac{(\nu)(F_L^2/\rho^2)\langle u_L^2\rangle}{(1-F_LG_L\delta_L)^2+F_L^4\delta_L^2}, \tag{1}$$

where

$$\langle u_L^2\rangle=\int_0^b w_Lu_L^2dr;\quad \int_0^b w_L(r)dr=1. \tag{1.1}$$

Here the function w_L is the relative intrinsic probability of inducing the disintegration in dr at r as in Bloch, Hull, Broyles, Bouricius, Freeman, and Breit,[8] and in this note will be assumed to be a constant, $1/b$, for simplicity, as in OBJ.

Yost, Wheeler and Breit[7] gave an expansion for Φ and sufficient relations to obtain Φ^* as a power series in $1/\eta^2$ (proportional to energy) and Breit and Hull[9] obtained a corresponding expansion for Θ where the coefficients are simple expressions involving Bessel functions of imaginary argument as defined by Whittaker and Watson.[10]

These expansions were introduced into Eq. (1) in order to obtain the second term in an asymptotic expansion about zero energy of the cross section. The quantity

$$C_0^2=2\pi\eta/(e^{2\pi\eta}-1),$$

which enters through the F^2 in the numerator of the cross-section formula, contains the main energy dependence and was kept intact. Except for the case where a resonance occurs at a very low energy, the term $F^4\delta^2$ is small enough to be neglected and it has therefore been dropped. The result of the calculation thus performed is

$$\sigma=\frac{2\pi P}{v}\frac{H\beta}{(R+S\alpha)^2}\left\{1+(1/\eta^2)\left[\frac{M+N\alpha+O\beta}{R+S\alpha}+\left(\frac{x}{2}\right)^4\frac{\gamma}{\beta}\right]+\cdots\right\}\frac{2\pi\eta}{e^{2\pi\eta}-1}, \tag{2}$$

where

$$H\equiv\nu b^3(x/2)^{-2}I_\nu^2(x)=(\nu/8)a^3(x/2)^4I_\nu^2(x), \tag{2.1}$$

$$R\equiv[\nu+1+2(x/2)^2/(\nu+1)]I_\nu(x)K_\nu(x)-[2(x/2)^2/(\nu+1)]I_\nu(x)K_{\nu+2}(x), \tag{2.2}$$

$$S\equiv-2I_\nu(x)K_\nu(x), \tag{2.3}$$

$$M\equiv\left[\frac{(\nu+2)(x/2)^4}{3(\nu+1)}-\frac{\nu(\nu-1)(x/2)^2}{12}-\frac{\nu(\nu-1)(\nu+1)^2}{24}\right]I_\nu(x)K_\nu(x)+\left[-\frac{(x/2)^4}{3(\nu+1)}+\frac{(\nu-1)(x/2)^2}{12}\right]I_\nu(x)K_{\nu+2}(x), \tag{2.4}$$

$$N\equiv\left[-\frac{(x/2)^4}{3(\nu+1)}+\frac{\nu(\nu-1)(\nu+1)}{12}\right]I_\nu(x)K_\nu(x)+\left[\frac{(x/2)^4}{3(\nu+1)}-\frac{(\nu-1)(x/2)^2}{6}\right]I_\nu(x)K_{\nu+2}(x), \tag{2.5}$$

$$O\equiv(x/2)^4S/4. \tag{2.6}$$

[7] Yost, Wheeler, and Breit, Phys. Rev. **49**, 174 (1936).
[8] Bloch, Hull, Broyles, Bouricius, Freeman, and Breit, Revs. Modern Phys. **23**, 147 (1951).
[9] G. Breit and M. H. Hull, Jr., Phys. Rev. **80**, 561 (1950).
[10] E. T. Whittaker and G. N. Watson, *Modern Analysis* (Cambridge University Press, Cambridge, 1927), Sec. 17.7.

TABLE I. Values of parameters corresponding to typical nuclear interactions.[a]

Reaction	$\eta^2 E$	x	E/ρ^2	x	E/ρ^2	x	E/ρ^2
		$10^{13}r_0=1.4$		$10^{13}r_0=1.7$		$10^{13}r_0=2.1$	
$\alpha+p$	0.0991	1.027	5.70	1.132	3.87	1.258	2.533
$C^{13}+p$	0.892	2.241	2.264	2.469	1.535	2.744	1.006
$Ne^{20}+p$	2.477	3.183	1.545	3.51	1.049	3.90	0.687
$S^{32}+p$	6.34	4.38	1.102	4.83	0.747	5.37	0.490
Li^7+d	0.446	1.935	2.034	2.133	1.379	2.370	0.904
$O^{16}+d$	3.171	3.79	0.983	4.18	0.666	4.64	0.437
$Al^{27}+d$	8.37	5.35	0.649	5.90	0.442	6.56	0.2898
$Li^7+\alpha$	3.92	3.62	1.464	3.99	0.994	4.43	0.651
$C^{13}+\alpha$	15.70	5.91	0.822	6.52	0.557	7.24	0.365
$Ne^{20}+\alpha$	43.6	8.61	0.508	9.49	0.344	10.55	0.2257

[a] The nuclear boundary is given by $b=r_0A^{\frac{1}{3}}$ where A is the sum of the mass numbers of the incident and the bombarded nuclei and $10^{13}r_0$ is 1.4, 1.7, and 2.1. Lengths are in centimeters and energies in Mev.

H, R, S, M, N, and O are functions only of the external region, and the other parameters in (2) are defined by the expansions

$$\rho u'/u=\alpha+(1/\eta^2)[-\beta(x/2)^4/8]+\cdots, \tag{3}$$

$$2\langle u^2\rangle=\beta+(1/\eta^2)[\gamma(x/2)^4]+\cdots, \tag{3.1}$$

with energy-independent α, β, and γ. It has been assumed that the nuclear potential does not extend beyond b.

The relation of η to the bombarding energy in Mev is[8]

$$E=(0.1574ZZ')^2M_i/\eta^2, \tag{4}$$

where M_i is the mass of the incident particle. The choice of a nuclear radius b determines

$$\rho\eta=ZZ'\mu b/(2.905\times10^{-12}\text{ cm}), \tag{4.1}$$

and thus x, and establishes the relation between E and ρ^2. The phase z of the wave function at b can be obtained from the knowledge of the internal potential. Thus if U is the depth of a square well potential inside b, the ratio of the square of the phase of the wave function at b to $E+U$ is the same as that of ρ^2 to E, and for zero energy $z^2/U=\rho^2/E$. In Table I values of the parameters are given for various reactions.

The functions defined by Eqs. (2.2)–(2.6) are tabulated in Table II for values of x less than 10. The functions α, β, and γ are obtainable from their definitions, Eqs. (3) and (3.1).

This expansion was compared for a simple case with calculations using the Coulomb function tables.[8] The parameters chosen, $x=2.76$ and $z=4$, correspond to $C^{12}+p$ with a square well potential of depth, $U=14.75$ Mev and range, $b=4.99\times10^{-13}$ cm. The proton energy is obtainable as $E=0.892/\eta^2$ Mev.

The solid straight lines in Fig. 1 represent the correction to the one-term low-energy formula due to terms linear in energy in this case. For $L=0$ accurate computations of σ using the Coulomb function tables give the same result as the expansion. The agreement is fortuitous in this case, as an examination of the energy dependence of $1-FG\delta$ indicates that the nonlinearity of $\rho\delta$ tends to cancel that of FG/ρ. For $L=1$ the difference of 10 percent when $1/\eta^2=0.5$ between the result of the computations using the Coulomb function tables and those using the expansion is largely due to the nonlinearity of $1-FG\delta$. The results of obtaining the values of the various components of the cross section, $2\langle u^2\rangle$, $1-FG\delta$, and F/ρ, from their low-energy expansions at $1/\eta^2=0.5$ and then combining these numbers directly indicate that terms of order $1/\eta^4$ are large enough to be seen on an ordinary graph even at this energy.

TABLE II. Values of coefficients $\begin{pmatrix} R & S \\ M & [N] \end{pmatrix}$ for different L.[a]

x \ L	0		1		2		3		4	
0	0	1.000	0.333	0.3333	0.400	0.2000	0.429	0.1429	0.444	0.1111
	0	[0]	0.333	[0.333]	2.000	[1.000]	6.00	[2.000]	13.33	[3.333]
1	0.238	0.680	0.353	0.3149	0.404	0.1960	0.430	0.1414	0.445	0.1104
	0.0312	[−0.0383]	0.354	[0.311]	2.020	[0.979]	6.02	[1.979]	13.35	[3.312]
2	0.362	0.445	0.383	0.2754	0.414	0.1853	0.434	0.1372	0.447	0.1084
	0.0604	[−0.1345]	0.395	[0.251]	2.064	[0.913]	6.07	[1.915]	13.40	[3.249]
3	0.412	0.3175	0.412	0.2345	0.426	0.1711	0.439	0.1312	0.450	0.1054
	0.00567	[−0.2736]	0.396	[0.110]	2.091	[0.799]	6.11	[1.806]	13.46	[3.143]
4	0.436	0.2437	0.432	0.1995	0.437	0.1558	0.446	0.1239	0.454	0.1015
	−0.197	[−0.453]	0.277	[−0.0665]	2.035	[0.635]	6.10	[1.651]	13.47	[2.991]
5	0.449	0.1968	0.446	0.1713	0.447	0.1412	0.452	0.1161	0.457	0.0971
	−0.609	[−0.673]	−0.0360	[−0.288]	1.795	[0.422]	5.96	[1.448]	13.39	[2.795]
6	0.458	0.1649	0.455	0.1491	0.455	0.1279	0.457	0.1083	0.461	0.0924
	−1.292	[−0.934]	−0.612	[−0.553]	1.378	[0.163]	5.62	[1.197]	13.13	[2.551]
7	0.464	0.1417	0.462	0.1314	0.461	0.1161	0.462	0.1010	0.464	0.0877
	−2.308	[−1.237]	−1.516	[−0.860]	0.629	[−0.140]	5.02	[0.902]	12.66	[2.263]
8	0.469	0.1243	0.467	0.1170	0.466	0.1060	0.466	0.0940	0.468	0.0830
	−3.72	[−1.581]	−2.813	[−1.208]	−0.495	[−0.487]	4.07	[0.559]	11.86	[1.925]
9	0.472	0.1106	0.471	0.1055	0.470	0.0971	0.470	0.0875	0.471	0.0784
	−5.60	[−1.969]	−4.57	[−1.600]	−2.062	[−0.880]	2.70	[0.1690]	10.67	[1.540]
10	0.475	0.0996	0.474	0.0958	0.473	0.0894	0.474	0.0817	0.474	0.0741
	−7.98	[−2.394]	−6.84	[−2.027]	−4.14	[−1.308]	0.859	[−0.2557]	8.27	[1.118]

[a] Graphical or parabolic interpolation is recommended.

The expansion has been used to investigate the effect of decreasing the nuclear radius while increasing the well depth so as to keep the same zero-energy value of the logarithmic derivative of the wave function at b. This makes z, and thus α, β, and γ remain unchanged. The correction to the one-term formula due to the second term is given in Fig. 1 by the solid straight lines when $x=2.76$, the dashed lines when $x=2.48$, and the dotted lines when $x=2.25$. The corresponding radii b are 4.99×10^{-13} cm, 4.04×10^{-13} cm and 3.32×10^{-13} cm, and the well depths are 14.75 Mev, 22.5 Mev and 33.2 Mev, respectively. For these cases $H\beta/(R+S\alpha)^2$ is given by $3.25b^3$, $2.18b^3$, and $1.55b^3$ for $L=0$, and $1.80b^3$, $0.409b^3$, and $0.150b^3$ for $L=1$.

Sawyer and Phillips[11] have measured cross sections at 90° for several of the reactions which occur when lithium or beryllium is bombarded by protons or deuterons in the 30- to 250-kev energy range. By assuming an isotropic distribution of the reaction particles they obtained values for the total cross sections. For most of their reactions $\ln(\sigma E)$ was a linear function of $E^{-\frac{1}{2}}$ with a slope not far from that predicted by the one-term asymptotic formula

$$\sigma E = Ae^{-2\pi\eta}. \tag{5}$$

The slope corresponding to the two-term formula is

$$d\ln(\sigma E)/dE^{-\frac{1}{2}} = -2\pi\eta E^{\frac{1}{2}}[1+\Xi E/\eta\pi], \tag{5.1}$$

where

$$\Xi = \left[\frac{M+N\alpha+O\beta}{R+S\alpha} + \left(\frac{x}{2}\right)^4\frac{\gamma}{\beta}\right]/\eta^2 E. \tag{5.2}$$

For reasonable models the ratio of this slope to that of the one-term formula was found to be of the same order of magnitude as the ratio obtained from the experimental curves. In the case of $Li^6(p,\alpha)He^3$ the ratio from experiment was 1.024 while the ratio computed from the two-term formula varied from 1.020 when $E=20$ kev to 1.118 when $E=250$ kev. These values were very insensitive to the nuclear radius chosen, showing little change as the radius was increased from 2.87×10^{-13} cm to 4.02×10^{-13} cm. The order of magnitude is not very sensitive to the well depth in the region of good convergence of Eqs. (3) and (3.1). For the ratio quoted, the well depth had been adjusted for a phase of 1.7 radians at the nuclear radius. The ratio obtained from experiment for the $Li^6(d,\alpha)He^4$ reaction was 0.967. If the well is adjusted to give a phase of about 1.7 radian at a nuclear radius of 4×10^{-13} cm, the calculated ratio varies from 1 to about 0.97 in the energy range considered. The calculated ratio shows considerable sensitivity both to the radius and the depth in this case. These calculations were made for $L=0$. No significance is being attached to the possibility of fitting experimental values exactly.

[11] G. A. Sawyer and J. A. Phillips, Los Alamos Report LA-1578 (unpublished).

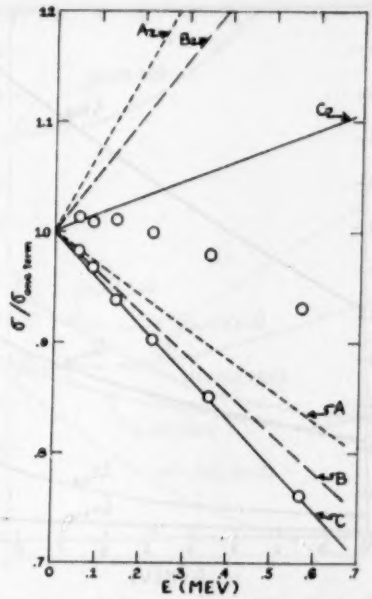

FIG. 1. Correction factor, $\{1+(1/\eta^2)[(M+N\alpha+O\beta)/(R+S\alpha)+(x/2)^4\gamma/\beta]\}$, to the one-term formula for the reaction cross section for $C^{12}+p$ as a function of the bombarding energy E. The dotted lines A correspond to a nuclear well of range $b=3.32\times10^{-13}$ cm and depth $U=33.2$ Mev, the dashed lines B to $b=4.04\times10^{-13}$ cm, $U=22.5$ Mev, and the solid lines C to $b=4.99\times10^{-13}$ cm, $U=14.75$. The points marked by circles represent the results of an exact calculation using the Coulomb function tables for parameters corresponding to lines C. The lower curves are for $L=0$ and the upper for $L=1$.

It appears appropriate to state again that in the correction terms discussed above, the decay of the wave function inside the nucleus is not taken into account.

Behavior of the f Function

Breit[6] has generalized the f function for cases where $L>0$:

$$f_L = [\nu C_L^2 \cot K_L - p_L \ln\eta + q_L]/\eta^\nu. \tag{6}$$

This function was computed for some one-body models for reactions between protons, deuterons, or alpha particles and nuclei smaller than Si^{28}. Values of f and $\nu C^2\cot K/\eta^\nu$ were compared for several choices of $\rho\eta$, keeping $U=0$. For $\rho\eta=0.1$, f_0 and f_1 are almost constant, f_0 increasing from 79 to 81 as $1/\eta^2$ goes from 0 to 10 and f_1 changing from 5.4×10^4 to 5.5×10^4 in the same range. When $\rho\eta=0.538$, which represents the interaction of a deuteron with Li^7, f_0 changes almost linearly from 1.5 to 3.4 while f_1 goes from 41 to 60 with some curvature as $1/\eta^2$ goes from 0 to 10. These curves are not illustrated but are similar to those for $\rho\eta=0.952$ which corresponds to a proton incident on C^{12} where $b=4.99\times10^{-13}$ cm. The $\rho\eta=0.952$ curves, presented in Fig. 2, illustrate the effect produced by changing L

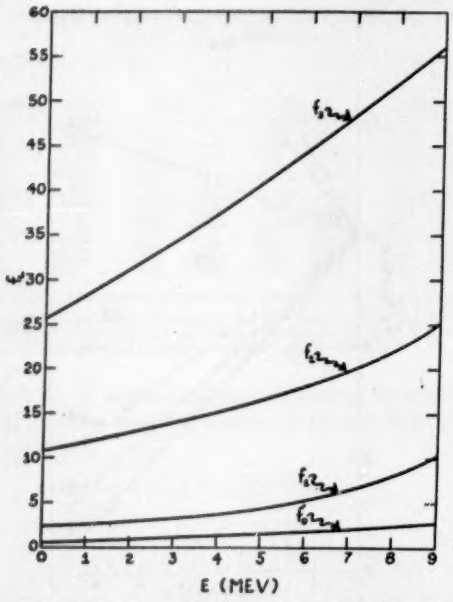

FIG. 2. The f_L function as a function of the bombarding energy, E, for $C^{12}+p$ with $b=4.99\times10^{-13}$ cm($\rho\eta=.952$) and $U=0$.

and are reasonably well represented by the series:

$$f_0=0.50+0.175/\eta^2+0.005/\eta^4; \quad (7)$$

$$f_1=2.45+0.055/\eta^2+0.055/\eta^4; \quad (7.1)$$

$$f_2=10.70+0.713/\eta^2+0.072/\eta^4; \quad (7.2)$$

$$f_3=25.70+2.24/\eta^2+0.084/\eta^4. \quad (7.3)$$

For values of $\rho\eta$ greater than 2, the term $(-p\ln\eta+q)/\eta^r$ tends to mask all the effects of the phase shift. In these cases a simple plot of $C_L^2\cot K_L/\eta^r$ used in the spirit of Breit, Thaxton, and Eisenbud[12] could still be useful.

In order to facilitate the use of the f function, values of the term $(-p\ln\eta+q)/\eta^r$ have been computed for $L\leq4$ for values of $1/\eta^2<40$ and are presented in Table III.

For the case $L=1$, calculations were performed to see the effect of varying the range of the nuclear well. The well depth was adjusted in each case to restore the f function at zero energy to its previous value. The well depth is increased to 5.05 Mev when $\rho\eta$ is decreased to 0.72 which corresponds to $C^{12}+p$ where $b=3.77\times10^{-13}$ cm. Similarly $U=24.16$ Mev when $\rho\eta=0.50$ for which $b=2.62\times10^{-13}$ cm. The results are shown in Fig. 3. The straight lines indicate the f function as found from an expansion in powers of the energy similar to Eq. (2). The slope at zero energy rapidly steepens as the nuclear radius is decreased, illustrating the fact, pointed out by Breit,[6] that for zero range $\partial f/\partial E=-\infty$ for $L>0$.

In order to investigate the effect of changing the Coulomb field, the effect of changing a proton to a neutron in a reaction was considered. As f is proportional to η^{-r} it was necessary to introduce a modification for zero charge. The function, $(e^2/mc^2a)^r f_L$, was used, the dependence of a on the charge Z canceling that of η, and the length, e^2/mc^2, being introduced to reduce the function to a convenient order of magnitude. For zero charge the term, $-p\ln\eta+q$, reduces to zero. In Fig. 4, comparisons are made for $L=1$ between $C^{12}+p$ and $C^{12}+n$, the nuclear radii and the potentials inside the nuclear boundary being the same as those of the lower two curves in Fig. 3. The case corresponding to $\rho\eta=0.952$ is not shown, as the phase shift would vanish since $U=0$ so that the modified f function would be infinite.

In changing from a proton to a neutron reaction some consideration must be made of the effect of the change in the internal potential. To estimate this the potential corresponding to a uniform distribution of charge inside the nucleus was calculated. The average value of this potential was then added to the depth of the internal well for the neutron reaction calculations. The modified f functions are shown by dotted lines in Fig. 4 for the same radii as above but with larger well depths. When $b=3.77\times10^{-13}$ cm the well depth is increased to 8.15 Mev and for $b=2.62\times10^{-13}$ cm, $U=28.61$ Mev.

The cross section of $H^3(d,n)He^4$ has recently been studied at energies below 120 kev by Arnold, Phillips,

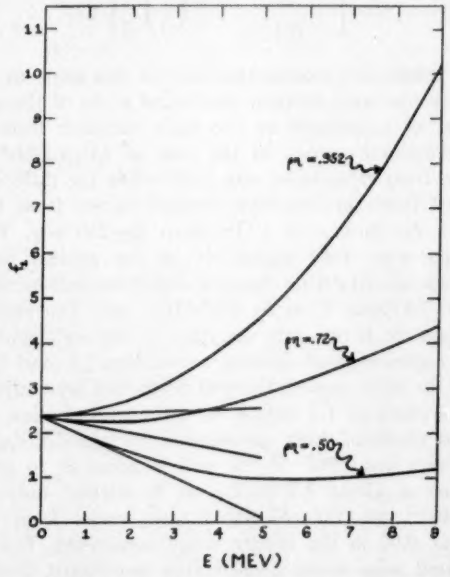

FIG. 3. The effect on the f function for $L=1$ of decreasing b and increasing U to keep the same zero-energy intercept. The curves, representing $C^{12}+p$, have parameters: $b=4.99\times10^{-13}$ cm ($\rho\eta=0.952$), $U=0$; $b=3.77\times10^{-13}$ cm ($\rho\eta=0.72$), $U=5.05$ Mev; and $b=2.62\times10^{-13}$ cm ($\rho\eta=0.50$), $U=24.16$ Mev. The straight lines indicate the zero-energy slopes as obtained from an asymptotic expansion.

[12] Breit, Thaxton, and Eisenbud, Phys. Rev. 55, 1018 (1939).

Sawyer, Stovall, and Tuck,[13] as well as by Argo, Taschek, Agnew, Hemmendinger, and Leland[14] and by Conner, Bonner, and Smith.[15] At the peak of the 107-kev resonance the total cross section is 4.95 barns. Within experimental error it is isotropic[16] with angle at the resonance as well as at lower energies. There is no special objection therefore to assuming the reaction to be caused by incident deuterons in s states. Since in the comparison of resonance and potential well effects one is primarily interested in relative values the exact interpretation of the cross section in terms of contributions from different values of total angular momentum J is probably not too important. For this reason only the two extremes were tried in assignments of partial cross sections to $J=\frac{1}{2}$ and $\frac{3}{2}$, it being assumed that the whole cross section at resonance is associated with one or the other of these values of J. The experimental value of 4.95 barns is large enough to exclude the assignment of the reaction to $J=\frac{1}{2}$.[14,15] For $J=\frac{3}{2}$, the resonance denominator has the approximate form

$$(44 \text{ kev})^2+(E-E_0)^2,$$

giving a variation in σ of a factor $\frac{5}{2}$ as one changes E from about 60 kev to 20 kev. The denominator of the Breit-Wigner formula is readily seen to give a sufficiently strong dependence on E to make the direct application of Eq. (2) difficult. No attempt is being made here to find the best one-level formula fit since it is desired to illustrate the lack of constancy of the denominator. Even if one were to use 88 kev in place of 44 kev with constant Γ and no energy-dependent level shift, the factor $\frac{5}{2}$ would change to about 1.6 which is still larger than the one-body effects unless the latter are made to have distinct resonance features.

TABLE III. Values[a] of $(-p_L \ln\eta+q_L)/\eta^2$.

$1/\eta^2$	$L=0$	$L=1$	$L=2$	$L=3$	$L=4$
0	0.3089	−0.453	−0.013		
1	0.4982	−0.612	−0.091	−0.004	
2[b]	0.697	−0.632	−0.200	−0.012	
3[b]	0.875	−0.540	−0.303	−0.040	−0.003
4[b]	1.037	−0.383	−0.409	−0.074	−0.007
6[b]	1.300	0.138	−0.552	−0.170	−0.020
8[b]	1.510	0.851	−0.531	−0.271	−0.049
10	1.679	1.711	−0.364	−0.399	−0.099
12	1.828	2.689	0.050	−0.477	−0.162
14	1.956	3.777	0.712	−0.480	−0.235
16[b]	2.071	4.94	1.66	−0.370	−0.310
18	2.172	6.211	2.914	−0.082	−0.363
20	2.265	7.517	4.463	0.410	−0.381
22	2.350	8.915	6.425	1.199	−0.325
24[b]	2.429	10.36	8.85	2.30	−0.140
26[b]	2.503	11.84	11.50	3.03	0.180
28	2.569	13.39	14.34	5.873	0.695
30	2.633	14.98	17.78	8.406	1.502
32	2.693	16.63	21.71	11.54	2.617
34	2.750	18.30	25.94	15.33	4.159
36	2.802	20.00	30.60	19.82	6.172
38	2.855	21.80	35.86	25.29	8.861
40[b]	2.900	23.40	41.37	30.65	11.67

[a] Linear interpolation is accurate to ±0.03.
[b] Values were not calculated directly but were obtained graphically from neighboring calculated values.

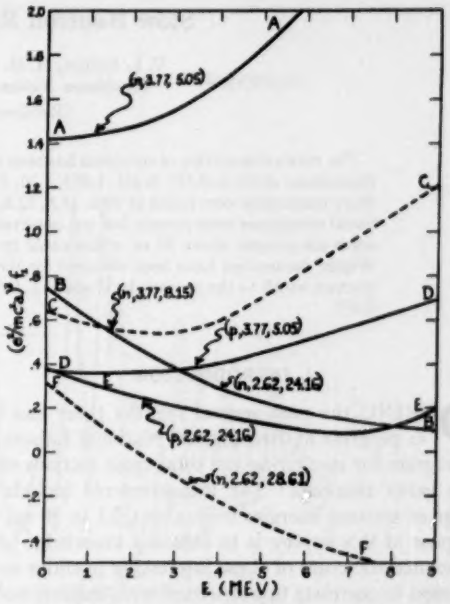

FIG. 4. Comparison of $(e^2/mc^2a)^2 f_L$ for $C^{12}+p$ and $C^{12}+n$ reactions. For the solid curves the parameters representing the nuclear well are the same as for the two bottom curves in Fig. 3, *viz.*, curves D and E represent a proton reaction where $b=3.77\times10^{-13}$ cm ($\rho\eta=0.72$), $U=5.05$ Mev, and $b=2.62\times10^{-13}$ cm ($\rho\eta=0.50$), $U=24.16$ Mev, and the curves A and B represent the corresponding neutron reactions ($\rho\eta=0$). For the dotted curves the well depths have been increased so as to take approximate account of the Coulomb potential inside the nucleus. Thus for curve C the well depth has been increased to 8.15 Mev, the radius being kept at $b=3.77\times10^{-13}$ cm, and for curve F where $b=2.62\times10^{-13}$ cm the well depth is 28.61 Mev. In order to ensure positive identification of the graphs the triplet of symbols consisting of the designation of the reaction particle (p or n), the radius in 10^{-13} cm and the well depth in Mev are used as an additional label for each graph. Thus graph A has the additional identification (n, 3.77, 5.05).

ACKNOWLEDGMENTS

We are greatly indebted to Professor G. Breit for initiating and guiding this work and for much assistance in the preparation of this note. We are also very grateful to Mr. W. Huebner and Mr. W. S. Porter for assistance in the reduction of the experimental material.

[13] Stovall, Arnold, Phillips, Sawyer, and Tuck, Phys. Rev. **88**, 159 (1952).
[14] Argo, Taschek, Agnew, Hemmendinger, and Leland, Phys. Rev. **87**, 612 (1952).
[15] Conner, Bonner, and Smith, Phys. Rev. **88**, 468 (1952).
[16] E. Bretscher and A. P. French, Phys. Rev. **75**, 1154 (1949); D. L. Allan and M. J. Poole, Proc. Roy. Soc. (London) **A204**, 500 (1951).

Slow Neutron Resonances in Europium*

V. L. SAILOR, H. H. LANDON, AND H. L. FOOTE, JR. †
Brookhaven National Laboratory, Upton, New York
(Received December 11, 1953)

The total cross section of europium has been measured over a range of neutron energy from 0.08 to 58 ev. Resonances occur at 0.327, 0.461, 1.055, 1.76, 2.46 2.73, 3.35, 3.84, 6.25, 7.36, and 8.98 ev. Between 10- and 20-ev resonances were found at 10.6, 11.8, 12.8, 15.1, and ~19.5; however, it is probable that several additional resonances were present but not observed because of insufficient instrument resolution. Many resonances are present above 20 ev which could not be resolved. The strength, $\sigma_0\Gamma^0$, and various other Breit-Wigner parameters have been obtained for the resonances below 10 ev. The ratio of the average reduced neutron width to the average level spacing, Γ_n^0/D, was found to be 3.5×10^{-4} for Eu^{151} and 3.3×10^{-4} for Eu^{153}.

I. INTRODUCTION

DURING the past several months there has been in progress at Brookhaven National Laboratory a program for measuring the total cross sections of the rare earth elements.[1] The measurements include the range of neutron energies from about 0.1 to 50 ev. One purpose of this survey is to obtain a knowledge of the resonance structure of these interesting nuclides and to attempt to correlate this structure with existing nuclear theory. One can compare for example, the average spacing and strengths of resonances with theoretical predictions based on specific nuclear models. The rare earth region is particularly sensitive for comparison with the so-called "cloudy crystal-ball" model of Feshbach, Porter, and Weisskopf.[2]

Europium has two stable isotopes, Eu^{151} and Eu^{153}, having abundances[3] of 47.77 percent and 52.23 percent, respectively. Both are odd-even isotopes, and experience indicates that odd-even isotopes in this region of the nuclear periodic table are characterized by relatively closely spaced slow-neutron resonances of moderate strength. Previous measurements[4,5] of the europium cross section disclosed a complicated resonance structure including one resonance in[4] Eu^{151} which lies at approximately "zero" energy.[5] There appeared to be several additional resonances below 5 ev, with evidence for one of these at approximately 3.3 ev belonging[6] to Eu^{151}. The earlier measurements were made with insufficient instrument resolution to permit the details of the structure to be observed.

II. EXPERIMENTAL DETAILS

The total cross section measurements were made with the BNL crystal spectrometer, which has been described in detail previously.[7] The crystals used for the monochromator were as follows: 0.08 to 0.2 ev, NaCl (220); 0.1 to 0.4 ev, NaCl (240); 0.3 to 58 ev, Be ($12\bar{3}1$).

Three europium samples from two independent sources were used in the measurements. Samples 0.0509 and 0.0117 g/cm² in thickness were prepared from Johnson, Matthey, and Company, Ltd. "Specpure" Europium Oxide. Spectroscopic analysis of this material disclosed no significant impurities. A third sample 0.1747 g/cm² in thickness was prepared from europium oxide obtained from Research Chemicals, Inc. This oxide had a nominal purity of better than 99.8 percent. Before preparing the samples it was necessary to bake the oxides for several hours at approximately 800°C to remove water. The material for each sample was then placed in a 5-ml volumetric flask for weighing and processing. After being weighed the oxide was converted to the nitrate by dissolving it in nitric acid; hydrogen in the sample (the water of crystallization of the nitrate) was displaced by deuterium by means of several stages of dissolving it in D_2O and evaporating it to dryness; and finally the "deuterated" nitrate was dissolved in D_2O and diluted to standard volume. In this manner the concentration of the solution was accurately determined. For the measurement, an aliquot was transferred to a precision quartz cell. Transmission measurements were made against an identical cell filled with D_2O. It is estimated that the error in determining the thickness of each sample was approximately ±1 percent. A small correction to the observed transmission was needed in the case of the 0.1747-g/cm² sample to correct for the presence of the $(NO_3)_3$ radical in the solution.

III. RESULTS

Total Cross Section

The observed total cross section of europium (uncorrected for the effects of instrument resolution or Doppler broadening) is shown in Fig. 1. The resonances which were observed are listed in Table I. In addition

* Research performed under contract with the U. S. Atomic Energy Commission.
† Doctoral candidate from the University of Utah, Salt Lake City, Utah.
[1] Foote, Landon, and Sailor, Phys. Rev. **92**, 656 (1953); Sailor, Landon, and Foote, Phys. Rev. **91**, 450 (1953); Foote, Sailor, and Landon, Phys. Rev. **90**, 362 (1953); Sailor, Foote, and Landon, Phys. Rev. **89**, 904 (1953).
[2] Feshbach, Porter, and Weisskopf, Phys. Rev. **90**, 166 (1953); Nuclear Development Associates, Inc., Report NYO-3076, 1953 (unpublished).
[3] D. C. Hess, Jr., Phys. Rev. **74**, 773 (1948).
[4] Borst, Ulrich, Osborne, and Hasbrouck, Phys. Rev. **70**, 557 (1946).
[5] W. J. Sturm, Phys. Rev. **71**, 757 (1947).
[6] M. Goldhaber (unpublished). See reference 20 in W. J. Sturm, Phys. Rev. **71**, 757 (1947).
[7] L. B. Borst and V. L. Sailor, Rev. Sci. Instr. **24**, 141 (1953).

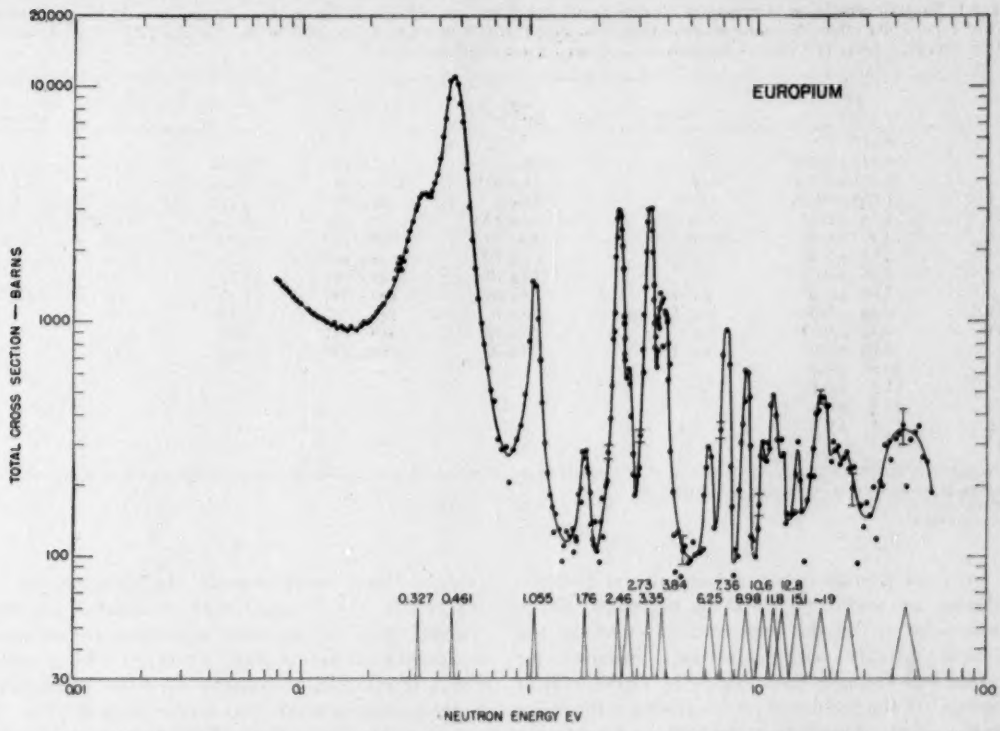

FIG. 1. Total cross section of europium. The location of each resonance is indicated by the triangle and the value of E_0. The width of the triangle represents the width of the instrument resolution function at that energy. Uncertainties due to counting statistics are, in general, smaller than the plotted points, except in the regions where typical errors are shown.

to those listed in the table it is probable that several more resonances occur between 10 and 20 ev which could not be observed because of insufficient resolution. Above 20 ev many resonances are present but are unresolved.

The resonances at 1.76 and 2.73 ev are markedly weak, and at first sight would appear to be due to impurities. It is possible in principle to identify impurities by means of the resonance spectrum, because the line structure of each element is unique. The most probable impurities in europium would be other rare earth elements, which are generally difficult to detect by ordinary chemical or spectroscopic means. However, the cross sections of all of the rare earths, with the exception of terbium,[1] have been carefully studied below 10 ev; and it is found that no rare earth impurity (with possible exception of Tb) can account for the two lines in question.[8] In fact, a search among all those elements for which the resonance structure has been determined[9] (the majority of the 92 elements), discloses no impurities which could reasonably account for the 1.76- and 2.73-ev resonances. Probably both of these resonances belong to europium. Further evidence in regard to the 2.73-ev line is obtained from activation measurements which indicate that it belongs to Eu^{151}, although the identification is not certain.

In an independent study,[10] Wood has determined which of the resonances below 10 ev belong to Eu^{151}. The assignment was made by measuring the amount of 9-hour Eu^{152} activity produced by the irradiation of a Eu sample with monochromatic neutrons. The isotopic assignments of Wood are listed in Table I.

Analysis of Resonances

Except at very low energies the experimentally observed shape of a neutron resonance is not the same as the theoretical shape because of the effects of instrument resolution and Doppler broadening. With the BNL crystal spectrometer these distortions are appreciable at 1 ev and become increasingly more severe at higher energies. Several methods are available for obtaining various combinations of the "true" Breit-Wigner parameters of a resonance. These are as follows: (1) A direct fit of the experimental curve to a theore-

[8] Dysprosium, for example, has strong resonances at 1.7 and 2.7 ev, but an additional very strong resonance at 5.5 ev. If the 1.76- and 2.73-ev resonances in the europium sample were due to a small dysprosium impurity, then the resonance at 5.5 ev would also have been observed.

[9] *Neutron Cross Sections*, U. S. Atomic Energy Commission Report, AECU-2040 (U. S. Government Printing Office, Washington, D. C., 1952).

[10] R. E. Wood (to be published).

TABLE I. Neutron resonances in europium. Entries containing σ_0 are isotopic values. Parameters obtained directly from analysis are in normal type, while values derived from the assumption that $\Gamma_\gamma = 0.09$ ev are in italics. The "reduced width", $\Gamma_n^0 = \Gamma_n/E_0^{\frac{1}{2}}$, was computed by assuming $g = \frac{1}{2}$. The various methods for analysis are described in the text.

	E_0 (ev)	Isotope[a]	$\sigma_0\Gamma^2$ barn ev^2	$\sigma_0\Gamma$ barn ev	$10^3 g\Gamma_n$ ev	$10^3\Gamma_n^0$ ev	Method of analysis
1	−0.011[b]	151[c]	...	...	...	...	...
2	+0.327±0.001	151	30.0±1.5	347±14	0.044	0.15	1
3	0.461±0.001	151	213±10	2230±60	0.396	1.11	1
4	1.055±0.005	151	35±6	330±50	0.136	0.25	1
5	1.76 ±0.02	Not 151	*4.6±1.5*	53±14	0.034	0.06	4
6	2.46 ±0.01	Not 151	86±10	*960±120*	0.90	1.20	3, 4
7	2.73 ±0.05	151(?)	*3.8±1.5*	42±10	0.04	0.05	4
8	3.35 ±0.01	151	113±12	1340±140	1.72	1.80	4
9	3.84 ±0.02	Not 151	73±16	*800±200*	1.19	1.26	4
10	6.25 ±0.04	Not 151(?)	*16±4*	184±20	0.44	0.37	4
11	7.36 ±0.03	151	126±15	*1380±140*	3.91	2.76	4
12	8.98 ±0.05	Not 151	95±20	*1050±300*	3.63	2.53	4
13	10.6 ±0.2	...	...	...	...	...	...
14	11.8 ±0.1						
15	12.8 ±0.3						
16	15.1 ±0.2						
17	~19.5						

[a] Isotopic assignments of R. E. Wood (see reference 10).
[b] See reference 5.
[c] See reference 4.

tical one-level formula when resolution and Doppler broadening are small enough to be neglected; (2) A point-by-point fit of the experimental curve to the theoretical formula with corrections included for resolution and Doppler broadening;[11] (3) Direct fit of the "wings" of the resonance (in the region of the curve where the effects of resolution and Doppler broadening are negligible) to the theoretical formula; and (4) The "area analysis" method as refined by Melkonian *et al.*[12]

The choice of the method of analysis to be applied to a particular resonance depends on many practical considerations; e.g., the proximity of other resonances and the resolution width at E_0. In the case of the europium spectrum the method selected for the analysis of each resonance is noted in Table I.

The resonances at 0.327 and 0.461 ev lie at a low enough energy so that the effects of instrument resolution and Doppler broadening are negligible. Therefore, the Breit-Wigner formula can be fitted directly to these resonances [(i.e., method (1) above)]. Note, however, that they lie so close together that it is necessary to analyze them simultaneously. In carrying out this analysis it was assumed that resonant scattering is negligible and that all other resonances are far enough separated so as to contribute a background cross section which is essentially constant over the energy range under consideration. It was further assumed that each resonance satisfies a Breit-Wigner single-level formula and that the resultant cross section can be obtained by adding the individual cross sections. This implies that the resonances do not mutually fulfill the rather stringent requirements of the many-level formula in regard to identity of the entrance and exit channels and hence do not exhibit interference effects.

The curve fitting was accomplished by using the method of least squares to solve for E_0, Γ, and σ_0 for each resonance plus the constant background contribution from other resonances. The final solution involved a seventh-order determinant. The results of the analysis are presented in Table II, and the individual and combined theoretical curves are shown with the experimental points in Fig. 2. It is believed that the excellent

TABLE II. Precise Breit-Wigner parameters for three of the europium resonances. These results were derived by fitting the experimental points to the single-level formula by the method of least squares. The entry $F\sigma_0$ is the total cross section at resonance for the element. All other entries are corrected for the isotopic abundance F.

	No. 2	No. 3	No. 4
E_0	0.327±0.001	0.461±0.001	1.055±0.005
Isotope[a]	151	151	151
$F\sigma_0$(barns)	1930±50	11 100±100	1500±70
σ_0(barns)	4040±100	23 230±200	3100±150
Γ_γ(ev)	0.086±0.002	0.096±0.002	0.105±0.010
$g\Gamma_n$(ev)	(0.044±0.002)×10^{-3}	(0.395±0.010)×10^{-3}	(0.14±0.02)×10^{-3}
$g\Gamma_n/\Gamma$	(0.51±0.02)×10^{-3}	(4.1±0.2)×10^{-3}	(1.3±0.2)×10^{-3}

[a] Isotopic assignments of R. E. Wood (see reference 10).

[11] V. L. Sailor, Phys. Rev. 91, 53 (1953).
[12] Melkonian, Havens, and Rainwater, Phys. Rev. 92, 702 (1953).

agreement between the calculated and experimental curves justifies the assumption of the applicability of the single-level formula; and, that if interference effects were present, a marked misfit would have resulted in the region between the two resonances.

The 1.055-ev resonance was analyzed by method (1) after correcting for the contributions of the 0.327- and 0.461-ev resonances. The results of this analysis are less accurate because resolution and Doppler broadening, though small, are appreciable. To reduce the effects of resolution and Doppler broadening, points near the center of the resonance were not used in the analysis because the smearing effects are largest at the center. The parameters for the 1.055-ev resonance are also listed in Table II.

Less precise results were obtained for the resonances at higher energies because of the close spacing of levels and the correspondingly poorer resolution. Unfortunately, the close spacing prevented full advantage to be taken of the refinements of the "area method." Results for these resonances are summarized in Table I.

Several additional parameters of interest may be computed and are listed in Table I. The product, $\sigma_0\Gamma$, can be used to obtain $g\Gamma_n$ for each resonance. In several cases only $\sigma_0\Gamma^2$ was measured from the area analysis; so in order to compute $g\Gamma_n$, Γ must be estimated. The value $\Gamma=0.09$ ev appeared to be a resonable estimate for Eu, and was arbitrarily assumed when necessary. The statistical weight factor g cannot be uniquely determined from total cross section measurements; however, it should be noted that the spin[13] of both Eu^{151} and Eu^{153} is 5/2 permitting g to be either 5/12 or 7/12. Thus the error is small if g is assumed to be $\frac{1}{2}$ in all cases. A more useful quantity for comparing the strength of resonances is the "reduced neutron width", defined as $\Gamma_n^0\equiv\Gamma_n/E^{\frac{1}{2}}$. This parameter permits the strength of all resonances to be compared at a reference energy of 1 ev with all energy-dependent factors in the parameters eliminated.

IV. DISCUSSION OF RESULTS

Comparison of the values of Γ_n^0 in Table I shows a range of variation of more than a factor of ten. Large and apparently random fluctuations of Γ_n^0 in an individual isotope are not uncommon, and on the contrary appear to be the usual case.[14,15] At the present time there is no theory sufficiently detailed to account for this behavior.

The ratio of the average "reduced neutron width" to the average level spacing $\bar{\Gamma}_n^0/D$ is of importance to the choice of nuclear models in theories relating to the formation of the compound nucleus.[16] In the "extreme compound nucleus" model of Feshbach, Peaslee, and Weisskopf,[17] $\bar{\Gamma}_n^0/D$ is expected to be independent of the atomic weight and approximately equal to 1.45×10^{-4}. The more recent "cloudy crystal-ball" model of Feshbach, Porter, and Weisskopf predicts variations in $\bar{\Gamma}_n^0/D$ as a function of A. With their present choice of the well depth $V_0=19$ Mev and nuclear absorption coefficient $\xi=0.05$, a large increase in $\bar{\Gamma}_n^0/D$ is expected in the vicinity of an atomic weight of 160.

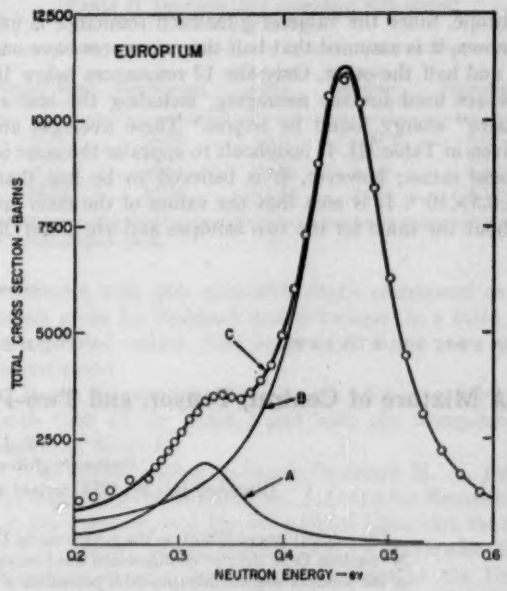

FIG. 2. Theoretical fit to the experimental points for the 0.327- and 0.461-ev resonances. Curves A and B are the best Breit-Wigner curves for the two resonances, and curve C is the sum of A and B.

Only rough averages of the ratio can be obtained from the present data partly because of the small sampling of levels and partly because of the lack of knowledge of the proper value of g for each level. The averaging was carried out for the element as well as for the individual isotopes to serve as a comparison. The averaging of Γ_n^0 for the element is not sensitive to isotopic assignment in Eu because the isotopes are almost equally abundant. The quantity D is defined as the average spacing between resonances of the same g in a given

TABLE III. Average reduced neutron widths and level spacings for europium. These averages are based on the twelve resonances below 10 ev. The averages for the element serve merely as a comparison.

	$\bar{\Gamma}_n^0$, ev	D, ev	$\bar{\Gamma}_n^0/D$
Eu (element)	1.05×10^{-3}	3.3	3.2×10^{-4}
Eu^{151}	1.02×10^{-3}	2.9	3.5×10^{-4}
Eu^{153}	1.08×10^{-3}	3.3	3.3×10^{-4}

[13] H. Schuler and T. Schmidt, Z. Physik 94, 457 (1935).
[14] V. L. Sailor and L. B. Borst, Phys. Rev. 87, 161 (1952).
[15] R. L. Christensen, Phys. Rev. 92, 1510 (1953).
[16] C. Porter (private communication). See also J. M. Blatt and V. F. Weisskopf, *Theoretical Nuclear Physics* (John Wiley and Sons, Inc., New York, 1952), p. 462 ff. Similar importance is attached to this ratio in the theory of the compound nucleus developed by R. G. Thomas (private communication).
[17] Feshbach, Peaslee, and Weisskopf, Phys. Rev. 71, 145 (1947).

isotope. Since the value of g for each resonance is unknown, it is assumed that half the resonances have one g and half the other. Only the 12 resonances below 10 ev are used for the averaging, including the one at "zero" energy found by Sturm.[5] These averages are given in Table III. It is difficult to appraise the error in these ratios; however, it is believed to be less than $\pm 0.5\times 10^{-4}$. It is seen that the values of the ratio are about the same for the two isotopes and are about $2\frac{1}{2}$ times larger than the estimated 1.45×10^{-4} derived from the "extreme compound nucleus" model. Specific information for comparison with the "cloudy crystal-ball" model is not available at this time.

V. ACKNOWLEDGMENTS

The authors wish to thank R. E. Wood for permitting his results on the isotopic assignments to be quoted prior to publication.

PHYSICAL REVIEW VOLUME 93, NUMBER 6 MARCH 15, 1954

A Mixture of Central, Tensor, and Two-Particle Spin-Orbit Interactions for N^{14} and D^2

W. J. Robinson
University of Reading, Reading, England

(Received July 27, 1953; revised manuscript received November 30, 1953)

The calculations of Elliott on the p-shell nuclei Li^6, Li^7, and B^{10} have been extended by the author to the N^{14} nucleus. Only the s^4p^{10} configuration was considered. The central and tensor potentials were taken to be of the Yukawa shape while spin-orbit potentials of both the Yukawa and Case-Pais forms were considered, the ranges being assumed equal. The conclusions are similar to those of Elliott.

The object of the deuteron work was to discover whether the conclusions drawn from the p-shell calculations were consistent with the deuteron data. Here the potentials were taken to be of the Yukawa form throughout with almost equal ranges. Only one calculation has been carried out, but it indicates that the data required by the p-shell nuclei are not inconsistent for the deuteron.

INTRODUCTION

It has been shown by Elliott[1] that a mixed central, tensor, and spin-orbit interaction of the form

$$V(\mathbf{r})=\tfrac{1}{2}(\tau_1\cdot\tau_2)[V_cC_{12}f_0(r/r_0)+V_tS_{12}f(r/r_t)+V_sM_{12}f_s(r/r_0)],$$

with

$$C_{12}=1+\tfrac{1}{2}g(\sigma_1\cdot\sigma_2-1);\quad S_{12}=[3(\sigma_1\cdot\mathbf{r})(\sigma_2\cdot\mathbf{r})/r^2]-(\sigma_1\cdot\sigma_2);$$

$$M_{12}=3\hbar^{-1}(\sigma_1+\sigma_2)(\mathbf{r}\times\mathbf{p}_{12});$$

$$f_0(z)=\frac{e^{-z}}{z};\qquad f_s(z)=-\frac{1}{z}\frac{d}{dz}\left(\frac{e^{-z}}{z}\right);$$

$$r_0=r_t=1.18\times 10^{-13}\text{ cm},$$

may be used with a suitable value of g and of central, tensor, and spin-orbit depths V_c, V_t, and V_s to fit the ground-state total angular momentum, magnetic moment, and quadrupole moment of the p-shell nuclei Li^6, Li^7, and B^{10}, subject to the various assumptions which he makes.

TABLE I. Values of interaction parameters in N^{14}.

Case (1)	$r_0=1.18^-\times 10^{-13}$ cm	$2.28>g>0.63$	$x=-0.46+1.24\,g$ $y=-0.034-0.053g$
	$r_0=1.35^-\times 10^{-13}$ cm	$2.25>g>0.5$	$x=-0.32+1.40\,g$ $y=-0.024-0.043g$
Case (2)	$r_0=1.18^-\times 10^{-13}$ cm	$g>0$	$x=0.21+2.30\,g$ $y=-0.098-0.153g$
	$r_0=1.35^-\times 10^{-13}$ cm	$g>-0.12$	$x=0.55+2.90\,g$ $y=-0.112-0.190g$

N^{14} CALCULATION

Subject to these same assumptions, and restricted to the configuration s^4p^{10}, the author has shown that the total angular momentum, magnetic moment, and quadrupole moment of N^{14} may be achieved under the conditions set out in Table I, where x and y are defined by the relationships

$$x=V_t/V_c,\quad y=V_s/V_c.$$

In Case (1),

$$f_0(z)=\frac{e^{-z}}{z},\qquad f_s(z)=-\frac{1}{z}\frac{d}{dz}\left(\frac{e^{-z}}{z}\right),\qquad r_0=r_t.$$

In Case (2),

$$f_0(z)=f_s(z)=\frac{e^{-z}}{z},\qquad r_0=r_t.$$

It may be noted with regard to these calculations that, although the matrix elements of the tensor force are identical for the p^2 and p^{10} configurations, the matrix elements of the spin-orbit interaction for the two configurations are entirely different. These matrix elements were evaluated using the $\langle p^{10}|p^8,p^2\rangle$ fractional per-

[1] J. P. Elliott, Proc. Roy. Soc. (London) **A218**, 345 (1953).

centage coefficients of Elliott, Hope, and Jahn[2] and were checked independently by Hope[3] using his tensor-operator method.

For a symmetric-type interaction it has been found that a single configuration is inadequate for the binding energy of N^{14}. Consequently further calculations with the present model have not been undertaken. Work is in progress at Southampton on improving the wave functions. When this has been completed more detailed calculations will be possible.

DEUTERON CALCULATION

It was thought desirable to investigate whether, with an interaction of the above kind, it would be possible to fit the deuteron data. With $f_0(z)=f_s(z)=e^{-z}/z$, $r_0=1.35\times10^{-13}$ cm, $r_0/r_t=0.978$, the coupled differential equations for the deuteron $^3S_1$ and $^3D_1$ states were solved by the standard variation method and by a numerical method based on that of Hartree, the depths being adjusted to give the correct binding energy. Table II contains the results obtained. The constants with zero spin-orbit depth correspond to a result given by Feshbach and Schwinger[4] in a table of interpolated values. The deuteron P states were not investigated.

TABLE II. Deuteron data consistent with correct binding energy.

Central depth V_c(Mev)	Tensor depth V_t(Mev)	Spin-orbit depth V_s(Mev)	Quadrupole moment (10^{-27} cm^2)	Percentage D state
25.51	45.56	0	2.60	4.2
26.80	40.20	−2.68	2.81	4.9
27.91	39.07	−2.79	2.76[a]	4.8[a]
33.36	33.36	−3.34	2.56	4.1

[a] Interpolated values.

It can be seen that $x=1.4$, $y=-0.1$ is consistent with Case (1) in Table I and with the interpolated values of Table II.

The author wishes to thank Professor H. A. Jahn for suggesting the problem, Dr. J. Irving for discussions on the deuteron, and the Ministry of Education for an F.E.T. award which enabled him to undertake the investigation as a postgraduate student at the University of Southampton.

[2] Elliott, Hope, and Jahn, Trans. Roy. Soc. (London) **A246**, 241 (1953).
[3] J. Hope, Ph.D. thesis, London, 1952 (unpublished).
[4] H. Feshbach and J. Schwinger, Phys. Rev. **84**, 194 (1951).

PHYSICAL REVIEW VOLUME 93, NUMBER 6 MARCH 15, 1954

The Odd-Nucleon-Plus-Liquid-Drop-Model of Heavy Odd Nuclei*

F. J. MILFORD
Department of Physics, Case Institute of Technology, Cleveland, Ohio
(Received October 5, 1953)

The odd-nucleon-plus-liquid-drop-model of the heavy odd nuclei is considered using the techniques developed by Racah in the construction of the nuclear ground states. The odd nucleon-core interaction is treated perturbation-wise, and the nuclear magnetic moments, quadrupole moments, and the energies of the excited states are investigated. The results are not wholly satisfactory; however, some indications of improvement may be seen.

I. INTRODUCTION

THE analogy of the atomic nucleus to a liquid drop has been successful in accounting for a considerable fraction of the experimental data regarding nuclei.[1–3] In particular this analogy has been successful in the fields of nuclear reactions, nuclear fission, and nuclear binding energies. An alternative approach, the shell model,[4] has been similarly successful in accounting for the properties of nuclear ground states, spins, parities, etc., and in explaining the "magic" behavior of certain nuclei containing closed shells of neutrons or protons. Neither model has, however, been completely successful in explaining nuclear moments. The main features of the variation of the nuclear magnetic moments with nuclear spin is correctly given by Schmidt limits; however, there are appreciable deviations from these predictions for several nuclei. The variation of the quadrupole moment with the number of odd nucleons is partially accounted for by the shell model. On the other hand, however, the shell model gives too small a value for the quadrupole moment of some nuclei. A spheroidal liquid drop model[5,6] is capable of giving the larger quadrupole moments required for these nuclei but tends to give quadrupole moments which increase monotonically

* Supported by the U. S. Atomic Energy Commission.
[1] N. Bohr, Nature **137**, 344, 351 (1936).
[2] N. Bohr and F. Kalckar, Kgl. Danske Videnskab. Selskab Mat.-fys. Medd. **14**, No. 10 (1937).
[3] N. Bohr and J. A. Wheeler, Phys. Rev. **56**, 426 (1939).
[4] M. G. Mayer, Phys. Rev. **78**, 16, 22 (1950). Haxel, Jensen, and Suess, Z. Physik **128**, 295 (1950).
[5] J. Rainwater, Phys. Rev. **79**, 432 (1950).
[6] E. Feenberg and K. C. Hammack, Phys. Rev. **81**, 285 (1951).

with increasing Z in contradiction with the experimental data.

These observations lead one to attempt to combine the two models in such a way as to preserve the essential features of both. The particular combination of the models which we wish to consider is the odd-nucleon-plus-liquid-drop-model of an odd nucleus which has been the subject of several recent papers.[7-9] In particular we consider a liquid core containing all but the odd nucleon; the core liquid will be considered to be incompressible and to move with an irrotational velocity. Such a liquid drop possesses certain modes of oscillation which may be excited by interaction with the odd nucleon. As a result of this excitation there will be a sharing of the nuclear spin between the odd nucleon and the core. This sharing of angular momentum leads to deviations of the magnetic moments from the Schmidt limits which are substantially in the correct direction but too small in magnitude to fit the experimental observations. There also results a distortion of the core to a spheroidal shape which gives rise to a large quadrupole moment, somewhat too large in fact to fit the experimental values for most nuclei. The specifically shell model effects are also absent since only one nucleon has been treated on an individual basis.

This model is quite similar to that of Bohr, the principal difference being that we treat the odd nucleon-core coupling as weak while Bohr uses a strong coupling approximation analogous to that used in molecular structure studies. The results of the perturbation calculation indicate that the coupling is actually intermediate and thus the results of both the weak and strong coupling calculations may be pertinent.

In spite of the shortcomings mentioned above, we feel that these calculations together with those of Bohr,[8] Davidson and Feenberg,[9] and Hill and Wheeler[10] give some insight into the nature of the modifications required to fit the experimental data.

II. THE LIQUID-DROP CORE

In this section we will recapitulate the properties of a drop of incompressible liquid as applied to the construction of a nuclear model. In particular we will consider the surface waves or phonons[11] that may be excited by the interaction of the drop with an odd nucleon.

Let the surface of the drop be given by $R(\vartheta,\varphi)$.[12] We may expand $R(\vartheta,\varphi)$ in a series of spherical harmonics:

$$R(\vartheta,\varphi)=R_0\{1+\sum \alpha_l^m Y_l^m(\vartheta,\varphi)\}.$$

R_0 is the radius of the undeformed drop, i.e., $(3V/4\pi)^{\frac{1}{3}}$ with V the volume of liquid in the drop. This radius is also given by

$$R_0=1.5\times10^{-13}A^{\frac{1}{3}}\text{ cm}.$$

The Y_l^m's are normalized spherical harmonics with the conventional (Condon and Shortley) choice of phase. Since the radius is real, the coefficients α_l^m must satisfy

$$\alpha_l^m=(-1)^m\alpha_l^{-m*}.$$

We may note at this point that the incompressibility assumption implies that $\alpha_0^0=0$ and that the α_1^m's correspond to a rigid displacement of the drop. In consequence the terms with $l=0$ and $l=1$ may be dropped from the sum without losing interesting features of the drop model.

A straightforward calculation of the quantity

$$T=\frac{1}{2}\int_V d\tau\rho_0\mathbf{v}^2$$

gives the kinetic energy. If $\mathbf{v}$ the velocity vector is assumed to be irrotational, one finds

$$T=\tfrac{1}{2}\rho_0R_0^5\sum(\dot{\alpha}_l^{m*}\dot{\alpha}_l^m/l),$$

where ρ_0 is the mass density of the fluid and terms of the third and higher orders in $\dot{\alpha}_l^m$ have been dropped.

The potential energy consists of two terms, one corresponding to the surface energy and the other to the Coulomb energy. If the coefficient of surface tension is S, one finds

$$V_s=S\sum(l+2)(l-1)R_0^2\alpha_l^{m*}\alpha_l^m,$$

for the change (to second order in α_l^m) of the surface energy due to a deformation characterized by the α's. For the change in the Coulomb energy one finds

$$V_c=-\frac{4\pi}{3}\rho_e^2R_0^5\sum\frac{l-1}{2l+1}\alpha_l^{m*}\alpha_l^m,$$

where ρ_e is the charge density (assumed to be constant) within the drop and again the expression is correct to second order in the α's.

The total energy of the core due to the deformation is then

$$H_c=\tfrac{1}{2}\rho_0R_0^5\sum\frac{\dot{\alpha}_l^{m*}\dot{\alpha}_l^m}{l}+\sum\left[R_0^2S(l+2)(l-1)-\frac{4\pi}{3}\rho_e^2R_0^5\frac{l-1}{2l+1}\right]\alpha_l^{m*}\alpha_l^m.$$

It is convenient to define

$$B_l=\rho_0R_0^5/l$$

and

$$C_l=2R_0^2S(l+2)(l-1)-(8\pi/3)\rho_e^2R_0^5(l-1)/(2l+1).$$

In terms of the B_l's and C_l's we have

$$H_c=\tfrac{1}{2}\sum\{B_l\dot{\alpha}_l^{m*}\dot{\alpha}_l^m+C_l\alpha_l^{m*}\alpha_l^m\}.$$

[7] L. L. Foldy and F. J. Milford, Phys. Rev. **80**, 751 (1950).
[8] A. Bohr, Kgl. Danske Videnskab. Selskab Mat.-fys. Medd. **26**, No. 14 (1952).
[9] J. P. Davidson and E. Feenberg, Phys. Rev. **89**, 856 (1953).
[10] D. L. Hill and J. A. Wheeler, Phys. Rev. **89**, 1102 (1953).
[11] The name surfon has been coined for these waves by V. F. Weisskopf.
[12] We use the notation of Bohr (see reference 8) where appropriate.

The momentum canonically conjugate to α_l^m is easily found to be

$$\pi_l^m = \partial H_c/\partial \dot{\alpha}_l^m = B_l \dot{\alpha}_l^{m*}.$$

Expressed in terms of π's and α's, H_c becomes

$$H_c = \sum \left\{ \frac{\pi_l^{m*}\pi_l^m}{2B_l} + \frac{C_l}{2}\alpha_l^{m*}\alpha_l^m \right\}.$$

It is clear from the form of the Hamiltonian that the surface oscillations may be considered as a system of harmonic oscillators with mass coefficients B_l and spring constants C_l. The corresponding frequencies are just

$$\omega_l = (C_l/B_l)^{\frac{1}{2}}.$$

This system of harmonic oscillators is easily quantized by reinterpreting π_l^m and α_l^m as quantum-mechanical operators satisfying the canonical commutation rules:

$$[\pi_l^m, \alpha_{l'}^{m'}]_- = (\hbar/i)\delta_{ll'}\delta_{mm'},$$
$$[\pi_l^{m*}, \alpha_{l'}^{m'*}]_- = (\hbar/i)\delta_{ll'}\delta_{mm'},$$
$$[\pi_l^m, \pi_{l'}^{m'}]_- = [\alpha_l^m, \alpha_{l'}^{m'}]_- = 0.$$

It is convenient to introduce creation operators $c_l^{m\dagger}$ and destruction operators c_l^m according to

$$c_l^{m\dagger} = \tfrac{1}{2}[(2C_l/\hbar\omega_l)^{\frac{1}{2}}\alpha_l^{m*} - i(2/\hbar\omega_l B_l)^{\frac{1}{2}}\pi_l^m],$$
$$c_l^m = \tfrac{1}{2}[(2C_l/\hbar\omega_l)^{\frac{1}{2}}\alpha_l^m + i(2/\hbar\omega_l B_l)^{\frac{1}{2}}\pi_l^{m*}].$$

The commutation rules for the c's are

$$[c_l^m, c_{l'}^{m'\dagger}]_- = \delta_{ll'}\delta_{mm'}.$$

The representation in which the operator $c_l^{m\dagger}c_l^m$ is diagonal is particularly useful, for in this representation $c_l^{m\dagger}c_l^m$ is not only diagonal but also has integral eigenvalues which may be interpreted as occupation numbers; i.e., as the number of l, m phonons which are present in a given state.

In terms of the c's and $c^\dagger$'s, the Hamiltonian is

$$H_c = \sum (\hbar\omega_l/2)[c_l^m c_l^{m\dagger} + c_l^{m\dagger}c_l^m].$$

The angular momentum operator can be found by evaluating the integral

$$\boldsymbol{\lambda} = \int_V d\tau \rho_0 \mathbf{r} \times \mathbf{v}.$$

The detailed evaluation of this integral is tedious; we give only the result for λ_z in terms of the creation and destruction operators.

$$\lambda_z = (\hbar/2)\sum m[c_l^m c_l^{m\dagger} + c_l^{m\dagger}c_l^m].$$

The magnitude of $\hbar\omega_l$ is interesting as it gives the separation of the energy levels corresponding to the change of N_l by one. This quantity is easily found by using the value of S obtained from the empirical binding energy formula, namely,

$$4\pi R_0^2 S = 15.4A^{\frac{1}{3}} \text{ Mev}.$$

One finds for $A=100$, $Z=50$:

$$\hbar\omega_2 = 2.25 \text{ Mev}.$$

For $l=4$ the value of $\hbar\omega$ is larger than this by a factor of greater than 3. Since to first approximation an odd nucleon will interact only with deformations of even order, we neglect the deformations of order three, and, furthermore, because of the larger excitation energy, we neglect deformations of all higher orders.

We consider then only deformations of order two and further restrict ourselves to two phonons of this order. This latter restriction is introduced in order to make the problem tractable; calculations involving more than two phonons appear to be prohibitively complicated. With these restrictions, the specification of five occupation numbers completely specifies the state of the core. It is in fact not necessary to specify five quantum numbers; if the sum of the occupation numbers is less than two, specifying the sum and the one or two nonvanishing quantum numbers is sufficient. Rather than specifying these three quantum numbers, one may specify the sum of the occupation numbers, the total angular momentum of the core, and the z component of the core angular momentum. The states so specified are of course not eigenstates of the occupation number operators but linear combinations of these eigenstates. As a convenient notation we introduce $\chi_{\lambda,\mu}^{\nu}$ to represent the state with ν phonons excited, total angular momentum λ, and z-component of angular momentum μ.

III. THE INTERACTION ENERGY

We consider now the interaction of the odd nucleon with the liquid drop core assuming that this interaction can be described by an interaction potential for the nucleon and a volume element of the drop depending only on the distance between them. Let $\mathbf{r}$ be the radius vector to the odd nucleon and $\mathbf{r}'$ the radius vector to the volume element dv' of the core. The assumption is that the interaction may be described by

$$U(\rho) = \sum g_n(r', r) Y_n^0(\Theta),$$

where $\rho = |\mathbf{r} - \mathbf{r}'|$ and Θ is the angle between $\mathbf{r}$ and $\mathbf{r}'$. The addition theorem for spherical harmonics enables us to write

$$U(\rho) = \sum_{nm} g_n(r', r)\left(\frac{4\pi}{2n+1}\right)^{\frac{1}{2}} Y_n^{m*}(\vartheta', \varphi') Y_n^m(\vartheta, \varphi).$$

The total interaction energy is

$$V(\mathbf{r}) = \int U(\rho)dv' = \sum_{nm}\left(\frac{4\pi}{2n+1}\right)^{\frac{1}{2}} \int d\Omega \times \int_0^R r'^2 dr' g_n(r', r) Y_n^{m*}(\vartheta', \varphi') Y_n^m(\vartheta, \varphi).$$

Let

$$G_n(R, r) = \int_0^R r'^2 dr' g_n(r', r) = G_n(R_0, r) + \left.\frac{\partial G_n}{\partial R}\right|_{R_0} (R - R_0).$$

One readily finds from this and

$$R=R_0[1+\sum_{n'm'}\alpha_{n'}{}^{m'}Y_{n'}{}^{m'}(\vartheta',\varphi')]$$

that

$$G_n(R,r)=G_n(R_0,r)+g_n(R_0,r)R_0{}^2\sum_{n'm'}\alpha_{n'}{}^{m'}Y_{n'}{}^{m'}(\vartheta',\varphi').$$

Using this in the expression for $V(\mathbf{r})$ gives

$$V(\mathbf{r})=(4\pi)^{\frac{1}{2}}G_0(R_0,r)+\sum_{nm}\left(\frac{4\pi}{2n+1}\right)^{\frac{1}{2}}R_0{}^3g_n(R_0,r)\alpha_n{}^mY_n{}^m(\vartheta,\varphi).$$

If $U(\rho)$ is taken as

$$U(\rho)=-U_0\delta(\rho),$$

one finds

$$V(\mathbf{r})=-U_0R_0\delta(R_0-r)\sum\alpha_n{}^mY_n{}^m(\vartheta,\varphi)\begin{cases}-U_0, & r<R_0;\\ -0, & r>R_0.\end{cases}$$

This expression is easily interpreted: the second term represents the interaction of the odd nucleon with the undistorted core (i.e., a spherical well of depth U_0), and the first term describes the interaction with the surface waves. This division of $V(\mathbf{r})$ leads us to consider the motion of an odd nucleon in a spherical well as the unperturbed odd-nucleon problem and to treat the interaction of the nucleon with the surface waves as a perturbation.

IV. THE ODD NUCLEON

The interaction of the odd nucleon with the core consists, as we have seen, of two terms, a spherical well term and a term describing the interaction of the odd nucleon with the surface waves. An "unperturbed" odd-nucleon Hamiltonian,

$$H_P=T_P+V_P(\mathbf{r})+D(\mathbf{l}\cdot\mathbf{s}),$$

can be readily formed. In this expression T_P is the odd-nucleon kinetic energy, $V_P(\mathbf{r})$ the spherical well potential arising from the interaction energy and $D(\mathbf{l}\cdot\mathbf{s})$ a spin-orbit coupling term. The eigenfunctions of the Hamiltonian are well known; they may be designated by $\Phi_{jn}{}^m$, where $j=l\mp\frac{1}{2}$ is the total angular momentum with z component m, and n is the radial quantum number. This designation of the eigenfunctions implies that the spin-orbit coupling is sufficiently strong, compared to the interaction with the surface oscillations, to insure that j is an approximate constant of the motion.

In the perturbation calculations which we will make later, it will be necessary to evaluate matrix elements of the odd nucleon-surface wave interaction between nuclear states. These matrix elements are largely determined by the angular momenta involved in the initial and final states; however, the square of the magnitude of the radial part of the odd-nucleon wave function is also involved. This quantity may be estimated, following Feenberg and Hammack,[6] by a straightforward boundary condition perturbation calculation. The result of the calculation is

$$\tfrac{1}{2}U_0R_0{}^3|\,\mathfrak{R}_{nl}(R_0)\,|^2\approx T_{nl}[x_0/(1+x_0)]^2,$$

where $\mathfrak{R}_{nl}$ is the radial wave function, T_{nl} is the kinetic energy of a nucleon in the n, l state of an infinite spherical well and $x_0{}^2=2mR_0{}^2U_0/\hbar^2$. For $l=4$, $n=1$, $A=100$, and $U=28.3$ Mev, one finds

$$\tfrac{1}{2}U_0R_0{}^3|\,\mathfrak{R}_{nl}(R_0)\,|^2\approx 25\text{ Mev},$$

which is too large, compared to the exact value, by about twenty-five percent. In spite of this and in spite of the variation with l, we will use 25 Mev as an estimate of $\frac{1}{2}U_0R_0{}^3|\,\mathfrak{R}_{nl}(R_0)\,|^2$.

V. THE NUCLEAR STATES

The Hamiltonian for the entire nucleus consists of three terms: the core Hamiltonian H_c, the odd-nucleon Hamiltonian H_P, and the interaction Hamiltonian H_{int}. In treating the last of these as a perturbation, one writes the nuclear state as a sum of products of core state functions by odd-nucleon state functions. In this form the nuclear state appears as a very complicated sum. This complexity can be reduced by forming substates of definite angular momentum One forms the states $\psi_{J\lambda j\nu n}{}^M=\sum_{m\mu}b_{Jm\mu}{}^M\chi_{\lambda\nu}{}^\mu\Phi_{jn}{}^m$, which correspond to definite values of the core angular momentum λ the odd-nucleon angular momentum j, and the total angular momentum J. This is of course nothing more than the vector addition of $\mathbf{j}$ and $\boldsymbol{\lambda}$ to get $\mathbf{J}$. This addition is easily accomplished by means of the Clebsch-Gordon coefficients although the explicit construction will not be necessary. In terms of these substates, the nuclear state function may be written as

$$\Psi_{Jjn}{}^M=\sum_{\lambda\nu}c_{\lambda\nu}\psi_{J\lambda j\nu n}{}^M,$$

where it is assumed that j and n are good quantum numbers. Considering only states for which ν is less than or equal to two it is easily seen that only five substates ($\nu=0,\lambda=0$; $\nu=1,\lambda=2$; $\nu=2,\lambda=0,2,4$) are involved. The virtue of expressing the nuclear state in this way is that Racah[13] has given a set of explicit formulas for calculating the matrix elements of tensor operators (i.e., operators which transform like the Y_2's) between such states.

In order to determine the $c_{\lambda\nu}$'s which appear in the nuclear state, the eigenvalue problem

$$\sum(n,\nu;J,M;j,\lambda|H|n',\nu';J,M;j,\lambda')c_{\lambda'\nu'}=Ec_{\lambda\nu}$$

must be solved. The matrix element of H_c+H_P is readily evaluated; it is just

$$(n,\nu;J,M;j,\lambda|H_c+H_P|n',\nu';J,M;j,\lambda')=(\nu\hbar\omega_2+E_{nl})\delta_{\nu\nu'}\delta_{\lambda\lambda'},$$

[13] G. Racah, Phys. Rev. 62, 438 (1942).

where E_{nl} is the energy of the odd nucleon in the n,l state. The remainder of the matrix element is evaluated by means of Racah's formulas.[13]

The part of Racah's work which is of interest in this connection concerns the matrix elements of the scalar product of two tensor operators of the second rank. The two tensor operators are Y_2^μ and α_2^μ. According to Racah, the matrix element of the interaction Hamiltonian is given by

$$(n',\nu';J,M;j,\lambda'|\{-U_0R_0\delta(r-R_0)\times\textstyle\sum_\mu\alpha_2^\mu Y_2^\mu\}|n,\nu;J,M;j,\lambda)$$
$$=(-1)^\lambda\textstyle\sum_{n'',\nu''}(n',\nu',j\|-U_0R_0\delta(r-R_0)Y_2\|n'',\nu'',j)\times(n'',\nu'',\lambda'\|\alpha_2\|n,\nu,\lambda)W(j,\lambda';j,\lambda;J,2),$$

where $(n',\nu',j'\|-U_0R_0\delta(r-R_0)Y_2\|n,\nu,j)$ is defined by

$$(n',\nu',j',m'|-U_0R_0\delta(r-R_0)Y_2^\mu|n,\nu,j,m)=(-1)^{j+m}(n',\nu',j'\|-U_0R_0\delta(r-R_0)Y_2\|n,\nu,j)\times V(j',j,2;-m',m,\mu),$$

and a similar expression defines $(n'',\nu'',\lambda'\|\alpha_2\|n,\nu,\lambda)$. V and W are functions of their arguments which are explicitly given in Racah's papers and which have been tabulated in several places. The "double-bar" matrix elements are readily found by evaluating V, and the left-hand side of the defining equation for particular states chosen to simplify the evaluation of the left hand side. The remainder of the evaluation of the matrix element is straightforward.

$$(00|H_{\rm int}|21)=\tfrac{1}{2}U_0R_0^3|\mathfrak{R}_{nl}(R_0)|^2\times\left(\frac{5}{4\pi}\frac{\hbar\omega_2}{2C_2}\frac{(2J+3)(2J-1)}{(2J+2)(2J)}\right)^{\frac{1}{2}},$$

$$(21|H_{\rm int}|42)=\tfrac{1}{2}U_0R_0^3|\mathfrak{R}_{nl}(R_0)|^2\times\left(\frac{5}{4\pi}\frac{\hbar\omega_2}{2C_2}\frac{(2J+3)(2J+1)}{2J(2J+2)}(2J-1)\times\frac{(2J+5)!}{(2J-4)!}\right)^{\frac{1}{2}}\frac{(2J-2)!}{(2J+3)!}\frac{6}{\sqrt{35}},$$

$$(21|H_{\rm int}|22)=\tfrac{1}{2}U_0R_0^3|\mathfrak{R}_{nl}(R_0)|^2\times\left(\frac{5}{4\pi}\frac{\hbar\omega_2}{2C_2}\frac{(2J+3)(2J+1)}{2J(2J+2)}(2J-1)\times\frac{(2J-2)!}{(2J+3)!}\right)^{\frac{1}{2}}(2J-3)(2J+5)\sqrt{\frac{8}{7}},$$

$$(21|H_{\rm int}|02)=\tfrac{1}{2}U_0R_0^3|\mathfrak{R}_{nl}(R_0)|^2\times\left(\frac{5}{4\pi}\frac{\hbar\omega_2}{2C_2}\frac{(2J+3)(2J+1)}{2J(2J+2)}(2J-1)\right)^{\frac{1}{2}}\times\frac{1}{(2J+1)^{\frac{1}{2}}}\sqrt{\frac{4}{5}},$$

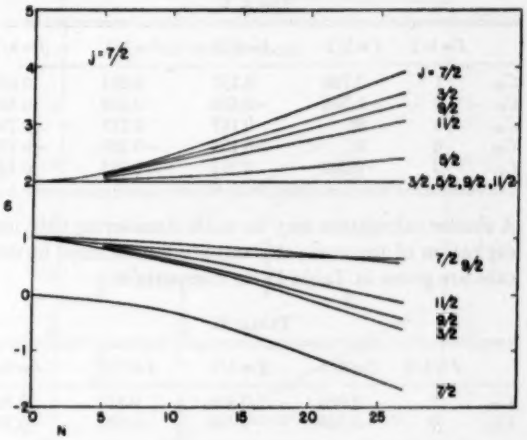

FIG. 1. Energy levels in odd nucleus as functions of the odd-nucleon liquid-drop coupling parameter $N=U_0R_0^3|\mathfrak{R}_{nl}(R_0)|^2\times(\hbar\omega_2/2C_2)^{\frac{1}{2}}/\hbar\omega_2$.

where the states are specified by simply giving λ and ν in this order. These matrix elements, together with the diagonal elements which have already been given, form the matrix of H. This matrix leads to a fifth-order secular equation which, however, reduces to a cubic by virtue of a doubly-degenerate unperturbed root $E=2\hbar\omega_2$. This cubic may be solved exactly by means of the standard tables for the solution of cubics. These solutions are the energy levels of the nucleus for $J=j$. A similar procedure can be carried through to obtain the energy levels for $J=j\mp n$, $n\lesssim 4$. The results of all of these calculations are given in Fig. 1 where the energy levels are plotted in units of $\hbar\omega_2$ as functions of $N=U_0R_0^3|\mathfrak{R}_{nl}(R_0)|^2(\hbar\omega_2/2C_2)^{\frac{1}{2}}/\hbar\omega_2$ for $j=7/2$. The value 2.0 for N corresponds to 25 Mev for $\frac{1}{2}U_0R_0^3|\mathfrak{R}_{nl}(R_0)|^2$. It is interesting to note that the lowest energy level is a $j=J$ level which develops from the zero-interaction state with an unexcited core. The first five excited states develop from the fivefold degenerate state with one core phonon excited and correspond to $J=j-2$, $j+1$, $j+2$, $j-1$, and j in that order. It may be possible to incorporate in this theory the electromagnetic interactions of nuclei and thus provide another explanation of the long-lived isomers. In this connection it should be noted that the energy separations, about 2.2 Mev, shown in Fig. 1 are appreciably larger than the gamma-ray energies involved in most isomeric transitions. However, the large spin change between the ground state and the first excited state compares favorably with the prediction of the shell model. A more detailed investigation of these points is being made.

Having obtained the lowest energy level it is a simple matter to obtain the amplitudes of the five substates involved in the nuclear ground state. These amplitudes are given in Table I for $J=j=1/2$, $3/2$, $5/2$, $7/2$, and $9/2$.

TABLE I.

	$J=1/2$	$J=3/2$	$J=5/2$	$J=7/2$	$J=9/2$
C_{00}	1	0.780	0.757	0.654	0.629
C_{21}	0	−0.588	−0.576	−0.660	−0.669
C_{41}	0	0	0.167	0.211	0.230
C_{22}	0	0	−0.151	−0.208	−0.230
C_{02}	0	0.208	0.212	0.223	0.223

A similar calculation may be made considering only one excitation of the core; the amplitudes obtained in this case are given in Table II for comparison.

TABLE II.

	$J=1/2$	$J=3/2$	$J=5/2$	$J=7/2$	$J=9/2$
C_{00}	1	0.826	0.826	0.817	0.816
C_{21}	0	−0.563	−0.563	−0.577	−0.578

The amplitudes of the excited states are relatively large, indicating that states involving more than two core phonons are probably of some importance. The calculations for three excitations, however, appear to be prohibitively complicated.

VI. THE NUCLEAR MAGNETIC MOMENTS

Each nuclear substate $\psi_{J\lambda j/n}{}^{J}$ has a magnetic moment $\mathfrak{M}_{J\lambda j}$. This magnetic moment can be expressed in nuclear magnetons as the product of J and a gyromagnetic ratio $g_{J\lambda j}$. The gyromagnetic ratio is readily found either from the vector model or by a formal quantum-mechanical calculation to be

$$g_{J\lambda j}=g_j+\frac{\lambda(\lambda+1)}{2J(J+1)}(g_c-g_j),$$

where g_c is the gyromagnetic ratio for the core ($g_c\approx Z/A\approx 0.5$) and g_j is the gyromagnetic ratio for the odd nucleon. g_j depends on the charge of the odd nucleon and on whether j equals $l+\frac{1}{2}$ or $l-\frac{1}{2}$. The four possibilities are

	Odd proton	Odd neutron
$j=l+\frac{1}{2}$	$g_j=\frac{2j-1}{2j}+\frac{1}{2j}g_p$	$g_j=\frac{1}{2j}g_n$
$j=l-\frac{1}{2}$	$g_j=\frac{2(j+1)}{2j+3}-\frac{1}{2(j+1)}g_p$	$g_j=-\frac{1}{2(j+1)}g_n$

Here $g_p=5.58$ is the spin gyromagnetic ratio for the proton and $g_n=-3.82$ is the spin gyromagnetic ratio for the neutron. These g_j's evaluated for $j=J$ give the gyromagnetic ratios for the substates.

The expectation value of the nuclear magnetic moment is given, in terms of the $g_{J\lambda j}$'s, by

$$\langle\mathfrak{M}\rangle=\sum_{\lambda\nu}|c_{\lambda\nu}|^2 g_{J\lambda J}.$$

The results are shown in Figs. 2 and 3 for the four cases considered above. Also shown are the Schmidt limits and the observed magnetic moments for most of the nuclei for which measurements have been made. It may be noted that the deviations from the Schmidt lines are in the correct direction in most cases. On the other hand the deviations are too small for large spin values and the magnetic moments coincide with the Schmidt values for spin $\frac{1}{2}$.

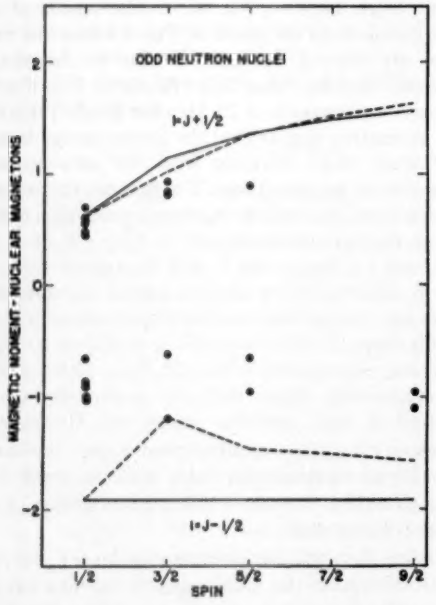

FIG. 2. Nuclear magnetic moments for odd-proton nuclei. Solid lines are Schmidt limits; broken lines represent this theory; dots are experimental points.

VII. QUADRUPOLE MOMENTS

The quadrupole moment operator for a nucleus is conventionally taken to be

$$Q=\int d\tau\rho(\mathbf{r})(3z^2-r^2),$$

where $\rho(\mathbf{r})$ is the charge density operator. The charge density operator can be divided into two parts, a core part and an odd-nucleon part. In this way one writes

$$Q=Q_c+Q_P,$$

where Q_c is the core contribution and Q_P the odd-nucleon contribution to the quadrupole moment operator.

In the core term, $\rho(\mathbf{r})$ is a constant inside the core and zero outside. The integral for Q_c is readily found to be

$$Q_c=\frac{2Ze}{(4/3)\pi R_0{}^3}\int d\Omega\int_0^R drr^4\left(\frac{4\pi}{5}\right)^{\frac{1}{2}}Y_2{}^0(\vartheta,\varphi),$$

where again $R=R_0\{1+\sum_{nm}\alpha_n{}^m Y_n{}^m(\vartheta,\varphi)\}$ is the distance from the center of gravity of the core to a point on surface. To second order in the α's, this can be evaluated

and found to be

$$Q_c=\frac{6Ze}{4\pi R_0^3}\left(\frac{4\pi}{5}\right)^{\frac{1}{2}}\frac{R_0^5}{5}\left\{5\alpha_2^0-\left(\frac{5}{4\pi}\right)^{\frac{1}{2}}\sum_m\frac{m^2-2}{7}\alpha_2^{-m}\alpha_2^m\right\},$$

where only terms for which $n=2$ have been retained. The term quadratic in the α's contains an extra factor of $(\hbar\omega_2/2c_2)^{\frac{1}{2}}\approx 0.18$ as compared to the α_2^0 term. It may consequently be dropped without essential loss of accuracy. Thus we take

$$Q_c=\frac{6Ze}{4\pi}\left(\frac{4\pi}{5}\right)^{\frac{1}{2}}R_0^2\alpha_2^0$$

as the core contribution to the quadrupole moment operation.

The odd-nucleon charge density operator is zero if the odd nucleon is a neutron, and $e\delta(\mathbf{r}-\mathbf{r}')$ if it is a proton. The odd-nucleon position coordinate is $\mathbf{r}'$. This charge density operator gives

$$Q_P=Ze\left(\frac{4\pi}{5}\right)^{\frac{1}{2}}\mathbf{r}'^2Y_2^0(\vartheta',\varphi')$$

for the odd-nucleon quadrupole moment operator. The expectation value of this operator is essentially bounded by eR_0^2 which is small compared to the expectation value of Q_c for moderately large values of Z. For smaller values of Z the model is undoubtedly very poor, and a comparison in this region consequently pointless.

The quantity which is to be compared with experiment is the expectation value of the operator Q for the nuclear ground states determined in part five. If Q_p and terms of quadratic and higher order in the α's are neglected, Q is given by

$$Q=\frac{6Ze}{4\pi}\left(\frac{4\pi}{5}\right)^{\frac{1}{2}}R_0^2\alpha_2^0.$$

This is a tensor operator to which the results obtained by Racah apply. Racah has given, in fact, explicit formulas for the matrix elements of such operators between states such as our nuclear substates. These matrix elements and the amplitudes which have already been found suffice to determine the expectation value of the quadrupole moments. The results are given in Table III.

TABLE III.

J	$\langle Q\rangle/eR_0^2$
1/2	0
3/2	$0.069Z$
5/2	$0.101Z$
7/2	$0.132Z$
9/2	$0.146Z$

The magnitudes of these quadrupole moments are, in general, larger than the observed moments by a factor of about two. Lu and Ta are exceptions; for these nuclei the calculated and observed moments are in good agreement. A more serious difficulty is the failure of the model to give small quadrupole moments in the neighborhood of the magic numbers.

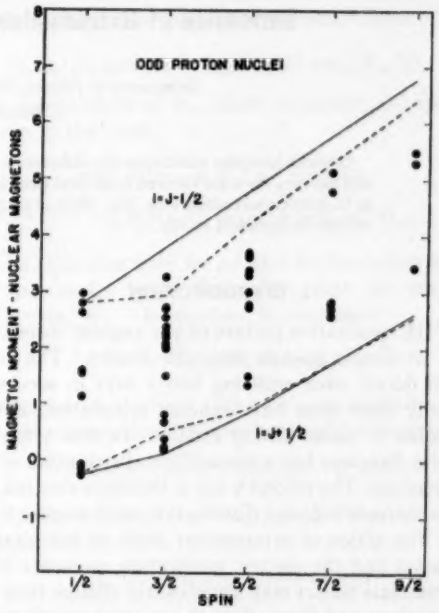

FIG. 3. Nuclear magnetic moments for odd-neutron nuclei. Solid lines are Schmidt limits; broken lines represent this theory; dots are experimental points.

VIII. CONCLUSIONS

The model of an odd nucleon coupled to a liquid-drop core gives deviations of the nuclear magnetic moments from the Schmidt limits which are in the correct direction but too small in magnitude, especially for the larger nuclear spins. The nuclear quadrupole moments are for the most part too large; this is particularly evident in the neighborhood of the magic numbers, where the observed quadrupole moments are quite small. As possible modifications of the model which could alleviate these difficulties, the use of some type of intermediate coupling might be suggested. This suggestion is based on the moderate amplitude of the excited states found in the nuclear ground states. As a further possibility one might attempt to take into account the partially filled outer shells. This, however, appears to be a rather formidable computational task.

IX. ACKNOWLEDGMENT

The author would like to acknowledge the importance of Professor L. L. Foldy's advice and assistance with difficult portions of this work and to thank both him and Professor E. Feenberg for critical readings of the manuscript.

Note added in proof.—Recent papers by A. Bohr and B. R. Mottelson, Kgl. Danske Videnskab. Selskab. Mat.-fys. Medd. **27**, No. 16 (1953) and by A. K. Kerman, Phys. Rev. **92**, 1196 (1953) contain calculations of interest in connection with the model used in this paper.

Influence of Extranuclear Fields on Angular Correlations*

F. COESTER
Department of Physics, State University of Iowa, Iowa City, Iowa
(Received October 5, 1953)

General formulas exhibiting the influence of extranuclear fields on angular correlations of two or three successive γ rays are derived from first principles. They are applicable to polarization correlations as well as to directional correlations. The effect of transitions in the electron shell during the life of the intermediate nucleus is discussed briefly.

I. INTRODUCTION

THE qualitative picture of γ-γ angular correlations is simple enough and well known.[1] The source nuclei decay, each emitting two γ rays in succession. Initially their spins have random orientation, but the ensemble of nuclei having emitted the first γ ray in a definite direction has a nonuniform distribution of spin orientations. The second γ ray is therefore emitted with a nonisotropic angular distribution with respect to the first. The action of extranuclear fields on the magnetic moments and the electric quadrupole moments of the intermediate nuclei may significantly change their spin orientations and thus affect the angular correlation.

In the quantitative theory first given by Hamilton[2] and refined by many authors[3] one does not have, however, a detailed description of the time development corresponding to the picture just sketched. One merely calculates from the time-dependent Schrödinger equation the relative probability for having two γ rays emitted in specified directions during a long time t. Goertzel's theory[4] of the influence of extranuclear fields follows the same lines. The splitting of the nuclear levels rather than any spin reorientation in time appears to be directly responsible for the influence of extranuclear fields on angular correlations. This theory is necessarily restricted to time independent interactions. Recently Abragam and Pound[5] have given a prescription which modifies Hamilton's formula on the basis of the physical picture in order to describe the influence of time-dependent extranuclear fields as well. Fano[6] has suggested a different approach which promises a consistent quantitative theory in close parallel to the physical picture. The decaying nuclei and the emitted radiation can be described by a density matrix.[7] When extranuclear fields are negligible it suffices to consider only the initial and final density matrix connected by the S matrix.[8] In any case the angular correlation can be written in the form

$$W=\mathrm{Tr}(\epsilon\rho), \tag{1}$$

[see Eq. (I2)], where ρ is the final density matrix. But if extranuclear fields are effective, the final density matrix must be obtained in terms of an explicit description of the intermediate stages.

It is the purpose of this note to provide an explicit description in time of the decaying nuclei along the lines suggested by Fano. While many of our considerations apply to all kinds of cascade decay, we restrict ourselves at first to γ decay of long-lived isomers for the sake of definiteness in the exposition. Gamma cascades preceded by β decay or K capture are discussed in Sec. IV.

II. DENSITY MATRICES IN SUCCESSIVE γ DECAY

The density matrix ρ in (1) describes the ensemble of all the nuclei in the source. It can be written in the form

$$\rho=\frac{1}{N}\sum_{\alpha=1}^{N}\rho^{\alpha},$$

where α labels the individual nuclei in the source and ρ^{α} is the density matrix describing the αth nucleus.

We consider a sequence of nuclear levels a,b,c with angular momentum j_a, $m_a\cdots$. The density matrix ρ^{α} describes the system containing the nucleus α, its environment and the emitted radiation. The matrix $\bar{\rho}^{\alpha}$ is obtained by taking the trace of ρ^{α} with respect to all photon energies. Since ϵ is the unit matrix with respect to the photon energies it is $\bar{\rho}^{\alpha}$ which we need to calculate the angular correlation. We assume for the sake of simplicity that only transitions between adjacent levels are possible. At the time $t=0$ all the nuclei are in the level a and no photons are present. The matrix $\bar{\rho}^{\alpha}(t)$ then has no off-diagonal elements connecting different nuclear levels and may be written in the form

$$\bar{\rho}^{\alpha}=\rho_a{}^{\alpha}+\rho_b{}^{\alpha}+\rho_c{}^{\alpha}+\cdots. \tag{2}$$

Each term on the right-hand side of (2) has only matrix elements with respect to the substates of one level $a,b,c\cdots$, respectively. If the nucleus is in b there is always one photon, in c there are two photons and so

* Supported in part by the U. S. Atomic Energy Commission.
[1] See, for instance, H. Fraunfelder, Ann. Rev. Nuclear. Sci. **2**, 129 (1953).
[2] D. R. Hamilton, Phys. Rev. **58**, 122 (1940).
[3] For references see reference 1.
[4] G. Goertzel, Phys. Rev. **70**, 897 (1946). See, also, K. Alder, Helv. Phys. Acta **25**, 235 (1952).
[5] A. Abragam and R. V. Pound, Phys. Rev. **92**, 943 (1953).
[6] U. Fano, Natl. Bur. Standards Rept. 1214, 1951 (unpublished); Phys. Rev. **90**, 577 (1953).
[7] For a definition see, for instance, R. C. Tolman, *Principles of Statistical Mechanics* (Oxford University Press, London, 1938), Chap. 9.
[8] F. Coester and J. M. Jauch, Helv. Phys. Acta **26**, 3 (1953) quoted as I in the following.

on. The Hamiltonian of the system is $H_0+H_e^\alpha(t)+H$, where H_0 is the energy of the bare nucleus and the free photons, H is the interaction of the nucleus with the radiation field, and $H_e^\alpha(t)$ is the Hamiltonian of the environment in interaction with the nucleus. It has an index α since different nuclei do not in general have identical environments. In the interaction representation the Schrödinger equation is

$$i\partial\Psi^\alpha/\partial t=[H_e^\alpha+H(t)]\Psi^\alpha, \tag{3}$$

where

$$H(t)=e^{iH_0t}He^{-iH_0t}. \tag{4}$$

H_e^α commutes with H_0. It is therefore the same in the interaction representation and in the Schrödinger representation. As a consequence of (3) ρ^α satisfies the equation[9]

$$i\partial\rho^\alpha/\partial t=[(H_e^\alpha+H(t)),\rho^\alpha(t)]. \tag{5}$$

No attempt is made to integrate (5) from $t=0$ to large t. In fact this solution would not describe the physical situation since the system is under continuous observation. The emitted photons are at least in principle observed at all times; the system is therefore described by a density matrix $\rho^\alpha(t)$ which is diagonal in the photon numbers.

In order to get a useful equation for $\bar\rho^\alpha(t)$ from (5), we integrate (5) by perturbation theory between t and $t+\delta t$. The interval δt is so small that $\langle\delta tH_e^\alpha\rangle\ll1$, and $H_e^\alpha(t)$ is approximately constant in this interval. Further δt is small compared to the lifetimes of the nuclear levels but large compared to the reciprocal frequency of the γ rays. We have then

$$\rho^\alpha(t+\delta t)=\rho^\alpha(t)-i\delta t[H_e^\alpha,\rho^\alpha]-i\int_t^{t+\delta t}dt'[H(t'),\rho^\alpha(t)]$$
$$-\int_t^{t+\delta t}dt'\int_t^{t'}dt''[H(t'),[H(t''),\rho^\alpha(t)]]. \tag{6}$$

Since the time dependence of $H(t)$ is known according to (4) we can carry out the integrations in (6) explicitly and then take the trace with respect to the photon energies. The matrix $\rho^\alpha(t)$ is diagonal with respect to the photon number; therefore the first-order term in H does not contribute and the result is

$$\bar\rho^\alpha(t+\delta t)-\bar\rho^\alpha(t)=-\{i[H_e^\alpha,\bar\rho^\alpha]+\gamma\bar\rho^\alpha-2\pi H\bar\rho^\alpha H\}\delta t, \tag{7}$$

where γ is a diagonal matrix whose eigenvalues $\gamma_a,\gamma_b\cdots$ are the reciprocal lifetimes of the nuclear levels. For instance,

$$\gamma_a=2\pi\sum_\xi\sum_M\sum_{m_b}|(m_aj_a|H|j_b\xi m_bM)|^2; \tag{8}$$

ξ and M are photon quantum numbers.[10] Since

$$(j_am_a|H|j_b\xi m_bM)=(j_bLm_bM|j_am_a)H_{ba}(\xi), \tag{9}$$

γ_a is independent of m_a. More explicitly, (7) may be written in the form

$$\partial\rho_a^\alpha/\partial t=-i[H_e^\alpha,\rho_a^\alpha]-\gamma_a\rho_a^\alpha, \tag{10a}$$

$$\partial\rho_b^\alpha/\partial t=-i[H_e^\alpha,\rho_b^\alpha]-\gamma_b\rho_b^\alpha+2\pi\mathbf{H}_{ba}\rho_a^\alpha\mathbf{H}_{ab}. \tag{10b}$$

Similar equations hold for ρ_c^α and further terms if any. One can easily verify from (10) that the trace of $\bar\rho^\alpha=\rho_a^\alpha+\rho_b^\alpha+\cdots$ is constant in time since

$$2\pi\,\mathrm{Tr}(\mathbf{H}_{ba}\rho_a^\alpha\mathbf{H}_{ab})=\gamma_a\rho_a^\alpha. \tag{11}$$

The solution of (10a), (10b), $\cdots$ can easily be given in terms of a matrix $U^\alpha(t,t_0)$ which satisfies the equation

$$i\partial U^\alpha(t,t_0)/\partial t=H_e^\alpha U^\alpha(t,t_0),\quad (t>t_0), \tag{12}$$

and the initial condition $U^\alpha(t_0,t_0)=1$. From (10a) and (12) we find

$$\rho_a^\alpha(t)=e^{-\gamma_at}U^\alpha(t,0)\rho_a^\alpha(0)U^\alpha(t,0)^+. \tag{13a}$$

Since $\rho_a^\alpha(t)$ is known, (10b) can be integrated. The result is

$$\rho_b^\alpha(t)=2\pi\int_0^t dt'e^{-\gamma_b(t-t')}U^\alpha(t,t')\mathbf{H}_{ba}\rho_a^\alpha(t')\mathbf{H}_{ab}U^\alpha(t,t')^+. \tag{13b}$$

In the same way we obtain the density matrix at any level. For instance we get $\rho_c^\alpha(t)$ by substituting $a\to b$, $b\to c$ in Eq. (13b).

III. EXPLICIT ANGULAR CORRELATION FUNCTIONS

If the level c is the ground level ($\gamma_c=0$), the correlation of the two γ rays is, according to (1),

$$W=\text{const}\,\mathrm{Tr}\{\epsilon(\Omega_1\Omega_2)\rho_c(t)\}, \tag{14}$$

where ϵ is the unit matrix with respect to all variables except those describing the observed photons,

$$\rho_c=\frac{1}{N}\sum_\alpha\rho_c^\alpha, \tag{15}$$

and t is in (14) by definition the total duration of the experiment. We shall see later that the angular correlation is actually independent of t, as expected. From (14), (15), and (13c) (not written out) it follows that

$$W=\text{const}\,\mathrm{Tr}\left\{\epsilon(\Omega_1\Omega_2)\int_0^t dt'\mathbf{H}_{cb}\rho_b(t')\mathbf{H}_{bc}\right\}. \tag{16}$$

We assume that for every environment there is a large number of nuclei uniformly distributed over the sub-

[9] A similar equation has been discussed recently by R. K. Wangsness and F. Bloch, Phys. Rev. 89, 728 (1953) [Eq. (2.4)]. Our treatment is analogous to theirs in many respects.

[10] We follow the notation of I.

states of the level a and find from (13a) and (13b)

$$\rho_b(t)=\frac{1}{N}\sum_a 2\pi\int_0^t dt' e^{-\gamma_b(t-t')}e^{-\gamma_a t'}\rho_a(0) \times U^a(t,t')\mathbf{H}_{ba}\mathbf{H}_{ab}U^a(t,t')^+. \quad (13b')$$

$\rho_a(0)$ is here merely a normalization factor. Inserting (13b') in (16) we write W in the form

$$W=\text{const}\int_0^t dt'\int_0^{t'} dt'' e^{-\gamma_b(t'-t'')}e^{-\gamma_a t''} \times\frac{1}{N}\sum_a \mathrm{Tr}\{\epsilon(\Omega_1\Omega_2)\mathbf{H}_{cb}U^a(t',t'') \times\mathbf{H}_{ba}\mathbf{H}_{ab}U^a(t',t'')^+\mathbf{H}_{bc}\}. \quad (17)$$

If c is not the ground level, but further decays are not observed we must replace (14) by

$$W=\text{const}\,\mathrm{Tr}\{\epsilon(\Omega_1\Omega_2)(\rho_c+\rho_d+\cdots)\}. \quad (18)$$

Equation (18) leads again to (17) since by (10) and (11)

$$\partial\,\mathrm{Tr}\{\epsilon(\rho_d+\cdots)\}/\partial t=\gamma_c\,\mathrm{Tr}(\epsilon\rho_c). \quad (19)$$

In order to evaluate the trace in (17) we use a representation specified by the quantum numbers jm for the nucleus, ξM for the photons, and κ for the atomic environment. The efficiency matrix is in this representation:

$$\begin{aligned}(\kappa m_e\xi_2M_2\xi_1M_1|\,\epsilon(\Omega_1\Omega_2)\,|\kappa' m_e'\xi_2'M_2'\xi_1'M_1')&=\delta(\kappa,\kappa')\delta(m_e,m_e')\sum_{k_1n_1}(-1)^{L_1'-M_1'}\\ &\times(L_1L_1'M_1-M_1'|k_1n_1)(\xi_1|\,\epsilon(k_1,n_1;\Omega_1)\,|\xi_1')\\ &\times\sum_{k_2n_2}(-1)^{L_2'-M_2'}(L_2L_2'M_2-M_2'|k_2n_2)\\ &\times(\xi_2|\,\epsilon(k_2,n_2;\Omega_2)\,|\xi_2'). \quad (20)\end{aligned}$$

The matrix elements of U^a describing the influence of the extranuclear fields are combined in the expression

$$\begin{aligned}(\bar{k}\bar{n}\bar{\kappa}'|G^a(t',t'')|kn\kappa\kappa')&=\sum_{m_bm_b'}\sum_{\bar{m}_b\bar{m}_b'}(\bar{m}_b\bar{\kappa}|\,U^a(t',t'')\,|m_b\kappa)^*\\ &\times(\bar{m}_b'\bar{\kappa}'|\,U^a(t',t'')\,|m_b'\kappa')(-1)^{j_b-m_b'}\\ &\times(j_bj_bm_b-m_b'|kn)(-1)^{j_b-\bar{m}_b'}\\ &\times(j_bj_b\bar{m}_b-\bar{m}_b'|\bar{k}\bar{n}). \quad (21)\end{aligned}$$

The matrix elements of the Hamiltonian are given by (9) and a similar expression for the second transition. All sums over magnetic quantum numbers are carried out using Eq. (IB6).[11] The result is

$$W(\Omega_1\Omega_2)=\text{const}\sum_{kn}\sum_{\bar{k}\bar{n}}(00|F_{cb}(\Omega_2)|\bar{k}\bar{n}) \times(\bar{k}\bar{n}|G|kn)(kn|F_{ba}(\Omega_1)|00), \quad (22)$$

where

$$(\bar{k}\bar{n}|G|kn)=\frac{1}{N}\sum_a\sum_{\kappa\bar{\kappa}}\int_0^t dt'\int_0^{t'}dt''\gamma_b e^{-\gamma_b(t'-t'')} \times\gamma_a e^{-\gamma_a t''}(\bar{k}\bar{n}\bar{\kappa}\bar{\kappa}|G^a(t',t'')|kn\kappa\kappa), \quad (23)$$

and

$$\begin{aligned}(kn|F_{ba}(\Omega_1)|k'n')&=\sum_{k_1n_1}H_{ba}(\xi_1)H_{ba}(\xi_1')(\xi_1|\,\epsilon(k_1,n_1;\Omega_1)\,|\xi_1')\\ &\times(kk_1nn_1|k'n')(j_aj_a|\Gamma(j_bj_bL_1L_1'k')|kk_1). \quad (24)\end{aligned}$$

The matrix element $H_{ba}(\xi)$ is real.[12] F_{cb} is obtained by substituting $a\to b$, $b\to c$, and $1\to 2$ in (24). For directional correlations,[13]

$$(\xi|\,\epsilon(k,n;\Omega)\,|\xi')=[4\pi/(2k+1)]^{\frac{1}{2}}C_k(\xi,\xi')Y_k^n(\Omega)^*. \quad (25)$$

In the absence of any interaction of the nucleus with its environment U^a is the unit matrix. Equation (22) reduces then to the unperturbed correlation:

$$W(\Omega_1\Omega_2)=\text{const}\sum_{kn}(00|F_{cb}(\Omega_2)|kn)(kn|F_{ba}(\Omega_1)|00). \quad (26)$$

If H_e^a is time-independent, the eigenvalues of $U^a(t',t'')$ are of the form $e^{i\omega(t'-t'')}$. $U^a(t',t'')$ and therefore $G^a(t',t'')$ depend only on the difference $t'-t''$ and not on t' and t'' separately. If on the other hand H_e^a is the interaction with randomly fluctuating fields such as occur in liquids, $G(t't'')=N^{-1}\sum_a G^a(t',t'')$ again depends only on the difference $t'-t''$. This is a consequence of the ergodic hypothesis which says that the ensemble average $N^{-1}\sum_a$ is equivalent to a time average. Equation (23) may then be simplified somewhat. The duration of the experiment is always long compared to the lifetime of the intermediate state $\gamma_b t\gg 1$. If it is also long compared to the lifetime of the source $\gamma_a t\gg 1$ we may replace t in (23) by ∞ and use the

[11] There is a misprint in the last line of (IB6). Instead of $W(acbf';b\kappa)$ read $W(acb'f;b\kappa)$. Delete the equality sign at the end of the previous line.

Note added in proof.—Coefficients closely related to the Γ coefficients of I have been introduced independently by many authors in unpublished papers. Several of these definitions and their relations are given by H. A. Jahn and J. Hope [Phys. Rev. **93**, 318 (1954)]. The Γ coefficients are related to the Wigner $9j$ symbol according to

$$(cc'|\Gamma(aa'bb'd)|ef)=\{(2e+1)(2f+1)(2c'+1)(2c+1)\}^{\frac{1}{2}}\begin{Bmatrix}a'e\ a\\ b'f\ b\\ c'd\ c\end{Bmatrix}.$$

The Wigner $9j$ symbol is identical with Fano's x coefficient (Natl. Bur. Standards Report 1214, 1951, unpublished).

[12] S. P. Lloyd, Phys. Rev. **81**, 161 (1951); F. Coester, Phys. Rev. **89**, 619 (1953).

[13] See Eqs. (I32) (I23), and (IC3).

relation

$$\int_0^\infty dt' \int_0^{t'} dt'' \cdots = \int_0^\infty dt'' \int_0^\infty d(t'-t'') \cdots, \quad (27)$$

which gives

$$(\bar{k}\bar{n}|G|kn) = \sum_{\kappa\bar{\kappa}} \int_0^\infty dt \gamma_b e^{-\gamma_b t} (\bar{k}\bar{n}\bar{\kappa}\bar{\kappa}|G(t)|kn\kappa\kappa). \quad (28)$$

At this point we establish the connection with the work of Abragam and Pound[5] by the relation

$$\sum_{\kappa\bar{\kappa}} (k_2\mu_2\bar{\kappa}\bar{\kappa}|G(t)|k_1\mu_1\kappa\kappa) = \frac{[(2k_1+1)(2k_2+1)]^{\frac{1}{2}}}{2j_b+1} \times \mathrm{III}(k_1,k_2,\mu_1,\mu_2,t). \quad (29)$$

The assumption $\gamma_a t \gg 1$ which led to (28) is in general not justified. On the other hand the lifetime of the source is large compared to that of the intermediate state, $\gamma_a \ll \gamma_b$. We may therefore use in (22) the transformation

$$\int_0^t dt' \int_0^{t'} dt'' \cdots = \int_0^t dt'' \int_0^t d(t'-t'') \cdots - \int_0^t dt'' \int_{t-t''}^t d(t'-t'') \quad (30)$$

and neglect the second term on the right-hand side, since it is small of order γ_a/γ_b compared to the first one. Since the factor $1-e^{-\gamma_a t}$ does not affect the correlation, we may still use (28) in (22).

So far we have assumed that the resolving time of the coincidence circuit is large compared to the lifetime of the intermediate nucleus. If this is not the case and delayed coincidences are counted, we have, instead of (28):

$$(\bar{k}\bar{n}|G|kn) = \sum_{\kappa\bar{\kappa}} \int_{\tau_1}^{\tau_2} dt e^{-\gamma_b t} \gamma_b (\bar{k}\bar{n}\bar{\kappa}\bar{\kappa}|G(t)|kn\kappa\kappa), \quad (31)$$

where τ_1 and τ_2 are the minimum and maximum delay times; that means the second quantum is delayed with respect to the first by a time t between τ_1 and τ_2.[14]

Triple correlation functions can easily be derived with the same methods. In analogy to (17), we get

$$W = \text{const} \int_0^t dt' \int_0^{t'} dt'' \int_0^{t''} dt''' e^{-\gamma_c(t'-t'')} \times e^{-\gamma_b(t''-t''')} e^{-\gamma_a t'''} \frac{1}{N} \sum_\alpha \mathrm{Tr}\{\epsilon(\Omega_1\Omega_2\Omega_3) \times \mathbf{H}_{dc} U^\alpha(t',t'') \mathbf{H}_{cb} U^\alpha(t'',t''') \mathbf{H}_{ba} \mathbf{H}_{ab} \times U^\alpha(t'',t''')^+ \mathbf{H}_{bc} U^\alpha(t',t'')^+ \mathbf{H}_{cd}\}. \quad (32)$$

[14] For a time-independent interaction L. C. Biedenharn and M. E. Rose [Revs. Modern Phys. **25**, 729 (1953)] have derived a formula for delayed coincidence angular correlations [Eq. (125)]. Integrating this formula over t from τ_1 to τ_2 we obtain the same angular correlation formula as (22) with (31). See also S. P. Lloyd, Phys. Rev. **82**, 277 (1951).

The evaluation of the trace gives, in analogy to (22),

$$W = \text{const} \sum_{\kappa\kappa} \sum_{\kappa'\kappa''} \int_0^t dt' \int_0^{t'} dt'' \int_0^{t''} dt''' e^{-\gamma_c(t'-t'')} \times e^{-\gamma_b(t''-t''')} e^{-\gamma_a t'''} \frac{1}{N} \sum_\alpha \sum_{k_c\bar{n}_c} \sum_{k_c n_c} \sum_{k_b\bar{n}_b} \sum_{k_b n_b} \times (00|F_{dc}(\Omega_3)|\bar{k}_c\bar{n}_c)(\bar{k}_c\bar{n}_c\bar{\kappa}\bar{\kappa}|G_c^\alpha(t',t'')|k_c n_c \kappa'\kappa'') \times (k_c n_c|F_{cb}(\Omega_2)|\bar{k}_b\bar{n}_b) \times (\bar{k}_b\bar{n}_b\kappa'\kappa''|G_b^\alpha(t'',t''')|k_b n_b\kappa\kappa) \times (k_b n_b|F_{ba}(\Omega_1)|00), \quad (33)$$

where G_b^α is given by (21) and G_c^α is the corresponding expression for the level c. For time independent interactions, G_b^α and G_c^α are functions of $t''-t'''$ and $t'-t''$, respectively. For liquid sources with randomly fluctuating fields, $\sum_\alpha G_c^\alpha(t',t'') G_b^\alpha(t'',t''')$ is a function of $t'-t''$ and $t''-t'''$ only. In both cases we can simplify (33) by changing the time integration according to

$$\int_0^t dt' \int_0^{t'} dt'' \int_0^{t''} dt''' \cdots \rightarrow \int_0^t dt''' \int_0^\infty d(t'-t'') \times \int_0^\infty d(t''-t''') \cdots. \quad (34)$$

This is not rigorous but only terms which are small, of the order γ_a/γ_b or γ_a/γ_c, are neglected.

IV. γ CASCADES PRECEDED BY β DECAY OR K CAPTURE

In many instances the initial state of a γ cascade is not a long-lived isomeric state, but a short-lived excited state reached by β decay or K capture from a long-lived state, labeled 0 in the following. β decay or K capture leaves the electron shell in an excited state which may decay by x-ray or Auger emission during the nuclear decay. We must then find a way to describe simultaneous decay of the nuclei and their electron shells. Actually the electron shell decays through a sequence of excited states which begins with very short-lived states and may proceed through intermediate states with lifetimes comparable to those of the nuclear levels. For the sake of simplicity, however, we assume only one excited electron state.

The symbols a, b, c label the three nuclear levels with the electrons in the ground state; a', b', c' are the same nuclear levels with the electrons in the excited state. $\mathbf{H}'$ is the matrix for the electronic transition. γ is the reciprocal lifetime of the excited electron state. The correlation formula corresponding to (16) is now

$$W = \text{const}\, \mathrm{Tr}\left\{\epsilon(\Omega_1\Omega_2) \int_0^t dt' \mathbf{H}_{cb} (\rho_b(t') + \rho_{b'}(t')) \mathbf{H}_{bc},\right\} \quad (35)$$

where $\rho_b(t)$ and $\rho_{b'}(t)$ are to be determined from the following set of equations corresponding to (10):

$$\partial\rho_{a'}{}^a/\partial t = -i[H_e{}^a,\rho_{a'}{}^a] - (\gamma_a+\gamma)\rho_{a'}{}^a + 2\pi\mathbf{H}_{a0}\rho_0{}^a\mathbf{H}_{0a}, \quad (36a')$$

$$\partial\rho_a{}^a/\partial t = -i[H_e{}^a,\rho_a{}^a] - \gamma_a\rho_a{}^a + 2\pi\mathbf{H}'\rho_{a'}{}^a\mathbf{H}', \quad (36a)$$

$$\partial\rho_{b'}{}^a/\partial b = -i[H_e{}^a,\rho_{b'}{}^a] - (\gamma_b+\gamma)\rho_{b'}{}^a + 2\pi\mathbf{H}_{ba}\rho_{a'}{}^a\mathbf{H}_{ab}, \quad (36b')$$

$$\partial\rho_b{}^a/\partial t = -i[H_e{}^a,\rho_b{}^a] - \gamma_b\rho_b{}^a + 2\pi\mathbf{H}'\rho_{b'}{}^a\mathbf{H}' + 2\pi\mathbf{H}_{ba}\rho_a{}^a\mathbf{H}_{ab}. \quad (36b)$$

In the average over α, $\rho_0(t)$ is proportional to the unit matrix and its time dependence is given by the factor $e^{-\gamma_0 t}$. Since the decay $0\rightarrow a$ is not observed and $\gamma_0 \ll \gamma_a$, this is still true for $\rho_{a'}(t)$. The desired solutions of the Eqs. (36b') and (36b) are then

$$\rho_{b'}(t) = \text{const}\frac{1}{N}\sum_\alpha \int_0^t dt' e^{-(\gamma_a+\gamma)(t-t')}e^{-\gamma_0 t'} \times U^\alpha(t,t')\mathbf{H}_{ba}\mathbf{H}_{ab}U^\alpha(t,t')^+ \quad (37)$$

and

$$\rho_b(t) = \text{const}\left\{\frac{1}{N}\sum_\alpha \int_0^t dt' \frac{\gamma}{\gamma_a} e^{-\gamma_b(t-t')}e^{-\gamma_0 t'}U^\alpha(t,t') \times \mathbf{H}_{ba}\mathbf{H}_{ab}U^\alpha(t,t')^+ + \frac{1}{N}\sum_\alpha \int_0^t dt' \int_0^{t'} dt'' \times 2\pi e^{-\gamma_b(t-t')}e^{-(\gamma_a+\gamma)t'-t''}e^{-\gamma_0 t''}U^\alpha(t,t') \times \mathbf{H}'U^\alpha(t',t'')\mathbf{H}_{ba}\mathbf{H}_{ab}U^\alpha(t',t'')^+\mathbf{H}'U^\alpha(t,t')^+\right\}. \quad (38)$$

Inserting (37) and (38) in (35), we have clearly three terms in the correlation function. The first term in (38) describes those cases where the electron shell decays while the nucleus is still in the level a; the second term describes decays of the electrons during the life of the state b; (37) describes the nuclei whose electrons remain in the excited state during the life of the state b. For large γ, the first term in (38) is predominant; for small γ, (37) is predominant. In both cases we have the same correlation function as in Sec. III.

I wish to thank Dr. H. Frauenfelder for several stimulating discussions.

PHYSICAL REVIEW VOLUME 93, NUMBER 6 MARCH 15, 1954

Gamma Radiation from Proton Bombardment of Li^7†

ALFRED A. KRAUS, JR.*
Kellogg Radiation Laboratory, California Institute of Technology, Pasadena, California
(Received December 7, 1953)

The capture γ rays from the reaction $Li^7(p,\gamma)$ have been investigated by measuring excitation functions and angular distributions. In addition to the well-known resonance at 441 kev, the excitation curve exhibits resonance at 1030 kev in proton bombarding energy corresponding to an excited state at 18.14 Mev in Be^8. Near this resonance the γ rays have a nonisotropic angular distribution with fore-and-aft asymmetry. The yield integrated over this resonance corresponds to a radiation width given by $\omega\Gamma_\gamma = 2$ ev.

IN the bombardment of Li^7 by protons, γ rays of 15- and 18-Mev energy are produced in the capture reaction, $Li^7(p,\gamma)$. In addition, the first excited state of Li^7 is produced by inelastic scattering of the protons and the decay of this state results in the emission of 478-kev γ rays, the over-all process being indicated by $Li^7(p,p'\gamma)$. The excitation curve for the 478-kev γ rays exhibits resonance[1] at 1030-kev bombarding energy and the behavior of the inelastically scattered protons near this resonance has recently been studied in this laboratory.[2] In addition, the cross section for the protons elastically scattered by Li^7 shows a strong anomaly near this resonance.[3] The present investigation was conducted to determine whether or not the capture γ rays for $Li^7(p,\gamma)$ are resonant at this energy.

Evaporated lithium targets were bombarded with protons from the 2-Mev electrostatic accelerator of the Kellogg Radiation Laboratory. The γ rays were detected with a scintillation counter made of a NaI(Tl) crystal $1\frac{1}{2}$ in. in diameter and 2 in. long, cemented to a 5819 photomultiplier tube. The output was fed into a linear amplifier and to two discriminators, each having its output pulses counted on decade scalers. The system was unable to discriminate between the 15- and 18-Mev γ rays from the $Li^7(p,\gamma)$ reaction. One discriminator was set to count all events over 5 Mev, and the second was set to count the 478-kev (soft) γ rays from the

† This work was supported by the joint program of the U. S. Office of Naval Research and the U. S. Atomic Energy Commission.
* G. E. Fellow in Physics, 1952–1953 academic year. Now at the Department of Physics, The Rice Institute, Houston, Texas.
[1] Brown, Snyder, Fowler, and Lauritsen, Phys. Rev. **82**, 159 (1951).
[2] Mozer, Fowler, and Lauritsen, Phys. Rev. **93**, 829 (1954).
[3] Waters, Fowler, and Lauritsen, Phys. Rev. **91**, 917 (1953).

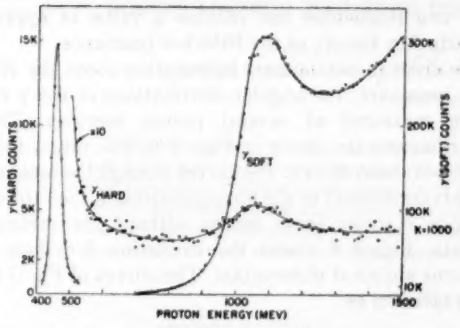

FIG. 1. The excitation function for the various γ rays from the reaction Li^7+p. The soft γ rays are from $Li^7(p,p'\gamma)Li^7$. The hard γ rays are from $Li^7(p,\gamma)$.

reaction $Li^7(p,p'\gamma)$. Typical excitation curves are shown in Fig. 1. The soft γ-ray excitation function agrees with that of Brown, Snyder, Fowler, and Lauritsen.[1] The rise in cross section beyond the reso-

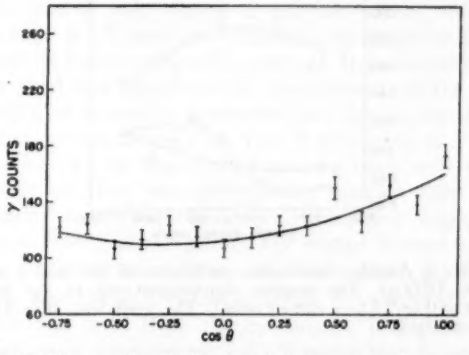

FIG. 2. The angular distribution of hard γ rays at a proton energy of 880 kev. The curve is $W(\theta)=112+16\cos\theta+32\cos^2\theta$.

nance is mainly due to the rapid increase in penetration factor with energy of the outgoing proton. The hard γ rays from the reaction $Li(p,\gamma)$ show the well known 441-kev resonance and the 1030-kev resonance as well.

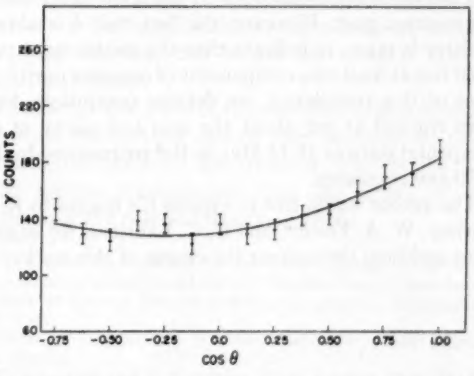

FIG. 3. The angular distribution of hard γ rays at a proton energy of 960 kev. The curve is $W(\theta)=130+18\cos\theta+36\cos^2\theta$.

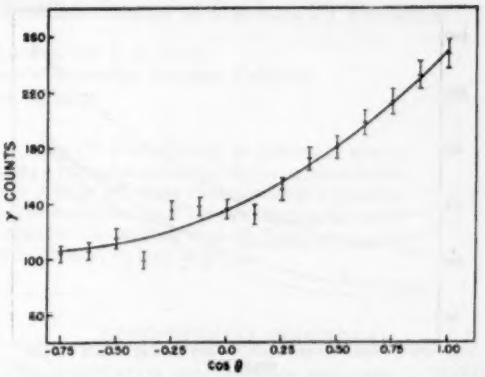

FIG. 4. The angular distribution of hard γ rays at a proton energy of 1060 kev. The curve is $W(\theta)=134+70\cos\theta+44\cos^2\theta$.

The target thickness was about 30 kev. The hard γ-ray counts are the measured number corrected for a small background and the scattering of the points is to be expected from the small number of counts. The soft

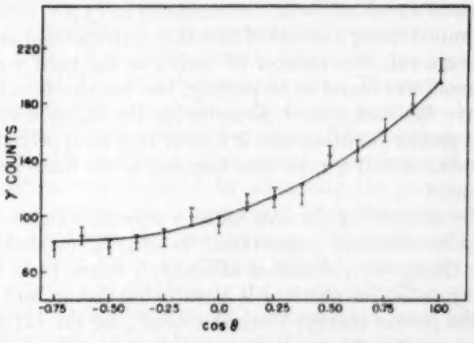

FIG. 5. The angular distribution of hard γ rays at a proton energy of 1140 kev. The curve is $W(\theta)=98+56\cos\theta+40\cos^2\theta$.

γ-ray counts are the measured number corrected for background and hard γ-ray counts.

In order to show that the observed resonance of the hard γ rays was not due to pile-up of the soft γ-ray

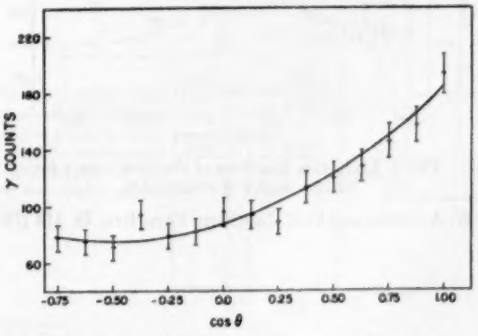

FIG. 6. The angular distribution of hard γ rays at a proton energy of 1240 kev. The curve is $W(\theta)=88+48\cos\theta+48\cos^2\theta$.

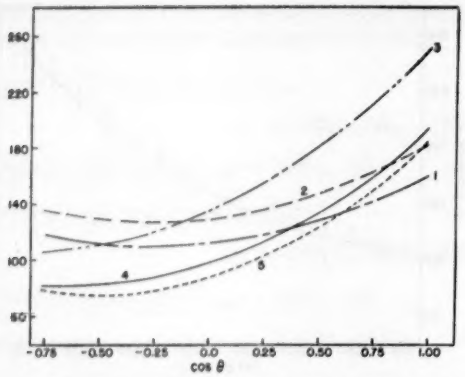

FIG. 7. The curves of Figs. 2–6. Curve 1 is for a proton energy of 880 kev; curve 2 for 960 kev; curve 3 for 1060 kev; curve 4 for 1140 kev; and curve 5 for 1240 kev.

counts, an experiment was devised to determine the importance of pile-up counts. A Cs^{137} source, which emits 661-kev γ rays, was put near the counter at a distance such that the counting rate in the soft γ-ray channel was about twice the maximum $Li^7(p,p'\gamma)$ counting rate. During a period of time that corresponded to an average run, the number of counts in the hard γ-ray channel was found to be slightly, but not significantly, above the background. Considering the higher energy and greater counting rate, it is clear that no appreciable number of soft γ rays were counted in the hard γ-ray channel.

By integrating the area under a resonance curve one obtains numbers proportional to $\omega\Gamma_\gamma/E_p$ (neglecting the change of γ-detection efficiency), where Γ_γ is the γ-ray radiation width, ω is a statistical factor, and E_p is the proton energy. The value of $\omega\Gamma_\gamma$ for the 441-kev resonance[4] is 9.4 ev. Performing the integrations over the two resonances one obtains a value of approximately 2 ev for $\omega\Gamma_\gamma$ at the 1030-kev resonance.

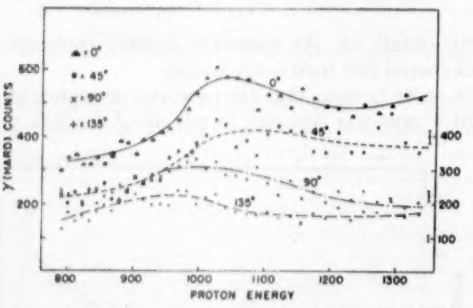

FIG. 8. Excitation functions of the hard γ rays for various angles of observation.

[4] W. A. Fowler and C. C. Lauritsen, Phys. Rev. **76**, 314 (1949).

In order to obtain more information about the 1030-kev resonance, the angular distributions of the γ rays were measured at several proton energies. These distributions are shown in Figs. 2–6. The target thickness was about 60 kev. The curves through the measured points correspond to the formulas given in the captions. Figure 7 shows these curves without the measured points. Figure 8 shows the excitation functions for various angles of observation. The curves of Fig. 7 can be expressed as

$$W(\theta)=W(\pi/2)[1+a\cos\theta+b\cos^2\theta],$$

where $W(\theta)$ is the number of counts at the angle of observation θ. Figure 9 is a plot of $W(\pi/2)$, a, and b for the different energies.

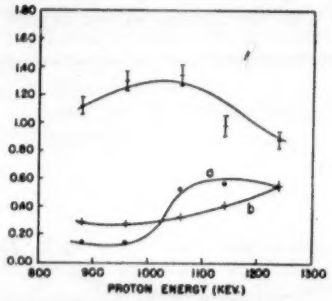

FIG. 9. Angular distribution coefficients of the hard γ rays from $Li^7(p,\gamma)$. The angular distributions are of the form $W(\theta)=W(\pi/2)[1+a\cos\theta+b\cos^2\theta]$. The coefficient $W(\pi/2)$ is divided by 100.

One important feature of Fig. 9 is the shape of the curve for a. The coefficient a is positive throughout the resonance, although the shape is approximately that to be expected from a resonance interfering with a nonresonant state of opposite parity. A simple interpretation is that the resonant part of the γ-ray cross section gives rise to a change in the coefficient a by the interference with a nonresonant part. However, the fact that a is always positive is taken to indicate that the nonresonant part itself has at least two components of opposite parity. In view of this complexity, no definite conclusions have been reached as yet about the spin and parity of the compound state at 18.14 Mev in Be^8 represented by the 1030-kev resonance.

The author would like to express his thanks to R. F. Christy, W. A. Fowler, and C. C. Lauritsen for suggestions and help throughout the course of this work.

Low-Energy Gamma Radiation from the Bombardment of Carbon by Protons*

H. H. WOODBURY,† A. V. TOLLESTRUP, AND R. B. DAY‡
Kellogg Radiation Laboratory, California Institute of Technology, Pasadena, California
(Received December 14, 1953)

Weak, low-energy capture radiation has been observed when C^{12} is bombarded by protons of energy 1–3 Mev. From the observed dependence of gamma-ray energy on proton bombarding energy, it is concluded that the radiation arises from a transition to the 2.369-Mev level in N^{13}. Since the latter level is unstable to proton emission a second gamma ray is not observed. The excitation curve for this reaction shows an anomaly in the neighborhood of 1.7 Mev, which can be explained as resulting from the interference of a nonresonant p-wave radiation with the radiation from the 3.511-Mev, $P_{\frac{1}{2}}$ level in N^{13}.

INTRODUCTION

IN the course of an investigation of the gamma radiation from the reaction $C^{12}(p,\gamma)N^{14}$ a very weak, low-energy gamma ray was found which could not be fitted into the level scheme of N^{14} as then known. The energy of this gamma ray changed from about 0.75 Mev to 2 Mev as the bombarding energy changed from 1.3 Mev to 2.7 Mev. In investigating the origin of this gamma ray, targets of normal carbon, carbon enriched in C^{13}, and bare tantalum, the target backing material, were bombarded by protons. It was found that the yield was approximately proportional to the C^{12} content of the carbon targets and zero for the tantalum target; hence, it was clear that it originated in a C^{12} reaction. At the bombarding energies used, only two proton reactions were energetically possible with C^{12}, namely, elastic scattering and radiative capture. Measurement of the gamma-ray energy showed that this was a capture radiation reaction in which the final state was the 2.369-Mev level[1] of N^{13} (see Fig. 1). Since this level is in the continuum, it decays by breaking up into a proton and C^{12}, rather than by emission of a second gamma ray to the ground state of N^{13}. The reaction may thus be designated as

$$H^1+C^{12}\rightarrow(N^{13})\rightarrow N^{13*}+\gamma$$
$$\searrow$$
$$C^{12}+H^1,$$

or, in briefer notation, $C^{12}(p,\gamma p')C^{12}$. Although the end products of the reaction are the same as in an inelastic scattering reaction, this is just an unusual case of radiative capture.

The energy and yield of this gamma ray as a function of proton bombarding energy were investigated using a NaI(Tl) scintillation spectrometer. The results have given further confirmation that the origin of the radiation is the reaction described above.

EXPERIMENTAL PROCEDURE

The scintillation spectrometer employed a NaI(Tl) crystal 1½ inches long and 1½ inches in diameter mounted on an RCA 5819 photomultiplier. The counter and associated electronic equipment have been described briefly in another paper,[2] together with the procedures followed in obtaining pulse-height spectra.

Since the background radiation from the electrostatic accelerator and from other reactions in the target was generally very much more intense than the gamma ray of interest here, it was necessary to identify the latter by means of its characteristic photopeak produced in the NaI(Tl) scintillation counter. Therefore, the measurements required a pulse-height spectrum to be obtained at each bombarding energy. Three such spectra are shown in Fig. 2. The energy dependence of the radiation was obtained by observing the position of the photopeak and comparing it with the photopeaks from Cs^{137} and Na^{22} gamma rays. The yield measurements were made by integrating the area under the photopeak and dividing by the photopeak efficiency.

Since a calculation of the photopeak efficiency would be extremely tedious because of the secondary processes that take place in the crystal,[3] it was determined semiempirically. Pulse-height distributions were obtained for gamma rays of the following energies: 0.661 Mev (Cs^{137}), 1.277 Mev (Na^{22}), 1.63 Mev [$Na^{22}(p,\alpha\gamma)Ne^{20}$], and 2.615 Mev (ThC″). The ratio of the area under the photopeak to the total area under the

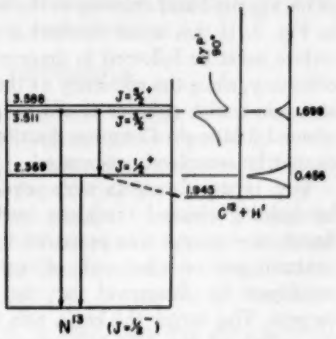

FIG. 1. Energy level diagram of N^{13}. Energy levels are given in Mev. The angular momentum (J) and parity of the levels are shown above each level.

* This work was assisted by the joint program of the U. S. Office of Naval Research and the U. S. Atomic Energy Commission.
† Now at General Electric Research Laboratory, Schenectady, New York.
‡ Now at Los Alamos Scientific Laboratory, Los Alamos, New Mexico.
[1] F. Ajzenberg and T. Lauritsen, Revs. Modern Phys. **24**, 321 (1952).
[2] Woodbury, Day, and Tollestrup, Phys. Rev. **92**, 1199 (1953).
[3] D. Maeder and V. Wintersteiger, Phys. Rev. **87**, 537 (1952).

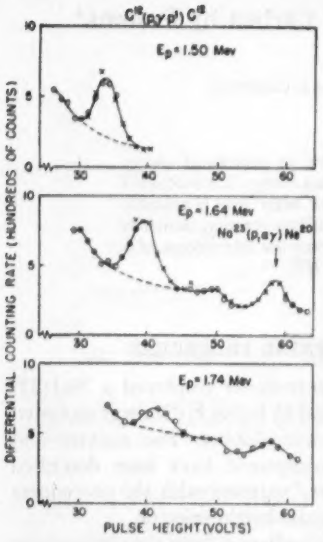

FIG. 2. Typical pulse-height spectra obtained for the reaction $C^{13}(p,\gamma p')C^{13}$. The photopeak for the gamma ray of interest is shown to move from 33.5 volts to 39 volts to 41 volts corresponding to the increase in bombarding energy as noted. The peak at 58 volts is the photopeak corresponding to the 1.63-Mev radiation from the reaction $Na^{23}(p,\alpha\gamma)Ne^{20}$.

pulse-height curve was measured for each of these gamma rays. The photopeak efficiency was then found by multiplying this ratio by the calculated probability that a gamma ray would interact in the crystal. The ratio of the photopeak efficiencies at 0.511 Mev and 1.277 Mev was also determined experimentally with a Na^{22} source. The results of these determinations are plotted in Fig. 3. It can be seen from the graph that the energy variation of the photopeak efficiency follows a power law within the experimental error.

In practice it is sometimes difficult to obtain a clear separation of the photopeak from the Compton distribution and from the pulse distribution due to background radiation. However, reproducible results can be obtained in such cases if one follows the criterion that the photopeak corrected for background be symmetrical. Such an analysis is independent of the resolution of the counter but is quite tedious if many data have to be handled. It has been found that results that are just as reproducible can be obtained by considering the front part of the Compton distribution as background and drawing in the background as shown in Fig. 2. If this latter method is used, the same procedure must be followed in determining the photopeak efficiency, since the efficiency as thus determined varies somewhat with counter resolution. The reason is that above 1.5 Mev the Compton distribution and photopeak cannot be completely separated.

Two types of targets were used. One was prepared by holding cleaned tantalum over a smoky benzene flame; the second was prepared by cracking methane (natural gas) on a hot strip of tantalum in the manner employed by Seagrave[4] for the preparation of C^{13} targets. The target thickness was found by measuring the width of the 1.76-Mev resonance in $C^{13}(p,\gamma)N^{14}$. This resonance is strong enough to be easily observable in normal carbon, and since it has a width of only 2 kev, while the targets were 20 to 100 kev thick, the observed resonance width was equal to the target thickness. Knowing the target thickness in kev, one could then calculate the number of carbon atoms per square centimeter by dividing by the stopping cross section of carbon[5] at the average proton bombarding energy used in determining the target thickness.

It was found that the targets were easily contaminated, either by handling or by simply leaving them uncovered in the laboratory. This contamination resulted in a 1.63-Mev gamma ray from the strong reaction[1] $Na^{23}(p,\alpha\gamma)Ne^{20}$ (see Fig. 2). Although the intensity of this gamma ray was usually small compared to the other background radiation, the fact that the gamma ray being investigated had the same energy at a proton bombarding energy of 2.2 Mev meant that its photopeak was distorted by the photopeak from this sodium contamination. To check on this and other possible contaminants, pulse-height spectra were often taken up to pulse heights of 3–4 Mev to make sure that there was no structure except for the smoothly varying background.

A second contaminant producing high-energy gamma rays is believed to be fluorine in the tantalum used for the target backing. Since the 6- and 7-Mev radiation from the $F^{19}(p,\alpha\gamma)O^{16}$ reaction produces a smoothly varying pulse-height distribution in the region of interest, this contaminant was not a problem below 2.2-Mev bombarding energy. However, above 2.5 Mev the yield from this reaction increased so greatly that it proved troublesome.

There was also a background from the proton capture radiation reactions in C^{12} and C^{13}, but since it was mostly composed of higher-energy gamma rays it did not cause difficulty. However, the annihilation radiation

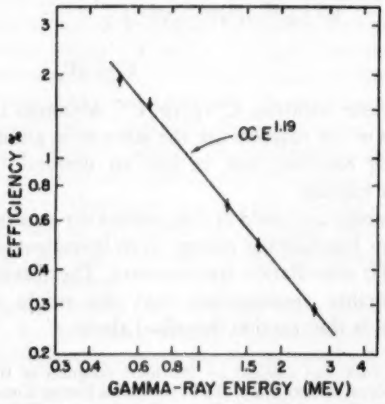

FIG. 3. Photopeak efficiency of the NaI (Tl) scintillation counter for a source 0.75 inch from the top of the crystal. The crystal is 1.50 inches long and 1.50 inches in diameter.

[4] J. D. Seagrave, Phys. Rev. 85, 197 (1952).

[5] J. O. Hirschfelder and J. L. Magee, Phys. Rev. 83, 207 (1948).

resulting from the positron decay of the N^{13} formed in the $C^{12}(p,\gamma)N^{13}$ reaction made it impossible to observe the gamma ray of interest when its energy was less than about 0.6 Mev.

The proton currents normally used were between 3 and 5 microamperes, with the maximum value being limited by the heating of the target. The current was measured by means of a standard current integrator in which a 10-microfarad capacitor was charged to a fixed voltage. Even though a large capacitor was used the integrator was often cycled as much as six times a run (corresponding to a beam charge of about 0.003 coulomb). A constant current source of known magnitude was used to calibrate the integrator and to take into account the capacitor soakage effects when the integrator was cycled.

RESULTS

With the scintillation counter at 90° to the proton beam, a number of measurements of the gamma-ray energy were made at various proton bombarding energies. The results of these are plotted in Fig. 4 as a function of the effective proton energy, which has been taken as the bombarding energy minus half of the target thickness. It can be seen that the gamma-ray energy increases linearly with proton energy. A least squares fit to these data gives

$$E_\gamma = 0.88(E_p - 0.45),$$

where E_γ and E_p are in Mev. If the final state in the capture radiation reaction is indeed the 2.369-Mev level in N^{13}, the expected variation of gamma-ray energy with proton energy would be

$$E_\gamma = 0.92(E_p - 0.456).$$

This agrees with the experimental result within the accuracy of the observations, hence it constitutes strong evidence that the proposed origin of the radiation is correct.

The gamma-ray yield was obtained as a function of proton energy by measuring the area under the photo-

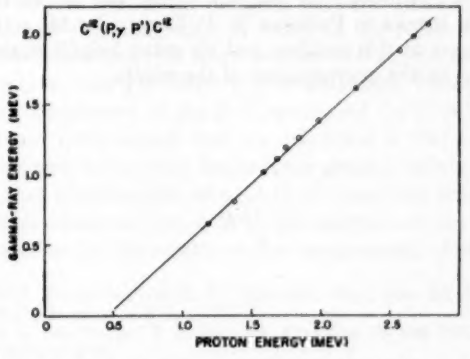

FIG. 4. Gamma-ray energy *versus* proton bombarding energy for the reaction $C^{12}(p,\gamma p')C^{12}$.

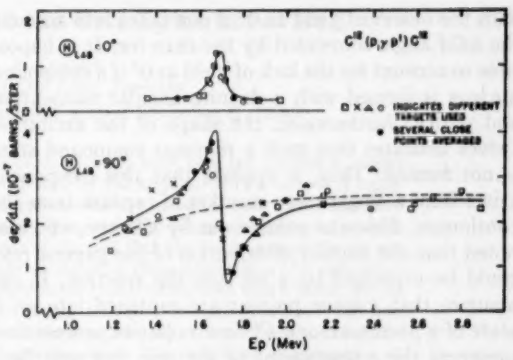

FIG. 5. Excitation curve for the reaction $C^{12}(p,\gamma p')C^{12}$. The upper and lower curves are for the counter at 0° and 90° with respect to the beam.

peak of the pulse-height distribution and dividing by the photopeak efficiency. In these measurements the counter was used at 0° and at 90° to the beam with the front face of the crystal $\frac{3}{4}$ inch from the target. The relative counter efficiency at 0° and 90° was checked in two ways. One was to replace the target by a Na^{22} source, while the other was to observe the relative intensity of the 2.4-Mev radiation at the 0.456-Mev resonance in $C^{12}(p,\gamma)N^{13}$ which is known to be isotropic.[6] To obtain the true yields it was also necessary to make a correction for absorption of the gamma rays in the target chamber. This was only 2 to 4 percent for the measurements at 90°, but amounted to approximately 20 percent at 0°. The gamma-ray interaction cross sections for these corrections were obtained from the work of Davisson and Evans.[7]

The procedure outlined above gave the total effective isotropic yield per proton $Y(E,\theta)$. The differential cross sections were then calculated from the relation

$$d\sigma(E,\theta)/d\Omega = Y(E,\theta)/4\pi n,$$

where n is the number of carbon nuclei per cm² in the target. The effective proton energy E is again taken as the bombarding energy minus half the target thickness. The cross sections at 0° and 90° are plotted in Fig. 5 and in the following section the behavior of these curves is considered in more detail.

DISCUSSION

From the excitation curves of Fig. 5 one can see that the radiation is composed of two parts—a slowly varying, nonresonant component, and one which is resonant at 1.7 Mev. Considering the first, it is seen to have approximately zero yield at 0°, and it is assumed for simplicity that it exhibits a $\sin^2\theta$ angular dependence although this cannot be demonstrated by measurements at only the two angles. This assumption is consistent

[6] S. Devons and M. G. N. Hine, Proc. Roy. Soc. (London) **A199**, 56 (1949).

[7] C. M. Davisson and R. D. Evans, Revs. Modern Phys. **24**, 79 (1952).

with the observed yield at 0° if one takes into account the solid angle subtended by the detector. It is impossible to account for the lack of yield at 0° if a compound nucleus is formed with a definite angular momentum and parity; furthermore, the shape of the excitation curves indicates that such a resonant compound state is not formed. Thus, it appears that this component arises from a single stage reaction of capture from the continuum. This was pointed out by Christy, who also noted that the angular distribution of the gamma rays could be explained by a no spin flip reaction. If one assumes that p-wave protons are captured into an S state of a proton around C^{12} in a radiative process that preserves the z component of the spin (no spin flip), then the expected angular distribution is $\sin^2\theta$. This assumption is further strengthened by the way in which it accounts for the interference near the 1.7-Mev resonance.

The scattering of protons by C^{12} shows a strong anomaly near 1.7 Mev[8] which has been shown by Jackson and Galonsky[9] to be due to two resonant levels, a $P_{\frac{1}{2}}$ state at $E_p=1.698$ Mev and a $D_{\frac{3}{2}}$ state at 1.748 Mev. Only the first of these appears in the reaction $C^{12}(p,\gamma)N^{13}$; the radiation from the second is expected to be much weaker, and so far has eluded detection.[10] Neglecting the latter, the combined gamma-ray intensity to be expected from the $P_{\frac{1}{2}}$ level and the nonresonant p-wave radiation suggested above was calculated and is easily shown to be proportional to the expression

$$I(E,\theta)=\left|\frac{(2/3)^{\frac{1}{2}}Ae^{i\delta}(\Gamma/2)}{E-E_r+i(\Gamma/2)}+1\right|^2\sin^2\theta+\left|\frac{(1/3)^{\frac{1}{2}}Ae^{i\delta}(\Gamma/2)}{E-E_r+i(\Gamma/2)}\right|^2\frac{(1+\cos^2\theta)}{2}.$$

Here A is the relative amplitude of the resonant and nonresonant gamma rays at $E=E_r$, δ is the relative phase excluding the resonance phase, and E_r and Γ are the proton resonance energy and width at half-maximum. When expanded, this expression becomes

$$I(E,\theta)=\sin^2\theta+\frac{(5/24)A^2\Gamma^2-(1/8)A^2\Gamma^2\cos^2\theta}{(E-E_r)^2+(\Gamma/2)^2}+\frac{[(2/3)^{\frac{1}{2}}A\Gamma\Delta E\cos\delta+(1/6)^{\frac{1}{2}}A\Gamma^2\sin\delta]\sin^2\theta}{(E-E_r)^2+(\Gamma/2)^2}.$$

The values used for the resonance parameters were $E_r=1.70$ Mev and $\Gamma=60$ kev.[9] The value of A was determined by comparing the relative amplitude of the 0° and 90° data. In doing this for the 0° data, θ was actually set equal to 20°, the average angle subtended by the counter in the forward direction. The value of δ was then determined by the best fit to the 90° data. Since the only criterion used in picking the values of A and δ was the best looking fit to the data, it was difficult to calculate limits on acceptable values for these parameters. However, from trying various combinations acceptable values for A and δ were found to be

$$A=1.1\pm0.1,$$
$$\delta=2.4\pm10°.$$

This expression for the intensity has been plotted in Fig. 5 using these values except that the nonresonant radiation is assumed to follow the dashed line rather than to be constant. The dashed curve was obtained by connecting the data on either side of the resonance with a smooth, slowly varying curve.

The gamma-emission width, Γ_γ, for the resonance transition from the 3.511-Mev level to the 2.369-Mev level (see Fig. 1) was found from the absolute yield to be 0.04 ev. For comparison, the ground-state transition from the 3.511-Mev level has a width of 0.7 ev.[4]

An attempt was also made to find the gamma radiation from a similar nonresonant reaction in which the final state of the radiative transition was the 3.511-Mev $P_{\frac{1}{2}}$ state in N^{13}. Because of the higher bombarding energy required, the conditions were not too favorable and the attempt failed. Proton energies up to 2.7 Mev were used here.

In conclusion, the authors would like to express their thanks to Professor R. F. Christy for his active interest in this problem and his many helpful suggestions on the interpretation of the results.

[8] Jackson, Galonsky, Eppling, Hill, Goldberg, and Cameron, Phys. Rev. 89, 365 (1953).
[9] H. L. Jackson and A. I. Galonsky, Phys. Rev. 89, 370 (1953).
[10] R. B. Day, Ph.D. thesis, California Institute of Technology, 1951 (unpublished); J. D. Seagrave, Phys. Rev. 84, 1219 (1951).

The Pseudoscalar Interaction and the Beta Spectrum of RaE

M. E. Rose and R. K. Osborn
Oak Ridge National Laboratory, Oak Ridge, Tennessee

(Received September 14, 1953; revised manuscript received December 17, 1953)

It is shown that the theory of forbidden beta transitions, as hitherto used, does not provide a correct treatment of the pseudoscalar interaction. This is demonstrated by the application of a canonical transformation to the Hamiltonian of interacting nucleons and leptons whereby all odd nuclear Dirac operators are eliminated from the theory. When this is done properly it is seen that the pseudoscalar interaction makes a contribution to the β-decay process only by virtue of the fact that the lepton covariants are not constant. The corresponding additional operators introduced in the other three interactions (S is pure even) are examined and it is shown that, except in one case, these make trivial corrections which would not be observed in practice. The exception occurs in second and higher forbidden transitions wherein the spin change (tensor rank, strictly speaking) is lower than the forbiddenness order. By virtue of present knowledge of the beta interaction these must be regarded as small correction terms. The possibility of calculating all nuclear matrix elements using nonrelativistic wave functions based on some coupling model is discussed. The results presented here also show that wherever P and T interactions interfere (spin change zero, first-forbidden transitions) it will be possible to obtain the ratio of coupling coefficients (g_P/g_T for example) by comparison with the observed spectral shapes. A method of reduction of the β-decay operators is described and it is pointed out that the same procedure is very convenient for obtaining the nuclear matrix elements. In this method the irreducible tensors are obtained automatically and the retardation expansion is a trivial operation performed at the end of the calculation rather than at the beginning. The correction factors for pseudoscalar (P) as well as P–T and P–A mixtures are obtained and the fact that the shape of the correction factor is strongly modified as compared to the customary result is observed. The correction factor is now more strongly Z dependent and this would perhaps account for the appearance of the P interaction only for heavy elements. The results of this investigation are applied to the RaE spectrum. No fit with the assumption of zero spin for RaE can be obtained. It is suggested that the spin of RaE is unity, and other evidence pointing in this direction is cited.

I. INTRODUCTION

THE somewhat anomalous beta-spectrum of RaE has attracted considerable attention in recent years. It is a well-known fact that despite several attempts to account for the observed spectrum, using the well-established theory of forbidden beta transitions,[1] no success could be claimed until the analysis of Petschek and Marshak[2] appeared. From that work one would conclude that the RaE spectrum demands the presence of the pseudoscalar (P) interaction in the beta-coupling and in fact, a tensor-pseudoscalar (T-P) mixture seemed to suffice to account for the observed results.[3]

The assumption upon which the aforementioned analysis of Petschek and Marshak is based is the assignment of zero spin to the decaying state and an a priori reason for this assignment is based on the Nordheim rule for minimum spin when neutron and proton configurations belong to different Schmidt groups. The odd parity assignment of the shell model and the ft value makes it quite certain that the transition is first forbidden and the fact that the spectrum shape is definitely not that characteristic of a $|\Delta J|=2$ transition limits the spin values to 0 or 1. With the exclusion of the A interaction by the results of the measurement of the He^6 angular correlation[4] and the shapes of other first forbidden spectra,[5] one is led to a P-T mixture as the only possible explanation of the spectrum if the spin 0 assignment is adopted.

Nevertheless, this analysis of the RaE spectrum in terms of the T-P mixture cannot be accepted, because the otherwise completely correct theory of forbidden beta transitions is not correct insofar as the pseudoscalar interaction is concerned. The reasons for this statement will be presented below in detail. At this point it suffices to say that the proper correction factor to be used for the P interaction and for all interference terms with the P interaction differs from those hitherto used in a major way. There are also other cases in which the correction factors are misrepresented in a non-trivial way but these arise in circumstances which are now known to be impractical. This remark will also be amplified in the following.

At this stage of the discussion we may indicate in what manner the customary treatment fails. The central point involved is that in all forbidden transitions wherein, in the conventional form of the theory, odd Dirac operators are involved, one cannot make the usual categorical statement that the nuclear matrix elements are certain numbers independent of the parameters describing the lepton field. Actually, in such operators the small component of the nuclear wave function is involved and this implies that the momentum

[1] E. J. Konopinski and G. E. Uhlenbeck, Phys. Rev. **60**, 308 (1941), referred to as KU.
[2] A. G. Petschek and R. E. Marshak, Phys. Rev. **85**, 698 (1952), referred to as PM.
[3] For example, L. M. Langer and H. C. Price, Jr., Phys. Rev. **76**, 461 (1949).
[4] B. M. Rustad and S. L. Ruby, Phys. Rev. **89**, 880 (1952).
[5] H. M. Mahmoud and E. J. Konopinski, Phys. Rev. **85**, 1266 (1952).

of the decaying nucleon appears. Because of the point-coupling of the beta interaction, this will introduce terms directly dependent on the momenta of the leptons (more exactly, the gradient operator acting on the lepton covariant is introduced). Because the lepton de Broglie wavelengths are so large compared to the nuclear radius, such terms are always rejected. This, it turns out, is completely justified in all but two cases and one of these is the pseudoscalar interaction. In this case, if one follows the usual treatment, there is *no contribution from the pseudoscalar interaction at all.*[6] In this respect the pseudoscalar interaction is unique. In fact, the word "peculiar" may be an appropriate description of such interactions.

The validity of statements made above become apparent if one carries out a thorough reduction of the beta-decay problem to the nonrelativistic limit so far as the nucleon space is concerned. This is done in Sec. II in such a way that one can see exactly what is neglected. The error involved in such a step is exceedingly minute so that the beta-decay problem can be described in a greatly simplified representation which is virtually exact.

A particularly interesting advantage which accrues from this procedure is the possibility of calculating nuclear matrix elements in terms of nonrelativistic wave functions. The implication here is that one adopts a specific coupling model (*j-j* or *L-S*, for example). This representation of the beta-decay operators in even form may be compared to the usual representation where it is necessary to calculate matrix elements of odd operators; the usual representation therefore requires relativistic wave functions concerning which one must profess almost complete ignorance. While our change of representation is a formal step, it facilitates the application of what one *does* know concerning nuclear forces from a phenomenological point of view. In some cases, (for mirror nuclei, say) no detailed knowledge of nuclear forces is necessary, just as was the case for certain even operators.[7]

Finally, we mention the fact that initial attempts in the direction we have here indicated were made by others.[8] However, these investigations did not lead to correct results because the reduction to the nonrelativistic case was not made consistently.

II. THE CANONICAL TRANSFORMATION OF THE BETA-DECAY OPERATORS

Since, as implied above, the difficulty in the conventional formalism lies in the occurrence of odd Dirac operators, we eliminate these by a canonical transformation (FW).[9] Alternatively, one can proceed by the method of elimination of small components in the nuclear wave function. However, this procedure is cumbersome to apply in the case of a many-particle nucleus and is also somewhat less desirable from a theoretical point of view.[9]

For the system of nuclear sources coupled to the lepton field the Hamiltonian is

$$H=H_N+H_\beta+H_l, \tag{1}$$

where

$$H_N=-\boldsymbol{\alpha}\cdot\mathbf{p}-\frac{\beta}{2}[M_n(1+\tau_z)+M_p(1-\tau_z)]+V \tag{2}$$

is the nuclear Hamiltonian, and

$$H_\beta=\sum_X g_X\Omega_{X^\mu}(N)\Omega_{X^\mu}(l)Q \tag{3}$$

is the β coupling while H_l is the Hamiltonian for the lepton field alone. In (2) as in all the subsequent formalism, our notation is that the operator product $\omega\omega'\omega''\cdots$ means $\sum_k \omega_k\omega_k'\omega_k''\cdots$, where k is a particle label. The only exception to this rule is the minor one that wherever V, the nuclear force operator, occurs a double summation is implied. Thus, in explicit form,

$$V=\sum_{ij}{}' V_{ij}=\sum_{ij}{}' V_iV_j, \tag{4}$$

where the prime means that $i=j$ is excluded. Then, in the following discussion, where commutators with V appear, we recognize that

$$\begin{aligned}(V,\omega)&=\sum_{ij}{}'(V_{ij},\omega_i+\omega_j)\\&=\sum_{ij}{}'[(V_i,\omega_i)V_j+V_i(V_j,\omega_j)],\end{aligned} \tag{5}$$

where $(A,B)\equiv AB-BA$ and again $\omega=\sum_k\omega_k$. But

$$(\omega,\omega')=\sum_k(\omega_k,\omega_k'). \tag{6}$$

Our units are such that $c=\hbar=1$ and later, when the β-particle wave functions are introduced, $m=1$. In Eq. (2), M_n and M_p are the neutron and proton masses, respectively.

In (3) only electron emission is represented explicitly. The positron emission is obtained of course by adding the hermitian conjugate of H_β. In the following we consider electron emission wherever it is necessary to be explicit. For positron emission the results are obtained as usual by changing Z to $-Z$ (and introducing the sign changes in the Fierz interference terms[10]) or, if the central field in which the β particle moves is not a Coulomb field but is V_e, one changes V_e to $-V_e$. The operators $\Omega_{X^\mu}(N)\Omega_{X^\mu}(l)$ in (3) are the usual contracted tensors in nucleon (N) and lepton (l) spaces and for convenience only a single tensor index (μ) is written explicitly. Of course, $X=S$, V, T, A, and P. If $\Omega_X(N)=\omega_\mu{}^N$, then $\Omega_{X^\mu}(l)=\psi^*\omega_\mu C\varphi=L(\omega_\mu)$, where ω_μ is

[6] This statement is almost rigorous. There may be extremely small contributions; see Sec. II.

[7] As a preliminary step we have investigated the matrix elements of the (formerly) odd operators in the one particle *j-j* coupling model, M. E. Rose and R. K. Osborn, following paper [Phys. Rev. **93**, 1326 (1954)].

[8] Ahrens, Feenberg, and Primakoff, Phys. Rev. **87**, 663 (1952); T. Ahrens, Phys. Rev. **90**, 974 (1953). Part of our results are contained in the results of the latter paper, but to obtain the proper correction factor large parts of Ahren's results are simply to be discarded.

[9] L. L. Foldy and S. A. Wouthuysen, Phys. Rev. **78**, 29 (1950), referred to as FW.

[10] M. Fierz, Z. Physik **104**, 553 (1937).

a Dirac operator in lepton space, φ is a positive energy neutrino wave function, and C ($=i\beta\alpha_2 K_0$ with K_0 meaning complex conjugation) is the charge conjugation operator. The lepton covariant, referred to above, is just $L(\omega_\mu)$. Q is the operator which changes neutron into proton. Except in special circumstances we need not make this operator explicit. We adopt the special representation

$$\alpha=\begin{pmatrix}0 & \sigma\\ \sigma & 0\end{pmatrix},\quad \beta=\begin{pmatrix}1 & 0\\ 0 & -1\end{pmatrix}, \tag{2'}$$

in the Dirac space notation. Then our sign convention is the one usually used in β-decay theory.

The FW transformation is applied to the total Hamiltonian H with the purpose of removing odd operators in H_N and H_β to a given order.[9] That is, the new Hamiltonian is

$$H'=e^S H e^{-S}=H+(S,H)+\tfrac{1}{2}(S,(S,H))+\cdots, \tag{7}$$

and we restrict our attention to just the three terms written. However, as is well known, consistent results are obtained if in the double commutator only the mass term ($\sim-\beta M$) is taken. To this order, the mass difference M_n-M_p is not essential for the new β-decay interaction (H_β') but it will be for some subsequent results (see Sec. III). Also, to this order the transformation of H_l does not contribute anything to H_β'. Superficially, it would appear that the expansion parameter is of order $p/M\sim v/c$ (v the nucleon velocity) but a more thorough investigation shows that, because of the parity properties of the $\mathbf{p}$ operator, the expansion parameter here is effectively $p^2/M^2\sim 10^{-2}$.

Writing

$$H_N=H_N(e)+O_1,\quad H_\beta=H_\beta(e)+O_2, \tag{8}$$

where $H_N(e)$, $H_\beta(e)$ are the respective even parts and O_1, O_2 the respective odd parts in Dirac space we have

$$S=-\frac{\beta}{2M}(O_1+O_2). \tag{9}$$

The commutator $(S,-\beta M)=-(O_1+O_2)$, so that these odd terms are removed by the canonical transformation. The commutator of S and an even operator is odd and can be removed by another canonical transformation of the type (9). The even terms thus generated are of order $1/M^2$ and are neglected.

For the nuclear force operator V it is legitimate to assume a sum over pairs of terms which are symmetrical between the interacting nucleons. Hence there should be two types of interaction operators: direct products of even operators and of odd operators. The direct product of two even operators, V_e, gives rise to no difficulty; see Eq. (11) below. The prescription (9) for removing odd operators does not apply directly in the case of two-particle operators (V_0). However, the removal of such terms can be effected[11] and the resulting transformed operators appear only in terms of order $1/M^2$. Consequently, these terms need not concern us further.

Applying successive transformations of the type (9) until all odd operators to the prescribed order disappear, we find

$$H'=H_N'+H_\beta'+H_l, \tag{10}$$

with

$$H_N'=-\frac{\beta p^2}{2M}-\beta M-\tfrac{1}{2}\Delta\beta\tau_z+V_e, \tag{11}$$

where $\Delta=M_n-M_p$ and

$$H_\beta'=-\frac{1}{2M}\beta(O_1,O_2)_+ +H_\beta(e) \tag{12}$$

where $(O_1,O_2)_+=O_1O_2+O_2O_1$. Of course, terms quadratic in the coupling constants g_X are dropped. The results given in (11) and (12) are identical with those obtained by the method of elimination of small components when carried out to the same order in $1/M$.

With the representation (2') the positive energy solutions correspond to $\beta=-1$. We set $\beta=-1$ (in the nuclear space) from this point on, realizing that no approximation is involved other than that involved in terminating the development given by (7). The zero order nuclear wave functions are now truly nonrelativistic ones. From (12) it is apparent that the β interaction contains only even operators and that $H_\beta(e)$ which accounts for allowed transitions as well as unique matrix element transitions, is unaffected.

At this point one can begin to discern the role of the lepton covariant. The S operator involves $\beta\boldsymbol{\alpha}\cdot\mathbf{p}/2M$ and a gradient operation on L appears. In the pseudoscalar case this is *all* that appears. This fact becomes apparent below when we explicitly compute the anticommutator of (12). However, it is enlightening to see how this happens when one uses the method of elimination of small components. For this purpose we use a simplified one-particle model, but this simplification does not change the essential ideas. Then, with the nuclear wave function in the form

$$\Psi=\begin{pmatrix}v\\ u\end{pmatrix}, \tag{13}$$

where u, v are the large and small components, respec-

[11] In the case of a two-particle Hamiltonian it has been shown by Z. V. Chraplyvy, Phys. Rev. **91**, 388 (1953), that a canonical transformation which removes V_0 can be constructed. While the generating function S given in this reference is singular in the case of two particles of equal mass, this difficulty disappears if the canonical transformation is required to separate only states in which both particles have the same sign of the energy. Extension to the case of many particles presents no difficulty. [See Z. V. Chraplyvy, Phys. Rev. **92**, 1310 (1953).] We wish to express our thanks to Dr. Chraplyvy for communicating these results before publication.

tively, we have

$$\int \beta\gamma_5 L \equiv \int \Psi_f^* \beta\gamma_5 L \Psi_i = -\int (v_f^* L u_i - u_f^* L v_i), \quad (14)$$

where $L=L(\beta\gamma_5)$. Eliminating v by

$$v=-(W+M-V)^{-1}\boldsymbol{\sigma}\cdot\mathbf{p}u \approx -\frac{1}{2M}\boldsymbol{\sigma}\cdot\mathbf{p}u \quad (14a)$$

since $W-M-V \ll 2M$, we have

$$\int \beta\gamma_5 L = \frac{1}{2M}\int u_f^*(\boldsymbol{\sigma}\cdot\mathbf{p}L)u_i, \quad (15)$$

where $\mathbf{p}$ acts *only* on L. The way in which the momentum of the nucleon, entering through the small component, introduces the lepton parameters (energy and V_e) is now clear.

For simplicity, we consider plane waves

$$L=L_P e^{-i\mathbf{P}\cdot\mathbf{r}}, \quad (16)$$

where L_P contains the lepton spinor amplitudes, and[12]

$$\mathbf{P}=\mathbf{p}_e+\mathbf{q}, \quad (17)$$

with $\mathbf{p}_e$, $\mathbf{q}$ the electron and neutrino momenta, respectively. Then, with a retardation expansion,

$$\int \beta\gamma_5 L = -\frac{1}{2M}\int \boldsymbol{\sigma}\cdot\mathbf{P}L_P(1-i\mathbf{P}\cdot\mathbf{r}\cdots). \quad (18)$$

The first term,

$$-\frac{1}{2M}L_P\mathbf{P}\cdot\int\boldsymbol{\sigma},$$

gives rise to the second forbidden transitions and corresponds exactly to the contribution of $\int\beta\gamma_5\mathbf{r}$ in the KU representation. The second term gives rise to two terms:

$$\frac{i}{4M}\sum_{ij}B_{ij}P_iP_j,$$

and

$$\frac{i}{6M}P^2\int\boldsymbol{\sigma}\cdot\mathbf{r}.$$

The correction factor associated with the first is the same as that associated with $R_{ij}{}^{\beta\gamma_5}$ in the KU representation. The second part has a correction factor which is the same as that associated with the matrix element of $\beta\gamma_5 r^2$. In fact, we would say that

$$i\int\boldsymbol{\sigma}\cdot\mathbf{r}\leftrightarrow-\int\beta\gamma_5 r^2, \quad (19)$$

in the sense that the matrix element on the left replaces that on the right with the same correction factor associated with each. In the KU theory the $\int\beta\gamma_5 r^2$ term is supposed to be only a small correction to the $\int\beta\gamma_5$ contribution. It would there be called a third forbidden correction. However, there is *no* term corresponding to $\int\beta\gamma_5$, which is the matrix element appearing in the RaE analysis. Of course, we are using plane waves but the results shown below verify that this is no real restriction. The results obtained with this simplified model are fully substantiated by the application of the less restrictive FW transformation.

The question now arises as to whether the 0→0, *yes*, transition should be called third or first forbidden. We postpone the discussion of this until Sec. IV where the pseudoscalar correction factor is obtained. For leptons in a central field we shall show that the situation is very different and that for a Coulomb field, for example, one gets a correction factor whose largest contribution ($Z\neq 0$) indeed vanishes in the $Z=0$ limit and it has been verified that the results reduce (for $Z=0$) to the correction factor implied by the above. The matrix element for the zero-rank tensor for nonfree leptons is again $\int\boldsymbol{\sigma}\cdot\mathbf{r}$. We expect to find the correction factor for this term, which makes the sole contribution to 0→0, *yes*, in the pseudoscalar case, to be strongly Z- and energy-dependent.

III. THE BETA-DECAY OPERATORS IN NONRELATIVISTIC FORM

The recasting of the operators for forbidden transitions resulting from Eq. (12) may now be exhibited explicitly. The transformed (formerly odd) part of the interaction now consists of two types of terms: $\mathcal{E}$ operators in which there appears a $\mathbf{p}$ operator acting on the nuclear wave function and $\mathcal{E}'$ operators in which $\mathbf{p}$ acts only on the lepton covariant. That is, we write (12) in the form

$$H_\beta' = H_\beta(e)+\frac{1}{2M}\sum_X g_X(\mathcal{E}_X+\mathcal{E}_X')Q, \quad (20)$$

and

$$H_\beta(e)=[-g_S L(\beta)+g_V L(1)-g_T\boldsymbol{\sigma}\cdot L(\beta\boldsymbol{\sigma})+g_A\boldsymbol{\sigma}\cdot L(\boldsymbol{\sigma})]Q. \quad (20')$$

In Table I we list the odd part of $\Omega_X{}^\mu(N)\Omega_X{}^\mu(l)$ before and after the canonical transformation. Of course, we we may set $\beta=-1$ only for $\mathcal{E}$ and $\mathcal{E}'$.

TABLE I. Beta-interaction operators in odd and even form.

Interaction	$[\Omega_X{}^\mu(N)\Omega_X{}^\mu(l)]_{\text{odd}}$	$\mathcal{E}_X$	$\mathcal{E}_X'$
V	$-L(\boldsymbol{\alpha})\cdot\boldsymbol{\alpha}$	$2L(\boldsymbol{\alpha})\cdot\mathbf{p}$	$\mathbf{p}\cdot L(\boldsymbol{\alpha})$ $+i\boldsymbol{\sigma}\cdot\mathbf{p}\times L(\boldsymbol{\alpha})$
T	$L(\beta\boldsymbol{\alpha})\cdot\beta\boldsymbol{\alpha}$	$-2iL(\beta\boldsymbol{\alpha})\cdot(\boldsymbol{\sigma}\times\mathbf{p})$	$-\mathbf{p}\cdot L(\beta\boldsymbol{\alpha})$ $-i\boldsymbol{\sigma}\cdot\mathbf{p}\times L(\beta\boldsymbol{\alpha})$
A	$-L(\gamma_5)\gamma_5$	$-2L(\gamma_5)\boldsymbol{\sigma}\cdot\mathbf{p}$	$-\boldsymbol{\sigma}\cdot\mathbf{p}L(\gamma_5)$
P	$L(\beta\gamma_5)\beta\gamma_5$	0	$-\boldsymbol{\sigma}\cdot\mathbf{p}L(\gamma_5)$

[12] In order to avoid confusion with the $\mathbf{p}$ operator we attach a subscript to the electron momentum. Later, where no confusion will arise we drop this subscript.

The vanishing of $\mathcal{S}_P$ confirms the results of the elementary considerations given above. In a formal manner of expression this result arises whenever one deals with a nonvector operator of the form of a direct product of a Pauli operator and the Dirac operator ρ_2. The only operator of this form is $\beta\gamma_5$. It is also obvious that, if $L(\beta\gamma_5)$ were treated as a constant, the pseudoscalar contribution disappears. The fact that the only nonvanishing term contains $\boldsymbol{\sigma}\cdot\mathbf{p}L(\beta\gamma_5)$ and not $L(\beta\gamma_5)$ implies that the correction factors may very well be changed in a serious manner, as turns out to be the case.

We shall show in succeeding paragraphs that, except for the pseudoscalar interaction, only the (originally) even operators $H_\beta(e)$ and the $\mathcal{S}$ operators are important. Thus, leaving aside the $\mathcal{S}'$ operators for the moment, it is clear that for the S, V, T, A interactions the correction factors are identical with the well-known results.[1] The only change, as is evident from Table I, is a replacement of every odd operator by an even one. Thus, we make the replacements:[13]

$$\boldsymbol{\alpha}\rightarrow-(1/M)\mathbf{p},\quad i\beta\boldsymbol{\alpha}\rightarrow(1/M)\boldsymbol{\sigma}\times\mathbf{p},\qquad \gamma_5\rightarrow(1/M)\boldsymbol{\sigma}\cdot\mathbf{p}. \tag{21}$$

This correspondence between operators, and of course between matrix elements, extends to all higher rank tensors formed by adjoining the position vector $\mathbf{r}$. In so doing $\mathbf{p}$ must operate to the right of $\mathbf{r}$. Thus [see Eq. (26d) below],

$$A_{ij}\rightarrow-\frac{1}{M}\mathcal{T}_{ij}(\mathbf{r},\mathbf{p});\ A_{ij}{}^{\beta}\rightarrow\frac{i}{M}\mathcal{T}_{ij}(\mathbf{r},\boldsymbol{\sigma}\times\mathbf{p}), \tag{22}$$

et simile. Here $\mathcal{T}_{ij}(\mathbf{a},\mathbf{b})$ is the matrix element of the ij component of a symmetrical second rank tensor with vanishing trace.

$$\mathcal{T}_{ij}(\mathbf{a},\mathbf{b})=\int(a_ib_j+a_jb_i-\tfrac{2}{3}\mathbf{a}\cdot\mathbf{b}\delta_{ij}). \tag{23}$$

Particular attention must be given to the order of the operators because of the noncommutation of $\mathbf{r}$ and $\mathbf{p}$.

One may now raise the question as to whether the $\mathcal{S}_X'$ operators effect an appreciable change in the correction factors for interactions other than P. The first answer which one is tempted to give is that, since $\mathcal{S}'$ involves the lepton momenta while $\mathcal{S}$ involves the nucleon momentum, the former should make very small contributions in comparison with the latter. Actually, this reasoning is not entirely correct although, for all practical purposes, the conclusion is correct. In order to investigate this question it suffices to treat the leptons as free particles. Then a term-by-term comparison of the matrix elements, together with correction factors, for the conventional and transformed operators, may be made. For example, for the tensor interaction, the customary matrix element would be written, with $L(\beta\boldsymbol{\alpha})=\mathbf{L}_Te^{-i\mathbf{P}\cdot\mathbf{r}}$,

$$\begin{aligned}M_T(KU)&=\int\beta\boldsymbol{\alpha}\cdot\mathbf{L}_T(1-i\mathbf{P}\cdot\mathbf{r}\cdots)\\&=\mathbf{L}_T\cdot\int\beta\boldsymbol{\alpha}-\frac{i}{2}\sum_{ij}P_iL_{Tj}\\&\quad\times\left[A_{ij}{}^{\beta}+\int\beta(\boldsymbol{\alpha}\times\mathbf{r})_{ij}+\frac{2}{3}\int\beta(\boldsymbol{\alpha}\cdot\mathbf{r})\delta_{ij}\right]\\&=\mathbf{L}_T\cdot\int\beta\boldsymbol{\alpha}-\frac{i}{3}\mathbf{P}\cdot\mathbf{L}_T\int\beta\boldsymbol{\alpha}\cdot\mathbf{r}+\frac{i}{2}(\mathbf{P}\times\mathbf{L}_T)\\&\quad\cdot\int\beta\boldsymbol{\alpha}\times\mathbf{r}-\frac{i}{2}\sum_{ij}P_iL_{Tj}A_{ij}{}^{\beta}.\end{aligned} \tag{24}$$

For the matrix element of the transformed operators one finds

$$\begin{aligned}M_T&=\frac{1}{2M}\int(1-i\mathbf{P}\cdot\mathbf{r})[\mathbf{P}\cdot\mathbf{L}_T+i\boldsymbol{\sigma}\cdot\mathbf{P}\times\mathbf{L}_T-2i\mathbf{L}_T\cdot\boldsymbol{\sigma}\times\mathbf{p}]\\&=\frac{1}{2M}\Big\{\mathbf{P}\cdot\mathbf{L}_T\int1+i\mathbf{P}\times\mathbf{L}_T\cdot\int\boldsymbol{\sigma}-2i\mathbf{L}_T\cdot\int\boldsymbol{\sigma}\times\mathbf{p}\\&\quad+\sum_{ij}L_{Ti}P_i\mathcal{T}_{ij}(\mathbf{r},\boldsymbol{\sigma}\times\mathbf{p})+\mathbf{P}\times\mathbf{L}_T\\&\quad\cdot\int\mathbf{r}\times(\boldsymbol{\sigma}\times\mathbf{p})-\tfrac{2}{3}\mathbf{L}_T\cdot\mathbf{P}\int\boldsymbol{\sigma}\cdot\mathbf{r}\times\mathbf{p}\Big\}.\end{aligned} \tag{25}$$

The comparison shows that the correspondence between operators is

$$i\int\beta\boldsymbol{\alpha}\rightarrow\frac{1}{M}\int\boldsymbol{\sigma}\times\mathbf{p}, \tag{26a}$$

$$i\int\beta\boldsymbol{\alpha}\cdot\mathbf{r}\rightarrow-\frac{3}{2M}\int(1-\tfrac{2}{3}\boldsymbol{\sigma}\cdot\mathbf{r}\times\mathbf{p}), \tag{26b}$$

$$i\int\beta\boldsymbol{\alpha}\times\mathbf{r}\rightarrow\frac{1}{M}\int[i\boldsymbol{\sigma}+\mathbf{r}\times(\boldsymbol{\sigma}\times\mathbf{p})], \tag{26c}$$

$$-iA_{ij}{}^{\beta}\rightarrow\frac{1}{M}\mathcal{T}_{ij}(\mathbf{r},\boldsymbol{\sigma}\times\mathbf{p}). \tag{26d}$$

It is seen that in the second and third of these (26b and 26c) both $\mathcal{S}$ and $\mathcal{S}'$ operators contribute. The reason is almost trivial from a consideration of parity. The $\mathcal{S}$ operators involving $\mathbf{p}$ must combine with the $\mathbf{P}\cdot\mathbf{r}$ term of the retardation expansion while the $\mathcal{S}'$ operators combine with the first term. Note that both $\beta\boldsymbol{\alpha}\cdot\mathbf{r}$ and $\beta\boldsymbol{\alpha}\times\mathbf{r}$ correspond to second-order forbidden. For $\beta\boldsymbol{\alpha}$,

[13] Essentially the same results were given by T. Ahrens and E. Feenberg, Phys. Rev. **86**, 64 (1951). We do not check their sign in the case of γ_5 and, moreover, we feel that the present procedure places the operator correspondence on a firmer foundation where whatever approximation is involved may be explicitly brought to light

TABLE II. Transformation of $\mathcal{E}$ operators, see Eq. (29).

Interaction	n	χ	χ'
V	1	$\mathbf{p}$	$\mathbf{r}$
	2	$\mathcal{T}_{ij}(\mathbf{r},\mathbf{p})$	$\frac{1}{2}\mathcal{T}_{ij}(\mathbf{r},\mathbf{r})=R_{ij}$
T	1	$\boldsymbol{\sigma}\times\mathbf{p}$	$\boldsymbol{\sigma}\times\mathbf{r}$
A	1	$\boldsymbol{\sigma}\cdot\mathbf{p}$	$\boldsymbol{\sigma}\cdot\mathbf{r}$

which enters in first-order forbidden, the $\mathcal{E}$ operator can combine with the large leading term of the exponential and the $\mathcal{E}'$ operator makes an extremely trivial correction. For the case of the second rank tensor $\mathcal{T}_{ij}(\mathbf{r},\boldsymbol{\sigma}\times\mathbf{p})$ which is, of course, a second forbidden matrix element, the $\mathcal{E}'$ operator does not contribute a like term until one includes $(\mathbf{P}\cdot\mathbf{r})^2$ terms from the exponential which, again, would constitute a very small correction. We therefore conclude that for first forbidden transitions the $\mathcal{E}'$ operators are unimportant while for second forbidden transitions they are unimportant for $|\Delta J|=2$; but for tensors of zero and first rank (maximum $\Delta J=0, 1$) they must be considered and both $\mathcal{E}$ and $\mathcal{E}'$ enter. That they make contributions of comparable magnitude is obvious from the fact that for low-lying β-emitting states $p\rho\sim 1$, ρ being the nuclear radius. Also, both $\mathcal{E}$ and $\mathcal{E}'$ operators are necessary in order that the canonical transformation preserve the hermitian character of the operators.

The same conclusion follows with the vector and axial vector interactions. The $\mathcal{E}$ and $\mathcal{E}'$ operators are equally involved for second forbidden transitions with tensors of rank 0 or 1. Thus, for the V interaction,

$$\int \boldsymbol{\alpha}\cdot\mathbf{r}\rightarrow\frac{3i}{2M}\int(1+\tfrac{2}{3}i\mathbf{r}\cdot\mathbf{p}),\quad \int\boldsymbol{\alpha}\times\mathbf{r}\rightarrow\frac{1}{M}\int(\boldsymbol{\sigma}+\mathbf{r}\times\mathbf{p})$$

and for the A interaction

$$\int\gamma_5\mathbf{r}\rightarrow-\frac{i}{2M}\int[\boldsymbol{\sigma}+2i\mathbf{r}(\boldsymbol{\sigma}\cdot\mathbf{p})].$$

These conclusions are not changed when one removes the restriction of free leptons and considers the fact that the electron moves in some central field. Moreover, one can easily extend the rule to the effect that for all orders of forbiddenness n equal to or higher than second, the correction factors would be appreciably modified for $(\Delta J)_{\max}<n$. However, if one accepts the present experimental evidence that the beta interaction contains *both* Fermi and Gamow-Teller constitutents and that both types are present in appreciable amount, then all these types of transitions with a modified correction factor become academic. They represent small contributions to a lower order of forbiddenness where the $\mathcal{E}'$ operator makes a negligible contribution and the correction factor is, to a very high degree of accuracy, just that given in the usual theory.[1,14]

[14] See also E. Greuling, Phys. Rev. **61**, 568 (1942). Also D. L. Pursey, Phil. Mag. **42**, 1193 (1951); A. M. Smith, Phys. Rev. **82**, 955 (1951).

It will be recognized that the transformation of the operators carried out above does not depend on any detailed knowledge of the nuclear forces.[11] It is possible to simplify some of the $\mathcal{E}$ operators introduced above but this simplification does depend on more specific assumptions concerning these forces. Thus, for any operator χ' one may write

$$(W_f-W_i)\int\chi'=\int(H,\chi'),\tag{27}$$

where W_f and W_i are the final and initial eigenvalues of the nuclear Hamiltonian $H=H_N'$, see Eq. (11). One now attempts to find an operator χ' such that $(p^2,\chi')=-2i\chi$ for a given χ. The term $\frac{1}{2}\Delta\tau_z$ in (11) contributes to (H_N',χ') and now the charge transformation operator Q must be placed in evidence.

$$\tfrac{1}{2}\Delta(\tau_z,\chi'Q)=\tfrac{1}{2}\Delta\chi'(\tau_z,Q)=-\Delta\chi'Q,\tag{28}$$

since χ' is charge independent. Then, it follows that

$$\int\chi=iM\left\{(\Delta-W_0)\int\chi'-\int(V,\chi')\right\},\tag{29}$$

where $W_0=W_i-W_f$ is the β-energy release.

The χ operators ($\mathcal{E}$ type) to be considered are $\mathbf{p}$, $\mathcal{T}_{ij}(\mathbf{r},\mathbf{p})$ from the V interaction; $\boldsymbol{\sigma}\times\mathbf{p}$, $\mathcal{T}_{ij}(\mathbf{r},\boldsymbol{\sigma}\times\mathbf{p})$ from the T interaction and $\boldsymbol{\sigma}\cdot\mathbf{p}$ from the A interaction. We limit our consideration to first and second forbidden transitions. Then with the aid of

$$(\mathbf{p}^2,\mathbf{r})=-2i\mathbf{p},\quad (p^2,r_jr_k)=-2\delta_{jk}-2i(r_jp_k+r_kp_j),\tag{30}$$

one can find the appropriate χ' operator for all these tensors with the exception of $\mathcal{T}_{ij}(\mathbf{r},\boldsymbol{\sigma}\times\mathbf{p})$. The results are exhibited in Table II. For the tensor $\mathcal{T}_{ij}(\mathbf{r},\boldsymbol{\sigma}\times\mathbf{p})$ one would expect that the χ' operator is $\mathcal{T}_{ij}(\mathbf{r},\boldsymbol{\sigma}\times\mathbf{r})=T_{ij}$, in the usual notation.[1] Actually,

$$(p^2,\mathcal{T}_{ij}(\mathbf{r},\boldsymbol{\sigma}\times\mathbf{r}))=-4i\mathcal{T}_{ij}(\mathbf{r},\boldsymbol{\sigma}\times\mathbf{p})+2i\mathcal{T}_{ij}(\boldsymbol{\sigma},\mathbf{L}),$$

where $\mathbf{L}=\mathbf{r}\times\mathbf{p}$ is the orbital angular momentum operator.

If one assumes that the nuclear force operator is velocity-independent, which is plausible as a first approximation,[15] the $\boldsymbol{\alpha}\rightarrow-\mathbf{p}/M$ operator is replaced by $-i(\Delta-W_0)\mathbf{r}$. Thus, the Λ introduced by Feenberg[13] is given by[16]

$$\Lambda=\frac{-2i\rho}{\alpha Z}\frac{\int\boldsymbol{\alpha}}{\int\mathbf{r}}=\frac{2\rho}{\alpha Z}(W_0-\Delta)\approx\frac{A^{\frac{1}{3}}}{Z}(W_0-\Delta).\tag{31}$$

[15] Strictly speaking, the commutator $(V,\mathbf{r})$ does not vanish unless one can also neglect the nuclear Coulomb energy or the charge dependent interactions. Here we recall the suppressed Q operator, see Ahrens and Feenberg (reference 13). The comments based on the assumption that $(V,\mathbf{r})=0$ should therefore be applicable to light nuclei.

[16] See also D. L. Pursey, reference 14.

The same assumption of velocity independence of the forces permits the elimination of $\mathcal{T}_{ij}(\mathbf{r},\mathbf{p})$ which is replaced by iMR_{ij} which also appears from the even part $H_\beta(e)$ of the interaction. The number of operators involved in forbidden transitions is thus somewhat reduced and there is less arbitrariness in fitting β spectra than was hitherto supposed. If one considers a mixture of two interactions, the ratio of matrix elements multiplied with coupling constants is, in some cases, reduced to simply the ratio of coupling constants. In this way, one may obtain vital information concerning the composition of the β interaction from the shapes of some forbidden spectra.

It may be seen that for zero spin change, parity change yes, transitions, the only operator involved in both P and T interactions is $\boldsymbol{\sigma}\cdot\mathbf{r}$. This will appear explicitly in Sec. IV. Thus, the RaE spectrum provides the possibility of fixing g_P/g_T if the transition corresponds to $\Delta J=0$. Here *no* assumption about nuclear forces is involved. For the A interaction there are two zero rank, odd parity tensors: $\boldsymbol{\sigma}\cdot\mathbf{r}$ and $\boldsymbol{\sigma}\cdot\mathbf{p}$. Only if one assumes that $(V,\boldsymbol{\sigma}\cdot\mathbf{r})=0$ (spin-dependent nuclear forces are sufficient but may not be necessary) could one reduce these two operators to a single one.

IV. THE CORRECTION FACTORS

The calculation of the correction factors, which are presumably pertinent for RaE, is a fairly simple one. However, we do not wish to restrict our consideration to this case and prefer to consider a more general situation in which one need not specify the parity or spin change (tensor rank) at the start. Instead, the general correction factor for the P, or any other, interaction can be given with no more effort than is involved in calculating special cases. The formalism which is ideally suited for our purpose is that which is involved in a complete utilization of the angular momentum representation. We have found this procedure to be highly useful not only for the calculation of correction factors but also for the determination of nuclear matrix elements. The formalism is therefore presented in the following in some detail.

We designate the quantum numbers for the electron and neutrino by κ, μ, and κ_ν, μ_ν, respectively. Here κ, a nonzero integer, gives both the angular momentum j according to

$$j=|\kappa|-\tfrac{1}{2}, \tag{32}$$

and the parity $(-)^{l_\kappa+1}$ according to

$$l_\kappa=|\kappa|+\tfrac{1}{2}(S_\kappa-1), \tag{33}$$

where S_κ is the sign of κ. Thus, $j=l_\kappa-\frac{1}{2}S_\kappa$ and $|l_\kappa-l_{-\kappa}|=1$. The eigenvalue of j_z is μ, the magnetic quantum number.

In terms of this notation the differential energy spectrum is

$$N(W)=\frac{2}{\pi}\frac{W}{p}\sum_{\kappa\kappa_\nu}\sum_{\mu\mu_\nu}\left|\int H_\beta'\right|^2, \tag{34}$$

and the correction factor is

$$C_\beta=\frac{4\pi^2}{p^2q^2F_0}\sum_{\kappa\kappa_\nu}\sum_{\mu\mu_\nu}\left|\int H_\beta'\right|^2. \tag{35}$$

Here F_0 is the well-known Fermi function.[14]

In an arbitrary central field the electron wave functions are

$$\psi=\begin{pmatrix} -if_\kappa\chi_{-\kappa}^\mu \\ g_\kappa\chi_\kappa^\mu \end{pmatrix}, \tag{36}$$

and a similar representation of the neutrino wave function φ with radial wave functions F_{κ_ν} and G_{κ_ν} in place of f_κ, g_κ. With the usual sign convention $[H\psi=(-\boldsymbol{\alpha}\cdot\mathbf{p}-\beta+V_e)\psi]$, the radial wave equation, of which explicit use is made below, is

$$\frac{d}{dr}\begin{pmatrix} f \\ g \end{pmatrix}=\begin{pmatrix} (\kappa-1)/r & -(W-1-V_e) \\ W+1-V_e & -(\kappa+1)/r \end{pmatrix}\begin{pmatrix} f \\ g \end{pmatrix}, \tag{37}$$

and for the neutrino we set the central field $V_e=0$ and replace $W\pm1$ by q. The f_κ and g_κ are real and, for a Coulomb field are just $(\pi p/W)^{\frac{1}{2}}$ times those explicitly given elsewhere.[17] For the neutrino,

$$F_\kappa=S_\kappa qj_{l(-\kappa)}(qr), \quad G_\kappa=qj_{l(\kappa)}(qr), \tag{38}$$

where j_l is the spherical Bessel function. Throughout, the normalization corresponds to one particle in a sphere of unit radius.

In Eq. (36) the spin-angular functions are the usual Pauli spinors:

$$\chi_\kappa^\mu(\mathbf{r})=\textstyle\sum_\tau C(l_\kappa\tfrac{1}{2}j;\mu-\tau,\tau)\chi_{\frac{1}{2}}^\tau Y_{l_\kappa}^{\mu-\tau}(\mathbf{r}), \tag{39}$$

where the C coefficients are the usual vector addition coefficients

$$[C(j_1j_2j_3;m_1m_2)\equiv(j_1j_2j_3m_1+m_2|\,j_1j_2m_1m_2)].$$

Their properties as well as those of the χ_κ^μ spinors are summarized elsewhere.[18] In (39) $\mathbf{r}$ is the unit vector. Also $\chi_{\frac{1}{2}}^\tau$ is a spin eigenfunction ($\tau=\pm\frac{1}{2}$).

In forming the pseudoscalar lepton covariant we use

$$\beta\gamma_5C=i\sigma_2K_0=T, \tag{40}$$

where T is the time-reversal operator, and observe that

$$T\chi_\kappa^\mu=(-)^{l_\kappa-j+\mu+1}\chi_\kappa^{-\mu}. \tag{40'}$$

The procedure for evaluating matrix elements of any operator (such as those of Table I) is simplified enormously if one avoids a retardation expansion. This expansion, which is simply carried out at the end of

[17] M. E. Rose, Phys. Rev. **51**, 484 (1937). Our present notation differs only in the explicit use of κ as an index and also in that Y_l^m as here defined differs by a factor $(-)^m$ from the definition in Eq. (2) of this reference.

[18] G. Racah, Phys. Rev. **62**, 438 (1942); L. C. Biedenharn and M. E. Rose, Revs. Modern Phys. **25**, 729 (1953) and Rose, Biedenharn, and Arfken, Phys. Rev. **85**, 5 (1952).

the calculation, would, if performed at the beginning, necessitate a separate treatment of each term and the rather involved procedure whereby irreducible tensors are introduced. In our case these irreducible tensors appear automatically. For purposes of illustration the calculation of the pseudoscalar matrix element is displayed.

We use the notation

$$H_P=\frac{1}{2M}\boldsymbol{\sigma}\cdot\mathbf{p}L(\beta\gamma_5)$$

$$=\frac{1}{2M}\sum_\xi(-1)^\xi\sigma_{-\xi}p_\xi L(\beta\gamma_5), \tag{41}$$

where $\xi=\pm1$, 0 and for any operator

$$A_{\pm1}=\mp2^{-\frac{1}{2}}(A_x\pm iA_y), \quad A_0=A_z.$$

Then from (36), (40), and (40′),

$$L(\beta\gamma_5)=\exp[i\pi(l_{\kappa_\nu}-j_\nu-\mu_\nu)][g_\kappa G_{\kappa_\nu}(\chi_\kappa{}^\mu,\chi_{\kappa_\nu}{}^{-\mu_\nu})$$
$$-f_\kappa F_{\kappa_\nu}(\chi_{-\kappa}{}^\mu,\chi_{-\kappa_\nu}{}^{-\mu_\nu})]. \tag{42}$$

The inner product of the spinors is readily evaluated from (39) and the coupling relation

$$Y_l{}^m(\mathbf{r})Y_{l'}{}^{m'}(\mathbf{r})=\sum_\lambda\left[\frac{(2l+1)(2l'+1)}{4\pi(2\lambda+1)}\right]^{\frac{1}{2}}C(ll'\lambda,00)$$
$$\times C(ll'\lambda;mm')Y_\lambda{}^{m+m'}(\mathbf{r}). \tag{43}$$

The vector addition coefficients imply that l, l', and λ form a triangle. That is, $|l-l'|\leqslant\lambda\leqslant l+l'$, etc. In general, we refer to such a triangle relation by stating that $\Delta(ll'\lambda)$ exists. Also, $C(ll'\lambda;00)=0$ unless the parity rule ($l+l'+\lambda=$ even integer) is satisfied.

The spin projection quantum number sum is readily carried out by using the orthonormal properties of the unitary C coefficients after one performs a Racah[18] recoupling according to the prescription:

$$C(j_1j_2j;m_1m_2)C(jj_3j_4;m_1+m_2,m_3)$$
$$=\sum_s[(2s+1)(2j+1)]^{\frac{1}{2}}C(j_2j_3s;m_2m_3)$$
$$\times C(j_1sj_4;m_1,m_2+m_3)W(j_1j_2j_4j_3;js), \tag{44}$$

where $W(abcd;ef)$ is a Racah coefficient,[19] implying the existence of $\Delta(abe)$, $\Delta(cde)$, $\Delta(acf)$, $\Delta(bdf)$. The result to be used in (42) is

$$(\chi_\kappa{}^\mu,\chi_{\kappa'}{}^{\mu'})=(4\pi)^{-\frac{1}{2}}(-)^{l_{\kappa'}-j'+\mu+1}\sum_\lambda R_\lambda(\kappa\kappa')$$
$$\times C(jj'\lambda;-\mu,\mu')Y_\lambda{}^{\mu'-\mu}(\mathbf{r}), \tag{45}$$

where[19]

$$R_\lambda(\kappa\kappa')=(-)^{l_\kappa+j'-\lambda-\frac{1}{2}}$$
$$\times\left[\frac{(2j+1)(2j'+1)(2l_\kappa+1)(2l_{\kappa'}+1)}{2\lambda+1}\right]^{\frac{1}{2}}$$
$$\times C(l_\kappa l_{\kappa'}\lambda;00)W(jj'l_\kappa l_{\kappa'};\lambda\tfrac{1}{2}). \tag{46}$$

To apply the $\boldsymbol{\sigma}\cdot\mathbf{p}$ operator to $L(\beta\gamma_5)$, we use

$$\nabla_m Y_l{}^M(\mathbf{r})\Phi(r)$$
$$=\left(\frac{l+1}{2l+3}\right)^{\frac{1}{2}}C(l1l+1;Mm)Y_{l+1}{}^{M+m}D_-(l)\Phi$$
$$-\left(\frac{l}{2l-1}\right)^{\frac{1}{2}}C(l1l-1;Mm)Y_{l-1}{}^{M+m}D_+(l)\Phi, \tag{47}$$

where Φ is any radial function and

$$D_-(l)=\frac{d}{dr}-\frac{l}{r}, \quad D_+(l)=\frac{d}{dr}+\frac{l+1}{r}. \tag{47′}$$

We are now in a position to introduce the irreducible tensors $T_{Ll}{}^m(\mathbf{A},\mathbf{B})$ for any two vector operators $\mathbf{A}$, $\mathbf{B}$. These are defined by

$$T_{Ll}{}^m(\mathbf{A},\mathbf{B})=\sum_{m'}C(1lL;-m',m+m')$$
$$\times\mathcal{Y}_l{}^{m'+m}(\mathbf{A})\mathcal{Y}_1{}^{-m'}(\mathbf{B}), \tag{48}$$

and hence the inverse

$$\mathcal{Y}_l{}^m(\mathbf{A})\mathcal{Y}_1{}^{m'}(\mathbf{B})=\sum_L C(1lL;m'm)T_{Ll}{}^{m+m'}(\mathbf{A},\mathbf{B}). \tag{48′}$$

Here $\mathcal{Y}_l{}^m(\mathbf{A})$ is a solid harmonic of degree l. Where $\mathbf{A}=\mathbf{r}$, $\mathcal{Y}_l{}^m=Y_l{}^m$, of course. The rank of the tensor $T_{Ll}{}^m$ is L, corresponding to the fact that $T_{Ll}{}^m$ transforms under 3-space rotations according to the $2L+1$ dimensional representation of the rotation group.[20] The condition that $\Delta(Ll1)$ exists will be noted. The parity of $T_{Ll}{}^m(\mathbf{AB})$ is $\pi_A{}^l\pi_B$, so that if $\mathbf{A}=\mathbf{r}$, $\mathbf{B}=\boldsymbol{\sigma}$ the parity is $(-)^l$ while for $\mathbf{A}=\mathbf{r}$, $\mathbf{B}=\mathbf{p}$ or $\boldsymbol{\sigma}\times\mathbf{p}$ the parity is $(-)^{l+1}$.

Applying (48′) to (47), one obtains for any $\mathbf{B}$ but with $\mathbf{A}=\mathbf{r}$,

$$\mathbf{B}\cdot\mathbf{p}Y_l{}^M\Phi=i\left(\frac{4\pi}{3}\right)^{\frac{1}{2}}\left\{\left(\frac{l+1}{2l+1}\right)^{\frac{1}{2}}D_-(l)\Phi T_{l,\,l+1}{}^M(\mathbf{r},\mathbf{B})\right.$$
$$\left.-\left(\frac{l}{2l+1}\right)^{\frac{1}{2}}D_+(l)\Phi T_{l,\,l-1}{}^M(\mathbf{r},\mathbf{B})\right\}. \tag{49}$$

[19] The properties of these coefficients are discussed in Biedenharn, Blatt, and Rose, Revs. Modern Phys. **24**, 249 (1952). See also G. Racah, reference 18. Numerical values are given by L. C. Biedenharn, Oak Ridge National Laboratory Report ORNL-1098 (unpublished). These tables also give numerical values of $Z(abcd;ef)$ see J. M. Blatt and L. C. Biedenharn, Revs. Modern Phys. **24**, 258 (1952) which is related to our R coefficients, introduced in Eqs. (45) and (46), by

$$R_\lambda(\kappa\kappa')=(-)^{l_{\kappa'}+j'-\frac{1}{2}}2^{\lambda-l_\kappa-l_{\kappa'}}(2\lambda+1)^{-\frac{1}{2}}Z(l_\kappa jl_{\kappa'}j';\tfrac{1}{2}\lambda).$$

In all applications $\lambda-l-l_{\kappa'}$ is an even integer so that both R and Z coefficients are real.

[20] E. P. Wigner, *Gruppentheorie* (Friedrich Vieweg und Sohn, Braunschweig, 1931).

Then the operator H_P becomes

$$H_P=\frac{(-)^{m}3^{-\frac{1}{2}}i}{2M}\sum_{\lambda}C(jj_\nu\lambda;-\mu,-\mu_\nu)(2\lambda+1)^{-\frac{1}{2}}$$
$$\times[(\lambda+1)^{\frac{1}{2}}T_{\lambda\lambda+1}{}^{-m}(\mathbf{r},\boldsymbol{\sigma})D_-(\lambda)$$
$$-\lambda^{\frac{1}{2}}T_{\lambda\lambda-1}{}^{-m}(\mathbf{r},\boldsymbol{\sigma})D_+(\lambda)]$$
$$\times[R_\lambda(-\kappa,-\kappa_\nu)f_\kappa F_{\kappa_\nu}-R_\lambda(\kappa,\kappa_\nu)g_\kappa G_{\kappa_\nu}], \quad (50)$$

where $m=\mu+\mu_\nu$.

Each term in the λ summation corresponds to the angular momentum selection rule that $\Delta(jj_\nu\lambda)$ exists and the parity selection rule $\pi=(-)^{\lambda+1}$, that is, $\pi_i\pi_f=\pi$, where π_i and π_f are initial and final state parities. The order of forbiddenness is, in this case, $n=\lambda+1$. On forming the square of the matrix element and summing over μ and μ_ν, it is seen that tensors of different rank cannot interfere, as expected. In fact, if we use the notation

$$H_P=i\sum_\lambda(S_\lambda{}^+T_{\lambda\lambda+1}{}^{-m}+S_\lambda{}^-T_{\lambda\lambda-1}{}^{-m})$$

and

$$I_\lambda(a,b)=\sum_m\int T_{\lambda\lambda+a}{}^{-m}\left(\int T_{\lambda\lambda+b}{}^{-m}\right)^*,$$

which is the (real) invariant combination of matrix elements, one obtains

$$\sum_{\mu\mu_\nu}\left|\int H_P\right|^2=\sum_\lambda[(S_\lambda{}^+)^2I_\lambda(11)+2S_\lambda{}^+S_\lambda{}^-I_\lambda(1-1)$$
$$+(S_\lambda{}^-)^2I_\lambda(-1-1)]. \quad (51)$$

Designating the angular momenta and magnetic quantum numbers for the initial and final nuclear states by $J_i m_i$ and $J_f m_f$, respectively, one has, by the Wigner-Eckart theorem[20]

$$\int T_{\lambda,\lambda\pm1}{}^{-m}(\mathbf{A},\mathbf{B})=C(J_i\lambda J_f;$$
$$m_i-m)(J_f\|T_{\lambda,\lambda\pm1}\|J_i), \quad (52)$$

where the vector addition coefficient contains all the magnetic quantum number dependence and the remaining factor is a so-called reduced matrix element. The conditions that $\Delta(J_i\lambda J_f)$ and $\Delta(jj_\nu\lambda)$ exist express the over-all angular momentum conservation

$$\mathbf{J}_i+\mathbf{J}_f=\boldsymbol{\lambda}=\mathbf{j}+\mathbf{j}_\nu. \quad (53)$$

Also $m_i=m_f+m=m_f+\mu+\mu_\nu$. For the quantity which should actually appear in the β-transition probability, one sums (51) over m_f and averages over m_i. Thus, using (52), the pertinent quantity is

$$\frac{1}{2J_i+1}\sum_{m_im_f}I_\lambda(11)=\frac{2J_f+1}{2J_i+1}|(J_f\|T_{\lambda\lambda+1}\|J_i)|^2, \quad (54)$$

etc.

As an aid in transcription of notation we append the following useful relations:

$$T_{0l}(\mathbf{A},\mathbf{B})=-\frac{3^{\frac{1}{2}}}{4\pi}\mathbf{A}\cdot\mathbf{B}\delta_{l1},$$
$$T_{\lambda0}{}^m(\mathbf{A},\mathbf{B})=\frac{3^{\frac{1}{2}}}{4\pi}B_m\delta_{\lambda1}, \quad (55)$$
$$T_{11}{}^m(\mathbf{A},\mathbf{B})=-\frac{i}{\sqrt{2}}\left(\frac{3}{4\pi}\right)(\mathbf{A}\times\mathbf{B})_m.$$

For second rank tensors one needs

$$T_{21}{}^{\pm2}(\mathbf{AB})=\frac{3}{4\pi}A_{\pm1}B_{\pm1},$$
$$T_{21}{}^{\pm1}(\mathbf{AB})=\frac{1}{\sqrt{2}}\frac{3}{4\pi}(A_0B_{\pm1}+A_{\pm1}B_0), \quad (56)$$
$$T_{21}{}^0(\mathbf{AB})=\frac{3}{8\pi}\left(\frac{2}{3}\right)^{\frac{1}{2}}(3A_0B_0-\mathbf{A}\cdot\mathbf{B}).$$

Thus, for any two operators $\mathbf{A}$, $\mathbf{B}$ one has

$$I_0(11)=\frac{3}{16\pi^2}\left|\int\mathbf{A}\cdot\mathbf{B}\right|^2,$$
$$I_1(-1-1)=\frac{3}{16\pi^2}\left|\int\mathbf{B}\right|^2,$$
$$I_1(00)=\frac{9}{32\pi^2}\left|\int\mathbf{A}\times\mathbf{B}\right|^2, \quad (57)$$
$$I_2(-1-1)=\frac{9}{64\pi^2}\sum_{ij}|\mathcal{T}_{ij}(\mathbf{A},\mathbf{B})|^2.$$

We now turn our attention to the correction factors for zero rank tensors. For $\lambda=0$ we may write (35) in the simple form[21]

$$C_{1P}=\frac{\pi^2}{3p^2q^2F_0M^2}\left|\int T_{01}(\mathbf{r},\boldsymbol{\sigma})\right|^2\sum_\kappa(2j+1)$$
$$\times[(f_\kappa F_\kappa)'+(g_\kappa G_\kappa)']_{r=\rho}{}^2 \quad (58)$$

since $R_0(\kappa\kappa_\nu)=(-)^{l_\kappa}(2j+1)^{\frac{1}{2}}\delta_{\kappa\kappa_\nu}=-R_0(-\kappa,-\kappa_\nu)$. In (58) the prime denotes d/dr. The change in the correction factor, as previously noted, is directly traceable to the appearance of these derivatives.

The result (58) expresses the correction factor in the most compact form and the retardation expansion can

[21] Note that

$$W(abcd;Of)=(-)^{b+c-f}\delta_{ad}\delta_{cf}[(2b+1)(2c+1)]^{-\frac{1}{2}}.$$

be made by taking only the terms[22] $\kappa=\pm 1$. Consistently, one replaces $j_l(x)$ by the first term in its series expansion; $j_l(x)\to x^l[(2l+1)!!]^{-1}$. We carry out this operation and in addition we use (37) to replace f', g' in terms of f and g. In this way the correction factor is expressed in terms of well-tabulated quantities.[23] These are[14]

$$\begin{aligned}
L_{k-1}&=(2p^2F_0)^{-1}\rho^{2-2k}(g_{-k}^2+f_k^2),\\
M_{k-1}&=(2p^2F_0)^{-1}\rho^{-2k}(g_k^2+f_{-k}^2),\\
N_{k-1}&=(2p^2F_0)^{-1}\rho^{1-2k}(f_{-k}g_{-k}-f_kg_k),\\
P_{k-1}&=(2p^2F_0)^{-1}\rho^{2-2k}(g_{-k}^2-f_k^2),\\
Q_{k-1}&=(2p^2F_0)^{-1}\rho^{-2k}(g_k^2-f_{-k}^2),\\
R_{k-1}&=(2p^2F_0)^{-1}\rho^{1-2k}(f_{-k}g_{-k}+f_kg_k).
\end{aligned}\tag{59}$$

Thus, L_0, M_0, etc., are exactly the same quantities which these symbols have hitherto denoted. Using (55), the correction factor becomes

$$\begin{aligned}
C_{1P}=\frac{1}{4M^2}\Big\{&(U^2+1)M_0-2UQ_0\\
&+\tfrac{2}{3}q[(U^2-1)N_0+4(UM_0-Q_0)]\\
&+\frac{q^2}{9}[(U^2+1)L_0-2UP_0+16M_0\\
&\qquad+8(UN_0-R_0)]\Big\}\left|\int\boldsymbol{\sigma}\cdot\mathbf{r}\right|^2.
\end{aligned}\tag{60}$$

Here $U=W-V_c-q$ and for most cases $U\approx -V_c$. In (60) the term U^2M_0 is dominant while the terms UQ_0, UM_0, and U^2N_0 each make about a ten percent correction for $\alpha Z/\rho W_0\gg 1$. The remaining terms contribute one percent or less. This statement is borne out by a numerical calculation. This calculation also shows that the coefficient of $|\int\boldsymbol{\sigma}\cdot\mathbf{r}|^2$ in C_{1P} (K_{1P}, say) is a monotonically increasing function of energy and that for RaE it rises by 35 percent over the spectrum. This is in contrast to L_0, which represents the shape of the hitherto used correction factor. Over the range of energies corresponding to the RaE spectrum L_0 increases monotonically by 4 percent.

Proceeding in exactly the same manner as described above, we find the correction factors for P-X mixtures. For the T interaction the only zero rank tensor with parity change, yes, is clearly $T_{01}(\mathbf{r},\boldsymbol{\sigma})$ or $\boldsymbol{\sigma}\cdot\mathbf{r}$. From $T_{\lambda 1}(\mathbf{r},\boldsymbol{\sigma}\times\mathbf{p})$ the only zero rank tensor is $\mathbf{r}\cdot(\boldsymbol{\sigma}\times\mathbf{p})$ which has even parity. The interference term is now

$$\begin{aligned}
C_{1PT}=-\frac{1}{M}\Big\{&UM_0-Q_0+\frac{2q}{3}(2M_0+UN_0)\\
&+\frac{q^2}{9}(UL_0-P_0+4N_0)\Big\}\left|\int\boldsymbol{\sigma}\cdot\mathbf{r}\right|^2.
\end{aligned}\tag{61}$$

For the A interaction, which is given for the sake of completeness, both $\boldsymbol{\sigma}\cdot\mathbf{r}$ and $\boldsymbol{\sigma}\cdot\mathbf{p}$ are possible with the specified rank and parity, and the correction factor for the A-P mixture is

$$\begin{aligned}
C_{1PA}=\frac{1}{M}\Big\{&-UQ_0+M_0-\frac{2q}{3}(2Q_0+N_0)\\
&+\frac{q^2}{9}(L_0-UP_0-4R_0)\Big\}\left|\int\boldsymbol{\sigma}\cdot\mathbf{r}\right|^2\\
&+\frac{3^{\frac{1}{2}}}{M^2}\Big\{UR_0+N_0+\frac{q}{3}[UP_0-L_0+4R_0\\
&-\rho^2(UQ_0-M_0)]-\frac{q^2\rho^2}{9}(4Q_0-UR_0+N_0)\Big\}\\
&\times i\int\boldsymbol{\sigma}\cdot\mathbf{r}\left(\int\boldsymbol{\sigma}\cdot\mathbf{p}\right)^*.
\end{aligned}\tag{62}$$

From the discussion given in Sec. III, it follows that both matrix element products are of the same order of magnitude. However, for $\alpha Z/\rho\gg 1$ the part of the correction factor associated with the second matrix element product is relatively unimportant.

To these mixture terms one must add the pure T and A contributions[1]

$$C_{1T}=\left|\int\boldsymbol{\sigma}\cdot\mathbf{r}\right|^2(\tfrac{1}{9}q^2L_0+M_0+\tfrac{2}{3}qN_0),\tag{63}$$

and

$$\begin{aligned}
C_{1A}=\left|\int\boldsymbol{\sigma}\cdot\mathbf{r}\right|^2&(\tfrac{1}{9}q^2L_0+M_0-\tfrac{2}{3}qN_0)+\frac{1}{M^2}\left|\int\boldsymbol{\sigma}\cdot\mathbf{p}\right|^2L_0\\
&-\frac{2i}{M}\int\boldsymbol{\sigma}\cdot\mathbf{r}\left(\int\boldsymbol{\sigma}\cdot\mathbf{p}\right)^*(\tfrac{1}{3}qL_0-N_0).
\end{aligned}\tag{64}$$

In (62) and (64) we have used the fact that the cross product of matrix elements of $\boldsymbol{\sigma}\cdot\mathbf{r}$ and $\boldsymbol{\sigma}\cdot\mathbf{p}$, when multiplied with i, is real.[24]

[22] However, to check the $Z=0$ limit it is necessary to take $\kappa=\pm 2$ in those terms which vanish for $|\kappa|=1$. This peculiarity of the pseudoscalar factor is responsible for the appearance of a correction factor which has the energy dependence characteristic of third forbidden for $Z=0$.

[23] Rose, Perry, and Dismuke, Oak Ridge National Laboratory Report ORNL-1459 (unpublished). These tables are for Coulomb field wave functions. Corrections for finite nuclear size have been given by M. E. Rose and D. K. Holmes, Phys. Rev. 83, 190 (1951) and Oak Ridge National Laboratory Report ORNL-1022 (unpublished).

[24] By application of the time-reversal operator T, one can show that all the cross products of matrix elements (with the factors of i where they appear) are real; see C. L. Longmire and A. M. L. Messiah, Phys. Rev. 83, 464 (1951) for a special case. See also L. C. Biedenharn and M. E. Rose, reference 18.

V. APPLICATION TO THE RaE SPECTRUM

The correction factor for a T-P mixture is given by (60), (61), and (63) in the form

$$C=g_P^2C_{1P}+g_Pg_TC_{1PT}+g_T^2C_{1T}. \quad (65)$$

Using this correction factor we have attempted to fit the RaE spectrum, wherein comparison is made with the data of Langer and Price[25] and of Neary.[26] The observed spectrum $N(W)$ is compared with $\lambda N_0(W)C$ where N_0 is the allowed shape, λ is a scale factor and C is given by Eq. (65). In minimizing

$$\epsilon^2=\sum[N(W)-\lambda N_0(W)C]^2,$$

where the sum is over the experimental points ($1.20\leqslant W\leqslant 2.97$), the parameters λ and g_P/g_T are available as adjustable quantities. The best fit gives $\epsilon=0.14\times[\sum N^2(W)]^{\frac{1}{2}}$. A relative root-mean-square error of 14 percent implies that the spectrum cannot be fitted with a T-P mixture.

The conclusion to which this result leads is that the spin of RaE is not zero but *unity*. That this is not an isolated item of evidence leading to this conclusion can be seen from the following considerations.

(a) If the RaE spin is unity it should be possible to fit the spectrum with an S-T, or, less likely,[5] with a V-T mixture. Actually, Yamada[27] has obtained a fit of the spectrum with an S-T mixture.

(b) The existence of a group of highly favored first forbidden transitions ($\log ft=5$–6) between nuclei near the doubly magic 82–126 shell seems to point strongly to the rule that such transitions are characterized by $\Delta J=0$. On the other hand transitions in similar nuclei with $|\Delta J|=1$ show normal first forbidden ft values about 100 times larger. Examples of the first group together with $\log ft$ values and the most plausible assignment of orbitals are: $Tl^{207}\rightarrow Pb^{207}(5.16)s_{\frac{1}{2}}\rightarrow p_{\frac{1}{2}}$; $Pb^{209}\rightarrow Bi^{209}(5.59)g_{9/2}\rightarrow h_{9/2}$; $Tl^{206}\rightarrow Pb^{206}(5.18)s_{\frac{1}{2}}$ proton, $p_{\frac{1}{2}}$ neutron coupling to spin 0 in Tl^{206}; $Hg^{205}\rightarrow Tl^{205}(5.52)p_{\frac{1}{2}}\rightarrow s_{\frac{1}{2}}$. On the other hand for the second group one may cite $Pb^{205}\rightarrow Tl^{205}$ (large ft)[28] $p_{\frac{3}{2}}\rightarrow s_{\frac{1}{2}}$; and several other transitions between slightly lighter nuclei; e.g., $Au^{199}\rightarrow Hg^{199}(7.73)d_{\frac{5}{2}}\rightarrow p_{\frac{1}{2}}$; $Hf^{181}\rightarrow Ta^{181}(7.2)^{29}p_{\frac{7}{2}}\rightarrow d_{\frac{5}{2}}$. The decay scheme[30] of RaE shows that the spins of the 46.5-kev state and ground state of RaE should be different; i.e., either 0 and 1, respectively, or 1 and 0. The β transition from the 0^+ state of RaD with a $\log ft\sim 5$–6 and the 5-day transition from the ground state with $\log ft=8$ both fit into the above if and only if the RaE spin is unity. The transitions $Pb^{212}\rightarrow Bi^{212*}(5.17)0^+\rightarrow 0^-$ and $Bi^{212}\rightarrow Po^{212}(7.22)1^-\rightarrow 0^+$ also fit into the same scheme for similar reasons.

(c) The optical spectrum of RaE as investigated by Fred[31] shows that the $\lambda 3067$ line of Bi^{210} shows no hfs splitting. The conclusion from this, that the magnetic moment of the RaE ground state <0.18 nuclear magneton, is at least consistent with a spin 1 assignment ($h_{9/2}$ proton, $g_{9/2}$ neutron orbitals).

It is of interest to note that a natural explanation of the favored $\Delta J=0$ first forbidden transitions in heavy elements is afforded by the interaction as described above. From Eq. (60) the correction factor is fairly accurately represented by

$$g_P^2C_{1P}\approx(\alpha Z/2\rho)^4(g_P^2/M^2).$$

The strong Z dependence exhibited by the P interaction contribution which would enhance transitions of the aforementioned type, could be cited as evidence for the existence of the P interaction. However, in order that the P contribution be comparable with that arising from the T interaction, it is necessary that $g_P/g_T\sim 50$. It should be emphasized that this conclusion is not a necessary one and if $g_P/g_T\ll 50$, which would require an independent explanation of the favored first forbidden transitions, one would conclude that the P interaction plays no practical role in the β interaction.

VI. ACKNOWLEDGMENTS

It is a pleasure to record our thanks to Dr. Z. V. Chraplyvy, Dr. M. Fred, Dr. A. de-Shalit, Dr. M. Goldhaber, Dr. R. W. King, and Dr. M. Yamada for making the results of their research available to us before publication. We are indebted to Dr. O. Kofoed-Hansen and Dr. A. Winther for correspondence.

[25] L. M. Langer and H. C. Price, Jr., Phys. Rev. **76**, 461 (1949).
[26] G. J. Neary, Proc. Roy. Soc. (London) **A175**, 71 (1940).
[27] M. Yamada, Progr. Theoret. Phys. (Japan) **10**, 245 (1953).
[28] C. D. Coryell, quoted by A. de-Shalit and M. Goldhaber, Phys. Rev. **92**, 1211 (1953).
[29] This distinction between $\Delta J=0$ and $|\Delta J|=1$ transitions has already been noted by L. W. Nordheim (Indiana Conference on the Shell Model) and by R. W. King.
[30] Wu, Boehm, and Nagel, Phys. Rev. **91**, 319 (1953).
[31] Fred, Tomkins, and Barnes, Phys. Rev. **92**, 1324 (1953), and private communication from M. Fred.

Nuclear Matrix Elements in Beta Decay

M. E. Rose and R. K. Osborn
Oak Ridge National Laboratory, Oak Ridge, Tennessee
(Received October 13, 1953)

By using the j-j coupling model, all the β-decay nuclear matrix elements are calculated (in terms of radial integrals) for one- and two-nucleon configurations. The operators in terms of which one can describe the entire theory are of five types. Three of these, involving the nucleon momentum operator, replace the operators which, in the conventional representation of the theory, appeared as odd Dirac operators. The operators in the present representation, which is most naturally expressed in terms of spherical notation and angular momentum eigenfunctions are explicitly related to those which appeared in the older notation as cartesian tensor components. The results for both one- and two-nucleon configurations are expressed in terms of reduced matrix elements which, in turn, can be written in terms of Racah coefficients and other coefficients derived from them. All these coefficients, and thereby the reduced matrix elements, can be written in terms of comparatively simple algebraic formulas which cover all cases of interest. A brief discussion of the implications of these results for spectral shapes and comparative half-lives is given.

I. INTRODUCTION AND DEFINITION OF MATRIX ELEMENTS

IN the preceding paper[1] it has been shown that the entire theory of forbidden transitions can be formulated in terms of a representation in which only even Dirac operators occur in the nucleon space. This reformulation, which proceeds by means of a Foldy-Wouthuysen transformation,[2] implies that one needs only nonrelativistic nuclear wave functions for the description of all beta transitions. More specifically, if one adopts a particular coupling model, the opportunity for calculating nuclear matrix elements for forbidden as well as for allowed transitions is at hand. As has been emphasized by others, a particularly valuable application of the theory and experimental results of beta decay lies in the possibility of obtaining information of greater detail with regard to nuclear forces, by comparing ratios of matrix elements deduced from observed shapes of spectra with the results calculated on the basis of some model. The results presented below should facilitate such a comparison.

One should distinguish between a physical model in which an assertion is made concerning the coupling of the angular momentum vectors, and one in which additional assumptions concerning nuclear forces are made. We shall make a specific assumption concerning the vector coupling and shall consider the j-j coupling model in this paper. However, unless additional information descriptive of the nuclear force model is introduced, the matrix elements are reduced to radial integrals about which no very quantitative statements can be made. For specified angular momenta of the initial and final states, there are only a comparatively small number of such radial integrals (three for a given order of forbiddenness). In one well-known case the radial integral, in fact, reduces to the normalization integral.[3] Of greater interest is the fact that for a number of cases the radial integrals, associated with two interfering matrix elements, are identical, so that the shape of the spectrum can be specified with no arbitrariness. A comparison with experimental spectra in such cases provides a check on the validity of the coupling model. In all remaining cases the radial integrals play a nontrivial role and the shape of the beta spectrum is conditioned by the more detailed aspect of nuclear forces. The problem of evaluating the radial integrals by more detailed assumptions concerning nuclear forces is deferred for later consideration. In any case the results presented below exhibit explicitly the nuclear-force parameter (ratio of radial integrals) which may be ascertained from the analysis of observed shapes of beta spectra.

In Sec. II the nuclear matrix elements are expressed in terms of reduced matrix elements and the latter are evaluated for the single particle case (closed shells$\pm$one nucleon). In Sec. III it is shown that for even-mass nuclei, where two nucleons may participate in the beta transition, the nuclear matrix elements may be easily obtained from the single particle reduced matrix elements of Sec. II. In the remainder of this section we define the matrix elements, or combinations thereof, which are pertinent for our considerations. For this purpose we restrict our attention to forbiddenness order $n \leqslant 2$, although it is a trivial matter to extend the discussion to higher n.

It was shown in I, Eq. (21I), that in the new (even) formulation of the theory one makes the following replacements for the odd operators: $\boldsymbol{\alpha} \rightarrow -\mathbf{p}/M$, $i\beta\boldsymbol{\alpha} \rightarrow \boldsymbol{\sigma}\times\mathbf{p}/M$, $\gamma_5 \rightarrow \boldsymbol{\sigma}\cdot\mathbf{p}/M$, where M is the nucleon mass and $\mathbf{p}=-i\nabla$. Then, all higher-rank tensors are

[1] M. E. Rose and R. K. Osborn [Phys. Rev. **93**, 1315 (1953)]. References to this paper are denoted by I.
[2] L. L. Foldy and S. A. Wouthuysen, Phys. Rev. **78**, 29 (1950).
[3] Allowed transitions and light nuclei for which Coulomb effects are of minor importance and for which charge symmetry seems to be justified; see O. Kofoed-Hansen and A. Winther, Phys. Rev. **86**, 428 (1952). The allowed matrix elements, in the j-j coupling model, have also been thoroughly investigated by I. Talmi, Phys. Rev. **91**, 122 (1953).

formed exactly as usual.[4] Of course, some care must be exercised because of the noncommutability of $\mathbf{r}$ and the operators involving $\mathbf{p}$.

The exact correspondence between operators can easily be obtained. One may use the Cartesian notation [see (23I)]

$$\mathcal{T}_{ij}(\mathbf{a},\mathbf{b})=\int(a_ib_j+a_jb_i-\tfrac{2}{3}\mathbf{a}\cdot\mathbf{b}\delta_{ij}), \quad (1)$$

for second-rank tensors, for example. However, we find it far more convenient to represent the tensor in the spherical form:

$$T_{\lambda L}{}^{m}(\mathbf{r},\mathbf{B}) =\sum_{m'}C(1L\lambda;-m',m+m')\mathcal{Y}_L{}^{m'+m}(\mathbf{r})\mathcal{Y}_1{}^{-m'}(\mathbf{B}), \quad (2)$$

where $\mathcal{Y}_L$ is a solid spherical harmonic of degree L and the C coefficient is a vector addition (Wigner or Clebsch-Gordan) coefficient. All the tensors with which we have to deal can be represented in the form (2) or simply as a solid harmonic $\mathcal{Y}_\lambda(\mathbf{r})$, or finally as $\mathcal{Y}_\lambda(\mathbf{r})\boldsymbol{\sigma}\cdot\mathbf{p}$. Throughout the notation is such that λ is the tensor rank and L gives the parity π'. For $\mathbf{B}=\mathbf{p}$ and $\boldsymbol{\sigma}\times\mathbf{p}$, $\pi=(-)^{L+1}$ while for $\mathbf{B}=\boldsymbol{\sigma}$, $\pi=(-)^{L}$.

The matrix element combinations are then conveniently given in terms of the following notation:

$$\sum_m\int T_{\lambda L}{}^{m}(\mathbf{r},\mathbf{A})\left[\int T_{\lambda L'}{}^{m}(\mathbf{r},\mathbf{B})\right]^*\equiv I_\lambda(LL';\mathbf{AB}), \quad (3a)$$

where, to avoid redundancy, we write $I_\lambda(LL,\mathbf{AA})\equiv I_\lambda(L;\mathbf{A})$; and

$$\sum_m\int\mathcal{Y}_\lambda{}^{m}(\mathbf{r})\left[\int T_{\lambda L}{}^{m}(\mathbf{r},\mathbf{A})\right]^*\equiv J_\lambda(L;\mathbf{A}); \quad (3b)$$

$$\sum_m\left|\int\mathcal{Y}_\lambda{}^{m}(\mathbf{r})\right|^2\equiv K_\lambda; \quad (3c)$$

$$\sum_m\left|\int\mathcal{Y}_\lambda{}^{m}(\mathbf{r})\boldsymbol{\sigma}\cdot\mathbf{p}\right|^2\equiv\mathcal{K}_\lambda. \quad (3d)$$

Of course, the parity of the interfering operators must be the same. In all cases $-\lambda\leqslant m\leqslant\lambda$. The quantity $\mathcal{K}_\lambda$ enters in only the A interaction and with the restriction $n\leqslant 2$ only $\mathcal{K}_0$ is needed. We also write $\mathcal{K}_0{}^{\frac{1}{2}}\equiv\int\boldsymbol{\sigma}\cdot\mathbf{p}/(4\pi)^{\frac{1}{2}}$. In Tables I and II we give the relation between these quantities and the corresponding invariant matrix element combinations in the customary notation.[4,5] In each case we have given the normalization constant $\mathfrak{N}$ so defined that $\mathfrak{N}$ is the ratio of the entry in the first column to that in the second. Thus, as an example,

$$I_2(11;\boldsymbol{\sigma}\boldsymbol{\sigma})=I_2(1;\boldsymbol{\sigma})=\frac{9}{64\pi^2}\sum_{ij}|B_{ij}|^2.$$

The tables also indicate the order of forbiddenness and the interactions in which the particular combination occurs. For convenience, the tabulation is separated into two parts: Table I for the square terms, Table II for the interference terms. Throughout we omit consideration of tensors of rank 0 and 1 for second forbidden transitions. These should be small corrections to the

TABLE I. Square matrix element combinations for order of forbiddenness $n\leqslant 2$. The normalization constant $\mathfrak{N}$ in column 3 is the ratio of first to second column entries. Column 5 gives the pertinent interactions.

Spherical notation	Cartesian notation	$\mathfrak{N}$	n	Interactions
$I_1(0;\boldsymbol{\sigma})$	$\lvert\int\boldsymbol{\sigma}\rvert^2$	$3/16\pi^2$	0	T, A
K_1	$\lvert\int\mathbf{r}\rvert^2$	$3/4\pi$	1	S, V
$I_1(0,\mathbf{p})$	$\lvert\int\boldsymbol{\alpha}\rvert^2$	$3M^2/(4\pi)^2$	1	V
$I_1(0,\boldsymbol{\sigma}\times\mathbf{p})$	$\lvert\int\beta\boldsymbol{\alpha}\rvert^2$	$3M^2/(4\pi)^2$	1	T
$\mathcal{K}_0$	$\lvert\int\gamma_5\rvert^2$	$M^2/4\pi$	1	A
$I_0(1;\boldsymbol{\sigma})$	$\lvert\int\boldsymbol{\sigma}\cdot\mathbf{r}\rvert^2$	$3/16\pi^2$	1	T, A, P
$I_1(1;\boldsymbol{\sigma})$	$\lvert\int\boldsymbol{\sigma}\times\mathbf{r}\rvert^2$	$9/32\pi^2$	1	T, A
$I_2(1;\boldsymbol{\sigma})$	$\Sigma_{ij}\lvert B_{ij}\rvert^2$	$9/64\pi^2$	1	T, A
K_2	$\Sigma_{ij}\lvert R_{ij}\rvert^2$	$15/8\pi$	2	S, V
$I_2(1;\mathbf{p})$	$\Sigma_{ij}\lvert A_{ij}\rvert^2$	$9M^2/64\pi^2$	2	V
$I_2(1;\boldsymbol{\sigma}\times\mathbf{p})$	$\Sigma_{ij}\lvert A_{ij}{}^{\beta}\rvert^2$	$9M^2/64\pi^2$	2	T
$I_2(2;\boldsymbol{\sigma})$	$\Sigma_{ij}\lvert T_{ij}\rvert^2$	$15/64\pi^2$	2	T, A
$I_3(2;\boldsymbol{\sigma})$	$\Sigma_{ijk}\lvert S_{ijk}\rvert^2$	$15/96\pi^2$	2	T, A

TABLE II. Interfering matrix element combinations for order of forbiddenness $n\leqslant 2$. The normalization constant $\mathfrak{N}$ in column 3 is the ratio of first to second column entries. X-Y in column 5 indicates that the matrix element product in column 1 (or 2) occurs in the interference between X and Y interactions. X indicates the appearance of interference for the pure interaction.

Spherical notation	Cartesian notation	$\mathfrak{N}$	n	Interactions
$J_1(0;\mathbf{p})$	$i\int\mathbf{r}\cdot\int\boldsymbol{\alpha}^*$	$3iM/(4\pi)^{\frac{1}{2}}$	1	V, S-V
$J_1(0;\boldsymbol{\sigma}\times\mathbf{p})$	$i\int\mathbf{r}\cdot\int\beta\boldsymbol{\alpha}^*$	$-3M/(4\pi)^{\frac{1}{2}}$	1	S-T, V-T
$J_1(1;\boldsymbol{\sigma})$	$i\int\mathbf{r}\cdot\int\boldsymbol{\sigma}\times\mathbf{r}^*$	$-(27/2)^{\frac{1}{2}}/16\pi^2$	1	S-T, S-A V-T, V-A
$I_1(01;\mathbf{p},\boldsymbol{\sigma})$	$\int\boldsymbol{\alpha}\cdot\int\boldsymbol{\sigma}\times\mathbf{r}^*$	$iM(27/2)^{\frac{1}{2}}/16\pi^2$	1	V-T, V-A
$I_1(01;\boldsymbol{\sigma}\times\mathbf{p},\boldsymbol{\sigma})$	$\int\beta\boldsymbol{\alpha}\cdot\int\boldsymbol{\sigma}\times\mathbf{r}^*$	$M(27/2)^{\frac{1}{2}}/16\pi^2$	1	T, T-A
$\mathcal{K}_0{}^{\frac{1}{2}*}T_{01}{}^0(\mathbf{r},\boldsymbol{\sigma})$	$i\int\boldsymbol{\sigma}\cdot\mathbf{r}\int\gamma_5{}^*$	$iM3^{\frac{1}{2}}/(4\pi)^{\frac{1}{2}}$	1	A, T-A, P-A
$I_1(00;\mathbf{p},\boldsymbol{\sigma}\times\mathbf{p})$	$\int\boldsymbol{\alpha}\cdot\int\beta\boldsymbol{\alpha}^*$	$3iM^2/16\pi^2$	1	V-T
$J_2(2;\boldsymbol{\sigma})$	$i\Sigma_{ij}R_{ij}T_{ij}{}^*$	$15/(8\pi)^{\frac{1}{2}}$	2	S-T, S-A V-T, V-A
$J_2(1;\mathbf{p})$	$i\Sigma_{ij}R_{ij}A_{ij}{}^*$	$iM(135)^{\frac{1}{2}}/(8\pi)^{\frac{1}{2}}$	2	S-V, V
$J_2(1;\boldsymbol{\sigma}\times\mathbf{p})$	$i\Sigma_{ij}R_{ij}A_{ij}{}^{\beta*}$	$M(135)^{\frac{1}{2}}/(8\pi)^{\frac{1}{2}}$	2	S-T, V-T
$I_2(21;\boldsymbol{\sigma},\mathbf{p})$	$\Sigma_{ij}T_{ij}A_{ij}{}^*$	$-iM(135)^{\frac{1}{2}}/(8\pi)^2$	2	V-T, V-A
$I_2(21;\boldsymbol{\sigma},\boldsymbol{\sigma}\times\mathbf{p})$	$\Sigma_{ij}T_{ij}A_{ij}{}^{\beta*}$	$M(135)^{\frac{1}{2}}/(8\pi)^2$	2	T, T-A
$I_2(11;\boldsymbol{\sigma}\times\mathbf{p},\mathbf{p})$	$\Sigma_{ij}A_{ij}{}^{\beta}A_{ij}{}^*$	$-9iM^2/64\pi^2$	2	T-A

[4] E. J. Konopinski and G. E. Uhlenbeck, Phys. Rev. **60**, 308 (1941). For interaction mixtures, see D. L. Pursey, Phil. Mag. **42**, 1193 (1951), and A. M. Smith, Phys. Rev. **82**, 955 (1951). While one can set $\beta=-1$ in our representation, this is not permissible in the conventional formulation, and appropriate changes are necessary in the results of the first and third of these references.

[5] In the customary (or cartesian) notation we have used such symbols as $\boldsymbol{\alpha}$ and A_{ij} to make comparison easier. Of course, the representations for the nuclear wave functions involved in the matrix elements of columns 1 and 2 are not the same.

contribution to the allowed matrix elements if both Fermi and Gamow-Teller interactions are present in appreciable strength. Otherwise, if these terms are considered it must be remembered that the conventional theory does not represent them properly.[1]

As an aid in the construction of Tables I and II we note that (see Appendix A),

$$T_{\lambda\lambda-1}^{m}(\mathbf{r}, \mathbf{r}\times\mathbf{A}) = i[6(2\lambda-1)]^{\frac{1}{2}}C(1\lambda-1\lambda; 00) \times W(11\lambda\lambda-1; \lambda 1)T_{\lambda\lambda}^{m}(\mathbf{r}, \mathbf{A}) \quad (4)$$
$$= i[(\lambda+1)/(2\lambda+1)]^{\frac{1}{2}}T_{\lambda\lambda}^{m}(\mathbf{r}, \mathbf{A}).$$

Here W is a Racah coefficient,[6] and in this case a particularly simple one. We also observe that every entry in the second column in both Tables I and II is real and that therefore the corresponding statement applies to the first-column entry divided by $\mathfrak{R}$. In general, we recognize five different types of tensors:[7]

$$\begin{array}{ll} \mathcal{Y}_{\lambda}^{M}(\mathbf{r}) & \text{Type I,} \\ T_{\lambda L}^{m}(\mathbf{r}, \boldsymbol{\sigma}) & \text{Type II,} \\ T_{\lambda L}^{m}(\mathbf{r}, \mathbf{p}) & \text{Type III,} \\ \mathcal{Y}_{\lambda}^{m}(\mathbf{r})\boldsymbol{\sigma}\cdot\mathbf{p} & \text{Type IV,} \\ T_{\lambda L}^{m}(\mathbf{r}, \boldsymbol{\sigma}\times\mathbf{p}) & \text{Type V.} \end{array} \quad (A)$$

If these are respectively designated as τ_{I}, τ_{II}, $\cdots\tau_{\mathrm{V}}$, then one gets real matrix element products for interference between any one of $i\tau_{\mathrm{I}}$, $i\tau_{\mathrm{II}}$, τ_{III}, τ_{IV}, and $i\tau_{\mathrm{V}}$, and the complex conjugate of any other.[8] Our results confirm this statement.

The order of forbiddenness for the five types of operators is $n=\lambda$, L, $L+1$, $\lambda+1$, and $L+1$, respectively.

II. SINGLE-PARTICLE MATRIX ELEMENTS IN j-j COUPLING

We now consider any one of the five operator types listed in Part A at the end of the foregoing section. Then, for $T_{\lambda L}^{-m}(\mathbf{r}, \mathbf{B})$, say, the matrix element can always be expressed in the form

$$\int T_{\lambda L}^{-m}(\mathbf{r}, \mathbf{B}) \equiv (f|T_{\lambda L}^{-m}(\mathbf{r}, \mathbf{B})|i) = C(j'\lambda j; \mu', -m)(f\|T_{\lambda L}\|i), \quad (5)$$

which is the Wigner-Eckart theorem. In (5) the entire magnetic quantum number dependence is contained in the vector addition coefficient and the remaining factor is a reduced matrix element. Also, j and $\mu=\mu'-m$ are the final state (f) quantum numbers; j', μ' refer to the initial state (i). Thus, m is the total z component of the angular momentum carried off by the electron and neutrino.[1] The parity quantum number, for which we have no immediate need, will be expressed explicitly in subsequent developments. A relation exactly like (5) holds for each of the other four types of operators.

What is pertinent for the transition probablity is the absolute square or cross product of two matrix elements summed over final magnetic substates (μ) and averaged over initial substates (μ'). Therefore we define

$$\langle I_{\lambda}(LL'; \mathbf{AB})\rangle = \frac{1}{2j'+1}\sum_{m\mu\mu'}(j\mu|T_{\lambda L}^{-m}(\mathbf{r}, \mathbf{A})|j'\mu') \times (j\mu|T_{\lambda L'}^{-m}(\mathbf{r}, \mathbf{B})|j'\mu')^{*}. \quad (6)$$

Using (5), we can reduce Eq. (6) to

$$\langle I_{\lambda}(LL'; \mathbf{AB})\rangle = \frac{2j+1}{2j'+1}(j\|T_{\lambda L}(\mathbf{r}, \mathbf{A})\|j') \times (j\|T_{\lambda L}(\mathbf{r}, \mathbf{B})\|j')^{*}. \quad (7)$$

Similarly,

$$\langle J_{\lambda}(L; A)\rangle = \frac{2j+1}{2j'+1}(j\|\mathcal{Y}_{\lambda}\|j')(j\|T_{\lambda L}(\mathbf{r}, \mathbf{A})\|j')^{*} \quad (7a)$$

is the pertinent quantity for interference between type I and type II, III, or V operators. Note that type I and type IV operators cannot interfere. In the same way one finds

$$\langle K_{\lambda}\rangle = \frac{2j+1}{2j'+1}|(j\|\mathcal{Y}_{\lambda}\|j')|^{2}, \quad (7b)$$

etc. Thus, all that are required are the reduced matrix elements which we proceed to calculate by establishing the Wigner-Eckart theorem in each case. That is, we calculate $(f|T_{\lambda L}^{-m}|i)$ and compare the result with the right-hand side of Eq. (5). This is done in the following for each of the five types of operators.

For a single particle the final-state wave function may be written in the form [see (I39)],

$$\psi_f = \mathfrak{R}(r)\textstyle\sum_{\tau} C(l\tfrac{1}{2}j; \mu-\tau, \tau)\chi_{\frac{1}{2}}^{\tau}Y_{l}^{\mu-\tau}(\mathbf{r}). \quad (8)$$

Here $\mathfrak{R}$ is a real radial wave function, $\chi_{\frac{1}{2}}^{\tau}$ (with $\tau=\pm\frac{1}{2}$) a spin eigenfunction, and $\mathbf{r}$ is the unit vector. For the initial state we replace $\mathfrak{R}$, μ, l, j by $\mathfrak{R}'$, μ', l', j', respectively. Since these single-particle wave functions are eigenfunctions of j, l, μ (for ψ_f), we write the matrix elements in the form $(jl\mu|T_{\lambda L}^{-m}|j'l'\mu')$ and the reduced matrix elements as $(jl\|T_{\lambda L}\|j'l')$, and similarly for the other tensor operators.

It should be noted that the reduced matrix elements are not Hermitian.[9] In fact, if we consider Eq. (5)

[1] G. Racah, Phys. Rev. 62, 438 (1942); see also Biedenharn, Blatt, and Rose, Revs. Modern Phys. 24, 249 (1952) (referred to as BBR), and L. C. Biedenharn, Oak Ridge National Laboratory Report ORNL-1098 (unpublished). The properties of the C coefficients needed here are also given by Racah. See also Rose, Biedenharn, and Arfken, Phys. Rev. 85, 5 (1952).

[7] The tensors of types II and III are exactly those which occur in the emission of electromagnetic radiation by particles with spin.

[8] These results follow directly by using the properties of the time-reversal operator; see C. L. Longmire and A. M. L. Messiah, Phys. Rev. 83, 464 (1951).

[9] Compare G. Racah, reference 6, Eqs. (31) and (31'). Our normalization of the reduced matrix elements differs from that

together with

$$(i|T_{\lambda L}{}^{m}|f)^{*}=(f|T_{\lambda L}{}^{m\dagger}|i)=(-)^{j'-j+m}\left(\frac{2j'+1}{2j+1}\right)^{\frac{1}{2}}\times C(j'\lambda j;\mu'-m)(i\|T_{\lambda L}\|f)^{*}, \quad (9)$$

and similar relations for the other tensor operators, we find the relation between a reduced matrix element and its Hermitian conjugate by considering $T_{\lambda L}{}^{m\dagger}$. In general, if Ω^{m} denotes any one of the five types of operators, we find

$$\Omega^{m\dagger}=(-)^{m}\{(-)^{\eta}\Omega^{-m}+\Gamma\Omega'^{-m}\}, \quad (10)$$

where Γ is a constant (including zero) and Ω' is another tensor operator listed in A. Thus,

$$\left(\frac{2j'+1}{2j+1}\right)^{\frac{1}{2}}(-)^{j'-j}(i\|\Omega\|f)^{*}=(-)^{\eta}(f\|\Omega\|i)+\Gamma(f\|\Omega'\|i). \quad (11)$$

For each of the five operators we give the results for $(-)^{\eta}$, Γ and Ω' in Table III. Of course, the parity and rank of Ω' is exactly the same as in Ω. In connection with the type III operator we shall not be interested in $T_{\lambda\lambda+1}(\mathbf{r},\mathbf{p})$ since this occurs in terms which are small corrections to $T_{\lambda\lambda-1}(\mathbf{r},\mathbf{p})$. The orders of forbiddenness corresponding to these two operators are $\lambda+2$ and λ, respectively. Also, the type IV operator, occurring in the A interaction, is of interest for the case $\lambda=0$ only. Thus, $\Gamma=0$ effectively for all but type V operators.[10] The appearance or absence of factors i is just what is required for the reality theorem quoted at the end of Sec. I. A derivation of a typical one of the results is given in Appendix A.

The results of Table III are useful as a check and also provide relationships between reduced matrix elements which simplifies the calculations and presentation of results. We now consider the explicit calculations of the matrix elements of the five operator types. We do not restrict the order of forbiddenness wherever it is just as convenient to give general results.

A. Type I Operator

We consider the $\mathcal{Y}_{\lambda}(\mathbf{r})$ operator which occurs in the S and V interactions. Then

$$(f|\mathcal{Y}_{\lambda}{}^{-m}|i)=\int r^{\lambda+2}\mathfrak{R}\mathfrak{R}'dr\int d\omega(\chi_{\kappa'}{}^{\mu'}|V_{\lambda}{}^{-m}|\chi_{\kappa}{}^{\mu}),$$

where $\chi_{\kappa}{}^{\mu}$ is the 2-component spinor which represents the spin angular part of ψ_{f} [see Eqs. (2) and (39I)], κ represents both j and l, and $[j=|\kappa|-\frac{1}{2}=l-\frac{1}{2}\kappa/|\kappa|]$.

used by Racah; see his Eq. (29). Actually, all but one (type I) of the tensors listed above are more general than those discussed by Racah, and his rule for Hermitian conjugation does not apply in all cases. See Table III.

[10] Operators such as $\mathcal{Y}_{1}(\mathbf{r})\boldsymbol{\sigma}\cdot\mathbf{p}$ constitute second forbidden corrections to allowed transitions. However, such operators may play an important role in so-called l forbidden transitions.

TABLE III. Properties of the tensor operators under Hermitian conjugation; see Eq. (11).

Type	Ω^{m}	$(-)^{\eta}$	Γ	Ω'^{-m}
I	$\mathcal{Y}_{\lambda}{}^{m}$	1	0	
II	$T_{\lambda L}{}^{m}(\mathbf{r},\boldsymbol{\sigma})$	$(-)^{L+\lambda+1}$	0	
III	$T_{\lambda L}{}^{m}(\mathbf{r},\mathbf{p})$	$(-)^{L+\lambda+1}$	$i\left(\frac{3}{4\pi}\right)^{\frac{1}{2}}\left(\frac{L}{2L-1}\right)^{\frac{1}{2}}\times(2L+1)\delta_{\lambda L-1}$	$\mathcal{Y}_{\lambda}{}^{-m}$
IV	$\mathcal{Y}_{\lambda}{}^{m}\boldsymbol{\sigma}\cdot\mathbf{p}$	1	$-i\left[\frac{4\pi}{3}\lambda(2\lambda+1)\right]^{\frac{1}{2}}$	$T_{\lambda\lambda-1}{}^{-m}(\mathbf{r},\boldsymbol{\sigma})$
V	$T_{\lambda L}{}^{m}(\mathbf{r},\boldsymbol{\sigma}\times\mathbf{p})$	$(-)^{L+\lambda+1}$	$(6L)^{\frac{1}{2}}(2L+1)\times W(11L-1L;1\lambda)$	$T_{\lambda L-1}{}^{-m}(\mathbf{r},\boldsymbol{\sigma})$

Using Eq. (45I), we find immediately that

$$(jl\|\mathcal{Y}_{\lambda}\|j'l')=(4\pi)^{-\frac{1}{2}}(-)^{l'+j-\frac{1}{2}}[(2\lambda+1)(2l+1)(2j'+1)]^{\frac{1}{2}}\times C(l0\lambda';00)W(ljl'j';\tfrac{1}{2}\lambda)\mathfrak{F}_{\lambda}, \quad (12)$$

where (5) has been used and $\mathfrak{F}_{\lambda}$ is a radial integral:[11]

$$\mathfrak{F}_{\lambda}=\int r^{\lambda+2}\mathfrak{R}\mathfrak{R}'dr. \quad (12')$$

Using the well-known symmetry properties of the Racah coefficients, we check the Hermitian conjugation property of Table III at once.

The special values in which we are interested correspond to $\lambda=0$, 1, and 2. For $\lambda=0$ we get $(4\pi)^{-\frac{1}{2}}\int 1=(4\pi)^{-\frac{1}{2}}\mathfrak{F}_{0}$. For $\lambda=1$ one obtains $\int\mathbf{r}$ using Table I and the definitions given in Eq. (3); see also Eq. (7b). Similarly, for $\lambda=2$ one obtains R_{ij}. The specific results are easily obtained by using Table I of BBR[4] for the W coefficient with the following transcription of notation $(ljl'j'\lambda\leftrightarrow l_1J_1l_2J_2L)$ and

$$C(l1l';00)=\begin{cases}[(l+1)/(2l+1)]^{\frac{1}{2}}, & l'=l+1\\ -[l/(2l+1)]^{\frac{1}{2}}, & l'=l-1,\end{cases} \quad (13a)$$

$$C(l2l';00)=\begin{cases}\left[\frac{3}{2}\frac{(l+1)(l+2)}{(2l+1)(2l+3)}\right]^{\frac{1}{2}}, & l'=l+2\\ -\left[\frac{l(l+1)}{(2l-1)(2l+3)}\right]^{\frac{1}{2}}, & l'=l\\ \left[\frac{3}{2}\frac{l(l-1)}{(2l-1)(2l+1)}\right]^{\frac{1}{2}}, & l'=l-2.\end{cases} \quad (13b)$$

For higher than second forbidden transitions one needs the corresponding results for $L>2$. These can be easily obtained from BBR, Eq. (5). Of course, we have the

[11] These radial integrals have been evaluated by S. A. Moszkowski, Phys. Rev. 89, 474 (1952), using a number of rather simple models. See also H. Brysk, Phys. Rev. 86, 996 (1952). The use of relativistic nuclear wave functions as in this last reference is unnecessary here.

condition $\Delta(jj'\lambda)$ in all cases; i.e.,

$$|j-j'|\leqslant\lambda\leqslant j+j'. \tag{14}$$

As an example, we give $\langle|R_{ij}|^2\rangle$ (averaged and summed over initial and final states, respectively) for $l-\frac{1}{2}=j=j'+2=l'+\frac{3}{2}$. This is

$$\langle\sum_{ij}|R_{ij}|^2\rangle=\frac{l(l-1)}{(2l-1)(2l-3)}\mathfrak{F}_2^2. \tag{15}$$

As is to be expected, this vanishes for the specified quantum numbers unless $l\geqslant 2$.

B. Type II Operator

The operator $T_{\lambda L}^{m}(\mathbf{r},\boldsymbol{\sigma})$ occurs in T, A, and P interactions and, of course, in all interference terms of these among themselves and with S and V interactions. Here, and in the following, we give the results for the reduced matrix elements without exhibiting any of the details of the derivation. Such details for the type II operator matrix element are presented in Appendix B. The procedure for the remaining cases is very much the same.

As shown in Appendix B we have

$$(jl\|T_{\lambda L}(\mathbf{r}\boldsymbol{\sigma})\|j'l')=\frac{3\sqrt{2}}{4\pi}(-)^{l'-j}[(2L+1)(2\lambda+1)(2l+1)(2j'+1)]^{\frac{1}{2}}\times C(lLl';00)X(\tfrac{1}{2}1\tfrac{1}{2};j\lambda j';lLl')\mathfrak{F}_L. \tag{16}$$

In (16) the X coefficient is a combination of Racah coefficients originally defined by Fano.[12] The precise relation is exhibited in Appendix B. All the X coefficients which may ever arise in β transitions can be expressed in comparatively simple algebraic form as follows. We consider four cases:

$$\begin{aligned}&\text{Case 1.}\quad j=l+\tfrac{1}{2},\quad j'=l'+\tfrac{1}{2};\\&\text{Case 2.}\quad j=l+\tfrac{1}{2},\quad j'=l'-\tfrac{1}{2};\\&\text{Case 3.}\quad j=l-\tfrac{1}{2},\quad j'=l'+\tfrac{1}{2};\\&\text{Case 4.}\quad j=l-\tfrac{1}{2},\quad j'=l'-\tfrac{1}{2}.\end{aligned} \tag{17}$$

Since we are interested in T_{10}, T_{11}, T_{22}, T_{21}, T_{32} whose matrix elements are related to $\int\boldsymbol{\sigma}$, $\int\boldsymbol{\sigma}\times\mathbf{r}$, T_{ij}, B_{ij}, S_{ijk}, respectively, in the usual notation (see Tables I and II) we consider $\lambda=L$ and $\lambda=L+1$. There is one further case of interest which corresponds to $\lambda=L-1$; $T_{01}(\mathbf{r},\boldsymbol{\sigma})\sim\boldsymbol{\sigma}\cdot\mathbf{r}$. This case is quite trivial. In fact,

$$(jl\|T_{01}(\mathbf{r},\boldsymbol{\sigma})\|j'l')=\frac{\sqrt{3}}{4\pi}\delta_{\kappa,-\kappa'}\mathfrak{F}_1, \tag{18}$$

where $\delta_{\kappa,-\kappa'}$ is the same as $\delta_{jj'}\delta_{|l-l'|,\pm1}$. Thus, all remaining cases can be classified as above.

For the four cases listed in (17) and for $\lambda=L$, $L+1$ (with $\lambda\geqslant 1$ throughout), we have:

Case 1, $\lambda=L+1$,

$$X=-\frac{1}{4}\left[\frac{2}{3}\frac{(l+l'+\lambda+2)(l+l'+\lambda+1)(l-l'+\lambda)(l'-l+\lambda)}{(l+1)(l'+1)(2l+1)(2l'+1)\lambda(2\lambda-1)(2\lambda+1)}\right]^{\frac{1}{2}}; \tag{18a}$$

Case 1, $\lambda=L$,

$$X=-\frac{1}{4}\left[\frac{2}{3}\frac{(l+l'+\lambda+2)(l+l'-\lambda+1)}{(l+1)(l'+1)(2l+1)(2l'+1)\lambda(\lambda+1)(2\lambda+1)}\right]^{\frac{1}{2}}(l-l'); \tag{18b}$$

Case 2, $\lambda=L+1$,

$$X=-\frac{1}{4}\left[\frac{2}{3}\frac{(l+l'+\lambda+1)(l-l'+\lambda+1)(l-l'+\lambda)(l'+l-\lambda+1)}{l'(l+1)(2l+1)(2l'+1)\lambda(2\lambda-1)(2\lambda+1)}\right]^{\frac{1}{2}}; \tag{18c}$$

Case 2, $\lambda=L$,

$$X=-\frac{1}{4}\left[\frac{2}{3}\frac{(\lambda-l+l')(\lambda-l'+l+1)}{l'(l+1)(2l+1)(2l'+1)\lambda(\lambda+1)(2\lambda+1)}\right]^{\frac{1}{2}}(l+l'+1); \tag{18d}$$

Case 3, $\lambda=L+1$,

$$X=-\frac{1}{4}\left[\frac{2}{3}\frac{(l'+l-\lambda+1)(l'+l+\lambda+1)(l'-l+\lambda+1)(l'-l+\lambda)}{l(l'+1)(2l+1)(2l'+1)\lambda(2\lambda-1)(2\lambda+1)}\right]^{\frac{1}{2}}; \tag{18e}$$

Case 3, $\lambda=L$,

$$X=-\frac{1}{4}\left[\frac{2}{3}\frac{(l+\lambda-l')(l'+\lambda-l+1)}{l(l'+1)(2l+1)(2l'+1)\lambda(\lambda+1)(2\lambda+1)}\right]^{\frac{1}{2}}(l+l'+1); \tag{18f}$$

Case 4, $\lambda=L+1$,

$$X=-\frac{1}{4}\left[\frac{2}{3}\frac{(l'+l-\lambda+1)(l'+l-\lambda)(l'-l+\lambda)(l-l'+\lambda)}{ll'(2l+1)(2l'+1)\lambda(2\lambda-1)(2\lambda+1)}\right]^{\frac{1}{2}}; \tag{18g}$$

Case 4, $\lambda=L$,

$$X=-\frac{1}{4}\left[\frac{2}{3}\frac{(l'+l+\lambda+1)(l'+l-\lambda)}{ll'(2l+1)(2l'+1)\lambda(\lambda+1)(2\lambda+1)}\right]^{\frac{1}{2}}(l'-l). \tag{18h}$$

[12] U. Fano, National Bureau of Standards Report NBS-1214 (unpublished), p. 48; also A. Simon, Phys. Rev. **90**, 1036 (1953). The pertinent properties of this coefficient are as follows: Write the coefficient as $X(a_{11}a_{12}a_{13};\ a_{21}a_{22}a_{21};\ a_{31}a_{32}a_{33})$ and consider the

Returning to (16), one observes that again $\Delta(lLl')$ exists and that, moreover, $l+l'+L=$even integer. However, for even L one of the possibilities ($l=l'$) is ruled out for $\lambda=L$, cases 1 and 4. This implies the exclusion of $j=j'$ for T_{ij}. The other triangular rule expressing conservation of angular momentum $\Delta(jj'\lambda)$ is fulfilled automatically by virtue of the fact that the X coefficients either vanish or become imaginary when this conservation rule is violated. The X coefficients, like the Racah coefficients, are defined to vanish under such circumstances so that they are always real.

The results given in (18) and (13) define the type II reduced matrix element completely in terms of the radial integral $\mathfrak{F}_L$. The special case $\lambda=1$, $L=0$, giving the matrix element $\int\boldsymbol{\sigma}$, yields results which agree completely with those previously published,[3] except that we have not assumed complete overlap of the radial wave functions ($\mathfrak{F}_0\neq 1$ necessarily). To what extent the distinction between favored allowed and ordinary allowed transitions can be attributed to the radial matrix element is not yet clear.

C. Type III Operator

The operator $T_{\lambda L}{}^{m}(\mathbf{r},\mathbf{p})$, which occurs in the V interaction only, gives rise to the reduced matrix element

$$(jl\|T_{\lambda L}(\mathbf{r},\mathbf{p})\|j'l')$$
$$=\frac{\sqrt{3}i}{4\pi}(-)^{l'+j'-\frac{1}{2}}[(2L+1)(2\lambda+1)(2l+1)(2j'+1)]^{\frac{1}{2}}$$
$$\times W(ljl'j';\tfrac{1}{2}\lambda)\{(l'+1)^{\frac{1}{2}}C(lLl'+1;00)$$
$$\times W(L\lambda l'+1l';1l)\mathcal{G}_{Ll'}{}^{-}$$
$$-l'^{\frac{1}{2}}C(lLl'-1;00)W(L\lambda l'-1l';1l)\mathcal{G}_{Ll'}{}^{+}\},\quad(19)$$

where two new radial matrix elements have been introduced

$$\mathcal{G}_{Ll'}{}^{-}=\int r^{L+2}\mathfrak{R}\left(\frac{d}{dr}-\frac{l'}{r}\right)\mathfrak{R}'dr,\quad(20a)$$

$$\mathcal{G}_{Ll'}{}^{+}=\int r^{L+2}\mathfrak{R}\left(\frac{d}{dr}+\frac{l'+1}{r}\right)\mathfrak{R}'dr.\quad(20b)$$

Since these are real, interchange of initial and final states is equivalent to Hermitian conjugation and

$$(\mathcal{G}_{Ll'}{}^{-})^{\dagger}=-\mathcal{G}_{L,\,l'+L+1}{}^{+},\quad(20c)$$

$$(\mathcal{G}_{Ll'}{}^{+})^{\dagger}=-\mathcal{G}_{L,\,l'-L-1}{}^{-}.\quad(20d)$$

In (19) the C coefficients can be obtained from (13) (note the parity rule: $l+L+l'=$odd integer), while the Racah coefficients can be obtained from Tables I and II of BBR with the notation transcription $(L\lambda l'\pm 1l'l)$ $\leftrightarrow(l_1J_1l_2J_2L)$ for the second and third W's. We again note that $\Delta(\lambda L1)$ exists and that for our purposes ($n\leqslant 2$) only T_{10} and T_{21} (giving $-\int\mathbf{p}/M$, corresponding to $\boldsymbol{\alpha}$, and $\mathcal{T}_{ij}(\mathbf{r},\mathbf{p})$, corresponding to A_{ij}) are needed. For the first case ($L=0$) the results become much simpler:

$$(jl\|T_{10}(\mathbf{r},\mathbf{p})\|j'l')$$
$$=\frac{i(-)^{l+l'+j'-\frac{1}{2}}}{4\pi}[3(2j'+1)]^{\frac{1}{2}}W(ljl'j';\tfrac{1}{2}1)$$
$$\times\{l^{\frac{1}{2}}\mathcal{G}_{0l'}{}^{-}\delta_{l'+1,\,l}-l'^{\frac{1}{2}}\mathcal{G}_{0l'}{}^{+}\delta_{l'-1,\,l}\}.\quad(21)$$

The results of Table III are checked from (19) by using (20c) as well as Table II and Eq. (5) of BBR.

D. Type IV Operator

The operator $\mathcal{Y}_{\lambda}(\mathbf{r})\boldsymbol{\sigma}\cdot\mathbf{p}$ occurs in the A interaction only. The reduced matrix element is

$$(jl\|\mathcal{Y}_{\lambda}(\mathbf{r})\boldsymbol{\sigma}\cdot\mathbf{p}\|j'l')$$
$$=i(-)^{l-l'}\left[\frac{3}{2\pi}(2l+1)(2\lambda+1)(2j'+1)\right]^{\frac{1}{2}}$$
$$\times\{(l'+1)^{\frac{1}{2}}C(l\lambda l'+1;00)W(1\tfrac{1}{2}l'j';\tfrac{1}{2}l'+1)$$
$$\times W(l'+1\,j'lj;\tfrac{1}{2}\lambda)\mathcal{G}_{\lambda\,l'}{}^{-}-l'^{\frac{1}{2}}C(l\lambda l'-1;00)$$
$$\times W(1\tfrac{1}{2}l'j';\tfrac{1}{2}l'-1)W(l'-1\,j'lj;\tfrac{1}{2}\lambda)\mathcal{G}_{\lambda l'}{}^{+}\}.\quad(22)$$

Again the C coefficient may be obtained from (13) and the parity rule is $l+\lambda+l'=$odd integer, as expected. The Racah coefficients can be obtained directly from Table I of BBR.

For $\lambda=0$ the result (22) simplifies to

$$(jl\|\mathcal{Y}_{0}(\mathbf{r})\boldsymbol{\sigma}\cdot\mathbf{p}\|j'l')$$
$$=-i\left(\frac{3}{2\pi}\right)^{\frac{1}{2}}(-)^{l+l'-\frac{1}{2}}\delta_{jj'}W(1\tfrac{1}{2}l'j';\tfrac{1}{2}l)$$
$$\times[l^{\frac{1}{2}}\delta_{L\,l'+1}\mathcal{G}_{0l'}{}^{-}-l'^{\frac{1}{2}}\delta_{L\,l'-1}\mathcal{G}_{0l'}{}^{+}].\quad(22a)$$

E. Type V Operator

The operator $T_{\lambda L}{}^{m}(\mathbf{r},\boldsymbol{\sigma}\times\mathbf{p})$ occurs in only the T interaction. In the calculation of the reduced matrix element the operator $\mathcal{Y}_1(\boldsymbol{\sigma}\times\mathbf{p})$ is replaced by $T_{11}(\boldsymbol{\sigma},\mathbf{p})$ as in Appendix A, and finally by a product of two solid harmonics $\mathcal{Y}_1(\boldsymbol{\sigma})\mathcal{Y}_1(\mathbf{p})$. The essential complication introduced by the form of this operator is reflected in the fact that the magnetic quantum number sums involve seven C coefficients. [These may be indicated schematically by the couplings $\mathbf{l}+\frac{1}{2}\rightarrow\mathbf{j}$, $\mathbf{l}'+\frac{1}{2}\rightarrow\mathbf{j}'$, $\mathbf{l}+\mathbf{L}\rightarrow\boldsymbol{\lambda}$, $\mathbf{l}+\mathbf{1}\rightarrow\mathbf{1}$, $\mathbf{l}'+\mathbf{1}\rightarrow(\mathbf{l}'+\mathbf{b})$, $\mathbf{l}+(\mathbf{l}'+\mathbf{b})\rightarrow\mathbf{L}$, and $\frac{1}{2}+\frac{1}{2}\rightarrow\mathbf{1}$. All of these are intended as vector additions.

---

nine arguments arranged in a square array like the matrix a_{ij}. Then, the interchange of any two rows or columns multiplies X by $(-)^{E}$ where $E=\sum_{ij}a_{ij}$. Interchange of rows and columns ($a\rightarrow$transpose of a) leaves X unchanged. With the aid of this rule one verifies the result of Table III. A triangular condition exists between the elements of any row or any column of the matrix a. If one element of a is zero, one has

$$X=X(a_{11}a_{12}a_{13};\,a_{21}a_{22}a_{23};\,a_{31}a_{32}0)$$
$$=(-)^{a_{11}+a_{21}-a_{31}-a_{32}}[(2a_{31}+1)(2a_{32}+1)]^{-\frac{1}{2}}W(a_{11}a_{12}a_{21}a_{22};\,a_{13}a_{31}).$$

The coupling $l'+1\to(l'+b)$ with $b=\pm1$ is the result of the **p** operator acting on the orbital angular momentum of the initial state and $l+(l'+b)\to L$ implies that $Y_{l'+b}$ is coupled to Y_l of the final state to give a resultant Y_L, so that orbital angular momentum and parity are conserved. The coupling $\frac{1}{2}+\frac{1}{2}\to1$ represents the fact that the initial and final spin functions $\chi_{\frac{1}{2}}^{\nu}$ and $\chi_{\frac{1}{2}}^{\nu'}$ must couple together to make a resultant with intrinsic spin of 1.] As a consequence it is not surprising that the reduced matrix element in this case is somewhat more complex than any previously encountered. A new combination of Racah coefficients enters and this new coefficient (M coefficient) will be defined below.

The reduced matrix element is

$$(jl\|T_{\lambda L}(\mathbf{r},\boldsymbol{\sigma}\times\mathbf{p})\|j'l')=(-)^{l'+1+\lambda}(3/2\pi)\times[3(2\lambda+1)(2L+1)(2l+1)(2j'+1)]^{\frac{1}{2}}\{(l'+1)^{\frac{1}{2}}C(lL\lambda'+1;00)M(l\lambda l'+1,1L\tfrac{1}{2},j'jl')\mathcal{G}_{Ll'}^{-}-l'^{\frac{1}{2}}C(lL\lambda'-1;00)M(l\lambda l'-1,1L\tfrac{1}{2},j'jl')\mathcal{G}_{Ll'}^{+}. \quad (23)$$

Here the only new quantity is the M coefficient which is defined as[13]

$$M(l\lambda l'+b,1L\tfrac{1}{2},j'jl')=\sum_s(-)^s(2s+1)W(l\lambda l'+b1;sL)W(l\lambda\tfrac{1}{2}j';sj)\times W(1l'\tfrac{1}{2}j';s\tfrac{1}{2})W(1l'1l'+b;s1). \quad (24)$$

If we do not consider any transitions beyond second forbidden, we are interested in the reduced matrix elements for $\lambda=1$, $L=0$ (giving $\int\boldsymbol{\sigma}\times\mathbf{p}/M$ corresponding to $i\int\beta\boldsymbol{\alpha}$) and for $\lambda=2$, $L=1$ (corresponding to $A_{ij}^{(2)}$). For $L=0$, $\lambda=1$ one has

$$M(l1l'+b,10\tfrac{1}{2},j'jl')=(-)^{l'}\delta_{l,l'+b}[3(2l+1)]^{-\frac{1}{2}}X(\tfrac{1}{2}1\tfrac{1}{2};j1j';l1l'), \quad (25)$$

and numerical values can thus be obtained from (18b, d, f, h) with $\lambda=L=1$. For any other case it is possible to find a fairly simple algebraic form for the M coefficient. This is obtained by noting that in (24) one has $s=j'\pm\frac{1}{2}$. The two-term sum is then simplified by the use of Tables I and II of BBR. One finds, with the designations (17):

Case 1, $b=1$,

$$M=\frac{(-)^{l'}}{24}\frac{3l'-l+\lambda+1}{(l'+1)(2l'+1)}\left[\frac{(l+l'+\lambda+2)(l-l'+\lambda-1)(l+l'-\lambda+2)(l-l'+\lambda)}{\lambda(2\lambda-1)(2\lambda+1)(l+1)(2l+1)(2l'+3)}\right]^{\frac{1}{2}}; \quad (26a)$$

Case 1, $b=-1$,

$$M=\frac{(-)^{l'+1}}{24(2l'+1)}\left[\frac{(l+l'+\lambda+2)(l+l'+\lambda+1)(l+l'+\lambda)(l+l'-\lambda+1)(l'-l+\lambda)(l'-l+\lambda-1)}{\lambda(2\lambda-1)(2\lambda+1)l'(l'+1)(l+1)(2l'-1)(2l+1)}\right]^{\frac{1}{2}}; \quad (26b)$$

Case 2, $b=1$,

$$M=\frac{(-)^{l'+1}}{24(2l'+1)}\left[\frac{(l+l'-\lambda+2)(l+l'-\lambda+1)(l-l'+\lambda+1)(l-l'+\lambda)(l-l'+\lambda-1)(l'-l+\lambda)}{\lambda(2\lambda-1)(2\lambda+1)l'(l'+1)(l+1)(2l+1)(2l'+3)}\right]^{\frac{1}{2}}; \quad (26c)$$

Case 2, $b=-1$,

$$M=\frac{(-)^{l'}(3l'+l-\lambda+2)}{24l'(2l'+1)}\left[\frac{(l+l'+\lambda+1)(l+l'+\lambda)(l'-l+\lambda-1)(l-l'+\lambda+1)}{\lambda(2\lambda-1)(2\lambda+1)(l+1)(2l+1)(2l'-1)}\right]^{\frac{1}{2}}; \quad (26d)$$

Case 3, $b=1$,

$$M=\frac{(-)^{l'}(3l'+l+\lambda+2)}{24(l'+1)(2l'+1)}\left[\frac{(l'+l-\lambda+2)(l'-l+\lambda+1)(l-l'+\lambda-1)(l+l'-\lambda+1)}{\lambda(2\lambda-1)(2\lambda+1)l(2l+1)(2l'+3)}\right]^{\frac{1}{2}}; \quad (26e)$$

Case 3, $b=-1$,

$$M=\frac{(-)^{l'}}{24(2l'+1)}\left[\frac{(l+l'+\lambda+1)(l+l'+\lambda)(l'-l+\lambda)(l'-l+\lambda-1)(l'-l+\lambda+1)(l-l'+\lambda)}{\lambda(2\lambda-1)(2\lambda+1)ll'(l'+1)(2l+1)(2l'-1)}\right]^{\frac{1}{2}}; \quad (26f)$$

Case 4, $b=1$,

$$M=\frac{(-)^{l'-1}}{24(2l'+1)}\left[\frac{(l+l'-\lambda+2)(l+l'-\lambda+1)(l-l'+\lambda)(l-l'+\lambda-1)(l+l'+\lambda+1)(l+l'-\lambda)}{\lambda(2\lambda-1)(2\lambda+1)ll'(l'+1)(2l+1)(2l'+3)}\right]^{\frac{1}{2}}; \quad (26g)$$

Case 4, $b=-1$,

$$M=\frac{(-)^{l'}}{24l'(2l'+1)}(3l'-l-\lambda+1)\left[\frac{(l'+l+\lambda)(l'-l+\lambda)(l'-l+\lambda-1)(l'+l-\lambda)}{\lambda(2\lambda-1)(2\lambda+1)l(2l+1)(2l'-1)}\right]^{\frac{1}{2}}. \quad (26h)$$

[13] There is no special significance about the ordering of the nine arguments on the left-hand side of Eq. (24) nor is there any reason, other than convenience of reading, for separating the arguments into triads by commas. The M coefficient is a special

Here we have used the parity rule: $l+l'+\lambda=$even integer. These results, which apply for $\lambda=L+1$, together with Eq. (5) of BBR, are all that is needed to obtain the reduced matrix elements in terms of the radial integrals for any order of forbiddenness.

It is of interest to note that on the basis of the present model we can confirm certain results which have been quoted in the literature. We designate the terms in the β interaction which were originally even by e and those which were originally odd by o. Then the contributions of e terms to the transition probability will be denoted by ee, those of the o terms alone by oo, and the cross terms by eo. For first-forbidden transitions with $|\Delta j|=0$ or 1, it is well known that the correction factors are of order $(\alpha Z/\rho)^2$, where ρ is the nuclear radius. For most spectra of interest $\alpha Z/\rho W_0\gg 1$, and this is of decisive importance for explaining the allowed shape of first forbidden spectra[14] (except RaE[1]). For eo terms and oo terms the correction factors are of order $\alpha Z/\rho$ and 1, respectively. This is valid for pure as well as mixed interactions. Nevertheless, all three types of terms are of the same order and, leaving aside the P interaction, are essentially energy independent. This comes about because the o-matrix elements are larger than the e matrix elements by a factor of order $\alpha Z/\rho$. This has already been pointed out in the literature.[15] In the present model this result may be seen as follows. The e and o matrix elements involve $\mathfrak{F}_1$ and $\mathfrak{G}_{0l'}{}^{\pm}$, respectively. A relation between these is derived by forming the radial wave equations from Eq. (11 I). With

$$U_f=(\chi_{\kappa}{}^{\mu},\ V_f\chi_{\kappa}{}^{\mu}),\qquad U_i=(\chi_{\kappa'}{}^{\mu'},\ V_i\chi_{\kappa'}{}^{\mu'}),\tag{27}$$

where angular integration is included in the scalar product, one finds

$$\frac{d^2\mathfrak{R}}{dr^2}+\frac{2}{r}\frac{d\mathfrak{R}}{dr}+\left[2M(W_f+\Delta-U_f)-\frac{l(l+1)}{r^2}\right]\mathfrak{R}=0,\tag{28a}$$

and

$$\frac{d^2\mathfrak{R}'}{dr^2}+\frac{2}{r}\frac{d\mathfrak{R}'}{dr}+\left[2M(W_i-U_i)-\frac{l'(l'+1)}{r^2}\right]\mathfrak{R}=0,\tag{28b}$$

with $\Delta=M_n-M_p$, the neutron-proton mass difference. Using the fact that U_i and U_f are Hermitian radial operators, elementary operations yield

$$\begin{aligned}(L+1)\mathfrak{G}_{Ll'}{}^{-}&=\tfrac{1}{2}(l-l'-L-1)(l+l'+L+2)\mathfrak{F}_{L-1}\\&\quad+M(W_i-W_f-\Delta)\mathfrak{F}_{L+1}-M\mathfrak{D}_L,\\(L+1)\mathfrak{G}_{Ll'}{}^{+}&=\tfrac{1}{2}(l-l'+L+1)(l+l'-L)\mathfrak{F}_{L-1}\\&\quad+M(W_i-W_f-\Delta)\mathfrak{F}_{L+1}-M\mathfrak{D}_L,\end{aligned}\tag{29}$$

where

$$\mathfrak{D}_L=\int\mathfrak{R}(r^{L+1}U_i-U_fr^{L+1})\mathfrak{R}'dr.\tag{29a}$$

If one defines[15]

$$\frac{1}{2}\Lambda\frac{\alpha Z}{\rho}=\frac{-i\int\alpha}{\int\mathbf{r}}=\frac{-i\int\gamma_5}{\int\boldsymbol{\sigma}\cdot\mathbf{r}}=\frac{-\int\beta\alpha}{\int\boldsymbol{\sigma}\times\mathbf{r}},\tag{30}$$

then from the results of this section one has for these first forbidden matrix elements, $l=l'\mp 1$,

$$\Lambda=\frac{2\rho}{\alpha ZM}\frac{\mathfrak{G}_{0l'}{}^{\pm}}{\mathfrak{F}_1}.\tag{31}$$

In this model one can envisage three possible contributions to $\mathfrak{D}_0$. The first is the Coulomb interaction between odd nucleon and core which contributes zero to V_i and $\alpha Z/r$ to V_f. The second is the spin-orbit coupling which we write as $V_0\boldsymbol{\sigma}\cdot\mathbf{r}\times\mathbf{p}$. The third, which is rather unlikely and will be ignored, is the possible appearance of the radial component of the momentum operator in V. From the first, one obtains a contribution $-\alpha Z\mathfrak{F}_0$ to $\mathfrak{D}_0$ and from the second $-(\kappa-\kappa')\Delta E/(2l+1)$, where $\Delta E=E_{j=l-\frac{1}{2}}-E_{j=l+\frac{1}{2}}$ is the spin-orbit splitting. Consequently, from (29) and (31) one finds in all cases:

$$\Lambda=2\left\{\rho\frac{\mathfrak{F}_0}{\mathfrak{F}_1}+\frac{\rho}{\alpha Z}\left[\frac{\kappa-\kappa'}{2l+1}\Delta E+W_i-W_f-\Delta\right]\right\}.\tag{32}$$

Roughly $\rho\mathfrak{F}_0/\mathfrak{F}_1\approx 1$ and $\Delta E\approx 2$ Mev (i.e., ≈ 4 in our units); the second and third terms are negligible and $\Lambda\sim 1$ to 3. Since $\mathfrak{F}_1$ is the average value of r (with $\mathfrak{R}\mathfrak{R}'$ as a weight function), one would expect $\rho\mathfrak{F}_0/\mathfrak{F}_1>1$, if anything ($\rho\mathfrak{F}_0/\mathfrak{F}_1=4/3$ for $\mathfrak{R}\mathfrak{R}'=$const), and the upper value appears somewhat more plausible. This slightly weakens the argument against rejection of the V-T mixture in the β interaction.[14]

A similar situation holds for second forbidden transitions so far as the relative order of magnitude of the ee, eo, and oo contributions is concerned. Thus, for S-T interference, which is the interesting case, we can obtain the ratio of squares of o-matrix elements to e-matrix elements. These are matrix elements of $T_{21}(\mathbf{r},\boldsymbol{\sigma}\times\mathbf{p})$ and $\mathcal{Y}_2$, respectively. For simplicity, we consider the two cases $l-\frac{1}{2}=j=l'+\frac{3}{2}=j'+2$ and $l-\frac{1}{2}=j=l'-5/2=j'-2$, in which cases only one term of (29) enters. The terms in $\mathfrak{F}_{L-1}$ in (29) also vanish. Then, for both

case of a more general coefficient of the form given by the right-hand side of Eq. (24) but with fewer relations between the arguments. For instance, in the coupling of particles with intrinsic spin other than $\frac{1}{2}$ (arbitrary channel spin, say) a more general coefficient would appear. Note that the application of the results shown in Table III would provide a relation between M coefficients and the X coefficient.

[14] H. M. Mahmoud and E. J. Konopinski, Phys. Rev. **88**, 1266 (1952).

[15] D. L. Pursey, Phil. Mag. **42**, 1193 (1951); T. Ahrens and E. Feenberg, Phys. Rev. **86**, 64 (1952).

cases, we obtain

$$\sum_{ij}|A_{ij}^{\rho}|^2/\sum_{ij}|R_{ij}|^2\cong\left(\frac{\alpha Z}{\rho}\right)^2\left(\frac{\rho\mathfrak{F}_1}{\mathfrak{F}_2}\right)^2, \quad (33)$$

where only the dominant Coulomb contribution has been considered in $\mathfrak{D}_1$, and the relatively small contribution of $\mathfrak{F}_2$ has also been neglected. The ratio $\rho\mathfrak{F}_1/\mathfrak{F}_2$ should be about unity or somewhat larger. The correction factors contain $\alpha Z/\rho$ in such a way as to cancel the dominance of the *o-o* matrix element over the *e-e* matrix element. Similar results apply to the cross term and to the comparison of other pairs of second-rank tensors. For example, for the cases cited above,[16]

$$k^2\equiv\sum_{ij}|A_{ij}^{\rho}|^2/\sum_{ij}|T_{ij}|^2=\left(\frac{\alpha Z}{2\rho}\right)^2\left(\frac{\rho\mathfrak{F}_1}{\mathfrak{F}_2}\right)^2. \quad (33a)$$

If one considers different orbitals, the first term of (29) need not vanish and an extra term $\mathfrak{F}_{L-1}/M\mathfrak{F}_{L+1}$ is added to the Coulomb contribution. This added term is of order $1/M\rho^2$ (i.e., essentially the kinetic energy of a nucleon at the nuclear surface), which is $\sim 40/A^{\frac{1}{3}}$, and this is almost always small compared to $\alpha Z/\rho \sim 2Z/A^{\frac{1}{3}}$ for all but the very light nuclei.

For the ratio of two *e*-matrix elements one notes that the radial integrals cancel out for the following cases: (a) the ratio of $(f\|\mathbf{r}\|i)$ to $(f\|\boldsymbol{\sigma}\times\mathbf{r}\|i)$ in first forbidden, and (b) the ratio of $(f\|\mathcal{Y}_2\|i)$ to $(f\|T_{22}(\mathbf{r},\boldsymbol{\sigma})\|i)$ in second forbidden. The ratio (*a*) is obtained from Eq. (12) for $\lambda=1$, and Eq. (16) for $\lambda=L=1$ [see Eq. (55 I)], and results for special cases previously given are confirmed.[15] The ratio (*b*), which is obtained from Eq. (12) with $\lambda=2$ and Eq. (16) with $\lambda=L=2$, gives $\sum_{ij}R_{ij}T^{*}_{ij}/\sum_{ij}|T_{ij}|^2$ or $\sum_{ij}|R_{ij}|^2/\sum_{ij}|T_{ij}|^2$, which is involved in *S* and/or *V* interactions mixed with *T* and/or *A*.

A second question is the matter of fluctuation of *ft* values for a given order of forbiddenness. One may ask whether this fluctuation is or is not almost entirely due to the radial integrals. To take a simple case, it is clear that for unique spectra (G-T transitions with $|\Delta j|=n+1$), one obtains a measure of the radial integrals by comparison of the foregoing results with measured values of $\log_{10}ft$ or, somewhat better, $\log_{10}[(W_0^2-1)ft]$. Thus, if the transition probability is represented in terms of

$$\frac{2j+1}{2j'+1}(jl\|T_{\lambda L}(\mathbf{r},\boldsymbol{\sigma})\|j'l')^2=A(jl,j'l')\mathfrak{F}_L^2,$$

one could compute the values of $\log_{10}[(W_0^2-1)ftA]$. As is to be expected, the scatter is not much improved as compared to the values with $A=1$.[17] For example, with $\lambda=2$, $L=1$, $A=15/22\pi^2$ for a $g_{7/2}\rightarrow h_{11/2}$ transition, and $A=9/10\pi^2$ for a $p_{\frac{1}{2}}\rightarrow d_{3/2}$ transition. Thus, on the basis of the *j-j* coupling model, and for the cases wherein a one- or two-particle configuration (see Sec. III) is applicable, one can obtain, from a comparison of $\log[(W_0^2-1)ft]$ values, an indication of differences in nuclear structure as reflected in the radial integrals.

III. MATRIX ELEMENTS FOR TWO-NUCLEON CONFIGURATIONS

We employ the isotopic spin notation and designate the charge wave function for a single nucleon by φ_i^{ν} with $i=\frac{1}{2}$. The values $\nu=\frac{1}{2}$, $-\frac{1}{2}$ correspond to neutron, proton, respectively. For the two-nucleon configuration the isotopic spin wave function is Φ_I^N, with $I=0$ or 1 and $N=\frac{1}{2}(N_n-N_p)$, where N_n and N_p are, respectively, the number of neutrons and protons in the configuration. As before, primes are used for the initial state. Then, for the final state,

$$\Phi_I^N=\sum_{\nu}C(\tfrac{1}{2}\tfrac{1}{2}I;\nu N-\nu)\varphi_i^{\nu}(1)\varphi_i^{N-\nu}(2). \quad (34)$$

On interchange of the arguments 1 and 2, which designate the two particles, Φ_{ν}^N goes to $(-)^{I+1}\Phi_I^N$ as expected.

The total wave function for the final state with total angular momentum J and projection quantum number M is now

$$\Psi_f=\Phi_I^N\Psi_J^M=\frac{1}{\sqrt{2}}\Phi_I^N\sum_m C(j_1j_2J;mM-m)$$
$$\times[\psi_{\kappa_1}^m(1)\psi_{\kappa_2}^{M-m}(2)+(-)^I\psi_{\kappa_1}^{M-m}(2)\psi_{\kappa_2}^m(1)], \quad (35)$$

which is antisymmetric with respect to interchange of all coordinates. In Eq. (35) κ_i stands for j_i, l_i. The wave function Ψ_f is normalized to unity if $\kappa_1\neq\kappa_2$ (i.e., $j_1\neq j_2$ and/or $l_1\neq l_2$). If $\kappa_1=\kappa_2$, one has $(\Psi_f,\Psi_f)=2$ and the normalization factor is to be changed, see Eq. (36) below.

If, in the initial state, $\kappa_1'\neq\kappa_2'$, the wave function Ψ_i is obtained from (35) by priming all the quantum numbers. On the other hand, let us assume that $\kappa_1'=\kappa_2'$; that is, the two nucleons in the initial state are in the same orbital. Then,

$$\Psi_i=\Phi_{I'}^{N'}\Psi_{J'}^{M'}=\Phi_{I'}^{N'}\sum_{m'}C(j'j'J';m'M'-m')$$
$$\times\psi_{\kappa'}^{m'}(1)\psi_{\kappa'}^{M'-m'}(2), \quad (36)$$

and over all antisymmetry is assured if

$$(-)^{J'+I'}=-1.$$

We consider three cases: (a) In the initial state the two orbitals are identical and in the final state they are different. (b) The orbitals are the same for the final state and different in the initial state. (c) Both initial and final states are characterized by different orbitals but at least one orbital in initial and final states must

[16] While we recognize that the single-particle model cannot be directly applied to Cl^{36} or Tc^{99}, it is interesting to note that (33a) gives $k^2\cong 30$ and $k^2\cong 90$ ($\rho\mathfrak{F}_1/\mathfrak{F}_2=1$), respectively, while the empirical values are $k^2=18$ and 45, respectively; see L. Feldman and C. S. Wu, Phys. Rev. **87**, 1091 (1952). One does not expect the order of magnitude to change radically when more complicated configurations are considered. In fact, it is fairly easy to see that the results given above [Eq. (31)–(33a)] also hold for two-nucleon configurations; see Sec. III.

[17] See, e.g., Mayer, Moszkowski, and Nordheim, Revs. Modern Phys. **23**, 315 (1951).

be the same. Where $\kappa_1=\kappa_2$ and $\kappa_1'=\kappa_2'$, the matrix elements are easily obtained as special cases of the result of (a) or (b).

Considering any operator of the five types listed in A and designating the operator by $\Omega_\lambda^{-M''}$, one has

$$(f|\sum_k \Omega_\lambda^{-M''}(k)Q_k|i) = C(J'\lambda J; M', -M'')\delta_{M'-M'',M}(J\|\Omega_\lambda\|J'), \quad (37)$$

where the sum over k is over particles 1 and 2. For the transition probability, one needs

$$\langle|(f|\sum\Omega_\lambda^{-M''}(k)Q_k|i)|^2\rangle=\frac{2J+1}{2J'+1}|(J\|\Omega_\lambda\|J')|^2. \quad (38)$$

This is what one designates by $|f\Omega_\lambda|^2$ in the usual notation. For interference terms between operators Ω and Ω' the absolute square of the reduced matrix element is replaced by $(J\|\Omega_\lambda\|J')(J\|\Omega_\lambda'\|J')^*$.

Considering case (a) first, the wave functions (35) and (36) are substituted in (37) and the result is reduced to the form of the right-hand side, whereby identification of the reduced matrix element is made. Using

$$Q_k\varphi_\frac{1}{2}^\nu(k)=(\nu+\tfrac{1}{2})\varphi_\frac{1}{2}^{-\nu}(k), \quad (39)$$

and with the notation

$$\Theta=\frac{1}{\sqrt{2}}[(\Phi_I{}^N, Q_1\Phi_{I'}{}^{N'})+(-)^{I+I'}(\Phi_I{}^N, Q_2\Phi_{I'}{}^{N'})],$$

one finds that $\Theta=1$ for the transitions $I'=1$, $N'=1\to I=1$, $N=0$; $(I'N')=(10)\to(IN)=(1-1)$; $(I'N')=(00)\to(IN)=(1-1)$. For the only other transition possible, $(I'N')=(11)\to(IN)=(00)$, one has $\Theta=-1$. It can be seen that Θ occurs as a factor of the reduced matrix element in every case, and we can take $\Theta=1$ since a phase which is the same for all interfering matrix elements is irrelevant.

Using Eq. (5), together with the orthonormality of the single nucleon $\psi_\kappa{}^m$, a simple Racah recoupling gives

$$\begin{aligned}(f\|\Omega_\lambda\|i)=(-)^{\lambda-J}(2J'+1)^\frac{1}{2}\{&(2j_1+1)^\frac{1}{2}\delta_{\kappa_2\kappa'}\\ &\times W(j'j_1J'J;\lambda j')(\kappa_1\|\Omega_\lambda\|\kappa')\\ &+(2j_2+1)\delta_{\kappa_1\kappa'}(-)^{j_2+j'+J+I}\\ &\times W(j'j_2J'J;\lambda j')(\kappa_2\|\Omega_\lambda\|\kappa')\}. \quad (40)\end{aligned}$$

In (40) the single-particle reduced matrix elements are $(\kappa_1\|\Omega_\lambda\|\kappa')\equiv(j_1l_1\|\Omega_\lambda\|j'l')$ and similarly for $(\kappa_2\|\Omega_\lambda\|\kappa')$. These are given in Sec. II. Under the assumption that $\kappa_1\neq\kappa_2$, only one term of (40) will be nonvanishing in any particular case. If, however, $\kappa_1=\kappa_2=\kappa$ (i.e., $j_1=j_2=j$, $l_1=l_2=l$), one obtains

$$\begin{aligned}(f\|\Omega_\lambda\|i)=(-)^{\lambda-J}&[(2J'+1)(2j+1)]^\frac{1}{2}\\ &\times W(j'jJ'J;\lambda j')(\kappa\|\Omega_\lambda\|\kappa'). \quad (40a)\end{aligned}$$

For tensors of rank $\lambda\leq 2$ the Racah coefficient can be obtained from BBR, Tables II and IV. For higher-rank tensors the numerical tables may be used.[6] If one or more of j_1, j_2, $j'=\frac{3}{2}$, Table III of BBR may be used.

For case (b), where the orbitals are identical in the final state, one finds

$$\begin{aligned}(f\|\Omega_\lambda\|i)=(-)^\lambda&[(2J'+1)(2j+1)]^\frac{1}{2}\\ &\times\{(-)^{j-j_1'-J}\delta_{\kappa\kappa_2'}W(j_1'jJ'J;\lambda j)(\kappa\|\Omega_\lambda\|\kappa_1')\\ &+(-)^{J'+I'+I}\delta_{\kappa\kappa_1'}W(j_2'jJ'J;\lambda j)(\kappa\|\Omega_\lambda\|\kappa_2')\}. \quad (41)\end{aligned}$$

Here $\kappa_i'=j_i'$, l_i' which designate the orbital of particle i in the initial state. Again, with $\kappa_1'\neq\kappa_2'$ only one term enters and the Racah coefficients can be obtained as described above. For $\kappa_1'=\kappa_2'$, the result (41) reduces to (40a) when proper account is taken of the necessary renormalization of Ψ_i.

Finally, the case (c) we use a wave function like (35) for both initial and final states. The reduced matrix element is

$$\begin{aligned}(f\|\Omega_\lambda\|i)=(-)^{\lambda+1}(2J'+1)^\frac{1}{2}\{&(-)^{J+j_2'+j_1'}(2j_1+1)^\frac{1}{2}\\ &\times\delta_{\kappa_2\kappa_2'}W(j_1j_1'JJ';\lambda j_2)(\kappa_1\|\Omega_\lambda\|\kappa_1')\\ &+(-)^{I+I'+j_1+j_2+J'}(2j_2+1)^\frac{1}{2}\delta_{\kappa_1\kappa_1'}\\ &\times W(j_2j_2'JJ';\lambda j_1)(\kappa_2\|\Omega_\lambda\|\kappa_2')\\ &+(-)^{I'+J+J'}(2j_1+1)^\frac{1}{2}\delta_{\kappa_2\kappa_1'}\\ &\times W(j_1j_2'JJ';\lambda j_2)(\kappa_1\|\Omega_\lambda\|\kappa_2')\\ &+(-)^{I-j_2+j_1'}(2j_2+1)^\frac{1}{2}\delta_{\kappa_1\kappa_2'}\\ &\times W(j_2j_1'JJ';\lambda j_1)(\kappa_2\|\Omega_\lambda\|\kappa_1')\}. \quad (42)\end{aligned}$$

The reduced matrix element (42) vanishes if all four κ's are different, as is obvious from the fact that the beta interaction is a sum of single-particle operators. A nonvanishing result with $\kappa_1\neq\kappa_2$ and $\kappa_1'\neq\kappa_2'$ is obtained if: $\kappa_1=\kappa_1'$ and $\kappa_2=\kappa_2'$ in which the first two terms coexist, $\kappa_1'=\kappa_2$, $\kappa_2'=\kappa_1$, for which case the last two terms contribute; or only one pair of κ's can be equal, in which case any one of the four terms may contribute. Thus, at most, two terms contribute.

For configurations of more than two nucleons the procedure is somewhat more complicated but the reduced matrix elements can still be expressed as linear combinations of single-nucleon reduced matrix elements. For this purpose one may use the coefficients of fractional parentage[18] as explained by Talmi.[3] Further applications to experimental results must await a continuation of the calculations along these lines.

APPENDIX A. HERMITIAN CONJUGATION PROPERTY OF THE TENSOR OPERATORS

As an illustration of the derivation of the results given in Table III, we consider the case of the type V operator: $T_{\lambda L}{}^m(\mathbf{r}, \boldsymbol{\sigma}\times\mathbf{p})$. From Eq. (2),

$$\begin{aligned}T_{\lambda L}{}^{m\dagger}(\mathbf{r}, \boldsymbol{\sigma}\times\mathbf{p})=(-)^m&\textstyle\sum_{m'}C(1L\lambda;-m', m+m')\\ &\times\mathcal{Y}_1{}^{m'}(\boldsymbol{\sigma}\times\mathbf{p})\mathcal{Y}_L{}^{-m'-m}(\mathbf{r}). \quad (A.1)\end{aligned}$$

[18] See, for example, A. R. Edmonds and B. H. Flowers, Proc. Roy. Soc. (London) 214, 515 (1952).

From Eq. (I 55), we obtain

$$\mathcal{Y}_1{}^{m'}(\sigma\times\mathbf{p})=(3/4\pi)^{\frac{1}{2}}(\sigma\times\mathbf{p})_{m'}$$
$$=\sqrt{2}i(4\pi/3)^{\frac{1}{2}}T_{11}{}^{m'}(\sigma,\mathbf{p}), \quad \text{(A.2)}$$

and if Eq. (2) is used to express $T_{11}(\sigma,\mathbf{p})$ in terms of $\mathcal{Y}_1(\sigma)$, $\mathcal{Y}_1(\mathbf{p})$, we find

$$T_{\lambda L}{}^{m\dagger}(\mathbf{r},\sigma\times\mathbf{p})=\sqrt{2}i(4\pi/3)^{\frac{1}{2}}(-)^m$$
$$\times\textstyle\sum_{m'M} C(1L\lambda,-m',m+m')C(111;-m,m'+M)$$
$$\times\mathcal{Y}_1{}^{m'+M}(\sigma)\mathcal{Y}_1{}^{-M}(\mathbf{p})\mathcal{Y}_L{}^{-m'-m}(\mathbf{r}). \quad \text{(A.3)}$$

We note that $\mathcal{Y}_1(\sigma)$ commutes with the other operators in (A.3) and from Eq. (I 47) we have

$$(\mathcal{Y}_1{}^{\mu}(\mathbf{p}),\mathcal{Y}_L{}^{\mu'}(\mathbf{r}))=i\left(\frac{3}{4\pi}\right)^{\frac{1}{2}}(2L+1)\left(\frac{L}{2L-1}\right)^{\frac{1}{2}}$$
$$\times C(1LL-1;\mu\mu')\mathcal{Y}_{L-1}{}^{\mu+\mu'}(\mathbf{r}), \quad \text{(A.4)}$$

where (A,B) is the commutator of A and B. Using (A.4) in (A.3) and the symmetry relations of the C coefficients,[6] one finds that

$$T_{\lambda L}{}^{m\dagger}(\mathbf{r},\sigma\times\mathbf{p})=(-)^{m+L+\lambda+1}T_{\lambda L}{}^{-m}(\mathbf{r},\sigma\times\mathbf{p})$$
$$+(-)^m\Gamma\Omega'^{-m}, \quad \text{(A.5)}$$

where, with $M+m'=M'$,

$$\Gamma\Omega'^{-m}=-\left(\frac{2L}{2L-1}\right)^{\frac{1}{2}}(2L+1)$$
$$\times\sum_{m'M'} C(1L\lambda;-m',m+m')C(111;-M'+m',M')$$
$$\times C(1LL-1;-M'+m',-m'-m)$$
$$\times\mathcal{Y}_{L-1}{}^{-m-M'}(\mathbf{r})\mathcal{Y}_1{}^{M'}(\sigma). \quad \text{(A.6)}$$

We now use Eq. (I 44) applied to the second and third C coefficients so as to produce one C coefficient free of m'. The sum over m' is then easily carried out by the orthogonality property of the unitary C coefficients, and the sum over M' is used with Eq. (2) to introduce the tensor operator $\Omega'=T_{\lambda L-1}(\mathbf{r},\sigma)$. One then finds

$$\Gamma=(6L)^{\frac{1}{2}}(2L+1)W(11L-11;1\lambda). \quad \text{(A.7)}$$

Thus, $\Gamma\neq 0$ only if $\lambda=L$ or $L-1$, $(L>0)$. For type V operators the practical case is $\lambda=L+1$.

APPENDIX B. THE MATRIX ELEMENT OF THE TYPE II OPERATOR

Employing Eqs. (2) and (8), one may immediately write

$$(jl\mu|T_{\lambda L}{}^{-m}(\mathbf{r},\sigma)|j'l'\mu')$$
$$=\sum_{\tau\tau'm'} C(l\tfrac{1}{2}j;\mu-\tau,\tau)C(l'\tfrac{1}{2}j';\mu'-\tau',\tau')$$
$$\times C(1L\lambda;-m',m'-m)(\chi_1{}^{\tau},\mathcal{Y}_1{}^{-m'}(\sigma)\chi_1{}^{\tau'})$$
$$\times\mathfrak{F}_L(Y_l{}^{\mu-\tau},Y_L{}^{m'-m}Y_{l'}{}^{\mu'-\tau'}), \quad \text{(B.1)}$$

where the notation of Eq. (12′) has been used. The scalar product in spin-space is readily evaluated, yielding

$$(\chi_1{}^{\tau},\mathcal{Y}_1{}^{-m'}(\sigma)\chi_1{}^{\tau'})$$
$$=\frac{3}{(4\pi)^{\frac{1}{2}}}(-1)^{-m'}C(\tfrac{1}{2}1\tfrac{1}{2};\tau'-m',m')\delta_{\tau,\tau'-m'}. \quad \text{(B.2)}$$

Using this result, along with Eq. (I 43) for the coupling between a product of two orbital angular momentum wave functions in the same space, one obtains, after performing the trivial sum over τ,

$$(jl\mu|T_{\lambda L}{}^{-m}(\mathbf{r}\sigma)|j'l'\mu')$$
$$=\frac{3}{4\pi}(2L+1)^{\frac{1}{2}}(-)^{l+l'}C(lL l';0,0)$$
$$\times\delta_{m,\mu'-\mu}\mathfrak{F}_L\textstyle\sum_{m'}(-)^{m'}C(1L\lambda;-m',m'-m)$$
$$\times\textstyle\sum_{\tau'} C(l\tfrac{1}{2}j;\mu-\tau'+m',\tau'-m')$$
$$\times C(l'\tfrac{1}{2}j';\mu'-\tau',\tau')C(\tfrac{1}{2}1\tfrac{1}{2};\tau'-m',m')$$
$$\times C(Ll'l;m'-m,\mu'-\tau'). \quad \text{(B.3)}$$

Employing Eq. (I 44) twice, the four Clebsch-Gordan coefficients in the τ' sum may be transformed to a new set of four C coefficients and two Racah coefficients. Only two of the new Clebsch-Gordan coefficients depend upon τ', and these yield an orthogonality relation enabling the τ' sum and one of the recoupling sums to be done immediately. The remaining two C coefficients depend upon m' and after using (I 44) once more one is able, in an entirely similar fashion, to carry out the m' sum and another recoupling sum. One then finds

$$(jl\mu|T_{\lambda L}{}^{-m}(\mathbf{r}\sigma)|j'l'\mu')$$
$$=(3\sqrt{2}/4\pi)[(2L+1)(2j'+1)(2\lambda+1)(2l+1)]^{\frac{1}{2}}$$
$$\times C(lLl';0,0)\delta_{m,\mu'-\mu}(-)^{\lambda+1}$$
$$\times C(j'\lambda j;\mu',-m)\mathfrak{F}_L\textstyle\sum_s(2s+1)W(1jLj';s\lambda)$$
$$\times W(j1l\tfrac{1}{2};s\tfrac{1}{2})W(j'L\tfrac{1}{2}l;sl'). \quad \text{(B.4)}$$

One now notes that the sum over s yields, by definition,[12]

$$(-1)^{\lambda+L+j'+j+l'+l}X(\tfrac{1}{2}1\tfrac{1}{2};j\lambda j';lLl'),$$

so that finally the reduced matrix element becomes

$$(jl\|T_{\lambda L}(\mathbf{r},\sigma)\|j'l')$$
$$=(3\sqrt{2}/4\pi)[(2\lambda+1)(2L+1)(2l+1)(2j'+1)]^{\frac{1}{2}}$$
$$\times(-)^{j'-j}C(lLl';0,0)X(\tfrac{1}{2}1\tfrac{1}{2};j\lambda j';lLl')\mathfrak{F}_L, \quad \text{(B.5)}$$

in accordance with Eq. (16).

The Natural Distribution of Tritium*

SHELDON KAUFMAN† AND W. F. LIBBY
Department of Chemistry and Institute for Nuclear Studies, University of Chicago, Chicago, Illinois

(Received December 14, 1953)

The abundance of cosmic-ray-produced tritium has been measured in a variety of natural waters in the Mississippi Valley, the Chicago area, and in a few places elsewhere in the northern hemisphere. Contents ranging between 0.5 and 67 tritium atoms per 10^{18} hydrogen atoms have been found. These correspond to an average cosmic-ray production rate of about 0.12 tritium atoms per cm^2 per second if the total rate of transfer of tritium into the oceans by oceanic rain and snow and by rivers carrying continental water is taken as being equal to the total production rate. This is equivalent to assuming short land storage time in terms of eighteen years—the tritium average life. This production rate corresponds to an inventory of about 1800 g, with only about one percent of this in the atmosphere.

The tritium contents of vintage wines appear to agree with the time elapsed since bottling, indicating the tritium abundances over the last eighteen years to have been essentially equal to the present ones. Some of the possible applications of natural tritium to problems of hydrology and meteorology are discussed. The present production rate for tritium corresponds to an He^3 escape rate from the earth of about 5×10^7 years or less.

I. INTRODUCTION

THE probability of the occurrence of tritium in nature[1,2] as a disintegration product of the bombardment of the air by cosmic rays and as an explanation of the occurrence of helium-3 in the helium of the atmosphere at a higher abundance than in terrestrial or oil-well helium, the discovery of tritium in nature which resulted from testing Norwegian lake water[3] and atmospheric hydrogen,[4] as well as the potential usefulness of natural tritium[5] all have led to intensification of the study of natural tritium.

Since it seems clear that most of any tritium produced by the cosmic rays probably would soon be oxidized to form water, it follows that cosmic-ray tritium should be found in rain and snow. The dominance in magnitude of the cosmic-ray source as compared to the direct generation in the rocks and oceans is not obvious so we consider briefly the magnitude of the terrestrial ray sources. Since the helium in natural gas does contain helium-3 in an abundance of about 10 percent of that at which it occurs in atmospheric helium,[6,7] the production of tritium in the earth itself seems to be very likely, since helium-3 is the radioactive decay product. The production of tritium in rocks can occur by neutrons which are generated by the spontaneous fission of uranium and by the (α,n) reactions. The neutrons so generated then react with lithium traces in the rocks to form tritium, which decays with a half-life of 12.5 years[8] to form helium-3. The fission reaction is probably a less important source than the bombardment of the rocks with the alpha particles from the uranium and thorium via the (α,n) reactions.[9,10] Using the cross sections for thermal neutrons[11] and the composition of igneous rock,[12] one can calculate the probability that a neutron liberated in igneous rock will form tritium. The result is about six percent. This together with the abundance of uranium and thorium allows a calculation of the ratio of the helium-3 to helium-4 production rates due to fission alone. The result is about 0.5×10^{-7}, which compares favorably with the values of about 1.7×10^{-7} actually found.[6,7] The variation in composition of rock is such that this must be taken only as an average figure and the tritium production in the earth's crust as a whole is difficult to estimate except as an order of magnitude. It does seem clear, however, from the theory outlined[9] that there is no essential mystery about the occurrence of helium-3 in terrestrial rock helium and that it must have been produced by the radioactive and fission disintegration of the uranium and thorium in the earth's surface via tritium. In terms of tritium production the terrestrial source is very small. In fact a layer of igneous rock one kilometer deep has a production rate of only 0.001 T atoms per cm^2 per second, whereas we shall see later that it is very likely that the cosmic ray production is 0.1 or higher. The production in sea water by a similar mechanism is completely negligible since the proton capture of the neutrons will prevent the absorption by lithium due to the great abundance of ordinary hydrogen in sea water. One concludes therefore that the production of tritium in the earth's crust constitutes a negligible source of tritium for natural waters. It is

* This research was supported by the United States Air Force under a contract monitored by the Office of Scientific Research, Air Research and Development Command.

† Now in United States Army.

[1] W. F. Libby, Phys. Rev. **69**, 671 (1946).
[2] E. L. Fireman, Phys. Rev. **91**, 922 (1953).
[3] Grosse, Johnston, Wolfgang, and Libby, Science **113**, 1 (1951).
[4] V. Faltings and P. Harteck, Z. Naturforsch. **5A**, 438 (1950).
[5] W. F. Libby, Proc. Nat. Acad. Sci. **39**, 245 (1953).
[6] L. T. Aldridge and A. O. Nier, Phys. Rev. **74**, 1590 (1948).
[7] J. H. Coon, Phys. Rev. **75**, 1355 (1949).
[8] Jenks, Ghormley, and Sweeton, Phys. Rev. **75**, 701 (1949).
[9] P. Morrison and D. B. Beard, Phys. Rev. **75**, 1332 (1949).
[10] M. G. Inghram (private communication).
[11] *Nuclear Data*, National Bureau of Standards Circular No. 499 (U. S. Government Printing Office, Washington, D. C., 1950) and Supplements 1–3.
[12] K. Rankama and T. G. Sahama, *Geochemistry* (The University of Chicago Press, Chicago, 1950), pp. 39–40.

interesting that the consideration of natural spontaneous fission and (α,n) reactions[9,10] gives essentially quantitative explanation of the helium-3 content of well helium.

The half-life of tritium[8] fixes the time scale for the natural phenomena associated with the cosmic-ray tritium. For example, rain water bottled should lose its radioactivity at the rate of 50 percent every 12.5 years and one should expect therefore that natural products such as wine and other agricultural products which are fed essentially by rain water should be datable by their tritium content. Data reported in this paper seem to substantiate this. In addition it is clear that the terrestrial underground waters which have been out of atmospheric contact for several years should be distinguishable from rain water. This may well afford an opportunity to measure the flow of underground water and to determine storage time for underground reservoirs. Experiments checking these expectations are in progress, but no definitive results have been obtained as yet. In the field of meteorology it is clear that the tritium assay for a given storm depends not only on the cosmic ray intensity, but also on such meteorological factors as the trajectory of the air mass and its water content. Further studies of these factors reveal the potential usefulness of natural tritium for meteorology.

II. MEASUREMENT OF TECHNIQUE

A. Enrichment Process

The water sample to be assayed for tritium content is first distilled in a standard two gallon gas-fired still, mixed with sodium hydroxide to produce a 3 percent by weight solution, electrolyzed in an iron-nickel anode plant[13] to a final volume of about 1 cc or less, and the deuterium and tritium content of the final product determined. In addition it has been the custom to remove samples during the course of the enrichment to obtain confirmatory evidence as to the correctness of the assay and assurance of freedom from tritium contamination. The plant consists of 38 water-cooled steel cells of 3-liter capacity each operated in series at 100 amperes and 100 volts and arranged in three stages. A series of smaller cells constitute the final stages. The gases generated at each stage are collected by iron header pipes and conducted out of doors or simply allowed to escape into a lightly constructed drafty shed which houses the electrolytic plant. The cells are constructed of Shelby seamless steel tubing, four inches in diameter and eighteen inches in length. A bottom plate and a central tie-rod which secures the head are attached by arc welding. The head carries the gas outlet tube and the tube through which the cell is filled. The cell itself, insulated from the cooling water by paint and electrical tape, serves as the cathode. The anode consists of a perforated cylinder of sheet nickel, 3.5 inches in diameter and 5 inches high, attached by welding to the flat end of a $\frac{1}{2}$ inch nickel rod which passes through an inverted rubber stopper in the head part of the cell. The nickel cylinder is insulated from the cell wall by small pieces of hard rubber. The small cell which constitutes the fourth and final stage in the large plant is constructed on the same design, but the material is 2.5-inch iron pipe.

The water cooling is achieved by placing the cells in a trough through which the cooling water is circulated. The electrical insulation between ground potential water and the cell wall is achieved by painting the cells with three coats of Tygon paint, series TP, then wrapping with Scotch Electrical Tape (No. 33).

The source of electrical power is a 10-kw direct-current generator capable of delivering up to 125 amperes at 100 volts. The plant is located in a lightly constructed wooden shack next to the Jones Chemical Laboratory at the University of Chicago. In order to avoid freezing of the solutions including water during winter, a steam radiator has been installed. During the summer time the cooling water is cooled by a commercial refrigerating unit. During winter, tap water is sufficiently cold. Because of the possibility of explosion in the enclosure of the shack, the closure has purposely been made poor so a considerable air circulation takes place. The plant design is such that in case all the hydrogen and oxygen gas in the plant should explode at once it would do relatively little damage.

The thirty cells of the first stage are filled with three liters of a three percent sodium hydroxide solution made up of the water sample. The sodium hydroxide is a CP electrolytic grade and the water is distilled before use.

When the electrolysis has proceeded for about 72 hours, the initial charge, totaling 90 liters, is reduced to about $\frac{1}{3}$ of its original volume. It then is removed, neutralized and distilled, and transferred to the second stage. Similarly, the residue from the second stage is transferred to the third stage, etc. The whole plant is a direct reproduction of that constructed by Brown and Daggett[13] with the exception of a few minor changes such as the use of Tygon paint and electrical tape wrapping to insure the insulation between the cell wall and the cooling water.

The final stages of the enrichment are accomplished on laboratory bench cells made by the use of iron and nickel strips and glass containers. The current supply found to be most satisfactory for the laboratory cells has been commercial battery chargers. An important factor in the attainment of large fractionation has proved to be the cooling of the water. One notes that in the method of separation used in this work in which the hydrogen and oxygen gases are discarded without recirculation and no attempt is made to remove the water vapor from them the volume of electrolytic vapor is so large that a moderate vapor pressure of the liquid water makes the removal of water by volatiliza-

[13] W. G. Brown and A. F. Daggett, J. Chem. Phys. 3, 216 (1935).

tion appreciable relative to that removed by the electrolysis.

The deuterium assays have been used to measure the tritium separation actually obtained, it being assumed and confirmed experimentally that alterations in conditions which would change the deuterium enrichment would alter the tritium enrichment proportionately (see Table I). These assays were made by the falling drop technique.[14] It was found possible to determine deuterium contents as low as 0.1 percent with an accuracy of about 0.01 percent. The concentration range normally encountered was between 1 and 4 percent where the accuracy is about 0.02 percent. The more highly enriched water samples were diluted down to this concentration with ordinary water. This dilution also tends to reduce the error due to O^{18} accumulation to less than 1 percent in the deuterium content.

The equations governing electrolytic separation of the hydrogen isotopes are easily derived. The heavy isotopes are discharged at the cathode more slowly than protium. Labelling the number of moles of protium, deuterium, and tritium isotope as p, d, and t, respectively, we can write

$$d\ln p=\alpha d\ln d=\beta d\ln t, \tag{1}$$

where α and β are the separation factors for deuterium and tritium, respectively, with respect to protium. It was assumed that α is independent of the deuterium concentration, a fact for which experimental evidence exists,[15] and it was further assumed that β would also be independent of isotopic content. This allows Eq. (1) to be integrated to give

$$\ln(p/p_0)=\alpha\ln(d/d_0)=\beta\ln(t/t_0), \tag{2}$$

where the subscript indicates the initial condition. Since the mole volumes of H_2O and D_2O are almost identical, we can write

$$V=18(p+d), \tag{3}$$

where V is the volume of solution in cc. At the start of the electrolysis the concentration of D_2O is only 0.015 percent for normal water.[16] For solutions low in deuterium, the enrichment equations are

$$V/V_0=p/p_0=(d/d_0)^{\alpha}=(t/t_0)^{\beta}. \tag{4}$$

If the concentration or specific activity of tritium is denoted by τ, the tritium enrichment is

$$\tau/\tau_0=(t/t_0)(V_0/V)=(V_0/V)^{1-1/\beta}, \tag{5}$$

and

$$\tau/\tau_0\cong V_0/V,$$

since β is nearly always larger than 10. If N denotes the mole fraction of deuterium, so that $N=d/18V$, an expression for the tritium enrichment valid at all deuterium concentrations is,

$$\frac{\tau}{\tau_0}=\frac{V_0}{V}\left(\frac{d}{d_0}\right)^{\alpha/\beta}=\frac{V_0}{V}\left(\frac{N\times V}{N_0\times V_0}\right)^{\alpha/\beta}. \tag{6}$$

One previous measurement of β has been reported in the literature by Eidinoff.[17] Values of about 15 were obtained.

Using standard tritium solutions made by diluting tritium obtained from the U.S. Atomic Energy Commission and conducting electrolyses in the same way as for natural water samples, experimental values for α and β/α as shown in Table I were obtained.

It is clear from these data that the value of β/α is nearly constant while the value of α can fluctuate widely. This of course is to be expected since the effective separation depends on a variety of conditions which would hardly be expected to affect the relative separation factor, β/α. The data have been computed on the assumption that $\beta/\alpha=2.1\pm0.10$.

TABLE I. Experimental values of β/α (10°–25°C).

Standard	V_0/V	% D_2O	Sp. activity (counts min^{-1} cm^{-1})	α	β/α
No. 2	1	0.16	5.8		
	3.8	0.47	19.2	5.2 ±1.3	1.9 ±0.8
	14.5	1.32	59.6	4.4 ±0.6	1.5 ±0.4
No. 3	1	1.48	4.64		
	7.60	6.42	27.3	3.7 ±0.1	2.18±0.20
	47.2	28.0	138	5.9 ±0.2	1.75±0.16
	186	70.7	440	5.14±0.18	2.16±0.18
No. 4	1	1.94	10.03		
	8.01	10.85	67.7	6.1 ±0.3	2.08±0.19
	52.2	49.8	371	7.0 ±0.3	2.01±0.18
	239	96.5	1178	...	2.34±0.13
No. 5	1	1.89	11.65		
	6.55	9.75	71.2	8.2 ±1.4	3.5 ±1.4
	214	83.5	1268	3.9 ±0.1	2.20±0.11
No. 6	1	0.0148	0.002875		
	1070	5.18	1.93	6.3 ±0.2	2.4 ±0.3
	3420	12.4	5.05	6.0 ±0.2	2.10±0.15
	1650	11.20	3.15	9.7 ±0.6	1.91±0.19
	3170	20.3	6.29	10.0 ±0.6	2.22±0.25
	1300	10.40	2.70	12.0 ±0.5	1.86±0.19
	3060	17.1	5.63	8.4 ±0.3	2.18±0.15
	1190	7.60	2.15	8.5 ±0.3	1.81±0.18
	2650	15.3	5.23	8.5 ±0.3	2.45±0.25
Weighted average					2.10±0.10

B. Counting

The measurement of the tritium content of the enriched water samples consists in the conversion of water to hydrogen gas and its measurement in a low-level Geiger counter. The procedure has been described previously.[3,18] Further utilization of it has revealed no essential weaknesses. The technique for the conversion of water to gaseous hydrogen[3] consists of the use of finely divided zinc dust at about 500°C. The zinc dust

[14] I. Kirshenbaum, *Physical Properties and Analysis of Heavy Water* (McGraw-Hill Book Company, Inc., New York, 1951), National Nuclear Energy Series, Plutonium Project Record, Vol. III, Div. IVA, p. 324.
[15] A. Farkas, Trans. Faraday Soc. **33**, 552 (1937).
[16] I. Kirshenbaum (see reference 14).
[17] M. L. Eidinoff, J. Am. Chem. Soc. **69**, 977, 2507 (1947).
[18] R. L. Wolfgang and W. F. Libby, Phys. Rev. **85**, 437 (1952).

is mixed with freshly dehydrated calcium oxide into which the water sample is distilled at room temperature. When this step has been completed, the mixture is heated in a Pyrex tube to about 500°C to cause the evolution of hydrogen gas. It has been found that the conversion is essentially quantitative by this technique and the isotopic fractionation therefore is of no consequence. The gaseous hydrogen is stored in a bulb and transferred to the vacuum line used for filling counters.

The counting technique consists in the use of an ordinary Geiger counter with flat ends in order that a known correction might be made for the end loss.[19] The gaseous mixture consisted of about 2.0-cm Hg pressure of ethylene gas, 3.0-cm Hg pressure of argon gas, and 0- to 20- or 30-cm pressure of hydrogen gas in which the tritium is contained. The counters used in our research were 2 in. in inside diameter and 18 inches in length. They were made of brass tubing with Lucite ends waxed in place. The center wire was No. 28 copper. The counter voltages depended a great deal on the pressure of hydrogen and ethylene, and ranged from 1500 to 3000 volts. An anticoincidence shield together with an 8-inch thick iron shield was customarily used.[20] The background for our counters in the iron shield with the anticoincidence shielding counters disconnected was 160 counts per minute. It was about 8 counts/min with these connected in the full shielding arrangement. We normally did not measure a sample with less than 1 count/min of radioactivity. In general, the activities were at least 5 to 10 counts per minute above background. Small corrections were made for the end losses to convert to absolute tritium contents. Normal measurements can be completed in about half an hour.

III. EXPERIMENTAL RESULTS

The experimental data are given in Tables II, III, and IV, and in Fig. 1. In Table II are given the detailed data and calculations of the tritium content for a series of samples, and in Table III are given the summarizing data for all the samples measured. The errors quoted are standard deviations taken principally from the counting errors, that is, the errors in measurement of radioactivity. The error in the volume enrichment alone is about 3 percent. This relatively large error is due to the accumulation of small errors in the individual volume measurements. In addition other errors are present such as the variation in initial abundance of deuterium. In a few cases, as indicated in Table II, the initial deuterium abundances were measured directly, but in the other cases the abundance was taken as 0.015 percent, the average based on the careful study made several years ago.[16] An additional error lay in a failure to remove thoroughly all moisture from the hydrogen generation equipment in one or two instances. This introduced diluting nonradioactive hydrogen into the samples, as shown by a decrease in the deuterium content of the gases generated as compared to that of the water used in the generation. Correction was made for this whenever the effect was discovered; however, it may have been present in one or two undiscovered instances. It seems likely that the entire error is perhaps twice the error quoted.

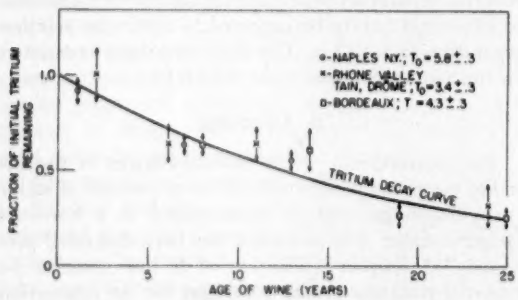

FIG. 1. Tritium content of vintage wines vs age.

The data in Fig. 1, taken from the wine data listed in Table III, have been computed by using the mean of the calculated initial assays for the wine as shown in the last column of Sec. E of Table III. This last column containing parenthetical figures consists of the calculated initial assays assuming that the tritium present has decayed at the 12.5-year half-life rate. Taking the weighted average, the weighting being done according to the inverse square of the counting errors as indicated, we deduce the average effective initial assays given in Table IV, and using these as the standard basis, the fraction of tritium remaining in the various wines is calculated and the data derived is shown in Fig. 1.

It appears that the data do agree with the curve within the rather large experimental errors. In spite of these errors, which are largely due to the fact that limited quantities of the wine were available for measurement, the agreement between the tritium content and the expected curve is quite satisfactory and we do find that we probably can date wine, agricultural products, and water in general, in the sense of measuring the time elapsed since the last precipitation as rain or snow, i.e., the last contact with atmospheric moisture.

IV. DISCUSSION

A. Tritium Production Rate $\bar{Q}$

It would seem reasonable that whatever the mechanism by which the cosmic rays produce tritium by bombarding the air—whether by the (n,t) reaction of fast secondary neutrons on nitrogen[1,2] or by direct production in cosmic ray "stars"[2,9]—the production rate should vary with latitude in a manner not too dissimilar from that in which the secondary neutrons

[19] A. G. Engelkemeir and W. F. Libby, Rev. Sci. Instr. **21**, 550 (1950).
[20] Anderson, Arnold, and Libby, Rev. Sci. Instr. **22**, 225 (1951).

TABLE II. Typical experimental results.

No.	$\frac{V_0}{V}$	$\frac{\tau}{\tau_0}$	% D_2O	Sp. activity (counts min^{-1} cm^{-1})	α	$\left(\frac{T}{H}\right)\times10^{18}$	Av.
5	1560	948	8.10	1.51 ±0.2	5.7±0.3	32 ±4	
	6250	3660	30.0	6.15 ±0.38	11 ±2	34 ±2	
	18 500	9300	64.5	15.3 ±0.2	7.1±1.3	33.5 ±3	33 ±2
14	1	1	0.0138				
	786	546	4.83	0.714±0.06	7.8±0.2	24 ±3	
	3420	2130	17.5	2.43 ±0.09	9.0±0.9	19.8 ±0.8	
	23 800	11 600	72.2	12.6 ±0.2	5.9±0.3	20.0 ±0.3	
	696	479	4.39	0.58 ±0.02	7.7±0.3	21 ±2	
	2240	1450	12.4	1.43 ±0.07	9.6±1.5	17.2 ±1.1	
	14 500	6860	43.7	8.03 ±0.18	3.8±0.3	21.3 ±0.5	20.4 ±0.7
16	2830	1875	17.6	4.45 ±0.17	9.4±0.4	41.1 ±1.7	
	21 000	11 500	72.3	21.7 ±1.1	5.3±0.7	35.0 ±2	37 ±3
17	1660	1150	11.3	4.08 ±0.23	9.7±0.6	65.0 ±2.5	
	12 800	7160	56.2	27.4 ±0.5	6.3±0.7	66.8 ±0.7	66.0 ±1.0
18	1	1	0.0147				
	1400	850	7.20	0.89 ±0.11	6.9±0.8	19.3 ±2.4	
	890	605	5.80	0.63 ±0.10	8.3±0.5	19.4 ±3.0	19.3 ±1.5
19	1	1	0.0132				
	1160	850	8.00	0.61 ±0.05	9.2±0.4	13.2 ±1.2	13.2 ±1.2
21	1	1	0.0129				
	1700	1170	10.0	0.48 ±0.03	7.5±0.2	7.1 ±0.5	7.1 ±0.5
22	1	1	0.0137				
	1600	1070	9.42	0.54 ±0.05	8.1±0.7	9.0 ±1.0	9.0 ±1.0
30	1	1	0.0148				
	1730	1130	10.4	0.33 ±0.05	8.4±0.3	5.0 ±0.7	5.0 ±0.7
33	1	1					
	2100	1760	18.7	1.14 ±0.09	16 ±2	10.8 ±1.0	11.9 ±1.0
34	1	1	0.0148				
	1860	1190	10.8	0.15 ±0.05	8.1±0.3	2.4 ±0.8	
	6800	3880	31.0	0.70 ±0.06	6.5±0.5	3.3 ±0.3	3.3 ±0.3
38	4290	2730	24.4	1.39 ±0.14	9.0±0.4	9.4 ±1.0	9.4 ±1.0
39	3190	1970	17.2	1.04 ±0.08	8.2±0.4	9.6 ±0.8	9.6 ±0.8
40	5050	3090	26.7	0.82 ±0.15	8.5±0.3	4.6 ±0.8	
	25 300	12 200	81.5	3.30 ±0.15	6.1±0.3	4.75±0.21	4.75±0.20

vary. Simpson[21] has published data for the variation of neutron intensity with latitude at 30 000-feet altitude (22.5-cm Hg pressure). Using these data we can calculate the ratio of the expected world-wide average production rate of tritium, $\bar{Q}$ (T atoms/cm² sec), to the local production rate Q to be 0.58 at Lake Mösvann, Norway, 0.64 at 48°N geomagnetic latitude, the approximate mean latitude of the Mississippi Valley, and 0.58 for Chicago.

If we suppose that the tritium produced is converted into water which is precipitated as rain or snow, equating the production rate to the rate of precipitation into the sea plus the rate of transport by rivers into the sea gives

$$\tfrac{1}{4}\bar{\rho}\bar{T}_l+\tfrac{3}{4}\bar{r}_s\bar{T}_s=4.7\bar{Q}. \qquad (7)$$

In Eq. (7) $\bar{\rho}$ is the annual run-off from the world's land areas in meters, $\bar{r}_s$ is the annual precipitation over the oceans in meters, $\bar{T}_l$ and $\bar{T}_s$ are the tritium contents of the run-off waters and ocean rain waters, respectively, in units of T atoms per 10^{18} H atoms, and $\bar{Q}$ is the world wide average tritium production rate in atoms per cm² per second. The factors $\frac{1}{4}$ and $\frac{3}{4}$ are the fractional land and ocean areas. The factor 4.7 is a numerical constant arising from the units selected. Equation (7) simply states that the tritium is transported into the oceans where it is absorbed and that this transport occurs in the first year or two before any appreciable decay into He^3 could occur. From the Norwegian Lake Mösvann datum (Table IV), which probably is typical of sea precipitation since it derives almost entirely from the sea saturated air masses which roll over the Norwegian coast, we can calculate $\bar{T}_s$ to be $(0.8\pm0.1)\times(0.58)\times(0.9/0.77)$ or 0.54 ± 0.07, where

[21] J. A. Simpson, Jr., Phys. Rev. 83, 1175 (1951).

TABLE III. Summary of data.

Sample No.	Description of sample	$(T/H)\times10^{18}$
	A. Chicago rains and snows	
5	May 11, 1951. Collected from 1000 to 1200. Storm lasted from evening of 10th to afternoon of 11th. 3.81 in. rain.	33 ±2
14	October 14, 1952. Collected throughout storm. Storm lasted from 1700 to 2400. 0.70 in. rain.	20.4 ±0.7
16	November 17, 1952. Collected throughout storm. Storm lasted from 0030 to 0100; 0600 to 0630. 0.31 in. rain.	37 ±3
17	November 18, 1952. Collected throughout storm. Storm lasted from 2100 of 17th to 1200 of 18th. 0.70 in. rain.	66.0 ±1.0
18	November 22–24–25, 1952. Collected throughout storms. Rained afternoon of 22nd, evening of 24th, all day 25th. 1.13 in. rain.	19.3 ±1.5
19	December 2, 1952. Fell during night. 0.29 in. snow.	13.2 ±1.2
21	January 6, 1953. Fell during afternoon. 0.05 in. snow.	7.1 ±0.5
22	January 23, 1953. Collected from 1515 to 1530. Storm lasted from 1200 to 1900. 0.32 in. rain.	9.0 ±1.0
30	February 11, 1953. Collected from 0930 to 1245. Light rain all morning. 0.03 in. rain.	5.0 ±0.7
33	February 16, 1953. Collected 1030. Fell from 0300 to 1400. 0.19 in. snow.	10.8 ±1.0
34	February 20, 1953. Collected 1615. Storm lasted from 1530 to 1645. 0.94 in. rain.	3.3 ±0.3
38	March 3, 1953. Collected throughout storm. Rain, sleet and snow fell from 1300 to 2000. 0.38 in. rain.	9.4 ±1.0
39	March 7, 1953. Collected 1200. Fell from 0800 to 1500. 0.18 in. snow.	9.6 ±0.8
40	March 12, 1953. Collected 1030. Storm lasted from 0900 to 1700. 0.98 in. rain.	4.75±0.20
45	March 14, 1953. Collected throughout storm. Rained from 1000 to 1600; 2000 to 2200. 1.05 in. rain.	1.16±0.18
46	March 18, 1953. Collected throughout storm. Light rain from 1300 to 1700. 0.13 in. rain.	7.9 ±0.3
48	March 21–22, 1953. Collected throughout storms. Rained night of 21st, night of 22nd. 0.06 in. rain.	3.10±0.13
50	March 31, 1953. Collected from 1030 to 1100. Rained lightly from 1000 to 1200. 0.07 in. rain.	9.5 ±0.4
	Wtd. Ave. (December to March):	5.5
	B. Rains and snows from other areas	
42	Fayetteville, Arkansas, snow. January 23, 1953. 1.17 in. snow.	5.5 ±0.6
49	Honolulu, Hawaii, rain. March 26, 1953. Collected in morning. Trace rain.	0.61±0.10

the world wide average,[22] ξ_ρ, of 0.77 is used to correct for the unusually high precipitation on the mountain plateau, Hardangervidda, east of Bergen which feeds Lake Mösvann. For the value of $\bar{T}_l$ we take the Mississippi Valley average of 5.2±0.2 (Table IV) and correct it for the latitudinal effect with the factor 0.64. Substituting in Eq. (7) and using a value[22] of 0.28 for $\bar{\rho}$, we find $\bar{Q}$ to be 0.12 T atoms per cm² per second, to an accuracy of about 30 percent.

B. Meteorology

Having evaluated the tritium production rate Q, we can calculate the expected value of T, the tritium concentration in water in an air mass, in terms of the amount of water w, (meters per cm²) and the time τ, in years, elapsed since the water evaporated from the oceans. For a given latitude we would write

$$Tw=4.7Q\tau \qquad (8)$$

For example, if the water content of the average air mass traveling over the Hardangervidda is 3 g per cm², τ would be on the average 0.024 years, or about nine days.

The much larger values of the tritium concentration found in the rain and run-off waters over the land masses (Table IV) as contrasted to sea rains and snows undoubtedly are due to longer exposure of these waters to atmospheric tritium. The average length of exposure is to be calculated from Eq. (8) in which the total water, atmospheric plus run-off is to be included as w. Estimating the surface and ground water in the Mississippi Valley to average about 7 g per cm² we estimate w to be 0.10 and τ is 0.9 year. In other words, the water flowing into the Gulf of Mexico at New Orleans left the ocean about eleven months earlier. More accurate values of w should be used to improve this calculation. This time, while somewhat surprisingly long, still does not violate our primary assumption that the tritium reaches the great depths of the oceans before decaying appreciably.

The data on the individual storms in the Chicago area for the past year reveal no obvious correlations of real importance. Averaging the rains from December 1, 1952 through March, 1953, and excluding the fall rains which followed an unusually dry summer and fall in the Northwest gives a value of 5.2—a value not only in good agreement with the Mississippi River waters collected over essentially the same period, but also with the Lake Michigan value of 7.7±0.3 which is an average for approximately the last 18 years calculated from the

[22] Reference 12, pp. 39–40.

TABLE III.—*Continued.*

Sample No.	Description of sample	$(T/H)\times10^{18}$
	C. Mississippi and other rivers	
24	Mississippi River, Rock Island, January 29, 1953.	2.5 ±0.3
27	Mississippi River, Rock Island, February 6, 1953.	3.7 ±0.4
37	Mississippi River, Rock Island, February 24, 1953.	4.4 ±0.2
23	Mississippi River, St. Louis, January 31, 1953.	5.6 ±0.6
26	Mississippi River, St. Louis, February 4, 1953.	4.5 ±0.6
31	Mississippi River, St. Louis, February 10, 1953.	6.0 ±0.9
36	Mississippi River, St. Louis, February 20, 1953.	6.4 ±0.5
28	Mississippi River, Memphis, February 4, 1953.	6.0 ±1.0
29	Mississippi River, New Orleans, February 8, 1953.	4.7 ±0.3
	Wtd. Ave. for St. Louis, Memphis, and New Orleans:	5.2 ±0.2
15	Sangamon River, Decatur, August 6, 1952.	1.15±0.08
52	Arkansas River, Conway, Arkansas, March 20, 1953.	3.12±0.10
	D. Lake Michigan	
8	Jones Laboratory, Tap water, July 7, 1952.	1.35±0.25
32	Jones Laboratory, Tap water, February 13–16, 1953.	1.73±0.06
13	Oak Park tap, hot water heater, *ca* 12 years old.	0.62±0.06 (1.2)
	E. Vintage wines	
55	Widmer's New York Riesling wine, Vintage 1940, Naples, New York.	3.2 ±0.2 (6.6±0.4)
62	Widmer's New York Riesling wine, Vintage 1946, Naples, New York.	3.63±0.16 (5.4±0.3)
54	Widmer's New York Riesling wine, Vintage 1952, Naples, New York.	5.3 ±0.3 (5.6±0.3)
63	Hermitage Rhone wine, Vintage 1929, Tain, Drôme, France.	1.13±0.38 (4.3±1.4)
64	Hermitage Rhone wine, Vintage 1942, Tain, Drôme, France.	2.15±0.21 (3.92±0.4)
65	Hermitage Rhone wine, Vintage 1947, Tain, Drôme, France.	2.15±0.28 (3.0±0.3)
66	Hermitage Rhone wine, Vintage 1951, Tain, Drôme, France.	3.4 ±0.4 (3.8±0.5)
69	Chateau Laujac Bordeaux wine, Vintage 1928, France.	1.16±0.16 (4.6±0.7)
70	Chateau Laujac Bordeaux wine, Vintage 1934, France.	1.16±0.30 (3.3±0.9)
71	Chateau Laujac Bordeaux wine, Vintage 1939, France.	2.6 ±0.4 (5.6±0.9)
72	Chateau Laujac Bordeaux wine, Vintage 1945, France.	2.70±0.18 (4.2±0.3)
	F. Miscellaneous	
9	Cistern, Decatur, collected August 6, 1952. Covered loosely about 29 years ago.	5.9 ±0.5
12	Cistern, Sullivan, Illinois, collected August 6, 1952. Covered with tight iron lid about 14 years ago.	2.9 ±0.2 (6.3±0.4)
20	Fire extinguisher, Skokie, Illinois. Filled June 5, 1936.	12.5 ±0.5 (32±1.2)
75	Pacific Ocean, Santa Monica, California, June 8, 1953.	0.54±0.02

1.7 assay of the lake water as explained in the next paragraph. In addition the Naples, New York, wine datum of 5.8±0.3 is in agreement.

The Lake Michigan rainfall value of 7.7 is calculated from the observed assay for the Lake of 1.7 (Table III) by use of the factor 4.5 for the storage and hydrologic effects. The factor of 4.5 is obtained as follows: The drainage area feeding Lake Michigan is 43 148 square miles, excluding lakes, and the annual run-off is 14.5 inches.[22] The annual rainfall over the lake itself is 31.3 inches, and the lake area is 22 336 square miles. The mean depth of the lake is 312.56 feet.[23] It is well known that the lake has complete vertical mixing each year, since the water inverts once each year as shown by the temperature gradient reversal. We therefore assume that the lake is perfectly mixed on the time scale of the lifetime of tritium. We further assume that the lake level is fixed and that the annual rainfall is exactly balanced by outflow and evaporation and that these processes do not fractionate the hydrogen isotopes appreciably. With these assumptions, we set up the equation for the steady condition that the rate of introduction of tritium into Lake Michigan must equal that at which it leaves the lake both by overflow and evaporation, and the radioactive decay into helium-3. The resulting equation is

$$[(T_r)-(T_l)]\left(31.3+14.5\times\frac{43148}{22336}\right)=(T_l)\frac{312.56\times12}{18}. \quad (8)$$

This equation gives the expected ratio of the tritium content of rain (T_r) to that of lake water (T_l) as 4.5.

TABLE IV. Average T content for precipitation in the northern hemisphere.

Location	Latitude (geomagnetic)	Precipitation (meters/year)	T content (T atoms/10^{18} H's)
Lake Michigan	~54°N	0.80	7.7 ±0.3
Mississippi Basin	48°N	0.76 (0.19 run-off)	5.2 ±0.2
Naples, New York (wine)	~54°N	1.0	5.8 ±0.3
Rhone Valley, Tain, Drôme, France (wine)	~54°N	0.8	3.4 ±0.3
Bordeaux, France (wine)	~54°N	0.8	4.3 ±0.3
Lake Mösvann, Norway	55°N	0.9	0.8 ±0.1[a]

[a] See reference 3.

[22] "Hydrology of the Great Lakes," Report of the Engineering Board of Review on the Sanitary District of Chicago for the year 1927, Horton.

C. The Age of Waters and Agricultural Products and Hydrology

Clearly the data on vintage wines given in Tables III and IV and Fig. 1 show that the tritium content of rain waters probably disappears at the tritium decay rate and that waters more than a few decades old in the sense of exposure to contamination by atmospheric water will show an undetectably low tritium content. Therefore it appears likely that we can distinguish underground from surface run-off water. Similarly, deep lake waters in which the storage time is appreciable relative to the life time of tritium (eighteen years, average) will be distinguishable. Michigan is such a lake. The possibility of making such distinctions should have application to hydrology. In particular the storage times for underground reservoirs would appear to be measurable in this way.

D. Escape Time for He^3 from the Earth; World Tritium Inventory

If $\bar{Q}$ be 0.12 ± 0.04, there must be $5.7\times10^8\times0.12$ T atoms per cm^2 to maintain a steady-state balance guaranteeing equality of the rates of production and radioactive decay of tritium. This corresponds to a total inventory of 1800 ± 600 grams of tritium in the world distributed about in the following way: 11 grams in the atmosphere ($w=0.03$) and 13 grams in the ground waters (10 grams per cm^2 of ground water assumed), with the remainder in the ocean depths.

Since the abundance of He^3 in the atmosphere is known[6,7] to be 1.8×10^{14} atoms/cm^2, $\bar{Q}$ gives an upper limit to the rate at which He^3 must escape from the earth. Being nonradioactive and chemically inert, physical escape is the only way in which the low atmospheric abundance can be maintained in view of the tritium production $\bar{Q}$. In fact the escape time τ (years) will be given by

$$\tau\leq\frac{1.8\times10^{14}}{0.12\times3.16\times10^7} \quad \text{or} \quad 4.7\times10^7\pm1.6\cdot10^7 \text{ years.}$$

Since it seems extremely likely that cosmic-ray stars may be involved in the production mechanism for tritium and it is difficult to imagine tritium being produced in the star mechanism method without helium-3 also being formed, we can expect that the true value of the escape time is less than 47 million years by perhaps thirty percent. Of course this assumes constant cosmic-ray intensity over this time, τ.

V. ACKNOWLEDGMENTS

The authors are extremely indebted to the Office of Scientific Research of the Air Research and Development Command of the U. S. Air Force for support of this research. We wish to thank, also, the many individuals who offered samples of old water in response to a public appeal. Mr. B. O. Caplener, Port Captain of the Federal Barge Lines and the U. S. Army Engineers kindly furnished our Mississippi Water Samples.

The vintage wines were selected by Professor M. Amerine of the University of California at Davis and were furnished by the cooperation of vintners, wholesalers, and tax authorities. We wish to thank all of these and in particular Mr. William Widmer who furnished the New York wines.

The Decay of Ho^{166}†

A. W. SUNYAR
Brookhaven National Laboratory, Upton, New York
(Received November 25, 1953)

The disintegration of Ho^{166} (27.3 hr) has been studied by scintillation counter coincidence techniques. Gamma rays of 1.53 Mev and 1.61 Mev are present in low intensity, in addition to the previously identified 80-kev and 1.36-Mev transitions. Both the 1.36-Mev and the 1.53-Mev gamma rays are in coincidence with the 80-kev transition. For the 80-kev $E2$ transition the K-conversion coefficient has been measured as 1.9 ± 0.2 and the total conversion coefficient as 7.6 ± 1.5. The β branching has been determined from $\beta-\gamma$ and $\gamma-\gamma$ coincidence measurements and by a comparison of the $\beta-\gamma$ coincidences with Tm^{170}. The results indicate a ground state branch of ~25 percent, a branch of ~74 percent to the 80-kev state, a branch of ~1 percent to a state at 1.44 Mev and a branch of ~0.3 percent to a state at 1.61 Mev in Er^{166}. The spin of Ho^{166} is probably 2−.

AN investigation of the continuous β spectrum of Ho^{166} (27.3 hr) by several workers[1] has shown that the principal β^- component has an end point energy of ~1.84 Mev. Two γ rays were known to be present in the disintegration scheme. The more intense 80.8-kev $E2$ transition[2,3] to the ground state of Er^{166} has a half-life[4] of 1.7×10^{-9} sec and a K-shell conversion coefficient[5] of 1.9. The number of L-conversion electrons of this transition per disintegration of Ho^{166} has been given[6,7] as about 0.3. Two intensity measurements of the 1.36-Mev γ ray are in disagreement. Grant and Hill[6] gave its intensity as ~1.5 percent, whereas Siegbahn and Slätis[7] quote a value of ~11 percent. It was not known whether the 1.36-Mev transition takes place to the 80-kev excited state or to the ground state of Er^{166}.[7]

TABLE I. Relative γ-ray intensities in the decay of Ho^{166}.

E_γ (Mev)	Relative intensity
0.080	8.5±2
1.36	1
1.53	0.2±0.05
1.61	~0.1

A study has been made of the decay of Ho^{166} by scintillation counter techniques. The γ-ray pulse-height distribution as observed from a 3-cm diameter and 2-cm thick crystal of NaI(Tl) on a Dumont type 6292 photomultiplier is shown in Fig. 1. The γ spectrum was measured through a Lucite absorber of ~1100 mg/cm² to eliminate the hard β rays from the counter. A comparison of the unconverted 80-kev γ-ray intensity to the K x-ray intensity after corrections for K-shell fluorescent yield and for absorption in the Lucite absorber gives a value of 1.92 ± 0.20 for the K-shell conversion coefficient, in complete agreement with the measurement of McGowan.[5] The photopeaks in the high-energy portion of the γ-ray spectrum show the 1.36-Mev γ ray and a peak near 1.55 Mev. The latter peak is considerably too broad to be attributed to a single γ ray and may be decomposed into photopeaks at 1.53 and 1.61 Mev. The counting geometry used in the measurement insures that the broad photopeak is not due to addition of two pulses in the phosphor. After correcting for detection efficiency in our phosphor we obtain the γ-ray intensities listed in Table I.

$\gamma-\gamma$ coincidence measurements imposing pulse-height selection upon both γ counters have shown that both the 1.36-Mev and 1.53-Mev γ rays are in coincidence with the 80-kev γ ray or its associated K x-rays (see Fig. 2). The drop in the coincidence rate per recorded γ ray on the high-energy side of the 1.53-Mev photopeak suggests that the 1.61-Mev γ ray is not in coincidence with the 80-kev γ ray. We tentatively

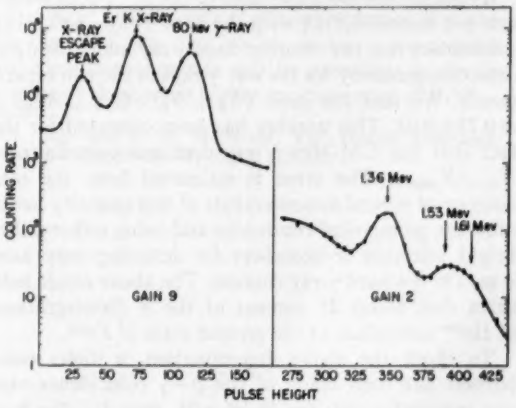

FIG. 1. Pulse-height distribution of γ-ray spectrum observed with NaI(Tl) scintillation counter. Note the change in pulse-height scale and amplifier gain for high-energy region.

† Work supported by the U. S. Atomic Energy Commission.
[1] For a complete list of authors see *Nuclear Data*, National Bureau of Standards Circular 499 (U. S. Government Printing Office, Washington, D. C., 1950), and its supplements or Hollander, Perlman, and Seaborg, Revs. Modern Phys. **25**, 469 (1953).
[2] M. Goldhaber and A. W. Sunyar, Phys. Rev. **83**, 906 (1951).
[3] M. Goldhaber and R. D. Hill, Revs. Modern Phys. **24**, 179 (1952).
[4] F. K. McGowan, Phys. Rev. **80**, 923 (1950).
[5] F. K. McGowan, Phys. Rev. **85**, 690 (1952).
[6] P. J. Grant and J. M. Hill, Nature **163**, 524 (1949).
[7] K. Siegbahn and H. Slätis, Arkiv Fysik **1**, 559 (1950).

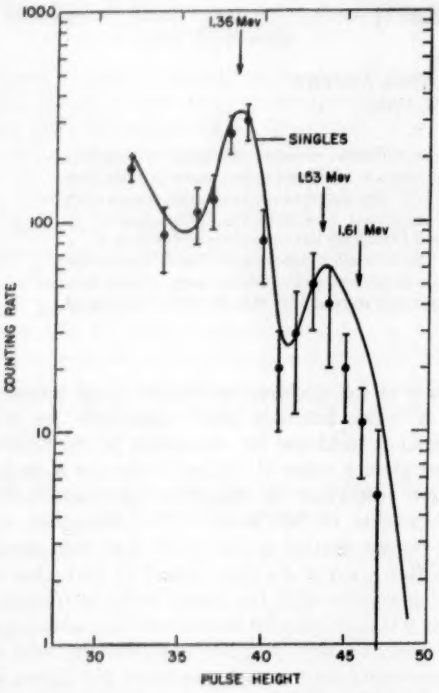

FIG. 2. Spectrum of γ radiation in coincidence with K x-rays and 80-kev γ ray. The solid curve is the singles spectrum in this region.

interpret this γ ray as a cross-over γ ray to the ground state of Er^{166}, as was suggested by its measured energy. A search has been made for a γ ray near 170 kev with negative results. If present, its photon intensity is less than 1 percent of the intensity of the 80-kev γ ray. There is also no evidence for a γ ray of 1.44 Mev. If present, its intensity is less than 20 percent of the 1.36-Mev γ-ray intensity.

A comparison has been made of the $\beta-\gamma$ coincidence rate per recorded β ray with the hard γ-ray—soft γ-ray coincidence rate per recorded hard γ ray under identical detection geometry for the soft γ rays in the two experiments. We find the ratio $(N_{\beta-\gamma}/N_\beta)\div(N_{\gamma-\gamma}/N_{\text{hard }\gamma})=0.74\pm0.03$. This number has been corrected for the fact that the 1.61-Mev γ ray does not contribute to $N_{\gamma-\gamma}/N_{\text{hard }\gamma}$. The error is estimated from the consistency of several measurements of this quantity under different geometrical conditions and using either pulse-height selection or absorbers for detecting only hard γ rays in the hard γ-ray counter. The above result indicates that about 25 percent of the β disintegrations of Ho^{166} take place to the ground state of Er^{166}.

To check the above determination, a direct comparison has been made of the $\beta-\gamma$ coincidence rate per recorded β ray for Ho^{166} with that for Tm^{170} in identical geometry. Tm^{170} was chosen as a standard for comparison for the following reasons:

(1) The β branching in Tm^{170} is known with good precision.[8]

(2) The γ ray of 84 kev and Yb K x-rays arising from its conversion are very similar to the 80-kev γ ray and Er K x-rays following the Ho^{166} decay.

(3) The conversion coefficients of the 84-kev γ ray following the Tm^{170} decay are known[8] for the K, L, and M shells.

(4) The total conversion coefficients for the 84-kev and 80-kev γ rays are expected to be very similar since both are $E2$ transitions[2,3] with nearly the same energy in elements of similar Z.

We find $(N_{\beta-\gamma}/N_\beta)_{\text{Ho}}/(N_{\beta-\gamma}/N_\beta)_{\text{Tm}}=2.9$. After making a small correction for the difference in absorption in Lucite ($\sim$1 percent) of the soft γ radiation from the two sources and taking 24 percent as the β branch to the 84-kev excited state in Yb^{170}, we obtain 71 percent for the β branch to the 80-kev state in Er^{166}. This assumes that the quantity $(1+F_K\alpha_K)/(1+\alpha_T)$ is the same for both transitions. F_K denotes the K-shell fluorescent yield, α_K the K-shell conversion coefficient, and α_T the total conversion coefficient. Since this quantity is not expected to differ much for these transitions, we conclude that the agreement between the two methods is satisfactory and adopt (74 ± 3) percent as the value of the β branch to the 80-kev state in Er^{166}.

To obtain α_T for the 80-kev transition we have compared the Ho^{166} soft γ—hard γ coincidence rate per recorded hard γ ray with the Tm^{170} $\beta-\gamma$ coincidence rate per recorded β ray in identical geometry for detection of soft γ rays. We denote the soft γ counter geometry factor by Ω_γ, the Tm^{170} β branch by f_β, and the fraction of hard γ rays giving coincidences in the Ho^{166} source by f_γ. We assume unit intrinsic efficiency for detection of the low-energy γ and K radiation in our phosphor and for purposes of clarity neglect small differences ($\sim$1 percent) in absorption in Lucite for the Ho^{166} and Tm^{170} soft γ radiation. Then,

$$\left(\frac{N_{\beta-\gamma}}{N_\beta}\right)_{\text{Tm}}=f_\beta\Omega_\gamma\left(\frac{1+F_K\alpha_K}{1+\alpha_T}\right)_{\text{Tm}}$$

and

$$\left(\frac{N_{\gamma-\gamma}}{N_{\text{hard }\gamma}}\right)_{\text{Ho}}=f_\gamma\Omega_\gamma\left(\frac{1+F_K\alpha_K}{1+\alpha_T}\right)_{\text{Ho}}.$$

TABLE II. Conversion coefficients for the 80-kev γ ray in Er^{166} and the 84-kev γ ray in Yb^{170}.[a]

Isotope	E_γ (kev)	α_K	α_L	α_M	α_T
$_{68}Er^{166}$	80.8	1.9±0.2	$\alpha_{L+M}=5.7\pm1.5$		7.6±1.5
$_{70}Yb^{170}$	84.1	1.6±0.15	4.1±0.5	1.2±0.2	6.9±0.6

[a] The Yb^{170} measurements are taken from reference 8.

[8] Graham, Wolfson, and Bell, Can. J. Phys. **30**, 459 (1952).

Finally,

$$(1+\alpha_T)_{Ho}=\frac{f_\gamma}{f_\beta}\left(\frac{N_{\beta-\gamma}}{N_\beta}\right)_{Tm}\left(\frac{N_{\text{hard }\gamma}}{N_{\gamma-\gamma}}\right)_{Ho}\times\frac{(1+F_K\alpha_K)_{Ho}}{(1+F_K\alpha_K)_{Tm}}(1+\alpha_T)_{Tm}.$$

We take $f_\beta=0.24$, $f_\gamma=0.92$, $F_K(Z=68)=0.922$, $F_K(Z=70)=0.93$, $(1+\alpha_T)_{Tm}=6.9$, $\alpha_K(Ho^{166})=1.9$, and $\alpha_K(Tm^{170})=1.6$. We find $\alpha_T=7.6\pm1.5$ for the 80-kev transition in Er^{166}. Thus $\alpha_K/\alpha_{L+M}=0.33\pm0.08$. The errors are estimated from consideration of the uncertainties in all factors entering into the determination. It may be noted here that if one takes an L/M ratio of ~3.5 as was found[8] for the Yb^{170} $E2$ transition, $\alpha_L\simeq4.5$. This agrees well with an estimate of $\sim(4.5-5)$ obtained by interpolation of the computations of Gellman, Griffith, and Stanley.[9] However, the inferred K/L ratio of 0.43 ± 0.12 is in disagreement with a previous determination.[10] Our conversion measurements for the 80-kev γ ray in Er^{166} and the measurements of Graham, Bell, and Wolfson[8] for the 84-kev γ ray in Yb^{170} are shown in Table II.

A decay scheme consistent with our data is shown in Fig. 3. The low-energy β branches are computed from the γ-ray intensity ratios, the total conversion coefficient of the 80-kev γ ray and the β branching to the ground state and first excited state of Er^{166}. The logft of ~8.4 for the ground-state transition is in the right range for a $\Delta I=2$ (yes) transition. The quantity $ft(W_0^2-1)\simeq0.5\times10^{10}$, in accord with most $\Delta I=2$ (yes) transitions. A spin of two and odd parity in accordance with Nordheim's rule[11] seems likely for the Ho^{166} ground state. A measurement of the shape of the ground-state β transition could of course decide this question.

It is interesting to note that in the case of Tm^{170}, for which an assignment of $1-$ has been made to the ground state,[8] the β-branching ratio between the $2+$ state and the $0+$ ground state of Yb^{170} is just reversed from that in $Ho^{166}\rightarrow Er^{166}$. The ratio of ft values in the Tm^{170} decay are in accord[12] with computations based on the collective nuclear model of Bohr and Mottelson[13] assuming a spin $1-$ for Tm^{170}, Gamow-Teller selection rules, and pure tensor coupling. Under such conditions a value of 2 is expected[12] for the ft ratio $[(1-)\rightarrow(2+)]/[(1-)\rightarrow(0+)]$. For Ho^{166} this ft ratio is ~0.2. Since the spin of Ho^{166} may be $2-$, the same ft ratio is not necessarily expected to hold. In any event, the Ho^{166} spin can be determined unambiguously by a measurement of the shape of the ground-state transition or by a direct-spin measurement. The parity is almost certainly odd from the ft values of the β transitions.

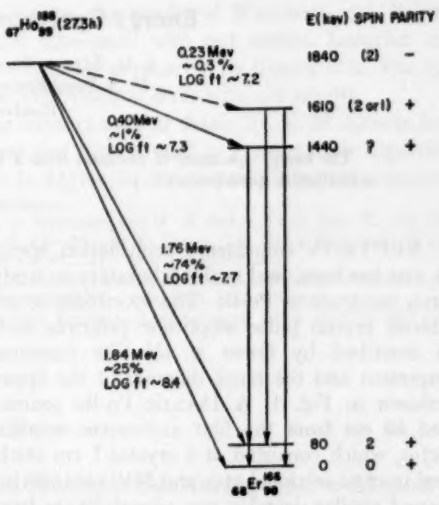

FIG. 3. Disintegration scheme for $Ho^{166}\xrightarrow{\beta-}Er^{166}$.

The spins of the excited states of Er^{166} at 1.44 Mev and 1.61 Mev cannot be stated with any degree of certainty. The parities of both states are probably even in view of the approximate ft values for the β transitions to these states. The fact that the 1.61-Mev state emits γ radiation to both the $0+$ ground state and $2+$ excited state of Er^{166} with comparable probability suggests that this spin may be $2+$ or $1+$. $\gamma-\gamma$ angular correlation measurements will be necessary to decide the spins of these more highly excited states of Er^{166}.

[9] Gellman, Griffith, and Stanley, Phys. Rev. **85**, 944 (1952).
[10] J. W. Mihelich and E. L. Church, Phys. Rev. **85**, 690 (1952).
[11] L. W. Nordheim, Revs. Modern Phys. **23**, 322 (1951).
[12] B. R. Mottelson (private communication).
[13] A. Bohr and B. R. Mottelson, Kgl. Danske Videnskab. Selskab Mat.-fys. Medd. **27**, No. 16 (1953).

Energy Spectrum of Neutrons from Po-Be

J. O. Elliot, W. I. McGarry, and W. R. Faust
U. S. Naval Research Laboratory, Washington, D. C.

(Received November 17, 1953)

The energy spectrum of neutrons from a Po-Be source has been observed by means of a coincidence scintillation spectrometer.

A NEUTRON coincidence scintillation spectrometer has been used in this laboratory to study the neutron spectrum of Po-Be. The spectrometer utilizes the recoil proton pulse amplitude principle and has been described by Owen *et al.*[1] The experimental arrangement and the block diagram of the apparatus are shown in Fig. 1. A 15-curie Po-Be source was placed 40 cm from the first anthracene scintillation detector, which consisted of a crystal 1 cm thick and 16 cm² in cross-sectional area and 5819 photomultiplier. A second similar detector was placed 50 cm from the first at a laboratory scattering angle of 60°. Pulse-height analysis was performed upon the signals from the first detector, and signals from the two detectors placed in coincidence defined the angle of scattering by supplying a triggering pulse to the electronic analyzer. Suitable delays were inserted in the first channel of the coincidence circuit to compensate for the neutron time-of-flight between the two detectors.

Energy calibration of the instrument was accomplished by comparing the pulse height produced by protons with the pulse height produced by internal conversion electrons of Cs^{137}. Data obtained by Taylor *et al.*[2] for anthracene were then used to convert proton pulse height into energy.

Owen has described the energy dependence of the efficiency of this type of spectrometer in terms of the n-p cross-section of the crystals and the coincidence circuit discrimination against small pulses arising in the second crystal as the result of proton recoils occurring at all possible angles. The cutoff due to the coincidence circuit was approximated by obtaining an upper bound for the effect. A linear extrapolation to zero counting rate at the low-energy end of the spectrum provided this upper bound and gave the cut-off energy as 0.6 Mev. In the present analysis additional energy-dependent corrections were introduced to account for the attenuation of the primary beam in the first crystal and the attenuation of the scattered beam in escaping the first crystal and entering the second crystal.

The differential counting rate data obtained were treated using the above corrections. The resulting neutron spectrum is shown in Fig. 2; the vertical bars indicate the probable errors in the mean, and the horizontal bars indicate the electronic channel widths used in the experiment. Two possible distortions in the spectrum result from the detection of the Po-Be gamma rays and from neutron reactions with the carbon in the anthracene detectors. The 4.45-Mev gamma ray[3] of Po-Be detected by the Compton effect would apparently alter the neutron spectrum near 9.96 Mev. However, two experimental arrangements tend to suppress this distortion. The delay which was inserted in the first coincidence channel to insure neutron coincidences acts together with the 15-millimicrosecond resolving time to suppress gamma coincidences. Also background data in this experiment were taken by inserting 40 cm of paraffin between the detectors while leaving the source in place; this procedure would tend to cancel in part the effect of the gamma rays. An energetically possible neutron reaction with the carbon content of the first

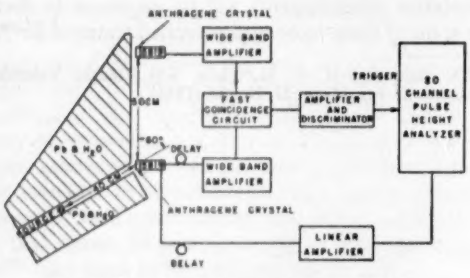

FIG. 1. Experimental arrangement and block diagram of the apparatus.

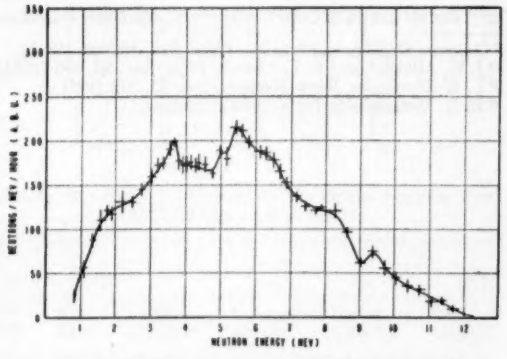

FIG. 2. Neutron spectrum of Po-Be as observed by coincidence spectrometer.

[1] Owen, Neiler, and Wheatley, Fast Neutron Spectrometer Project, Report No. 1, Radiation Laboratory, University of Pittsburgh, June, 1951 (unpublished).

[2] Taylor, Jentschke, Remley, Eby, and Kruger, Phys. Rev. 84, 1034 (1951).

[3] J. Terrell, Phys. Rev. 80, 1076 (1950).

anthracene crystal, which would also produce a coincident particle for the second detector, is $C^{12}(n,n)3\alpha$ having a threshold of 7.88 Mev as computed from the isotopic mass values.[4] It can be shown that such processes may distort the neutron spectrum below 1.3 Mev.

Various spectral distributions obtained for Po-Be neutrons have been reported in the literature.[5–10] Of these spectra the results of Whitmore and Baker are in good agreement with our results. Location of intensity maxima as reported by Gursky *et al.* also agrees within experimental error with our results.

The authors wish to thank Dr. E. H. Krause for his interest and support and to express their appreciation to W. L. Myers for aid in performing the experiment.

[4] E. Segrè, *Experimental Nuclear Physics* (John Wiley and Sons, Inc., New York, 1953), Vol. I.
[5] H. T. Richards, U. S. Atomic Energy Commission Report MDDC-1504, 1944 (unpublished).
[6] P. Demers, Report MP-74, National Research Council of Canada, Division of Atomic Energy, 1945 (unpublished).
[7] B. G. Whitmore and W. B. Baker, Phys. Rev. **78**, 799 (1950).
[8] B. R. Gossick and K. Henry, Oak Ridge National Laboratory Report ORNL-711, 1950 (unpublished).
[9] R. G. Cochran and K. M. Henry, Oak Ridge National Laboratory Report ORNL-1479, 1953 (unpublished).
[10] Gursky, Winnemore, and Cowan, Phys. Rev. **91**, 209 (1953).

PHYSICAL REVIEW VOLUME 93, NUMBER 6 MARCH 15, 1954

Some Possible Relationships between π-Meson Nucleon Scattering and π-Meson Production in Nucleon-Nucleon Collisions

A. Aitken and H. Mahmoud, *Indiana University, Bloomington, Indiana,*
E. M. Henley, *Columbia University, New York, New York,*
M. A. Ruderman, *University of California, Berkeley, California,*
and
K. M. Watson, *University of Wisconsin, Madison, Wisconsin*

(Received December 3, 1953)

For a reaction such as $p+p\rightarrow\pi^{+}+n+p$, it is known that the interaction of the emitted neutron and proton will frequently result in the formation of a deuteron. An analogous effect is that of the interaction of the π meson with either the neutron or the proton. This interaction is known to be strong from studies of meson-nucleon scattering. Explicit calculations are made, which indicate that pronounced qualitative effects may indeed result from the meson-nucleon interaction. In particular, the $p+p\rightarrow\pi^{+}$ cross section is expected to be considerably larger than is the $n+p\rightarrow\pi^{+}$ cross section.

I. INTRODUCTION

As is well known, there is an implication from strong coupling meson theory[1] that the state of the meson-nucleon system which has an isotopic spin of $\frac{3}{2}$ and a spin of $\frac{3}{2}$ [to be designated as the $(\frac{3}{2},\frac{3}{2})$ state] should be one of strong interaction. An analysis accepting this possibility for the pion-nucleon scattering[2] made by Brueckner[3] has led to a very reasonable qualitative explanation of the magnitudes of these cross sections. A field-theoretic calculation by Chew[4] has led to results in general agreement with these suggestions.

Further implications of a strong interaction in the $(\frac{3}{2},\frac{3}{2})$, state of the meson-nucleon system have been suggested[5] for photomeson production. These have been in not unreasonable agreement with observed[6] angular distributions and magnitudes of the cross sections.

The modest successes of these suggestions would seem to indicate that it is worth seeking further implications of the hypothesized strong $(\frac{3}{2},\frac{3}{2})$ interaction. In this connection two suggestions have been made in respect to pion production in nucleon-nucleon collisions. The first of these[5] concerned the reactions

$$p+p\rightarrow\pi^{+}+d, \tag{A}$$

$$p+p\rightarrow\pi^{+}+n+p. \tag{A'}$$

To a first approximation, the angular distribution in the rest system and near the energetic threshold should be of the form

$$1+3\cos^{2}\theta,$$

where θ is the angle between the meson momentum vector and that of one of the incident protons. This is in rough agreement with measured cross sections.[7] The second suggestion in this connection[8] was that for the

[1] W. Pauli and S. Dancoff, Phys. Rev. **62**, 85 (1942).
[2] Anderson, Fermi, Martin, and Nagle, Phys. Rev. **91**, 155 (1953).
[3] K. A. Brueckner, Phys. Rev. **86**, 106 (1952).
[4] G. F. Chew, Phys. Rev. **89**, 591 (1953).
[5] K. A. Brueckner and K. M. Watson, Phys. Rev. **86**, 923 (1952). B. T. Feld, Phys. Rev. **89**, 330 (1953); S. Matsuyama and H. Miyazawa, Prog. Theoret. Phys. (Japan) **8**, 141 (1952).
[6] A. Silverman and M. Sterns, Phys. Rev. **88**, 1228 (1952); G. Cocconi and A. Silverman, Phys. Rev. **88**, 1230 (1952); Goldschmidt-Clermont, Osborne, and Scott, Phys. Rev. **89**, 329 (1953); Walker, Oakley, and Tollestrup, Phys. Rev. **89**, 1301 (1953).
[7] Cartwright, Richman, Whitehead, and Wilcox, Phys. Rev. **91**, 677 (1953).
[8] M. A. Ruderman, Phys. Rev. **88**, 1427 (1952).

reactions

$$n+p\rightarrow\pi^{+}+n+n, \quad \text{(B)}$$

$$n+p\rightarrow\pi^{-}+p+p, \quad \text{(B')}$$

the $(\frac{3}{2},\frac{3}{2})$ state of the meson with respect to either nucleon is expected to be inhibited near energetic threshold because of angular momentum and parity considerations.[9] This might be expected to lead to qualitative differences between these and reactions (A) and (A'). Indeed, a study of pion production from the bombardment of deuterons by protons[10] suggests that the ratio of cross sections (A) and (A') to the cross sections (B) or (B') may be as great as 20:1 (see reference 8). In any case, the cross sections (B) and (B') (these are expected by charge symmetry to be equal, except for Coulomb effects) are subject to direct measurement, although this does not seem to have been done as yet.

The above suggestions concerning the role played by the $(\frac{3}{2},\frac{3}{2})$ state in pion production by nucleon collisions were purely qualitative, there being no explicit calculations. The purpose of the present note is to present such a calculation much along the lines of that of Chew[4] for the pion-nucleon scattering. This analysis will fall into the general category known as the "Tamm-Dancoff" method and will be carried out along specific lines recently suggested.[11]

The results do, indeed, bear out the expected qualitative features, both as to the angular distributions and the magnitudes of the cross sections. The approximate cross sections are summarized in Eqs. (46) and Fig. 3.

II. CALCULATION OF THE SCATTERING AMPLITUDE

It is clearly impossible at present to make any calculation in meson field theory which can strictly be termed "quantitative." On the other hand, semiquantitative and qualitative field theoretic analyses have been of considerable use in the planning and analyzing of experiments. It is in the spirit of this latter category that the present work is presented.

Various perturbation calculations[12] of the nuclear production of mesons have been made. These have been in "order of magnitude" agreement with the observed cross sections and their dependence upon energy. Among the perturbation transitions is one which describes the emission of a meson by one nucleon, which is then "scattered" by the second nucleon before finding itself "free." We shall treat this "scattering" by the Tamm-Dancoff method along the lines used by Chew.[4] Aside from this, the calculation will be simply a third order (i.e., lowest order) perturbation calculation, except for our treatment of the nuclear force between the nucleons.

In the subsequent analysis we shall, for instance, (1) neglect multiple meson exchanges between the two nucleons; (2) treat all but the meson scattering in the $(\frac{3}{2},\frac{3}{2})$ state as a weak perturbation; (3) neglect radiative corrections; (4) treat the nucleons nonrelativistically and neglect their recoil except where this is most obviously unreasonable.

Our primary justification for such arbitrary omissions is that it seems difficult, if not impossible, to make a completely consistent calculation of any one of these effects. Consequently, we shall concentrate only on the "final scattering" of this emitted meson, which provides the motivation for the present work. Neglect of effects (1) and (3) above did not seem to change the qualitative features of the calculation in an analysis of the low-energy nuclear forces.[13] The approximation (2) would not seem to change Chew's conclusions in a qualitative manner. Finally, one can probably justify the neglect of nucleon recoil in a theory which cuts off momentum space integrals at sufficiently low values.

A. Formulation of the Problem

We suppose the Hamiltonian describing the meson-nucleonic system to be

$$H=H_0+H', \quad (1)$$

where H_0 is the energy of the noninteracting mesons and nucleons and

$$H'=h_1+h_2, \quad (2)$$

with

$$h_1=\frac{g}{2M}[\boldsymbol{\sigma}^{(1)}\cdot\nabla_1\boldsymbol{\phi}(\mathbf{z}_1)\cdot\boldsymbol{\tau}^{(1)}],$$

$$h_2=\frac{g}{2M}[\boldsymbol{\sigma}^{(2)}\cdot\nabla_2\boldsymbol{\phi}(\mathbf{z}_2)\cdot\boldsymbol{\tau}^{(2)}]. \quad (3)$$

M is the nucleonic mass, $\mathbf{z}_1$ and $\mathbf{z}_2$ are the space coordinates of the two nucelons and the $\boldsymbol{\sigma}$'s and $\boldsymbol{\tau}$'s are their respective spin and isotopic spin operators. We may suppose Eqs. (3) to have been derived from the pseudoscalar coupling term by the Dyson[14] transformation, if we care to consider the higher-order terms as negligible.[15]

The process to be considered is that in which the two nucleons with respective momenta $\mathbf{p}_1$ and $\mathbf{p}_2$ collide to produce a meson with momentum $\mathbf{q}$, leaving the two nucleons with final momenta $\mathbf{p}_1'$, and $\mathbf{p}_2'$. It will be convenient to consider the process in the rest system:

$$\mathbf{p}_1+\mathbf{p}_2=0, \quad \text{or} \quad \mathbf{p}_1\equiv\mathbf{p}=-\mathbf{p}_2, \quad (4)$$

$$\mathbf{p}_1'+\mathbf{p}_2'+\mathbf{q}=0. \quad (5)$$

[9] This is because the final nucleons are expected to be primarily in a ^1S state and the meson in a P state with respect to these. Consequently, the initial state must be an admixture of $^3S_1$ and $^3D_1$, or an isotopic spin zero state. However a final state of total isotopic spin zero cannot be formed if the meson forms a state of isotopic spin $\frac{3}{2}$ with either nucleon.

[10] Passman, Bloch, and Havens, Phys. Rev. 85, 370 (1952); J. Carothers and C. Andrè, Phys. Rev. 88, 1426 (1952).

[11] K. Brueckner and K. Watson, Phys. Rev. 90, 699 (1953).

[12] K. Brueckner, Phys. Rev. 82, 598 (1951).

[13] K. Brueckner and K. Watson, Phys. Rev. 92, 1023 (1953).

[14] F. J. Dyson, Phys. Rev. 73, 929 (1948).

[15] See, for instance, Brueckner, Gell-Mann, and Goldberger, Phys. Rev. 90, 476 (1953).

The relative momentum of the two nucleons in the final state is

$$\mathbf{p}'=\tfrac{1}{2}(\mathbf{p}_1'-\mathbf{p}_2'). \tag{6}$$

$\mathbf{q}$ will be taken as the relative momentum of the meson with respect to the center of mass of the two nucleons. (We shall consistently drop terms of relative order $\mu/2M$, where μ is the rest mass of the meson.)

The total energy of the system is

$$E_a=p^2/M, \tag{7}$$

and we shall suppose this to be sufficiently near the energetic threshold that terms of relative order $(E_a-\mu c^2)/\mu c^2$ can be neglected.

Following the notation of Brueckner and Watson[11] we define

$$a\equiv E_a+i\eta-H_0, \tag{8}$$

where η is an infinitesimal positive parameter. The part of the Møller wave matrix which describes meson production is

$$\Omega_p=\Omega_s(1/a)H', \tag{9}$$

where Ω_s is diagonal in particle occupation numbers and H' produces a meson [see Eq. (28) of reference 11]. We may describe Eq. (9) by saying that H' produces the meson, after which Ω_s scatters the meson and the two nucleons into the final observed state. Equation (9) is formally exact if Ω_s satisfies the Lippmann-Schwinger equation:

$$\Omega_s=1+(1/a)\mathcal{U}\Omega_s, \tag{10}$$

where $\mathcal{U}$ is the interaction potential between the three particles.

There will be contained in $\mathcal{U}$ the nuclear force interaction V_N between the two nucleons.[16] We define the remainder of $\mathcal{U}$ to be v by the equation

$$\mathcal{U}\equiv V_N+v. \tag{11}$$

By means of a little algebraic manipulation we can rewrite Eq. (9) as

$$\Omega_p=\frac{1}{a-\mathcal{U}}H'=\frac{1}{a}w^{(-)\dagger}\left[1+v\frac{1}{a-V_N-v}\right]H'. \tag{12}$$

$w^{(-)\dagger}$ satisfies the Lippmann-Schwinger equation:

$$w^{(-)\dagger}=1+w^{(-)\dagger}V_N\,1/a, \tag{13}$$

and so describes the scattering of the two nucleons in the final state. Indeed, if we define the final state nuclear wave function to be[17]

$$\phi^{(-)}=w^{(-)}\chi_{p'},$$

with

$$\chi_{p'}=(2\pi)^{-\frac{3}{2}}\exp\{i\mathbf{p}'\cdot(\mathbf{z}_1-\mathbf{z}_2)\}, \tag{14}$$

then $\phi^{(-)}$ satisfies the Schrödinger equation (in a momentum representation):

$$\left[\frac{l^2}{M}-\frac{p'^2}{M}\right]\phi^{(-)}(l)=-\int V_N(\mathbf{l},\mathbf{l}')\phi^{(-)}(l')d^3l'. \tag{15}$$

We designate the plane wave function for the relative motion of the incoming nucleons and the outgoing meson by χ_p and χ_q, respectively. The coefficient of $1/a$ in Eq. (12) is the transition matrix T. For our process this is then:

$$T=\left(\phi^{(-)}\chi_q,\left[1+v\frac{1}{a-V_N-v}\right]H'\chi_p\right). \tag{16}$$

Although this has been derived only when $\phi^{(-)}$ describes a scattering state of the two nucleons, the result is easily seen to hold when they are bound to form a deuteron.[18] In this case, $\phi^{(-)}$ is just the deuteron wave function.

To simplify Eq. (16), we consider the term

$$\begin{aligned}(\phi^{(-)}\chi_q,H'\chi_p)&=\phi^{(-)}(\mathbf{p}\pm\mathbf{q})(\mathbf{q},\mathbf{p}\pm\mathbf{q}\,|\,H'\,|\,\mathbf{p})\\&\simeq\phi^{(-)}(\mathbf{p})(\mathbf{q},\mathbf{p}\pm\mathbf{q}\,|\,H'\,|\,\mathbf{p}).\end{aligned} \tag{17}$$

Now for $p'^2/M\ll p^2/M$, it is reasonable to neglect the l' in V_N in Eq. (15)[19] and to write that equation as

$$\begin{aligned}\frac{p^2}{M}\phi(p)&\simeq-V_N(p)\int\phi(l')d^3l'\\&=-V_N(p)(2\pi)^{\frac{3}{2}}\Phi_0.\end{aligned} \tag{18}$$

where Φ_0 is the value of ϕ in a coordinate representation evaluated for $\mathbf{z}_1=\mathbf{z}_2$. Then,

$$\begin{aligned}\phi(p)&\simeq(2\pi)^{\frac{3}{2}}\Phi_0\left[-V_N\Big/\frac{p^2}{M}\right]\\&\simeq(2\pi)^{\frac{3}{2}}\Phi_0V_N(1/a).\end{aligned} \tag{19}$$

The last step is seen to be approximately valid near threshold when substituted into Eq. (17). A similar argument for the remainder of Eq. (16) leads to[19]

$$T\simeq(2\pi)^{\frac{3}{2}}\Phi_0\left(\chi_{p'}\chi_q,\left[V_N\frac{1}{a}+v\frac{1}{a-V_N-v}\right]H'\chi_p\right), \tag{20}$$

where p' is considered to be negligibly small. The values of Φ_0 appropriate to our problem have been considered previously in detail.[19]

The potential v in Eq. (20) will be evaluated to order

[16] More specifically, we may consider V_N to be that part of $\mathcal{U}$ which introduces momentum transfers between the nucleons, but is diagonal in the momentum of the meson.

[17] We suppose the fact that $w^{(-)\dagger}$ is to be operating on the wave function of a meson of momentum $\mathbf{q}$ to have been taken into account in eliminating the meson field variables from H_0 in $w^{(-)\dagger}$.

[18] See N. C. Francis and K. M. Watson, Phys. Rev. **93**, 313 (1954). Here the same formal problem was considered in connection with the deuteron stripping reaction.

[19] The separation of the final state interaction of the two nucleons has been much discussed [see, for instance, K. M. Watson, Phys. Rev. **88**, 1163 (1952)]. Our purpose at present is not to repeat the detailed physical arguments, but to show how this arises in a consistent field-theoretic treatment of the problem.

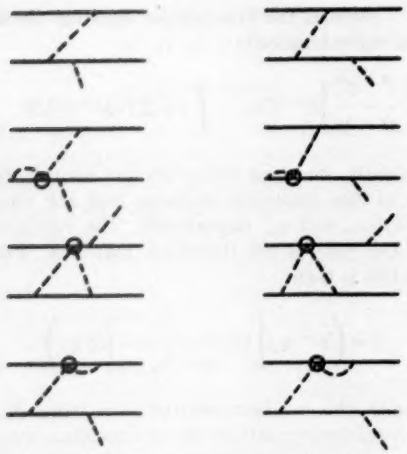

FIG. 1. Some typical processes arising in connection with the first term in expression (23). Heavy lines represent nucleons, dotted lines mesons. Time is considered to be increasing to the right.

g^2 only. From reference 11 and Eq. (3), we have

$$v=v^{(1)}+v^{(2)}+v^{(3)}+v^{(4)}, \tag{21}$$

where the superscripts $(+)$ or $(-)$ designate the matrix elements of h which create or absorb one meson, respectively,

$$\begin{aligned}
v^{(1)}&=h_1^{(-)}\frac{1}{a}h_2^{(+)}+h_2^{(-)}\frac{1}{a}h_1^{(+)},\\
v^{(2)}&=h_1^{(-)}\frac{1}{a}h_1^{(+)}+h_2^{(-)}\frac{1}{a}h_2^{(+)},\\
v^{(3)}&=h_1^{(+)}\frac{1}{a}h_1^{(-)}+h_2^{(+)}\frac{1}{a}h_2^{(-)},\\
v^{(4)}&=h_1^{(+)}\frac{1}{a}h_2^{(-)}+h_2^{(+)}\frac{1}{a}h_1^{(-)}.
\end{aligned} \tag{22}$$

We have already included in V_N that part of $v^{(1)}$ which refers to emission and absorption of the *same* meson and so must omit this from the definition of $v^{(1)}$ above.

In accordance with the approximation (1) described at the beginning of this section we shall neglect the V_N in the denominator of Eq. (20). That in the numerator will be included only to order g^2, and so is obtainable from the expression written for $v^{(1)}$ in Eq. (22). A further consequence of our assumption that many meson exchanges between the nucleons are to be neglected is that $v^{(1)}$ and $v^{(4)}$ may be treated as small perturbations. Thus we must consider T [Eq. (20)]:

$$[v^{(1)}+v^{(4)}]\frac{1}{a-v^{(2)}-v^{(3)}}+[v^{(2)}+v^{(3)}]\frac{1}{a-v^{(2)}-v^{(3)}}. \tag{23}$$

Now, $v^{(2)}+v^{(3)}$ is the interaction for scattering a meson by either of the two nucleons (except for some renormalization effects). We may thus write

$$\frac{1}{a-v^{(2)}-v^{(3)}}=\frac{1}{a}+\frac{1}{a}t_s\frac{1}{a},$$

where t_s is the scattering matrix for the meson from the two nucleons. As we are to neglect multiple scattering,[20] t_s is the sum of amplitudes for scattering from the individual nucleons. The types of transitions resulting from the first term in expression (23) are indicated in Fig. 1. (The interaction t_s is represented by an intersecting meson and nucleon line with a circle drawn through the point of intersection). The corrections involving t_s are seen to involve either multiple meson exchanges between the nucleons or radiative corrections to the upper diagram, both of which we are ignoring.

We also note that $v^{(3)}$ contributes to meson-nucleon scattering only in the $J=\frac{1}{2}$, $J=\frac{1}{2}$ [i.e., $(\frac{1}{2},\frac{1}{2})$] state and so may be treated as a perturbation by the assumptions made at the beginning of this section. Then the second term in expression (23) is

$$v^{(3)}\frac{1}{a-v^{(2)}}+v^{(2)}\frac{1}{a-v^{(2)}}.$$

Now the $v^{(2)}$ in the denominator of the first term may be neglected for the same reason: this term is nonvanishing only in the $(\frac{1}{2},\frac{1}{2})$ scattering state. But this state is to be treated by perturbation theory, so the $v^{(2)}$ can be neglected.

We finally summarize the above arguments by rewriting Eq. (20) as

$$T=(2\pi)^{\frac{1}{2}}\Phi_0\left(\chi_p\chi_q,\left[(V_N+v^{(1)}+v^{(3)}+v^{(4)})\frac{1}{a}+v^{(2)}\frac{1}{a-v^{(2)}}\right]H'\chi_p\right). \tag{24}$$

Were we to drop the $v^{(2)}$ in the denominator of the last last term we would arrive at the perturbation expression used by Brueckner,[12] except that he did not give a field theoretic justification for his use of Φ_0. The term $v^{(2)}[1/(a-v^{(2)})]$ may be written as $t(1/a)$, where

$$t=v^{(2)}+v^{(2)}(1/a)t \tag{25}$$

is the Lippmann-Schwinger integral equation for the scattering matrix t. Equation (25) is to be resolved into four equations for the four substates of spin and isotopic spin for the scattering of a meson from either nucleon. By assumption (2) we set $t=v^{(2)}$ for all but the $(\frac{3}{2},\frac{3}{2})$ state.

[20] K. Watson, Phys. Rev. 89, 575 (1953).

Equation (24) is then expressed as

$$T=(2\pi)^{\frac{1}{2}}\Phi_0\Big(\chi_p'\chi_q,\ \times[V_N+v^{(1)}+v^{(3)}+v^{(4)}+t]\frac{1}{a}H'\chi_p\Big). \quad (26)$$

It must be admitted that it is not easy to justify neglecting the terms which were omitted in obtaining Eq. (26) from Eq. (20). However, we are interested in what is essentially a qualitative feature of the cross sections. Equation (26) permits us to develop this point [the effect of the scattering of the emitted meson in the $(\frac{3}{2},\frac{3}{2})$ state] without obscuring the result with questionable and detailed calculations of correction terms. Whether or not these may predominate over the effects included in our calculations may, perhaps, best be answered by experiment.

B. Evaluation of the Matrix t

The evaluation of Eq. (26) is the same as that of Brueckner[12] except for the treatment of t as the solution to Eq. (25). We shall consequently discuss only the determination of t.

The potential $v^{(2)}$ is

$$v^{(2)}=v_1^{(2)}+v_2^{(2)}, \quad (27)$$

where $v_1^{(2)}$ is the interaction for scattering the meson by nucleon "1", etc. As we are neglecting multiple meson exchanges, we write

$$t=t_1+t_2, \quad (28)$$

where

$$t_1=v_1^{(2)}+v_1^{(2)}(1/a)t_1, \quad (29)$$

with a corresponding equation for t_2 in terms of $v_2^{(2)}$.

The potentials $v_1^{(2)}$ and $v_2^{(2)}$ have been given by Brueckner and Watson[13] as

$$(\mathbf{k}'|v_1^{(2)}|\mathbf{k})=\lambda\frac{k'k}{(\omega_{k'}\omega_k)^{\frac{1}{2}}}[E_a+i\eta-\omega_{k'}-\omega_k]^{-1}$$
$$\times\{E_1F_1-\tfrac{1}{2}E_1F_3-\tfrac{1}{2}E_3F_1+\tfrac{1}{4}E_3F_3\}, \quad (30)$$

etc. Here $\omega_k=[\mu^2+k^2]^{\frac{1}{2}}$, etc., the E_I's and F_J's are projection operators for the substates of isotopic spin and angular momentum.[13] Also

$$\lambda\equiv\left(\frac{g^2}{4\pi}\right)\frac{1}{3\pi}\frac{1}{M^2}. \quad (31)$$

We can express the scattering matrices t_1 and t_2 as

$$t_1=t_1(\tfrac{3}{2}\tfrac{3}{2})E_3F_3+t_1(\tfrac{3}{2}\tfrac{1}{2})E_3F_1$$
$$+t_1(\tfrac{1}{2}\tfrac{3}{2})E_1F_3+t_1(\tfrac{1}{2}\tfrac{1}{2})E_1F_1, \quad (32)$$

with a similar expression for t_2, the scattering from nucleon "2". The integral equation (29) for $t_1(\frac{3}{2}\frac{3}{2})$ is (the nucleon recoil energy is dropped from this equation):

$$(k'|t_1(\tfrac{3}{2}\tfrac{3}{2})|k^0)=\lambda\frac{k'k^0}{(\omega_{k'}\omega_{k^0})^{\frac{1}{2}}}[E_a-\omega_{k'}-\omega_{k^0}]^{-1}$$
$$+\lambda\int\frac{k'k}{(\omega_{k'}\omega_k)^{\frac{1}{2}}}\frac{k^2dk}{[E_a-\omega_{k'}-\omega_k][E_a+i\eta-\omega_k]}$$
$$\times(k|t_1(\tfrac{3}{2}\tfrac{3}{2})|k^0), \quad (33)$$

using the expression (30) for the potential. Before attempting to solve this equation we observe the approximate magnitudes of the momentum variables. Reference to Fig. 2 indicates that the initial meson momentum $\mathbf{k}^0$ is

$$\mathbf{k}^0\simeq\pm\mathbf{p}, \quad (34)$$

the initial nucleon momentum, since the nucleons are brought to rest in a first approximation by the event under consideration.

The final meson momentum $\mathbf{k}'$ is just:

$$\mathbf{k}'=\mathbf{q}. \quad (35)$$

Thus,

$$\omega_{k'}\simeq p\simeq(M\mu)^{\frac{1}{2}}. \quad (36)$$

The integral in Eq. (33) is assumed to be cut off at a value

$$k=k_c\simeq M. \quad (37)$$

We now attempt to solve Eq. (33) with a trial function of the form

$$(k'|t_1(\tfrac{3}{2}\tfrac{3}{2})|k^0)=-\lambda\Delta\frac{k'k^0}{(\omega_{k'}\omega_{k^0})^{\frac{1}{2}}}\times\begin{cases}\dfrac{1}{\omega_{k^0}} & \text{for } \omega_{k^0}>\omega_k\\ \dfrac{1}{\omega_k} & \text{for } \omega_{k^0}<\omega_k\end{cases} \quad (38)$$

where Δ is a constant to be determined. We substitute this into Eq. (33) and evaluate the integral, keeping in mind the magnitudes of the parameters of Eqs. (34)–(37). If we keep only the leading term proportional to k_c in the integral [this implies an error of the order of 20 percent according to Eq. (37)], we obtain the following algebraic equation for Δ:

$$\Delta=1+\Delta\lambda\omega_{k^0}k_c, \quad (39)$$

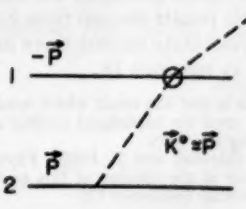

FIG. 2. Diagrammatic representation of the term $t_1(1/a)h_2^{(+)}$ in the transition operator T [Eq. (26)]. The scattering matrix t_1 is represented by a circle. Momenta are indicated, the final nucleons being nearly brought to rest by the event.

or

$$\Delta=\left[1-\frac{g^2}{4\pi}\frac{1}{3\pi}\left(\frac{\mu}{M}\right)^{\frac{1}{2}}\frac{k_0}{M}\right]^{-1}, \tag{40}$$

by Eqs. (31) and (36). In evaluating the integral in Eq. (33) we have dropped an imaginary term which is negligible for our purposes, but which prevents Eq. (40) from becoming infinite.

We finally obtain[21]

$$(q|t_1(\tfrac{3}{2}\tfrac{3}{2})|p)\simeq-\left[\frac{g^2}{4\pi}\frac{1}{3\pi}\frac{q}{M^2\mu}\right]\left(\frac{\mu}{M}\right)^{\frac{1}{2}}\Delta. \tag{41}$$

The other submatrices t of Eq. (32) are easily obtained in first Born approximation from Eq. (30). The evaluation of the remainder of Eq. (26) has been given several times in the literature[12] and will not be repeated here.

III. THE CROSS SECTIONS

The differential cross sections are obtained from Eq. (26) as

$$d\sigma=(2\pi)^4\frac{dJ}{v_r}S|T|^2. \tag{42}$$

Here S is the appropriate sum and average over final and initial spin substates and v_r is the relative velocity of the colliding nucleons; dJ is the volume in momentum space available to the particles in the final state. For a final state containing a deuteron and a pion of momentum $\mathbf{q}$:

$$dJ\simeq q\mu d\Omega, \tag{43}$$

where $d\Omega$ is the solid angle into which $\mathbf{q}$ is directed. For a final state in which the nucleons are not bound,

$$dJ\simeq\frac{(\mu M)^{\frac{1}{2}}}{\sqrt{2}}[T_k(T_0-T_k)]^{\frac{1}{2}}dT_k d\Omega d\Omega_{p'}. \tag{44}$$

In this equation T_k is the kinetic energy of the meson, T_0 is its maximum energy, and $d\Omega_{p'}$ is the solid angle into which the nucleonic relative momentum $\mathbf{p}'$ is directed.

We shall here present the cross sections in the Marshak-Foldy[22] approximation. This involves dropping terms with somewhat larger energy denominators than those which are kept [according to Brueckner's arguments in reference 12 this may involve errors of the order of 20 percent in T as defined by Eq. (26)]. This approximation is reasonable for the magnitudes of the cross sections, but is dangerous for a discussion of angular distributions. In the Appendix we present the complete results derived from Eq. (26). The evaluation of the final state nuclear wave function Φ_0 has been discussed in reference 18.

[21] This is just the result which would also have been obtained had we used the variational method used by Chew (reference 4) in solving Eq. (33).

[22] R. Marshak and L. Foldy, Phys. Rev. 75, 1493 (1949). A discussion of the relation of this to field theory has been given by Brueckner (reference 12).

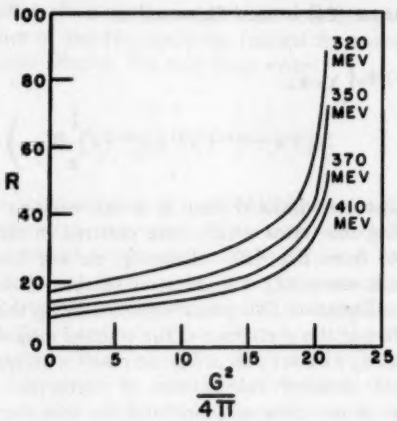

FIG. 3. The ratio R of Eq. (47) is plotted against the coupling constant for several values of the nucleon bombarding energy (in the laboratory system).

If we define

$$\sigma_0\equiv 2\pi\left(\frac{g^2}{4\pi}\right)^3\left(\frac{\mu}{M}\right)^{\frac{1}{2}}\frac{1}{M^2}, \tag{45}$$

the total cross sections are approximately[23]

$$\begin{aligned}
&\sigma[p+p\to\pi^++d]\\
&\quad=\sigma_0\left[\frac{\gamma/M}{1-r_0\gamma}\right]\left(\frac{q}{\mu}\right)^3\left[1+\frac{4}{9}\left(\frac{\mu}{M}\right)^{\frac{1}{2}}\Delta\right]^2,\\
&\sigma[p+p\to\pi^++n+p]\\
&\quad=\frac{3\sqrt{2}}{8}\sigma_0\left[\frac{T_0^2}{\mu M}\right]\left(\frac{M}{\mu}\right)^{\frac{1}{2}}\left[1+\frac{4}{9}\left(\frac{\mu}{M}\right)^{\frac{1}{2}}\Delta\right]^2,\\
&\sigma[n+p\to\pi^++n+n]=\frac{3\sqrt{2}}{16}\sigma_0\left[\frac{T_0^2}{\mu M}\right]\left(\frac{M}{\mu}\right)^{\frac{1}{2}}.
\end{aligned} \tag{46}$$

Here $\gamma=(M\times\text{deuteron binding energy})^{\frac{1}{2}}$ and r_0 is the ^3S-state effective range for low-energy $n-p$ scattering. Δ is given by Eq. (40) and represents the effect of the scattering of the meson in the $(\frac{3}{2}\frac{3}{2})$ state as indicated in Fig. 2.

The energy spectrum of the mesons is given in reference 19. The angular distribution of the mesons is, in the Marshak-Foldy approximation from which Eq. (46) has been obtained, $1+3\cos^2\theta$, where θ is the angle between $\mathbf{q}$ and $\mathbf{p}$. This angular distribution is not to be taken seriously for the $n+p\to\pi^++n+n$ process, as is

[23] The T_0^3 energy dependence (rather than a T_0^5 dependence) for the last two cross sections in Eq. (46) is due to the strong interaction between the outgoing nucleons. The differential cross section to be integrated has the form of Eq. (47) of reference 19. Equation (46) represents a sufficient approximation to this integral. A common normalization factor for the three Eqs. (46) has also been approximated. That is, the evaluation of Φ_0 in Eq. (26) has been done as in reference 19 with the $[f(r)]^{-1}$ of Eq. (44) in reference 19 replaced by the "impact parameter" $(M\mu)^{\frac{1}{2}}$.

indicated in the Appendix. However, if Δ is large the angular distribution is of this form on the basis of symmetry arguments only.[5]

The ratio,

$$R=\frac{\sigma[p+p\rightarrow\pi^{+}+d]+\sigma[p+p\rightarrow\pi^{+}+n+p]}{\rho[n+p\rightarrow\pi^{+}+n+n]}, \quad (47)$$

is plotted in Fig. 3 for several values of the total energy in the (laboratory system) as a function of $g^2/4\pi$. For a cutoff $k_c=M$, both the meson-nucleon scattering and the low energy nuclear forces are fitted by $g^2/4\pi\simeq 15-18$. Reference to Fig. 3 indicates that for an energy of 340 Mev (the energy of the Berkeley cyclotron) the ratio R may be of the order of 20 or 30 which is reasonable.[8]

Since the R *versus* $g^2/4\pi$ curve is rather steep in this region, it is difficult to accept the numerical values too literally. On the other hand, observation of an experimental ratio of R which is clearly larger than would be expected on the basis of deuteron formation alone[24] might be interpreted as giving an indication that the strong meson-nucleon interaction in the $(\frac{3}{2},\frac{3}{2})$, state does play an important role in the $p+p\rightarrow\pi^{+}$ reaction. A measurement of the energy variation of R might also provide a reasonable test of the present theory, since this predicts that R should vary only with the relative probability for deuteron formation at various energies near threshold.

IV. CONCLUSIONS

Although our calculations have depended on the rather specific form of meson field theory, it is likely that the role played by the meson scattering in the final state has a more general validity. Indeed, this effect seems to be analogous to the interaction of the neutron and the proton in the reaction,

$$p+p\rightarrow\pi^{+}+n+p,$$

by which a deuteron is formed. This is to a certain extent suggested by the appearance of t in Eq. (26). We have not, however, been able to find a satisfactory general formulation of this effect and so present the calculation given above.

Rough estimates of the energy dependence of Δ seem to indicate Δ should increase with energy and thus may be larger than its value at the energetic threshold, as given by Eq. (40).

[24] This effect is approximately indicated in Fig. 3 by the value of R for $g^2/4\pi=0$.

The differential cross section for the reactions,

$$n+p\rightarrow\pi^{0}+n+p$$
$$\rightarrow\pi^{0}+d,$$

need not be calculated, since they can be obtained from Eqs. (46) using charge-independence arguments.[25]

APPENDIX

The angular distribution of the meson as obtained from Eq. (26) are of the form

$$A+B\cos^2\theta. \quad (A-1)$$

For the reactions $p+p\rightarrow\pi^{+}$:

$$A=\left[1+\left(\frac{\mu}{M}\right)^{\frac{1}{2}}\left(\frac{4}{9}\Delta+\frac{5}{9}\right)\right]^2,$$

$$B=3\left[1+\left(\frac{\mu}{M}\right)^{\frac{1}{2}}\left(\frac{4}{9}\Delta+\frac{1}{18}\right)\right]\times\left[1+\left(\frac{\mu}{M}\right)^{\frac{1}{2}}\left(\frac{4}{9}\Delta-\frac{17}{18}\right)\right]. \quad (A-2)$$

For the reactions $n+p\rightarrow\pi^{+}$:

$$A=\left[1-\left(\frac{\mu}{M}\right)^{\frac{1}{2}}\right]^2,$$

$$B=3\left[1-\frac{4}{9}\left(\frac{\mu}{M}\right)^{\frac{1}{2}}\right]\left[1+\frac{2}{3}\left(\frac{\mu}{M}\right)^{\frac{1}{2}}\right]. \quad (A-3)$$

To obtain the approximation of Eqs. (46), we replace Eq. (A-2) by

$$\tfrac{1}{3}B=A=\left[1+\frac{4}{9}\Delta\left(\frac{\mu}{M}\right)^{\frac{1}{2}}\right]^2. \quad (A-4)$$

Equations (A-3) should be replaced by

$$A=1, \quad B=3. \quad (A-5)$$

The normalization of the differential cross sections can easily be obtained by comparison of these equations with Eqs. (46).

Note added in proof.—J. L. Gammel [Phys. Rev. (to be published)] has numerically integrated Eq. (33) on the Los Alamos MANIAC to find R [Eq. (47)]. With $(g^2/4\pi)$ chosen to fit the pion-nucleon scattering, he finds that $R\simeq 18$ for energies less than 380 Mev and increases appreciably for higher energies. We are indebted to Dr. Gammel for informing us of his work.

[25] K. Watson and K. Brueckner, Phys. Rev. 83, 1 (1951). See Eq. (21) of this reference.

A Cloud-Chamber Investigation of Nuclear Interactions of Cosmic Rays*

N. R. WHETTEN,† R. S. PRESTON, R. V. ADAMS,‡ R. M. WALKER, AND H. L. KRAYBILL
Yale University, New Haven Connecticut

(Received November 24, 1953)

A magnet cloud chamber recently constructed at Yale University was operated at mountain altitudes (Climax, Colorado, elev. 11 200 feet) during the late fall of 1952. The cloud chamber was electronically controlled to photograph penetrating shower events initiated by high-energy cosmic rays. Five examples of neutral V-particle decays have been observed. One photograph reveals the decay of two V_2^0 particles that probably originated in a single nuclear interaction.

Secondary particles in the penetrating showers have been examined for sign of charge. From the positive-to-negative ratio of charge of the secondary particles, it has been determined that 30 percent of the observed proton-plus-meson secondary particles are protons. This percentage is a lower limit, but is probably close to the actual value.

I. INTRODUCTION

IN recent years cloud chambers have been used[1–11] to determine properties of very high-energy nuclear interactions of cosmic rays. This article reports an investigation of nuclear interactions of high-energy cosmic rays carried out at mountain altitudes during the late fall of 1952. During the course of this study, five neutral V-particle decays have been observed. Secondary particles arising from observed high-energy nuclear interactions have been analyzed with respect to sign of charge. From the ratio of the number of positive-to-negative charges of the secondary penetrating particles, a proton-to-meson ratio has been determined for the observed secondary particles of high-energy nuclear interactions. Results are largely in agreement with conclusions of the sea-level cloud-chamber experiments of Rochester, Barker, Rosser, and Butler.[1–3]

II. THE MAGNET CLOUD CHAMBER

The magnet cloud chamber utilized in this experiment is a double chamber of the expansion type, composed of two separate chambers, each rectangular in cross section. The two chambers are separated by a $\frac{7}{8}$-inch gap. The gap may be used to accommodate a proportional counter to assist with the triggering arrangement, or may be used for easy insertion of absorbing material between the two chambers. The chamber walls are constructed of aluminum. Total illuminated dimensions of the double chamber are 25 cm×25 cm×8 cm in depth.

A strong magnetic field is provided across the chamber by a large six-ton electromagnet. The yoke of soft iron supports a large coil on each pole piece, and power is supplied by a 25-kva motor generator. The magnetic field strength across the chamber has been measured by three separate methods—with a flip coil and galvanometer arrangement, with measurements of the curvature of a current-bearing wire suspended in the magnetic field, and with a commercially available "fluxmeter," or rotating flip coil. The magnetic field strength was found to be 8200 oersted across the gap between the pole pieces, and to be homogeneous across the illuminated region of the cloud chamber to within plus or minus 5 percent.

Stereoscopic photographs of the cloud chamber are obtained with a single lens and camera system. In order to photograph along the direction of the magnetic field, and consequently to record the curvature of trajectories of particles traversing the magnetic field, a large hole was cut in the front pole piece. This hole, rectangular in cross section, is lined along two sides with aluminized mirrors. The lens and camera mounted in the hole photograph both mirror views of the chamber in addition to the direct view. The spatial representation of tracks may be determined by reprojecting the film image through an identical optical system, using the original lens. Photographs are recorded on 35-mm Linagraph Pan film, with a Baltar 40-mm, $f/2.3$ lens.

Illumination is provided with xenon-filled Edgerton-type flash tubes constructed in this laboratory. The flash tubes are constructed from Vycor tubing to withstand the intense heat of the discharge. Two flash tubes are discharged simultaneously, dissipating 800 joules each. Uniform illumination across the chamber

* This work was supported in part by the joint program of the U. S. Office of Naval Research and the U. S. Atomic Energy Commission.

† This paper is based on a dissertation by N.R.W. in partial fulfillment of the requirements for the degree of Doctor of Philosophy in Yale University. N.R.W. is now at General Electric Research Laboratory, Schenectady, New York.

‡ Now at Physics Department, Mt. Holyoke College, South Hadley, Massachusetts.

[1] G. D. Rochester and C. C. Butler, Proc. Phys. Soc. (London) **61**, 535 (1948).

[2] Butler, Rosser, and Barker, Proc. Phys. Soc. (London) **A63**, 145 (1950).

[3] K. H. Barker and C. C. Butler, Proc. Phys. Soc. (London) **A64**, 4 (1950).

[4] W. B. Fretter, Phys. Rev. **76**, 511 (1949).

[5] G. D. Rochester and C. C. Butler, Nature **160**, 855 (1947).

[6] Seriff, Leighton, Hsaio, Cowan, and Anderson, Phys. Rev. **78**, 290 (1950).

[7] Armenteros, Barker, Butler, and Cachon, Phil. Mag. **42**, 113 (1951).

[8] Fretter, May, and Nakada, Phys. Rev. **89**, 168 (1953).

[9] Leighton, Wanlass, and Anderson, Phys. Rev. **89**, 148 (1953).

[10] Thompson, Cohn, and Flum, Phys. Rev. **83**, 175 (1951).

[11] Bridge, Peyrou, Rossi, and Safford, Phys. Rev. **91**, 362 (1953).

is obtained with a lens system utilizing the aplanatic points of a cylindrical Lucite rod as suggested by Lofgren, Ney, and Oppenheimer.[12] An electric sweeping field of 300 volts clears the chamber gas of old ions. This electric sweeping field is removed from the chamber within a microsecond after the coincidence circuits have been actuated.

The chamber is filled with helium and argon to nine lb/in.^{2} above atmospheric pressure, in the ratio of three parts helium to one part argon by pressure, and absolute alcohol provides the vapor. To prevent gas in the chamber from leaking through the semiporous aluminum castings, it was found necessary to line the chambers with a thin sheet of rubber. No absorber was placed between the two chambers during this experiment.

III. THE PENETRATING SHOWER DETECTOR

The cloud chamber and accessory equipment were mounted in a 22-foot trailer and transported to mountain altitudes at Climax, Colorado (elev. 11 200 feet). The cloud chamber was electronically controlled to photograph secondary particles occurring in penetrating showers resulting from nuclear interactions of high-energy cosmic rays in the lead absorber placed directly above the chamber. The penetrating shower detector is presented in Fig. 1. In order that the nuclear interactions could occur as close as possible to the chamber, 12 cm of lead was placed immediately above the cloud chamber. Above this was located a tray containing four Geiger counters followed by 20 more cm of lead. Below the chamber was placed a tray of four Geiger counters, followed by 10 cm of lead and another tray of counters.

To select penetrating shower events, it was required that at least one counter in tray *a*, two counters in tray *b*, and one counter in tray *c* be discharged simultaneously. The counting rate with this triggering arrangement was 10 per hour of sensitive time. Two thousand pictures were obtained with this experimental arrangement, 1200 of them of suitable quality for accurate momentum measurements. Twenty percent of the two thousand photographs contained two or more collimated particles that could have been secondary particles originating in penetrating showers, indicating that the efficiency of this equipment for penetrating shower detection is twenty percent. As will be shown later (Sec. V) the efficiency of this arrangement for detecting penetrating showers is actually much better.

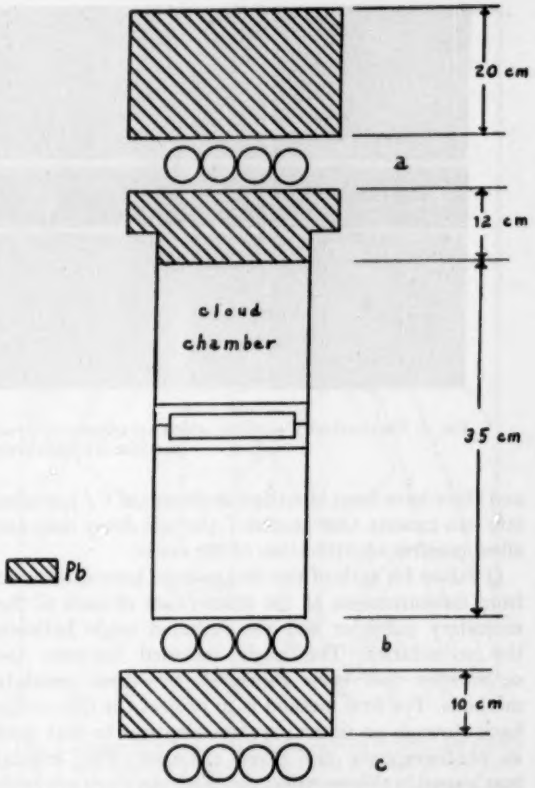

FIG. 1. Side view of penetrating shower detector and Yale cloud chamber.

IV. THE DECAY OF NEUTRAL *V* PARTICLES

Five decays of neutral *V* particles have been observed in photographs of sufficiently good quality that momentum measurements are obtainable. Information derived from these neutral *V*-particle decays largely agrees with results and conclusions of other workers.[4–11] One of the decays has been identified as the decay of a V_1^0 particle into a proton and a negative pi meson,

TABLE I. V^0 particle data.

Particle No.	Event	Classification	Momentum of positive secondary (Mev/*c*)	Momentum of negative secondary (Mev/*c*)	θ (degrees)	Q (Mev)
I	4–278	V_1^0	625±200	170±50	53.5°	49±20
		V_2^0				162±55
II	6–89	V_1^0	450±200	600±250	40.7°	176±75
III	6–89	V_2^0	875±300	700±400	31°	221±100
IV	11–40	V_1^0	180±50	230±40	24°	76±30
V	6–28	V_2^0	800±400	800±400	38°	312±170

[12] Lofgren, Ney, and Oppenheimer, Rev. Sci. Instr. **19**, 271 (1948).

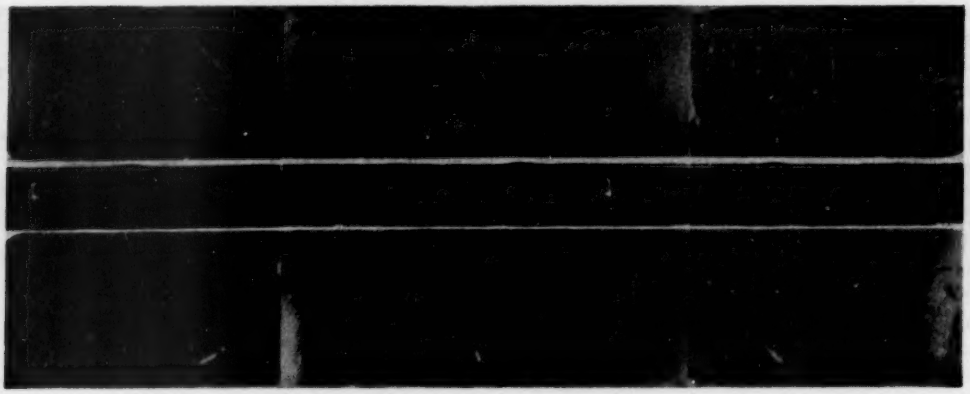

FIG. 2. Two neutral V particles which are apparently produced in the same event. From their momenta and angles these particles are tentatively classified as V_2^0 particles.

and three have been identified as decays of V_2^0 particles into two mesons. One neutral V-particle decay does not allow positive identification of the event.

Q values for each of the decays have been calculated from measurements of the momentum of each of the secondary particles and the included angle between the secondaries. The angle included between the secondaries has been measured by three separate methods. The first method is to project the film image back through an optical system identical to that used in photographing the cloud chamber. The original lens is used in this reprojection. With the three available views, the spatial representation of the tracks is obtained. The included angle may be measured directly on a small screen, equipped with many degrees of freedom of rotation, which has been adjusted until all of the secondary track images have been brought into proper alignment.

The second method used to measure the included angle between the secondary particles is similar to that described by Campbell and Welch,[13] and utilizes descriptive geometry techniques to obtain orthographic views of the decay and the true angle between the secondaries. The third method obtains algebraic equations for the trajectories of the secondaries from the projected views of the film image. The included angle may then be easily calculated. All three of these methods usually agree to within less than one degree. The data for the five measurable V-particle decays are presented in Table I.

Photograph 6–89 shows the decay of two neutral V particles that probably originated in a single nuclear interaction. (Fig. 2). Both V particles decay near the front glass of the chamber, and the secondaries slope downward and toward the back of the chamber. The upper decay occurs $\frac{1}{8}$ inch behind the front glass. Both decays may be seen well in stereoscopic reprojection. When the value[14] $\alpha=(P_+^2-P_-^2)/P^2$ is plotted *versus* P_t (transverse momentum), both V^0 particles are consistent with the decay scheme $\pi^++\pi^-+220$ Mev. (See Fig. 3.) Although the errors in the momentum measurements are large, it does not seem possible to interpret either of these as V_1^0 particles. This event can therefore be interpreted as the production of two V_2^0 particles in the same nuclear interaction.

Photograph 4–278 contains a decay which can be interpreted as a V_2^0 as well as a V_1^0 decay. The calculated value of alpha for this decay is 0.73 ± 0.08. On the assumption of a V_1^0 decay the calculated Q value is 49 ± 20 Mev, and on the assumption of a V_2^0 decay the calculated Q value is 162 ± 55 Mev. The plane of the V-particle secondaries is coplanar to within two degrees with the point of nuclear interaction determined by reprojecting the other tracks in the shower back to their common origin.

Photograph 11–40 contains a decay which has been classified as a V_1^0 decay since one of the secondaries is identified as a proton on the basis of ionization and momentum. The Q value calculated for this decay is 76 ± 30 Mev.

V. THE SECONDARY PARTICLES IN THE PENETRATING SHOWERS

The 1200 good quality photographs were analyzed with respect to the secondary particles of the penetrating showers. Photographs showing penetrating showers with two or more well-collimated particles produced in the lead above the chamber were first selected. Particles in this category having momentum greater than 125 Mev/c and not occurring in identifiable electronic showers were analyzed for sign of charge. It was required that all particles traverse the entire chamber and not interact in the $\frac{1}{2}$-inch aluminum wall

[13] J. S. Campbell and D. F. Welch, Nucleonics **10**, 62 (1952).

[14] C. C. Butler, *Progress in Cosmic Ray Physics*, edited by J. G. Wilson (North-Holland Publishing Company, Amsterdam, 1952), Chap. 2.

between the two chambers. The data for this group are given in Table II. It should be pointed out that no lead was used between the chambers to select penetrating particles. However, all photographs containing a recognizable electronic component were excluded. Three hundred and seventy-eight particles were included in this group in 120 penetrating-shower photographs. Two hundred and thirty-five of the secondary particles could be classified as to sign of charge.

The ratio of positively charged secondaries to negatively charged secondaries is 1.83. If one assumes that positive and negative mesons are present in equal numbers, that a negligible number of electrons is present, and that the excess positive particles are protons, then the ratio of protons to mesons is 0.42. The percentage of protons among the observed secondary particles is therefore 30 percent. If electron-positron pairs are present, or if many electrons are present, this percentage would represent a lower limit for the protons present among the penetrating particles (protons plus mesons). This result agrees well with the results of Barker, Rosser, and Butler,[2,3] in which they conclude in a similar experiment at sea level with lead in their chamber to select penetrating secondary particles, that about half of the penetrating secondary particles observed by them are protons, and that between 25 and 50 percent of all penetrating shower particles are probably protons.

In addition, all singly-occurring particles observed in this experiment, or particles not appearing to come from a single point of nuclear interaction and therefore rejected in the first selection have been analyzed for sign of charge. All photographs containing an identifiable electronic component were again rejected. Two hundred-ninety particles of measurable sign and having momenta greater than 125 Mev/c are included in this group (Table III). The ratio of positively charged particles to negatively charged particles in this case is 1.84, which is remarkably close to the corresponding value of 1.83 in the much more stringently selected group. This provides strong evidence that the penetrating shower detector is much more efficient for selecting penetrating shower events than the 20 percent figure given in Sec. III would indicate.

TABLE II. Analysis of the collimated secondary particles in definite penetrating shower events.

Total number of penetrating showers:	120
Total number of secondaries from penetrating showers:	378
Total number of secondaries with measurable sign of charge:	235
Total number of positive secondaries:	152
Total number of negative secondaries:	83
Excess of positive particles:	69
Ratio of positive secondaries to negative secondaries:	1.83
Ratio of protons to mesons and electrons:	0.42

TABLE III. Analysis of singly-occurring particles and groups of particles that are not collimated.

Particles with measured sign of charge:	290
Total number of positive particles:	188
Total number of negative particles:	102
Excess of positive particles:	86
Ratio of positive to negative particles:	1.84
Ratio of protons to mesons and electrons:	0.42

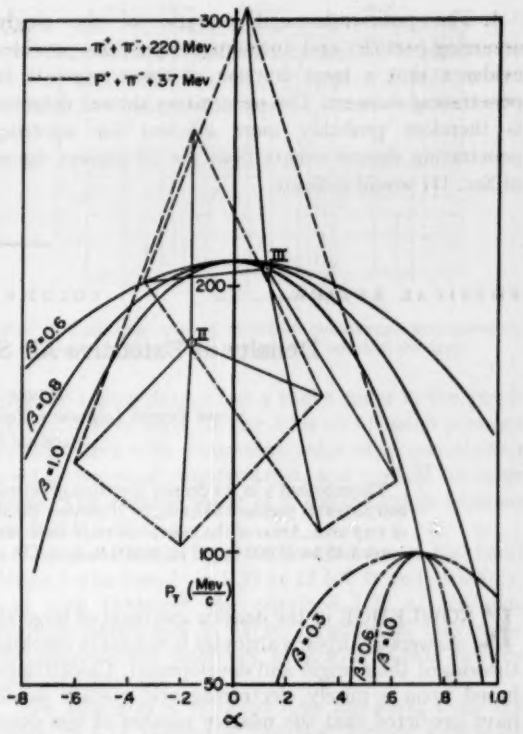

FIG. 3. Graph of α *versus* P_T for the neutral V particles shown in Fig. 2 and listed as II and III in Table I. $\alpha=(P_+^2-P_-^2)/P_0^2$ where P_+, P_-, P_0 are momenta of the positive, negative, and neutral particles, respectively. P_T is the component of momentum of either of the charged particles perpendicular to the direction of travel of the neutral particle. The dashed trapezoids represent the possible range of the plotted points, due to errors in the momenta of the decay products.

VI. CONCLUSIONS

1. Five decays of neutral V particles have been observed and analyzed. One of these is a decay of a V_1^0 particle, three of V_2^0 particles, and one does not permit definite identification.

2. A single photograph shows the decay of two V_2^0 particles that probably originated in a single nuclear interaction.

3. The proton component of the proton-plus-meson secondary particles in the penetrating showers observed in this experiment has been determined to be 30 percent. This figure is a lower limit, but is probably close to the actual value.

4. The positive-to-negative ratio of the singly occurring particles and uncollimated particles provides evidence that a large fraction of these originate in penetrating showers. The penetrating shower detector is therefore probably more efficient for selecting penetrating shower events than the 20 percent figure of Sec. III would indicate.

ACKNOWLEDGMENTS

The work at Climax, Colorado was facilitated by the generous cooperation of the Climax Molybdenum Company, and of the High Altitude Observatory of the University of Denver and Harvard University. Analysis of the results was aided by helpful discussions with Professor Earle C. Fowler.

PHYSICAL REVIEW VOLUME 93, NUMBER 6 MARCH 15, 1954

Density of Extensive Air Showers at Airplane Altitudes*

HENRY L. KRAYBILL
Sloane Physics Laboratory, Yale University, New Haven, Connecticut
(Received October 30, 1953)

The exponent γ in the density spectrum of extensive air showers has been measured at 25 000-ft, 30 000-ft, and 33 000-ft pressure altitude, by observing the threefold coincidence rate of counter trays as a function of tray area. Areas of the individual trays were varied by factors up to eight. The measured mean values of γ are 1.45 at 25 000 ft, 1.5 at 30 000 ft, and 1.56 at 33 000 ft.

KNOWLEDGE of the density spectrum of large air showers at airplane altitudes is helpful in checking theories of their origin and development. Calculations[1] based upon a purely electromagnetic cascade model have predicted that the relative number of less dense showers should increase with altitude, and that γ, the exponent in the integral density spectrum,[2] should increase from 1.4 near sea level to about 1.9 near 30 000 feet. This prediction conflicts with measurements by Maze *et al.*,[3] by Biehl and Neher,[4] and by Hodson,[5] who have found values of γ at airplane altitudes which are not much different from the sea-level values. The method used in most cases was to observe the change of counting rate of a coincidence detector when the counter area was changed (method *B*). Early measurements of this author,[6] obtained by varying the number of counters in coincidence (method *A*), indicated that γ increases with altitude, in qualitative agreement with the predictions of the above theory. However, it has been pointed out[7] that method *A* is unreliable, because it is susceptible to density gradients in the showers, which become more serious at high altitudes. Therefore, I have remeasured γ in a series of airplane flights during the summer of 1951, using method *B*. The counter areas were varied by factors as high as eight. Curves of counting rate *versus* counter area were plotted from which the applicability of the power law to the density spectrum was ascertained and the values of γ were determined. This procedure differs from other reported measurements at these altitudes, in which the power law was assumed, and the value of γ was deduced by comparing the counting rates for two different counter areas.

The data reported here were taken in a B-29 airplane during two round trips at constant altitude between Rome, New York, and Lima, Peru. The variation in latitude, which was required by other experiments carried out in the airplane, did not adversely affect these measurements, since the extensive shower rate is constant with latitude.[4,6]

The location of the counter trays in the airplane is shown in Fig. 1. The active dimensions of the cylindrical counters were 2.4 cm×32 cm. A space of one inch was provided between adjacent counters in each tray, to avoid overlapping of their areas for showers incident from angles other than the zenith. In this way, a tray of several counters is made to have the same effective shape as a single counter. Calculations by Biehl and

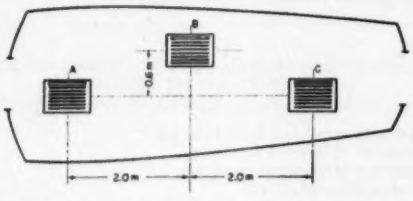

FIG. 1. Top view of rear pressurized compartment of B-29 airplane, showing location of shower counter trays. Each tray was connected to a channel of a threefold coincidence circuit.

* The work was supported in part by the joint program of the U. S. Office of Naval Research and the U. S. Atomic Energy Commission.
[1] M. M. Mills, Ph.D. thesis, California Institute of Technology, 1948 (unpublished).
[2] $N = K\Delta^{-\gamma}$, where N is the number of showers with density greater than Δ, and K and γ are constants.
[3] R. Maze and A. Frèon, J. phys. radium **10**, 85 (1949).
[4] A. Biehl and H. V. Neher, Phys. Rev. **83**, 1169 (1950).
[5] A. L. Hodson, Proc. Phys. Soc. (London) **A66**, 49 (1953).
[6] H. L. Kraybill, Phys. Rev. **76**, 1092 (1949).
[7] J. Ise and W. Fretter, Phys. Rev. **76**, 993 (1949).

Neher[4] and measurements by Hodson[5] indicate that the above spacing is sufficient for this purpose. The trays were mounted just under the roof of the plane, with an estimated 2 g/cm² of aluminum and insulating fiber above them.

The three trays were connected to four different threefold coincidence circuits. By connecting a different number of counters per tray to each circuit, it was possible to record coincidence rates for four different counter areas simultaneously. Coincidences were recorded as marks on a moving film.

The rates were not corrected for accidental coincidences, since these were considered negligible. All coincidence circuits had resolving times less than 1.5 microsecond. The highest single counting rate of a tray of eight counters was 500 per second. The threefold accidental rate under these conditions is less than 0.05 counts per minute, compared with a coincidence rate of 9 counts per minute. For lower altitudes and smaller tray areas, accidentals are even less frequent.

TABLE I. Counting rates of threefold coincidence arrangement shown in Fig. 1.

Altitude	No. of counters per tray	Time (min)	Rate (min⁻¹)
25 000 ft	1	1580	0.43±0.02
	2	857	1.34±0.04
	3	767	2.89±0.06
	4	813	3.64±0.07
	5	767	4.98±0.08
	7	723	7.16±0.10
	8	90	9.02±0.32
30 000 ft	1	884	0.42±0.02
	2	650	1.12±0.04
	3	559	1.96±0.06
	5	39	4.97±0.36
33 000 ft	1	740	0.35±0.02
	2	55	1.19±0.15
	3	55	2.04±0.20
	4	685	3.13±0.07
	5	55	3.56±0.25
	7	450	7.30±0.13

Most data were taken at 25 000-ft pressure altitude, but smaller amounts of time were also spent at 30 000 ft and at 33 000 ft. The results are given in Table I, and are plotted in Fig. 2.

From Fig. 2, it is apparent that the results at 33 000 ft and 30 000 ft are consistent with the equation $C=KA^{\gamma}$, where C is the coincidence counting rate, A is counter area, and K and γ are constants. The value of γ is 1.5 at 30 000 ft and 1.56 at 33 000 ft. The exponent γ, obtained in this way, has been shown to be identical with the exponent in the density spectrum of the showers.

The results at 25 000 ft, where more time was available for taking data, show a slight curve in the graph of log$C$ *versus* log$A$. If one tries to fit small portions of this curve with a constant value of γ, one obtains $\gamma=1.65$ for small counter areas, and $\gamma=1.25$ for large areas. The average value of γ for the range of areas studied is 1.45.

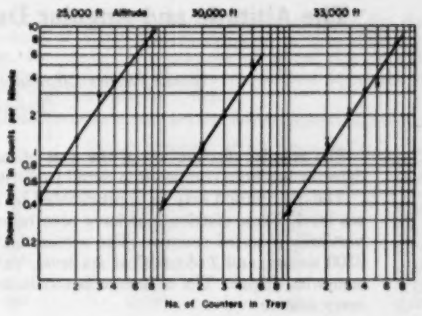

FIG. 2. Counting rate of threefold coincidence arrangement, shown in Fig. 1, *versus* number of counters per tray.

The above results agree well with those of Biehl and Neher,[4] who found $\gamma=1.50$ at 22 500 ft and 30 000 ft, and with Hodson,[5] who obtained 1.55 at altitudes between 20 000 and 33 500 ft. In addition, they show the approximate constancy of γ with shower density and with altitude.

The values of γ reported here are lower than the value of 1.73 previously obtained by the author at 30 000 ft, by varying the number of counters in coincidence (method A). Part of this difference is due to the inadequacy of method A for determining shower density, unless the counter geometry be very carefully chosen. However, some of the difference may also be due to the use of single counters with very small area (75 cm²) for which the value of γ, as suggested by the results of the present experiment at 25 000 ft, may be higher.

The above results confirm that the density spectrum of large air showers does not change markedly from sea level to 33 000-ft pressure altitude. The variation of γ with altitude is slight. As Hodson[5] has pointed out, this is in conflict with predictions based on the model of a pure electronic cascade, and is more readily reconciled with a mixed nucleonic and electronic cascade theory of the extensive air showers.

I wish to acknowledge the indispensable assistance of Irwin Tessman, who constructed the Geiger counters for this experiment. I am also grateful to the officers and airmen of the Griffiss Air Force Base, Rome, New York, for their cooperation and skill in flying the B-29 airplane for these flights.

The Altitude and Angular Dependence of Cosmic-Ray Air Showers*

H. L. KRAYBILL
Sloane Physics Laboratory, Yale University, New Haven, Connecticut
(Received November 4, 1954)

The angular distribution of the axes of large air showers incident upon a typical coincidence counter detector has been computed in detail from the altitude dependence.

The distribution may be approximated by the function $\cos^{5.4}\theta$ at 3500 meters elevation and by $\cos^{7.4}\theta$ at sea level. These distributions have been tested experimentally by comparing the rates of horizontally and vertically oriented counters. The vertical-horizontal counting ratio (R) was measured to be 2.12 ± 0.07 at 3500 meters, and 2.68 ± 0.07 at sea level. Values of R calculated from the above angular distributions are somewhat higher. The difference is attributed principally to scattering of shower particles about the primary axis.

THE angular distribution of extensive air showers is related to the processes involved in their formation. If they are formed solely by interactions with the matter of the atmosphere, the angular distribution must be related to their altitude dependence by a transformation similar to that first given by Gross. If, on the other hand, decay processes are important in transferring energy into or out of the showers, these decay processes will be more prevalent in the rare atmosphere traversed at large zenith angles, than in the same mass of air traversed vertically, and the angular dependence of the showers may be different from that deducible from the altitude variation by a Gross transformation.

Previous measurements[1–5] of the angular distribution of air showers, performed mostly with cloud chambers, have yielded varying results. The results of Deutschmann, Daudin, and McKay and Brown are in approximate agreement with a Gross transformation from the known altitude dependence. Other observers,[3,5] however, have found distributions considerably steeper. I have, therefore, undertaken to examine closely the relation between angular distribution and altitude dependence of air showers, and to investigate the angular distribution by a different experimental method from those used previously.

This method consists of comparing the shower counting rate of long cylindrical Geiger counters with their axes oriented horizontally, to the rate of the same counters when their axes are vertical. This horizontal-vertical ratio is quite sensitive to the steepness of the zenith angle distribution of the incident showers. It was measured at mountain altitudes and at sea level, and it has been compared with values calculated theoretically from the angular distributions deduced from the altitude curve of large air showers. Results obtained at mountain altitudes have been reported previously.[6] Since then, measurements based upon the same method have been reported by Bassi *et al.*[7] The present work includes additional measurements at sea level, and explains the method of calculating the angular dependence from the altitude dependence.

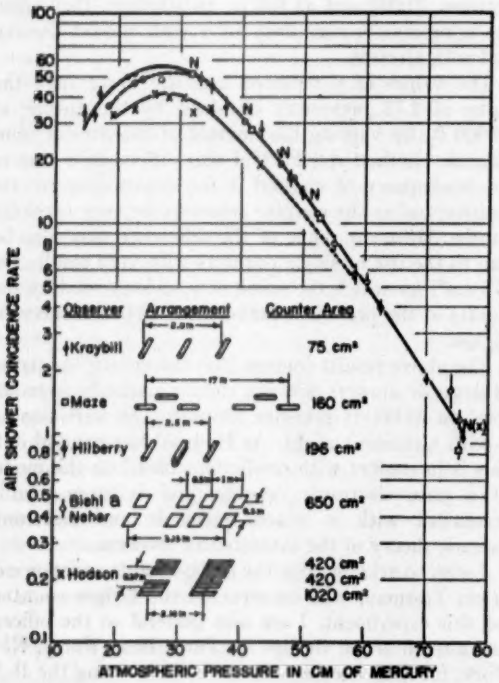

FIG. 1. Altitude dependence of extensive air showers. Each observer's data are normalized to the solid curve at the point marked N. The solid curve is normalized to unity at 76 cm of mercury.

* This work was supported in part by the joint program of the U. S. Office of Naval Research and U. S. Atomic Energy Commission.

[1] J. Daudin, J. phys. radium **6**, 302 (1945).
[2] M. Deutschmann, Z. Naturforsch. **2**, 61 (1947).
[3] R. W. Williams, Phys. Rev. **74**, 1689 (1948).
[4] W. W. Brown and A. S. McKay, Phys. Rev. **76**, 1034 (1949).
[5] E. W. Cowan, Ph.D. thesis, California Institute of Technology, 1948 (unpublished); M. M. Mills, Phys. Rev. **74**, 1555 (1948).
[6] H. L. Kraybill, Phys. Rev. **77**, 410 (1950).
[7] Bassi, Bianchi, Cadorin, and Manduchi, Nuovo cimento **9**, 1037 (1952).

ALTITUDE DEPENDENCE OF AIR SHOWERS

In Fig. 1, measurements of air shower altitude dependence by different observers,[8–12] using coincidence counters, are plotted on the same graph. Each observer's data are normalized to fit the solid curve at a single point. The solid curve has been drawn to fit all of the data as well as possible, and has been normalized to unity at 76 cm of mercury. In spite of differences in experimental arrangements, it is possible to draw a curve which is reasonably consistent with most of the data below 22 000-ft altitude. An altitude curve is thus determined which is insensitive to detector geometry within rather wide limits in the lower atmosphere.

This insensitivity of the altitude variation to counter geometry is related to the empirical observation that the variation of shower rate with counter area and with counter separation is similar at different altitudes, especially between mountain altitude and sea level.[13,14] This is particularly true for counter areas between 10 and 1000 cm² and for separations between 2 and 10 meters. All of the experimental arrangements used for the data of Fig. 1 fall within these ranges. On the other hand, the angular distribution changes with altitude, as shown in this paper. This factor should cause single horizontal cylinders to have a slightly steeper altitude variation in counting rate than a closely packed tray of cylinders, but the difference is only a few percent in the ratio of rates between sea level and mountain altitudes. At higher elevations, the zenith angle distribution should change rapidly near the maximum of the altitude curve. This will cause counter trays to show a maximum rate at lower altitudes than single cylinders, and a more rapid decrease in rate at altitudes above the maximum. The existence of this effect at altitudes above 22 000 ft is apparent in Fig. 1.

CALCULATION OF ANGULAR DISTRIBUTION

Shower detectors usually have a sensitivity which varies with incident direction of the shower axis. Therefore the angular distribution of showers counted by a detector will depend on its anisotropy. To obtain an angular distribution which is independent of detector shape, we will make the following definition. The angular distribution of showers *incident upon* a given detector is defined as: the directional variation of showers recorded by an isotropic detector having the same sensitivity in every direction which the actual detector has towards the zenith direction. This distribution will be denoted by the function $M(x,t)$, where

[8] N. Hilberry, Phys. Rev. **60**, 1 (1941).
[9] H. L. Kraybill, Phys. Rev. **73**, 632 (1948); Phys. Rev. **76**, 1093 (1949).
[10] R. Maze and A. Freon, J. phys. radium **10**, 85 (1949).
[11] A. T. Biehl and H. V. Neher, Phys. Rev. **83**, 1169 (1951).
[12] A. L. Hodson, Proc. Phys. Soc. (London) **A66**, 49 (1953).
[13] G. Cocconi and V. Cocconi Tongiorgi, Phys. Rev. **75**, 1058 (1951).
[14] J. Wei and C. G. Montgomery, Phys. Rev. **76**, 1488 (1949).

TABLE I. Comparison of normalized values of the directional dependence of Auger showers, deduced for three different counter shapes, for atmospheric pressure of 50-cm Hg. $M(x,t)$ is the directional dependence of showers incident upon the detector. $x=\cos\theta$, and $t=$atmospheric depth.

Zenith angle	$M(x,t)$, assuming isotropic detector	$M(x,t)$, assuming cylindrical counters	$M(x,t)$, assuming trays of counters
0°	1.000	1.000	1.000
10°	0.940	0.937	0.935
20°	0.750	0.746	0.742
30°	0.497	0.493	0.485
40°	0.238	0.235	0.229
50°	0.070	0.067	0.064

t is the depth below the top of the atmosphere, and $x=\cos\theta$ ($\theta=$zenith angle).

The angular distribution defined in the above manner should be nearly independent of counter area and spacing for most commonly used areas (between 10 cm² and 1000 cm²) and separations (between 2 m and 10 m) in the lower atmosphere. If this were not so, the change in counting ratio of different detectors with zenith direction would imply a corresponding change in their counting ratio with altitude. However, it has been noted above that this ratio is nearly constant with altitude.

The altitude curve of Fig. 1 was used to compute the angular dependence of air showers *incident upon* the detector at 50 cm and at 75 cm of Hg. Details of the computation are given in Appendix I. The results at 50 cm are given in Table I. This table shows that the deduced angular variation depends very weakly on the shape of detector.

The computation was based upon the following premises: (1) the shower primaries are isotropic at the top of the atmosphere, (2) the multiplication and disappearance of the particles depends only on the mass traversed, not upon the air density or time of traversal, and (3) the shower particles have the same direction as the incident primary. Further assumptions, which were used in refining the calculations, are (4) the shape of the lateral structure of the showers depends only upon the mass of air traversed, and the extent of the lateral structure is inversely proportional to the air density, (5) the variation of counting rate (C) with counter area (A), for showers incident from the zenith only, is given by $C\propto A^{1.5}$ at all atmospheric depths, and (6) the variation of counting rate with counter separation (S) for showers incident from the vertical direction is given by $C\propto S^{-0.2}$ at all atmospheric depths.

Assumption (5) is supported by the work of Cocconi *et al.*[13] Although they actually measured γ for showers from all directions rather than those incident only vertically, showers in the lower atmosphere come mostly from small zenith angles. Also, the near constancy of γ with atmospheric depth implies that it is also constant with direction at a given altitude. Assumption (6) is obtained from the work of Wei.[14] Deviations from

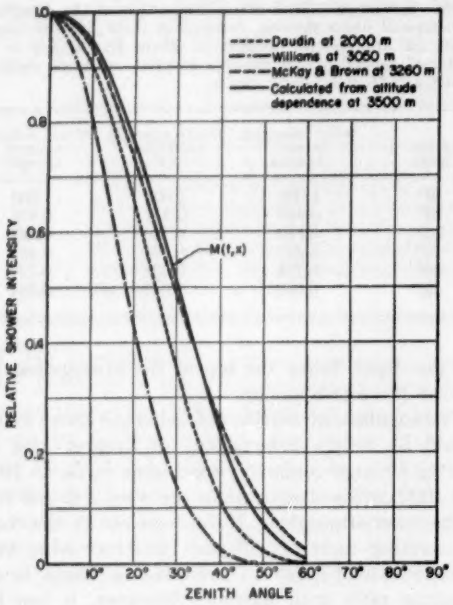

FIG. 2. Calculated and measured zenith angle dependence of extensive air showers at mountain altitudes.

assumption (3) certainly exist, but merely change slightly the effective directional sensitivity of the detector, to which the calculated angular distribution is quite insensitive (see Table I).

The computed angular distributions of the shower axes are represented by the solid curves in Figs. 2 and 3. Since the shower rate is not known for atmospheric depths greater than 76 cm, the sea level calculation had to be based upon an extrapolation of the altitude curve to greater depths. This was done by extending the lower part of the curve of Fig. 1, as a straight line on the semilogarithmic graph.

Experimental curves of the directional distribution, obtained by Deutschmann,[2] Daudin,[1] Williams,[3] and McKay and Brown[4] are also plotted in Figs. 2 and 3. The distributions deduced from the altitude curve are similar to those measured by Deutschmann, and by McKay and Brown, at sea level and at mountain altitude, respectively. The distribution found by Daudin is slightly steeper, and the distribution of Williams is considerably steeper, than the calculated curve.

EXPERIMENTAL RESULTS

Measurements of the shower rate of horizontal and vertical cylindrical counters were carried out at Climax, Colorado,[6] (49.5 cm of Hg) and at New Haven, Connecticut (76 cm of Hg). The arrangement at sea level is shown in Fig. 4. The geometry at Climax was similar, except that smaller counters were used and the counters at D were located at D' in Fig. 4. To minimize the effects of surrounding materials, the counters were placed under a light canvas tarpaulin at Climax. At New Haven they were placed in the open air on the flat roof of the Sloane Physics Laboratory, encased in light plastic bags. To avoid effects of inequalities of counter construction, vertical and horizontal counters were alternated periodically. The results are given in Table II. Table III shows values of R computed for assumed angular distributions of the form x^n ($x \equiv \cos\theta$). In Table IV, the measured horizontal-to-vertical counting ratios (R) are compared with values computed from the angular distributions of Figs. 2 and 3. In these computations, scattering of shower particles in the air was neglected, and all particles were assumed to move parallel to the shower axis. Details of computing these ratios are given in Appendix II.

The measured and computed horizontal-vertical ratios both indicate a steeper angular distribution at sea level than at mountain altitude. The measured ratios are lower than the ratios computed from the angular variation derived from the altitude curve, by about the same amount at each altitude. Before attributing significance to this difference, however, the following effects must be considered: (1) scattering of shower particles about the direction of their axis, (2) absorption and multiplication of particles in the counter walls, (3) backscattering from material below the counters.

Approximate calculations have been made of the effect of each of these factors on the value of (R). The

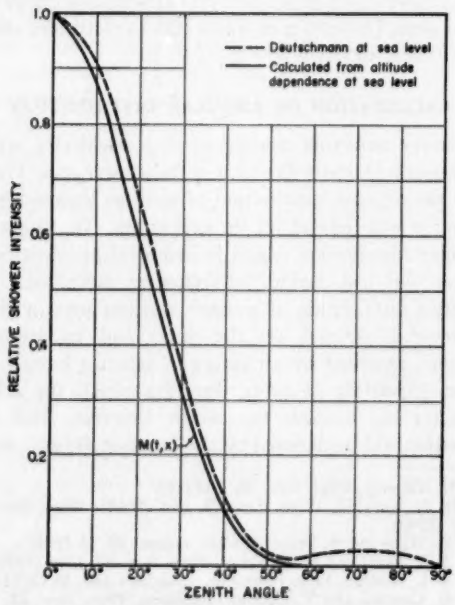

FIG. 3. Calculated and measured zenith angle dependence of extensive air showers at sea level.

numerical results of Richards, Roberg, and Nordheim,[15] on the number and angular distribution of low energy cascade electrons, were used. The calculations indicate a reduction in R of about 7 percent due to scattering in air, and a further reduction of 2 percent due to multiplication and absorption in counter walls. A very crude estimate of the effect of backscattering from the ground suggests a reduction in R of another 2 percent. The values of R, after these approximate corrections have been applied, are given in Table IV.

SUMMARY

The angular variation of the axes of extensive air showers incident upon Geiger counter detectors in the lower atmosphere has been computed in detail from the altitude dependence. This variation may be approximated by the function $\cos^{5.4}\theta$ at 3500 meters elevation and by $\cos^{7.4}\theta$ at sea level. An experimental test of these distributions, by comparing the rates of horizontally and vertically oriented counters, shows the predicted steepening of the angular distribution with increasing atmospheric depth. The measured horizontal-vertical counting ratios (R) are in fair agreement with the values calculated from the altitude dependence, after corrections for secondary effects, such as scattering of shower particles, have been considered. The results are consistent with the cloud chamber observations of McKay and Brown at 3250 meters, and with those of Deutschmann at sea level. They also agree well with results[16] recently obtained at 2000 m by Cresti, Loria, and Zago, who find a distribution of the form $\cos^n\theta$ with n in the range of 4 to 5, for the shower particles. There is fairly good agreement with the results of Bassi *et al.*[7] at 2000 m, although at sea level the angular distribution found here is steeper.

The absence of a marked discrepancy between the calculated and measured values of R suggests that decay processes do not greatly affect the angular distribution of air showers in the lower atmosphere.

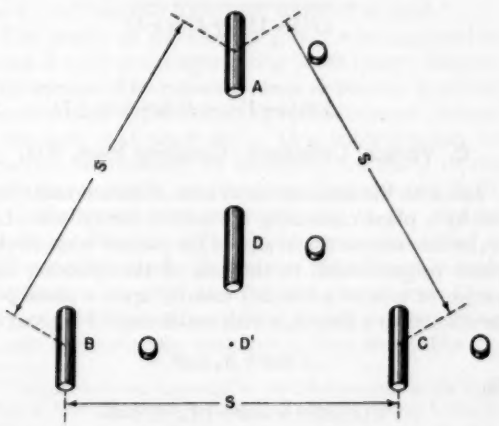

FIG. 4. Vertical view of coincidence counter arrangement used to test zenith angle dependence of air showers at sea level. Coincidence rates ABC and $ABCD$ of the horizontal counters were compared with the corresponding rates for the vertical counters. At sea level, $S=4$ meters. At 3500 m, $S=2.8$ meters, and the counter at D was at D'.

TABLE II. Counting rates of arrangement of Fig. 4. The counters used at 3500 meters had active dimensions of 2.5 cm ×32 cm. Those used at sea level had dimensions of 5 cm×100 cm.

Coincidence combination	Vertical rate (hr^{-1})	Horizontal rate (hr^{-1})	Horizontal-to-vertical ratio (R)
	3500 meters elevation		
$D'BC$	3.47±0.12	7.37±0.18	2.13
ABC	3.35±0.12	7.11±0.18	2.12
$ABCD'$	2.15±0.11	4.63±0.15	2.15
	Sea level		
ABC	2.17±0.07	7.38±0.12	2.71
$ABCD$	1.78±0.06	4.83±0.10	2.66

TABLE III. Computed values of the ratio (R) of horizontal to vertical counting rates of cylindrical counters at atmospheric pressures of 50-cm Hg and at sea level. The counters at sea level have a ratio of 0.038 between their minimum and lateral cross sections. For the counters at 50-cm Hg, the ratio is 0.058.

$M(x,l)$	R(50 cm Hg)	R(sea level)
x^3	1.86	1.89
x^5	2.33	2.39
x^7	2.76	2.82
x^9	3.16	3.23

TABLE IV. Comparison of computed and measured values of R.

R, computed from angular distribution deduced from altitude curve	2.56	3.15
Computed R, after correcting for scattering and counter walls	2.31	2.84
Measured value of R	2.13±0.07	2.68±0.07

APPENDIX I. DEDUCTION OF ANGULAR VARIATION FROM ALTITUDE DEPENDENCE

Let: t be the atmospheric depth measured along the vertical direction; x represent $\cos\theta$, where θ is the angle between the axis of a shower and the zenith; φ represent the azimuthal angle of the shower axis; β represent the angle between the direction of the shower axis and the direction of the axis of the horizontal counters; $N(t,x)$ be the counting rate per steradian of the shower detector at atmospheric depth t, averaged over all azimuths (φ) at constant zenith angle θ; $\rho(t)$ be the air density at depth t; and $f(x)$ represent the directional sensitivity of the detector, which is assumed the same at all altitudes. Then

$$N(t,x)=N(t/x,1)f(x)[\rho(t)/\rho(t/x)]^{2(\gamma-1)-0.2}f(x). \quad (1)$$

[15] J. A. Richards and L. W. Nordheim, Phys. Rev. **74**, 1106 (1948); J. Roberg and L. W. Nordheim, Phys. Rev. **75**, 444 (1949).

[16] Cresti, Loria, and Zago, Nuovo cimento **10**, 779 (53).

The factor involving the air density can be deduced from assumptions 1 to 6, by reasoning given elsewhere.[17] Taking the values given in assumptions 5 and 6, using the empirical expression $\rho \propto t^{0.9}$, one finds this factor is $x^{0.72}$. This was rounded to $x^{0.7}$.

It was found that $x^{0.5}$ is a good empirical approximation for $f(x)$ for the arrangement of Fig. 4, for zenith angles smaller than 60 degrees. The deduced angular dependence at 50 cm of Hg is in any case very insensitive to inaccuracy in this function. (See Table I.) Thus,

$$N(t,x)=N(t/x,\,1)x^{1.2}. \tag{2}$$

Let $C(t)$ be counting rate of the shower detector at depth t. Then,

$$C(t)=2\pi\int_0^1 N(t/x,\,1)x^{1.2}dx. \tag{3}$$

The expression for $C(t)$ can be integrated by parts, following the standard procedure of the gross transformation.

One then obtains

$$N(t,1)=[2.2C(t)-tC'(t)]/2\pi. \tag{4}$$

Finally, from Eq. (2):

$$N(t,x)=N(t/x,\,1)x^{1.2}=[2.2C(t/x)-(t/x)C'(t/x)]x^{1.2}/2\pi. \tag{5}$$

To obtain the zenith angle dependence of the incident showers, we must divide $N(t,x)$ by the directional sensitivity ($x^{0.5}$) of the detector, to get the zenith angle dependence:

$$M(t,x)=[2.2C(t/x)-(t/x)C'(t/x)]x^{0.7}/2\pi. \tag{6}$$

APPENDIX II. CALCULATION OF RELATIVE COUNTING RATES OF DIFFERENT SHAPED COUNTERS, FROM THE ZENITH ANGLE DEPENDENCE

A. General Method

The shower rate per steradian detected by an isotropic detector has been calculated in Appendix I, as $M(t,x)$. If the particles in the atmosphere are not scattered, the sensitivity of a set of counters to showers from a single direction will depend upon (1) the projected area $A(x,\varphi)$ of the counters on the plane perpendicular to the shower axis, and (2) the geometrical configuration and spacing of the projections of the counters upon that plane. Now, from assumption (5), the showers counted will vary as $A^{\gamma}(\gamma=1.5)$. The effect of the change in counter spacing with zenith angle is very small for the geometry used, and it will be neglected. Hence, the total counting rate is obtained as

$$C(t)=\int_{x=0}^{1}\int_{\varphi=0}^{2\pi}M(t,x)\left[\frac{A(x,\varphi)}{A(1,0)}\right]^{1.5}d\varphi dx.$$

[17] A. Daudin and J. Daudin, J. phys. radium **10**, 394 (1950). Compare also reference 11.

B. Horizontal Cylinders—Counting Rate, $H(t)$

$$A(x,\varphi)/A(1,0)=\sin\beta=(1-\cos^2\beta)^{\frac{1}{2}}=(1-\sin^2\theta\,\sin^2\varphi)^{\frac{1}{2}},$$

and

$$H(t)=\int_0^1 M(t,x)\int_0^{2\pi}[1-(1-x^2)\sin^2\varphi]^{0.75}d\varphi dx.$$

Expanding by binomial theorem and letting $(1-x^2)\equiv y^2$:

$$(1-y^2\sin^2\varphi)^{0.75}=1-0.75(y^2\sin^2\varphi)-(0.75)(0.25)(y^4\sin^4\varphi)/2-(0.75)(0.25)(1.25)(y^6\sin^6\varphi)/6-\cdots;$$

$$\int_0^{2\pi}(1-y^2\sin^2\varphi)^{0.75}d\varphi=2\pi[1-(3/8)y^2-(9/256)y^4-(25/2048)y^6-\cdots]=2\pi f(x).$$

So,

$$H(t)=2\pi\int_0^1 M(t,x)f(x)dx.$$

This equation can be integrated numerically. If the directional distribution $M(t,x)$ is some power α of $\cos\theta$, then,

$$H(t)=2\pi\int_0^1 x^{\alpha}[1-(3/8)(1-x^2)-(9/256)(1-x^2)^2-(25/2048)(1-x^2)^3\cdots]dx$$

$$=2\pi\left[\frac{1}{\alpha+1}-\frac{3}{4(\alpha+1)(\alpha+3)}-\frac{9}{32(\alpha+1)(\alpha+3)(\alpha+5)}-\frac{75}{128(\alpha+1)(\alpha+3)(\alpha+5)(\alpha+7)}-\cdots\right].$$

C. Vertical Cylinders—Counting Rate, $V(t)$

Let A be the cross-sectional area of the counter when cut by a plane containing the axis of the cylinder. Let A_e be the cross-sectional area of the counter when cut by plane perpendicular to the axis of the cylinder. The projected area of a vertical counter upon a plane perpendicular to a direction with zenith angle θ is given by

$$A\sin\theta+A_e\cos\theta.$$

So,

$$A(x,\varphi)/A=\sin\theta+(A_e/A)\cos\theta.$$

For the counters used at Climax, $A_e/A=0.058$. (For the counters used at New Haven, $A_e/A=0.038$.) So,

$$V(t)=2\pi\int^1 M(t,x)(\sin\theta+0.058\cos\theta)^{1.5}dx.$$

This equation can be integrated numerically without difficulty.

Scattering of 65-Mev Pions in Hydrogen*

D. BODANSKY, A. M. SACHS, AND J. STEINBERGER
Columbia University, New York, New York

(Received November 30, 1953)

A measurement has been made at approximately 65 Mev of the differential cross sections in the processes $\pi^+ + p \to \pi^+ + p$, $\pi^- + p \to \pi^- + p$ and $\pi^- + p \to \pi^0 + n$ using a liquid hydrogen target and scintillation counter detectors. The measured cross sections in the center-of-mass system are

$\pi^+ + p \to \pi^+ + p$ (58 Mev)		$\pi^- + p \to \pi^- + p$ (65 Mev)	
θ	$d\sigma/d\Omega$ (mb)	θ	$d\sigma/d\Omega$ (mb)
36	0.24±0.11	42	0.91±0.13
47	0.48±0.08	53	0.51±0.08
64	0.66±0.06	70	0.29±0.06
101	1.24±0.07	101	0.23±0.06
129	2.10±0.11	151	−0.01±0.11
155	2.79±0.15		

$$d\sigma/d\Omega(\pi^- \to \pi^0) = \left[0.96\pm0.03 - (1.38\pm0.09)\cos\theta + (0.14\pm0.24)\frac{3\cos^2\theta - 1}{2}\right](1\pm0.10) \quad \text{(at 65 Mev)}.$$

Because of Coulomb interference effects, the experiment, affords the opportunity of determining the signs as well as the magnitudes of the phase shifts in an analysis including only s and p waves. It is found that two very markedly different sets of phase shifts fit the data. Each of these sets includes subsets of the Fermi and Yang type. The results of this experiment, in conjunction with those of similar experiments, favor a set characterized by a strong attractive p wave interaction in the $T = \frac{3}{2}$ isotopic spin state.

I. INTRODUCTION

THE angular distribution in the three scattering processes $\pi^+ + p \to \pi^+ + p$, $\pi^- + p \to \pi^- + p$, and and $\pi^- + p \to \pi^0 + n$, has been studied by Anderson, Fermi, Martin, and Nagle[1] at 120 and 135 Mev. The information has been extended to lower energy by several groups,[1–6] chiefly for positive pions. We present here a rather detailed study of the three processes at approximately 65 Mev. The experimental results for the $\pi^+ \to \pi^+$ reaction have been reported in brief.[7]

The results of the Chicago group were analyzed in terms of s and p wave scattering in the charge independent theory.[1] The reported phase shifts are, however, indeterminate with respect to a simultaneous reversal of the signs of all phase shifts. This ambiguity may, in principle, be removed by extending the study of the scattering to angles for which the Coulomb amplitude is of the same order of magnitude as the nuclear amplitude. This encounters experimental difficulties at high energies, because the angles of prominent Coulomb interference are small and the background from Coulomb and diffraction scattering in the beam-defining system and hydrogen container is then large. The situation is more favorable at lower energies, because small nuclear and larger Coulomb amplitudes both act to increase the angles at which the interference is appreciable. At 65 Mev, for example, the total cross section for positive pions is 20 mb, compared to approximately 90 mb at 120 Mev, while the differential Coulomb cross section at 30° is 0.14 mb per steradian at 65 Mev compared to 0.06 mb per steradian at 120 Mev.

In this experiment, therefore, the effects of the Coulomb field are quite large. Nevertheless, we find it possible to fit the experimental results with two sets of phase shifts differing in sign, but the magnitudes in one set differ considerably from those in the other. It may be possible to remove the ambiguity in sign by arguments as to magnitude. In the last section of this report we discuss an attempt to select one set by extrapolating the results at other energies.

II. EXPERIMENTAL ARRANGEMENT

A. Meson Beams

The positive-meson scattering experiment was performed in the meson beam of lowest energy at the Columbia Nevis Cyclotron. The mesons are produced at an internal beryllium target, are analyzed in the fringing field of the cyclotron magnet, and emerge through a channel in the 8-ft iron shielding.

For negative-meson scattering, an attempt was made to use the corresponding beam obtained by reversing the current in the cylcotron magnet. The negative mesons are, however, accompanied by a large number of electrons, probably due to the production of neutral mesons and conversion in the target of the resultant γ rays. The dependence of this contamination on meson

* This research was supported by the joint program of the U. S. Office of Naval Research and the U. S. Atomic Energy Commission.

[1] Anderson, Fermi, Martin, and Nagle, Phys. Rev. **91**, 155 (1953).
[2] Fowler, Fowler, Schutt, Thorndyke, and Whittemore, Phys. Rev. **86**, 1053 (1952); **91**, 135 (1953).
[3] G. Goldhaber, Phys. Rev. **89**, 1187 (1953).
[4] Minguzzi, Puppi, and Ranzi (to be published). We wish to thank Professor Puppi for a prepublication copy of this work.
[5] A. Roberts and J. Tinlot, Phys. Rev. **90**, 951 (1953).
[6] J. P. Perry and C. E. Angell, Phys. Rev. **91**, 1289 (1953).
[7] Bodansky, Sachs, and Steinberger, Phys. Rev. **90**, 996 (1953); **90**, 997 (1953).

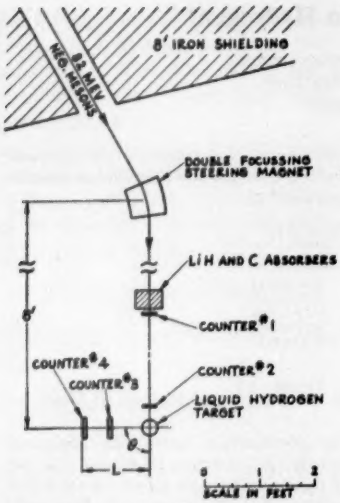

FIG. 1. Experimental arrangement ($\pi^- + p \rightarrow \pi^- + p$).

sign is then related to the fact that the collimated negative particles are emitted in the forward direction and the positive particles in the backward direction with respect to the proton beam. In the region of interest the number of conversion electrons is a rapidly decreasing function of electron momentum. It is, therefore, possible to reduce this contamination by using a meson beam of higher energy and then decreasing the energy with absorbers.

Each beam is further analyzed in a double-focusing magnet (Fig. 1). The mesons are bent through 30°, and a parallel, monochromatic beam is focused in both planes at a distance of 10 ft from the magnet. The beam is defined in the scintillation counter 1–2 telescope. In the case of the negative meson scattering, an absorber of 4 in. of lithium hydride (density$\sim$0.5) and $\frac{1}{2}$-in. of carbon is inserted before the first counter to reduce the beam energy without excessive Coulomb scattering. In the position of Fig. 1 the absorber reduces the intensity by 30 percent. If the absorber, instead, is placed between the shielding and the analyzing magnet, the intensity is reduced to less than $\frac{1}{10}$.

B. Liquid Hydrogen Target

The liquid hydrogen scatterer[8] is contained in the 3.1-in. diameter cylindrical cup of the metal Dewar shown in Fig. 2. The target cup, made from stainless steel tubing turned to 0.004-in. wall thickness, is soldered to the bottom of the larger liquid hydrogen reservoir. The hydrogen in the reservoir can be admitted to the target cup by means of a standpipe of thin wall tubing extending to the bottom of the cup. It may be returned by increasing the pressure in the cup relative to that in the reservoir. This is accomplished by closing the cup exhaust and heating a resistance element at the bottom of the cup (not shown).

The hydrogen reservoir is surrounded by a container of liquid nitrogen which serves as a radiation shield. The target cup itself is shielded by a foil of 0.001-in. aluminum fastened to the bottom of the nitrogen reservoir. The design of the vacuum chamber surrounding the cup represents a compromise between conflicting requirements. In particular, it is desirable to be able to place the defining telescope near the cup, to be able to detect particles over a wide angular region, and to have the walls of the chamber as thin as possible to minimize pion scattering and γ-ray conversion. The thin wall of the vacuum chamber is a U-shaped aluminum foil, $3\frac{3}{4}$-in. high and 0.007 in. thick. The cup may be viewed through the thin window over an angle of 300° (see Fig. 2).

The liquid levels in the cup and reservoirs are indicated on oil manometers. The hydrogen capacity of the reservoir is 4 liters; the rate of loss is approximately 0.1 liter per hour.

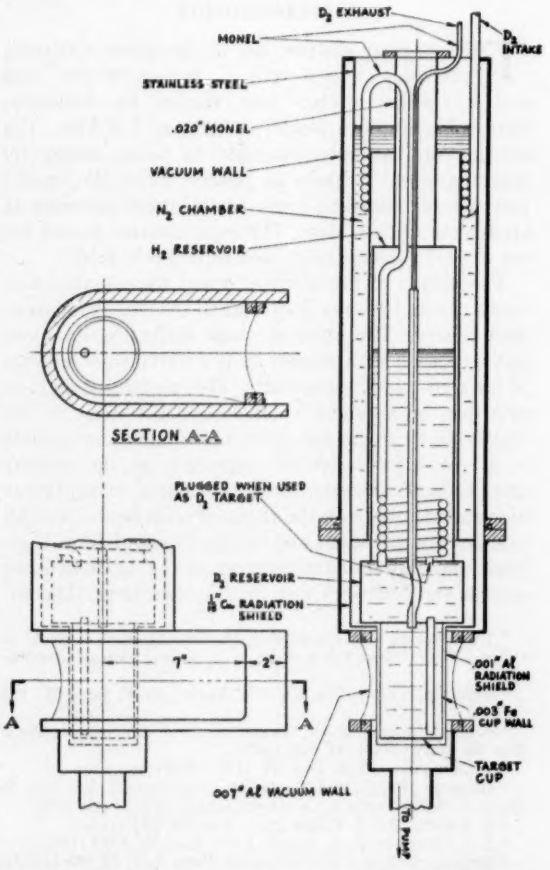

FIG. 2. Liquid hydrogen target. May also be used with deuterium.

[8] Lindenfeld, Sachs, and Steinberger, Phys. Rev. 89, 531 (1951).

C. Counters

The two stilbene crystals defining the incident beam are each viewed from the side by two 1P21 photomultipliers. Counter 1 is $3\frac{1}{4}$ in.$\times 2\frac{1}{2}$ in.$\times\frac{1}{8}$ in. Counter 2 is $2\frac{1}{4}$ in.$\times 2\frac{3}{4}$ in.$\times\frac{1}{16}$ in., and is located as close to the target as possible to insure that most of the incident beam enters the hydrogen. Counter 2 is thin to minimize the diffraction scattering from the crystal, since this contributes strongly to the background at small angles.

The scattered particles are detected in the larger liquid scintillation counters 3 and 4. In $\pi^+\rightarrow\pi^+$ and $\pi^-\rightarrow\pi^-$ scattering, the mesons are detected in two counters, 4 in.$\times$8 in.$\times$1 in., illustrated in Fig. 3. The scintillating liquid, phenylcyclohexane with terphenyl and diphenylhexatriene, is held in a Lucite container. The Lucite fits into a metal frame, with aluminum foil covering the faces, and with iron shields to hold 1P21

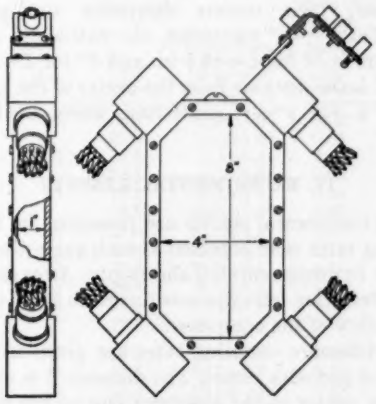

FIG. 3. Liquid scintillation counter used in detection telescope for elastic scattering.

phototubes at each of the four corners. The light collection is poor compared to that in the smaller counters, and this is probably responsible for the rather low detection efficiency ($\sim$95 percent for the 2-counter telescope; see Sec. V). On the other hand, for a given angular resolution the large size (in comparison to the size of the scatterer) and rectangular shape of the counters result in a larger counting rate than would be obtained with smaller or circular counters.

In the charge-exchange scattering, single γ rays are detected in the telescope shown in Fig. 4. The γ rays are converted primarily in the $\frac{1}{4}$-in. lead. Counter 3 is a $4\frac{1}{2}$-in. diameter circular liquid counter, viewed from the side by three 1P21 photomultipliers. Counter 4 is large in order to accept electrons scattered in the converter. It is 8 in. in diameter, liquid-filled, and viewed from the back by 4 1P21's.[9] The beryllium and polyethylene absorbers are placed in front of the converter in order to

[9] Durbin, Loar, and Havens, Phys. Rev. 88, 179 (1952).

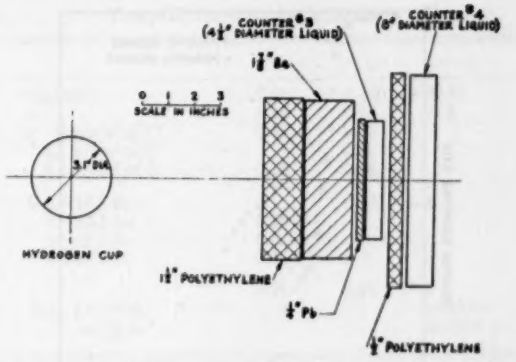

FIG. 4. γ-ray detection telescope used in charge-exchange scattering.

stop ionizing particles. The absorber between counters 3 and 4 is intended to stop protons from low-energy neutron interactions in either counter.

D. Electronics

A block diagram of the electronics is shown in Fig. 5. Signals are taken in parallel from the phototubes of each counter and fed into Hewlett Packard wide-band amplifiers. Coincidences are made between pairs of the amplified signals in diode bridge circuits with a resolving time of 10^{-8} sec. The coincidence signals are then amplified to a level of approximately 10 v, discriminated in a diode circuit, and then formed to uniform negative pulses 5×10^{-8} sec long and 15 v high. The dead time of the pulse former is $\sim10^{-7}$ sec.[10] The outputs are again paired in diode coincidence circuits, as shown in Fig. 5. The 1–2 pulse is scaled in a system with 10^{-7} sec dead time.[11] All other circuits are commercially available through the Atomic Instrument Company. Inspection of the block diagram shows that the resolving time for accidental coincidences between 1–2 counts and 3–4 counts is just that of the 1–3 coincidence, $\sim10^{-8}$ sec. Several intermediate coincidence rates are scaled to check the operation of the equipment, but the pertinent

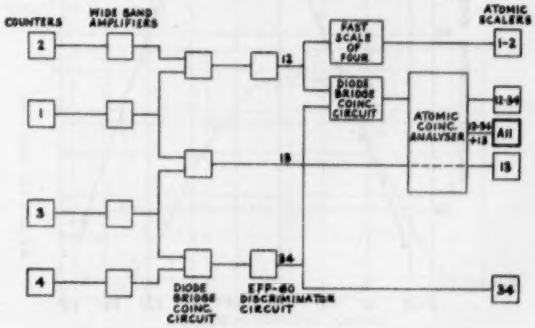

FIG. 5. Block diagram of electronics.

[10] We are indebted to V. Fitch for the design of this circuit.
[11] V. Fitch, Rev. Sci. Instr. 20, 942 (1949).

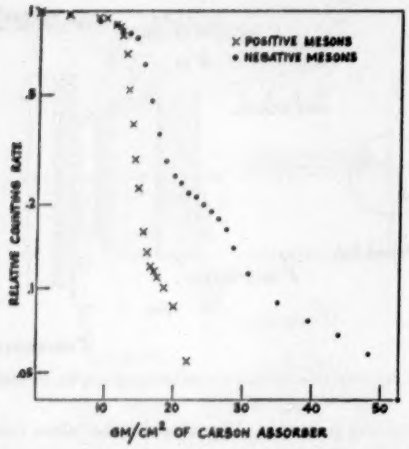

FIG. 6. Range curves for positive and negative meson beams.

data are the over-all quadruple counts and the 1–2 counts.

III. CALIBRATION MEASUREMENTS

A. Beam Energy

The integral range distributions of the two beams were determined by placing counter 3 in line with counters 1 and 2, ~12 in. behind counter 2, and measuring the ratio of rates 1–2–3 and 1–2 as a function of the thickness of carbon absorber placed in front of counter 3. The results are given in Fig. 6 for the positive and negative meson beams. Each of these curves exhibits the characteristic initial slope due to nuclear interactions of the pions and a sharp drop as the pions reach the end of their range in the absorbers. A second drop occurs at a higher range corresponding to μ mesons with the same momentum. The remainder of the beam is attributed to electrons.

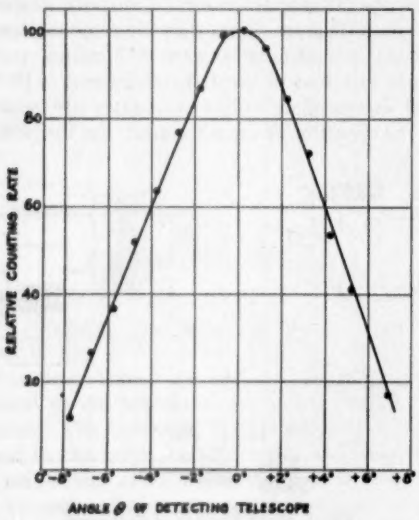

FIG. 7. Angular resolution in elastic scattering, measured by rotating detecting telescope through forward angles. (For $\pi^+ + p \rightarrow \pi^+ + p$, with $L = 27.5$ inches.)

Using Aron's tabulation[12] of the range-energy relationships, the mean energy of the pions at the center of the target is determined to be 58 Mev for the positive and 65 Mev for the negative mesons. The half-width of the energy distribution at half-maximum is esitmated to be 3 Mev for the positive mesons and 5 Mev for the negative mesons and is due to the initial beam spread, ionization loss in the target, and the effect of the absorbers in the negative beam.

B. Angular Resolution

By rotating the detecting telescope through the forward angles, curves like the one shown in Fig. 7 are obtained for each geometry in the $\pi^+ \rightarrow \pi^+$ and $\pi^- \rightarrow \pi^-$ scattering. These curves are a measure of the angular resolution; their centers determine the positions $\theta = 0°$. For $\pi^+ \rightarrow \pi^+$ scattering, the half-width at half-maximum is 7° for $L = 18.5$ in. and 5° for $L = 27.5$ in. where L is the distance from the center of the target to counter 4. For $\pi^- \rightarrow \pi^-$ scattering, where $L = 15.5$ in., it is 11°.

IV. EXPERIMENTAL RESULTS

The experimental results are presented in Table I. Counting rates were obtained at each angle alternately with the hydrogen cup full and empty. After each such set the detecting telescope was turned to $\theta = 0°$ to check the stability of the equipment.

The difference counting rates are given with their statistical probable errors. The distance L is measured from the center of the hydrogen cup to the center of counter 4 for the elastic scattering and to the front of counter 3 for the charge-exchange scattering measurements. In some measurements, carbon absorber was placed in front of counter 4 to reduce the background from short-range particles. The thickness of the absorber is indicated in the last column.

With average cyclotron conditions, 10^8 particles passed through the defining telescope in about 10 minutes for both the positive and negative beams. With this intensity, approximately 110 hours of operation were required to make the measurements listed in Table I.

V. CALCULATION OF CROSS SECTIONS

The differential cross sections in the laboratory system are calculated using the relation

$$\frac{d\sigma'}{d\Omega} = \frac{10^{-6}n}{N_0 A^{-1} t \rho (1-\alpha)\epsilon \Omega'}, \qquad (1)$$

[12] W. A. Aron, University of California Radiation Laboratory UCRL 1325 (unpublished).

where $d\sigma'/d\Omega$=uncorrected differential cross section, n=counting rate per 10^6 incident particles, N_0=Avogadro's number, A=atomic weight of hydrogen, t=average thickness of hydrogen target (g/cm²), ρ=fraction of incident particles which are π mesons, α=attenuation of scattered mesons caused by nuclear absorption, ϵ=efficiency of detector telescope, and Ω=solid angle of detector telescope. The counting rates, n, are obtained from Table I. The values used for the other relevant quantities are listed in Table II and are discussed below.

A. Target Thickness

In order to determine the average thickness of the liquid hydrogen in the path of the mesons counted in the incident telescope, the lateral extension of the positive and negative beams was scanned with a $\frac{1}{8}$-in. wide crystal directly behind the target. The experimental curve taken in the positive beam is shown in Fig. 8. By extrapolating this curve to the center of the hydrogen cup and folding it into a circle of diameter 3.1 in. (the horizontal cross section of the cup), the relevant weighted average of the distance through the cup is obtained. The net thickness t of the liquid hydrogen minus that of gas remaining in the cup when the liquid is removed is 0.460 g/cm² for the positive and 0.440 g/cm² for the negative beam.

Table I. Experimental data.

	θ_{lab} (deg)	L (in.)	Counts from hydrogen per 10^6 incident particles	Ratio of counts from hydrogen to background	Carbon absorber (g/cm²)
$\pi^+\to\pi^+$	30	32.5	1.5±1.6	0.02	0
		27.5	2.1±1.4	0.04	4.4
	40	27.5	5.2±0.8	0.19	0
		18.5	4.2±4.8	0.05	0
	55	27.5	4.5±1.6	0.26	0
		18.5	14.0±1.3	0.47	0
	90	27.5	11.5±1.2	1.96	0
		18.5	20.4±1.1	1.11	0
	120	27.5	11.9±1.4	1.44	0
		18.5	30.5±1.6	1.36	0
	150	27.5	12.0±1.5	1.04	0
		18.5	32.2±1.5	0.92	0
$\pi^-\to\pi^-$	35	15.5	29.4±3.8	0.10	4.4
	45	15.5	16.7±2.3	0.13	4.4
	60	15.5	10.1±1.3	0.23	4.4
	90	15.5	8.0±1.0	0.26	2.2
	145	15.5	3.6±1.3	0.06	0
$\pi^-\to\gamma$	45	11	7.6±0.6	0.68	
	90	11	15.2±0.6	2.53	
	145	11	20.2±1.5	1.75	
		14	12.1±0.9	1.12	

B. Beam Purity

The composition of the incident beam is determined from the range curves of Fig. 6. The μ mesons and electrons, which are assumed to undergo negligible scattering in hydrogen, are estimated to comprise 11 percent of the positive and 22 percent of the negative beam. The remainder consists of pions.

Table II. Experimental parameters.

	$\pi^+\to\pi^+$	$\pi^-\to\pi^-$	$\pi^-\to\gamma$
t(g/cm²)	0.460	0.440	0.440
ρ	0.89	0.78	0.78
α 0 g/cm² of C	0.03	0.03	
2.2 g/cm² of C		0.06	
4.4 g/cm² of C	0.08	0.08	
Ω L=15.5 in.		0.123	
L=18.5 in.	0.0860		
L=27.5 in.	0.0389		
L=32.5 in.	0.0229		
ϵ	0.91	0.97	
$(\epsilon\Omega)_1$ L=11 in.			0.0357[a]
L=14 in.			0.0220[a]

[a] For γ rays from stopped mesons.

C. Nuclear Attenuation

A fraction, α, of the scattered mesons will not be counted by the detection telescope because of interactions in counter 3 and in the carbon absorbers which were at times placed in front of counter 4. Counter 3 contains 2.2 g/cm² of carbon. The values listed in Table II are calculated using a mean free path in carbon of 80 g/cm² for the loss of mesons from the detecting system.[13]

D. Solid Angle and Efficiency—Elastic Scattering

In the elastic scattering measurements the solid angle Ω is defined by counter 4. It is estimated that, on the average, a meson must penetrate $\frac{1}{4}$-in. into counter 4 to be detected, and, therefore, the appropriate distance in calculating the solid angle is $L-\frac{1}{4}$ in. A small correction is made to account for the fact that the average distance from the target to the counter is greater than the distance along the central axis. The solid angles calculated from these considerations are listed in Table II.

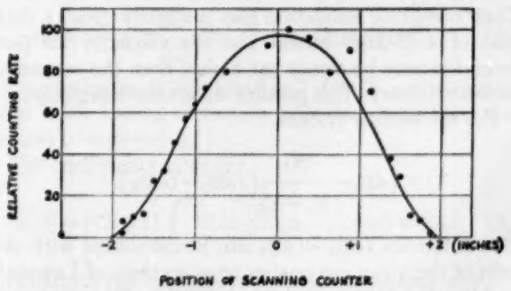

Fig. 8. Lateral distribution of positive meson beam directly behind hydrogen target measured with small scanning counter.

[13] Isaacs, Sachs, and Steinberger, Phys. Rev. 85, 803 (1952).

The efficiency ϵ of the detecting telescope for counting charged mesons is measured by placing the larger counters 3 and 4 between counters 1 and 2, and finding the ratio of over-all quadruple coincidences to 1–2 coincidences. For positive mesons this ratio is found to be 0.91, while for negative mesons it is 0.97. The improvement in the latter case is believed due to a change of phototubes.

E. Solid Angle and Efficiency—Charge Exchange Scattering

In order to maximize the efficiency for gamma rays, a lead converter is used which is $\frac{1}{4}$ in. thick (1.2 radiation lengths) and covers the area of counter 3. As a consequence, the complications of multiple processes and scattering of the resulting electrons prevent a simple and accurate calculation of the efficiency or solid angle. In fact, the quantities ϵ and Ω cannot here be independently defined, It is, therefore, advantageous to determine experimentally the product $\epsilon\Omega$.

The calibration of $\epsilon\Omega$ is obtained by comparing the counting rate of the normal system with that in a detection system for which the efficiency can be calculated rather accurately. γ rays from negative pions stopped in hydrogen are used in the comparison, providing a high flux with known energy distribution.[14] Absorbers are therefore placed in the incident beam and the resulting γ rays are detected in three different geometries: (1) the system normally used (see Fig. 4); (2) the same geometry with the exception that the absorbers and converter are replaced by a thin lead converter, 0.97 g/cm^2 thick and 4 in. in diameter, directly in front of counter 3; (3) the same geometry as in (2), but with the thin lead converter replaced by a polyethylene absorber in which ionization losses are the same. Counting rates for the events from hydrogen are $N_1=764\pm12$, $N_2=296\pm6$, and $N_3=160\pm5$ per 10^6 incident particles. In addition, we require the efficiency of the 3–4 telescope for counting electron pairs. The efficiency for counting mesons is found to be 84 percent by the method used in the elastic scattering experiments. In most cases two electrons pass through the telescope for each γ ray converted in the thin lead. Their combined ionization loss is slightly greater than that of a 65-Mev meson and the efficiency for pair detection may be somewhat higher than the measured meson efficiency. This possible difference is neglected.

For the normal system,

$$(\epsilon\Omega)_1=\frac{N_1}{N_2-N_3}[(\epsilon\Omega)_2-(\epsilon\Omega)_3].$$

The difference $(\epsilon\Omega)_2-(\epsilon\Omega)_3$ can be calculated with the help of the γ-ray conversion cross sections of Lawson[15] and Dewire, Ashkin, and Beach.[16] With thin converters, multiple processes can be neglected and, in the geometry used, scattering corrections are unnecessary. For the γ rays from stopped mesons, the effective mean free path in lead is 11.4 g/cm^2, corresponding to a conversion efficiency of 0.082 in the thin lead converter. The conversion efficiency of the polyethylene is calculated to be 0.007. Therefore, for $L=11$ in., $(\epsilon\Omega)_2-(\epsilon\Omega)_3=0.00655$ and $(\epsilon\Omega)_1=0.0368$ steradian.

This efficiency, together with the corresponding value for $L=14$ in., is listed in Table II. The values include an additional small correction, 3 ± 2 percent, for the effects of γ ray conversion in the heavy members of the target. These values are for the γ rays from stopped mesons and must be adjusted to account for the different energies in the scattering experiment.

The quantities in Table II, other than the γ-ray efficiency-solid angle products, are believed to be sufficiently well known that errors in their determination do not contribute significantly to the errors in the determination of the cross sections. The γ-ray products $(\epsilon\Omega)_1$ have three principle sources of error: (1) A statistical probable error of 6 percent due to errors in the counting rates N_1, N_2, and N_3; (2) An uncertainty in the efficiency for pair detection which is estimated to be $+5$ to -3 percent; (3) The 2 percent uncertainty in the correction for electrons converted in the heavy parts of the target. The over-all probable error in the products $(\epsilon\Omega)_1$ is therefore about ±10 percent.

F. Corrections

Several corrections are applied to the cross sections calculated from Eq. (1). Correction 1 is applied to the $\pi^+\rightarrow\pi^+$ cross sections at all angles in an attempt to correct for the decrease in background counts when hydrogen is in the cup. One would like to assume in a subtraction procedure that the background is unaffected by the presence of the target—in this case the liquid hydrogen. This is not always justifiable. For instance, a meson star in the wall of the target cup could have a proton prong which will be detected if the cup is empty, but, due to additional ionization loss in the hydrogen, will not be detected if the cup is full. Inelastic meson scattering can give rise to similar events. An attempt to set an upper limit on this effect was made by comparing the background counting rates with different amounts of carbon absorber in the path of the background particles. It was found on this basis that if half of the background traverses the entire cup, then the measured laboratory differential cross sections decrease by about 0.12 mb. This is probably an overestimate of the effect as some of the background does not arise in the walls of the cup. Therefore, a small correction of 0.08 ± 0.06 mb/steradian is added to the cross sections. In the $\pi^-\rightarrow\pi^-$ scattering the same problem exists, but to a smaller extent, since the number of protons from negative meson stars is considerably less than from positive meson stars. The correction is expected to be small and,

[14] Panofsky, Aamodt, and Hadley, Phys. Rev. **81**, 565 (1951).
[15] J. L. Lawson, Phys. Rev. **75**, 433 (1949).
[16] Dewire, Ashkin, and Beach, Phys. Rev. **83**, 505 (1951).

since it requires untested assumptions about the nature of the background, no similar correction is made.

Correction 2 is applied to the $\pi^-\to\gamma$ cross sections to account for the γ rays from the radiative capture of the meson. The cross section for this process is calculated from that of the inverse process, which is taken to be equal[17] to the cross section for the process $\gamma+p\to\pi^+ +n$.[18] The correction is 0.06 mb/steradian.

Correction 3 is applied to the $\pi^-\to\pi^-$ cross sections to account for the detection of converted γ rays. 1.1 percent of the γ rays produced in charge-exchange scattering are internally converted in the hydrogen[8,19] and an additional 2.4 percent are converted in passing through the target. An approximate calculation indicates that electrons from γ rays converted in the heavy brass parts of the target contribute an additional flux in the detecting telescope equal to 2.5±1.5 percent of the γ-ray flux. Thus at each angle we subtract from the observed $\pi^-\to\pi^-$ cross section 0.06±0.02 of the $\pi^-\to\gamma$ cross section.

Correction 4 is applied only to the 150° point in the $\pi^+\to\pi^+$ scattering. Mesons detected in the backward direction have about one-half the energy of the incident mesons. In the arrangement used, those mesons which traverse most of the hydrogen target are then scattered at 150°, and have to pass again through most of the target before reaching the telescope, may have insufficient range to be counted. The correction for this effect required the addition of 10±5 percent to the measured cross section at 150°. No similar correction is required in the $\pi^-\to\pi^-$ scattering, as the incident meson energy is greater.

G. Calculated Cross Sections

The laboratory cross sections for the elastic scattering processes, as calculated from Eq. (1) and including the corrections discussed above, are presented in Table III. The corresponding center-of-mass angles and cross sections are also given. The errors include only the probable statistical errors and the probable errors in the corrections. Other uncertainties are thought to be small.

In charge-exchange scattering the neutral pion distribution is related to the γ-ray counting rate, $n(\theta)$, by

$$n(\theta)=Cq(\theta)\int\frac{d\sigma(\theta')}{d\Omega'}W(\alpha)\epsilon\Omega(E)d\Omega', \qquad (2)$$

where θ=angle of detected γ ray in the laboratory system, $\theta'=\pi^0$ angle in the center-of-mass system, $\theta''=\gamma$-ray angle in the center-of-mass system. α=angle between π^0 and γ ray in the center-of-mass system, βc=velocity of $\pi^\pm$ in the center-of-mass system, $\beta_0 c$ =velocity of center of mass, $d\sigma(\theta')/d\Omega'=\pi^0$ differential cross section in the center-of-mass system, $W(\alpha)$ =probability that a π^0 emits a γ ray at an angle α $=(1-\beta^2)/2\pi(1-\beta\cos\alpha)^2$,

$E(\theta,\alpha)=\gamma$-ray energy in the laboratory system

$$=\frac{m_\pi c^2}{2}\left(\frac{1-\beta^2}{1-\beta_0^2}\right)^{\frac{1}{2}}\frac{1+\beta_0\cos\theta''}{1-\beta\cos\alpha},$$

$$C=10^4/N_0A^{-1}\rho,$$

$$q(\theta)=\left(\frac{d\sigma_\gamma}{d\Omega}\right)_{\text{lab}}\Big/\left(\frac{d\sigma_\gamma}{d\Omega}\right)_{\text{c.m.}}=(1-\beta_0^2)/(1-\beta_0\cos\theta)^2.$$

To integrate Eq. (2) we use an expansion in Legendre polynominals similar to that of Anderson, Fermi, Martin, and Nagle,[1] but with the explicit consideration of the variation with energy of γ-ray detection efficiency. If pion scattering occurs only in the s and p states (see Sec. VI), the cross section can be expressed as

$$\frac{d\sigma(\theta')}{d\Omega'}=\sum_{l=0}^{2}\sigma_lP_l(\cos\theta').$$

Similarly,

$$W(\alpha)\epsilon\Omega(\theta,\alpha)=\sum\omega_l(\theta)P_l(\cos\alpha).$$

Then

$$n(\theta)=4\pi Cq(\theta)\sum_{l=0}^{2}(2l+1)^{-1}\sigma_l\omega_l(\theta)P_l(\cos\theta''). \qquad (3)$$

The counting rates $n(\theta)$ listed in Table IV, are obtained from Table I using correction 2 for the γ rays from the process $\pi^-+p\to\gamma+n$.

The coefficients $\omega_l(\theta)$ are

$$\omega_l(\theta)=\tfrac{1}{2}(2l+1)\int_0^\pi W(\alpha)\epsilon\Omega(\theta,\alpha)P_l(\cos\alpha)\sin\alpha d\alpha. \qquad (4)$$

To evaluate the coefficients we must determine $\epsilon\Omega(\theta,\alpha)$, i.e., determine the energy dependence of the efficiency. Silverman and Cocconi[20] have found in a similar teles-

TABLE III. Differential cross sections.

	Laboratory system		Center-of-mass system	
	θ(deg)	$\frac{d\sigma}{d\Omega}$ (mb/sterad)	θ(deg)	$\frac{d\sigma}{d\Omega}$ (mb/sterad)
$\pi^+\to\pi^+$	30	0.33±0.15	36	0.24±0.11
58 Mev	40	0.64±0.10	47	0.48±0.08
	55	0.81±0.08	64	0.66±0.06
	90	1.21±0.06	101	1.24±0.07
	120	1.68±0.09	129	2.10±0.11
	150	1.95±0.10	155	2.79±0.15
$\pi^-\to\pi^-$	35	1.24±0.17	42	0.91±0.13
65 Mev	45	0.66±0.10	53	0.51±0.08
	60	0.35±0.07	70	0.29±0.06
	90	0.22±0.06	101	0.23±0.06
	145	−0.01±0.07	151	−0.01±0.11

[17] The experimental evidence on the equality of the $\gamma+p$ and $\gamma+n$ photoproduction rests on the near-unity ratio of π^-/π^+ photoproduction in deuterium. See, e.g., White, Jacobson, and Schultz, Phys. Rev. **88**, 836 (1952), and R. M. Littauer and D. Walker, Phys. Rev. **86**, 838 (1952).

[18] Luckey, Jenkins, and Wilson, Phys. Rev. **91**, 468 (1953); G. Bernardini (private communication).

[19] Cornelius, Sargent, Rinehart, Lederman, and Rogers, Phys. Rev. **92**, 1583 (1953).

[20] G. Cocconi and A. Silverman, Phys. Rev. **88**, 1230 (1952).

cope that the detection efficiency may be represented by

$$\epsilon = \text{const} \times (1 - e^{-(E-2\delta)/40}), \tag{5}$$

where E is in Mev. Ignoring the slight difference in geometry, we assume the same energy dependence but determine the constant from the measured value of $(\epsilon\Omega)_1$ for γ rays from stopped mesons. Using the known energy spectrum of these γ rays[14] the proportionality constant for $\epsilon\Omega$ is calculated to be 0.0471 steradian.

Inspection of (5) shows that the detection efficiency is an increasing function of γ-ray energy, and its inclusion in (4) has the effect of favoring the detection of γ rays with small correlation angles α. The correlation between γ ray and π^0 is, therfore, somewhat better than would be obtained with a detection system of uniform efficiency. If the energy dependent $\epsilon\Omega$ is replaced by some average value, at best chosen to give the same total cross section, the correlation coefficients ω_0 remain essentially the same, but ω_1 is depressed approximately by the factor 1.3 and ω_2 by 1.5.

Equation (4) is integrated numerically and the resulting coefficients are listed in Table IV. Equation

TABLE IV. Corrected γ-ray counting rates $n(\theta)$ and correlation coefficients $\omega_l(\theta)$.

Lab. angle θ	$n(\theta)$	Correlation coefficients $\omega_l(\theta)$ $l=0$	$l=1$	$l=2$
45°	7.0±0.8	5.76×10^{-3}	11.12×10^{-3}	9.54×10^{-3}
90°	14.6±0.9	5.46	10.83	9.40
145°	19.3±1.6	5.12	10.49	9.18

(3) is evaluated at the three experimental angles θ. We find $\sigma_0 = 0.96\pm0.03$ mb/sterad, $\sigma_1 = -1.38\pm0.09$ mb/sterad, $\sigma_2 = 0.14\pm0.24$ mb/sterad. The errors correspond to the statistical probable errors in $n(\theta)$. The previously discussed 10 percent uncertainty in detection efficiency is not included. The error due to possible inadequacy of the assumed energy dependence of the efficiency is believed to be small, since the calibration is performed at an intermediate energy. We therefore find for the center-of-mass system,

$$d\sigma(\theta)/d\Omega(\pi^-\to\pi^0) = (1\pm0.10)[0.96\pm0.03 - (1.38\pm0.09)\cos\theta + (0.14\pm0.24)(3\cos^2\theta-1)/2].$$

The corresponding center-of-mass γ-ray cross section is

$$d\sigma(\theta)/d\Omega(\pi^-\to\gamma) = (1\pm0.10)[1.98\pm0.6 - (1.41\pm0.09)\cos\theta + (0.07\pm0.11)(3\cos^2\theta-1)/2].$$

VI. PHASE-SHIFT ANALYSIS

We have attempted to express the experimental results in terms of phase shifts. Following the Chicago group,[1] the analysis is performed assuming (a) that the meson-nucleon coupling is charge-independent, and (b) only s and p states scatter appreciably. There is a growing body of evidence[21] to support (a), chiefly the experiments on nucleon-nucleon meson production,[22] the level structure of isobaric nuclei,[23] and perhaps also the success of the assumption in this and preceding experiments.[1] In support of (b) we note that in this experiment the meson momentum is 0.88 $m_\pi c$, and if the meson-nucleon interaction has a range not in excess of the mson Compton wavelength ($\sim1.4\times10^{-13}$ cm) the scattering in higher angular momentum states may be expected to be small. Nevertheless, appreciable d scattering, even at this low energy, is entirely possible. The experiment does not permit the determination of the relative importance of higher orbital states. On the other hand, the pronounced asymmetries about 90° do make it necessary to combine at least one even and one odd state.

In the analysis of the higher energy experiments the magnitudes of the phase shifts were determined, but an ambiguity remained which permitted the simultaneous reversal of the signs of all phase shifts. This ambiguity may, in principle, be removed by studying the scattering in situations in which the Coulomb interference enters significantly, since the Coulomb amplitudes are known. At the smallest angles of this experiment the Coulomb amplitudes are of the same order of magnitude as the observed amplitudes and, therefore, effect the scattering strongly.

An analysis of pion-nucleon scattering with the inclusion of Coulomb effects has been made by Van Hove.[24] For the present purposes it is necessary to retain only first-order Coulomb terms and to consider the phase shifts small. In this approximation the cross sections are

$$\frac{d\sigma}{d\Omega} = \lambda^2\left\{\left[\sum_{l=1}^{4}\xi^l\left(\frac{\alpha}{2\sin^2(\theta/2)}+X^l+Y^l\cos\theta\right)\right]^2 + \left(\sum_{l=1}^{4}\xi^l Z^l\right)^2\sin^2\theta\right\}, \tag{6}$$

where $\lambda = (2\pi)^{-1}\times$wavelength in the center-of-mass system, $X^l=\delta(S^l)$, $Y^l=2\delta(P_{\frac{3}{2}}{}^l)+\delta(P_{\frac{1}{2}}{}^l)$, $Z^l=\delta(P_{\frac{3}{2}}{}^l)-\delta(P_{\frac{1}{2}}{}^l)$, and for $\pi^+\to\pi^+$: $\xi^1=0$, $\xi^3=1$, $\alpha=-e^2/\hbar v$; for $\pi^-\to\pi^-$: $\xi^1=\frac{2}{3}$, $\xi^3=\frac{1}{3}$, $\alpha=+e^2/\hbar v$; for $\pi^-\to\pi^0$: $\xi^1=-\sqrt{2}/3$ $\xi^3=\sqrt{2}/3$, $\alpha=0$. The precise determination of v in the Coulomb term requires solution of the relativistic two-body problem, but according to Van Hove the relative velocity in the center of mass may be expected to be nearly correct.

The degree of agreement between the observed cross sections and calculated ones can be quantitatively expressed in terms of

$$\omega = \sum_{i=1}^{14}\left(\frac{\Delta_i}{\text{PE}_i}\right)^2,$$

[21] Henley, Ruderman, and Steinberger, Ann. Rev. Nuclear Sci. (to be published).

[22] R. H. Hildebrand, Phys. Rev. 89, 1090 (1953).

[23] Ajzenberg and Lauritsen, Revs. Modern Phys. 24, 321 (1952).

[24] L. Van Hove, Phys. Rev. 88, 1358 (1952).

where Δ_i is the difference between the observed and calculated cross sections at the ith point and PE_i is the probable error of the cross section at the ith point. The best fit is the one which minimizes ω, but any fit which gives a sufficiently small value of ω is an acceptable fit. The determination of the phase shifts which give the best fit and an analysis of the possible deviation of the phase shifts from the best-fit values is difficult without the aid of computing machines. Mr. N. Mitropoulos has kindly consented to investigate this problem using the Los Alamos computer. Pending the completion of this more thorough analysis, a preliminary study has been made.

It will be noticed that the experimental cross sections are obtained at two energies, 65 and 58 Mev. The phase shifts were calculated to apply at 65 Mev, and were extrapolated for the purpose of comparison with the $\pi^+ \rightarrow \pi^+$ results at 58 Mev. In the absence of information on the energy dependence of the individual phases, we have decreased all phase shifts in proportion to the cube of the center-of-mass momentum, in accord with the observed energy dependence of the total cross section.

TABLE V. Phase shifts at 65 Mev.

	Phase shifts in degrees					
	$\delta(S_{\frac{1}{2}})$	$\delta(P_{\frac{3}{2}})$	$\delta(P_{\frac{1}{2}})$	$\delta(S_{\frac{3}{2}})$	$\delta(P_{\frac{3}{2}})$	$\delta(P_{\frac{1}{2}})$
Fermi type:						
Set IA	−6.2	−1.9	+9.1	+10.9	+0.4	−2.6
Set IIA	+14.5	−1.4	−2.8	−4.6	−1.3	+7.1
Yang type:						
Ste IB	−6.2	+12.8	+1.7	+10.9	−3.6	−0.6
Set IIB	+14.5	−3.2	−1.9	−4.6	+9.9	+1.5

There are four sets of phase shifts which give reasonably good fits. It is believed that the data preclude sets of phase shifts radically different from these. These phase shifts are listed in Table V.[25] Sets A and B differ in the reversal of the signs of the spin-flip terms Z^1 and correspond to the types first discussed by Fermi and Yang, respectively.[1] For small phase shifts the Fermi and Yang solutions lead to identical cross sections, and no choice can be made between them.

The cross sections determined by these phase shifts are compared with the experimental results in Figs. 9, 10, and 11. In the charge-exchange scattering the comparison is made directly with the counting rates using Eq. (3) and the σ's determined by the phase shifts: in Set I, $\sigma_0=0.98$, $\sigma_1=-1.24$, $\sigma_2=+0.29$, and in Set II, $\sigma_0=0.97$, $\sigma_1=-1.31$, $\sigma_2=0.34$. Set I gives an appreciably better fit than Set II for the $\pi^+ \rightarrow \pi^+$ cross sections but a slightly poorer fit for the $\pi^- \rightarrow \pi^-$ and $\pi^- \rightarrow \pi^0$ cross sections. Both sets give acceptable over-all fits and are characterized by deviation parameters ω of 14 for Set I and 20 for Set II. Slight changes in the phase shifts within each set can probably lead to smaller values of ω, but a great improvement is unlikely. The fits can be judged in terms of the median deviation $\omega_{\frac{1}{2}}$ expected in fitting 14 experimental points in a theory with 6 free parameters. $\omega_{\frac{1}{2}}$ is approximately 15. It should be noted that the significance of the comparison of ω with the expected $\omega_{\frac{1}{2}}$ is limited by the uncertainties in the stated errors. Thus, although Set I is the better fit, Set II is not excluded.

[25] The $\pi^+ \rightarrow \pi^+$ phase shifts of Table V differ from those previously reported (see reference 7). This difference is in part due to the difference in relevant energy, but, in Set II particularly, there are additional differences due to the inclusion of the π^- data in the best fit.

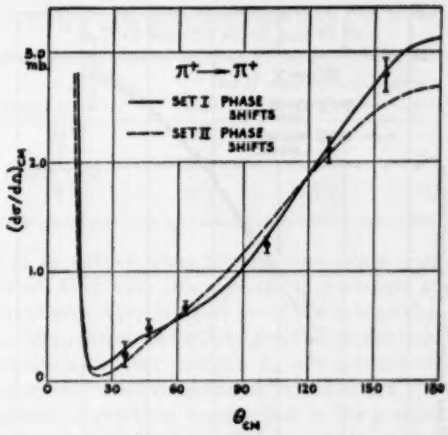

FIG. 9. Comparison of experimental cross sections of $\pi^+ \rightarrow \pi^+$ scattering at 58 Mev with results from phase shifts of Sets I and II. Experimental points are given with probable errors.

In the Fermi-type solutions, both in Set IA here and in the Chicago analysis,[1] the phase shifts $\delta(P_{\frac{1}{2}}{}^1)$, $\delta(P_{\frac{3}{2}}{}^1)$ and $\delta(P_{\frac{3}{2}}{}^1)$ are small. Because of the possible theoretical importance we have attempted to fit the experimental results under the assumption that these phase shifts are identically zero. Such a fit is characterized by a

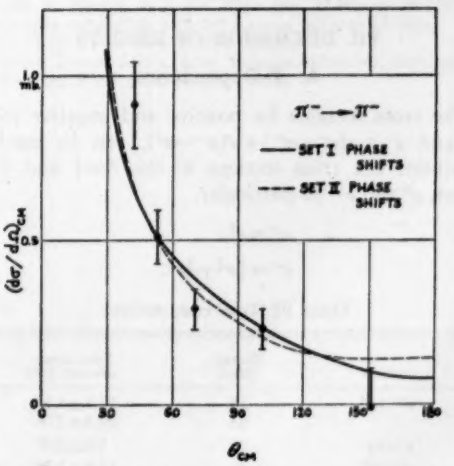

FIG. 10. Comparison of experimental cross sections of $\pi^- \rightarrow \pi^-$ scattering at 65 Mev with results from phase shifts of Sets I and II. Experimental points are given with probable errors.

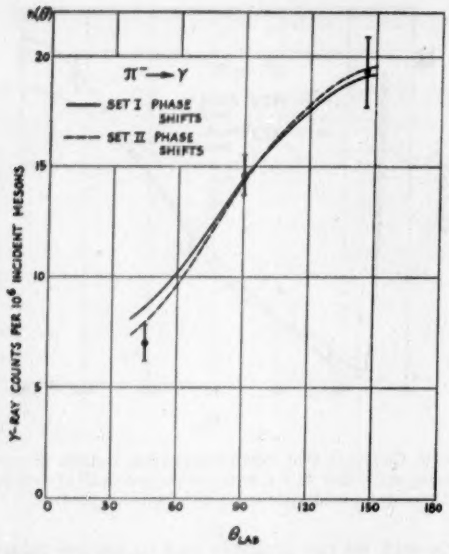

FIG. 11. Comparison of observed γ-ray counting rates in $\pi^-\to\pi^0$ scattering at 65 Mev with results from phase shifts of Sets I and II. The probable errors indicated for the experimental points do not include an over-all uncertainty of ± 10 percent in γ-ray efficiency determination.

deviation ω of the order of 50, and we consider it unlikely that our results are in error by such an amount. Therefore, we are of the opinion that although the interaction in these states is weak, it is nonvanishing.

The total cross section cannot be simply defined because of the small-angle Coulomb scattering. A measure of the nuclear contribution to the total cross section may be given by integration of Eq. (6) with the Coulomb term omitted. These cross sections, for the three scattering processes, are presented in Table VI with estimated probable errors.

VII. DISCUSSION OF RESULTS

A. T-Dependence

The cross sections for positive and negative pions, σ^+ and $\sigma^-=\sigma(\pi^-\to\pi^-)+\sigma(\pi^-\to\pi^0)$, can be used to determine the cross sections in the $T=\frac{1}{2}$ and $T=\frac{3}{2}$ states, $\sigma^{\frac{1}{2}}$ and $\sigma^{\frac{3}{2}}$. In particular,

$$\sigma^+=\sigma^{\frac{3}{2}},$$
$$\sigma^-=\tfrac{2}{3}\sigma^{\frac{3}{2}}+\tfrac{1}{3}\sigma^{\frac{1}{2}}.$$

TABLE VI. Total cross sections.

Process	Energy (Mev)	Total cross section (mb)
$\pi^+\to\pi^+$	58	15.8 ± 1.5[a]
	65	20.4 ± 2.0[b]
$\pi^-\to\pi^-$	65	2.9 ± 0.5[b]
$\pi^-\to\pi^0$	65	12.4 ± 1.5[b]

[a] From phase shifts corresponding to 58-Mev $\pi^+\to\pi^+$ scattering.
[b] From phase shifts of Table V, Set I.

At higher energy the scattering is almost entirely in the $T=\frac{3}{2}$ state, corresponding to the 3-to-1 ratio of the total cross sections σ^+ and σ^-. This is no longer the case at 65 Mev. The ratio of total cross sections is about 4 to 3, and this corresponds to $\sigma^{\frac{1}{2}}=1.6\sigma^{\frac{3}{2}}$. In the phase shift Set I this increase in the relative importance of the $T=\frac{1}{2}$ state is reflected in $\delta(S^{\frac{1}{2}})$, which is the largest single phase shift. The contributions of s- and p-wave phase shifts to $\sigma^{\frac{1}{2}}$ and $\sigma^{\frac{3}{2}}$ are given in Table VII.

B. Discrimination Between Set I and Set II Solutions

We have attempted to select between Sets I and II by extraploating the phase shifts at higher and lower energies. For $T=\frac{3}{2}$ the main difference between the two sets is that the scattering is mainly in the p state in I and in the s state in II. At higher energies the p state is known to be dominant over the s state, and if this could be shown to persist to 65 Mev, Set II would definitely be excluded. There are, however, serious difficulties in this procedure: (a) in the absence of an adequate theory on the energy dependence of meson-nucleon scattering, any extrapolation is necessarily based on questionable preconceptions; (b) the reported phase shifts are best fits to the data, but may often be seriously altered without exceeding the limits imposed by the experimental results; (c) the neglect of higher angular momentum states may be misleading.

TABLE VII. Contributions of s and p waves to $\sigma^{\frac{1}{2}}$ and $\sigma^{\frac{3}{2}}$ at 65 Mev for phase shifts of Sets I and II (mb).[a]

	Set I		Set II	
	S	P	S	P
$T=\frac{1}{2}$	11.6	1.3	2.1	10.1
$T=\frac{3}{2}$	3.7	16.7	20.5	1.7

[a] Solutions of Yang and Fermi types give same results for contributions from s and p states.

Subject to these reservations we have assembled in Table VIII the relevant published phase shifts. On this basis we would reject Set II because of the abruptly large s-wave and small $p_{\frac{1}{2}}$-wave phase shifts in the $T=\frac{3}{2}$ state. However, if the experimental results at other energies can be reasonably fitted with phase shifts with a large $s^{\frac{1}{2}}$ and small $p^{\frac{1}{2}}$ interaction, this rejection of Set II is impossible. A re-examination of the results at 40[6] and 78[1] Mev shows that it is quite possible to find such phase shifts (see Table IX).[26] We do not know whether or not this is also possible at higher energies.

Other experimental results which might provide a basis for the choice between Sets I and II are the measurements of 60-Mev pion scattering in carbon by Byfield Kessler, and Lederman,[27] and of 40-Mev pion scattering

[26] In a preliminary report of this work [Bodansky, Sachs, and Steinberger, Phys. Rev. 93, 918(A) 1954] we had not considered this possibility.
[27] Byfield, Kessler, and Lederman, Phys. Rev. 86, 17 (1952).

in hydrogen by Perry and Angell.[6] In the carbon experiments it was found that the scattering in the forward directions corresponds to that of an attractive potential. The same concludion is valid for both Sets I and II of the data presented here. Bethe[28] has pointed out that if the p-state interaction is dominant then it is attractive, in agreement with our Set I. Similarly, the Rochester group have noted that if either (a) $\delta(P_{\frac{3}{2}}{}^{\frac{1}{2}})$ is greater than $\delta(S^{\frac{1}{2}})$[6] or (b) $\delta(P_{\frac{1}{2}}{}^{\frac{1}{2}})$, $\delta(P_{\frac{3}{2}}{}^{\frac{1}{2}})$ and $\delta(P_{\frac{3}{2}}{}^{\frac{3}{2}})$ are all very small,[29] the signs can be determined. In both cases the results correspond to Set I. However, if Set II were indeed correct, these arguments would fail. Therefore, they do not provide an independent basis for selection.

TABLE VIII. Published phase shifts at various energies (deg). At 78, 120, and 135 Mev only the relative sign is determined.

Energy	40 Mev[a]	65 Mev		78 Mev[b]	120 Mev[b]	135 Mev[b]
$\frac{P}{mc}$	0.68	0.88		0.97	1.24	1.32
		Set I	Set II			
S wave						
$\delta(s^{\frac{1}{2}})$	−2	−6.2	14.5	−6	−15	−14
$\delta(s^{\frac{3}{2}})$		10.9	−4.6		9	10
Fermi-type p wave						
$\delta(p_{\frac{1}{2}}{}^{\frac{1}{2}})$	6	9.1	−2.8	13	30	38
$\delta(p_{\frac{3}{2}}{}^{\frac{1}{2}})$	0.7	−1.9	−1.4	−3	4	5
$\delta(p_{\frac{3}{2}}{}^{\frac{3}{2}})$		−2.6	7.1		2	2
$\delta(p_{\frac{1}{2}}{}^{\frac{3}{2}})$		0.4	1.3		−3	−5
Yang-type p wave						
$\delta(p_{\frac{1}{2}}{}^{\frac{1}{2}})$	2.5	1.7	−1.8	2	13	17
$\delta(p_{\frac{3}{2}}{}^{\frac{1}{2}})$	7.8	12.8	−3.2	18	39	49
$\delta(p_{\frac{3}{2}}{}^{\frac{3}{2}})$		−0.6	1.8		−1	−3
$\delta(p_{\frac{1}{2}}{}^{\frac{3}{2}})$		−3.5	9.9		4	6

[a] See reference 6.
[b] See reference 1.

If the pion-nucleon scattering were characterized by phase shifts similar to those of our Set II and Table IX, that is, by a large $S^{\frac{1}{2}}$ and small $p^{\frac{1}{2}}$ interaction, a fairly radical departure from present viewpoints would be required. However, although the experiments are not conclusive on this point,† we are of the opinion that they establish a preference for Set I and the similar published phase shifts at other energies. In this case the signs of the phase shifts are determined. In particular, the most important interaction, namely that in the p state with isotopic spin $\frac{3}{2}$, is attractive. This is a result which should be of considerable theoretical interest, since it verifies a prediction of the pseudoscalar meson theory (with either form of the coupling).[30,31] This particular theoretical result, namely the sign of the interaction in the $P_{\frac{1}{2}}{}^{\frac{1}{2}}$ state, is probably insensitive to the inadequacy of the calculational methods which makes more quantitative theoretical deductions uncertain. Experimental verification of this theoretical prediction is, therefore, believed to be significant.

TABLE IX. Alternative phase shifts (Set II) in $T=\frac{1}{2}$ state for 40, 65, and 78 Mev.

Energy in Mev	Set II phase shifts in degrees $\delta(S^{\frac{1}{2}})$	$\delta(P_{\frac{1}{2}}{}^{\frac{1}{2}})$	$\delta(P_{\frac{3}{2}}{}^{\frac{1}{2}})$
40	9	−2	−2
65 (Fermi type)	14.5	−2.8	−1.4
78	19	−2.5	−2.5

We wish to extend our thanks to Professor H. A. Boorse for the use of a hydrogen liquefaction apparatus, to Mr. E. Ihasz for the construction of the Dewar, and to Mr. W. Chinowsky and H. Wolfe for assistance in the liquefaction operations.

† *Note added in proof.*—Recently, better data have been obtained on the scattering of pions 200 Mev [J. Ashkin, Rochester Conference on High Energy Physics, Rochester, New York (1954), and M. Glicksman, private communication]. These results make it very probable that there is indeed a resonance in $\delta(P_{3/2}{}^{3/2})$ near 200 Mev [M. Glicksman, private communication; see, also, R. Martin, Bull. Am. Phys. Soc. **29**, No. 1, 28 (1954)]. This is only compatible with Set I phase shifts at 65 Mev.

[28] H. A. Bethe, Phys. Rev. **90**, 994 (1953).
[29] Barnes, Angell, Perry, Miller, Ring, and Nelson, Phys. Rev. **92**, 1327 (1953).
[30] G. Chew, Phys. Rev. **89**, 591 (1953).
[31] Bethe, Dyson, Mitra, Ross, Salpeter, Schweber, Sundaresan, and Visscher, Phys. Rev. **90**, 372 (1953).

Space-Charge Forces in Strong-Focusing Synchrotrons

S. E. BARDEN
University of Glasgow, Glasgow, Scotland
(Received October 22, 1953)

A new principle, strong focusing, has recently been put forward as the basis for the design of synchrotrons, particularly proton synchrotrons in the energy range above about 10 Bev. In this new proposal the field gradient index, n, is alternatively positive and negative and has a numerical value of some thousands as opposed to conventional, weak-focusing synchrotrons and betatrons, where $0<n<1$. The object of this note is to examine the effect of space-charge forces in strong-focusing synchrotrons on the stability of the radial and axial motion of the particles being accelerated.

It is shown that, by virtue of the decrease of these forces as the particle velocity approaches that of light, the average field index is gradually altered throughout the cycle of acceleration. Such modulation, if sufficiently large, can make it impossible to provide radial and axial stability for the whole of this cycle. If the number of sectors, N, is much greater than 10, however, much smaller amounts of modulation may create conditions favorable for forced radial or axial resonances in the presence of inevitable magnet alignment errors, and it is this effect which places stringent limits on the strength of space charge forces permitted in a strong-focusing accelerator. The limitations discussed are far more serious in the case of proton beams than in the case of electron beams.

IN the first-order theory of the strong-focusing synchrotron,[1] stability of particle orbits with respect to radial and axial perturbations is shown to occur for values of the average field gradient index, n, lying within certain limits. It is the purpose of this note to show how such stability limits are modified by space-charge forces in such machines and the effect on the choice of design parameters promoted by such considerations. The increased importance of space-charge forces in strong-focusing, as against such forces in weak-focusing synchrotrons, arises out of the large number of resonances[2] that may obtain between forced and free oscillations in the former, which results in a building up of the amplitude of the free oscillations and a rapidly decreasing accelerating efficiency.

In strong-focusing synchrotrons the field gradient is a function of the azimuthal angle, ϕ, and is of the form

$$n(\phi)=\langle n\rangle+\sum_{k=1}^{K}\alpha_k\cos(k\phi+\gamma_k), \tag{1}$$

where

$$\langle n\rangle=(1/2\pi)\int_0^{2\pi}n(\phi)d\phi, \tag{2}$$

and $K=N/2$, N representing the number of magnet sectors. Thus, $n(\phi)$ always lies within a range bounded by the limiting values, n_1 and n_2, given by the equations

$$n_1=\langle n\rangle+\textstyle\sum_k\alpha_k,\quad n_2=\langle n\rangle-\sum_k\alpha_k. \tag{3}$$

Two cases are of special interest, namely, when $\alpha_j=\alpha$, $\alpha_{k\neq j}=0$, and, secondly, when $\alpha_{k=2p}=0$, $\alpha_{k=2p+1}=(-1)^{(k-1)/2}(\alpha/k)$, k and p being positive integers, when $n(\phi)$ has a rectangular distribution, alternating in magnitude discontinuously from $n_1=\langle n\rangle+(4/\pi)\alpha$ to $n_2=\langle n\rangle-(4/\pi)\alpha$. In the second case, the radial and axial equations of motion are known as Hill-Meissner differential equations, and their application to the theory of the strong-focusing synchrotron has been treated by Courant *et al.*[1] In the first case we have a sinusoidal distribution of the field gradient, and the radial and axial equations of motion are of the form known as Mathieu's equation[3] and may be written

$$d^2\zeta/d\chi^2+(a-2q\cos2\chi)\zeta=0. \tag{4}$$

ζ represents the fractional radial deviation of the particle from its circular instantaneous orbit, and the fractional axial deviation of the particle from the median plane for the radial and axial equations, respectively; $\chi=0.5[(N\phi/2)+\gamma_{(N/2)}]$, $q=8\alpha/N^2$, while for $N\gg1$,

$$a=\mp(16/N^2)\langle n\rangle \tag{5}$$

in the radial and axial cases, respectively.

It is well known from the theory of Mathieu's equation that radial and axial motion are both stable (bounded) if the inequalities

$$0<\beta_r<1,\quad 0<\beta_z<1 \tag{6}$$

are simultaneously satisfied, where, provided

$$\langle n\rangle/N^2\ll\alpha/N^2\ll5,$$

β_r and β_z are constants given by the equations

$$\begin{aligned}(\beta_r^2/16)-(8\alpha^2/N^4)(\beta_r^2+4)/(\beta_r^2-4)^2&\\=(8\alpha^2/N^4)(\beta_z^2+4)/(\beta_z^2-4)^2-(\beta_z^2/16)&\\=-\langle n\rangle/N^2,&\end{aligned} \tag{7}$$

to a sufficiently good approximation. The boundaries of the radial and axial stable regions in α, $\langle n\rangle$ space, or n_1, n_2 space are therefore defined by the equations obtained by replacing the inequalities in Eq. (6) by equalities. The stable region so defined is shown enclosed by dashed lines in Fig. 1. For comparison the

[1] Courant, Livingston, and Snyder, Phys. Rev. **88**, 1190 (1952).
[2] E. D. Courant (private communication).
[3] E. T. Whittaker and G. N. Watson, *A Course of Modern Analysis* (Cambridge University Press, Cambridge, 1950), fourth edition, p. 404.

stable region obtained from the theory of the Hill-Meissner equation and given by Courant *et al.*[1] is shown enclosed by the dotted lines in Fig. 1. Space-charge forces have so far been omitted.

Assume now that the charged particles at injection lie within a toroid of circular cross section, radius κ cm and diameter $2r$. Space-charge forces on peripheral electrons result then from an electric field, E_r, obtained from Gauss's theorem to be

$$E_r = 2\pi\eta\zeta r, \tag{8}$$

η representing the charge density in esu. If the current density per unit cylinder length is written in the form, $I(\text{amps})/\pi\kappa^2$ amp/cm^2, it can be shown that the field gradient index is modulated between the limits

$$n_1 = (\langle n\rangle' + \alpha), \quad n_2 = (\langle n\rangle' - \alpha), \tag{9}$$

where

$$\langle n\rangle' = \langle n\rangle \pm S, \tag{10}$$

in the radial and axial cases, respectively, with

$$S = 6(e/m)v^{-3}\zeta^{-2}I(\text{amp})[1-(v/c)^2]\times 10^9. \tag{11}$$

v is the velocity of the particles, whose ratio of charge to mass in esu is given by e/m.

The most significant feature of Eq. (11) is the dependence of S on v/c, the ratio of particle velocity to the velocity of light, and $S(v)_{v\sim c} \ll S(v)_{v\ll c}$. Thus for particles injected with velocities, $v \ll c$, and accelerated to velocities, $v \sim c$, $(n_1+n_2)/2$ is modulated from $\langle n\rangle'$ at injection to nearly $\langle n\rangle$ when the particles are extracted from the accelerator. In such circumstances, the most obvious effect of the modulation of $\langle n\rangle$ by the space-charge term, S, is a reduction of the stable region in strong-focusing accelerators. Figure 1 shows the net stable region if $S_{v\ll c} = 0.1(N^2/16)$. The space-charge limit is attained only when $S = 0.024N^2$ at injection.

A more important though less obvious result of such modulation of $\langle n\rangle$ is the presence of forced resonances due to imperfections in magnet alignment causing azimuthal variations in either the axial or radial component of field, or both. Thus, if a Fourier analysis of such variations gives rise to term in the series of harmonic order, m, the radial or axial motion of the particles becomes unbounded if

$$\beta_r = 4m/N, \quad \text{or} \quad \beta_z = 4m/N, \tag{12}$$

respectively. If $\beta_r = \beta_z = 0.5$, $m/N = \frac{1}{8}$; radial or axial instability could occur for β_r or β_z equal to the rational fractions

$$\cdots (4/N)(m-1),\ (4/N)(m),\ (4/N)(m+1), \cdots. \tag{13}$$

Consequently, the change in β_r or β_z during the acceleration cycle should be much less than $(4/N)$ if the absence of forced resonances is to be ensured during the whole of this period. By virtue of its inverse dependence

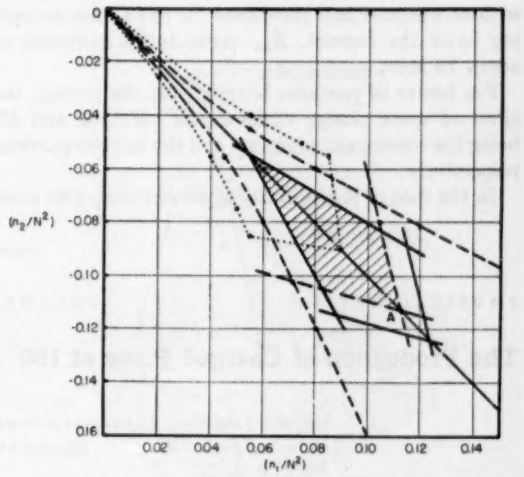

FIG. 1. Stable regions in strong-focusing synchrotrons, showing the effect of space-charge forces in proton beams. The dashed lines indicate the boundary of the stable region for sinusoidal variation of n, without space-charge effects. The solid lines show the boundary of the stable region for sinusoidal variation of n, the space-charge term: $S = 0.1(N^2/16)$ being taken into account. The shaded area is the net stable region over a cycle of acceleration in the presence of space charge. The dotted lines indicate the boundary of the stable region for a discontinuous variation of n without space-charge effects (see reference 1).

on N, this is clearly a far greater restriction on the magnitude of space-charge forces than the effect on the boundaries of the stable region mentioned above, for $N \gg 10$. To ensure, from this point of view, that modulation of $\langle n\rangle$ by space-charge forces is not excessive, S, defined in Eq. (11), should satisfy the inequality,

$$S_{v\ll c} - S_{v\sim c} \ll 1. \tag{14}$$

This problem is clearly more important in the case of heavy particle beams than in the case of electrons, and for proton beams in particular we have

$$(S_{v\ll c} - S_{v\sim c}) = 6.3I(\text{amp})\cdot\zeta^{-2}E_{\text{inj}}^{-\frac{1}{2}}\cdot 10^{-4}, \tag{15}$$

where E_{inj} represents the energy of the protons, in Mev, at injection. Combining relations (14) and (15) we obtain

$$[I(\text{amp})/\zeta^2] \ll 1.6E_{\text{inj}}^{\frac{1}{2}}\times 10^3, \tag{16}$$

a relationship independent of N.

If $E_{\text{inj}} = 4$ Mev, the right-hand side of Eq. (16) becomes about 1.3×10^4, and $I(\text{amp})/\zeta^2 \lesssim 2000$. If a current of protons of 100 microamperes wants accelerating, then an aperture, both radially and axially, of $\zeta = 5\times 10^{-4}$ must be provided. If the radius of the accelerator is 300 ft,[1] then the radial and axial apertures should be not much less than 2 in. The most economical way of increasing the magnitude of the current accelerated is to increase E_{inj}, and not ζ, in a magnet of this size. Thus,

with an aperture half the size of the one above, accepting twice the current, E_{inj} needs to be increased to about 16 Mev.

For beams of particles heavier than the proton, the effect of space charge varies as $(M'/M)^{\frac{1}{2}}$, M and M' being the masses of the proton and the heavier particle, respectively.

In the case of strong-focusing accelerators with comparatively small apertures it may be said, in conclusion, that the possibility of radial or axial instability caused by forced resonances places stringent limits on the magnitude of the current that may be stably accepted in any given magnet. This magnitude is independent of the strength of radial and axial focusing and depends only on the radial and axial apertures available and the energy of the particles at injection

PHYSICAL REVIEW VOLUME 93, NUMBER 6 MARCH 15, 1954

The Production of Charged Pions at 180° to the Beam by 340-Mev Protons on Carbon

STANLEY L. LEONARD*
Radiation Laboratory, Department of Physics, University of California, Berkeley, California
(Received October 13, 1953)

The yield of charged pions at 180°±5° to the beam produced by 340-Mev protons on carbon has been measured, using nuclear emulsion techniques. Nuclear emulsions embedded in copper, aluminum, or Lucite absorber blocks were exposed to magnetically separated positive and negative pions emitted at 180° by graphite targets bombarded in the electrically deflected proton beam of the Berkeley synchrocyclotron. Plates were exposed for a series of pion energies from 9 to 118 Mev. The developed emulsions were examined with a microscope under high magnification and meson track endings were identified and counted. The values of $d\sigma/d\Omega dT$ as a function of pion energy and the values of $d\sigma/d\Omega$ were calculated for both positive and negative pions. Corrections were made for errors resulting from pion decay in flight, the finite thickness of the target, nuclear interaction of pions in the target and absorber blocks, and background pions. The corrected integrated cross sections are

$$d\sigma/d\Omega(\pi^+)=1.77\pm0.27\times10^{-28}\ \text{cm}^2/(\text{sterad nucleus}) \quad \text{and}$$
$$d\sigma/d\Omega(\pi^-)=1.90\pm0.38\times10^{-29}\ \text{cm}^2/(\text{sterad nucleus}),$$

yielding a positive-negative ratio of 9.3±2.3. An attempt has been made to interpret the positive pion spectrum in terms of existing information on the production of positive pions by protons on hydrogen.

I. INTRODUCTION

A NUMBER of observers have studied the cross sections for production of positive and negative pions when carbon is bombarded by high-energy protons. In particular, the differential cross sections have been measured for pions produced at 0° and 90° to the proton beam, in the laboratory system. These measurements show that the ratio of the differential cross section (integrated over pion energy) for positive pions to that for negative pions at 90° to the beam is either about 5,[1] or about 10,[2] but that this ratio is much larger at 0°, being about 28.[3] The positive pion cross section itself at 0° is either 3 or 6 times as great as at 90°, while the negative cross section is about the same at 0° as at 90°.

In considering these results, it is commonly assumed that the production of pions occurs in the interaction of the incident protons with individual nucleons of the target nucleus. The proton-proton interaction gives rise to positive pions only, by charge conservation, while the proton-neutron interaction gives rise to pions of both signs. Since the carbon nucleus consists of equal numbers of protons and neutrons, positive pion production would be expected to predominate. If the proton-proton and proton-neutron pion production cross sections inside the nucleus are the same, one would expect the ratio of the total production cross section (integrated over the solid angle) for positive pions to that for negative pions to be about three.

It is, therefore, of interest to measure the production cross sections for pions emerging in the backward direction in order that the total cross sections may be calculated and the positive-negative ratio found for these total cross sections. In addition, such a measurement helps to round out existing information on the production of pions by protons on carbon, and thus on any complex nucleus to the extent that carbon may be considered typical.

II. EXPERIMENTAL METHOD

The technique used in this experiment is essentially the same as that originated by Richman and Wilcox[1] and modified by Cartwright, Richman, Whitehead, and Wilcox[4] in their measurement of the cross section for

* Now at Principia College, Elsah, Illinois.
[1] Richman, Weissbluth, and Wilcox, Phys. Rev. 85, 161 (1952); C. Richman and H. A. Wilcox, Phys. Rev. 78, 496 (1950).
[2] Block, Passman, and Havens, Phys. Rev. 88, 1239 (1952); Passman, Block, and Havens, Phys. Rev. 88, 1247 (1952).
[3] W. Dudziak (private communication).
[4] Cartwright, Richman, Whitehead, and Wilcox, Phys. Rev. 91, 677 (1953).

the production of positive pions by protons on protons at 0°. The 340-Mev electrically deflected proton beam of the 184-in. Berkeley synchrocyclotron was used. This beam was collimated in passing through the cyclotron shielding and emerged into the so-called cave area. There (Fig. 1) it passed through an ion chamber and struck a carbon target situated at the farther edge of a region of strong magnetic field.

Pions created in this target and emerging at 180° to the proton beam were deflected by the magnetic field. Those pions in the desired momentum interval passed down channels in brass shielding blocks and struck absorber blocks in which were embedded Ilford C-2 nuclear emulsions. These emulsions were subsequently developed and examined with a microscope under sufficiently high power. The tracks left by negative and positive pions could be recognized, and the number of pion tracks which stopped in the body of the emulsion in a given region was determined. The energy of these mesons was determined by the amount of absorber material they passed through in reaching the region of emulsion scanned. The tables and graphs of the range-energy relation calculated by W. Aron[6] were used. The number of pions reaching the end of their range and stopping in a given region of the emulsion was a measure of the population density of mesons stopped in that region of the absorber block during bombardment. From the number of meson endings in a given section of the plate, then, the number of pions in the corresponding energy interval emerging from the target at 180° was calculated.

The current from the ion chamber was integrated during the run. Since this instrument had been accurately calibrated by comparison with a Faraday cup, the total number of protons which passed through the target during the bombardment was then known. From these values were calculated the positive and negative pion production cross sections in each energy interval.

The pion detectors in this experiment were, as has been mentioned, nuclear emulsions embedded in blocks of absorber material. The absorber blocks (Fig. 2) were thick enough to stop pions of the energy being investigated.The plates were inclined at an angle of 15° to the horizontal, and, therefore, to the direction of the incoming pions. The angle was chosen somewhat arbitrarily, being small enough that the pions might leave long tracks in the emulsion in order to facilitate identification, and yet larger than 0° so that the mesons might pass directly from absorber to emulsion prior to stopping. This was necessary in order to make it possible to assume that practically the entire path of a pion was in the single medium of the absorber (rather than partly in absorber and partly in the glass backing of the plate), so that the energy could be reliably calculated from the depth in absorber.

[6] Aron, Hoffman, and Williams, U. S. Atomic Energy Commission Report 663 (unpublished); W. A. Aron, thesis, University of California Radiation Laboratory Report No. 1325 (unpublished).

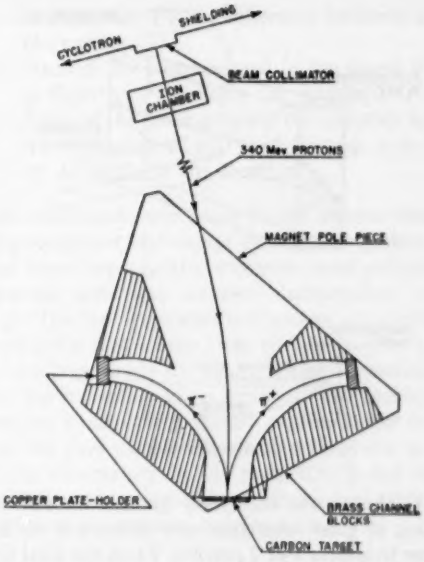

FIG. 1. Schematic diagram of typical experimental arrangement.

The absorber materials were chosen, at the various energies, mainly for convenience. At all high enough energies, copper was used. For the low-energy measurements, it was necessary to use lighter absorber materials (aluminum at 18 Mev and Lucite at 9 Mev) since otherwise the pions in the desired energy interval would have stopped too near the front edge of the emulsion for accurate scanning. Furthermore, the section of the plate corresponding to the desired energy interval would have been so small as to render small uncertainties in its location important. The methods of identification and counting of the tracks of positive and negative pions in the plates under high magnification have been very completely covered elsewhere[1,4] and will not be further discussed.

In the determination of the number of stopped pions per unit volume of emulsion, it is obviously necessary to know accurately the total volume occupied at the time of exposure by that region of the emulsion which was subsequently scanned. The emulsions are manufactured with a glass backing so that development causes no significant changes in dimensions except in thickness. The surface area of emulsion scanned was measured in conjunction with the scanning operation with the aid of an accurately calibrated microscope stage.

To determine the thickness of the emulsion a series of measurements of the thickness of glass plus emulsion were made on each plate before and after development, using a spring-loaded thickness gauge mounted on a rigid frame with a movable stage. The postdevelopment thickness of the emulsion was measured with the aid of a scale on the fine focus control of the microscope. This scale had been calibrated to ± 2 percent by using it in the measurement of the thickness of a cover glass

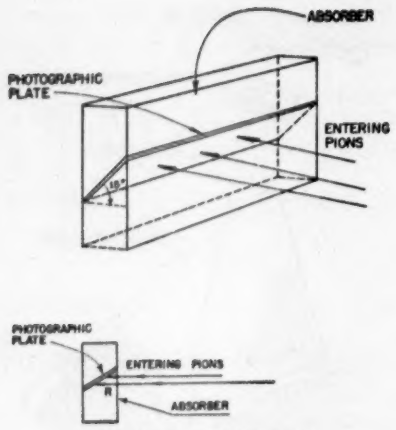

FIG. 2. Absorber block.

whose thickness was accurately known, the indices of refraction of glass, emulsion, and immersion oil being the same to within 1 or 2 percent. From the final thickness and the shrinkage of the thickness at the time of exposure was calculated, the estimated accuracy of the resulting value being ± 3 percent.

The magnetic field used to deflect the pions into the detectors was provided by a large electromagnet originally designed for use as a pair spectrometer. With the pole pieces used in this experiment, the magnet gives a field which is uniform to about 5 percent over a region which extends to within 2 in. of the edges of the pole pieces on all sides. The maximum field which can be maintained over a period of many hours is about 14.3 kilogauss. The gap is 3.4 in.

In the gap between the pole pieces were placed brass channel pieces. These were simply brass shielding blocks with channels cut into them. The channels were designed so that pions in the desired energy interval could emerge from any point of the bombarded area of the target within $\pm 5°$ of 180° and reach any point of the channel exit without striking the channel walls. The brass served to shield the detectors (placed at the channel exits) from stray particles of different momentum, and from pions of the same momentum emitted at angles other than $180° \pm 5°$. The channels thus selected and collimated a rather broad energy interval of pions emitted at 180° into a broad beam of roughly uniform density at the channel exit. In order to obviate the necessity of correcting the results for multiple Coulomb scattering, the direction setup was so arranged that the scanned area of emulsion was effectively in an infinite sea of absorber material during exposure. This was accomplished by seeing that the portions of emulsion scanned were chosen to be at least five times $\sqrt{y^2}$ from either edge of the channel exit during exposure, where $\sqrt{y^2}$ is the rms average lateral displacement from its initial trajectory of a pion of the desired energy at the end of its range in the absorber. As a result of this "bad geometry" arrangement, the number of pions lost from the scanned area by multiple Coulomb scattering in the absorber material was equal, to the first order, to the number of slightly more energetic pions which were scattered into the scanned area. The value of $\sqrt{y^2}$ was calculated for the various absorber materials and pion energies from a formula of L. Eyges[6] and was of the order of 0.1 cm. The greatest value, at the 118-Mev point, was 0.27 cm.

It is important, of course, to know the solid angle subtended at the target by the scanned volume of emulsion. It can be shown that, in a uniform magnetic field, the solid angle is related to ρ, the radius of curvature of the pion, and to ϕ, the angle through which the pions are turned in passing from the target to the absorber block, by the equation[7]

$$d\Omega/dA = 1/(\rho^2\phi \sin\phi),$$

where $d\Omega/dA$ is the solid angle per unit projected area perpendicular to the path of the pions.

The error introduced into the calculation of the solid angle by the nonuniformity in the field near the edges of the pole pieces is negligible even though the plate holders were placed at or near the edge of the pole pieces during several of the exposures. The effect of a variation in the radius of curvature caused by this decrease in field strength near the edge is only to shift by a small amount (less than 1°) the angle at which pions of the desired energy must leave the target in order to get down the channel. Since the cross section varies only slowly with laboratory angle (as is seen by comparing the cross sections measured in this experiment with those measured at 90°), a small shift in the angle has a completely negligible effect on the result. The effect of this variation in ρ on the solid angle is likewise negligible, the effective distance of the emulsion from the target being changed by only an infinitesimal amount.

The magnetic field has another possible effect on the result. If the curvature of the pion path in the absorber block is appreciable, the actual length of path of the pion in the absorber may be longer than the apparent value as measured from the front face of the absorber. This difference between actual and measured pion range can be shown to be negligible.[8] The variation of the field strength with time during any run was less than 1 percent.

III. CROSS-SECTION FORMULA

It can be shown[4] that the cross section may be expressed in terms of the density of stopped pions by the

[6] L. Eyges, Phys. Rev. 74, 1534 (1948).
[7] W. F. Cartwright, thesis, University of California Radiation Laboratory Report No. 1278 (unpublished).
[8] M. N. Whitehead, thesis, University of California Radiation Laboratory Report No. 1828 (unpublished).

following relation:

$$\frac{d\sigma}{d\Omega dT}(T)=q\Big/\left(\frac{N\rho t}{A}A_0\frac{d\Omega}{dA}\frac{dT}{dx}\frac{R_{ab}}{R_{em}}\right),$$

where q=density of stopped pions per unit volume of emulsion; N=total number of protons passing through the target; ρt=target thickness in g/cm²; A=atomic weight of target material; A_0=Avogadro's number; dT/dx=rate of pion energy loss per cm of absorber at energy T; $d\Omega/dA$=solid angle per unit projected area perpendicular to the pion path; and $R_{em}=t\csc\alpha$, where t=thickness of emulsion and α is the angle at which the emulsion is inclined to the path of the pions. R_{ab} is the range in the absorber material of a pion whose range in emulsion is R_{em}. The values of R_{ab}/R_{em} are: for copper, 0.414; for aluminum, 1.14; and for Lucite, 2.02.

IV. CORRECTIONS

Because of the smallness of the production cross section at 180°, particularly for negative pions, it was necessary that the proton beam flux be as large as possible. As a result, the collimators used had fairly large diameter (usually two inches) and some protons in the wings of the beam struck the pole pieces of the magnet before reaching the production target. Some pions were produced in the iron of the pole pieces at such energies and angles as to be able to travel down the channels into the detectors. There were thus background pions of both signs in both positive and negative detectors. To correct for this flux of background pions, plates were exposed in the same geometry as the plates used for the cross-section measurement, but with the production target removed. The background plates were developed and scanned with the others, and the contribution from the background flux to the total density of stopped pions was subtracted. At two of the energies, 75 and 118 Mev, it was inconvenient to expose background plates. For the 75-Mev cross sections, the correction was estimated from the measured corrections at the other energies by comparing the numbers of positive pions found in the negative pion plates. At the 118-Mev point no negative plate was exposed, so that the correction had to be estimated from the corrections at other energies on the basis of the total number of pions found. Very little error was introduced in this way, since the background correction is relatively small at all energies. Furthermore, the cross sections themselves are relatively quite small at 75 and 118 Mev, so that uncertainties in the correction are less important than at the lower energies.

In addition, the cross sections were corrected for the following effects:

(a) Pions emerging from the target at energy T in an interval ΔT were created at different depths of the target in different energy intervals $\delta T'$. Since we measure ΔT, we must correct the calculated cross section for the difference between ΔT and the various $\delta T'$.

(b) Some of the pions created in the target decayed in flight before reaching the detector.

(c) Some of the pions entering the absorber material were absorbed or scattered through large angles by the nuclei in the absorber.

These corrections were made in the manner described by Cartwright *et al.*,[4] except that in the nuclear interaction correction a total attenuation cross section equal to nuclear area was assumed, independent of pion energy. This last correction is of course not precise, but the available data on the cross section for pion absorption and large-angle scattering are still insufficient to make the correction more accurate. Fortunately, this correction is important mainly at the higher energies where the pion production cross sections are so small that the uncertainty in the correction is not serious. Even though the percentage uncertainty is rather large, the absolute uncertainty is quite small.

V. RESULTS

The measured cross sections are given in Tables I and II, along with the various correction factors; for target thickness, k_{th}; for pion decay in flight, k_{dec}; and for nuclear interaction, k_{nuc}.

The errors given are probable errors of purely statistical origin. In addition, the results are subject to a number of systematic errors. Among these are the scanning efficiency of the observer, inaccuracies in the ion chamber calibration, uncertainties in the stopping power of emulsion, and uncertainties in the emulsion thickness measurements. The energy width shown for each of the points is the larger of the widths ΔT and δT, where ΔT is the energy interval determined by the width of the region scanned in the emulsion, and δT is the energy width of the target.

The calculated values of $d\sigma/d\Omega dT$ are plotted *versus* T in Figs. 3 and 4. The curves drawn through the points are merely smooth curves fitted by eye and have no theoretical significance. The integrated cross sections have been obtained by integrating the area under these curves, as corrected for nuclear interaction. The systematic errors mentioned above are estimated to give a net uncertainty of ±10 percent to the results. Because of these errors, as well as the lack of precision of the nuclear interaction correction, an error of ±15 percent is assigned to the value of $d\sigma/d\Omega$ for positive pions, and an error of ±20 percent of the value of $d\sigma/d\Omega$ for negative pions. These values are intended to include the statistical errors and should be considered probable errors. The results for the differential cross sections integrated over pion energy are

$$d\sigma/d\Omega(\pi^+)=1.77\pm0.27\times10^{-28}\ \text{cm}^2/(\text{sterad nucleus}),$$

$$d\sigma/d\Omega(\pi^-)=1.90\pm0.38\times10^{-29}\ \text{cm}^2/(\text{sterad nucleus}).$$

TABLE I. Positive pion cross sections.

T	$\left(\frac{d\sigma}{d\Omega dT}\right)_{\text{uncorr}}$		K_{th}	K_{dec}	$\left(\frac{d\sigma}{d\Omega dT}\right)_{\text{corr}^a}$	K_{nuc}	$\left(\frac{d\sigma}{d\Omega dT}\right)_{\text{corr}}$
9.2±1.2 Mev	2.01 ±0.18×10^{-30}	cm^2 / sterad Mev nucleus	1.10	1.091	2.41±0.21×10^{-30}	1.008	2.43 ±0.21×10^{-30}
17.8±2.8	2.83 ±0.21		1.16	1.122	3.68±0.28	1.026	3.78 ±0.29
31.9±1.9	2.60 ±0.18		1.04	1.095	2.97±0.20	1.064	3.16 ±0.21
51.5±1.5	1.33 ±0.11		1.00	1.073	1.42±0.12	1.143	1.62 ±0.14
75 ±5.0	0.56 ±0.05		1.00	1.074	0.60±0.05	1.278	0.77 ±0.06
118.6±8.6	0.056±0.014		1.00	1.072	0.06±0.015	1.627	0.097±0.024

[a] Corrected for everything except nuclear interaction.

The positive-negative ratio at 180° is thus equal to 9.3±2.3. These results are based on a total of 570 pion-muon decay events and 136 negative pion stars.

Using the values of $d\sigma/d\Omega$ measured in this experiment along with those for pions emerging at 0°[3] and 90°[1] to the beam, one can integrate roughly over the entire solid angle to obtain the total cross sections. The results are approximately $\sigma(\pi^-)=5.7\times10^{-28}$ cm^2 and $\sigma(\pi^+)=47.6\times10^{-28}$ cm^2, giving a positive-negative ratio of 8.4. Since this is much larger than three, it is clear that the proton-proton and proton-neutron pion production cross sections inside the carbon nucleus are not the same.

The salient differences in the spectra for positive and negative pions (Figs. 3 and 4) are the differences in the location of the peak and in the location of the high-energy cutoff. It is seen that the negative spectrum peaks at a lower pion energy and has a high-energy cutoff at a lower pion energy than is the case for positive pions. These features, which are also found in the positive and negative spectra at 0° and 90°, can be understood tentatively in terms of a nucleon-nucleon picture of the production process. Energetic pions could not be produced at 180° to the beam if it were not for the fact that the individual nucleons in the carbon nucleus have fairly large internal momenta. It then appears that the creation process for positive pions may have a steeper excitation function than that for negative pions, so that the positive pion process takes greater advantage of the higher momentum components of the nucleons in carbon. The large positive-negative production ratio may also be understood in terms of this picture. Thus, there seems to be a fundamental difference between the primary production processes for positive and negative pions. This may perhaps be explained in terms of a difference between the $p-n$ interaction and the $p-p$ interaction. One may imagine that the $p-p$ interaction can result in a closely associated pair of nucleons, in analogy to the free nucleon reaction $p+p=\pi^++d$. An attempt to analyze the positive spectrum in terms of such a picture is described in the next section.

VI. ANALYSIS OF POSITIVE PION SPECTRUM ON NUCLEON-NUCLEON MODEL

An attempt has been made to interpret the positive pion spectrum measured in this experiment in terms of pion production in nucleon-nucleon collisions. Similar analyses have been carried out by Henley[9] for positive pion production at 0° and 90° by protons on carbon, by Passman, Block, and Havens[2] in the case of positive pion production at 90° by protons on various nuclei, and also by Neher[10] in the case of positive and negative pion production at 90° by neutrons on carbon.

If one assumes that negative pion production in proton-neutron collisions is roughly as probable as is the production of positive pions in the same type of collision, then it is clear that most of the positive pions produced by proton bombardment of carbon must result from proton-proton collisions. This is to be inferred from the fact that the positive-negative ratio has been found to be about 9 and the additional fact that negative pions in this experiment can only result from $p-n$ collisions. It has therefore been assumed in this analysis that only $p-p$ collisions are involved in the production of positive pions from carbon.

It has also been assumed that in each pion-producing collision the resulting nucleons leave in such a way

TABLE II. Negative pion cross sections.

T	$\left(\frac{d\sigma}{d\Omega dT}\right)_{\text{uncorr}}$		K_{th}	K_{dec}	$\left(\frac{d\sigma}{d\Omega dT}\right)_{\text{corr}^a}$	K_{nuc}	$\left(\frac{d\sigma}{d\Omega dT}\right)_{\text{corr}}$
9.6±1.6 Mev	3.67±0.60×10^{-31}	cm^2 / sterad Mev nucleus	1.10	1.091	4.41±0.72×10^{-31}	1.008	4.47±0.73×10^{-31}
17.8±2.8	2.64±0.43		1.16	1.122	3.44±0.56	1.026	3.53±0.57
31.9±1.9	2.63±0.30		1.04	1.095	3.00±0.34	1.064	3.19±0.36
51.5±1.5	1.66±0.28		1.00	1.073	1.78±0.30	1.143	2.03±0.34
75 ±5.0	0.30±0.08		1.00	1.074	0.32±0.09	1.278	0.41±0.12

[a] Corrected for everything except nuclear interaction.

[9] E. Henley, Phys. Rev. 85, 204 (1952).
[10] L. Neher, thesis, University of California Radiation Laboratory Report No. 2191 (unpublished).

that the pion gets the maximum possible kinetic energy—that is, that the resulting nucleons form a deuteron. This has been assumed for several reasons. First, it is known that in the bombardment of free protons by protons, the deuteron-forming reaction produces ~70 percent of the positive pions.[4] In addition, the analysis of Passman, Block, and Havens, which gives a reasonably good fit to the experimental data on pion production from carbon at 90°, is based on the same assumption. Further still, the analysis of Henley involves the assumption that the deuteron-producing reaction does not contribute appreciably, and that analysis fails to account for the positive pion spectrum from carbon at 0° or for the positive-negative ratio at that angle. Moreover, a compelling reason for making this assumption is that it results in a considerable simplification of the calculations.

Such an analysis as this involves knowledge of the momentum distribution of the nucleons in the carbon nucleus and of the energy dependence of the nucleon-nucleon pion production cross section. This calculation has been carried out for two types of momentum distributions, the Chew-Goldberger distribution,[11] and a Gaussian distribution with a width corresponding to 16 Mev. This last distribution was chosen because Cladis, Hess, and Moyer[12] have found that Gaussians of widths ranging from 14 to 19 Mev can be used to fit their measured values for the cross sections at various angles for quasi-elastic scattering of protons in carbon. Two different excitation functions were also used, with energy dependences of T'^2 and T'^4, where T' is the maximum energy of the pion resulting from the nucleon-nucleon interaction, expressed in the center-of-mass system of the two interacting nucleons. These excitation functions were adjusted for approximate fit to the experimental points for production at 0° from free protons as measured by Schulz[13] and calculated by him from the data of Durbin, Loar, and Steinberger[14] on the inverse reaction. The energy-dependence values were chosen for the following reasons: the T'^2 dependence because Passman, Block, and Havens[2] found that it gave best agreement with their experimental data, the T'^4 dependence because it is the steepest energy dependence which has any relation to the phenomenological matrix elements obtained by Passman *et al.*, in extending the treatment of Watson and Brueckner.[15]

In addition to variations in excitation functions and momentum distributions, the analysis has been carried out for two different models of the kinematic situation. One can assume that the incoming nucleon selects one of the nucleons of the carbon nucleus, and interacts with it, with the resulting pion emerging so rapidly

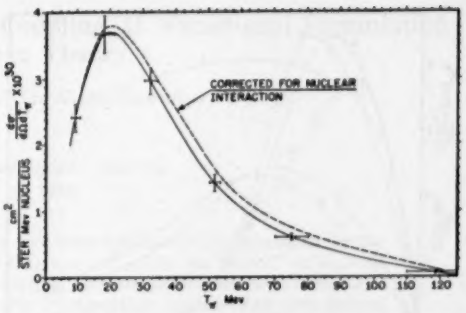

FIG. 3. Plot of differential cross section for production of positive pions as a function of energy. The solid curve has not been corrected for nuclear interaction. The dashed curve has been so corrected.

that the reaction is over, as far as the pion is concerned, before the rest of the nucleus can react in any way. In this "impulse-approximation" model, the calculation is carried out as if the nucleus consists merely of a set of particles whose relationship to each other has the sole effect of imparting to each a momentum relative to the others. When energy and momentum are balanced, only the two interacting nucleons are considered. This model, of course, overestimates the energy available to produce pions, since in reality the rest of the nucleus does absorb some energy and momentum, as is shown by the experiment of Ford [16] on the production of pions by neutrons on oxygen in a cloud chamber. In addition, the momentum distribution gives a finite probability that the struck nucleon has sufficient internal momentum to permit the production of a pion whose kinetic energy is so large as to violate over-all energy conservation. In the case of production at 180°, however, the pion energies considered are all well below the limiting value determined by over-all energy conservation.

The other model for the kinematics used in this analysis is essentially that used by Neher[10] and involves

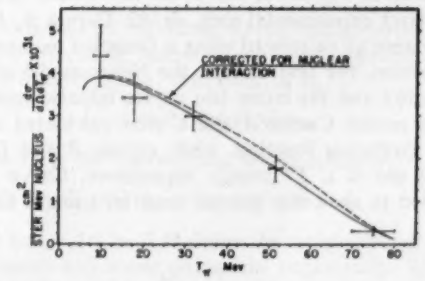

FIG. 4. Plot of differential cross section for production of negative pions as a function of energy. The solid curve has not been corrected for nuclear interaction. The dashed curve has been so corrected.

[11] G. F. Chew and M. L. Goldberger, Phys. Rev. **77**, 470 (1950).
[12] Cladis, Hess, and Moyer, Phys. Rev. **87**, 425 (1952); P. Wolff, Phys. Rev. **87**, 434 (1952).
[13] A. G. Schulz, Jr., thesis, University of California Radiation Laboratory Report No. 1756 (unpublished).
[14] Durbin, Loar, and Steinberger, Phys. Rev. **84**, 581 (1951).
[15] K. Watson and K. Brueckner, Phys. Rev. **83**, 1 (1951).
[16] F. C. Ford, thesis, University of California Radiation Laboratory Report No. 2148 (unpublished); F. C. Ford (private communication).

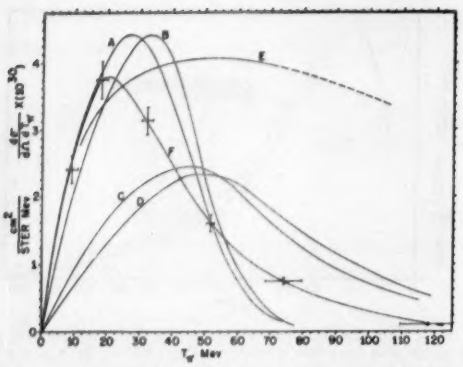

FIG. 5. Experimental spectrum of positive pions with theoretical spectra calculated on a nucleon-nucleon model and normalized to the area of the experimental curve.

considering the rest of the nucleus in the energy and momentum balance. The incoming nucleon is assumed, as before, to select for interaction one of the nucleons of the target nucleus. If this struck nucleon has a momentum p, then the rest of the nucleus must be recoiling with momentum $-p$. After the collision, the residual nucleus, with changed mass, carries off kinetic energy and momentum, as do the pion and deuteron. The selection of an appropriate average value for the new mass of the residual nucleus involves an estimate of its average excitation. The new mass M' was set equal to $M-m+\epsilon/c^2$, where M is the mass of the C^{12} nucleus, m is the proton mass, and ϵ is 20 Mev. The value of 20 Mev was chosen to include 8-Mev binding energy for the removed proton (carried off in the deuteron), plus about 12-Mev excitation for the residual nucleus, a figure arrived at from a consideration of the data of Ford.[16]

These calculated spectra were corrected for the attenuation of the incident protons and the reabsorption of the pions in nuclear matter.

The theoretical spectra resulting from this analysis are shown in Fig. 5. All curves are normalized to have the correct experimental area, $d\sigma/d\Omega$. Curves A, B, C, and D were all calculated using a Gaussian momentum distribution, the first two on the Neher model of the kinematics and the latter two on the impulse-approximation model. Curves A and C were calculated using a T'^1 excitation function, while curves B and D involved use of a T'^2 energy dependence. Curve E is intended to show the general result of using a Chew-Goldberger momentum distribution with either of the kinematic models and either of the excitation functions. The exact values for the cross sections could not be calculated in the case of the Chew-Goldberger distribution without much additional work. However, the analysis was carried far enough to show that the result is in general the deplorable one shown in the diagram. Curve F is the experimentally measured spectrum. It must be remarked that the area under the curves before normalization differed widely. Curves A, B, C, and D had to be multiplied by factors of 31.3, 17.4, 9.3, and 4.1, respectively, to normalize them.

It is seen that the Neher model gives a better fit to the experimental spectrum shape than does the impulse approximation, but that only the impulse approximation with a T'^2 excitation gives anything like the experimental value of the integrated area before normalization. It is clear, then, that none of the variations makes possible a really adequate interpretation of the carbon spectrum in terms of the proton-proton spectrum. Even use of the Chew-Goldberger momentum distribution was found not to change the values of $d\sigma/d\Omega dT$ in the region of interest (at the few values of the pion energy for which the exact value could be obtained) by a factor of more than about 1.2, though the values of $d\sigma/d\Omega dT$ at higher energies are changed considerably, in a direction in disagreement with the experimental results.

It is difficult to see how any variation in kinematic model or momentum distribution could bring the calculated spectrum into reasonable agreement with the observed one. It is believed to be possible (on the basis of several attempts in this direction) to pick an arbitrary excitation function such that a good fit could be obtained, but such a function would be so steep (proportional to T'^n, where $n\geq 8$) and so arbitrary in shape as to be meaningless.

VII. ACKNOWLEDGMENTS

This experiment was first suggested by Professor C. Richman, whose constant encouragement and advice throughout the course of the work have been greatly appreciated.

I would like to thank Dr. S. Bludman for many stimulating discussions about the theoretical aspects of the paper.

The assistance of Miss I. D'Arche and Mrs. B. Baldridge in scanning some of the plates is gratefully acknowledged.

Neutron-Proton Scattering with Spin-Orbit Coupling. II. Variational Formulation and Effective Range Theory

L. C. BIEDENHARN, *Yale University,** *New Haven, Connecticut*

AND

J. M. BLATT, *University of Sydney, Sydney, Australia*

(Received November 23, 1953)

The variational methods of Schwinger *et al.* are used to give variationally correct expressions for the three independent real parameters in the scattering matrix ($\delta_{J\alpha}$, $\delta_{J\beta}$, and ϵ_J) for the "mixed" states, such as ${}^3S_1+{}^3D_1$, of the neutron-proton system with spin-orbit coupling. The relation between these variational principles and the effective range theory is discussed briefly. The effective range expansions are then derived nonvariationally. The two leading terms are given for $k^5\cot\delta_{1\beta}$ and for $k^{-2}\tan\epsilon_1$. The three leading terms are given for $k\cot\delta_{1\alpha}$.

1. INTRODUCTION

IN a previous paper,[1] henceforth referred to as I, we have given the scattering matrix theory of neutron-proton scattering with spin-orbit coupling. The possible triplet states of the neutron-proton system fall into two categories: single-channel states such as ${}^3P_1$, in which the spin-orbit interaction cannot admix any other state because of conservation of total angular momentum and parity; and two-channel states, such as ${}^3S_1+{}^3D_1$, in which the spin-orbit interaction admixes the other state even if the ingoing wave contains only one of the two states. The analysis of the single-channel states is simple; in particular, the scattering matrix for such a state contains only one real parameter, a phase shift, and this phase shift can be found by the usual variational methods.[2] This paper is devoted to a discussion of the two-channel states, in particular the ${}^3S_1+{}^3D_1$ state which makes the dominant contribution to (triplet) low-energy neutron-proton scattering.

The general considerations in I have shown that the scattering matrix for a two-channel state depends on three real parameters, δ_α, δ_β, and ϵ. The first two are eigenphase shifts, the last is a "mixture parameter" which specifies which particular superpositions of ${}^3S_1$ and ${}^3D_1$ wave functions are eigenfunctions of the scattering matrix. Paper I contains an explicit formula for the scattering cross section in terms of these parameters. We were also able to determine the behavior of δ_α, δ_β, and ϵ close to zero energy. Beyond that, however, the general theory is powerless; more specific assumptions must be made about the nuclear forces in order to get useful answers.

Section 2 is devoted to the variational formulation of the problem of finding the parameters δ_α, δ_β, and ϵ. Variational principles for the two eigenphase shifts have been given by Schwinger,[3] and in that respect our work represents only a slight modification of his. The variational principle for ϵ given here has not been published previously, to our knowledge.[4]

In Sec. 3 we determine the coefficients of a series expansion of the parameters $k\cot\delta_\alpha$, $k\cot\delta_\beta$, and $\tan\epsilon$. We choose to expand around zero energy, hence our zero-order trial functions are the ones appropriate to zero energy. Their asymptotic dependence for large r has been given in I. We get an effective range expansion for δ_α (we recall that the α wave is by definition predominantly of ${}^3S_1$ type at low energies), and similar expansions for δ_β and for ϵ. The trial functions can be improved systematically, using the results of calculations with lower-order trial functions, thereby yielding a step-by-step procedure for finding higher terms in the various series.

2. VARIATIONAL PRINCIPLES FOR THE SCATTERING MATRIX PARAMETERS

In order to fix our ideas, let us restrict ourselves to the ${}^3S_1+{}^3D_1$ state, and to a spin-orbit coupling of the tensor force type, i.e., the potential is

$$V=V_c(r)+V_t(r)S_{12}, \tag{2.1}$$

where S_{12} is the conventional tensor operator,

$$S_{12}=3(\boldsymbol{\sigma}_1\cdot\mathbf{r})(\boldsymbol{\sigma}_2\cdot\mathbf{r})/r^2-(\boldsymbol{\sigma}_1\cdot\boldsymbol{\sigma}_2). \tag{2.2}$$

$V_c(r)$ and $V_t(r)$ in (2.1) define the radial dependence of the central and tensor potentials, respectively. We emphasize, though, that the contents of this section are *not* restricted to tensor forces; any Hermitian operator leading to spin-orbit coupling may be substituted for $V_t(r)S_{12}$. Furthermore, only trivial modifications are

* Assisted by the joint program of the U. S. Office of Naval Research and the U. S. Atomic Energy Commission and by the Office of Ordnance Research, U. S. Army.

[1] J. M. Blatt and L. C. Biedenharn, Phys. Rev. **86**, 399 (1952). General references to the literature on neutron-proton scattering with spin-orbit coupling will be found in this paper.

[2] J. Schwinger, Phys. Rev. **78**, 135 (1950); **72**, 749 (1947); L. Hulthèn, Kgl. Fysiograf. Sällskap. Lund, Förh. **14**, No. 21, 257 (1944); Skand. Mat. Kongres 1946, Copenhagen, 201 (1947); B. Lippmann and J. Schwinger, Phys. Rev. **79**, 469 (1950); W. Kohn, Phys. Rev. **74**, 1763 (1948); S. Huang, Phys. Rev. **76**, 1878 (1949); Toraldo di Francia, Phys. Rev. **78**, 298 (1950); T. Kato, Phys. Rev. **80**, 475 (1950); H. Feshbach and S. I. Rubinow, Phys. Rev. **88**, 484 (1952).

[3] J. Schwinger, lectures, Harvard University, 1947 (unpublished).

[4] A brief report was made at the Cambridge Meeting of the American Physical Society [Phys. Rev. **90**, 365 (1953)].

required to make the variation principles derived here applicable to other two-channel states (e.g., the ${}^3P_2+{}^3F_2$ state).

Let $u(r)$ and $w(r)$ be the radial wave functions for the ${}^3S$ and ${}^3D$ states, respectively, defined in the conventional way.[5] Let M be the nucleon mass, and E be the energy in the center-of-gravity system. Then u and w satisfy the coupled differential equations

$$-(\hbar^2/M)(d^2u/dr^2)+V_c(r)u(r) +8^{\frac{1}{2}}V_t(r)w(r)=Eu(r), \quad (2.3a)$$

$$-(\hbar^2/M)(d^2w/dr^2)+(6\hbar^2/Mr^2)w(r) +[V_c(r)-2V_t(r)]w(r)+8^{\frac{1}{2}}V_t(r)u(r)=Ew(r). \quad (2.3b)$$

We introduce a simplified notation in order to write the formulas more compactly. We define the column vector ψ by

$$\psi=\begin{pmatrix} u(r) \\ w(r) \end{pmatrix}. \quad (2.4)$$

The scalar product between two vectors ψ_1 and ψ_2 is defined by

$$(\psi_1,\psi_2)=\int_0^\infty [u_1^*(r)u_2(r)+w_1^*(r)w_2(r)]dr. \quad (2.5)$$

We also introduce the wave number k,

$$k^2=ME/\hbar^2, \quad (2.6)$$

and the kinetic energy operator T,

$$T=\begin{pmatrix} -d^2/dr^2 & 0 \\ 0 & -d^2/dr^2+6/r^2 \end{pmatrix}. \quad (2.7)$$

Finally, we introduce an operator W which corresponds to $-(M/\hbar^2)$ times the potential energy (the negative sign is chosen so that W is positive for attractive potentials, and the factor $M/\hbar^2$ ensures that W has the dimension cm^{-2}),

$$W=-(M/\hbar^2)\begin{pmatrix} V_c(r) & 8^{\frac{1}{2}}V_t(r) \\ 8^{\frac{1}{2}}V_t(r) & V_c(r)-2V_t(r) \end{pmatrix}. \quad (2.8)$$

With this notation, Eqs. (2.3) can be rewritten as

$$(T-k^2)\psi=W\psi. \quad (2.9)$$

The operator $T-k^2$ can be inverted. We look for standing-wave solutions (i.e., solutions of type $\Psi_a^{(1)}$ in the notation of Lippmann and Schwinger[2]). The Green's function operator then is

$$\mathcal{G}=\text{principal value of}\left(\frac{1}{T-k^2}\right) =k^{-1}\begin{pmatrix} F_0(r_<)G_0(r_>) & 0 \\ 0 & F_2(r_<)G_2(r_>) \end{pmatrix}, \quad (2.10)$$

where $F_l(r)$ and $G_l(r)$ are the regular and irregular solutions of the radial wave equation for a free particle of orbital angular momentum l and wave number k (as defined in I, for example), and $r_<$ is the smaller one of r, r'; $r_>$ is the larger one of r, r'. To avoid misunderstanding, we write out explicitly the effect of the operation $\mathcal{G}$ on the state vector ψ,

$$\mathcal{G}\psi=\begin{bmatrix} k^{-1}G_0(r)\int_0^r F_0(r')u(r')dr' \\ \qquad +k^{-1}F_0(r)\int_r^\infty G_0(r')u(r')dr' \\ k^{-1}G_2(r)\int_0^r F_2(r')w(r')dr' \\ \qquad +k^{-1}F_2(r)\int_r^\infty G_2(r')w(r')dr' \end{bmatrix}. \quad (2.11)$$

Let ϕ_a be any solution of the force-free radial wave equation regular at the origin; i.e.,

$$\phi_a=\begin{pmatrix} A_0k^{-1}F_0(r) \\ A_2k^{-1}F_2(r) \end{pmatrix}, \quad (T-k^2)\phi_a=0, \quad (2.12)$$

where A_0 and A_2 are arbitrary constants. Then the standing wave solution ψ_a of the complete problem associated with the free state ϕ_a satisfies the integral equation,

$$\psi_a=\phi_a+\mathcal{G}W\psi_a. \quad (2.13)$$

It will prove convenient to introduce an explicit notation for the free-state solutions ϕ associated with pure S waves and pure D waves. We define

$$\phi_0=\begin{pmatrix} k^{-1}F_0(r) \\ 0 \end{pmatrix}, \quad \phi_2=\begin{pmatrix} 0 \\ k^{-1}F_2(r) \end{pmatrix}. \quad (2.14)$$

In this notation (2.12) becomes

$$\phi_a=A_0\phi_0+A_2\phi_2. \quad (2.12a)$$

We now determine the asymptotic form of ψ_a for large values of r. We use the asymptotic forms of $F(r)$ and $G(r)$ given in I as well as formulas (2.11) and (2.13) to get

$$\psi_a(r)=\begin{pmatrix} A_0k^{-1}\sin(kr) \\ A_2k^{-1}\sin(kr-\pi) \end{pmatrix} +\begin{pmatrix} (\phi_0, W\psi_a)\cos(kr) \\ (\phi_2, W\psi_a)\cos(kr-\pi) \end{pmatrix}, \quad (2.15)$$

where the scalar products $(\phi_0,W\psi_a)$ and $(\phi_2,W\psi_a)$ are defined by (2.5), (2.8), and (2.14).

We now look for eigenstates of the scattering matrix. The eigenstates can be characterized by the requirement

[5] J. M. Blatt and V. F. Weisskopf, *Theoretical Nuclear Physics* (John Wiley and Sons, Inc., New York, 1952), Chap. II, Sec. 5D.

that the asymptotic form for large r is

$$\psi_a(r)\sim\begin{pmatrix} B_0k^{-\frac{1}{2}}\sin(kr+\delta) \\ B_2k^{-\frac{1}{2}}\sin(kr-\pi+\delta)\end{pmatrix}, \tag{2.16}$$

where the eigenphase shift δ is the *same* for both components of ψ_a. The two eigenphase shifts δ_α and δ_β are associated with different ratios of B_2 to B_0. Comparing (2.15) and (2.16), we get

$$A_0=k\cot\delta(\phi_0,W\psi_a), \qquad A_2=k\cot\delta(\phi_2,W\psi_a), \tag{2.17}$$

and hence (2.13) can be rewritten, for the special case of eigenstates of the scattering matrix, as

$$\psi_a=k\cot\delta[(\phi_0,W\psi_a)\phi_0+(\phi_2,W\psi_a)\phi_2]+\mathcal{G}W\psi_a. \tag{2.18}$$

This equation has the tremendous advantage that it is homogeneous in ψ_a and may therefore be considered an eigenvalue problem with $k\cot\delta$ as the eigenvalue. We simplify the notation by introducing the projection operator $\mathcal{F}$,

$$\mathcal{F}\psi=(\phi_0,\psi)\phi_0+(\phi_2,\psi)\phi_2. \tag{2.19}$$

The matrix form of the operator $\mathcal{F}$ is

$$\mathcal{F}=\begin{pmatrix} k^{-2}F_0(r)F_0(r') & 0 \\ 0 & k^{-2}F_2(r)F_2(r')\end{pmatrix}. \tag{2.19a}$$

This operator satisfies the operator equation $(T-k^2)\mathcal{F}=0$, whereas the Green's function operator $\mathcal{G}$ (2.10) satisfies the operator equation $(T-k^2)\mathcal{G}=\mathbf{1}$ where $\mathbf{1}$ is the unit operator. We can now rewrite (2.18) as an eigenvalue equation for $k\cot\delta$,

$$(1-\mathcal{G}W)\psi=k\cot\delta\,\mathcal{F}W\psi. \tag{2.10}$$

This equation still suffers from one defect: the operators $1-\mathcal{G}W$ and $\mathcal{F}W$ are not Hermitian. We can remedy this defect by premultiplying both sides of (2.20) by the operator W. We therefore define the two Hermitian operators,

$$Z=W-W\mathcal{G}W \quad \text{and} \quad Y=W\mathcal{F}W, \tag{2.21}$$

to get

$$Z\psi=(k\cot\delta)Y\psi. \tag{2.20a}$$

From this it follows immediately that a variationally correct form for the eigenvalue $k\cot\delta$ is

$$k\cot\delta=\frac{(\psi,Z\psi)}{(\psi,Y\psi)}=\frac{(\psi,W\psi)-(\psi,W\mathcal{G}W\psi)}{(\psi,W\mathcal{F}W\psi)}. \tag{2.22}$$

Writing out the denominator explicitly, we find that (2.22) becomes

$$k\cot\delta=\frac{(\psi,W\psi)-(\psi,W\mathcal{G}W\psi)}{|(\phi_0,W\psi)|^2+|(\phi_2,W\psi)|^2}. \tag{2.22a}$$

This variational expression for the eigenphase shifts was first given by Schwinger[3] and the derivation presented here is identical with his except for notation.

In order to put the calculation of the scattering matrix on a completely variational basis, we still need a variation principle for the mixture parameter ϵ defined in I. Two *nonvariational* expressions for $\tan\epsilon$ follow from (2.17). Let δ be the α-wave eigenphase shift δ_α and ψ_a be the corresponding eigensolution ψ_α. Then according to Eq. (2.17) of I, the ratio of A_2/A_0 is equal to $\tan\epsilon$; i.e.,

$$\tan\epsilon=(\phi_2,W\psi_\alpha)/(\phi_0,W\psi_\alpha). \tag{2.23}$$

Now let δ be the other eigenphase shift δ_β and compare with Eq. (2.18) of I. The ratio of A_2/A_0 is now $-\cot\epsilon$, so that

$$\tan\epsilon=-(\phi_0,W\psi_\beta)/(\phi_2,W\psi_\beta). \tag{2.24}$$

Expressions (2.23) and (2.24) are homogeneous in ψ, so that both are independent of the normalization of ψ. We now search for a variational expression for $\tan\epsilon$ which preserves this property.

It is well known that two eigenfunctions of the usual eigenvalue problem $H\psi=\lambda\psi$, belonging to two different eigenvalues λ_1 and λ_2, are orthogonal to each other; i.e., $(\psi_1,\psi_2)=0$ and also $(\psi_1,H\psi_2)=\lambda_2(\psi_1,\psi_2)=0$. By an obvious extension of the usual proof to the modified eigenvalue problem $Z\psi=\lambda Y\psi$, we find that eigenfunctions ψ_α and ψ_β of (2.21) belonging to two different eigenvalues $k\cot\delta_\alpha$ and $k\cot\delta_\beta$, respectively, satisfy the relations

$$(\psi_\alpha,Y\psi_\beta)=0, \quad (\psi_\alpha,Z\psi_\beta)=0. \tag{2.25}$$

Let us now consider trial wave functions ψ_a and ψ_b which are close to the eigenfunctions ψ_α and ψ_β, respectively. That is, we assume

$$\psi_a=\psi_\alpha+\eta E_a, \quad \psi_b=\psi_\beta+\eta E_b, \tag{2.26}$$

where E_a and E_b are arbitrary vectors and η is a small parameter. If we compute $(\psi_a,Z\psi_b)$ we find, using (2.22) and (2.25),

$$\begin{aligned}(\psi_a,Z\psi_b)&=(\psi_b,Z\psi_a)\\&=\eta(\psi_a,ZE_b)+\eta(\psi_\beta,ZE_\alpha)+O(\eta^2)\\&=\eta k\cot\delta_\alpha(\psi_a,YE_b)+\eta k\cot\delta_\beta(\psi_\beta,YE_\alpha)+O(\eta^2),\end{aligned}$$

so that

$$\begin{aligned}(\psi_a,Z\psi_b)=k\cot\delta_\alpha&(\psi_a,Y\psi_b)\\&+k\cot\delta_\beta(\psi_\beta,Y\psi_a)+O(\eta^2).\end{aligned} \tag{2.27}$$

We now use the definition of the operator Y and Eq. (2.23) in order to get an explicit form for $(\psi_a,Y\psi_b)$; that is,

$$\begin{aligned}(\psi_a,Y\psi_b)&=(\phi_0,W\psi_a)(\phi_0,W\psi_b)+(\phi_2,W\psi_a)(\phi_2,W\psi_b)\\&=(\phi_0,W\psi_a)(\phi_2,W\psi_b)\left[\frac{(\phi_0,W\psi_b)}{(\phi_2,W\psi_b)}+\tan\epsilon\right].\end{aligned} \tag{2.28a}$$

Similarly, using (2.21) and (2.24), we get

$$\begin{aligned}(\psi_\beta,Y\psi_a)&\\&=(\phi_0,W\psi_\beta)(\phi_0,W\psi_a)+(\phi_2,W\psi_\beta)(\phi_2,W\psi_a)\\&=(\phi_0,W\psi_a)(\phi_2,W\psi_\beta)\left[-\tan\epsilon+\frac{(\phi_2,W\psi_a)}{(\phi_0,W\psi_a)}\right].\end{aligned} \tag{2.28b}$$

According to Eq. (2.23) the expression $(\phi_2,W\psi_a)/(\phi_0,W\psi_a)$ is an approximation to $\tan\epsilon$ homogeneous in the trial function ψ_a with an error of first order. We use the symbol t for this expression, i.e.,

$$t\equiv(\phi_2,W\psi_a)/(\phi_0,W\psi_a)=\tan\epsilon+O(\eta). \quad (2.29a)$$

We also introduce the symbol t' for

$$t'\equiv-(\phi_0,W\psi_b)/(\phi_2,W\psi_b)=\tan\epsilon+O(\eta). \quad (2.29b)$$

Thus to an error of second order, we may write for (2.28)

$$\begin{aligned}(\psi_a,Y\psi_b)&=(\phi_0,W\psi_a)(\phi_2,W\psi_b)[-t'+\tan\epsilon]+O(\eta^2)\\(\psi_\beta,Y\psi_a)&=(\phi_0,W\psi_a)(\phi_2,W\psi_b)[t-\tan\epsilon]+O(\eta^2).\end{aligned} \quad (2.30)$$

Substituting this into Eq. (2.27) and solving for $\tan\epsilon$, we find an expression for $\tan\epsilon$ accurate to an error of second order in η, i.e., *a variational expression for $\tan\epsilon$ homogeneous in the trial wave functions*

$$\tan\epsilon=(k\cot\delta_\beta-k\cot\delta_a)^{-1}\left[tk\cot\delta_\beta-t'k\cot\delta_a-\frac{(\psi_a,Z\psi_b)}{(\phi_0,W\psi_a)(\phi_2,W\psi_b)}\right]. \quad (2.31)$$

In this expression ψ_a must be chosen close to ψ_a, ψ_b close to ψ_β, t and t' are defined by (2.29), and $k\cot\delta_a$ and $k\cot\delta_\beta$ are defined by (2.22) with ψ_a and ψ_b, respectively. Since (2.22) is itself a variational form, the error introduced by its use is also of the order of the square of the errors in ψ_a and ψ_b.

Expressions (2.22) and (2.31) put the calculation of the scattering matrix on a completely variational basis, in terms of the minimum number of parameters.[6] Just as the Schwinger variational principle for the diagonal elements of the scattering matrix (the eigenphase shifts essentially) is not confined to a two-channel system, so the variational principle in (2.31) can be generalized for determining the $N(N-1)/2$ remaining independent parameters of the scattering matrix for an N-channel problem. This will be treated in a separate paper.

3. THE EFFECTIVE RANGE EXPANSION AND THE VARIATION PRINCIPLE

The general considerations of Sec. 4 of I have determined the behavior of the parameters δ_a, δ_β, and ϵ near zero energy. The same considerations moreover fixed the asymptotic behavior of the zero energy eigenfunctions.[7] Restricting our attention to $J=1$ ($^3S_1+^3D_1$ state), we find the following asymptotic forms for the zero energy wave functions:

$$\psi_{0a}\sim\psi_{0a}^{(\infty)}=\begin{pmatrix}u_{0a}^{(\infty)}\\w_{0a}^{(\infty)}\end{pmatrix}=\begin{pmatrix}r-a_a\\-3qa_a/r^2\end{pmatrix}, \quad (3.1a)$$

$$\psi_{0\beta}\sim\psi_{0\beta}^{(\infty)}=\begin{pmatrix}u_{0\beta}^{(\infty)}\\w_{0\beta}^{(\infty)}\end{pmatrix}=\begin{pmatrix}-15qr\\r^3-a_\beta^5/5r^2\end{pmatrix}. \quad (3.1b)$$

Utilizing the above as a boundary condition on the two independent zero energy solutions of the wave equation (2.9) leads to the desired zero energy eigenfunctions. With these as trial functions in the variational expressions (2.22) and (2.31) we can determine $k\cot\delta$ and $\tan\epsilon$ to an error of order k^4—the square of the error in the trial functions. Greater accuracy can be obtained with iterated solutions (see below) of the Schrödinger equation (2.9) accurate to an error of order k^4, and we can thus systematically improve our results.

The variational approach leads in a natural fashion to expressions of the form

$$k\cot\delta=\frac{a_0+a_1k^2+a_2k^4+\cdots}{b_0+b_1k^2+b_2k^4+\cdots}, \quad (3.2)$$

where a_0, a_1, b_0, b_1 can be found from the zero energy trial functions. Trial functions correct to order k^2 can be used to obtain expressions for a_2, a_3, b_2, b_3, and so on.

The effective range theory is obtained by rewriting (3.2) as a power series in k^2; i.e.,

$$k\cot\delta_a=c_0+c_1k^2+c_2k^4+\cdots. \quad (3.2a)$$

It should be emphasized, perhaps, that (3.2a) is equivalent to (3.2) only within the radius of convergence (in the k^2 plane) of (3.2a). In general, this radius of convergence is very much smaller than the radii of convergence of the series in the numerator and denominator of (3.2). Thus, the reduction of (3.2) to (3.2a) gives rise to an appreciable reduction in the range of validity of the expression for $k\cot\delta_a$.

The nonvariational derivations current in the literature[8] all lead to expressions of the form (3.2a). To the extent that the variational form (3.2) is reduced to (3.2a), the nonvariational formulations of the theory are equivalent to the variational formulation. However, this reduction need not be made in the variational formulation, whereas it is made automatically [i.e., (3.2) is never obtained] in the nonvariational formulation. Thus, the two formulations of the effective range theory are not equivalent, the variational one being rather more powerful.

For example, the series (3.2a) breaks down if the scattering length is zero, i.e., if the coefficient c_0 in (3.2a) becomes infinite. This can happen when there

[6] The calculation of Rohrlich and Eisenstein (see reference 1) was variational only to the extent that the eigenphase shifts were computed variationally. The mixture parameters found by them are correct only to a first-order error.

[7] Note the misprint in Eq. 4.22 of I. The superscript $2J+1$ should be $2J+3$.

[8] H. A. Bethe, Phys. Rev. **76**, 38 (1949); R. E. Peierls and M. A. Preston, Phys. Rev. **72**, 250 (1947); Hatcher, Arfken, and Breit, Phys. Rev. **75**, 1389 (1949); G. F. Chew and M. L. Goldberger, Phys. Rev. **75**, 250 (1947); see also G. Breit, Revs. Modern Phys. **23**, 238 (1951).

is a repulsive core and an attractive outside region. Expression (3.2), however, retains its usefulness even when the scattering length vanishes.

Since wells with hard repulsive cores are becoming increasingly fashionable, we may be forced to use expressions of type (3.2) rather than (3.2a), in spite of their more awkward form. In this paper, however, we shall reduce all results to the power series form (3.2a).

We write these expansions in the form

$$k\cot\delta_\alpha=-1/a_\alpha+r_\alpha k^2/2-Pr_\alpha^3k^4+\cdots, \tag{3.3}$$

$$k^5\cot\delta_\beta=(225/a_\beta^4)[-1/a_\beta+r_\beta k^2/2+\cdots], \tag{3.4}$$

$$\tan\epsilon=qk^2+q_1k^4+\cdots. \tag{3.5}$$

The lowest-order terms are known from Sec. 4 of I. The coefficient a_α is the usual triplet scattering length, while r_α is the triplet effective range. Tanϵ is a measure of the mixing of the S and D states in the deuteron problem, and to a first approximation, q is proportional to the quadrupole moment of the deuteron. The coefficients a_β and r_β are the analogs of the a_α and r_α, respectively.

The proportionality of Q and q can be seen in the following way.[9] The quadrupole moment is given by the expression

$$Q=(\sqrt{2}/10)\int_0^\infty r^2(uw-8^{-\frac{1}{2}}w^2)dr.$$

Because of the smallness of the percentage D state in the deuteron problem, it is a good approximation to neglect the w^2 term in this expression. Furthermore the factor r^2 insures the major contribution (~90 percent in actual cases) will come from large distances, outside the nuclear interaction, but still in the region where the centrifugal well dominates the behavior of the D state. Thus it is sufficient to use the asymptotic forms:

$$u=Ae^{-\gamma r}, \qquad w=A\times C\times e^{-\gamma r}(1+3/\gamma r+3/\gamma^2r^2),$$

$$\gamma=(M|E_d|)^{\frac{1}{2}}/\hbar, \quad E_d=\text{deuteron binding energy}.$$

The normalization can be determined approximately from the effective range by neglecting the effects of the D state (this procedure compensates slightly for the neglect of w^2 in Q). Thus we take

$$A^{-2}\cong(1-\gamma r_\alpha)/2\gamma,$$

and then find that

$$C\cong(1-\gamma r_\alpha)^{\frac{1}{2}}\times\sqrt{2}\times Q\gamma^2.$$

But the constant C is the asymptotic ratio of D to S state, i.e., just the quantity denoted by tanϵ for positive energy states. Hence C is tanϵ for the negative energy given by $k=-i\gamma$, $k^2=-\gamma^2$.[9] We therefore get

$$(\tan\epsilon)_{k^2=-\gamma^2}=-q\gamma^2+q_1\gamma^4-\cdots\cong(1-\gamma r_\alpha)^{\frac{1}{2}}\sqrt{2}Q\gamma^2.$$

To the rather moderate (perhaps 10 percent) accuracy of the approximations made already, we can ignore the term in q_1 and obtain

$$q\cong-(1-\gamma r_\alpha)^{\frac{1}{2}}\times\sqrt{2}Q. \tag{3.5a}$$

[9] This extension of positive-energy relations to include ground-state properties is valid only for a restricted class of potentials V; see R. Jost and W. Kohn, Kgl. Danske Videnskab. Selskab Mat.-fys. Medd. **27**, No. 9, 1–19 (1953), and other papers referred to there. For central forces, a sufficient (but not necessary) condition upon V is that V must decrease, for large r, faster than the probability density $u^2(r)$ in the ground state; i.e.,

$$\lim_{r\to\infty}[e^{2\gamma r}V(r)]=0.$$

Presumably a similar condition exists for tensor forces. Whatever it is, we shall presume it to be satisfied for our present purpose.

The coefficients r_α, r_β, and q_1 can be obtained explicitly in terms of the wave functions $\psi_{0\alpha}$ and $\psi_{0\beta}$ by means of (2.22) and (2.31). Some care in carrying out this reduction must be exercised in order not to misuse the variational principle.[10] Let us denote by $\mathcal{V}_\alpha(k^2\psi_\alpha)$ the variational principle for $k\cot\delta_\alpha$ given by (2.22). Then, according to (3.3) we have

$$\begin{aligned}\tfrac{1}{2}r_\alpha&=\lim_{k^2\to0}\left(\frac{d\mathcal{V}_\alpha}{dk^2}\right)\\&=\lim_{k^2\to0}\left(\frac{\partial\mathcal{V}_\alpha}{\partial k^2}+\frac{\delta\mathcal{V}_\alpha}{\delta\psi_\alpha}\cdot\frac{\partial\psi_\alpha}{\partial k^2}\right)\\&=\lim_{k^2\to0}\left(\frac{\partial\mathcal{V}_\alpha}{\partial k^2}\right).\end{aligned} \tag{3.6}$$

The last equation results from the fact that $\delta\mathcal{V}_\alpha/\delta\psi_\alpha=0$ for all values of k^2 by the stationary property of (2.22). The limit $k^2\to0$ was taken in order to determine a value for $\frac{1}{2}r_\alpha$. If we do *not* take this limit, however, Eq. (3.6) yields an *exact* expression for $d(k\cot\delta_\alpha)/dk^2$ in terms of ψ_α alone, which is, to be sure, no longer a variationally stationary result. The expression obtained is, in fact, the precise equivalent to the usual starting point for the nonvariational approach to the effective range expansion.[8]

We do not give this derivation in this paper, however, for the following reason: if the effective range expansion (3.2a) is all that is desired, it is simpler and more straightforward to derive it directly from the differential equations satisfied by the wave functions u and w, along the lines of Bethe.[8] We therefore do so in the following section, and we would like to thank Professor Bethe for permission to publish this material.[11] All results have been checked independently by rederiving them directly from the variational expressions given in Sec. 2; however, since this derivation is much more lengthy, we do not give it here.

4. THE EFFECTIVE RANGE EXPANSION: NONVARIATIONAL DERIVATION

We shall normalize the α-wave functions ψ_α so that in the limit of zero energy, the normalization agrees with (3.1a); that is, for large values of r ($r>b$), we have

$$u_\alpha^{(\infty)}=-a_\alpha\cos\epsilon(\cot\delta_\alpha F_0+G_0), \tag{4.1a}$$

$$w_\alpha^{(\infty)}=-a_\alpha\sin\epsilon(\cot\delta_\alpha F_2+G_2). \tag{4.1b}$$

[10] The point at issue here is that $k\cot\delta$ and tanϵ, as defined by (2.22) and (2.31), are both *explicit* functions of k^2, through the operators $\mathfrak{F}$ and $\mathfrak{G}$, and *implicit* functions of k^2, through the wave functions ψ. The stationary property asserts only that the first-order variations in ψ cancel out. If one labels this variation by k^2, it is clear that confusion with the explicit dependence on k^2 might arise.

[11] Professor Bethe has obtained Eq. (4.11) and its consequences independently. We believe that Eqs. (4.19) and (4.26) represent new contributions.

Denote by $\psi_{\alpha 1}$ the α-wave function, normalized in this way, at energy E_1, and by $\psi_{\alpha 2}$ the α-wave function at energy E_2. They satisfy the differential equations

$$(T-k_1^2)\psi_{\alpha 1}=W\psi_{\alpha 1}, \tag{4.2a}$$

$$(T-k_2^2)\psi_{\alpha 2}=W\psi_{\alpha 2}, \tag{4.2b}$$

each set of two differential equations being written in abbreviated form. We multiply the u part of (4.2a) by $u_{\alpha 2}$, the w part by $w_{\alpha 2}$; we multiply the u part of (4.2b) by $u_{\alpha 1}$, the w part by $w_{\alpha 1}$. Subtraction then gives

$$\begin{aligned} &u_{\alpha 2}d^2u_{\alpha 1}/dr^2+w_{\alpha 2}d^2w_{\alpha 1}/dr^2-u_{\alpha 1}d^2u_{\alpha 2}/dr^2-w_{\alpha 1}d^2w_{\alpha 2}/dr^2 \\ &\quad=(d/dr)(u_{\alpha 2}u'_{\alpha 1}+w_{\alpha 2}w'_{\alpha 1}-u_{\alpha 1}u'_{\alpha 2}-w_{\alpha 1}w'_{\alpha 2}) \\ &\quad=(k_2^2-k_1^2)(u_{\alpha 1}u_{\alpha 2}+w_{\alpha 1}w_{\alpha 2}). \end{aligned} \tag{4.3}$$

A similar expression can be derived for the asymptotic forms (4.1). However, this is not very useful because $w_\alpha^{(\infty)}$ diverges at $r=0$. It is more useful to define a set of functions, related to (4.1), with the property that they are finite both as r approaches zero and as r approaches infinity. These functions will be distinguished by bars, and are defined as follows:

$$\begin{aligned} &\bar{u}_\alpha=u_\alpha^{(\infty)}, \\ &\bar{w}_\alpha=w_\alpha^{(\infty)}+3a_\alpha\sin\epsilon(kr)^{-2} \\ &\qquad=-a_\alpha\sin\epsilon[\cot\delta_\alpha F_2+G_2-3(kr)^{-2}]. \end{aligned} \tag{4.4}$$

The differential equations satisfied by $\bar{\psi}_\alpha$ are, again in the abbreviated notation,

$$(T-k^2)\bar{\psi}_\alpha=\begin{pmatrix}0\\-3a_\alpha\sin\epsilon\, r^{-2}\end{pmatrix}. \tag{4.5}$$

By a procedure analogous to the one followed to derive (4.3), we get

$$\begin{aligned} &(d/dr)[\bar{u}_{\alpha 1}\bar{u}'_{\alpha 2}+\bar{w}_{\alpha 1}\bar{w}'_{\alpha 2}-\bar{u}'_{\alpha 1}\bar{u}_{\alpha 2}-\bar{w}'_{\alpha 1}\bar{w}_{\alpha 2}] \\ &\qquad=(k_1^2-k_2^2)(\bar{u}_{\alpha 1}\bar{u}_{\alpha 2}+\bar{w}_{\alpha 1}\bar{w}_{\alpha 2}) \\ &\qquad\quad+3a_\alpha r^{-2}(\sin\epsilon_2\,\bar{w}_{\alpha 1}-\sin\epsilon_1\,\bar{w}_{\alpha 2}), \end{aligned} \tag{4.6}$$

where ϵ_1 stands for the value of the mixture parameter ϵ at energy E_1. In spite of appearances, the last term of (4.6) is finite as r approaches zero. This can be seen by using the series expansions of F_2 and G_2 in the second equation (4.4).

Following Bethe, we now combine (4.3) and (4.6) and integrate the resulting expression from zero to infinity. This yields

$$\begin{aligned} &[\bar{u}_{\alpha 1}\bar{u}'_{\alpha 2}+\bar{w}_{\alpha 1}\bar{w}'_{\alpha 2}-\bar{u}'_{\alpha 1}\bar{u}_{\alpha 2}-\bar{w}'_{\alpha 1}\bar{w}_{\alpha 2} \\ &\quad-u_{\alpha 1}u'_{\alpha 2}-w_{\alpha 1}w'_{\alpha 2}+u'_{\alpha 1}u_{\alpha 2}+w'_{\alpha 1}w_{\alpha 2}]_0^\infty \\ &\qquad=(k_1^2-k_2^2)[(\bar{\psi}_{\alpha 1},\bar{\psi}_{\alpha 2})-(\psi_{\alpha 1},\psi_{\alpha 2})] \\ &\qquad\quad+3a_\alpha\int_0^\infty dr\, r^{-2}(\sin\epsilon_2\,\bar{w}_{\alpha 1}-\sin\epsilon_1\,\bar{w}_{\alpha 2}). \end{aligned} \tag{4.7}$$

The terms on the left side of (4.7) all vanish at infinity, and only the barred functions contribute at $r=0$. By using (4.4) and (4.1), we get

left side of (4.7)

$$=a_\alpha^2\cos\epsilon_1\cos\epsilon_2(k_1\cot\delta_{\alpha 1}-k_2\cot\delta_{\alpha 2}). \tag{4.8}$$

It remains to evaluate the integral on the right side of (4.7). We use the identities

$$\begin{aligned} &\int_a^\infty dr\, r^{-2}F_2(r)=F_1(a)/ka^2, \\ &\int_a^\infty dr\, r^{-2}G_2(r)=G_1(a)/ka^2, \end{aligned} \tag{4.9}$$

in order to get

$$\begin{aligned} &3a_\alpha\int_0^\infty dr\, r^{-2}(\sin\epsilon_2\,\bar{w}_{\alpha 1}-\sin\epsilon_1\,\bar{w}_{\alpha 2}) \\ &\qquad=-a_\alpha^2\sin\epsilon_1\sin\epsilon_2(k_1\cot\delta_{\alpha 1}-k_2\cot\delta_{\alpha 2}). \end{aligned} \tag{4.10}$$

We combine (4.7), (4.8), and (4.10), divide both sides by $k_1^2-k_2^2$, and take the limit as k_1 approaches k_2. The final result is

$$\begin{aligned} \frac{d(k\cot\delta_\alpha)}{d(k^2)}=a_\alpha^{-2}\int_0^\infty&[(\bar{u}_\alpha)^2+(\bar{w}_\alpha)^2 \\ &-(u_\alpha)^2-(w_\alpha)^2]dr. \end{aligned} \tag{4.11}$$

This identity forms the basis for the nonvariational approach to the effective range theory. As remarked before, the same identity can be derived from the explicit derivative of the variational expression (2.22), after a fair amount of manipulation.

The determination of the effective range r_α from (4.11) is immediate. All we have to do is to take the limit as the energy approaches zero. The left side is then equal to $\frac{1}{2}r_\alpha$, as can be seen from (3.3). On the right side, the function $\bar{w}_\alpha$ vanishes in this limit, and $\bar{u}_\alpha=u_\alpha^{(\infty)}$ becomes equal to $u_{0\alpha}=r-a_\alpha$, according to (3.1a). We therefore get (denoting zero energy functions by the subscript 0)

$$r_\alpha=2(a_\alpha)^{-2}\int_0^\infty[(u_{0\alpha}^{(\infty)})^2-(u_{0\alpha})^2-(w_{0\alpha})^2]dr. \tag{4.12}$$

We now turn to the beta-wave solution, and the expansion (3.4). We again normalize the function ψ_β at arbitrary energy E so that it reduces to the standard zero energy solution (3.1b) at $E=0$. That means

$$u_\beta^{(\infty)}=(1/15)k^2a_\beta^5\sin\epsilon(\cot\delta_\beta F_0+G_0), \tag{4.13a}$$

$$w_\beta^{(\infty)}=-(1/15)k^2a_\beta^5\cos\epsilon(\cot\delta_\beta F_2+G_2), \tag{4.13b}$$

and we define the barred functions, which are regular at zero, by

$$\bar{u}_\beta=u_\beta^{(\infty)}, \tag{4.14a}$$

$$\bar{w}_\beta=w_\beta^{(\infty)}+a_\beta^5\cos\epsilon/(5r^2). \tag{4.14b}$$

By using the same methods as before, we obtain an equation entirely analogous to (4.11), namely,

$$k^4\frac{d(k\cot\delta_\beta)}{d(k^2)}=\frac{225}{a_\beta^{10}}\int_0^\infty[(\bar{u}_\beta)^2+(\bar{w}_\beta)^2-(u_\beta)^2-(w_\beta)^2]dr. \quad (4.15)$$

Equation (4.15) is valid for all positive energies. However, difficulties arise when we try to go to the limit as the energy approaches zero, in order to obtain the quantity r_β in (3.4).

Looking back at Eq. (3.4), the quantity

$$k^4\frac{d}{d(k^2)}(k\cot\delta_\beta)=\frac{225}{a_\beta^4}\left[\frac{2}{a_\beta k^2}-\frac{1}{2}r_\beta+\cdots\right],$$

and hence diverges as $k^2\to 0$. The quantity of interest to us is not this, but rather

$$\frac{d}{dk^2}(k^5\cot\delta_\beta)=k^4\frac{d}{d(k^2)}(k\cot\delta_\beta)+2k^3\cot\delta_\beta. \quad (4.16)$$

In order to obtain an equation involving this quantity, we examine the integral on the right side of (4.15) in the limit as $k^2\to 0$. In that limit, the integrand is

$$(\bar{u}_{0\beta})^2-(u_{0\beta})^2+(\bar{w}_{0\beta})^2-(w_{0\beta})^2=(-15qr)^2-(u_{0\beta})^2+r^6-(w_{0\beta})^2. \quad (4.17)$$

For large values of r, (4.17) becomes

$$0+r^6-(w_{0\beta}{}^{(\infty)})^2=r^6-[r^3-(a_\beta{}^5/5r^2)]^2,$$

and this contains a term proportional to r. In order to avoid this difficulty, we add and subtract in the integrand the term

$$2(\bar{w}_\beta-w_\beta{}^{(\infty)})\left(-\frac{a_\beta{}^5\cos\epsilon}{15}k^2\cot\delta_\beta F_2\right),$$

which is that part of the cross term causing the trouble. (The complete cross term is $2(\bar{w}_\beta-w_\beta{}^{(\infty)})\bar{w}_\beta$, but using this would introduce a divergence at the origin.) The integral of this added term can be evaluated from (4.9) and is

$$\int_0^\infty 2(\bar{w}_\beta-w_\beta{}^{(\infty)})\left(-\frac{k^2a_\beta{}^5\cos\epsilon}{15}\cot\delta_\beta F_2\right)dr=-2\frac{a_\beta{}^{10}}{225}\cos^2\epsilon\,k^3\cot\delta_\beta. \quad (4.18)$$

By combining (4.15), (4.16), and (4.18) we obtain the equation

$$\frac{d(k^5\cot\delta_\beta)}{d(k^2)}=2k^3\sin^2\epsilon\cot\delta_\beta+\frac{225}{a_\beta{}^{10}}\int_0^\infty[(\bar{u}_\beta)^2+(\bar{w}_\beta)^2+(2/15)(\bar{w}_\beta-w_\beta{}^{(\infty)})\times(a_\beta{}^5\cos\epsilon\,k^2\cot\delta_\beta F_2)-(u_\beta)^2-(w_\beta)^2]dr, \quad (4.19)$$

or, equivalently (using 4.14)

$$\frac{d(k^5\cot\delta_\beta)}{d(k^2)}=2k^3\sin^2\epsilon\cot\delta_\beta+\frac{225}{a_\beta{}^{10}}\int_0^\infty\left[(u_\beta{}^{(\infty)})^2+(w_\beta{}^{(\infty)})^2-(u_\beta)^2-(w_\beta)^2+\frac{a_\beta{}^{10}\cos^2\epsilon}{75}\left(\frac{3}{r^4}-\frac{2k^2G_2}{r^2}\right)\right]dr. \quad (4.19')$$

Unlike (4.15), this equation is also valid in the limit as the energy (k^2) approaches zero. In this limit the first term on the right of (4.19) vanishes, and we get the following expression for r_β in (3.4):

$$r_\beta=2a_\beta{}^{-6}\int_0^\infty[(u_{0\beta}{}^{(\infty)})^2+r^3(2w_{0\beta}{}^{(\infty)}-r^3)-(u_{0\beta})^2-(w_{0\beta})^2]dr. \quad (4.20)$$

It remains now to determine the coefficient q_1 in the expansion for $\tan\epsilon$, Eq. (3.5). Again the nonvariational derivation of such a limited result is more straightforward than the derivation starting from the variational expression (2.31). By methods entirely analogous to the ones used so far, we derive

$$k_2{}^2\frac{a_\alpha a_\beta{}^5}{15}\cos\epsilon_1\cos\epsilon_2(k_2\cot\delta_{\beta 2}-k_1\cot\delta_{\alpha 1})(\tan\epsilon_2-\tan\epsilon_1)=(k_1{}^2-k_2{}^2)\int_0^\infty(\bar{u}_{\alpha 1}\bar{u}_{\beta 2}+\bar{w}_{\alpha 1}\bar{w}_{\beta 2}-u_{\alpha 1}u_{\beta 2}-w_{\alpha 1}w_{\beta 2})dr. \quad (4.21)$$

Dividing (4.21) by $(k_1{}^2-k_2{}^2)$ and going to the limit $k_1\to k_2$ yields

$$k^{-2}\frac{d}{dk^2}(\tan\epsilon)=15[a_\alpha a_\beta{}^5\cos^2\epsilon(k^5\cot\delta_\alpha-k^5\cot\delta_\beta)]^{-1}\times\int_0^\infty(\bar{u}_\alpha\bar{u}_\beta+\bar{w}_\alpha\bar{w}_\beta-u_\alpha u_\beta-w_\alpha w_\beta)dr. \quad (4.22)$$

Again we encounter difficulties in going to the limit $k^2\to 0$. We really need

$$\frac{d}{d(k^2)}\left(\frac{\tan\epsilon}{k^2}\right)=k^{-2}\frac{d}{d(k^2)}(\tan\epsilon)-k^{-4}\tan\epsilon. \quad (4.23)$$

In the limit $k^2\to 0$, the integrand in (4.22) becomes, for large values of r,

$$\bar{w}_{0\alpha}\bar{w}_{0\beta}-w_{0\alpha}{}^{(\infty)}w_{0\beta}{}^{(\infty)}=0-\left(\frac{-3qa_\alpha}{r^2}\right)\left(r^3-\frac{a_\beta{}^5}{5r^2}\right). \quad (4.24)$$

This contains a term proportional to r, which can be considered as the limit of a cross term between F_2 and

$1/r^2$, just as in (4.17). If we add in, and subtract from, the integrand the terms,

$$(-a_\alpha \sin\epsilon \cot\delta_\alpha F_2)(w_\beta^{(\infty)}-w_\beta)$$
$$+\left(\frac{-a_\beta^5}{15}\cos\epsilon\, k^3 \cot\delta_\beta F_2\right)(w_\alpha^{(\infty)}-w_\alpha),$$

then these troublesome cross terms are cancelled, and the integrals still remain well behaved at the origin. Using (4.9), the integral of these added terms is found to be

$$\int_0^\infty\Big[-a_\alpha \sin\epsilon \cot\delta_\alpha F_2(w_\beta^{(\infty)}-w_\beta)$$
$$-\frac{a_\beta^5}{15}\cos\epsilon\cdot k^3 \cot\delta_\beta F_2(w_\alpha^{(\infty)}-w_\alpha)\Big]dr$$
$$=\frac{a_\alpha a_\beta^5 \sin\epsilon\cos\epsilon}{15}(k\cot\delta_\alpha+k\cot\delta_\beta). \quad (4.25)$$

Combining (4.22), (4.23), and (4.25), we get

$$\frac{d}{d(k^2)}\left(\frac{\tan\epsilon}{k^3}\right)=15[a_\alpha a_\beta^5\cos^2\epsilon(k^5\cot\delta_\alpha-k^5\cot\delta_\beta)]^{-1}$$
$$\times\Big\{-\frac{2}{15}a_\alpha a_\beta^5\cos\epsilon\sin\epsilon\cdot k\cot\delta_\alpha$$
$$+\int_0^\infty\Big[\bar{u}_\alpha\bar{u}_\beta+\bar{w}_\alpha\bar{w}_\beta-u_\alpha u_\beta-w_\alpha w_\beta$$
$$-a_\alpha\sin\epsilon\cdot\cot\delta_\alpha\cdot F_2(w_\beta^{(\infty)}-w_\beta)$$
$$-\frac{a_\beta^5}{15}\cos\epsilon\cdot k^2\cot\delta_\beta\cdot F_2(w_\alpha^{(\infty)}-w_\alpha)\Big]dr\Big\}. \quad (4.26)$$

We can now go to the limit $k^2\to 0$, to obtain the coefficient q_1 in Eq. (3.5):

$$q_1=(15a_\alpha)^{-1}\int_0^\infty[u_{0\alpha}^{(\infty)}u_{0\beta}^{(\infty)}-3qa_\alpha r$$
$$-u_{0\alpha}u_{0\beta}-w_{0\alpha}w_{0\beta}]dr. \quad (4.27)$$

Equations (4.12), (4.20), and (4.27) give the first two terms in the power series (3.3) to (3.5). For purposes of estimating the error in this approximation higher terms are needed. We shall confine our attention to the "P" term in (3.3), the so-called "well shape parameter." According to the stationary property of (2.22), both P and the term of order k^6 can be determined exactly from trial functions accurate through order k^2. It is probably simplest to proceed directly from the differential equation (2.9). Define

$$\psi_\alpha\equiv\psi_{0\alpha}+k^2\psi_{2\alpha}+k^4\psi_{4\alpha}+\cdots. \quad (4.28)$$

Then from (2.9) we have

$$(T-W)\psi_{2\alpha}=\psi_{0\alpha}. \quad (4.29)$$

The boundary conditions on $\psi_{2\alpha}$ are first that it vanish at the origin, and second that it have the asymptotic behavior specified by (4.1). Expanding (4.1) in powers of k^2 and using (3.3), (3.5) we get

$$\psi_{2\alpha}\sim\begin{pmatrix}-r^3/6+a_\alpha r^2/2-r_\alpha a_\alpha r/2\\ -a_\alpha q/2-3a_\alpha q_1 r^{-2}\end{pmatrix}. \quad (4.30)$$

Any solution to (4.29), vanishing properly at the origin, is equal to the desired solution $\psi_{2\alpha}$ plus undetermined amounts of the two independent solutions $\psi_{0\alpha}$ and $\psi_{0\beta}$ of the homogeneous equations. Let a solution of (4.29) be denoted by $\chi_{2\alpha}$. According to the differential equation (4.29), the asymptotic behavior for large r of the solution $\chi_{2\alpha}$ must be

$$\chi_{2\alpha}^{(\infty)}=\begin{pmatrix}A+Br+a_\alpha r^2/2-r^3/6\\ Cr^{-2}-a_\alpha q/2+Dr^3\end{pmatrix}, \quad (4.31)$$

where A, B, C, and D are constants which can be determined by a numerical integration. By comparing (3.1), (4.30), and (4.31), we see that

$$\psi_{2\alpha}=\chi_{2\alpha}+(A/a_\alpha)\psi_{C\alpha}-D\psi_{0\beta}. \quad (4.32)$$

Furthermore, comparing the coefficients of r and r^{-2} on both sides of (4.32), we get the identities

$$-r_\alpha a_\alpha/2=A/a_\alpha+15qD+B, \quad (4.33)$$
$$-3a_\alpha q_1=C-3qA+a_\beta^5 D/5. \quad (4.34)$$

In other words, a given solution to (4.29), $\chi_{2\alpha}$ (numerically determined for example) automatically yields a value for both r_α and q_1—quantities known already from the zero energy solutions $\psi_{0\alpha}$ and $\psi_{0\beta}$. This feature of the calculations affords a useful check on the numerical accuracy of the work.

An explicit formula for P utilizing $\psi_{2\alpha}$ is readily determined from (4.11). Differentiating this equation, and taking the limit for $k^2\to 0$, one finds

$$P=-a_\alpha^{-2}r_\alpha^{-3}\int_0^\infty[u_{0\alpha}^{(\infty)}u_{2\alpha}^{(\infty)}-u_{0\alpha}u_{2\alpha}$$
$$-w_{0\alpha}w_{2\alpha}]dr. \quad (4.35)$$

Similar coefficients can be determined for $k\cot\delta_\beta$ and $\tan\epsilon$, by using (4.19) and (4.26), respectively, but we shall not consider them in this paper.

Operators and Observables in Isotopic Spin Space*

LESLIE L. FOLDY†
Case Institute of Technology, Cleveland, Ohio
(Received November 23, 1953)

The usefulness of the conventional isotopic spin formalism is somewhat marred by the fact that it contains superfluous formal elements which have no physical counterpart. It is demonstrated that application of the "superselection principle" for total electric charge, recently suggested by Wick, Wightman, and Wigner, is sufficient to eliminate these superfluous elements and thus reduce the content of the theory to that of the more conventional formalism in which neutrons and protons are distinguished *ab initio*. This superselection principle applied to the conventional state-function representation of quantum mechanics requires that admissable state functions be eigenfunctions of the total charge and that operators representing observables commute with the total charge. The disjointness of the various subspaces in Hilbert space corresponding to different total charge eigenvalues, demanded by the superselection principle, leads to the result that many observables which are outwardly different in form are actually essentially equivalent. The construction of all inequivalent observables compounded from nucleonic isotopic spin operators only is carried out and it is shown that all such observables are simply functions of the square of the total isotopic spin and its z component. The essentially uniqueness of the charge parity operator introduced by Kroll and Foldy is established.

1. INTRODUCTION

THE isotopic spin formalism[1] has proved to be a very convenient means of dealing with the similarities in properties of the proton and neutron, and its employment has paid ample rewards as an aid in recognizing and formulating the consequences of these similarities for nuclear structure, nuclear interactions, and meson-nucleon interactions.[2–5] However, these advantages are partly cancelled by the fact that the isotopic spin formalism contains superfluous formal elements which have no known physical counterparts. These difficulties are best known in the following formulation: while the projection of a vector in isotopic spin space on the z axis has a definite physical interpretation in terms of the electric charge of the system being described, still the azimuth of the vector appears to have no such absolute significance and only relative azimuths of vectors having the same z component have at present a clearly identifiable physical meaning.

The program of the present paper consists in the separation of the physical from the nonphysical elements in the isotopic spin formalism by application of the recently suggested[6] "superselection principle" for electric charge. It is likely that many, if not all, of the specific results obtained here represent a transcription into isotopic spin notation of well-known results from the theory of symmetry groups. However, since the avowed purpose of the present paper is to learn how to work within the isotopic spin formalism itself, and since all of our results are obtained by the use of rather elementary operator algebra without direct resort to formal group-theoretical concepts, we feel that no apology is necessary in case of such duplication.

2. THE SUPERSELECTION PRINCIPLE FOR ELECTRIC CHARGE

One of the fundamental principles of quantum mechanics is the principle of superposition of states according to which the states of a system form a linear vector space. Thus if ψ and ϕ represent two possible states of a system then a linear combination of them,

$$\Psi = a\psi + b\phi,$$

where a and b are complex numbers, is also a possible state of the system. It is usually understood that two distinct state vectors represent two different physical states of the system except when one is a complex numerical multiple of the other, in which case they represent exactly the same state. Thus the linear vector space is to be interpreted as a "ray space" in which different rays are associated with physically distinct states. Hence a second linear combination of the states ψ and ϕ,

$$\Psi' = a'\psi + b'\phi,$$

will represent a different physical state than that represented by Ψ if, and only if, $(a'/b') \neq (a/b)$. The existence of an experiment which allows one to measure the *relative* phase of any two states of a physical system is therefore usually regarded as a necessary implication of the conventional formulation of quantum mechanics.

Recently, Wick, Wightman, and Wigner[6] have pointed out that there exist situations in which the above conditions are not satisfied. They have shown, in particular, that in a situation in which the system described has accessible to it both integral and half (odd) integral eigenvalues of the total angular momentum, to grant the possibility of measuring the relative phase of two states, one belonging to an

* Work supported by the U. S. Atomic Energy Commission.
† Present address: Institute for Theoretical Physics, Copenhagen, Denmark.
[1] B. Cassen and E. U. Condon, Phys. Rev. **50**, 846 (1936).
[2] E. P. Wigner, Phys. Rev. **51**, 106 (1937).
[3] K. M. Watson, Phys. Rev. **85**, 852 (1952).
[4] R. K. Adair, Phys. Rev. **87**, 1044 (1952).
[5] N. M. Kroll and L. L. Foldy, Phys. Rev. **88**, 1177 (1952).
[6] Wick, Wightman, and Wigner, Phys. Rev. **88**, 101 (1952).

integral, the other to a half-integral, value for the total angular momentum, would be tantamount to a violation of covariance with respect to Lorentz transformations. They also suggest that a similar situation may arise with respect to systems which have accessible to them different eigenvalues of the total electric charge (or different numbers of "heavy particles"), in that it may be impossible to measure the relative phase of states belonging to different eigenvalues of these quantities. Thus, within the usual framework of quantum electrodynamics, this inability to measure the relative phase of states of different total charge follows directly from gauge invariance considerations. For by a gauge transformation of a particularly simple character (constant gauge function) which reflects no physical change in a system but only a change in its *description* the relative phase of two states of different total charge may be changed arbitrarily.

To describe the situation arising when for some reason it is impossible to measure the relative phase of certain states of a system these authors have coined the phrase: a "superselection principle" operates with respect to the quantity whose eigenvalues distinguish the states whose relative phase cannot be measured. To understand clearly the nature of a superselection principle it is imperative to distinguish between it and a universal conservation law. A conservation law, such as that for total momentum, total angular momentum, electric charge, space parity, energy, etc., is a condition which is satisfied by the Hamiltonian of the system being described. It does not of itself inhibit the measurement of relative phases; in fact, the measurement of such relative phases of states belonging to different eigenvalues of conserved quantities is a regular concomitant of many physical measurements. For example, the measurement of an angular distribution in a scattering experiment determines the relative phases of states of different angular momentum. But a superselection principle is more than a condition satisfied by the Hamiltonian describing a system; it denies the existence of apparatus which is capable of performing certain types of measurements on the system. Some understanding of how such limitations on the intrinsic capacity of available measuring apparatus may arise in a natural way has been obtained by Wigner in a recent investigation.[7]

The existence of a superselection principle for the total electric charge of a system (which is the only superselection principle with which we shall be concerned in this paper) has a profound influence on the quantum-mechanical interpretation of a system which is being described by means of the isotopic spin representation. The object of the isotopic spin representation is to encompass the dynamical behavior of systems of different particles in a single dynamical scheme by treating the different particles as different states of the same particle. Such a general scheme has decided advantages in at least two cases (which often occur together). The first occurs when the different particles, though distinguishable, possess certain similarities which it is of interest to exploit in the development of the theory, while the second occurs when actual transformations of a particle from one type to another is a natural part of the dynamical development of the system. Since in the principal applications of this formalism the different particles which are identified as different states of the same particle possess different electric charges, the abstract composite system with which one then deals has accessible to it states of different total electric charge; hence the superselection principle for electric charge immediately comes into play.

To prevent our considerations from becoming too abstract we shall limit ourselves now to the only case which we shall discuss in detail in the later parts of this paper, namely that in which we have a system of nucleons only, described in an isotopic spin formalism with neutron and proton regarded as two states of a nucleon. We consider first the case of a single nucleon, and in the familiar manner, represent the proton state of the nucleon by the function α and the neutron state by the function β. A state function representing a proton in a space-spin state $\phi(r,\sigma)$ would then be written $\phi\alpha$, while the state function representing a neutron in the same space-spin state would be written $\phi\beta$. The superposition principle would then suggest that $\phi(\alpha+\beta)$ is also a possible state function for the system. However, since the states $\phi\alpha$ and $\phi\beta$ are states of different total charge, their relative phase cannot be discerned by an experiment and hence the state $\phi(\alpha+\beta)$ would be indiscernable from the state $\phi(\alpha-\beta)$. In fact each of these would now be interpretable only as a statistical mixture (in contrast to a pure state) with equal probabilities of the system consisting of a proton or a neutron in the space-spin state ϕ. That one can hardly treat such state functions in the familiar manner in which one usually operates in quantum mechanics is made trivially, but strikingly, evident if one applies the usual rule for obtaining the probability than an observation will reveal that the system is in the state $\phi(\alpha-\beta)$ when it has been projected into the state $\phi(\alpha+\beta)$ by a previous preparation. In the customary procedure one forms the inner product of the two state functions (after they have been normalized) and identifies its absolute square with the desired probability. In this case such an inner product has the value zero; this in spite of the fact that the two states described by these functions are *observationally indistinguishable.*

In view of these difficulties it would seem appropriate to avoid the state function representation of the state of a physical system altogether and pass over to the statistical matrix representation which can cope with equanimity with both pure states and statistical

[7] E. P. Wigner, Z. Physik 133, 101 (1952).

mixtures.[6] However, if one desires to remain on the more familiar quantum-mechanical ground of state function representations, it is obvious that one must modify the rules of the quantum-mechanical game. The simplest such change, and one which is tacitly observed when one works in situations where superselection principles operate, consists in limiting considerations to state functions which are eigenstates of the quantity with respect to which the superselection principle operates—in our particular case, the total electric charge. While state functions which have not this character might still be given interpretations as representing statistical mixtures, one nevertheless simply ignores them and omits them from the theory.

Now the simple change suggested above has some consequences for the theory which are not trivially evident. These arise with respect to the role played by Hermitian operators as representatives of observables in the theory. It is immediately evident that if a superselection principle operates with respect to a quantity Q, then no operator which has matrix elements connecting states belonging to different eigenvalues of Q can represent an observable; otherwise the measurement of such an observable would be tantamount to an observation of the relative phase of the two states, in contradiction to the superselection principle. Hence, in general, only Hermitian operators which commute with Q, the total charge in our case, represent observables, and, in the absence of any other superselection principle, we assume that every Hermitian operator which does commute with Q does indeed represent an observable. In actuality, however, in working in an isotopic spin representation another principle closely akin to a superselection principle does intervene. For if one is working in such a representation it is essential that the antisymmetrization (Pauli) principle be observed if one is working with a system of particles satisfying Fermi-Dirac statistics or that the symmmetrization principle be observed in the case of Bose-Einstein statistics if one is to obtain only the manifold of state functions which one finds by observation. This then means that, provided no further superselection principle intervenes, only *symmetric* Hermitian operators which commute with Q will represent observables and conversely.

Now the observation which is not so trivially evident is that within these restrictions many operators which satisfy the above criteria and which are outwardly quite different in form actually represent essentially the same observable. To economize in our language concerning this point let us regard the function space for the system under consideration as decomposed into the various subspaces each associated with a given eigenvalue of Q, or in view of our later considerations, a given eigenvalue of the z component of isotopic spin T_z which is linearly related to the total charge Q. Then the admissible state functions lie entirely in one or another of these subspaces T_z. Let $\mathcal{O}$ be a symmetric Hermitian operator which commutes with T_z and consequently represents an observable. Then the operator $\mathcal{O}f(T_z)=f(T_z)\mathcal{O}$ where $f(T_z)$ is any real function of its argument, is also an observable which is essentially equivalent to $\mathcal{O}$ in the following sense. In each subspace T_z, $\mathcal{O}f(T_z)$ is simply a numerical multiple of $\mathcal{O}$ itself, though it will in general be a different numerical multiple in each different subspace. Since one admits state functions lying entirely in one of these subspaces only, nothing is essentially gained by discriminating between these operators, and it becomes of some importance to recognize whether two outwardly different operators represent equivalent observables.

Actually our restriction that in order for an operator to represent an observable it must commute with T_z and hence leave all the subspaces T_z invariant is more stringent than is necessary. It is certainly necessary if the operator is to represent an observable in all subspaces T_z. Such observables we shall call complete observables. On the other hand there may exist operators which leave one or more, but not all, subspaces T_z invariant and these will represent perfectly good observables in these particular subspaces. Such observables we shall call incomplete observables; an example is provided by the charge-parity operator.[5] Actually the distinction between complete and incomplete observables is largely a matter of convenience, since to every incomplete observable we can always find an equivalent complete observable which vanishes in all subspaces which the original does not leave invariant. One has simply to postmultiply such an incomplete observable by a polynomial in T_z which vanishes in every such noninvariant subspace.

Before proceeding further we make some remarks concerning our notation. We employ the conventional Pauli matrices to represent the three components τ_x^n, τ_y^n, τ_z^n of the isotopic spin vector of the nth nucleon, and in addition we shall sometimes use the notation τ_0^n for the unit isotopic spin matrix. The total isotopic spin vector $\mathbf{T}$ is defined by

$$\mathbf{T}=\tfrac{1}{2}\sum_n \boldsymbol{\tau}^n,$$

and its components are designated by T_x, T_y, and T_z. In addition we shall write

$$\tau_\pm^n=\tfrac{1}{2}(\tau_x^n\pm i\tau_y^n), \quad T_\pm=T_x\pm iT_y.$$

While our earlier remarks are applicable to systems composed of both nucleons and mesons, or perhaps even more general systems, our further considerations will be limited to nuclear systems composed of a number A of nucleons.

3. INEQUIVALENT OBSERVABLES

We shall first determine all of the *linearly independent* observables formed from the isotopic spin operators only. To do this we note that the most general operator formed from isotopic spin operators will be a linear

combination of terms, each of which consists of A (the total number of nucleons in the system) factors chosen from the τ_0^n, τ_+^n, τ_-^n, τ_z^n with one and only one τ for each nucleon. All such terms are clearly linearly independent and their total number is 4^A. The linearly independent observables must then be *symmetric* functions formed from these by linear combination. Each such linearly independent symmetric function can clearly be designated by giving only the total number of τ_0's, τ_+'s, τ_-'s, and τ_z's occurring in each term of the sum; that is, by a *partition* $n_0+n_++n_-+n_z=A$. We denote each such symmetrical operator (with unit coefficient for each term) by the symbol (n_0,n_+,n_-,n_z).

However, not all of these symmetrical operators will be observables since they do not all commute with T_z. In view of the discussion in the last section we may limit our attention to complete observables. A simple calculation gives us for the commutator of any of these operators with T_z:

$$[(n_0,n_+,n_-,n_z),\ T_z]=(n_--n_+)(n_0,n_+,n_-,n_z),$$

whence it immediately follows that to obtain complete observables which do not vanish in *every* subspace T_z we must include in our basic linearly independent set only those (n_0,n_+,n_-,n_z) for which $n_+=n_-=N\leqslant A/2$. Hence we may now designate our basic set by (n_0,N,n_z), each associated with a partition $n_0+2N+n_z=A$.

Now, while each of the operators of our basic set are observable, many of these will be equivalent in the sense of the discussion in the preceding section. To select a basic set of observables which are inequivalent we note that

$$(n_0,N,n_z)T_z=\tfrac{1}{2}n_0(n_0-1,N,n_z+1)+\tfrac{1}{2}n_z(n_0+1,N,n_z-1).$$

Therefore $(n_0-1,N,1)$ is equivalent to $(n_0,N,0)$ except possibly in the subspace $T_z=0$ where the first vanishes while the second may not. Repeated application of the above recursion relation allows us to express (n_0,N,n_z) as $(n_0+n_z,N,0)$ multiplied by a function of T_z. Examination of these results shows that we will lose no non-vanishing observables in any subspace if we choose as a basic set of inequivalent observables the operators $(n_0,N,0)$ with n_0 running through all integral values from 0 to A. In other words, any observable in any particular subspace T_z can be written as a linear combination of the $(n_0,N,0)$ with fixed coefficients, or any complete observable can be written as a linear combination of the $(n_0,N,0)$ in all subspaces with coefficients which are functions (polynomials) in T_z. We may now designate our basic set of linearly independent inequivalent observables simply by $[N]$, where N designates the number of τ_+'s and τ_-'s occurring as factors in each term. The total number of observables $[N]$ will be $(A+1)/2$ or $(A+2)/2$ according as A is odd or even ($[0]$ is included in this count).

While we have determined the linearly independent, inequivalent observables, it does not follow that they are completely independent. Actually they are not, for we shall now show that all of them may be written as functions of T^2 and T_z from which it follows that any complete observable composed of isotopic spin operators only can be expressed as functions of T^2 and T_z.

For the proof we shall require the following lemma: any polynomial in the operators T_+, T_-, and T_z in which each term is of equal degree in T_+ and T_- is a function of T^2 and T_z only. The proof is very elementary. We begin by noting that $T^2=\frac{1}{2}(T_+T_-+T_-T_+)+T_z^2$, whence, in view of the commutation relations satisfied by these operators, $T_+T_-=T^2-T_z^2+T_z$. Now in the given polynomial consider first the terms of highest degree, say s, in T_+ and T_-. By the use of the commutation relations rearrange each such term so that all of the T_z's stand to the right of all T_+'s and T_-'s. All terms resulting from this process will still be of degree s in T_+ and T_-. Now by further use of the commutation relations rearrange each such term so that it is of the form $T_+T_-T_+\cdots T_+T_-$ times a power of T_z standing to the right. In this process new terms will be generated which are of degree s-1, s-2,$\cdots$ in T_+ and T_-. The terms of degree s will now be functions of (T_+T_-) and T_z only, and consequently by our earlier result can be written as functions of T^2 and T_z only. One now carries out the same process on terms of degree s-1, s-2, etc., whereupon the lemma is established.

Finally, to prove our main theorem we note that $[N]$ can be written as the coefficient of p^Nq^N in the expansion of

$$S=\prod_{n=1}^{A}(1+p\tau_+^n+q\tau_-^n).$$

Letting

$$p=(x/y)^{\frac{1}{2}}\tanh(xy)^{\frac{1}{2}},\quad q=(y/x)^{\frac{1}{2}}\tanh(xy)^{\frac{1}{2}},$$

we may rewrite S as follows:

$$S=[\cosh(xy)^{\frac{1}{2}}]^{-A}\prod_{n=1}^{A}\left[\cosh(xy)^{\frac{1}{2}}+(x\tau_+^n+y\tau_-^n)\frac{\sinh(xy)^{\frac{1}{2}}}{(xy)^{\frac{1}{2}}}\right]$$

$$=[\cosh(xy)^{\frac{1}{2}}]^{-A}\prod_{n=1}^{A}\exp(x\tau_+^n+y\tau_-^n)$$

$$=[\cosh(xy)^{\frac{1}{2}}]^{-A}\exp[2(xT_+^n+yT_-^n)].$$

Note that xy is a function of pq only, and that x and y are equal to p and q, respectively, divided by a function of pq. Then it follows that the expansion of S in powers of p and q will have for the coefficient of p^Nq^N a polynomial formed from the sum of terms in each of which the degrees of T_+ and T_- are equal. The theorem then follows from our lemma.

4. UNIQUENESS OF THE CHARGE PARITY OPERATOR

As an example of the preceding ideas, we shall consider the question[8] of the uniqueness of the charge parity operator[5] introduced by Kroll and Foldy as a formal means of expressing the consequences of charge symmetry for nuclear structure and nuclear reactions. Formally this operator is defined to be one which for a particular nuclear system changes all neutrons to protons and all protons to neutrons. The above authors elected to write this operator as

$$P_x=\prod_{n=1}^{A}(i\tau_x^n)=\exp(i\pi T_x),$$

in which case it may be interpreted as the operator which performs a rotation of 180° about the x axis in isotopic spin space. It is clearly an observable only in the subspace $T_z=0$, and is therefore an incomplete observable. Applied to a state function of a nucleus in a state of nonvanishing T_z it generates a state function representing the corresponding state of the mirror nucleus.

Now it is readily observed that there exist many operators which perform the same function of changing all protons to neutrons and all neutrons to protons. In fact any product of A factors chosen from the τ_x^n and τ_y^n with one and only one τ referring to each nucleon will accomplish this result, as will any linear combination of such products. Since there are 2^A such operators which are linearly independent it is not at all clear that the charge parity operator is a unique quantity, and questions may be raised as to whether a unique charge parity assignment can be made for states of a self-conjugate nucleus when charge symmetry obtains.

In the present section we shall show that no real ambiguity exists and that the charge parity operator is essentially unique. We note first that all of the 2^A operators formed as above are not observables since they are not symmetric. However, by forming linear combinations one can obtain $A+1$ linearly independent symmetric operators each of which may be specified by the number n_z of τ_z's and the number $A-n_z$ of τ_y's contained in each term of the symmetric sum. We shall now show that all of these symmetric operators are equivalent in the sense defined earlier. Thus, take any of these symmetric operators and replace in each term each of the τ_y's contained in it by its equivalent $-i\tau_x\tau_z$. This symmetric operator then takes the form of the operator P_x above multiplied by a symmetric function of the τ_z's. To complete our proof we show that every symmetric function of the τ_z's is a function simply of T_z. To accomplish this we note that the linearly independent symmetric functions of the τ_z's can be obtained as the coefficients of x^s in the expansion of

$$Q=\prod_{n=1}^{A}(1+ix\tau_z^n).$$

However, the following manipulations indicate that this generating function is a function of T_z only:

$$Q=(1+x^2)^{A/2}\prod_{n=1}^{A}(\cos\theta+i\tau_z^n\sin\theta)$$

$$=(1+x^2)^{A/2}\prod_{n=1}^{A}\exp(i\theta\tau_z^n)$$

$$=(1+x^2)^{A/2}\exp(i\theta T_z),$$

where $\sin\theta=x/(1+x^2)^{\frac{1}{2}}$. Our result then follows.

Thus all of the $A+1$ symmetric operators are simply multiples of the Kroll-Foldy parity operator[9] in the subspace $T_z=0$. The argument further demonstrates the essential uniqueness of the operator which transforms any nucleus into its mirror nucleus, apart from an irrelevant (because of the superselection principle for total charge) phase factor. This last fact is useful in establishing relationships between matrix elements referring to pairs of mirror nuclei.

We may note also that the charge parity operator may be converted into a complete observable by multiplying it by the factor:

$$(T_z^2-1)(T_z^2-4)(T_z^2-9)\cdots(T_z^2-A^2).$$

Our results obtained in Sec. 5 also tell us that this complete observable (which now vanishes in every subspace except $T_z=0$) should be a function of T^2 only. That this is the case was noted in reference 5 where it was shown that in the subspace $T_z=0$, P_z has the eigenvalue $+1$ in a state in which $T^2=t(t+1)$ with t an even integer and the eigenvalue -1 in a state in which t is an odd integer.

5. CONCLUSION

We may summarize our results by the statement that the overgenerality of the usual isotopic spin formalism represents a purely formal difficulty which can easily be overcome without destroying the conveniences of the formalism. The apparently superfluous elements contained in the usual isotopic spin formalism may be

[8] The question of the uniqueness of the charge parity operator was raised with the author by Professor E. L. Hill.

[9] Of course the uniqueness of the charge parity operator is established here only to within a constant multiplying factor (of, say, P_z). If one further requires the operator to be unitary, that is that it preserve the normalization of the wave function, then the constant multiplying factor is restricted to modulus unity. If the operator is further restricted to be hermitian (in the subspace $T_z=0$) then the factor must be ±1. The choice between these two is a matter of convention. The important point is that the operator discriminate through its eigenvalues states of different parity. However, note that if the charge parity operator is defined as a rotation of 180° about an axis lying in the x-y plane in isotopic spin space, then there exists no ambiguity, even with respect to sign, to be resolved by convention.

eliminated by proper application of the superselection principle for electric charge and the recognition of the consequent existence of equivalent observables. Under these restrictions the isotopic spin formalism becomes equivalent to a conventional representation in which neutrons and protons are discriminated *ab initio*. It is conceivable that someday new phenomena may appear which will require the full potential content of the isotopic spin formalism for its description, but at present this does not appear likely.

Part of this work was performed while the author was a summer visitor at Brookhaven National Laboratory during the summer of 1953. The manuscript was completed at the Institute for Theoretical Physics, Copenhagen, Denmark, under a Fulbright Research Fellowship and a John Simon Guggenheim Memorial Fellowship. The hospitality offered to the author by these institutions is gratefully acknowledged. The author also wishes to acknowledge the benefits of discussion of some of these questions with Dr. N. M. Kroll and of correspondence with Professor E. L. Hill.

PHYSICAL REVIEW VOLUME 93, NUMBER 6 MARCH 15, 1954

Multipole Singularities of Classical Scalar and Pseudoscalar Meson Fields*

PETER HAVAS
Department of Physics, Lehigh University, Bethlehem, Pennsylvania
(Received October 13, 1953)

The general form of the equations of motion of a particle possessing multipole singularities of a neutral scalar or pseudoscalar meson field has been found by Harish-Chandra on the basis of Dirac's method. In this paper the general form of the multipole moment compatible with these equations is established under the assumption that the spin and the 2^n-pole moments of the particle are of constant magnitude and have only spatial components in the system in which the particle is at rest. Then the general form of the equations of motion and of the multipole moment compatible with them is established for point particles interacting with a charge-symmetric scalar or pseudoscalar meson field. It is found that 2^n-pole moments of different types are possible for arbitrary n, and that a particle can carry an arbitrary combination of such moments.

1. INTRODUCTION

SEVERAL methods have been suggested recently to avoid the infinities associated with point singularities in classical field theory. The method first used by Dirac[1] for the case of point charges interacting with an electromagnetic field was extended by Harish-Chandra[2] to fields of any integral spin. He succeeded in obtaining the general form of the equations of motion of point multipoles of such (neutral) fields and the explicit form of the equations for point charges and dipoles in fields of spin zero and one.

Although the general form of the equations of motion is thus known, this in itself does not mean that a self-consistent theory of arbitrary point singularities is possible. Except in the case of spin zero, the field equations impose certain restrictions on the charge density; furthermore the equations of motion interrelate the momentum, angular momentum, and charge density of the particle. In addition it appears to be desirable for the physical interpretation of the theory to impose further restrictions on the spin and the 2^n-pole moments of the particle. It is not inherent in the method that it should be possible to satisfy all these relations for any type of charge singularity.

Although many different types of "elementary" particles have been found in nature, it appears that present theories (quantum as well as classical) are far too wide in allowing an infinite variety of such particles. The present study was undertaken in the hope that it might be possible to exclude at least some types of particles by proving that they could not satisfy all the conditions required. In the case of the scalar and pseudoscalar meson fields it was found, on the contrary, that all the conditions can be fulfilled for multipole singularities of arbitrary order and also for arbitrary combinations of such poles by explicit construction of the most general form of such poles. The results obtained in the case of neutral fields are summarized in Theorems I–IV of Secs. III–VI. Then the theory is extended to charge-symmetric fields; the results are summarized in Theorem V of Sec. VII.

II. THE EQUATIONS OF MOTION IN NEUTRAL FIELDS

We shall first outline the field-theoretical derivation of the general form of the equations of motion of a point particle interacting with a neutral scalar or pseudoscalar meson field as given by Harish-Chandra.[2] Except for minor changes we shall use his notation.

We consider a four-space with coordinates x_μ, Greek letters taking the values 0, 1, 2, 3, where x_0 is the time coordinate. Repetition of an index implies summation

* Assisted by the National Science Foundation.
[1] P. A. M. Dirac, Proc. Roy. Soc. (London) **A167**, 148 (1938).
[2] Harish-Chandra, Proc. Roy. Soc. (London) **A185**, 269 (1946).

over this range. The velocity of light is taken as unity. The metric tensor $g_{\mu\nu}$ is given by

$$g_{\mu\nu}=0 \text{ if } \mu\neq\nu, \quad g_{00}=-g_{11}=-g_{22}=-g_{33}=1. \quad (1)$$

The meson field is described by a scalar or pseudoscalar potential U which satisfies the equation

$$\partial^2U/\partial x_\mu\partial x^\mu+\chi^2U=4\pi\rho, \quad (2)$$

where χ is a reciprocal length (equal to $1/\hbar$ times the meson mass in the quantized theory). All the results of this paper also hold in the limit $\chi=0$. ρ is the mesonic charge density, which is taken to be of the form

$$\rho=\sum_n \partial_{\alpha\beta\cdots\nu}\mathfrak{S}^{\alpha\beta\cdots\nu}. \quad (3)$$

Here

$$\partial_{\alpha\beta\cdots\nu}\equiv\partial_\alpha\partial_\beta\cdots\partial_\nu\equiv\partial^n/\partial x^\alpha\partial x^\beta\cdots\partial x^\nu, \quad (4)$$

and the tensor of rank n $\mathfrak{S}^{\alpha\beta\cdots\nu}$ is the 2^n-pole density. It can clearly always be chosen to be completely symmetric. For a point particle we take

$$\mathfrak{S}^{\alpha\beta\cdots\nu}=\int_{-\infty}^{\infty}S^{\alpha\beta\cdots\nu}(\tau)\delta(x_0-z_0)\delta(x_1-z_1)\times\delta(x_2-z_2)\delta(x_3-z_3)d\tau, \quad (5)$$

where τ and $z_\mu(\tau)$ are the proper time and the coordinates of the particle and δ is Dirac's δ function. We call $S^{\alpha\beta\cdots\nu}$ the 2^n-pole moment.

Particular solutions of Eq. (2) are given by the retarded potential

$${}_{\text{ret}}U=\sum_n \partial_{\alpha\beta\cdots\nu}\left[\left(\frac{S^{\alpha\beta\cdots\nu}}{\kappa}\right)_{\tau_r}-\chi\int_{-\infty}^{\tau_r}S^{\alpha\beta\cdots\nu}\frac{J_1(\chi s)}{s}d\tau\right], \quad (6)$$

and the advanced potential

$${}_{\text{adv}}U=\sum_n \partial_{\alpha\beta\cdots\nu}\left[-\left(\frac{S^{\alpha\beta\cdots\nu}}{\kappa}\right)_{\tau_a}-\chi\int_{\tau_a}^{\infty}S^{\alpha\beta\cdots\nu}\frac{J_1(\chi s)}{s}d\tau\right]. \quad (7)$$

Here we have used the abbreviations

$$s_\mu=x_\mu-z_\mu, \quad s=(s_\mu s^\mu)^{\frac{1}{2}}, \quad \kappa=s_\mu v^\mu, \quad (8)$$

with

$$v_\mu=\dot{z}_\mu, \quad v_\mu v^\mu=1, \quad v_\mu\dot{v}^\mu=0, \quad (9)$$

where the dot indicates differentiation with respect to the proper time. τ_r and τ_a are the proper times of the "retarded" and "advanced" points, respectively, i.e., the points on the world line of the particle such that $s=0$ and $s_0>0$ and <0, respectively. J_1 is the Bessel function of order 1.

The energy-momentum tensor of the field is given by

$$4\pi T_{\mu\nu}=\partial_\mu U\partial_\nu U-\tfrac{1}{2}g_{\mu\nu}(\partial_\sigma U\partial^\sigma U-\chi^2U^2), \quad (10)$$

and the angular momentum tensor by

$$M_{\mu\nu\lambda}=x_\mu T_{\nu\lambda}-x_\nu T_{\mu\lambda}. \quad (11)$$

Here we have to insert the total potential, due both to the particle itself and to other sources. Following the method of Dirac[1] the world line of the particle is enclosed by a narrow tube, the radius of which will in the end be made to tend to zero. The equations of motion are then derived from the condition that the flow of energy, momentum and angular momentum out of a portion of the tube in the presence of an external field, as calculated by using Eqs. (10) and (11), shall only depend on the conditions at the ends of the tube, i.e., that the rates of flow shall be perfect differentials.

The equation of translational motion obtained is

$$\dot{A}_\mu=\sum_n(-1)^{n+1}S^{\alpha\beta\cdots\nu}\partial_{\alpha\beta\cdots\nu\mu}U', \quad (12)$$

and that of rotational motion is

$$\dot{B}_{\mu\rho}=\sum_n n(-1)^{n+1}(S_\mu{}^{\beta\cdots\nu}\partial_{\rho\beta\cdots\nu}U'-S_\rho{}^{\beta\cdots\nu}\partial_{\mu\beta\cdots\nu}U')-(v_\mu A_\rho-v_\rho A_\mu). \quad (13)$$

A_μ is the energy-momentum four-vector of the particle. $B_{\mu\rho}$ is an antisymmetric tensor which we, following Harish-Chandra, shall interpret as the particle's spin angular momentum. In analogy to the case of an extended body, whose spin has only three spatial components in the system in which the center of mass is at rest, we assume that

$$B_{\mu\rho}v^\rho=0. \quad (14)$$

We also postulate that the magnitude of the spin should be constant:

$$B_{\mu\rho}B^{\mu\rho}=\text{constant}, \quad B_{\mu\rho}\dot{B}^{\mu\rho}=0. \quad (15)$$

The value of U' in the equations of motion (12) and (13) depends on the assumptions made concerning the total potential. For the case that it is taken as the sum of the external potential ${}_{\text{ext}}U$ and of the retarded potential of the particle itself, it has been shown by Bhabha and Harish-Chandra[2] that

$$U'={}_{\text{ext}}U+\tfrac{1}{2}({}_{\text{ret}}U-{}_{\text{adv}}U)-\frac{\chi}{2}\sum_n\partial_{\alpha\beta\cdots\nu}\int_{-\infty}^{\infty}S^{\alpha\beta\cdots\nu}\frac{J_1(\chi s)}{s}d\tau. \quad (16)$$

We can also put the total potential equal to the external one plus half the sum of the retarded and advanced

[2] H. J. Bhabha and Harish-Chandra, Proc. Roy. Soc. (London) A185, 250 (1946). As discussed in reference 4, we identify the "ingoing field" of these authors and of Dirac (see reference 1) with the external field.

potentials of the particle. This differs from the previous assumption by $\frac{1}{2}({}_{\rm ret}U-{}_{\rm adv}U)$, an expression which has been shown to be finite on the world line together with all its derivatives.[3] Thus we obtain now

$$U'={}_{\rm ext}U-\frac{\chi}{2}\sum_n \partial_{\alpha\beta\cdots\nu}\int_{-\infty}^{\infty} S^{\alpha\beta\cdots\nu}\frac{J_1(\chi s)}{s}d\tau. \quad (17)$$

As discussed elsewhere,[4] self-action terms like those involving the integrals over the entire motion of the particle are not consistent with the point of view of an action-at-a-distance theory. In such a theory we have to omit these terms and thus have

$$U'={}_{\rm ext}U, \quad (18)$$

where the external potential is equal to half the sum of the retarded plus advanced potentials of all other particles. All the potentials appearing in the equations of motion have to be evaluated at the position of the particle under consideration.

All the considerations of this paper are independent of the form of U'; our results hold for a field theory with retarded or time-symmetric interactions as well as for a theory of action at a distance. To simplify the notation we shall hereafter write U for the different forms of U'. In the mathematical arguments to be presented U is treated as an arbitrary function of the x_μ.

It is physically reasonable to require that the magnitude of each 2^n-pole moment should be constant:

$$S^{\alpha\beta\cdots\nu}S_{\alpha\beta\cdots\nu}=\text{constant}, \quad S^{\alpha\beta\cdots\nu}\dot{S}_{\alpha\beta\cdots\nu}=0. \quad (19)$$

Furthermore we can impose the constraint

$$v_\alpha S^{\alpha\beta\cdots\nu}=0; \quad (20)$$

the following proof of this is analogous to the one presented by Harish-Chandra[2] for the case of a dipole.

We write the part of the 2^n-pole moment not satisfying condition (20) as

$$v^\alpha T^{\beta\cdots\nu}(\tau). \quad (21)$$

The retarded potential due to this part equals

$${}_{\rm ret}U=\partial_{\alpha\beta\cdots\nu}\left[\left(\frac{v^\alpha T^{\beta\cdots\nu}}{\kappa}\right)_{\tau_r} -\chi\int_{-\infty}^{\tau_r} v^\alpha T^{\beta\cdots\nu}\frac{J_1(\chi s)}{s}d\tau\right], \quad (22)$$

from Eq. (6). In carrying out the differentiations it has to be kept in mind that the retarded time τ_r also depends on x_μ. We have [see reference 3, Eq. (31)]

$$\partial_\mu\tau_r=(s_\mu/\kappa)_{\tau_r}. \quad (23)$$

[4] P. Havas, Phys. Rev. 87, 309 (1952); a paper extending the results of this work to spinning particles will be published shortly.

Therefore we obtain, using (9),

$${}_{\rm ret}U=\partial_{\beta\cdots\nu}\left[\frac{v^\alpha\dot{T}^{\beta\cdots\nu}s_\alpha+\dot{v}^\alpha T^{\beta\cdots\nu}s_\alpha}{\kappa^2}-\frac{v^\alpha T^{\beta\cdots\nu}s_\alpha}{\kappa^3}\right.$$
$$\times\left(-1+s_\mu\dot{v}^\mu\right)-\frac{T^{\beta\cdots\nu}}{\kappa^2}-\chi v^\alpha T^{\beta\cdots\nu}\frac{J_1(\chi s)}{s}\frac{s_\alpha}{\kappa}$$
$$\left.-\chi\int_{-\infty}^{\tau_r} v^\alpha T^{\beta\cdots\nu}\partial_\alpha\frac{J_1(\chi s)}{s}d\tau\right]. \quad (24)$$

Using

$$v^\alpha\partial_\alpha\frac{J_1(\chi s)}{s}=-\frac{d}{d\tau}\frac{J_1(\chi s)}{s},$$

we can carry out an integration by parts. Remembering definition (8), we obtain, after simplification,

$${}_{\rm ret}U=\partial_{\beta\cdots\nu}\left[\left(\frac{\dot{T}^{\beta\cdots\nu}}{\kappa}\right)_{\tau_r}-\chi\int_{-\infty}^{\tau_r}\dot{T}^{\beta\cdots\nu}\frac{J_1(\chi s)}{s}d\tau\right]. \quad (25)$$

This is of the form (6) of a retarded potential for a 2^{n-1}-pole of moment $\dot{T}^{\beta\cdots\nu}$. Similarly the advanced potential of the 2^n-pole (21) is reducible to that of the 2^{n-1}-pole $\dot{T}^{\beta\cdots\nu}$. Therefore regardless of our assumptions on the potential of the particle, the part of the 2^n-pole moment not satisfying condition (20) acts like a 2^{n-1}-pole and thus can be included in the 2^{n-1}-pole moment of the particle; any pure 2^n-pole has to obey (20).

According to our interpretation, the spin $B_{\mu\rho}$ and the multipole moments $S^{\alpha\beta\cdots\nu}$ are intrinsic properties of the particle; the energy-momentum vector A_μ on the other hand is only required to be a function of τ alone and thus can depend on it not only through properties of the particle, but also through the values of the potential U and its derivatives at the position of the singularity. All of these quantities are interrelated through the equations of motion (12) and (13), and further restricted by Eqs. (14), (15), (19), and (20). As noted before, it is not inherent in Dirac's method that it is possible to satisfy all of these requirements for multipoles of any order.

In the following three sections it is shown that this is indeed possible for three special forms of the 2^n-pole moment of a particle possessing only a moment of a single, but arbitrary, order. Using the methods developed in these sections, the most general form of the multipole moment compatible with all the requirements of the theory is presented in Sec. VI.

III. AXIAL 2^n-POLES

In this section we establish

Theorem I: Let a point particle be characterized by two four-vectors z_μ and A_μ, an antisymmetric tensor $B_{\mu\rho}$ and a symmetric tensor of rank n $S^{\alpha\beta\cdots\nu}$, which are functions of the proper time τ and are

subject to the constraints

$$B_{\mu\rho}v^\rho=0, \quad v_\mu v^\mu=1, \tag{A}$$

where $v_\mu\equiv\dot{z}_\mu$, and to the equations of motion

$$\dot{B}_{\mu\rho}=n(-1)^{n+1}(S_\mu{}^{\beta\cdots\nu}\partial_{\rho\beta\ldots\nu}U-S_\rho{}^{\beta\cdots\nu}\partial_{\mu\beta\ldots\nu}U) -(v_\mu A_\rho-v_\rho A_\mu), \tag{B}$$

and

$$A_\mu=(-1)^{n+1}S^{\alpha\beta\cdots\nu}\partial_{\alpha\beta\ldots\nu\mu}U, \tag{C}$$

where U is an arbitrary function of x_μ whose derivatives are evaluated at $z_\mu(\tau)$. It is required that $S^{\alpha\beta\cdots\nu}$ be of such a form that the conditions

$$B^{\mu\rho}\dot{B}_{\mu\rho}=0, \tag{a}$$

$$v_\alpha S^{\alpha\beta\cdots\nu}=0, \tag{b}$$

$$S^{\alpha\beta\cdots\nu}\dot{S}_{\alpha\beta\ldots\nu}=0 \tag{c}$$

are valid and that A_μ becomes identically equal to a function of the other particle variables, of U and of their derivatives at $z_\mu(\tau)$ by virtue of Eqs. (A)–(C).

Then a possible form of the multipole moment $S^{\alpha\beta\cdots\nu}$ satisfying these requirements is given for any n by

$$S^{\alpha\beta\cdots\nu}=f_n\prod_{\sigma=\alpha\cdots\nu}S^\sigma, \quad S^\sigma=\epsilon^{\sigma\kappa\lambda\mu}B_{\kappa\lambda}v_\mu, \tag{I}$$

(to be called an axial 2^n-pole), where $\epsilon^{\sigma\kappa\lambda\mu}$ is a pseudotensor antisymmetric in each pair of indices, with $\epsilon^{0123}=1$, and f_n is an arbitrary constant. A_μ is then of the form

$$A_\mu=[m+(-1)^{n+1}S^{\alpha\beta\cdots\nu}\partial_{\alpha\beta\ldots\nu}U]v_\mu-B_{\mu\rho}\dot{v}^\rho -n(-1)^{n+1}S_\mu{}^{\beta\cdots\nu}\partial_{\beta\ldots\nu}U, \tag{α}$$

where m is an arbitrary constant.

We first list a number of relations, which we have to use frequently in our proofs, and which are either well known or easy to verify. We have

$$\epsilon_{\mu\nu\rho\sigma}\epsilon^{\mu\nu\alpha\beta}=-2(\delta_\rho{}^\alpha\delta_\sigma{}^\beta-\delta_\sigma{}^\alpha\delta_\rho{}^\beta), \tag{26}$$

and

$$\epsilon_{\mu\nu\rho\sigma}\epsilon^{\mu\alpha\beta\gamma}=-\sum\pm\delta_\nu{}^\alpha\delta_\rho{}^\beta\delta_\sigma{}^\gamma, \tag{27}$$

where $\delta_\beta{}^\alpha$ is the Kronecker δ, the summation extends over all permutations of α, β, and γ, and the positive or negative sign has to be taken for even or odd permutations, respectively. Furthermore

$$P^{\cdots\mu\nu\cdots}Q_{\ldots\mu\nu\ldots}=0 \tag{28}$$

for any two tensors of arbitrary ranks which are contracted in a pair of indices which is symmetric for one tensor and antisymmetric for the other. We also have

$$v^\alpha\partial_\alpha U=\dot{U}. \tag{29}$$

We choose a "standard rest system" such that in this system

$$v_1=v_2=v_3=0, \ v_0=1, \text{ all } B_{\mu\rho}=0 \text{ except } B_{12}=-B_{21}. \tag{30}$$

The possibility of choosing such an orientation of the coordinate axes is a consequence of the constraints (A). The name "axial 2^n-pole" has been chosen for a pole of type (I), because in the standard rest system only its 3-components do not vanish, and it can thus be regarded as the limit of a distribution of charge along the 3-axis.

In the rest system we have

$$\dot{v}_0=0, \quad \partial_0 U=\dot{U}. \tag{31}$$

Furthermore we have for any tensor

$$T_{\alpha\beta\ldots}=0 \text{ in all systems, if all its components vanish in the standard rest system.} \tag{32}$$

Therefore

$$S^\alpha B_{\alpha\beta}=0. \tag{33}$$

Furthermore, introducing

$$C_q{}^{\alpha\beta}\equiv B^{\alpha\lambda}B_\lambda{}^\kappa B_\kappa{}^\sigma\cdots B_\tau{}^\beta=(-1)^q C_q{}^{\beta\alpha}, \quad K\equiv\tfrac{1}{2}B_{\mu\nu}B^{\mu\nu}, \tag{34}$$

where q is the number of factors B and K is constant by (a), we get, using (32),

$$C_{2m+1}{}^{\alpha\beta}=K^m B^{\alpha\beta}, \quad C_{2m}{}^{\alpha\beta}=K^{m-1}B^{\alpha\lambda}B_\lambda{}^\beta, \quad C_{2m\,\alpha}{}^\alpha=2K^m. \tag{35}$$

We shall now verify conditions (a)–(c). Multiplying the rotational equation (B) by $B^{\mu\rho}$ we obtain, using (A),

$$B^{\mu\rho}\dot{B}_{\mu\rho}=-2n(-1)^{n+1}B^{\mu\rho}S_\rho{}^{\beta\cdots\nu}\partial_{\mu\beta\ldots\nu}U, \tag{36}$$

which vanishes by (33), proving condition (a). Condition (b) is satisfied from (28). To prove (c), it is sufficient to show that

$$S^\alpha\dot{S}_\alpha=\epsilon^{\alpha\kappa\lambda\mu}B_{\kappa\lambda}v_\mu\epsilon_{\alpha\rho\sigma\tau}(\dot{B}^{\rho\sigma}v^\tau+B^{\rho\sigma}\dot{v}^\tau)=0. \tag{37}$$

Now we have from (27)

$$\epsilon_{\alpha\rho\sigma\tau}\epsilon^{\alpha\kappa\lambda\mu}B_{\kappa\lambda}v_\mu=-2(B_{\rho\sigma}v_\tau+B_{\tau\rho}v_\sigma+B_{\sigma\tau}v_\rho), \tag{38}$$

and therefore we obtain, using (A),

$$S^\alpha\dot{S}_\alpha=-2[B_{\rho\sigma}\dot{B}^{\rho\sigma}+(B_{\tau\rho}v_\sigma+B_{\sigma\tau}v_\rho)B^{\rho\sigma}\dot{v}^\tau] =-2B_{\rho\sigma}\dot{B}^{\rho\sigma}, \tag{39}$$

which equals zero because of (a).

To derive (α), we put

$$A_\mu=\bar{A}_\mu+Mv_\mu, \text{ with } M=A_\mu v^\mu \text{ and } \bar{A}_\mu v^\mu=0. \tag{40}$$

Multiplying (B) by v^ρ and using (A), (b), and (29) we get

$$\bar{A}_\mu=-n(-1)^{n+1}S_\mu{}^{\beta\cdots\nu}\partial_{\beta\ldots\nu}\dot{U}-B_{\mu\rho}\dot{v}^\rho. \tag{41}$$

Thus, using (40) and (28), we obtain

$$\dot{A}_\mu v^\mu = -\bar{A}_\mu \dot{v}^\mu = n(-1)^{n+1}\dot{v}^\mu S_\mu{}^{\beta\cdots\nu}\partial_{\beta\ldots\nu}\dot{U}. \quad (42)$$

On the other hand we get from the translational equation (C), multiplying by v^μ, and using (29)

$$\dot{A}_\mu v^\mu = (-1)^{n+1}S^{\alpha\beta\cdots\nu}\partial_{\alpha\beta\ldots\nu}\dot{U}. \quad (43)$$

Subtracting (42) from (43) and using (40), (A), and (b) we get

$$\begin{aligned}\dot{M} &= (-1)^{n+1}(S^{\alpha\beta\cdots\nu}\partial_{\alpha\beta\ldots\nu}\dot{U} - n\dot{v}^\mu S_\mu{}^{\beta\cdots\nu}\partial_{\beta\ldots\nu}\dot{U}) \\ &= (-1)^{n+1}[(d/d\tau)(S^{\alpha\beta\cdots\nu}\partial_{\alpha\beta\ldots\nu}U) \\ &\quad - \dot{S}^{\alpha\beta\cdots\nu}\partial_{\alpha\beta\ldots\nu}U] + n(-1)^{n+1}v^\alpha \dot{S}_\alpha{}^{\beta\cdots\nu}\partial_{\beta\ldots\nu}\dot{U}. \quad (44)\end{aligned}$$

Now from (I) we have

$$\dot{S}^{\alpha\beta\cdots\nu}\partial_{\alpha\beta\ldots\nu}U = n\dot{S}^\alpha \prod_{\sigma=\beta\cdots\nu} S^\sigma \partial_{\alpha\beta\ldots\nu}U, \quad (45)$$

and also, using (b),

$$v^\alpha \dot{S}_\alpha{}^{\beta\cdots\nu} = v_\alpha \dot{S}^\alpha \prod_{\sigma=\beta\cdots\nu} S^\sigma. \quad (46)$$

Substituting these expressions in Eq. (44), we obtain

$$\begin{aligned}\dot{M} &= (-1)^{n+1}(d/d\tau)(S^{\alpha\beta\cdots\nu}\partial_{\alpha\beta\ldots\nu}U) \\ &\quad - n(-1)^{n+1}\epsilon^\alpha{}_{\lambda\mu}(\dot{B}^{\alpha\lambda}v^\mu + B^{\alpha\lambda}\dot{v}^\mu) \\ &\quad \times \prod_{\sigma=\beta\cdots\nu} S^\sigma(\partial_{\alpha\beta\ldots\nu}U - v_\alpha\partial_{\beta\ldots\nu}\dot{U}). \quad (47)\end{aligned}$$

The last term of this expression will now be shown to vanish. We have

$$\epsilon^\alpha{}_{\lambda\mu}B^{\alpha\lambda}\dot{v}^\mu(\partial_{\alpha\beta\ldots\nu}U - v_\alpha\partial_{\beta\ldots\nu}\dot{U}) \prod_{\sigma=\beta\cdots\nu} S^\sigma = 0 \quad (48)$$

from (31) and (32). Furthermore Eq. (B) becomes, on substitution of (41),

$$\begin{aligned}\dot{B}_{\mu\rho} &= n(-1)^{n+1}(S_\mu{}^{\beta\cdots\nu}\partial_{\rho\beta\ldots\nu}U - S_\rho{}^{\beta\cdots\nu}\partial_{\mu\beta\ldots\nu}U) \\ &\quad + n(-1)^{n+1}(v_\mu S_\rho{}^{\beta\cdots\nu}\partial_{\beta\ldots\nu}\dot{U} - v_\rho S_\mu{}^{\beta\cdots\nu}\partial_{\beta\ldots\nu}\dot{U}) \\ &\quad - (v_\mu\dot{v}^\sigma B_{\sigma\rho} - v_\rho\dot{v}^\sigma B_{\sigma\mu}). \quad (49)\end{aligned}$$

Substituting this expression after changing dummy indices and using (48) and (28), we get for the last term of (47)

$$\begin{aligned}&-n(-1)^{n+1}\epsilon^\alpha{}_{\lambda\mu}(\dot{B}^{\alpha\lambda}v^\mu + B^{\alpha\lambda}\dot{v}^\mu) \\ &\quad \times \prod_{\sigma=\beta\cdots\nu} S^\sigma(\partial_{\alpha\beta\ldots\nu}U - v_\alpha\partial_{\beta\ldots\nu}\dot{U}) \\ &= -2n^2\epsilon^\alpha{}_{\lambda\mu}v^\mu S^{\alpha\beta'\cdots\nu'}\partial^\lambda{}_{\beta'\ldots\nu'}U\partial_{\alpha\beta\ldots\nu}U \prod_{\sigma=\beta\cdots\nu} S^\sigma. \quad (50)\end{aligned}$$

Defining the differential operator D by

$$D = (S^\sigma\partial_\sigma)^{n-1}, \quad (51)$$

we can write the expression

$$-2n^2\epsilon^\alpha{}_{\lambda\mu}v^\mu\epsilon^{\kappa\rho\sigma\tau}B_{\rho\sigma}v_\tau(D\partial^\lambda U)(D\partial_\alpha U). \quad (52)$$

From (38) and (A) this is equal to

$$-4n^2B^{\alpha\lambda}(D\partial_\lambda U)(D\partial_\alpha U), \quad (53)$$

which equals zero from (28). Thus the last term of Eq. (47) vanishes.

This allows us to integrate Eq. (47) and we obtain

$$M = m + (-1)^{n+1}S^{\alpha\beta\cdots\nu}\partial_{\alpha\beta\ldots\nu}U, \quad (54)$$

where m is a constant of integration. Substituting this and Eq. (41) into (40), we obtain the required expression ($\mathfrak{a}$). This completes the proof of the theorem.

IV. PLANAR 2^n-POLES

Now we establish

Theorem II: A possible form of the multipole moment satisfying the requirements stated in Theorem I is given for even n by

$$S^{\alpha\beta\cdots\nu} = g_n \sum B^\alpha{}_\lambda B^{\lambda\beta}B^\gamma{}_\sigma B^{\sigma\delta}\cdots B^{\rho-1}{}_\tau B^{\tau\nu}, \quad (II)$$

(to be called a planar 2^n-pole), where the summation extends over all permutations of $\alpha, \beta\cdots\nu$, and g_n is an arbitrary constant. A_μ is then again of the form ($\mathfrak{a}$) of Theorem I.

The name "planar 2^n-pole" has been chosen for a pole of type (II), because in the standard rest system all of its 3-components vanish, and it can thus be regarded as the limit of a distribution of charge in the 1–2 plane. It is not necessary to include all permutations of $\alpha, \beta\cdots\nu$ to make form (II) symmetric in the indices; it is, however, more convenient for our proof to define $S^{\alpha\beta\cdots\nu}$ in this manner.

To verify condition (a) we can obtain Eq. (36) as before. This expression becomes, on substitution of (II),

$$-2n(-1)^{n+1}n!B^{\mu\rho}B_{\rho\lambda}B^{\lambda\beta}B^\gamma{}_\sigma B^{\sigma\delta}\cdots B^{\tau\nu}\partial_{\mu\beta\ldots\nu}U \quad (55)$$

and thus vanishes because of (28). Condition (b) is a direct consequence of the constraint (A). Condition (c) implies, because of the symmetry of $S^{\alpha\beta\cdots\nu}$,

$$\begin{aligned}&(\dot{B}_{\alpha\mu}B^\mu{}_\beta\cdots B^{\rho-1}{}_\tau B^{\tau\nu})(\sum B^\alpha{}_\lambda B^{\lambda\beta}\cdots B^{\rho-1}{}_\tau B^{\tau\nu}) \\ &\qquad \equiv \dot{B}_{\alpha\mu}T^{\mu\alpha} = 0. \quad (56)\end{aligned}$$

Here $T^{\mu\alpha}$ consists of a series of terms each containing $2n-1$ factors B grouped together in some manner and, by Eqs. (35), reducible to a constant times $B^{\mu\alpha}$; thus condition (c) holds because of condition (a), which has been proved above.

To derive ($\mathfrak{a}$), we can proceed up to Eq. (44) as for Theorem I. From (II) we have now

$$\dot{S}^{\alpha\beta\cdots\nu}\partial_{\alpha\beta\ldots\nu}U = n!ng_n\dot{B}^{\alpha\lambda}B_\lambda{}^\beta\cdots B^{\rho-1}{}_\tau B^{\tau\nu}\partial_{\alpha\beta\ldots\nu}U, \quad (57)$$

and, applying (A),

$$v^\alpha\dot{S}_\alpha{}^{\beta\cdots\nu}\partial_{\beta\ldots\nu}\dot{U} = n!g_n\dot{B}^{\alpha\lambda}B_\lambda{}^\beta\cdots B^{\rho-1}{}_\tau B^{\tau\nu}v_\alpha\partial_{\beta\ldots\nu}\dot{U}. \quad (58)$$

Substituting these expressions into Eq. (44) we get

$$\dot{M}=(-1)^{n+1}\frac{d}{d\tau}(S^{\alpha\beta\cdots\nu}\partial_{\alpha\beta\ldots\nu}U)-(-1)^{n+1}n!ng_n \times\dot{B}^{\alpha\lambda}B_{\lambda}{}^{\beta}\cdots B^{\nu-1}{}_{\tau}B^{\tau\nu}(\partial_{\alpha\beta\ldots\nu}U-v_{\alpha}\partial_{\beta\ldots\nu}\dot{U}). \quad (59)$$

The last term of this expression will be shown to vanish. From Eq. (49), which holds regardless of the form of $S^{\alpha\beta\cdots\nu}$, we obtain by multiplication with $B^{\lambda}{}_{\beta}$, using (A) and changing dummy indices,

$$\dot{B}_{\alpha\lambda}B^{\lambda}{}_{\beta}=n(-1)^{n+1}(S_{\alpha}{}^{\beta'\cdots\nu'}\partial_{\lambda\beta'\ldots\nu}U -S_{\lambda}{}^{\beta'\cdots\nu'}\partial_{\alpha\beta'\ldots\nu}U)B^{\lambda}{}_{\beta}+n(-1)^{n+1} \times v_{\sigma}S_{\lambda}{}^{\beta'\cdots\nu'}\partial_{\beta'\ldots\nu}UB^{\lambda}{}_{\beta}-v_{\alpha}\dot{v}^{\sigma}B_{\sigma\lambda}B^{\lambda}{}_{\beta}. \quad (60)$$

Therefore we have

$$\begin{aligned}&-(-1)^{n+1}(\partial_{\alpha\beta\ldots\nu}U-v_{\alpha}\partial_{\beta\ldots\nu}\dot{U})\dot{B}^{\alpha\lambda}B_{\lambda}{}^{\beta}\\ &=-n(\partial_{\alpha\beta\ldots\nu}U-v_{\alpha}\partial_{\beta\ldots\nu}\dot{U})(S^{\alpha\beta'\cdots\nu'}\partial^{\lambda}{}_{\beta'\ldots\nu}U\\ &\quad-S^{\lambda\beta'\cdots\nu'}\partial^{\alpha}{}_{\beta'\ldots\nu}U)B_{\lambda}{}^{\beta}\\ &\quad-n(\partial_{\alpha\beta\ldots\nu}U-v_{\alpha}\partial_{\beta\ldots\nu}\dot{U})v^{\alpha}S^{\lambda\beta'\cdots\nu'}\partial_{\beta'\ldots\nu}UB_{\lambda}{}^{\beta}\\ &\quad+(-1)^{n+1}(\partial_{\alpha\beta\ldots\nu}U-v_{\alpha}\partial_{\beta\ldots\nu}\dot{U})v^{\alpha}\dot{v}^{\sigma}B_{\sigma}{}^{\lambda}B_{\lambda}{}^{\beta}. \quad (61)\end{aligned}$$

But the last two terms vanish, as

$$(\partial_{\alpha\beta\ldots\nu}U-v_{\alpha}\partial_{\beta\ldots\nu}\dot{U})v^{\alpha}=v^{\alpha}\partial_{\alpha\beta\ldots\nu}U-\partial_{\beta\ldots\nu}\dot{U}=0 \quad (62)$$

from (29). Multiplying Eq. (61) by the remaining $(n-2)$ B's appearing in the last term of (59), and applying (b) and (29), we obtain

$$\begin{aligned}&-(-1)^{n+1}(\partial_{\alpha\beta\ldots\nu}U-v_{\alpha}\partial_{\beta\ldots\nu}\dot{U})\dot{B}^{\alpha\lambda}B_{\lambda}{}^{\beta}\cdots B^{\nu-1}{}_{\tau}B^{\tau\nu}\\ &=-n[\partial_{\alpha\beta\ldots\nu}US^{\alpha\beta'\cdots\nu'}\partial^{\lambda}{}_{\beta'\ldots\nu}U\\ &\quad-\partial_{\alpha\beta\ldots\nu}US^{\lambda\beta'\cdots\nu'}\partial^{\alpha}{}_{\beta'\ldots\nu}U\\ &\quad+\partial_{\beta\ldots\nu}\dot{U}S^{\lambda\beta'\cdots\nu'}\partial_{\beta'\ldots\nu}\dot{U}]B_{\lambda}{}^{\beta}\cdots B^{\nu-1}{}_{\tau}B^{\tau\nu}. \quad (63)\end{aligned}$$

After substitution of the form (II) for the multipole moments, this reduces to

$$\begin{aligned}&-n!ng_n[(D^*\partial_{\alpha\beta}U)B^{\alpha\mu}B_{\mu}{}^{\beta'}B^{\lambda\beta}(D^*\partial_{\lambda\beta'}U)\\ &+(D^*\partial_{\alpha\beta}U)B^{\beta}{}_{\lambda}B^{\lambda\mu}B_{\mu}{}^{\beta'}(D^*\partial^{\alpha}{}_{\beta'}U)\\ &\quad-(D^*\partial_{\beta}\dot{U})B^{\beta}{}_{\lambda}B^{\lambda\mu}B_{\mu}{}^{\beta'}(D^*\partial_{\beta'}\dot{U})], \quad (64)\end{aligned}$$

where the differential operator D^* is given by

$$D^*=B^{\tau}{}_{\sigma}B^{\sigma\delta}\cdots B^{\nu-1}{}_{\tau}B^{\tau\nu}\partial_{\gamma\delta\ldots\nu} \quad (65)$$

and the factor $n!$ results from the permutation of the indices in (II).

Each of the three terms of expression (64) vanishes separately because of (34) and (28) and thus the last term of Eq. (59) vanishes. But then we can integrate $\dot{M}$ and derive (α) as in Sec. III. This completes the proof of Theorem II.

V. GENERAL 2^n-POLES

Now we consider a more general form of 2^n-poles, of which the axial and planar 2^n-poles are special cases. The most general form of 2^n-poles is a linear combination of poles of the type considered in the following Theorem III; the possibility of such a combination will be proved in Theorem IV of Sec. VI, together with the possibility of combining poles of different orders. Thus we first establish

Theorem III: A possible form of the multipole moment satisfying the requirements stated in Theorem I is given for any n by

$$S_p{}^{\alpha\beta\cdots\nu}=g_{np}\sum B^{\alpha}{}_{\lambda}B^{\lambda\beta}B^{\gamma}{}_{\rho}B^{\rho\delta}\cdots B^{\nu-1}{}_{\psi}B^{\psi\nu}\prod_{\sigma=\nu+1,\ldots,\nu}S^{\sigma}, \quad (III)$$

where the summation extends over all permutations of $\alpha, \beta\cdots\nu$, the number of factors B is any even number $p\leqslant n$, and g_{np} is an arbitrary constant. A_n is then again of the form (α) of Theorem I.

Just as in form (II) of the multipole moment it is not necessary to include all permutations of $\alpha, \beta\cdots\nu$ to make form (III) symmetric in the indices; this is merely done for convenience. $S_0{}^{\alpha\beta\cdots\nu}$ and $S_n{}^{\alpha\beta\cdots\nu}$ are, respectively, the axial and planar 2^n-poles considered previously, with $g_{n0}=f_n/n!$ and $g_{nn}=g_n$.

To a considerable extent the subsequent proofs require only a simultaneous application of the arguments used in proving Theorems I and II. Thus we find on substitution of (III) into Eq. (36) that we obtain a number of terms, some of which vanish because of Eq. (33) (as for Theorem I) and the remaining ones because of (28) (as for Theorem II), which proves condition (a). Similarly we find on contracting (III) with v_{α} that each term of the resulting sum vanishes separately, either from (28) or from (A), which proves condition (b). Condition (c) requires

$$\{B^{\alpha}{}_{\lambda}B^{\lambda\beta}\cdots B^{\nu-1}{}_{\tau}B^{\tau\nu}\prod_{\sigma=\nu+1,\ldots,\nu}S^{\sigma}\}\frac{d}{d\tau}\{\sum B_{\alpha\rho}B^{\rho}{}_{\beta}\cdots B_{\nu-1}{}_{\rho}B^{\rho}{}_{\nu}\prod_{\sigma=\nu+1,\ldots,\nu}S_{\sigma}\}=0. \quad (66)$$

This expression consists of a number of terms, each of which contains a factor of the form (39), or one of the form (33) (or both), or one of the form (56). All of these factors vanish as before, and thus condition (c) holds.

To derive (α), we can again proceed up to Eq. (44) as for Theorem I. However, we have now by (III), changing dummy indices,

$$\dot{S}_p{}^{\alpha\beta\cdots\nu}\partial_{\alpha\beta\ldots\nu}U=n!g_{np}\{(n-p)B^{\nu+1}{}_{\lambda}B^{\lambda\beta}\cdots B^{\nu-1}{}_{\psi}B^{\psi\nu}\dot{S}^{\alpha}\prod_{\sigma=\nu+1,\ldots,\nu}S^{\sigma}+p\dot{B}^{\alpha}{}_{\lambda}B^{\lambda\beta}\cdots B^{\nu-1}{}_{\psi}B^{\psi\nu}\prod_{\sigma=\nu+1,\ldots,\nu}S^{\sigma}\}\partial_{\alpha\beta\ldots\nu}U, \quad (67)$$

and, applying (28) and (A),

$$nv_\alpha \dot{S}_p{}^{\alpha\beta\cdots\nu}\partial_\beta\ldots_\nu\dot{U}=n!g_{np}\{(n-p)v_\alpha\dot{S}^\alpha B^{\pi+1}{}_\lambda B^{\lambda\beta}\ldots B^{\pi-1}{}_\eta B^{\eta\pi}\prod_{\sigma=\pi+2,\ldots,\nu}S^\sigma$$
$$+pv_\alpha\dot{B}^\alpha{}_\lambda B^{\lambda\beta}\ldots B^{\pi-1}{}_\eta B^{\eta\pi}\prod_{\sigma=\pi+1,\ldots,\nu}S^\sigma\}\partial_\beta\ldots_\nu\dot{U}. \quad (68)$$

Substituting these expressions into Eq. (44) we obtain

$$\dot{M}=(-1)^{n+1}\frac{d}{d\tau}(S_p{}^{\alpha\beta\cdots\nu}\partial_{\alpha\beta}\ldots_\nu U)-(-1)^{n+1}n!pg_{np}\dot{B}^\alpha{}_\lambda B^{\alpha\lambda\beta}\ldots B^{\pi-1}{}_\eta B^{\eta\pi}\prod_{\sigma=\pi+1,\ldots,\nu}S^\sigma(\partial_{\alpha\beta}\ldots_\nu U-v_\alpha\partial_\beta\ldots_\nu\dot{U})$$
$$-(-1)^{n+1}n!(n-p)g_{np}B^{\pi+1}{}_\lambda B^{\lambda\beta}\ldots B^{\pi-1}{}_\eta B^{\eta\pi}\dot{S}^\alpha\prod_{\sigma=\pi+2,\ldots,\nu}S^\sigma(\partial_{\alpha\beta}\ldots_\nu U-v_\alpha\partial_\beta\ldots_\nu\dot{U}). \quad (69)$$

We shall now show that the sum of the last two terms vanishes. For the last term we can follow the procedure leading to Eq. (50); we find that it equals

$$-2n\,n!(n-p)g_{np}\epsilon^\alpha{}_{\lambda\mu}v^\mu S_p{}^{\kappa\beta'\cdots\nu'}\partial^\lambda{}_{\beta'\ldots\nu'}U\partial_{\alpha\beta}\ldots_\nu UB^{\pi+1}{}_\kappa B^{\kappa\beta}\ldots B^{\pi-1}{}_\eta B^{\eta\pi}\prod_{\sigma=\pi+2,\ldots,\nu}S^\sigma. \quad (70)$$

We now substitute (III) for $S_p{}^{\kappa\beta'\cdots\nu'}$. Those terms of the resulting expression which contain a factor S^κ reduce to the form (53) (except for a constant factor), but with the differential operator

$$D_{np}=(B^\alpha{}_\lambda B^{\lambda\beta}\ldots B^{\pi-1}{}_\eta B^{\eta\pi}\partial_{\alpha\beta}\ldots_\pi)(S^\rho\partial_\rho)^{n-p-1} \quad (71)$$

replacing the operator $D(\equiv D_{n0})$; thus they vanish by (28). The remaining $(n-1)!p$ terms add up to

$$-2(n!)^2p(n-p)g^2{}_{np}\epsilon^\alpha{}_{\lambda\mu}v^\mu B^\kappa{}_\rho B^{\rho\beta'}(D_{np}\partial_\alpha U)(D^*{}_{np}\partial^\lambda{}_{\beta'}U), \quad (72)$$

where the differential operator $D^*{}_{np}$ is given by

$$D^*{}_{np}=(B^\gamma{}_\tau B^{\tau\delta}\ldots B^{\pi-1}{}_\eta B^{\eta\pi}\partial_{\gamma\delta}\ldots_\pi)(S^\rho\partial_\rho)^{n-p}. \quad (73)$$

In the standard rest system the only nonvanishing terms of expression (72) are those with $\kappa=\beta'=1$ or 2 (but $\neq\alpha$), and α and $\lambda=1$, 2 or 3 (but $\alpha\neq\lambda\neq\kappa$). Among these, the terms with $\alpha=3$ add up to zero; those with $\alpha=1$ or 2 are left over.

For the next to last term of Eq. (69) we can follow the procedure leading to Eq. (63); we obtain now

$$-(-1)^{n+1}n!pg_{np}(\partial_{\alpha\beta}\ldots_\nu U-v_\alpha\partial_\beta\ldots_\nu\dot{U})\dot{B}^\alpha{}_\lambda B^{\lambda\beta}\ldots B^{\pi-1}{}_\eta B^{\eta\pi}\prod_{\sigma=\pi+1,\ldots,\nu}S^\sigma$$
$$=-n!npg_{np}[\partial_{\alpha\beta}\ldots_\nu US_p{}^{\alpha\beta'\cdots\nu'}\partial^\lambda{}_{\beta'\ldots\nu'}U-\partial_{\alpha\beta}\ldots_\nu US_p{}^{\lambda\beta'\cdots\nu'}\partial^\alpha{}_{\beta'\ldots\nu'}U$$
$$+\partial_\beta\ldots_\nu\dot{U}S_p{}^{\lambda\beta'\cdots\nu'}\partial_{\beta'\ldots\nu'}\dot{U}]B_\lambda{}^\beta\ldots B^{\pi-1}{}_\eta B^{\eta\pi}\prod_{\sigma=\pi+1,\ldots,\nu}S^\sigma, \quad (74)$$

where we have to substitute (III) for the multipole moments. The terms resulting from the substitution for $S_p{}^{\lambda\beta'\cdots\nu'}$ either contain a factor S^λ, and thus vanish by (33), or have a factor $B^\lambda{}_\tau$. Similarly the terms resulting from the substitution for $S_p{}^{\alpha\beta'\cdots\nu'}$ contain either a factor S^α or a factor $B^\alpha{}_\tau$. The terms involving $B^\lambda{}_\tau$ or $B^\alpha{}_\tau$ add up to $(n-1)!p^2$ times expression (64), with g_n and D^* replaced by their generalizations g_{np} and $D^*{}_{np}$. Thus they vanish by (28). The remaining $(n-1)!(n-p)$ terms, involving S^α, add up to

$$-(n-1)!(n-p)(n!np)g^2{}_{np}\partial_{\alpha\beta}\ldots_\nu UB^{\beta'}{}_\mu B^{\mu\gamma'}\ldots B^{\pi\pi'+1}S^\alpha\prod_{\sigma'=\pi'+2,\ldots,\nu'}S^{\sigma'}\partial^\lambda{}_{\beta'\ldots\nu'}UB_\lambda{}^\beta\ldots B^{\pi-1}{}_\eta B^{\eta\pi}\prod_{\sigma=\pi+1,\ldots,\nu}S^\sigma$$
$$=-(n!)^2p(n-p)g^2{}_{np}S^\alpha B_\lambda{}^\beta(D_{np}\partial^\lambda U)(D_{np}{}^*\partial_{\alpha\beta}U), \quad (75)$$

with the same differential operators as in expression (72). In the standard rest system the only nonvanishing terms of (75) are those with $\alpha=3$, and $\beta=1$, $\lambda=2$ or $\beta=2$, $\lambda=1$; but these just cancel the terms left over from expression (72). By (32), this completes the proof of the vanishing of the sum of the last two terms of Eq. (69); but then we can integrate $\dot{M}$ and derive the expression ($\mathfrak{A}$) for A_μ as in Sec. III. This completes the proof of Theorem III.

VI. COMBINATIONS OF MULTIPOLES

The most general form of the multipole moments of a point particle in a neutral scalar or pseudoscalar meson field is given in

Theorem IV: Let a point particle be characterized by the variables z_μ, A_μ, and $B_{\mu\rho}$ subject to the constraints (A) as in Theorem I, and by N symmetric tensors $S^{\alpha\beta\cdots\nu}(\tau)$ of ranks $n=0, 1, \cdots N-1$, subject to the equations of motion

$$\dot{B}_{\mu\rho}=\sum_n n(-1)^{n+1}(S_\mu{}^{\beta\cdots\nu}\partial_{\rho\beta\ldots\nu}U-S_\rho{}^{\beta\cdots\nu}\partial_{\mu\beta\ldots\nu}U) - (v_\mu A_\rho-v_\rho A_\mu), \quad (B')$$

and

$$\dot{A}_\mu=\sum_n(-1)^{n+1}S^{\alpha\beta\cdots\nu}\partial_{\alpha\beta\ldots\nu\mu}U, \quad (C')$$

with U as in Theorem I. It is required that the 2^n-pole moments $S^{\alpha\beta\cdots\nu}$ be of such a form that the condition on A_μ and the conditions (a)–(c) of Theorem I ((b) and (c) holding for each $S^{\alpha\beta\cdots\nu}$ separately) are a consequence of Eqs. (A), (B'), and (C').

Then the most general form of the 2^n-pole moments satisfying these requirements is given by

$$S^{\alpha\beta\cdots\nu}=\sum_p S_p{}^{\alpha\beta\cdots\nu}, \quad (IV)$$

where $S_p{}^{\alpha\beta\cdots\nu}$ is of the form (III) of Theorem III, for all n. Conditions (b) and (c) hold for each $S_p{}^{\alpha\beta\cdots\nu}$ separately. A_μ is of the form

$$A_\mu=[m+\sum_n(-1)^{n+1}S^{\alpha\beta\cdots\nu}\partial_{\alpha\beta\ldots\nu}U]v_\mu-B_{\mu\rho}v^\rho - \sum_n n(-1)^{n+1}S_\mu{}^{\beta\cdots\nu}\partial_{\beta\ldots\nu}\dot{U}, \quad (\alpha')$$

where m is an arbitrary constant.

Equations (B') and (C') differ from Eqs. (B) and (C) only by a summation over n in each term depending explicitly on n. Therefore we obtain now instead of Eqs. (36), (41)–(44), and (49) new expressions differing from the original ones only by having each term depending explicitly on n replaced by a summation over N such terms. We denote these new equations by the same number as the original ones, with a prime attached.

To prove condition (a), we have to consider Eq. (36') instead of Eq. (36). Apart from this the proof is identical with the corresponding proof for Theorem III, as is the proof of condition (b) holding for each $S_p{}^{\alpha\beta\cdots\nu}$ separately. To show that condition (c) holds for $S^{\alpha\beta\cdots\nu}$ as well as for each $S_p{}^{\alpha\beta\cdots\nu}$ separately, it is sufficient to show that

$$S_{p_1}{}^{\alpha\beta\cdots\nu}\dot{S}_{p_2\alpha\beta\cdots\nu}=0, \quad (76)$$

where p_1 and p_2 can take any of the values allowed for p. If $p_1\neq p_2$, each of the terms in Eq. (76) resulting from the substitution of the form (III) for the moments contains at least one factor of the form $S^\alpha B_{\alpha\lambda}$, which vanishes by (33). If $p_1=p_2$, expression (76) reduces to (66), which vanishes as before.

To derive expression (α'), we substitute Eqs. (67) and (68) into Eq. (44') and obtain

$$\dot{M}=\sum_{n_1,p_1}(-1)^{n_1+1}\frac{d}{d\tau}(S_{p_1}{}^{\alpha\beta\cdots\nu_1}\partial_{\alpha\beta\cdots\nu_1}U)$$
$$-\sum_{n_1,p_1}(-1)^{n_1+1}n_1!p_1g_{n_1p_1}\dot{B}^\alpha{}_\lambda B^{\lambda\beta}\cdots B^{\nu_1-1}{}_\nu B^{\nu\nu_1}\prod_{\sigma=\nu_1+1,\cdots\nu_1}S^\sigma(\partial_{\alpha\beta\cdots\nu_1}U-v_\alpha\partial_{\beta\cdots\nu_1}\dot{U})$$
$$-\sum_{n_1,p_1}(-1)^{n_1+1}n_1!(n_1-p_1)g_{n_1p_1}B^{\nu_1+1}{}_\lambda B^{\lambda\beta}\cdots B^{\nu_1-1}{}_\nu B^{\nu\nu_1}\dot{S}^\alpha\prod_{\sigma=\nu_1+2,\cdots\nu_1}S^\sigma(\partial_{\alpha\beta\cdots\nu_1}U-v_\alpha\partial_{\beta\cdots\nu_1}\dot{U}). \quad (77)$$

We shall again show that the sum of the last two terms vanishes. For the last term we can again follow the procedure leading to Eq. (50); we obtain now

$$\sum_{n_1,n_2,p_1,p_2}(-1)^{n_1+n_2+1}2n_2n_1!(n_1-p_1)g_{n_1p_1}\epsilon^\alpha{}_{\lambda\mu}v^\mu S_{p_2}{}^{\kappa\beta'\cdots\nu_2'}\partial^\lambda{}_{\beta'\cdots\nu_2'}U \times\partial_{\alpha\beta\cdots\nu_1}UB^{\nu_1+1}{}_\rho B^{\rho\beta}\cdots B^{\nu_1-1}{}_\nu B^{\nu\nu_1}\prod_{\sigma=\nu_1+2,\cdots\nu_1}S^\sigma. \quad (78)$$

We now substitute (III) for the moments $S_{p_2}{}^{\kappa\beta'\cdots\nu_2'}$. The resulting expression contains $(n_2-1)!(n_2-p_2)$ terms with a factor S^κ for each pair of values n_2, p_2. These terms add up to

$$\sum_{n_1,n_2,p_1,p_2}(-1)^{n_1+n_2+1}4n_1!n_2!(n_1-p_1)(n_2-p_2)g_{n_1p_1}g_{n_2p_2}B^\alpha{}_\lambda(D_{n_1p_1}\partial_\alpha U)(D_{n_2p_2}\partial^\lambda U), \quad (79)$$

and thus vanish by (28). The remaining terms add up to

$$\sum_{n_1,n_2,p_1,p_2}(-1)^{n_1+n_2+1}2n_1!n_2!p_2(n_1-p_1)g_{n_1p_1}g_{n_2p_2}\epsilon^\alpha{}_{\lambda\mu}v^\rho B^\kappa{}_\rho B^{\lambda\beta'}(D_{n_2p_2}\partial_\alpha U)(D^*{}_{n_1p_1}\partial^\lambda{}_{\beta'}U). \quad (80)$$

For the next to last term of Eq. (77) we obtain, by again following the procedure leading to Eq. (63),

$$-\sum_{n_1,p_1}(-1)^{n_1+1}n_1!p_1g_{n_1p_1}(\partial_{\alpha\beta\cdots\nu_1}U-v_\alpha\partial_{\beta\cdots\nu_1}\dot{U})\dot{B}^\alpha{}_\lambda B^{\lambda\beta}\cdots B^{\nu_1-1}{}_\nu B^{\nu\nu_1}\prod_{\sigma=\nu_1+1,\cdots\nu_1}S^\sigma$$
$$=\sum_{n_1,n_2,p_1,p_2}(-1)^{n_1+n_2+1}n_1!n_2p_1g_{n_1p_1}[\partial_{\alpha\beta\cdots\nu_1}US_{p_2}{}^{\alpha\beta'\cdots\nu_2'}\partial^\lambda{}_{\beta'\cdots\nu_2'}U-\partial_{\alpha\beta\cdots\nu_1}US_{p_2}{}^{\lambda\beta'\cdots\nu_2'}\partial^\alpha{}_{\beta'\cdots\nu_2'}U$$
$$+\partial_{\beta\cdots\nu_1}\dot{U}S_{p_2}{}^{\lambda\beta'\cdots\nu_2'}\partial_{\beta'\cdots\nu_2'}\dot{U}]B_\lambda{}^\beta\cdots B^{\nu_1-1}{}_\nu B^{\nu\nu_1}\prod_{\sigma=\nu_1+1,\cdots\nu_1}S^\sigma. \quad (81)$$

Those terms resulting from the substitution of (III) for $S_{p_2}{}^{\lambda\beta'\cdots\nu'}$ in this expression which contain a factor S^λ vanish as before. Those which contain a factor $B^\lambda{}_\tau$, together with those terms resulting from the substitution for $S_{p_2}{}^{\alpha\beta'\cdots\nu'}$ which contain a factor $B^\alpha{}_\tau$, add up to

$$\sum_{n_1,n_2,p_1,p_2}(-1)^{n_1+n_2+1}n_1!n_2!p_1p_2g_{n_1p_1}g_{n_2p_2}[(D^*{}_{n_1p_1}\partial_{\alpha\beta}U)B^{\alpha\mu}B_\mu{}^{\beta'}B^{\lambda\beta}(D^*{}_{n_2p_2}\partial_{\lambda\beta'}U)$$
$$+(D^*{}_{n_1p_1}\partial_{\alpha\beta}U)B^\beta{}_\lambda B^{\lambda\mu}B_\mu{}^{\beta'}(D^*{}_{n_2p_2}\partial^\alpha{}_{\beta'}U)-(D^*{}_{n_1p_1}\partial_\beta\dot{U})B^\beta{}_\lambda B^{\lambda\mu}B_\mu{}^{\beta'}(D^*{}_{n_2p_2}\partial_{\beta'}\dot{U})], \quad (82)$$

and thus again vanish by (28). The remaining terms resulting from the substitution for $S_{p_2}{}^{\alpha\beta'\cdots\nu'}$ contain a factor S^α. They add up to

$$\sum_{n_1,n_2,p_1,p_2}(-1)^{n_1+n_2+1}n_1!n_2!p_1(n_2-p_2)g_{n_1p_1}g_{n_2p_2}S^\alpha B_\lambda{}^\beta(D_{n_1p_1}\partial^\lambda U)(D^*{}_{n_2p_2}\partial_{\alpha\beta}U). \quad (83)$$

Because of the summation we can interchange n_1,p_1, and n_2,p_2 in this expression; then we add it to expression (80). In the resulting sum each part belonging to a set of values n_1,n_2,p_1,p_2 only differs by a factor from the sum of the expressions (72) and (75), which has been shown to be zero. Thus the sum of the last two terms of Eq. (77) vanishes; integrating $\dot{M}$ we obtain

$$M=m+\sum_n(-1)^{n+1}S^{\alpha\beta\cdots\nu}\partial_{\alpha\beta\ldots\nu}U, \quad (54')$$

where m is a constant of integration. Substituting this and Eq. (41′) into (40) we obtain the required expression (α′).

It remains to be shown that (IV) is indeed the most general form of the 2^n-pole moment satisfying the requirement of Theorem IV.

We first consider condition (b). $S^{\alpha\beta\cdots\nu}$ may consist of a series of terms; however, it follows from the considerations of Sec. II that each term must vanish separately on contraction of any index λ with v_λ, as any part of the 2^n-pole moment for which this does not hold is equivalent to a 2^{n-1}-pole moment.

Condition (a) requires, by (36), that

$$B^\mu{}_\alpha S^{\alpha\beta\cdots\nu}\partial_{\beta\ldots\nu\mu}U=0 \quad (84)$$

for arbitrary U. This expression may consist of several terms, some of which may vanish because the product of $B^\mu{}_\alpha$ and the corresponding term of $S^{\alpha\beta\cdots\nu}$ is itself zero (case 1), and others, by (28), because some terms in $B^\mu{}_\alpha S^{\alpha\beta\cdots\nu}$ may be antisymmetric in μ and another index, while $\partial_{\beta\ldots\nu\mu}U$ is symmetric in these indices (case 2). Because of the symmetry of $S^{\alpha\beta\cdots\nu}$ similar considerations apply for any other index λ contracted with $B^\mu{}_\lambda$; but as not every term in $S^{\alpha\beta\cdots\nu}$ has to be symmetric in the indices by itself, it may be that for a single term case 1 applies to some indices, and case 2 to the others. Because of the arbitrariness of U there are no other possibilities of satisfying Eq. (84).

In case 1 we consider the part of $S^{\alpha\beta\cdots\nu}$ which vanishes by contraction with either v_α or $B^\mu{}_\alpha$; it can be put equal to $\epsilon^{\alpha\lambda\rho}B_{\lambda\lambda}v_\rho T^{\beta\cdots\nu}(\tau)$ without loss of generality.

In case 2 we consider the part $P^{\alpha\beta}Q^{\gamma\cdots\nu}(\tau)$ of $S^{\alpha\beta\cdots\nu}$ which is symmetric in α and β, vanishes after contraction with v_α or v_β, and is antisymmetric in μ and α or β after contraction with $B^\mu{}_\beta$ or $B^\mu{}_\alpha$. Apart from additive terms of the form considered in case 1, $P^{\alpha\beta}$ must then be equal to a function of τ times $C_{2m}{}^{\alpha\beta}$ (in the notation of (34)); thus, by (35), the part of $S^{\alpha\beta\cdots\nu}$ under consideration must contain α and β in the combination $B^{\alpha\lambda}B_\lambda{}^\beta$.

This leaves (IV) as the most general form of the 2^n-pole moment, where, however, the g_{np} may still be functions of τ. Our previous consideration of condition (c) has shown the vanishing of all the terms of $S^{\alpha\beta\cdots\nu}\dot{S}_{\alpha\beta\ldots\nu}$ in which g_{np} is not differentiated. All the terms of this expression containing a factor $g_{np_1}\dot{g}_{np_2}$ (with $p_1\neq p_2$) also contain at least one factor $S^\alpha B_{\alpha\lambda}$ and thus vanish by (33). Therefore condition (c) reduces to

$$\sum_p\frac{\dot{g}_{np}}{g_{np}}S_p{}^{\alpha\beta\cdots\nu}S_{p\alpha\beta\ldots\nu}=0. \quad (85)$$

Furthermore, if the g_{np}'s are not constant, Eq. (77) will contain an additional term

$$-\sum_{n,p}(-1)^{n+1}\frac{\dot{g}_{np}}{g_{np}}S_p{}^{\alpha\beta\cdots\nu}\partial_{\alpha\beta\ldots\nu}U \quad (86)$$

on the right-hand side. $\dot{M}$ and thus $\dot{A}_\mu$ cannot be integrated unless this is a perfect differential. Because of the arbitrariness of U this requires that all the $\dot{g}_{np}$ are zero, instead of just their linear combinations (85). This completes the proof of Theorem IV.

VII. MULTIPOLE SINGULARITIES OF CHARGE-SYMMETRIC FIELDS

The charge-symmetric meson theory, which describes a combination of charged and neutral mesons, was developed originally in quantum theory by Kemmer[5] and by Møller and Rosenfeld.[6] A corresponding classical field theory was developed for point particles interacting through retarded vector meson fields by Le Couteur.[7] This theory was extended to scalar fields and to time-symmetric interactions in a recent paper,[8] which also contained an action-at-a-distance formulation of the theory. Only simple poles were considered in this paper; therefore we first have to find the general form of the

[5] N. Kemmer, Proc. Cambridge Phil. Soc. **34**, 354 (1938).
[6] C. Møller and L. Rosenfeld, Kgl. Danske Videnskab. Selskab, Mat.-fys. Medd. **17**, No. 8 (1940); **20**, No. 12 (1943).
[7] K. J. Le Couteur, Proc. Cambridge Phil. Soc. **45**, 429 (1949).
[8] P. Havas, Phys. Rev. **91**, 997 (1953).

equations of motion for multipoles of any order before we can apply the methods developed in the preceding sections to find the explicit expressions for the multipole moments.

The charge-symmetric meson theory treats all field quantities as three-component vectors in "charge space." We denote all such vectors by boldface letters. Two components of such field quantities describe the charged mesons, and the third component the neutral mesons. The neutral theory discussed in the preceding sections can be obtained from the charge-symmetric theory by setting the first two components of all field quantities equal to zero.

The scalar or pseudoscalar potential $\mathbf{U}$ satisfies the equation

$$\partial^2\mathbf{U}/\partial x_\mu\partial x^\mu+\chi^2\mathbf{U}=4\pi\varrho, \tag{87}$$

where the mesonic charge density is given by

$$\varrho=\sum_n \partial_{\alpha\beta\cdots\nu}\mathfrak{S}^{\alpha\beta\cdots\nu}, \tag{88}$$

with the multipole density

$$\mathfrak{S}^{\alpha\beta\cdots\nu}=\int_{-\infty}^{\infty}\mathbf{S}^{\alpha\beta\cdots\nu}(\tau)\delta(s_0)\delta(s_1)\delta(s_2)\delta(s_3)d\tau. \tag{89}$$

Particular solutions of Eq. (87) are given by the retarded and the advanced potential, which are the vector analogs of Eqs. (6) and (7), respectively. The energy-momentum tensor of the field is given by

$$4\pi T_{\mu\nu}=\partial_\mu\mathbf{U}\cdot\partial_\nu\mathbf{U}-\tfrac{1}{2}g_{\mu\nu}(\partial_\sigma\mathbf{U}\cdot\partial^\sigma\mathbf{U}-\chi^2\mathbf{U}^2), \tag{90}$$

where the dot denotes a scalar product in charge space; the angular momentum tensor is related to it by Eq. (11) as before. In addition we can define an electric charge-current density vector by

$$4\pi\mathbf{J}_\mu=e\mathbf{U}\wedge\partial_\mu\mathbf{U}, \tag{91}$$

where $\wedge$ denotes a vector product in charge space and e is an arbitrary constant.

The equations of motion are again obtained by an application of the method of Dirac[1] to the energy-momentum and angular momentum tensors. Because of the similarity of the tensors (10) and (90) only minor modifications of the calculations of Harish-Chandra for neutral fields[2] are necessary. The resultant translational and rotational equations of motion differ from Eqs. (12) and (13) of the neutral theory only in the replacement of each product of a multipole moment and a field quantity by the corresponding scalar product in charge space. A new equation is obtained, however, by applying Dirac's method to the electric charge-current density vector (91). By (87) we have

$$\partial^\mu\mathbf{J}_\mu=e\mathbf{U}\wedge\varrho, \tag{92}$$

from which it follows by a calculation similar to that leading to the equations of motion, that the requirement of conservation of electric charge implies

$$d\mathbf{Q}/d\tau=e\sum_n(-1)^{n+1}\partial_{\alpha\beta\ldots\nu}\mathbf{U}'\wedge\mathbf{S}^{\alpha\beta\cdots\nu}. \tag{93}$$

Here $\mathbf{Q}(\tau)$ is a vector whose third component is interpreted as the electric charge of the particle; its explicit form, just like that of the particle momentum A_μ, is restricted only by the requirement that all the equations of the theory ought to be compatible.

The potential $\mathbf{U}'$ appearing in Eq. (93) and in the equations of motion has to be taken as the vector analog of Eqs. (16) or (17) in a field theory with retarded or time-symmetric interactions; in an action-at-a-distance formulation of the theory the vector analog of Eq. (18) must be used.

As in the neutral theory, we require the constancy of the magnitude of the 2^n-pole moments; their components can always be restricted by the vector analog of condition (20), by an argument analogous to the one presented in establishing this condition in Sec. II. We also maintain the conditions imposed on the spin.

In the neutral theory the form of the multipole moment determines the energy-momentum vector A_μ completely. In the charge-symmetric theory, however, the form of A_μ depends not only on the multipole moment, but also on the charge vector $\mathbf{Q}$, which is not determined uniquely by the requirements of the theory presented here. In the following theorem we establish the most general form of the multipole moment, but derive only a particular form of A_μ and $\mathbf{Q}$. Other, more complicated, forms of these quantities can be found easily by the method presented in proving the theorem.

Theorem V: Let a point particle be characterized by the variables z_μ, A_μ, and $B_{\mu\rho}$ subject to the constraints (A) as in Theorem I, by a vector in charge-space $\mathbf{Q}(\tau)$ and by N vectors in charge-space $\mathbf{S}^{\alpha\beta\cdots\nu}(\tau)$ whose vector components are symmetric tensors of ranks $n=0, 1, \cdots N-1$, subject to the equations

$$\dot{B}_{\mu\rho}=\sum_n n(-1)^{n+1}(\mathbf{S}_\mu^{\beta\cdots\nu}\cdot\partial_{\rho\beta\ldots\nu}\mathbf{U}-\mathbf{S}_\rho^{\beta\cdots\nu}\cdot\partial_{\mu\beta\ldots\nu}\mathbf{U})-(v_\mu A_\rho-v_\rho A_\mu), \tag{B''}$$

$$\dot{A}_\mu=\sum_n(-1)^{n+1}\mathbf{S}^{\alpha\beta\cdots\nu}\cdot\partial_{\alpha\beta\cdots\nu\mu}\mathbf{U}, \tag{C''}$$

and

$$d\mathbf{Q}/d\tau=e\sum_n(-1)^{n+1}\partial_{\alpha\beta\ldots\nu}\mathbf{U}\wedge\mathbf{S}^{\alpha\beta\cdots\nu}, \tag{D}$$

where the vector components of $\mathbf{U}$ are arbitrary functions of x_μ whose derivatives are evaluated at $z_\mu(\tau)$, and e is a constant. It is required that the 2^n-pole moments $\mathbf{S}^{\alpha\beta\cdots\nu}$ be of such a form that the conditions (a) of Theorem I and

$$v_\alpha\mathbf{S}^{\alpha\beta\cdots\nu}=0 \tag{b''}$$

and

$$\mathbf{S}^{\alpha\beta\cdots\nu}\cdot\dot{\mathbf{S}}_{\alpha\beta\ldots\nu}=0 \tag{c''}$$

are valid and that A_μ and $\mathbf{Q}$ become identically equal to some functions of the other particle variables, of

U and of their derivatives at $z_\mu(\tau)$ by virtue of Eqs. (A), (B″), (C″), and (D).

Then the most general form of the 2^n-pole moments satisfying these requirements is given by

$$\mathbf{S}^{\alpha\beta\cdots\nu}=\tau\sum_p S_p^{\alpha\beta\cdots\nu}, \tag{Va}$$

where $S_p^{\alpha\beta\cdots\nu}$ is of the form (III) of Theorem III, and

$$\tau\cdot d\tau/d\tau=0. \tag{Vb}$$

Conditions (b″) and (c″) hold for each moment $\tau S_p^{\alpha\beta\cdots\nu}$ separately. A possible form of A_μ and $\mathbf{Q}$ is given by

$$A_\mu=[m+\textstyle\sum_n(-1)^{n+1}\mathbf{S}^{\alpha\beta\cdots\nu}\cdot\partial_{\alpha\beta\ldots\nu}\mathbf{U}$$
$$-\tfrac{1}{4}L(d\tau/d\tau)^2]v_\mu-B_{\mu\rho}\dot{v}^\rho$$
$$-\sum_n n(-1)^{n+1}\mathbf{S}_\mu{}^{\beta\cdots\nu}\cdot\partial_{\beta\ldots\nu}\frac{d\mathbf{U}}{d\tau}, \tag{C″}$$

and

$$\mathbf{Q}=\xi+c\tau-\tfrac{1}{2}eL\tau\wedge d\tau/d\tau, \tag{B″}$$

where m, c, L, and the components of ξ are arbitrary constants and $c\neq 0$.

A consideration entirely analogous to the one carried out in Sec. VI shows that the most general form of the 2^n-pole moment compatible with conditions (a) and (b″) is given by

$$\mathbf{S}^{\alpha\beta\cdots\nu}=\textstyle\sum_p\tau_{np}(\tau)S_p^{\alpha\beta\cdots\nu}, \tag{94}$$

where $S_p^{\alpha\beta\cdots\nu}$ is of the form (III) of Theorem III; because of the presence of the as yet arbitrary factors τ_{np} the g_{np}'s can be taken as constant without loss of generality. From (III) it follows that condition (b″) holds for each moment $\tau_{np}S_p^{\alpha\beta\cdots\nu}$ separately. By considerations analogous to those leading to Eq. (85) we find that condition (c″) requires

$$\sum_p\tau_{np}\cdot\frac{d\tau_{np}}{d\tau}S_p^{\alpha\beta\cdots\nu}S_{p\alpha\beta\ldots\nu}=0. \tag{95}$$

By a procedure analogous to the one leading from Eqs. (B′) and (C′) to Eq. (77), we obtain now from Eqs. (B″) and (C″), using expression (94) for the 2^n-pole moments

$$\dot{M}=\sum_n(-1)^{n+1}\frac{d}{d\tau}(\mathbf{S}^{\alpha\beta\cdots\nu}\cdot\partial_{\alpha\beta\ldots\nu}\mathbf{U})$$
$$-\sum_{n,p}(-1)^{n+1}n!pg_{np}\dot{B}^\alpha{}_\lambda B^{\lambda\beta}\cdots B^{\tau-1}{}_\varphi B^{\varphi\nu}\prod_{\sigma=\tau+1,\ldots,\nu}S^\sigma\left(\partial_{\alpha\beta\ldots\nu}\mathbf{U}-v_\alpha\partial_{\beta\ldots\nu}\frac{d\mathbf{U}}{d\tau}\right)\cdot\tau_{np}$$
$$-\sum_{n,p}(-1)^{n+1}n!(n-p)g_{np}B^{\tau+1}{}_\lambda B^{\lambda\beta}\cdots B^{\tau-1}{}_\varphi B^{\varphi\nu}\dot{S}^\alpha\prod_{\sigma=\tau+2,\ldots,\nu}S^\sigma\left(\partial_{\alpha\beta\ldots\nu}\mathbf{U}-v_\alpha\partial_{\beta\ldots\nu}\frac{d\mathbf{U}}{d\tau}\right)\cdot\tau_{np}$$
$$-\sum_{n,p}(-1)^{n+1}S_p^{\alpha\beta\cdots\nu}\partial_{\alpha\beta\ldots\nu}\mathbf{U}\cdot\frac{d\tau_{np}}{d\tau}. \tag{96}$$

The sum of the second and third series in this expression can be shown to vanish by a proof analogous to the one for the corresponding terms of Eq. (77). Therefore Eq. (96) can be integrated, provided that

$$-\sum_{n,p}(-1)^{n+1}S_p^{\alpha\beta\cdots\nu}\partial_{\alpha\beta\ldots\nu}\mathbf{U}\cdot\frac{d\tau_{np}}{d\tau} \tag{97}$$

is a perfect differential. Because of the scalar product this condition is less stringent than the corresponding one for expression (86). Furthermore we have the additional information available from Eq. (D) that

$$d\mathbf{Q}/d\tau=e\sum_{n,p}(-1)^{n+1}S_p^{\alpha\beta\cdots\nu}\partial_{\alpha\beta\ldots\nu}\mathbf{U}\wedge\tau_{np} \tag{98}$$

also has to be a perfect differential. However, it is only possible to draw conclusions about the series (97) from the single equation (98) if it involves just a single vector function, i.e., if all τ_{np} are proportional to a single vector $\tau(\tau)$. The constants of proportionality can be absorbed in the g_{np}'s without loss of generality. This reduces the 2^n-pole moments (94) to the form (Va) and the requirement (95) to Eq. (Vb), which has to be assured by the proper choice of $\mathbf{Q}$. If (Vb) is valid' condition (c″) holds for each moment $\tau S_p^{\alpha\beta\cdots\nu}$ separately. From (Va) expression (97) reduces to

$$-\frac{d\tau}{d\tau}\cdot\sum_{n,p}(-1)^{n+1}S_p^{\alpha\beta\cdots\nu}\partial_{\alpha\beta\ldots\nu}\mathbf{U}, \tag{99}$$

and Eq. (98) to

$$d\mathbf{Q}/d\tau=-e\tau\wedge\sum_{n,p}(-1)^{n+1}S_p^{\alpha\beta\cdots\nu}\partial_{\alpha\beta\ldots\nu}\mathbf{U}. \tag{100}$$

The simplest possibility of satisfying our requirements is given by $\mathbf{Q}=\tau$. Then Eq. (Vb) follows from Eq. (100) by scalar multiplication with τ; scalar multiplication with $\sum(-1)^{n+1}S_p^{\alpha\beta\cdots\nu}\partial_{\alpha\beta\ldots\nu}\mathbf{U}$ shows that expression (99) equals zero. A more general solution is provided by choosing expression (B″) for $\mathbf{Q}$. Then we get from Eq. (100),

$$\frac{d\tau}{c\,d\tau}=-e\tau\wedge\left[\sum_{n,p}(-1)^{n+1}S_p^{\alpha\beta\cdots\nu}\partial_{\alpha\beta\ldots\nu}\mathbf{U}-\tfrac{1}{2}L\frac{d^2\tau}{d\tau^2}\right], \tag{101}$$

which implies condition (Vb) as before, and from which it follows by scalar multiplication with the factor [ ] that

$$-\frac{d\tau}{d\tau}\cdot\sum_{n,p}(-1)^{n+1}S_p^{\alpha\beta\cdots\nu}\partial_{\alpha\beta\ldots\nu}\mathbf{U}=-\tfrac{1}{2}L\frac{d\tau}{d\tau}\cdot\frac{d^2\tau}{d\tau^2}, \quad (102)$$

provided that $c\neq 0$. Substituting this into Eq. (96) and integrating we get

$$M=m+\sum_n(-1)^{n+1}\mathbf{S}^{\alpha\beta\cdots\nu}\cdot\partial_{\alpha\beta\ldots\nu}\mathbf{U}-\tfrac{1}{4}L(d\tau/d\tau)^2. \quad (103)$$

Combining this with Eq. (40) and the equation of the charge-symmetric theory analogous to Eq. (41), we obtain expression (α''). This completes the proof of Theorem V.

VIII. DISCUSSION

In the preceding sections we have established the most general form of the multipole moment compatible with all the conditions of the theory in form (IV) of Theorem IV for the neutral theory and in form (V) of Theorem V for the charge-symmetric theory. It then follows from Theorem III that there are $\frac{1}{2}n+1$ essentially different 2^n-poles for even n, and $\frac{1}{2}(n+1)$ different ones for odd n, characterized by the constants g_{np}, and from Theorems IV and V, that a point particle can carry an arbitrary combination of such poles of any order. By Theorem IV, in the neutral theory a point particle is completely characterized by the constants g_{np} and m and the variables z_μ and $B_{\mu\rho}$; in the charge-symmetric theory, additional constants and a new variable τ are needed because of the electric charge, a simple form of which is given in Theorem V.

However, within the framework of the charge-symmetric theory considered here, the presence of an electric charge and current manifests itself only in the appearance of a new conservation law for the charge, but not in the production of electromagnetic fields. It is possible that the nonlinearity of the equations of a theory which includes electromagnetic fields would reduce the variety of possible expressions for the electric charge. Another possibility of reducing this variety may be provided by requiring that the equations of motion of the special theory of relativity considered here fit into the framework of the general theory, instead of basing their derivation on the ambiguous information provided by the conservation laws for the fields.[9] This has been discussed for the case of a simple pole of the neutral meson field in a recent paper;[10] the general case is being investigated at present.

It appears noteworthy that all multipole moments with $n>0$ vanish if $B_{\mu\rho}=0$. Thus all except the simplest of the particles discussed here would be eliminated from the theory if it could be shown that a point particle cannot possess an intrinsic angular momentum in the classical theory.

In the preceding investigation we have made no distinction between scalar and pseudoscalar fields. The tensor or pseudotensor character of the multipole moments is determined by their constituents (III) of Theorem III. As v_μ and $B_{\mu\rho}$ are tensors and $\epsilon^{\sigma\lambda\lambda\rho}$ is a pseudotensor, we can conclude that all 2^n-pole moments of even n are tensors, and of odd n are pseudotensors, if the constants g_{np} are scalars, and vice versa, if they are pseudoscalars. Thus, in the customary case of scalar coupling constants, scalar or pseudoscalar meson fields can only have 2^n-pole singularities of even or odd n, respectively.

[9] P. Havas, Phys. Rev. 87, 898 (1952).
[10] F. R. Crownfield, Jr., and P. Havas, Phys. Rev. (to be published).

Letters to the Editor

PUBLICATION of brief reports of important discoveries in physics may be secured by addressing them to this department. The closing date for this department is five weeks prior to the date of issue. No proof will be sent to the authors. The Board of Editors does not hold itself responsible for the opinions expressed by the correspondents. Communications should not exceed 600 words in length and should be submitted in duplicate.

Elastic Scattering of 1-Mev Electrons from Aluminum and Gold

ROBERT T. BAYARD, *University of Pittsburgh, Pittsburgh, Pennsylvania and Westinghouse Electric Corporation, Pittsburgh, Pennsylvania*

AND

J. L. YNTEMA, *University of Pittsburgh, Pittsburgh, Pennsylvania*

(Received December 10, 1953)

KINZINGER and Bothe[1] have reported significant deviations from Mott theory in the large-angle scattering of 245-kev electrons from heavy nuclei. For gold at 150° they found that the scattering is more than 35 percent low. Subsequent measurements by Kinzinger[2] at 120° show a consistent deviation which is 25 percent low and is independent of energy between 150 and 400 kev. Paul and Reich[3] report similar behavior for 2.2-Mev electrons, the deviation being about 15 percent for platinum at 90° and 120°.

A preliminary measurement of the scattering of 1-Mev electrons by aluminum and gold has been made. Electrons from a Van de Graaff generator are focused on Parlodion (0.006 mg/cm²) backed foils of aluminum (0.22 mg/cm²) and gold (0.02 mg/cm²), and the relative number of electrons scattered at 30°, 60°, 90°, 120°, and 150° is measured. The two detectors are photomultipliers with anthracene crystals mounted at the end of collimators. An integral pulse-height discriminator is biased to minimize the x-ray and low-energy electron background so that the electrons elastically scattered from the foil nuclei are counted. The ratios of scattering at 30°, 60°, 120°, and 150° to that at 90° are measured and compared with the theoretically predicted values. Account has been taken of background counting rate, counting losses due to finite resolving time of the scaling circuits, multiple scattering, plural scattering (transmission-reflection asymmetry), and scattering in the Parlodion foil support. The maximum contribution for each of these was of the order of one percent and was in most cases less than this.

The results for aluminum and gold are given in Table I. The uncertainties shown are the standard deviations associated with counting. The results for aluminum are compared with the α^4 approximation to the Mott series given by McKinley and Feshbach[4] rather than the α^2 approximation formula, since the latter does not fit the experimental values as well as the more accurate α^4 approximation. For gold, the α^4 approximation is not sufficiently accurate, since $\alpha=Z/137=0.58$ and the series does not converge rapidly enough. The theoretical values given in Table I for gold were obtained by interpolating the calculations of Bartlett and Watson[5] for mercury and multiplying the result by the ratio of gold to mercury scattering given by the α^4 approximation. This procedure should give results accurate to about 1 percent.[4] As may be seen in Table I, the experimental results do not differ from these theoretical values by more than 1.5 percent and the differences exhibit no systematic trend. Thus, there is no evidence for deviation from the Mott theory of electron scattering at 1 Mev. Work is continuing on the measurement of relative scattering at other energies as well as of the absolute scattering.

TABLE I. Relative scattering with respect to 90°.

Angle	Aluminum Experimental	Theoretical	Deviation (%)
30°	89.06 ±0.27	89.08	−0.0
60°	5.504 ±0.011	5.496	+0.2
120°	0.2654 ±0.0007	0.2665	−0.4
150°	0.08572 ±0.00029	0.08544	+0.3
Angle	**Gold Experimental**	**Theoretical**	**Deviation (%)**
30°	39.50 ±0.12	39.87	−0.9
60°	3.898 ±0.009	3.840	+1.5
120°	0.3204 ±0.0008	0.3178	+0.8
150°	0.09610 ±0.00039	0.09693	−0.9

[1] E. Kinzinger and W. Bothe, Z. Naturforsch. **7a**, 390 (1952).
[2] E. Kinzinger, Z. Naturforsch. **8a**, 312 (1953).
[3] W. Paul and H. Reich, Z. Physik **131**, 326 (1952).
[4] W. A. McKinley, Jr., and H. Feshbach, Phys. Rev. **74**, 1759 (1948).
[5] J. H. Bartlett and R. E. Watson, Proc. Am. Acad. Arts Sci. **74**, 53 (1940).

Feynman's Theory of Liquid Helium

G. V. CHESTER

Radar Research Establishment, Ministry of Supply, St. Andrew's Road, Malvern, Worcestershire, England

(Received January 18, 1954)

RECENTLY, Feynman[1] has developed a new theory of liquid helium. In the present note we wish to show how the approximations that Feynman has to make to evaluate the partition function may be related to well-known approximations in statistical mechanics. We should also like to point out that Matsubara[2] has developed a theory of liquid helium using almost the same mathematical approximations as Feynman. It appears to us that the relationships that exist between Feynman's approximations and the standard approximations of statistical mechanics throw new light on the nature of Feynman's work.

We shall confine ourselves in this note to the first of Feynman's papers—hereafter referred to as I—in which he discusses the origin of the lambda transition of liquid helium. In I, three approximations are made in order to evaluate the partition function for the system. Feynman first argues that it is very reasonable to assume that the helium atoms move about as if they were practically free, and therefore that to a high degree of accuracy the distribution function in configuration space will be essentially the same as that for an ideal Bose-Einstein gas. This distribution function is proportional to

$$\Sigma_P \exp\left[-(\pi/\lambda^2)\sum_{i=1}^{N}|\mathbf{z}_i-P\mathbf{z}_i|^2\right],$$

where $\mathbf{z}_i$ is the coordinate of the ith atom, P is any permutation of the N indices, $\lambda^2=h^2/2\pi mkT$, and Σ_P stands for a summation over all permutations P. In order to take into account the effects of the interactions between the atoms Feynman proposes to modify this distribution function by replacing the true mass m by an effective mass m' and by multiplying it by an additional distribution function $K_\beta\cdot\rho_N(\mathbf{z}_1\cdots\mathbf{z}_N)$, where K_β is a normalization constant. The function ρ_N is stated to be "··· qualitatively very similar to the distribution function for a classical gas." We can therefore write it in the form $\exp[-\beta V'(\beta)]$, where $V'(\beta)$ is a quasi-interaction potential, with properties similar to that for a classical system except that it depends slightly on the temperature. With these approximations the partition function reduces to

$$Q'=\lambda'^{3N}\frac{K_\beta}{N!}\int_{\mathbf{z}}\exp[-\beta V'(\beta)]\times\sum_P\exp\left[-(\pi/\lambda'^2)\sum_{i=1}^{N}|\mathbf{z}_i-P\mathbf{z}_i|^2\right]d\mathbf{z}, \quad (1)$$

where $\lambda'^2=h^2/2\pi m'kT$ and $\mathbf{z}$ stands for the set of all coordinates $(\mathbf{z}_i)$. We now wish to compare this approximate partition function with another that can be obtained from the semiclassical expansion due to Wigner[3] and Kirkwood.[4] These authors showed that the

partition function can be written in the form,

$$Q=(\lambda^{3N}/N!)\int_z \exp(-\beta V)\Big[\sum_P \exp\Big[-(\pi/\lambda^2)\times\sum_{i=1}^{N}|\mathbf{z}_i-P\mathbf{z}_i|^2\Big]+O(\hbar^2)+O(\hbar^4)\cdots\Big]d\mathbf{z}, \quad (2)$$

where V is the interaction potential of the atoms. If we ignore the terms of order $\hbar^2,\hbar^4\cdots$, etc., in the above expansion we get

$$Q'=(\lambda^{3N}/N!)\int_z \exp(-\beta V)\times\sum_P \exp\Big[-(\pi/\lambda^2)\sum_{i=1}^{N}|\mathbf{z}_i-P\mathbf{z}_i|^2\Big]d\mathbf{z}. \quad (3)$$

It is seen that Q' only differs from Q'' in that m is replaced by m' and $\exp(-\beta V)$ by $K_\beta\exp[-\beta V'(\beta)]$. In I it is stated that m' will probably not differ very much from the true mass m, near the λ temperature, and that K_β can be ignored as far as the nature of the transition is concerned. We have already noted that $V'(\beta)$ is fairly insensitive to changes in β and is qualitatively similar to the actual potential V. In other words the modifications to the zero-order term in Eq. (2) proposed by Feynman are quite small; we therefore have to consider whether the effects of all the other terms, that have been omitted, can be supposed to be small. This question is very difficult to decide, although it is quite easy to show that the coefficients of the leading terms of the series are large. However, even if we cannot evaluate any of the higher-order terms rigorously we can still argue that they are unlikely to remove any discontinuities that may be present in the derivatives of the first term of the series. This follows from the fact that the above series is an expansion in powers of $\Lambda^{*2}(=\hbar^2/\sigma^2 m\epsilon)$, and therefore if the higher-order terms were to remove any discontinuities predicted from the first term this would imply a critical dependence on Λ^*. This would seem to be unreasonable on physical grounds. We therefore conclude that although the first term may be a poor approximation quantitatively it may still yield useful qualitative information.

Feynman next considers a typical term in the summation over all the permutations P in Eq. (1). Let us suppose that in this particular term there are m_l cycles of l "atoms" so that $\sum_l lm_l=N$. Then a typical term in the sum in Eq. (2) can be written,

$$\int_z \rho_N(\mathbf{z}_1\cdots\mathbf{z}_N)\prod_l\prod_{k=j}^{j+m_l l}\prod_{p=1}^{l}\exp[-(\pi/\lambda^2)|\mathbf{z}_{k+p}-\mathbf{z}_{k+p+1}|^2]d\mathbf{z}, \quad (4)$$

where the product Π_l is over a set of values of l such that $\sum_l lm_l=N$ and $\mathbf{z}_{k+l+1}\equiv\mathbf{z}_{k+1}$, Feynman now approximates to ρ_N by the product

$$\prod_l\prod_{k=j}^{j+m_l l}\prod_{p=1}^{l}\rho_2(\mathbf{z}_{k+p},\mathbf{z}_{k+p+1}),$$

where ρ_2 is proportional to the pair or "radial" distribution function. Clearly with this approximate form for ρ_N each of the terms in the sum of permutations can be evaluated explicitly, provided the form of ρ_2 is assumed. We shall now show that this approximation is closely related to the well-known superposition approximation of Kirkwood.[5] The superposition approximation can be formulated by saying that we approximate to ρ_N by the product

$$\prod_{i\le j=1}^{N}\rho_2(\mathbf{z}_i,\mathbf{z}_j).$$

Basically, therefore, Feynman's approximation rests on this approximation. However, Feyman has also replaced all factors of the form $\rho_2(\mathbf{z}_i,\mathbf{z}_{i+p}),p>1$, in the superposition approximation, by unity. As he has pointed out, this means that we are completely neglecting (a) correlations between atoms that are not 'nearest neighbors' in a cycle and (b) correlations between all the atoms in any one cycle and those in any other cycle. It is well known that it is very difficult to estimate the validity of the superposition approximation. However it is very reasonable to assume that the more "gas-like" the structure of the liquid the more accurate the approximation will be. We may therefore be reasonably sure that for helium, which is a "gas-like" liquid with an abnormally low density, the approximation will be quite accurate. This conclusion lends support to Feynman's basic approximation and we would agree with him that the neglect of correlations between atoms in different cycles is probably much more important; it may be vital in deciding the order of the lambda transition. It is interesting to note that for a "classical liquid" the superposition approximation is, by itself, sufficient to allow us to calculate many of its properties. This is unfortunately not so for a "quantum liquid."

Finally we would like to mention that Matsubara[2] has developed a similar theory of liquid helium using essentially the same mathematical approximations as Feynman. Equations (4.13) and (4.14) of Matsubara's paper are equivalent to Eqs. (25) and (26) of Feynman's. Matsubara concludes that the lambda transition predicted by his theory is of the second order: this conclusion appears to us to be due to an error in the later stages of his analysis.

Acknowledgment is made to the Chief Scientist, Ministry of Supply, and the Controller, H. Britannic M. Stationery Office for permission to publish this paper.

[1] R. P. Feynman, Phys. Rev. 91, 1291 (1953).
[2] T. Matsubara, Progr. Theoret. Phys. (Japan) 6, 714 (1951).
[3] E. P. Wigner, Phys. Rev. 40, 749 (1932).
[4] J. A. Kirkwood, Phys. Rev. 41, 31 (1933).
[5] J. A. Kirkwood, J. Chem. Phys. 3, 300 (1935).

Speculations on the Behavior of Positrons in Superconductors

M. DRESDEN
Department of Physics, University of Kansas, Lawrence, Kansas
(Received January 26, 1954)

THE measurements of Graham and Bell[1] and those of Ferguson and Lewis[2] indicate that the mean lifetime of positrons in metals is constant and roughly independent of the metal. In other materials one may describe the observed facts by using two separate lifetimes for the positrons, indicating two distinct modes of annihilation. Inasmuch as there appears to be some empirical connection between the characteristics of the material and the type of positron annihilation process, one may inquire whether the annihilation characteristics of positrons are affected when a metal goes over from the normal to the superconductive state. A precise calculation of these characteristics should be based on a detailed description of the thermalization and annihilation processes in superconductive solids. Since even for a normal solid the mechanisms involved in these processes are only partially known[3,4] and since there does not appear to be a completely satisfactory wave function of a superconductor, it seems best to investigate the qualitative features of these processes. Several of the results are amenable to experimental verification, so one may decide on the basis of the experimental result whether a more detailed treatment is worth while.

1. It would appear that in so far as the lifetime of positrons depends on the average electron density only, the lifetime should not change in a superconductive transition, since the electron density is the same in the two phases (unless one wanted to exclude the "super electrons" *a priori* from taking part in the annihilation process, which seems unreasonable). It should be stressed however that even for normal metals the relationship between lifetime and electron density is not completely clear. In fact the experimentally obtained lifetimes are constant, whereas the electron densities may vary by a factor 20.[1] It may be shown[3] that the annihilation mechanism of a thermalized positron in a solid is determined by the matrix element $M_{ij}(p)=\int u_i^* v_j \times\exp(ipx/\hbar)dx$. Here p is the total momentum of the annihilating pair, u_i and v_j are the wave functions of the electron and positron in the lattice (specified by wave numbers i and j). To obtain a mean lifetime from this matrix element, one has to perform certain averaging processes over the electron and positron distributions. Now the wave functions u_i and v_j certainly change when the solid

goes from a normal to a superconductive state, and the electron distribution will be affected to some extent. Since the factors on which the lifetime depends change in the superconductive transition, it seems quite possible that the lifetime itself changes. Crude estimates indicate the lifetime might be lengthened.

2. It seems quite certain now[1,4] that positronium formation plays an important role in the annihilation process. In fact the experimental data can be explained best by assuming that the positrons slow down rapidly, then form positronium, and finally annihilation takes place from the ground state of the positronium. The long-lived triplet state of positronium will be converted rapidly to the singlet state, by the interaction of the positronium with the lattice vibrations, or by collisions with other electrons. One of the typical features of the superconductive state is the inability of the electron system to exchange energy with the lattice system or with impurities. It has been recognized[5] that in the superconductive state one has to deal with a wave function which is "adjusted" to the electron-lattice interaction, the electron-electron interaction and also to the interaction between the electron system and impurities. ("Adjusted" is used here in the sense that these interactions cannot cause transitions.) It seems quite possible therefore that the positronium exists in the system as some kind of impurity. In that case the interactions responsible for the conversion from the triplet to the singlet state would not operate, or would operate much less efficiently, in the superconductive state. Consequently the triplet state would persist longer in a superconductor than in a normal conductor. This would give rise to a complex lifetime decay of positrons in a superconductor. It is true that a second electron could in principle annihilate with the positron in the positronium; one finds, however, that when positronium formation itself is likely, this pick-off annihilation probability becomes quite small. Further, the average electron density around positronium is smaller than that around a positron, and this too reduces the efficiency of the "pick-off annihilations." (This type process was in fact invoked by Garwin[4] to explain the long-lived component of the positron lifetime in some materials.)

3. Experiments done by Stump and Talley[6] and independently by Millett[7] indicate that the decay of positrons in lead at liquid nitrogen temperatures differs from that at liquid helium temperatures. The experiments at liquid nitrogen temperature yield the usual one-lifetime annihilation process (with the usual numerical value for metals), whereas those at liquid helium temperatures indicate a complex lifetime scheme with a longer-lived component.

4. On the basis of the model developed, one would expect more three-quantum annihilation processes in a superconductor since the triplet state has less chance to be converted. Experiments to check this feature are now in progress. If these same lifetime measurements were made at liquid helium temperatures in lead and if a magnetic field strong enough to destroy the superconductive state were applied, one should on the basis of previous considerations reobtain one-lifetime type annihilation. This last experiment would also decide whether the effects already observed are indeed characteristic of the superconductive state, or whether they represent some general property of metals at low temperatures.

Further details will be published in a more extensive communication.

The author wants to thank many members of the "Third International Conference of Low Temperature Physics," held at The Rice Institute, for many stimulating conversations, in particular Professors Marcus, Price, Bardeen, Feynman, Pippard, and Mendelssohn. Special thanks are due Professor Robert Stump for many illuminating discussions.

[1] R. L. Graham and R. E. Bell, Phys. Rev. 90, 644 (1953).
[2] A. T. G. Ferguson and G. M. Lewis, Phil. Mag. 44, 1339 (1953).
[3] S. de Benedetti *et al.* Phys. Rev. 77, 205 (1950).
[4] This point of view was expressed by Bohr in a discussion remark. [See Physica 19, 762 (1953).]
[5] R. L. Garwin, Phys. Rev. 91, 1571 (1953).
[6] The author is indebted to these authors for communicating their results before publication. These experiments will be reported at the Austin Meeting of the American Physical Society.
[7] The author wants to express his gratitude to Dr. Millett for informing him about these results in advance of publication. These results, too, will be reported at the Austin Meeting.

Creation of Displacements in Radiation Damage*

H. B. HUNTINGTON†
Brookhaven National Laboratory, Upton, New York
(Received January 20, 1954)

A THEORETICAL investigation has been started into the formation and character of the displacements created in face-centered cubic metals by radiation damage. (Displacements, or Frenkel defects, are caused when energetic particles drive atoms of the lattice to interstitial sites leaving vacancies in their original positions.) Attention has been concentrated here on low-energy collisions because most of the displacements are generally created by collisions with energies only a few times the threshold—in the range of one or two hundred electron volts. The procedure has been to consider that an atom at a lattice site, or in an interstitial position, receives a considerable amount of energy at a given instant and to attempt to determine the end state of the lattice as a function of the magnitude and direction of the original impulse. In this way the threshold energy for displacement creation can be calculated and presumably, for a given distribution of primary particle energies, the distribution in length of the resulting displacements, their spatial distribution, and their total number could be obtained.

It has been assumed that for close-packed metals at low energies the principal interaction between colliding atoms is the repulsion of closed shells, which may be approximated by a semiempirical formula of the Born-Mayer type, $V(r)=A\exp\{-(r-r_0)\rho/r_0\}$. The constants in the closed-shell repulsive potential depend to some extent on the assumptions used in determining them. It has been shown[1] that for copper the value for ρ can be bracketed between 13 and 17. Since this force law is very short-range, the procedure has been to predict the result of a particular collision on the basis of a billiard ball model where the size of the balls is determined by the interatom distance at the instant of contact, i.e., when the relative kinetic energy vanishes. At these low energies many-body collisions are important, and reasonable techniques have been evolved to treat such cases in a manner consistent with the rigid sphere model. So far only collisions have been considered where the high-energy particle moves in a crystallographic direction. The high degree of symmetry in these cases facilitates their treatment. From their study, one finds two close competitors for the mechanism of displacement creation with minimum energy.

For ρ equals 13 (for which the corresponding value of A is 0.053 ev), it is found that an atom at a lattice site needs about 18.5 ev to move in the (111) direction through the triangle formed by three of its nearest neighbors to the interstitial position. Comparable energy (17.5 ev) is required by a lattice atom moving in the (100) direction for displacement creation in a "knock-on" mechanism where the original fast atom moves to another lattice site displacing its neighbor to an interstitial position. The history of all these collisions is rather complex and we have had to resort to reasonable, though somewhat arbitrary, criteria for determining the thresholds. A further difficulty is introduced by uncertainty as to the equilibrium configuration of the interstitial atom.[1]

Rough estimates have been made on the magnitude of these threshold energies on the basis of an alternate force law with $\rho=17$ and $A=0.038$ ev. They give 43 ev for the (111) mechanism and 34 ev for the knock-on collision. Experiments with electron radiation by Eggen and Laubenstein[2] report a threshold value of 25 ± 1 ev. Apparently this value lies well inside the rather wide limits set by the foregoing alternate calculations.

It was mentioned above that consideration was also being given to the history of energetic interstitial atoms. Such interstitials can be studied as typical atoms undergoing displacements longer then the minimum stable length. It appears that displacement length increases somewhat more rapidly than the logarithm of the energy.

Among the subjects planned for future study are (1) the replacement of the rigid body model by an improved treatment, and (2) the investigation of collisions undergone by atoms moving along directions of low symmetry. It appears that the rigid body

assumption may give rise to larger errors than were first anticipated. Information on collisions as a function of the general direction of the initial impulse is useful in establishing the displacement yield as a function of energy above threshold.

The writer wishes to express his appreciation to Dr. G. J. Dienes for his interest in this work and to the Brookhaven National Laboratory for the opportunity to carry on the research.

* Work done under contract with the U. S. Atomic Energy Commission.
† On summer leave from Rensselaer Polytechnic Institute, Troy, New York.

[1] H. B. Huntington, Phys. Rev. **91**, 1092 (1953).
[2] D. T. Eggen and M. J. Laubenstein, Phys. Rev. **91**, 238 (1953).

Superconducting Compounds

B. T. Matthias, E. Corenzwit, and C. E. Miller
Bell Telephone Laboratories, Murray Hill, New Jersey
(Received January 25, 1954)

In a previous paper[1] an outline was given of the necessary[2] though not always sufficient, conditions for the occurrence of superconductivity in compounds. Following the hypothesis of an optimum number of valence electrons per atom and of the increase of the transition temperature with an increase of volume, a variety of new superconducting binary and ternary systems have been found. They confirm the assumption that deviation from an essentially metallic bond is a necessity for superconductivity.

(a) *Phosphides.*—Until now, no superconducting phosphides have been known. Recently we have found that Mo_3P becomes superconducting near 7°K and Rh_3P_4 at 1.22°K. We are not quite certain yet whether these compositions correspond to a single phase and rely thus far on the reported crystallographic investigations.[3,4]

X-ray patterns showed that in general we were unable to obtain these phases completely pure. In the case of Mo_3P, MoP was always present, and in Rh_3P_4 we always detected Rh_2P. Both MoP and Rh_2P, however, can be prepared without any other phases present and neither becomes superconducting above 1.03°K.

(b) *The* NiAs *Structure.*—As mentioned before,[1] several intermetallic compuonds with this type structure have been reported as superconductors. However, no superconducting arsenides had previously been found. NiAs by itself does not show superconductivity above 1.28°K.[4,5] Assuming now that the transition temperature, if present, could be raised by enlarging the crystal lattice (as pointed out before[1]), we substituted the larger Pd partially for the Ni. This, however, cannot go all the way to PdAs, as this alloy is not isomorphous with NiAs, nor does PdAs become superconducting above 1.02°K. This attempt to enforce superconductivity was successful: the solid solutions from $(Ni_{0.75}Pd_{0.25})As$ to $(Ni_{0.12}Pd_{0.88})As$ become superconducting above 1.06°K. The maximum transition temperature is reached for $(Ni_{0.25}Pd_{0.75})As$ at 1.6°K and decreases with either increasing or decreasing Pd amount.

(c) *The* Rh-X *System.* X=S, Se, Te.—From our previous considerations it had seemed likely that compounds of Rh with S, Se, or Te should also become superconducting.

We have found that Rh_9S_8, which is a well-defined compound,[6] becomes superconducting at 5.8°K.

According to Woehler[7] and Biltz,[8] the only compound in the Rh-Se system is supposed to be Rh_2Se_3. Now Rh_2Se_3 does not become superconducting above 1.04°K, whereas compounds with an approximate composition between 2Rh:3.4Se and 2Rh:4Se do become superconducting. In this Rh-Se system one does not seem to have a well-defined phase with respect to composition, as one does in the Rh_9S_8 case. The x-ray patterns indicate identical lattice structure for all those alloys whose composition lies between 2Rh:3.2Se and 2Rh:5Se. The lattice constant, however, rises as the Se content decreases. On both ends of the homogeneity range no superconductivity can be observed any longer above 1.02°K.

We seem to have here an example of the hypothesis according to which the transition temperature depends strongly upon the volume and the number of valence electrons per atom.[1] Whereas an increase in Se decreases the volume and raises the number of electrons, an increase in Rh has the opposite effect, and one therefore seems to be able to cover the whole range in which superconductivity can occur. Consequently, the transition temperature rises and falls between 1°K and 6°K with varying selenium content. The optimum condition seems to be 2Rh:3.5Se with a transition temperature at ~6°K.

In the Rh-Te system the situation is similar but extends over a smaller range, as Te cannot replace Rh to the same amount as Se. The optimum condition is 2Rh:4Te, which becomes superconducting at 1.51°K.

It is our hope that more systematic measurements on the Rh-Se system will reveal the critical electronic condition for superconductivity in a given crystal lattice.

The x-ray identification and structure studies which Dr. S. Geller has made on these compounds have been most helpful. We are grateful to him for his interest and his assistance, and to Mr. A. N. Holden for valuable discussions.

[1] B. T. Matthias, Phys. Rev. **92**, 874 (1953).
[2] F. E. Faller and W. Biltz, Z. anorg. Chem. **248**, 209 (1941).
[3] Faller, Strotzer, and Biltz, Z. anorg. Chem. **244**, 317 (1940).
[4] B. T. Matthias and J. K. Hulm, Phys. Rev. **87**, 799 (1952).
[5] Meissner, Franz, and Westerhoff, Ann. Physik **17**, 593 (1933).
[6] Juza, Hülsmann, Meisel, and Biltz, Z. anorg. Chem. **225**, 369 (1935).
[7] Woehler, Ewald, and Krall, Ber. deut. chem. Ges. **66**, 1638 (1933).
[8] W. Biltz, Z. anorg. Chem. **233**, 282 (1937).

X-Ray Coloring of 400-Mev Proton-Irradiated KCl*

W. Leivo and R. Smoluchowski
Carnegie Institute of Technology, Pittsburgh, Pennsylvania
(Received February 1, 1954)

The total number of lattice defects produced by particle irradiation is an important quantity in the study of radiation effects in solids. In this connection, a possible correlation of the large decrease of density produced by 400-Mev protons in KCl with measurements of optical abosrption is of interest since both effects may be interpreted in terms of a concentration of vacancies. An appreciable coloring of KCl crystals with the high-energy protons, however, is obtained in our experimental setup only at low intensity of irradiation ($nvt=1\times10^{15}$) which produces rather small changes in density. At intensities about five times higher, on the other hand, the density is altered considerably but the crystals are almost completely bleached, which is presumably because of a stronger heating of the crystals in the higher-intensity beam. In order to use this high-intensity irradiation, it appeared thus advisable to try to color the crystals with x-rays after they have been irradiated in a proton beam which is strong enough to produce large density changes. In a normal crystal, the coloring produced by x-rays falls off rapidly with distance attaining a value of $1/e$ at about 0.05 mm below the surface.[1] Thus, if the proton-irradiated crystals could be bodily colored by x-rays, then this would indicate that vacancies produced by protons can be subsequently filled by x-ray photoelectrons. It would provide also a further evidence for the basic role of the soft component of the x-ray radiation in producing color centers.

To test these ideas, crystals, which were essentially uncolored by proton irradiation in the Carnegie Institute of Technology cyclotron, were exposed to x-rays from a molybdenum target tube which had a beryllium window and was operated at 45 kv and 18 ma. A similar crystal which had not been previously irradiated on the cyclotron was placed on the opposite window of the x-ray tube. To compensate for any possible differences in the beam intensities between the two windows, the crystals were periodically interchanged giving each crystal the same length of time on each window. It was found that crystals which had been irradiated on the cyclotron could be colored much more readily than the ones which had not previously been irradiated and, furthermore, the crystals could be actually bodily colored. The crystals, which were abour 3 mm thick, were cleaved after exposure to x-rays into three

sections perpendicular to the direction of the x-ray beam. All three sections of the crystal, which had a previous proton irradiation, showed strong coloring, whereas, in crystals which had been exposed only to x-rays, only a thin surface layer of the first section was colored, the other two sections showing negligible color-center concentration. This indicates absence of any spurious effects due to scattered x-rays, etc.

Changes in density of the clear crystals were observed after cyclotron irradiation but before irradiation with x-rays. The observed decrease in density was about four times greater than had been previously reported for heavily[2] colored crystals. A more detailed quantitative study of these effects is underway.

* This work was supported by contract with the U. S. Atomic Energy Commission.

[1] Estermann, Leivo, and Stern, Phys. Rev. 75, 627 (1949).
[2] W. J. Leivo, Phys. Rev. 91, 245 (1953).

Coefficient of Expansion of Liquid Helium II

K. R. Atkins and M. H. Edwards
Department of Physics, University of Toronto, Toronto, Canada
(Received January 25, 1954)

We have measured the coefficient of thermal expansion of liquid helium II from the λ point down to 0.85°K. The dilatometer was a closed system consisting of a copper chamber full of liquid helium attached to the lower end of a glass capillary in which the surface of the liquid could be viewed. The whole was immersed in a bath of liquid helium II and the procedure was to make a small measured change in bath temperature while observing the change in the position of the meniscus in the capillary. Temperatures below 1.2°K were obtained by pumping on the bath with a large diffusion pump and were measured by a carbon resistance thermometer which had been calibrated against the magnetic susceptibility of ferric alum.

Earlier density measurements[1] showed that the expansion coefficient is positive above the λ point but negative just below the λ point. Our extended measurements show that it becomes positive again below 1.12°K (Fig. 1). This was not unexpected,[2,3] since liquid helium below 1°K is very similar to a Debye solid.[4] In fact, the positive contribution which the phonons make to the expansion coefficient can be calculated from a form of Gruneisen's law,[3]

$$\alpha_{ph}=\frac{16\pi^5}{15}\frac{k^4}{h^3c^3}\left(\frac{1}{c}\frac{\partial c}{\partial p}+\frac{1}{3\rho c^2}\right)T^3, \tag{1}$$

in which α_{ph} is the phonon coefficient of expansion, c the velocity of first sound, and $\partial c/\partial p$ the variation of this velocity with pressure. This expression reduces to

$$\alpha_{ph}=1.08\pm0.04\times10^{-3}T^3\text{deg}^{-1}, \tag{2}$$

and is plotted as the dashed curve in Fig. 1.

If it is permissible to divide the measured coefficient of expansion α into separate phonon and roton contributions α_{ph} and α_r, then α_{ph} can be calculated from Eq. (2) and subtracted from α to give α_r. A calculation of $\alpha_r=-\rho(\partial S_r/\partial p)_T$, by using Landau's expression[5] for S_r and keeping his notation, yields

$$\alpha_r=\frac{2(k\mu)^{\frac{1}{2}}p_0^2\Delta}{(2\pi)^{\frac{1}{2}}\rho T^{\frac{1}{2}}\hbar^3c^2}\left(1+\frac{3kT}{2\Delta}\right)\exp\left(-\frac{\Delta}{kT}\right)\times\left[\tfrac{1}{2}\frac{\rho}{\mu}\frac{\partial\mu}{\partial\rho}+2\frac{\rho}{p_0}\frac{\partial p_0}{\partial\rho}+\frac{\Delta}{\rho}\frac{\partial\Delta}{\partial\rho}-1-\frac{\rho}{\Delta}\frac{\partial\Delta}{\partial\rho}\frac{\Delta}{kT}\times\left\{1+\frac{\frac{3}{2}(kT/\Delta)^2}{1+\frac{3}{2}kT/\Delta}\right\}\right]. \tag{3}$$

Within the limits imposed by the experimental errors in the various quantities, this expression is consistent with the measurements below 1.6°K if

$$[\tfrac{1}{2}(\rho/\mu)(\partial\mu/\partial\rho)+2(\rho/p_0)(\partial p_0/\partial\rho)+(\rho/\Delta)(\partial\Delta/\partial\rho)]\sim-1.5$$

and $(\rho/\Delta)(\partial\Delta/\partial\rho)\sim-0.65$.

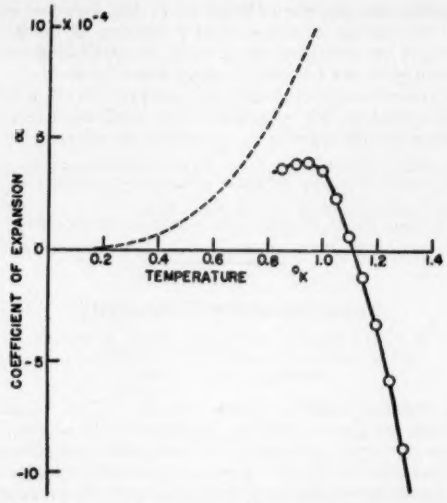

FIG. 1. The coefficient of thermal expansion of liquid helium II below 1.4°K. ○, Experimental. – – –, Phonon contribution.

Integrating α gives an accurate curve for the variation of density with temperature, and again this may be divided into phonon and roton parts,

$$\rho=\rho_0+\delta\rho_{ph}+\delta\rho_r. \tag{4}$$

By calculating $\delta\rho_{ph}$ from (2) and using it to derive $\delta\rho_r$ from (4), it appears that $\delta\rho_r$ is very nearly a linear function of the density of the normal component ρ_n. It is not possible to say whether this fact has any more fundamental significance than the approximate agreement with Landau's theory. A careful comparison of theory and experiment must await more accurate values of certain quantities, in particular the entropy, which at present is uncertain to about 10 percent.[6]

[1] W. H. Keesom, *Helium* (Elsevier Publishing Company, Inc., Amsterdam, 1942), p. 206.
[2] L. Goldstein, Phys. Rev. 89, 597 (1953).
[3] K. R. Atkins and R. A. Stasior, Can. J. Phys. 31, 1156 (1953).
[4] Kramers, Wasscher, and Gorter, Physica 18, 329 (1952).
[5] L. Landau, J. Phys. U.S.S.R. 11, 91 (1947).
[6] G. R. Hercus and J. Wilks, in *Proceedings of the Third International Conference on Low Temperature Physics and Chemistry* (The Rice Institute, Houston, Texas, 1953), p. 65.

Temperature Measurement below 1°K*

D. H. Howling,† *H. H. Wills Physical Laboratory, University of Bristol, Bristol, England*
and
F. J. Darnell and E. Mendoza,‡ *Department of Physics, Carnegie Institute of Technology, Pittsburgh, Pennsylvania*
(Received January 18, 1954)

Usually the thermometric parameters used for temperature measurements below 1°K are magnetic in character—the susceptibility, the remanence, and the area of the hysteresis loop have been so used. By carrying out thermodynamic cycles or by equivalent means, these parameters can be calibrated absolutely.[1] For temperatures down to a little way below the Curie point the results are most often presented as a $T-T^*$ relation, T being the absolute temperature, T^* the Curie temperature proportional to the reciprocal of the susceptibility. When a secondary thermometer, such as a resistance thermometer in thermal contact with the paramagnetic salt, is to be calibrated absolutely, it is usual to calibrate the resistance against T^* and then to apply the $T-T^*$ relation, usually determined in another experiment or taken from previously published data. Though there is a good deal of evidence

that the $T-T^*$ relation at the very lowest temperatures depends markedly upon the thermal treatment of the salt,[2] calibrations by this method should be accurate within a few percent down to the region of, say, 0.1°K using iron or chrome alum.

The purpose of this note is to point out that it is possible to simplify this procedure and to perform the $R-T$ calibration without the need for magnetic measurements. Well-known methods can be adapted by substituting resistance measurements for susceptibility measurements, with certain practical restrictions to insure a good degree of thermodynamic reversibility. For example, using the fundamental relation $dQ=T\cdot dS$, and regarding R as a reversible temperature dependent parameter, we obtain $T=(dR/dS)/(dR/dQ)$, all referred to zero field. This is applied as follows. A series of demagnetizations is performed from known values of H/T_i (H being the magnetic field suitably corrected, T_i a temperature near 1°K), and the values of R determined at the low temperatures T attained after demagnetization. Assuming the value of the susceptibility at temperatures above T_i to be known, the entropy S at a temperature T can be calculated as a function of H/T_i and hence $(dR/dS)_{H=0}$ can be determined. The quantity $(dR/dQ)_{H=0}$ is then determined from observations of the changes of resistance produced by known heat inputs dQ at several points below 1°K.

This procedure does of course depend on a knowledge of the magnetic susceptibility of the salt above 1°K. It may be noted, however, that it is very rare indeed for an absolute susceptibility measurement to be performed as part of a $T-T^*$ calibration, the value being most often taken from other work, so the present method is no worse than usual in this respect. Deterioration of the salt—for example, as a result of prolonged exposure to a dry atmosphere—can affect the susceptibility.

This method was used for the absolute calibration, Fig. 1, of a nominal ½-watt, 100-ohm Erie "Ceramicon" radioresistor, which was soldered to metal fins embedded in a cylinder of powdered and compressed ferric ammonium alum. The cylindrical specimen of salt was of mass 6.5 g; the copper fins were of surface area 12 cm² and were 0.04 mm thick.

The points to be considered in such a system are (a) the rapidity of diffusion of transient temperature inhomogeneities within the salt, (b) the attainment of temperature equality between resistor and salt, (c) the temperature homogeneity within the resistor, (d) the effect on the final equilibrium temperature of the finite heat capacity of the fins and resistor, and (e) eddy current heat generation in the fins produced during demagnetization. We will now consider the conditions at 0.1°K. At this temperature the resistance of the resistor was 285 ohms and the measuring voltage across it was 100 μv. The thickness of the slabs of salt between successive pairs of fins was about 2 mm. Then (a) the observed thermal relaxation time for the thermometer to reach its steady state temperature, within the accuracy of measurement, was 7

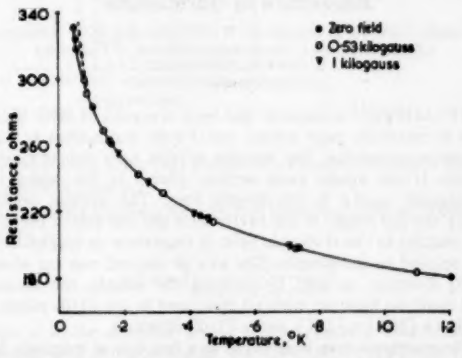

FIG. 1. Calibration curve of Erie "Ceramicon" ½-watt 100-ohm resistor.

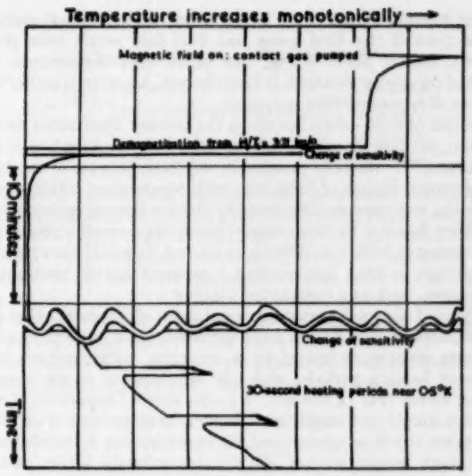

FIG. 2. Temperature changes of iron alum specimen with Allen Bradley 10-ohm resistor, taken from recording millivoltmeter.

minutes (increasing to 14 minutes at 0.05°K). This long time can however be decreased considerably by growing the crystals of salt around the fins and thus producing crystallites of large size with correspondingly larger thermal diffusivity. (b) The persistent temperature difference between the fins and the interior of the salt, caused by the steady outflow of heat from the resistor and fins into the badly conducting salt—a temperature difference which behaves as if it were due to the presence of a badly conducting layer between fins and salt—was reduced to a calculated value of not more than 0.01 percent of the absolute temperature.[3] The smallness of this difference depended on the use of a small measuring current and on the minimization of the inflow of heat down the electrical leads; these leads were constantan wires brought into thermal contact with the salt before reaching the fins. (c) Taking the thermal conductivity of the graphite of the resistor as 10^{-5} watt-unit,[4] the specific heat as 2 ergs g^{-1} deg^{-1} (using an unfavorable T^3 extrapolation of the data above 10°K),[5] the thermal relaxation time of the resistor was calculated to be less than 1 second and the temperature inhomogeneity inside it about 0.1 percent of the absolute temperature. (d) The mass of copper was 1.5 g, so the effect of the fins and resistor was to cause an increase of 0.3 percent in the final equilibrium temperature reached by a demagnetization to 0.1°K. It should be noted that this effect, in contrast to (a), (b), and (c), becomes more serious the higher the temperature, though never exceeding 1 percent. (e) Eddy current heat generation in the fins was made negligible by arranging the plane of the fins to be parallel to the magnetic field and by performing the act of demagnetization very slowly. The stray heat inflow into the salt was so small that, during tests of the reversibility of the demagnetization, times as long as 2 minutes could be taken to reduce the field to zero; further, several cycles of demagnetization and magnetization in the same field could be performed with good reproducibility of the final temperatures.

In Fig. 1 the points are those at which tangent lines to the smoothed $S-R$ graphs were drawn. In addition to demagnetizations to zero field, final fields of 0.53 and 1.00 kilogauss were also used; the curve shows that the magnetoresistive increases of this resistor were small in these fields even at the lowest temperatures. One further point concerning the experiment is that if the salts were reproducible from run to run, there should be no reason why the value of T should not be a unique function of H/T_i; that is, in principle there should be no need to make temperature measurements on the salt at all at the low temperatures if H/T_i is known.

Using smoothed data based on published work,[8] "blind" demagnetizations of this kind using zero final field would have given correct results above 0.1°K, but below that temperature the dashed curve was obtained. It is not known, however, whether this degree of reproducibility is typical.

In the (dR/dQ) determinations the resistor itself acted as the heater, but this proved something of an oversimplification of the apparatus. It was only possible in any case because of the relatively small change of resistance with temperature which meant that the temperature difference (b) did not become serious; with an Allen Bradley 10-ohm resistor, which has a much higher slope, the measurements were difficult to control. It would have been an advantage to have incorporated a separate heater, constant in resistance, such as a constantan winding.

Figure 2 shows the temperature changes on magnetization and demagnetization of an iron alum specimen, using an Allen Bradley 10-ohm resistor, as traced by a recording millivoltmeter; subsequent heating periods, with the temperature of the resistor rising above that of the salt, are also shown. Apparatus of this kind is simple and rugged and shows a large amount of detail of behavior; it will be appreciated, for example, that a knowledge of the exact temperature of the salt immediately before demagnetization is valuable in leading to reproducible results.

* Supported in part by the U. S. Office of Naval Research.
† In receipt of a grant for Further Education and Training from the Ministry of Education.
‡ Now returned to H. H. Wills Laboratory, University of Bristol, Bristol, England.
[1] For example, see de Klerk, Steenland, and Gorter, Physica **15**, 649 (1949).
[2] B. Bleaney and R. P. Penrose, Proc. Phys. Soc. (London) **A60**, 395 (1948). See also discussion at Proceedings of the International Conference on Low Temperature Physics, edited by R. Bowers (1951), p. 144.
[3] B. B. Goodman, thesis, Cambridge University, 1952 (unpublished).
[4] R. Berman, Proc. Phys. Soc. (London) **A65**, 1029 (1952).
[5] W. de Sorbo and W. W. Tyler, J. Chem. Phys. **21**, 1660 (1953).
[6] Casimir, de Haas, and de Klerk, Physica **6**, 241 (1939); A. H. Cooke, Proc. Phys. Soc. (London) **A62**, 269 (1949).

The Specific Heat of Liquid He^3*

T. R. Roberts and S. G. Sydoriak
Los Alamos Scientific Laboratory, Los Alamos, New Mexico
(Received January 18, 1953)

THE specific heat of saturated liquid He^3 containing less than 0.1 percent He^4 has been measured from 0.54°K to 1.7°K. The results were presented at the Third International Conference on Low Temperature Physics and Chemistry and are in general agreement with data reported there by two other groups of workers.[1]

The warmup rate $\dot{T}$ of liquid He^3 in a vacuum-jacketed ¼-cc copper sphere was measured as a function of N, the total number of moles of He^3 in the system. The He^3 was cooled below the surrounding He^4 bath temperature by pumping. The heat flux to the liquid $\dot{Q}$ was measured and a plot of $\dot{Q}/\dot{T}$ *versus* N yielded a straight line. The slope, when corrected[2] for vapor warming and for evaporation into the changing amount of vapor space within the sphere, equals the specific heat. This correction varied from 2.5±0.05 percent of C at 0.54°K to 40±1 percent at 1.7°K. With this method the effects of the noxious volume outside of the sphere and of the specific heat of the calorimeter are eliminated because they do not depend upon liquid level.

Measurements were made from 1.05°K to 1.7°K with $\dot{Q}$ supplied by an electrical heater. $\dot{T}$ was measured by the vapor pressure rise and averaged about 1° per hour. Each point is based on six warmups. The results are given in Table I.

TABLE I. Liquid He^3 specific heats measured with heater.

T°K	1.069	1.157	1.256	1.364	1.453	1.528	1.609	1.695
C cal/mole deg	1.06	1.12	1.19	1.25	1.35	1.44	1.46	1.54

TABLE II. Liquid He^3 specific heats measured without heater.

T°K	0.540	0.629	0.748	0.804	0.872	1.251
C/L deg^{-1}	0.109	0.110	0.110	0.107	0.111	0.123
C cal/mole deg	0.83	0.89	0.92	0.92	0.98	1.22

To reach lower temperatures, the heater was removed and $\dot{Q}$ derived from the measured normal heat leak. The sphereas w filled with iron ammonium alum at 55 percent packing for temperature measurement by the standard ballistic method. The salt was calibrated above 1°K against the Argonne He^3 vapor pressure equation.[3]

The average heat leak was determined from: ΔN, the number of moles of He^3 pumped during cooldown between successive warmups over the same 0.05° interval; the time between identical temperatures on these warmups; and the average latent heat over the interval. A correction was applied to the observed average heat flux for the measured 2 percent reduction in flux during cooldown. Since $\dot{Q} \propto L$, only C/L is measured directly. For L we used values calculated from an equation fitting preliminary vapor pressures measured down to 0.5°K. Each point is based on at least twelve warmups. The results are given in Table II.

Entropy differences in the range 0.5 to 1.7°K can be calculated from these data. When combined with our preliminary vapor pressure data we find the value of entropy at 0.50°K to be 1.38 ±0.04 cal mole^{-1} deg^{-1}. By coincidence this is just equal to the nuclear spin entropy, $R \ln 2$. Data from a few warmups starting at 0.4°K indicate that the entropy has decreased to 1.20±0.06 at 0.4°K, a value significantly below $R \ln 2$. Hence, as qualitatively predicted by Pomeranchuk,[4] nuclear spin alignment must begin at or above 0.5°K, and a melting-pressure minimum would be expected at this temperature. The reported[3] apparent constancy of melting pressures below 0.5°K is consistent with the existence of a minimum, since the blocked-capillary technique used could not detect a rise in melting pressures below the temperature of a minimum.

* This paper is based on work performed under a University of California contract with the U. S. Atomic Energy Commission.
[1] G. de Vries and J. G. Daunt; Osborne, Abraham, and Weinstock; Abstracts of Third International Conference on Low Temperature Physics and Chemistry, The Rice Institute, Dec. 17–22, 1953 (unpublished).
[2] Hull, Wilkinson, and Wilks, Proc. Phys. Soc. (London) **A64**, 379 (1951).
[3] Weinstock, Abraham, and Osborne, Phys. Rev. **89**, 787 (1953).
[4] I. Pomeranchuk, J. Exptl. Theoret. Phys. (U.S.S.R.) **20**, 919 (1950).

Directional Properties of the Cyclotron Resonance in Germanium*

Benjamin Lax, H. J. Zeiger, R. N. Dexter, and E. S. Rosenblum
Lincoln Laboratory, Massachusetts Institute of Technology, Cambridge, Massachusetts
(Received January 25, 1954)

CYCLOTRON resonance[1] has been observed at 8895 Mc/sec in relatively pure n-type and p-type germanium at liquid helium temperatures. The samples studied were rods of approximately 1 mm square cross section, placed in the center of a rectangular cavity ¾ wavelength long. The sample occupied nearly the full height of the cavity with the rod axis in the direction parallel to the rf electric field. A transverse dc magnetic field was applied to the sample. The axis of the rod was cut along a [110] direction, so that by rotating the sample, the magnetic field could be lined up with all directions in the (110) plane, including a [100], a [111], and a [110] direction.

The resonance data were taken as a function of magnetic field, by means of an automatic recording system. The rf power down

the guide was kept at a low level, so that the electric field in the cavity was ~0.1 volt/cm. This field is well below "avalanche ionization,"[1,2] which was observed at ~4 volts/cm.

The resonance curves obtained in the n-type Ge sample show a marked dependence on sample orientation, as shown in Fig. 1. The effect differs from the previously reported results on cyclotron resonance[1] in $n-$Ge.

The positions of the resonance peaks observed in n-type germanium seem inconsistent with the model[3,4] of six ellipsoidal energy surfaces along the [100] directions in reciprocal lattice space. The data are well described by a conduction band structure in which the Brillouin energy surfaces consist of eight ellipsoids of revolution lying along [111] axes, with a longitudinal mass m_1 and a transverse mass m_2.

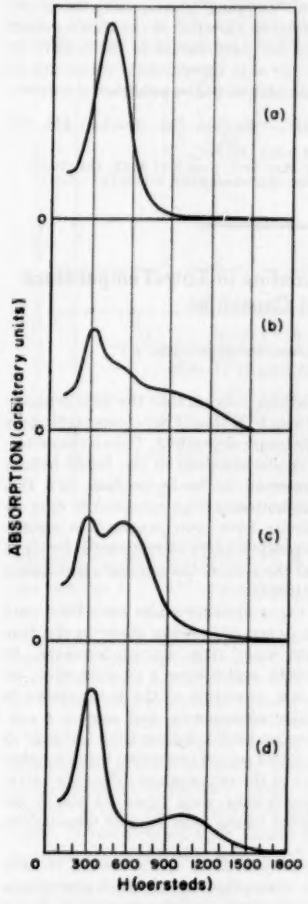

FIG. 1. Resonance absorption in intrinsic n-type Ge at 4.2 °K. The curves show data taken at four values of θ in the (110) plane as a function of the external magnetic field intensity H. θ is the angle between H and the [100] direction. (a) $\theta=0°$, [100]. (b) $\theta=37°$. (c) $\theta=55°$, [111]. (d) $\theta=90°$, [110].

For a single ellipsoid, the effective mass for cyclotron resonance is given by:

$$m^*=m_2\left(\frac{m_1}{m_1\alpha^2+m_2(1-\alpha^2)}\right)^{\frac{1}{2}}, \qquad (1)$$

where α is the direction cosine of the magnetic field with the principal axis of the ellipsoid. For the [100], [111], and [110] directions, Eq. (1) gives the following effective cyclotron masses and weightings:

$$[100]: m^*=m_2[3m_1/(m_1+2m_2)]^{\frac{1}{2}}, \quad \text{(8 times)}$$

$$[111]: \begin{cases} m^*=m_2, & \text{(2 times)} \\ m^*=3m_2[m_1/(m_1+8m_2)]^{\frac{1}{2}}, & \text{(6 times)} \end{cases}$$

$$[110]: \begin{cases} m^*=m_2[3m_1/(2m_1+m_2)]^{\frac{1}{2}}, & \text{(4 times)} \\ m^*=[m_1m_2]^{\frac{1}{2}}. & \text{(4 times)} \end{cases}$$

Although in general the assumed band structure predicts four effective masses in an arbitrary direction, two of these coincide in the (110) plane. This is consistent with the appearance of 3 "bumps" in the resonance curve of Fig. 1(c). The half-width was observed to increase with the effective mass, as shown in Fig. 1. The width in the [100] direction, where the effective mass is $\sim 0.12m_0$, is ~50 percent wider than that previously reported in $n-$Ge, where the effective mass was $0.11m_0$.[1]

The values of m_1 and m_2 were calculated from the resonance peaks in the [110] direction. The values obtained were:

$$m_1=1.3m_0, \quad m_2=0.08m_0,$$

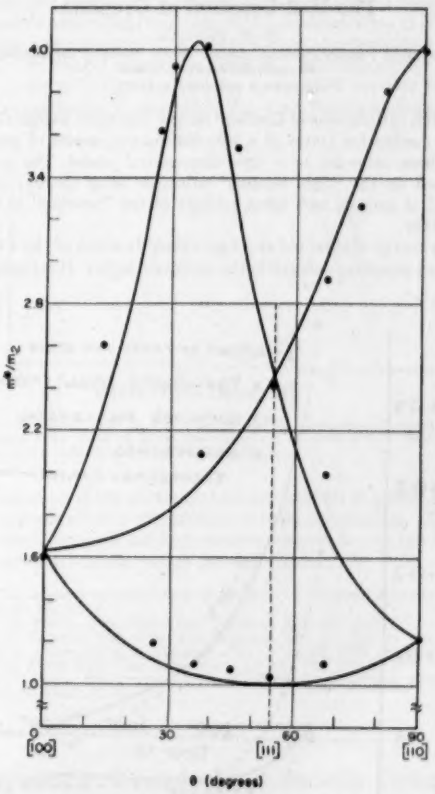

FIG. 2. Variation of the effective electronic mass m^* in a (110) plane as a function of θ. m^* is rationalized by the transverse mass $m_2=0.08\ m_0$. The solid lines are theoretical curves. The dots are experimental points.

where m_0 is the free electron mass. Figure 2 shows a comparison of theoretical and experimental values of m^*/m_2 as a function of sample orientation for these values of m_1 and m_2.

Similar resonance experiments in a relatively pure p-type Ge sample showed no directional effects. The peak positions for resonance, corresponding to $0.04m_0$ and $0.30m_0$, are consistent with those observed earlier by Dresselhaus, Kip, and Kittel.[1] The line breadths of ~250 and 580 oersteds are broader than theirs.

To exclude possible errors due to "dimensional resonances," the sample was reduced in size to 0.6 mm square cross section. The resonance lines were not affected. It is also reasonable to exclude the effect of sample shape on the spectra, since p-type samples of the same shape show no directional effects. No difference in the results was observed for etched or unetched samples.

We would like to thank Professors H. Brooks, N. Bloembergen, and Dr. G. Koster for several helpful discussions. We are indebted to Dr. H. F. Priest for providing the Ge samples, to Dr. D. Tuomi for orienting the crystals, and to other members of the solid state groups of Lincoln Laboratory for their cooperation.

* The research in this document was supported jointly by the U. S. Army, Navy, and Air Force under contract with the Massachusetts Institute of Technology.

[1] Dresselhaus, Kip, and Kittel, Phys. Rev. **92**, 547 (1953).
[2] Sclar, Burstein, Turner, and Davisson, Phys. Rev. **91**, 215 (1953).
[3] W. Shockley, Phys. Rev. **90**, 393 (1953).
[4] F. Herman, Phys. Rev. **88**, 1210 (1953).

The Hall Constant of Graphite

D. F. JOHNSTON
Theoretical Physics Division, Atomic Energy Research Establishment, Harwell, Berkshire, England
(Received February 2, 1954)

THE calculations of Coulson[1] on the electronic energies of the conduction states of a two-dimensional model of graphite have been extended to a three-dimensional model. The method is based on the "tight-binding" principle using the $2p_z$ atomic orbital of carbon, and takes account of the "overlap" of many neighbors.

The energy is obtained as a four-valued function of the k vector within a primitive unit cell in the reciprocal lattice. It is found that the first of these "bands" of states is effectively fully occupied, the second is almost fully occupied, the third is almost empty, and the fourth is effectively empty. The first and second bands "touch" all over the upper and lower faces of this primitive unit cell and so do the third and fourth bands. The second and third bands "touch" along certain lines parallel to the c axis in the reciprocal lattice. The lowest energy of the third band comes just below the highest energy of the second band, so there are "free" electrons even at absolute zero.

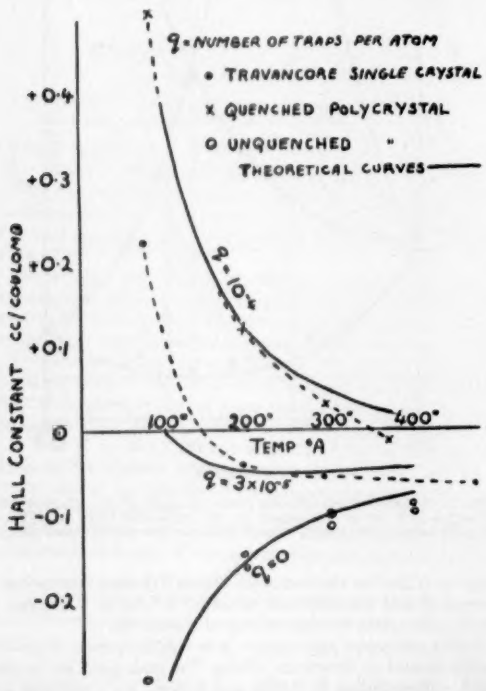

FIG. 1. Hall constant as a function of temperature. The experimental values are those of Kinchin.

This presentation of the energy levels in k space was adopted in order to overcome the difficulties associated with the extended zone scheme commented on by Mrozowski in a recent letter in this journal.[2]

This knowledge of the electronic energies has been used as the basis for a calculation of the Hall constant of graphite as a function of temperature and number of "trapping" states, using the model of Jones and Zener.[3] The theoretical variation of the Hall constant as a function of temperature for given values of the density of traps is shown in Fig. 1 together with experimental values due to Kinchin.[4] The details of the calculation will be published elsewhere.

[1] C. A. Coulson and R. Taylor, Proc. Phys. Soc. (London) **A65**, 815 1952).
[2] S. Mrozowski, Phys. Rev. **92**, 1320 (1953).
[3] H. Jones and C. Zener, Proc. Roy. Soc. (London) **A145**, 268 (1934).
[4] G. H. Kinchin, Proc. Roy. Soc. (London) **A217**, 9 (1953).

Some Apparent Anomalies in Low-Temperature Heat Capacities

J. R. CLEMENT
Naval Research Laboratory, Washington, D.C.
(Received January 27, 1954)

THEORETICAL calculations indicate that the heat capacity of a crystalline lattice near 0°K should be representable by a smooth, monotonically temperature dependent, Debye characteristic temperature.[1] Certain results obtained in the liquid helium temperature range have appeared to be in conflict with this prediction, two notable examples being some calorimetric data on KCl[2] and Ag.[3] Various schemes have been proposed to explain these discrepancies,[4] but the possible effect of systematic errors in the temperature scale used at the time of the original experiments seems not to have been investigated.

Numerous liquid helium vapor pressure scales have been used in the past,[5] each new scale presumably being closer to the true thermodynamic temperature scale than its predecessors. In calorimetry, differences between scales have a twofold effect on resultant data. First there is a correction of the temperature to which the heat capacity value corresponds, and second, a correction of the heat capacity value itself resulting from a change in the temperature rise involved, this second correction being roughly proportional to the derivative of the temperature difference curve. Before testing theoretical predictions, data based on one of the older scales should be corrected to the most reliable temperature scale known.

Because of the necessity for secondary thermometers in calorimetry, a difficulty arises in attempting to make such corrections, namely, an uncertainty concerning possible smoothing of the secondary thermometer calibration data. Nevertheless, it seemed worth while to study the effect on calorimetric data of improvements in the temperature scale, assuming the secondary thermometer to reproduce exactly the vapor pressure scale (except for slight smoothing near the λ point in some cases). Evidence favoring this assumption follows. In 1932 Keesom and Kok[6] measured the atomic heat of tin very thoroughly in the neighborhood of the transition from the superconducting to the normal state, using a phosphor bronze thermometer calibrated according to the "1929" scale. They concluded that the transition from the superconducting to the normal state (in an applied field of 2 gauss) occurred at 3.705(±0.006)°K. Correcting their observed transition

for the 2-gauss field and for the difference between the "1929" and "1949" scales gives a zero field transition on the "1949" scale of 3.731(±0.006)°K, a value in perfect agreement with that which can be deduced for natural tin from recent, precise isotope measurements based on the "1949" scale.[7,8]

Employing the above assumption, the pertinent KCl and Ag calorimetric data[2,3] were corrected to the "1949" scale (below 4.3°K). The results for KCl are shown in Fig. 1B, the original uncorrected data being reproduced for comparison in Fig. 1A. What appeared to be a significant "anomaly" in the original data has been essentially removed. Some recent data[9] have also been included in Fig. 1B and are in excellent agreement with the older corrected data. The result for Ag was practically equivalent to that for KCl, a strikingly similar "anomaly" in the characteristic temperatures being effectively removed.[10]

Finally it may be noted that the Debye characteristic temperatures obtained by Keesom and Pearlman[9] for KCl (using the "1949" scale) show a sharp rise below 2.2°K. The data on which

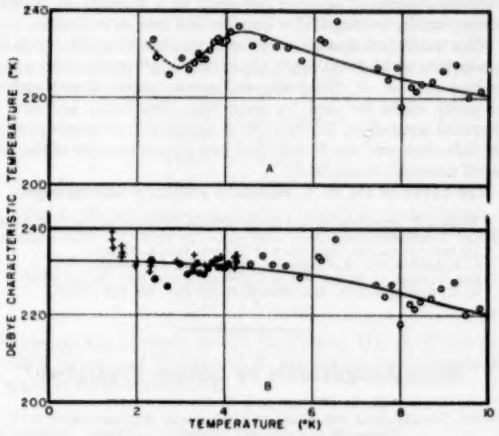

FIG. 1. Debye characteristic temperature of KCl. ○ Uncorrected data of Keesom and Clark (see reference 2); ● data of Keesom and Clark (see reference 2); corrected to "1949" scale; + data of Keesom and Pearlman (see reference 2) ("1949" scale).

the "1949" scale is based have been questioned by Kistemaker,[11] and it is interesting to note that if Kistemaker's results are used to determine a new vapor pressure scale and the KCl data of Keesom and Pearlman corrected to this new scale, the sudden rise in their characteristic temperatures is substantially reduced.

The principal conclusion to be drawn here is that systematic differences between an actual temperature scale and the true thermodynamic scale may cause apparently significant "anomalies" in calorimetric results, so that the presence of systematic errors in temperature scale should at least be investigated as a possible source of small "anomalies" when they occur.

[1] M. Blackman, Repts. Progr. Phys. **8**, 11 (1941).
[2] W. H. Keesom and C. W. Clark, Physica **2**, 698 (1935).
[3] W. H. Keesom and J. A. Kok, Proc. Amsterdam Acad. Sci. **35**, 301 (1932); Physica **1**, 770 (1934).
[4] See, e.g., P. H. Keesom and N. Pearlman, Phys. Rev. **88**, 140 (1953).
[5] These scales are: "1924," "1929," "1932" [see W. H. Keesom, Leiden Comm. Suppl. 71d (1932)], "1937" [G. Schmidt and W. H. Keesom, Physica **4**, 971 (1937)], "1939" [R. Bleaney and F. Simon, Trans. Faraday Soc. **35**, 1205 (1939)], and "1949" [H. van Dijk and D. Schoenberg, Nature **164**, 151 (1949)]. See also W. H. Keesom, *Helium* (Elsevier Publishing Company, Amsterdam, 1942), pp. 186–201.
[6] W. H. Keesom and J. A. Kok, Proc. Amsterdam Acad. Sci. **35**, 743 (1932).
[7] E. Maxwell, Phys. Rev. **86**, 235 (1952).
[8] Lock, Pippard, and Shoenberg, Proc. Cambridge Phil. Soc. **47**, 811 (1951).
[9] P. H. Keesom and N. Pearlman, Phys. Rev. **91**, 1354 (1953).
[10] Compare Debye characteristic temperature curves given by Keesom and Clark (see reference 2).
[11] J. Kistemaker, Physica **12**, 272, 281 (1946).

Further Evidence for the Energy Gap of Lead Sulfide*

GEORGE R. MITCHELL AND ARTHUR E. GOLDBERG
Chicago Midway Laboratories, Chicago, Illinois
(Received February 1, 1954)

THERE has been some question regarding the value of the energy gap for PbS. The thermal activation energy (1.17 ev) disagrees with the adsorption edge of single crystals and the long-wavelength limit of photoresponse of PbS thin films.[1–3] Recently, Moss published curves showing the wavelength dependence of the photoelectromagnetic effect in natural galena and gave evidence that the quantum efficiency of the photoresponse is of the order of unity.[4] He concluded that the energy gap is very close to 0.41 ev.

In the course of growing PbS single crystals from the vapor phase, a *p-n* junction was found that exhibited a small photovoltaic effect. The response time was not greater than 150μ sec, thus ruling out the possibility of a thermal effect. According to present theory the photovoltage results mainly from the production of minority carriers.[5] It is most probable that the minority carriers are produced by band-to-band transitions. Conceivably, minority carriers could be produced by photoexcitation of impurity centers. Since the activation energy for impurity ionization is very small, the energy required to produce a minority carrier in this way is virtually that required for a transition between full and conduction bands. Compared in Fig. 1 are the equal-energy spec-

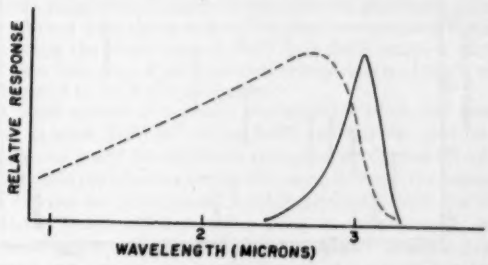

FIG. 1. Photoeffects in PbS: dashed curve, photoelectromagnetc effect in galena from data of Moss (see reference 4); solid curve, photovoltaic effect in *p-n* junction in synthetic single crystal.

tral responses of the photoelectromagnetic effect in galena and the photovoltaic effect in the junction at room temperature. The good agreement between the long-wavelength cutoffs supplies further confirmation that the energy gap is 0.4 ev.

* This research was supported in whole by a contract with the United States Air Force.
[1] E. H. Putley, Proc. Phys. Soc. (London) **B65**, 388 (1952).
[2] A. F. Gibson, Proc. Phys. Soc. (London) **B65**, 378 (1952).
[3] M. A. Clark and R. J. Cashman, Phys. Rev. **85**, 1043 (1952).
[4] T. S. Moss, Proc. Phys. Soc. (London) **B66**, 993 (1953).
[5] T. S. Moss, *Photoconductivity in the Elements* (Academic Press, Inc., New York, 1952), p. 50.

Temperature Dependence of Periodic Deviations from the Schottky Line*

G. A. HAAS† AND E. A. COOMES
University of Notre Dame, Notre Dame, Indiana
(Received February 1, 1954)

ALTHOUGH the importance of the $1/T$ dependence of the amplitude in periodic Schottky deviations to electron emission theory has been stressed,[1] a completely satisfactory experimental study of this effect has been hindered by patch effects. Recent Schottky data taken on a specimen of polished molybdenum wire revealed a long patch-free region $100<\xi<300$ (volts cm^{-1})$^{\frac{1}{2}}$. This allowed a precise separation of deviations from

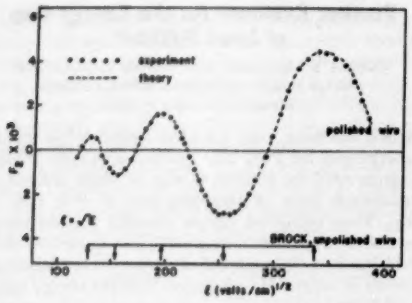

FIG. 1. Periodic deviations in the Schottky effect for a polished molybdenum filament, at 1600°K.

which accurate amplitude determinations could be made, an example of which is given in Fig. 1. In this figure the points are experimental, the dotted curve theoretical,[2] while the arrows along the axis of abscissas mark experimental extrema obtained for unpolished molybdenum filaments.[3] The amplitude maximum taken at $\xi=200$ from deviation curves for various temperatures is plotted against $1/T$ in Fig. 2. While some uncertainty is involved

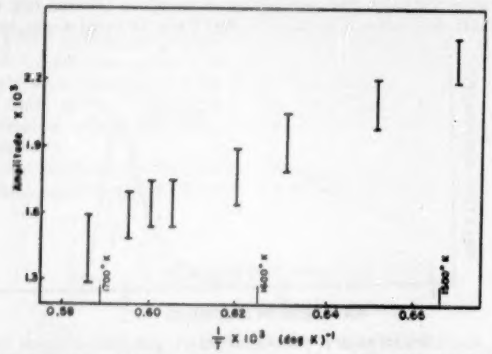

FIG. 2. Periodic deviation amplitude maximum at $\xi=200$, plotted against $1/T$. The range in amplitude indicates uncertainty in locating extrema on the deviation plot. (See Fig. 1.)

in locating the exact maximum of deviations, as indicated by the range at a given temperature, the tendency to increase with $1/T$ seems definitely apparent.

* Sponsored by the U. S. Navy Bureau of Ships.
† Now at the U. S. Naval Research Laboratory, Washington, D.C.
[1] W. B. Nottingham, Phys. Rev. 57, 935 (1940); E. Guth and C. Mullin, Phys. Rev. 60, 535 (1941).
[2] Juenker, Colladay, and Coomes, Phys. Rev. 90, 772 (1953).
[3] Brock, Houde, and Coomes, Phys. Rev. 89, 851 (1953).

Radioactive Isotope Separation by Nuclear Recoil*

H. MORINAGA† AND D. J. ZAFFARANO
Institute for Atomic Research and Department of Physics, Iowa State College, Ames, Iowa
(Received January 13, 1954)

NUCLEAR reactions such as (γ,n), (d,p), and $(\alpha,2p)$ lead to product nuclides with the same atomic number as the initial nuclides. Unless the Szilard-Chalmers process[1] is practicable, it is usually difficult to achieve high specific activity for the product isotope. With light nuclei, however, the recoil momentum of the product nucleus can afford sufficient range to allow physical separation, as is clearly visible in nuclear emulsions.[2] When the ranges of the product nuclei are of the order of a micron, i.e., the size of colloidal particles, one may expect that in a fine powder mixture or in a colloidal suspension one phase or element can act as donor and the other as catcher. If the grain size of the donor is comparable to or smaller than the range of the recoiling product nucleus, the probability of stopping the radioactive nucleus within the "catcher phase" becomes high. Therefore, radioactive atoms will be transferred to the catcher phase from the donor phase.

To verify this experimentally, a preliminary experiment has been done using the $C^{12}(\gamma,n)C^{11}$ reaction in colloidal graphite solution. "Aquadag" solution of about 0.5-percent carbon by weight was bombarded by x-rays from the 70-Mev bremsstrahlung beam from the Iowa State College synchrotron, together with a control sample of powdered carbon. The colloid was precipitated and identical counting samples were prepared from the two target materials. It was found that the carbon bombarded as a colloid lost as much as 80 percent of its activity into the water phase. This result is understandable, since the carbon particles in "Aquadag" consist of small slabs with an approximate diameter of $\frac{1}{10}$ micron and much smaller thickness. The energies of recoiling C^{11} nuclei are expected to be of the order of a fraction of a Mev, corresponding to ranges of a fraction of a micron in carbon.

This method of separating isotopes may have importance in the production of Mg^{28} by $Mg^{26}(\alpha,2p)$.[3] For Mg^{28} production, a compressed powder of mixed Mg and some catcher metal such as tungsten might be used for good heat dissipation and ease of chemical separation. In the case of alpha-particle bombardment, particle sizes need not be less than one micron because of the high recoil momentum available.

The advice of Dr. R. S. Hansen is gratefully acknowledged.

* Work was performed in part in the Ames Laboratory of the U. S. Atomic Energy Commission.
† On leave from the University of Tokyo, Tokyo, Japan.
[1] L. Szilard and T. A. Chalmers, Nature 134, 462 (1934).
[2] For example, C. Millar and A. Cameron, Phys. Rev. 78, 78 (1950).
[3] R. K. Sheline and N. R. Johnson, Phys. Rev. 89, 520 (1953).

Mass Assignments by Isotope Separation*

M. C. MICHEL AND D. H. TEMPLETON
Radiation Laboratory and Department of Chemistry, University of California, Berkeley, California
(Received January 19, 1954)

A TIME-OF-FLIGHT isotope separator constructed in this laboratory[1] has been used to assign mass numbers to several radioactive isotopes produced in cyclotron bombardments. Atoms of the mass numbers in question have been separated and the corresponding activity observed with a Geiger counter or other counting equipment.

The essential features of the instrument are high transmission (about 20 percent) at a resolution such that the separation factor between adjacent isotopes in the mass range 100–250 is about 100 or larger. In addition, the instrument is calibrated absolutely so that any desired mass number can be selected without the necessity of observing ion currents due either to the isotope being separated or to added stable isotopes.

Several isotopes of cesium (formed by α,xn reactions on iodine) have been separated in the course of work on their decay properties. Chemically separated carrier-free cesium sulfate fractions were ionized from a surface ionization source for this work. The previous assignments[2] of Cs^{127} and Cs^{129} were verified, with sufficient activity separated to establish the half-life of Cs^{127} as 6.1 ± 0.2 hours instead of the previously reported 5.5 hours. In addition, Cs^{130} has been separated and its half-life observed to be 30 minutes, in agreement with the previous result.[2]

A new isotope of cesium found by Mathur and Hyde of this laboratory, has been assigned to mass 125 and its half-life observed (from separated samples) to be 45 ± 1 minutes.

In connection with an investigation of the decay scheme of Cs^{136} by Olsen and O'Kelley[3] a large quantity of this isotope was separated for use in a beta spectrometer study of its decay. On the basis of the decay of part of the separated sample over nine half-

lives, the half-life has been determined by Olsen and O'Kelley as 12.9 days.

The neutron deficient thallium isotopes formed by bombardment of thick gold targets with 40-Mev helium ions have been separated and assigned directly. The activities at mass 199 and 200 have half-lives of 7.4±0.2 hours and 27±1 hours, respectively, and show gamma spectra in excellent agreement with the conversion electron work of Israel and Wilkinson.[4] The activity associated with mass 198 showed two distinct periods of 1.75 and 5.3 hours. These have been assigned to Tl^{198m} and Tl^{198}, respectively, by observation of the isomeric transition in the shorter isomer.[5] The ground state was independently discovered by Bergstrom, Hill, and de Pasquali at the University of Illinois.

Tl^{204}, produced by neutron capture in natural thallium, has recently been separated to test if an isomer of Tl^{206} is the cause of the various reports[7-9] of the half-life of Tl^{204}. Direct observation of the ion current due to Tl^{204} has also been made in a conventional magnetic mass spectrometer. No long-lived Tl^{206} could be detected by either method.

Considerable work with the heavy rare earth elements has been done with Nervik and Seaborg and will be reported separately. However, the following previously known isotopes have been assigned in the course of this work (half-lives are by direct observation of the decay of separated samples):

Yb^{166}	58±1 hours,
Yb^{169}	32 days,
Tm^{166}	7.7 hours,
Tm^{167}	9.6 days.

In addition, the following new isotopes formed in the spallation of tantalum with 350-Mev protons have been assigned:[10]

Tm^{165}	29 hours,
Er^{160}	30 hours,
Er^{161}	3.5 hours.

We would like to thank Mr. H. B. Mathur, Mr. W. E. Nervik, Dr. E. K. Hyde, and Professor G. T. Seaborg for their cooperation in many of these experiments.

* This work was done under the auspices of the U. S. Atomic Energy Commission.

[1] M. C. Michel and D. H. Templeton (to be published).
[2] Fink, Reynolds, and Templeton, Phys. Rev. 77, 614 (1950).
[3] J. L. Olsen and G. D. O'Kelley (to be published).
[4] H. I. Israel and R. G. Wilkinson, Phys. Rev. 83, 1051 (1951).
[5] Passell, Michel, and Bergstrom (unpublished).
[6] Bergstrom, Hill, and de Pasquali, Phys. Rev. 92, 918 (1953).
[7] Hollander, Perlman, and Seaborg, Revs. Modern Phys. 25, 469 (1953).
[8] K. Fajans and A. F. Voight, Phys. Rev. 60, 619 (1941).
[9] G. Harbottle, Phys. Rev. 91, 1234 (1953).
[10] The decay curves in these cases gave no evidence of the growth of daughter activities. If such growth occurred, the reported half-lives are too long.

Decay Properties of Am^{243} and Possible Rotational Bands in the Alpha Spectra of Odd-Even Nuclei

FRANK ASARO AND I. PERLMAN
Radiation Laboratory and Department of Chemistry, University of California, Berkeley, California
(Received January 20, 1954)

THE principal aim of this note is to show the close similarity in the alpha spectra of Am^{242} and Am^{241} insofar as comparison is possible and to suggest an interpretation for some of the observed levels. In earlier publications[1,2] the similarities in the spectra of even-even alpha emitters were demonstrated, and it now appears that alpha emitters with odd nucleons have points of similarity with each other but have a distinctly different pattern than the even-even nuclei.

The alpha-emitter Am^{242} was first prepared[3] through neutron capture by Am^{241} and its presence detected by observing the growth of Np^{239}. From mass spectrographic analysis of the americium and the amount of Np^{239} which grew, the half-life was estimated to be $\sim 10^4$ years.[3] The neutron irradiation of plutonium containing Pu^{242} creates Am^{243} through the intermediary Pu^{243} which is a short-lived β^- emitter,[4] and sufficient Am^{242} relative to Am^{241} could be produced in this way to measure the alpha-particle energy (5.27 Mev) with an ionization chamber.[5,6]

The sample of Am^{243} used for magnetic analysis in the present study was prepared by plutonium (Pu^{239}) irradiation. Only about 2 percent of the alpha activity was due to Am^{242} and the rest was Am^{241}.[7] Nevertheless, the more prominent features of the Am^{243} alpha spectrum could be measured. From the resolved alpha spectra and the isotopic abundance of Am^{242} in the sample, the half-life was calculated to be 7.6×10^3 years. The magnetic spectrograph has been described in earlier publications.[5,6]

Three alpha groups attributable to Am^{243} were observed with energies and abundances as indicated in Fig. 1. The alpha groups of Am^{241} were used as energy standards.[8] In comparing the spectrum with that of Am^{241}, it will be noted that the main group of Am^{241} (84 percent abundance) populates a state 60 kev above the ground state,[10] and the main group of Am^{243} (84 percent abundance) leads to an excited state of 75 kev. The alpha-gamma coincidence measurements which established this decay sequence will be mentioned presently. Each alpha emitter has a transition in about 14 percent abundance of some 40-kev lower energy than the main alpha transition and each has a low-intensity group of about 55-kev still lower energy. It is seen that the parallelism is close for those transitions which can be compared.

The ground-state alpha transition for Am^{243} was not observed, but the limit of detection was 2.5 percent and it will be noted that the corresponding transition for Am^{241} is found in only 0.3 percent abundance. Similarly, if there is a low-abundance transition (energy level shown as a broken line) corresponding to that populating the 33-kev state of Np^{237} from Am^{241} decay, it would not have been seen. Purer and more intense souces of Am^{243} will be required to see if this state exists.

A small amount of a sample was available which had about twice as much Am^{243} activity as Am^{241}, and this was used for a gamma-ray study. A scintillation spectrometer triggered by coincident alpha particles was employed in order to obtain the gamma-ray energies and abundances. A single prominent peak was obtained at 75 kev which showed a hump on the low-energy side presumably due to the 60-kev gamma ray of Am^{241}. Since the Am^{241} content was known, its contribution to the gamma-ray peak could be subtracted. The result was that the 75-kev gamma ray was found to accompany 80 percent of the total Am^{243} alpha particles. This means that the conversion coefficient cannot be greater than 0.25 and fixes this transition as $E1$ just as is the case for the 60-kev transition of Am^{241}.[11] (The conversion coefficients of 75-kev $M1$ and $E2$ transitions should be 10 or greater.[12])

If we consider those components of the Am^{243} spectrum which lead to the 75-kev state and to the next two higher states, we note a marked resemblance to the ground state and first two excited states of an even-even alpha emitter like Cm^{242}.[13] The similarity includes energy level spacings and the intensities of the alpha groups. In the case of an even-even nucleus this type of spectrum has been interpreted as a rotational band comprising the states 0+, 2+, and 4+.[13]

According to the theory of Bohr and Mottelson,[14] the rotational states of an odd-nucleon case could have the following energy and

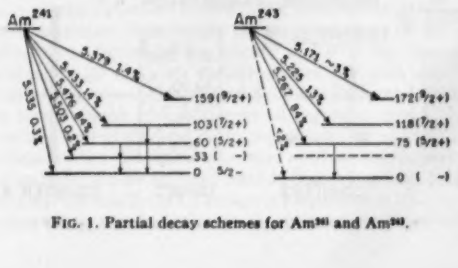

FIG. 1. Partial decay schemes for Am^{241} and Am^{243}.

spin sequence:

$$E_I=\frac{\hbar^2}{2\mathcal{I}}[I(I+1)-I_0(I_0+1)];\quad I=I_0,\quad I_0+1,\quad I_0+2,\cdots,$$

where I_0 is the spin of the lowest state in the band.

If one has three adjacent states belonging to a rotational band, it should be possible to calculate I_0 (and therefore I_0+1 and I_0+2) as well as the quantum of rotation, $\hbar^2/2\mathcal{I}$. On this basis the spins of the states reached by Am^{241} α_{60} and Am^{243} α_{75} were calculated to be 2.3 and 2.8, respectively. Since the spins must be half-integral, the closest value is 5/2. This same treatment of Am^{241} data was made by Rasmussen[15] who arrived at similar conclusions for the spin numbers of the excited states. It should be mentioned that the calculated spin number is sensitive to the accuracy of the energies of the states. If the measured energy difference between Am^{241} α_{60} and α_{103} were 44 kev instead of 43 kev, the value obtained for I_0 would have been 2.8 instead of 2.3.

From shell-model considerations, the ground states of Np^{237} and Np^{239} are assigned odd parity. Since the 60-kev and 75-kev transitions are $E1$, the levels belonging to the rotational band have even parity. The spin and parity assignments made on this basis are shown in Fig. 1. The spin number 5/2 for the ground state of Np^{237} is a measured value.[16]

[1] F. Asaro and I. Perlman, Phys. Rev. **87**, 393 (1952).
[2] F. Asaro and I. Perlman, Phys. Rev. **91**, 763 (1953).
[3] Street, Ghiorso, and Seaborg, Phys. Rev. **79**, 530 (1950).
[4] Thompson, Street, Ghiorso, and Reynolds, Phys. Rev. **84**, 165 (1951).
[5] A. Ghiorso (unpublished). (See reference 6.)
[6] Hollander, Perlman, and Seaborg, Revs. Modern Phys. **25**, 459 (1953).
[7] We wish to thank Dr. S. G. Thompson and Dr. G. H. Higgins for making this sample, and others, available to us and Mr. F. L. Reynolds for making the mass spectrographic analysis. This sample was prepared by the irradiation of a plutonium sample in the Chalk River pile and we wish to thank the staff of Atomic Energy of Canada Ltd., for making this irradiation.
[8] F. L. Reynolds, Rev. Sci. Instr. **22**, 749 (1951).
[9] Asaro, Reynolds, and Perlman, Phys. Rev. **87**, 277 (1952).
[10] It was earlier reported (reference 9), that the 60-kev transition did not lead to the ground state of Np^{237} but to an ~10-kev excited state. This was based on the observation of a low-intensity alpha group of 10-kev higher energy than the one now thought to be the most energetic group. A change in the baffle system of the spectrograph eliminated this group as well as fictitious high-energy groups noted with some other alpha emitters.
[11] Beling, Newton, and Rose, Phys. Rev. **87**, 670 (1952); **86**, 797 (1952).
[12] Gellman, Griffith, and Stanley, Phys. Rev. **85**, 944 (1952).
[13] Asaro, Thompson, and Perlman, Phys. Rev., **92**, 694 (1953).
[14] A. Bohr and B. R. Mottelson, Phys. Rev. **89**, 316 (1953); Kgl. Danske Videnskab. Selskab, Mat.-fys. Medd. **27**, No. 16 (1953).
[15] J. O. Rasmussen, Jr., Arkiv Fysik (to be published).
[16] F. S. Tomkins, Phys. Rev. **73**, 1214 (1948).

Cross Sections for p-p Scattering at 330 and 225 Mev*

O. Chamberlain, G. Pettengill, E. Segrè, and C. Wiegand
Radiation Laboratory and Department of Physics, University of California, Berkeley, California
(Received January 25, 1954)

THE total cross sections for scattering of high-energy protons by protons have been directly measured at the full and at one reduced energy of the Berkeley synchrocyclotron. Attenuation of the external proton beam in liquid hydrogen was measured with standard counting techniques in order to check, by an independent method, the results obtained in previous differential scattering experiments.

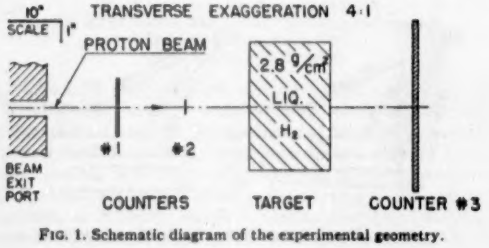

FIG. 1. Schematic diagram of the experimental geometry.

Figure 1 shows the experimental setup. The counting rate of counters 1–2–3 in coincidence was subtracted from the 1–2 coincidence rate and divided by the latter to obtain the attenuation occurring between counters 2 and 3. The difference in this quantity for the target filled with liquid hydrogen and for the empty target is attributed to scattering of the beam through an angle greater than the average half-angle subtended by the rear counter (No. 3).

The experiments were made with the full-energy beam (340 Mev) and at an energy of 240 Mev. Reduction of the beam energy was achieved by inserting 7¼ inches of beryllium in the path of the emerging beam before the existing analyzing magnet inside the shielding. Counting difficulties arising from the low duty cycle of the synchrocyclotron were minimized by holding the average external beam level below 10 protons per second. The use of scintillation counters ensured counting efficiencies of substantially 100 percent and also allowed a pulse-height investigation of beam homogeneity. The target is constructed of polystyrene foam.

Thus we have measured directly the attenuation f and may calculate:

$$\sigma_{\rm obs}=\frac{M(f_H-f_B)}{\rho l[1-\frac{1}{2}(f_H+f_B)]},$$

where the subscripts H and B refer to target filled and empty, respectively, M is the mass of the hydrogen atom, and ρl is the surface density of the liquid hydrogen in the target. The small values of f obtained (not exceeding 0.05) justify the degree of approximation involved in the equation. $\sigma_{\rm obs}$ is related to the differential scattering cross section through the expression

$$\sigma_{\rm obs}=\int_{\theta_{\rm min}}^{90^\circ}\frac{d\sigma}{d\Omega}2\pi\sin\theta d\theta=2\pi\cos\theta_{\rm min}\left\langle\frac{d\sigma}{d\Omega}\right\rangle_{Av},$$

where $\theta_{\rm min}$ is the average half-angle subtended by the rear counter in the center-of-mass system and was varied around 18° in this experiment. It should be noted that this angle is too large to include the Rutherford scattering at either energy, or the small contribution from the inelastic reaction $p+p\rightarrow\pi^++d$ at the full energy. The values obtained were

Mean energy (Mev)	$\langle d\sigma/d\Omega\rangle_{Av}$ in units of 10^{-27} cm²/sterad
330	3.72±0.15
225	3.56±0.15

The errors shown include statistical and target-thickness uncertainties.

Since previous differential scattering work has shown, for the energies considered here, that $d\sigma/d\Omega$ is essentially constant over the range of angles included in $\sigma_{\rm obs}$, $\langle d\sigma/d\Omega\rangle_{Av}$ may be compared directly with the corresponding differential data. In this comparison our experimental results are consistent with those of a previous paper[1] and those of Marshall *et al.*,[2] but seem at variance with the results of Oxley and Schamberger[3] and Towler.[4]

Extension of this method to a lower energy is planned in the near future, after which a complete report will be submitted.

* This work was done under the auspices of the U. S. Atomic Energy Commission.
[1] Chamberlain, Segrè, and Wiegand, Phys. Rev. **83**, 923 (1951).
[2] Marshall, Marshall, and Nedzel, Phys. Rev. **92**, 834 (1953).
[3] C. L. Oxley and R. D. Schamberger, Phys. Rev. **85**, 416 (1952).
[4] O. A. Towler, Phys. Rev. **85**, 1024 (1952).

Neutral-to-Charge Ratio in High-Energy Interactions*

M. F. Kaplon, W. D. Walker, and M. Koshiba
University of Rochester, Rochester, New York
(Received January 18, 1954)

ONE of the problems of primary interest in the study of elementary particles is the determination of their production efficiency as a function of energy. At energies well removed from threshold, cosmic rays furnish the only source of high-energy

interactions. At the present time it is practically impossible to make a direct determination of mass by the usual techniques for particles whose velocities are greater than $0.95c$. For interactions of energies $>10^{12}$ ev, almost all of the secondary particles have relativistic velocities and, consequently, indirect methods must be used to determine the constitution of the shower particles.

A possible method of studying the relative production of pions and other mesons at these very high energies lies in determining the ratio R of neutral π mesons to charged shower particles. $R=N_{\pi^0}/(N_{\pi^\pm}+N_{s'})$, where $N_{s'}$ is the number of charged shower particles not $\pi^\pm$ mesons and the total number of charged shower particles $N_s=N_{\pi^\pm}+N_{s'}$. Letting $R(\pi)=N_{\pi^0}/N_{\pi^\pm}$, we find $N_{s'}/N_{\pi^\pm}=[R(\pi)/R]-1$. Thus if $R(\pi)$ and R are known, we have a measure of the relative production of shower particles which are not π mesons, to charged π mesons.

To determine R, we have studied in stripped emulsion, a group of very high energy interactions ($E\gtrsim 10^{13}$ ev per nucleon). If we assume for the moment that π^0 decay is the only source of high-energy γ rays in these interactions, then a determination of the number of high-energy electron pairs (N_p) is a measure of the number of π^0 mesons emitted in the interaction. In order to minimize the effect of cascade multiplication, we have restricted our search for electron pairs to distances from the shower origin small in comparison to the conversion length in emulsion (3.75 cm), and to assure more efficient pair detection we restrict our scanning to the more local region of the central core part of the shower. Table I summarizes the results of our observations. Column 1 gives the number of black prongs (N_h) associated with the star, 2 gives the primary (P means singly charged), 3 gives the total number of charged shower particles (N_s^T), 4 gives the number of charged shower particles (N_s) for each star in the region searched for pairs, 5 gives the total length of charged shower particles in the area scanned, and column 6 gives the total number of accepted pairs in this area.

Since it is expected that bremsstrahlung will accompany meson production,[1] we have accepted only those pairs of high enough energy (determined by multiple scattering or opening angle) to be consistent with ultimate nuclear origin; there will however still be some contribution from bremsstrahlung. With our restriction to distances small compared to the conversion length (λ) we can write

$$N_p=2N_{\pi^0}\frac{\Delta x}{\lambda}+\alpha N_{\pi^0}+\sum_i \frac{N_\gamma{}^i}{\lambda}\Delta x_i,$$

where α is the probability for the decay $\pi^0\to\gamma+e^++e^-$, Δx is the distance scanned, $N_s(i)$ is the number of charged shower particles of length Δx_i in the area scanned, and $N_\gamma{}^i$ is the number of high-energy bremsstrahlung γ rays accompanying the ith charged shower particle. On substituting $N_{\pi^0}=RN_s$, we find

$$R=\frac{N_p-\frac{1}{\lambda}\sum_i N_\gamma{}^i\Delta x_i}{\frac{2}{\lambda}\sum_i N_s(i)\Delta x_i+\alpha N_s}.$$

The correction for bremsstrahlung amounts to a spurious neutral-to-charged ratio of at most 0.03 for shower particles of spin 0, $\frac{1}{2}$, or 1. (See reference 2 for details.) This derivation assumes a zero lifetime for the π^0 (for a finite lifetime the measured R is a lower limit); this may be compensated for by some slight cascade multiplication. Substituting from Table I and applying the slight correction for bremsstrahlung, we find $R=0.46\pm0.09$.[2]

In order to obtain an estimate for $N_{s'}/N_{\pi^\pm}$ we must know $R(\pi)$. Van Hove[3] has predicted on the basis of charge independence $R(\pi)=0.5$ for multiple meson processes if the sample represents a statistical ensemble of nucleon-nucleon interactions. If we further assume the fluctuations $R(\pi)$ are $\sim\sqrt{N_\pi}$, we find $N_{s'}/N_{\pi^\pm}=0.09\pm0.25$. This implies that particles other than π mesons may be relatively inefficiently produced in very high energy interactions. This conclusion rests upon the validity of the charge independence hypothesis and the assumption that π^0 mesons are the sole source of high-energy γ rays in these interactions; if there exist other sources, this conclusion does not hold and appreciable production of particles other than π mesons may occur. However, this requires that any other particles unstable to γ decay must have lifetimes of $\lesssim 10^{-14}$ second if they are to serve as an additional source of high-energy γ rays.

TABLE I. Characteristics of high-energy interactions.

N_h	Primary	N_s^T	N_s	L(cm)	N_p
0	P	16	11	5.0	2
1	P	16	8	2.40	0
2	P	19	11	8.0	3
3	P	36	24	30.7	10
4	P	12	6	5.2	2
6	P	15	9	2.9	2
15	P	16	11	10.0	2
5	α	49	49	23.3	5
14	α	90	45	12.0	2
			174	99.5	28

We wish to express our thanks to Miss Barbara Hull for her assistance in scanning.

* This research was supported in part by the United States Air Force under a contract monitored by the Office of Scientific Research, Air Research and Development Command.

[1] L. Schiff, Phys. Rev. **76**, 89 (1949).

[2] M. F. Kaplon and D. M. Ritson, Phys. Rev. **88**, 386 (1952); the figure derived above is in excellent agreement with the value of 0.49 obtained in this paper.

[3] Van Hove, Marshak, and Pais, Phys. Rev. **85**, 1211 (1952).

K-Conversion Electron-Gamma Angular Correlation Measurements in Te^{121} and Te^{123}†

NORMAN GOLDBERG AND SHERMAN FRANKEL
Randal Morgan Laboratory, University of Pennsylvania, Philadelphia, Pennsylvania
(Received January 27, 1954)

THIS note describes preliminary measurements of K-conversion electron-gamma correlation measurements in the two-step isomers, Te^{121} and Te^{123}. In order to separate unambiguously the K and L correlations, a lens spectrometer has been employed for electron detection. To date, theoretical correlation coefficients are only available for the K shell. The isomers studied are of interest since conversion coefficient measurements[1] indicate the second transition is predominately magnetic dipole, whereas shell model assignments ($d_{\frac{1}{2}}\to s_{\frac{1}{2}}$; $\Delta l=2$) would forbid ordinary $M1$ transitions. Partial breakdown of this selection rule would yield depressed $M1$ transition probabilities (as observed in the measurements of the lifetime of Te^{123} by Graham and Bell[2]) and might allow competition by the slower electric quadrupole transition.

Angular correlation measurements are extremely sensitive to a small mixture of $E2$ in $M1$ transitions. The expected correlation for the K-conversion electron-gamma cascade is

$$W(\theta)=1+b_2a_2g_2h_2j_2[1-2\sqrt{3}\delta(1-\delta^2)^{\frac{1}{2}}-2\delta^2]P_2(\cos\theta)$$
$$=1+a_2'f(\delta)P_2(\cos\theta).$$

We have assumed here that the first transition is pure $M4$; $a_2=-0.1545$ is the theoretical $\gamma-\gamma$ correlation coefficient,[3] $b_2=1.065$ is the modification introduced because the transition is K converted,[4] $g_2=0.982$ represents the effect of the finite φ-symmetric gamma detector,[5] $h_2=0.971$ the effect of the finite φ-symmetric acceptance cone of the spectrometer, $j_2=1.00$ the effect of electron scattering in the source,[6] and δ^2 is the ratio of the intensity of $E2$ radiation to intensity of $M1$ plus $E2$. These values lead to $a_2=-0.157$. Mixed Te^{121} and Te^{123}, made by cyclotron bombardment with deuterons on antimony, was separated chemically and evaporated on formvar films ($<9\ \mu g/cm^2$), which had been coated with either aluminum or silver conducting layers ($<4\ \mu g/cm^2$). The source itself was less than $0.5\ \mu g/cm^2$. Pertinent results are listed in Table I. The sign of δ is positive in both isomers. The possibility of perturbations on the intermediate state producing

TABLE I. Summary of data.

Isotope	Backing material	Theoretical $a_4'f(0)$	Experimental $\frac{W(\pi)}{W(\pi/2)}-1$	Experimental $a_4'f(\delta)$	Experimental δ^2
Te^{121}	Al		-0.023 ± 0.010	-0.015 ± 0.007	0.055 ± 0.005
Te^{123}	Al	-0.157	-0.133 ± 0.005	-0.093 ± 0.004	0.012 ± 0.001
Te^{123}	Ag		-0.143 ± 0.020	-0.100 ± 0.016	0.009 ± 0.004

the reduced correlation, rather than the presence of $E2$ mixtures, is unlikely in these isomers because of their short lifetime (half-life of $Te^{123}=1.9\times10^{-10}$ sec).[3] In addition, Weisskopf's formula[6] for transition probabilities predicts a shorter lifetime for Te^{121}, yet the Te^{121} has a much smaller anisotropy. Also δ^2 should have a dependence on the energy of the transition which is in the proper direction.

From the measured lifetime of Te^{123} (the empirical lifetime formula of Graham and Bell[2] was used for Te^{121}) and the mixture ratio, the $E2$ matrix elements can be calculated. Comparing these matrix elements (M) with the Weisskopf formula as modified for odd-neutron nuclei,[7,8] we obtain $M^2(\text{theor.})/M^2(\text{exp.})=K(A^2/Z)^2$, where $K=0.12$ for Te^{121} and 0.34 for Te^{123}. The term $(A^2/Z)^2$ is the factor determining the depression of $E2$ matrix elements for odd-neutron transitions over odd-proton transitions. Thus $E2$ is enhanced by a factor of approximately 10^4 over the prediction of the single-particle model.

A detailed treatment of these experiments including $L-\gamma$ and $K-K$ measurements now being completed will appear in a subsequent paper. We wish to thank Dr. A. J. Allen for the bombardment of Sb in the University of Pittsburgh cyclotron.

† This work is supported in part by the U. S. Office of Ordnance Research.

[1] Katz, Hill, and Goldhaber, Phys. Rev. **78**, 9 (1950).
[2] R. L. Graham and R. E. Bell, Can. J. Phys. **31**, 377 (1953).
[3] S. P. Lloyd, Phys. Rev. **83**, 904 (1952).
[4] Rose, Biedenharn, and Arfken, Phys. Rev. **85**, 5 (1952).
[5] S. Frankel, Phys. Rev. **83**, 673 (1951).
[6] J. M. Blatt and V. F. Weisskopf, *Theoretical Nuclear Physics* (John Wiley and Sons, Inc., New York, 1952), p. 627.
[7] M. Goldhaber and A. W. Sunyar, Phys. Rev. **83**, 906 (1951).
[8] S. A. Moszkowski, Phys. Rev. **89**, 474 (1953).

A Photon Monochromator for Bremsstrahlung Radiation*

J. GOLDEMBERG
Department of Physics, University of Illinois, Champaign, Illinois, and Department of Physics, University of Sao Paulo, Sao Paulo, Brazil
(Received December 28, 1953)

USING the external beam of electrons of the 22-Mev betatron of the University of Illinois an attempt has been made to select monochromatic γ rays from the bremsstrahlung radiation. A similar experiment using the internal beam of a synchrotron has been tried by Weil and McDaniel.[1] To achieve this purpose coincidences between the straggled electron and the corresponding photon have been measured. A general diagram of the experimental arrangement is shown in Fig. 1. Monoenergetic electrons accelerated by the betatron to energies up to 22 Mev are extracted from the acceleration chamber by means of a "peeler," collimated, and focused externally in a gold foil. This foil, 1/100 of a radiation length thick, is situated at the edge of a permanent magnet 180° β spectrometer able to detect β rays of 3 Mev. In this β spectrometer, that had good collection efficiency, the electrons are detected by a stilbene crystal $2\times2\times2$ cm³ and a 5819 photomultiplier. If the betatron is run at an energy E_0 (Mev), the γ ray corresponding to a straggled electron of 3 Mev has an energy of (E_0-3), and it travels about 100 cm to a liquid scintillator cell where it is detected. This liquid cell is 4 cm in diameter and 20 cm long and it is filled with phenylcyclohexane with terphenyl (3 g per liter) and diphenyl hexatriene (10 mg per liter). The efficiency of such a γ-ray detector is of the order of 10 percent for 10-Mev photons incident on it; a fast pulse rather than high efficiency was sought. The coincidence circuit has a resolving time of $\sim10^{-8}$ sec and consists essentially of chains of distributed amplifiers feeding the Z and X axis of a 5XP15 DuMont oscillograph tube. A coincidence brings the oscilloscope spot out from behind a mask and brightens it. A 1P21 photomultiplier counter records these flashes.

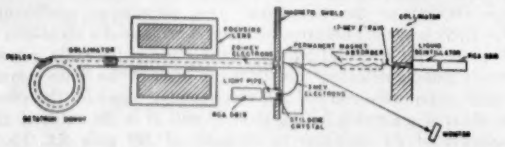

FIG. 1. The photon monochromator: diagram of experimental arrangement.

The betatron was run at a level at least 10 times lower than normal in order to have desirable counting rates. This corresponds to a current of $\sim10^{-10}$ ampere incident on the gold radiator.

The behavior of the electron counter and β spectrometer were examined by running the betatron at 3 Mev and shooting the electrons into it with the radiator in place. This gave ±0.15 Mev for the actual resolution of the β spectrometer. This can be seen in Fig. 2 as well as an integral and differential bias curve for the detected electrons.

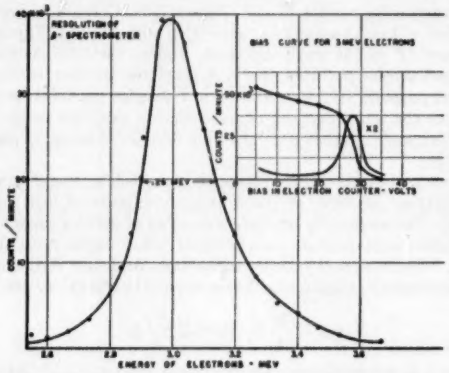
RESOLUTION OF β- SPECTROMETER
BIAS CURVE FOR 3 MEV ELECTRONS
COUNTS / MINUTE
BIAS IN ELECTRON COUNTER - VOLTS
ENERGY OF ELECTRONS - MEV

FIG. 2. Behavior of β spectrometer: resolving power and bias curve for electron counter.

The electron and γ counters were biased conveniently in order to get the best ratio of true to accidental coincidences. Since a bremsstrahlung spectrum enters in the γ detector the accidentals were a serious problem. A ratio of 4.5 to 1 for true to accidental counts was obtainable at a counting rate of 50 true coincidences per minute. In order to reduce accidentals a 200-μsec pulse of electrons was extracted from the betatron using the method of Keegan.[2] Delay lines in either of the detectors gave the characteristic curves for correlated events. By changing the maximum energy of the betatron, γ rays of energies between zero and 19 Mev could be obtained, the spectral band being determined essentially by the resolution at the β spectrometer. The external electrons from the betatron have a total intrinsic spread of 1 percent when a long pulse is employed. Thus the energy band is about ±0.2 Mev in this experiment.

With the system described, absorption coefficients were measured in carbon by using a block of pure graphite of 111.5 g/cm². The original beam of electrons that passed through the gold foil was slightly bent by the magnetic field of the β spectrometer, collected, and measured for monitoring purposes. The preliminary results obtained show that the absorption coefficients are within 3 percent (the statistical error) of those calculated excluding nuclear excitation.[3] Most of the measurements were made between 13.5 and 16.5 Mev in less than 0.15-Mev steps. In this

region the absorption coefficient appeared to change smoothly with energy. Only 1.5 percent of the transmitted photons could be accounted for by bad geometry effects. These photons were at most 0.5 Mev outside the selected energy bin. Room background consisted essentially of x-rays and it was easily shielded. With the coincidence arrangement this background did not amount to more than 1 percent of the true coincidences.

Coincidences between the straggled electrons and neutrons emitted in photonuclear processes seems to be within the possibilities of the monochromator scheme. In this kind of experiment where a counter is not exposed to the total bremsstrahlung spectrum the possibility exists of using the full yield of the betatron before jamming the electron counter.

The author wishes to express his sincere acknowledgments to Professor D. W. Kerst for the hospitality extended to him at the University of Illinois, and for stimulating discussions and encouragement. He acknowledges also the invaluable help of Dr. M. Miwa, B. M. Spicer, and A. S. Penfold who made available the counting equipment.

* This work supported in part by the U. S. Atomic Energy Commission and the U. S. Office of Naval Research.

[1] J. W. Weil and B. D. McDaniel, Phys. Rev. **92**, 391 (1953).
[2] T. J. Keegan, Rev. Sci. Instr. **24**, 472 (1953).
[3] G. R. White, *X-ray Attenuation Coefficients* (National Bureau of Standards Report 1003, U. S. Government Printing Office, Washington, D. C., 1952).

Negative π-μ Meson Decays in Photographic Emulsion*

W. F. FRY, *University of Wisconsin, Madison, Wisconsin*
AND
GEORGE R. WHITE,† *Iowa State College, Ames, Iowa*
(Received February 2, 1954)

IT is generally believed that a slow negative π meson which stops in an emulsion will be captured into mesonic orbits of an atom and then absorbed by the nucleus. Experimental observations[1-3] have shown that nuclear absorption of slow negative π mesons in photographic emulsion completely predominates over π-μ decay. However, several negative decays in emulsion have been observed recently.

Electron-sensitive G-5 plates were exposed behind absorbers to slow negative π mesons from the various channels of the University of Chicago cyclotron. Among 40 000 meson endings, 18 π-μ meson decays were observed. The μ meson stopped in the emulsion in 11 of these 18 cases. The characteristics of these 11 π-μ decays are given in Table I. A histogram of the μ meson range distribution for these decays is shown in Fig. 1.

In 5 of the 11 cases where the μ meson stopped in the emulsion, the range of the μ meson is outside the limits of the experimental μ meson range distribution from positive π-μ decays;[4,5] thus it is highly improbable that these 5 events are positive decays. Also, 5 of the 11 decays (events 1, 3, 6, 7, and 11) show no decay electron from the μ-meson ending; thus it is very improbable that these 5

TABLE I. Characteristics of negative π-μ decays.

Event	Range of μ meson	μ-e decay?
1[a]	320	(one-prong star)
2	443	yes
3	580	no
4	581	yes
5	598	yes
6	610	no
7	615	no
8	647	yes
9	687	yes
10	720	yes
11	780	no

[a] An electron track is observed at the π-μ junction. The energy of the electron is about 25 kev.

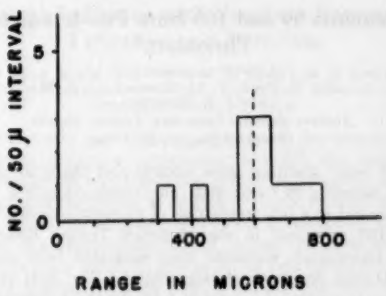

FIG. 1. The μ-meson range distribution from negative π-meson decays is shown in the histogram. The mean range from positive π-meson decays is 597 microns.

are positive π-meson events.[6] In fact, this fraction of μ-e decays is reasonable if it is assumed that the μ mesons are negative.[7] There is no correlation of the μ-meson range with the presence of a decay electron. Of the 6 events where the range of the μ meson is within the distribution from 1000 positive π-meson decays, the decay-electron track is observed in only 3 cases. Therefore, it is improbable that more than 2 events are positive decays; however, it is possible that all are negative. The π and μ mesons in event No. 1 are undoubtedly negative, as shown by the 1-prong star caused by the μ meson.

The spead of the μ-meson range distribution from negative π decays is significantly greater than the spread from positive π decays. This fact suggests that the negative π mesons did not decay from rest. The μ-meson range distribution implies that the average momentum of the π meson at the time of decay was about 3.3 Mev/c. The stopping time in an emulsion for a π meson of this momentum (E_π=40 kev) is estimated to be about 10^{-13} sec. The probability of decay in flight is the ratio of the moderation time to the mean lifetime (5×10^{-6}). This probability is too small to account for the number of π-μ decays observed.

The events are interpreted as π-meson decays from negative energy states where the average momentum is about 3.3 Mev/c. The relative scanning efficiency for π-μ decays in comparison to π-meson stars is estimated to be 75 percent. Thus, the probability that a slow negative meson will decay in a photographic emulsion is $(18/40\,000)(4/3)=6\times10^{-4}$. It is not known whether the decays follow the atomic capture in the heavy or the light elements. From a previous study of μ-meson phenomena it was found that 61 percent of the slow μ mesons stop in Ag or Br and that 39 percent stop in the light elements (C,N,O).[7] These same percentages should apply to slow negative π mesons. If the π-meson decays follow the stopping in Ag or Br, the ratio of decay to nuclear absorption is $(18/40\,000\times0.61)(4/3)=1.0\times10^{-3}$. If the decays follow the stopping in the light elements, the ratio of decay to nuclear absorption is $(18/40\,000\times0.39)(4/3)=1.5\times10^{-3}$.

The authors are indebted to Professor H. L. Anderson and Mr. Lester Kornblith for their assistance in obtaining the cyclotron exposures. Many discussions with Dr. Jay Orear and Dr. A. H. Rosenfeld were very valuable and stimulating.

* Supported in part by the Graduate Committee from funds supplied by the Wisconsin Alumni Research Foundation.
† National Science Foundation Predoctoral Fellow. This work was performed at the University of Wisconsin, Madison, Wisconsin.

[1] Menon, Muirhead, and Rochat, Phil. Mag. **41**, 583 (1950).
[2] F. L. Adelman, Phys. Rev. **85**, 249 (1952).
[3] W. F. Fry, Phys. Rev. **84**, 385 (1951). A negative π-μ decay was observed where the range of the μ meson is 820 microns. This event, previously interpreted as a decay in flight, is more likely due to the same cause as the above events.
[4] Walter H. Barkas, Am. J. Phys. **20**, 5 (1952).
[5] W. F. Fry and G. R. White, Phys. Rev. **90**, 207 (1953). The range distribution of 1000μ mesons from π-meson decay has a mean of 597 ± 1 microns. No events were found where the range was less than 504 microns or greater than 681 microns.
[6] W. F. Fry, Phys. Rev. **85**, 676 (1952). The decay-electron track was not observed in 2 of 38 positive π-μ decays, probably caused by unfavorable orientation of the electron track.
[7] W. F. Fry, Nuovo cimento **10**, 490 (1953). In emulsion, 36 ± 2 percent of stopped negative μ mesons decay into an electron.

Elements 99 and 100 from Pile-Irradiated Plutonium*

M. H. Studier, P. R. Fields, H. Diamond, J. F. Mech, A. M. Friedman
P. A. Sellers, G. Pyle, C. M. Stevens, L. B. Magnusson,
and J. R. Huizenga
Argonne National Laboratory, Lemont, Illinois
(Received January 25, 1954)

THIS note[1] describes some nuclear and chemical properties of elements 99[2] and 100. The transcalifornium elements were produced in a pile irradiation of plutonium (integrated flux of 1.0×10^{23} neutrons) in the Materials Testing Reactor. The purified transcurium elements were separated from each other with a Dowex 50 cation citrate column.[3] The final element-99 peak (Fig. 1) contained a total of 3.3×10^4 alpha disintegrations/minute. The energy of the prominent alpha group was measured by pulse analysis to be 6.64 Mev. The alpha spectrum of this isotope appears to exhibit fine structure which is characteristic for odd-even nuclides, e.g., similar to Np^{237} and Am^{241}. In the final californium peak were 2.3×10^3 alpha disintegrations/minute as well as 4.6×10^2 spontaneous fission disintegrations/minute. Alpha pulse analysis of the californium fraction showed at least two alpha groups of 6.01 and 6.10 Mev. These alpha groups chemically follow the large spontaneous fission activity as shown in Fig. 1 and are in the ratio of forty-five californium alpha disintegrations to one spontaneous fission disintegration. The presence of short spontaneous fission half-lives in the californium fraction is supporting evidence for the recently published spontaneous fission systematics.[4]

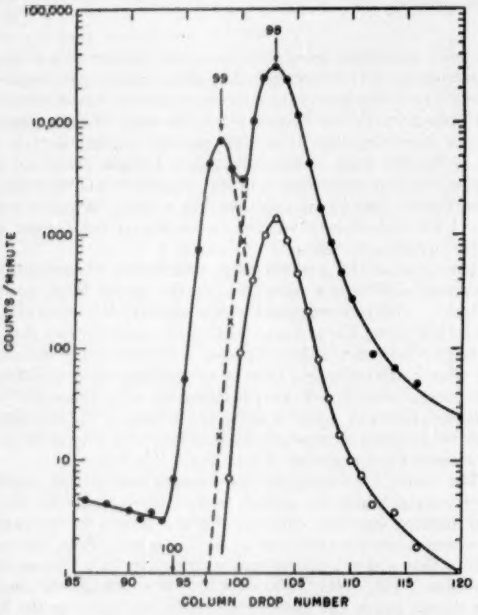

FIG. 1. The solid points represent the total activity in counts/minute (alpha particles plus spontaneous fissions) of successive drops from the Dowex 50 cation citrate column. The open circles give the spontaneous fissions in counts/minute as a function of drop number. The dashed lines give the respective amounts of californium and element-99 activities in the drops which contain alpha activity from both elements. The curium began to elute at drop 170 in this column run.

The small amount of spontaneous fission activity on plates containing the 6.64-Mev alpha particles is a measure of the excellent separation of element 99 from 98 (see Fig. 1). Drop 97 contained 8600 disintegrations/minute of 6.64-Mev alpha particles and about 0.004 ± 0.002 fission disintegrations/minute. Assigning all of the fissions to californium gives a limit of 0.2 disintegrations/minute of californium alpha particles on the above plate.

The observed half-life of the 6.64-Mev alpha-emitting isotope of element 99 is 20 ± 2 days (the decay was over a period of 8 days). By using a 20-day decay half-life for the above element-99 isotope, the spontaneous fission half-life is calculated to be greater than 10^5 years. This half-life limit can be increased if the spontaneous fissions do not decay with the 6.64-Mev alphas. Such a long spontaneous fission half-life (compared to even-even nuclides) for a 99 isotope is consistent with expectations for an odd-Z element. The 6.64-Mev alpha has grown in drop 109 from 2 counts/minute (at the time of the first alpha pulse analysis) to 13 counts/minute in six days, establishing its genetic relationship to californium. A number of arguments[1] indicate that the probable mass assignment of the element-99 isotope is 253.

Alpha pulse analysis showed the presence of an energy group of 7.20 Mev and possibly another group (one-third the abundance of the 7.20-Mev group) approximately 170 kev lower in energy in the element-99 fraction. From the energies of these groups one may deduce that they represent isotopes of $Z>99$ in equilibrium with β^--emitting element-99 isotopes. The ratio of 6.64-Mev activity to the 7.20-Mev activity is about 5000. An alpha group of approximately 7.1 Mev was shown to elute from a Dowex 50 cation citrate column ahead of the 6.64-Mev alpha group, which is evidence for assigning at least one of the energetic groups to element 100. The short half-life of the ~7.1-Mev alpha group which eluted ahead of element 99 prevented a possible resolution of this group in the absence of the element-99 activity.

Several chemical experiments on elements 99 and 100, in addition to the previously mentioned cation citrate elution behavior, have been performed. Both elements carry on LaF_3 and $La(OH)_3$, and solvent extract into tributyl phosphate from a highly salted, dilute nitric acid solution. In concentrated hydrochloric acid, element 99 behaves like curium with both Dowex A-1 anion and Dowex 50 cation resins.

The valuable assistance in these experiments by C. H. Youngquist, R. K. Sjoblom, James Gindler, and D. W. Engelkemeir is gratefully acknowledged. We also wish to thank W. M. Manning for guidance and many stimulating discussions.

* These elements (99 and 100) have previously been discovered in other work at Argonne National Laboratory, University of California Radiation Laboratory, and Los Alamos Scientific Laboratory, not yet published.

[1] A manuscript containing details of these experiments as well as a number of additional experiments is in preparation.

[2] The production of lighter isotopes of element 99 by nitrogen-ion bombardment of uranium has recently been described: Ghiorso, Harvey, Rossi, and Thompson, Phys. Rev. **93**, 257 (1954).

[3] B. H. Ketelle and G. E. Boyd, J. Am. Chem. Soc. **69**, 2800 (1947); K. Street, Jr., and G. T. Seaborg, J. Am. Chem. Soc. **72**, 2790 (1950).

[4] J. R. Huizenga, Phys. Rev. (to be published).

The Nuclear Spin of Si^{29}†

G. A. Williams, D. W. McCall,* and H. S. Gutowsky
Noyes Chemical Laboratory, University of Illinois, Urbana, Illinois
(Received January 15, 1954)

SEVERAL attempts have been made to determine the spin of Si^{29} with either inconclusive,[1] conflicting,[2] or rather indirect[3] results. The consensus favors the value 1/2. Nuclear shell theory gives 1/2, 3/2, and 5/2 as the only possibilities.[1] We have eliminated values greater than 1, thereby establishing the spin of Si^{29} as 1/2. This was accomplished by resolving the multiplet structure produced in the fluorine nuclear magnetic resonance by the electron coupled interaction[4] of the Si^{29} spin with the F^{19} spins, using isotopically enriched $Si^{29}F_4$.

In pure liquid or gaseous $Si^{29}F_4$, the fluorine resonance should be a multiplet, with $2I(Si^{29})+1$ equally spaced components of the same intensity.[4] The SiF_4 actually used was prepared[5] from a sample of SiO_2 whose composition was given as 30, 69, and 1 percent, respectively, of Si^{28}, Si^{29}, and Si^{30}. The enriched sample of SiO_2 was supplied by the Oak Ridge National Laboratory. The

spins of Si^{28} and Si^{30} are presumably zero so the $Si^{29}F_4$ and $Si^{30}F_4$ should give a single fluorine resonance with 31 percent of the total absorption, located at the center of the $Si^{29}F_4$ multiplet. The high-resolution spectrometer and experimental procedures used have been described elsewhere.[6] A typical oscilloscope photograph of the fluorine resonance observed in the liquefied sample of SiF_4 is reproduced in Fig. 1.

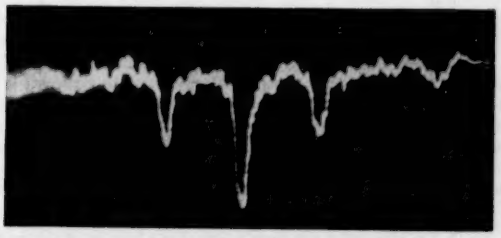

FIG. 1. The F^{19} nuclear magnetic resonance in a mixture of $Si^{28}F_4$ and $Si^{29}F_4$. The center line is from the $Si^{28}F_4$. The two outer lines are from the $Si^{29}F_4$; their separation is 46 milligauss. A sawtooth sweep of 135 milligauss was used; the pip on the far right is from the return trace.

Figure 1 shows a symmetrical multiple resonance of three components with approximate *peak* intensities of 1:2:1. The separation of the two outer components is 46 milligauss. The number of lines observed is compatible with a spin of either 1/2 or 1. For a spin of 1/2 the predicted *integrated* absorption of the components should be 34.5:31:34.5, and for a spin of 1, 23:54:23; in the latter case the $Si^{28}F_4$ and $Si^{30}F_4$ lines overlap the center component of the $Si^{29}F_4$ triplet. The observed *peak* intensities correspond more closely to the spin 1 case than to the spin 1/2. However, a spin of 1 is eliminated by the shell theory; moreover, there is a convenient mechanism to explain the intensities observed.

In aqueous, concentrated $H_2Si^{29}F_6$ the fluorine resonance was not split by the Si^{29} spin but was broadened to about 4 milligauss compared to 2 milligauss in $H_2Si^{28}F_6$. This effect[4] is produced most likely by fast chemical exchange[7] involving the fluorines. In the case of SiF_4, hydrolysis would result from a trace of water, giving HF which would catalyze exchange of the fluorines. Depending upon the exchange rate, there can be a significant reduction in the peak intensities and some broadening of the component lines. In Fig. 1 noise obscures any broadening of the outer components, but this explanation is supported by the observation that the ratio of the intensity of the outer components to that of the center line decreased at higher temperatures, for which chemical exchange would be faster. The isotopic composition of the SiF_4 was checked by an infrared analysis which gave 28 ± 2 percent $Si^{28}F_4$.

Figure 1 suggests an amusing and direct way to set an experimental maximum for the gyomagnetic ratio of Si^{29}. The splitting in gauss of the fluorine resonance in $Si^{29}F_4$ is given as[4] $\delta H = C\gamma \times (Si^{29})/\hbar$, where C is a constant determined by the electronic structure of SiF_4. The central component in Fig. 1 is from the $Si^{28}F_4$ and splitting of it greater than 2 milligauss would be discernible. If we take the ratio of the equations for the splitting in $Si^{28}F_4$ and $Si^{29}F_4$, introduce the values of 2 and 46 milligauss for the splitting and the experimental value[1] for $\gamma(Si^{29})$, we find $\gamma(Si^{29})<0.05$. This value could be improved by taking greater pains to obtain maximum resolution and to minimize the effects of chemical exchange. Similar experiments are feasible in several other cases, including $C^{13}H_4-C^{12}H_4$ and $H_2S^{33}-H_2S^{32}$ mixtures.

† Assisted by the U. S. Office of Naval Research and a Grant-in-Aid from du Pont and Company.

* National Science Foundation predoctoral fellow; now at Bell Telephone Laboratories, Murray Hill, New Jersey.

[1] H. E. Weaver, Phys. Rev. **89**, 923 (1953).
[2] R. H. Sands and G. E. Pake, Phys. Rev. **89**, 896 (1953).
[3] R. L. White and C. H. Townes, Phys. Rev. **92**, 1256 (1953).
[4] Gutowsky, McCall, and Slichter, J. Chem. Phys. **21**, 279 (1953).
[5] C. J. Hoffman and H. S. Gutowsky, Inorg. Syntheses **4**, 145 (1953).
[6] Gutowsky, Meyer, and McClure, Rev. Sci. Instr. **24**, 644 (1953).
[7] H. S. Gutowsky and A. Saika, J. Chem. Phys. **21**, 1688 (1953).

Nuclear Induction with Separate Regions of Excitation and Detection

CHRISTOPHER SHERMAN
Princeton University, Princeton, New Jersey
(Received February 2, 1954)

A FEW years ago Purcell[1] pointed out the possibility of a nuclear induction experiment in which the sample is a flowing stream of water and the detection occurs at a location downstream of the region of excitation. More recently Benedek,[2] working under the direction of Purcell, investigated this possibility and in an unpublished report derived the expected form of the signal in some detail, as well as listing experimental conditions which are required in order that a nuclear induction signal be obtained.

This letter reports the performance of such an experiment. The essential details of the nuclear induction head are shown in Fig. 1.

The block is milled (unhatched section) of a solid piece of aluminum, and the wall separating the exciting and detecting coils is $\frac{1}{8}$ inch thick, with a $\frac{1}{16}$-inch hole drilled through for the water tube. These dimensions were chosen with a mind to keeping the direct electromagnetic coupling from excitor to detector down to a low level. A 30-cycle/sec lock-in detecting system with a 1-cycle/sec band width was used, the modulation being obtained with two coils, one fastened on the bottom of the block, the other on a cover plate. Except for water and electrical lead-ins, the block and cover enclosed the system completely.

The details of the water system, made of Lucite, are: Distance between centers of excitor and detector coils $=\frac{1}{4}$ inch; inner diameter of excitor tube $=0.016$ inch; inner diameter of detector tube $=0.040$ inch.

The excitor and detector coils are closewound of 0.003-inch copper wire, have 20 turns, and diameters of 0.072 inch and 0.062 inch, respectively. They are matched to coaxial cables by use of the condenser-transformer networks shown in the diagram.

From the foregoing data, the effective detector sample volume is slightly greater than 10^{-3} cc.

With a flow rate of 0.6 cc/sec, and a resonant frequency of 15 Mc/sec, a signal-to-noise power ratio of roughly 50 db was obtained. With decreasing flow rates, the signal drops off rapidly, so that at a flow rate of 1 cc/min noise is definitely visible on the resonant response.

The shape of the resonance curves has not yet been interpreted on a theoretical basis. There are several factors which hinder this, among them being the complicated flow pattern caused by the abrupt change in tube diameter, and complications introduced by the 30-cycle/sec modulation frequency. The theoretical prediction of a signal frequency equal to the driving frequency rather than any dipole precession frequency determined by the magnetic field has been verified.

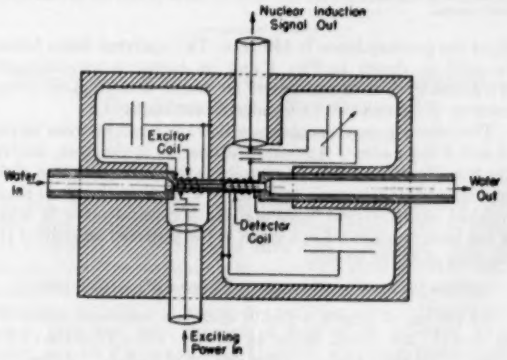

FIG. 1. Details of nuclear induction head.

This work is being continued in the direction of increasing the path length (and also the time spent) between exciting and detecting coils, with a view to possibly obtaining narrower resonant responses.

The author wishes to thank Professor R. H. Dicke for frequent advice during the course of the work.

[1] E. M. Purcell (private communication).
[2] George Benedek, "An Experiment to Determine With High Precision the Average Value of a Magnetic Field Over an Extended Path in Space," Harvard University, June 4th, 1952 (unpublished).

Experiments with High-Energy Polarized Protons*

O. CHAMBERLAIN, E. SEGRÈ, R. TRIPP, C. WIEGAND, AND T. YPSILANTIS
Radiation Laboratory and Department of Physics, University of California, Berkeley, California
(Received January 25, 1954)

THERE have been recent reports[1,2] on high-energy polarized proton beams and their scattering properties. We also have been scattering protons in the Berkeley cyclotron and investigating their polarization by double-scattering experiments and we wish to give at this time a progress report because the data so far collected appear of interest.

The beam is polarized by scattering on target A of beryllium or carbon (Fig. 1) and is deflected by a steering magnet into the shielded experimental area (cave).

The angle of scattering Ψ in a horizontal plane and at target A varies between 17° and 20° in different experiments. The energy

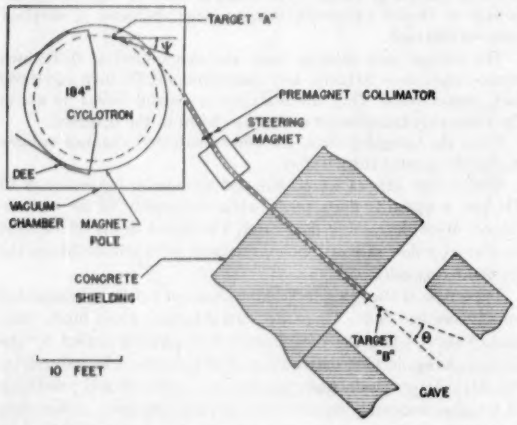

FIG. 1. Plan view of the experimental arrangement showing the angles Ψ and Θ at the first and second targets. The angle Φ, measuring rotation of the apparatus in the cave around the beam, is equal to zero for the configuration shown.

E_0 of the primary beam is 340 Mev. The scattered beam follows an orbit as drawn in Fig. 1 and its energy is approximately $E=E_0\cos^3\Psi$ as if it underwent an elastic scattering on a free nucleon. E is measured by a range determination.

The following experiments show that the beam between targets A and B is polarized: A second scatterer B, in the cave, scatters the beam by an angle Θ. To completely define the direction of the scattered beam we need also an angle Φ between the plane of the incident and scattered beam and the horizontal plane in which Ψ has been measured. For a given Θ the scattered intensity I is a function of Φ and we call

$$\epsilon(\Theta)=[I(\Phi=0°)-I(\Phi=180°)]/[I(\Phi=0°)+I(\Phi=180°)].$$

By the use of targets A and B of carbon, measured values of I at $\Theta=15°$ are found to be as follows: $I(\Phi=0°)=134.1\pm4.0$, $I(\Phi=90°)=101.8\pm3.7$, $I(\Phi=180°)=59.3\pm4.3$, $I(\Phi=270°)=104.7\pm3.3$, from which $\epsilon=0.39\pm0.04$; and $[I(\Phi=90°)-I(\Phi=270°)]/[I(\Phi=90°)+I(\Phi=270°)]=0.01\pm0.02$, which is a satisfactory check indicating that the polarization is a real effect.

When liquid hydrogen was used as scatterer B, we found that $\epsilon(\vartheta)$, where ϑ is the scattering angle in the c.m. system, is given by the curve of Fig. 2. It will be noticed that $\epsilon(90°$ c.m.) is consistent

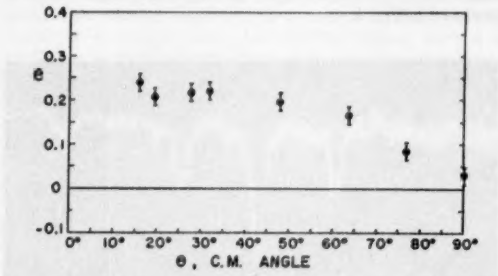

FIG. 2. The asymmetry parameter ϵ plotted as a function of the center-of-mass scattering angle ϑ for proton-proton scattering at target B. The errors shown include only counting statistics.

with zero as it should be for reasons of symmetry. These checks and an accurate study of the alignment, geometry, and counter properties, which we do not now report, have convinced us that the polarization effect is real. Furthermore we have checked that the external beam extracted in the ordinary way shows no asymmetry with either hydrogen or carbon as target B. (This confirms the fact that our p-p scattering experiments[3] were not influenced by polarization effects.)

The absolute intensity of the polarized beam entering the cave was approximately 2×10^5 protons per second over an area of 5 cm^2.

In order to use the polarized beam for quantitative measurements we would like to know its degree of polarization $P=(F_+-F_-)/(F_++F_-)$, where $F_\pm$ is the intensity of the protons with spin up or down, respectively. If the scatterings in targets A and B were elastic, and the targets were of the same material, and if Θ equals Ψ, then P equals $\sqrt{\epsilon}$ at least approximately. (We neglect the degradation of energy.) At present we have no completely satisfactory way of knowing the degree of polarization of the beam.

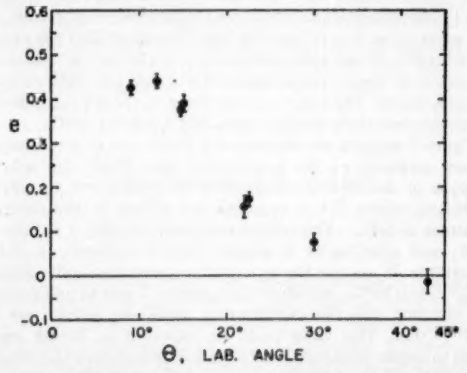

FIG. 3. The asymmetry parameter ϵ plotted as a function of the laboratory angle Θ for scattering from a carbon target at position B. Different absorbers were used in the counter telescope at different angles as outlined in the text. The errors shown indicate counting statistical errors.

A curve with targets A and B of carbon is given in Fig. 3. This curve is obtained with an absorber in the telescope which would cut off protons with an energy smaller than $\frac{1}{4}$ of the energy $E\cos^2\Theta$ which would obtain in an elastic nucleon-nucleon scattering. It shows that at 30° the polarization is sufficiently small to have escaped Marshall, Nedzel, and Marshall.

Since in the case of carbon a large part of the scattering might be inelastic, especially at large Θ, it is important to investigate ϵ not only as a function of Θ but also of the energy of the protons detected. We have started this investigation by taking measurements with various energy cutoff values by inserting various absorber thicknesses in our counter telescope at $\Theta=15°$ and 9°. In each case the lowest energy group of scattered protons (0 to 210 Mev) shows no observable asymmetry. For $\Theta=15°$ the intermediate energy group (210 to 280 Mev, quasielastic scattering) gives large asymmetry with $\epsilon=0.37\pm0.04$, and the elastically scattered protons (290 Mev) indicate $\epsilon=0.45\pm0.04$. For $\Theta=9°$, the elastically scattered protons show $\epsilon=0.43\pm0.02$.

If the beam polarization P were known, we could determine the polarization in scattering by hydrogen P_H from the relation $\epsilon_H=P\,P_H$. If we tentatively assume that $\epsilon_C=P^2$ (even though the carbon scattering is not elastic) then we obtain from the data for $\Psi=\Theta=20°$ the result $P=0.5$, and $P_H=2\epsilon_H$. This allows a provisional interpretation of the data of Fig. 2. Quite aside from the absolute value of P_H, its angular distribution is given in Fig. 2 and this indicates a more complex dependence than the $\sin(2\vartheta)$ dependence obtained by considering only s and p waves.

* This work was done under the auspices of the U. S. Atomic Energy Commission.

[1] Oxley, Cartwright, Rouvina, Baskir, Klein, Ring, and Skillman, Phys. Rev. 91, 419 (1953).

[2] Marshall, Nedzel, and Marshall, Phys. Rev. 93, 927 (1954). Chicago meeting.

[3] Chamberlain, Segrè, and Wiegand, Phys. Rev. 83, 923 (1951).

Polarization by p-p Collision at 310 Mev*

J. MARSHALL, L. MARSHALL, AND H. G. DE CARVALHO
Institute for Nuclear Studies, University of Chicago, Chicago, Illinois
(Received January 25, 1954)

THE discovery of polarized protons at 240 Mev by Oxley and co-workers[1] led us to look for similar phenomena at 320 to 430 Mev. For angles and energies consistent with quasi-free nucleon scattering inside the beryllium nucleus from 25° to 35°, we have reported an unsuccessful search.[2] We are grateful to Segrè for telling us of preliminary results at Berkeley indicating production of a polarized 340-Mev proton beam by small-angle scattering from carbon. Following this lead, we have obtained a polarized proton beam of about 310 Mev by scattering of 322-Mev average energy protons at 14° to the right from a beryllium target inside the cyclotron. The polarization has been demonstrated by a second scattering on a beryllium target outside the cyclotron giving asymmetries as high as 80 percent. The polarization increases as shown in Fig. 1 with thickness of absorber as if the main polarized component were the elastic scattering. We estimate a rough value of the amount of polarization of the beam as ($\frac{1}{3}$ asymmetry)[1] (see definitions in reference 1), where the asymmetry is measured at 14° excluding the nucleon-scattered component, these conditions being true for both first and second scatterings. Our beam therefore is believed to be ~60 percent polarized.

Liquid hydrogen was substituted for the second beryllium target, and the asymmetry of scattering was measured as shown in Fig. 2. The polarization due to hydrogen, P_H, is obtained from the data of Fig. 2 according to the relation $0.6\,P_H=\frac{1}{3}$ asymmetry. A phase shift analysis indicates that the asymmetric part of the p-p scattering should vary as $\sin\theta\cos\theta$, where θ is the barycentric angle if only ^3P states act, but if ^3P and ^3F states both are important, the asymmetry should vary as $\sin\theta\cos\theta(a+b\cos^2\theta+c\cos^4\theta)$. The singlet states do not give asymmetric terms. The data of Fig. 2 indicate large values of b and c and a small value of a. We are investigating the effect of this result on the phase shifts.

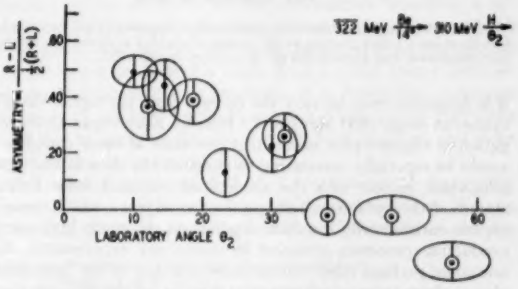

FIG. 2. Asymmetry produced by second scattering from liquid hydrogen of estimated 60 percent polarized 310-Mev proton beam.

The values of p-p differential scattering cross section previously reported by us[3] were for a beam scattered first to the right at a small angle and scattered externally always to the left. The evidence of Fig. 1 is that a similar beam at 310 Mev is polarized. The evidence of Fig. 2 is that cross sections measured to the left will be lower than the cross sections for a nonpolarized beam. Consequently our cross sections at 420 Mev may have been low at small angles. This point is under further investigation.

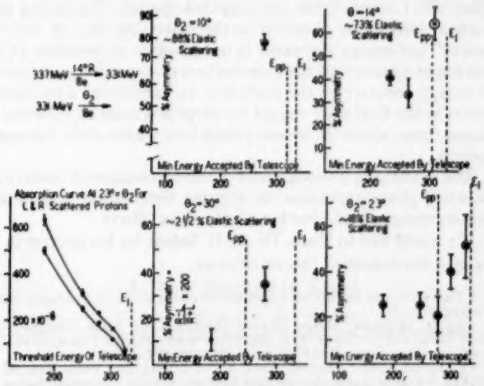

FIG. 1. Dependence of polarization of beryllium-scattered protons on scattering angle θ_2 and on energy of scattered protons. E_1 is the energy of protons incident on the second beryllium target. E_{pp} is the energy a proton would have if scattered by a free nucleon. The high absorption curve at $23°=\theta_2$ is for right-scattered protons, the lower for left. The percent elastic scattering is estimated by using the elastic scattering cross sections measured by Moyer *et al.* (see reference 4) at 340 Mev.

* Research supported by a joint program of the U. S. Office of Naval Research and the U. S. Atomic Energy Commission.

[1] Oxley, Cartwright, Rouvina, Baskir, Klein, Ring, and Skillman, Phys. Rev. 91, 419 (1953).

[2] Marshall, Nedzel, and Marshall, Phys. Rev. 93, 927 (1954).

[3] Marshall, Marshall, and Nedzel, Phys. Rev. 93, 927 (1954).

[4] Richardson, Ball, Leith, and Moyer, Phys. Rev. 86, 29 (1952).

Energy Spectrum of Negative Pions Produced in Beryllium by 2.3-Bev Protons*

LUKE C. L. YUAN AND S. J. LINDENBAUM
Brookhaven National Laboratory, Upton, New York
(Received January 5, 1954)

THE study of pion production by nucleon-nucleon and nucleon-nucleus collisions is of considerable basic interest, and a number of experiments have been performed[1] both at comparatively low-incident nucleon energies (up to 440 Mev) with particles produced by particle accelerators and at extremely relativistic energies with cosmic-ray particles. The existing experimental data have shed considerable light on the nature of the π meson and its interaction with nucleons. Since the Brookhaven Cosmotron produces protons of energies up to about 2.3 Bev and

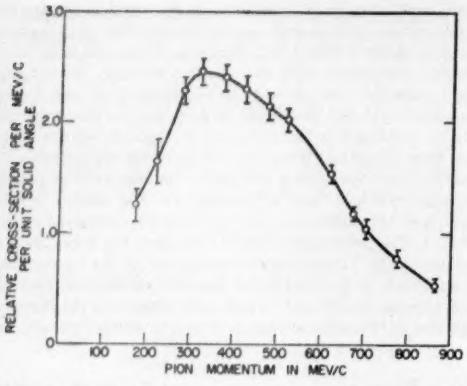

FIG. 1. The relative momentum spectrum of negative pions produced in beryllium by 2.3-Bev protons at 32° in the laboratory system. The momentum resolution was approximately 10 percent (total width).

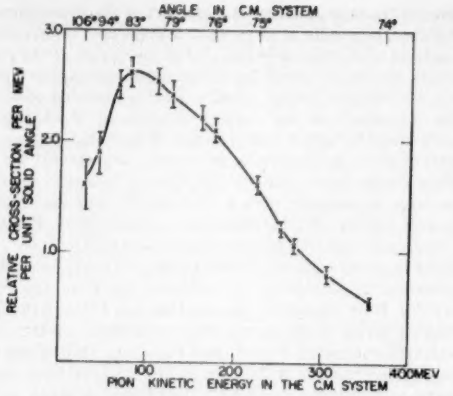

FIG. 2. The relative energy spectrum of negative pions, transformed to the proton-nucleon center-of-mass system (assuming that the pions are produced effectively by proton-nucleon interaction in beryllium.

it is relatively easy to vary the energy[2] from the top of the FM cyclotron range (400 Mev) to 2.3 Bev, we have begun an investigation of charged-pion production processes at these energies. It would be especially interesting to compare the data in this near-relativistic region with the predictions obtained from Fermi's statistical theory[3] for multiple production of pions, which seems to explain satisfactorily the data obtained on extremely high-energy production processes observed in cosmic-ray experiments. Also one could perhaps expect to see some evidence of the "apparent" pion-nucleon resonance interactions[4] in the production processes.

We have obtained preliminary results for the energy spectrum of negative pions emitted at 32° (laboratory angle) from a 2×2×6 inch beryllium target when bombarded by 2.3-Bev protons. The experimental arrangement was similar to that previously described.[4] A 3-inch collimator looked directly at the beryllium target (in a straight section outside the magnet quadrant) at an angle of 32° from the incident beam direction. A double-coincidence counter telescope defined and monitored the incident beam. An analyzing magnet followed by a third counter, displaced by 30°, in triple coincidence measured the relative fraction of negative particles of a particular momentum range. By varying the magnet current, the relative momentum spectrum of the negative particles issuing from the target was determined. The percentage of pions at each momentum was determined by range-curve analysis of the beam as previously described.[4] A correction for the π-μ decay in flight was applied to the data. The relative momentum spectrum deduced for negative pions in the laboratory system at 32° is shown in Fig. 1. The momentum resolution was approximately constant and about 10 percent (total width) for all points.

If one makes the assumption that beryllium is a light enough nucleus so that one is essentially observing the elementary proton-nucleon production of mesons, without appreciable subsequent scattering and reabsorption of the mesons produced, one can transform the observed spectrum in the laboratory system back to the proton-nucleon center-of-mass system. This has been done in Fig. 2, neglecting the Fermi momentum distribution of the nucleons involved. An analysis of the effect of the Fermi motion demonstrates that the energy transformation back to the c.m. system is affected only slightly (a few percent) by the Fermi motion.

The angular range seen in the c.m. system is rather narrow (between 74 and 80°) except for the lower-energy points where the angle rises rapidly to about 105° for the lowest-energy point observed. The effect of the Fermi motion is only to smear out the angular region observed by a few degrees. Hence one is essentially observing the energy spectrum in the region near 90° in the c.m. system. The most striking feature of the energy spectrum is the dominance of low-energy mesons and the existence of a well-defined peak in the region of 75–100 Mev. The total energy available in the c.m. system is 930 Mev. The mean total energy of the negative pions is ~300 Mev. Therefore, if one assumes that all of the available energy in the c.m. system went into meson production and that the π^+ and π^0 spectra are similar to the π^- spectrum, we might expect a mean multiplicity of ~3. However, the nucleons carry away some kinetic energy, and therefore the mean multiplicity probably is less than three.

The general shape of the energy spectrum as shown in Fig. 2 suggests a comparison with the Fermi statistical type of meson production process. Christian and Yang[5] have calculated the spectra for one-, two-, and three-meson production processes according to the Fermi theory.[3] Our results appear to be consistent with a mixture of mostly double and some (~10 percent) triple meson production.[6] Christian and Yang[5] have recalculated the relative weights of the various multiplicities predicted by the Fermi theory using more exact statistical weight expressions and taking into account the rest mass of the meson. They concluded that one-meson production should be highly dominant. The predicted spectrum would then favor a peak at much higher energies in the c.m. system and hence be in disagreement with our results.

If one assumes that the spectra for the different multiplicities predicted by the Fermi theory are correct, one concludes that double and triple production are favored for some other reason than the simple statistical factors considered. Of course, some other effect could distort the expected spectra. The strong pion-nucleon interaction observed in the scattering data at the "apparent" low-energy resonance is one possible explanation. In fact one might assume that the pion-nucleon cross section, as a function of energy (relative to the nucleons), be considered a multiplying factor in the final state weight for these processes and thereby enhance those modes of meson production which yield low-energy mesons.

The continuing investigations of the dependence of positive and negative pion production on angular distribution and incident proton energy should further clarify these effects.

We would like to thank Dr. E. O. Salant for his interest in and helpful discussions of this experiment.

* This work was performed under the auspices of the U. S. Atomic Energy Commission.

[1] See R. Marshak, *Meson Physics* (McGraw-Hill Book Company, Inc., New York, 1952), Chaps. 2, 3, and 8, for work prior to July 1, 1952.

[2] Cosmotron Issue, Rev. Sci. Instr. **24**, 723–898 (1953).

[3] E. Fermi, Progr. Theoret. Phys. **5**, 570 (1951), and Phys. Rev. **92**, 452 (1953). Fermi's statistical weights require a $1/n!$ correction factor [E. Fermi, Phys. Rev. **93**, 1434(E) (1954)].

[4] S. J. Lindenbaum and L. C. L. Yuan, Phys. Rev. **92**, 1578 (1953).

[5] R. Christian and C. N. Yang (private communication).

[6] Fowler, Shutt, Thorndike, and Whittemore, Phys. Rev. **91**, 758 (1953), have observed considerable double meson production (16 of 24 three-prong events produced by 1.5–2.3 Bev neutrons in a hydrogen-filled diffusion cloud chamber), but not one example of triple meson production in 100 cases.

Plutonium-244 from Pile-Irradiated Plutonium

M. H. Studier, P. R. Fields, P. H. Sellers, A. M. Friedman, C. M. Stevens, J. F. Mech, H. Diamond, J. Sedlet, and J. R. Huizenga
Argonne National Laboratory, Lemont, Illinois
(Received February 1, 1954)

THE high neutron flux of the Materials Testing Reactor (MTR) enhances by manyfold the possibility of multiple-order neutron-capture reactions. For plutonium-239 irradiations, Studier and Manning[1] in a detailed calculation have plotted the expected yields of mass numbers up to 244 as a function of integrated flux. In a program designed to follow up these calculations, several plutonium-239 samples have been irradiated in the MTR for progressively longer periods of time, the sample described here having an integrated flux of 4×10^{21} neutrons. Details of the experimental assembly in which the plutonium is irradiated are given elsewhere.[2]

The chemical procedure used was one which separated the plutonium from the *trans*-plutonium elements and the bulk of the fission products in the early stages of purification by utilizing the multivalency of plutonium. The separated plutonium fraction was then further purified by precipitations and solvent extractions.

The plutonium was analyzed in a 12-inch, 60-degree mass spectrometer using a multiple-filament source. The isotopic distribution agreed very well with the calculations of Fields and Weiss[3] in which they used more recent cross-section values than the earlier values used by Studier and Manning. In addition to the plutonium isotopes 239, 240, 241, 242, previously produced and identified in pile irradiations, this plutonium sample also contained Pu^{244}.[4] The Pu^{244}/Pu^{242} mole ratio was 0.0036 percent. Plutonium-244 is produced from Pu^{239} in the pile by the reactions shown in Fig. 1. The solid arrows represent the predominant reactions causing the production of the higher masses in the MTR. The dashed arrows indicate reaction paths of secondary importance. Plutonium-244 is formed by $Pu^{243}(n,\gamma)Pu^{244}$ reaction and possibly by electron capture of Am^{244}.

On the basis of a predicted alpha disintegration energy of 4.7 Mev for Pu^{244}, a closed cycle shows Pu^{244} to be approximately 1.3 Mev heavier than Cm^{244}. If the β^- energy of Am^{244} is greater than 1.3 Mev, it will be electron-capture unstable. If the β^- energy of Am^{244} is less than 1.3 Mev, Pu^{244} will be β^- unstable. In any case arguments from heavy element systematics indicate that the energies will be small (i.e., either the β^- energy of Pu^{244} or the electron-capture energy of Am^{244}). Other experiments have shown the β^- half-life of Pu^{244} to be greater than 1000 years[5] (the alpha half-life of Pu^{244} is estimated to be approximately 10^7 years). The capture cross section of Pu^{242} calculated from the data of this irradiation is 30 ± 10 barns in agreement with the earlier value.[6] Assuming all of the Pu^{244} to be produced by the $Pu^{243}(n,\gamma)Pu^{244}$, reaction and Pu^{242} to have a 30-barn capture cross section, the pile neutron-capture cross section of Pu^{243} is about 100 barns. On the other hand, if one assumes all the Pu^{244} to come from electron capture of Am^{244}, the electron-capture branching is approximately 0.5 percent. Assuming the tentative assignment[7] of a 25-minute β^- half-life for Am^{244} to be correct, the electron-capture half-life is greater than 3.4 days. Since a much longer electron-capture half-life would be predicted, it is reasonable to assume that most of the Pu^{244} comes from neutron capture by Pu^{243}. The possibility of energetic isomers of Am^{244} does, however, cast some doubt on the above assumption.

The technical assistance of C. H. Youngquist in the engineering aspects of these experiments is gratefully acknowledged. We also wish to thank W. M. Manning for many stimulating discussions.

[1] M. H. Studier and W. M. Manning (unpublished).
[2] A. B. Shuck (unpublished).
[3] P. R. Fields and M. A. Weiss (unpublished).
[4] This isotope was previously discovered by Hess, Fried, Pyle, and Ingram (unpublished).
[5] Fried, Pyle, and Fields (private communication).
[6] Pyle, Fields, and Huizenga (unpublished).
[7] Street, Ghiorso, and Seaborg, Phys. Rev. 79, 530 (1950).

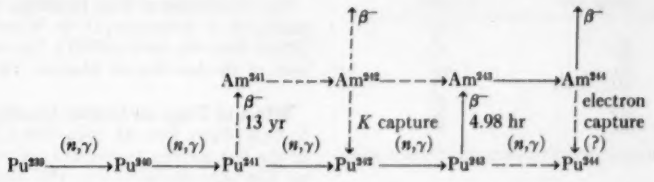

FIG. 1. Reactions in pile-irradiated Pu^{239}.

A New Isomer in Lead

D. Maeder* and A. H. Wapstra
Instituut voor Kernphysisch Onderzoek, Amsterdam, The Netherlands
(Received January 27, 1954)

IN irradiations of Tl with 26-Mev deuterons, a new 3.5 ± 0.1 hr activity appeared in the Pb fraction. Its excitation curve, compared with those of 1.1-hr Pb^{204*} and 2.3-day Pb^{203} pointed to the reaction $Tl^{205}(d,3n)Pb^{203*}$. This activity has been studied with NaI scintillation spectrometers and a β-ray spectrometer. The γ rays, found in this isomer, are collected in Table I, together with their assignments, [based on $K/(L+M)$ ratios, conversion coefficients and half-lives] and the relative intensities of the transitions (γ rays+conversion electrons).

A decay scheme, derived from these data, is shown in Fig. 1. This decay scheme is consistent with the results of γ-γ coincidence measurements made with two scintillstion spectrometers in coincidence. The relative position of the 956-kev and 416-kev transitions is not determined; comparison with the first excited state in Pb^{204} and Pb^{206} suggests that the 416-kev transition should be the lower one. An $E1$ γ ray of 200 kev with an intensity of about 8 percent should also be present. Its K conversion line coincides

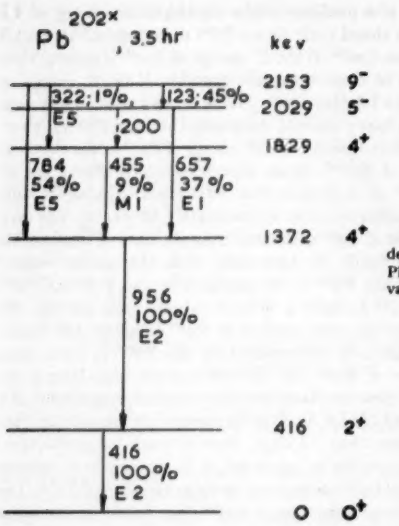

FIG. 1. Proposed decay scheme of Pb^{202*} (energy values in kev).

with the strong M conversion line of the 123-kev γ ray, and the L conversion line with the 196-kev conversion line of Pb^{203}, which was also present in the sample; in the scintillation spectrum the 277-kev Pb^{203} γ ray and the backscattering peak hinder the detection of this γ ray.

A more extensive report will be published in Physica. We thank Dr. C. J. Bakker and Dr. A. H. W. Aten, Jr., for their interest,

TABLE I. γ rays in Pb^{202*}.

Energy (kev)	Assignment	Intensity
XK	—	~15
123 ±2	$E3,4$	45
322 ±4	$E5$	1.2
416 ±3	$E2$	102
455 ±4	$M1(+E2?)$	9
657 ±5	$E1$	40
784 ±4	$E5$	54
957 ±5	$E2$	98

R. H. Nussbaum, G. J. Nijgh, and L. T. M. Ornstein for help with the measurements, Mrs. T. de Vries-Hamerling for performing the chemical separations, and the Foundation for Fundamental Research of Matter (F.O.M.) of the Organization for Pure Scientific Research (Z.W.O.) for their support.

* On leave from the Eidgenossische Technische Hochschule in Zürich, Switzerland.

Errata

Interpretation of Electron Scattering Experiments, L. I. SCHIFF [Phys. Rev. 92, 988 (1953)]. The last sentence at the end of the first paragraph: "This effect was noted earlier by M. Goldhaber and A. W. Sunyar [Phys. Rev. 83, 906 (1951)]" should have been placed at the end of footnote 3B.

Neutron Capture γ Rays from Scandium, Vanadium, Manganese, Cobalt, and Copper, G. A. BARTHOLOMEW AND B. B. KINSEY [Phys. Rev. 89, 386 (1953)]. Because of a regrettable oversight, the intensities for the vanadium γ rays given in Tables II and III of this paper are too large by a factor of 1.56. However, this error does not apply to Fig. 4. We are indebted to Dr. P. S. Mittelman for drawing our attention to this point.

Effects of the Atmosphere on the Penetrating Cosmic Radiation, ROBERT L. CHASSON [Phys. Rev. 89, 1255 (1953)]. In Table I, the signs of the temperature coefficients of Duperier and Chasson should be + rather than −.

The Energy Loss of a Fast Charged Particle by Čerenkov Radiation, R. M. STERNHEIMER [Phys. Rev. 91, 256 (1953)]. In this paper a dimensionless quantity b_p was defined as $b/(c/\nu_p)$, where b is the impact parameter. This definition should be $b/(c/2\pi\nu_p)$. All of the equations are unaffected, in particular Eqs. (1), (35), and (36) for the Čerenkov loss W_b. However, Eq. (24) for κ_p gives the absorption coefficient for a length $c/2\pi\nu_p$ instead of c/ν_p. The numerical values of b_p for the examples considered are increased by a factor 2π. As a result W_b is smaller than the values given in the paper. The case of emulsion [also reported in Phys. Rev. 89, 1148 (1953)] was recalculated using $b_p=31.4$. This gives $W_b(\infty)\cong 0.4\times 10^{-3}$ Mev/g cm^{-2}. The values of W_b for gases given in Table II should be decreased by $\frac{1}{2}Af_j \ln(2\pi)$, which is 0.104 Mev/g cm^{-2} for H_2, 0.052 Mev/g cm^{-2} for He, and 0.0135 Mev/g cm^{-2} for O_2 (model II). The resulting values of $W_b(\infty)$ (in Mev/g cm^{-2}) are 0.128 for H_2, 0.088 for He, and 0.0165 for O_2. $W_b(\infty)$ for Xe becomes 0.058 Mev/g cm^{-2}. Figure 1 for the Čerenkov loss J in emulsion pertains to $b=0.02\mu$ (instead of 0.13μ) and Fig. 3 pertains to $b=0.013$ cm (instead of 0.081 cm).

In the second line below Eq. (6), ν_{18} should be ν_{14}.

A Precision Measurement at 24 500 Volts of the Conversion Constant λv, GAELEN L. FELT, JOHN N. HARRIS, AND JESSE W. M. DUMOND [Phys. Rev. 92, 1160 (1953)]. The title should read: "A Precision Measurement at 24 500 Volts of the Conversion Constant λV."

The Scattering of Fast Neutrons by Iron, Lead, and Chromium, M. A. ROTHMAN, D. W. KENT, AND C. E. MANDEVILLE [Phys. Rev. 92, 1097 (1953)]. The word "unresolved" on the next to the last line of Abstract P6 should read "resolved."

Effect of Traps on Carrier Injection in Semiconductors, H. Y. FAN [Phys. Rev. 92, 1424 (1953)]. The factor τ_g appearing in the last section on the drift of injected carriers should be τ_f. The term dn_t/dt in Eqs. (18) and (26) should be replaced by $(R_{et}-R_{te})$, if the electron transitions between the traps and the conduction band were to be taken into account. In that case, the coefficient of Δn_t in (21) and the coefficient of Δp in (27) will become $[(1/\tau_f\tau_r)+(1/\tau_c\tau_t)]$ instead of $(1/\tau_f\tau_r)$, where $1/\tau_c=r_c(n_0+n_1)$.

A Binding Energy Calculation on He^4 with Single-Particle Wave Functions, P. G. WAKELY [Phys. Rev. 90, 724 (1953)]. The third square bracket in the wave function Ψ_2 should read $[\sqrt{\frac{1}{2}}\Phi(sp[2]^3P,sp[2]^3P,{}^1S)-\sqrt{\frac{1}{2}}\Phi(sp[2]^1P,sp[2]^1P,{}^1S)]$. The state referred to earlier as $(9s)^2(2p)^2[4]^1S$ should of course be $(1s)^2(2p)^2[4]^1S$.

Multiple Production of Pions in Nucleon-Nucleon Collisions at Cosmotron Energies, E. FERMI [Phys. Rev. 92, 452 (1953)]. In computing the statistical weights of the various states discussed in this paper, a factor $1/n!$ (n = number of pions) was omitted. For this reason, the statistical weights given in column 2 of Table II and in columns 2 and 3 of Table III should be divided by the factorials of the number of pions given in column 3 of Table II and column 4 of Table III. Corresponding changes should be made in the computed probabilities for the two cases. This correction has the effect of reducing the probability of events with high multiplicity. For example, for a neutron-proton collision, the probabilities of stars with 1, 3,

THE PHYSICAL REVIEW

A journal of experimental and theoretical physics established by E. L. Nichols in 1893

VOLUME 93

Second Series

JANUARY 1–MARCH 15, 1954

Published for the

AMERICAN PHYSICAL SOCIETY

by the

AMERICAN INSTITUTE OF PHYSICS

Incorporated

THE PHYSICAL REVIEW

A journal of experimental and theoretical physics established by E. L. Nichols in 1893

Published by the American Institute of Physics for the

AMERICAN PHYSICAL SOCIETY

Officers

President

ENRICO FERMI
Institute for Nuclear Studies
University of Chicago
Chicago 37, Illinois

Vice-President

H. A. BETHE
Cornell University
Ithaca, New York

Secretary

K. K. DARROW
Bell Telephone Laboratories
Office:
Columbia University
New York 27, New York

Treasurer

G. B. PEGRAM
Columbia University
New York 27, New York

Local Secretary for the Pacific Coast

J. KAPLAN
University of California at Los Angeles
Los Angeles, California

Managing Editor

S. A. GOUDSMIT
Brookhaven National Laboratory
Upton, Long Island
New York

BOARD OF EDITORS

Editor

S. A. GOUDSMIT

Assistant Editor

S. PASTERNACK

Associate Editors

1951–1953	*1952–1954*	*1953–1955*
C. L. CRITCHFIELD	W. P. ALLIS	W. A. FOWLER
M. DEUTSCH	F. G. BRICKWEDDE	KENNETH GREISEN
M. GOLDHABER	W. B. FRETTER	CHARLES KITTEL
T. H. JOHNSON	CONYERS HERRING	R. E. MARSHAK
R. SERBER	H. W. LEVERENZ	W. K. H. PANOFSKY
C. H. TOWNES	ARNOLD NORDSIECK	V. F. WEISSKOPF

Manuscripts for publication should be submitted to S. A. GOUDSMIT, Brookhaven National Laboratory, Upton, Long Island, New York. The authors' institutions are requested to pay a publication charge of $15 per page which, if honored, entitles them to 100 free reprints. Instructions will be sent with galley proofs.

Proof and all correspondence concerning papers in the process of publication should be addressed to the Publication Manager, American Institute of Physics, 57 East 55 Street, New York 22, New York.

Subscription Price

United States and Canada $30.00
Elsewhere $32.00

Back Numbers [1]

Yearly back number rate when complete year is available:
Prior to 1949: $25.00
Thereafter: $33.00
Single copies: $3.00 each, prior to July, 1929;
$1.50 each, July, 1929–December, 1941;
$3.00 each, January, 1942–December, 1946;
$1.50 each, thereafter.
General index, 1893–1920: $4.00.

Subscriptions, renewals, and orders for back numbers should be addressed to the American Institute of Physics, 57 East 55 Street, New York 22, New York.

Changes of address in the case of members of the American Physical Society should be addressed to the Treasurer; in the case of other subscribers to the American Institute of Physics.

[1] For Series 1 inquire of Physics Department, Cornell University, Ithaca, New York.

The Physical Review is published semi-monthly at Prince and Lemon Streets, Lancaster, Pennsylvania.

Entered as second-class matter March 6, 1947, at the Post Office at Lancaster, Pennsylvania, under the Act of March 3, 1879.

Acceptance for mailing at special rate of postage provided for in paragraph (d-2), section 34.40, P. L. & R. of 1948, authorized January 27, 1933.

or 5 prongs for 1.75-Bev bombarding energy become 68, 32, and 0.13 percent; for bombarding energy of 2.2 Bev, the probabilities are 62, 38, and 0.3 percent. For 3-pronged stars the probabilities of a star containing a single negative pion, or at least a negative and a neutral pion, or at least a positive and a negative pion, for bombarding energy of 1.75-Bev energy are 61, 11, and 28 percent; and for 2.2-Bev bombarding energy 47, 14, and 39 percent.

In this computation the possibility of deuteron formation by proton-neutron binding, as well as the elastic shadow scattering have been neglected.

Production of Polarized Particles in Nuclear Reactions, A. SIMON AND T. A. WELTON [Phys. Rev. 90, 1036 (1953)] and **Theory of Polarized Particles and Gamma Rays in Nuclear Reactions,** ALBERT SIMON [Phys. Rev. 92, 1050 (1953)]. In these two papers (hereafter referred to as I and II, respectively), the operators T_s^q were assumed to be tensor operators defined by the commutation relations given by Racah[1] and were normalized by the requirement that $T_0^q = P_q \times([i_s/i(i+1)]^{\frac{1}{2}})$. Innes[2] has kindly pointed out that the normalization of the operators T_s^q cannot be correct for $q>2$ since for these cases the matrix element[3] $(ii|T_0^q|ii)$ has nonzero values for $2i<q$ and hence the operator will not be irreducible. The difficulty appears to lie in the circumstance that the commutation relations of Racah[1] are a necessary but not a sufficient condition for the irreducibility of the tensor operators. In our papers the operator T_s^q was assumed to transform irreducibly and the only use of the definition of T_0^q was in normalizing the final result. Hence all general results such as angular dependences, selection rules, etc., are correct and all that must be changed is the coefficient preceding the summation symbol in several of the equations.

A suitable normalization of the tensor operators may be obtained by defining

$$T_0^q = \Sigma_m (iqm0|iqim)\chi_m^{i}\chi_m^{i*}, \tag{1}$$

where χ_m^i is a state vector of spin i and z component m. This operator is irreducible by construction. It is identical to the previous operator for $q=0$ and 1 and differs only by the constant factor $[4i(i+1)/[(2i-1)(2i+3)]]^{\frac{1}{2}}$ for $q=2$. Since all special cases discussed in the papers involve $q \leq 2$, all results for these cases will still be correct with the understanding that T_0^2 is as defined previously.

Equations involving the general operator T_s^q will have a changed coefficient which is easily found by the use of Eq. (1) and the procedure of Appendix A of I. The reduced matrix element of T_s^q is now $(2i+1)^{\frac{1}{2}}$ rather than $[(2i-q)!(2i+q+1)!]^{\frac{1}{2}}P_q([i/(i+1)]^{\frac{1}{2}})/(2i)!$ Hence the coefficient of Eq. (6.3) of I becomes $(\pi)^{\frac{1}{2}}\lambda_a^2(2i+1)^{\frac{1}{2}}/[2(2I+1)(2i+1)]$ rather than the more complicated expression given previously. The new coefficient of Eq. (3.2) of II is

$$\lambda_a^2[(2i'+1)(2q+1)]^{\frac{1}{2}}/\{4(2I+1)[(2i+1)(2q+1)]^{\frac{1}{2}}\}.$$

The correction for the remaining equations is similar.

We wish to take this opportunity to thank Dr. Innes for calling our attention to this point.

[1] G. Racah, Phys. Rev. 62, 442 (1942).
[2] F. R. Innes (private communication).
[3] See Appendix A of I.

Total Cross Section for Positive Pions in Hydrogen, STANLEY L. LEONARD AND DONALD H. STORK [Phys. Rev. 93, 568 (1954)]. In the issue, the word "Pions" in the title appeared incorrectly as "Ions."

Author Index to Volume 93

References with (A) are to abstracts of papers presented at meetings of the American Physical Society; references with (T) are to titles of invited papers; references with (L) are to Letters to the Editor; references with (E) are to Errata.

Abeles, B. (see Meiboom, S.)—1121(L)

Abell, D. F. and W. D. Knight. Saturation behavior of Gaussian magnetic resonance line—940(A)

Adair, R. K. (see Darden, S. E.)—931(A)

Adams, Raymond V. Decay of elementary particles—363(T)

—— (see Whetten, N. R.)—1356

Aden, A. L. (see Faire, A. C.)—650(A)

Aitken, A., H. Mahmoud, E. M. Henley, M. A. Ruderman, and K. M. Watson. Some possible relationships between π-meson nucleon scattering and π-meson production in nucleon-nucleon collisions—1349

Ajzenberg, F., W. Franzen, and J. G. Likely. Neutrons from proton bombardment of N^{15}—925(A)

Alger, R. S. Coloring and bleaching of alkali halide crystals containing U centers—953(A)

Allen, J. R. Specific ionization and energy loss of fast charged particle—353(L)

Allis, W. P. and D. J. Rose. Transition from free to ambipolar diffusion—84

Amin, M. R. Fast time analysis of burst pulse, Preonset streamer, and Trichel pulse point-to-plane coronas—649(A)

Andersen, E. (see McReynolds, A. W.)—195

Anderson, A. B. C. Jet-tone orifice number for orifices of small thickness-diameter ratio—946(A)

Anderson, J. D., C. A. McDonald, Jr., and R. F. Post. Triplet production in H_2 at 300 Mev by a total absorption method—948(A)

Anderson, J. M. and L. Goldstein. Phenomena associated with small temperature variations of electron gas in discharge plasmas around 300°K. I. Cross modulation—648(A)

—— (see Goldstein, L.)—648(A)

Anderson, K. (see Winckler, J. R.)—596

Anderson, P. W., F. R. Merritt, J. P. Remeika, and W. A. Yager. Magnetic resonance in αFe_2O_3—717

Andre, C. G. and J. R. Huizenga. Neutron binding energy in Bi^{210}—931(A)

——, **W. J. Ramler, E. G. Rauh, R. J. Thorn, and J. R. Huizenga.** Proton-induced reactions in Bi—925(A)

Ang, C. and C. Wert. Internal friction of alloys Au and Ni—922(A)

Arnold, J. S. (see Sherburne, R. K.)—946(A)

Arnold, James R. Energy levels in Lu^{176} and Hf^{176}—743

Arnold, W. R., J. A. Phillips, G. A. Sawyer, E. J. Stovall, Jr., and J. L. Tuck. Cross sections for reactions $D(d,p)T$, $D(d,n)He^3$, $T(d,n)He^4$, and $He^3(d,p)He^4$ below 120 kev—483

Arroe, Hack. Isotope shift in $_{58}$Ce II spectrum—94

—— Isotope shift in spectra of some elements of intermediate atomic number—933(T)

Asaro, Frank and I. Perlman. Decay properties of Am^{243} and possible rotational bands in α spectra of odd-even nuclei—1423(L)

Ashkin, J., J. P. Blaser, F. Feiner, J. Gorman, and M. O. Stern. Total cross sections of 135-Mev to 250-Mev negative pions in H—1129(L)

Atkins, K. R. and M. H. Edwards. Coefficient of expansion of liquid He II—1416(L)

Atterling, Hugo (see Slätis, Hilding)—646(L)

Aukerman, L. W. Photoinduced conductivity in solutions of anthracene in n-hexane—929(A)

Austern, N. (see Butler, S. T.)—355(L)

Azumi, K. and J. E. Goldman. Volume magnetostriction in Ni and Bethe-Slater interaction curve—630(L)

Backman, M. E. and H. L. Morrison. Measurements of Rittenger's number for glass and decomposed granite—953(A)

Baez, A. V. and M. Weissbluth. X-ray microscope mirror systems—942(A)

Ballam, J. and P. G. Lichtenstein. Interaction and production of cosmic-ray protons in C—851

Band, William. Low-temperature diamagnetism of electrons in cylinder—350(L)

Bandel, H. W. Current growth in formative time lag of sparks—944(A); 649(A)

Banta, H. E. (see Macklin, R. L.)—924(A)

Baranger, Elizabeth Urey. Scattering of high-energy electrons by heavy nuclei—1127(L)

—— (see Yennie, D. R.)—1128(L)

Barber, W. C. Specific ionization of high-energy electrons in H_2 and N_2—942(A)

Barbour, Ian G. Emulsion studies of cosmic-ray stars produced in metal foils—535

Barbour, J. P. (see Dolan, W. W.)—943(A)

Barden, S. E. Space-charge forces in strong-focusing synchrotrons—1378

Barnes, B. T. Physical processes in fluorescent lamps—359(T)

Barnes, C. A. (see Peterson, R. W.)—951(A)

Barnes, C. B. (see Heer, C. V.)—362(A)

Barnes, R. G. and W. V. Smith. Electric field gradients of atomic p electrons—95

Barnett, C. F. (see Stier, P. M.)—926(A)

Barschall, H. H. Interactions of fast neutrons with heavy nuclei—917(T)

—— (see Walt, M.)—1062

Bartholomew, G. A. and B. B. Kinsey. Neutron capture γ rays from Sc, V, Mn, Co, and Cu—1434(E)

—— (see Kinsey, B. B.)—1260

Barut, A. O. Mechanism of secondary electron emission—981

Batzel, R. E. and G. H. Coleman. Cross sections for formation of Na^{22} from Al and Mg bombarded with protons—280

Bayard, Robert T. and J. L. Yntema. Elastic scattering of 1-Mev electrons from Al and Au—1412(L)

Beard, David Breed. Interpretation of experiments on nuclear temperatures—950(A)

Bearden, J. A., M. D. Earle, J. M. Minkowski, and J. S. Thomson. Present status of atomic constants—629(L)

Becker, E. W., R. Misenta, and F. Schmeissner. Viscosity of gaseous He^3 and He^4 between 1.3° and 4.2°K—244(L)

Bedard, F. D. (see Gallagher, J. J.)—729

Beeninga, D. E. Opportunities for physics graduates in General Electric—360(T)

Beer, A. C., R. K. Willardson, and A. E. Middleton. Degeneracy in high-purity InSb—912(A)

—— (see Harman, R. K.)—912(A)

—— (see Willardson, R. K.)—912(A)

Belinfante, F. J. Positon theory without "holes"—935(A)

Bell, E. E. (see Burstein, E.)—65

Belser, Richard B. and Margaret C. Chester. Observation of diffusion effects occurring during artificial aging of dual layer bi-metal films—937(A)

—— **and Margaret C. Chester.** Electrical resistances of dual layer and simultaneously evaporated bi-metal films before and after artificial aging—930(A)
—— **and Walter H. Hicklin.** Effects of alloying actions of dual-layer bi-metal electrodes on frequencies of piezoelectric quartz resonators—937(A)
—— (see Raudebaugh, Robert J.)—930(A)
—— (see Woolf, William E.)—930(A)
Bengston, J. (see Thaler, R. M.)—643(L); 644(L)
Bennett, W. E., P. A. Roys, and B. J. Toppel. Low-energy yield of (α,n) reactions—924(A)
—— (see Bradford, C. E.)—921(A)
Berlincourt, D. A. Low-temperature coefficient ceramics—362(A)
Berlincourt, Ted G. and John K. Logan. Further correlation between magnetoresistance variations and de Haas-van Alphen effect—348(L)
Bernardini, Gilberto. Photomesons near production threshold—930(T)
Bernstein, Richard B. (see Cleveland, Forrest F.)—933(A)
Bernstein, Seymour (see Roberts, L. D.)—917(T)
—— (see Stanford, C. P.)—931(A)
Bernstein, W., S. S. Markowitz, and S. Katcoff. Radiations of 13.9-min Ce^{148} and 24.4-min Pr^{146}—1073
—— (see Markowitz, S. S.)—178
Bessey, William H. and Harold Weisbrod. Thermal conductivity of NaCl—923(A)
Bethe, H. A. and L. C. Maximon. Theory of bremsstrahlung and pair production. I. Differential cross section—768
—— (see Breit, G.)—888
—— (see Davies, Handel)—788
Bhatnagar, P. L. (see Krook, M.)—936(A)
Biedenharn, L. C. and J. M. Blatt. n-p scattering with spin-orbit coupling. II. Variational formulation and effective range theory—1387
—— **and J. M. Blatt.** Variation principle for eigenfunctions—230
—— (see Sack, S.)—321
Biondi, Manfred A. Diffusion cooling of electrons in ionized gases—1136
—— Doppler broadening of dissociative recombination lines—650(A)
Birnbaum, Milton. Precision determination of photoneutron thresholds—146
Blair, J. M. (see Hintz, N. M.)—924(A)
Blanchard, C. H. (see Spencer, L. V.)—114
Blaser, J. P. (see Ashkin, J.)—1129(L)
Blatt, J. M. (see Biedenharn, L. C.)—230; 1387
Blau, Henry H., Jr., John H. Shaw, and Dudley Williams. Study of pressure broadening in near infrared—360(A)
Blau, M. (see Caulton, M.)—919(A)
Blewitt, T. H., R. R. Coltman, Jr., and J. K. Redman. Structural defects in Cu and the electrical resistivity minimum—891(L)
Blizard, J. B. European and American productivity in basic science—364(A)
Bloch, Claude. Theory of nuclear level density—1094
Bloch, Felix. Recent developments in nuclear induction—944(T)
Bloembergen, N. and S. Wang. Relaxation effects in para- and ferromagnetic resonance—72
Bloom, Arnold and Dolan Mansir. Measurement of nuclear induction relaxation times in weak magnetic fields—941(A)
Bloom, David S. Specific heat of alloy $FeNi_3$ and of sigma phase FeCr—953(A)
——, **H. S. Gutowsky, D. W. McCall, and J. G. Powles.** Effect of molecular motion on intensity of pure quadrupole resonances—920(A)
—— **and R. E. Norberg.** Transient nuclear induction signals associated with pure quadrupole interactions—638(L)
Boato, G. Primeval cosmic abundance of deuterium—640(L)
Bodansky, D., A. M. Sachs, and J. Steinberger. Scattering of 65-Mev pions in H—918(A); 1367
Boehm, F. and C. S. Wu. Internal bremsstrahlung and ionization accompanying β decay—518
Boorse, H. A. (see Worley, R. D.)—45
Borowitz, Sidney and Bernard Friedman. Three-body scattering problems—251(L)
—— (see Boyet, Howard)—1225
Bortner, T. E. and G. S. Hurst. Ionization of pure gases and mixtures of gases by 5-Mev α particles—1236
Boyet, Howard and Sidney Borowitz. Variational calculation of elastic scattering of electrons by H atoms—1225
Brachman, Malcolm K. Generalized Fermi-Thomas theory—636(L)
—— (see Smaller, B.)—940(A)
Bradford, C. E., T. Kikuchi, and W. E. Bennett. Ion source for doubly charged He—921(A)
Bradley, Richard C. Sputtering of alkali atoms by inert gas ions of low energy—719
—— Sputtering of alkali metals by inert gas ions of low energy—652(A)
Bramley, Arthur. Wavelength of scattered radiation—246(L)
Branscomb, Lewis M. and Wade L. Fite. Photodetachment of H_2 negative ion—651(A)
Breen, R. J. and A. H. Weber. Neutron diffraction in vitreous silica—923(A)
Breit, G. and H. A. Bethe. Ingoing waves in final state of scattering problems—888
—— (see Sack, S.)—321
—— (see Thaler, R. M.)—644(L)
Brice, M. K. (see Cork, J. M.)—1059
Briggs, H. B., R. F. Cummings, H. J. Hrostowski, and M. Tanenbaum. Optical properties of some group III-group V compounds—912(A)
Brinkman, J. A. Effect of temperature gradients on diffusion in crystals—345(L)
Brockhouse, B. N., L. M. Corliss, and J. M. Hastings. Diffuse magnetic scattering of neutrons: zinc ferrite—923(A)
Brode, Robert B. Cosmic-ray transition phenomena due to electrons, photons, and mesons—947(A)
Brodie, Laird C. Hall effect in Bi at low temperatures—935(A)
Broecker, W. S. (see Grosse, A. V.)—250(L)
Brooks, R. A. (see Dunlap, W. C., Jr.)—911(A)
Brown, Fielding and David Park. Magnetic resonance phenomena in ferrites—381
Brown, Karl L. and Richard Wilson. Electrodisintegration of Cu^{65}, Zn^{64}, Ag^{109}, and Ta^{181}—443
Brown, R. J. S. (see Famularo, K. F.)—928(A)
Brown, S. LeRoy (see Lee, Chu Jui)—945(A)
Brown, Sanborn C. Microwave studies of electron diffusion in gases—943(T)
—— (see Looney, Duncan H.)—649(A); 965
Brown, W. B. (see Hendee, C. F.)—651(A)
Brown, W. W. Cosmic-ray nuclear interactions in gases—518
——, **J. Oeser, H. H. Staub, and C. G. Telschow.** Nuclear magnetic moments of Xe^{129} and Xe^{131}—904(L)
Brun, E., J. Oeser, H. H. Staub, and C. G. Telschow. Nuclear magnetic moments of K^{41}, Y^{89}, Ag^{107}, and Ag^{109}—172
Burch, D. S., R. C. Irick, and R. Geballe. Further studies of photon production in externally sustained discharges—650(A)
Burger, E. E. (see Cobine, J. D.)—653(A)

Burke, Bernard F., M. W. P. Strandberg, Victor W. Cohen, and Walter S. Koski. Nuclear magnetic moment of S^{33} by microwave spectroscopy—193
Burke, W. H., Jr., and W. G. Meinschein. Methane proportional counter method for C^{14} age determinations—915(A)
——, **J. R. Risser, and G. C. Phillips.** Angular distributions and excitation curves for $B^{10}(d,p)B^{11}$ and $B^{10}(d,n)$ and $B^{11}(d,n)$ reactions below 2-Mev bombarding energy—188
Burrus, Charles A. and Walter Gordy. Sub-millimeter wave spectroscopy—897(L)
—— (see Gordy, Walter)—419
Burson, S. B. (see LeBlanc, J. M.)—916(A); 1124(L)
Burstein, Elias. Anomalous optical absorption limit in InSb—632(L)
——, **J. W. Davisson, E. E. Bell, W. J. Turner, and H. G. Lipson.** Infrared photoconductivity due to neutral impurities in Ge—65
Butler, S. T. and N. Austern. Coulomb corrections in stripping—355(L)

Caird, R. S. and Allan C. G. Mitchell. Disintegration of Co^{58}—916(A)
Caldwell, David O., J. Reginald Richardson, and Herbert N. Royden. Proton-deuteron scattering at 20 Mev—942(A)
Cameron, A. G. W. Origin of anomalous abundances of elements in giant stars—932(A)
Cap, Ferdinand. New spinor theory of elementary particles—907(L)
Caretto, Albert A., Jr., and Edwin O. Wiig. New neutron-deficient isotope of Kr—175
Carlson, B. C. (see Rohrlich, F.)—38
Carmichael, H. and J. F. Steljes. Cosmic-ray ionization bursts in eight-inch sphere at sea level—913(A)
—— (see Steljes, J. F.)—913(A)
Carpenter, Robert and Dudley Williams. Proton line shapes in magnetic resonance spectra of NH_4 salts—360(A)
Carr, H. E. (see Donnally, B. L.)—111
Carroll, K. G. (see Fisher, R. M.)—921(A)
Cartwright, W. F. (see Oxley, C. L.)—806
Cashman, R. J. (see Soule, D. E.)—635(L)
Caulton, M., M. Blau, and J. E. Smith. Interactions of 500-Mev negative pions with emulsion nuclei—919(A)
Chamberlain, O. G., G. Pettengill, E. Segrè, and C. Wiegand. Cross sections for p-p scattering at 330 and 225 Mev—1424(L)
——, **E. Segrè, R. Tripp, C. Wiegand, and T. Ypsilantis.** Experiments with high-energy polarized protons—1430(L)
Charbonnier, Francis M. (see Miller, Charles E.)—590
Chasson, Robert L. Effects of atmosphere on penetrating cosmic radiation—1434(E)
Ch'en, Shang-Yi and William J. Parker. Shift and broadening of blue Cs doublet produced by A and He—946(A)
—— (see Takeo, Makoto)—420
Chester, G. V. Feynman's theory of liquid He—1412(L)
—— Quantum-mechanical partition function—606
Chester, Margaret C. (see Belser, Richard B.)—930(A); 937(A)
Cheston, W. (see Primakoff, H.)—908(L)
Chetham-Strode, A., Jr., and E. M. Kinderman. Half-life of Y^{90}—1029
Chew, Geoffrey F. One of Schwinger's variational principles for scattering—341
Chiarotti, G. and L. Giulotto. Proton relaxation in water—1241
Chilton, Arthur B., John N. Cooper, and James C. Harris. Stopping powers of various elements for protons of energies from 400 to 1050 kev—413
Chinowsky, William, A. Sachs, and J. Steinberger. Mass difference of neutral and negative π mesons—917(A)
—— **and Jack Steinberger.** Mass difference of neutral and negative π mesons—586
Choppin, Gregory R. (see Harvey, Bernard G.)—1129(L)
—— (see Thompson, S. G.)—908(L)
Clay, W. G. (see Hendricks, C. D., Jr.)—952(A)
Cleland, J. W. and J. H. Crawford, Jr. Radiation effects in InSb—894(L)
Clement, J. R. Apparent anomalies in low temperature heat capacities—1420(L)
Cleveland, Forrest F., Richard B. Bernstein, and Fred L. Voelz. Raman and infrared spectra of $C^{13}H_3I$—933(A)
—— (see Weber, Alfons)—933(A)
Cobine, J. D. and E. E. Burger. High-pressure arc anode phenomena—653(A)
Coburn, T. J., H. H. Nielsen, and Dudley Williams. New vacuum near-infrared spectrometer—360(A)
Cocconi, Giuseppe. Influence of earth's magnetic field on extensive air showers—646(L)
—— Nucleon-nucleus collisions at relativistic energies—1107
Cochran, L. W. (see Stanford, C. P.)—931(A)
Coensgen, F. H. Compton effect at 250 Mev—948(A)
Coester, F. Influence of extranuclear fields on angular correlations—1304
Cohen, Bernard L. and T. H. Handley. Experimental studies of (p,t) reactions—514
—— **and Rodger V. Neidigh.** Angular distributions of 22-Mev protons elastically scattered by various elements—282
Cohen, S. G. and A. Weinreb. Energy transfer from solvent to solute in liquid organic solutions under ultraviolet excitation—1117(L)
Cohen, Victor W., Noel R. Corngold, and Norman F. Ramsey. Experiment for measurement of magnetic moment of neutron—941(A)
—— (see Burke, Bernard F.)—193
—— (see Kikuchi, C.)—394
Cole, C. D. and S. Mrozowski. Forbidden lines in spectrum of Bi II—933(A)
Coleman, G. H. (see Batzel, R. E.)—280
Collins, R. J. and H. Y. Fan. Infrared lattice absorption bands in Ge, Si, and diamond—674
Coltman, R. R., Jr. (see Blewitt, T. H.)—891(L)
Condit, Richard I. Shock-wave valve—945(A)
Conger, R. L. and L. E. Schilberg. Photosensitive cell response to sinusoidally varying light flux—943(A)
Conwell, Esther M. Experimental evidence concerning degeneracy in Ge—1118(L)
—— (see Debye, P. P.)—693
Cool, R. L., L. Madansky, and O. Piccioni. Total cross section of pions at 1.5 Bev—249(L)
——, **L. Madansky, and O. Piccioni.** Total interaction cross section of negative pions at kinetic energies of 1.0 and 1.45 Bev—918(A)
——, **L. Madansky, and O. Piccioni.** Total interaction cross section of pions with protons and deuterons at 1.0 Bev—637(L)
Coomes, E. A. (see Haas, G. A.)—930(A); 1421(L)
—— (see Kruse, P. W.)—929(A)
Cooper, Duane H., David C. Oakley, and Robert L. Walker. 500-Mev pair spectrometer—950(A)
Cooper, John N. (see Chilton, Arthur B.)—413
—— (see Taylor, Warren E.)—1056
Copeland, Paul L. (see DeLany, B. Pearson)—926(A)
—— (see Kouba, J. T.)—926(A)
Corenzwit, E. (see Matthias, B. T.)—1415(L)
Cork, J. M., M. K. Brice, G. D. Hickman, and L. C. Schmid. Radiation from Sb^{120}—1059
—— (see LeBlanc, J. M.)—916(A); 1124(L)
Corliss, L. M., J. M. Hastings, and J. E. Goldman. Neutron diffraction study of anisotropy transition in α-Fe_2O_3—893(L)

—— (see Brockhouse, B. N.)—923(A)
Cornelius, R. C. (see Sargent, C. P.)—917(A)
Corngold, Noel R. (see Cohen, Victor W.)—941(A)
Cotts, R. M. and W. D. Knight. Nuclear resonance of Nb^{93} in $KNbO_3$—940(A)
Cox, Mason C., Jan J. van Loef, and D. A. Lind. γ rays from inelastic scattering of protons by Ne—925(A)
Crane, H. R. Method of eliminating cathode activation effects in G-M counter—921(A)
Crasemann, Bernd. Isomeric state of Ga^{69}—1034
Crawford, J. H., Jr. (see Cleland, J. W.)—894(L)
Creedon, John E. (see Udelson, Burton J.)—648(A)
Cronemeyer, D. C. (see Johnston, R. W.)—634(L)
Crouch, M. F. (see Diller, D. E.)—362(A)
Crussard, J., M. F. Kaplon, J. Klarmann, and J. H. Noon. Observation of new decay mode of heavy meson—253(L)
Culp, Richard and Bernard Hamermesh. Determination of energy of Sb-Be photoneutrons—1025
Cummings, R. F. (see Briggs, H. B.)—912(A)

Dabbs, J. W. T. and L. D. Roberts. Thermodynamic properties of $Mn(ND_4)_2(SO_4)_2 \cdot 6D_2O$ below 1°K—935(A)
Dalby, F. W., F. P. Dickey, and Dudley Williams. Infrared emission spectrum of CO in 2.4 μ region—361(A)
Dalitz, R. H. Angular correlations in τ-meson decay—914(A)
Daniels, R. D. and R. W. Hoffman. Formation of dislocation rings by vacancy migration—361(A)
Danielson, G. C. (see Gardner, W. R.)—46
Danner, H. (see Shirane, G.)—672
Darden, S. E., R. E. Fields, and R. K. Adair. Scattering of polarized neutrons from heavy nuclei—931(A)
—— (see Okazaki, A.)—461
Darken, L. S. (see Fisher, R. M.)—921(A)
Darnell, F. J. (see Howling, D. H.)—1416(L)
Das, T. P. and A. K. Saha. Mathematical analysis of Hahn spin-echo experiment—749
Daunt, J. G. (see De Vries, G.)—361(A); 631(L)
—— (see Heer, C. V.)—362(A)
Davidson, R. A. (see Hendricks, C. D., Jr.)—952(A)
Davies, Handel, H. A. Bethe, and L. C. Maximon. Theory of bremsstrahlung and pair production. II. Integral cross section for pair production—788
Davies, R. W. Connection between Smoluchowski equation and Kramers-Chandrasekhar equation—1169
Davis, Leverett, Jr. Fermi's theory of origin of cosmic rays—947(A)
Davis, R. E. and Colman Goldberg. New galvanomagnetic effect. II. Experiments with Ge—913(A)
Davis, Robert H. (see Divatia, Ajay S.)—926(A)
Davis, Sumner P. Nuclear spins and band spectra of Se isotopes—159
Davis, William R. (see Miller, Charles E.)—590
Davisson, J. W. (see Burstein, E.)—65
Dawson, Maynard and George Finn. Capacity measurements on point contact Ge diodes—913(A)
Day, R. B. (see Woodbury, H. H.)—1311
DeBenedetti, S. (see Stearns, M. B.)—1123(L)
deBretteville, A., Jr., and E. D. Harris. Threshold field *vs* temperature slope for paraelectric-ferroelectric change in $BaTiO_3$—934(A)
Debye, P. P. and E. M. Conwell. Electrical properties of *n*-type Ge—693
de Carvalho, H. G. (see Marshall, J.)—1431(L)
Dehmelt, H. G., H. G. Robinson, and Walter Gordy. Nuclear quadrupole resonance of Hg^{201}—480; 920(A)
De Juren, James A. and Hyman Rosenwasser. Pulse height measurements of recoils from $B^{10}(n,\alpha)Li^7$—831
de Klerk, D., R. P. Hudson, and J. R. Pellam. Second sound propagation below 1°K—28
DeLany, B. Pearson and Paul L. Copeland. Use of pinhole for producing glow to arc transitions—926(A)
de Launay, Jules. Isotope effect in superconductivity—661
Delbecq, C. J., J. E. Robinson, and P. H. Yuster. Iodide impurity absorption in KBr and NaBr—262
Demichelis, F. and R. Malvano. Angular correlation of cascade γ rays from decay of $_{84}Po^{214}$—526
Deser, Stanley. Radiative effects in meson-nucleon scattering—612
de-Shalit, A. (see Gillon, L. P.)—124
—— (see Mihelich, J. W.)—135
Deutsch, Martin (see Kendall, H. W.)—932(A)
de Vries, G. and J. G. Daunt. Specific heat of 96 percent He^3 below 1°K—631(L)
—— **and J. G. Daunt.** Specific heat of 96 percent liquid He^3 between 1.3°K and 2.3°K—361(A)
Dexter, D. L. *F*-center wave functions in alkali halides—244(L)
—— X-ray coloration of alkali halides—985
Dexter, R. N. (see Lax, Benjamin)—1418(L)
Diamond, H. (see Studier, M. H.)—1428(L)
Diamond, R. M. (see Sharp, R. A.)—358(L)
Dicke, R. H. Coherence in spontaneous radiation processes—99
Dickey, F. P., R. V. Zumstein, and Dudley Williams. Atomic spectra in infrared and electrodeless discharge source—361(A)
—— (see Dalby, F. W.)—361(A)
Dienes, G. J. (see Vineyard, G. H.)—265
Diller, D. E. and M. F. Crouch. Branching ratio of $Be^9(\alpha,n)C^{12*}$—362(A)
Dillon, John A., Jr., and H. E. Farnsworth. Improved radiotracer technique for study of gaseous adsorption on metals—364(A)
Ditzenberger, J. A. (see Fuller, C. S.)—1182
Divatia, Ajay S., Robert H. Davis, and R. G. Herb. Evapor-ion pump—926(A)
Diven, B. C. (see Martin, H. C.)—199
Dolan, W. W., W. P. Dyke, J. K. Trolan, and J. P. Barbour. Effect of temperature on field emission—943(A)
Donnally, B. L. and H. E. Carr. Metastable negative ions—111
Douglas, R. A. (see Galonsky, A.)—928(A)
—— (see Goldberg, E.)—799
Dresden, M. Speculations on behavior of positrons in superconductors—1413(L)
Dresselhaus, G. (see Kip, A. F.)—952(A)
Dudley, John M. (see Kenney, Robert W.)—951(A)
Dudziak, Walter F. and Ryokichi Sagane. Dependence of relative low-energy $\pi^{\pm}$ production cross section on atomic and neutron numbers—948(A)
—— (see Sagane, Ryokichi)—948(A)
Duffendack, C. S. and C. F. Hendee. X-ray absorption processes in proportional counter gases—653(A)
Duller, N. M. and W. D. Walker. High-energy meson production—284
DuMond, Jesse W. M. (see Felt, Gaelen L.)—1434(E)
Dunlap, W. C., Jr., D. E. McMillan, and R. A. Brooks. Conduction properties of *p*-type Ge between 25°C and 925°C—911(A)
Dyke, W. P. (see Dolan, W. W.)—943(A)
Dzimianski, J. W. (see Jones, T. B.)—654(A)

Earle, M. D. (see Bearden, J. A.)—629(L)
Ebel, A. A. and Clark Goodman. Inelastic scattering of neutrons by In^{115} and Au^{197}—197
Eby, F. S., R. D. Hill, and W. K. Jentschke. Angular distribution of protons from $Zn^{66}(d,p)Zn^{66}$—925(A)
Edwards, M. H. (see Atkins, K. R.)—1416(L)

Efremov, N. New method of calculation of effective ionic radii of lanthanides—934(A)
—— Numerical regularities in periodic system of ions—945(A)
Eggleston, R. R. (see Meechan, C. J.)—953(A)
Eisberg, R. M. and G. Igo. Inelastic scattering of 31-Mev protons from heavy elements—1039
Eisenstein, Albert S. X-ray-induced photostimulated conductivity in MgO—1017
Elder, S. A., J. Kolb, and W. L. Nyborg. Physical factors involved in sonic irradiation of liquids—364(A)
Elliot, J. O., W. I. McGarry, and W. R. Faust. Energy spectrum of neutrons from Po-Be—1348
Elliott, J. Is electroluminescence practical light source?—360(T)
Elliott, L. G., R. L. Graham, J. Walker, and J. L. Wolfson. Spins and parities of energy levels in Pb^{208}—356(L)
Elsken, R. H. and T. M. Shaw. Quantitative measurement of magnetic absorption utilizing null-balance system—943(A)
Emigh, C. R. and L. R. Megill. Long-lived phosphorescent components of Tl-activated NaI—1190
English, W. N. Thermal microstructure in ocean—945(A)
Epstein, A. and H. Fritzsche. Electrical resistivity of pure Te at the melting point and in liquid state—922(A)
Epstein, Saul T. Deriving Schrödinger's equation—364(A)
Ergen, William Krasny. Kinetics of circulating-fuel nuclear reactor—920(A)
Erickson, R. A. and L. D. Roberts. Measurement and calculation of liquid He vapor pressure-temperature scale from 1° to 4.2°K—957
Ernst, H. (see Hayward, R. W.)—916(A)
Evans, G. E. (see Stier, P. M.)—926(A)

Fairbank, Henry A. (see King, J. C.)—21
Faire, A. C., O. T. Fundingsland, and A. L. Aden. Measurement of dissociative recombination in N_2^+—650(A)
Falkoff, D. L. Impedance concept in nuclear scattering—364(A)
Famularo, K. F., R. J. S. Brown, H. D. Holmgren, and T. F. Stratton. Differential cross sections for elastic scattering of protons by He^6—928(A)
Fan, H. Y. Effect of traps on carrier injection in semiconductors—1434(E)
—— (see Collins, R. J.)—674
—— (see Kaiser, W.)—911(A); 977
—— (see Navon, D.)—911(A)
Fankuchen, Isador. New applications of x-ray diffraction—359(T)
Fano, U. Inelastic collisions in Molière theory of multiple scattering—117
—— Stokes parameter technique for treatment of polarization in quantum mechanics—121
— (see Spencer, L. V.)—1172
Farnsworth, H. E. (see Dillon, John A., Jr.)—364(A)
Farwell, George W. and Harvey E. Wegner. Elastic scattering of intermediate-energy α particles by Au—356(L)
Faust, W. R. (see Elliot, J. O.)—1348
Feher, G. and T. W. Griswold. Electron-spin resonance absorption in bulk and dispersed Li and Na—952(A)
Feiner, F. (see Ashkin, J.)—1129(L)
Feld, B. T. (see Wattenberg, A.)—915(A)
Feldman, David. Interaction between two nucleons at low energies—935(A)
Feldmann, W. L. (see Tanenbaum, M.)—912(A)
Felt, Gaelen L., John N. Harris, and Jesse W. M. DuMond. Precision measurement at 24 500 volts of conversion constant λV—1434(E)
Ferguson, A. J. (see Gove, H. E.)—928(A)
Ferigle, Salvador M. (see Weber, Alfons)—933(A)
Fermi, Enrico. Multiple production of pions in nucleon-nucleon collisions at cosmotron energies—1434(E)
—— Pion-hydrogen scattering—917(T)
Fields, P. R. (see Studier, M. H.)—1428(L); 1433(L)
Fields, R. E. (see Darden, S. E.)—931(A)
Fine, S. Proportional counter "escape" peak resolution and fine structure—653(A)
Finn, George (see Dawson, Maynard)—913(A)
Firor, J., F. Jory, and S. B. Treiman. Solar magnetic moment and diurnal variation in cosmic-ray intensity—551
Fisher, L. H. (see Lessin, I.)—649(A)
—— (see Mayer, Alex)—649(A)
Fisher, R. M., L. S. Darken, and K. G. Carroll. Accelerated growth of Sn whiskers—921(A)
Fite, Wade L. (see Branscomb, Lewis M.)—651(A)
Foldy, Leslie L. Elementary particles and Lamb-Retherford line shift—880
—— Operators and observables in isotopic spin space—1395
Foley, H. M., R. M. Sternheimer, and D. Tycko. Nuclear quadrupole coupling in polar molecules—734
Foote, H. L., Jr. (see Sailor, V. L.)—1292
Forro, M. End-point energy determination of β emitters—915(A)
Forsbergh, P. W., Jr. Effect of two-dimensional pressure on Curie point of $BaTiO_3$—686
Foster, B. P., G. S. Stanford, and L. L. Lee, Jr. γ rays from Ne^{22}—1069
Fowler, W. A. (see Mozer, F.)—829
—— (see Peterson, R. W.)—951(A)
Fowler, W. B., R. P. Shutt, A. M. Thorndike, and W. L. Whittemore. Production of heavy unstable particles by negative pions—861
Francis, N. C. and K. M. Watson. Theory of deuteron stripping reactions—313
Franck, Kurt. Prismatic light control—360(T)
Frank, R. M. and J. L. Gammel. Inelastic scattering of protons and neutrons by deuterons—463
Frankel, Sherman (see Goldberg, Norman)—1425(L)
Franzen, W. (see Ajzenberg, F.)—925(A)
Fraser, J. S. and J. C. D. Milton. Distribution of prompt neutron emission probability for fission fragments of U^{233}—818
Frauenfelder, H., J. S. Lawson, Jr., and W. Jentschke. Magnetic moment of first excited state of Pb^{204}—1126(L)
Freier, G. and H. Holmgren. Interaction between D^2 and He^3 in neighborhood of 18.6-Mev level of Li^{5*}—825
Friedland, Stephen S. (see Katzenstein, Henry S.)—363(A)
—— (see Lane, George H.)—363(A)
—— (see Ogushwitz, Howard)—363(A)
Friedman, A. M. (see Studier, M. H.)—1428(L); 1433(L)
Friedman, Bernard (see Borowitz, Sidney)—251(L)
Fritzsche, H. (see Epstein, A.)—922(A)
Frizzell, C. 701 calculator—359(T)
Fry, W. F. Inelastic scattering of 220-Mev π^- mesons in emulsions—845
—— **and George R. White.** Negative π-μ meson decays in photographic emulsion—1427(L)
Frye, Glenn M., Jr. Charged particles from interaction of 14-Mev neutrons with Li^6 and Li^7—1086
Fuller, C. S., J. D. Struthers, J. A. Ditzenberger, and K. B. Wolfstirn. Diffusivity and solubility of Cu in Ge—1182
Fulton, Thomas and Robert Karplus. Bound state corrections in two-body systems—1109
—— **and Paul C. Martin.** Radiative corrections in positronium—903(L)
Fundingsland, O. T. (see Faire, A. C.)—650(A)

Gallagher, J. J., F. D. Bedard, and C. M. Johnson. Microwave spectrum of $N^{14}O^{16}$—729
Galonsky, A. I., R. Douglas, W. Haeberli, M. McEllistrem, and H. T. Richards. Elastic scattering of deuterons by He—928(A)
—— (see Goldberg, E.)—799
Galt, J. K., W. A. Yager, and F. R. Merritt. Temperature dependence of ferromagnetic resonance line width in nickel iron ferrite: new loss mechanism—1119(L)
Gammel, J. L. (see Frank, R. M.)—463
Gardner, W. R. and G. C. Danielson. Electrical resistivity and Hall coefficient of sodium tungsten bronze—46
Garrison, Gerald R. (see Miller, Charles E.)—590
Garstens, M. A. Paramagnetic resonance in gases at low fields—1228
Gasiorowicz, S. Production of positive mesons in heavy nuclei—843
Geballe, R. (see Burch, D. S.)—650(A)
Gellman, H. (see McManus, H.)—924(A)
Gell-Mann, Murray. Theoretical speculations about new unstable particles—930(T)
Gerjuoy, E. (see Stein, S.)—934(A)
Ghiorso, Albert, G. Bernard Rossi, Bernard G. Harvey, and Stanley G. Thompson. Reactions of U^{238} with cyclotron-produced nitrogen ions—257(L)
—— (see Harvey, Bernard G.)—1129(L)
—— (see Thompson, S. G.)—908(L)
Ghosh, S. N. Charge transfer in upper atmosphere—650(A)
Gilbert, F. C. Range distribution of α particles following decays of Li^9 and B^8—499
Gillon, L. P., K. Gopalakrishnan, A. de-Shalit, and J. W. Mihelich. Nuclear spectroscopy of neutron-deficient Hg isotopes—124
Giulotto, L. (see Chiarotti, G.)—1241
Glass, Neel W. and J. Reginald Richardson. Radiations from Sc^{46}, Cl^{32}, P^{29}, and Al^{24}—942(A)
Goertzel, G. (see Spruch, Larry)—642(L)
Goldberg, Arthur E. (see Mitchell, George R.)—1421(L)
Goldberg, Colman. New galvanomagnetic effect. I. Theory—913(A)
—— (see Davis, R. E.)—913(A)
Goldberg, E., W. Haeberli, A. I. Galonsky, and R. A. Douglas. Elastic scattering of α particles by Ne—799
Goldberg, Norman and Sherman Frankel. *K*-conversion electron-γ angular correlation measurements in Te^{123} and Te^{125}—1425(L)
Goldemberg, J. Photon monochromator for bremsstrahlung radiation—1426(L)
Goldhaber, Gerson (see Homa, George)—554
Goldman, J. E. (see Azumi, K.)—630(L)
—— (see Corliss, L. M.)—893(L)
Goldsmith, G. J. Photoconductivity of single crystals of anthracene—929(A)
Goldstein, L. and J. M. Anderson. Phenomena associated with small temperature variations of electron gas in discharge plasmas around 300°K. II. Afterglow quenching—648(A)
—— (see Anderson, J. M.)—648(A)
Gomer, Robert. Chemisorption of O_2 on W—926(A)
Good, R. H., Jr. Hamiltonian mechanics of fields—239
Goodman, Clark (see Ebel, A. A.)—197
—— (see Kiehn, Robert M.)—177
—— (see McClelland, C. L.)—904(L)
Goodrich, Max and Wilbur B. Payne. Inner bremsstrahlung from P^{32}—916(A)
Gopalakrishnan, K. (see Gillon, L. P.)—124
Gordy, Walter and Charles A. Burrus. Spectrum of DBr in 1-mm wave region—419
—— (see Burrus, Charles A.)—897(L)
—— (see Dehmelt, H. G.)—480; 920(A)
—— (see Hill, Robert M.)—1019
—— (see King, William C.)—407
Gorman, J. (see Ashkin, J.)—1129(L)
Gould, Lawrence. Microwave measurement of velocity dependence of collision cross section of slow electrons in He—648(A)
Gove, H. E., A. J. Ferguson, and J. T. Sample. Elastic scattering of protons by N_2—928(A)
Graham, R. L. (see Elliott, L. G.)—356(L)
Graham, Walter J. and Arthur J. Ruhlig. Calculated values of parameters of noble gas discharges—647(A)
Green, Louis C., Margaret N. Lewis, Marjorie M. Mulder, Cynthia W. Wyeth, and John W. Woll, Jr. Correlation energies and angular components of wave functions of ground states of H^-, He I, and Li II—757
——, **Marjorie M. Mulder, Margaret N. Lewis, and John W. Woll, Jr.** Discussion of analytic and Hartree-Fock wave functions for $1s^2$ configurations from H^- to C V—757
Greenstadt, John. Variational formulas in evaporation theory—1140
Gregg, E. C. (see Tucker, B. L.)—362(A)
Griffel, M., R. E. Skochdopole, and F. H. Spedding. Heat capacity of gadolinium from 15 to 355°K—657
Griswold, T. W. (see Feher, G.)—952(A)
Groetzinger, G. (see Wiener, B.)—922(A)
Gross, E. P. Solution of Boltzmann equation for Maxwellian molecules—347(L)
—— **and M. Krook.** Kinetic approach to collision processes in gases—936(A)
—— (see Krook, M.)—936(A)
Grosse, A. V., A. D. Kirshenbaum, J. Laurence Kulp, and W. S. Broecker. Natural tritium content of atmospheric hydrogen—250(L)
Grossweiner, L. I. and M. S. Matheson. Luminescent centers in x-ray excited fluorescence of ice—929(A)
Grove, G. R. and L. N. Russell. Thin lens β-ray spectrometer—361(A)
Gugelot, P. C. Level densities of nuclei from inelastic scattering of 18-Mev protons—425
Guth, Eugene. Nuclear magnetism study of polymers—944(T)
Gutowsky, H. S. (see Bloom, Myer)—920(A)
—— (see McGarvey, B. R.)—940(A)
—— (see Williams, G. A.)—1428(L)
Gyorgy, E. M. and G. G. Harvey. Spectroscopy of solid state: some of transition elements—365

Haas, G. A. and E. A. Coomes. Effect on periodic Schottky deviations resulting from SrO layer deposited on clean Mo—930(A)
—— **and E. A. Coomes.** Temperature dependence of periodic deviations from Schottky line—1421(L)
Haeberli, W. (see Galonsky, A.)—928(A)
—— (see Goldberg, E.)—799
Hagstrum, Homer D. Reflection of ions as ions or as metastable atoms at metal surface—652(A)
Hahn, Erwin L. Free nuclear induction experiments involving pure nuclear electric quadrupole interactions—944(T)
—— **and B. Herzog.** Anisotropic relaxation of quadrupole spin echoes—639(L)
Halpern, J. (see Nathans, R.)—437
Halsted, R. E. and L. R. Koller. Electroluminescence in thin films of ZnS: Mn—349(L); 929(A)
Hamermesh, Bernard (see Culp, Richard)—1025
Hamermesh, Morton and James Monahan. Non-single scattering of electrons at oblique incidence—963
Hamilton, Joseph G. (see Rossi, G. Bernard)—256(L)
Handley, Thomas H. and Elmer L. Olson. New radioactive nuclides of rare earths—524

—— (see Cohen, B. L.)—514
Hardy, George F. and John K. Hulm. Superconductivity of some transition metal compounds—1004
Harlow, Francis H. and Boris A. Jacobsohn. Nucleon isobars in intermediate coupling—333
Harman, T. C., R. K. Willardson, and A. C. Beer. Temperature dependence of transverse magnetoresistance effect in InSb—912(A)
Harris, E. D. (see deBretteville, A., Jr.)—934(A)
Harris, James C. (see Chilton, Arthur B.)—413
Harris, John N. (see Felt, Gaelen L.)—1434(E)
Harrison, Don E., Jr. Statistical mechanics of cathode sputtering—652(A)
Harrison, Sol E. Conductivity and Hall effect of ZnO at low temperatures—52
Hartzler, A. J. and R. T. Siegel. n-p scattering at 395 Mev —928(A)
—— (see Siegel, R. J.)—928(A)
Harvey, Bernard G., Stanley G. Thompson, Albert Ghiorso, and Gregory R. Choppin. Further production of transcurium nuclides by neutron irradiation—1129(L)
—— (see Ghiorso, Albert)—257(L)
—— (see Thompson, S. G.)—908(L)
Harvey, G. G. (see Gyorgy, E. M.)—365
Hastings, J. M. (see Brockhouse, B. N.)—923(A)
—— (see Corliss, L. M.)—893(L)
Haugsnes, J. (see Roberts, James H.)—920(A)
Havas, Peter. Classical theory of particles interacting with electromagnetic and mesonic fields—882
—— Multipole singularities of classical scalar and pseudoscalar meson fields—1400
Haxby, R. O. (see Voss, J. R.)—918(A)
Hayden, R. J. (see Wasserburg, G. J.)—645(L)
Hayward, Evans and John Hubbell. Albedo of various materials for 1-Mev photons—955
Hayward, R. W., D. D. Hoppes, and H. Ernst. Disintegration of 10-yr Ba^{133}—916(A)
Hazen, W. E., R. W. Williams, and C. A. Randall, Jr. Structure of air showers—578
Heer, C. V., C. B. Barnes, and J. G. Daunt. Operational data for magnetic refrigerator for maintaining temperatures below 1°K—362(A)
Heller, J. and H. Keller. Direct integration of neutron transport equation—932(A)
Hemstreet, H. W. (see Reynolds, J. M.)—247(L)
Hendee, C. F. and W. B. Brown. Time-resolved spectroscopy of N_2 and H_2—651(A)
—— (see Duffendack, C. S.)—653(A)
Henderson, Joseph E. Recent developments in field emission—943(T)
—— (see Miller, Charles E.)—590
Hendrick, Roy W., Jr. Measurements of reflection of 8A x-rays by mirror surfaces—942(A)
Hendricks, C. D., Jr., M. E. Van Valkenburg, W. G. Clay, and R. A. Davidson. Ionization by ultra-speed pellets—952(A)
Henley, E. M. (see Aitken, A.)—1349
Henry, Warren E. Strong-field induced paramagnetic anomaly in $NiSiF_6 \cdot 6H_2O$—935(A)
Herb, R. G. (see Divatia, Ajay S.)—926(A)
Herman, Frank. Calculation of energy band structures of diamond and Ge crystals by method of orthogonalized plane waves—1214
Herring, Conyers. Correlation of electronic band structure with properties of Si and Ge—943(T)
Hershberger, W. D. (see Hurd, F. Kenneth)—373; 919(A)
Herwig, Lloyd O., G. H. Miller, and N. G. Utterback. Characteristics of gridded parallel-plate ionization chambers—926(A)
—— (see Miller, Glenn H.)—932(A)
Herzog, B. (see Hahn, E. L.)—639(L)
Heydenburg, N. P. and G. M. Temmer. Coulomb excitation of heavy and medium heavy nuclei by α particles—906(L)
—— (see Temmer, G. M.)—351(L)
Hickam, W. M. Ionization probability curves near threshold for Hg, Cd, and Zn—652(A)
Hicklin, Walter H. (see Belser, Richard B.)—937(A)
Hickman, G. D. (see Cork, J. M.)—1059
Hildebrand, Roger H. Measurement of fraction of $n + p \rightarrow \pi^0$ events in which deuteron is formed—918(A)
Hill, David L. Nuclear Coulomb excitation by heavy particles—923(A)
Hill, R. D. (see Eby, F. S.)—925(A)
Hill, Robert M. and Walter Gordy. Zeeman effect and line breadth studies of microwave lines of O_2—1019
—— (see Mizushima, Masataka)—745
Hintermann, K. Angle of divergence of pairs produced by photons—898(L)
Hintz, N. M., J. M. Blair, and D. M. Van Patter. γ radiation from excited state of Li^8—924(A)
Hochman, R. (see Kuczynski, G. C.)—952(A)
Hoffman, R. W. (see Daniels, R. D.)—361(A)
Holcomb, D. F. and R. E. Norberg. Effects of imperfections and of electron interactions on magnetic resonance in alkali metals—919(A)
Hollander, Jack M. (see Rossi, G. Bernard)—256(L)
Holmgren, H. D. (see Famularo, K. F.)—928(A)
—— (see Freier, G.)—825
Holstein, T. (see Stein, S.)—934(A)
Holton, Gerald. Are we achieving our aims in general education?—363(T)
Homa, George, Gerson Goldhaber, and Leon M. Lederman. Scattering of 151 and 188-Mev positive pions by protons—554
Honig, A., M. Mandel, M. L. Stitch, and C. H. Townes. Pure rotational spectra of alkali halides—953(A)
Hope, J. (see Jahn, H. A.)—318
Hoppes, D. D. (see Hayward, R. W.)—916(A)
Horn, F. Hubbard (see Taft, E. A.)—64
Hornbostel, J. and E. O. Salant. Artificially-produced negative heavy meson—902(L)
Horton, G. K. and G. E. Tauber. Electrical conductivity of graphite—911(A)
Howling, D. H., F. J. Darnell, and E. Mendoza. Temperature measurement below 1°K—1416(L)
Hrostowski, H. J. (see Briggs, H. B.)—912(A)
Hubbell, John (see Hayward, Evans)—955
Huber, Elsa L. Velocity of spread of burst pulses in air with coaxial cylindrical geometry—950(A)
Hudson, A. M. and F. X. Roser. Uniformity of pulse heights from a large-area photomultiplier—941(A)
Hudson, G. E. and D. H. Potts. Class of solutions of Maxwell's equations—936(A)
Hudson, R. P. (see de Klerk, D.)—28
Hughes, D. J. (see Kato, W. Y.)—931(A)
Huizenga, John R. (see Andre, C. G.)—925(A); 931(A)
—— (see Studier, M. H.)—1428(L); 1433(L)
Hulm, John K. (see Hardy, George F.)—1004
Hunter, L. P. Transistor physics—359(T)
Huntington, H. B. Creation of displacements in radiation damage—1414(L)
Hurd, F. Kenneth, Mendel Sachs, and W. D. Hershberger. Paramagnetic resonance absorption of Mn^{++} in single crystals of $CaCO_3$—373; 919(A)
Hurst, G. S. (see Bortner, T. E.)—1236
Huxford, W. S. Time constants of self-sustained Townsend discharges—652(A)

Igo, G. (see Eisberg, R. M.)—1039
Ilakovac, K. and P. B. Moon. Resonant scattering of recoil-broadening γ rays—254(L)
Irick, R. C. (see Burch, D. S.)—650(A)
Ito, Takashi, Yukito Tanabe, and Masataka Mizushima. Line width of rotational spectra of some symmetric top molecules due to nuclear quadrupole moments—1242

Jacobs, I. S. Effect of pressure on *F*-center absorption in alkali halides—993
Jacobsohn, Boris A. (see Harlow, Francis H.)—333
Jahn, H. A. and J. Hope. Symmetry properties of Wigner $9j$ symbol—318
Jakobson, M. J. and F. H. Schmidt. Characteristics of proposed double-mode cyclotron—303
James, Ralph A. Excitation functions of proton-induced reactions of Nb^{93}—288
Janes, G. Sargent and William L. Kraushaar. Photoproduction of π^+ mesons from H and C—900(L)
Jastram, P. S. Elastic scattering of positive and negative electrons from nuclei—928(T)
Jeffries, C. D. (see Sogo, P. B.)—174
Jeffries, Carson. Recent measurements of nuclear moments—944(T)
Jentschke, W. K. (see Eby, F. S.)—925(A)
—— (see Eby, F. S.)—925(A)
—— (see Frauenfelder, H.)—1126(L)
—— (see Kreger, W. E.)—837
Johnson, C. H. and C. C. Trail. Yields near threshold for (p,n) reactions in intermediate nuclei—924(A)
Johnson, C. M. (see Gallagher, J. J.)—729
Johnson, J. B. and K. G. McKay. Secondary electron emission from Ge—668
Johnson, J. L. and H. M. Jones. Nuclear cross sections at low energies—1286
Johnson, M. H. and E. Teller. Classical theory of heavy nuclei—947(A)
—— **and E. Teller.** Proton distribution in heavy nuclei—357(L)
—— (see Teller, E.)—947(A)
Johnston, D. F. Hall constant of graphite—1420(L)
Johnston, R. W. and D. C. Cronemeyer. Infrared absorption of NiO—634(L)
Jones, H. M. (see Johnson, J. L.)—1286
Jones, Shannon. Physical characteristics of phosphors for fluorescent lamps—360(T)
Jones, T. B. and J. W. Dzimianski. Equation for V-I curve of high current A arc—654(A)
Jones, William B. (see Rossi, G. Bernard)—256(L)
Jordan, W. C. (see LeBlanc, J. M.)—1124(L)
Jory, F. (see Firor, J.)—551
Julian, A. (see Wattenberg, A.)—915(A)
Jungerman, J. and H. Steiner. Photofission produced by 335-Mev bremsstrahlung—949(A)

Kaiser, W. and H. Y. Fan. Infrared absorption, photoconductivity, and impurity states in Ge—911(A); 977
Kaplon, M. F., G. W. Racette, and D. M. Ritson. Light elements of the primary cosmic radiation—interpretation—914(A)
——, **W. D. Walker, and M. Koshiba.** Neutral-to-charge ratio in high-energy interactions—1424(L)
—— (see Crussard, J.)—253(L)
—— (see Racette, G. W.)—914(A)
Karash, W. J. Critical effects of electric fields in fluorescent lamp starting and their use in new lamp design—360(T)
Karplus, Robert (see Fulton, Thomas)—1109
Katcoff, S. (see Bernstein, W.)—1073
—— (see Markowitz, S. S.)—178
Kato, W. Y., D. J. Hughes, and J. S. Levin. Determination of scattering resonance parameters from total cross section—931(A)
Katz, Robert (see Lee, Milford R.)—155
Katzenstein, Henry S. and Stephen S. Friedland. Time-of-flight mass spectrometer—363(A)
—— (see Lane, George H.)—363(A)
Kaufman, Sheldon and W. F. Libby. Natural distribution of tritium—1337
Keck, J., R. M. Littauer, G. K. O'Neill, A. M. Perry, and W. M. Woodward. Photodisintegration of deuteron by 180-Mev and 260-Mev γ rays—827
Keister, G. L. and F. H. Schmidt. Second-forbidden β spectra of Co^{60} and Sc^{46}—140
Keller, H. (see Heller, J.)—932(A)
Kendall, H. W. and Martin Deutsch. Annihilation of positrons in flight—932(A)
Kenney, Robert W., John M. Dudley, and Charles A. McDonald, Jr. Absolute photon attenuation cross section for non-pair processes in Be at 300 Mev—951(A)
—— (see McDonald, C. A., Jr.)—951(A)
Kent, D. W. (see Rothman, M. A.)—1434(E)
Kenty, Carl. New method for exciting metallic spectra by active N_2. Excitation of Xe—651(A)
Kiehn, Robert M. and Clark Goodman. Neutron inelastic scattering—177
Kierstead, Henry A. (see McDonell, William R.)—247(L)
Kikuchi, C. Dielectric absorption of liquid crystalline biaxial molecules—934(A)
—— **and V. W. Cohen.** Paramagnetic resonance absorption of carbazyl and hydrazyl—394
Kikuchi, T. (see Bradford, C. E.)—921(A)
Kinderman, E. M. (see Chetham-Strode, A., Jr.)—1029
Kling, D. T., N. Seeman, and M. M. Shapiro. K^+ mesons from "fundamental" nuclear collisions—914(A)
—— (see Shapiro, M. M.)—914(A)
—— (see Wada, W. W.)—914(A)
King, J. C. and Henry A. Fairbank. Second sound in He^3–He^4 mixtures below 1°K—21
King, William C. and Walter Gordy. 1–2 mm wave spectroscopy. IV. Experimental methods and results for OCS, CH_3F, and H_2O—407
Kingston, R. H. Water vapor and "channel" effect in *n-p-n* junction transistors—346(L)
Kinsey, B. B. and G. A. Bartholomew. Dipole and quadrupole transition probabilities in neutron-capture γ radiation—1260
—— (see Bartholomew, G. A.)—1434(E)
Kip, A. F., G. Dresselhaus, and C. Kittel. Cyclotron resonance in Ge crystals—952(A)
Kirby, H. W. and Murrell L. Salutsky. Half-life of La^{140}—1051
Kirshenbaum, A. D. (see Grosse, A. V.)—250(L)
Kittel, C. (see Kip, A. F.)—952(A)
Klarmann, J. (see Crussard, J.)—253(L)
Knight, W. D. Nuclear magnetic resonance phenomena in metals and alloys—944(T)
—— (see Abell, D. F.)—940(A)
—— (see Cotts, R. M.)—940(A)
Koehler, W. F. Aging of evaporated Ag films—953(A)
Kohman, Truman P. (see Waldron, Esther C.)—254(L)
Kolb, J. (See Elder, S. A.)—364(A)
Koller, L. R. (see Halsted, R. E.)—349(L); 929(A)
Konopinski, E. J. Universal Fermi interaction—936(T)
Koshiba, M. (see Kaplon, M. F.)—1424(L)
Koski, Walter S. (see Burke, Bernard F.)—193
Kouba, J. T. and P. L. Copeland. Stability of low-pressure Hg arcs with positive conducting rod—926(A)
Kovacs, J. S. Angular correlation of mesons produced in inelastic meson-nucleon collisions—252(L)

Kraus, Alfred A., Jr. γ radiation from proton bombardment of Li^7—1308
Kraushaar, William L. and Lawrence J. Marks. Meson production in high-energy nucleon-nucleon collisions—326
—— (see Janes, G. Sargent)—900(L)
Kraybill, H. L. Altitude and angular dependence of cosmic-ray air showers—1362
—— Density of extensive air showers at airplane altitudes—1360
—— (see Whetten, N. R.)—1356
Kreger, W. E., W. Jentschke, and P. G. Kruger. Elastic scattering of protons by He at 5.78 Mev—837
—— **and L. McIsaac.** NaI counting response for γ rays—943(A)
Kroll, Norman M. and Malvin A. Ruderman. Theorem on photomeson production near threshold and suppression of pairs in pseudoscalar meson theory—233
Krone, R. W. (see Teener, J. W.)—1035
Krook, M., P. L. Bhatnagar, and E. P. Gross. Kinetic approach to collision processes in gases—936(A)
—— (see Gross, E. P.)—936(A)
Krueger, Helmut. Mechanical properties of ceramic $BaTiO_3$—362(A)
Kruger, P. G. (see Kreger, W. E.)—837
Krumhansl, J. A. Theoretical calculations of F-center energy levels—245(L)
Kruse, P. W. and E. A. Coomes. Study of SrO on Mo by use of field emission microscope—929(A)
Kuczynski, G. C. Strain sensitivity of AuCu and $AuCu_3$ alloys—922(A)
—— **and R. Hochman.** Kinetics of ordering in AuCu alloys—952(A)
Kulp, J. Laurence (see Grosse, A. V.)—250(L)
Kusch, P. Observations of double and triple quantum transitions—1022

Landon, H. H. Doppler effect in slow neutron resonance of Rh—931(A)
—— **and V. L. Sailor.** Slow neutron resonances in Cs, Pd, and Au—1030
—— (see Sailor, V. L.)—1292
Landsberg, P. T. Quantum statistics of closed and open systems—1170
Lane, George H., Henry S. Katzenstein, and Stephen S. Friedland. Mass spectrometry of low vapor-pressure molecules—363(A)
Lane, R. O. and D. J. Zaffarano. Transmission of 0–50 kev electrons by thin films with applications to β spectra—916(A)
Langer, L. M. and J. W. Starner. Triple γ-ray cascade in Sb^{124}—245(L)
Lauritsen, C. C. (see Mozer, F.)—829
—— (see Peterson, R. W.)—951(A)
Lawson, A. W. and Lothar Meyer. Light scattering in liquid He—259
Lawson, J. S., Jr. (see Frauenfelder, H.)—1126(L)
Lax, Benjamin, H. J. Zeiger, R. N. Dexter, and E. S. Rosenblum. Directional properties of cyclotron resonance in Ge—1418(L)
Lazarus, David. Effect of screening on solute diffusion in metals—973
LeBlanc, J. M., J. M. Cork, S. B. Burson, and W. C. Jordan. Decay of V^{48}—1124(L)
——, **J. M. Cork, and S. B. Burson.** γ spectra of Cd^{117} and In^{117}—916(A)
LeClaire, A. D. Predicted effects of temperature gradients on diffusion in crystals—344(L)
Lederman, Leon M. (see Homa, George)—554
—— (see Sargent, C. P.)—917(A)
Lee, Chu Jui and S. LeRoy Brown. Response currents in coupled circuits by Laplace transformation and mechanical harmonic synthesizer—945(A)
Lee, L. L., Jr. (see Foster, B. P.)—1069
Lee, Milford R. and Robert Katz. Radioactivity of Sm^{156} and Eu^{155}—155
Leinhardt, T. E. (see Reynolds, J. M.)—247(L)
Leipuner, L. (see Stearns, M. B.)—1123(L)
Leivo, W. and R. Smoluchowski. γ-ray coloring of 400-Mev proton-irradiated KCl—1415(L)
Leonard, Stanley L. Production of charged pions at 180° to beam by 340-Mev protons on C—1380
—— **and Donald H. Stork.** Total cross section for positive pions in H—568; 1435(E)
Lessin, I. and L. H. Fisher. Formative time lags of uniform field breakdown in H_2—649(A)
Letaw, Harry, Jr., Lawrence M. Slifkin, and William M. Portnoy. Self-diffusion in Ge—892(L)
Levin, J. S. (see Kato, W. Y.)—931(A)
Levinger, J. S. Harmonic mean energy of nuclear photoeffect—932(A)
Levy, Henri A., S. W. Peterson, and S. H. Simonsen. Neutron diffraction study of ferroelectric modification of KH_2PO_4—1120(L)
Lewis, Margaret N. (see Green, Louis C.)—757; 757
Liao, T. W. Impulse corona and breakdown of a point-plane gap—650(A)
Libby, W. F. (see Kaufman, Sheldon)—1337
Lichtenstein, Philip G. Differential range spectrum of cosmic-ray mesons at sea level—858
—— (see Ballman, J.)—851
Likely, J. G. (see Ajzenberg, F.)—925(A)
Lind, D. A. (see Cox, Mason C.)—925(A)
Lindenbaum, S. J. and Luke C. L. Yuan. Energy spectrum of negative pions produced in Be by 2.3-Bev protons—917(A)
—— (see Yuan, Luke C. L.)—917(A); 1431(L)
Lindener, Arthur (see Robson, J. W.)—362(A)
Lindstrom, G. (see Meyerhof, W. E.)—949(A)
Linlor, W. I. and B. Ragent. Neutron total cross section for Bi and U between 45 and 130 Mev—951(A)
—— (see Ragent, B.)—951(A)
Linsley, John. Čerenkov counter-cloud chamber measurement of multiply charged primary cosmic rays—899(L)
Lipson, H. G. (see Burstein, E.)—65
Littauer, R. M. (see Keck, J.)—827
Loeb, Leonard B. Hitherto unrecognized aspects of breakdown streamers—649(A)
Loferski, Joseph J. Infrared optical properties of single crystals of Te—707
Logan, John K. (see Berlincourt, Ted G.)—348(L)
Looney, Duncan H. and Sanborn C. Brown. Excitation of plasma oscillations—649(A); 965
Lord, J. J. (see Orear, Jay)—575
Lukesh, Joseph S. Structure of vitreous silica—264
Lynch, F. J. New fluorescence photometer—926(A)
Lyon, W. S. and J. J. Manning. Radioactive Si^{31}—501

Mackin, R. J., Jr., W. B. Mims, and W. R. Mills. γ radiation from $C^{13} + D^2$—950(A)
Macklin, R. L. and H. E. Banta. $Li^7(d,t)Li^6$—924(A)
Madansky, L. (see Cool, R. L.)—249(L); 637(L); 918(A)
Maeder, D. and A. H. Wapstra. New isomer in Pb—1433(L)
Magnusson, L. B. (see Studier, M. H.)—1428(L)
Mahmoud, H. (see Aitken, A.)—1349
Malvano, R. (see Demichelis, F.)—526
Mandel, M. (see Honig, A.)—953(A)
Mandeville, C. E. (see Rothman, M. A.)—796; 1434(E)
Manning, J. J. (see Lyon, W. S.)—501

Manring, Edward, Yu Ting, and Dudley Williams. Nuclear quadrupole transition in single crystal of $NaClO_3$—360(A)
Mansir, Dolan (see Bloom, Arnold)—941(A)
Margolis, B. Inelastic scattering of neutrons near thresholds—204
Mark, Hans (see McClelland, C. L.)—904(L)
Markowitz, S. S., W. Bernstein, and S. Katcoff. New 3.0-min Ce fission product and its 5.95-hr Pr daughter—178
—— (see Bernstein, W.)—1073
Marks, Lawrence J. (see Kraushaar, William L.)—326
Marshall, J., L. Marshall, and H. G. de Carvalho. Polarization by p-p collision at 310 Mev—1431(L)
——, **L. Marshall, and V. A. Nedzel.** p-p elastic scattering and pion production at 419 Mev—927(A)
—— (see Marshall, L.)—927(A)
—— (see Nedzel, V. A.)—927(A)
Marshall, L., V. A. Nedzel, and J. Marshall. Search for polarization of protons from 450-Mev synchrocyclotron—927(A)
—— (see Marshall, J.)—927(A); 1431(L)
—— (see Nedzel, V. A.)—927(A)
Martin, H. C. Cross sections for $O^{16}(n,p)N^{16}$ from 12 to 18 Mev—498
——, **B. C. Diven, and R. F. Taschek.** Cross sections for production of In^{115m} and Au^{197m} by inelastic scattering of neutrons—199
Martin, Paul C. (see Fulton, Thomas)—903(L)
Matheson, M. S. (see Grossweiner, L. I.)—929(A)
Matossi, Frank (see Nudelman, Sol)—929(A)
Matthias, B. T., E. Corenzwit, and C. E. Miller. Superconducting compounds—1415(L)
Maunsell, C. D. Absorption cross sections for photoionizing radiations in low-pressure gases—943(A)
Maximon, L. C. (see Bethe, H. A.)—768
—— (see Davies, Handel)—788
Mayer, Alex and L. H. Fisher. Buildup times of glow discharges in air—649(A)
McCall, D. W. (see Bloom, Myer)—920(A)
—— (see Williams, G. A.)—1428(L)
McClelland, C. L., Hans Mark, and Clark Goodman. Electric excitation of low-lying levels in separated W isotopes—904(L)
McCoubrey, A. O. Band fluorescence of Hg vapor—1249
McDonald, Charles A., Jr., R. W. Kenney, and R. F. Post. Monitor for high-energy photons—951(A)
—— (see Anderson, J. D.)—948(A)
—— (see Kenney, Robert W.)—951(A)
McDonell, William R. and Henry A. Kierstead. Expansion of Cu bombarded by 21-Mev deuterons—247(L)
McEllistrem, M. (see Galonsky, A.)—928(A)
McGarry, W. I. (see Elliot, J. O.)—1348
McGarvey, B. R. and H. S. Gutowsky. Temperature dependence of the nuclear resonance shift in metals—940(A)
McGowan, F. K. Angular correlations of γ rays in Ta^{181}—471
—— Measurement of K-shell internal conversion coefficients with coincidence scintillation spectrometer—163
McGuire, Thomas R. Microwave resonance absorption in Ni ferrite-aluminate—682
McIsaac, L. (see Kreger, W. E.)—943(A)
McKay, K. G. (see Johnson, J. B.)—668
McKay, R. E. Science day program for high-school students in Ohio—360(T)
McManus, H., W. T. Sharp, and H. Gellman. Nuclear interactions of high-energy nucleons—924(A)
McMillan, D. E. (see Dunlap, W. C., Jr.)—911(A)
McReynolds, A. W. and E. Andersen. Thermal neutron resonance of Sm—195
Mech, J. F. (see Studier, M. H.)—1428(L); 1433(L)
Medicus, G. Electron current saturation in a ball-of-fire diode—649(A)
Meechan, C. J. and R. R. Eggleston. Formation energy of vacancies in Cu—953(A)
Megill, L. R. (see Emigh, C. R.)—1190
Meiboom, S. and B. Abeles. Theory of galvanomagnetic effects in N-Ge—1121(L)
Meinschein, W. G. (see Burke, W. H., Jr.)—915(A)
Mendoza, E. (see Howling, D. H.)—1416(L)
Merritt, F. R. (see Anderson, P. W.)—717
—— (see Galt, J. K.)—1119(L)
Meshkov, Sydney. d^9 and d^4 configurations of V—270
Meyer, Lothar. Thickness of He film—655
—— (see Lawson, A. W.)—259
Meyer, Robert A. Influence of deuteron bombardment and strain hardening on mild steel—953(A)
Meyerhof, W. E. and G. Lindstrom. Decay of Cl^{38}—949(A)
Michel, L. and A. Wightman. μ-meson decay, β radioactivity, and universal Fermi interaction—354(L)
Michel, M. C. and D. H. Templeton. Mass assignments by isotope separation—1422(L)
Middleton, A. E. (see Beer, A. C.)—912(A)
—— (see Willardson, R. K.)—912(A)
Mihelich, J. W. and A. de-Shalit. Irregularities in nuclear level spacings of Hg, Au, and Pt—135
—— (see Gillon, L. P.)—124
Milford, F. J. Odd-nucleon-plus-liquid-drop model of heavy odd nuclei—1297
Miller, C. G. and N. L. Sanders. Motion of arc cathode spot in magnetic field—654(A)
Miller, Charles E., Joseph E. Henderson, David S. Potter, Jay Todd, Jr., Wayne M. Sandstrom, Gerald R. Garrison, William R. Davis, and Francis M. Charbonnier. Zenith angle dependence of cosmic-ray protons—590
—— (see Matthias, B. T.)—1415(L)
Miller, Frank N. Improved high-intensity short-duration light source—945(A)
Miller, Glenn H. and Lloyd O. Herwig. Ionization yields for fission fragments—932(A)
—— (see Herwig, L. O.)—926(A)
Miller, R. H. (see Sherr, R.)—1076
Mills, W. R. (see Mackin, R. J., Jr.)—950(A)
Milne, Edmund A. Energy levels in N^{14} from scattering of protons by C^{13}—762
Milton, J. C. D. (see Fraser, J. S.)—818
Mims, W. B. (see Mackin, R. J., Jr.)—950(A)
Minkowski, J. M. (see Bearden, J. A.)—629(L)
Misenta, R. (see Becker, E. W.)—244(L)
Mitchell, Allan C. G. (see Caird, Robert S.)—916(A)
Mitchell, George R. and Arthur E. Goldberg. Further evidence for energy gap of PbS—1421(L)
Mittleman, M. H. Higher-order potential effects in radiative correction to scattering of slow electrons—453
Mizushima, Masataka and Robert M. Hill. Microwave spectrum of O_3—745
—— (see Ito, Takashi)—1242
Molière, G. Spread of soft component of cosmic radiation—636(L)
Monahan, James (see Hamermesh, Morton)—963
Moon, P. B. (see Ilakovac, K.)—254(L)
Morin, F. J. Electrical properties of α-Fe_2O_3—1195
—— Electrical properties of NiO—1199
—— Lattice-scattering mobility in Ge—62
—— (see Pearson, G. L.)—666
Morinaga, H. and D. J. Zaffarano. Radioactive isotope separation by nuclear recoil—1422(L)
Morrison, G. L. and G. J. Plain. Limiting range of Reynolds' number in determining flow permeability—945(A)
Morrison, H. L. (see Backman, M. E.)—953(A)

Moszkowski, S. A. and D. C. Peaslee. Isotopic spin and odd-odd $N = Z$ nuclei—941(A); 455
—— **and C. H. Townes.** Tendency for positive nuclear quadrupole moments—306
Motz, Henry T. Slow neutron capture γ rays from Ti—925(A)
Motz, Lloyd. Nonconservation of rest mass and Dirac equation—901(L)
Mozer, F., W. A. Fowler, and C. C. Lauritsen. Inelastic scattering of protons by Li^7—829
Mrozowski, S. Forbidden line in spectrum of P I—933(A)
—— "Magnetic scanning" method for investigating hfs and isotope shift—641(L)
—— (see Cole, C. D.)—933(A)
Muether, H. R. (see Palevsky, H.)—920(A)
Mulder, Marjorie M. (see Green, Louis C.)—757; 757
Müller, Ralph H. Interaction of β particles with matter—891(L)
Murakawa, Kiyoshi. Hfs in spectra of Sb, Sm, Hg, and Cd—1232

Nachtrieb, N. H. Effect of pressure on self-diffusion of Na—926(T)
Nagle, D. E. Scattering of negative pions by deuterium—918(A)
Nathans, R. and J. Halpern. Systematics of photoneutron reactions—437
Navon, D. and H. Y. Fan. Low-temperature recombination and trapping in Ge—911(A)
Neamtan, S. M. Čerenkov effect and dielectric constant—932(A)
Nedzel, V. A., J. Marshall, and L. Marshall. p-p differential elastic scattering cross sections at 144, 271, and 429 Mev—927(A)
—— (see Marshall, J.)—927(A)
—— (see Marshall, L.)—927(A)
Neidigh, Rodger V. (see Cohen, Bernard L.)—282
Nicolet, Marcel. Origin of emission of oxygen green line in airglow—633(L)
Nielsen, H. H. (see Coburn, T. J.)—360(A)
Nigam, B. P. V_0^1 particle as high angular state of meson-nucleon system—914(A)
Nijgh, G. J. (see van Lieshout, R.)—255(L)
Noel, E. B. Physics problems in high-pressure Hg-vapor light sources—360(T)
Noon, J. H. (see Crussard, J.)—253(L)
Norberg, R. E. (see Bloom, M.)—638(L)
—— (see Holcomb, D. F.)—919(A)
Nordsieck, A. Reduction of integral in theory of bremsstrahlung—785
Novey, T. B. Influence of electric quadrupole interaction on angular correlation—916(T)
Nudelman, Sol and Frank Matossi. Electroluminescence with nonsinusoidal electric fields—929(A)
Nussbaum, R. H. (see van Lieshout, R.)—255(L)
Nyborg, W. L. (see Elder, S. A.)—364(A)

Oakley, David C., R. L. Walker, J. G. Teasdale, and J. I. Vette. Photoproduction of neutral pions at high energies—949(A)
—— (see Cooper, Duane H.)—950(A)
Oberly, John J. Photoelectric Hall effect in Ge single crystals—911(A)
Odian, A. (see Wattenberg, A.)—915(A)
Oeser, J. (see Brun, E.)—172; 904(L)
O'Friel, Z. (see Sturcken, E. F.)—1053
Ogushwitz, Howard and Stephen S. Friedland. Improved chronotron for time-of-flight measurements—363(A)
Okazaki, A., S. E. Darden, and R. B. Walton. Total cross sections of rare earths for fast neutrons—461
O'Kelley, G. D. (see Olsen, J. L.)—1125(L)
Olsen, J. L. and G. D. O'Kelley. β-ray spectrum of Mg^{28}—1125(L)
Olsen, L. O. G.E.-Case fellowship program for high-school physics teachers—360(T)
Olson, Elmer L. (see Handley, Thomas H.)—524
O'Neill, G. K. (see Keck, J.)—827
Orear, Jay. Signs of phase shifts in pion-proton scattering—918(A)
——, **J. J. Lord, and A. B. Weaver.** Scattering of 45-Mev positive pions by H—575
Ortel, William C. G. Neutron production by cosmic rays—561
Osborn, R. K. (see Rose, M. E.)—1315; 1326
Osborne, L. S. (see Wattenberg, A.)—915(A)
Oxley, C. L. Double scattering of protons at high energies—928(T)
——, **W. F. Cartwright, and J. Rouvina.** Double scattering of high-energy protons—806
Ozarow, Vernon. Electrical properties of Ge crystals containing compensated impurities—371

Pack, J. L. (see Phelps, A. V.)—652(A)
Packard, Martin and Russell Varian. Free nuclear induction in earth's magnetic field—941(A)
Pake, G. E. Paramagnetic relaxation in free radical solutions exhibiting hfs—944(T)
Palevsky, H., H. R. Muether, and A. Stolovy. Scintillation detector for Brookhaven fast chopper—920(A)
Palfrey, T. R. (see Voss, J. R.)—918(A)
Panofsky, Wolfgang K. H. Achromatic translation system for high-energy beams—949(A)
Park, David (see Brown, Fielding)—381
Parker, James H., Jr. Electron ejection by slow positive ions incident on flashed and gas-covered metallic surfaces—652(A); 1148
Parker, William J. (see Ch'en, Shang-Yi)—946(A)
Patrick, Lyle. Antiferromagnetism of Mn—370
—— Change of ferromagnetic Curie points with hydrostatic pressure—384
Pavlovic, A. (see Shirane, G.)—672
Payne, Wilbur B. (see Goodrich, Max)—916(A)
Pearson, G. L., W. T. Read, Jr., and F. J. Morin. Dislocations in plastically-deformed Ge—666
—— (see Tanenbaum, M.)—912(A)
Peaslee, D. C. (see Moszkowski, S. A.)—455; 941(A)
Pellam, J. R. (see de Klerk, D.)—28
Pepinsky, R. (see Shirane, G.)—672
Perlman, I. (see Asaro, Frank)—1423(L)
Perry, A. M. (see Keck, J.)—827
Peter, Brother Simon. Nuclear resonance of P^{31} in CS_2 solutions—940(A)
Peterson, R. W., C. A. Barnes, W. A. Fowler, and C. C. Lauritsen. Inelastic scattering of protons by F^{19}—951(A)
Peterson, S. W. (see Levy, Henri A.)—1120(L)
Pettengill, G. (see Chamberlain, O.)—1424(L)
Phelps, A. V. and J. L. Pack. Improved optical absorption technique for study of metastable atoms—652(A)
Phillips, G. C. (see Burke, W. H.)—188
Phillips, J. A. (see Arnold, W. R.)—483
Piccioni, O. (see Cool, R. L.)—249(L); 637(L); 918(A)
Placzek, G. Incoherent neutron scattering by polycrystals—895(L)
—— **and L. Van Hove.** Crystal dynamics and inelastic scattering of neutrons—1207
Plain, G. J. (see Morrison, H. L.)—945(A)
Polkinghorne, J. C. Identity for S matrix for finite time interval—228

Pond, T. A. Annihilation of positrons in condensed materials —478
Poritsky, A. Spectroscopy in manufacture of W—360(T)
Portnoy, William M. (see Letaw, Harry, Jr.)—892(L)
Post, R. F. (see Anderson, J. D.)—948(A)
—— (see McDonald, C. A., Jr.)—951(A)
Potter, David S. (see Miller, Charles E.)—590
Potter, Roy F. Cross sections for charge transfer collisions of low-energy ions in N_2 and O_2—650(A)
Potts, D. H. (see Hudson, G. E.)—936(A)
Pound, R. V. Recent results in nuclear magnetism—944(T)
Powles, J. G. (see Bloom, Myer)—920(A)
Pratt, William W. Angular distribution of protons from $B^{10}(d,p)B^{11}$—816
Preston, R. S. (see Whetten, N. R.)—1356
Price, Glenn A. Energy spectra and angular distributions of photoneutrons from heavy nuclei—1279
Primakoff, H. and W. Cheston. "*V* dinucleons"—908(L)
Prince, M. B. Drift mobilities in semiconductors. II. Si—1204
Proctor, D. G. and T. A. Romanowski. Study of α-particle pulse heights from organic scintillators—362(A)
Pyle, G. (see Studier, M. H.)—1428(L)

Racette, G. W., M. F. Kaplon, and D. M. Ritson. Light elements of the cosmic radiation—experimental—914(A)
—— (see Kaplon, M. F.)—914(A)
Ragent, B. and W. I. Linlor. Total neutron cross sections for C, Fe, Sb, and Ta from 35 to 180 Mev—951(A)
—— (see Linlor, W. I.)—951(A)
Ramler, W. J. (see Andre, C. G.)—925(A)
Ramsey, Norman F. Nuclear interactions in molecules—944(T)
—— (see Cohen, Victor W.)—941(A)
Randall, C. A., Jr. (see Hazen, W. E.)—578
Rappaport, P. Electron-voltaic effect in *p-n* junctions induced by β-particle bombardment—246(L)
Rasmussen, John O., Jr. (see Slätis, Hilding)—646(L)
Raudebaugh, Robert J. and Richard B. Belser. Metallographic studies of dual layer and simultaneously evaporated bimetal films after artificial aging by heating—930(A)
Rauh, E. G. (see Andre, C. G.)—925(A)
Ravenhall, D. G., D. R. Yennie, and R. N. Wilson. Phase-shift calculation of high-energy electron scattering by nuclei—949(A)
—— (see Yennie, D. R.)—948(A); 1128(L)
Read, W. T., Jr. (see Pearson, G. L.)—666
Reagan, Daryl. Photospallation yields of N^{17}—947(A)
Redman, J. K. (see Blewitt, T. H.)—891(L)
Remeika, J. P. (see Anderson, P. W.)—717
Reynolds, Charles A. "Closed" fountain effect in liquid He II—363(A); 1118(L)
Reynolds, J. M., T. E. Leinhardt, and H. W. Hemstreet. Hall effect in Bi at 1.4°K—247(L)
Rhodes, J. Elmer, Jr. Thermal energy in almost normal modes—1
Rice, O. K. Nature of higher-order phase transitions with application to liquid He—1161
Richards, H. T. (see Galonsky, A.)—928(A)
Richardson, J. Reginald (see Caldwell, David O.)—942(A)
—— (see Glass, Neel W.)—942(A)
Rinehart, M. C. (see Sargent, C. P.)—917(A)
Risser, J. R. (see Burke, W. H.)—188
Ritson, D. M. (see Kaplon, M. F.)—914(A)
—— (see Racette, G. W.)—914(A)
Roberts, James H., J. Haugsnes, and D. E. Wood. Loading of nuclear emulsions with Li gloss specks—920(A)
—— (see Weddell, James B.)—924(A)
Roberts, L. D. and Seymour Bernstein. Capture of polarized neutrons by polarized Mn^{55} and Sm^{149} nuclei; (a) Production of nuclear polarization. (b) Observation of effects due to nuclear polarization—917(T)
—— (see Dabbs, J. W. T.)—935(A)
—— (see Erickson, R. A.)—957
Roberts, T. R. and S. G. Sydoriak. Specific heat of liquid He^3—1418(L)
Robinson, H. G. (see Dehmelt, H. G.)—480; 920(A)
Robinson, J. E. (see Delbecq, C. J.)—262
Robinson, W. J. Mixture of central, tensor, and two-particle spin-orbit interactions for N^{14} and D^2—1296
Robson, A. E. and A. von Engel. Origin of retrograde motion of arc cathode spots—1121(L)
Robson, J. W., R. L. Stearns, and Arthur Lindener. Energy loss and scattering of 0.624-Mev electrons—362(A)
Rogers, K. (see Sargent, C. P.)—917(A)
Rogers, T. F. Absolute intensity of water vapor absorption at microwave frequencies—248(L)
Rohrlich, Fritz and B. C. Carlson. Positron-electron differences in energy loss and multiple scattering—38
—— (see Warner, Charles, III)—406
Romanowski, T. A. (see Proctor, D. G.)—362(A)
Roos, Charles E. New method for measuring Auger transitions—401
Rose, D. J. (see Allis, W. P.)—84
Rose, M. E. Mixed γ-mixed γ angular correlation—477
—— **and R. K. Osborn.** Nuclear matrix elements in β decay—1326
—— **and R. K. Osborn.** Pseudoscalar interaction in β decay —1315
Rosen, Arthur Z. Proton intensities at sea level and 9000 feet—280
Rosenblum, E. S. (see Lax, Benjamin)—1418(L)
Rosendorff, S., R. Stahl, and G. Yekutieli. Double star connected by heavy meson—901(L)
Rosenstock, Herbert B. Quantization of nonlinear field theory—331
Rosenwasser, Hyman (see De Juren, James A.)—831
Roser, F. X. (see Hudson, A. M.)—941(A)
Ross, S. W., E. Tochilin, and B. W. Shumway. Measurements of cyclotron neutron and γ fields for animal irradiation studies—945(A)
Rossi, G. Bernard, William B. Jones, Jack M. Hollander, and Joseph G. Hamilton. Acceleration of nitrogen 14 (+6) ions in 60-inch cyclotron—256(L)
—— (see Ghiorso, Albert)—257(L)
M. A. Rothman, D. W. Kent, and C. E. Mandeville. Scattering of fast neutrons by Fe, Pb, and Cr—1434(E)
—— **and C. E. Mandeville.** γ rays excited by inelastic scattering of neutrons in Pb, Bi, Fe, Ni, and Cr—796
Rothstein, J. Analogies between lattice defects and current carriers in semiconductors—912(A)
Rouvina, J. (see Oxley, C. L.)—806
Royden, Herbert N. (see Caldwell, David O.)—942(A)
Roys, P. A. (see Bennett, W. E.)—924(A)
Ruderman, Malvin A. (see Aitken, A.)—1349
—— (see Kroll, Norman M.)—233
Ruhlig, Arthur J. (see Graham, Walter J.)—647(A)
Russell, F. N. (see Grove, G. R.)—361(A)
Russell, Leonard N. (see Taylor, Warren E.)—1056

Sachs, A. M. (see Bodansky, D.)—918(A); 1367
—— (see Chinowsky, W.)—917(A)
Sachs, Mendel (see Hurd, F. Kenneth)—373; 919(A)
Sack, S., L. C. Biedenharn, and G. Breit. Elastic scattering of protons by α particles—321

Sagane, Ryokichi and Walter F. Dudziak. Relative low-energy pion production cross sections by photons on H—948(A)
—— (see Dudziak, Walter F.)—948(A)
Saha, A. K. (see Das, T. P.)—749
Sailor, V. L., H. H. Landon, and H. L. Foote, Jr. Slow neutron resonances in Eu—1292
—— (see Landon, H. H.)—1030
Salant, E. O. (see Hornbostel, J.)—902(L)
Salkowitz, E. I. (see Weertman, J.)—922(A)
Salutsky, Murrell L. (see Kirby, H. W.)—1051
Sample, J. T. (see Gove, H. E.)—928(A)
Sanders, N. L. (see Miller, C. G.)—654(A)
Sandstrom, Wayne M. (see Miller, Charles E.)—590
Sargent, C. P., M. C. Rinehart, R. C. Cornelius, L. M. Lederman, and K. Rogers. Internal conversion of mesic γ rays—917(A)
Savitt, Jacob. Velocity attenuation of explosive-produced air shocks—927(A)
Sawyer, G. A. (see Arnold, W. R.)—483
Schardt, A. W. and Joan P. Welker. Decay scheme of Se^{75} and Ge^{75}—916(A)
Schein, Marcel. Reports on the cosmic-ray conferences held in July, 1953, at Bagnères-de-Bigorre. (b) Conference on fundamental particles—930(T)
Schiff, L. I. Interpretation of electron scattering experiments —1434(E)
Schilberg, L. E. (see Conger, R. L.)—943(A)
Schild, A. New modification of classical electromagnetic theory—936(A)
Schmeissner, F. (see Becker, E. W.)—244(L)
Schmid, L. C. (see Cork, J. M.)—1059
Schmidt, F. H. (see Jakobson, M. J.)—303
—— (see Keister, G. L.)—140
Schneider, E. E. Hfs in paramagnetic resonance of x-rayed LiF—919(A)
Schultz, Virginia A. (see Waldron, Esther C.)—254(L)
Schulz, L. G. Reflectivity of Ag in near infrared—922(A)
Schwinger, Julian. Theory of quantized fields. V—615
Seagondollar, L. W. (see Teener, J. W.)—1035
Sears, G. W. Hg whiskers—921(A)
Sedlet, J. (see Studier, M. H.)—1433(L)
Seeman, N. (see King, D. T.)—914(A)
—— (see Shapiro, M. M.)—914(A)
Segrè, Emilio (see Chamberlain, O.)—1424(L); 1430(L)
Seidl, F. G. P. Recent measurements of lowest neutron scattering resonance in Co—931(A)
Sellers, P. A. (see Studier, M. H.)—1428(L); 1433(L)
Shapiro, M. M., D. T. King, and N. Seeman. Charged particles intermediate in mass between protons and deuterons—914(A)
—— (see King, D. T.)—914(A)
Shapiro, Philip. Angular distribution of protons from $Na^{23}(d,p)Na^{24}$—290
Sharp, R. A. and R. M. Diamond. New Ti nuclide: Ti^{44}—358(L)
Sharp, W. T. (see McManus, H.)—924(A)
Shaw, John H. (see Blau, Henry H., Jr.)—360(A)
Shaw, T. M. (see Elsken, R. H.)—943(A)
—— (see Windle, J. J.)—952(A)
Sherburne, R. K. and J. S. Arnold. New observations of hydrocarbon flame growth—946(A)
Sherman, Christopher. Nuclear induction with separate regions of excitation and detection—1429(L)
Sherman, Noah. Atmospheric temperature effect for μ mesons observed at depth of 846 m.w.e.—277
Sherr, R. and R. H. Miller. Electron capture in decay of Na^{22}—1076
Sherrill, F. A. (see Wittels, M.)—1117(L)
Shirane, G., H. Danner, A. Pavlovic, and R. Pepinsky. Phase transitions in ferroelectric $KNbO_3$—672
Shockley, W. Predicted effects of temperature gradients on diffusion in crystals—345(L)
Shumway, B. W. (see Ross, S. W.)—945(A)
Shutt, R. P. (see Fowler, W. B.)—861
Siegel, R. T. and A. J. Hartzler. Neutron-proton scattering at 395 Mev—928(A)
—— (see Hartzler, A. J.)—928(A)
Simon, Albert. Theory of polarized particles and γ rays in nuclear reactions—1435(E)
—— **and T. A. Welton.** Production of polarized particles in nuclear reactions—1435(E)
Simonsen, S. H. (see Levy, Henri A.)—1120(L)
Simpson, J. A. Reports on the cosmic-ray conferences held in July, 1953, at Bagnères-de-Bigorre. (a) Conference on intensity-time variations—930(T)
Sinclair, Rolf M. γ radiation from certain nuclear reactions —1082
Singer, L. S. Magnetic resonance in some Cr^{++} complexes —919(A)
Skochdopole, R. E. (see Griffel, M.)—657
Skolnik, M. I. Rf noise from low-current, atmospheric-pressure arc discharges in air—648(A)
Slätis, Hilding, John O. Rasmussen, Jr., and Hugo Atterling. β decay of Np^{239}—646(L)
Slichter, C. P. Polarization of nuclear spins in metals by Overhauser method—920(T)
Slifkin, Lawrence M. (see Letaw, Harry, Jr.)—892(L)
—— (see Sonder, E.)—970
Smaller, B., E. Yasaitis, and M. Brachman. Paramagnetic resonance of Mn^{++} at radiofrequencies—940(A)
Smith, Alan W. Thermal conductivity of graphite—952(A)
Smith, Charles G. Orderly subdivision of Hg arc cathode spot—653(A)
Smith, J. E. (see Carlton, M.)—919(A)
Smith, R. E. Glass absorption factors in light bulbs—360(T)
Smith, R. W. Radiation from CdS crystals generated by dc electric fields—347(L)
Smith, Robert D. and Dudley Williams. Total emission of HCl and CO in region of their fundamentals—361(A)
Smith, W. V. (see Barnes, R. G.)—95
Smoluchowski, R. Influence of pressure on Curie temperature of Fe and Ni—392
—— (see Leivo, W.)—1415(L)
Sogo, P. B. and C. D. Jeffries. Magnetic moments of Ag^{107} and Ag^{109} and hfs anomaly—174
Sonder, E., L. Slifkin, and C. T. Tomizuka. Diffusion of Sb in Ag—970
Soule, D. E. and R. J. Cashman. Bulk photoconductivity in PbS—635(L)
Spedding, F. H. (see Griffel, M.)—657
Spencer, L. V. and C. H. Blanchard. Multiple scattering of relativistic electrons—114
—— **and U. Fano.** Energy spectrum resulting from electron slowing-down—1172
Spruch, Larry and G. Goertzel. Internal Compton effect in Ba^{137}—642(L)
Stahl, R. (see Rosendorff, S.)—901(L)
Stanford, C. P., T. E. Stephenson, F. W. Cochran, and S. Bernstein. Polarization of neutrons—931(A)
Stanford, G. S. (see Foster, B. P.)—1069
Starner, J. W. (see Langer, L. M.)—253(L)
Staub, H. H. (see Brun, E.)—172; 904(L)
Stearns, M. (see Stearns, M. B.)—1123(L)
Stearns, M. B., S. DeBenedetti, M. Stearns, and L. Leipuner. Relative intensities of π and μ meson x-rays of K and L series in low Z elements—1123(L)
Stearns, R. L. (see Robson, J. W.)—362(A)

Steeb, E. S. Problems in evaluating radiant energy from light sources—360(T)
Steenberg, N. R. Nuclear alignment at low temperatures —678
Steffen, R. M. Influence of extra-nuclear fields on angular correlation of nuclear radiation—916(T)
Stehn, J. R. Nuclear energy surface and isotopic mass values —932(A)
Stein, S., E. Gerjuoy, and T. Holstein. Rotational excitation of homonuclear molecules—934(A)
Steinberger, Jack (see Bodansky, D.)—918(A); 1367
—— (see Chinowsky, William)—586; 917(A)
Steiner, H. (see Jungerman, J.)—949(A)
Steljes, J. F. and H. Carmichael. Influence of Pb shielding on ionization bursts at sea level—913(A)
—— (see Carmichael, H.)—913(A)
Stelson, P. H. Angular distribution of α particles from $Na^{23}(p,\alpha)Ne^{20}$—925(A)
Stephenson, T. E. (see Stanford, T. E.)—931(A)
Stern, M. O. (see Ashkin, J.)—1129(L)
Sternglass, Ernest J. Energy distribution of secondary electrons from solids—929(A)
Sternheimer, R. M. Density effect for ionization loss at low energies—351(L)
—— Energy loss of fast charged particle by Čerenkov radiation—1434(E)
—— Kinematic criterion for meson production in fundamental particle collisions—642(L)
—— (see Foley, H. M.)—734
Stevens, C. M. (see Studier, M. H.)—1428(L); 1433(L)
Stier, P. M., C. F. Barnett, and G. E. Evans. Charge states of ion beams in various gases—926(A)
Stitch, M. L. (see Honig, A.)—953(A)
St. John, Robert and J. G. Winans. Retrograde motion of cathode spot in transverse magnetic fields—653(A)
Stolovy, A. (see Palevsky, H.)—920(A)
Stork, Donald Harvey. Interaction of pions with complex nuclei—868
—— (see Leonard, Stanley L.)—568; 1435(E)
Stovall, E. J., Jr. (see Arnold, W. R.)—483
Strandberg, M. W. P. (see Burke, Bernard F.)—193
Stratton, T. F. (see Famularo, K. F.)—928(A)
Struthers, J. D. (see Fuller, C. S.)—1182
Studier, M. H., P. R. Fields, H. Diamond, J. F. Mech, A. M. Friedman, P. A. Sellers, G. Pyle, C. M. Stevens, L. B. Magnusson, and J. R. Huizenga. Elements 99 and 100 from pile-irradiated plutonium—1428
——, **P. R. Fields, P. H. Sellers, A. M. Friedman, C. M. Stevens, J. E. Mech, H. Diamond, J. Sedlet, and J. R. Huizenga.** Pu^{244} from pile-irradiated Pu—1433(L)
Sturcken, E. F., Z. O'Friel, and A. H. Weber. Internal conversion coefficients of Nb^{95}, Zn^{65}, and Sc^{46}—1053
Sueoka, Seiichi. Matrix elements of spin-orbit interaction in d^2d configuration—302
Sunyar, A. W. Decay of Ho^{166}—1345
—— Short-lived metastable states of W^{180}—1122(L)
Swann, W. F. G. Alfvén's theory of effect of magnetic storms on cosmic-ray intensity—905(L)
Sydoriak, S. G. (see Roberts, T. R.)—1418(L)

Taft, E. A. and F. Hubbard Horn. Au as donor in Si—64
Takeda, Gyo. High-energy protons in nuclear interaction of 220-Mev π^- mesons in nuclear emulsions—848
Takeo, Makoto and Shang-Yi Ch'en. Theory of fine structure pressure broadening of spectral lines—420
Tamor, S. Scattering of many-particle systems—227
Tanabe, Yukito (see Ito, Takashi)—1242
Tanaka, Katsumi. Čerenkov radiation—459
Tanaka, Yoshio and Murray Zelikoff. Continuous emission spectra of Kr and Xe in vacuum uv region—933(A)
Tanenbaum, M., G. L. Pearson, and W. L. Feldmann. Magnetoresistance in InSb and GaSb single crystals—912(A)
—— (see Briggs, H. B.)—912(A)
Tannenwald, L. M. Asymptotic spherical shock decay—946(A)
—— (see Martin, H. C.)—199
Tauber, G. E. and Ta-You Wu. Energies of excited states of nuclei—434
—— **and Ta-You Wu.** *p*- and *d*-shell nuclei in intermediate coupling—295
—— (see Horton, G. K.)—911(A)
Taylor, Warren E., Leonard N. Russell, and John N. Cooper. Resonance capture of protons by Mg^{25}—1056
Tchen, Chan-Mou. Transport processes as foundations of Heisenberg and Obukhoff theories of turbulence—4
Teasdale, J. G. (see Oakley, D. C.)—949(A)
Teener, J. W., L. W. Seagondollar, and R. W. Krone. γ rays from proton bombardment of Na—1035
Telegdi, Valentine L. (see Thirion, Jacques)—950(A)
Teller, E. and M. H. Johnson. Classical theory of heavy nuclei—947(A)
—— (see Johnson, M. H.)—357(L); 947(A)
Telschow, C. G. (see Brun, E.)—172; 904(L)
Temmer, G. M. and N. P. Heydenburg. Coulomb excitation of heavy and medium heavy nuclei by α particles—351(L)
—— (see Heydenburg, N. P.)—906(L)
Templeton, D. H. (see Michel, M. C.)—1422(L)
Thaler, R. M. and J. Bengston. Phase shift analysis of high-energy nucleon-nucleon scattering—643(L)
——, **J. Bengston, and G. Breit.** Effect of $^3P_2$–$^3F_2$ coupling on nucleon-nucleon scattering—644(L)
Thayer, R. N. Physics and physicists in Ohio industry—electric lamps—359(T)
Thirion, Jacques and Valentine L. Telegdi. Lifetime measurements for first excited states of O^{17} and B^{10} from recoil studies—950(A)
Thompson, R. W. Evidence for existence of V_1 particle—930(T)
Thompson, Stanley G., A. Ghiorso, B. G. Harvey, and G. R. Choppin. Transcurium isotopes produced in neutron irradiation of Pu—908(L)
—— (see Ghiorso, Albert)—257(L)
—— (see Harvey, Bernard G.)—1129(L)
Thomson, J. S. (see Bearden, J. A.)—629(L)
Thorn, R. J. (see Andre, C. G.)—925(A)
Thorndike, A. M. (see Fowler, W. B.)—861
Ting, Yu (see Manring, Edward)—360(A)
Tochilin, E. (see Ross, S. W.)—945(A)
Todd, Jay, Jr. (see Miller, Charles E.)—590
Tollestrup, A. V. and W. A. Wentzel. Monitor for high-energy electron or γ-ray beams—950(A)
—— (see Woodbury, H. H.)—1311
Tomizuka, C. T. Diffusion of Cd, In, and Sn in single crystals of Ag—922(A)
—— (see Sonder, E.)—970
Toppel, B. J. (see Bennett, W. E.)—924(A)
Townes, C. H. (see Honig, A.)—953(A)
—— (see Moszkowski, S. A.)—306
Trail, C. C. (see Johnson, C. H.)—924(A)
Treiman, S. B. Cosmic radiation in trapped orbits of solar magnetic dipole field—544
—— (see Firor, J.)—551
Tripp, R. (see Chamberlain, O.)—1430(L)
Trolan, J. K. (see Dolan, W. W.)—943(A)
Tuck, J. L. (see Arnold, W. R.)—483
Tucker, B. L. and E. C. Gregg. Resonances in $Li^7(\gamma,p)He^6$ cross section and high-energy limit of bremsstrahlung spectra—362(A)

Turner, W. J. (see Burstein, E.)—65
Tweet, Arthur G. Small angle x-ray scattering from liquid He I and liquid He II—15
Tycko, D. (see Foley, H. M.)—734

Udelson, Burton J. and John E. Creedon. Microwave measurements of properties of a dc H_2 discharge—648(A)
Utterback, N. G. (see Herwig, L. O.)—926(A)

Vachaspati. Elastic scattering of electrons by Coulomb field of nuclei using Born approximations—502
Van Hove, Leon. Temperature variation of magnetic inelastic scattering of slow neutrons—268
—— (see Placzek, G.)—1207
van Lieshout, R., R. H. Nussbaum, G. J. Nijgh, and A. H. Wapstra. Decay of Cu^{60} and nuclear levels in Ni^{60}—255(L)
van Loef, Jan J. (see Cox, Mason C.)—925(A)
Van Patter, D. M. (see Hintz, N. M.)—924(A)
Van Valkenburg, M. E. (see Hendricks, C. D., Jr.)—952(A)
Varian, Russell (see Packard, Martin)—941(A)
Varney, Robert N. Liberation of electrons by positive ion impact on cathode of pulsed Townsend discharge tube—1156
Vette, J. I. (see Oakley, D. C.)—949(A)
Vineyard, G. H. and G. J. Dienes. Theory of defect concentration in crystals—265
Voelker, W. H. Angular distribution of Compton scattered γ rays—362(A)
Voelz, Fred L. (see Cleveland, Forrest F.)—933(A)
Volkoff, G. M. Quadrupole splitting of nuclear magnetic resonance lines in single crystals—944(T)
von Engel, A. (see Robson, A. E.)—1121(L)
von Krzywoblocki, M. Z. Application of solutions of Boltzmann equation to turbulence—927(A)
Voss, J. R., T. R. Palfrey, and R. O. Haxby. Photoproduction of low-energy charged π mesons—918(A)

Wada, W. W. and D. T. King. Cross section for trident production by electrons of cosmic radiation—914(A)
Wainfan, N., W. C. Walker, and G. L. Weissler. Photoionization in atmospheric gases—651(A)
—— (see Walker, W. C.)—651(A)
Wakely, P. G. Binding energy calculation on He^4 with single-particle wave functions—1434(E)
Waldron, Esther C., Virginia A. Schultz, and Truman P. Kohman. Natural α activity of Nd—254(L)
Walker, J. (see Elliott, L. G.)—356(L)
Walker, R. (see Whetten, N. R.)—1356
Walker, Robert L. (see Cooper, Duane H.)—950(A)
—— (see Oakley, D. C.)—949(A)
Walker, W. C., N. Wainfan, and G. L. Weissler. Photoelectric yields of some metals in vacuum uv—651(A)
—— (see Wainfan, N.)—651(A)
Walker, W. D. (see Duller, N. M.)—284
—— (see Kaplon, M. F.)—1424(L)
Wallace, Robert. High-frequency performance of junction tetrode transistors—363(T)
Walt, M. and H. H. Barschall. Scattering of 1-Mev neutrons by intermediate and heavy elements—1062
Walton, R. B. (see Okazaki, A.)—461
Wang, S. (see Bloembergen, N.)—72
Wangsness, Roald K. Magnetic resonance in ferrimagnetics—68
Wapstra, A. H. (see Maeder, D.)—1433(L)
—— (see van Lieshout, R.)—255(L)
Warner, Charles, III, and Fritz Rohrlich. Energy loss and straggling of electrons—406
Warren, Roger W. Refined electron beam probe studies in glow discharges—943(A)
Wasserburg, G. J. and R. J. Hayden. Branching ratio of K^{40}—645(L)
Watson, K. M. (see Aitken, A.)—1349
—— (see Francis, N. C.)—313
Wattenberg, A., B. T. Feld, A. Julian, A. Odian, and L. S. Osborne. Search for production of μ-meson pairs by 340-Mev bremsstrahlung—915(A)
Weaver, A. B. (see Orear, Jay)—575
Weber, A. H. (see Breen, R. J.)—923(A)
—— (see Sturcken, E. F.)—1053
Weber, Alfons, Forrest F. Cleveland, and Salvador M. Ferigle. Raman and infrared spectra of dimethyltriacetylene—933(A)
Weddell, James B. and James H. Roberts. Angular distribution of $Li^6(n,\alpha)H^3$ for fast neutrons—924(A)
Weertman, J. and E. I. Salkowitz. Internal friction of dilute alloys of Pb—922(A)
Wegner, Harvey E. (see Farwell, George W.)—356(L)
Wehner, Gottfried K. Sputtering by ion bombardment—momentum transfer problem—653(A)
—— Threshold energies for sputtering and sound velocity in metals—633(L)
Weinreb, A. (see Cohen, S. G.)—1117(L)
Weisbrod, Harold (see Bessey, William H.)—923(A)
Weissbluth, M. (see Baez, A. V.)—942(A)
Weissler, G. L. (see Wainfan, N.)—651(A)
—— (see Walker, W. C.)—651(A)
Welker, Joan P. (see Schardt, A. W.)—916(A)
Welton, T. A. (see Simon, A.)—1435(E)
Wentzel, W. A. (see Tollestrup, A. V.)—950(A)
Wert, C. (see Ang, C.)—922(A)
Westerkamp, J. F. Variation of l-type doubling constant in HCN—716
Westermark, Torbjörn. Energy loss of charged relativistic particles and periodicity of elements—400
—— Influence of chemical state on stopping of fast charged particles—835
Wexler, S. Average charge of recoil atoms from several nuclear transitions—182
Weymouth, John. Simple bent-crystal x-ray spectrograph for senior experiment—359(T)
Whetten, N. R., R. S. Preston, R. V. Adams, R. Walker, and H. L. Kraybill. Cloud-chamber investigation of nuclear interactions of cosmic rays—1356
White, George R. (see Fry, W. F.)—1427(L)
Whittemore, W. L. (see Fowler, W. B.)—861
Wiegand, Clyde (see Chamberlain, O.)—1424(L); 1430(L)
Wiener, B. and G. Groetzinger. Variation of magnetoresistivity and resistivity of AuCu during annealing from cold-worked and thermally-disordered states—922(A)
Wightman, A. (see Michel, L.)—354(L)
Wiig, Edwin O. (see Caretto, Albert A., Jr.)—175
Wiles, Donald R. Search for $p_{1/2}$ isomeric state in Tc^{101} and identification of energy levels—181
Willardson, R. K., A. C. Beer, and A. E. Middleton. Magnetic field dependence of Hall coefficient in InSb—912(A)
—— (see Beer, A. C.)—912(A)
—— (see Harman, T. C.)—912(A)
Williams, Dudley (see Blau, Henry H., Jr.)—360(A)
—— (see Carpenter, Robert)—360(A)
—— (see Coburn, T. J.)—360(A)
—— (see Dalby, F. W.)—361(A)
—— (see Dickey, F. P.)—361(A)
—— (see Manring, Edward)—360(A)
—— (see Smith, Robert D.)—361(A)
—— (see Wolfe, Peter N.)—360(A)

Williams, G. A., D. W. McCall, and H. S. Gutowsky. Nuclear spin of Si^{29}—1428(L)
Williams, R. W. (see Hazen, W. E.)—578
Willig, F. J. Fast jet actuated shock tubes—946(A)
Wilson, R. N. Second Born approximation to the scattering of fast electrons and positrons by nuclei—949(A)
—— (see Ravenhall, D. G.)—949(A)
—— (see Yennie, D. R.)—948(A)
Wilson, Richard (see Brown, Karl L.)—443
Winans, J. G. (see St. John, Robert)—653(A)
Winckler, J. R. and K. Anderson. Geomagnetic and albedo studies with Čerenkov detector at 40° geomagnetic latitude—596
Windle, J. J. and T. M. Shaw. Slotted resonant cavity for dielectric measurements—952(A)
Winsberg, Lester. Interaction of μ^- mesons with I^{127}—937(A)
—— Pure negative muon beam—915(A)
Wittels, M. and F. A. Sherrill. Radiation damage in SiO_2 structures—1117(L)
Witten, Louis. Generalization of Yang and Lee's theory of condensation—1131
Wolfe, Peter N. and Dudley Williams. Microwave spectrum of O_2—360(A)
Wolfson, J. L. (see Elliott, L. G.)—356(L)
Wolfstirn, K. B. (see Fuller, C. S.)—1182
Woll, John W., Jr. (see Green, Louis C.)—757; 757
Wood, D. E. (see Roberts, James H.)—920(A)
Woodbury, H. H., A. V. Tollestrup, and R. B. Day. Low-energy γ radiation from bombardment of C by protons—1311
Woodruff, Truman O. OPW method for calculating energy eigenvalues extended to crystals of compounds—947(A)
Woodward, Ervin C., Jr. Isotope displacement in λ4415A Cd II—948(A)
—— Nuclear spins of Mo^{95} and Mo^{97}—954(A)
Woodward, W. M. (see Keck, J.)—827
Woolf, William E. and Richard B. Belser. X-ray diffraction studies of dual layer and simultaneously evaporated bimetal films after artificial aging by heating—930(A)
Worley, R. D., M. W. Zemansky, and H. A. Boorse. Vapor pressure curve of He between 4.2°K and 4.8°K—45
Wu, C. S. (see Boehm, F.)—518
Wu, Ta-You (see Tauber, G. E.)—295; 434
Wyeth, Cynthia W. (see Green, Louis C.)—757

Yager, W. A. (see Anderson, P. W.)—717
—— (see Galt, J. K.)—1119(L)
Yalow, Rosalyn. Use of radioactive I in the study of thyroid function—359(T)
Yasaitis, E. (see Smaller, B.)—940(A)
Yekutieli, G. (see Rosendorff, S.)—901(L)
Yennie, D. R., D. G. Ravenhall, and E. Baranger. Sign of phase shift in elastic scattering of electrons—1128(L)
——, **R. N. Wilson, and D. G. Ravenhall.** Phase-shift calculation of high-energy electron scattering by nuclei—948(A)
—— (see Ravenhall, D. G.)—949(A)
Yntema, J. L. (see Bayard, Robert T.)—1412(L)
Yokota, Ryosuke. Color centers in alkali silicate glasses—896(L)
Young, D. R. Dielectric constant measurements of $BaTiO_3$—359(T)
Ypsilantis, T. (see Chamberlain, O.)—1430(L)
Yuan, Luke C. L. Meson-nucleon interaction experiments at Brookhaven cosmotron—363(T)
—— **and S. J. Lindenbaum.** Energy spectrum of negative pions produced in Be by 2.3-Bev protons—1431(L)
—— **and S. J. Lindenbaum.** Total interaction cross section of hydrogen for positive and negati[illegible]200–700 Mev pions—917(A)
—— (see Lindenbaum, S. J.)—917(A)
Yuster, P. H. (see Delbecq, C. J.)—20

Zaffarano, D. J. (see Lane, R. O.)—916(A)
—— (see Morinaga, H.)—1422(L)
Zeiger, H. J. (see Lax, Benjamin)—1418(L)
Zelikoff, Murray (see Tanaka, Yoshio)—933(A)
Zemansky, M. W. (see Worley, R. D.)—45
Zumstein, R. V. (see Dickey, F. P.)—361(A)
Zweifel, Paul F. Positron-capture branching ratios—915(A)
Zwicky, F. Atmospheric disturbances and stellar scintillations—946(A)

Analytic Subject Index to Volume 93

References with (A) are to abstracts of papers presented at meetings of the American Physical Society: references with (L) are to Letters to the Editor; references with (E) are to Errata. Items are listed under the following categories:

Acoustics
Astrophysics
Atomic and Molecular Beams
Atomic Mass and Abundance
Atomic Structure and Spectra
Biophysics
Chemical Effects and Properties
Constants, Standards, Units
Cosmic Radiation
Crystalline State
Dielectrics and Dielectric Properties
Diffraction
Diffusion
Elasticity and Plasticity
Electrical Conductivity and Resistance
Electrical Discharges
Electrical Properties
Electromagnetic Theory and Electrodynamics
Electrons and Positrons
Elementary Particle Interactions
Errata
Field Theory
Films, Properties
Fluid Dynamics
Gamma Rays
Gases
Geophysics
Helium, Liquid
Imperfections in Solids
Ionization
Ions
Ions and Electrons, Mobility
Liquids
Luminescence
Magnetic Properties
Magnetic Resonance
Mathematical Methods
Mechanics
Mesons
Methods and Instruments
Microwaves
Miscellaneous
Molecular Aggregates
Molecular Structure and Spectra
Neutrino
Noise
Nuclear Fission
Nuclear Moments and Spin
Nuclear Photoeffects
Nuclear Reactions, General
Nuclear Reactions Induced by α Particles and He^3
Nuclear Reactions Induced by Deuterons and Tritons
Nuclear Reactions Induced by Mesons
Nuclear Reactions Induced by Neutrons
Nuclear Reactions Induced by Protons
Nuclear Spectra
Nuclear Structure Theory
Optical Properties
Proceedings of the American Physical Society
Quantum Electrodynamics
Quantum Mechanics
Radiation
Radioactivity
Range and Energy Loss of Particles
Relativity and Gravitation
Scattering, General
Scattering of α Particles
Scattering of Deuterons
Scattering of Electrons and Positrons
Scattering of Mesons
Scattering of Neutrons
Scattering of Protons
Semiconductors
Spectra, General
Statistical Mechanics and Thermodynamics
Superconductivity
Thermal Properties
X-Rays

Absorption of Radiation (see **Radiation**)

Acoustics
- Physical factors involved in sonic irradiation of liquids, S. A. Elder, J. Kolb, and W. L. Nyborg—364(A)
- Threshold energies for sputtering and sound velocity in metals, Gottfried K. Wehner—633(L)

Adsorption (see **Gases**)

Aerodynamics (see **Fluid Dynamics**)

Afterglow (see **Electrical Discharges**)

Alloys (see **Crystalline State**)

Annihilation (see **Electrons and Positrons**)

Antiferroelectric Phenomena (see **Dielectrics and Dielectric Properties**)

Antiferromagnetism (see **Magnetic Properties**)

Arcs (see **Electrical Discharges**)

Astrophysics
- Atmospheric disturbances and stellar scintillations, F. Zwicky—946(A)
- Origin of anomalous abundances of elements in giant stars, A. G. W. Cameron—932(A)
- Primeval cosmic abundance of deuterium, G. Boato—640(L)

Atmosphere (see **Geophysics**)

Atomic and Molecular Beams
- Observations of double and triple quantum transitions, P. Kusch—1022

Atomic Mass and Abundance
- K^{40} branching ratio, G. J. Wasserburg and R. J. Hayden—645(L)
- Mass assignments by isotope separation, M. C. Michel and D. H. Templeton—1422(L)
- Natural distribution of tritium, Sheldon Kaufman and W. F. Libby—1337
- Natural tritium content of atmospheric hydrogen, A. V. Grosse, A. D. Kirshenbaum, J. Laurence Kulp, and W. S. Broecker—250(L)
- Nuclear energy surface and isotopic mass values, J. R. Stehn—932(A)
- Origin of anomalous abundances of elements in giant stars, A. G. W. Cameron—932(A)
- Primeval cosmic abundance of deuterium, G. Boato—640(L)

Atomic Structure and Spectra
- Atomic spectra in infrared and electrodeless discharge source, F. P. Dickey, R. V. Zumstein, and Dudley Williams—360(A)
- Continuous emission spectra of Kr and Xe in vacuum uv region, Yoshio Tanaka and Murray Zelikoff—933(A)
- Correlation energies and angular components of wave functions of ground states of H^-, He I, and Li II, Louis C. Green, Margaret N. Lewis, Marjorie M. Mulder, Cynthia W. Wyeth, and John W. Woll, Jr.—757
- d^9 and d^4 configurations of V, Sydney Meshkov—270
- Discussion of analytic and Hartree-Fock wave functions for $1s^2$ configurations from H^- to C V, Louis C. Green, Marjorie M. Mulder, Margaret N. Lewis, and John W. Woll, Jr.—757
- Electric field gradients of atomic p electrons, R. G. Barnes and W. V. Smith—95
- Forbidden line in spectrum of P I, S. Mrozowski—933(A)
- Forbidden lines in spectrum of Be II, C. D. Cole and S. Mrozowski—933(A)
- Hfs in spectra of Sb, Sm, Hg, and Cd, Kiyoshi Murakawa—1232
- Improved optical absorption technique for study of metastable atoms, A. V. Phelps and J. L. Pack—652(A)

Ionization probability curves near threshold for Hg, Cd, and Zn, W. M. Hickam—652(A)
Isotope displacement in λ4415A Cd II, Ervin C. Woodward, Jr.—948(A)
Isotope shift in $_{58}$Ce II spectrum, Hack Arroe—94
"Magnetic scanning" method for investigating hfs and isotope shift, S. Mrozowski—641(L)
Method for measuring Auger transitions, Charles E. Roos —401
New method for exciting metallic spectra by active N_2. Excitation of Xe, Carl Kenty—651(A)
Radiative corrections in positronium, Thomas Fulton and Paul C. Martin—903(L)
Relative intensities of π and μ meson x-rays of K and L series in low Z elements, M. B. Stearns, S. DeBenedetti, M. Stearns, and L. Leipuner—1123(L)
Shift and broadening of blue Cs doublet produced by A and He, Shang-Yi Ch'en and William J. Parker—945(A)
Theory of fine structure pressure broadening of spectral lines, Makoto Takeo and Shang-Yi Ch'en—420
Aurora (see **Astrophysics; Geophysics**)

Barkhausen Effect (see **Magnetic Properties**)
Biophysics
Measurements of cyclotron neutron and γ fields for animal irradiation studies, S. W. Ross, E. Tochilin, and B. W. Shumway—945(A)
Boson Theory (see **Field Theory**)
Bremsstrahlung (see **Radiation**)
Broadening of Spectral Lines (see **Atomic Structure and Spectra; Molecular Structure and Spectra; Spectra, General**)

Capture Cross Sections (see **Electrons and Positrons; Nuclear Reactions; Radiation**)
Čerenkov Effect (see **Radiation**)
Chemical Effects and Properties
Hydrocarbon flame growth, R. K. Sherburne and J. S. Arnold—946(A)
Chemical Reactions (see **Chemical Effects and Properties**)
Chemiluminescence (see **Luminescence**)
Cold Emission (see **Electrical Properties**)
Colloids (see **Chemical Effects and Properties; Molecular Aggregates**)
Compton Effect (see **Radiation**)
Conductivity, Electrical (see **Electrical Conductivity and Resistance**)
Conductivity, Thermal (see **Thermal Properties**)
Constants, Standards, Units
Precision measurement at 24 500 volts of conversion constant λV, Gaelen L. Felt, John N. Harris, and Jesse W. M. DuMond—1434(E)
Present status of atomic constants, J. A. Bearden, M. D. Earle, J. M. Minkowski, and J. S. Thomson—629(L)
Cosmic Radiation
Alfvén's theory of effect of magnetic storms on cosmic-ray intensity, W. F. G. Swann—905(L)
Altitude and angular dependence of air showers, H. L. Kraybill—1362
Angle of divergence of pairs produced by photons, K. Hintermann—898(L)
Atmospheric temperature effect for μ mesons observed at depth of 846 m.w.e., Noah Sherman—277
Čerenkov counter-cloud chamber measurement of multiply charged primary cosmic rays, John Linsley—899(L)
Charged particles intermediate in mass between protons and deuterons, M. M. Shapiro, D. T. King, and N. Seeman—914(A)
Cloud-chamber investigation of nuclear interactions of cosmic rays, R. N. Whetten, R. S. Preston, R. V. Adams, R. Walker, and H. L. Kraybill—1356
Cosmic radiation in trapped orbits of solar magnetic dipole field, S. B. Treiman—544
Cosmic-ray ionization bursts in an eight-inch sphere at sea level, H. Carmichael and J. F. Steljes—913(A)
Cosmic-ray nuclear interactions in gases, W. W. Brown —518
Cosmic-ray transition phenomena due to electrons, photons, and mesons, Robert B. Brode—947(A)
Cross section for trident production by electrons of cosmic radiation, W. W. Wada and D. T. King—914(A)
Density of extensive air showers at airplane altitudes, Henry L. Kraybill—1360
Differential range spectrum of cosmic-ray mesons at sea level, Philip G. Lichtenstein—858
Effects of atmosphere on penetrating cosmic radiation, Robert L. Chasson—1434(E)
Emulsion studies of cosmic-ray stars produced in metal foils, Ian G. Barbour—535
Fermi's theory of origin of cosmic rays, Leverett Davis, Jr. —947(A)
Geomagnetic and albedo studies with Čerenkov detector at 40° geomagnetic latitude, J. R. Winckler and K. Anderson—596
High-energy meson production, N. M. Duller and W. D. Walker—284
Influence of earth's magnetic field on extensive air showers, Giuseppe Cocconi—646(L)
Influence of Pb shielding on ionization bursts at sea level, J. F. Steljes and H. Carmichael—913(A)
Interaction and production of cosmic-ray protons in C, J. Ballam and P. G. Lichtenstein—851
$K^{\pm}$ mesons from "fundamental" nuclear collisions, D. T. King, N. Seeman, and M. M. Shapiro—914(A)
Light elements of the cosmic radiation—experimental, G. W. Racette, M. F. Kaplon, and D. M. Ritson—914(A); interpretation, M. F. Kaplon, G. W. Racette, and D. M. Ritson—914(A)
Neutral-to-charge ratio in high-energy interactions, M. F. Kaplon, W. D. Walker, and M. Koshiba—1424(L)
Neutron production by cosmic rays, William C. G. Ortel —561
Proton intensities at sea level and 9000 feet, Arthur Z. Rosen—280
Solar magnetic moment and diurnal variation in cosmic-ray intensity, J. Firor, F. Jory, and S. B. Treiman—551
Spread of soft component of cosmic radiation, G. Molière —636(L)
Structure of air showers, W. E. Hazen, R. W. Williams, and C. A. Randall, Jr.—578
Zenith angle dependence of cosmic-ray protons, Charles E. Miller, Joseph E. Henderson, David S. Potter, Jay Todd, Jr., Wayne M. Sandstrom, Gerald R. Garrison, William R. Davis and Francis M. Charbonnier—590
Cosmology (see **Astrophysics; Relativity and Gravitation**)
Critical Potentials (see **Atomic Structure and Spectra; Molecular Structure and Spectra**)
Cross Section (see **Electrons and Positrons; Nuclear Reactions; Radiation; Scattering**)
Crystal Counters (see **Methods and Instruments**)
Crystalline State (see also **Electrical Properties; Imperfections in Solids; Magnetic Properties; Semiconductors; etc.**)
Accelerated growth of Sn whiskers, R. M. Fisher, L. S. Darken, and K. G. Carroll—921(A)

Crystalline State (Continued)
Calculation of energy band structures of diamond and Ge crystals by method of orthogonalized plane waves, Frank Herman—1214
Coloring and bleaching of alkali halide crystals containing *U* centers, R. S. Alger—953(A)
Creation of displacements in radiation damage, H. B. Huntington—1414(L)
Crystal dynamics and inelastic scattering of neutrons, G. Placzek and L. Van Hove—1207
Degeneracy in Ge, Esther M. Conwell—1118(L)
Diffusion of Sb in Ag, E. Sonder, L. Slifkin, and C. T. Tomizuka—970
Effect of pressure on *F*-center absorption in alkali halides, I. S. Jacobs—993
Effect of screening on solute diffusion in metals, David Lazarus—973
Effect of two-dimensional pressure on Curie point of $BaTiO_3$, P. W. Forsbergh, Jr.—686
Electrical conductivity of graphite, G. K. Horton and G. E. Tauber—911(A)
Expansion of Cu bombarded by 21-Mev deuterons, William R. McDonell and Henry A. Kierstead—247(L)
F-center wave functions in alkali halides, D. L. Dexter—244
Formation energy of vacancies in Cu, C. J. Meechan and R. R. Eggleston—953(A)
Further evidence for energy gap of PbS, George R. Mitchell and Arthur E. Goldberg—1421(L)
Hg whiskers, G. W. Sears—921(A)
Incoherent neutron scattering by polycrystals, G. Placzek—895(L)
Influence of deuteron bombardment and strain hardening on mild steel, Robert A. Meyer—953(A)
Infrared absorption of NiO, R. W. Johnston and D. C. Cronemeyer—634(L)
Infrared lattice absorption bands in Ge, Si, and diamond, R. J. Collins and H. Y. Fan—674
Infrared optical properties of single crystals of Te, Joseph J. Loferski—707
Internal friction of alloys Au and Ni, C. Ang and C. Wert—922(A)
Internal friction of dilute alloys of Pb, J. Weertman and E. I. Salkowitz—922(A)
Iodide impurity absorption in KBr and NaBr, C. J. Delbecq, J. E. Robinson, and P. H. Yuster—262
Kinetics of ordering in AuCu alloys, G. C. Kuczynski and R. Hochman—952(A)
Nuclear alignment at low temperatures, N. R. Steenberg—678
OPW method for calculating energy eigenvalues extended to crystals of compounds, Truman O. Woodruff—947(A)
Radiation damage in SiO_2 structures, M. Wittels and F. A. Sherrill—1117(L)
Specific heat of alloy $FeNi_3$ and of sigma phase FeCr, David S. Bloom—953(A)
Spectroscopy of solid state; some of transition elements, E. M. Gyorgy and G. G. Harvey—365
Strain sensitivity of AuCu and $AuCu_3$ alloys, G. C. Kuczynski—922(A)
Structural defects in Cu and the electrical resistivity minimum, T. H. Blewitt, R. R. Coltman, Jr., and J. K. Redman—891(L)
Structure of vitreous silica, Joseph S. Lukesh—264
Theoretical calculations of *F*-center energy levels, J. A. Krumhansl—245(L)
Theory of defect concentration in crystals, G. H. Vineyard and G. J. Dienes—265
Threshold energies for sputtering and sound velocity in metals, Gottfried K. Wehner—633(L)
Variation of magnetoresistivity and resistivity of AuCu during annealing from cold-worked and thermally disordered states, B. Wiener and G. Groetzinger—922(A)
X-ray coloration of alkali halides, D. L. Dexter—985
X-ray coloring of 400-Mev proton-irradiated KCl, W. Leivo and R. Smoluchowski—1415(L)

Diamagnetism (see **Magnetic Properties**)
Dielectrics and Dielectric Properties
Čerenkov effect and dielectric constant, S. M. Neamtan—932(A)
Dielectric absorption of liquid crystalline biaxial molecules, C. Kikuchi—934(A)
Effect of two-dimensional pressure on Curie point of $BaTiO_3$, P. W. Forsbergh, Jr.—686
Effects of alloying actions of dual-layer bi-metal electrodes on frequencies of piezoelectric quartz resonators, Richard B. Belser and Walter H. Hicklin—937(A)
Low-temperature coefficient ceramics, D. A. Berlincourt—360(A)
Mechanical properties of ceramic $BaTiO_3$, Helmut Krueger—360(A)
Neutron diffraction study of ferroelectric modification of KH_2PO_4, Henri A. Levy, S. W. Peterson, and S. H. Simonsen—1120(L)
Phase transitions in ferroelectric $KNbO_3$, G. Shirane, H. Danner, A. Pavlovic, and R. Pepinsky—672
Slotted resonant cavity for dielectric measurements, J. J. Windle and T. M. Shaw—952(A)
Threshold field *vs* temperature slope for paraelectric-ferroelectric change in $BaTiO_3$, A. deBretteville, Jr., and E. D. Harris—934(A)
Diffraction (see also **Scattering**)
Neutron diffraction in vitreous silica, R. J. Breen and A. H. Weber—923(A)
Neutron diffraction study of anisotropy transition in α-Fe_2O_3, L. M. Corliss, J. M. Hastings, and J. E. Goldman—893(L)
Neutron diffraction study of ferroelectric modification of KH_2PO_4, Henri A. Levy, S. W. Peterson, and S. H. Simonsen—1120(L)
Structure of vitreous silica, Joseph S. Lukesh—264
X-ray diffraction studies of dual layer and simultaneously evaporated bimetal films after artificial aging by heating, William E. Woolf and Richard B. Belser—930(A)
Diffusion
Connection between Smoluchowski equation and Kramers-Chandrasekhar equation, R. W. Davies—1169
Diffusion cooling of electrons in ionized gases, Manfred A. Biondi—1136
Diffusion effects occurring during artificial aging of dual layer bi-metal films, Richard B. Belser and Margaret C. Chester—937(A)
Diffusion of Cd, In, and Sn in single crystals of Ag, C. T. Tomizuka—922(A)
Diffusion of Sb in Ag, E. Sonder, L. Slifkin, and C. T. Tomizuka—970
Diffusivity and solubility of Cu in Ge, C. S. Fuller, J. D. Struthers, J. A. Ditzenberger, and K. B. Wolfstirn—1182
Effect of screening on solute diffusion in metals, David Lazarus—973
Effect of temperature gradients on diffusion in crystals, A. D. LeClaire—344(L); J. A. Brinkman—345(L); W. Shockley—345(L)
Self-diffusion in Ge, Harry Letaw, Jr., Lawrence M. Slifkin, and William M. Portnoy—892(L)
Study of SrO on Mo by use of field emission microscope, P. W. Kruse and E. A. Coomes—929(A)

Transition from free to ambipolar diffusion, W. P. Allis and D. J. Rose—84
Discharge of Electricity in Gases (see **Electrical Discharges**)
Disintegration and Excitation of Nucleus (see **Nuclear Reactions**)
Dynamics (see **Mechanics**)

Elasticity and Plasticity
Effect of two-dimensional pressure on Curie point of $BaTiO_3$, P. W. Forsbergh—686
Formation of dislocation rings by vacancy migration, R. D. Daniels and R. W. Hoffman—360(A)
Internal friction of alloys Au and Ni, C. Ang and C. Wert —922(A)
Internal friction of dilute alloys of Pb, J. Weertman and E. I. Salkowitz—922(A)
Mechanical properties of ceramic $BaTiO_3$, Helmut Krueger —360(A)
Rittenger's number for glass and decomposed granite, M. E. Backman and H. L. Morrison—953(A)
Strain sensitivity of AuCu and $AuCu_3$ alloys, G. C. Kuczynski—922(A)
Electrical Breakdown (see **Dielectrics and Dielectric Properties; Electrical Discharges**)
Electrical Conductivity and Resistance (see also **Semiconductors; Superconductors**)
α-Fe_2O_3 electrical properties, F. J. Morin—1195
Bulk photoconductivity in PbS, D. E. Soule and R. J. Cashman—635(L)
Conduction properties of *p*-type Ge between 25°C and 925°C, W. C. Dunlap, Jr., D. E. McMillan, and R. A. Brooks—911(A)
Conductivity and Hall effect of ZnO at low temperatures, Sol E. Harrison—52
Electrical conductivity of graphite, G. K. Horton and G. E. Tauber—911(A)
Electrical properties of Ge crystals containing compensated impurities, Vernon Ozarow—371
Electrical properties of *n*-type Ge, P. P. Debye and E. M. Conwell—693
Electrical resistances of dual layer and simultaneously evaporated bimetal films before and after artificial aging, Richard B. Belser and Margaret C. Chester—930(A)
Electrical resistivity and Hall coefficient of sodium tungsten bronze, W. R. Gardner and G. C. Danielson—46
Electrical resistivity of pure Te at melting point and in liquid state, A. Epstein and H. Fritzsche—922(A)
Formation energy of vacancies in Cu, C. J. Meechan and R. R. Eggleston—953(A)
Further correlation between magnetoresistance variations and de Haas-van Alphen effect, Ted G. Berlincourt and John K. Logan—348(L)
Hall constant of graphite, D. F. Johnston—1420(L)
Hall effect in Bi at low temperatures, Laird C. Brodie—935(A)
Hall effect in Bi at 1.4°K, J. M. Reynolds, T. E. Leinhardt, and H. W. Hemstreet—247(L)
Infrared absorption, photoconductivity, and impurity states in Ge, W. Kaiser and H. Y. Fan—911(A); 977
Infrared optical properties of single crystals of Te, Joseph J. Loferski—707
Infrared photoconductivity due to neutral impurities in Ge, E. Burstein, J. W. Davisson, E. E. Bell, W. J. Turner, and H. G. Lipson—65
Magnetic field dependence of Hall coefficient in InSb, R. K. Willardson, A. C. Beer, and A. E. Middleton—912(A)
Magnetoresistance in InSb and GaSb single crystals, M. Tanenbaum, G. L. Pearson, and W. L. Feldmann—912(A)
New galvanomagnetic effect. I. Theory, Colman Goldberg—913(A); II. Experiments with Ge, R. E. Davis and Colman Goldberg—913(A)
NiO electrical properties, F. J. Morin—1199
Photoconductivity of single crystals of anthracene, G. J. Goldsmith—929(A)
Photoelectric Hall effect in Ge single crystals, John J. Oberly—911(A)
Photoinduced conductivity in solutions of anthracene in *n*-hexane, L. W. Aukerman—929(A)
Strain sensitivity of AuCu and $AuCu_3$ alloys, G. C. Kuczynski—922(A)
Structural defects in Cu and electrical resistivity minimum, T. H. Blewitt, R. R. Coltman, Jr., and J. K. Redman—891(L)
Temperature dependence of transverse magnetoresistance effect in InSb, T. C. Harman, R. K. Willardson, and A. C. Beer—912(A)
Variation of magnetoresistivity and resistivity of AuCu during annealing from cold-worked and thermally-disordered states, B. Wiener and G. Groetzinger—922(A)
X-ray-induced photostimulated conductivity in MgO, Albert S. Eisenstein—1017
Electrical Discharges
Aspects of breakdown streamers, Leonard B. Loeb—649(A)
Buildup times of glow discharges in air, Alex Mayer and L. H. Fisher—649(A)
Current growth in formative time lag of sparks, H. W. Bandel—944(A); 649(A)
Diffusion cooling of electrons in ionized gases, Manfred A. Biondi—1136
Dissociative recombinations in N_2, A. C. Faire, O. T. Fundingsland, and A. L. Aden—650(A)
Doppler broadening of dissociative recombination lines, Manfred A. Biondi—650(A)
Electron beam probe studies in glow discharges, Roger W. Warren—943(A)
Electron current saturation in ball-of-fire diode, G. Medicus —649(A)
Equation for *V-I* curve of high current A arc, T. B. Jones and J. W. Dzimianski—654(A)
Excitation of plasma oscillations, Duncan H. Looney and Sanborn C. Brown—649(A); 965
Fast time analysis of burst pulse, preonset streamer, and Trichel pulse point-to-plane coronas, M. R. Amin—649(A)
Formative time lags of uniform field breakdown in H_2, I. Lessin and L. H. Fisher—649(A)
High-pressure arc anode phenomena, J. D. Cobine and E. E. Burger—653(A)
Impulse corona and breakdown of point-plane gap, T. W. Liao—650(A)
Ion source for doubly-charged He, C. E. Bradford, T. Kikuchi, and W. E. Bennett—921(A)
Liberation of electrons by positive ion impact on cathode of pulsed Townsend discharge tube, Robert N. Varney—1156
Method of eliminating cathode activation effects in G-M counter, H. R. Crane—921(A)
Microwave measurement of velocity dependence of collision cross section of slow electrons in He, Lawrence Gould—648(A)
Microwave measurements of properties of dc hydrogen discharge, Burton J. Udelson and John E. Creedon—648(A)

Electrical Discharges (Continued)
Motion of arc cathode spot in magnetic field, C. G. Miller and N. L. Sanders—654(A)
New method for exciting metallic spectra by active N_2. Excitation of Xe, Carl Kenty—651(A)
Orderly subdivision of Hg arc cathode spot, Charles G. Smith—653(A)
Origin of emission of oxygen green line in airglow, Marcel Nicolet—633(L)
Origin of retrograde motion of arc cathode spots, A. E. Robson and A. von Engel—1121(L)
Parameters of noble gas discharges, Walter J. Graham and Arthur J. Ruhlig—647(A)
Phenomena associated with small temperature variations of electron gas in discharge plasmas around 300°K. I. Cross modulation, J. M. Anderson and L. Goldstein—648(A); II. Afterglow quenching, L. Goldstein and J. M. Anderson—648(A)
Photodetachment of H_2 negative ion, Lewis M. Branscomb and Wade L. Fite—651(A)
Photon production in externally-sustained discharges, D. S. Burch, R. C. Irick, and R. Geballe—650(A)
Retrograde motion of cathode spot in transverse magnetic fields, Robert St. John and J. G. Winans—653(A)
Rf noise from low-current, atmospheric-pressure arc discharges in air, M. I. Skolnik—648(A)
Sputtering of alkali atoms by inert gas ions of low energy, Richard C. Bradley—719
Stability of low-pressure Hg arcs with positive conducting rod, J. T. Kouba and P. L. Copeland—926(A)
Statistical mechanics of cathode sputtering, Don E. Harrison, Jr.—652(A)
Time constants of self-sustained Townsend discharges, W. S. Huxford—652(A)
Time-resolved spectroscopy of N_2 and H_2, C. F. Hendee and W. B. Brown—651(A)
Transition from free to ambipolar diffusion, W. P. Allis and D. J. Rose—84
Use of pinhole for producing glow-to-arc transitions, B. Pearson DeLany and Paul L. Copeland—926(A)
Velocity of spread of burst pulses in air with coaxial cylindrical geometry, Elsa L. Huber—950(A)

Electrical Properties (see also **Dielectrics and Dielectric Properties; Electrical Conductivity and Resistance; Semiconductors; Superconductors**)
α-Fe_2O_3 electrical properties, F. J. Morin—1195
Effect of temperature on field emission, W. W. Dolan, W. P. Dyke, J. K. Trolan, and J. P. Barbour—943(A)
Effect on periodic Schottky deviations resulting from SrO layer deposited on clean Mo, G. A. Haas and E. A. Coomes—930(A)
Electrical properties of *n*-type Ge, P. P. Debye and E. M. Conwell—693
Electron ejection by slow positive ions incident on flashed and gas-covered metallic surfaces, James H. Parker, Jr.—652(A); 1148
Energy distribution of secondary electrons from solids, Ernest J. Sternglass—929(A)
Further evidence for energy gap of PbS, George R. Mitchell and Arthur E. Goldberg—1421(L)
Mechanism of secondary electron emission, A. O. Barut—981
NiO electrical properties, F. J. Morin—1199
Photoelectric Hall effect in Ge single crystals, John J. Oberly—911(A)
Photoelectric yields of some metals in vacuum uv, W. C. Walker, N. Wainfan, and G. L. Weissler—651(A)
Reflection of ions as ions or as metastable atoms at metal surface, Homer D. Hagstrum—652(A)
Secondary electron emission from Ge, J. B. Johnson and K. G. McKay—668
Sputtering by ion bombardment—momentum transfer problem, Gottfried K. Wehner—653(A)
Sputtering of alkali atoms by inert gas ions of low energy, Richard C. Bradley—719; 652(A)
Study of SrO on Mo by use of field emission microscope, P. W. Kruse and E. A. Coomes—929(A)
Temperature dependence of periodic deviations from Schottky line, G. A. Haas and E. A. Coomes—1421(L)
Threshold energies for sputtering and sound velocity in metals, Gottfried K. Wehner—633(L)

Electrodisintegration (see **Nuclear Reactions, General**)
Electrodynamics (see **Electromagnetic Theory and Electrodynamics**)
Electroluminescence (see **Luminescence**)
Electrolysis (see **Chemical Effects and Properties**)
Electromagnetic Theory and Electrodynamics
Class of solutions of Maxwell's equations, G. E. Hudson and D. H. Potts—936(A)
Classical theory of particles interacting with electromagnetic and mesonic fields, Peter Havas—882
New modification of classical electromagnetic theory, A. Schild—936(A)
Response currents in coupled circuits by Laplace transformation and mechanical harmonic synthesizer, Chu Jui Lee and S. LeRoy Brown—945(A)
Space-charge forces in strong-focusing synchrotrons, S. E. Barden—1378

Electron Diffraction (see **Diffraction; Scattering of Electrons and Positrons**)
Electron Optics (see **Electromagnetic Theory and Electrodynamics**)
Electronic Tubes (see **Methods and Instruments**)
Electrons and Positrons (see also **Electromagnetic Theory and Electrodynamics; Elementary Particle Interactions; Scattering of Electrons and Positrons**)
Angle of divergence of pairs produced by photons, K. Hintermann—898(L)
Annihilation of positrons in condensed materials, T. A. Pond—478
Annihilation of positrons in flight, H. W. Kendall and Martin Deutsch—932(A)
Behavior of positrons in superconductors, M. Dresden—1413(L)
Cross section for trident production by electrons of cosmic radiation, W. W. Wada and D. T. King—914(A)
Energy spectrum resulting from electron slowing-down, L. V. Spencer and U. Fano—1172
Radiative corrections in positronium, Thomas Fulton and Paul C. Martin—903(L)
Theory of bremsstrahlung and pair production. I. Differential cross section, H. A. Bethe and L. C. Maximon—768; II. Integral cross section for pair production, Handel Davies, H. A. Bethe, and L. C. Maximon—788
Triplet production in H_2 at 300 Mev by total absorption method, J. D. Anderson, C. A. McDonald, Jr., and R. F. Post—948(A)

Electrons, Mobility (see **Ions and Electrons, Mobility**)
Electrons, Scattering of (see **Scattering of Electrons and Positrons**)
Electrons, Secondary (see **Electrical Properties**)
Electrons, Thermionic (see **Electrical Properties**)
Electro-Optical Effects (see **Optical Properties**)
Electrostriction (see **Dielectrics and Dielectric Properties**)

Elementary Particle Interactions
Angle of divergence of pairs produced by photons, K. Hintermann—898(L)

Angular correlation of mesons produced in inelastic meson-nucleon collisions, J. S. Kovacs—252(L)
Bound state corrections in two-body systems, Thomas Fulton and Robert Karplus—1126
Cross sections for p-p scattering at 330 and 225 Mev, O. Chamberlain, G. Pettengill, E. Segrè, and C. Wiegand—1424(L)
Dependence of relative low-energy π^+ production cross section on atomic and neutron numbers, Walter F. Dudziak and Ryokichi Sagane—948(A)
Effect of $^3P_2$—$^3F_2$ coupling on nucleon-nucleon scattering, R. M. Thaler, J. Bengston, and G. Breit—644(L)
Elementary particles and Lamb-Retherford line shift, Leslie L. Foldy—880
Fraction of $n + p \rightarrow \pi^0$ events in which deuteron is formed, Roger H. Hildebrand—918(A)
Interaction between two nucleons at low energies, David Feldman—935(A)
Internal conversion of mesic γ rays, C. P. Sargent, M. C. Rinehart, R. C. Cornelius, L. M. Lederman, and K. Rogers—917(A)
$K^{\pm}$ mesons from "fundamental" nuclear collisions, D. T. King, N. Seeman, and M. M. Shapiro—914(A)
Kinematic criterion for meson production in fundamental particle collisions, R. M. Sternheimer—642(L)
Mass difference of neutral and negative π mesons, W. Chinowsky, A. Sachs, and J. Steinberger—917(A)
Meson production in high-energy nucleon-nucleon collisions, William L. Kraushaar and Lawrence J. Marks—326
Multiple production of pions in nucleon-nucleon collisions at cosmotron energies, E. Fermi—1434(E)
Neutral-to-charge ratio in high-energy interactions, M. F. Kaplon, W. D. Walker, and M. Koshiba—1424(L)
n-p scattering at 395 Mev—I, A. J. Hartzler and R. T. Siegel—928(A); II, R. T. Siegel and A. J. Hartzler—928(A)
n-p scattering with spin-orbit coupling. II. Variational formulation and effective range theory, L. C. Biedenharn and J. M. Blatt—1387
Phase shift analysis of high-energy nucleon-nucleon scattering, R. M. Thaler and J. Bengston—643(L)
Photomeson production near threshold and suppression of pairs in pseudoscalar meson theory, Norman M. Kroll and Malvin A. Ruderman—233
Photoproduction of neutral pions at high energies, D. C. Oakley, R. L. Walker, J. G. Teasdale, and J. I. Vette—949(A)
Photoproduction of π^+ mesons from H and C, G. Sargent Janes and William L. Kraushaar—900(L)
Polarization by p-p collision at 310 Mev, J. Marshall, L. Marshall, and H. G. de Carvalho—1431(L)
Possible relationships between π-meson nucleon scattering and π-meson production in nucleon-nucleon collisions, A. Aitken, H. Mahmoud, E. M. Henley, M. A. Ruderman, and K. M. Watson—1349
p-p differential elastic scattering cross sections at 144, 271, and 429 Mev, V. A. Nedzel, J. Marshall, and L. Marshall—927(A)
p-p elastic scattering and pion production at 419 Mev, J. Marshall, L. Marshall, and V. A. Nedzel—927(A)
Production of heavy unstable particles by negative pions, W. B. Fowler, R. P. Shutt, A. M. Thorndike, and W. L. Whittemore—861
Radiative effects in meson-nucleon scattering, Stanley Deser—612
Relative low-energy pion production cross sections by photons on hydrogen, Ryokichi Sagane and Walter F. Dudziak—948(A)
Scattering of 45-Mev positive pions by H, Jay Orear, J. J. Lord, and A. B. Weaver—575
Scattering of 65-Mev pions in hydrogen, D. Bodansky, A. M. Sachs, and J. Steinberger—918(A)
Scattering of 151- and 188-Mev positive pions by protons, George Homa, Gerson Goldhaber, and Leon M. Lederman—554
Signs of phase shifts in pion-proton scattering, Jay Orear—918(A)
Total cross section for positive pions in hydrogen, Stanley L. Leonard and Donald H. Stork—568; 1435(E)
Total cross section of pions at 1.5 Bev, R. L. Cool, L. Madansky, and O. Piccioni—249(L)
Total cross sections of 135-Mev to 250-Mev negative pions in hydrogen, J. Ashkin, J. P. Blaser, F. Feiner, J. Gorman, and M. O. Stern—1129(L)
Total interaction cross section of H for positive and negative 200-700 Mev pions, Luke C. L. Yuan and S. J. Lindenbaum—917(A)
Total interaction cross section of negative pions at kinetic energies of 1.0 and 1.45 Bev, R. L. Cool, L. Madansky, and O. Piccioni—637(L)
Total interaction cross section of pions with protons and deuterons at 1.0 Bev, R. L. Cool, L. Madansky, and O. Piccioni—637(L)
V_s^1 particle as high angular state of meson-nucleon system, B. P. Nigam—914(A)
Elements (see **Atomic Mass and Abundance**)
Energy Loss of Particles (see **Range and Energy Loss of Particles**)
Energy States of Atoms (see **Atomic Structure and Spectra**)
Energy States of Molecules (see **Molecular Structure and Spectra**)
Energy States of Nucleus (see **Nuclear Reactions; Nuclear Spectra; Nuclear Structure Theory**)
Equations of State (see **Chemical Effects and Properties**)
Errata
Binding energy calculation on He^4 with single-particle wave functions, P. G. Wakely—1434(E)
Effect of traps on carrier injection in semiconductors, H. Y. Fan—1434(E)
Effects of atmosphere on penetrating cosmic radiation, Robert L. Chasson—1434(E)
Energy loss of fast charged particle by Čerenkov radiation, R. M. Sternheimer—1434(E)
Interpretation of electron scattering experiments, L. I. Schiff—1434(E)
Multiple production of pions in nucleon-nucleon collisions at cosmotron energies, E. Fermi—1434(E)
Neutron capture γ rays from Sc, V, Co, and Cu, G. A. Bartholomew and B. B. Kinsey—1434(E)
Precision measurement at 24 500 volts of conversion constant λV, Gaelen L. Felt, John N. Harris, and Jesse W. M. DuMond—1434(E)
Production of polarized particles in nuclear reactions, A. Simon and T. A. Welton—1435(E)
Scattering of fast neutrons by Fe, Pb, and Cr, M. A. Rothman, D. W. Kent, and C. E. Mandeville—1434(E)
Theory of polarized particles and γ rays in nuclear reactions, Albert Simon—1435(E)
Errors of Measurement (see **Methods and Instruments**)
Evaporation (see **Liquids**)
Excitation of Atoms (see **Atomic Structure and Spectra**)
Excitation of Molecules (see **Molecular Structure and Spectra**)
Excitation of Nucleus (see **Nuclear Reactions; Nuclear Spectra; Nuclear Structure Theory**)
Explosion Phenomena (see **Fluid Dynamics**)

Faraday Effect (see **Optical Properties**)
Ferroelectric Phenomena (see **Dielectrics and Dielectric Properties**)
Ferromagnetism (see **Magnetic Properties**)
Field Emission (see **Electrical Properties**)
Field Theory (see also **Quantum Electrodynamics**)
Classical theory of particles interacting with electromagnetic and mesonic fields. I, Peter Havas—882
Hamiltonian mechanics of fields, R. H. Good, Jr.—239
Identity for S matrix for finite time intervals, J. C. Polkinghorne—228
Interaction between two nucleons at low energies, David Feldman—935(A)
μ-meson decay, β radioactivity, and universal Fermi interaction, L. Michel and A. Wightman—345(L)
Multipole singularities of classical scalar and pseudoscalar meson fields, Peter Havas—1400
New spinor theory of elementary particles, Ferdinand Cap—907(L)
Nucleon isobars in intermediate coupling, Francis H. Harlow and Boris A. Jacobsohn—333
Photomeson production near threshold and suppression of pairs in pseudoscalar meson theory, Norman M. Kroll and Malvin A. Ruderman—233
Quantization of nonlinear field theory, Herbert B. Rosenstock—331
Theory of quantized fields. V, Julian Schwinger—615
V_0^1 particle as high angular state of meson-nucleon system, B. P. Nigam—914(A)
Films, Properties
Aging of evaporated Ag films, W. F. Koehler—953(A)
Diffusion effects occurring during artificial aging of dual layer bi-metal films, Richard B. Belser and Margaret C. Chester—937(A)
Effect on periodic Schottky deviations resulting from SrO layer deposited on clean Mo, G. A. Haas and E. A. Coomes—930(A)
Effects of alloying actions of dual-layer bi-metal electrodes on frequencies of piezoelectric quartz resonators, Richard B. Belser and Walter H. Hicklin—937(A)
Electrical resistances of dual layer and simultaneously-evaporated bimetal films before and after artificial aging, Richard B. Belser and Margaret C. Chester—930(A)
Formation of dislocation rings by vacancy migration, R. D. Daniels and R. W. Hoffman—360(A)
Metallographic studies of dual layer and simultaneously evaporated bimetal films after artificial aging by heating, Robert J. Raudebaugh and Richard B. Belser—930(A)
Thickness of He film, Lothar Meyer—655
Transmission of 0–50 kev electrons by thin films with applications to β spectra, R. O. Lane and D. J. Zaffarano—916(A)
X-ray diffraction studies of dual layer and simultaneously evaporated bimetal films after artificial aging by heating, William E. Woolf and Richard B. Belser—930(A)
Fine Structure (see **Atomic Structure and Spectra**)
Fission of Nucleus (see **Nuclear Fission**)
Fluctuation Phenomena (see **Noise**)
Fluid Dynamics
Application of solutions of Boltzmann equation to turbulence, M. Z. von Krzywoblocki—927(A)
Asymptotic spherical shock decay, L. M. Tannenwald—946(A)
Fast jet actuated shock tubes, F. J. Willig—946(A)
Ionization by ultra-speed pellets, C. D. Hendricks, Jr., M. E. Van Valkenburg, W. G. Clay, and R. A. Davidson—952(A)
Jet-tone orifice number for orifices of small thickness-diameter ratio, A. B. C. Anderson—946(A)
Limiting range of Reynolds' number in determining flow permeability, G. L. Morrison and G. J. Plain—945(A)
Physical factors involved in sonic irradiation of liquids, S. A. Elder, J. Kolb, and W. L. Nyborg—364(A)
Shock-wave value, Richard I. Condit—945(A)
Transport processes as foundations of Heisenberg and Obukhoff theories of turbulence, Chan-Mou Tchen—4
Velocity attenuation of explosive-produced air shocks, Jacob Savitt—927(A)
Viscosity of gaseous He^3 and He^4 between 1.3° and 4.2°K, E. W. Becker, R. Misenta, and F. Schmeissner—244(L)
Fluorescence (see **Luminescence**)
Friction (see **Mechanics**)

Galvanomagnetic Effect (see **Magnetic Properties**)
Gamma Rays (see also **Nuclear Reactions; Nuclear Spectra**)
Gases
Improved radiotracer technique for study of gaseous adsorption on metals, John A. Dillon, Jr., and H. E. Farnsworth—364(A)
Ionization of pure gases and mixtures of gases by 5-Mev α particles, T. E. Bortner and G. S. Hurst—1236
Kinetic approach to collision processes in gases. I, E. P. Gross and M. Krook—936(A); II, M. Krook, P. L. Bhatnagar, and E. P. Gross—936(A)
Paramagnetic resonance in gases at low fields, M. A. Garstens—1228
Solution of Boltzmann equation for Maxwellian molecules, E. P. Gross—347(L)
Variational formulas in evaporation theory, John Greenstadt—1140
Geophysics
Charge transfer in upper atmosphere, S. N. Ghosh—650(A)
Free nuclear induction in earth's magnetic field, Martin Packard and Russell Varian—941(A)
Natural distribution of tritium, Sheldon Kaufman and W. F. Libby—1337
Natural tritium content of atmospheric hydrogen, A. V. Grosse, A. D. Kirshenbaum, J. Laurence Kulp and W. S. Broecker—250(L)
Origin of emission of oxygen green line in airglow, Marcel Nicolet—633(L)
Thermal microstructure in ocean, W. N. English—945(A)
Glasses (see **Molecular Aggregates**)
Gravitation (see **Relativity and Gravitation**)
Gyromagnetization (see **Magnetic Properties**)

Hall Effect (see **Electrical Conductivity and Resistance**)
Heat Capacity (see **Thermal Properties**)
Heat Conduction (see **Thermal Properties**)
Heat of Dissociation and Formation (see **Molecular Structure and Spectra**)
Heat of Fusion (see **Thermal Properties**)
Heat of Vaporization (see **Thermal Properties**)
Helium, Liquid
"Closed" fountain effect in liquid He II, Charles A. Reynolds—363(A); 1118(L)
Coefficient of expansion of liquid He II, K. R. Atkins and M. H. Edwards—1416(L)
Feynman's theory of liquid He, G. V. Chester—1412(L)
Light scattering in liquid He, A. W. Lawson and Lothar Meyer—259
Measurement and calculation of liquid He vapor pressure-temperature scale from 1° to 4.2°K, R. A. Erickson and L. D. Roberts—958
Nature of higher-order phase transitions with application to liquid He, O. K. Rice—1161

Second sound in He^3–He^4 mixtures below 1°K, J. C. King and Henry Fairbank—21
Second sound propagation below 1°K, D. de Klerk, R. P. Hudson, and J. R. Pellam—28
Small-angle x-ray scattering from liquid He I and liquid He II, Arthur G. Tweet—15
Specific heat of liquid He^3, T. R. Roberts and S. G. Sydoriak—1418(L)
Specific heat of 96 percent He^3 below 1°K, G. de Vries and J. G. Daunt—631(L)
Specific heat of 96 percent liquid He^3 between 1.3°K and 2.3°K, G. de Vries and J. G. Daunt—360(A)
Thickness of He film, Lothar Meyer—655
Vapor pressure curve of He between 4.2°K and 4.8°K, R. D. Worley, M. W. Zemansky, and H. A. Boorse—45
Viscosity of gaseous He^3 and He^4 between 1.3° and 4.2°K, E. W. Becker, R. Misenta, and F. Schmeissner—244(L)

High-Voltage Tubes and Machines (see **Methods and Instruments**)

Hydrodynamics (see **Fluid Dynamics**)

Hyperfine Structure (see **Atomic Structure and Spectra**; **Molecular Structure and Spectra**; **Nuclear Moments and Spin**)

Imperfections in Solids (see also **Crystalline State**; **Electrical Conductivity and Resistance**; **Luminescence**; **Semiconductors**)
Analogies between lattice defects and current carriers in semiconductors, J. Rothstein—912(A)
Color centers in alkali silicate glasses, Ryosuke Yokota—896(L)
Coloring and bleaching of alkali halide crystals containing *U* centers, R. S. Alger—953(A)
Creation of displacements in radiation damage, H. B. Huntington—1414(L)
Diffusion of Sb in Ag, E. Sonder, L. Slifkin, and C. T. Tomizuka—970
Dislocations in plastically-deformed Ge, G. L. Pearson, W. T. Read, Jr., and F. J. Morin—666
Effect of pressure on *F*-center absorption in alkali halides, I. S. Jacobs—993
Effect of temperature gradients on diffusion in crystals, A. D. LeClaire—344(L); J. A. Brinkman—345(L); W. Shockley—345(L)
Effect of traps on carrier injection in semiconductors, H. Y. Fan—1434(E)
Effects of imperfections and of electron interactions on magnetic resonance in alkali metals, D. F. Holcomb and R. E. Norberg—919(A)
Electron-voltaic effect in *p-n* junctions induced by β-particle bombardment, P. Rappaport—246(L)
Expansion of Cu bombarded by 21-Mev deuterons, William R. McDonell and Henry A. Kierstead—247(L)
F-center wave functions in alkali halides, D. L. Dexter—244
Formation energy of vacancies in Cu, C. J. Meechan and R. R. Eggleston—953(A)
Formation of dislocation rings by vacancy migration, R. D. Daniels and R. W. Hoffman—360(A)
Hfs in paramagnetic resonance of x-rayed LiF, E. E. Schneider—919(A)
Influence of deuteron bombardment and strain hardening on mild steel, Robert A. Meyer—953(A)
Infrared absorption, photoconductivity, and impurity states in Ge, W. Kaiser and H. Y. Fan—911(A); 977
Internal friction of alloys Au and Ni, C. Ang and C. Wert—922(A)
Internal friction of dilute alloys of Pb, J. Weertman and E. I. Salkowitz—922(A)
Iodide impurity absorption in KBr and NaBr, C. J. Delbecq, J. E. Robinson, and P. H. Yuster—262
Radiation damage in SiO_2 structures, M. Wittels and F. A. Sherrill—1117(L)
Radiation effects in InSb, J. W. Cleland and J. H. Crawford, Jr.—894(L)
Structural defects in Cu and electrical resistivity minimum, T. H. Blewitt, R. R. Coltman, Jr., and J. K. Redman—891(L)
Theoretical calculations of *F*-center energy levels, J. A. Krumhansl—245(L)
Theory of defect concentration in crystals, G. H. Vineyard and G. J. Dienes—265
X-ray coloration of alkali halides, D. L. Dexter—985
X-ray coloring of 400-Mev proton-irradiated KCl, W. Leivo and R. Smoluchowski—1415(L)
X-ray-induced photostimulated conductivity in MgO, Albert S. Eisenstein—1017

Inelastic Scattering (see **Nuclear Reactions**; **Scattering**)

Instruments (see **Methods and Instruments**)

Internal Conversion (see **Nuclear Spectra**)

Ionization (see also **Electrical Discharges**; **Range and Energy Loss of Particles**)
Absorption cross sections for photoionizing radiations in low-pressure gases, C. D. Maunsell—943(A)
Characteristics of gridded parallel-plate ionization chambers, L. O. Herwig, G. H. Miller, and N. G. Utterback—926(A)
Density effect for ionization loss at low energies, R. M. Sternheimer—351(L)
Internal bremsstrahlung and ionization accompanying β decay, F. Boehm and C. S. Wu—518
Ionization by ultra-speed pellets, C. D. Hendricks, Jr., M. E. Van Valkenburg, W. G. Clay, and R. A. Davidson—952(A)
Ionization of pure gases and mixtures of gases by 5-Mev α particles, T. E. Bortner and G. S. Hurst—1236
Ionization probability curves near threshold for Hg, Cd, and Zn, W. M. Hickam—652(A)
Ionization yields for fission fragments, Glenn H. Miller and Lloyd O. Herwig—932(A)
Photoionization in atmospheric gases, N. Wainfan, W. C. Walker, and G. L. Weissler—651(A)
Specific ionization and energy loss of fast charged particle, J. R. Allen—353(L)
Specific ionization of high-energy electrons in H_2 and N_2, W. C. Barber—942(A)

Ionization Potentials of Atoms (see **Atomic Structure and Spectra**)

Ionization Potentials of Molecules (see **Molecular Structure and Spectra**)

Ionosphere (see **Geophysics**)

Ions (see also **Electrical Discharges**)
Acceleration of N^{14} (+6) ions in 60-inch cyclotron, G. Bernard Rossi, William B. Jones, Jack M. Hollander, and Joseph G. Hamilton—256(L)
Charge states of ion beams in various gases, P. M. Stier, C. F. Barnett, and G. E. Evans—926(A)
Cross sections for charge transfer collisions of low-energy ions in N_2 and O_2, Roy F. Potter—650(A)
Electron ejection by slow positive ions incident on flashed and gas-covered metallic surfaces, James H. Parker, Jr.—652(A); 1148
Liberation of electrons by positive ion impact on cathode of pulsed Townsend discharge tube, Robert N. Varney—1156
Metastable negative ions, B. L. Donnally and H. E. Carr—111
New method of calculation of effective ionic radii of lanthanides, N. Efremov—934(A)

Ions (Continued)
Numerical regularities in periodic system of ions, N. Efremov—945(A)
Reflection of ions as ions or as metastable atoms at metal surface, Homer D. Hagstrum—652(A)
Sputtering by ion bombardment, Gottfried K. Wehner—653(A)
Sputtering of alkali atoms by inert gas ions of low energy, Richard C. Bradley—719; 652(A)
Threshold energies for sputtering and sound velocity in metals, Gottfried K. Wehner—633(L)
Ions and Electrons, Mobility (see also **Semiconductors**)
Drift mobilities in semiconductors, II. Silicon, M. B. Prince—1204
Electrical properties of *n*-type Ge, P. P. Debye and E. M. Conwell—693
Lattice-scattering mobility in Ge, F. J. Morin—62
Isobars (see **Atomic Mass and Abundance**)
Isomers, Molecular (see **Molecular Structure and Spectra**)
Isotopes (see **Atomic Mass and Abundance; Radioactivity**)

Kerr Effect (see **Optical Properties**)
Kinetic Theory of Gases (see **Gases**)

Liquid Helium (see **Helium, Liquid**)
Liquids
Dielectric absorption of liquid crystalline biaxial molecules, C. Kikuchi—934(A)
Physical factors involved in sonic irradiation of liquids, S. A. Elder, J. Kolb, and W. L. Nyborg—364(A)
Variational formulas in evaporation theory, John Greenstadt—1140
Luminescence
α-particle pulse heights from organic scintillators, D. G. Proctor and T. A. Romanowski—360(A)
Band fluorescence of Hg vapor, A. O. McCoubrey—1249
Electroluminescence in thin films of ZnS: Mn, R. E. Halsted and L. R. Koller—349(L); 929(A)
Electroluminescence with nonsinusoidal electric fields, Sol Nudelman and Frank Matossi—929(A)
Energy transfer from solvent to solute in liquid organic solutions under uv excitation, S. G. Cohen and A. Weinreb—1117(L)
Fluorescence photometer, F. J. Lynch—926(A)
Long-lived phosphorescent components on Tl-activated NaI, C. R. Emigh and L. R. Megill—1190
Luminescent centers in x-ray excited fluorescence of ice, L. I. Grossweiner and M. S. Matheson—929(A)
NaI counting response for γ rays, W. E. Kreger and L. McIsaac—943(A)
Photoconductivity of single crystals of anthracene, G. J. Goldsmith—929(A)
Photoinduced conductivity in solutions of anthracene in *n*-hexane, L. W. Aukerman—929(A)

Magnetic Fields (see **Electromagnetic Theory and Electrodynamics**)
Magnetic Properties
Antiferromagnetism of Mn, Lyle Patrick—370
Change of ferromagnetic Curie points with hydrostatic pressure, Lyle Patrick—384
Diffuse magnetic scattering of neutrons: zinc ferrite, B. N. Brockhouse, L. M. Corliss, and J. M. Hastings—923(A)
Further correlation between magnetoresistance variations and de Haas-van Alphen effect, Ted G. Berlincourt and John K. Logan—348(L)
Heat capacity of Gd from 15 to 355°K, M. Griffel, R. E. Skochdopole, and F. H. Spedding—657
Influence of pressure on Curie temperature of Fe and Ni, R. Smoluchowski—392
Low-temperature diamagnetism of electrons in cylinder, William Band—350(L)
Magnetic resonance in αFe_2O_3, P. W. Anderson, F. R. Merritt, J. P. Remeika, and W. A. Yager—717
Magnetic resonance in ferrimagnetics, Roald K. Wangsness—68
Magnetic resonance in some Cr^{++} complexes, L. S. Singer—919(A)
Magnetic resonance phenomena in ferrites, Fielding Brown and David Park—381
Microwave resonance absorption in Ni ferrite-aluminate, Thomas R. McGuire—682
Neutron diffraction study of anisotropy transition in α-Fe_2O_3, L. M. Corliss, J. M. Hastings, and J. E. Goldman—893(L)
Spectroscopy of solid state; some of transition elements, E. M. Gyorgy and G. G. Harvey—365
Strong-field induced paramagnetic anomaly in $NiSiF_6 \cdot 6H_2O$, Warren E. Henry—935(A)
Temperature dependence of ferromagnetic resonance line width in nickel iron ferrite: New loss mechanism, J. K. Galt, W. A. Yager, and F. R. Merritt—1119(L)
Theory of galvanomagnetic effects in *n*-Ge, S. Meiboom and B. Abeles—1121(L)
Thermodynamic properties of $Mn(ND_4)_2(SO_4)_2 \cdot 6D_2O$ below 1°K, J. W. T. Dabbs and L. D. Roberts—935(A)
Volume magnetostriction in Ni and Bethe-Slater interaction curve, K. Azumi and J. E. Goldman—630(L)
Magnetic Resonance (see also **Nuclear Moments and Spin**)
Anisotropic relaxation of quadrupole spin echoes, E. L. Hahn and B. Herzog—639(L)
Cyclotron resonance in Ge crystals, A. F. Kip, G. Dresselhaus, and C. Kittel—952(A)
Directional properties of cyclotron resonance in Ge, Benjamin Lax, H. J. Zeiger, R. N. Dexter, and E. S. Rosenblum—1418(L)
Effect of molecular motion on intensity of pure quadrupole resonances, Myer Bloom, H. S. Gutowsky, D. W. McCall, and J. G. Powles—920(A)
Effects of imperfections and of electron interactions on magnetic resonance in alkali metals, D. F. Holcomb and R. E. Norberg—919(A)
Electron-spin resonance absorption in bulk and dispersed Li and Na, G. Feher and T. W. Griswold—952(A)
Experiment for measurement of magnetic moment of neutron, Victor W. Cohen, Noel R. Corngold, and Norman F. Ramsey—941(A)
Free nuclear induction in earth's magnetic field, Martin Packard and Russell Varian—941(A)
Hfs in paramagnetic resonance of x-rayed LiF, E. E. Schneider—919(A)
Hg^{201} nuclear quadrupole resonance, H. G. Dehmelt, H. G. Robinson, and Walter Gordy—480; 920(A)
K^{41}, Y^{89}, Ag^{107}, and Ag^{109} magnetic moments, E. Brun, J. Oeser, H. H. Staub, and C. G. Telschow—172
Magnetic moments of Ag^{107} and Ag^{109} and hfs anomaly, P. B. Sogo and C. D. Jeffries—174
Magnetic resonance in αFe_2O_3, P. W. Anderson, F. R. Merritt, J. P. Remeika, and W. A. Yager—717
Magnetic resonance in ferrimagnetics, Roald K. Wangsness—68
Magnetic resonance in some Cr^{++} complexes, L. S. Singer—919(A)
Magnetic resonance phenomena in ferrites, Fielding Brown and David Park—381
Mathematical analysis of Hahn spin-echo experiment, T. P. Das and A. K. Saha—749

Microwave resonance absorption in Ni ferrite-aluminate, Thomas R. McGuire—682
Nuclear induction relaxation times in weak magnetic fields, Arnold Bloom and Dolan Mansir—941(A)
Nuclear induction with separate regions of excitation and detection, Christopher Sherman—1429(L)
Nuclear quadrupole transition in single crystal of $NaClO_3$, Edward Manring, Yu Ting, and Dudley Williams—360(A)
Nuclear resonance of Nb^{93} in $KNbO_3$, R. M. Cotts and W. D. Knight—940(A)
Nuclear resonance of P^{31} in CS_2 solutions, Brother Simon Peter—940(A)
Observations of double and triple quantum transitions, P. Kusch—1022
Paramagnetic resonance absorption of carbazyl and hydrazyl, C. Kikuchi and V. W. Cohen—394
Paramagnetic resonance absorption of Mn^{++} in single crystals of $CaCO_3$, F. Kenneth Hurd, Mendel Sachs, and W. D. Hershberger—373; 919(A)
Paramagnetic resonance in gases at low fields, M. A. Garstens—1228
Paramagnetic resonance of Mn^{++} at radiofrequencies, B. Smaller, E. Yasaitis, and M. Brachman—940(A)
Proton line shapes in magnetic resonance spectra of NH_4 salts, Robert Carpenter and Dudley Williams—360(A)
Proton relaxation in water, G. Chiarotti and L. Giulotto—1241
Quantitative measurement of magnetic absorption utilizing null-balance system, R. H. Elsken and T. M. Shaw—943(A)
Relaxation effects in para- and ferromagnetic resonance, N. Bloembergen and S. Wang—72
Saturation behavior of Gaussian magnetic resonance line, D. F. Abell and W. D. Knight—940(A)
Si^{29} nuclear spin, G. A. Williams, D. W. McCall, and H. S. Gutowsky—1428(L)
Temperature dependence of nuclear resonance shift in metals, B. R. McCarvey and H. S. Gutowsky—940(A)
Transient nuclear induction signals associated with pure quadrupole interactions, M. Bloom and R. E. Norberg—638(L)
Xe^{129} and Xe^{131} magnetic moments, E. Brun, J. Oeser, H. H. Staub, and C. G. Telschow—904(L)

Magneto-Optical Effects (see **Optical Properties**)
Magnetoresistance (see **Electrical Conductivity and Resistance**)
Magnetostriction (see **Magnetic Properties**)
Mass Defects (see **Atomic Mass and Abundance**)
Mass Spectroscopy (see **Atomic Mass and Abundance; Methods and Instruments**)
Mathematical Methods
Stokes parameter technique for treatment of polarization in quantum mechanics, U. Fano—121
Measurements (see **Methods and Instruments**)
Mechanics
Kinematic criterion for meson production in fundamental particle collisions, R. M. Sternheimer—642(L)
Mechanics, Quantum—Atomic Structure and Spectra (see **Atomic Structure and Spectra**)
Mechanics, Quantum—General (see **Quantum Mechanics**)
Mechanics, Quantum—Molecular Structure and Spectra (see **Molecular Structure and Spectra**)
Mechanics, Quantum—Nuclear (see **Nuclear Structure Theory; Field Theory**)
Mechanics, Quantum—of Solid Bodies (see **Crystalline State**)
Mechanics, Statistical (see **Statistical Mechanics and Thermodynamics**)
Meson Field Theory (see **Field Theory**)

Mesons (see also **Cosmic Radiation; Elementary Particle Interaction; Nuclear Reactions Induced by Mesons; Scattering of Mesons**)
Angular correlation of mesons produced in inelastic meson-nucleon collisions, J. S. Kovacs—252(L)
Angular correlations in τ-meson decay, R. H. Dalitz—914(A)
Artificially-produced negative heavy meson, J. Hornbostel and E. O. Salant—902(L)
Atmospheric temperature effect for μ mesons observed at depth of 846 m.w.e., Noah Sherman—277
Charged particles intermediate in mass between protons and deuterons, M. M. Shapiro, D. T. King, and N. Seeman—914(A)
Cloud-chamber investigation of nuclear interactions of cosmic rays, N. R. Whetten, R. S. Preston, R. V. Adams, R. Walker, and H. L. Kraybill—1356
Dependence of relative low-energy $\pi^{\pm}$ production cross section on atomic and neutron numbers, Walter F. Dudziak and Ryokichi Sagane—948(A)
Differential range spectrum of cosmic-ray mesons at sea level, Philip G. Lichtenstein—858
Double star connected by heavy meson, S. Rosendorff, R. Stahl, and G. Yekutieli—901(L)
Energy spectrum of negative pions produced in Be by 2.3-Bev protons, S. J. Lindenbaum, and Luke C. L. Yuan—917(A); Luke C. L. Yuan and S. J. Lindenbaum—1431(L)
High-energy meson production, N. M. Duller and W. D. Walker—284
Internal conversion of mesic γ rays, C. P. Sargent, M. C. Rinehart, R. C. Cornelius, L. M. Lederman, and K. Rogers—917(A)
$K^{\pm}$ mesons from "fundamental" nuclear collisions, D. T. King, N. Seeman, and M. M. Shapiro—914(A)
Kinematic criterion for meson production in fundamental particle collisions, R. M. Sternheimer—642(L)
Mass difference of neutral and negative π mesons, William Chinowsky and Jack Steinberger—586; W. Chinowsky, A. Sachs, and J. Steinberger—917(A)
Meson production in high-energy nucleon-nucleon collisions, William L. Kraushaar and Lawrence J. Marks—326
Multiple production of pions in nucleon-nucleon collisions at cosmotron energies, E. Fermi—1434(E)
μ-meson decay, β radioactivity, and universal Fermi interaction, L. Michel and A. Wightman—354(L)
Negative π-μ meson decays in photographic emulsion, W. F. Fry and George R. White—1427(L)
Neutral-to-charge ratio in high-energy interactions, M. F. Kaplon, W. D. Walker, and M. Koshiba—1424(L)
New decay mode of heavy meson, J. Crussard, M. F. Kaplon, J. Klarmann, and J. H. Noon—253(L)
Nucleon-nucleus collisions at relativistic energies, Giuseppe Cocconi—1124
Photomeson production near threshold and suppression of pairs in pseudoscalar meson theory, Norman M. Kroll and Malvin A. Ruderman—233
Photoproduction of low-energy charged π mesons, J. R. Voss, T. R. Palfrey, and R. O. Haxby—918(A)
Photoproduction of neutral pions at high energies, D. C. Oakley, R. L. Walker, J. G. Teasdale, and J. I. Vette—949(A)
Photoproduction of π^0 mesons from H and C, G. Janes and William L. Kraushaar—900(L)
p-p elastic scattering and pion production at 419 Mev, J. Marshall, L. Marshall, and V. A. Nedzel—927(A)
Production of charged pions at 180° to beam by 340-Mev protons on C, Stanley L. Leonard—1380

Mesons (Continued)
Production of heavy unstable particles by negative pions, W. B. Fowler, R. P. Shutt, A. M. Thorndike, and W. L. Whittemore—861
Production of positive mesons in heavy nuclei, S. Gasiorowicz—843
Pure negative muon beam, Lester Winsberg—915(A)
Relative low-energy pion production cross sections by photons on hydrogen, Ryokichi Sagane and Walter F. Dudziak—948(A)
Search for production of μ-meson pairs by 340-Mev bremsstrahlung, A. Wattenberg, B. T. Feld, A. Julian, A. Odian, and L. S. Osborne—915(A)
Some possible relationships between π-meson nucleon scattering and π-meson production in nucleon-nucleon collisions, A. Aitken, H. Mahmoud, E. M. Henley, M. A. Ruderman, and K. M. Watson—1349
"V dinucleons," H. Primakoff and W. Cheston—908(L)
V_0^1 particle as high angular state of meson-nucleon system, B. P. Nigam—914(A)
Metals (see **Crystalline State**)
Metastable Atoms (see **Atomic Structure and Spectra**)
Metastable Molecules (see **Molecular Structure and Spectra**)
Meteorology (see **Geophysics**)
Methods and Instruments
Acceleration of N^{14} $(+6)$ ions in 60-inch cyclotron, G. Bernard Rossi, William B. Jones, Jack M. Hollander, and Joseph G. Hamilton—256
Achromatic translation system for high-energy beams, Wolfgang K. H. Panofsky—949(A)
α-particle pulse heights from organic scintillators, D. G. Proctor and T. A. Romanowski—360(A)
Atomic spectra in infrared and electrodeless discharge source, F. P. Dickey, R. V. Zumstein, and Dudley Williams—360(A)
Characteristics of gridded parallel-plate ionization chambers, L. O. Herwig, G. H. Miller, and N. G. Utterback—926(A)
Effects of alloying actions of dual-layer bi-metal electrodes on frequencies of piezoelectric quartz resonators, Richard B. Belser and Walter H. Hicklin—937(A)
Evapor-ion pump, Ajay S. Divatia, Robert H. Davis, and R. G. Herb—926(A)
Fast jet actuated shock tubes, F. J. Willig—946(A)
500-Mev pair spectrometer, Duane H. Cooper, David C. Oakley, and Robert L. Walker—950(A)
Fluorescence photometer, F. J. Lynch—926(A)
High-intensity short-duration light source, Frank N. Miller—945(A)
Improved chronotron for time-of-flight measurements, Howard Ogushwitz and Stephen S. Friedland—363(A)
Improved optical absorption technique for study of metastable atoms, A. V. Phelps and J. L. Pack—652(A)
Improved radiotracer technique for study of gaseous adsorption on metals, John A. Dillon, Jr., and H. E. Farnsworth—364(A)
Ion source for doubly-charged He, C. E. Bradford, T. Kikuchi, and W. E. Bennett—921(A)
Kinetics of circulating-fuel nuclear reactor, William Krasny Ergen—920(A)
Loading of nuclear emulsions with Li gloss specks, J. H. Roberts, J. Haugsnes, and D. E. Wood—920(A)
"Magnetic scanning" method for investigating hfs and isotope shift, S. Mrozowski—641(L)
Methane proportional counter method for C^{14} age determinations, W. H. Burke, Jr., and W. G. Meinschein—915(A)
Method for measuring Auger transitions, Charles E. Roos—401
Method of eliminating cathode activation effects in G-M counter, H. R. Crane—921(A)
Monitor for high-energy electron or γ-ray beams, A. V. Tollestrup and W. A. Wentzel—950(A)
Monitor for high-energy photons, C. A. McDonald, Jr., R. W. Kenney, and R. F. Post—951(A)
NaI counting response for γ rays, W. E. Kreger and L. McIsaac—943(A)
New vacuum near-infrared spectrometer, T. J. Coburn, H. H. Nielson, and Dudley Williams—360(A)
Operational data for magnetic refrigerator for maintaining temperatures below 1°K, C. V. Heer, C. B. Barnes, and J. G. Daunt—360(A)
Photon monochromator for bremsstrahlung radiation, J. Goldemberg—1426(L)
Photosensitive cell response to sinusoidally varying light flux, R. L. Conger and L. E. Schilberg—943(A)
Proportional counter "escape" peak resolution and fine structure, S. Fine—653(A)
Proposed double-mode cyclotron, M. J. Jakobson and F. H. Schmidt—303
Quantitative measurement of magnetic absorption utilizing null-balance system, R. H. Elsken and T. M. Shaw—943(A)
Radioactive isotope separation by nuclear recoil, H. Morinaga and D. J. Zaffarano—1422(L)
Response currents in coupled circuits by Laplace transformation and mechanical harmonic synthesizer, Chu Jui Lee and S. LeRoy Brown—945(A)
Scintillation detector for Brookhaven fast chopper, H. Palevsky, H. R. Muether, and A. Stolovy—920(A)
Shock-wave valve, Richard I. Condit—945(A)
Slotted resonant cavity for dielectric measurements, J. J. Windle and T. M. Shaw—952(A)
Space-charge forces in strong-focusing synchrotrons, S. E. Barden—1378
Temperature measurement below 1°K, D. H. Howling, F. J. Darnell, and E. Mendoza—1416(L)
Thin lens β-ray spectrometer, G. R. Grove and L. N. Russell—360(A)
Time-of-flight mass spectrometer, Henry S. Katzenstein and Stephen S. Friedland—363(A)
Uniformity of pulse heights from large-area photomultiplier, A. M. Hudson and F. K. Roser—941(A)
Use of pinhole for producing glow to arc transitions, B. Pearson DeLany and Paul L. Copeland—926(A)
X-ray absorption processes in proportional counter gases, C. S. Duffendack and C. F. Hendee—653(A)
X-ray microscope mirror systems, A. V. Baez and M. Weissbluth—942(A)
Microwaves (see also **Atomic Structure and Spectra; Magnetic Resonance; Molecular Structure and Spectra; Nuclear Moments and Spin**)
Absolute intensity of water vapor absorption at microwave frequencies, T. F. Rogers—248(L)
Microwave resonance absorption in Ni ferrite-aluminate, Thomas R. McGuire—682
Slotted resonant cavity for dielectric measurements, J. J. Windle and T. M. Shaw—952(A)
Zeeman effect and line breadth studies of microwave lines of O_2, Robert M. Hill and Walter Gordy—1019
Miscellaneous
European and American productivity in basic science, J. B. Blizard—364(A)
Mobility of Ions and Electrons (see **Ions and Electrons, Mobility**)
Molecular Aggregates
Color centers in alkali silicate glasses, Ryosuke Yokota—896(L)

Neutron diffraction in vitreous silica, R. J. Breen and A. H. Weber—923(A)
Rittenger's number for glass and decomposed granite, M. E. Backman and H. L. Morrison—953(A)
Structure of vitreous silica, Joseph S. Lukesh—264
Molecular Beams (see **Atomic and Molecular Beams**)
Molecular Structure and Spectra
Absolute intensity of water vapor absorption at microwave frequencies, T. F. Rogers—248(L)
Band fluorescence of Hg vapor, A. O. McCoubrey—1249
DBr spectrum in one-mm wave region, Walter Gordy and Charles A. Burrus—419
Dissociative recombinations in N_2, A. C. Faire, O. T. Fundingsland, and A. L. Aden—650(A)
Doppler broadening of dissociative recombination lines, Manfred A. Biondi—650(A)
Infrared emission spectrum of CO in 2.4 μ region, F. W. Dalby, F. P. Dickey, and Dudley Williams—360(A)
Line width of rotational spectra of some symmetric top molecules due to nuclear quadrupole moments, Takashi Ito, Yukito Tanabe, and Masataka Mizushima—1242
Mass spectrometry of low vapor-pressure molecules, George H. Lane, Henry S. Katzenstein, and Stephen S. Friedland—363(A)
Microwave spectrum of $N^{14}O^{16}$, J. J. Gallagher, F. D. Bedard, and C. M. Johnson—729
Microwave spectrum of O_3, Masataka Mizushima and Robert M. Hill—745
Microwave spectrum of O_3, Peter N. Wolfe and Dudley Williams—360(A)
Nuclear quadrupole coupling in polar molecules, H. M. Foley, R. M. Sternheimer and D. Tycko—734
Nuclear spins and band spectra of Se isotopes, Sumner P. Davis—159
1–2 mm wave spectroscopy, IV. OCS, CH_3F, and H_2O, William C. King and Walter Gordy—407
Pressure broadening in near infrared, Henry H. Blau, Jr., John H. Shaw, and Dudley Williams—360(A)
Pure rotational spectra of alkali halides, A. Honig, M. Mandel, M. L. Stitch, and C. H. Townes—953(A)
Raman and infrared spectra of $C^{13}H_3I$, Forrest F. Cleveland, Richard B. Bernstein, and Fred L. Voelz—933(A)
Raman and infrared spectra of dimethyltriacetylene, Alfons Weber, Forrest F. Cleveland, and Salvador M. Ferigle —933(A)
Rotational excitation of homonuclear molecules, S. Stein, E. Gerjuoy, and T. Holstein—934(A)
S^{33} nuclear magnetic moment by microwave spectroscopy, Bernard F. Burke, M. W. P. Strandberg, Victor W. Cohen, and Walter S. Koski—193
Sub-millimeter wave spectroscopy, Charles A. Burrus and Walter Gordy—897(L)
Time-resolved spectroscopy of N_2 and H_2, C. F. Hendee and W. B. Brown—651(A)
Total emission of HCl and CO in region of their fundamentals, Robert D. Smith and Dudley Williams—360(A)
Variation of *l*-type doubling constant in HCN, J. F. Westerkamp—716
Zeeman effect and line breadth studies of microwave lines of O_2, Robert M. Hill and Walter Gordy—1019
Moments, Nuclear (see **Nuclear Moments and Spin**)
Moments of Molecules (see **Molecular Structure and Spectra**)

Neutrino (see also **Nuclear Spectra; Radioactivity**)
Neutron Diffraction (see **Diffraction; Scattering of Neutrons**)
Neutrons (see **Elementary Particle Interactions**)
Noise
Rf noise from low-current, atmospheric-pressure arc discharges in air, M. I. Skolnik—648(A)
Nuclear Fission
Distribution of prompt neutron emission probability for fission fragments of U^{235}, J. S. Fraser and J. C. D. Milton—818
Ionization yields for fission fragments, Glenn H. Miller and Lloyd O. Herwig—932(A)
Photofission produced by 335-Mev bremsstrahlung, J. Jungerman and H. Steiner—949(A)
Nuclear Forces (see **Elementary Particle Interactions; Field Theory; Nuclear Structure Theory**)
Nuclear Induction (see **Magnetic Resonance; Nuclear Moments and Spin**)
Nuclear Isomers (see **Nuclear Spectra; Radioactivity**)
Nuclear Moments and Spin
Anisotropic relaxation of quadrupole spin echoes, E. L. Hahn and B. Herzog—639(L)
Experiment for measurement of magnetic moment of neutron, Victor W. Cohen, Noel R. Corngold, and Norman F. Ramsey—941(A)
Hfs in spectra of Sb, Sm, Hg, and Cd, Kiyoshi Murakawa —1232
Hg^{201} nuclear quadrupole resonance, H. G. Dehmelt, H. G. Robinson, and Walter Gordy—480; 920(A)
K^{41}, Y^{89}, Ag^{107}, and Ag^{109} magnetic moments, E. Brun, J. Oeser, H. H. Staub, and C. G. Telschow—172
Magnetic moments of Ag^{107} and Ag^{109} and hfs anomaly, P. B. Sogo and C. D. Jeffries—174
Mo^{95} and Mo^{97} nuclear spins, Ervin C. Woodward, Jr.— 954(A)
Nuclear alignment at low temperatures, N. R. Steenberg —678
Nuclear quadrupole coupling in polar molecules, H. M. Foley, R. M. Sternheimer, and D. Tycko—734
Nuclear quadrupole transition in single crystal of $NaClO_3$, Edward Manring, Yu Ting, and Dudley Williams— 360(A)
p- and *d*-shell nuclei in intermediate coupling, G. E. Tauber and Ta-You Wu—295
Pb^{204} magnetic moment of first excited state, H. Frauenfelder, J. S. Lawson, Jr., and W. Jentschke—1126(L)
S^{33} nuclear magnetic moment by microwave spectroscopy, Bernard F. Burke, M. W. P. Strandberg, Victor W. Cohen, and Walter S. Koski—193
Se isotopes, nuclear spins and band spectra, Sumner P. Davis—159
Si^{29} nuclear spin, G. A. Williams, D. W. McCall, and H. S. Gutowsky—1428(L)
Tendency for positive nuclear quadrupole moments, S. A. Moszkowski and C. H. Townes—306
Transient nuclear induction signals associated with pure quadrupole interactions, M. Bloom and R. E. Norberg —638(L)
Xe^{129} and Xe^{131} magnetic moments, E. Brun, J. Oeser, H. H. Staub, and C. G. Telschow—904(L)
Nuclear Photoeffects
Absolute photon attenuation cross section for non-pair processes in Be at 300 Mev, Robert W. Kenney, John M. Dudley, and Charles A. McDonald, Jr.—951(A)
Energy of Sb-Be phononeutrons, Richard Culp and Bernard Hamermesh—1025
Energy spectra and angular distributions of photoneutrons from heavy nuclei, Glenn A. Price—1279
Harmonic mean energy of nuclear photoeffect, J. S. Levinger—932(A)
Photodisintegration of deuteron by 180-Mev and 260-Mev γ rays, J. Keck, R. M. Littauer, G. K. O'Neill, A. M. Perry, and W. M. Woodward—827

Nuclear Photoeffects (Continued)
Photofission produced by 335-Mev bremsstrahlung, J. Jungerman and H. Steiner—949(A)
Photomeson production near threshold and suppression of pairs in pseudoscalar meson theory, Norman M. Kroll and Malvin A. Ruderman—233
Photoproduction of low-energy charged π mesons, J. R. Voss, T. R. Palfrey, and R. O. Haxby—918(A)
Photoproduction of neutral pions at high energies, D. C. Oakley, R. L. Walker, J. G. Teasdale, and J. I. Vette —949(A)
Photoproduction of π^+ mesons from H and C, G. Sargent Janes and William L. Kraushaar—900(L)
Photospallation yields of N^{17}, Daryl Reagan—947(A)
Precision determination of photoneutron thresholds, Milton Birnbaum—146
Relative low-energy pion production cross sections by photons on hydrogen, Ryokichi Sagane and Walter F. Dudziak—948(A)
Resonances in $Li^7(\gamma,p)He^6$ cross section and high-energy limit of bremsstrahlung spectra, B. L. Tucker and E. C. Gregg—360(A)
Search for production of μ-meson pairs by 340-Mev bremsstrahlung, A. Wattenberg, B. T. Feld, A. Julian, A. Odian, and L. S. Osborne—915(A)
Systematics of photoneutron reactions, R. Nathans and J. Halpern—437

Nuclear Reactions, General (see also **Elementary Particle Interactions; Scattering**)
Cosmic-ray nuclear interactions in gases, W. W. Brown —518
Electric excitation of low-lying levels in separated W isotopes, C. L. McClelland, Hans Mark, and Clark Goodman—904(L)
Electrodisintegration of Cu^{63}, Zn^{64}, Ag^{109}, and Ta^{181}, Karl L. Brown and Richard Wilson—443
Interpretation of experiments on nuclear temperatures, David Breed Beard—950(A)
Meson production in high-energy nucleon-nucleon collisions, William L. Kraushaar and Lawrence J. Marks—326
Multiple production of pions in nucleon-nucleon collisions at cosmotron energies, E. Fermi—1434(E)
Neutral-to-charge ratio in high-energy interactions, M. F. Kaplon, W. D. Walker, and M. Koshiba—1424(L)
Nuclear Coulomb excitation by heavy particles, David L. Hill—923(A)
Nuclear cross sections at low energies, J. L. Johnson and H. M. Jones—1286
Nuclear interaction of high-energy nucleons, H. McManus, W. T. Sharp, and H. Gellman—924(A)
Nucleon-nucleus collisions at relativistic energies, Giuseppe Cocconi—1124
Production of polarized particles in nuclear reactions, A. Simon and T. A. Welton—1435(E)
Reactions of U^{238} with cyclotron-produced nitrogen ions, Albert Ghiorso, G. Bernard Rossi, Bernard G. Harvey, and Stanley G. Thompson—257(L)
Theory of polarized particles and γ rays in nuclear reactions, Albert Simon—1435(E)

Nuclear Reactions Induced by α Particles and He^3 (see also **Scattering of α Particles**)
$Be^9(\alpha,n)C^{12*}$ reaction, D. E. Diller and M. F. Crouch—360(A)
Coulomb excitation of heavy and medium heavy nuclei by α particles, G. M. Temmer and N. P. Heydenburg—351(L); II, N. P. Heydenburg and G. M. Temmer—906(L)
Double star connected by heavy meson, S. Rosendorff, R. Stahl and G. Yekutieli—901(L)
Energy spectrum of neutrons from Po-Be, J. O. Elliot, W. I. McGarry, and W. R. Faust—1348
Low-energy yield of (α,n) reactions, W. E. Bennett, P. A. Roys, and B. J. Toppel—924(A)

Nuclear Reactions Induced by Deuterons and Tritons (see also **Scattering of Deuterons**)
Angular distribution of protons from $B^{10}(d,p)B^{11}$, William W. Pratt—816
Angular distribution of protons from $Na^{23}(d,p)Na^{24}$, Philip Shapiro—290
Angular distribution of protons from $Zn^{66}(d,p)Zn^{67}$, F. S. Eby, R. D. Hill, and W. K. Jentschke—925(A)
Angular distributions and excitation curves for $B^{10}(d,p)B^{11}$ and $B^{10}(d,n)$ reactions below 2-Mev bombarding energy, W. H. Burke, J. R. Risser, and G. C. Phillips—188
Coulomb corrections in stripping, S. T. Butler and N. Austern—355(L)
Cross sections for reactions $D(d,p)T$, $D(d,n)He^3$, $T(d,n)He^4$ and $He^3(d,p)He^4$ below 120 kev, W. R. Arnold, J. A. Phillips, G. A. Sawyer, E. J. Stovall, Jr., and J. L. Tuck—483
γ radiation from $C^{12}+D^2$, R. J. Mackin, Jr., W. B. Mims, and W. R. Mills—950(A)
γ radiation from certain nuclear reactions, Rolf M. Sinclair —1082
γ radiation from excited state of Li^6, N. M. Hintz, J. M. Blair, and D. M. Van Patter—924(A)
Interaction between D^2 and He^3 in neighborhood of 18.6-Mev level of Li^{5*}, G. Freier and H. Holmgren—825
$Li^7(d,t)Li^6$, R. L. Macklin and H. E. Banta—924(A)
Lifetime measurements for first excited states of O^{17} and B^{10} from recoil studies, Jacques Thirion and Valentine L. Telegdi—950(A)
Nuclear cross sections at low energies, J. L. Johnson and H. M. Jones—1286
Pb, new isomer, D. Maeder and A. H. Wapstra—1433(L)
Theory of deuteron stripping reactions, N. C. Francis and K. M. Watson—313

Nuclear Reactions Induced by Mesons (see also **Elementary Particle Interactions; Mesons; Scattering of Mesons**)
Angular correlation of mesons produced in inelastic meson-nucleon collisions, J. S. Kovacs—252(L)
High-energy protons in nuclear interaction of 220-Mev π^- mesons in nuclear emulsions, Gyo Takeda—848
Inelastic scattering of 220-Mev π^- mesons in emulsions, W. F. Fry—845
Interaction of μ^- mesons with I^{127}, Lester Winsberg—937(A)
Interaction of pions with complex nuclei, Donald Harvey Stork—868
Interactions of 500-Mev negative pions with emulsion nuclei, M. Caulton, M. Blau, and J. E. Smith—919(A)
Internal conversion of mesic γ rays, C. P. Sargent, M. C. Rinehart, R. C. Cornelius, L. M. Lederman, and K. Rogers—917(A)
Production of heavy unstable particles by negative pions, W. B. Fowler, R. P. Shutt, A. M. Thorndike, and W. L. Whittemore—861
Total cross section for positive pions in hydrogen, Stanley L. Leonard and Donald H. Stork—568; 1435(E)
Total cross section of pions at 1.5 Bev, R. L. Cool, L. Madansky, and O. Piccioni—249(L)
Total cross sections of 135-Mev to 250-Mev negative pions in H, J. Ashkin, J. P. Blaser, F. Feiner, J. Gorman, and M. O. Stern—1129(L)
Total interaction cross section of H for positive and negative 200-700 Mev pions, Luke C. L. Yuan and S. J. Lindenbaum—917(A)

Total interaction cross section of negative pions at kinetic energies of 1.0 and 1.45 Bev, R. L. Cool, L. Madansky, and O. Piccioni—918(A)
Total interaction cross section of pions with protons and deuterons at 1.0 Bev, R. L. Cool, L. Madansky, and O. Piccioni—637(L)

Nuclear Reactions Induced by Neutrons (see also **Elementary Particle Interactions; Scattering of Neutrons**)

Angular distribution of $Li^6(n,\alpha)H^3$ for fast neutrons, James B. Weddell and James H. Roberts—924(A)
Charged particles from interaction of 14-Mev neutrons with Li^6 and Li^7, Glenn M. Frye, Jr.—1086
Cross sections for production of In^{115m} and Au^{197m} by inelastic scattering of neutrons, H. C. Martin, B. C. Diven, and R. F. Taschek—199
Determination of scattering resonance parameters from total cross section, W. Y. Kato, D. J. Hughes, and J. S. Levin—931(A)
Dipole and quadrupole transition probabilities in neutron-capture γ radiation, B. B. Kinsey and G. A. Bartholomew—1260
Doppler effect in slow neutron resonance of Rh, H. H. Landon—931(A)
Energy of Sb-Be photoneutrons, Richard Culp and Bernard Hamermesh—1025
Fraction of $n+p \rightarrow \pi^0$ events in which deuteron is formed, Roger H. Hildebrand—918(A)
Further production of transcurium nuclides by neutron irradiation, Bernard G. Harvey, Stanley G. Thompson, Albert Ghiorso, and Gregory R. Choppin—1129(L)
γ rays excited by inelastic scattering of neutrons in Pb, Bi, Fe, Ni, and Cr, M. A. Rothman and C. E. Mandeville—796
Inelastic scattering of neutrons by In^{115} and Au^{197}, A. A. Ebel and Clark Goodman—197
Inelastic scattering of neutrons near thresholds, B. Margolis—204
Inelastic scattering of protons and neutrons by deuterons, R. M. Frank and J. L. Gammel—463
Lowest neutron scattering resonance in Co, F. G. P. Seidl—931(A)
Neutron-capture γ rays from Sc, V, Mn, Co, and Cu, G. A. Bartholomew and B. B. Kinsey—1434(E)
Neutron inelastic scattering, Robert M. Kiehn and Clark Goodman—177
Neutron total cross section for Bi and U between 45 and 130 Mev, W. I. Linlor and B. Ragent—951(A)
Nuclear interactions of high-energy nucleons, H. McManus, W. T. Sharp, and H. Gellman—924(A)
$O^{16}(n,p)N^{16}$ cross sections from 12 to 18 Mev, H. C. Martin—498
Pu^{244} from pile-irradiated Pu, M. H. Studier, P. R. Fields, P. H. Sellers, A. M. Friedman, C. M. Stevens, J. F. Mech, H. Diamond, J. Sedlet, and J. R. Huizenga—1433(L)
Pulse-height measurements of recoils from $B^{10}(n,\alpha)Li^7$, James A. De Juren and Hyman Rosenwasser—831
Radioactive Si^{31}, W. S. Lyon and J. J. Manning—501
Slow neutron capture γ rays from Ti, Henry T. Motz—925(A)
Slow neutron resonances in Cs, Pd, and Au, H. H. Landon and V. L. Sailor—1030
Slow neutron resonances in Eu, V. L. Sailor, H. H. Landon, and H. L. Foote, Jr.—1292
Thermal neutron resonance of Sm, A. W. McReynolds and E. Andersen—195
Total cross sections of rare earths for fast neutrons, A. Okazaki, S. E. Darden, and R. B. Walton—461
Total neutron cross sections for C, Fe, Sb, and Ta from 35 to 180 Mev, B. Ragent and W. I. Linlor—951(A)
Transcurium isotopes produced in neutron irradiation of Pu, S. G. Thompson, A. Ghiorso, B. G. Harvey, and G. R. Choppin—908(L)

Nuclear Reactions Induced by Protons (see also **Elementary Particle Interactions; Scattering of Protons**)

Angular distribution of α particles from $Na^{23}(p,\alpha)Ne^{20}$, P. H. Stelson—925(A)
Artificially-produced negative heavy meson, J. Hornbostel and E. O. Salant—902(L)
Cross sections for formation of Na^{22} from Al and Mg bombarded with protons, R. E. Batzel and G. H. Coleman—280
Cross sections for p-p scattering at 330 and 225 Mev, O. Chamberlain, G. Pettengill, E. Segrè, and C. Wiegand—1424(L)
Dependence of relative low-energy π^+ production cross section on atomic and neutron numbers, Walter F. Dudziak and Ryokicki Sagane—948(A)
Emulsion studies of cosmic-ray stars produced in metal foils, Ian G. Barbour—535
Energy spectrum of negative pions produced in Be by 2.3-Bev protons, S. J. Lindenbaum and Luke C. L. Yuan—917(A); Luke C. L. Yuan and S. J. Lindenbaum—1431(L)
Excitation functions of proton-induced reactions of Nb^{93}, Ralph A. James—288
γ radiation from proton bombardment of Li^7, Alfred A. Kraus, Jr.—1308
γ rays from inelastic scattering of protons by Ne, Mason C. Cox, Jan J. van Loef, and D. A. Lind—925(A)
γ rays from proton bombardment of Na, J. W. Teener, L. W. Seagondollar, and R. W. Krone—1035
Inelastic scattering of protons and neutrons by deuterons, R. M. Frank and J. L. Gammel—463
Inelastic scattering of protons by F^{19}, R. W. Peterson, C. A. Barnes, W. A. Fowler, and C. C. Lauritsen—951(A)
Inelastic scattering of protons by Li^7, F. Mozer, W. A. Fowler, and C. C. Lauritsen—829
Inelastic scattering of 31-Mev protons from heavy elements, R. M. Eisberg and G. Igo—1039
Kr neutron-deficient isotope, Albert A. Caretto, Jr., and Edwin O. Wiig—175
Level densities of nuclei from inelastic scattering of 18-Mev protons, P. C. Gugelot—425
Low-energy γ radiation from bombardment of C by protons, H. H. Woodbury, A. V. Tollestrup, and R. B. Day—1123
Neutron binding energy in Bi^{210}, C. G. Andre and J. R. Huizenga—931(A)
Neutrons from proton bombardment of N^{14}, F. Ajzenberg, W. Franzen, and J. G. Likely—925(A)
Nuclear cross sections at low energies, J. L. Johnson and H. M. Jones—1286
Nuclear interactions of high-energy nucleons, H. McManus, W. T. Sharp, and H. Gellman—924(A)
p-p elastic scattering and pion production at 419 Mev, J. Marshall, L. Marshall, and V. A. Nedzel—927(A)
Production of charged pions at 180° to beam by 340-Mev protons on C, Stanley L. Leonard—1380
Production of positive mesons in heavy nuclei, S. Gasiorowicz—843
Proton-induced reactions in Bi, C. G. Andre, W. J. Ramler, E. G. Rauh, R. J. Thorn, and J. R. Huizenga—925(A)
(p,t) reactions, B. L. Cohen and T. H. Handley—514

Nuclear Reactions Induced by Protons (Continued)
Resonance capture of protons by Mg^{25}, Warren E. Taylor, Leonard N. Russell, and John N. Cooper—1056
Yields near threshold for (p,n) reactions in intermediate nuclei, C. H. Johnson and C. C. Trail—924(A)
Nuclear Scattering (see **Scattering**)
Nuclear Spectra (see also **Nuclear Isomers; Nuclear Reactions; Radioactivity**)
Angular correlation of cascade γ rays from decay of $_{84}Po^{214}$, F. Demichelis and R. Malvano—526
Angular correlations of γ rays in Ta^{181}, F. K. McGowan—471
Ba^{140} 10-yr disintegration, R. W. Hayward, D. D. Hoppes, and H. Ernst—916(A)
Cd^{117} and In^{117} γ spectra, J. M. LeBlanc, J. M. Cork, and S. B. Burson—916(A)
Cl^{39} decay, W. E. Meyerhof and G. Lindstrom—949(A)
Co^{60} disintegration, R. S. Caird and Allan C. G. Mitchell—916(A)
Coulomb excitation of heavy and medium heavy nuclei by α particles, G. M. Temmer and N. P. Heydenburg—351(L)
Cu^{60} decay and nuclear levels in Ni^{60}, R. van Lieshout, R. H. Nussbaum, G. J. Nijgh, and A. H. Wapstra—255(L)
Decay properties of Am^{242} and possible rotational bands in α spectra of odd-even nuclei, Frank Asaro and I. Perlman—1423(L)
Dipole and quadrupole transition probabilities in neutron-capture γ radiation, B. B. Kinsey and G. A. Bartholomew—1260
Electric excitation of low-lying levels in separated W isotopes, C. L. McClelland, Hans Mark, and Clark Goodman—904(L)
Electron capture in decay of Na^{22}, R. Sherr and R. H. Miller—1076
End-point energy determination of β emitters, M. Forro—915(A)
Energies of excited states of nuclei, G. E. Tauber and Ta-You Wu—434
Ga^{65} isomeric state, Bernard Crasemann—1034
γ radiation from $C^{13} + D^2$, R. J. Mackin, Jr., W. B. Mims, and W. R. Mills—950(A)
γ radiation from certain nuclear reactions, Rolf M. Sinclair—1082
γ radiation from proton bombardment of Li^7, Alfred A. Kraus, Jr.—1308
γ rays excited by inelastic scattering of neutrons in Pb, Bi, Fe, Ni, and Cr, M. A. Rothman and C. E. Mandeville—796
γ rays from proton bombardment of Na, J. W. Teener, L. W. Seagondollar, and R. W. Krone—1035
Ho^{166} decay, A. W. Sunyar—1345
Influence of extranuclear fields on angular correlations, F. Coester—1304
Inner bremsstrahlung from P^{32}, Max Goodrich and Wilbur B. Payne—916(A)
Internal bremsstrahlung and ionization accompanying β decay, F. Boehm and C. S. Wu—518
Internal Compton effect in Ba^{137}, Larry Spruch and G. Goertzel—642(L)
Internal conversion coefficients of Nb^{95}, Zn^{65}, and Sc^{46}, E. F. Sturcken, Z. O'Friel, and A. H. Weber—1053
Irregularities in nuclear level spacings of Hg, Au, and Pt, J. W. Mihelich and A. de-Shalit—135
Isotopic spin and odd-odd $N = Z$ nuclei, S. A. Moszkowski and D. C. Peaslee—941(A)
K-conversion electron-γ angular correlation measurements in Te^{121} and Te^{123}, Norman Goldberg and Sherman Frankel—1425(L)
K-shell internal conversion coefficients using coincidence scintillation spectrometer, F. K. McGowan—163
Lifetime measurements for first excited states of O^{17} and B^{10} from recoil studies, Jacques Thirion and Valentine L. Telegdi—950(A)
Lu^{176} and Hf^{176} energy levels, James R. Arnold—743
Mg^{28} β-ray spectrum, J. L. Olsen and G. D. O'Kelley—1125(L)
Mixed γ-mixed γ angular correlation, M. E. Rose—477
N^{14} energy levels from scattering of protons by C^{13}, Edmund A. Milne—762
Ne^{20} γ rays, B. P. Foster, G. S. Stanford, and L. L. Lee, Jr.—1069
Neutron-capture γ rays from Sc, V, Mn, Co, and Cu, G. A. Bartholomew and B. B. Kinsey—1434(E)
New radioactive nuclides of rare earths, Thomas H. Handley and Elmer L. Olson—524
Np^{238} β decay, Hilding Slatis, John O. Rasmussen, Jr., and Hugo Atterling—646(L)
Nuclear matrix elements in β decay, M. E. Rose and R. K. Osborn—1326
Nuclear spectroscopy of neutron-deficient Hg isotopes, L. P. Gillon, K. Gopalakrishnan, A. de-Shalit, and J. W. Mihelich—124
Pb, new isomer, D. Maeder and A. H. Wapstra—1433(L)
Pb^{208} spins and parities of energy levels, L. G. Elliott, R. L. Graham, J. Walker, and J. L. Wolfson—356(L)
Positron-capture branching ratios, Paul F. Zweifel—915(A)
Radiations of 13.9-min Ce^{146} and 24.4-min Pr^{146}, W. Bernstein, S. S. Markowitz, and S. Katcoff—1073
Resonant scattering of recoil-broadened γ rays, K. Ilakovac and P. B. Moon—254(L)
Sb^{125} radiation, J. M. Cork, M. K. Brice, G. D. Hickman, and L. C. Schmid—1059
Sb^{124} triple γ-ray cascade, L. M. Langer and J. W. Starner—245(L)
Sc^{40}, Cl^{38}, P^{38}, and Al^{28} radiations, Neel W. Glass and J. Reginald Richardson—942(A)
Se^{75} and Ge^{75} decay scheme, A. W. Schardt and Joan P. Welker—916(A)
Search for $p_{1/2}$ isomeric state in Tc^{101} and identification of energy levels, Donald R. Wiles—181
Second-forbidden β spectra of Co^{60} and Sc^{46}, G. L. Keister and F. H. Schmidt—140
Si^{31}, W. S. Lyon and J. J. Manning—501
Slow neutron capture γ rays from Ti, Henry T. Motz—925(A)
Sm^{153} and Eu^{155} radioactivity, Milford R. Lee and Robert Katz—155
Symmetry properties of Wigner $9j$ symbol, H. A. Jahn and J. Hope—318
Theory of polarized particles and γ rays in nuclear reactions, Albert Simon—1435(E)
Ti^{44}, new Ti nuclide, R. A. Sharp and R. M. Diamond—358(L)
Transmission of 0–50 kev electrons by thin films with applications to β spectra, R. O. Lane and D. J. Zaffarano—916(A)
V^{52} decay, J. M. LeBlanc, J. M. Cork, S. B. Burson, and W. C. Jordan—1124(L)
W^{182} short-lived metastable states, A. W. Sunyar—1122(L)
Nuclear Structure Theory (see also **Nuclear Reactions; Nuclear Spectra**)
Binding energy calculation on He^4 with single-particle wave functions, P. G. Wakely—1434(E)

Classical theory of heavy nuclei, I, E. Teller and M. H. Johnson—947(A); II, M. H. Johnson and E. Teller—947(A)
Energies of excited states of nuclei, G. E. Tauber and Ta-You Wu—434
Harmonic mean energy of nuclear photoeffect, J. S. Levinger—932(A)
Interpretation of electron scattering experiments, L. I. Schiff—1434(E)
Interpretation of experiments on nuclear temperatures, David Breed Beard—950(A)
Irregularities in nuclear level spacings of Hg, Au, and Pt, J. W. Mihelich and A. de-Shalit—135
Isotopic spin and odd-odd $N = Z$ nuclei, S. A. Moszkowski and D. C. Peaslee—941(A)
Matrix elements of spin-orbit interaction in d^n configuration, Seiichi Sueoka—302
Mixture of central, tensor, and two-particle spin-orbit interactions for N^{14} and D^2, W. J. Robinson—1296
Nuclear energy surface and isotopic mass values, J. R. Stehn—932(A)
Nuclear matrix elements in β decay, M. E. Rose and R. K. Osborn—1326
Odd-nucleon-plus-liquid-drop model of heavy odd nuclei, F. J. Milford—1297
p- and d-shell nuclei in intermediate coupling, G. E. Tauber and Ta-You Wu—295
Production of positive mesons in heavy nuclei, S. Gasiorowicz—843
Proton distribution in heavy nuclei, M. H. Johnson and E. Teller—357(L)
Pseudoscalar interaction in β decay, M. E. Rose and R. K. Osborn—1315
Theory of nuclear level density, Claude Bloch—1094

Optical Instruments (see **Methods and Instruments**)
Optical Properties (see also **Luminescence**)
Anomalous optical absorption limit in InSb, Elias Burstein—632(L)
Color centers in alkali silicate glasses, Ryosuke Yokota—896(L)
Coloring and bleaching of alkali halide crystals containing U centers, R. S. Alger—953(A)
Effect of pressure on F-center absorption in alkali halides, I. S. Jacobs—993
F-center wave functions in alkali halides, D. L. Dexter—244(L)
Infrared absorption of NiO, R. W. Johnston and D. C. Cronemeyer—634(L)
Infrared absorption, photoconductivity, and impurity states in Ge, W. Kaiser and H. Y. Fan—911(A); 977
Infrared lattice absorption bands in Ge, Si, and diamond, R. J. Collins and H. Y. Fan—674
Infrared optical properties of single crystals of Te, Joseph J. Loferski—707
Infrared photoconductivity due to neutral impurities in Ge, E. Burstein, J. W. Davisson, E. E. Bell, W. J. Turner, and H. G. Lipson—65
Iodide impurity absorption in KBr and NaBr, C. J. Delbecq, J. E. Robinson, and P. H. Yuster—262
NiO electrical properties, F. J. Morin—1199
Optical properties of some group III—group V compounds, H. B. Briggs, R. F. Cummings, H. J. Hrostowski, and M. Tanenbaum—912(A)
Reflectivity of Ag in near infrared, L. G. Schulz—922(A)
Spectroscopy of solid state; some of transition elements, E. M. Gyorgy and G. G. Harvey—365
Theoretical calculations of F-center energy levels, J. A. Krumhansl—245(L)
X-ray coloration of alkali halides, D. L. Dexter—985
X-ray coloring of 400-Mev proton-irradiated KCl, W. Leivo and R. Smoluchowski—1415(L)
X-ray-induced photostimulated conductivity in MgO, Albert S. Eisenstein—1017

Pair Production (see **Electrons and Positrons**)
Phosphors and Phosphorescence (see **Luminescence**)
Photoconductivity (see **Electrical Conductivity and Resistance**)
Photodisintegration (see **Nuclear Photoeffects**)
Photoelasticity (see **Elasticity and Plasticity**)
Photoelectric Effect (see **Electrical Properties**)
Photography and Photographic Emulsions (see **Methods and Instruments**)
Photometry (see **Methods and Instruments**)
Photons (see **Radiation**)
Photovoltaic Effect (see **Electrical Properties**)
Piezoelectric Effect (see **Dielectrics and Dielectric Properties**)
Plasticity (see **Elasticity and Plasticity**)
Polarization, Electrical (see **Dielectrics and Dielectric Properties**)
Polymers (see **Molecular Aggregates**)
Positrons (see **Electrons and Positrons**)
Probability (see **Mathematical Methods**)
Proceedings of the American Physical Society
Autumn Meeting of the New York State Section at Poughkeepsie, October 16 and 17, 1953—359
Sixth Annual Conference on Gaseous Electronics held at Washington, D. C., October 22-24, 1953—647
Autumn Meeting of the Ohio Section at General Electric Light Institute, Nela Park, Cleveland, Ohio, October 23 and 24, 1953—359
Autumn Meeting of the New England Section at Storrs, Connecticut, November 7, 1953—363
Thanksgiving Meeting at Chicago, Illinois, November 27 and 28, 1953 [Bull. Am. Phys. Soc. 28, No. 6 (1953)]—909
Winter Meeting in the West at Stanford University, Stanford, California, December 28, 29, and 30, 1953 [Bull. Am. Phys. Soc. 28, No. 7 (1953)]—939
Protons (see **Elementary Particle Interactions**)

Quantum Electrodynamics (see also **Field Theory**)
Bound state corrections in two-body systems, Thomas Fulton and Robert Karplus—1126
Elementary particles and Lamb-Retherford line shift, Leslie L. Foldy—880
Positron theory without "holes," F. J. Belinfante—935(A)
Radiative corrections in positronium, Thomas Fulton and Paul C. Martin—903(L)
Theory of bremsstrahlung and pair production. I. Differential cross section, H. A. Bethe and L. C. Maximon—768; II. Integral cross section for pair production, Handel Davies, H. A. Bethe, and L. C. Maximon—788
Theory of quantized fields. V, Julian Schwinger—615
Quantum Mechanics
Deriving Schrödinger's equation, Saul T. Epstein—364(A)
Discussion of analytic and Hartree-Fock wave functions for $1s^2$ configurations from H^- to C v, Louis C. Green, Marjorie M. Mulder, Margaret N. Lewis, and John W. Woll, Jr.—757
Generalized Fermi-Thomas theory, Malcolm K. Brachman—636(L)
Nonconservation of rest mass and Dirac equation, Lloyd Motz—901(L)
Operators and observables in isotopic spin space, Leslie L. Foldy—1395

Quantum Mechanics (Continued)
Stokes parameter technique for treatment of polarization in quantum mechanics, U. Fano—121
Quenching of Radiation (see **Radiation**)

Radar (see **Methods and Instruments; Radiation**)
Radiation
Absolute photon attenuation cross section for non-pair processes in Be at 300 Mev, Robert W. Kenney, John M. Dudley, and Charles A. McDonald, Jr.—951(A)
Absorption cross sections for photoionizing radiations in low-pressure gases, C. D. Maunsell—943(A)
Albedo of various materials for 1-Mev photons, Evans Hayward and John Hubbell—955
Angular distribution of Compton-scattered γ rays, W. H. Voelker—360(A)
Band fluorescence of Hg vapor, A. O. McCoubrey—1249
Čerenkov effect and dielectric constant, S. M. Neamtan—932(A)
Čerenkov radiation, Katsumi Tanaka—459
Coherence in spontaneous radiation processes, R. H. Dicke—99
Compton effect at 250 Mev, F. H. Coensgen—948(A)
Energy loss of fast charged particle by Čerenkov radiation, R. M. Sternheimer—1434(E)
High-intensity short-duration light source, Frank N. Miller—945(A)
Ingoing waves in final state of scattering problems, G. Breit and H. A. Bethe—888
Inner bremsstrahlung from P^{32}, Max Goodrich and Wilbur B. Payne—916(A)
Internal bremsstrahlung and ionization accompanying β decay, F. Boehm and C. S. Wu—518
Internal Compton effect in Ba^{137}, Larry Spruch and G. Goertzel—642(L)
Light scattering in liquid He, A. W. Lawson and Lothar Meyer—259
"Magnetic scanning" method for investigating hfs and isotope shift, S. Mrozowski—641(L)
Monitor for high-energy photons, C. A. McDonald, Jr., R. W. Kenney, and R. F. Post—951(A)
Photon monochromator for bremsstrahlung radiation, J. Goldemberg—1426(L)
Reduction of integral in theory of bremsstrahlung, A. Nordsieck—785
Resonant scattering of recoil-broadened γ rays, K. Ilakovac and P. B. Moon—254(L)
Theory of bremsstrahlung and pair production, I. Differential cross section, H. A. Bethe and L. C. Maximon—768; II. Integral cross section for pair production, Handel Davies, H. A. Bethe, and L. C. Maximon—788
Wavelength of scattered radiation, Arthur Bramley—246(L)
Radio Waves (see **Radiation**)
Radioactivity (see also **Nuclear Spectra**)
Average charge of recoil atoms from several nuclear transitions, S. Wexler—182
Decay properties of Am^{234} and possible rotational bands in α spectra of odd-even nuclei, Frank Asaro and I. Perlman—1423(L)
End-point energy determination of β emitters, M. Forro—915(A)
Further production of transcurium nuclides by neutron irradiation, Bernard G. Harvey, Stanley G. Thompson, Albert Ghiorso, and Gregory R. Choppin—1129
Internal bremsstrahlung and ionization accompanying β decay, F. Boehm and C. S. Wu—518
K^{40} branching ratio, G. J. Wasserburg and R. J. Hayden—645(L)
Kr neutron-deficient isotope, Albert A. Caretto, Jr., and Edwin O. Wiig—175
La^{140} half-life, H. W. Kirby and Murrell L. Salutsky—1051
Measurements of cyclotron neutron and γ fields for animal irradiation studies, S. W. Ross, E. Tochilin, and B. W. Shumway—945(A)
Methane proportional counter method for C^{14} age determinations, W. H. Burke, Jr., and W. G. Meinschein—915(A)
Natural tritium content of atmospheric hydrogen, A. V. Grosse, A. D. Kirshenbaum, J. Laurence Kulp, and W. S. Broecker—250(L)
Nd natural α activity, Esther C. Waldron, Virginia A. Schultz, and Truman P. Kohman—254(L)
New radioactive nuclides of rare earths, Thomas H. Handley and Elmer L. Olson—524
New 3.0-min Ce fission product and its 5.95-hr Pr daughter, S. S. Markowitz, W. Bernstein, and S. Katcoff—178
Pseudoscalar interaction in β decay, M. E. Rose and R. K. Osborn—1315
Pu^{244} from pile-irradiated Pu, M. H. Studier, P. R. Fields, P. H. Sellers, A. M. Friedman, C. M. Stevens, J. F. Mech, H. Diamond, J. Sedlet, and J. R. Huizenga—1433(L)
Radioactive isotope separation by nuclear recoil, H. Morinaga and D. J. Zaffarano—1422(L)
Range distribution of α particles following decays of Li^8 and B^8, F. C. Gilbert—499
Sm^{150} and Eu^{150} radioactivity, Milford R. Lee and Robert Katz—155
Ti^{44}, new Ti nuclide, R. A. Sharp and R. M. Diamond—358(L)
Transcurium isotopes produced in neutron irradiation of Pu, S. G. Thompson, A. Ghiorso, B. G. Harvey, and G. R. Choppin—908(L)
Y^{90} half-life, A. Chetham-Strode and E. M. Kinderman—1029
Raman Spectra (see **Molecular Structure and Spectra**)
Range and Energy Loss of Particles (see also **Scattering**)
Density effect for ionization loss at low energies, R. M. Sternheimer—351(L)
Energy loss and scattering of 0.624-Mev electrons, J. W. Robson, R. L. Stearns, and Arthur Lindener—360(A)
Energy loss and straggling of electrons, Charles Warner, III and Fritz Rohrlich—406
Energy loss of charged relativistic particles and periodicity of elements, Torbjörn Westermark—400
Energy loss of fast charged particle by Čerenkov radiation, R. M. Sternheimer—1434(E)
Energy spectrum resulting from electron slowing-down, L. V. Spencer and U. Fano—1172
Influence of chemical state on stopping of fast charged particles, Torbjörn Westermark—835
Ionization of pure gases and mixtures of gases by 5-Mev α particles, T. E. Bortner and G. S. Hurst—1236
Positron-electron differences in energy loss and multiple scattering, F. Rohrlich and B. C. Carlson—38
Range distribution of α particles following decays of Li^8 and B^8, F. C. Gilbert—499
Rotational excitation of homonuclear molecules, S. Stein, E. Gerjuoy, and T. Holstein—934(A)
Specific ionization and energy loss of fast charged particle, J. R. Allen—353(L)
Stopping powers of various elements for protons of energies from 400 to 1050 kev, Arthur B. Chilton, John N. Cooper, and James C. Harris—413
Transmission of 0–50 kev electrons by thin films with applications to β spectra, R. O. Lane and D. J. Zaffarano—916(A)

Recombination (see **Molecular Structure and Spectra**)
Rectifiers (see **Electrical Conductivity and Resistance; Semiconductors**)
Relativity and Gravitation
Resistance, Electrical (see **Electrical Conductivity and Resistance**)
Resonance Radiation (see **Radiation**)

Scattering, General (see also **Diffraction; Elementary Particle Interactions; Nuclear Reactions; Range and Energy Loss of Particles**)
Effect of $^3P_2 - {}^3F_2$ coupling on nucleon-nucleon scattering, R. M. Thaler, J. Bengston, and G. Breit—644(L)
Impedance concept in nuclear scattering, D. L. Falkoff—364(A)
Inelastic collisions in Molière theory of multiple scattering, U. Fano—117
Ingoing waves in final state of scattering problems, G. Breit and H. A. Bethe—888
One of Schwinger's variational principles for scattering, Geoffrey F. Chew—341
Phase shift analysis of high-energy nucleon-nucleon scattering, R. M. Thaler and J. Bengston—643(L)
Scattering of many-particle systems, S. Tamor—227
Three-body scattering problems, Sidney Borowitz and Bernard Friedman—251(L)
Scattering of α Particles (see also **Nuclear Reactions Induced by α Particles and He^3**)
Elastic scattering of α particles by Ne, E. Goldberg, W. Haeberli, A. I. Galonsky, and R. A. Douglas—800
Elastic scattering of intermediate-energy α particles by Au, George W. Farwell and Harvey E. Wegner—356(L)
Scattering of Atoms and Molecules (see **Atomic and Molecular Beams**)
Scattering of Deuterons (see also **Nuclear Reactions Induced by Deuterons and Tritons**)
Elastic scattering of deuterons by He, A. Galonsky, R. Douglas, and W. Haeberli—928(A)
Scattering of Electrons and Positrons (see also **Electrons and Positrons**)
Elastic scattering of electrons by Coulomb field of nuclei using Born approximations, Vachaspati—502
Elastic scattering of 1-Mev electrons from Al and Au, Robert T. Bayard and J. L. Yntema—1412(L)
Energy loss and scattering of 0.624-Mev electrons, J. W. Robson, R. L. Stearns, and Arthur Lindener—362(A)
Higher-order potential effects in radiative correction to scattering of slow electrons, M. H. Mittleman—453
Interaction of β particles with matter, Ralph H. Müller—891(L)
Interpretation of electron scattering experiments, L. I. Schiff—1434(E)
Microwave measurement of velocity dependence of collision cross-section of slow electrons in He, Lawrence Gould—648(A)
Multiple scattering of relativistic electrons, L. V. Spencer and C. H. Blanchard—114
Non-single scattering of electrons at oblique incidence, Morton Hamermesh and James Monahan—963
Phase shift calculation of high-energy electron scattering by nuclei, D. R. Yennie, R. N. Wilson, and D. G. Ravenhall—948(A); II, D. G. Ravenhall, D. R. Yennie, and R. N. Wilson—949(A)
Positron-electron differences in energy loss and multiple scattering, F. Rohrlich and B. C. Carlson—38
Rotational excitation of homonuclear molecules, S. Stein, E. Gerjuoy, and T. Holstein—934(A)
Scattering of high-energy electrons by heavy nuclei, Elizabeth Urey Baranger—1127(L)
Second Born approximation to scattering of fast electrons and positrons by nuclei, R. N. Wilson—949(A)
Sign of phase shift in elastic scattering of electrons, D. R. Yennie, D. G. Ravenhall, and E. Baranger—1128(L)
Variational calculation of elastic scattering of electrons by H atoms, Howard Boyet and Sidney Borowitz—1225
Scattering of Mesons (see also **Mesons; Nuclear Reactions Induced by Mesons**)
Inelastic scattering of 220-Mev π^- mesons in emulsions, W. F. Fry—845
Interaction of pions with complex nuclei, Donald Harvey Stork—868
Possible relationships between π-meson nucleon scattering and π-meson production in nucleon-nucleon collisions, A. Aitken, H. Mahmoud, E. M. Henley, M. A. Ruderman, and K. M. Watson—1349
Radiative effects in meson-nucleon scattering, Stanley Deser—612
Scattering of 45-Mev positive pions by hydrogen, Jay Orear, J. J. Lord, and A. B. Weaver—575
Scattering of negative pions by deuterium, D. E. Nagle—918(A)
Scattering of 151- and 188-Mev positive pions by protons, George Homa, Gerson Goldhaber, and Leon M. Lederman—554
Scattering of 65-Mev pions in hydrogen, D. Bodansky, A. M. Sachs, and J. Steinberger—918(A)
Signs of phase shifts in pion-proton scattering, Jay Orear—918(A)
Scattering of Neutrons (see also **Nuclear Reactions Induced by Neutrons**)
Cross sections for production of In^{115m} and Au^{197m} by inelastic scattering of neutrons, H. C. Martin, B. C. Diven, and R. F. Taschek—199
Crystal dynamics and inelastic scattering of neutrons, G. Placzek and L. Van Hove—1207
Determination of scattering resonance parameters from total cross section, W. Y. Kato, D. J. Hughes, and J. S. Levin—931(A)
Diffuse magnetic scattering of neutrons: zinc ferrite, B. N. Brockhouse, L. M. Corliss, and J. M. Hastings—923(A)
Direct integration of neutron transport equation, J. Heller and H. Keller—932(A)
γ rays excited by inelastic scattering of neutrons in Pb, Bi, Fe, Ni, and Cr, M. A. Rothman and C. E. Mandeville—796
Incoherent neutron scattering by polycrystals, G. Placzek—895(L)
Inelastic scattering of neutrons by In^{115} and Au^{197}, A. A. Ebel and Clark Goodman—197
Inelastic scattering of neutrons near thresholds, B. Margolis—204
Inelastic scattering of protons and neutrons by deuterons, R. M. Frank and J. L. Gammel—463
Lowest neutron scattering resonance in Co, F. G. P. Seidl—931(A)
Neutron diffraction in vitreous silica, R. J. Breen and A. H. Weber—923(A)
Neutron inelastic scattering, Robert M. Kiehn and Clark Goodman—177
n-p scattering at 395 Mev. I, A. J. Hartzler and R. T. Siegel—928(A); II, R. T. Siegel and A. J. Hartzler—928(A)
n-p scattering with spin-orbit coupling, II. Variational formulation and effective range theory, L. C. Biedenharn and J. M. Blatt—1387

Scattering of Neutrons (Continued)
Polarization of neutrons, C. P. Stanford, T. E. Stephenson, F. W. Cochran, and S. Bernstein—931(A)
Scattering of fast neutrons by Fe, Pb, and Cr, M. A. Rothman, D. W. Kent, and C. E. Mandeville—1434(E)
Scattering of 1-Mev neutrons by intermediate and heavy elements, M. Walt and H. H. Barschall—1062
Scattering of polarized neutrons from heavy nuclei, S. E. Darden, R. E. Fields, and R. K. Adair—931(A)
Temperature variation of magnetic inelastic scattering of slow neutrons, Leon Van Hove—268
Thermal neutron resonance of Sm, A. W. McReynolds and E. Andersen—195
Scattering of Protons (see also **Nuclear Reactions Induced by Protons**)
Angular distributions of 22-Mev protons elastically scattered by various elements, Bernard L. Cohén and Rodger V. Neidigh—282
Cross sections for p-p scattering at 330 and 225 Mev, O. Chamberlain, G. Pettengill, E. Segrè, and C. Wiegand—1424(L)
Differential cross sections for elastic scattering of protons by He^4, K. F. Famularo, R. J. S. Brown, H. D. Holmgren, and T. F. Stratton—928(A)
Double scattering of high-energy protons, C. L. Oxley, W. F. Cartwright, and J. Rouvina—806
Effect of $^3P_2 - {}^3F_2$ coupling on nucleon-nucleon scattering, R. M. Thaler, J. Bengston, and G. Breit—644(L)
Elastic scattering of protons by α particles, S. Sack, L. C. Biedenharn, and G. Breit—321
Elastic scattering of protons by He at 5.78 Mev, W. E. Kreger, W. Jentschke, and P. G. Kruger—837
Elastic scattering of protons by N, H. E. Gove, A. J. Ferguson, and J. T. Sample—928(A)
Experiments with high-energy polarized protons, O. Chamberlain, E. Segrè, R. Tripp, C. Wiegand, and T. Ypsilantis—1430(L)
γ rays from inelastic scattering of protons by Ne, Mason C. Cox, Jan J. van Loef, and D. A. Lind—925(A)
Inelastic scattering of protons and neutrons by deuterons, R. M. Frank and J. L. Gammel—463
Inelastic scattering of protons by F^{19}, R. W. Peterson, C. A. Barnes, W. A. Fowler, and C. C. Lauritsen—951(A)
Inelastic scattering of protons by Li^7, F. Mozer, W. A. Fowler, and C. C. Lauritsen—829
Inelastic scattering of 31-Mev protons from heavy elements, R. M. Eisberg and G. Igo—1039
Level densities of nuclei from inelastic scattering of 18-Mev protons, P. C. Gugelot—425
N^{14} energy levels from scattering of protons by C^{13}, Edmund A. Milne—762
Phase shift analysis of high-energy nucleon-nucleon scattering, R. M. Thaler and J. Bengston—643(L)
Polarization by p-p collision at 310 Mev, J. Marshall, L. Marshall, and H. G. de Carvalho—1431(L)
p-p differential elastic scattering cross sections at 144, 271, and 429 Mev, V. A. Nedzel, J. Marshall, and L. Marshall—927(A)
p-p elastic scattering and pion production at 419 Mev, J. Marshall, L. Marshall, and V. A. Nedzel—927(A)
Proton-deuteron scattering at 20 Mev, David O. Caldwell, J. Reginald Richardson, and Herbert N. Royden—942(A)
Search for polarization of protons from 450-Mev synchrocyclotron, L. Marshall, V. A. Nedzel, and J. Marshall—927(A)
Scattering of Radiation (see **Radiation; X-Rays**)
Scintillation Counters (see **Methods and Instruments**)
Secondary Emission (see **Electrical Properties**)
Semiconductors
Analogies between lattice defects and current carriers in semiconductors, J. Rothstein—912(A)
Anomalous optical absorption limit in InSb, Elias Burstein—632(L)
Au as donor in Si, E. A. Taft and F. Hubbard Horn—64
Bulk photoconductivity in PbS, D. E. Soule and R. J. Cashman—635(L)
Calculation of energy band structures of diamond and Ge crystals by method of orthogonalized plane waves, Frank Herman—1214
Capacity measurements on point contact Ge diodes, Maynard Dawson and George Finn—913(A)
Conduction properties of p-type Ge between 25°C and 925°C, W. C. Dunlap, Jr., D. E. McMillan, and R. A. Brooks—911(A)
Cyclotron resonance in Ge crystals, A. F. Kip, G. Dresselhaus, and C. Kittel—952(A)
Degeneracy in Ge, Esther M. Conwell—1118(L)
Degeneracy in high-purity InSb, A. C. Beer, R. K. Willardson, and A. E. Middleton—912(A)
Diffusivity and solubility of Cu in Ge, C. S. Fuller, J. D. Struthers, J. A. Ditzenberger, and K. B. Wolfstirn—1182
Directional properties of cyclotron resonance in Ge, Benjamin Lax, H. J. Zeiger, R. N. Dexter, and E. S. Rosenblum—1418(L)
Dislocations in plastically-deformed Ge, G. L. Pearson, W. T. Read, Jr., and F. J. Morin—666
Drift mobilities in semiconductors. II. Si, M. B. Prince—1204
Effect of traps on carrier injection in semiconductors, H. Y. Fan—1434(E)
Electrical properties of Ge crystals, containing compensated impurities, Vernon Ozarow—371
Electrical properties of n-type Ge, P. P. Debye and E. M. Conwell—693
Electron-voltaic effect in p-n junctions induced by β-particle bombardment, P. Rappaport—246(L)
Infrared absorption of NiO, R. W. Johnston and D. C. Cronemeyer—634(L)
Infrared absorption, photoconductivity, and impurity states in Ge, W. Kaiser and H. Y. Fan—911(A); 977
Infrared lattice absorption bands in Ge, Si, and diamond, R. J. Collins and H. J. Fan—674
Infrared photoconductivity due to neutral impurities in Ge, E. Burstein, J. W. Davisson, E. E. Bell, W. J. Turner, and H. G. Lipson—65
Lattice-scattering mobility in Ge, F. J. Morin—62
Low-temperature recombination and trapping in Ge, D. Navon and H. Y. Fan—911(A)
Magnetic field dependence of Hall coefficient in InSb, R. K. Willardson, A. C. Beer, and A. E. Middleton—912(A)
Magnetoresistance in InSb and GaSb single crystals, M. Tanenbaum, G. L. Pearson, and W. L. Feldmann—912(A)
New galvanomagnetic effect, I. Theory, Colman Goldberg—913(A); II. Experiments with Ge, R. E. Davis and Colman Goldberg—913(A)
Optical properties of some group III-group V compounds, H. B. Briggs, R. F. Cummings, H. J. Hrostowski, and M. Tanenbaum—912(A)
OPW method for calculating energy eigenvalues extended to crystals of compounds, Truman O. Woodruff—947(A)
Photoelectric Hall effect in Ge single crystals, John J. Oberly—911(A)
Radiation effects in InSb, J. W. Cleland and J. H. Crawford, Jr.—894(L)

Secondary electron emission from Ge, J. B. Johnson and K. G. McKay—668
Self-diffusion in Ge, Harry Letaw, Jr., Lawrence M. Slifkin, and William M. Portnoy—892(L)
Temperature dependence of transverse magnetoresistance effect in InSb, T. C. Harman, R. K. Willardson, and A. C. Beer—912(A)
Theory of galvanomagnetic effects in N-Ge, S. Meiboom and B. Abeles—1121(L)
Water vapor and "channel" effect in *n-p-n* junction transistors, R. H. Kingston—346(L)
Shock Waves (see **Fluid Dynamics**)
Solid State (see **Crystalline State**)
Solutions (see **Liquids**)
Sound (see **Acoustics**)
Spallation (see **Nuclear Reactions**)
Spark Discharge (see **Electrical Discharges**)
Specific Heat (see **Thermal Properties**)
Spectra, Atomic (see **Atomic Structure and Spectra**)
Spectra, General
New method for exciting metallic spectra by active N_2. Excitation of Xe, Carl Kenty—651(A)
Theory of fine structure pressure broadening of spectral lines, Makoto Takeo and Shang-Yi Ch'en—420
Spectra, Molecular (see **Molecular Structure and Spectra**)
Spectra, Nuclear (see **Nuclear Spectra**)
Spectroscopy Technique (see **Methods and Instruments**)
Spinor Fields (see **Field Theory**)
Standards (see **Constants, Standards, Units**)
Stark Effect (see **Atomic Structure and Spectra**)
Statistical Mechanics and Thermodynamics
Connection between Smoluchowski equation and Kramers-Chandrasekhar equation, R. W. Davies—1169
Generalization of Yang and Lee's theory of condensation, Louis Witten—1131
Generalized Fermi-Thomas theory, Malcolm K. Brachman—636(L)
Kinetic approach to collision processes in gases. I, E. P. Gross and M. Krook—936(A); II, M. Krook, P. L. Bhatnagar, and E. P. Gross—936(A)
Nature of higher-order phase transitions with application to liquid He, O. K. Rice—1161
Quantum-mechanical partition function, G. V. Chester—606
Quantum statistics of closed and open systems, P. T. Landsberg—1170
Solution of Boltzmann equation for Maxwellian molecules, E. P. Gross—347(L)
Statistical mechanics of cathode sputtering, Don E. Harrison, Jr.—652(A)
Temperature measurement below 1°K, D. H. Howling, F. J. Darnell, and E. Mendoza—1416(L)
Thermal energy in almost-normal modes, J. Elmer Rhodes, Jr.—1
Variational formulas in evaporation theory, John Greenstadt—1140
Statistical Methods (see **Mathematical Methods**)
Superconductivity
Behavior of positrons in superconductors, M. Dresden—1413(L)
Isotope effect in superconductivity, Jules de Launay—661
Superconducting compounds, B. T. Matthias, E. Corenzwit, and C. E. Miller—1415(L)
Superconductivity of some transition metal compound, George F. Hardy and John K. Hulm—1006
Supersonics (see **Fluid Dynamics**)
Thermal Conductivity (see **Thermal Properties**)
Thermal Diffusion (see **Diffusion**)
Thermal Expansion (see **Thermal Properties**)
Thermal Properties
Apparent anomalies in low temperature heat capacities, J. R. Clement—1420(L)
Coefficient of expansion of liquid helium II, K. R. Atkins and M. H. Edwards—1416(L)
Heat capacity of Gd from 15 to 355°K, M. Griffel, R. E. Skochdopole, and F. H. Spedding—657
Specific heat of alloy $FeNi_3$ and of sigma-phase FeCr, David S. Bloom—952(A)
Specific heat of liquid He^3, T. R. Roberts and S. G. Sydoriak—1418(L)
Specific heat of 96 percent He^3 below 1°K, G. de Vries and J. G. Daunt—631(L)
Specific heat of 96 percent liquid He^3 between 1.3°K and 2.3°K, G. de Vries and J. G. Daunt—360(A)
Thermal conductivity of graphite, Alan W. Smith—952(A)
Thermal conductivity of NaCl, William H. Bessey and Harold Weisbrod—923(A)
Thermal microstructure in ocean, W. N. English—945(A)
Thermodynamic properties of $Mn(ND_4)_2(SO_4)_2 \cdot 6D_2O$ below 1°K, J. W. T. Dabbs and L. D. Roberts—935(A)
Thermal Radiation (see **Radiation**)
Thermionic Emission (see **Electrical Properties**)
Thermodynamics (see **Statistical Mechanics and Thermodynamics**)
Thermoelectric Effect (see **Electrical Properties**)
Thermoluminescence (see **Luminescence**)
Thermomagnetic Effect (see **Magnetic Properties**)
Total Cross Sections (see **Electrons and Positrons; Nuclear Reactions**)
Transmutation (see **Nuclear Reactions**)

Uncertainty Principle (see **Quantum Mechanics**)
Units (see **Constants, Standards, Units**)

Vacuum Tubes (see **Methods and Instruments**)
Van der Waals Forces (see **Molecular Structure and Spectra**)
Viscosity (see **Liquids**)

Wave Mechanics (see **Quantum Mechanics**)
Work Function (see **Electrical Properties**)
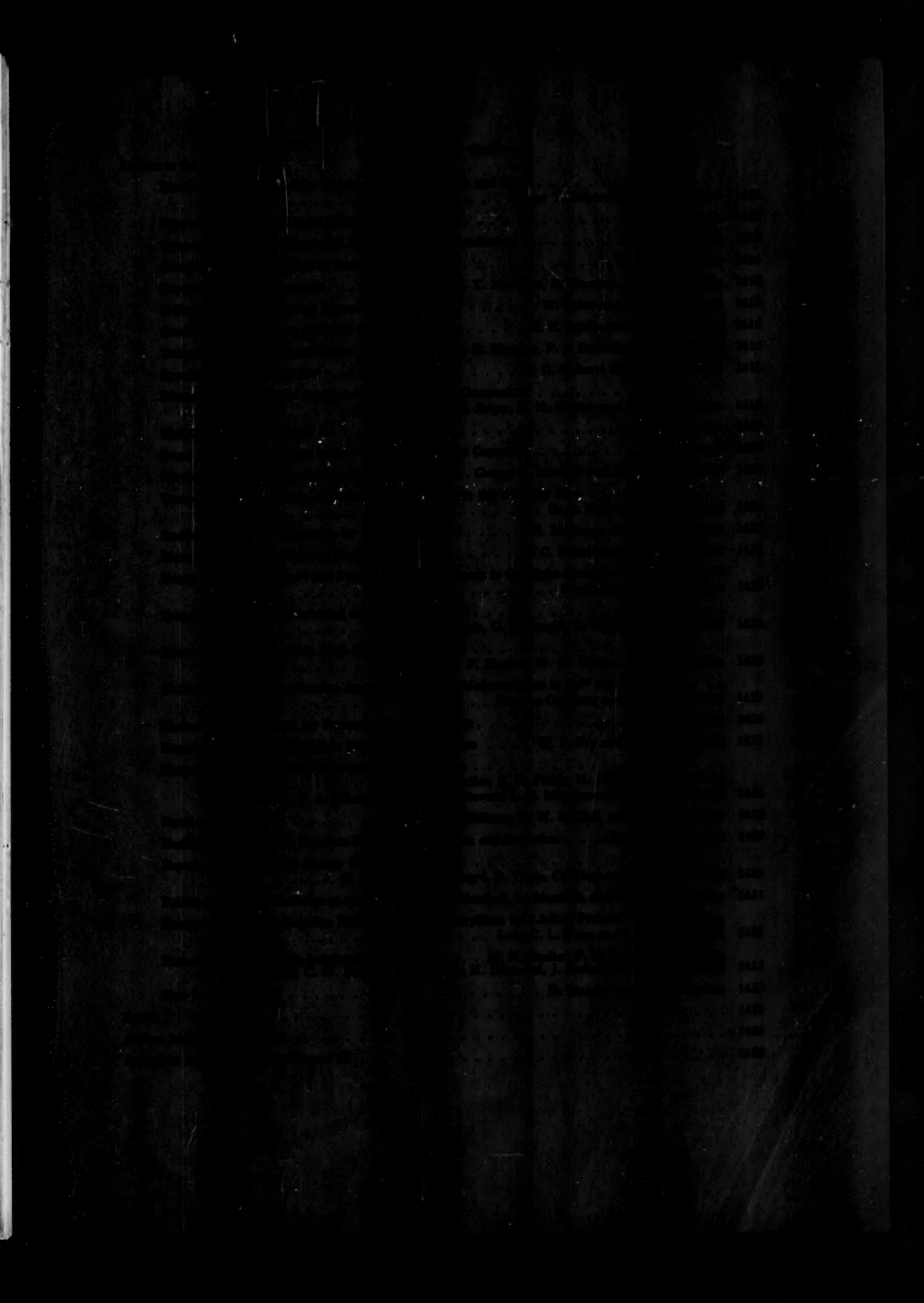
X-Rays
Method for measuring Auger transitions, Charles E. Roos—401
Precision measurement at 24 500 volts of conversion constant λV, Gaelen L. Felt, John N. Harris, and Jesse W. M. DuMond—1434(E)
Reflection of 8A x-rays by mirror surfaces, Roy W. Hendrick, Jr.—942(A)
Relative intensities of π- and μ-meson x-rays of K and L series in low Z elements, M. B. Stearns, S. DeBenedetti, M. Stearns, and L. Leipuner—1123(L)
Small angle x-ray scattering from liquid He I and liquid He II, Arthur G. Tweet—15
X-ray absorption processes in proportional counter gases, C. S. Duffendack and C. F. Hendee—653(A)
X-ray diffraction studies of dual layer and simultaneously evaporated bimetal films after artificial aging by heating, William E. Woolf and Richard B. Belser—930(A)
X-ray microscope mirror systems, A. V. Baez and M. Weissbluth—942(A)